frontiers | Research Topics

Immune modulation in tumor microenvironment: New perspectives for cancer immunotherapy

Edited by
Qian Xiao, Xuejun Sun, Zimu Deng and Jian Cao

Published in
Frontiers in Cell and Developmental Biology

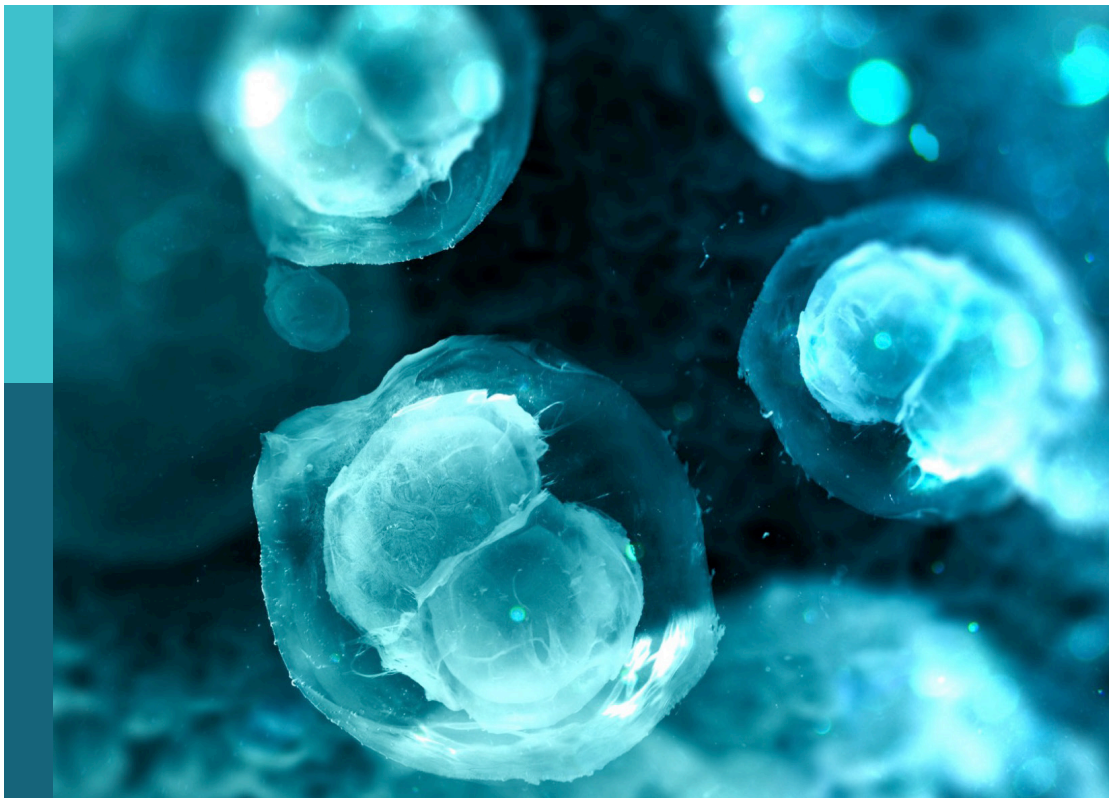

FRONTIERS EBOOK COPYRIGHT STATEMENT

The copyright in the text of individual articles in this ebook is the property of their respective authors or their respective institutions or funders. The copyright in graphics and images within each article may be subject to copyright of other parties. In both cases this is subject to a license granted to Frontiers.

The compilation of articles constituting this ebook is the property of Frontiers.

Each article within this ebook, and the ebook itself, are published under the most recent version of the Creative Commons CC-BY licence. The version current at the date of publication of this ebook is CC-BY 4.0. If the CC-BY licence is updated, the licence granted by Frontiers is automatically updated to the new version.

When exercising any right under the CC-BY licence, Frontiers must be attributed as the original publisher of the article or ebook, as applicable.

Authors have the responsibility of ensuring that any graphics or other materials which are the property of others may be included in the CC-BY licence, but this should be checked before relying on the CC-BY licence to reproduce those materials. Any copyright notices relating to those materials must be complied with.

Copyright and source acknowledgement notices may not be removed and must be displayed in any copy, derivative work or partial copy which includes the elements in question.

All copyright, and all rights therein, are protected by national and international copyright laws. The above represents a summary only. For further information please read Frontiers' Conditions for Website Use and Copyright Statement, and the applicable CC-BY licence.

ISSN 1664-8714
ISBN 978-2-83251-334-7
DOI 10.3389/978-2-83251-334-7

About Frontiers

Frontiers is more than just an open access publisher of scholarly articles: it is a pioneering approach to the world of academia, radically improving the way scholarly research is managed. The grand vision of Frontiers is a world where all people have an equal opportunity to seek, share and generate knowledge. Frontiers provides immediate and permanent online open access to all its publications, but this alone is not enough to realize our grand goals.

Frontiers journal series

The Frontiers journal series is a multi-tier and interdisciplinary set of open-access, online journals, promising a paradigm shift from the current review, selection and dissemination processes in academic publishing. All Frontiers journals are driven by researchers for researchers; therefore, they constitute a service to the scholarly community. At the same time, the *Frontiers journal series* operates on a revolutionary invention, the tiered publishing system, initially addressing specific communities of scholars, and gradually climbing up to broader public understanding, thus serving the interests of the lay society, too.

Dedication to quality

Each Frontiers article is a landmark of the highest quality, thanks to genuinely collaborative interactions between authors and review editors, who include some of the world's best academicians. Research must be certified by peers before entering a stream of knowledge that may eventually reach the public - and shape society; therefore, Frontiers only applies the most rigorous and unbiased reviews. Frontiers revolutionizes research publishing by freely delivering the most outstanding research, evaluated with no bias from both the academic and social point of view. By applying the most advanced information technologies, Frontiers is catapulting scholarly publishing into a new generation.

What are Frontiers Research Topics?

Frontiers Research Topics are very popular trademarks of the *Frontiers journals series*: they are collections of at least ten articles, all centered on a particular subject. With their unique mix of varied contributions from Original Research to Review Articles, Frontiers Research Topics unify the most influential researchers, the latest key findings and historical advances in a hot research area.

Find out more on how to host your own Frontiers Research Topic or contribute to one as an author by contacting the Frontiers editorial office: frontiersin.org/about/contact

Immune modulation in tumor microenvironment: New perspectives for cancer immunotherapy

Topic editors

Qian Xiao — The State University of New Jersey, United States
Xuejun Sun — Xi'an Jiaotong University, China
Zimu Deng — Shanghai Institute of Biochemistry and Cell Biology, Chinese Academy of Sciences (CAS), China
Jian Cao — The State University of New Jersey, United States

Citation

Xiao, Q., Sun, X., Deng, Z., Cao, J., eds. (2023). *Immune modulation in tumor microenvironment: New perspectives for cancer immunotherapy*. Lausanne: Frontiers Media SA. doi: 10.3389/978-2-83251-334-7

Table of contents

05 Editorial: Immune modulation in tumor microenvironment: New perspectives for cancer immunotherapy
Zimu Deng, Xuejun Sun, Jian Cao and Qian Xiao

09 Tumor Associated Macrophages, as the Dominant Immune Cells, Are an Indispensable Target for Immunologically Cold Tumor—Glioma Therapy?
Ni Tong, Zhenqiang He, Yujie Ma, Zheng Wang, Ziming Huang, Haihong Cao, Lanyang Xu, Yuheng Zou, Wanyu Wang, Chenpeng Yi, Zhixin Yin and Qirui Wang

26 BRAF Mutation as a Potential Therapeutic Target for Checkpoint Inhibitors: A Comprehensive Analysis of Immune Microenvironment in BRAF Mutated Colon Cancer
Shuyi Cen, Kun Liu, Yu Zheng, Jianzhen Shan, Chao Jing, Jiale Gao, Hongming Pan, Zhigang Bai and Zhen Liu

39 Two Similar Signatures for Predicting the Prognosis and Immunotherapy Efficacy of Stomach Adenocarcinoma Patients
Taohua Yue, Shuai Zuo, Jing Zhu, Shihao Guo, Zhihao Huang, Jichang Li, Xin Wang, Yucun Liu, Shanwen Chen and Pengyuan Wang

62 The Prognosis and Immune Checkpoint Blockade Efficacy Prediction of Tumor-Infiltrating Immune Cells in Lung Cancer
Xiangzheng Liu, Xueqian Shang, Jian Li and Shijie Zhang

82 Interleukin 32 Promotes Foxp3$^+$ Treg Cell Development and CD8$^+$ T Cell Function in Human Esophageal Squamous Cell Carcinoma Microenvironment
Li Han, Shiyu Chen, Zheyi Chen, Bingqian Zhou, Yingxia Zheng and Lisong Shen

92 Ferroptosis Driver *SOCS1* and Suppressor *FTH1* Independently Correlate With M1 and M2 Macrophage Infiltration in Head and Neck Squamous Cell Carcinoma
Zhang-Wei Hu, Yi-Hui Wen, Ren-Qiang Ma, Lin Chen, Xue-Lan Zeng, Wei-Ping Wen and Wei Sun

104 Characterization of Molecular Heterogeneity Associated With Tumor Microenvironment in Clear Cell Renal Cell Carcinoma to Aid Immunotherapy
Weimin Zhong, Yinan Li, Yichu Yuan, Hongbin Zhong, Chaoqun Huang, Jiwei Huang, Yao Lin and Jiyi Huang

122 Characterization of Immune-Related Long Non-coding RNAs to Construct a Novel Signature and Predict the Prognosis and Immune Landscape of Soft Tissue Sarcoma
Zhengjun Lin, Ke Pang, Hongli Li, Xianghong Zhang, Jia Wan, Tao Zheng, Tang Liu and Weijun Peng

137 Tumor Immune Microenvironment Landscape in Glioma Identifies a Prognostic and Immunotherapeutic Signature
Chunyu Zhang, Lirui Guo, Zhongzhou Su, Na Luo, Yinqiu Tan, Pengfei Xu, Liguo Ye, Shiao Tong, Haitao Liu, Xiaobin Li, Qianxue Chen and Daofeng Tian

153 Prognosis and Immunotherapy Significances of a Cancer-Associated Fibroblasts-Related Gene Signature in Gliomas
Zhimin Chen, Shenghua Zhuo, Guiying He, Jingzhi Tang, Weijie Hao, Wei-Qiang Gao, Kun Yang and Huiming Xu

167 Heme Oxygenase-1 Predicts Risk Stratification and Immunotherapy Efficacy in Lower Grade Gliomas
Wenrui Ye, Zhixiong Liu, Fangkun Liu and Cong Luo

186 Immune Landscape Refines the Classification of Colorectal Cancer With Heterogeneous Prognosis, Tumor Microenvironment and Distinct Sensitivity to Frontline Therapies
Zaoqu Liu, Yaxin Guo, Xiuxiu Yang, Chen Chen, Dandan Fan, Xiaoke Wu, Chaohua Si, Yanxin Xu, Bo shao, Zhuang Chen, Qin Dang, Wenming Cui, Xinwei Han, Zhenyu Ji and Zhenqiang Sun

200 Immune Characteristics of LYN in Tumor Microenvironment of Gliomas
Chonghua Jiang, Hao Zhang, Wantao Wu, Zeyu Wang, Ziyu Dai, Liyang Zhang, Zhixiong Liu and Quan Cheng

215 Identification of Tumor Antigens and Immune Subtypes in Lung Adenocarcinoma for mRNA Vaccine Development
Ran Xu, Tong Lu, JiaYing Zhao, Jun Wang, Bo Peng and LinYou Zhang

229 BCL2A1 and CCL18 Are Predictive Biomarkers of Cisplatin Chemotherapy and Immunotherapy in Colon Cancer Patients
Taohua Yue, Xiangzheng Liu, Shuai Zuo, Jing Zhu, Jichang Li, Yucun Liu, Shanwen Chen and Pengyuan Wang

252 Siglec Receptors Modulate Dendritic Cell Activation and Antigen Presentation to T Cells in Cancer
Jinyu Wang, Michela Manni, Anne Bärenwaldt, Ronja Wieboldt, Nicole Kirchhammer, Robert Ivanek, Michal Stanczak, Alfred Zippelius, David König, Natalia Rodrigues Manutano and Heinz Läubli

263 Key Players of the Immunosuppressive Tumor Microenvironment and Emerging Therapeutic Strategies
Kevin Park, Mysore S. Veena and Daniel Sanghoon Shin

287 ITGAL as a Prognostic Biomarker Correlated With Immune Infiltrates in Gastric Cancer
Junchang Zhang, Han Wang, Cheng Yuan, Jing Wu, Jiannan Xu, Songyao Chen, Changhua Zhang and Yulong He

frontiers | Frontiers in Cell and Developmental Biology

TYPE Editorial
PUBLISHED 04 January 2023
DOI 10.3389/fcell.2022.1103705

Check for updates

OPEN ACCESS

EDITED AND REVIEWED BY
Ramani Ramchandran,
Medical College of Wisconsin,
United States

*CORRESPONDENCE
Qian Xiao,
qx61@cinj.rutgers.edu

SPECIALTY SECTION
This article was submitted to Molecular and Cellular Pathology, a section of the journal Frontiers in Cell and Developmental Biology

RECEIVED 20 November 2022
ACCEPTED 19 December 2022
PUBLISHED 04 January 2023

CITATION
Deng Z, Sun X, Cao J and Xiao Q (2023), Editorial: Immune modulation in tumor microenvironment: New perspectives for cancer immunotherapy.
Front. Cell Dev. Biol. 10:1103705.
doi: 10.3389/fcell.2022.1103705

COPYRIGHT
© 2023 Deng, Sun, Cao and Xiao. This is an open-access article distributed under the terms of the Creative Commons Attribution License (CC BY). The use, distribution or reproduction in other forums is permitted, provided the original author(s) and the copyright owner(s) are credited and that the original publication in this journal is cited, in accordance with accepted academic practice. No use, distribution or reproduction is permitted which does not comply with these terms.

Editorial: Immune modulation in tumor microenvironment: New perspectives for cancer immunotherapy

Zimu Deng[1], Xuejun Sun[2], Jian Cao[3] and Qian Xiao[3]*

[1]Shanghai Institute of Biochemistry and Cell Biology, Chinese Academy of Sciences (CAS), Shanghai, China, [2]Xi'an Jiaotong University, Xi'an, China, [3]Rutgers Cancer Institute of New Jersey, Rutgers, The State University of New Jersey, New Brunswick, NJ, United States

KEYWORDS

tumor microenvironment, immunotherapy, immune suppression, inflammation, cancer progression

Editorial on the Research Topic
Immune modulation in tumor microenvironment and cancer immunotherapy

Introduction

The advances in immunotherapies in the last decades have brought new hope in the battle against cancer (Wang et al., 2019; Morad et al., 2021). These therapies include immune checkpoint blockade (ICB), chimeric antigen receptors T-cell (CAR-T), T-cell receptor (TCR)-based adoptive cell therapy, oncolytic virus, and cancer vaccine. Unfortunately, intrinsic and acquired resistance prevent most patients from benefiting from these emerging treatments (Majzner and Mackall, 2018; Morad et al., 2021). Tumor cells are heterogeneous and able to harness epigenomic alterations to alter the phenotype. Besides cancer cells, endothelial cells, immune cells, tumor-associated fibroblasts, extracellular matrix components, metabolic products, and signaling molecules form structurally complicated tissues known as the tumor microenvironment (TME) (Hu et al., 2022). The heterogeneity of TME provides unique opportunities for tumors to escape immune restriction through various mechanisms (Zhengxi Chen, 2020; Hu et al., 2022). Therefore, discovering and targeting these immune escape mechanisms have been a focused area in cancer immunology, aiming to develop new strategies to improve immunotherapies (Bader et al., 2020; Hu et al., 2020; Hu et al., 2022).

This Research Topic focuses on the immunosuppressive TME in tumor initiation, progression, and resistance to immunotherapies. 16 outstanding original studies and 2 review articles from 139 authors have been published, demonstrating emerging interest in cancer immunotherapy. This Research Topic contains studies on the following three topics.

Immune modulators in TME

Tumors are heterogeneous. It is a complex structure tissue comprised of various types of cells (Figure 1). Those immunosuppressive or immune escape mechanisms are initiated by

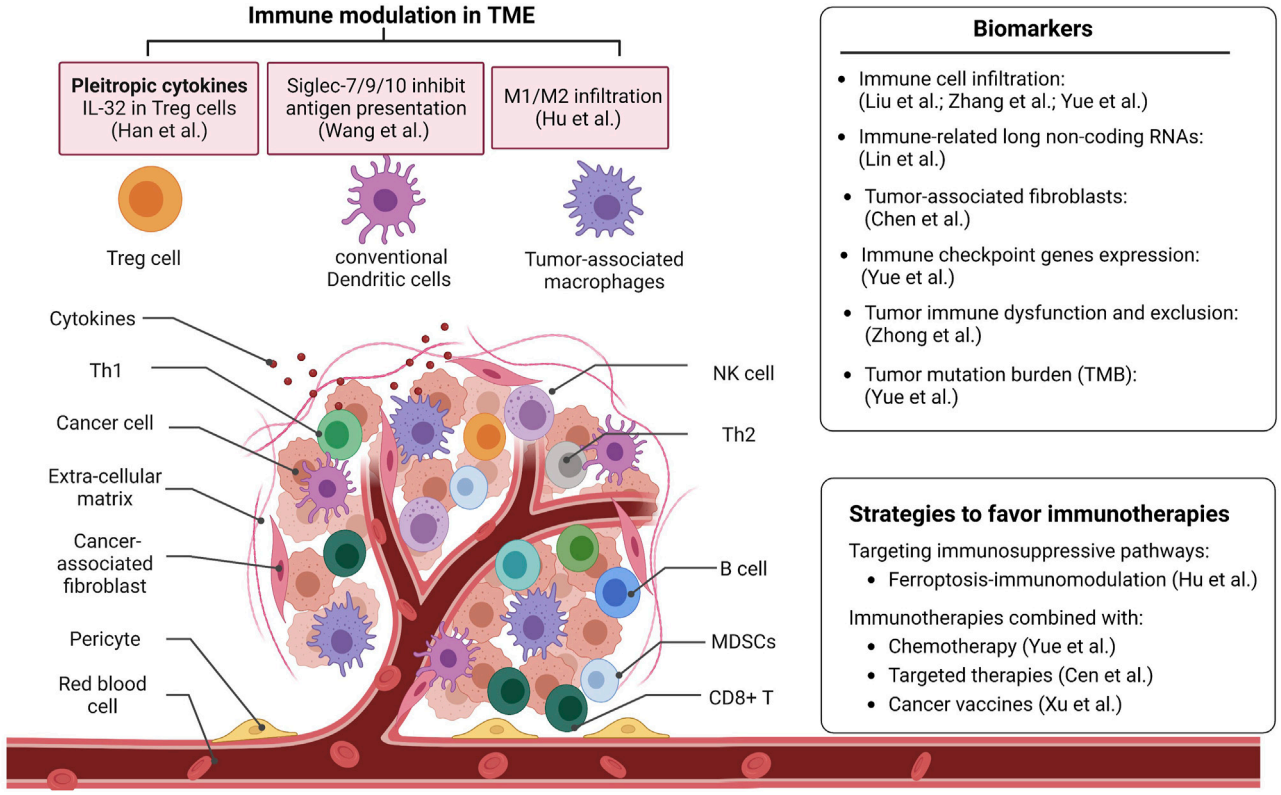

FIGURE 1
The representative studies from the Research Topic advance the understanding of the tumor microenvironment. This Research Topic also provides new biomarkers for predicting immune checkpoint blockade therapy and approaches to favor immunotherapies. NK cell: Natural Killer cell; Th1: Type 1T helper; Th2: Type 2 T helper; MDSCs: Myeloid-derived suppressor cells.

tumor cells or non-tumor cells to suppress the antitumor immune response. A comprehensive understanding of the TME favors effective immune therapy (Binnewies et al., 2018).

Abnormal cytokine secretion in TME is important in suppressing tumor immune response. In this Research Topic, Han et al. analyzed the single-cell RNA sequencing data to investigate the function of Interleukin-32 (IL-32) in the TME of esophageal squamous cell carcinoma (ESCC). They found that IL-32 is highly expressed in $CD4^+$ regulatory T cells (Treg cells). Knockdown of IL-32 reduced Foxp3 expressions in $CD4^+$ T cells, which indicates IL-32 may be used as a target for ESCC cancer immunotherapy.

Cell-cell interaction proteins, such as Siglecs (Sialic acid-binding immunoglobulin-like lectins), have also been reported as potential new ICB molecules. Wang et al. found that classical conventional dendritic cells (DCs) highly expressed inhibitory Siglecs, such as Siglec-7, Siglec-9, and Siglec-10, in human cancer samples. Consistently, they found that the expression of the Siglec-E receptor is upregulated on tumor-associated cDCs *in vivo* murine tumor models. Expressing these inhibitory Siglecs in DC cell lines and bone marrow-derived DCs showed impaired maturation states. Furthermore, depletion or inhibition of these inhibitory Siglecs on DCs enhanced the priming process of antigen-specific T cells and induced T cell proliferation. This study enhanced the understanding of the inhibitory functions of Siglecs on DCs and revealed new potential targets for cancer immunotherapy.

Biomarkers to predict immune checkpoint blockade (ICB) therapy

Identifying novel biomarkers to predict the response of cancer patients to ICB therapy is a challenge for immunotherapy (Crow et al., 2019). Immune cell infiltration is one of the most important signatures or indicators. A study from this Research Topic shows that myeloid dendritic cells and B cells are prognostic factors independently, which could predict ICB efficacy for lung adenocarcinoma and lung squamous cell carcinoma patients, respectively. Another study in colorectal cancers revealed two robust immune subtypes: the "immune cold subtype", characterized by the deficiency and depletion of immune cells; and the "immune hot subtype", characterized by the abundance of immune cell infiltration and ECM protein activation. Furthermore, they found that loss of MHC molecules and insufficient tumor antigen presentation are immune escape mechanisms in the "immune cold subtype" tumors. This study provided a deep understanding of TME in colorectal cancers. The abundance of macrophage (DeNardo and Ruffell, 2019) and some specific gene (PD-L1 and CD8A) signatures were identified and could be used to predict immunotherapy efficacy. Integrins, including Integrin alpha L, expressed in immune cells, were associated with cancer patient prognosis and potentially be applied to cancer therapy as biomarkers and targets (Hayat et al., 2020).

Besides immune cell infiltration signatures, other signatures are also being used as biomarkers. In this Research Topic, Lin et al. characterized that immune-related long non-coding RNAs (irlncRNAs) are correlated with immune cell infiltration signature and chemosensitivity in patients with soft tissue sarcoma. In addition, tumor-associated fibroblasts regulate the recruitment and function of immune cells *via* secreting cytokines/chemokines or remodeling the matrix, creating an immunosuppressive TME (Barrett and Pure, 2020). Here, Chen et al. found that the percentage of tumor-associated fibroblasts in the tumor tissue was associated with tumor immune characteristics and clinical outcomes of gliomas. They established a prediction model based on tumor-associated fibroblasts related gene signatures to predict the response of patients to immunotherapy.

Another important signature is the metabolism of cancer cells. The TME imposes massive metabolic restrictions on antitumor NK and T cells (DePeaux and Delgoffe, 2021). Heme oxygenase 1, an essential enzyme in heme catabolism, and HMOX1-related genes (HRGs) were found to regulate the immune-related pathways. HMOX1 expression could be used as a predictor for the response of immunotherapies in patients with Lower-grade glioma. Strategies or methods that target metabolic restrictions would break metabolic barriers of therapy.

TME signatures include immune cell infiltration score, tumor immune dysfunction and exclusion score, stromal score, tumor mutation burden value, and immune checkpoint genes expression score. Those emerging TME signatures have been identified in multiple tumor types with low or high immunogenicity. However, a systematic investigation of the TME needs to be validated to help clinicians predict the outcome of immunotherapy, facilitate clinical decision-making, and develop personalized treatment.

Strategies/approaches to favor immunotherapies

Tumor cells suppress the immune environment through different mechanisms (Zhou et al., 2021). Recently, diversified therapeutic strategies have been used to restore host immunity and enhance the sensitivity to immunotherapy (Binnewies et al., 2018; Hu et al., 2022). Ferroptosis in tumors, an iron-dependent non-apoptotic cell death, has a dual role in tumor promotion and suppression. The driver gene SOCS1 and suppressor gene FTH1 of ferroptosis are correlated with the infiltration of M1/M2 macrophage in the head and neck squamous cell carcinoma, respectively, which indicates ferroptosis-immunomodulation may be targeted and provide a new strategy for enhancing the efficacy of immunotherapy.

A major barrier to antitumor immunotherapies is acquired resistance (Schoenfeld and Hellmann, 2020). Numerous efforts have been made to find novel approaches to enhance immunotherapy, such as combination treatment of checkpoint inhibitors with chemotherapy or target therapy (Larkin et al., 2015; Hu et al., 2020). Chemotherapy such as cisplatin enhances antitumor T cell responses, leading to a better therapeutic effect when combined with ICB therapy. A study on this Research Topic showed that two cisplatin resistance-related genes, CCL18 and BCL2A1, are novel biomarkers for combined therapy of cisplatin and ICB in colorectal cancer patients. Targeted therapies inhibit oncogenic proteins and their regulated signaling pathways. Recently, more and more studies combined targeted therapies and immunotherapies to unleash patient antitumor immunity. A study from this Research Topic found more neutrophils and macrophages M1 infiltrate in BRAF-mutated colon tumors compared to BRAF-wt colon tumors. The immunotherapeutic molecules, including CTLA-4, PD-1, PD-L1, LAG-3, and TIM-3, were upregulated in BRAF-mutated tumors, which shed light on the combination therapy of ICB and BRAF inhibitors in this subgroup of patients.

Furthermore, cancer vaccines, especially mRNA vaccines, are emerging as a feasible strategy for cancer therapy (Sahin and Tureci, 2018; Miao et al., 2021). Xu et al. screened for genes positively correlated with antigen-presenting cell infiltration in lung adenocarcinoma. CBFA2T3 and KLRG1 are identified as potential tumor antigens used in mRNA vaccines in lung adenocarcinoma. They also identified the biomarkers to assess immunogenicity for mRNA vaccines. Overall, we expect a new perspective for combining mRNA vaccine and immunotherapy in future personalized cancer treatments.

Conclusion

This Research Topic presents recent discoveries on the immunomodulation of TME and its effects on immunotherapies (Figure 1). With these studies, this Research Topic aims to provide new prognostic biomarkers and novel insights into combination therapy strategies for cancer treatment.

Author contributions

All authors listed have made a substantial, direct, and intellectual contribution to the work and approved it for publication.

Conflict of interest

The authors declare that the research was conducted in the absence of any commercial or financial relationships that could be construed as a potential conflict of interest.

Publisher's note

All claims expressed in this article are solely those of the authors and do not necessarily represent those of their affiliated organizations, or those of the publisher, the editors and the reviewers. Any product that may be evaluated in this article, or claim that may be made by its manufacturer, is not guaranteed or endorsed by the publisher.

References

Bader, J. E., Voss, K., and Rathmell, J. C. (2020). Targeting metabolism to improve the tumor microenvironment for cancer immunotherapy. *Mol. Cell* 78 (6), 1019–1033. doi:10.1016/j.molcel.2020.05.034

Barrett, R. L., and Pure, E. (2020). Cancer-associated fibroblasts and their influence on tumor immunity and immunotherapy. *Elife* 9, e57243. doi:10.7554/eLife.57243

Binnewies, M., Roberts, E. W., Kersten, K., Chan, V., Fearon, D. F., and Merad, M. (2018). Understanding the tumor immune microenvironment (TIME) for effective therapy. *Nat. Med.* 24 (5), 541–550. doi:10.1038/s41591-018-0014-x

Crow, J., Samuel, G., and Godwin, A. K. (2019). Beyond tumor mutational burden: Potential and limitations in using exosomes to predict response to immunotherapy. *Expert Rev. Mol. Diagn* 19 (12), 1079–1088. doi:10.1080/14737159.2020.1688144

DeNardo, D. G., and Ruffell, B. (2019). Macrophages as regulators of tumour immunity and immunotherapy. *Nat. Rev. Immunol.* 19 (6), 369–382. doi:10.1038/s41577-019-0127-6

DePeaux, K., and Delgoffe, G. M. (2021). Metabolic barriers to cancer immunotherapy. *Nat. Rev. Immunol.* 21 (12), 785–797. doi:10.1038/s41577-021-00541-y

Hayat, S. M. G., Bianconi, V., Pirro, M., Jaafari, M. R., Hatamipour, M., and Sahebkar, A. (2020). CD47: Role in the immune system and application to cancer therapy. *Cell Oncol. (Dordr)* 43 (1), 19–30. doi:10.1007/s13402-019-00469-5

Hu, J., Wang, Z., Chen, Z., Li, A., Sun, J., and Zheng, M. (2020). DKK2 blockage-mediated immunotherapy enhances anti-angiogenic therapy of Kras mutated colorectal cancer. *Biomed. Pharmacother.* 127, 110229. doi:10.1016/j.biopha.2020.110229

Hu, X., Chen, Z., Wang, Z., and Xiao, Q. (2022). Cancer evolution: Special focus on the immune aspect of cancer. *Semin. Cancer Biol.* 86 (2), 420–435. doi:10.1016/j.semcancer.2022.05.006

Larkin, J., Hodi, F. S., Wolchok, J. D., Grob, J. J., Cowey, C. L., Lao, C. D., et al. (2015). Combined nivolumab and ipilimumab or monotherapy in untreated melanoma. *N. Engl. J. Med.* 373 (13), 23–34. doi:10.1056/NEJMoa1504030

Majzner, R. G., and Mackall, C. L. (2018). Tumor antigen escape from CAR T-cell therapy. *Cancer Discov.* 8 (10), 1219–1226. doi:10.1158/2159-8290.CD-18-0442

Miao, L., Zhang, Y., and Huang, L. (2021). mRNA vaccine for cancer immunotherapy. *Mol. Cancer* 20 (1), 41. doi:10.1186/s12943-021-01335-5

Morad, G., Helmink, B. A., Sharma, P., and Wargo, J. A. (2021). Hallmarks of response, resistance, and toxicity to immune checkpoint blockade. *Cell* 184 (21), 5309–5337. doi:10.1016/j.cell.2021.09.020

Sahin, U., and Tureci, O. (2018). Personalized vaccines for cancer immunotherapy. *Science* 359 (6382), 1355–1360. doi:10.1126/science.aar7112

Schoenfeld, A. J., and Hellmann, M. D. (2020). Acquired resistance to immune checkpoint inhibitors. *Cancer Cell* 37 (4), 443–455. doi:10.1016/j.ccell.2020.03.017

Wang, H., Kaur, G., Sankin, A. I., Chen, F., Guan, F., and Zang, X. (2019). Immune checkpoint blockade and CAR-T cell therapy in hematologic malignancies. *J. Hematol. Oncol.* 12 (1), 59. doi:10.1186/s13045-019-0746-1

Zhengxi Chen, Q. X. (2020). DKK2 mediated immunosuppressive pathway and angiogenesis for colon cancer progression. *J. Cancer Biol.* 1 (3), 57–60.

Zhou, B., Gao, Y., Zhang, P., and Chu, Q. (2021). Acquired resistance to immune checkpoint blockades: The underlying mechanisms and potential strategies. *Front. Immunol.* 12, 693609. doi:10.3389/fimmu.2021.693609

frontiers in Cell and Developmental Biology

REVIEW
published: 21 July 2021
doi: 10.3389/fcell.2021.706286

Tumor Associated Macrophages, as the Dominant Immune Cells, Are an Indispensable Target for Immunologically Cold Tumor—Glioma Therapy?

Ni Tong[1,2†], Zhenqiang He[3†], Yujie Ma[2†], Zheng Wang[4], Ziming Huang[2], Haihong Cao[1,2], Lanyang Xu[1,2], Yuheng Zou[1,2], Wanyu Wang[1,2], Chenpeng Yi[1,2], Zhixin Yin[5] and Qirui Wang[1,2]*

[1] Department of Pharmacy, Zhujiang Hospital of Southern Medical University, Guangzhou, China, [2] Department of Molecular Biology, State Administration of Traditional Chinese Medicine of the People's Republic of China, School of Traditional Chinese Medicine, Southern Medical University, Guangzhou, China, [3] State Key Laboratory of Oncology in South China, Department of Neurosurgery/Neuro-Oncology, Collaborative Innovation Center for Cancer Medicine, Sun Yat-sen University Cancer Center, Guangzhou, China, [4] Breast Surgery Department, Nanyang Central Hospital, Nanyang, China, [5] School of Basic Medical Science, Southern Medical University, Guangzhou, China

OPEN ACCESS

Edited by:
Qian Xiao,
Yale University, United States

Reviewed by:
Aleksandra Ellert-Miklaszewska,
Nencki Institute of Experimental Biology (PAS), Poland
Can Cui,
Yale University, United States
Lai Shi,
Boston Children's Hospital, United States

***Correspondence:**
Qirui Wang
wqrv@hotmail.com

[†] These authors have contributed equally to this work

Specialty section:
This article was submitted to Molecular and Cellular Pathology, a section of the journal Frontiers in Cell and Developmental Biology

Received: 07 May 2021
Accepted: 28 June 2021
Published: 21 July 2021

Citation:
Tong N, He Z, Ma Y, Wang Z, Huang Z, Cao H, Xu L, Zou Y, Wang W, Yi C, Yin Z and Wang Q (2021) Tumor Associated Macrophages, as the Dominant Immune Cells, Are an Indispensable Target for Immunologically Cold Tumor—Glioma Therapy? Front. Cell Dev. Biol. 9:706286. doi: 10.3389/fcell.2021.706286

Tumor microenvironment (TME) is the cornerstone of the occurrence, development, invasion and diffusion of the malignant central nerve system (CNS) tumor, glioma. As the largest number of inflammatory cells in glioma TME, tumor associated macrophages (TAMs) and their secreted factors are indispensable to the progression of glioma, which is a well-known immunologically "cold" tumor, including the growth of tumor cells, invasion, migration, angiogenesis, cancer immunosuppression and metabolism. TAMs intimately interface with the treatment failure and poor prognosis of glioma patients, and their density increases with increasing glioma grade. Recently, great progress has been made in TAM-targeting for anti-tumor therapy. According to TAMs' function in tumorigenesis and progression, the major anti-tumor treatment strategies targeting TAMs are to hinder macrophage recruitment in TME, reduce TAMs viability or remodel TAMs phenotype from M2 to M1. Different approaches offer unique and effective anti-tumor effect by regulating the phagocytosis, polarization and pro-tumor behaviors of macrophages in the therapy of glioma. The present review summarizes the significant characteristics and related mechanisms of TAMs and addresses the related research progress on targeting TAMs in glioma.

Keywords: glioma, tumor microenvironment, tumor associated macrophages, immunotherapy, TAM-targeting therapy

INTRODUCTION

Glioma, originated from neuroepithelial tissue, is one of the commonest primary and intractable central nerve system (CNS) malignant tumors with the highest incidence rate, rapidly progressive nature and dismal prognosis (Phillips et al., 2020; Wang et al., 2020). Glioblastoma multiforme [GBM, World Health Organization (WHO) grade IV] is a recalcitrant and incurable kind of glioma with the worst prognosis (Hambardzumyan and Bergers, 2015). Median overall survival (mOS) of GBM patients after comprehensive treatment, covering surgical carcinoma resection,

radiation therapy and chemotherapy, chemo-radiotherapy and novel schemes containing tumor-treating fields (TTFields), still hasn't broken through for 21 months (Pan, 2012; Tan et al., 2020). Complete surgical excision is impractical due to the particular physiological functions of brain tumors and the capacity of GBM to aggressively penetrate surrounding normal brain tissue. In spite of the latest progresses in standardized neurosurgery and the advancement of imaginative multidisciplinary comprehensive treatments against cerebral tumors in perioperative period, there has been exceptionally little enhancement in the treatment of intracranial malignancies. Therefore, huge clinical requirements urge researchers to explore the mechanism of tremendous invasion and recurrence process of glioma, clarify its occurrence and the development of pathogenesis, then find new effective therapies, in which immunologic treatment holds great promise for eradicating glioma (Hervey-Jumper and Berger, 2019; Nejo et al., 2020).

Till now, some seminal immunotherapy, such as immune checkpoint blockade (ICB) treatment (Ito et al., 2019), vaccination therapy (Hilf et al., 2019), chimeric antigen receptor (CAR) T-cell therapy (Bagley et al., 2018) and oncolytic virus therapy (Hua and Wakimoto, 2019), are constantly springing up for GBM treatment. However, these immunologic therapies have not resulted in substantial enhancement in progression-free survival (PFS) or OS (Bell et al., 2018). Pseudoprogression (Galldiks et al., 2017), hyperprogression (Wang Q. et al., 2018), cytokine release syndrome (CRS) (Pang et al., 2018) and high recurrence rate in the front of the operative cavity (Campos et al., 2016) can't be avoided yet.

For all we know, blood-brain-barrier (BBB), blood-cerebrospinal fluid barrier (BCB) and shortage of the framework for lymphatic drainage serving as a channel that transporting antigen-presenting cells (APC) to the lymph nodes, together engender the CNS immune privilege (Li et al., 2020). The unique physiological advantage of glioma establishes an immune-suppressive and cancer-permissive microenvironment that is featured with high resident and recruited myeloid cell substances, relatively hyporesponsive and exhausted state of tumor infiltrating lymphocyte (TIL), which makes glioma known as immunologically "cold" tumor (D'Alessio et al., 2019). This inherent characteristic makes brain tumors extremely difficult be targeted by T cells. Tumor microenvironment (TME) composing of cancer cells, infiltrating immune cells, endothelial cells, pericytes, fibroblasts, extracellular matrix (ECM) proteins and cytokines, is a complex cellular ecological environment, which evolves together with tumor cells and provides support throughout the transmutation to malignancy (Radin and Tsirka, 2020). Noteworthily, tumor associated macrophages (TAMs), characterized by the highest glucose uptake among TME cells (Reinfeld and Madden, 2021), dominate in number among the inflammatory cells which inhabit the glioma TME and perform a crucial role in neoplasm formation, growth, migration, angiogenesis, immunosuppression, treatment resistance and metabolism (Pan, 2012; Mira et al., 2013; Zhao et al., 2014; Li et al., 2015), and their numbers intimately correlate with glioma grade, suggesting that TAMs may represent an indispensable and pivotal target for brain cancer immunotherapy.

The innate immune system relies heavily on totipotent macrophages, which serve as the initial line of phylactery resisting cancer and infection attack. They are not only the front-line killer cells in infections, but also the maintainers of body homeostasis. They can phagocytize apoptotic cell fragments and secrete growth factors that promote tissue regeneration and angiogenesis, which helps the body constantly renew itself. So macrophages are pluralistic in function (Rothlin and Ghosh, 2020). TAMs are inflammatory infiltrating macrophages settled in the TME that play an integral part in tumor incidence and evolution. Unlike other malignancies, worthy of note is that TAMs in gliomas, generally identified as glioma associated microglia and macrophages (GAMs), originated from not only infiltrating myeloid cells, but also resident microglia. However, the distinction between macrophages and microglia is still being explored, as they can behave separately to different types of CNS injuries (Hambardzumyan et al., 2016). In common, macrophages are broadly classified into two categories depending on their activation status and functions, classic activation of macrophages (M1 macrophages) and alternative activation of macrophages (M2 macrophages) (Najafi et al., 2019). M1 macrophage phenotype can secrete C-X-C chemokine ligand (CXCL)-5, CXCL-9, CXCL-10 and other chemokines, express tumor necrosis factor (TNF)-α, interleukin (IL)-12, IL-2 and other proinflammatory cytokines simultaneously, promote antigen presentation and Th1 activation, and after that play essential roles in anti-tumor protection (Pan, 2012; Zhao et al., 2014). M2 macrophages secrete chemokine (C-C motif) ligand (CCL)-17, CCL-22, CCL-24 and other chemokines, but they are unable to be effectively engaged in antigen presentation. Through the production of inhibitory cytokines such as IL-4, IL-10, and transforming growth factor (TGF)-β, they suppress the immune response, encourage tumor invasion, development and infiltration, enhance angiogenesis, and prevent T cells from having an effective anti-tumor impact (Mira et al., 2013).

M1, M2 macrophages mainly exist in various stages of the tumor. In the early stage, M1 macrophages mediate anti-tumor effect, while M2 macrophages in the middle-late stage mediate pro-tumor effect. In addition, pro-tumorigenic M2 macrophages and anti-tumorigenic M1 macrophages are in a continuum of polarization states, they can reciprocally transform in the TME, which means there is a dynamic gene expression program (Li et al., 2015). An outline of the polarization mechanism of M1 macrophages and M2 macrophages is illustrated in **Figure 1**.

THE PERFORMANCE OF TAMs IN GLIOMA PROGRESSION

As a key segment of TME and the initial response of the host immune system's defense, TAMs are extremely powerful in tumor expansion and progress, including tumor genesis,

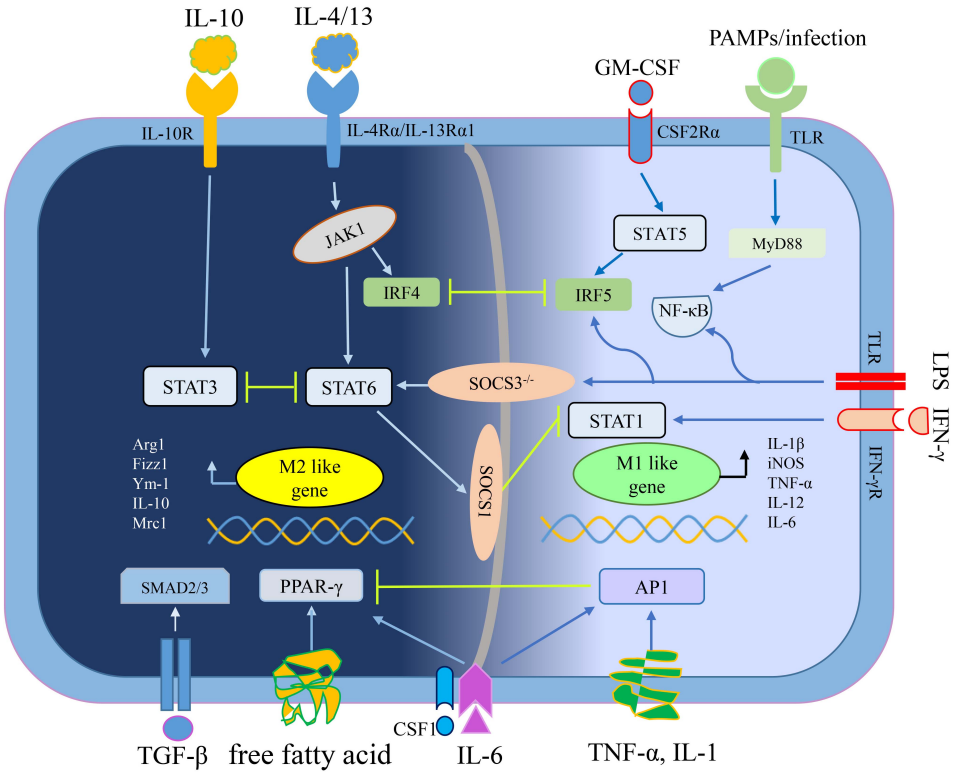

FIGURE 1 | The mechanisms of macrophage polarization. IL-4/13 mediates macrophage polarization toward M2 macrophages depending on STAT6 signaling, whereas IL-10 depending on STAT3 signaling (Lang et al., 2002; Sica and Mantovani, 2012). Free fatty acid or IL-6 plus CSF1 enhance PPAR-γ expression to educate M2 macrophage (Odegaard et al., 2007; Wang et al., 2018b). TGF-β secreted by tumor cells and M2 macrophages promoted M2 polarization of TAMs through Smad3 signaling pathways (Gordon and Martinez, 2010). Interferon-γ (IFN-γ) mediates macrophage polarization toward M1 macrophages relying on STAT1 signaling while other stimuli (like LPS and PAMPs/infections) convert macrophages into M1 phenotype relying on NF-κB signaling (Muraille et al., 2014). GM-CSF mediates macrophage polarization toward M1 macrophages through STAT5 signaling while pro-inflammatory cytokines (including TNF-α, IL-1, and IL-6) depending on AP1 signaling (Liu Y. C. et al., 2014; Wang N. et al., 2014). By the way, the crosstalk between activation of STAT3/STAT6 and STAT1, closely regulates macrophage polarization (Ohmori and Hamilton, 1997). Abbreviations: colony stimulating factor 1 (CSF1), esistin-like-α (Fizz1), Arginase1 (Arg1), chitinase 3-like 3 (Ym1), inducible nitric oxide synthase (iNOS), signal transducer and activator of transcription (STATs), interferon-regulatory factor (IRFs), nuclear factor (NF)-κB, activator protein (AP) 1, peroxisome proliferator-activated receptor (PPAR)-γ, pathogen associated molecular patterns (PAMPs), suppressor of cytokine signaling (SOCS), small mother against decapentaplegic (Smads).

invasion, migration, angiogenesis, immunosuppression and metabolism (**Figure 2**).

Tumor Growth

Both TAM master regulators and their effector genes are frequently associated with tumor growth and strongly linked to poor clinical outcomes. TAMs secrete effector cytokines such as epidermal growth factor (EGF), platelet derived growth factor (PDGF), basic fibroblast growth factor (bFGF), hepatocyte growth factor (HGF) and TGF-β, which can promote tumor cells proliferation and survival, based on a huge number of animal studies (Kennedy et al., 2013; Caux et al., 2016; Liu et al., 2018; Wang C. et al., 2018). McFarland et al. (2013) found TNF-α could stimulate IL-6 production and trigger NF-κB and STAT3 pathways to enhance glioma cells proliferation both *in vivo* and *in vitro*. Yan et al. (2015) and other researchers have verified that M2 macrophages residing in the tumor tissue showed high expression of Tim-3 gene. Knocking out Tim-3 in M2 macrophages inhibited the growth rate of cancerous cells. In glioma, glial TIM-3's level is diminished and several inflammation-related genes exhibit a lesser increase in Tim-3^{mut} glia compared to WT glia when exposed to glioma conditioned medium (GCM) (Kim et al., 2020). Normal macrophages synthesize NO by using iNOS and L-arginine as substrates, thereby acting as a cytotoxic effect. However, TAMs expressing Arg1 are strengthened by IL-4/13 signaling *via* the blocking effect of transcription factor STAT6, thus to reduce NO synthesis, promote the production of polyamines, and advance tumor progression (Pesce et al., 2009; Mantovani et al., 2013; Pires-Afonso et al., 2020).

Tumor Invasion and Migration

Glioblastoma multiforme has the characteristics of lethal intracranial invasion and rare extracranial metastases, and is often locally invasive (Rossi et al., 2020). Inside the brain, it may be due to the existence of BBB and the loss of a lymphatic drainage system, extra-neural metastases of glioma

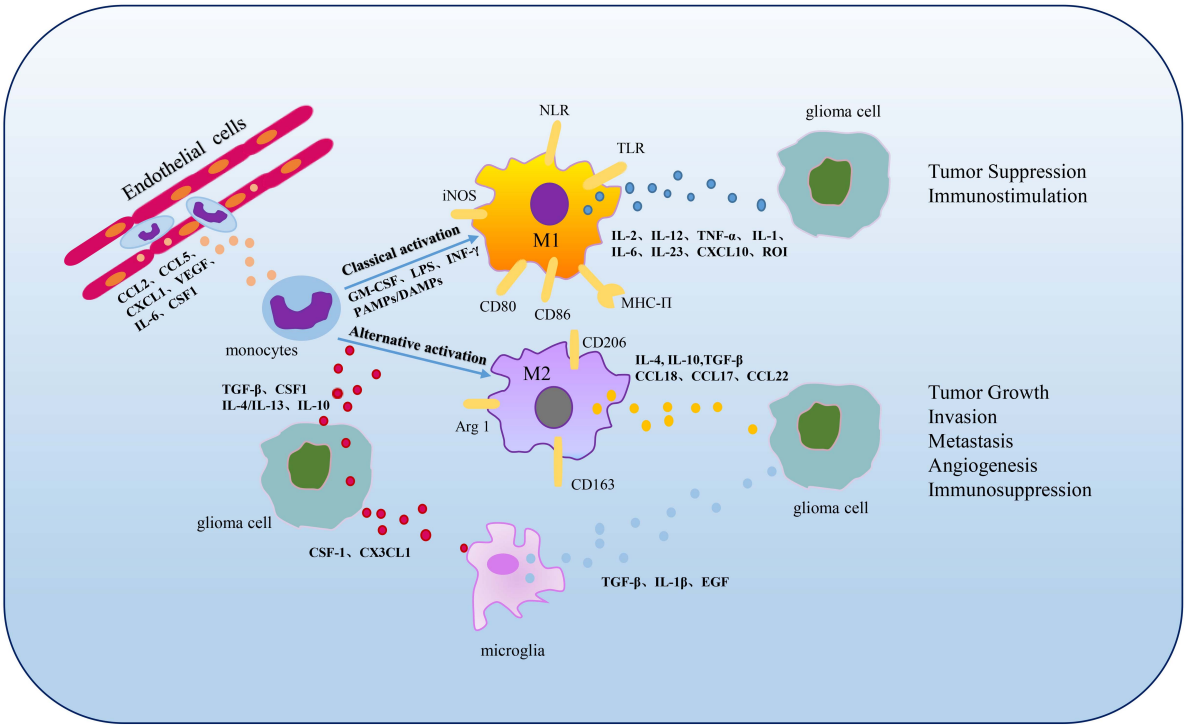

FIGURE 2 | Polarization and functions of GAMs. In the TME, when the BBB is impaired, monocytes infiltrate into tumors and can be differentiated into macrophages stimulated by cytokines involving CSF1, CCL2, CCL5, etc., (Chen and Hambardzumyan, 2018). M1 and M2 phenotypes are the two primary subpopulations of TAMs. M1 phenotype can be activated by cytokines such as GM-CSF, LPS, INF-γ or PAMPs/damage associated molecular patterns (DAMPs) and characterized by secretion of IL-2, IL-12, TNF-α, IL-1, IL-6, IL-23, CXCL10 and ROI, functioning in tumor suppression and immunostimulation (Lee et al., 2020; Xu et al., 2020). M2 phenotype can be activated by cytokines including TGF-β, CSF1, IL-4, IL-13 or IL-10 and secrete large amounts of IL-4, IL-10, TGF-β, CCL18, CCL17 and CCL22, contributing to tumor growth, invasion, metastasis, angiogenesis and immunosuppression (Xu et al., 2020). Microglia, the resident macrophages in CNS, can be activated by CSF1 and CX3CL1 secreted by glioma cells and up-regulate TGF-β, IL-1β, EGF expression to promote glioma development and migration (Marchesi et al., 2010; Hambardzumyan et al., 2016).

are rare, but still may occur in the later course of GBM. GBM metastases usually include the regional lymph nodes, lungs, and pleural cavity, as well as the bone and liver on rare occasions (Beauchesne, 2011). The degradation and damage of the basilar membrane of tumor vascular endothelial cells are the main factors leading to tumor cell infiltration and metastasis. In the TME, TAMs can disrupt cell-cell communication, destroy the basilar membrane by secreting serine proteases, matrix metalloproteinases (MMPs), cathepsins, etc., as well as promote endothelial cell viability, thus facilitating invasion and metastasis of tumors (Das et al., 2011; Yang et al., 2017; Quintero-Fabián et al., 2019). For example, MMPs are observed in a collection of malignancies, involving glioma, gastrointestinal stromal tumors, pancreatic cancer, breast cancer and other malignant tumors, and have been associated with tumor infiltration, metastasis and prognosis (Leifler et al., 2013; Liou et al., 2013; Wang C. et al., 2014). Growth factors, interleukin and extracellular matrix constituents (e.g., TGF-β, IL-6, PDGF, FGF and MMPs) generated by TAMs may cause tumor cells to go through GMT (glial-to-mesenchymal), as well as ease divergent invasions. Zhang et al. (2012) co-cultured $CCL2^{+}$ U87 glioma cells with microglia, and stated that microglia with CC chemokine receptor (CCR) 2 highly expressed IL-6, thus enhancing the aggressiveness of glioma cells.

Tumor Angiogenesis

During the development of the tumor, the newly generated blood arteries sustain oxygen and nutrition to tumor, authorizing it to grow and invade while macrophages secrete angiogenesis-promoting growth substances such as vascular epithelial growth factor (VEGF)-family members, CSF1, WNT family members etc., speeding the degradation of the perivascular extracellular matrix to assist tumor angiogenesis (De Palma et al., 2017). Studies have shown that TAMs infiltrated in tumor tissue accumulate in hypoxic regions with less micro vessels. Hypoxic niche induces TAMs to highly express numerous angiogenic and cytokines as well as a large number of angiogenic regulatory enzymes, such as VEGF, PDGF, fibroblast growth factor (FGF1, FGF2), placental growth factor (PIGF), HGF, (bFGF, IL-1, IL-8, MMP-9, MMP-2, TNF-α, urokinase plasminogen activator (uPA), adrenomedullin (ADM) etc., to spur tumor angiogenesis (Peng et al., 2005; Qian and Pollard, 2010; Wang et al., 2011; Zhang et al., 2011; Meng et al., 2012). In glioma, $CD163^{+}$ or tunica interna endothelial cell kinase 2 (Tie-2) positive TAMs are identified in parenchymal and perivascular niche.

Zhu et al. (2017) reviewed key roles of TAMs in angiogenesis through autocrine and paracrine. Take inflammatory cytokines for example, IL-1β synthesis by $COX2^+$ TAMs stimulated by GBM-derived C-reactive protein (CRP) can enhance the expression of pro-angiogenic factors in endothelial cells. TAMs can secret IL-6, which promotes GMT of high-grade gliomas. Moreover, IL-6 can recruit endothelial progenitor cells and promote vasculogenesis as well. Notably, it is interesting that in the previous study (Wang et al., 2018b), we found glioma endothelial cells can also secrete IL-6 and M-CSF to induce alternative macrophage activation through PPAR-γ/HIF 2α pathway. Thus, vascular niche and TAMs regulate each other positively, together promoting the formation and deterioration of glioma immunosuppressive microenvironment.

TAMs can also benefit lymph-angiogenesis by the expression of VEGF-C, VEGF-D, VEGFR3, and other diverse components involved in regulating this process. Kerjaschki (2005) proposed hypothesis that there may be two ways to induce lymph-angiogenesis by macrophages in TME. One is the direct *trans*-differentiation of macrophages into lymphatic endothelial cells, and the other is the stimulation of macrophages on the division and multiplication of lymphatic endothelial cells. Jung et al. (2016) discovered that multicellular signaling circuits were involved in flowing out sphingosine 1-phosphate (S1P) by dying human MCF-7 breast cancer cells, stimulating M2 macrophages to release lipocalin 2 (LCN2), and inspiring lymphatic endothelial cells to deliver lymph-angiogenic factor VEGF-C, thus promoting the growth of lymphatic vessels in the TME. Although there's little referring to GAMs, with the discovery of central nervous system lymphatic vessels, the relationship between GAMs and lymph-angiogenesis in gliomas may be a challenging research topic in the future (Louveau et al., 2015).

Immunosuppression in the TME

Immunosuppression is a prerequisite for tumor formation and growth. Macrophages are qualified of offering antigens to effector cells to turn on anti-tumor functions of T cells and NK cells. Whereas, alternative activated microglia/macrophages and inactivated T-killer cells, resulted in characteristic immunosuppressive TME. Single-cell transcriptomic atlas discovered inter-/intra-tumor heterogeneity, as well as enlarged depleted T cells, Tregs and other innate immune cells in GBM (Fu et al., 2020). Chen and Hambardzumyan (2018) reviewed the immunosuppressive functions of GAMs and mechanisms of GAMs inhibiting the functions of cytotoxic T cells (CTLs). As GAMs are remarkably plastic, M1 macrophages produce abundant pro-inflammatory cytokines (e.g., IL-1β, IL-6, IL-12, IL-23, and TNF-α) that support NK cells and Th1 cells mediate anti-tumor activity, while also promote $CD4^+$ T cells to release cytotoxic products to help achieve anti-tumor effect (Jiang et al., 2014; Shapouri-Moghaddam et al., 2018; Orecchioni et al., 2019). M2 macrophages can secrete human leukocyte antigen-G (HLA-G), IL-10, TGF-β, PGE2 and other immunosuppressive molecules, directly inhibiting immune response (Wu et al., 2010). IL-10 plays a negative role in regulating IL-12, which has the capacity to support Th2 cells differentiation, release notable quantities of IL-4 and IL-13 to convince regulatory T cells (Tregs) amplification and expedite TAMs development toward a pro-tumor phenotype. Besides, M2 macrophages can suppress CTLs *via* TGF-β and IL-10 production (van Dalen et al., 2018; DeNardo and Ruffell, 2019; **Figure 3**).

In animal experiments, IL-10 suppressed the immune response by inhibiting the NF-κB signaling route (Yang et al., 2014). Moreover, cancerous cells can secrete CSF1, which can bind to colony stimulating factor 1 receptor (CSF1R, also named as FMS) on macrophages, activating the downstream signaling pathway in charge of TAMs polarization toward the immunosuppressive M2 phenotype (Ramesh et al., 2019). TAMs and myeloid-derived suppressor cells (MDSCs) are powerful immunosuppressors in the glioma TME (Zinnhardt et al., 2020). STAT3 presents a prominent function in monitoring MDSC's differentiation into TAMs, together contributing to an immunosuppressive TME (Kumar et al., 2016; Pinton et al., 2020). Programmed death receptor-1 (PD-1) is an inhibitory immunological checkpoint on T cells which was originally obtained by subtracting hybridization techniques in apoptotic T cell hybridomas. Reacting with its ligand, PD-1 can regulate the body's immune system reaction. Programmed cell death ligand 1 (PD-L1), which aids tumor's immune evasion, is described on both tumor cells and TAMs in a collection of malignancies including glioma. PD-L1 on macrophages can lead to restraint of T cell activation (DeNardo and Ruffell, 2019), phagocytosis and tumor immunity (Hutchinson, 2017). TAM-derived PD-1 expression is negatively related to the macrophage phagocytosis against tumor cells. An excess of reactive oxygen species (ROS) and peroxynitrite can be produced to inhibit T cells-regulated anti-tumor responses (Kortylewski et al., 2005; Du et al., 2012). PD-1 blockade *in vivo* ameliorated macrophage phagocytosis against cancer cells, diminished tumor formation, and prolonged the survival of macrophage-dependent mouse models, which confirmed that PD-1/PD-L1 blockade could interfere with the tumor formation by direct action on macrophages (Gordon et al., 2017). The pre-existing tumor infiltration of CD8-positive cytotoxic T cells is a promising marker of ICB treatment response. By blocking Fcγ receptors (FcγRs) before the administration of anti-programmed cell death protein 1 monoclonal antibodies (aPD-1 mAb), time for aPD-1 mAb binding to tumor-infiltrating $CD8^+$ T cells perpetuated, which advanced tumor regression in mice treated with immunotherapy (Arlauckas and Garris, 2017).

The Crosstalk Between Glioma Stem Cells and TAMs

Cancer stem cells (CSCs), noted as tumor-propagating cells or tumor-initiating cells as well, refer to a distinct subset of cells holding many stem-like aspects such as tumorigenesis, self-renewal and multi-directional differentiation (Nassar and Blanpain, 2016). CSCs have been considered as a critical driver of tumor initiation. Detailed surveys have shown that TAMs can regulate the performances of CSCs in diverse carcinomas. Shi et al. (2017) reported that TAMs promoted GBM malignant growth by secreting pleiotrophin (PTN) in PTN–PTPRZ1 paracrine signaling to stimulate glioma stem

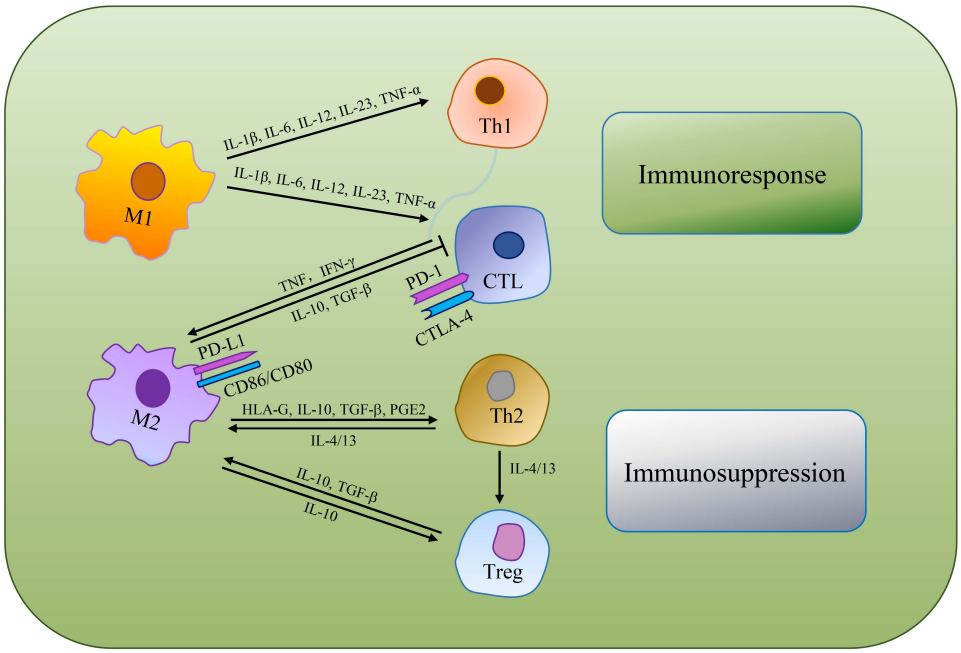

FIGURE 3 | The mechanisms of TAMs regulating tumoricidal T cells. TAMs can directly suppress CTLs or indirectly regulate the differentiation of Th cells and Tregs to make an immunosuppressive TME.

cells (GSCs) through its receptor PTPRZ1. Ye et al. (2012) revealed that TAMs enhanced the invasiveness of GSCs by expressing TGF-β1 to augment MMP-9 generation by stem-like cells in glioma. Zhang et al. (2017) labeled CD163 and CSC-related proteins by immunohistochemistry (IHC) and found that $CD163^{+}$ TAMs were excessive in gastric cancer (GC) tissues with invasive tendencies, which was an independent worse prognostic factor in GC. What's more, over-expression of CD163 in TAMs was linked to high levels of CSC markers, implying that CSCs in GC may act as a promoter for tumor progression and aggressiveness, and polarized $CD163^{+}$ TAMs may aid in the maintenance of CSCs in GC tumors (Zhang et al., 2017). According to Yang et al.'s research, TAMs can promote phosphorylation of STAT3 by activating EGF signaling in mouse breast cancer cells and induce SOX-2 expression which maintains tumor cell CSCs phenotype, and identified a novel role of TAMs in breast CSC regulation (Yang et al., 2013). However, the study of the relationship between macrophages and CSCs is still in its infancy so far and requires further study.

Macrophages Cell Fusion

Cell fusion is a unique cell biological phenomenon, referring to the process of re-integration of two or more cells into one cell, which is crucial in the body development and tissue repair. Cell fusion can be observed at various developmental stages, such as fertilization (sperm and egg fusion), bone development (macrophage differentiation into osteoclasts) and immune responses (macrophages fuse into megakaryocytes) (Bastida-Ruiz et al., 2016).

In the process of tumor development, cell fusion also plays an important part. As early as 1911, the German pathologist Otto Aichel proposed the cell fusion hypothesis that cancer cells can be fused with white blood cells to form malignant hybrid cells, leading to tumor development. Current studies have proved that tumor cells can be fused with a sort of bodily cells, covering interstitial cells, epithelial cells and endothelial cells. After fusion with normal leukocytes with low metastatic ability, the metastasis ability of tumor cell is enhanced (Bastida-Ruiz et al., 2016). When M2 macrophages and MCF-7 breast cancer cells were co-cultured, their fusion produced metastatic hybrids with maternal cytogenetic and phenotypic characteristics. By hybridizing with macrophages, MCF-7 cells gain CD163 and CD45 double markers, suggesting that cell fusion might result in tumor clonal explosion and heterogeneity (Shabo et al., 2015).

Metabolic Changes of TAMs in Glioma

In the early stage of tumor, TAMs mediate anti-tumor effect mainly through antioxidant function, displaying an active glycolytic metabolism. Within the progress of the tumor, malignant tumor cells constantly adjust their metabolic patterns to obtain sufficient nutrition and induce increased fatty acid oxidation of TAMs to promote the tumor development (Boscá et al., 2015). M1 macrophages have an enormous amount of aerobic glycolysis activity and can produce ROS to kill pathogens. M2 macrophages release substantial VEGF-A and IL-10 to support tumor cells proliferation mainly by oxidative phosphorylation. Under the stimulation of hypoxia and lactic acid, TAMs are easy to produce cytokines like IL-6, CCL5 and

CCL18. CCL5 and CCL18 up-regulate the activity of various glycolysis factors, including lactate dehydrogenase A (LDHA) and glucose-6-phosphate dehydrogenase (G6PD), which can advance glycolysis in tumor cells, lead to accumulation of lactic acid in TME and restrain the immune system's anti-tumor reaction (Colegio et al., 2014). M2 macrophages can serve tumor cells' evasion of immune detection by overexpressing Arg1 and catalyzing tryptophan metabolites, consuming amino acids in TME and challenging for nutrients with T and NK cells (Liu et al., 2017). Notably, for the latest survey data on myeloid cells, especially TAMs, showed the highest glucose uptake across a range of cancer models while cancer cells had the greatest capacity to take up glutamine. Cell-intrinsic programs derived cell-selective acquisition of glucose and glutamine by immune and cancer cells, respectively. Thus, a new therapy strategy could be exploited (Reinfeld and Madden, 2021).

THERAPY OF GLIOMA TARGETING TAMs

The leading anti-tumor treatment strategies targeting TAMs are updated and currently contain: (1) restricting macrophages entrance into TME or reducing TAMs viability; (2) reeducating TAMs phenotype to M1 phenotype exerting anti-cancer effects; (3) enhancing the phagocytosis and antigen presenting ability of macrophages or macrophage-mediated anti-cancer function. Current advances in TAM-targeting therapies are listed below (see **Table 1** for summary).

Inhibiting Macrophage Recruitment in TME or Reducing TAMs Viability

Reducing the Recruitment/Activation of TAMs

CD70, a TNF family member declared solely on tumor cells and not on macrophages, promotes tumor aggressiveness and immunosuppression by recruiting and activating TAMs (Bowman et al., 1994; Wischhusen et al., 2002). Ge et al. (2017) found that CD70 expression was strongly linked to the incidence of $CD163^+$ macrophages in GBM, indicating CD70 functioned by attracting TAMs to the tumor sites. It has been demonstrated that CD70-targeting therapy showed a profound anti-tumor effect in preclinical studies in orthotopic model of GBM, providing a ray of light for $CD70^+$ GBM patients. TAMs depend on CSF1 for proliferation, differentiation, survival and recruitment (Ramachandran et al., 2017; Peranzoni et al., 2018). One study of CSF1R restraint showed that TAMs were not depleted but M2 markers reduced in surviving TAMs in line with enhanced survival in GBM patients. The CSF1/CSF1R axis has gained a lot attention and clinical development is ongoing. BLZ945, as the inhibitor of CSF1R, prevented glioma progression and improved survival in animal experiments by perturbing macrophage survival (Pyonteck et al., 2013). What's more, a number of small molecules and mAbs targeting CSF1/CSF1R axis are being tested in melanoma, prostate cancer and other solid tumors (Cannarile et al., 2017).

Suppression of Macrophage Migration Into Tumors

ICAM-1, which is activated by pSTAT3 in hypoxic sites, facilitates glioma cell passage and carcinoma evolution. ICAM-1 knockdown decreased macrophages recruitment into carcinomas *in vivo*. *In vitro*, anti-ICAM-1 antibody inhibited tumor cell migration to macrophages (Yin et al., 2016). Besides, ICAM-1 was linked to the GAMs embroiled in resistance of glioma to antiangiogenic treatment. These findings suggested that ICAM-1 knockdown may be a helpful strategy for overcoming the resistance of GBM to antiangiogenic therapy (Piao et al., 2017). Blocking PD-1/PD-L1 has been announced directly effect on macrophages (Gordon et al., 2017). Monoclonal antibodies that point the PD-1/PD-L1 axis have been testified to be remarkably practical in clinical tumor cases. Pembrolizumab and nivolumab (NIVO, checkpoint inhibitor for PD-1) were authorized by the Food and Drug Administration (FDA) for melanoma and non-small cell lung cancer (NSCLC) treatment in 2014 and 2015 subsequently (Xue et al., 2017). The first large-scale phase III trial of NIVO in GBM patients (CheckMate 143, NCT02017717, initiated in January 2014 and data cutoff of January 20, 2017) showed a median follow-up of total 369 patients randomized to NIVO or bevacizumab. The results showed mOS was comparable and the safety profile of nivolumab was consistent with other tumor types (Reardon et al., 2020).

Increasing TAMs-Depletion Capability

Blood-brain-barrier, Blood-Brain tumor Barrier (BBTB), vasculogenic mimicry (VM) channels and TAMs are all natural restrictions of the therapeutic drugs for glioma. *In vitro* and *in vivo*, a synergistic anti-glioma activity was discovered when Lycobetaine (LBT) and octreotide (OCT) were combined. LBT and OCT co-loaded liposomes (LPs) showed outstanding anti-cancer and anti-angiogenesis efficacy. nRGD has the potential to improve selective glioma cell targeting efficiency, intra-glioma drug delivery and TAMs reduction. As a result, nRGD modified LPs proved to be a bright and flexible medicine delivery system for glioma treatment (Chen et al., 2017). Of note, latest investigation has indicated that macrophages were decisive in internalizing designed nanocarriers before being polarized or reprogrammed (Ye et al., 2019). Moreover, various liposomes have been designed to deplete or re-educate TAMs by targeting them through cell-specific surface receptors. Mukherjee et al. (2018) pointed out that liposomal TriCurin (TrLp), a mixture of curcumin, epicatechin gallate, and resveratrol, boosted activated p53 in GL261 cells, repolarized TAMs and eliminated glioblastoma cells as well as GSCs by triggering an apoptosis cascade.

Targeting Chemokines in Hypoxia-Niche of Glioma

Macrophage/microglial cells heavily infiltrate into most human glioma tumors, occupying up to 30% of the tumor's bulk. TAMs are attracted to the glioma community and secrete a variety of growth factors and cytokines in reaction to cancer cells stimuli and help tumor growth, survival, and relocation in a regurgitation-feeding way (Hambardzumyan et al., 2016).

TABLE 1 | Macrophages targeting therapies in cancers.

Substance	Target	Mechanisms	Tumor type / study type	Side effects	References
Nivolumab	*PD1*	Enhancing cytotoxic activity and phagocytosis to tumor cells	Glioma:Phase 3	Hypertension, fatigue	Reardon et al., 2020
WP1066	*STAT3*	Inducing costimulatory molecules expression and increasing immune-stimulatory cytokines production and T-cell proliferation	Glioma:preclinical trial melanoma:Phase 1	Unknown	Hussain et al., 2007
Anti-CD47 antibody	*CD47*	Enhancing cytotoxic activity and phagocytosis to tumor cells	Glioma:preclinical trial	Unknown	Hayat et al., 2020
OLA-PEG, NOX-A12	*SDF-1*	Inhibiting the recruitment of TAMs	Glioma:preclinical trial	Unknown	Deng et al., 2017
POL5551	*CXCR4*	Inhibiting hypoxia-induced glioma cell migration and reducing tumor-initiating GSCs and MGCs populations	Glioma:preclinical trial	Unknown	Gagner et al., 2017
ACF	*TGF-α*	Blocking hypoxia-induced POSTN over-expression by TGF-α through the RTK/PI3K pathway to inhibit the recruitment of macrophages.	Glioma:preclinical trial	Unknown	Guo et al., 2016
BLZ945	*CSF1R*	Inhibitor of CSF1R, preventing glioma progression	Glioma:preclinical trial	Unknown	Pyonteck et al., 2013
GK921	*TGM2*	Triggering MES transdifferentiation of GSCs	Glioma:preclinical trial	Unknown	Yin et al., 2016
STX-0119	*STAT3*	The STAT3 inhibitor, promoting TILs accumulation	Glioma:preclinical trial	Unknown	Akiyama et al., 2017
FLA-16	*CYP4A*	Inhibiting angiogenesis	Glioma:preclinical trial	Unknown	Wang et al., 2017
ISL	*Akt- FGF-2/ TGF-β/VEGF*	Inhibiting angiogenesis	Glioma:preclinical trial	Unknown	Wang et al., 2019
Flavonoid CH625	*CYP4X1*	Inhibiting angiogenesis	Glioma:preclinical trial	Unknown	Wang C. et al., 2018
TrLp	*p53*	Increasing the TAMs-depletion capability	Glioma:preclinical trial	Unknown	Mukherjee et al., 2018
miR-124	*STAT3*	Inhibiting the STAT3 pathway and reversing T-cell proliferation immunosuppression	Glioma:preclinical trial	Unknown	Wei et al., 2013
Trabectedin	*CCL2-CCR2 axis; caspase-8*	Inhibition of macrophage differentiation and cytokine production and improvement of the TAMs-depletion capability	Metastatic soft-tissue sarcomas:Phase 1/2 Breast cancer:Phase 2	Neutropenia, hepatic (transaminitis), fatigue, nausea, vomiting, constipation	Martin-Broto et al., 2020
PLX3397	*CSF1R*	Inducing gene expression of M2-like macrophages	Tenosynovial giant-cell tumors:Phase 1/2	Changes in hair color, fatigue, nausea, dysgeusia, periorbital edema, diarrhea, hyponatremia, etc.	Tap et al., 2015
AZD1480	*ICAM-1 and pSTAT3*	Suppressing macrophage infiltration into the tumor site	Lung cancer:Phase I	Dizziness, ataxia, hallucinations, and anxiety	Piao et al., 2017
Ablation of NRP-1	*NRP-1*	Inhibition of Angiogenesis and interfering the interaction of TAMs with the TME	Breast cancer:preclinical trial	Unknown	Kawaguchi et al., 2017
TMP195	*CSF1 and CSF2*	Regulating the polarization of TAMs	Breast cancer:preclinical trial	Unknown	Guerriero et al., 2017
Leg-3	*Legumain*	Activating the ablation of TAMs	Breast cancer:preclinical trial	Unknown	Lin et al., 2013
BLIMP1	*CCL8*	Suppressing CCL8 expression to modulate host defenses	*L. monocytogenes* infection:preclinical trial	Unknown	Severa et al., 2014

CXCR4, the receptor of stromal cell-derived factor (SDF)-1α, can be induced to overexpress on invading tumor, macrophages/microglia and GSCs in hypoxia-niche, and is a therapeutic target for patients suffering from GBM (Wang et al., 2012). Deng et al. (2017) demonstrated that SDF-1 blockade with olaptesed pegol (OLA-PEG, NOX-A12) impeded TAMs recruitment by VEGF blockage in GBM. POL5551, a potent CXCR4 antagonists, could decrease the populations of tumor-initiating GSCs and GAMs, as well as lessen hypoxia-induced uncontrolled multiplication and invasion of glioma (Gagner et al., 2017). Guo et al. (2016) discovered that the hypoxia-inducible factors (HIFs) inhibitor, acriflavine (ACF), blocked the over-expression of hypoxia-inducible POSTN by virtue of TGF-α through RTK/PI3K pathway.

Reeducating TAMs to M1 Macrophages

Minimizing the Immunosuppressive M2 Macrophages or Blocking the Signaling Pathways Displaying to CSCs

There was direct evidence that the existence of CSCs is the real driving force behind proceeded recurrence of brain tumors following chemotherapy (Hemmati et al., 2003). These cells have strong DNA repair, multipotency, self-renewal and tumor recapitulation ability *in vivo*. Even if the proportion of these cells in primary tumor cells is constrained, they have the capacity to fortify regrowth, and attack normal surrounding brain tissues to form local metastasis (Ortensi et al., 2013). MicroRNAs (miRNAs) are short non-coding RNAs that act *via* mRNA degradation, deadenylation or translational repression. Studies uncovered that miRNAs were fundamental for various pathophysiological processes, including cell proliferation, differentiation and apoptosis (Saliminejad et al., 2019; Zhang L. et al., 2019). Liu Y. et al. (2019) identified that miR-340-5p over-expression restrained TAMs thickness, M2 macrophages activation and tumorigenesis of glioma *in vivo*.

CSCs tend to regulate macrophage polarization by activating STAT3. TGF-β1 signaling allows M2 macrophages originating from peripheral blood monocytes to improve CSC functions. Moreover, siRNA-mediated STAT3 silencing could cut off CSC chemo-receptivity and migratory capacities. Suppressing immunosuppressive macrophages or disturbing the messages they send to CSCs may have unexpected effect in GBM combination therapies (Nusblat et al., 2017).

As a molecular chain, the PTN-PTPRZ1 paracrine signaling regulated M2 macrophages supportive ability on GBM destructive development and GSC maintenance. Disrupting PTN-PTPRZ1 signaling could effectively inhibit GSC-driven tumor development, and this result meant that targeting PTN-PTPRZ1 signaling therapy could enhance treatment for GBM and other malignant tumors (Shi et al., 2017).

As nanomedicine advances, sophisticated nanocarriers developed for specific receptors on TAMs are a very promising TAM-targeting technique. Ovais et al. (2019) reviewed the existing cancer immuno-nanomedicines, which mainly affect the survival of M2-like TAMs or their signaling pathways, prevent macrophages from recruiting to tumor sites and retrain M2-like macrophages to M1-like phenotype. One subject demonstrated that in a GBM model, transcribed mRNA encoding M1-polarizing transcription factors could be addressed by a specific nanocarrier to reprogram TAMs (Zhang F. et al., 2019).

Inducing M2-Like Gene Expression Changes in TAMs

TAMs could be depolarized from the initial M2-like state after being exposed to CSF1R inhibitors such as PLX3397, thus effectively impairing TAMs' pro-tumorigenic activities and further presumably led to reduction in tumor development or regression *in vivo* (Tap et al., 2015). Compared with PLX3397 monotherapy, it was found that combining PLX3397 with Dovitinib or Vatalanib further diminished M2-like genes expression, including Stab1, Irf4 and Ccl22 (Yan et al., 2017). Wei et al. (2013) identified a key candidate gene for regulating STAT3 signaling pathways, miR-124. STAT3 pathway could be blocked by upregulating miR-124 in GSCs. miR-124 inhibited T-cell proliferation and forkhead box P3 positive ($Foxp3^+$) Tregs activation through reversing GSCs-mediated immunosuppression. Zhang F. et al. (2019) introduced a specific nanocarrier, which could transport *in vitro*-transcribed mRNA to reprogram TAMs by encoding M1-polarizing transcription factors. By encoding IRF5 together with its activating kinase IKKβ, TAMs were reprogrammed to trigger anti-tumor response and facilitated tumor cell death after infused of nanoparticles formulated with mRNAs to reverse their immunosuppressive, tumor-supporting state.

Enhancing the Phagocytosis and Antigen Presenting Ability of Macrophages or Macrophage-Mediated Anti-cancer Function

Targeting Special Molecules Expressed on Macrophages

Mer tyrosine kinase (MerTK), expressed on GAMs, is a receptor tyrosine kinase (RTK) that activates efferocytosis (specific type of phagocytosis) and suppresses innate immune responses. Inhibition of MerTK combined with external beam radiotherapy (XRT) has been proved to be an effective way in treating a subset of GBMs (Wu et al., 2018). CCL2 (also named MCP-1), which is released by tumor cells, is a chemotactic factor that recruits $CCL2R^+$ monocytes, T cells and NK cells. Both antibodies against CCL2 as well as inhibitors of CCL2R have shown evidence of reducing cancer progression (Li et al., 2013; Cassetta and Pollard, 2018). Allavena et al. (2005) and Martin-Broto et al. (2020) detailed an imaginative anti-tumor item, yondelis (trabectedin), which inhibited macrophage differentiation and cytokine yield in metastatic soft-tissue sarcoma, ovarian and breast adenocarcinoma. Takenaka et al. (2019) reported that the production of kynurenine by glioma activated aryl hydrocarbon receptor (AHR), which drove TAMs enrollment in response to CCL2 and suppressed NF-κB activation in TAMs to modulate their functions.

Targeting Macrophages/Microglia-Derived Cytokines

Yin et al. (2017) reported that through NF-κB activation, macrophages/microglia-derived cytokines heightened transglutaminase 2 (TGM2, an inducible transamidating acyltransferase) expression. TGM2 is increased within the perinecrotic zone of GBM and promotes mesenchymal (MES) *trans*-differentiation in GSCs by controlling master transcription factors (TF) involving C/EBPβ, TAZ, and STAT3. It has been illustrated that TGM2 was a crucial switch protein in MES *trans*-differentiation triggered by necrosis, so it is a promising treatment target for MES GBM.

In the process of glioblastoma, TAMs are recruited and induced by cancer cells to enhance tumor development (Mantovani et al., 2002), that is, tumor cells inhibit the anti-tumor immunological reaction of TAMs and urge TAMs to secret IL-6, VEGF, MMPs, IL-10 and TGF-β1 to favor tumor cell expansion, angiogenesis, matrix degradation and invasion

(Joseph et al., 2015). TGF-β inducible protein (TGFBI) is one of many transduction regulatory molecules in TGF-β signal pathways relying on classical SMAD pathways and non-SMAD pathways (Rodríguez-García et al., 2017; Deng et al., 2018; Guo et al., 2018). One study discovered that there was a parallel relationship between the distribution of TGFBI and TAMs based on the inspection of tumor Genome Map Project (TCGA), Chinese Glioma Genome Map Project (CGGA), brain tumor Molecular Database (REMBRANDT) and Oncomine Database (Li and Graeber, 2012). Zhang et al. (2020) revealed that CCL8 (also referred to as MCP-2) delivered by TAMs promoted invasion and GBM cells stemness by mobilizing the phosphorylation of ERK1/2 in GBM cells. Severa et al. (2014) recorded the transcriptional repressor B lymphocyte-induced maturation protein 1 (BLIMP1) conditional knockout (CKO) mice showed stronger levels of circulating CCL8, uncovering that BLIMP1 performed a fundamental task in modifying host defense mechanisms by decreasing CCL8-expression.

Promotion of Tumor-Infiltrating Lymphocyte Accumulation and T Cell Activation

STAT3 participates in many of the widely active carcinogenic signaling as well as the transcriptional modulation of different tumor-promoting factors. STX-0119, the STAT3 inhibitor, demonstrates anti-tumor activity occurring through promoting TILs accumulation predominantly in the clonal expansion of CD8-postitive T cells and macrophages at TMZ-resistant U87 glioma tumor-site and humanized MHC-double knockout mouse (dKO-NOG) system, which has the potential to be a critical tool for assessing the impact of STAT3 inhibitors on human tumors (Akiyama et al., 2017). WP1066, a small-molecule STAT3 pathway inhibitor, increased the secretion of cytokines such as IL-2, IL-4, IL-12, IL-15, and T-cell proliferation by turning on co-stimulatory molecules expression on microglia and peripheral macrophages (Hussain et al., 2007).

Angiogenesis Inhibition in Glioma

VEGF and TGF-β are pivotal factors in glioma angiogenesis. Conditional medium collected from TAMs and EPCs that dealt with a flavonoid (FLA-16) caused pericyte cells relocation thus decreasing endothelial cells proliferation and migration, which could be shifted by cytochrome P450 (CYP) 4A (CYP4A) over-expression or exogenous supplement of 20-hydroxyeicosatetraenoic acid (20-HETE), VEGF or TGF-β. Moreover, FLA-16 inhibited crosstalk between TAM and EPC during angiogenesis. Repression of CYP4A by FLA-16 prolonged life and normalized tumor vasculature in GBM by hindering TAMs and EPC-derived VEGF and TGF-β through PI3K/Akt signaling (Wang et al., 2017). In addition, Arachidonic acid (AA) metabolic enzymes, including microsomal prostaglandin E synthase-1 (mPGES-1), cyclooxygenase-2 (COX-2) and CYP4A11, are vital to glioma angiogenesis. Wang et al. (2019) detailed that through the ceRNA effect of miR-194-5p and lncRNA NEAT1, flavonoid isoliquiritigenin (ISL) hindered the Akt/FGF-2/TGF-β/VEGF angiogenic signaling to reprogram AA metabolism mediated by COX-2, mPGES-1 and CYP4A in glioma. Wang C. et al. (2018) found that flavonoid CH625 (a flavonoid, 3-sulfanyl-1-triazene) inhibition of CYP4X1 in TAMs normalized tumor vasculature in glioma *via* cannabinoid receptors (CB) 2/EGFR-STAT3 axis, and this effect could be reversed by CYP4X1 and STAT3 over-expression, as well as external stimulants, such as 14,15-epoxyeicosatrienoic acid-ethanolamide (14,15-EET-EA), VEGF, TGF-β, EGF, and AM630 (the CB2 inhibitor) and so on. Neuropilin-1 (NRP-1), a transmembrane receptor, can amplify pro-angiogenic signaling in the TME. NRP-1 positive macrophages play an imperative role in antibody-mediated immune responses to fight cancer. Evidence showed that knockdown of NRP-1 on macrophages suppressed lymphocyte infiltration in TME. NRP-1 down-regulation on macrophages modulated tumoricidal function mediated by antibodies. *In vivo* studies with a human breast cancer xenograft model revealed that NRP-1 expression on macrophages was necessary for antibody-based tumoricidal activity and infiltration of $CD4^+$ T cell into tumor locations (Kawaguchi et al., 2017). Several experiments demonstrated that NRP-1 signaling in GAMs were essential for their intertwined links with the surrounding glioma microenvironment. Ablation of NRP-1 from GAMs exhibited less vascularity and slowed tumor progression (Miyauchi et al., 2016).

POTENTIAL TARGETS FOR TAMs IN OTHER TUMORS

Numerous investigations have described that TAMs are intimately linked to tumorigenesis. Hence, TAM-targeting immunotherapy shows great potential and promising prospects in tumor therapy. The potential targets of TAMs recently found in glioma and other cancer studies are listed below (**Table 1**), including TAMs activation inhibitor or direct targets for TAMs, in order to provide some inspiration in the subsequent treatment of glioma.

Enhancing Cytotoxic Activity and Phagocytosis to Tumor Cells

CD47

Macrophages never assault ordinary cells, since CD47 interacts with SIRP-1, a protein on its surface, and sends a negative signal back to macrophages, avoiding them from phagocytizing the target cells (Okazawa et al., 2005). Anti-CD47 antibody can block the interaction between CD47 and SIRPα, allowing phagocytes to selectively engulf tumor cells without damaging the surrounding healthy cells in melanoma and pediatric cancer (Uluçkan et al., 2009; Ridler, 2017; Hayat et al., 2020). *In vitro*, CD47 blockade triggered phagocytosis of cancer cells by macrophages, which has been thoroughly proved using microscopy and flow cytometry. *In vivo*, treatment of mice with liposomal clodronate, which exhausted macrophages, abolished the tumoricidal effects of CD47-blocking treatments, demonstrating macrophages were essential for robust anti-tumor responses (Xia et al., 2020). One inquiry supported that using a CpG oligodeoxynucleotide, a Toll-like receptor 9 agonist, to trigger macrophages could modify the metabolism of central carbon and strengthen the engulfment of $CD47^+$ cancerous cells

in pancreatic ductal adenocarcinoma models (PDAC) (Liu M. et al., 2019). Furthermore, *in situ* phagocytosis has been seen in leukemia, colon cancer, and breast cancer models (Weiskopf, 2017). However, a series of biosafety problems such as anemia should not be ignored.

Regulating the Polarization of TAMs

To reverse the polarization of TAMs, targeting the cytokines in TME is another potential method. The Th1 cytokine, IFN-γ could fuel macrophages to polarize toward M1 phenotype. On the other hand, M2 polarization was first discovered as a reaction to Th2 cytokine IL-4 (Stein et al., 1992). Anti-inflammatory molecules including glucocorticoids, IL-4, IL-13, and IL-10 were proved to be direct inhibitors of classical macrophage activation, since they caused distinct M2 activation programs (Biswas and Mantovani, 2010). Ramesh et al. (2019) reported that M2 macrophages were repolarized to M1 phenotype and demonstrated inferior phagocytic capabilities after self-assembled dual-inhibitor-loaded nanoparticles (DNTs). This kind of DNTs was designed to "target" M2 macrophages while concurrently inhibiting CSF1R and SHP2 pathways in breast cancer and melanoma mouse models. The inhibition of Class IIa histone deacetylase (HDAC) in breast tumors reduced monocyte responses to CSF1 and CSF2 *in vitro* and caused intensely phagocytic and stimulatory macrophages to be recruited and differentiated (Guerriero et al., 2017; Guerriero, 2018).

Activating the Ablation of TAMs

Legumain

Legumain, an asparaginyl endopeptidase, significantly expressed on M2 macrophages responding to the stimulation of Th2 cytokines in the TME. Legumain-ablated TAMs that directly triggered by a doxorubicin-based pro-drug could greatly inhibited tumor progress and metastases in breast carcinoma mouse models (Lin et al., 2013). Besides, alanine-alanine-asparagine (AAN), a substrate of endoprotease legumain, has also been identified as a specific ligand for TAMs (Liu Z. et al., 2014). To integrate AAN-based TAM-targeting and iRGD-based vascular and tumor permeability activities, nRGD was created by appending the substrate of endoprotease legumain (AAN) to the tumor homing peptide (iRGD). After loaded with Doxorubicin, liposomes that revised with nRGD (nRGD-Lipo-Dox) gained new skills by regulating TME with TAMs depletion, which explained the improved anti-tumor potency and long-term antiangiogenic effect in 4T1 breast cancer mice (Song et al., 2016).

Mannose Receptor

Macrophage mannose receptor, also called cluster of differentiation 206 (CD206), is a key promoter of tumor progression. Depleting $CD206^{+}$ TAMs is a critical approach to cancer therapy (De Vlaeminck et al., 2019). TPE-Man, a theranostic probe with mannose moieties attached to a red-emissive AIE (aggregation-induced emission)-active photosensitizer, pinpointed the over-expressed mannose receptor on TAMs and effectively eradicated TAMs when exposed to white light irradiation, similar to the mannose-receptor antibody (Gao et al., 2019).

Engineering CAR Macrophages With Tumor Specificity

Recently, adapting CAR strategies to macrophages have been demonstrated profitable. CAR macrophages (CAR-Ms) were designed to release pro-inflammatory cytokines and chemokines, convert M2 macrophages to M1, deliver a pro-inflammatory TME and increase T cells' anti-tumor activity (Morrissey and Williamson, 2018; Klichinsky and Ruella, 2020).

CONCLUSION

Over the last few years, with the constant emergence of modern technologies such as CRISPR/Cas9-mediated target gene activation (Xie et al., 2019; Morimoto and Nakazawa, 2021) and single cell RNA sequencing (Tirosh and Suvà, 2018), the characterization of GBM genome, epigenome, transcriptome revealed multiple subtypes and high inter- and intra-tumor heterogeneity of GBM (DeCordova et al., 2020). Glioma is a highly complex systemic disease that develops as a product of long-term Tumor/TME crosstalk between glioma cells and their local and distant microenvironments. TAMs, as one of the largest number of inflammatory cells in TME, perform a more fundamental and sophisticated character in glioma progression than previously thought (Li et al., 2021). Despite recent advances in T cell-based glioma therapy, accumulating evidence has showed that immunosuppressive microenvironment represents the main obstacle to maximize the effect of immunotherapies (Kwok and Okada, 2020; Mathewson et al., 2021). In view of the multi-dimensional influence of TAMs on tumor immunotherapies, TAMs, as the dominant immune cells in TME, are still indispensable targets for glioma therapy. So far, people have found that TAMs participate in the development and progression of glioma, and regulate tumor growth, invasion, angiogenesis, origin of GSCs and immune response. For these functions, numerous of experimental TAM-targeting strategies, such as macrophage elimination, recruitment inhibition and reprogramming, have been gradually developed. Some progress has been made in clinical and preclinical studies, but the prognosis of glioma patient is still unsatisfactory. Therefore, the function of TAMs in tumor progression needs more overall comprehension as well as the TAM-targeting strategies still need further development (Cassetta and Pollard, 2018). At present, there are still some questions that need to be forwarded.

(1) Recent data acquired utilizing unbiased large-scale techniques have discriminated that TAMs are not a simple binary M1-M2 typing, the intertwined relationships among each macrophage sub-populations' location, subphenotype, polarization, dynamic changes and heterogeneity, glioma's development and the efficacy of immunotherapy need to be fully unraveled by experimental research and clinical trials (Guillot and Tacke, 2019).

(2) Find highly specific molecular on TAMs that may be used as anti-glioma therapeutic objectives, to potentially low toxicity and side effects for successful therapy.
(3) The interaction between macrophages and other stromal cells should be further clarified to better understand the inter- and intra-driving force of the generation and maintenance of local glioma immunosuppressive microenvironment.
(4) What is the significance of macrophage subsets expressing different checkpoint receptors, such as PD-1 (Saha et al., 2017), T Cell Immunoglobulin and ITIM domain (TIGIT) (Chauvin and Zarour, 2020), or Lymphocyte-activation-gene-3 (LAG-3) (Maruhashi and Sugiura, 2020)? Is it possible to employ them to support T cell-targeting therapy?
(5) Governing the equilibrium between anti-cancer inflammatory response and pro-cancer inflammatory response is still an inherent problem to be solved.
(6) Recent multiple subclusters of TAMs have been established by single-cell RNA sequencing, suggesting that macrophage functionality is in a continuum of states. How to make TAM-targeting anti-glioma drugs get delivered through the BBB to act at the right point at the right time, and eliminate "bad" tumor-promoting TAMs without killing "good" macrophage in surrounding normal tissues?

In conclusion, at the genetic and immunological levels, the complicated and dramatic heterogeneity of malignant gliomas remains a profound challenge. As the dominant immune cells and indispensable target in immunologically cold tumor–glioma, TAMs' characteristics and their interaction with TME, combined with the progress of diagnosis and treatment technology, need more comprehensively understanding. It is believed that targeting TAMs residing in TME in various ways for anti-glioma treatment strategy, in combination with the introduction of other therapeutic approaches, such as the recently discovered "pan cancer therapy," combining SIRPα macrophage-based therapy with radiotherapy, miraculously activated tumor antigen-specific cytotoxic T cell in a broad spectrum of tumors including those at late-stage with low immunogenicity and metastases (Bian and Shi, 2021), may offer more and more innovative efficacious therapies for future glioma treatment and can be used as a realistic remedy for cancer patients.

AUTHOR CONTRIBUTIONS

All authors listed have made a substantial, direct and intellectual contribution to the work, and approved it for publication.

FUNDING

This work was financially supported by The National Natural Science Foundation of China (nos. 81873295 and 82074337), Natural Science Foundation of Guangdong Province (nos. 2018A030313106, 2019A1515012209, and 2020A1515110203), Special Funds for the Cultivation of Guangdong College Students' Scientific and Technological Innovation ("Climbing Program" Special Funds, no. pdjh2020b0120), and Fundamental Research Funds for Junior Teachers in Sun Yat-sen University, China (20ykpy163).

REFERENCES

Akiyama, Y., Nonomura, C., Ashizawa, T., Iizuka, A., Kondou, R., Miyata, H., et al. (2017). The anti-tumor activity of the STAT3 inhibitor STX-0119 occurs via promotion of tumor-infiltrating lymphocyte accumulation in temozolomide-resistant glioblastoma cell line. *Immunol. Lett.* 190, 20–25. doi: 10.1016/j.imlet.2017.07.005

Allavena, P., Signorelli, M., Chieppa, M., Erba, E., Bianchi, G., Marchesi, F., et al. (2005). Anti-inflammatory properties of the novel antitumor agent yondelis (trabectedin): inhibition of macrophage differentiation and cytokine production. *Cancer Res.* 65, 2964–2971. doi: 10.1158/0008-5472.can-04-4037

Arlauckas, S. P., and Garris, C. S. (2017). In vivo imaging reveals a tumor-associated macrophage-mediated resistance pathway in anti-PD-1 therapy. *Sci. Transl. Med.* 9:eaal3604. doi: 10.1126/scitranslmed.aal3604

Bagley, S. J., Desai, A. S., Linette, G. P., June, C. H., and O'rourke, D. M. (2018). CAR T-cell therapy for glioblastoma: recent clinical advances and future challenges. *Neuro Oncol.* 20, 1429–1438. doi: 10.1093/neuonc/noy032

Bastida-Ruiz, D., Van Hoesen, K., and Cohen, M. (2016). The dark side of cell fusion. *Int. J. Mol. Sci.* 17:638. doi: 10.3390/ijms17050638

Beauchesne, P. (2011). Extra-neural metastases of malignant gliomas: myth or reality? *Cancers (Basel)* 3, 461–477. doi: 10.3390/cancers3010461

Bell, E. H., Zhang, P., Fisher, B. J., Macdonald, D. R., Mcelroy, J. P., Lesser, G. J., et al. (2018). Association of MGMT promoter methylation status with survival outcomes in patients with high-risk glioma treated with radiotherapy and temozolomide: an analysis from the NRG oncology/RTOG 0424 trial. *JAMA Oncol.* 4, 1405–1409. doi: 10.1001/jamaoncol.2018.1977

Bian, Z., and Shi, L. (2021). Intratumoral SIRPα-deficient macrophages activate tumor antigen-specific cytotoxic T cells under radiotherapy. *Nat. Commun.* 12:3229. doi: 10.1038/s41467-021-23442-z

Biswas, S. K., and Mantovani, A. (2010). Macrophage plasticity and interaction with lymphocyte subsets: cancer as a paradigm. *Nat. Immunol.* 11, 889–896. doi: 10.1038/ni.1937

Boscá, L., González-Ramos, S., Prieto, P., Fernández-Velasco, M., Mojena, M., Martín-Sanz, P., et al. (2015). Metabolic signatures linked to macrophage polarization: from glucose metabolism to oxidative phosphorylation. *Biochem. Soc. Trans.* 43, 740–744. doi: 10.1042/bst20150107

Bowman, M. R., Crimmins, M. A., Yetz-Aldape, J., Kriz, R., Kelleher, K., and Herrmann, S. (1994). The cloning of CD70 and its identification as the ligand for CD27. *J. Immunol.* 152, 1756–1761.

Campos, B., Olsen, L. R., Urup, T., and Poulsen, H. S. (2016). A comprehensive profile of recurrent glioblastoma. *Oncogene* 35, 5819–5825. doi: 10.1038/onc.2016.85

Cannarile, M. A., Weisser, M., Jacob, W., Jegg, A. M., Ries, C. H., and Rüttinger, D. (2017). Colony-stimulating factor 1 receptor (CSF1R) inhibitors in cancer therapy. *J. Immunother. Cancer* 5:53. doi: 10.1186/s40425-017-0257-y

Cassetta, L., and Pollard, J. W. (2018). Targeting macrophages: therapeutic approaches in cancer. *Nat. Rev. Drug Discov.* 17, 887–904. doi: 10.1038/nrd.2018.169

Caux, C., Ramos, R. N., Prendergast, G. C., Bendriss-Vermare, N., and Ménétrier-Caux, C. (2016). A milestone review on how macrophages affect tumor growth. *Cancer Res.* 76, 6439–6442. doi: 10.1158/0008-5472.can-16-2631

Chauvin, J. M., and Zarour, H. M. (2020). TIGIT in cancer immunotherapy. *J. Immunother. Cancer* 8:e000957. doi: 10.1136/jitc-2020-000957

Chen, T., Song, X., Gong, T., Fu, Y., Yang, L., Zhang, Z., et al. (2017). nRGD modified lycobetaine and octreotide combination delivery system to overcome multiple barriers and enhance anti-glioma efficacy. *Colloids Surf. B Biointerfaces* 156, 330–339. doi: 10.1016/j.colsurfb.2017.05.038

Chen, Z., and Hambardzumyan, D. (2018). Immune microenvironment in glioblastoma subtypes. *Front. Immunol.* 9:1004. doi: 10.3389/fimmu.2018.01004

Colegio, O. R., Chu, N. Q., Szabo, A. L., Chu, T., Rhebergen, A. M., Jairam, V., et al. (2014). Functional polarization of tumour-associated macrophages by tumour-derived lactic acid. *Nature* 513, 559–563. doi: 10.1038/nature13490

D'Alessio, A., Proietti, G., Sica, G., and Scicchitano, B. M. (2019). Pathological and molecular features of glioblastoma and its peritumoral tissue. *Cancers (Basel)* 11:469. doi: 10.3390/cancers11040469

Das, G., Shiras, A., Shanmuganandam, K., and Shastry, P. (2011). Rictor regulates MMP-9 activity and invasion through Raf-1-MEK-ERK signaling pathway in glioma cells. *Mol. Carcinog.* 50, 412–423. doi: 10.1002/mc.20723

De Palma, M., Biziato, D., and Petrova, T. V. (2017). Microenvironmental regulation of tumour angiogenesis. *Nat. Rev. Cancer* 17, 457–474. doi: 10.1038/nrc.2017.51

De Vlaeminck, Y., Lecocq, Q., Giron, P., Heirman, C., Geeraerts, X., Bolli, E., et al. (2019). Single-domain antibody fusion proteins can target and shuttle functional proteins into macrophage mannose receptor expressing macrophages. *J. Control. Release* 299, 107–120. doi: 10.1016/j.jconrel.2019.02.023

DeCordova, S., Shastri, A., Tsolaki, A. G., Yasmin, H., Klein, L., Singh, S. K., et al. (2020). Molecular heterogeneity and immunosuppressive microenvironment in glioblastoma. *Front. Immunol.* 11:1402. doi: 10.3389/fimmu.2020.01402

DeNardo, D. G., and Ruffell, B. (2019). Macrophages as regulators of tumour immunity and immunotherapy. *Nat. Rev. Immunol.* 19, 369–382. doi: 10.1038/s41577-019-0127-6

Deng, G., Chen, L., Zhang, Y., Fan, S., Li, W., Lu, J., et al. (2018). Fucosyltransferase 2 induced epithelial-mesenchymal transition via TGF-β/Smad signaling pathway in lung adenocarcinaoma. *Exp. Cell Res.* 370, 613–622. doi: 10.1016/j.yexcr.2018.07.026

Deng, L., Stafford, J. H., Liu, S. C., Chernikova, S. B., Merchant, M., Recht, L., et al. (2017). SDF-1 blockade enhances anti-VEGF therapy of glioblastoma and can be monitored by MRI. *Neoplasia* 19, 1–7. doi: 10.1016/j.neo.2016.11.010

Du, J., Haile, L. A., Greten, T. F., and Korangy, F. (2012). Immune suppression: the hallmark of myeloid derived suppressor cells. *Cell Death Differ.* 41, 581–594. doi: 10.3109/08820139.2012.680635

Fu, W., Wang, W., Li, H., Jiao, Y., Huo, R., Yan, Z., et al. (2020). Single-cell atlas reveals complexity of the immunosuppressive microenvironment of initial and recurrent glioblastoma. *Front. Immunol.* 11:835. doi: 10.3389/fimmu.2020.00835

Gagner, J. P., Sarfraz, Y., Ortenzi, V., Alotaibi, F. M., Chiriboga, L. A., Tayyib, A. T., et al. (2017). Multifaceted C-X-C chemokine receptor 4 (CXCR4) inhibition interferes with anti-vascular endothelial growth factor therapy-induced glioma dissemination. *Am. J. Pathol.* 187, 2080–2094. doi: 10.1016/j.ajpath.2017.04.020

Galldiks, N., Kocher, M., and Langen, K. J. (2017). Pseudoprogression after glioma therapy: an update. *Expert Rev. Neurother.* 17, 1109–1115. doi: 10.1080/14737175.2017.1375405

Gao, X., Mao, D., Zuo, X., Hu, F., Cao, J., Zhang, P., et al. (2019). Specific targeting, imaging, and ablation of tumor-associated macrophages by theranostic mannose-AIEgen conjugates. *Anal. Chem.* 91, 6836–6843. doi: 10.1021/acs.analchem.9b01053

Ge, H., Mu, L., Jin, L., Yang, C., Chang, Y. E., Long, Y., et al. (2017). Tumor associated CD70 expression is involved in promoting tumor migration and macrophage infiltration in GBM. *Int. J. Cancer* 141, 1434–1444. doi: 10.1002/ijc.30830

Gordon, S., and Martinez, F. O. (2010). Alternative activation of macrophages: mechanism and functions. *Immunity* 32, 593–604. doi: 10.1016/j.immuni.2010.05.007

Gordon, S. R., Maute, R. L., Dulken, B. W., Hutter, G., George, B. M., Mccracken, M. N., et al. (2017). PD-1 expression by tumour-associated macrophages inhibits phagocytosis and tumour immunity. *Nature* 545, 495–499. doi: 10.1038/nature22396

Guerriero, J. L. (2018). Macrophages: the road less traveled, changing anticancer therapy. *Trends Mol. Med.* 24, 472–489. doi: 10.1016/j.molmed.2018.03.006

Guerriero, J. L., Sotayo, A., Ponichtera, H. E., Castrillon, J. A., Pourzia, A. L., Schad, S., et al. (2017). Class IIa HDAC inhibition reduces breast tumours and metastases through anti-tumour macrophages. *Nature* 543, 428–432. doi: 10.1038/nature21409

Guillot, A., and Tacke, F. (2019). Liver macrophages: old dogmas and new insights. *Hepatol. Commun.* 3, 730–743. doi: 10.1002/hep4.1356

Guo, S. K., Shen, M. F., Yao, H. W., and Liu, Y. S. (2018). Enhanced expression of TGFBI promotes the proliferation and migration of glioma cells. *Cell. Physiol. Biochem.* 49, 1097–1109. doi: 10.1159/000493293

Guo, X., Xue, H., Shao, Q., Wang, J., Guo, X., Chen, X., et al. (2016). Hypoxia promotes glioma-associated macrophage infiltration via periostin and subsequent M2 polarization by upregulating TGF-beta and M-CSFR. *Oncotarget* 7, 80521–80542. doi: 10.18632/oncotarget.11825

Hambardzumyan, D., and Bergers, G. (2015). Glioblastoma: defining tumor niches. *Trends Cancer* 1, 252–265. doi: 10.1016/j.trecan.2015.10.009

Hambardzumyan, D., Gutmann, D. H., and Kettenmann, H. (2016). The role of microglia and macrophages in glioma maintenance and progression. *Nat. Neurosci.* 19, 20–27. doi: 10.1038/nn.4185

Hayat, S. M. G., Bianconi, V., Pirro, M., Jaafari, M. R., Hatamipour, M., and Sahebkar, A. (2020). CD47: role in the immune system and application to cancer therapy. *Cell. Oncol. (Dordr.)* 43, 19–30. doi: 10.1007/s13402-019-00469-5

Hemmati, H. D., Nakano, I., Lazareff, J. A., Masterman-Smith, M., Geschwind, D. H., Bronner-Fraser, M., et al. (2003). Cancerous stem cells can arise from pediatric brain tumors. *Proc. Natl. Acad. Sci. U.S.A.* 100, 15178–15183. doi: 10.1073/pnas.2036535100

Hervey-Jumper, S. L., and Berger, M. S. (2019). Insular glioma surgery: an evolution of thought and practice. *J. Neurosurg.* 130, 9–16. doi: 10.3171/2018.10.jns181519

Hilf, N., Kuttruff-Coqui, S., Frenzel, K., Bukur, V., Stevanović, S., Gouttefangeas, C., et al. (2019). Actively personalized vaccination trial for newly diagnosed glioblastoma. *Nature* 565, 240–245. doi: 10.1038/s41586-018-0810-y

Hua, L., and Wakimoto, H. (2019). Oncolytic herpes simplex virus therapy for malignant glioma: current approaches to successful clinical application. *Expert Opin. Biol. Ther.* 19, 845–854. doi: 10.1080/14712598.2019.1614557

Hussain, S. F., Kong, L. Y., Jordan, J., Conrad, C., Madden, T., Fokt, I., et al. (2007). A novel small molecule inhibitor of signal transducers and activators of transcription 3 reverses immune tolerance in malignant glioma patients. *Cancer Res.* 67, 9630–9636. doi: 10.1158/0008-5472.can-07-1243

Hutchinson, L. (2017). Immunotherapy: exploiting PD-1 on TAMs for tumour cell kill. *Nat. Rev. Clin. Oncol.* 14, 392–393. doi: 10.1038/nrclinonc.2017.87

Ito, H., Nakashima, H., and Chiocca, E. A. (2019). Molecular responses to immune checkpoint blockade in glioblastoma. *Nat. Med.* 25, 359–361. doi: 10.1038/s41591-019-0385-7

Jiang, Z., Jiang, J. X., and Zhang, G. X. (2014). Macrophages: a double-edged sword in experimental autoimmune encephalomyelitis. *Immunol. Lett.* 160, 17–22. doi: 10.1016/j.imlet.2014.03.006

Joseph, J. V., Conroy, S., Pavlov, K., Sontakke, P., Tomar, T., Eggens-Meijer, E., et al. (2015). Hypoxia enhances migration and invasion in glioblastoma by promoting a mesenchymal shift mediated by the HIF1α-ZEB1 axis. *Cancer Lett.* 359, 107–116. doi: 10.1016/j.canlet.2015.01.010

Jung, M., Ören, B., Mora, J., Mertens, C., Dziumbla, S., Popp, R., et al. (2016). Lipocalin 2 from macrophages stimulated by tumor cell-derived sphingosine 1-phosphate promotes lymphangiogenesis and tumor metastasis. *Sci. Signal.* 9:ra64. doi: 10.1126/scisignal.aaf3241

Kawaguchi, K., Suzuki, E., Nishie, M., Kii, I., Kataoka, T. R., Hirata, M., et al. (2017). Downregulation of neuropilin-1 on macrophages modulates antibody-mediated tumoricidal activity. *Cancer Immunol. Immunother.* 66, 1131–1142. doi: 10.1007/s00262-017-2002-2

Kennedy, B. C., Showers, C. R., Anderson, D. E., Anderson, L., Canoll, P., Bruce, J. N., et al. (2013). Tumor-associated macrophages in glioma: friend or foe? *J. Oncol.* 2013:486912. doi: 10.1155/2013/486912

Kerjaschki, D. (2005). The crucial role of macrophages in lymphangiogenesis. *J. Clin. Invest.* 115, 2316–2319. doi: 10.1172/jci26354

Kim, H. S., Chang, C. Y., and Yoon, H. J. (2020). Glial TIM-3 modulates immune responses in the brain tumor microenvironment. *Cancer Res.* 80, 1833–1845. doi: 10.1158/0008-5472.can-19-2834

Klichinsky, M., and Ruella, M. (2020). Human chimeric antigen receptor macrophages for cancer immunotherapy. *Nat. Biotechnol.* 38, 947–953. doi: 10.1038/s41587-020-0462-y

Kortylewski, M., Kujawski, M., Wang, T., Wei, S., Zhang, S., Pilon-Thomas, S., et al. (2005). Inhibiting Stat3 signaling in the hematopoietic system elicits multicomponent antitumor immunity. *Nat. Med.* 11, 1314–1321. doi: 10.1038/nm1325

Kumar, V., Cheng, P., Condamine, T., Mony, S., Languino, L. R., Mccaffrey, J. C., et al. (2016). CD45 phosphatase inhibits STAT3 transcription factor activity in myeloid cells and promotes tumor-associated macrophage differentiation. *Immunity* 44, 303–315. doi: 10.1016/j.immuni.2016.01.014

Kwok, D., and Okada, H. (2020). T-Cell based therapies for overcoming neuroanatomical and immunosuppressive challenges within the glioma microenvironment. *J. Neurooncol.* 147, 281–295. doi: 10.1007/s11060-020-03450-7

Lang, R., Patel, D., Morris, J. J., Rutschman, R. L., and Murray, P. J. (2002). Shaping gene expression in activated and resting primary macrophages by IL-10. *J. Immunol.* 169, 2253–2263. doi: 10.4049/jimmunol.169.5.2253

Lee, H., Fessler, M. B., Qu, P., Heymann, J., and Kopp, J. B. (2020). Macrophage polarization in innate immune responses contributing to pathogenesis of chronic kidney disease. *BMC Nephrol.* 21:270. doi: 10.1186/s12882-020-01921-7

Leifler, K. S., Svensson, S., Abrahamsson, A., Bendrik, C., Robertson, J., Gauldie, J., et al. (2013). Inflammation induced by MMP-9 enhances tumor regression of experimental breast cancer. *J. Immunol.* 190, 4420–4430. doi: 10.4049/jimmunol.1202610

Li, J., Zhao, J., Tan, T., Liu, M., Zeng, Z., and Zeng, Y. (2020). Nanoparticle drug delivery system for glioma and its efficacy improvement strategies: a comprehensive review. *Int. J. Nanomedicine* 15, 2563–2582. doi: 10.2147/ijn.s243223

Li, M., Knight, D. A., Snyder, A. L., Smyth, M. J., and Stewart, T. J. (2013). A role for CCL2 in both tumor progression and immunosurveillance. *Oncoimmunology* 2:e25474. doi: 10.4161/onci.25474

Li, N., Qin, J., Lan, L., Zhang, H., Liu, F., Wu, Z., et al. (2015). PTEN inhibits macrophage polarization from M1 to M2 through CCL2 and VEGF-A reduction and NHERF-1 synergism. *Cancer Biol. Ther.* 16, 297–306. doi: 10.1080/15384047.2014.1002353

Li, W., and Graeber, M. B. (2012). The molecular profile of microglia under the influence of glioma. *Lab. Invest.* 14, 958–978. doi: 10.1093/neuonc/nos116

Li, X., Guo, X., Ling, J., Tang, Z., Huang, G., He, L., et al. (2021). Nanomedicine-based cancer immunotherapies developed by reprogramming tumor-associated macrophages. *Nanoscale* 13, 4705–4727. doi: 10.1039/d0nr08050k

Lin, Y., Wei, C., Liu, Y., Qiu, Y., Liu, C., and Guo, F. (2013). Selective ablation of tumor-associated macrophages suppresses metastasis and angiogenesis. *Cancer Sci.* 104, 1217–1225. doi: 10.1111/cas.12202

Liou, G. Y., Döppler, H., Necela, B., Krishna, M., Crawford, H. C., Raimondo, M., et al. (2013). Macrophage-secreted cytokines drive pancreatic acinar-to-ductal metaplasia through NF-κB and MMPs. *J. Cell Biol.* 202, 563–577. doi: 10.1083/jcb.201301001

Liu, D., Chang, C., Lu, N., Wang, X., Lu, Q., Ren, X., et al. (2017). Comprehensive proteomics analysis reveals metabolic reprogramming of tumor-associated macrophages stimulated by the tumor microenvironment. *J. Proteome Res.* 16, 288–297. doi: 10.1021/acs.jproteome.6b00604

Liu, M., O'connor, R. S., Trefely, S., Graham, K., Snyder, N. W., and Beatty, G. L. (2019). Metabolic rewiring of macrophages by CpG potentiates clearance of cancer cells and overcomes tumor-expressed CD47-mediated 'don't-eat-me' signal. *Nat. Immunol.* 20, 265–275. doi: 10.1038/s41590-018-0292-y

Liu, Y., Li, X., Zhang, Y., Wang, H., Rong, X., Peng, J., et al. (2019). An miR-340-5p-macrophage feedback loop modulates the progression and tumor microenvironment of glioblastoma multiforme. *Oncogene* 38, 7399–7415. doi: 10.1038/s41388-019-0952-x

Liu, Y. C., Zou, X. B., Chai, Y. F., and Yao, Y. M. (2014). Macrophage polarization in inflammatory diseases. *Int. J. Biol. Sci.* 10, 520–529. doi: 10.7150/ijbs.8879

Liu, Z., Kuang, W., Zhou, Q., and Zhang, Y. (2018). TGF-β1 secreted by M2 phenotype macrophages enhances the stemness and migration of glioma cells via the SMAD2/3 signalling pathway. *Int. J. Mol. Med.* 42, 3395–3403. doi: 10.3892/ijmm.2018.3923

Liu, Z., Xiong, M., Gong, J., Zhang, Y., Bai, N., Luo, Y., et al. (2014). Legumain protease-activated TAT-liposome cargo for targeting tumours and their microenvironment. *Nat. Commun.* 5:4280. doi: 10.1038/ncomms5280

Louveau, A., Smirnov, I., Keyes, T. J., Eccles, J. D., Rouhani, S. J., Peske, J. D., et al. (2015). Structural and functional features of central nervous system lymphatic vessels. *Nature* 523, 337–341. doi: 10.1038/nature14432

Mantovani, A., Biswas, S. K., Galdiero, M. R., Sica, A., and Locati, M. (2013). Macrophage plasticity and polarization in tissue repair and remodelling. *J. Pathol.* 229, 176–185. doi: 10.1002/path.4133

Mantovani, A., Sozzani, S., Locati, M., Allavena, P., and Sica, A. (2002). Macrophage polarization: tumor-associated macrophages as a paradigm for polarized M2 mononuclear phagocytes. *Trends Immunol.* 23, 549–555. doi: 10.1016/s1471-4906(02)02302-5

Marchesi, F., Locatelli, M., Solinas, G., Erreni, M., Allavena, P., and Mantovani, A. (2010). Role of CX3CR1/CX3CL1 axis in primary and secondary involvement of the nervous system by cancer. *J. Neuroimmunol.* 224, 39–44. doi: 10.1016/j.jneuroim.2010.05.007

Martin-Broto, J., Hindi, N., Lopez-Pousa, A., Peinado-Serrano, J., Alvarez, R., Alvarez-Gonzalez, A., et al. (2020). Assessment of safety and efficacy of combined trabectedin and low-dose radiotherapy for patients with metastatic soft-tissue sarcomas: a nonrandomized phase 1/2 clinical trial. *JAMA Oncol.* 6, 535–541. doi: 10.1001/jamaoncol.2019.6584

Maruhashi, T., and Sugiura, D. (2020). LAG-3: from molecular functions to clinical applications. *J. Immunother. Cancer* 8:e001014. doi: 10.1136/jitc-2020-001014

Mathewson, N. D., Ashenberg, O., Tirosh, I., Gritsch, S., Perez, E. M., Marx, S., et al. (2021). Inhibitory CD161 receptor identified in glioma-infiltrating T cells by single-cell analysis. *Cell* 184:1281-1298.e1226. doi: 10.1016/j.cell.2021.01.022

McFarland, B. C., Hong, S. W., Rajbhandari, R., Twitty, G. B. Jr., Gray, G. K., Yu, H., et al. (2013). NF-κB-induced IL-6 ensures STAT3 activation and tumor aggressiveness in glioblastoma. *PLoS One* 8:e78728. doi: 10.1371/journal.pone.0078728

Meng, C. D., Zhu, D. D., Jiang, X. D., Li, L., Sha, J. C., Dong, Z., et al. (2012). Overexpression of interleukin-l7 in tumor-associated macrophages is correlated with the differentiation and angiogenesis of laryngeal squamous cell carcinoma. *Chin. Med. J. (Engl.)* 125, 1603–1607.

Mira, E., Carmona-Rodríguez, L., Tardáguila, M., Azcoitia, I., González-Martín, A., Almonacid, L., et al. (2013). A lovastatin-elicited genetic program inhibits M2 macrophage polarization and enhances T cell infiltration into spontaneous mouse mammary tumors. *Oncotarget* 4, 2288–2301. doi: 10.18632/oncotarget.1376

Miyauchi, J. T., Chen, D., Choi, M., Nissen, J. C., Shroyer, K. R., Djordevic, S., et al. (2016). Ablation of neuropilin 1 from glioma-associated microglia and macrophages slows tumor progression. *Oncotarget* 7, 9801–9814. doi: 10.18632/oncotarget.6877

Morimoto, T., and Nakazawa, T. (2021). CRISPR-Cas9-mediated TIM3 knockout in human natural killer cells enhances growth inhibitory effects on human glioma cells. *Int. J. Mol. Sci.* 22:3489. doi: 10.3390/ijms22073489

Morrissey, M. A., and Williamson, A. P. (2018). Chimeric antigen receptors that trigger phagocytosis. *Elife* 7:e36688. doi: 10.7554/eLife.36688

Mukherjee, S., Baidoo, J. N. E., Sampat, S., Mancuso, A., David, L., Cohen, L. S., et al. (2018). Liposomal TriCurin, a synergistic combination of curcumin, epicatechin gallate and resveratrol, repolarizes tumor-associated microglia/macrophages, and eliminates glioblastoma (GBM) and GBM stem cells. *Molecules* 23:201. doi: 10.3390/molecules23010201

Muraille, E., Leo, O., and Moser, M. (2014). TH1/TH2 paradigm extended: macrophage polarization as an unappreciated pathogen-driven escape mechanism? *Front. Immunol.* 5:603. doi: 10.3389/fimmu.2014.00603

Najafi, M., Hashemi Goradel, N., Farhood, B., Salehi, E., Nashtaei, M. S., Khanlarkhani, N., et al. (2019). Macrophage polarity in cancer: a review. *J. Cell. Biochem.* 120, 2756–2765. doi: 10.1002/jcb.27646

Nassar, D., and Blanpain, C. (2016). Cancer stem cells: basic concepts and therapeutic implications. *Annu. Rev. Pathol.* 11, 47–76. doi: 10.1146/annurev-pathol-012615-044438

Nejo, T., Yamamichi, A., Almeida, N. D., Goretsky, Y. E., and Okada, H. (2020). Tumor antigens in glioma. *Semin. Immunol.* 47:101385. doi: 10.1016/j.smim.2020.101385

Nusblat, L. M., Carroll, M. J., and Roth, C. M. (2017). Crosstalk between M2 macrophages and glioma stem cells. *Cell. Oncol. (Dordr.)* 40, 471–482. doi: 10.1007/s13402-017-0337-5

Odegaard, J. I., Ricardo-Gonzalez, R. R., Goforth, M. H., Morel, C. R., Subramanian, V., Mukundan, L., et al. (2007). Macrophage-specific PPARgamma controls alternative activation and improves insulin resistance. *Nature* 447, 1116–1120. doi: 10.1038/nature05894

Ohmori, Y., and Hamilton, T. A. (1997). IL-4-induced STAT6 suppresses IFN-gamma-stimulated STAT1-dependent transcription in mouse macrophages. *J. Immunol.* 159, 5474–5482.

Okazawa, H., Motegi, S., Ohyama, N., Ohnishi, H., Tomizawa, T., Kaneko, Y., et al. (2005). Negative regulation of phagocytosis in macrophages by the CD47-SHPS-1 system. *Sci. Transl. Med.* 174, 2004–2011. doi: 10.4049/jimmunol.174.4.2004

Orecchioni, M., Ghosheh, Y., Pramod, A. B., and Ley, K. (2019). Macrophage polarization: different gene signatures in M1(LPS+) vs. classically and M2(LPS-) vs. alternatively activated macrophages. *Front. Immunol.* 10:1084. doi: 10.3389/fimmu.2019.01084

Ortensi, B., Setti, M., Osti, D., and Pelicci, G. (2013). Cancer stem cell contribution to glioblastoma invasiveness. *Stem Cell Res. Ther.* 4:18. doi: 10.1186/scrt166

Ovais, M., Guo, M., and Chen, C. (2019). Tailoring nanomaterials for targeting tumor-associated macrophages. *Adv. Mater.* 31:e1808303. doi: 10.1002/adma.201808303

Pan, X. Q. (2012). The mechanism of the anticancer function of M1 macrophages and their use in the clinic. *Chin. J. Cancer* 31, 557–563. doi: 10.5732/cjc.012.10046

Pang, Y., Hou, X., Yang, C., Liu, Y., and Jiang, G. (2018). Advances on chimeric antigen receptor-modified T-cell therapy for oncotherapy. *Mol. Cancer Res.* 17:91. doi: 10.1186/s12943-018-0840-y

Peng, S. H., Deng, H., Yang, J. F., Xie, P. P., Li, C., Li, H., et al. (2005). Significance and relationship between infiltrating inflammatory cell and tumor angiogenesis in hepatocellular carcinoma tissues. *World J. Gastroenterol.* 11, 6521–6524. doi: 10.3748/wjg.v11.i41.6521

Peranzoni, E., Lemoine, J., Vimeux, L., Feuillet, V., Barrin, S., Kantari-Mimoun, C., et al. (2018). Macrophages impede CD8 T cells from reaching tumor cells and limit the efficacy of anti-PD-1 treatment. *Proc. Natl. Acad. Sci. U.S.A.* 115, E4041–E4050. doi: 10.1073/pnas.1720948115

Pesce, J. T., Ramalingam, T. R., Mentink-Kane, M. M., Wilson, M. S., El Kasmi, K. C., Smith, A. M., et al. (2009). Arginase-1-expressing macrophages suppress Th2 cytokine-driven inflammation and fibrosis. *PLoS Pathog.* 5:e1000371. doi: 10.1371/journal.ppat.1000371

Phillips, R. E., Soshnev, A. A., and Allis, C. D. (2020). epigenomic reprogramming as a driver of malignant glioma. *Cancer Cell* 38, 647–660. doi: 10.1016/j.ccell.2020.08.008

Piao, Y., Henry, V., Tiao, N., Park, S. Y., Martinez-Ledesma, J., Dong, J. W., et al. (2017). Targeting intercellular adhesion molecule-1 prolongs survival in mice bearing bevacizumab-resistant glioblastoma. *Oncotarget* 8, 96970–96983. doi: 10.18632/oncotarget.18859

Pinton, L., Magri, S., Masetto, E., Vettore, M., Schibuola, I., Ingangi, V., et al. (2020). Targeting of immunosuppressive myeloid cells from glioblastoma patients by modulation of size and surface charge of lipid nanocapsules. *J. Nanobiotechnology* 18:31. doi: 10.1186/s12951-020-00589-3

Pires-Afonso, Y., Niclou, S. P., and Michelucci, A. (2020). Revealing and harnessing tumour-associated microglia/macrophage heterogeneity in glioblastoma. *Int. J. Mol. Sci.* 21:689. doi: 10.3390/ijms21030689

Pyonteck, S. M., Akkari, L., Schuhmacher, A. J., Bowman, R. L., Sevenich, L., Quail, D. F., et al. (2013). CSF-1R inhibition alters macrophage polarization and blocks glioma progression. *Nat. Med.* 19, 1264–1272. doi: 10.1038/nm.3337

Qian, B. Z., and Pollard, J. W. (2010). Macrophage diversity enhances tumor progression and metastasis. *Cell* 141, 39–51. doi: 10.1016/j.cell.2010.03.014

Quintero-Fabián, S., Arreola, R., Becerril-Villanueva, E., Torres-Romero, J. C., Arana-Argáez, V., Lara-Riegos, J., et al. (2019). Role of matrix metalloproteinases in angiogenesis and cancer. *Front. Oncol.* 9:1370. doi: 10.3389/fonc.2019.01370

Radin, D. P., and Tsirka, S. E. (2020). Interactions between tumor cells, neurons, and microglia in the glioma microenvironment. *Int. J. Mol. Sci.* 21:8476. doi: 10.3390/ijms21228476

Ramachandran, S. A., Jadhavar, P. S., Miglani, S. K., Singh, M. P., Kalane, D. P., Agarwal, A. K., et al. (2017). Design, synthesis and optimization of bis-amide derivatives as CSF1R inhibitors. *Bioorg. Med. Chem. Lett.* 27, 2153–2160. doi: 10.1016/j.bmcl.2017.03.064

Ramesh, A., Kumar, S., Nandi, D., and Kulkarni, A. (2019). CSF1R- and SHP2-inhibitor-loaded nanoparticles enhance cytotoxic activity and phagocytosis in tumor-associated macrophages. *Adv. Mater.* 31:e1904364. doi: 10.1002/adma.201904364

Reardon, D. A., Brandes, A. A., Omuro, A., Mulholland, P., Lim, M., Wick, A., et al. (2020). Effect of nivolumab vs bevacizumab in patients with recurrent glioblastoma: the checkmate 143 phase 3 randomized clinical trial. *JAMA Oncol.* 6, 1003–1010. doi: 10.1001/jamaoncol.2020.1024

Reinfeld, B. I., and Madden, M. Z. (2021). Cell-programmed nutrient partitioning in the tumour microenvironment. *Nature* 593, 282–288. doi: 10.1038/s41586-021-03442-1

Ridler, C. (2017). Neuro-oncology: CD47 antibody helps phagocytes fight paediatric cancer. *Nat. Rev. Neurol.* 13, 258–259. doi: 10.1038/nrneurol.2017.46

Rodríguez-García, A., Samsó, P., Fontova, P., Simon-Molas, H., Manzano, A., Castaño, E., et al. (2017). TGF-β1 targets Smad, p38 MAPK, and PI3K/Akt signaling pathways to induce PFKFB3 gene expression and glycolysis in glioblastoma cells. *FEBS J.* 284, 3437–3454. doi: 10.1111/febs.14201

Rossi, J., Giaccherini, L., and Cavallieri, F. (2020). Extracranial metastases in secondary glioblastoma multiforme: a case report. *BMC Neurol.* 20:382. doi: 10.1186/s12883-020-01959-y

Rothlin, C. V., and Ghosh, S. (2020). Lifting the innate immune barriers to antitumor immunity. *J. Immunother. Cancer* 8:e000695. doi: 10.1136/jitc-2020-000695

Saha, D., Martuza, R. L., and Rabkin, S. D. (2017). Macrophage polarization contributes to glioblastoma eradication by combination immunovirotherapy and immune checkpoint blockade. *Cancer Cell* 32:253-267.e255. doi: 10.1016/j.ccell.2017.07.006

Saliminejad, K., Khorram Khorshid, H. R., Soleymani Fard, S., and Ghaffari, S. H. (2019). An overview of microRNAs: biology, functions, therapeutics, and analysis methods. *J. Cell. Physiol.* 234, 5451–5465. doi: 10.1002/jcp.27486

Severa, M., Islam, S. A., Waggoner, S. N., Jiang, Z., Kim, N. D., Ryan, G., et al. (2014). The transcriptional repressor BLIMP1 curbs host defenses by suppressing expression of the chemokine CCL8. *J. Immunol.* 192, 2291–2304. doi: 10.4049/jimmunol.1301799

Shabo, I., Midtbö, K., Andersson, H., Åkerlund, E., Olsson, H., Wegman, P., et al. (2015). Macrophage traits in cancer cells are induced by macrophage-cancer cell fusion and cannot be explained by cellular interaction. *BMC Cancer* 15:922. doi: 10.1186/s12885-015-1935-0

Shapouri-Moghaddam, A., Mohammadian, S., Vazini, H., Taghadosi, M., Esmaeili, S. A., Mardani, F., et al. (2018). Macrophage plasticity, polarization, and function in health and disease. *J. Cell. Physiol.* 233, 6425–6440. doi: 10.1002/jcp.26429

Shi, Y., Ping, Y. F., Zhou, W., He, Z. C., Chen, C., Bian, B. S., et al. (2017). Tumour-associated macrophages secrete pleiotrophin to promote PTPRZ1 signalling in glioblastoma stem cells for tumour growth. *Nat. Commun.* 8:15080. doi: 10.1038/ncomms15080

Sica, A., and Mantovani, A. (2012). Macrophage plasticity and polarization: in vivo veritas. *J. Clin. Invest.* 122, 787–795. doi: 10.1172/jci59643

Song, X., Wan, Z., Chen, T., Fu, Y., Jiang, K., Yi, X., et al. (2016). Development of a multi-target peptide for potentiating chemotherapy by modulating tumor microenvironment. *Biomaterials* 108, 44–56. doi: 10.1016/j.biomaterials.2016.09.001

Stein, M., Keshav, S., Harris, N., and Gordon, S. (1992). Interleukin 4 potently enhances murine macrophage mannose receptor activity: a marker of alternative immunologic macrophage activation. *J. Exp. Med.* 176, 287–292. doi: 10.1084/jem.176.1.287

Takenaka, M. C., Gabriely, G., Rothhammer, V., Mascanfroni, I. D., Wheeler, M. A., Chao, C. C., et al. (2019). Control of tumor-associated macrophages and T cells in glioblastoma via AHR and CD39. *Nat. Neurosci.* 22, 729–740. doi: 10.1038/s41593-019-0370-y

Tan, A. C., Ashley, D. M., and López, G. Y. (2020). Management of glioblastoma: state of the art and future directions. *CA Cancer J. Clin.* 70, 299–312. doi: 10.3322/caac.21613

Tap, W. D., Wainberg, Z. A., Anthony, S. P., Ibrahim, P. N., Zhang, C., Healey, J. H., et al. (2015). Structure-guided blockade of CSF1R kinase in tenosynovial giant-cell tumor. *N. Engl. J. Med.* 373, 428–437. doi: 10.1056/NEJMoa1411366

Tirosh, I., and Suvà, M. L. (2018). Dissecting human gliomas by single-cell RNA sequencing. *Neuro Oncol.* 20, 37–43. doi: 10.1093/neuonc/nox126

Uluçkan, O., Becker, S. N., Deng, H., Zou, W., Prior, J. L., Piwnica-Worms, D., et al. (2009). CD47 regulates bone mass and tumor metastasis to bone. *Cancer Res.* 69, 3196–3204. doi: 10.1158/0008-5472.can-08-3358

van Dalen, F. J., Van Stevendaal, M., and Fennemann, F. L. (2018). Molecular repolarisation of tumour-associated macrophages. *Molecules* 24:9. doi: 10.3390/molecules24010009

Wang, C., Chen, Y., Wang, Y., Liu, X., Liu, Y., Li, Y., et al. (2019). Inhibition of COX-2, mPGES-1 and CYP4A by isoliquiritigenin blocks the angiogenic Akt signaling in glioma through ceRNA effect of miR-194-5p and lncRNA NEAT1. *J. Exp. Clin. Cancer Res.* 38:371. doi: 10.1186/s13046-019-1361-2

Wang, C., Li, Y., Chen, H., Huang, K., Liu, X., Qiu, M., et al. (2018). CYP4X1 inhibition by flavonoid CH625 normalizes glioma vasculature through reprogramming TAMs via CB2 and EGFR-STAT3 Axis. *J. Pharmacol. Exp. Ther.* 365, 72–83. doi: 10.1124/jpet.117.247130

Wang, C., Li, Y., Chen, H., Zhang, J., Zhang, J., Qin, T., et al. (2017). Inhibition of CYP4A by a novel flavonoid FLA-16 prolongs survival and normalizes tumor vasculature in glioma. *Cancer Lett.* 402, 131–141. doi: 10.1016/j.canlet.2017.05.030

Wang, C., Ma, H. X., Jin, M. S., Zou, Y. B., Teng, Y. L., Tian, Z., et al. (2014). Association of matrix metalloproteinase (MMP)-2 and -9 expression with extra-gastrointestinal stromal tumor metastasis. *Asian Pac. J. Cancer Prev.* 15, 4187–4192. doi: 10.7314/apjcp.2014.15.10.4187

Wang, H., Xu, T., Huang, Q., Jin, W., and Chen, J. (2020). Immunotherapy for malignant glioma: current status and future directions. *Trends Pharmacol. Sci.* 41, 123–138. doi: 10.1016/j.tips.2019.12.003

Wang, N., Liang, H., and Zen, K. (2014). Molecular mechanisms that influence the macrophage m1-m2 polarization balance. *Front. Immunol.* 5:614. doi: 10.3389/fimmu.2014.00614

Wang, Q., Gao, J., and Wu, X. (2018). Pseudoprogression and hyperprogression after checkpoint blockade. *Int. Immunopharmacol.* 58, 125–135. doi: 10.1016/j.intimp.2018.03.018

Wang, Q., He, Z., Huang, M., Liu, T., Wang, Y., Xu, H., et al. (2018b). Vascular niche IL-6 induces alternative macrophage activation in glioblastoma through HIF-2α. *Nat. Commun.* 9:559. doi: 10.1038/s41467-018-03050-0

Wang, R., Zhang, J., Chen, S., Lu, M., Luo, X., Yao, S., et al. (2011). Tumor-associated macrophages provide a suitable microenvironment for non-small lung cancer invasion and progression. *Lung Cancer* 74, 188–196. doi: 10.1016/j.lungcan.2011.04.009

Wang, S. C., Hong, J. H., Hsueh, C., and Chiang, C. S. (2012). Tumor-secreted SDF-1 promotes glioma invasiveness and TAM tropism toward hypoxia in a murine astrocytoma model. *Lab. Invest.* 92, 151–162. doi: 10.1038/labinvest.2011.128

Wei, J., Wang, F., Kong, L. Y., Xu, S., Doucette, T., Ferguson, S. D., et al. (2013). miR-124 inhibits STAT3 signaling to enhance T cell-mediated immune clearance of glioma. *Cancer Res.* 73, 3913–3926. doi: 10.1158/0008-5472.can-12-4318

Weiskopf, K. (2017). Cancer immunotherapy targeting the CD47/SIRPα axis. *Eur. J. Cancer* 76, 100–109. doi: 10.1016/j.ejca.2017.02.013

Wischhusen, J., Jung, G., Radovanovic, I., Beier, C., Steinbach, J. P., Rimner, A., et al. (2002). Identification of CD70-mediated apoptosis of immune effector cells as a novel immune escape pathway of human glioblastoma. *Cancer Res.* 62, 2592–2599.

Wu, A., Wei, J., Kong, L. Y., Wang, Y., Priebe, W., Qiao, W., et al. (2010). Glioma cancer stem cells induce immunosuppressive macrophages/microglia. *Neuro Oncol.* 12, 1113–1125. doi: 10.1093/neuonc/noq082

Wu, J., Frady, L. N., Bash, R. E., Cohen, S. M., Schorzman, A. N., Su, Y. T., et al. (2018). MerTK as a therapeutic target in glioblastoma. *Neuro Oncol.* 20, 92–102. doi: 10.1093/neuonc/nox111

Xia, Y., Rao, L., Yao, H., Wang, Z., Ning, P., and Chen, X. (2020). Engineering macrophages for cancer immunotherapy and drug delivery. *Adv. Mater.* 32:e2002054. doi: 10.1002/adma.202002054

Xie, B., Zhang, L., Hu, W., Fan, M., Jiang, N., Duan, Y., et al. (2019). Dual blockage of STAT3 and ERK1/2 eliminates radioresistant GBM cells. *Redox Biol.* 24:101189. doi: 10.1016/j.redox.2019.101189

Xu, F., Wei, Y., Tang, Z., Liu, B., and Dong, J. (2020). Tumor-associated macrophages in lung cancer: friend or foe? (Review). *Mol. Med. Rep.* 22, 4107–4115. doi: 10.3892/mmr.2020.11518

Xue, S., Hu, M., Iyer, V., and Yu, J. (2017). Blocking the PD-1/PD-L1 pathway in glioma: a potential new treatment strategy. *J. Hematol. Oncol.* 10:81. doi: 10.1186/s13045-017-0455-6

Yan, D., Kowal, J., Akkari, L., Schuhmacher, A. J., Huse, J. T., West, B. L., et al. (2017). Inhibition of colony stimulating factor-1 receptor abrogates microenvironment-mediated therapeutic resistance in gliomas. *Oncogene* 36, 6049–6058. doi: 10.1038/onc.2017.261

Yan, W., Liu, X., and Ma, H. (2015). Tim-3 fosters HCC development by enhancing TGF-β-mediated alternative activation of macrophages. *Gut* 64, 1593–1604. doi: 10.1136/gutjnl-2014-307671

Yang, H. Y., Fang, D. Z., Ding, L. S., Hui, X. B., and Liu, D. (2017). Overexpression of protease serine 8 inhibits glioma cell proliferation. Migration, and invasion via suppressing the Akt/mTOR signaling pathway. *Oncol. Res.* 25, 923–930. doi: 10.3727/096504016x14798241682647

Yang, J., Liao, D., Chen, C., Liu, Y., Chuang, T. H., Xiang, R., et al. (2013). Tumor-associated macrophages regulate murine breast cancer stem cells through a novel paracrine EGFR/Stat3/Sox-2 signaling pathway. *Stem Cells* 31, 248–258. doi: 10.1002/stem.1281

Yang, M., Shao, J. H., Miao, Y. J., Cui, W., Qi, Y. F., Han, J. H., et al. (2014). Tumor cell-activated CARD9 signaling contributes to metastasis-associated macrophage polarization. *Cell Death Differ.* 21, 1290–1302.

Ye, J., Yang, Y., Dong, W., Gao, Y., Meng, Y., Wang, H., et al. (2019). Drug-free mannosylated liposomes inhibit tumor growth by promoting the polarization of tumor-associated macrophages. *Int. J. Nanomedicine* 14, 3203–3220. doi: 10.2147/ijn.s207589

Ye, X. Z., Xu, S. L., Xin, Y. H., Yu, S. C., Ping, Y. F., Chen, L., et al. (2012). Tumor-associated microglia/macrophages enhance the invasion of glioma stem-like cells via TGF-β1 signaling pathway. *J. Immunol.* 189, 444–453. doi: 10.4049/jimmunol.1103248

Yin, J., Oh, Y. T., Kim, J. Y., Kim, S. S., Choi, E., Kim, T. H., et al. (2017). Transglutaminase 2 inhibition reverses mesenchymal transdifferentiation of glioma stem cells by regulating C/EBPβ signaling. *Int. J. Cancer* 77, 4973–4984. doi: 10.1158/0008-5472.CAN-17-0388

Yin, M., Li, X., Tan, S., Zhou, H. J., Ji, W., Bellone, S., et al. (2016). Tumor-associated macrophages drive spheroid formation during early transcoelomic metastasis of ovarian cancer. *J. Clin. Invest.* 126, 4157–4173. doi: 10.1172/jci87252

Zhang, F., Parayath, N. N., Ene, C. I., Stephan, S. B., Koehne, A. L., Coon, M. E., et al. (2019). Genetic programming of macrophages to perform anti-tumor functions using targeted mRNA nanocarriers. *Nat. Commun.* 10:3974. doi: 10.1038/s41467-019-11911-5

Zhang, J., Sarkar, S., Cua, R., Zhou, Y., Hader, W., and Yong, V. W. (2012). A dialog between glioma and microglia that promotes tumor invasiveness through the CCL2/CCR2/interleukin-6 axis. *Carcinogenesis* 33, 312–319. doi: 10.1093/carcin/bgr289

Zhang, L., Liao, Y., and Tang, L. (2019). MicroRNA-34 family: a potential tumor suppressor and therapeutic candidate in cancer. *J. Exp. Clin. Cancer Res.* 38:53. doi: 10.1186/s13046-019-1059-5

Zhang, W., Wang, L., Zhou, D., Cui, Q., Zhao, D., and Wu, Y. (2011). Expression of tumor-associated macrophages and vascular endothelial growth factor correlates with poor prognosis of peripheral T-cell lymphoma, not otherwise specified. *Leuk. Lymphoma* 52, 46–52. doi: 10.3109/10428194.2010.529204

Zhang, W. J., Zhou, Z. H., Guo, M., Yang, L. Q., Xu, Y. Y., Pang, T. H., et al. (2017). High infiltration of polarized CD163(+) tumor-associated macrophages correlates with aberrant expressions of CSCs markers, and predicts prognosis in patients with recurrent gastric cancer. *J. Cancer* 8, 363–370. doi: 10.7150/jca.16730

Zhang, X., Chen, L., Dang, W. Q., Cao, M. F., Xiao, J. F., Lv, S. Q., et al. (2020). CCL8 secreted by tumor-associated macrophages promotes invasion and stemness of glioblastoma cells via ERK1/2 signaling. *Lab. Invest.* 100, 619–629. doi: 10.1038/s41374-019-0345-3

Zhao, H., Zhang, X., Chen, X., Li, Y., Ke, Z., Tang, T., et al. (2014). Isoliquiritigenin, a flavonoid from licorice, blocks M2 macrophage polarization in colitis-associated tumorigenesis through downregulating PGE2 and IL-6. *Toxicol. Appl. Pharmacol.* 279, 311–321. doi: 10.1016/j.taap.2014.07.001

Zhu, C., Kros, J. M., Cheng, C., and Mustafa, D. (2017). The contribution of tumor-associated macrophages in glioma neo-angiogenesis and implications for anti-angiogenic strategies. *Neuro Oncol.* 19, 1435–1446. doi: 10.1093/neuonc/nox081

Zinnhardt, B., Müther, M., Roll, W., Backhaus, P., Jeibmann, A., Foray, C., et al. (2020). TSPO imaging-guided characterization of the immunosuppressive myeloid tumor microenvironment in patients with malignant glioma. *Neuro Oncol.* 22, 1030–1043. doi: 10.1093/neuonc/noaa023

Conflict of Interest: The authors declare that the research was conducted in the absence of any commercial or financial relationships that could be construed as a potential conflict of interest.

Copyright © 2021 Tong, He, Ma, Wang, Huang, Cao, Xu, Zou, Wang, Yi, Yin and Wang. This is an open-access article distributed under the terms of the Creative Commons Attribution License (CC BY). The use, distribution or reproduction in other forums is permitted, provided the original author(s) and the copyright owner(s) are credited and that the original publication in this journal is cited, in accordance with accepted academic practice. No use, distribution or reproduction is permitted which does not comply with these terms.

frontiers in Cell and Developmental Biology

ORIGINAL RESEARCH
published: 26 July 2021
doi: 10.3389/fcell.2021.705060

BRAF Mutation as a Potential Therapeutic Target for Checkpoint Inhibitors: A Comprehensive Analysis of Immune Microenvironment in BRAF Mutated Colon Cancer

Shuyi Cen[1†], Kun Liu[2,3,4,5†], Yu Zheng[1], Jianzhen Shan[6], Chao Jing[2,3,4,5], Jiale Gao[2,3,4,5], Hongming Pan[1], Zhigang Bai[2,3,4,5] and Zhen Liu[1*]*

[1] Department of Oncology, Sir Run Run Shaw Hospital, Zhejiang University School of Medicine, Hangzhou, China, [2] Department of General Surgery, Beijing Friendship Hospital, Capital Medical University, Beijing, China, [3] Clinical Center for Colorectal Cancer, Capital Medical University, Beijing, China, [4] Beijing Key Laboratory of Cancer Invasion and Metastasis Research, Beijing, China, [5] National Clinical Research Center for Digestive Diseases, Beijing, China, [6] Department of Oncology, The First Affiliated Hospital, Zhejiang University School of Medicine, Hangzhou, China

BRAF mutated colon cancer presents with poor survival, and the treatment strategies are controversial. The tumor microenvironment, which plays a key role in tumorigenesis as well as responses to treatments, of this subtype is largely unknown. In the present study, we analyzed the differences of immune microenvironments between BRAF mutated and BRAF wild-type colon cancer utilizing datasets from The Cancer Genome Atlas and Gene Expression Omnibus and confirmed the findings by tissue specimens of patients. We found that BRAF mutated colon cancer had more stromal cells, more immune cell infiltration, and lower tumor purity. Many immunotherapeutic targets, including PD-1, PD-L1, CTLA-4, LAG-3, and TIM-3, were highly expressed in BRAF mutated patients. BRAF mutation was also correlated with higher proportions of neutrophils and macrophages M1, and lower proportions of plasma cells, dendritic cells resting, and T cells CD4 naïve. In conclusion, our study demonstrates a different pattern of the immune microenvironment in BRAF mutated colon cancer and provides insights into the future use of checkpoint inhibitors in this subgroup of patients.

Keywords: BRAF, colon cancer, immune microenvironment, immunotherapy, therapeutic target

OPEN ACCESS

Edited by:
Qian Xiao,
Yale University, United States

Reviewed by:
Can Cui,
Yale University, United States
Xueyuan Jiang,
Merck, United States
Dipongkor Saha,
Texas Tech University Health Sciences Center, Abilene, United States

****Correspondence:***
Zhigang Bai
baizhigang@ccmu.edu.cn
Zhen Liu
liuzhen@zju.edu.cn

† These authors have contributed equally to this work

Specialty section:
This article was submitted to Molecular and Cellular Pathology, a section of the journal Frontiers in Cell and Developmental Biology

Received: *04 May 2021*
Accepted: *30 June 2021*
Published: *26 July 2021*

Citation:
Cen S, Liu K, Zheng Y, Shan J, Jing C, Gao J, Pan H, Bai Z and Liu Z (2021) BRAF Mutation as a Potential Therapeutic Target for Checkpoint Inhibitors: A Comprehensive Analysis of Immune Microenvironment in BRAF Mutated Colon Cancer. Front. Cell Dev. Biol. 9:705060. doi: 10.3389/fcell.2021.705060

INTRODUCTION

Colon cancer is one of the leading causes of cancer-related deaths worldwide. Colon cancer accounts for 6.0% of new cancer cases, with more than a million new cases of colon cancer identified in year 2020, and 5.8% of cancer deaths (Sung et al., 2021). Both environmental and genetic factors, such as mutated genes, inflammation, radiation, and hereditary disorders, contribute to tumorigenesis of colon cancer (Chan and Giovannucci, 2010).

The BRAF gene is one of the key genes in the RAS–RAF–MEK–ERK–MAP kinase pathway, which regulates many fundamental cellular processes such as cellular growth, proliferation, differentiation, migration, and apoptosis (Dhillon et al., 2007). There are several subtypes of BRAF

mutations, and the most common one lies at codon 600 (BRAF V600E), accounting for about 95% BRAF mutated cases (Molina-Cerrillo et al., 2020). The BRAF mutation accounts for around 10% cases of colon cancer and serves as a strong negative prognostic marker for patients (Davies et al., 2002; Gonsalves et al., 2014; Barras et al., 2017). Mutated BRAF tumors are prone to have elevated kinase activity and promoted cell proliferation through MAPK cascade, and therefore subject to a different pathological and immunological patterns (Davies et al., 2002). BRAF mutation is often associated with high microsatellite instability (MSI) and is frequently linked to proficient mismatched repair bases in DNA (Rajagopalan et al., 2002). BRAF mutated colon cancer often derives from sessile serrated adenoma and tends to be high grade, poorly differentiated, and located on right-sided colon, and has more mucinous component, more peritoneal and lymph node metastases, but less lung metastases (Matos and Jordan, 2018; Lee et al., 2019).

Tumor microenvironment plays an important role in tumorigenesis and cell proliferation. Aberrant infiltrated immune cells in human tumors not only fail to restrain tumor growth but also promote tumor escape from the host (Whiteside, 2008). Dysregulated molecular and cellular pathways in the tumor microenvironment also contribute to inhibition of apoptosis. T cells, natural killer (NK) cells, lymphocytes, fibroblasts, and many other immune cells have been proven to play important roles in tumor development in colon cancer patients (Kather and Halama, 2019). Recent studies demonstrated that immune microenvironment in BRAF mutated colon tumors might lead to resistance to conventional therapies through regulation of composition of immune cell infiltration and chemokines (Reddy et al., 2016; Croce et al., 2019). Mitogen-activated protein kinase (MAPK) inhibition gives rise to suppression of immunosuppressive factors such as interleukin-10 (IL-10), vascular endothelial growth factor (VEGF), programmed cell death protein 1 (PD-1), regulatory T cells, etc., and targeting BRAF mutation was associated with lower expression of these immunosuppressive factors (Reddy et al., 2016; Chen and Hurwitz, 2018; Yuan et al., 2018). However, despite the importance of the immune microenvironment in the development and treatment of BRAF mutated colon cancer, few studies have yet investigated the pattern of tumor microenvironment in BRAF mutated colon tumors. In the present study, we pooled The Cancer Genome Atlas (TCGA) and Gene Expression Omnibus (GEO) datasets to explore the immune landscape of BRAF mutated colon cancer and to validate the important immune markers in patient specimens.

MATERIALS AND METHODS

Gene Expression Datasets

Gene expression profiles of colon cancer were downloaded from the TCGA portal[1] and the GEO database (accession number: GSE39582) directly. Clinical information of patients were also obtained from the TCGA portal and GEO database, including gender, age at diagnosis, stage, mutation status, survival time, tumor location, as well as MSI status. Immune scores, stromal scores, ESTIMATE scores, and tumor purity were calculated using the ESTIMATE (Estimation of STromal and Immune cells in MAlignant Tumour tissues using Expression data) algorithm, which utilizes gene expression signatures of tumor cells to infer the fraction of stromal and immune cells in tumor samples (Yoshihara et al., 2013). This calculation was performed using estimate package in R software.

Identification of Differentially Expressed Genes (DEGs)

Data analysis was performed using R package limma (Ritchie et al., 2015). Fold change > 2 and multiple-testing adjusted p-value < 0.05 were set as the cutoffs to identify DEGs in both the TCGA and GEO cohorts.

Functional Analysis and Heatmaps

The Kyoto Encyclopedia of Genes and Genomes (KEGG) analysis was employed to understand the potential function and pathway enrichment of DEGs using the clusterProfiler package in R software (Yu et al., 2012). The adjusted p-value < 0.05 was considered statistically significant. Heatmaps were generated using TBtools[2] (Chen et al., 2018).

Survival Analysis

Log-rank test for Kaplan–Meier curve was applied to illustrate the association between overall survival of patients and gene mutation status using survival[3] and survminer[4] package in R software. A value of $p < 0.05$ was considered as statistically significant.

Overall Survival-Related Genes

The overall survival related genes were generated using the TIMER website, which is an online tool for analyzing genes and tumor-infiltrating immune cells in TCGA portal[5] (Li et al., 2017, 2020).

Immune Cell Analysis

Fractions of infiltrating immune cells of colon cancer patients were analyzed using Cibersort, an online tool to provide the estimation of the fraction of many immune cells using gene expression profiles[6] (Newman et al., 2015).

Tissue Immunohistochemistry (IHC)

Tissue samples were collected from 43 colon cancer patients receiving treatments at Beijing Friendship Hospital, Capital Medical University. The mutation status was determined by next-generation sequencing. All stainings used 4-μm-thick formalin-fixed paraffin-embedded tissue sections. The slides were baked,

[1]https://tcga-data.nci.nih.gov/tcga/

[2]https://github.com/CJ-Chen/TBtools

[3]https://github.com/therneau/survival

[4]http://www.sthda.com/english/rpkgs/survminer/

[5]http://timer.cistrome.org/

[6]https://cibersort.stanford.edu/

deparaffinized, rehydrated, washed, and then added with 0.3% hydrogen peroxide at room temperature to block the activity of endogenous peroxidase. For antigen retrieval, the sections were boiled for 25 min in citric acid-based buffer at pH 6.0 and EDTA-based buffer at pH 8.0, cooled to room temperature, and rinsed with PBS three times for 3 min. Slides were then incubated with primary antibodies, which were diluted using 1% BSA at 37°C for 1 h. After being rinsed, the sections were incubated in secondary antibodies (Maxim, Fuzhou, China) at room temperature for 15 min and stained with DAB detection kit (Gene Tech, Shanghai, China). Each section was washed as before and observed at ×200 magnification using a light microscope. Primary antibodies used included PD-1 (1:300, no. EM1707-60), PD-L1 (1:100, no. ET1701-41), TIM-3 (1:100, no. EM1701-19), BST2 (1:100, no. ET1706-46), CALB2 (1:100, no. ET1705-19), ENO2 (1:100, no. ET1610-96), Syndecan-1 (1:50, no. ET1703-42), HLA-DR (1:100, no. ET1702-51), Mye (1:100, no. ET1703-21) (all from Huabio, Hangzhou, China), and CTLA-4 (1:1,000, no. ab237712) and LAG-3 (1:1,000, no. ab180187) (both from Abcam, Cambridge, United Kingdom). For quantitative analysis, the staining scores were defined as 0 (negative), 1 (weak), 2 (moderate), and 3 (strong). Scores for the percentage of tumor cells for 0–10, 11–25, 26–50, 51–75, and >75% were classified as 0, 1, 2, 3, and 4, respectively. The scores of the staining intensity were multiplied by the scores of the percentage of stained cells.

Statistical Analysis

Univariate analyses between gene mutation and clinical characteristics were compared using the log-rank test. The Student's *t*-test was applied to analyze the association between gene mutation and stromal/immune/ESTIMATE scores and tumor purity. Log-rank test for Kaplan–Meier curves was conducted to assess the association between overall survival and gene mutations or expression levels. A value of $p < 0.05$ was considered statistically significant. The Venn diagram was plotted by R software.

RESULTS

Clinical Characteristics of Patients From the TCGA and GEO Dataset

There was a total of 396 patients from the TCGA cohort with available BRAF mutation status, and 59 (14.9%) patients were BRAF mutated, as shown in **Table 1**. Patients carrying BRAF mutant tend to be female ($p = 0.0029$) and older ($p = 0.0102$) compared to BRAF wild-type patients. The tumors are also more likely to be at an advanced stage ($p = 0.0226$), more often located in the right colon ($p < 0.0001$), and prone to be MSI-H ($p < 0.0001$). Similar results were found in patients from the GEO cohort; BRAF mutated patients were more likely to be female ($p = 0.0018$), older ($p < 0.0001$), and had the tumor at the right colon ($p < 0.0001$).

TABLE 1 | Patient characteristics in the TCGA and GEO dataset.

Patient characteristics		TCGA			GEO		
BRAF status		**Mut**	**WT**	***P*-value**	**Mut**	**WT**	***P*-value**
Total		59	337		51	461	
Gender	Female	39	150	0.0029	34	200	0.0018
	Male	20	185		17	261	
	NA		2				
Age	45	1	30	0.0102	0	35	<0.0001
	45–65	14	122		3	158	
	65+	44	183		48	267	
	NA		2			1	
Stage	Stage I	10	53	0.0226			
	Stage 2	32	118				
	Stage 3	14	95				
	Stage 4	3	57				
	NA		14				
T stage	T1	2	8	0.9609	2	8	0.4108
	T2	10	56		4	33	
	T3	40	225		29	299	
	T4	7	45		15	0.	
	NA		3		1	23	
Tumor location	right	49	176	<0.0001	44	164	<0.0001
	Left	4	145		7	297	
	NA	6	16		0	0	
MSI status	MSI-H	41	26	<0.0001			
	MSI-L	5	65				
	MSS	10	227				
	NA	3	19				

Immune Score Analysis

The ESTIMATE algorithm was established by Yoshihara et al. (2013) to predict the level of infiltrating stromal and immune cells. The levels of stromal cells and immune cells were defined as stromal score and immune score, respectively. These two scores form the basis for the ESTIMATE score to infer tumor purity. Stromal cells are one of the key players in tumor proliferation, invasion, and drug resistance, while infiltration of immune cells could serve as a prognostic indicator in cancer patients. We found that BRAF mutant colon cancer had higher stromal score ($p = 0.02$), immune score ($p < 0.0001$), ESTIMATE score ($p = 0.0001$), and lower tumor purity ($p = 0.0003$) (**Figure 1A**). The results suggest that BRAF mutant tumor tissues carry more stromal cells, more immune cell infiltration, and had lower tumor purity. Results from the GEO patients were in accordance with those of the TCGA patients. As shown in **Figure 1B**, BRAF mutated tumor had higher stromal score ($p = 0.0041$), immune score ($p < 0.0001$), ESTIMATE score ($p < 0.0001$), and lower tumor purity ($p < 0.0001$).

Overall Survival Analysis

The literature has reported that BRAF mutated colon cancer patients had a much poorer survival rate that wild-type patients (Phipps et al., 2015; Matos and Jordan, 2018; Taieb et al., 2019), we therefore analyzed overall survival in the two cohorts. However, as shown in **Figures 2A,C**, there was no significant survival difference between BRAF mutated and wild-type patients. Further analysis in patients with T3 or T4 stage

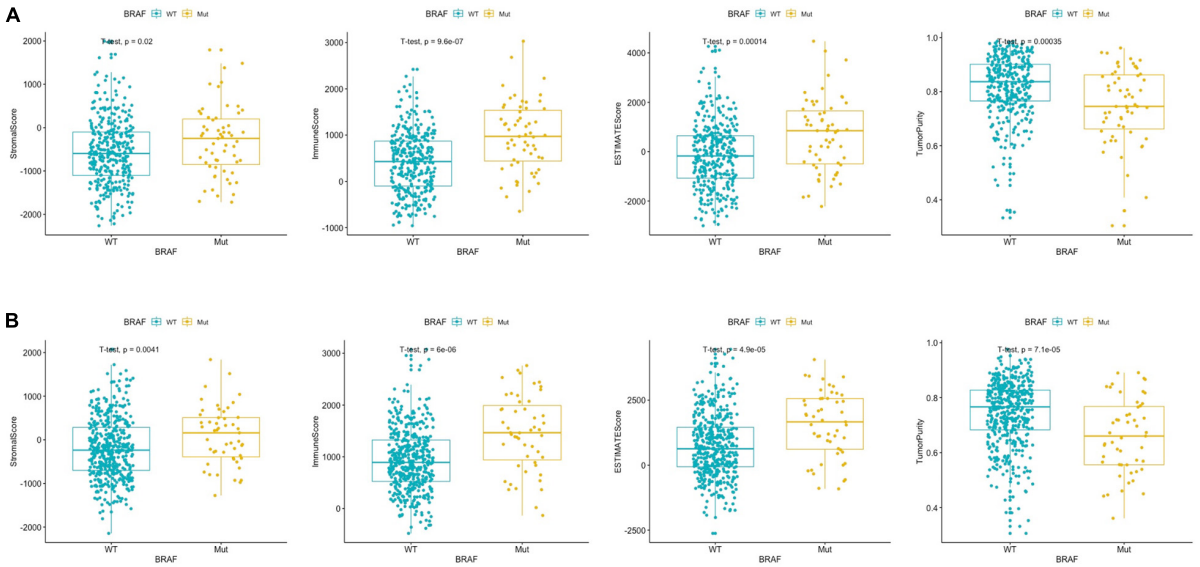

FIGURE 1 | BRAF mutation in colon cancer is presented with significantly different stromal scores, immune scores, ESTIMATE scores, and tumor purity in the TCGA dataset **(A)** and GEO dataset **(B)**. Student's *t*-tests were used for all analyses.

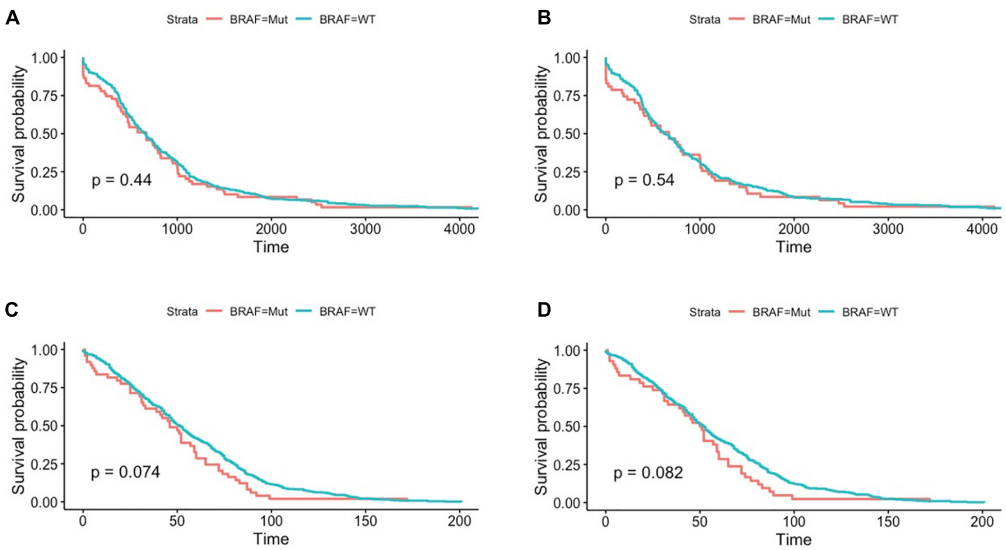

FIGURE 2 | Patients with BRAF mutation had no significant differences in terms of overall survival in the TCGA dataset, as shown in all-stage patients **(A)** and stage III/IV patients **(B)**. Similar results were found in GEO datasets, as shown in all-stage patients **(C)** and stage III/IV patients **(D)**. Student's *t*-tests were used for all analyses.

(**Figures 2B,D**) also revealed no difference in overall survival. This contradictory result may attribute to the fact that patients at these two cohorts were the ones who received radical surgery and were subjected to fewer metastasis. Brevity of patient survival information is another limitation of survival analysis in these two cohorts.

DEGs and Enrichment Analysis

A total of 973 genes in the TCGA cohort and 208 genes in the GEO cohort were found to have significantly different expression levels between BRAF mutated and BRAF wild-type tumors, respectively. Heatmaps of these genes are shown in **Figures 3A,B**. Among them, 144 genes are differentially expressed in both the TCGA and GEO cohorts. These overlapping 144 genes were selected to perform KEGG pathway enrichment analysis (**Figure 4A**). **Figures 4B,C** suggest that chemokine signaling pathway, cytokine receptor interaction, viral protein interaction with cytokine and cytokine receptors, and transcriptional misregulation in cancer might be the leading pathways that bring about alteration in tumorigenesis in BRAF mutated colon cancer.

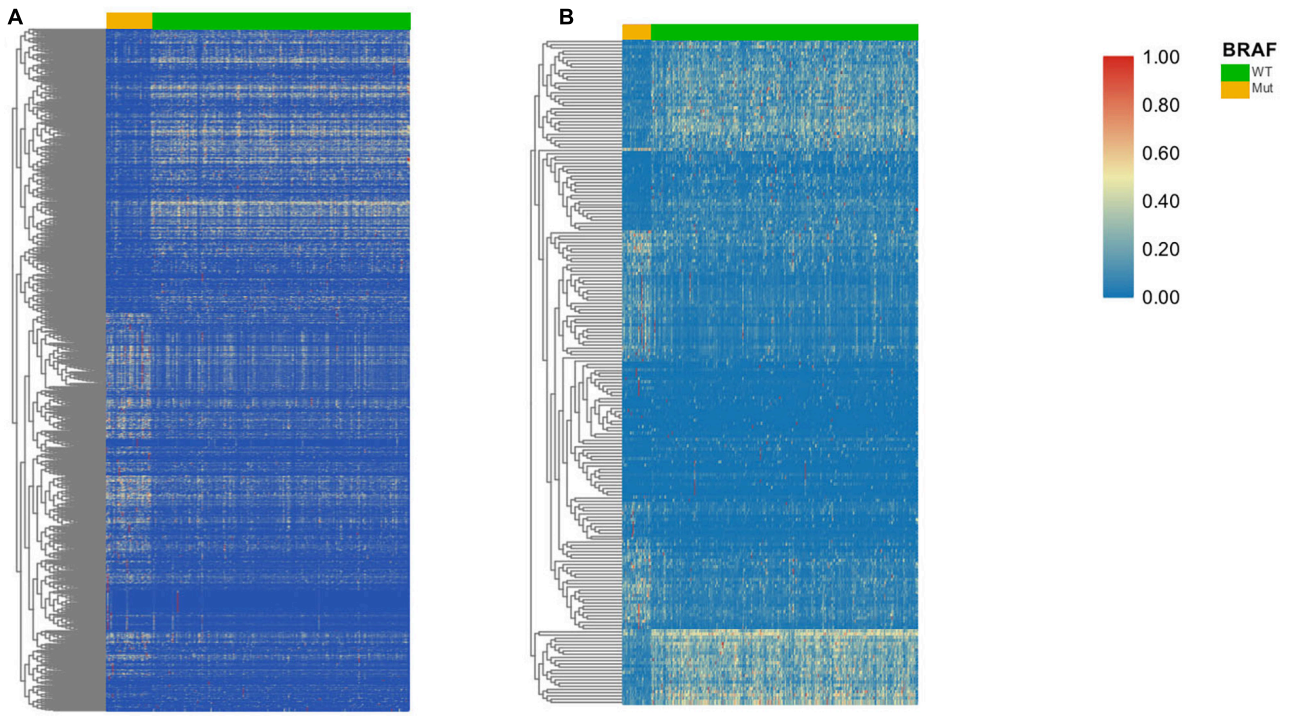

FIGURE 3 | Heatmaps of DEGs in the TCGA **(A)** and GEO dataset **(B)**.

Among the 144 DEGs, expression levels of six genes were found to associated with patient survival independently. Patients with lower expressions of BST2, CALB2, TNNT1, ENO2, HOXC6, and SYNGR3 had better cumulative survival than patients with higher expressions (**Figure 5**). Further, IHC of tissue samples suggested that in BRAF mutated colon samples, expression levels of BST2, CALB2, and ENO2 are significantly higher than those in BRAF wild-type tumor samples, as shown in **Figures 6A–F**, respectively.

BRAF Mutation and Immunotherapy-Related Genes

Immunotherapies, especially the use of immune checkpoint inhibitors, comprise an emerging strategy for the treatment of colon cancer patients. Therefore, we further analyzed the relationship between BRAF mutation and target genes of immunotherapy. It is detected that patients with BRAF mutation in the TCGA cohort had higher expression of PD-1 ($p = 0.0025$), PD-L1 ($p < 0.0001$), CTLA-4 ($p < 0.0001$), LAG-3 ($p = 0.0011$), and TIM-3 ($p < 0.0001$) (**Figures 7A–E**). In patients from the GEO dataset, BRAF mutation colon cancer also had higher expressions of CTLA-4 ($p = 0.031$) and LAG-3 ($p = 0.0011$), but had no significant expression of PD-1 ($p = 0.58$) (**Figures 7F–H**). Immunochemistry of tumor tissues of patients suggest that the expression levels of PD-1 (**Figures 8A,B**), PD-L1 (**Figures 8C,D**), CTLA-4 (**Figures 8E,F**), TIM-3 (**Figures 8G,H**), and LAG-3 (**Figures 8I,J**) are significantly higher in BRAF mutated samples than in BRAF wild-type samples.

BRAF Mutation Related Immune Cells

Using Cibersort algorithm, we identified the fraction of 22 immune cells in each tumor sample in the TCGA and GEO cohort. In TCGA samples, BRAF mutation was found to be significantly different in cell proportions of plasma cells, T cells CD8, T cells CD4 naïve, macrophages M0, macrophages M1, dendritic cells resting, and neutrophils (**Figure 9A**). In the GEO cohort, cell proportions of B cells memory, plasma cells, T cells CD4 naïve, T cells CD4 memory resting, T cells follicular helper, T cells gamma delta, macrophages M1, dendritic cells resting, and neutrophils were significantly different (**Figure 9B**). Therefore, the fractions of five immune cells, plasma cells, dendritic cells resting, neutrophils, macrophages M1, and T cells CD4 naïve were associated with BRAF mutation in both TCGA and GEO cohorts. Among these five immune cells, only the fraction of plasma cells was associated with patient survival (**Figure 10**) in the TCGA cohort. IHC staining proved that CD4 and CD8 cells are highly expressed in BRAF mutated samples, although the former did not illustrate statistical significance (**Figures 11A–D**). Interestingly, staining of Syndecan-1 (CD138), which is a cell surface heparan sulfate proteoglycan that could be used to detect plasma cells (Ajise et al., 2016), is highly expressed in BRAF wild-type tissues (**Figures 11E,F**). On the other hand, the staining intensity of HLA-DR, a common marker for macrophage M1 (Jayasingam et al., 2020), and myeloperoxidase (MPO), a biomarker for infiltrating neutrophils (Mariani and Roncucci, 2017), did not show significant difference between BRAF wild-type and BRAF mutated tissues (**Figures 11G–J**).

FIGURE 4 | DEGs between BRAF wild-type and BRAF mutated patients **(A)** and their KEGG graphs **(B,C)**.

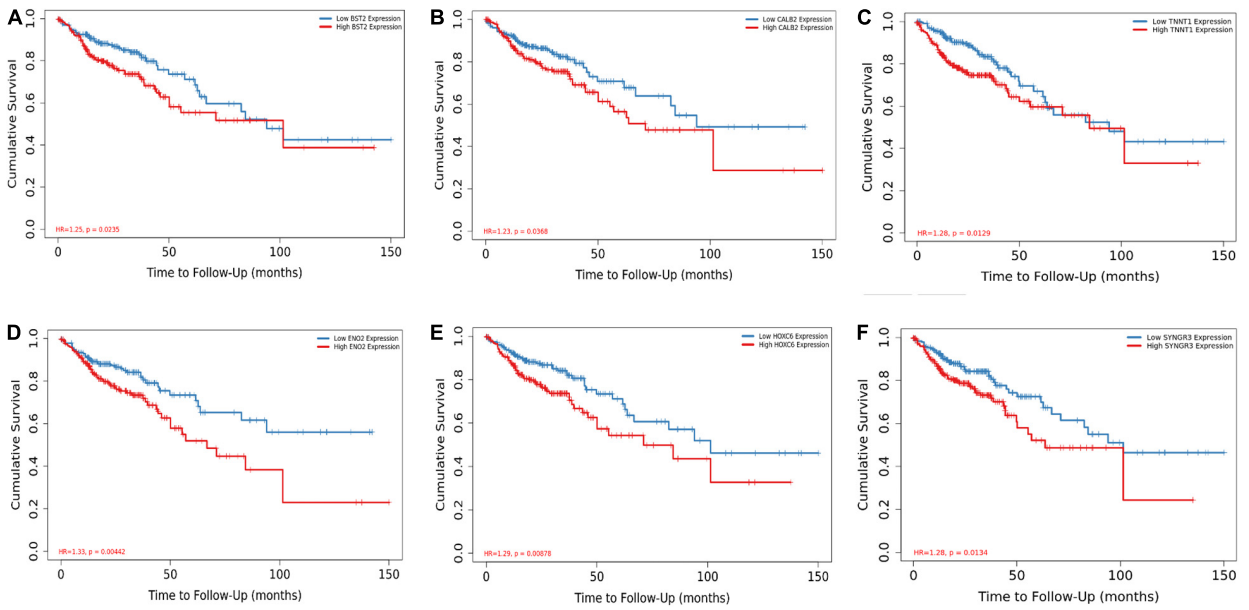

FIGURE 5 | BST2 **(A)**, CALB2 **(B)**, TNNT1 **(C)**, ENO2 **(D)**, HOXC6 **(E)**, and SYNGR **(F)** are associated with overall survival. Log-rank test for Kaplan–Meier curves was conducted to assess the association between overall survival and expression levels.

MSI Status in BRAF Mutated Colon Cancer

As mentioned above, BRAF mutated colon cancer is associated with higher MSI. We then divided the 59 BRAF mutated patients into microsatellite stable (MSS) subgroup and microsatellite instable (MSI) subgroup. We found that stromal score, immune score, ESTIMATE score, and tumor purity did not differ in these two groups (**Figures 12A–D**). PD-1 expression, CTLA expression, and TIM-3 expression did not illustrate significant difference in these subgroups either (**Figures 12E–H**). However, the MSI group showed significantly higher expression of PD-L1 ($p = 0.009$) (**Figure 12H**) and LAG-3 ($p = 0.011$) (**Figure 12I**) than the MSS group.

DISCUSSION

BRAF mutation is one of the most important mutation subtypes in colon cancer. Its unique tumorigenesis process suggests a different biological and pathological landscape from wild-type colon cancer. BRAF mutation is often associated with MSI, minimal chromosomal instability, and high rate of recurrence (Taieb et al., 2019). The presence of BRAF mutation is also correlated with CpG island methylator phenotype (CIMP), which can lead to the inactivation of the MLH1 promoter, resulting in an MMR deficiency. In the present study, we have identified immune characteristics of BRAF mutated colon cancer and have investigated the immune microenvironment of BRAF mutated colon tumors.

Through assessment of immune scores, we identified that BRAF mutated colon cancer had more stromal cells, more immune cell infiltration, and lower tumor purity in tumor tissue. Researches have suggested that stromal cells are often recruited by tumor cells from nearby stroma and play a critical role in tumor angiogenesis, proliferation, invasion, metastasis, and drug resistance (Bussard et al., 2016; Denton et al., 2018). The stromal cells could also transform into tumor-associated stromal cells, which would further secrete many cytokines to promote tumorigenesis such as IL-6, IL-8, and vascular endothelial growth factor (Bussard et al., 2016). Galland and Stamenkovic (2020) have indicated that stromal cells may have dual effects on tumor progression; that is, as stromal cells compromise several subgroups of cell populations, they could promote and constrain tumor growth at the same time. Reeducating and targeting stromal cells may both serve as effective strategy for antitumor therapies (Quail and Joyce, 2013). We have also found that BRAF mutation is correlated with higher proportions of neutrophils and macrophages M1, and lower proportions of plasma cells, dendritic cells resting, and T cells CD4 naïve. BRAF V600E mutation in colon cancer is often associated with consensus molecular subtype 1 (CSM1), which correlates with considerable immune infiltrations and activation of immune response pathways, especially with larger populations of type 1 T helper cells, cytotoxic T cells, and NK cells (Dienstmann et al., 2017). However, roles of these immune cells in the process of oncogenesis and their responses to chemotherapy, targeted therapy, and immunotherapy need further investigation.

Our pathway enrichment analysis reveals that cytokine-related pathways, such as chemokine signaling, cytokine receptor interaction, viral protein interaction with cytokine, and cytokine receptors, are differently expressed between BRAF mutated and BRAF wild-type tumors. The result is consistent with previous studies that BRAF mutant MSI-H colon cancer is associated with the overexpression of stromal cell-derived factor-1 (SDF-1;

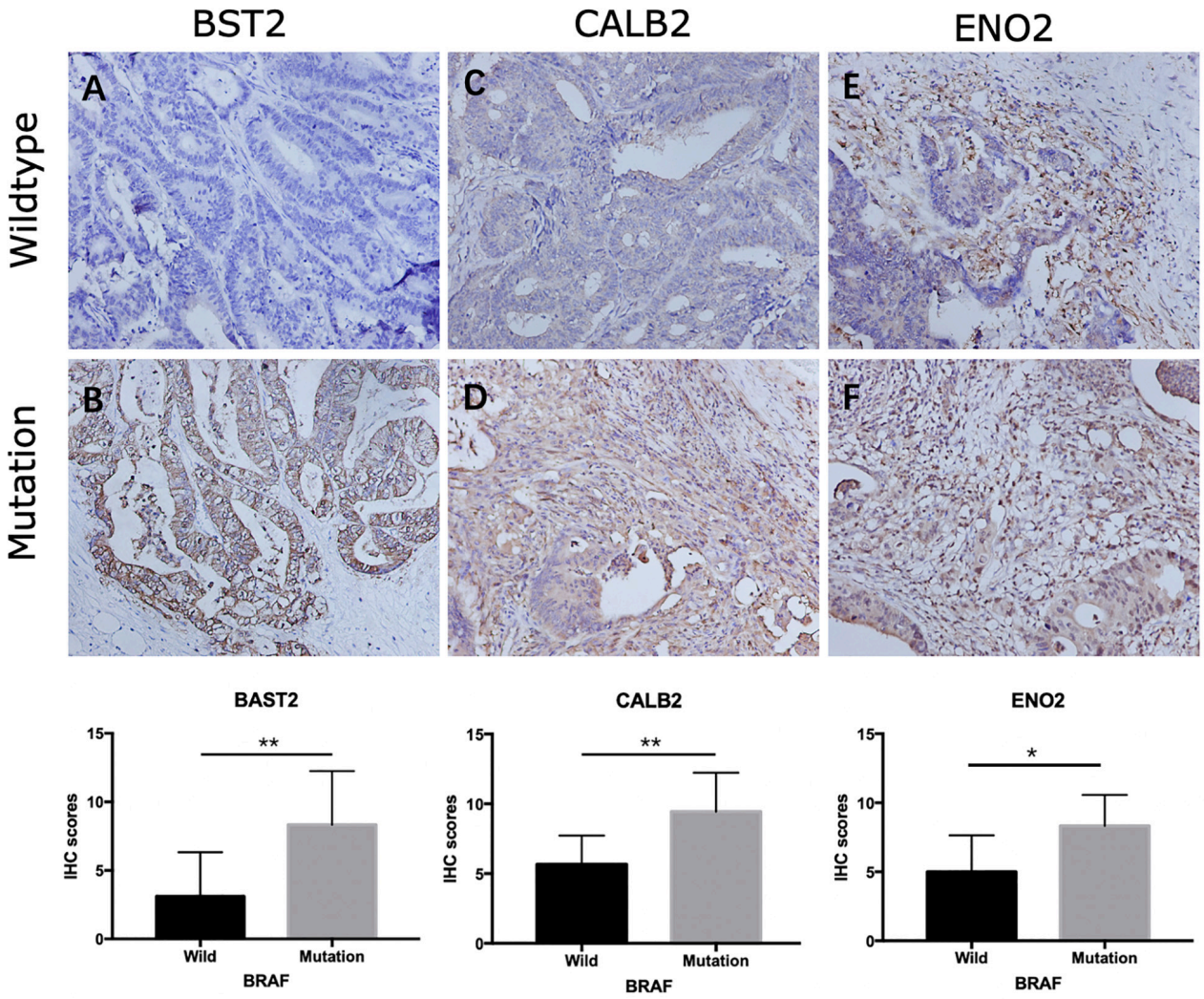

FIGURE 6 | Representative IHC staining showing expression of overall survival-related genes in colon cancer. Staining of BST2 **(A,B)**, CALB2 **(C,D)**, and ENO2 **(E,F)** in BRAF wild-type **(A,C,E)** and BRAF mutated **(B,D,F)** samples at magnification ×200. $^{*}p < 0.05$, $^{**}p < 0.01$, $^{***}p < 0.001$.

also called CXCL12) and chemokine (C-X-C motif) receptor 4 (CXCR4), thereby suggesting chemokines like CXCR4 may serve as future therapeutic targets (Molina-Cerrillo et al., 2020). Also, it is found that proangiogenic chemokines are highly expressed in BRAF mutated cell lines of colon cancer (Khan et al., 2014). Therefore, anti-VEGF therapies are recommended for BRAF mutated cancer patients. TRIBE study has proven the efficacy of FOLFOXIRI + bevacizumab as well for this subgroup of colon cancer patients (Cremolini et al., 2015). In addition to FOLFOXIRI chemotherapy, BRAF and MEK inhibitors are being tested in clinical trials to treat BRAF mutated colon cancer (Wu, 2018). The most recent therapy recommended for patients with BRAF mutant metastatic colon cancer is the binimetinib, encorafenib, and cetuximab triplet therapy from the BEACON Study (Kopetz et al., 2019).

Among the 144 DEGs between BRAF mutation and BRAF wild-type subtypes, BST2, CALB2, TNNT1, ENO2, HOXC6, and SYNGR3 were associated with overall survival in the TCGA dataset. Similar results were found that elevated BST2 level, HOXC6, and TNNT1 level are correlated with poor prognosis in colon cancer patients, while TNNT1 protein may be mediated through the process of epithelial–mesenchymal transition (Chiang et al., 2015; Hao et al., 2020; Yuan et al., 2020). CALB2 is a calcium binding protein from the EF hand family and is expressed in the majority of poorly differentiated colon cancer (Häner et al., 2010). It is also found that CALB2 may serve as a mediator for cell apoptosis in 5-FU-treated colon cancer through the mitochondrial pathway (Stevenson et al., 2011).

Interestingly, we also found that BRAF mutation was associated with overexpression in many immunotherapeutic targets, such as PD-1, PD-L1, CTLA-4, LAG-3, and TIM-3. Results from the IHC further prove that tumors with BRAF mutation have higher expression of these immunotherapy-related proteins. The Food and Drug Administration has already

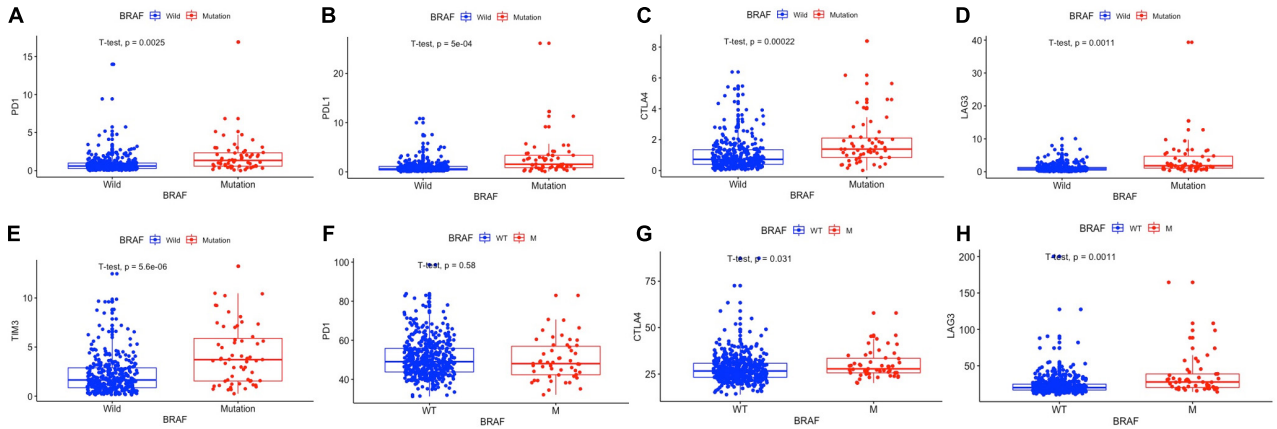

FIGURE 7 | BRAF mutation was correlated with the expression levels of PD-1 **(A)**, PD-L1 **(B)**, CTLA-4 **(C)**, LAG-3 **(D)**, and TIM-3 **(E)** in the TCGA cohort and the expression levels of PD-1 **(F)**, CTLA-4 **(G)**, and LAG-3 **(H)** in the GEO cohort. Student's *t*-tests were used for all analyses.

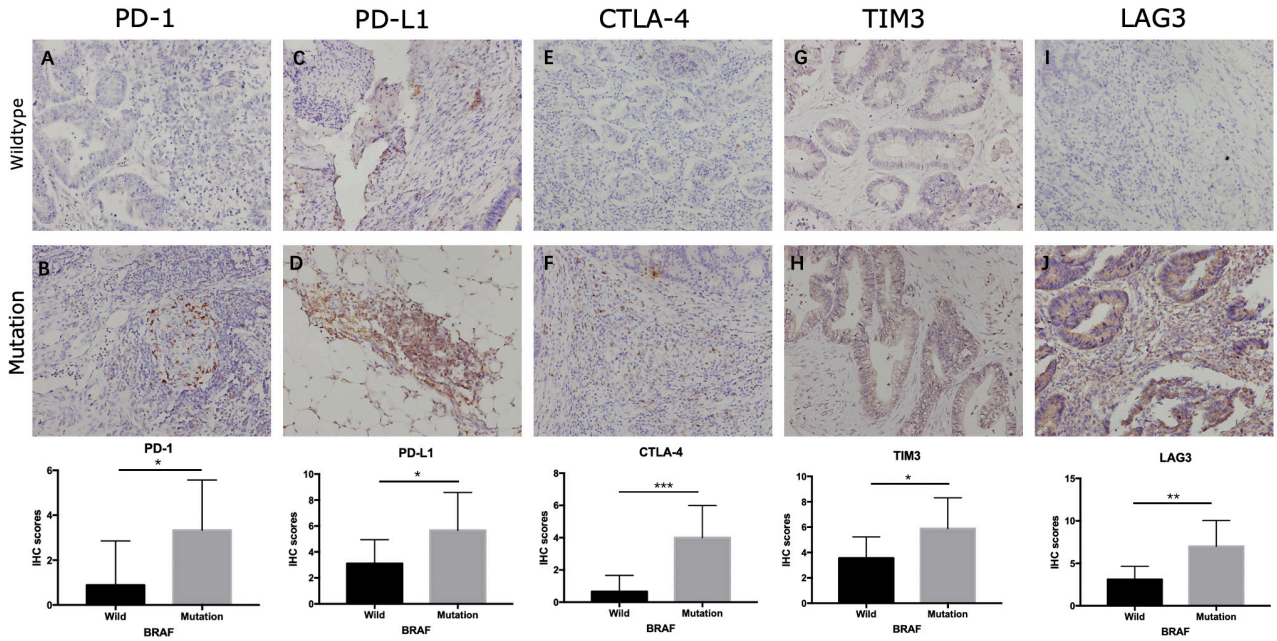

FIGURE 8 | Representative IHC staining showing expression of immunotherapy-related genes in colon cancer. Staining of PD-1 **(A,B)**, PD-L1 **(C,D)**, CTLA-4 **(E,F)**, TIM-3 **(G,H)**, and LAG-3 **(I,J)** in BRAF wild-type **(A,C,E,G,I)** and BRAF mutated **(B,D,F,H,J)** samples at magnification ×200. $^{*}p < 0.05$, $^{**}p < 0.01$, $^{***}p < 0.001$.

approved the clinical use of PD-1 inhibitors pembrolizumab and nivolumab for MSI-high tumors. Although the earlier Checkmate-142 study suggested that monotherapy of nivolumab has achieved an ORR of 25% in BRAF mutant tumors and 41% in KRAS/BRAF wild-type tumors, the most recent result has proven that nivolumab plus low-dose ipilimumab has achieved satisfying outcome for MSI-H/dMMR metastatic colorectal cancer (Overman et al., 2017; Lenz et al., 2020). The combination of two immunotherapies achieved an ORR of 71% in BRAF mutant tumors and an ORR of 60% in all patients (Lenz et al., 2020). In the phase II KEYNOTE-164 trial, ORRs of 20% and 55% were observed for second or further line treatment and third or further line treatment, respectively, for pembrolizumab-treated patients with BRAF mutant tumors who were resistant to chemotherapy (Le et al., 2020). This result demonstrated that combination immunotherapies had robust clinical benefit for colon cancer patients with high MSI, especially those with BRAF mutations. Since around 95% of metastatic colorectal cancer patients have MSS-type tumors, which act limited to single-agent immunotherapy, it is even inspiring that Japanese scientists reported an antitumor benefit from the combination of regorafenib plus nivolumab for advanced colorectal cancer patients in the phase Ib REGONIVO trial (Fukuoka et al., 2020).

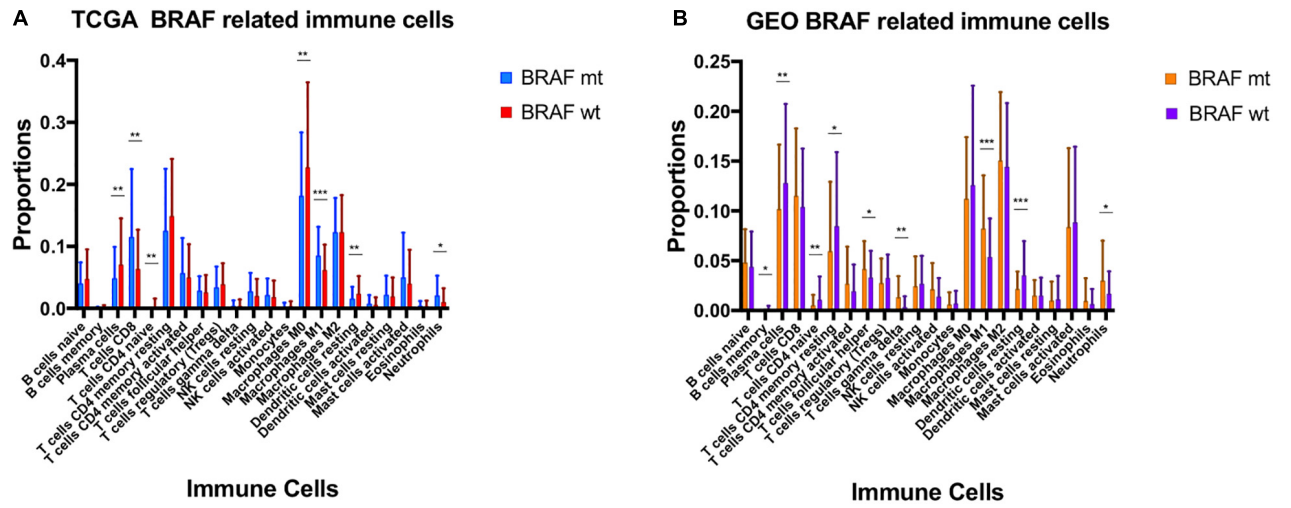

FIGURE 9 | BRAF mutation was correlated with the proportion of immune cells in TCGA **(A)** and GEO **(B)**.

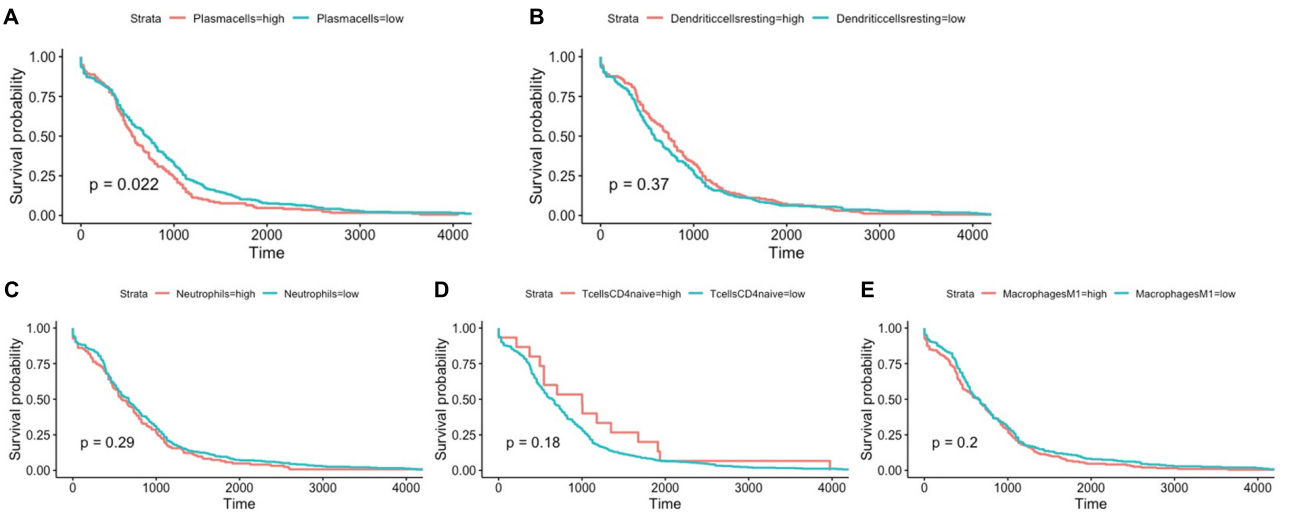

FIGURE 10 | BRAF mutation-related immune cells, including plasma cells **(A)**, dendritic cells resting **(B)**, neutrophils **(C)**, T cells CD4 naïve **(D)**, and macrophages M1 **(E)** and their association with overall survival. Log-rank test for Kaplan–Meier curves was conducted to assess the association between overall survival and expression levels.

Notably, although it is well acknowledged that dissimilar treatment strategies should be applied to MSS-type BRAF mutated colon cancer and MSI-type BRAF mutated colon cancer, no study has investigated tumor microenvironment among these subgroups yet. A review from Gelsomino et al. (2016) suggested that although patients with MSI-H generally had better prognosis than patients with MSS status, this favorable effect seemed to be partially mitigated by BRAF mutation. It should also be noted that the expression pattern of BRAF mutant colorectal cancer is very diverse, and several subtypes have been identified. Even two categories of BRAF V600E mutation have been identified with distinct molecular pattern, with one displaying high EMT activation and immune infiltration and the other one showing dysregulation in cell cycle checkpoints (Barras et al., 2017). Therefore, further researches may look into the precise targeted therapies to these subpopulations.

Recently, a follow-up study from the Checkmate-142 trial suggested that for patients who simultaneously had BRAF mutation and MSI status, nivolumab (NIVO) + low-dose ipilimumab (IPI) as first-line therapy received a remarkable ORR of 71% (12/17) (Lenz et al., 2020). Taking into account that BRAF mutated colon cancer tends to have higher expression levels of immunotherapy-related genes, such as PD-1, PD-L1, CTLA-4, and LAG-3, the use of checkpoint inhibitors in the Checkmate-142 trial was favorable and indicated that BRAF mutated colon cancer might present with an immunosuppressive microenvironment, which was in agreement with our conclusion.

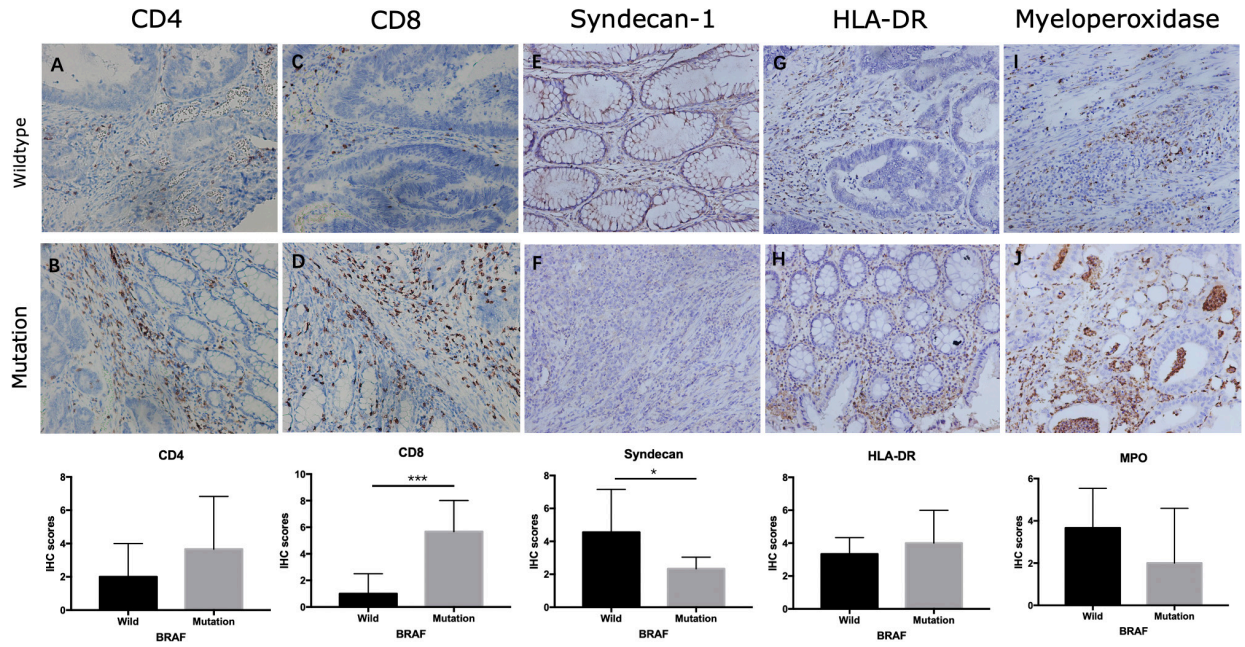

FIGURE 11 | Expression of immune cells in colon cancer. Staining of CD4 **(A,B)**, CD8 **(C,D)**, Syndecan-1 **(E,F)**, HLA-DR **(G,H)**, and myeloperoxidase **(I,J)** in BRAF wild-type **(A,C,E,G,I)** and BRAF mutated **(B,D,F,H,J)** samples at magnification ×200. $^{*}p < 0.05$, $^{**}p < 0.01$, $^{***}p < 0.001$.

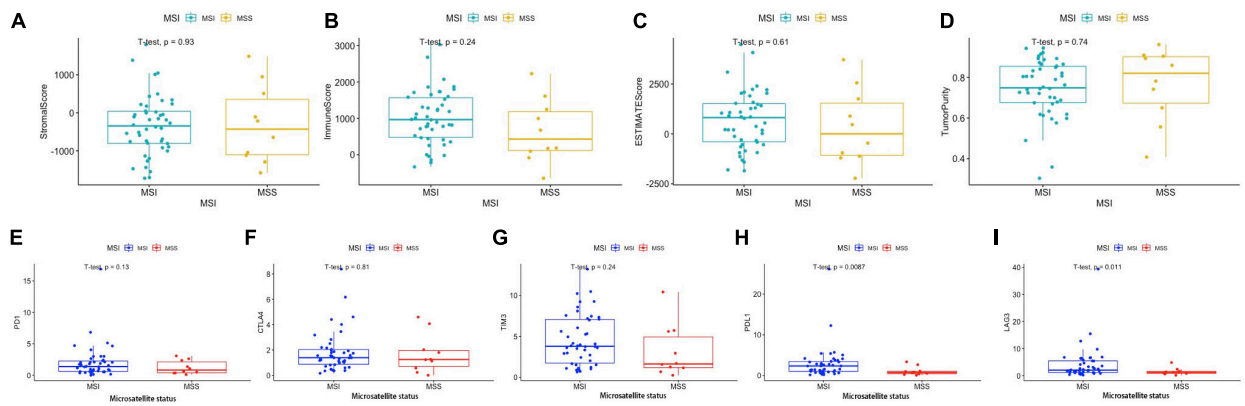

FIGURE 12 | Immune scores and immunotherapy-related genes according to MSI status. Stromal score **(A)**, immune score **(B)**, ESTIMATE score **(C)**, and tumor purity **(D)** in MSI and MSS groups. Expression levels of PD-1 **(E)**, CTLA-4 **(F)**, LAG-3 **(G)**, PD-L1 **(H)**, and TIM-3 **(I)** in the MSI and MSS groups. Student's *t*-tests were used for all analyses.

A limitation of our study was that the patients involved in our study, including patients from the TCGA dataset, the GEO dataset, and our hospital, are all postoperative ones. Hence, the patients with late-stage diseases were not included for analyses. In addition, information on postoperative treatments was not available. Further validation of the treatment efficacy in patients may provide more determined conclusions.

In conclusion, the present study provides insights into the tumor microenvironment in BRAF mutated colon cancer and discussed potential therapeutic targets from the perspective of immune biology. Immunotherapies may become fundamental treatments for BRAF mutated colon cancer in the future.

DATA AVAILABILITY STATEMENT

The datasets presented in this study can be found in online repositories. The names of the repository/repositories and accession number(s) can be found in the article/supplementary material.

ETHICS STATEMENT

The studies involving human participants were reviewed and approved by Research Ethics Committee of Beijing Friendship

Hospital. Written informed consent for participation was not required for this study in accordance with the national legislation and the institutional requirements.

AUTHOR CONTRIBUTIONS

ZL and ZB contributed to the conceptualization. SC and KL contributed to the investigation. SC, YZ, JS, CJ, and JG contributed to the analysis. SC, ZL, and KL contributed to the writing – original draft. ZL, ZB, and HP contributed to the writing – review and editing, and final approval. All authors contributed to the article and approved the submitted version.

FUNDING

This work was supported by the National Natural Science Foundation of China (Grant No. 81602635), Zhejiang Provincial Natural Science Foundation of China (Grant Nos. LY21H160042, LSY19H160006, and LGJ18H160001), Zhejiang Medical and Health Project (Grant No. 2019334185), and the National Key Technologies R&D Program (Grant No. 2015BAI13B09).

REFERENCES

Ajise, O. E., Roshal, M., Wang, L., Sukhram, G. N., Smith, K. M., Maslak, P., et al. (2016). Clinical utility of morphology, immunohistochemistry, flow cytometry, and FISH analysis in monitoring of plasma cell neoplasms in the bone marrow. *J. Hematopathol.* 9, 9–18. doi: 10.1007/s12308-015-0264-1

Barras, D., Missiaglia, E., Wirapati, P., Sieber, O. M., Jorissen, R. N., Love, C., et al. (2017). BRAF V600E mutant colorectal cancer subtypes based on gene expression. *Clin. Cancer Res.* 23, 104–115. doi: 10.1158/1078-0432.Ccr-16-0140

Bussard, K. M., Mutkus, L., Stumpf, K., Gomez-Manzano, C., and Marini, F. C. (2016). Tumor-associated stromal cells as key contributors to the tumor microenvironment. *Breast Cancer Res.* 18:84. doi: 10.1186/s13058-016-0740-2

Chan, A. T., and Giovannucci, E. L. (2010). Primary prevention of colorectal cancer. *Gastroenterology* 138, 2029–2043.e10. doi: 10.1053/j.gastro.2010.01.057

Chen, C., Xia, R., Chen, H., and He, Y. (2018). TBtools, a toolkit for biologists integrating various HTS-data handling tools with a user-friendly interface. *bioRxiv* [Preprint]. doi: 10.1101/289660 bioRxiv:289660

Chen, D. S., and Hurwitz, H. (2018). Combinations of bevacizumab with cancer immunotherapy. *Cancer J.* 24, 193–204. doi: 10.1097/ppo.0000000000000327

Chiang, S. F., Kan, C. Y., Hsiao, Y. C., Tang, R., Hsieh, L. L., Chiang, J. M., et al. (2015). Bone marrow stromal antigen 2 is a novel plasma biomarker and prognosticator for colorectal carcinoma: a secretome-based verification study. *Dis. Markers* 2015:874054. doi: 10.1155/2015/874054

Cremolini, C., Loupakis, F., Antoniotti, C., Lupi, C., Sensi, E., Lonardi, S., et al. (2015). FOLFOXIRI plus bevacizumab versus FOLFIRI plus bevacizumab as first-line treatment of patients with metastatic colorectal cancer: updated overall survival and molecular subgroup analyses of the open-label, phase 3 TRIBE study. *Lancet Oncol.* 16, 1306–1315. doi: 10.1016/s1470-2045(15)00122-9

Croce, L., Coperchini, F., Magri, F., Chiovato, L., and Rotondi, M. (2019). The multifaceted anti-cancer effects of BRAF-inhibitors. *Oncotarget* 10, 6623–6640. doi: 10.18632/oncotarget.27304

Davies, H., Bignell, G. R., Cox, C., Stephens, P., Edkins, S., Clegg, S., et al. (2002). Mutations of the BRAF gene in human cancer. *Nature* 417, 949–954. doi: 10.1038/nature00766

Denton, A. E., Roberts, E. W., and Fearon, D. T. (2018). Stromal cells in the tumor microenvironment. *Adv. Exp. Med. Biol.* 1060, 99–114. doi: 10.1007/978-3-319-78127-3_6

Dhillon, A. S., Hagan, S., Rath, O., and Kolch, W. (2007). MAP kinase signalling pathways in cancer. *Oncogene* 26, 3279–3290. doi: 10.1038/sj.onc.1210421

Dienstmann, R., Vermeulen, L., Guinney, J., Kopetz, S., Tejpar, S., and Tabernero, J. (2017). Consensus molecular subtypes and the evolution of precision medicine in colorectal cancer. *Nat. Rev. Cancer* 17, 79–92. doi: 10.1038/nrc.2016.126

Fukuoka, S., Hara, H., Takahashi, N., Kojima, T., Kawazoe, A., Asayama, M., et al. (2020). Regorafenib plus nivolumab in patients with advanced gastric or colorectal cancer: an open-label, dose-escalation, and dose-expansion phase Ib trial (REGONIVO, EPOC1603). *J. Clin. Oncol.* 38, 2053–2061.

Galland, S., and Stamenkovic, I. (2020). Mesenchymal stromal cells in cancer: a review of their immunomodulatory functions and dual effects on tumor progression. *J. Pathol.* 250, 555–572. doi: 10.1002/path.5357

Gelsomino, F., Barbolini, M., Spallanzani, A., Pugliese, G., and Cascinu, S. (2016). The evolving role of microsatellite instability in colorectal cancer: a review. *Cancer Treat. Rev.* 51, 19–26. doi: 10.1016/j.ctrv.2016.10.005

Gonsalves, W. I., Mahoney, M. R., Sargent, D. J., Nelson, G. D., Alberts, S. R., Sinicrope, F. A., et al. (2014). Patient and tumor characteristics and BRAF and KRAS mutations in colon cancer, NCCTG/Alliance N0147. *J. Natl. Cancer Inst.* 106:dju106. doi: 10.1093/jnci/dju106

Häner, K., Henzi, T., Pfefferli, M., Künzli, E., Salicio, V., and Schwaller, B. (2010). A bipartite butyrate-responsive element in the human calretinin (CALB2) promoter acts as a repressor in colon carcinoma cells but not in mesothelioma cells. *J. Cell. Biochem.* 109, 519–531. doi: 10.1002/jcb.22429

Hao, Y. H., Yu, S. Y., Tu, R. S., and Cai, Y. Q. (2020). TNNT1, a prognostic indicator in colon adenocarcinoma, regulates cell behaviors and mediates EMT process. *Biosci. Biotechnol. Biochem.* 84, 111–117. doi: 10.1080/09168451.2019.1664891

Jayasingam, S. D., Citartan, M., Thang, T. H., Mat Zin, A. A., Ang, K. C., and Ch'ng, E. S. (2020). Evaluating the polarization of tumor-associated macrophages into M1 and M2 phenotypes in human cancer tissue: technicalities and challenges in routine clinical practice. *Front. Oncol.* 9:1512. doi: 10.3389/fonc.2019.01512

Kather, J. N., and Halama, N. (2019). Harnessing the innate immune system and local immunological microenvironment to treat colorectal cancer. *Br. J. Cancer* 120, 871–882. doi: 10.1038/s41416-019-0441-6

Khan, S., Cameron, S., Blaschke, M., Moriconi, F., Naz, N., Amanzada, A., et al. (2014). Differential gene expression of chemokines in KRAS and BRAF mutated colorectal cell lines: role of cytokines. *World J. Gastroenterol.* 20, 2979–2994. doi: 10.3748/wjg.v20.i11.2979

Kopetz, S., Grothey, A., Yaeger, R., Van Cutsem, E., Desai, J., Yoshino, T., et al. (2019). Encorafenib, binimetinib, and cetuximab in BRAF V600E–mutated colorectal cancer. *N. Engl. J. Med.* 381, 1632–1643. doi: 10.1056/NEJMoa1908075

Le, D. T., Kim, T. W., Van Cutsem, E., Geva, R., Jäger, D., Hara, H., et al. (2020). Phase II open-label study of pembrolizumab in treatment-refractory, microsatellite instability-high/mismatch repair-deficient metastatic colorectal cancer: KEYNOTE-164. *J. Clin. Oncol.* 38, 11–19. doi: 10.1200/jco.19.02107

Lee, H. M., Morris, V., Napolitano, S., and Kopetz, S. (2019). Evolving strategies for the management of BRAF-mutant metastatic colorectal cancer. *Oncology* 33, 206–211.

Lenz, H.-J., Lonardi, S., Zagonel, V., Cutsem, E. V., Limon, M. L., Wong, K. Y. M., et al. (2020). Nivolumab plus low-dose ipilimumab as first-line therapy in microsatellite instability-high/DNA mismatch repair deficient metastatic colorectal cancer: clinical update. *J. Clin. Oncol.* 38(Suppl. 4):11. doi: 10.1200/JCO.2020.38.4_suppl.11

Li, T., Fan, J., Wang, B., Traugh, N., Chen, Q., Liu, J. S., et al. (2017). TIMER: a web server for comprehensive analysis of tumor-infiltrating immune cells. *Cancer Res.* 77, e108–e110. doi: 10.1158/0008-5472.Can-17-0307

Li, T., Fu, J., Zeng, Z., Cohen, D., Li, J., Chen, Q., et al. (2020). TIMER2.0 for analysis of tumor-infiltrating immune cells. *Nucleic Acids Res.* 48, W509–W514. doi: 10.1093/nar/gkaa407

Mariani, F., and Roncucci, L. (2017). Role of the vanins-myeloperoxidase axis in colorectal carcinogenesis. *Int. J. Mol. Sci.* 18:918. doi: 10.3390/ijms18050918

Matos, P., and Jordan, P. (2018). Targeting colon cancers with mutated BRAF and microsatellite instability. *Adv. Exp. Med. Biol.* 1110, 7–21. doi: 10.1007/978-3-030-02771-1_2

Molina-Cerrillo, J., San Román, M., Pozas, J., Alonso-Gordoa, T., Pozas, M., Conde, E., et al. (2020). BRAF mutated colorectal cancer: new treatment approaches. *Cancers* 12:1571. doi: 10.3390/cancers12061571

Newman, A. M., Liu, C. L., Green, M. R., Gentles, A. J., Feng, W., Xu, Y., et al. (2015). Robust enumeration of cell subsets from tissue expression profiles. *Nat. Methods* 12, 453–457. doi: 10.1038/nmeth.3337

Overman, M. J., McDermott, R., Leach, J. L., Lonardi, S., Lenz, H. J., Morse, M. A., et al. (2017). Nivolumab in patients with metastatic DNA mismatch repair-deficient or microsatellite instability-high colorectal cancer (CheckMate 142): an open-label, multicentre, phase 2 study. *Lancet Oncol.* 18, 1182–1191. doi: 10.1016/s1470-2045(17)30422-9

Phipps, A. I., Limburg, P. J., Baron, J. A., Burnett-Hartman, A. N., Weisenberger, D. J., Laird, P. W., et al. (2015). Association between molecular subtypes of colorectal cancer and patient survival. *Gastroenterology* 148, 77–87.e2. doi: 10.1053/j.gastro.2014.09.038

Quail, D. F., and Joyce, J. A. (2013). Microenvironmental regulation of tumor progression and metastasis. *Nat. Med.* 19, 1423–1437. doi: 10.1038/nm.3394

Rajagopalan, H., Bardelli, A., Lengauer, C., Kinzler, K. W., Vogelstein, B., and Velculescu, V. E. (2002). Tumorigenesis: RAF/RAS oncogenes and mismatch-repair status. *Nature* 418:934. doi: 10.1038/418934a

Reddy, S. M., Reuben, A., and Wargo, J. A. (2016). Influences of BRAF inhibitors on the immune microenvironment and the rationale for combined molecular and immune targeted therapy. *Curr. Oncol. Rep.* 18:42. doi: 10.1007/s11912-016-0531-z

Ritchie, M. E., Phipson, B., Wu, D., Hu, Y., Law, C. W., Shi, W., et al. (2015). limma powers differential expression analyses for RNA-sequencing and microarray studies. *Nucleic Acids Res.* 43:e47. doi: 10.1093/nar/gkv007

Stevenson, L., Allen, W. L., Proutski, I., Stewart, G., Johnston, L., McCloskey, K., et al. (2011). Calbindin 2 (CALB2) regulates 5-fluorouracil sensitivity in colorectal cancer by modulating the intrinsic apoptotic pathway. *PLoS One* 6:e20276. doi: 10.1371/journal.pone.0020276

Sung, H., Ferlay, J., Siegel, R. L., Laversanne, M., Soerjomataram, I., Jemal, A., et al. (2021). Global cancer statistics 2020: GLOBOCAN estimates of incidence and mortality worldwide for 36 cancers in 185 countries. *CA Cancer J. Clin.* 71, 209–249. doi: 10.3322/caac.21660

Taieb, J., Lapeyre-Prost, A., Laurent Puig, P., and Zaanan, A. (2019). Exploring the best treatment options for BRAF-mutant metastatic colon cancer. *Br. J. Cancer* 121, 434–442. doi: 10.1038/s41416-019-0526-2

Whiteside, T. L. (2008). The tumor microenvironment and its role in promoting tumor growth. *Oncogene* 27, 5904–5912. doi: 10.1038/onc.2008.271

Wu, C. (2018). Systemic therapy for colon cancer. *Surg. Oncol. Clin. N. Am.* 27, 235–242. doi: 10.1016/j.soc.2017.11.001

Yoshihara, K., Shahmoradgoli, M., Martínez, E., Vegesna, R., Kim, H., Torres-Garcia, W., et al. (2013). Inferring tumour purity and stromal and immune cell admixture from expression data. *Nat. Commun.* 4:2612. doi: 10.1038/ncomms3612

Yu, G., Wang, L. G., Han, Y., and He, Q. Y. (2012). clusterProfiler: an R package for comparing biological themes among gene clusters. *Omics* 16, 284–287. doi: 10.1089/omi.2011.0118

Yuan, X. H., Yang, J., Wang, X. Y., Zhang, X. L., Qin, T. T., and Li, K. (2018). Association between EGFR/KRAS mutation and expression of VEGFA, VEGFR and VEGFR2 in lung adenocarcinoma. *Oncol. Lett.* 16, 2105–2112. doi: 10.3892/ol.2018.8901

Yuan, Y., Chen, J., Wang, J., Xu, M., Zhang, Y., Sun, P., et al. (2020). Development and clinical validation of a novel 4-gene prognostic signature predicting survival in colorectal cancer. *Front. Oncol.* 10:595. doi: 10.3389/fonc.2020.00595

Conflict of Interest: The authors declare that the research was conducted in the absence of any commercial or financial relationships that could be construed as a potential conflict of interest.

Publisher's Note: All claims expressed in this article are solely those of the authors and do not necessarily represent those of their affiliated organizations, or those of the publisher, the editors and the reviewers. Any product that may be evaluated in this article, or claim that may be made by its manufacturer, is not guaranteed or endorsed by the publisher.

Copyright © 2021 Cen, Liu, Zheng, Shan, Jing, Gao, Pan, Bai and Liu. This is an open-access article distributed under the terms of the Creative Commons Attribution License (CC BY). The use, distribution or reproduction in other forums is permitted, provided the original author(s) and the copyright owner(s) are credited and that the original publication in this journal is cited, in accordance with accepted academic practice. No use, distribution or reproduction is permitted which does not comply with these terms.

frontiers in Cell and Developmental Biology

ORIGINAL RESEARCH
published: 03 August 2021
doi: 10.3389/fcell.2021.704242

Two Similar Signatures for Predicting the Prognosis and Immunotherapy Efficacy of Stomach Adenocarcinoma Patients

Taohua Yue, Shuai Zuo, Jing Zhu, Shihao Guo, Zhihao Huang, Jichang Li, Xin Wang, Yucun Liu, Shanwen Chen and Pengyuan Wang**

Division of General Surgery, Peking University First Hospital, Peking University, Beijing, China

OPEN ACCESS

Edited by:
Xuejun Sun,
Xi'an Jiaotong University, China

Reviewed by:
Hem Chandra Jha,
Indian Institute of Technology Indore, India
Jun Chen,
University of California, Berkeley, United States

***Correspondence:**
Shanwen Chen
shanwen_chen_bjmu@163.com
Pengyuan Wang
pengyuan_wang_bjmu@163.com

Specialty section:
This article was submitted to Molecular and Cellular Pathology, a section of the journal Frontiers in Cell and Developmental Biology

Received: *02 May 2021*
Accepted: *15 July 2021*
Published: *03 August 2021*

Citation:
Yue T, Zuo S, Zhu J, Guo S, Huang Z, Li J, Wang X, Liu Y, Chen S and Wang P (2021) Two Similar Signatures for Predicting the Prognosis and Immunotherapy Efficacy of Stomach Adenocarcinoma Patients. Front. Cell Dev. Biol. 9:704242. doi: 10.3389/fcell.2021.704242

Background: Globally, stomach adenocarcinoma (STAD)'s high morbidity and mortality should arouse our urgent attention. How long can STAD patients survive after surgery and whether novel immunotherapy is effective are questions that our clinicians cannot escape.

Methods: Various R packages, GSEA software, Metascape, STRING, Cytoscape, Venn diagram, TIMER2.0 website, TCGA, and GEO databases were used in our study.

Results: In the TCGA and GEO, macrophage abundance of STAD tissues was significantly higher than that of adjacent tissues and was an independent prognostic factor, significantly related to the overall survival (OS) of STAD patients. Between the high- and low- macrophage abundance, we conducted differential expression, univariate and multivariate Cox analysis, and obtained 12 candidate genes, and finally constructed a 3-gene signature. Both low macrophage abundance group and group D had higher TMB and PD-L1 expression. Furthermore, top 5 common gene-mutated STAD tissues had lower macrophage abundance. Macrophage abundance and 3 key genes expression were also lower in the Epstein-Barr Virus (EBV) and HM-indel STAD subtypes and significantly correlated with the tumor microenvironment score. The functional enrichment and ssGSEA revealed 2 signatures were similar and closely related to BOQUEST_STEM_CELL_UP, including genes up-regulated in proliferative stromal stem cells. Hsa-miR-335-5p simultaneously regulated 3 key genes and significantly related to the expression of PD-L1, CD8A and PDCD1.

Conclusion: macrophage abundance and 3-gene signature could simultaneously predict the OS and immunotherapy efficacy, and both 2 signatures had remarkable similarities. Hsa-miR-335-5p and BOQUEST_STEM_CELL_UP might be novel immunotherapy targets.

Keywords: stomach adenocarcinoma, macrophage abundance, 3-gene signature, prognosis, immunotherapy efficacy

INTRODUCTION

According to the Global Cancer Statistics 2020, the incidence and mortality of stomach adenocarcinoma (STAD) rank fifth and fourth, respectively (Sung et al., 2021). So far, the histology grades and TNM stages in the guidelines are still the primary standards for evaluating the prognosis of STAD patients (Salati et al., 2019). Glasgow Prognostic Score (GPS) that have not been included in the guidelines can be used as independent indicators for prognostic prediction of STAD patients without perioperative treatment (Melling et al., 2016). However, there are no satisfactory results in predicting the prognosis of STAD patients. Therefore, it is urgent to determine the potential factors for predicting prognosis in STAD.

Currently, the curative efficacies of comprehensive clinical treatments including surgery, radiotherapy, and chemotherapy, are not satisfactory (Kang et al., 2012). Molecularly targeted therapies, such as the human epidermal growth factor receptor 2 (HER2) monoclonal antibody, can improve the prognosis of advanced STAD. Still, they are only suitable for a small number of STAD patients and face the problem of drug resistance at the same time (Bang et al., 2010). Moreover, although PD-1/PD-L1 immune checkpoint inhibitors have opened up new ways to treat STAD patients (Kang et al., 2017), the positive response to immunotherapy was also limited to a small number of STAD patients, and the existing predictors of immunotherapy efficacy need to be improved (Salati et al., 2019).

In summary, we urgently needed an emerging method that could not only assess the prognosis of STAD patients, but also screen STAD patients suitable for immunotherapy.

In our research, compared with adjacent tissues, macrophage abundance was significantly increased in STAD tissues. In terms of prognosis, macrophage abundance was significantly related to the overall survival (OS) of STAD patients. Furthermore, the univariate and multivariate Cox analysis revealed that macrophage abundance was an independent prognostic factor for STAD patients. The higher the abundance of macrophages, the worse the prognosis of STAD patients. In the aspect of predicting the efficacy of immunotherapy, the low macrophage abundance group had a higher tumor mutational burden (TMB) and more PD-L1 (CD274) expression. Among the 6 most common gene mutations in the STAD, macrophage abundance in TTN/TP53/MUC16/LRP1B/SYNE1-mutant tissues was significantly lower than that of wild-type (WT) tissues.

To facilitate clinical quantification of macrophage abundance, based on the macrophage abundance of TCGA and GSE26899 data sets, we performed differential gene expression, univariate and multivariate Cox analysis, and finally obtained 12 candidate genes. With the help of the TIMER2.0 website, Kaplan-Meier (K-M), and Spearman correlation analysis, we identified 3 macrophage-related genes, including ABCA8, LUM, and SHC4 and further built a 3-gene signature. For convenience, we named them 3 key genes.

Among 5 molecular subtypes, Epstein-Barr virus (EBV) and HM-indel subtypes had the lowest macrophage abundance, 3 key genes expression, and the highest PD-L1 expression. The low macrophage group and group D had a higher proportion of EBV and HM-indel subtypes. Above results proved that these 2 subtypes were most suitable for immunotherapy.

Tumor purity as a prognosis and immunotherapy relevant feature in gastric cancer. We scored the stromal and immune components of tumor microenvironment (TME), and macrophage abundance and 3 key genes were all significantly negatively correlated with tumor purity and positively correlated with stromal scores. The 3-gene signature and macrophage abundance had similarities in predicting the OS, immunotherapy efficacy, and Gene Set Enrichment Analysis (GSEA).

To mine the molecular mechanisms of macrophage abundance and 3-gene signature in prognosis and immunotherapy efficacy prediction, we conducted functional enrichment analysis of 721 differentially expressed genes and 36 highly correlated genes, respectively. The up-regulated genes in proliferative stromal stem cells might be related to the above 2 signatures. For the regulatory network of microRNAs and RNA binding proteins of 3 key genes, on the Encyclopedia of RNA Interactomes (ENCORI) website, we unearthed 1 shared microRNAs and 8 RNA binding proteins (RBPs). Hsa-miR-335-5p was significantly related to PD-L1, CD8A and PDCD1.

In conclusion, we had built 2 similar signatures to evaluate the prognosis and immunotherapy efficacy of STAD patients. In terms of practicality, the 3-gene signature is more suitable for clinical application. Hsa-miR-335-5p and BOQUEST_STEM_CELL_UP might be novel immunotherapy targets that needed more verification.

MATERIALS AND METHODS

Ethics Statement

All data in our study were obtained from online public databases and did not involve any *in vitro* or *in vivo* experiments.

Study Samples

Specifically, 407, 357, 134, and 96 GC patients from the TCGA, GSE84433 (Yoon et al., 2020), GSE29272 (Wang et al., 2013), and GSE26899 (Oh et al., 2018), were enrolled in our study, respectively. Patients with a follow-up time <30 days or incomplete clinical information were excluded from the study. The detailed information was described in **Supplementary Table 1**. For normalization, the counts data of all genes in each sample of the TCGA database were transformed to transcripts per million (TPM) values for all the samples (Vera Alvarez et al., 2019).

Quantification of Immune Cell Infiltrations

The TIMER2.0[1] uses 6 kinds of the most advanced algorithms, including TIMER, CIBERSORT, quanTIseq, xCell, MCP counter, and EPIC algorithms, and provides a more reliable estimate of the immune infiltration level for the Cancer Genome Atlas (TCGA) or tumor atlas provided by users (Li et al., 2020c).

[1]http://timer.cistrome.org/

Besides, the TIMER2.0 also provides comprehensive analysis and visualization functions of tumor-infiltrating immune cells (Li et al., 2017). Based on gene expression matrix in the TCGA and GEO, the TIMER2.0 was used to quantify immune cell abundance both in STAD and normal samples. In the TCGA and GSE84433 data sets, based on the respective median macrophage abundance, we divided STAD patients into two groups, high and low macrophage infiltration groups. Then, we explored the associations between 12 candidate genes and clinical outcomes, 3 key genes and macrophage abundance in the pan-cancer on the TIMER2.0 website.

Prognostic Analysis

Based on "survival" and "survminer" packages, Kaplan–Meier (K–M) analysis and log-rank test were performed to evaluate the differences in the overall survival (OS) of STAD patients and establish survival curves (Li et al., 2020b). Furthermore, univariate and multivariate Cox regression analysis were used to identify independent prognostic factors and macrophage-related prognostic genes. $P < 0.05$ was set as the cut-off value.

Differential Expression Analysis

The Bioconductor packages "DESeq2"[2] (Love et al., 2014) (TCGA data set) and "limma"[3] (Ritchie et al., 2015) (GEO data set) were used to identify differentially expressed genes (DEGs) between high and low macrophage groups, group A and group D, with the criteria of $|\log_2(\text{fold-change})| > 1$ and false discovery rate < 0.05.

The ONCOMINE Database

The ONCOMINE database[4] is a friendly pan-cancer database that integrates RNA- and DNA-seq data from multiple sources, including GEO, TCGA, and published literature, designed to facilitate discovery from genome-wide expression analysis (Rhodes et al., 2004). The filter parameters were set as follows: *P*-value: 1E-4, Fold Change: 2, Gene Rank: Top 10%, Data Type: All.

Mutation Analysis

The TCGA mutation data were processed and visualized by R package "maftools" (Mayakonda et al., 2018).

Gene Set Enrichment Analysis (GSEA)

The "sva" package was used to remove batch effects and other unwanted variation in high-throughput data (Leek et al., 2012). In TCGA and GSE84433 joint data, to determine the significantly altered KEGG pathways and hallmark biological states or processes, we performed GSEA between high and low macrophage abundance, 3 key genes, group A and group D, using GSEA software 4.0.1. The (c2.cp.kegg.v7.2.symbols.gmt and h.all.v7.2.symbols.gmt) files were downloaded as the reference gene sets. The nominal (NOM) *P*-value < 0.05 and FDR *q*-value < 0.25 were set as the cut-off criteria.

UALCAN

The UALCAN[5] is a comprehensive, user-friendly, and interactive web resource for analyzing cancer OMICS data of TCGA and CPTAC (Chandrashekar et al., 2017). With the help of UALCAN, we analyzed mRNA expression levels of 3 key genes in normal tissues and different cancer stages or grades. The significant difference threshold was set to $P < 0.05$.

The cBioPortal for Cancer Genomics

The cBioPortal for Cancer Genomics[6] is an open-access resource for interactive exploration of multiple cancer genomics data sets, whose data derived from TCGA, ICGC, GEO, and other databases. The types of integrated genomic data include somatic mutations, DNA copy number changes (CNAs), mRNA and miRNA expression, DNA methylation, protein abundance, and phosphoprotein abundance (Cerami et al., 2012; Gao et al., 2013). Through this database, we obtained somatic mutation data of TCGA-STAD.

Expression Profiles of Predictive Biomarkers in Cancer Immunotherapy

In this study, based on non-parametric Mann–Whitney test, we quantified the expression differences of several key predictive biomarkers in cancer immunotherapy [Tumor Mutation Burden (TMB), PD-L1, GZMA, GZMB, PRF1, EOMES, IFNG, TNF, CXCL9, CXCL10, CD8A, CD4, FOXP3, ICOS, CTLA4, LAG3, CD276, VTCN1, CD70, HAVCR2, CD40, CD47, TNFRSF18, TIGIT, TNFSF14, ICAM1, and IL6] between high- and low-macrophage groups, and group A–D. $P < 0.05$ was considered to indicate a statistically significant difference.

Molecular Subtypes of TCGA-STAD

On the UCSC xena website, we mined the molecular subtypes of TCGA-STAD. Specifically, it included 5 molecular subtypes (GS, CIN, HM-indel, HM-SNV, and EBV) (version2017-06-25) (Liu et al., 2018).

The Tumor Microenvironment (TME) Score

An algorithm called ESTIMATE (Estimation of STromal and Immune cells in Malignant Tumor tissues using Expression data) was used for the estimation of stromal and immune cells in malignant tumor tissues based on the expression data. Stromal score represented the presence of stroma in tumor tissue, immune score captured the infiltration of immune cells in tumor tissue, and ESTIMATE score infers tumor purity (Yoshihara et al., 2013).

The Functional Enrichment Analysis

The Metascape[7] is a reliable, friendly tool for functional enrichment analysis, which integrates multiple databases, such as GO, KEGG, UniProt, and DrugBank (Zhou et al., 2019). The

[2]https://bioconductor.org/packages/release/bioc/html/DESeq2.html

[3]http://www.bioconductor.org/packages/release/bioc/html/limma.html

[4]www.oncomine.org/

[5]http://ualcan.path.uab.edu

[6]http://www.cbioportal.org/

[7]http://metascape.org

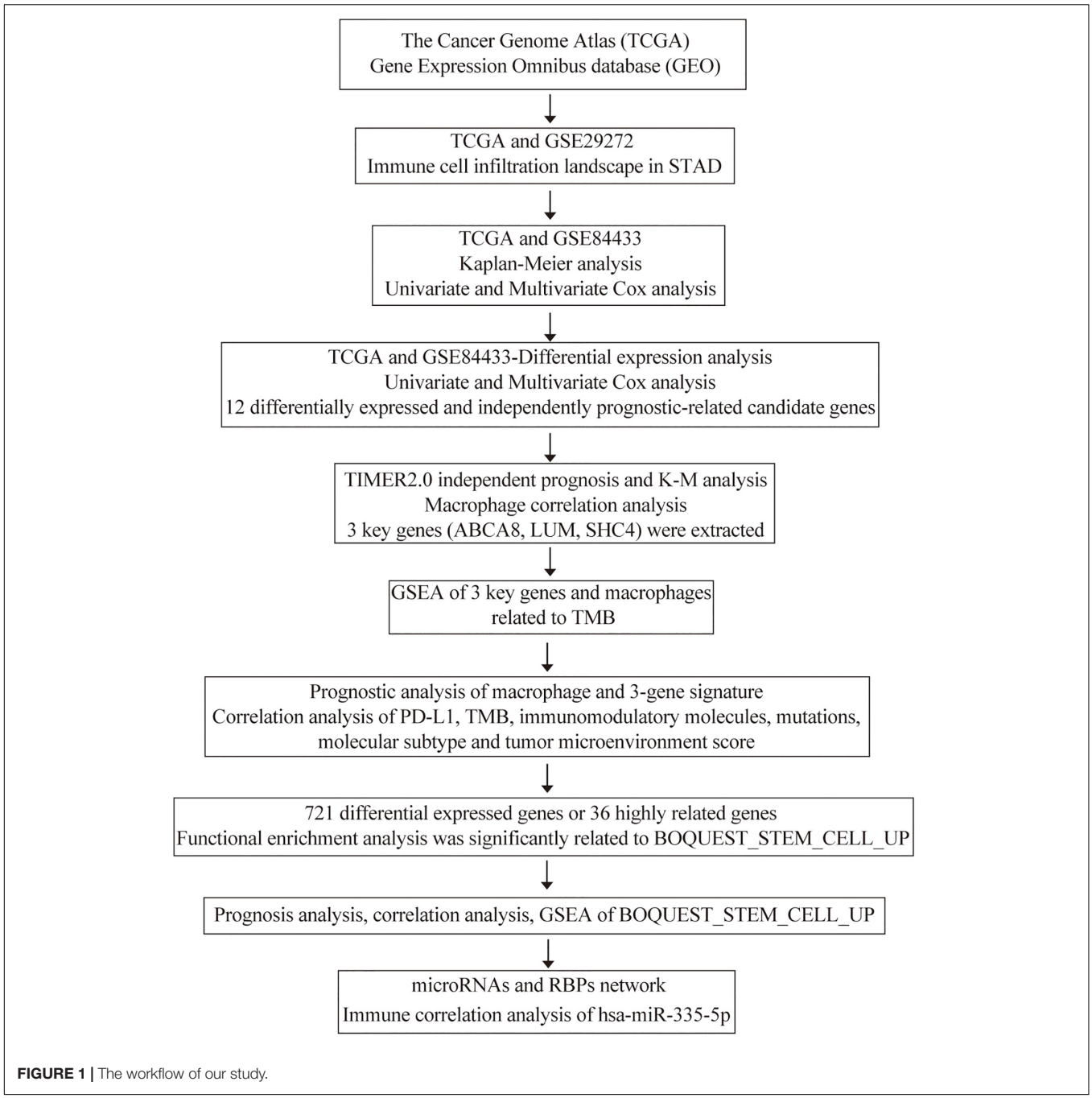

FIGURE 1 | The workflow of our study.

thresholds were set as follows: the number of min overlap and min enrichment were 3, and the P-value cutoff was 0.01.

The Single Sample Gene Set Enrichment Analysis (ssGSEA)

In our study, the ssGSEA was performed by package "gsva" (Hänzelmann et al., 2013), which was applied to the transcriptome of STAD samples to identify the association between 3 key genes, macrophage abundance and BOQUEST_STEM_CELL_UP score.

MicroRNA (miRNA) and RNA Binding Proteins (RBPs) Networks

On the ENCORI[8] and TarBase v.8[9], we obtains the microRNAs (miRNAs) and RNA binding proteins (RBPs) of 3 key genes (Li et al., 2014; Karagkouni et al., 2018). The Cytoscape is an open-source software platform for visualizing complex networks (Shannon et al., 2003). In this study, we constructed miRNA and

[8]http://starbase.sysu.edu.cn/

[9]http://carolina.imis.athena-innovation.gr/diana_tools/web/index.php?r=tarbasev8/index

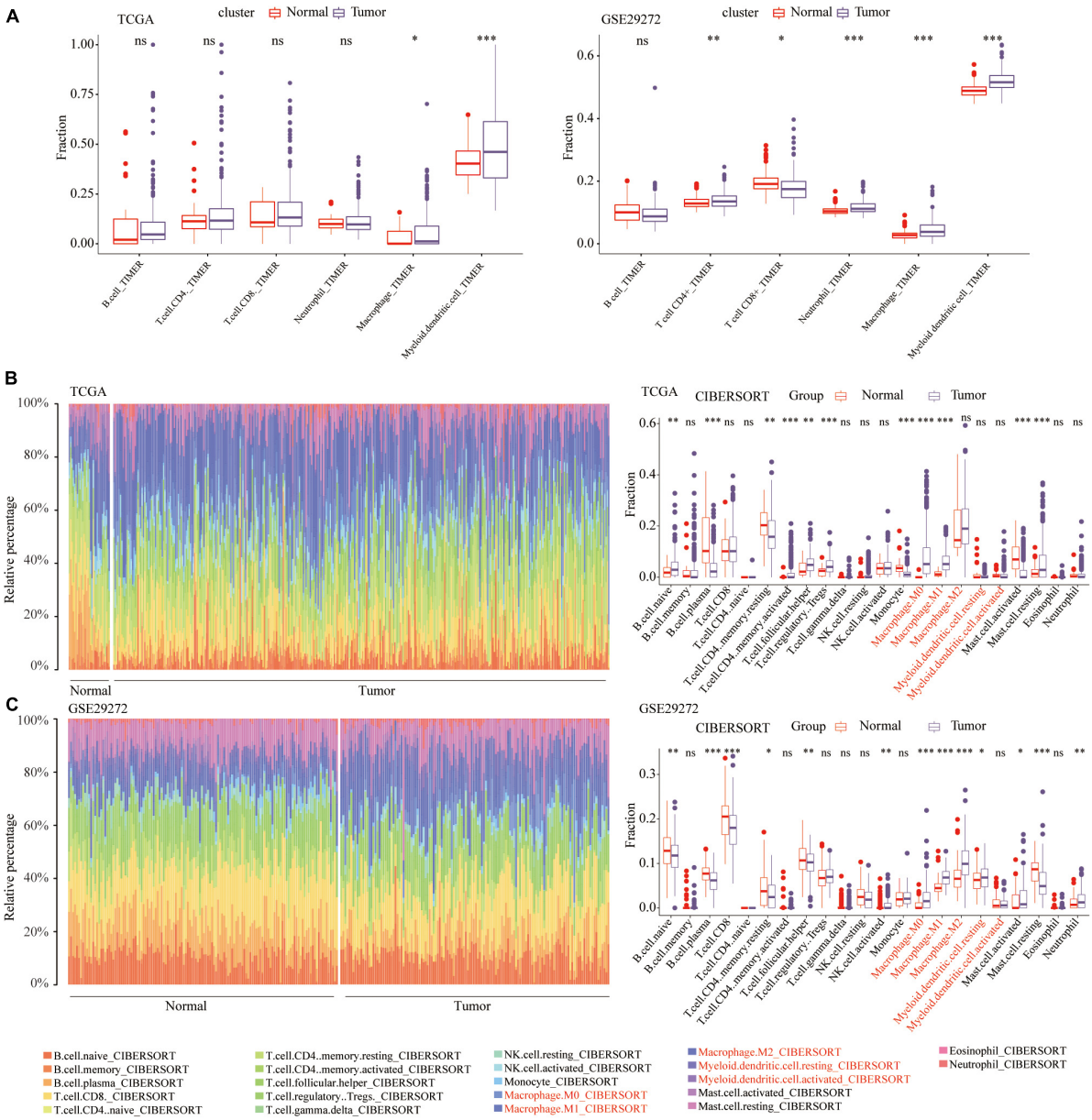

FIGURE 2 | Immune cell infiltration landscape in STAD patients. **(A)** Comparison of the abundance of six types of immune cells between normal and STAD tissues. The relative proportion and comparison of 22 immune cell between normal and STAD tissues in the **(B)** TCGA and **(C)** GSE29272. *$p < 0.05$, **$p < 0.01$, ***$p < 0.001$.

RBPs networks and cytoscape's plugin CytoHubba was used to discover key nodes in above networks (Chin et al., 2014).

Statistical Analysis

All of our analysis were conducted using R software version 3.6.1[10]. Since neither gene expression nor macrophage abundance obeyed a normal distribution, nonparametric Mann–Whitney test was used to compare variables between groups and spearman correlation analysis was used to analyze the correlation between genes and macrophage abundance. The threshold of significant difference was set to 0.05.

RESULTS

The Abundance of Tumor-Infiltrating Immune Cells (TIICs)

The workflow of our study was illustrated in **Figure 1**. Numerous studies have shown that the abundance of tumor infiltrating immune cells are closely related to the prognosis of cancer

[10]https://www.r-project.org/

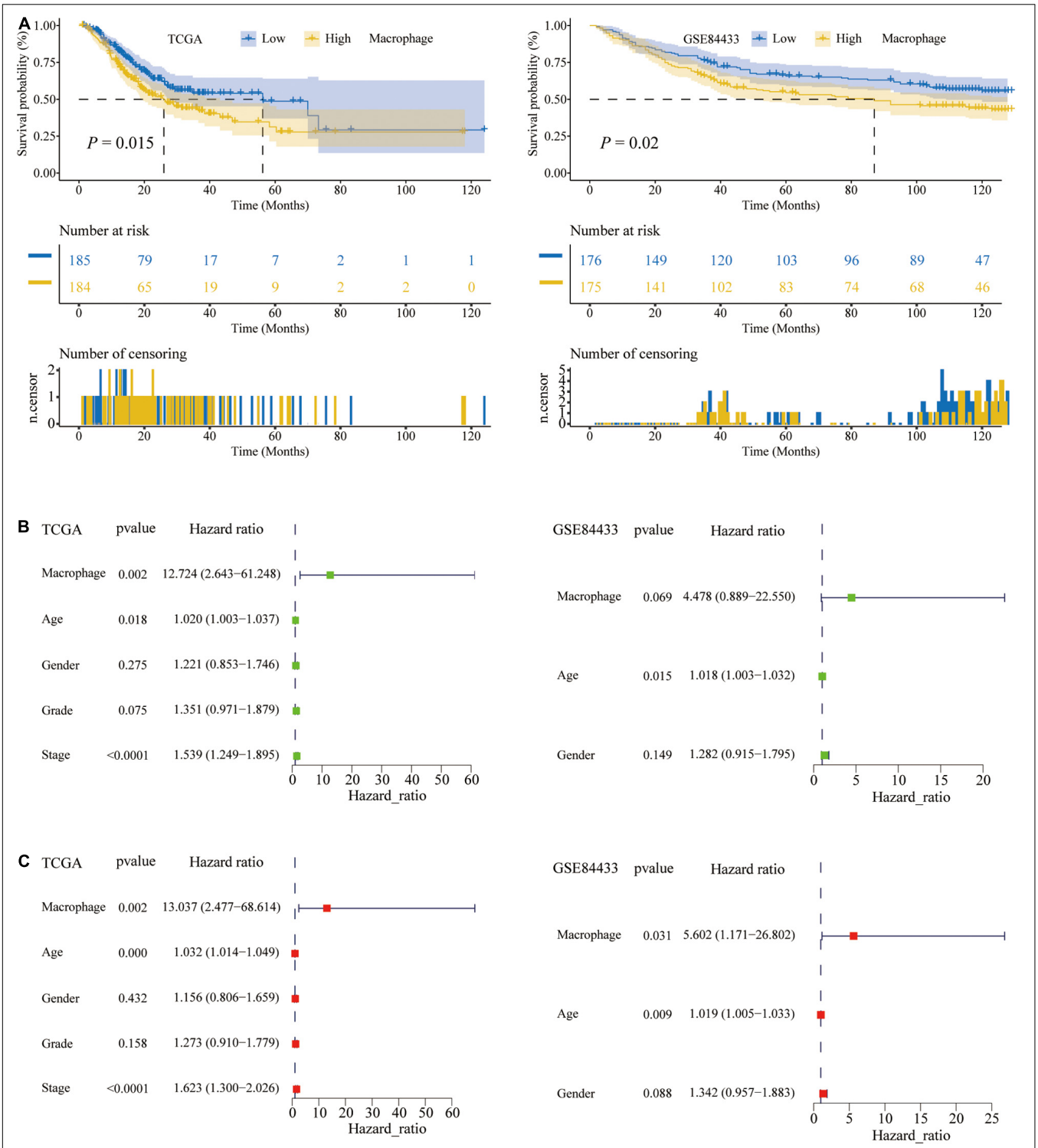

FIGURE 3 | The macrophage abundance was significantly related to the prognosis of STAD patients. **(A)** The higher the abundance of macrophages, the shorter the overall survival (OS) of STAD patients. **(B)** Univariate Cox regression analysis. **(C)** Multivariate Cox regression analysis.

patients and the efficacy of immunotherapy (Waniczek et al., 2017; Li et al., 2020c). The prognostic and therapeutic effects of tumor-infiltrating immune cells in stomach adenocarcinoma (STAD) have never been studied. Through the TIMER algorithm on the TIMER2.0 website, we quantitatively compared the abundance differences of 6 immune cell types between the STAD

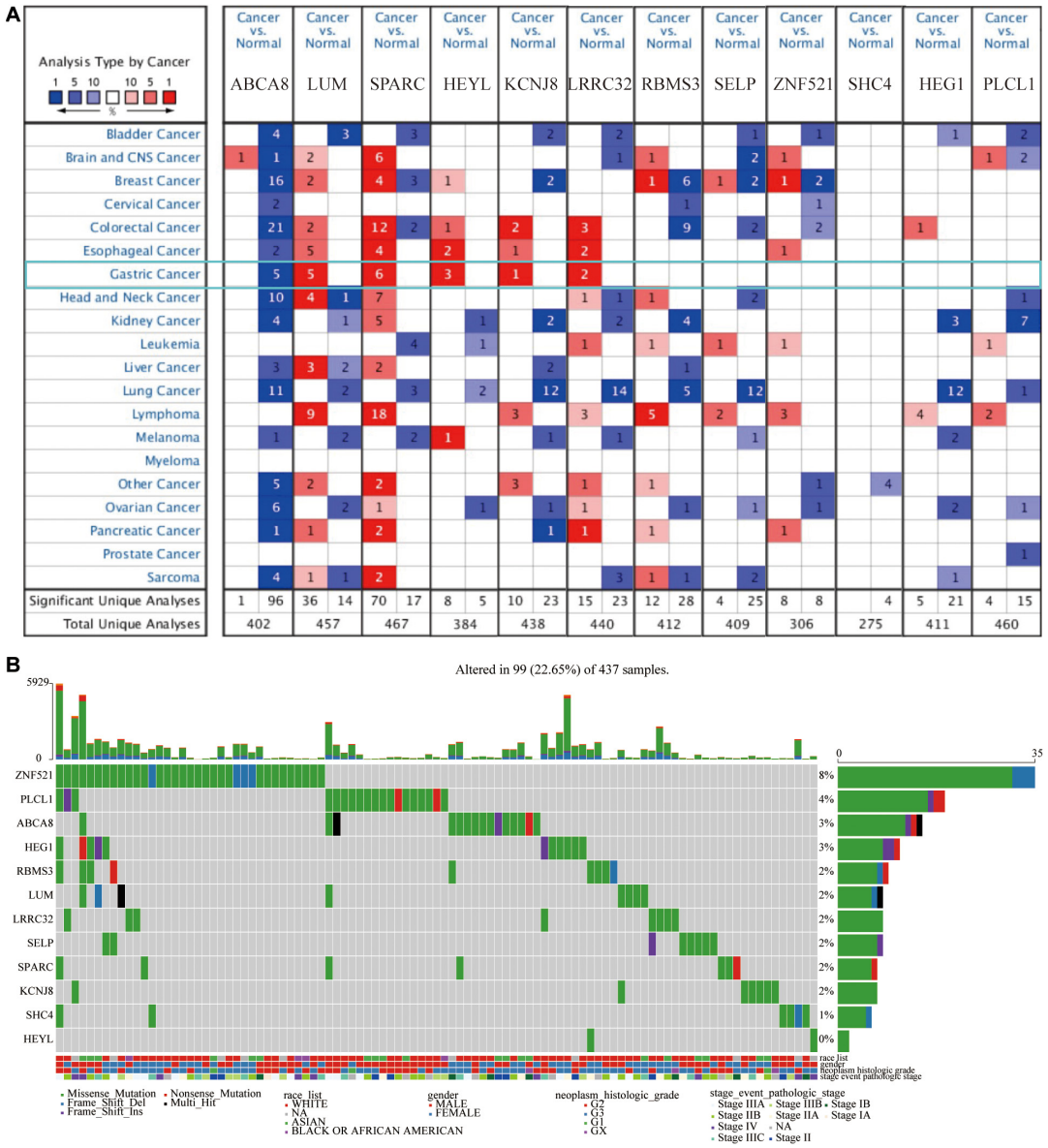

FIGURE 4 | Twelve candidate genes expression and mutation analysis. **(A)** Transcriptional expression of 12 candidate genes in pan-cancer on the ONCOMINE database. **(B)** Mutation analysis of 12 candidate genes in TCGA-STAD patients.

and normal samples, including $CD4^+$ T cells, $CD8^+$ T cells, B cells, neutrophils, macrophages, and myeloid dendritic cells. In the TCGA and GSE29272 data set, compared with normal samples, the abundance of macrophages and myeloid dendritic cells were significantly high in the STAD ($P < 0.05$) (**Figure 2A**). However, with regard to the infiltration of the other 4 immune cells, we did not draw a consistent conclusion.

To verify the results of the above TIMER algorithm, based on the CIBERSORT algorithm on the TIMER2.0 website, we further compared the abundance of macrophages and myeloid dendritic cells, including M0, M1, and M2 macrophages, resting and activated myeloid dendritic cells. In the TCGA (**Figure 2B**) and GSE29272 (**Figure 2C**), compared with normal samples, the proportions of M0 and M1 macrophages were significantly higher in STAD.

The Relationships Between the Abundance of Macrophages and the Prognosis of STAD Patients

Previous studies had confirmed that the abundance of immune cells in the tumor microenvironment (TME) were significantly related to the prognosis of cancer patients (Pagès et al., 2009). In the TCGA and GSE84433, K–M analysis was performed to determine the association between the overall survival (OS) and the abundance of 6 immune cell types. Among 6 types of TIICs,

the abundance of macrophages was significantly associated with the OS of STAD patients, and the higher the abundance of macrophages, the shorter the OS ($P < 0.05$) (**Figure 3A**). Besides, the abundance of the other 5 types of TIICs had no relationship with the OS of STAD patients (**Supplementary Figure 1**). For subpopulations of macrophages, the abundance of M0, M1, and M2 macrophage, calculated by CIBERSORT algorithm, had no relationships with the OS of STAD patients (**Supplementary Figure 2**). Therefore, M0, M1, and M2 macrophage could not predict the prognosis of STAD, while total macrophages were significantly related to the prognosis of STAD patients.

Given that the K–M analysis was a non-parametric test, the Cox parameter test was conducted. Also, in the above two data sets, TCGA and the GSE84433, we performed the univariate and multivariate Cox regression analysis and found that the abundance of macrophages was an independent prognostic factor for STAD patients ($P < 0.05$; **Figures 3B,C**). The green node represented the univariate Cox analysis, while the red represented the multivariate Cox analysis. Therefore, in STAD tissues, the abundance of macrophages was higher and related to a poor prognosis.

Identification of Differentially Expressed Genes (DEGs) and Prognostic Related Genes Related to Macrophage Infiltrations in STAD

To evaluate the biological functions of macrophage-related genes in the occurrence and development of STAD, we systematically performed the differential expression analysis between the high and low infiltration macrophage group in the TCGA and GSE84433 data sets, respectively. 1,727 and 8,606 differentially expressed genes were extracted from the TCGA and GSE84433, respectively. The shared 1,001 differentially expressed genes in the TCGA and GSE84433 were shown in heat maps, respectively (**Supplementary Figure 3A**).

Based on these 1,001 genes, we performed univariate Cox analysis in TCGA and GSE84433 and obtained 214 and 237 independent prognostic-related genes, respectively. The multivariate Cox analysis was then performed on these genes, respectively, and 37 and 227 independent prognostic-related genes were extracted. Finally, we obtained 12 shared independent prognostic macrophage-related genes and displayed them in forest plots (**Supplementary Figure 3B**).

The Expression and Mutation of 12 Macrophage-Related Genes

At the RNA level, to understand the differences in the expression of 12 macrophage-related genes between pan-cancer and adjacent normal tissues, we searched the ONCOMINE database. Among these 12 genes, multiple studies had shown that the expression of ABCA8 was significantly lower, and the expression of LUM, SPARC, HEYL, KCNJ, and LRRC32 were significantly higher in STAD than normal tissues. There was no significant difference in the expression of RBMS3, SELP, ZNF521, SHC4, HEG1, and PLCL1 between STAD and adjacent tissues (**Figure 4A**).

Numerous studies had shown that, at the DNA level, the gradual accumulation of mutations would promote the occurrence and development of cancer (Martincorena and Campbell, 2015). Therefore, we described the somatic mutation profiles of 12 macrophage-related genes in TCGA-STAD in detail. **Figure 4B** showed the mutation frequency and mutation types in detail. Among above 12 genes, the mutation frequency of ZNF521 was the highest, reaching 8%, and the mutation frequency of HEYL was the lowest. Frame shift deletion was the main type of mutation.

The Prognostic Significance of 12 Macrophage-Related Genes in STAD

Aiming to exclude the influence of STAD patients' age, gender, race, pathological American Joint Committee on Cancer (AJCC) stage and tumor purity on the prognosis of 12 macrophage-related genes, on the TIMER2.0 website, we performed multivariate Cox analysis. In **Figure 5A**, ABCA8, LUM, SPARC, LRRC32, RBMS3, ZNF521, SHC4, and PLCL1 were independent prognostic factors for STAD patients ($P < 0.05$). In addition, **Figure 5A** also clearly showed the prognostic performances of these 12 genes in pan-cancer.

Based on the TCGA and GSE84433, we further performed the K–M analysis and log-rank test among above 7 genes. The expression of ABCA8, LUM, and SHC4 were significantly related to the OS of STAD patients. The higher the expression, the worse the OS (**Figure 5B**). So far, we had captured 3 independent prognostic genes, ABCA8, LUM, and SHC4, among which there was no significant difference in the expression of SHC4 between STAD and normal tissues. For convenience, we called ABCA8, LUM, and SHC4 key genes.

Correlation Analysis of 3 Key Genes With Macrophage Infiltrations in STAD Patients

On the TIMER2.0 website, we reconfirmed the correlation of 3 key genes with macrophages and found that in TCGA pan-cancer, especially in the STAD, 3 key genes were significantly associated with macrophage infiltrations ($P < 0.05$) (**Figure 6A**).

We once again studied the correlation between 3 key genes and macrophage infiltrations in TCGA, GSE84433 and GSE26899, in the form of a scatter plot, and got the same conclusion that 3 key genes were significantly related to the infiltrations of macrophages ($P < 0.05$) (**Figure 6B**). Therefore, 3 key genes were independent prognostic factors related to macrophages. In addition to the 3 key genes mentioned above,the Spearman correlation between the other 9 genes and macrophage abundances was displayed in correlograms (**Figure 6C**).

Gene Set Enrichment Analysis (GSEA) of 3 Key Genes

Given that the 3 key genes and macrophage abundance were independent prognostic factors for STAD, we performed GSEA to determine the shared KEGG pathways and Hallmarks between low macrophage abundance/LUM/ABCA8/SHC4 groups and high macrophage abundance/LUM/ABCA8/SHC4 groups in the TCGA-GSE84433 joint cohort. Among the results of KEGG pathways enrichment, there were 10 significantly shared KEGG pathways. Among them, "KEGG_DNA_REPLICATION,"

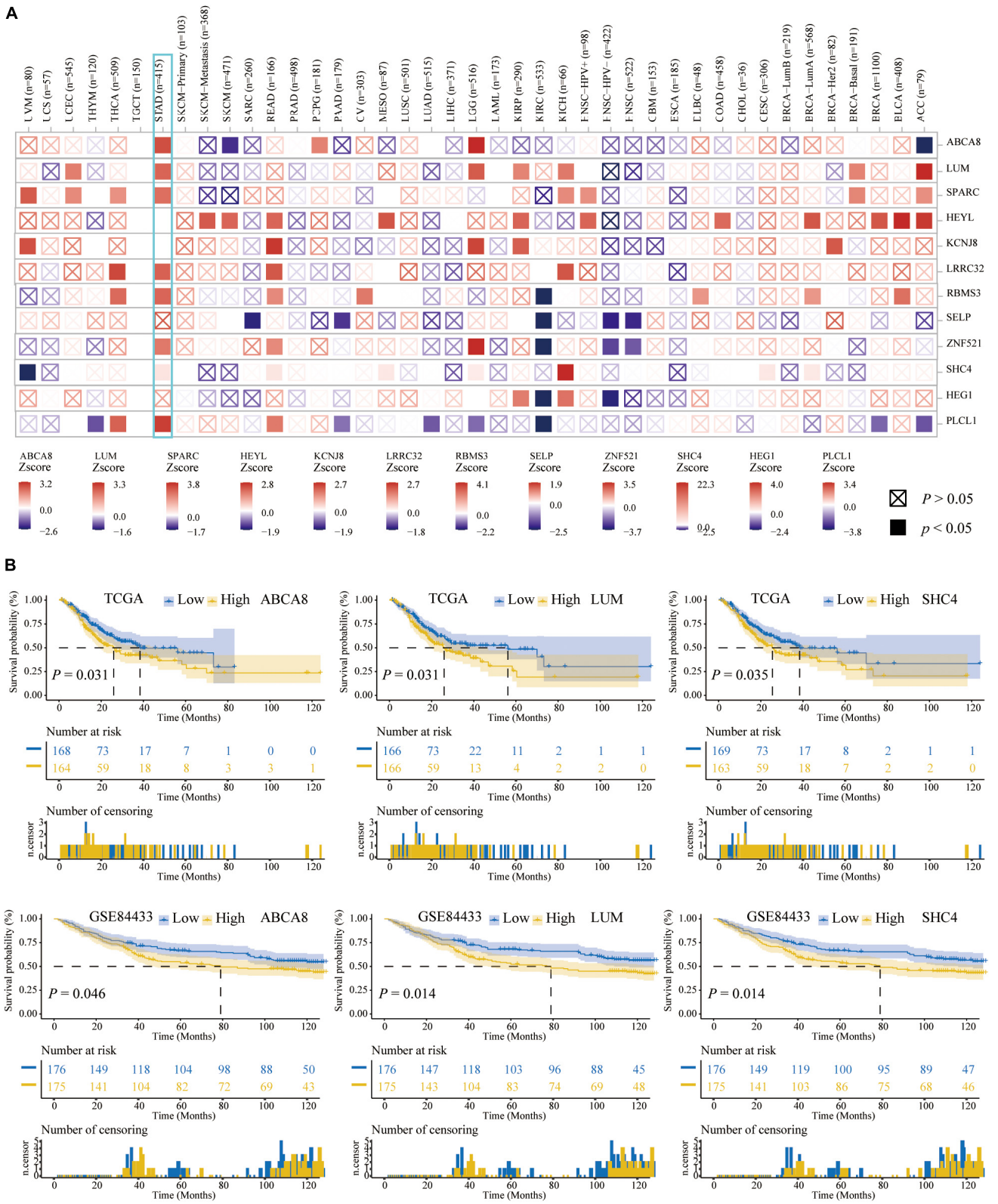

FIGURE 5 | Three key genes among 12 candidate genes. **(A)** Multivariate Cox analysis adjusted the influences of age, gender, race, stages, and tumor purity on the TIMER2.0 website. **(B)** Survival curves of the 3 key genes related to the OS of STAD patients among the 12 candidate genes. The higher the expression of 3 key genes, the shorter the OS of STAD patients.

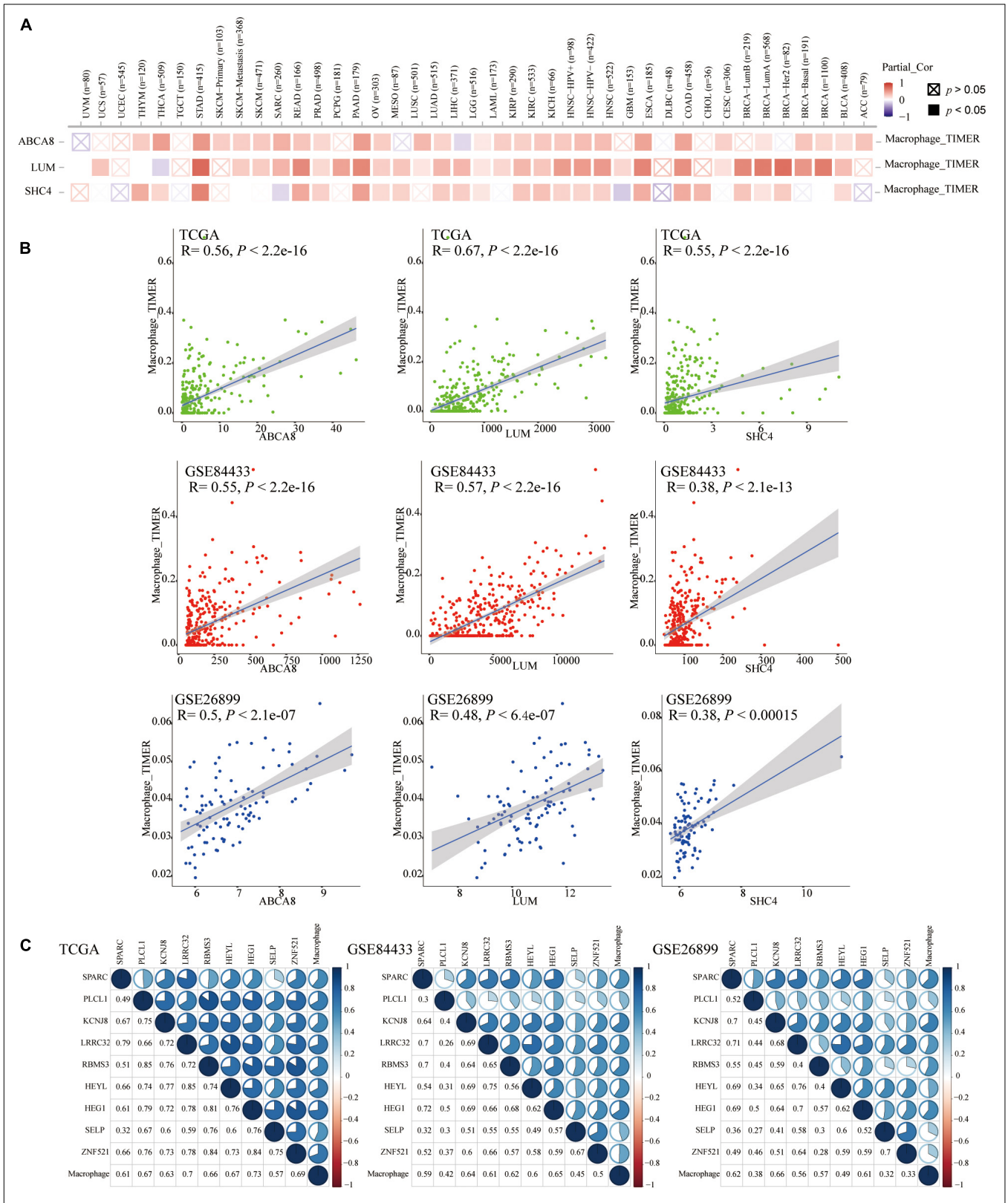

FIGURE 6 | Spearman correlation analysis between 3 key genes and the macrophage abundance. **(A)** In pan-cancer on the Timer2.0, Especially in STAD, 3 key genes were significantly correlated with the abundance of macrophages. **(B)** In TCGA and GEO data sets, 3 key genes were also significantly associated with macrophage abundance. **(C)** The Spearman correlation between the other 9 genes and macrophage abundances.

"KEGG_BASE_EXCISION_REPAIR," "KEGG_MISMATCH_REPAIR," and "KEGG_HOMOLOGOUS_RECOMBINATION" were tumor mutational burden (TMB) related pathways. For Hallmark enrichment results, there were 4 significantly shared enrichment Hallmarks. All results were shown in **Figure 7**, highlighted in red, as well as **Supplementary Tables 2, 3**. Results of GSEA suggested that 3 key genes and the abundance of macrophages might be related to the prediction of immunotherapy efficacy.

Associations Between 3 Key Genes and Clinical Characteristics and Prognosis

For STAD grades and stages, 3 key genes were differentially expressed in different STAD grades and stages ($P < 0.05$) (**Figure 8A**). So far we had found that 3 key genes had similarities in prognosis, molecular pathways, regulatory networks and relevance of stages and grades. In the following research, we tried to combine 3 key genes to predict the prognosis of STAD patients and the correlation of immunotherapy.

In terms of 3 key genes jointly predicting survival, based on the respective median of 3 key genes, STAD patients were divided into 4 group, specifically, High_SHC4_High_LUM_High_ABCA8, High_SHC4_Low_LUM_High_ABCA8/Low_SHC4_High_LUM_High_ABCA8/High_SHC4_High_LUM_Low_ABCA8, Low_SHC4_Low_LUM_High_ABCA8/High_SHC4_Low_LUM_Low_ABCA8/Low_SHC4_High_LUM_Low_ABCA8, and Low_SHC4_Low_LUM_Low_ABCA8. For convenience, let's call them groups A–D. In the single TCGA data set, the OS of group D was significantly longer than that of group A and group B ($P < 0.05$). In the single GSE84433 data set, the OS of group C and group D were significantly longer than that of group A ($P < 0.05$). Combining TCGA and GSE84433, the OS of group D was significantly longer than that of groups A and B, and the OS of group C was significantly longer than that of group A ($P < 0.05$) (**Figure 8B**). It was not difficult to see that the more the 3 key genes were highly expressed, the worse the prognosis of STAD patients.

The Correlation Between Macrophage Infiltrations, 3-Gene Signature, and Immunotherapy Predictors in STAD Patients

Immune checkpoint inhibitors have revolutionized cancer treatment and are approved for various cancer treatments (Duffy and Crown, 2019). Tumor mutation burden (TMB) and PD-L1 (CD274) expression are currently the main predictors of immunotherapy efficacy (Patel and Kurzrock, 2015; Chan et al., 2019). Our study revealed that the low macrophage group had higher TMB and higher PD-L1 expression (**Figure 9A**). We further speculated that the lower macrophage infiltrations, the better the efficacy of immunotherapy.

In terms of the combination of 3 key genes to predict the immunotherapy efficacy, since in the clinic, we could not directly score the macrophage infiltrations, and further studies show that the 3-gene signature could perfectly distinguish the macrophage abundance. For the degree of macrophage abundance, group A > group B > group C > group D (**Figure 9B**). The expression trends of TMB and PD-L1 in group A and D were also consistent with that of the high and low macrophage group (**Figure 9C**). We concluded that STAD patients in group D were most suitable for immunotherapy, while group A had the worst immunotherapy efficacy.

The Association Between Macrophage Infiltrations, 3-Gene Signature, and Immune-Related Molecules in STAD Patients

So far we had concluded that macrophages and 3-gene signature could predict the prognosis and efficacy of immunotherapy of STAD. With the deepening of research, in addition to TMB and PD-L1 expression, more and more immunotherapy biomarkers had appeared (Danilova et al., 2019). For macrophage infiltrations and 3-gene signature, including groups A–D, there were significant differences in the expression of GZMB, EOMES, CD8A, CD4, CD276, HAVCR2, and IL-6 ($P < 0.05$) (**Supplementary Figures 4A,B**), which once again verified that macrophages and 3-gene signature were immunotherapy biomarkers.

The Landscapes and Differences of Somatic Mutation of STAD

Gene mutations can cause cancer patients to be sensitive or resistant to immunotherapy, affecting the therapeutic effect (Rizvi et al., 2015). Using "maftools" package and mutation information in the cBioPortal database [Stomach Adenocarcinoma (TCGA, Firehose Legacy)], we first described the mutation of 30 genes with the highest mutation frequency of STAD (**Supplementary Figure 4C**). Taking the mutation frequency greater than 25% as the threshold, we extracted the top 6 genes, including TTN, TP53, MUC16, LRP1B, SYNE1, and ARID1A. Furthermore, TTN/TP53/MUC16/LRP1B/SYNE1-mutant tissues had significantly lower macrophage abundance than WT tissues ($P < 0.05$) (**Figure 10A**). These coincided with the impressive immunotherapy efficacy of STAD with TTN/TP53/MUC16/LRP1B/SYNE1-mutations mentioned in previous studies (Dong et al., 2017; Chen et al., 2019; Li et al., 2020a; Yang et al., 2020). It could be seen that STAD patients with low macrophage abundance could benefit more from immunotherapy.

Molecular Subtypes and Tumor Microenvironment (TME) Score of TCGA-STAD

To develop personalized treatment for STAD patients, previous studies had divided TCGA-STAD into different molecular subtypes, including Genome stable (GS), chromosomal instability (CIN), Hypermutated- insertion and deletion (HM-indel), Hypermutated-single nucleotide variants (HM-SNV), Epstein-Barr Virus (EBV) (Liu et al., 2018). To predict the immunotherapy effects of macrophages and 3 key genes, we analyzed their expression in different subtypes and compared

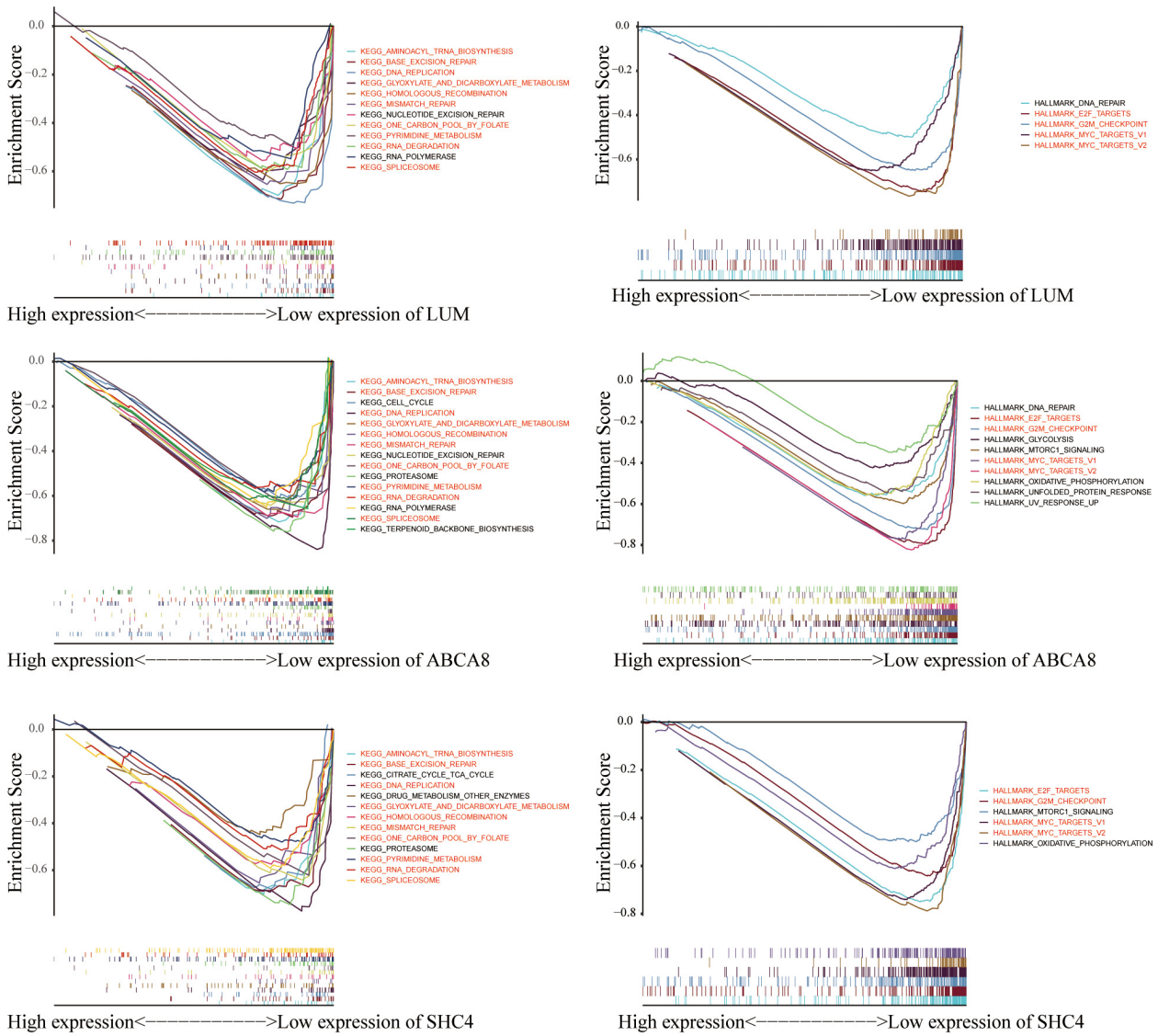

FIGURE 7 | Gene Set Enrichment Analysis (GSEA) of 3 key genes. 10 KEGG pathways and 4 hallmarks were significantly enriched in the low expression of macrophage abundance and 3 key genes.

them with the expression of PD-L1. Among 5 molecular subtypes, GS had higher macrophage abundance and 3 key genes expression and lower expression of PD-L1. The Epstein-Barr Virus (EBV) and HM-indel had lower macrophage abundance, 3 key genes expression and higher expression of PD-L1 (**Figure 10B**). The EBV and HM-indel subtypes could benefit more from immunotherapy. The expression trend of PD-L1 was opposite to that of macrophage abundance and 3 key genes. STAD tissues in the low macrophage group had higher proportions of HM-indel and EBV (**Figure 10C**). From group A to group D, the ratio of HM-indel and EBV gradually increased (**Figure 10D**).

The TME scores and tumor purity were also related to the efficacy of immunotherapy (Ren et al., 2020). Macrophage abundance, 3 key genes and PD-L1 were all significantly negatively correlated with tumor purity and positively correlated with stromal and ESTIMATE scores ($P < 0.05$) (**Figure 10E**). We concluded that macrophages and 3 key genes could predict the immunotherapy efficacy of STAD patients. STAD patients with of low macrophage group or group D were more suitable for immunotherapy.

Subtypes Analysis of Race and *Helicobacter pylori* (Hp) Infection

In view of the differences in clinical characteristics of different races (Asian, Black or African American, White), we studied the distribution ratio of races in 2 signatures. Among 3 races, STAD patients in low macrophage group and group D had higher proportions of Asian and Black or African American

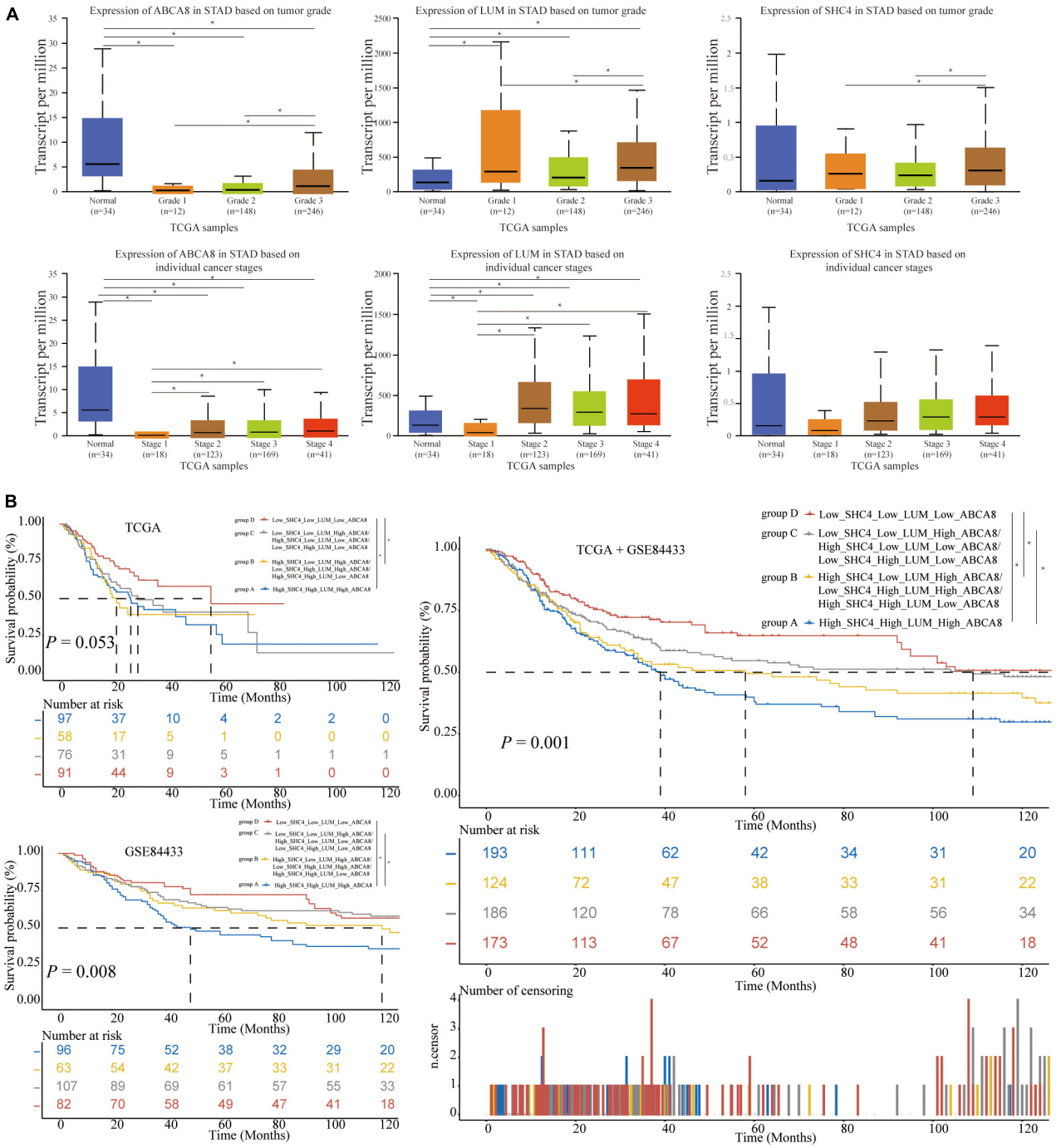

FIGURE 8 | The expression of 3 key genes among different grades and stages, and the construction of 3-gene signature. **(A)** In terms of grades, the higher the STAD patient's grade, the higher the expression of 3 key genes. In the aspect of stages, the higher the STAD patient's stage, the higher the expression of ABCA8 and LUM. **(B)** Based on the respective medians of 3 key genes, we divided the STAD patients of TCGA and GSE84433 into 4 groups. The more up-regulated genes in 3 key genes, the shorter the OS of STAD patients. The significant difference threshold was 0.05. *$p < 0.05$.

(**Supplementary Figure 5A**), which suggested that compared with white people, Asian and Black or African American people might be more suitable for immunotherapy.

Previous studies had shown that Hp infection affected the therapeutic efficacy of gastric cancer patients (Crowe, 2019). To understand the relationship between the Hp infection and the efficacy of immunotherapy, we explored the distribution ratio of the Hp infected and uninfected patients in 2 signatures. STAD patients in low macrophage group and groups B–D had higher proportions of the Hp uninfected patients

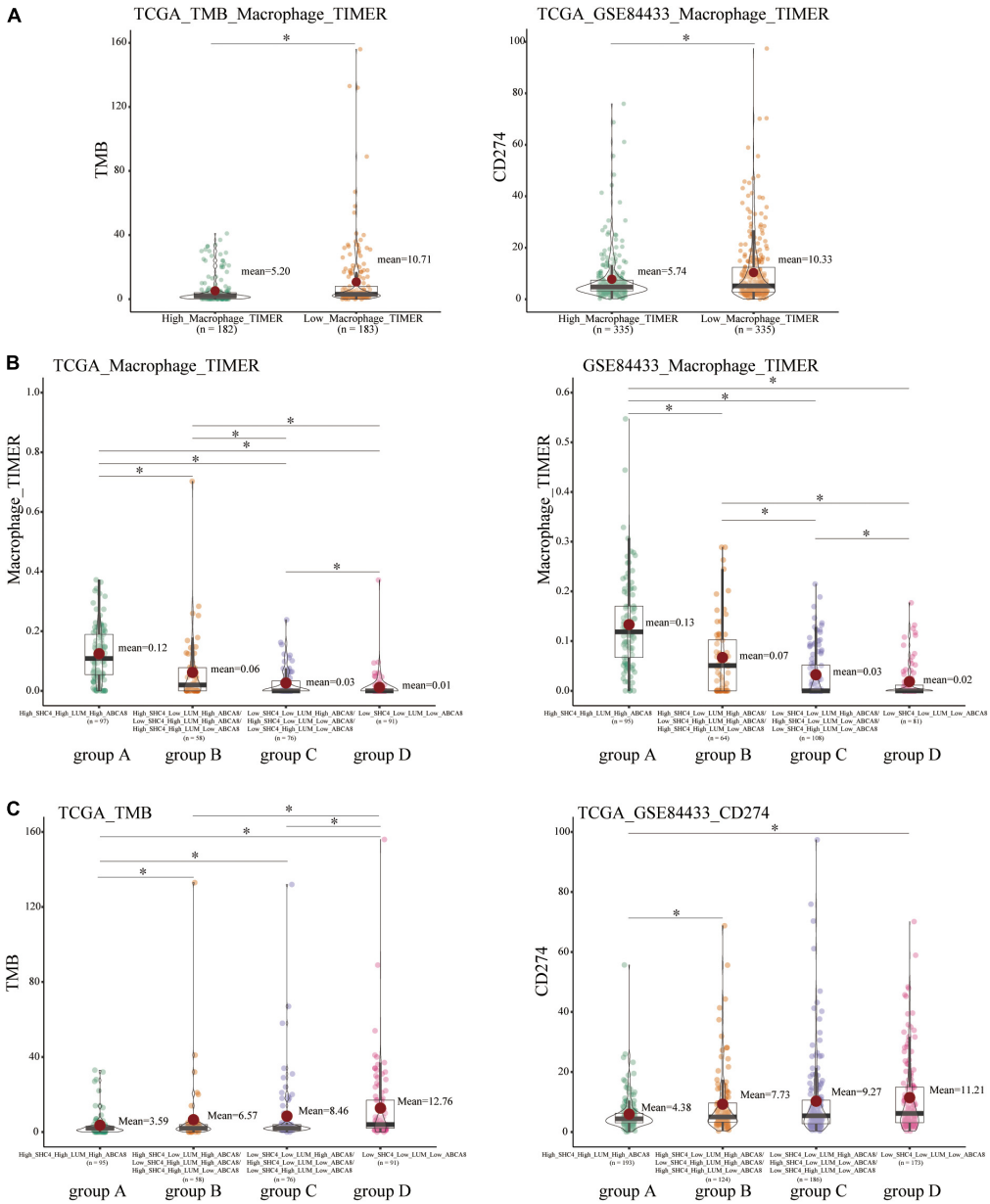

FIGURE 9 | Correlation of macrophage abundance, 3-gene signature, and immunotherapy biomarkers, including tumor mutational burden (TMB) and PD-L1 (CD274). **(A)** Compared with high macrophage group, low macrophage group had higher TMB and PD-L1 expression. **(B)** There were significant differences in the abundance of macrophages in 4 groups of STAD patients divided by the 3-gene signature. **(C)** Among 4 groups of STAD patients, there were significantly differences among group A, group B, and group D on the TMB and PD-L1. *$p < 0.05$.

(**Supplementary Figure 5B**), which indicated that the Hp uninfected patients might be more suitable for immunotherapy.

Enrichment Analysis of High and Low Macrophage Groups and the 3-Gene Signature Groups A and D

Through the above survival analysis and predictive significance of immunotherapy efficacy, we found that there were many similarities between macrophage abundance and the 3-gene signature. The GSEA was conducted between the high and low macrophage group and the 3-gene signature group A and group D. Results of hallmark and KEGG enrichment analysis were basically the same and further proved the similarities between macrophage abundance and group A and group D. All results of GSEA were shown in Venn diagrams in **Figure 11A** and **Supplementary Tables 2, 3**.

Functional enrichment analysis was used to reveal the potential and common biological mechanisms of macrophage abundance and 3-gene signature. On the one hand, in the

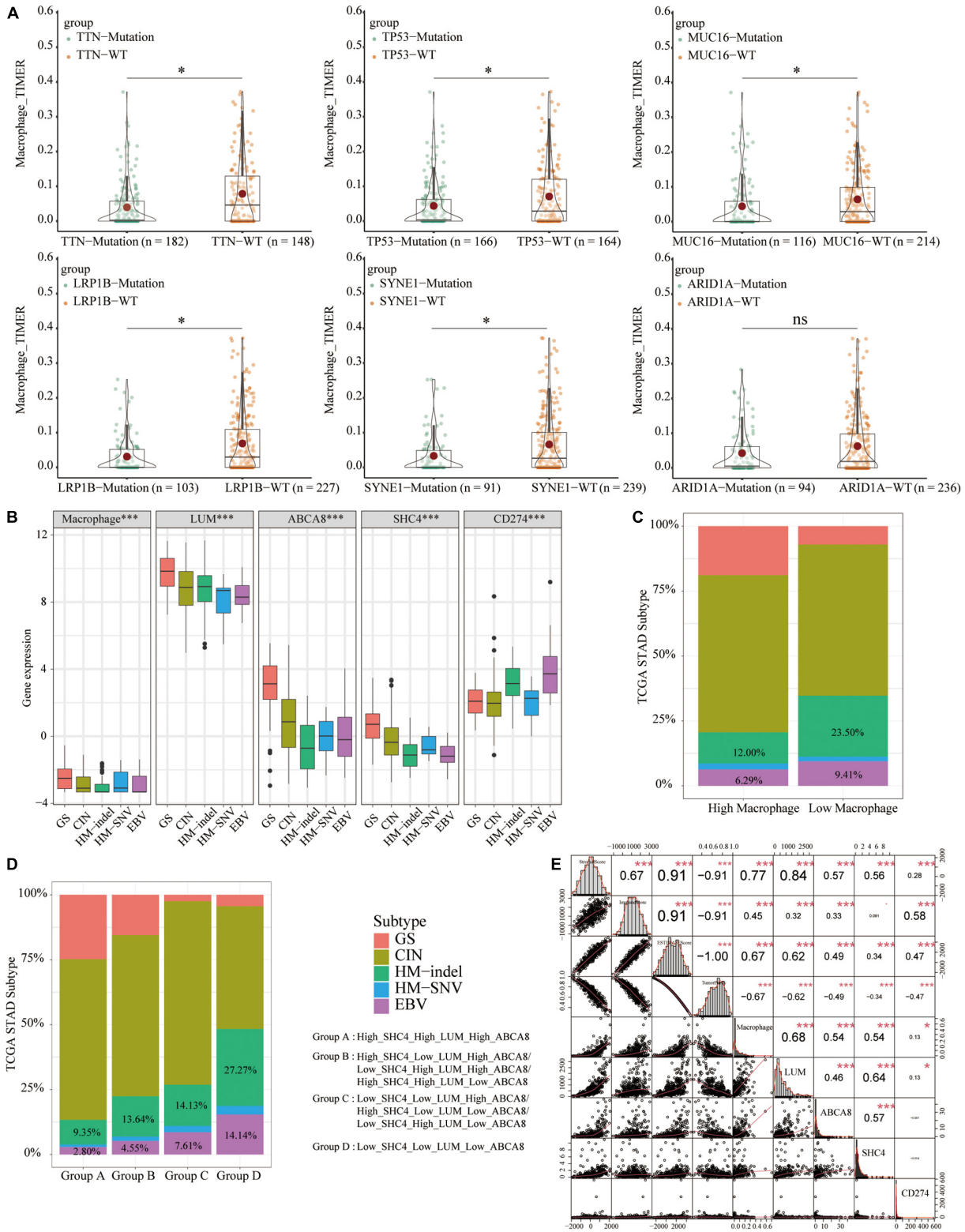

FIGURE 10 | Differences in the abundance of macrophages and 3 key genes and the correlation of tumor microenvironment score. **(A)** Among the 6 most frequently mutated genes, TTN/TP53/MUC16/LRP1B/SYNE1-mutant tissues had significantly lower macrophage abundance than WT tissues. **(B)** The EBV and HM-indel subtypes had lower macrophage abundance, expression of 3 key genes and higher expression of PD-L1. **(C)** STAD tissues in the low macrophage group had a higher proportion of HM-indel and EBV. **(D)** From group A to group D, the proportion of HM-indel and EBV significantly increased. **(E)** Macrophage abundance, 3 key genes and PD-L1 were all negatively correlated with tumor purity and positively correlated with stromal scores. $^{*}p < 0.05$, $^{***}p < 0.001$.

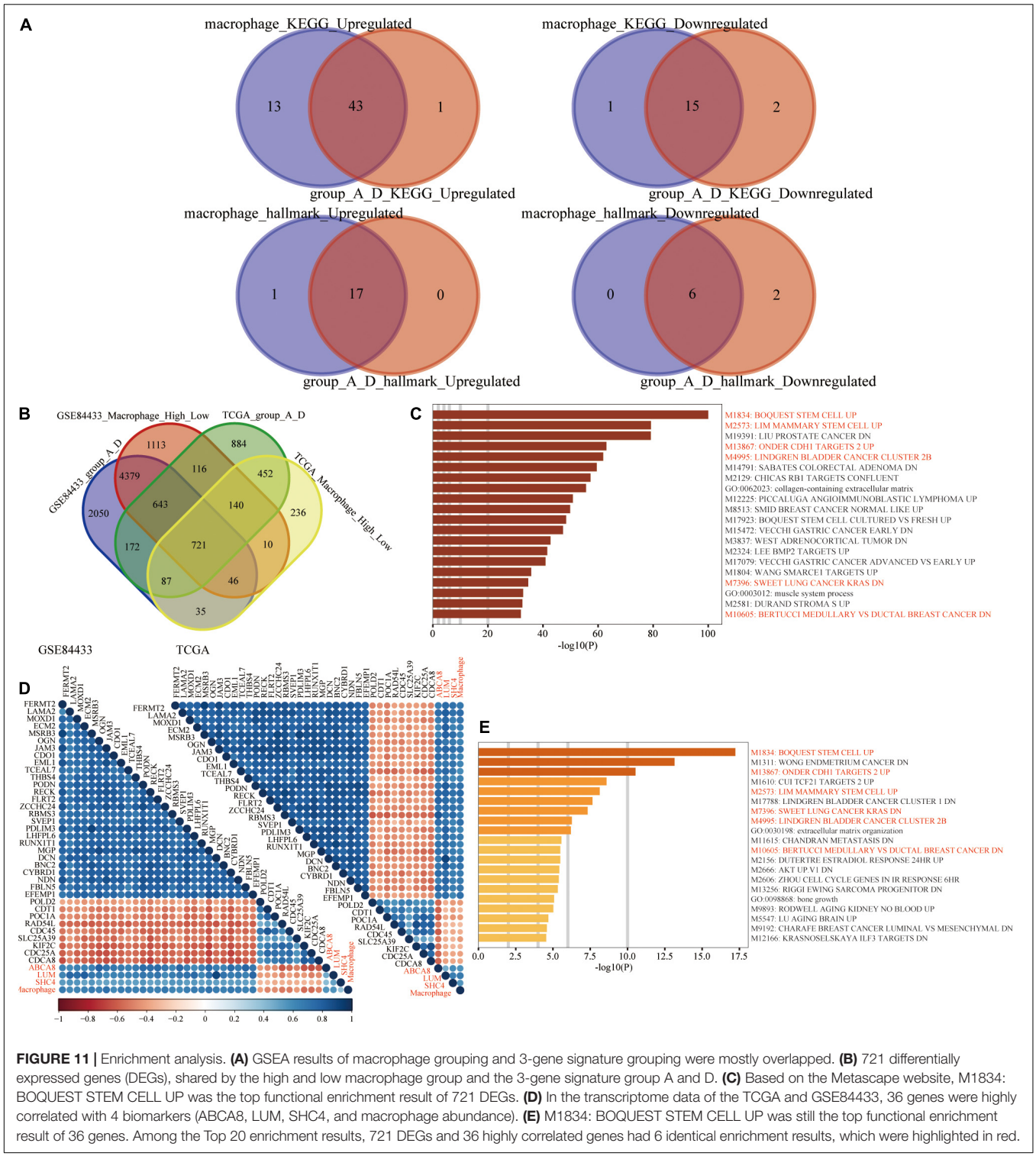

FIGURE 11 | Enrichment analysis. **(A)** GSEA results of macrophage grouping and 3-gene signature grouping were mostly overlapped. **(B)** 721 differentially expressed genes (DEGs), shared by the high and low macrophage group and the 3-gene signature group A and D. **(C)** Based on the Metascape website, M1834: BOQUEST STEM CELL UP was the top functional enrichment result of 721 DEGs. **(D)** In the transcriptome data of the TCGA and GSE84433, 36 genes were highly correlated with 4 biomarkers (ABCA8, LUM, SHC4, and macrophage abundance). **(E)** M1834: BOQUEST STEM CELL UP was still the top functional enrichment result of 36 genes. Among the Top 20 enrichment results, 721 DEGs and 36 highly correlated genes had 6 identical enrichment results, which were highlighted in red.

TCGA and GSE84433, between the high and low macrophage groups, groups A and D, differential expression analysis was performed, respectively. Based on the criteria of $|\log2(\text{fold-change})| > 1$ and false discovery rate < 0.05, we obtained 721 differentially expressed genes (**Figure 11B**). On the Metascape website, these 721 genes were mainly enriched in BOQUEST_STEM_CELL_UP (**Figure 11C**). Genes up-regulated in freshly isolated CD31- (stromal stem cells from adipose tissue) versus the CD31+ (non-stem) counterparts. On the other hand, we further performed Spearman correlation analysis among 19,584 protein-coding genes in the TCGA (Upper right) and 19,209 protein-coding genes in the GSE84433 (Bottom

left), respectively. Based on the following thresholds, Spearman correlation coefficients with 3 key genes, and macrophage abundance >0.5 or <-0.3, we finally obtained 36 genes (**Figure 11D**). Similarly, these 36 genes were still mainly enriched in BOQUEST_STEM_CELL_UP (**Figure 11E**).

Comparing the functional enrichment results of 721 shared differentially expressed genes and 36 highly correlated genes, macrophage abundance and the 3-gene signature were all enriched M1834: BOQUEST STEM CELL UP. We speculated that the molecular mechanisms by which macrophages and 3-gene signature worked were significantly related to the genes up-regulated by stromal stem cells.

The Prognosis and Correlation Significance of BOQUEST_STEM_CELL_UP

Based on the ssGSEA method, we calculated the scores of BOQUEST_STEM_CELL_UP in single STAD sample in the TCGA and GSE84433. Like the previous 2 signatures (macrophage abundance and 3-gene signature), the OS of low score group was significantly longer than that of high score group ($P < 0.05$) (**Figure 12A**). After calculating the Spearman correlation, BOQUEST_STEM_CELL_UP was significantly positively correlated with macrophage abundance and 3 key genes ($P < 0.05$) (**Figure 12B**). Similarly, for KEGG pathways and Hallmarks, GSEA results of low score group of BOQUEST_STEM_CELL_UP were consistent with that of low expression group of macrophage abundance and 3 key genes, all of which were highlighted in red (**Figure 12C**). Among them, "KEGG_DNA_REPLICATION," "KEGG_BASE_EXCISION_REPAIR," "KEGG_MISMATCH_REPAIR," and "KEGG_HOMOLOGOUS_RECOMBINATION" were TMB related pathways.

MicroRNA (miRNA) and RNA Binding Proteins (RBPs) Networks

To mine the connection between 3 key genes at the level of miRNA and RNA binding protein, we conducted the following research. On the Encyclopedia of RNA Interactomes (ENCORI) website, hsa-miR-335-5p was the only miRNA shared by 3 key genes (**Figure 13A**). Correlation analysis also revealed that hsa-miR-335-5p was negatively related to them ($P < 0.05$) (**Figure 13B**). This confirmed that 3 key genes might be target genes of Hsa-miR-335-5p. **Figure 13C** showed results of the KEGG enrichment pathways for the target genes of hsa-miR-335-5p. We also confirmed that hsa-miR-335-5p were significantly correlated with PD-L1 in 18 types of TCGA cancer including STAD (**Figure 14A**). As shown in **Figures 14B,C**, in STAD, hsa-miR-335-5p was also significantly correlated with CD8A and PDCD1. Hsa-miR-335-5p might be a novel immunotherapy targets.

In addition, there were 8 shared RBPs, namely IGF2BP2, UPF1, MBNL2, TAF15, PTBP1, EIF4A3, ELAVL1, and FUS, respectively (**Figure 13D**). In the TCGA (lower left) and GSE84433 (upper right) data sets, PTBP1 was the RBPs that were significantly negatively correlated with 3 key genes, while MBNL2 was positively correlated with them (**Figure 13E**).

DISCUSSION

Stomach adenocarcinoma (STAD) is one of the most common malignancies worldwide and is also a primary cause of cancer-related mortality (Cirri and Chiarugi, 2012). Recently, numerous of novel immune checkpoint inhibitors have been proposed to improve the survival rate (Kwak et al., 2020), however, which part of STAD patients is suitable for this therapy remains to be studied.

The abundance of immune cells in the tumor microenvironment (TME) strongly influence tumor progression and the efficacy of immunotherapy. Based on the above point of view, we designed 2 similar signatures to assess the prognosis and predict the immunotherapy efficacy of STAD patients at the same time. In terms of prognostic evaluation, the higher macrophage abundance, the shorter the overall survival (OS) of STAD patients. For 3-gene signature, the higher expression of 3 key genes, the shorter the OS of STAD patients. In the aspect of predicting the immunotherapy efficacy, the lower the abundance of macrophages, the better the efficacy of immunotherapy. STAD patients of the low macrophage group and group D were more suitable for immunotherapy and had a longer overall survival (OS).

Functional enrichment analysis and the ssGSEA algorithm showed that molecular mechanisms of 2 signatures for predicting prognosis and immunotherapy efficacy were significantly related to M1834: BOQUEST_STEM_CELL_UP, which represented genes up-regulated in freshly isolated CD31- (stromal stem cells) versus the CD31+ (non-stem) counterparts (Boquest et al., 2005). The direct molecular interaction mechanisms of BOQUEST_STEM_CELL_UP predicting prognosis and immune efficacy urgently needed more wet experimental research.

MicroRNA (miRNA) is a class of non-coding single-stranded RNA with a length of approximately 22 nucleotides encoded by endogenous genes. We found that Hsa-miR-335-5p could simultaneously regulate the expression of 3 key genes, PD-L1, CD8A and PDCD1, indicating that up-regulating the expression of Hsa-miR-335-5p might be a novel biomarker. Previous research had confirmed that 2 prognostic modules of osteosarcoma were regulated by Hsa-miR-335-5p (Chen et al., 2018) and Hsa-miR-335-5p was a protective factor for rectal cancer (Slattery et al., 2015). The therapeutic and prognostic roles of Hsa-miR-335-5p in the STAD urgently needed more experimental studies.

Gene Set Enrichment Analysis (GSEA) revealed that 2 signatures were similar in molecular mechanisms. GSEA between high expression of LUM/ABCA8/SHC4/macrophage abundance/BOQUEST_STEM_CELL_UP and low of that were focused on 10 KEGG pathways and 4 hallmark gene sets. Above 14 gene sets might play a crucial role in the prognosis and immunotherapy of STAD patients.

This study constructed a 3-gene signature associated with macrophage abundance for the first time. Previous studies had proved that 3 key genes were related to the prognosis

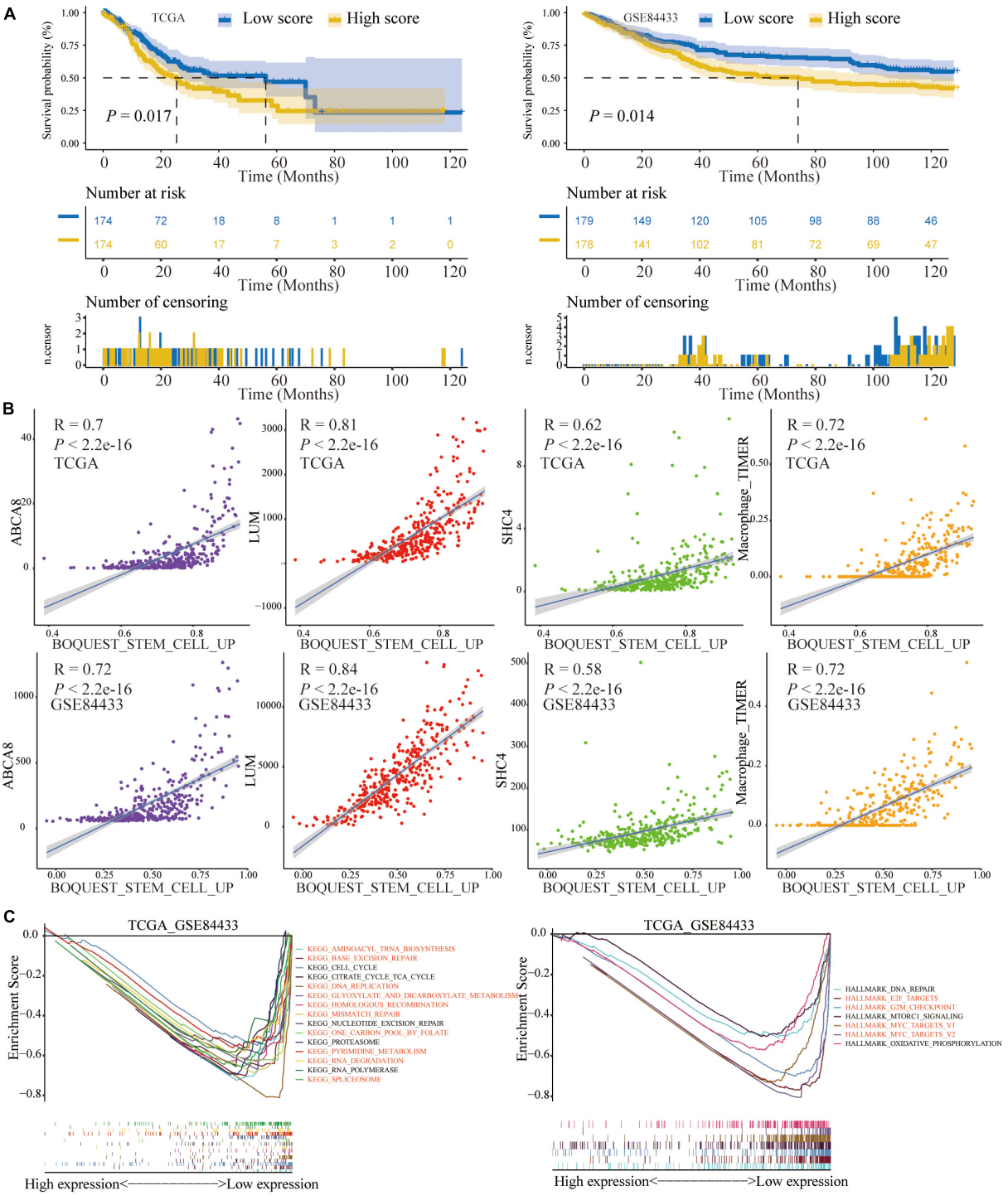

FIGURE 12 | The prognosis and correlation significance of BOQUEST_STEM_CELL_UP score. **(A)** The OS of low BOQUEST_STEM_CELL_UP group was significantly longer than that of high group. **(B)** Three key genes and macrophage abundance were significantly positively related with BOQUEST_STEM_CELL_UP score. **(C)** GSEA results between high and low BOQUEST_STEM_CELL_UP group, most of which were similar with that of 3 key genes and macrophage abundance and highlighted in red.

of GC patients, but the potential for predicting the efficacy immunotherapy had never been mentioned. Studies on these 3 genes were explicitly introduced as follows.

ATP Binding Cassette Subfamily A Member 8 (ABCA8) is a member of the superfamily of ATP-binding cassette (ABC) transporters. Members of the ABC1 subfamily comprise the

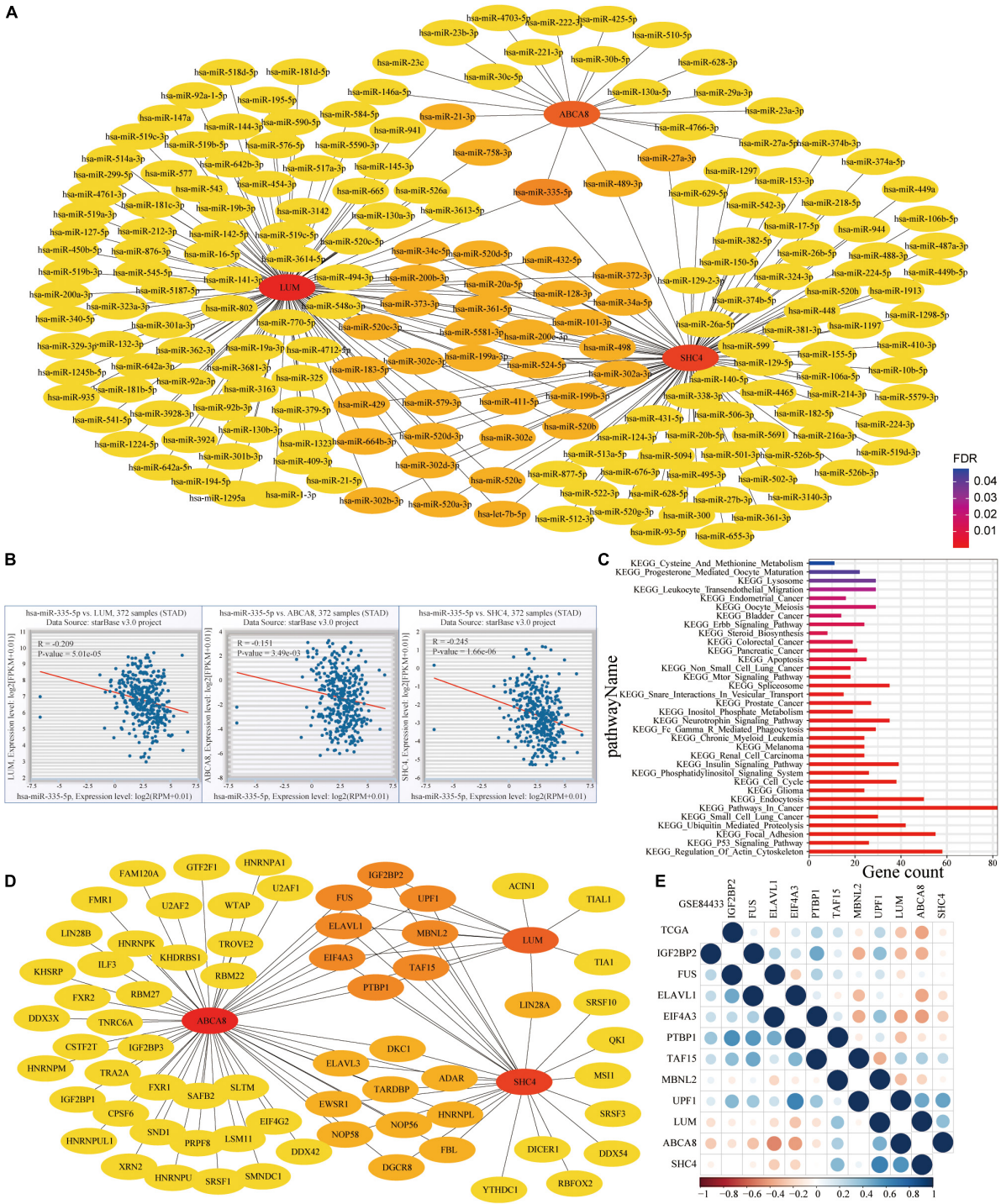

FIGURE 13 | MicroRNA (miRNA) and RNA binding proteins (RBPs) networks of 3 key genes. **(A)** MiRNAs of LUM, ABCA8 and SHC4. **(B)** Hsa-miR-335-5p, shared by 3 key genes, was significantly and negatively related to them. **(C)** KEGG enrichment results for the target genes of hsa-miR-335-5p. **(D)** RBPs of 3 key genes. **(E)** Spearman correlation between 3 key genes and 8 shared RBPs in the TCGA and GSE84433.

only major ABC subfamily found exclusively in multicellular eukaryotes (Tsuruoka et al., 2002). Specifically, ABCA8 regulated lipid metabolism and participated in the formation and maintenance of myelin (Kim et al., 2013). An article on its relevance to the prognosis of GC patients had been published in 2020 (Ding et al., 2020).

Lumican (LUM) is a member of the small leucine-rich proteoglycan family, which plays the dual role of oncogene

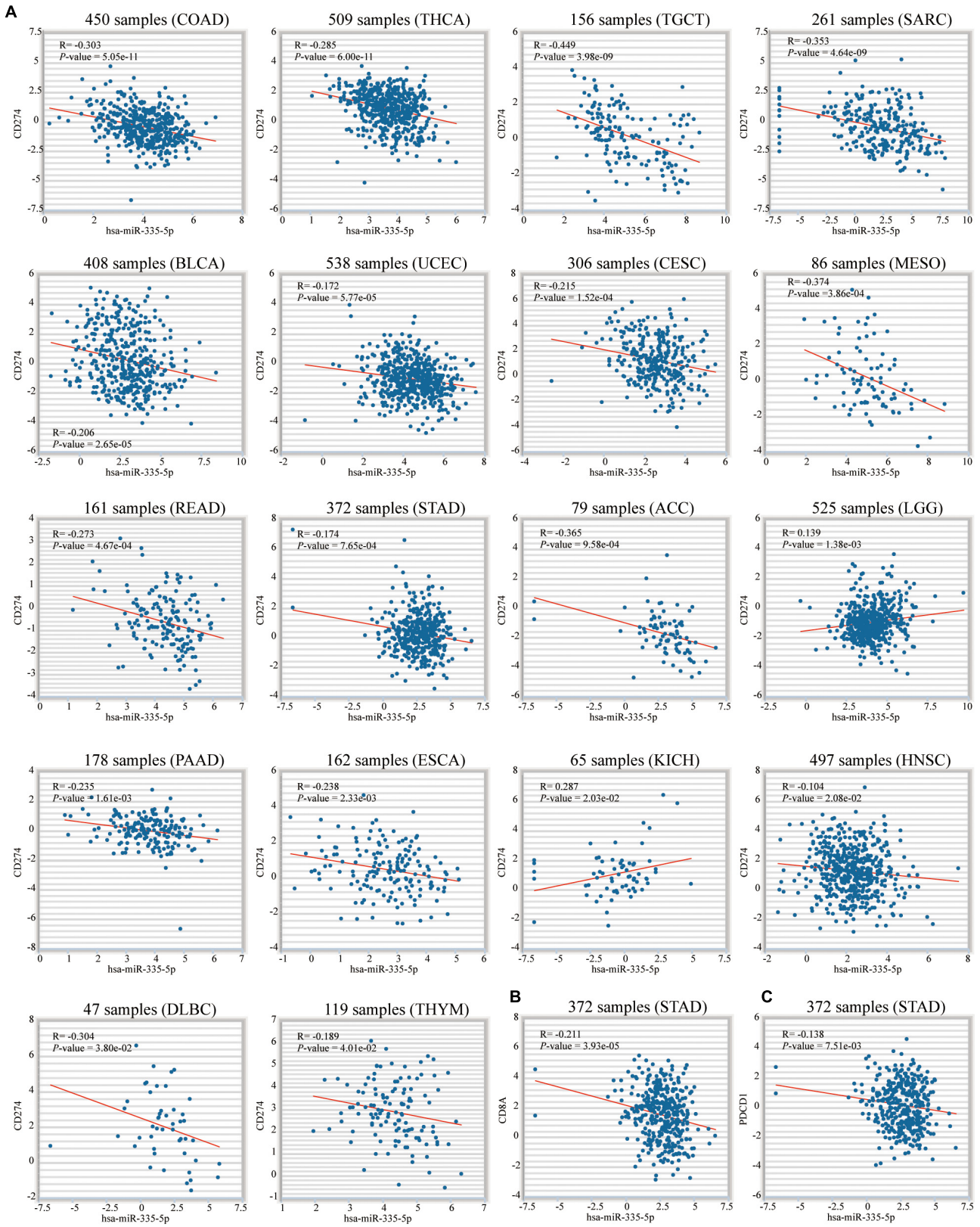

FIGURE 14 | Correlation between hsa-miR-335-5p and PD-L1, CD8A and PDCD1. **(A)** Among 18 TCGA cancers including STAD, hsa-miR-335-5p was significantly associated with PD-L1. In STAD, hsa-miR-335-5p is significantly related to **(B)** CD8A and **(C)** PDCD1.

and tumor suppressor gene (Nikitovic et al., 2008). In GC, LUM plays a role as an oncogene and may be regarded as a potential prognostic indicator and treatment target for GC patients (Chen et al., 2020).

SHC Adaptor Protein 4 (SHC4) is a member of the SHC adaptor protein family. SHC family proteins are implicated in the coupling of RTK to the Ras/mitogen-activated protein kinase signaling cascade (You et al., 2010). Overexpression of SHC4 in melanoma is a prerequisite for melanoma migration and invasion. And SHC4 nuclear translocation protects melanoma cells from DNA damage caused by oxidative stress (Ahmed and Prigent, 2014). In GC, SHC4 is an independent prognostic factor (Tian et al., 2020).

To further determine which types of macrophages were related to the prognosis of STAD patients, based on the CIBERSORT algorithm, we mined the correlation between M0, M1, and M2 macrophages and the prognosis of STAD patients and M0/M1/M2 macrophages alone could not predict the prognosis of GC patients. The role of macrophage subtypes M0/M1/M2 in prognosis and immunotherapy urgently needed more research.

In order to increase the credibility, our study included multiple data sets from different sources, including TCGA, GSE8444, GSE26899, and GSE29272. We had demonstrated the potential of macrophage abundance and 3-gene signature to predict the immunotherapy efficacy from multiple perspectives, such as Tumor Mutational Burden (TMB), PD-L1, immune-related liquid molecules, immune checkpoints, STAD molecular subtype analysis and gene mutation. However, the biggest shortcoming of this study was that no wet experiments verification was performed.

CONCLUSION

The macrophage abundance and 3-gene signature could predict the prognosis and immunotherapy efficacy of STAD patients. Besides, the 3-gene signature made the macrophage abundance more feasible to be used in clinical practice. Hsa-miR-335-5p and BOQUEST_STEM_CELL_UP might be novel immunotherapy targets.

DATA AVAILABILITY STATEMENT

The datasets presented in this study can be found in online repositories. The names of the repository/repositories and accession number(s) can be found in the article/ **Supplementary Material**.

AUTHOR CONTRIBUTIONS

PW, SC, and YL: idea and design. TY and SC: data analysis, processing, and mapping. TY: manuscript writing. TY, PW, SZ, XW, JZ, SG, ZH, and JL: manuscript revision. All authors approved the final manuscript.

FUNDING

This research was supported by the National Natural Science Foundation of China (Nos. 81902384 and 81770522), the National Science and Technology Major Project of China (No. 2018ZX10723204), and the Scientific Research Seed Fund of Peking University First Hospital (No. 2019SF01).

ACKNOWLEDGMENTS

We sincerely thank the developers of R packages and the maintainers of the TCGA and GEO database, the TIMER2.0, cBioPortal, ENCORI, ONCOMINE, UALCAN, TarBase v.8, STRING, and Metascape website.

SUPPLEMENTARY MATERIAL

The Supplementary Material for this article can be found online at: https://www.frontiersin.org/articles/10.3389/fcell.2021.704242/full#supplementary-material

REFERENCES

Ahmed, S. B., and Prigent, S. A. (2014). A nuclear export signal and oxidative stress regulate ShcD subcellular localisation: a potential role for ShcD in the nucleus. *Cell Signal.* 26, 32–40. doi: 10.1016/j.cellsig.2013.09.003

Bang, Y. J., Van Cutsem, E., Feyereislova, A., Chung, H. C., Shen, L., Sawaki, A., et al. (2010). Trastuzumab in combination with chemotherapy versus chemotherapy alone for treatment of HER2-positive advanced gastric or gastro-oesophageal junction cancer (ToGA): a phase 3, open-label, randomised controlled trial. *Lancet* 376, 687–697. doi: 10.1016/s0140-6736(10)61121-x

Boquest, A. C., Shahdadfar, A., Frønsdal, K., Sigurjonsson, O., Tunheim, S. H., Collas, P., et al. (2005). Isolation and transcription profiling of purified uncultured human stromal stem cells: alteration of gene expression after *in vitro* cell culture. *Mol. Biol. Cell* 16, 1131–1141. doi: 10.1091/mbc.e04-10-0949

Cerami, E., Gao, J., Dogrusoz, U., Gross, B. E., Sumer, S. O., Aksoy, B. A., et al. (2012). The cBio cancer genomics portal: an open platform for exploring multidimensional cancer genomics data. *Cancer Discov.* 2, 401–404. doi: 10.1158/2159-8290.cd-12-0095

Chan, T. A., Yarchoan, M., Jaffee, E., Swanton, C., Quezada, S. A., Stenzinger, A., et al. (2019). Development of tumor mutation burden as an immunotherapy biomarker: utility for the oncology clinic. *Ann. Oncol.* 30, 44–56. doi: 10.1093/annonc/mdy495

Chandrashekar, D. S., Bashel, B., Balasubramanya, S.a.H, Creighton, C. J., Ponce-Rodriguez, I., Chakravarthi, B., et al. (2017). UALCAN: a portal for facilitating tumor subgroup gene expression and survival analyses. *Neoplasia* 19, 649–658. doi: 10.1016/j.neo.2017.05.002

Chen, H., Chong, W., Wu, Q., Yao, Y., Mao, M., and Wang, X. (2019). Association of *LRP1B* Mutation with tumor mutation burden and outcomes in melanoma and non-small cell lung cancer patients treated with immune check-point blockades. *Front. Immunol.* 10:1113. doi: 10.3389/fimmu.2019.01113

Chen, X., Li, X., Hu, X., Jiang, F., Shen, Y., Xu, R., et al. (2020). LUM expression and its prognostic significance in gastric cancer. *Front. Oncol.* 10:605. doi: 10.3389/fonc.2020.00605

Chen, Y., Chen, Q., Zou, J., Zhang, Y., and Bi, Z. (2018). Construction and analysis of a ceRNA-ceRNA network reveals two potential prognostic modules regulated by hsa-miR-335-5p in osteosarcoma. *Int. J. Mol. Med.* 42, 1237–1246.

Chin, C. H., Chen, S. H., Wu, H. H., Ho, C. W., Ko, M. T., and Lin, C. Y. (2014). cytoHubba: identifying hub objects and sub-networks from complex interactome. *BMC Syst. Biol.* 8(Suppl. 4):S11. doi: 10.1186/1752-0509-8-S4-S11

Cirri, P., and Chiarugi, P. (2012). Cancer-associated-fibroblasts and tumour cells: a diabolic liaison driving cancer progression. *Cancer Metastasis Rev.* 31, 195–208. doi: 10.1007/s10555-011-9340-x

Crowe, S. E. (2019). *Helicobacter* pylori Infection. *N. Engl. J. Med.* 380, 1158–1165.

Danilova, L., Ho, W. J., Zhu, Q., Vithayathil, T., De Jesus-Acosta, A., Azad, N. S., et al. (2019). Programmed Cell Death Ligand-1 (PD-L1) and CD8 expression profiling identify an immunologic subtype of pancreatic ductal adenocarcinomas with favorable survival. *Cancer Immunol. Res.* 7, 886–895. doi: 10.1158/2326-6066.cir-18-0822

Ding, Y., Chen, Y., Wu, M., Li, L., Huang, Y., Wang, H., et al. (2020). Identification of genes associated with gastric cancer survival and construction of a nomogram to improve risk stratification for patients with gastric cancer. *Oncol. Lett.* 20, 215–225.

Dong, Z. Y., Zhong, W. Z., Zhang, X. C., Su, J., Xie, Z., Liu, S. Y., et al. (2017). Potential predictive value of TP53 and KRAS mutation status for response to PD-1 blockade immunotherapy in lung adenocarcinoma. *Clin. Cancer Res.* 23, 3012–3024. doi: 10.1158/1078-0432.ccr-16-2554

Duffy, M. J., and Crown, J. (2019). Biomarkers for predicting response to immunotherapy with immune checkpoint inhibitors in cancer patients. *Clin. Chem.* 65, 1228–1238. doi: 10.1373/clinchem.2019.303644

Gao, J., Aksoy, B. A., Dogrusoz, U., Dresdner, G., Gross, B., Sumer, S. O., et al. (2013). Integrative analysis of complex cancer genomics and clinical profiles using the cBioPortal. *Sci. Signal.* 6:l1.

Hänzelmann, S., Castelo, R., and Guinney, J. (2013). GSVA: gene set variation analysis for microarray and RNA-seq data. *BMC Bioinformatics* 14:7. doi: 10.1186/1471-2105-14-7

Kang, J. H., Lee, S. I., Lim, D. H., Park, K. W., Oh, S. Y., Kwon, H. C., et al. (2012). Salvage chemotherapy for pretreated gastric cancer: a randomized phase III trial comparing chemotherapy plus best supportive care with best supportive care alone. *J. Clin. Oncol.* 30, 1513–1518. doi: 10.1200/jco.2011.39.4585

Kang, Y. K., Boku, N., Satoh, T., Ryu, M. H., Chao, Y., Kato, K., et al. (2017). Nivolumab in patients with advanced gastric or gastro-oesophageal junction cancer refractory to, or intolerant of, at least two previous chemotherapy regimens (ONO-4538-12, ATTRACTION-2): a randomised, double-blind, placebo-controlled, phase 3 trial. *Lancet* 390, 2461–2471. doi: 10.1016/s0140-6736(17)31827-5

Karagkouni, D., Paraskevopoulou, M. D., Chatzopoulos, S., Vlachos, I. S., Tastsoglou, S., Kanellos, I., et al. (2018). DIANA-TarBase v8: a decade-long collection of experimentally supported miRNA-gene interactions. *Nucleic Acids Res.* 46, D239–D245.

Kim, W. S., Hsiao, J. H., Bhatia, S., Glaros, E. N., Don, A. S., Tsuruoka, S., et al. (2013). ABCA8 stimulates sphingomyelin production in oligodendrocytes. *Biochem. J.* 452, 401–410. doi: 10.1042/bj20121764

Kwak, Y., Seo, A. N., Lee, H. E., and Lee, H. S. (2020). Tumor immune response and immunotherapy in gastric cancer. *J. Pathol. Transl. Med.* 54, 20–33. doi: 10.4132/jptm.2019.10.08

Leek, J. T., Johnson, W. E., Parker, H. S., Jaffe, A. E., and Storey, J. D. (2012). The sva package for removing batch effects and other unwanted variation in high-throughput experiments. *Bioinformatics* 28, 882–883. doi: 10.1093/bioinformatics/bts034

Li, J. H., Liu, S., Zhou, H., Qu, L. H., and Yang, J. H. (2014). starBase v2.0: decoding miRNA-ceRNA, miRNA-ncRNA and protein-RNA interaction networks from large-scale CLIP-Seq data. *Nucleic Acids Res.* 42, D92–D97.

Li, P., Xiao, J., Zhou, B., Wei, J., Luo, J., and Chen, W. (2020a). SYNE1 mutation may enhance the response to immune checkpoint blockade therapy in clear cell renal cell carcinoma patients. *Aging (Albany NY)* 12, 19316–19324. doi: 10.18632/aging.103781

Li, S., Chen, S., Wang, B., Zhang, L., Su, Y., and Zhang, X. (2020b). A Robust 6-lncRNA prognostic signature for predicting the prognosis of patients with colorectal cancer metastasis. *Front. Med. (Lausanne)* 7:56. doi: 10.3389/fmed.2020.00056

Li, T., Fan, J., Wang, B., Traugh, N., Chen, Q., Liu, J. S., et al. (2017). TIMER: a web server for comprehensive analysis of tumor-infiltrating immune cells. *Cancer Res* 77, e108–e110.

Li, T., Fu, J., Zeng, Z., Cohen, D., Li, J., Chen, Q., et al. (2020c). TIMER2.0 for analysis of tumor-infiltrating immune cells. *Nucleic Acids Res.* 48, W509–W514.

Liu, Y., Sethi, N. S., Hinoue, T., Schneider, B. G., Cherniack, A. D., Sanchez-Vega, F., et al. (2018). Comparative molecular analysis of gastrointestinal adenocarcinomas. *Cancer Cell* 33, 721–735.e8.

Love, M. I., Huber, W., and Anders, S. (2014). Moderated estimation of fold change and dispersion for RNA-seq data with DESeq2. *Genome Biol.* 15:550.

Martincorena, I., and Campbell, P. J. (2015). Somatic mutation in cancer and normal cells. *Science* 349, 1483–1489. doi: 10.1126/science.aab4082

Mayakonda, A., Lin, D. C., Assenov, Y., Plass, C., and Koeffler, H. P. (2018). Maftools: efficient and comprehensive analysis of somatic variants in cancer. *Genome Res.* 28, 1747–1756. doi: 10.1101/gr.239244.118

Melling, N., Grüning, A., Tachezy, M., Nentwich, M., Reeh, M., Uzunoglu, F. G., et al. (2016). Glasgow Prognostic Score may be a prognostic index for overall and perioperative survival in gastric cancer without perioperative treatment. *Surgery* 159, 1548–1556. doi: 10.1016/j.surg.2016.01.018

Nikitovic, D., Katonis, P., Tsatsakis, A., Karamanos, N. K., and Tzanakakis, G. N. (2008). Lumican, a small leucine-rich proteoglycan. *IUBMB Life* 60, 818–823. doi: 10.1002/iub.131

Oh, S. C., Sohn, B. H., Cheong, J. H., Kim, S. B., Lee, J. E., Park, K. C., et al. (2018). Clinical and genomic landscape of gastric cancer with a mesenchymal phenotype. *Nat. Commun.* 9:1777.

Pagès, F., Kirilovsky, A., Mlecnik, B., Asslaber, M., Tosolini, M., Bindea, G., et al. (2009). In situ cytotoxic and memory T cells predict outcome in patients with early-stage colorectal cancer. *J. Clin. Oncol.* 27, 5944–5951. doi: 10.1200/jco.2008.19.6147

Patel, S. P., and Kurzrock, R. (2015). PD-L1 expression as a predictive biomarker in cancer immunotherapy. *Mol. Cancer Ther.* 14, 847–856. doi: 10.1158/1535-7163.mct-14-0983

Ren, Q., Zhu, P., Zhang, H., Ye, T., Liu, D., Gong, Z., et al. (2020). Identification and validation of stromal-tumor microenvironment-based subtypes tightly associated with PD-1/PD-L1 immunotherapy and outcomes in patients with gastric cancer. *Cancer Cell Int.* 20:92.

Rhodes, D. R., Yu, J., Shanker, K., Deshpande, N., Varambally, R., Ghosh, D., et al. (2004). ONCOMINE: a cancer microarray database and integrated data-mining platform. *Neoplasia* 6, 1–6. doi: 10.1016/s1476-5586(04)80047-2

Ritchie, M. E., Phipson, B., Wu, D., Hu, Y., Law, C. W., Shi, W., et al. (2015). limma powers differential expression analyses for RNA-sequencing and microarray studies. *Nucleic Acids Res.* 43, e47. doi: 10.1093/nar/gkv007

Rizvi, N. A., Hellmann, M. D., Snyder, A., Kvistborg, P., Makarov, V., Havel, J. J., et al. (2015). Cancer immunology. Mutational landscape determines sensitivity to PD-1 blockade in non-small cell lung cancer. *Science* 348, 124–128.

Salati, M., Orsi, G., Smyth, E., Aprile, G., Beretta, G., De Vita, F., et al. (2019). Gastric cancer: translating novels concepts into clinical practice. *Cancer Treat Rev* 79, 101889. doi: 10.1016/j.ctrv.2019.101889

Shannon, P., Markiel, A., Ozier, O., Baliga, N. S., Wang, J. T., Ramage, D., et al. (2003). Cytoscape: a software environment for integrated models of biomolecular interaction networks. *Genome Res.* 13, 2498–2504. doi: 10.1101/gr.1239303

Slattery, M. L., Herrick, J. S., Mullany, L. E., Valeri, N., Stevens, J., Caan, B. J., et al. (2015). An evaluation and replication of miRNAs with disease stage and colorectal cancer-specific mortality. *Int. J. Cancer* 137, 428–438. doi: 10.1002/ijc.29384

Sung, H., Ferlay, J., Siegel, R. L., Laversanne, M., Soerjomataram, I., Jemal, A., et al. (2021). Global cancer statistics 2020: GLOBOCAN estimates of incidence and mortality worldwide for 36 cancers in 185 countries. *CA Cancer J. Clin.* 71, 209–249. doi: 10.3322/caac.21660

Tian, R., Hu, J., Ma, X., Liang, L., and Guo, S. (2020). Immune-related gene signature predict overall survival of gastric cancer patients with varying microsatellite instability status. *Aging (Albany NY)* 13, 2418–2435. doi: 10.18632/aging.202271

Tsuruoka, S., Ishibashi, K., Yamamoto, H., Wakaumi, M., Suzuki, M., Schwartz, G. J., et al. (2002). Functional analysis of ABCA8, a new drug transporter. *Biochem. Biophys. Res. Commun.* 298, 41–45.

Vera Alvarez, R., Pongor, L. S., Mariño-Ramírez, L., and Landsman, D. (2019). TPMCalculator: one-step software to quantify mRNA abundance of genomic features. *Bioinformatics* 35, 1960–1962. doi: 10.1093/bioinformatics/bty896

Wang, G., Hu, N., Yang, H. H., Wang, L., Su, H., Wang, C., et al. (2013). Comparison of global gene expression of gastric cardia and noncardia cancers from a high-risk population in china. *PLoS One* 8:e63826.

Waniczek, D., Lorenc, Z., Śnietura, M., Wesecki, M., Kopec, A., and Muc-Wierzgoń, M. (2017). Tumor-associated macrophages and regulatory T cells infiltration and the clinical outcome in colorectal cancer. *Arch. Immunol. Ther. Exp. (Warsz)* 65, 445–454. doi: 10.1007/s00005-017-0463-9

Yang, Y., Zhang, J., Chen, Y., Xu, R., Zhao, Q., and Guo, W. (2020). MUC4, MUC16, and TTN genes mutation correlated with prognosis, and predicted tumor mutation burden and immunotherapy efficacy in gastric cancer and pan-cancer. *Clin. Transl. Med.* 10:e155.

Yoon, S. J., Park, J., Shin, Y., Choi, Y., Park, S. W., Kang, S. G., et al. (2020). Deconvolution of diffuse gastric cancer and the suppression of CD34 on the BALB/c nude mice model. *BMC Cancer* 20:314. doi: 10.1186/s12885-020-06814-4

Yoshihara, K., Shahmoradgoli, M., Martínez, E., Vegesna, R., Kim, H., Torres-Garcia, W., et al. (2013). Inferring tumour purity and stromal and immune cell admixture from expression data. *Nat. Commun.* 4:2612.

You, Y., Li, W., Gong, Y., Yin, B., Qiang, B., Yuan, J., et al. (2010). ShcD interacts with TrkB via its PTB and SH2 domains and regulates BDNF-induced MAPK activation. *BMB Rep.* 43, 485–490. doi: 10.5483/bmbrep.2010.43.7.485

Zhou, Y., Zhou, B., Pache, L., Chang, M., Khodabakhshi, A. H., Tanaseichuk, O., et al. (2019). Metascape provides a biologist-oriented resource for the analysis of systems-level datasets. *Nat. Commun.* 10:1523.

Conflict of Interest: The authors declare that the research was conducted in the absence of any commercial or financial relationships that could be construed as a potential conflict of interest.

Publisher's Note: All claims expressed in this article are solely those of the authors and do not necessarily represent those of their affiliated organizations, or those of the publisher, the editors and the reviewers. Any product that may be evaluated in this article, or claim that may be made by its manufacturer, is not guaranteed or endorsed by the publisher.

Copyright © 2021 Yue, Zuo, Zhu, Guo, Huang, Li, Wang, Liu, Chen and Wang. This is an open-access article distributed under the terms of the Creative Commons Attribution License (CC BY). The use, distribution or reproduction in other forums is permitted, provided the original author(s) and the copyright owner(s) are credited and that the original publication in this journal is cited, in accordance with accepted academic practice. No use, distribution or reproduction is permitted which does not comply with these terms.

frontiers in Cell and Developmental Biology

ORIGINAL RESEARCH
published: 03 August 2021
doi: 10.3389/fcell.2021.707143

The Prognosis and Immune Checkpoint Blockade Efficacy Prediction of Tumor-Infiltrating Immune Cells in Lung Cancer

*Xiangzheng Liu, Xueqian Shang, Jian Li and Shijie Zhang**

Department of Thoracic Surgery, Peking University First Hospital, Peking University, Beijing, China

Backgrounds: The high morbidity and mortality of lung cancer are serious public health problems. The prognosis of lung cancer and whether to apply immune checkpoint blockade (ICB) are currently urgent problems to be solved.

Methods: Using R software, we performed Kaplan–Meier (K-M) analysis, Cox regression analysis, functional enrichment analysis, Spearman correlation analysis, and the single-sample gene set enrichment analysis.

Results: On the Tumor IMmune Estimation Resource (TIMER2.0) website, we calculated the abundance of tumor-infiltrating immune cells (TIICs) of lung adenocarcinoma (LUAD) and lung squamous cell carcinoma (LUSC) patients. B cell and myeloid dendritic cell (DC1) were independent prognostic factors for LUAD and LUSC patients, respectively. Enrichment analysis confirmed that genes highly related to B cell or DC1 were closely related to the immune activation of lung cancer patients. In terms of adaptive immune resistance markers, CD8A, CD8B, immunomodulators (immunostimulants, major histocompatibility complex, receptors, and chemokines), immune-related pathways, tumor microenvironment score, and TIICs, high B cell/DC1 infiltration tissue was inflamed and immune-activated and might benefit more from the ICB. Genes most related to B cell [CD19, toll-like receptor 10 (TLR10), and Fc receptor-like A (FCRLA)] and DC1 (ITGB2, LAPTM5, and SLC7A7) partially clarified the roles of B cell/DC1 in predicting ICB efficacy. Among the 186 Kyoto Encyclopedia of Genes and Genomes (KEGG) pathways, there were three and four KEGG pathways, which partially explained the molecular mechanisms by which B cell and DC1 simultaneously predicted the prognosis and efficacy of immunotherapy, respectively. Among five immune subtypes, the abundance of B cell/DC1 and expression of six hub genes were higher in immune C2, C3, and C6.

Conclusion: B cell and DC1 could predict the prognosis and ICB efficacy of LUAD and LUSC patients, respectively. The six hub genes and seven KEGG pathways might be novel immunotherapy targets. Immune C2, C3, and C6 subtypes of lung cancer patients might benefit more from ICB therapy.

Keywords: lung cancer, B cell, myeloid dendritic cell, prognosis, immune checkpoint blockade

OPEN ACCESS

Edited by:
Zimu Deng,
Shanghai Institute of Biochemistry and Cell Biology, Chinese Academy of Sciences (CAS), China

Reviewed by:
Shasha Zhang,
Southeast University, China
Guangyu Wang,
Houston Methodist Research Institute, United States

***Correspondence:**
Shijie Zhang
shijie_zhang_bjmu@163.com

Specialty section:
This article was submitted to Molecular and Cellular Pathology, a section of the journal Frontiers in Cell and Developmental Biology

Received: *09 May 2021*
Accepted: *30 June 2021*
Published: *03 August 2021*

Citation:
Liu X, Shang X, Li J and Zhang S (2021) The Prognosis and Immune Checkpoint Blockade Efficacy Prediction of Tumor-Infiltrating Immune Cells in Lung Cancer. Front. Cell Dev. Biol. 9:707143. doi: 10.3389/fcell.2021.707143

INTRODUCTION

According to Global Cancer Statistics 2020, lung cancer is the most common cause of cancer-related deaths worldwide, whose incidence rate ranks second (second only to breast cancer). Specifically, in 2020, there were 2.2 million new cases and 1.8 million new deaths (Sung et al., 2021). Non-small cell lung cancer (NSCLC) is the main histologic subtypes (accounting for 85%) of lung cancer, of which approximately 50% are lung adenocarcinoma (LUAD) and approximately 30% are lung squamous cell carcinoma (LUSC) (Perez-Moreno et al., 2012).

The unoptimistic mortality rate makes lung cancer patients full of doubts about how long they can live, which is a problem that clinicians cannot avoid and facilitates the construction of various prognostic signatures (He and Zuo, 2019; Zuo et al., 2019). In terms of treatment, apart from traditional chemotherapy, targeted therapy, and antiangiogenesis therapy, novel immunotherapy based on programmed cell death ligand 1 (PD-L1, also called CD274)/ligand of programmed cell death 1 (PD-1), has attracted increasing attention. However, adhering to the principles of personalized medicine and precision medicine, which lung cancer patients might benefit more from immunotherapy, is a vital issue that urgently needs to be solved. Therefore, it is crucial to identify new targets or signatures that could predict both prognosis and immunotherapy efficacy of lung cancer patients.

In our study, based on the Tumor IMmune Estimation Resource (TIMER2.0), we quantified the abundance of tumor-infiltrating immune cells (TIICs) in the tumor microenvironment (TME) of The Cancer Genome Atlas (TCGA)-LUAD and TCGA-LUSC. Kaplan–Meier (K-M) and Cox regression analysis proved that B cell and myeloid dendritic cell (DC1) were independent prognostic factors for LUAD and LUSC patients, respectively. The functional enrichment analysis of genes highly related to B cell or DC1 (Spearman correlation coefficient >0.6) in lung cancer focused on B cell activation and T cell activation, respectively, indicating that the above two prognostic factors were significantly related to the activation of immune system of lung cancer. In terms of the expression of adaptive immune resistance markers, CD8A, CD8B, immunomodulators [immunostimulants, major histocompatibility complex (MHC), receptors, and chemokines], immune-related pathways, and TIICs, compared with tumor tissues in the low B cell/DC1 infiltration group, most immune biomarkers were significantly upregulated in the high B cell group (LUAD) or high DC1 group (LUSC). The above results indicated that high B cell/DC1 infiltration could shape an inflamed and immune-activated TME. We concluded that this part of lung cancer patients might benefit more from immune checkpoint blockade (ICB) therapy.

Abbreviations: TCGA, The Cancer Genome Atlas; GEO, Gene Expression Omnibus; LUAD, lung adenocarcinoma; LUSC, lung squamous cell carcinoma; TIICs, tumor-infiltrating immune cells; DC1, myeloid dendritic cell; OS, overall survival; TME, tumor microenvironment; ssGSEA, single-sample gene set enrichment analysis; ICB, immune checkpoint blockade.

For the convenience of clinical application, we then obtained genes most related to B cell [CD19, toll-like receptor 10 (TLR10), and FCRLA] or DC1 (ITGB2, LAPTM5, and SLC7A7). In pan-cancer, we confirmed that they were significantly related to CD8A, CD8B, and PD-L1. The protein–protein interaction (PPI) functional enrichment results were significantly related to the activation and proliferation of immune cells, which further confirmed that six hub genes were significantly related to the activation of immune system. Given the overall TME scores of LUAD and LUSC patients, B cell, DC1, and six hub genes, like CD8A, CD8B, and PD-L1, were significantly positively correlated with stromal score and immune score and significantly negatively correlated with tumor purity. Besides, compared with the ICB non-response group (NR), the response group (R) had higher expression of six hub genes and abundance of B cell and DC1. Among five immune subtypes of lung cancer, immune C2, C3, and C6 of LUAD and LUSC might be easier to benefit from ICB treatment.

To further explore the molecular mechanisms of B cell and DC1 in predicting the prognosis and the efficacy of immunotherapy at the same time, among 186 Kyoto Encyclopedia of Genes and Genomes (KEGG) pathways, we mined three KEGG pathways in LUAD tissues, which clarified the mechanisms by which B cell predicted the prognosis and ICB response of LUAD patients. Similarly, for LUSC patients, we investigated four KEGG pathways, elucidating the molecular pathways of DC1 predicting the overall survival (OS) and ICB reactivity.

In conclusion, through these three KEGG pathways, B cell abundance predicted the OS and ICB response of LUAD patients. For LUCS patients, four KEGG pathways were the molecular mechanisms of DC1 that both predicted the prognosis and the ICB efficacy. The above seven KEGG pathways were expected to become new immunotherapy targets. Among the five immune subtypes of lung cancer patients, immune C2, C3, and C6 subtypes might benefit more from ICB therapy.

MATERIALS AND METHODS

Data Source

The transcriptome expression profiles and clinical information of LUAD and LUSC were downloaded from TCGA[1] and Gene Expression Omnibus (GEO) database[2]. Fragment per kilobase of transcript per million mapped reads (FPKM) was converted to TPM (transcript per kilobase of exon model per million mapped reads) and used in this study. For TCGA-LUAD, 512 LUAD tissues and 58 adjacent normal tissues were included in our study. In terms of TCGA-LUSC, there were 497 LUSC samples and 49 LUSC adjacent normal samples. For GSE31210, there were 226 LUAD tissues and 20 normal tissues. For GSE157009, there were 249 LUSC tissues without normal samples. Specific

[1]https://portal.gdc.cancer.gov/

[2]https://www.ncbi.nlm.nih.gov/geo/

TABLE 1 | The clinical characteristics of lung cancer patients in our study.

Variables	TCGA LUAD	TCGA LUSC	GSE31210 LUAD	GSE157009 LUSC
Total	512	497	226	249
Female (%)	276 (53.9)	129 (26.0)	121 (53.5)	88 (35.3)
Male (%)	236 (46.1)	368 (74.0)	105 (46.5)	161 (64.7)
Age (median [IQR])	66.00 [59.00, 73.00]	68.00 [62.00, 73.00]	61.00 [55.00, 65.00]	70.00 [64.00, 76.00]
T (%)				
NA	3 (0.6)	0 (0.0)		
T1	168 (32.8)	112 (22.5)		
T2	277 (54.1)	292 (58.8)		
T3	45 (8.8)	70 (14.1)		
T4	19 (3.7)	23 (4.6)		
N (%)				
NA	12 (2.3)	5 (1.0)		
N0	328 (64.1)	317 (63.8)		
N1	96 (18.8)	130 (26.2)		
N2	74 (14.5)	40 (8.0)		
N3	2 (0.4)	5 (1.0)		
M (%)				
NA	142 (27.7)	83 (16.7)		
M0	345 (67.4)	407 (81.9)		
M1	25 (4.9)	7 (1.4)		
Stage (%)				
NA	7 (1.4)	4 (0.8)		
Stage i	274 (53.5)	242 (48.7)	168 (74.3)	123 (49.4)
Stage ii	121 (23.6)	160 (32.2)	58 (25.7)	108 (43.4)
Stage iii	84 (16.4)	84 (16.9)		18 (7.2)
Stage iv	26 (5.1)	7 (1.4)		

clinical information of LUAD and LUSC patients is shown in **Table 1**.

Quantification of TIICs

The TIMER2.0[3] is a friendly platform for systematical evaluations of the clinical impact of different immune cells in diverse cancer types (Li et al., 2020). The abundance of TIICs, including B cell, CD4 T cell, CD8 T cell, macrophage, neutrophil, and DC1, was estimated on the 2.0 version of this website. Gene_Corr module is used to explore the correlation between interested genes with a list of genes in pan-cancer.

The Prognostic Significance of Six Types of TIICs

Based on the median abundance of TIICs, we performed K-M analysis and log-rank test on the high- and low-infiltration groups. With the help of "survival" and "survminer" packages, we plotted survival curves. The Cox regression analysis was also included in our study and displayed in forest maps (In and Lee, 2019). Green represents univariate Cox analysis, whereas red represents multivariate Cox analysis.

[3]http://cistrome.dfci.harvard.edu/TIMER/

The Functional Enrichment Analysis

Among the transcriptome 19,464 protein-coding genes, taking the absolute Spearman correlation coefficient greater than 0.6 as the threshold (strong correlation) (Lin et al., 2016; Chen et al., 2017), we obtained genes that were highly related to B cell and DC1 in the TCGA-LUAD and TCGA-LUSC cohorts, respectively. Based on these highly related genes and "clusterProfiler" package, we performed Gene Ontology (GO) and KEGG analysis.

The Single-Sample Gene Set Enrichment Analysis

The single-sample gene set enrichment analysis (ssGSEA) is an extension of GSEA and calculates a separate enrichment score for each sample. Each ssGSEA enrichment score represents the degree to which the genes in a particular gene set are coordinately upregulated or downregulated within a sample (Subramanian et al., 2005). In our study, based on the "GSVA" package (Hänzelmann et al., 2013) and gene sets [30 immune-related pathways (Shang et al., 2020) and 186 KEGG pathways], the ssGSEA score was used to explore the differences in the activation status of immune system between the high and low B cell/DC1 groups and mine the molecular mechanisms of B cell and DC1 in predicting prognosis and ICB efficacy. The above gene sets were downloaded from the MSigDB database[4] (Liberzon et al., 2011).

The GeneMANIA Database

The GeneMANIA[5] is a database similar to STRING, based on which we can find genes with similar functions of interested genes and predict gene functions simultaneously (Warde-Farley et al., 2010).

The Stromal and Immune Scores of the TME and Tumor Purity

Infiltrating stromal cells and immune cells constitute the main part of normal cells in tumor tissues, which not only disrupt tumor signals in molecular research, but also play crucial roles in cancer biology. The abundance of non-tumor cells (stromal cells and immune cells) and tumor purity of lung cancer tissues could be evaluated by incorporating two gene signatures (the stromal and immune signatures) using the ESTIMATE (using expression data to estimate stromal cells and immune cells in malignant tumor tissue) algorithm (Yoshihara et al., 2013). The stromal signature was used to capture stromal cells in the TME, whereas the immune signature was designed to represent the immune cell abundance in tumor tissues. The results of ESTIMATE algorithm were presented as immune score, stromal score, and ESTIMATE score. The higher the score, the greater the ratio of the corresponding component in the TME. Based on the ESTIMATE score, we further inferred tumor purity in tumor tissues.

[4]https://www.gsea-msigdb.org/gsea/msigdb/index.jsp

[5]http://www.genemania.org

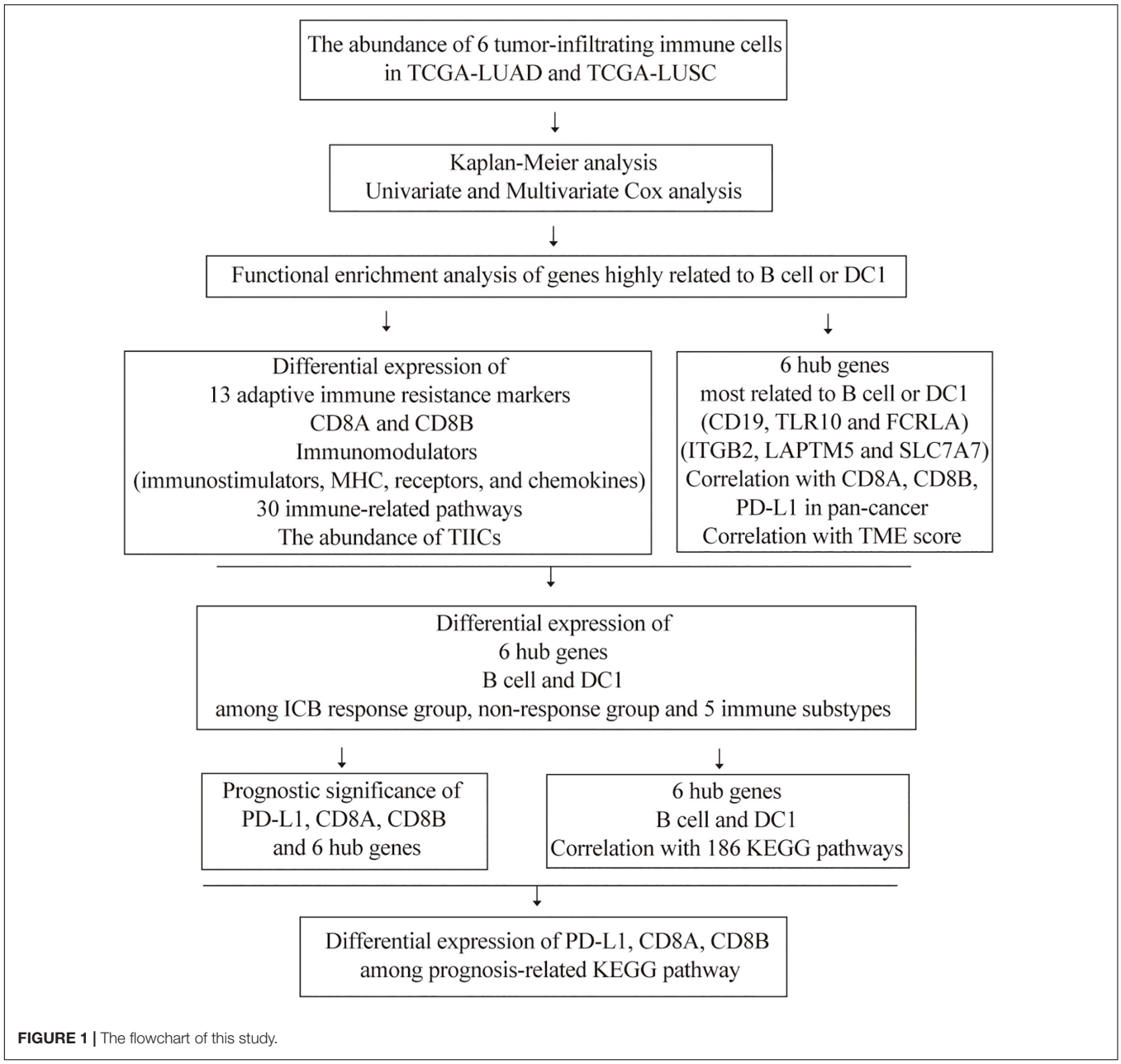

FIGURE 1 | The flowchart of this study.

The Efficacy Prediction of ICB

On the Immune Cell Abundance Identifier (ImmuCellAI) website[6], we predicted the ICB efficacy of lung cancer patients and divided them into the ICB response group and non-response group (Miao et al., 2020).

Correlation Diagram and Heatmap

In our research, we plotted correlation diagrams using "corrplot" and "PerformanceAnalytics" packages. With the "pheatmap" package, we draw heatmaps. To generate the heatmaps, data were log2-transformed. Each column represents a sample, and each row represents one of the immunomodulators. The levels of immunomodulators are displayed in different colors, which transition from blue to red with increasing expression.

Ethics Statement

All data in our study were obtained from the online public database, TCGA and GEO, and did not involve any *in vitro* or *in vivo* experiments.

Statistical Analysis

All statistical analyses were performed in R software (version 4.0.3). As gene expression and immune cell abundance did

[6]http://bioinfo.life.hust.edu.cn/web/ImmuCellAI/

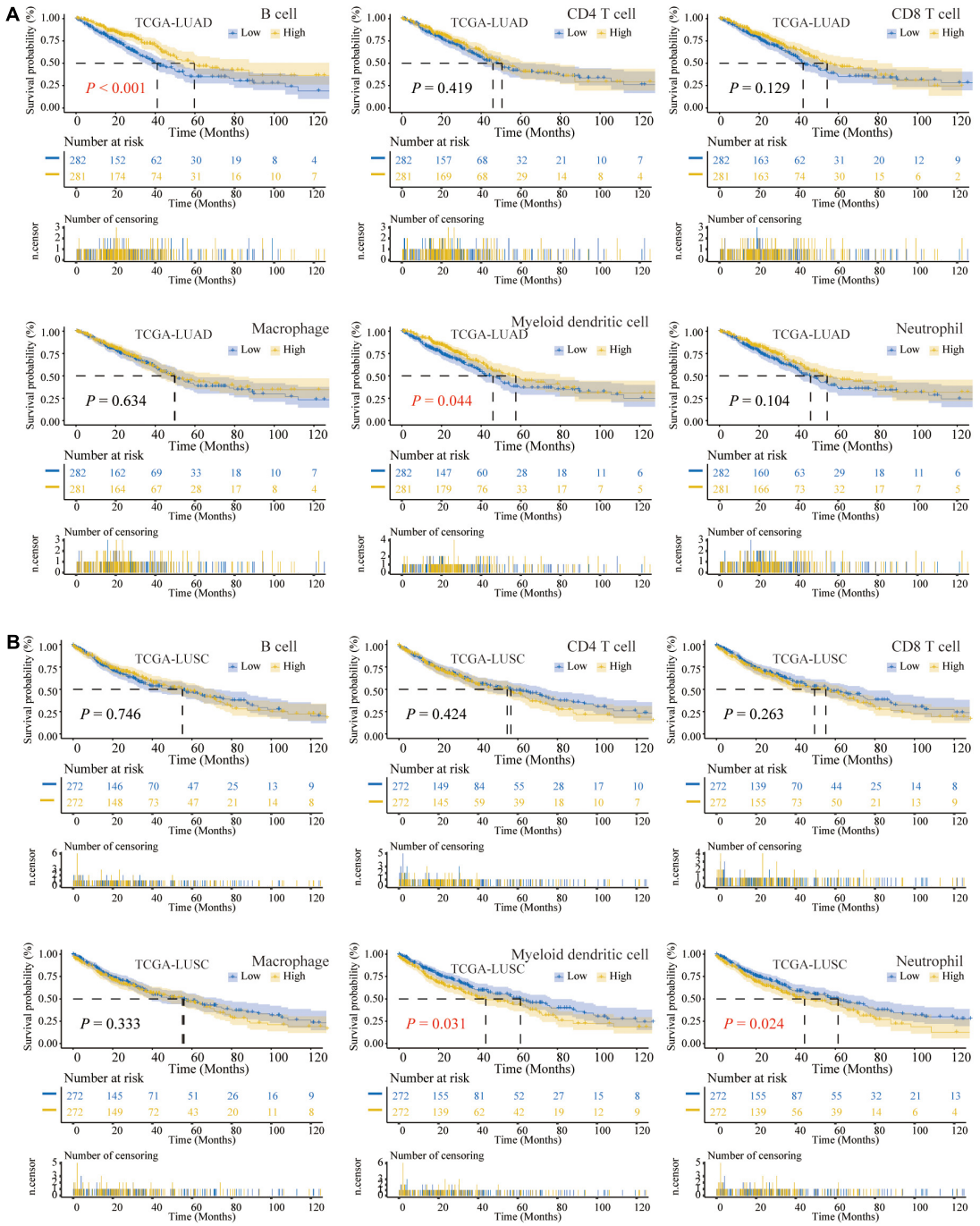

FIGURE 2 | The Kaplan–Meier (K-M) analysis and log-rank test of six types of tumor-infiltrating immune cells (TIICs) in lung cancer. **(A)** For TCGA-LUAD, the higher the abundance of B cell or DC1, the longer the overall survival (OS). **(B)** In TCGA-LUSC, the lower the infiltration of DC1 or neutrophil, the longer the OS.

not conform to the normal distribution, differences between two groups were tested by the Wilcoxon test, and differences between multiple groups were tested by the Kruskal–Wallis test. Based on the "ggstatsplot" package, the *P*-values were corrected for multiple testing using the Dunn test. $P < 0.05$ was considered statistically significant: $^{*}p < 0.05$, $^{**}p < 0.01$, $^{***}p < 0.001$.

RESULTS

The Survival Correlation of TIICs in Lung Cancer

The flowchart of our study is shown in **Figure 1**. Previous studies had confirmed that the abundance of TIICs was

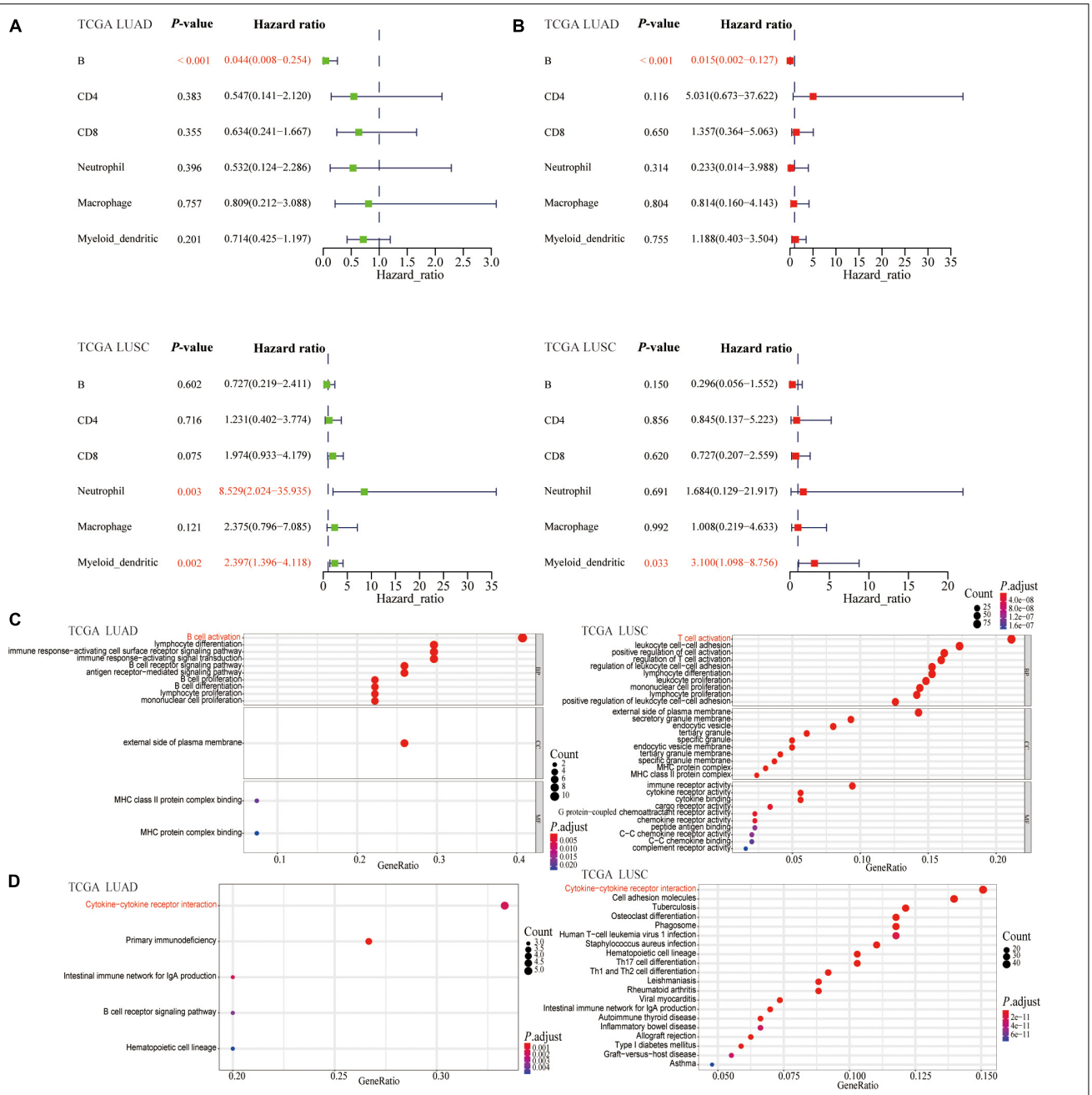

FIGURE 3 | The Cox regression analysis and function enrichment analysis. **(A)** The univariate Cox regression (green) and **(B)** multivariate Cox regression (red) analysis of six types of TIICs in LUAD and LUSC. The vertical dashed line represents HR = 1. B cell was a protective factor for LUAD (HR < 1), whereas DC1 was a harmful factor of LUSC (HR > 1). **(C)** GO and **(D)** KEGG enrichment analysis of 29 genes strongly related to B cell in TCGA-LUAD and 487 genes highly related to DC1 in TCGA-LUSC, respectively. The horizontal axis, gene ratio, represents the proportion of highly related genes contained in the corresponding term to the total highly related genes. The size of the dot indicates the number of highly related genes contained in the corresponding term.

closely related to the prognosis of cancer patients (Pagès et al., 2009; Waniczek et al., 2017). Based on the TIMER2.0, we quantified the abundance of TIICs in the TME of the TCGA-LUAD and TCGA-LUSC cohorts, including three types related to adaptive immunity: B cell, CD4 T cell, and CD8 T cell, as well as three types related to innate immunity: macrophage, DC1, and neutrophil. Among the above six TIICs, we performed K-M analysis and log-rank test. The OS of LUAD patients with high B cell or DC1 infiltration was longer than that of the low-infiltration group ($P < 0.05$) (**Figure 2A**), whereas compared with the high-infiltration group, LUSC patients with low DC1 or neutrophil infiltration had longer OS ($P < 0.05$) (**Figure 2B**). Therefore, B cell and DC1 were significantly related to the survival of LUAD patients, whereas

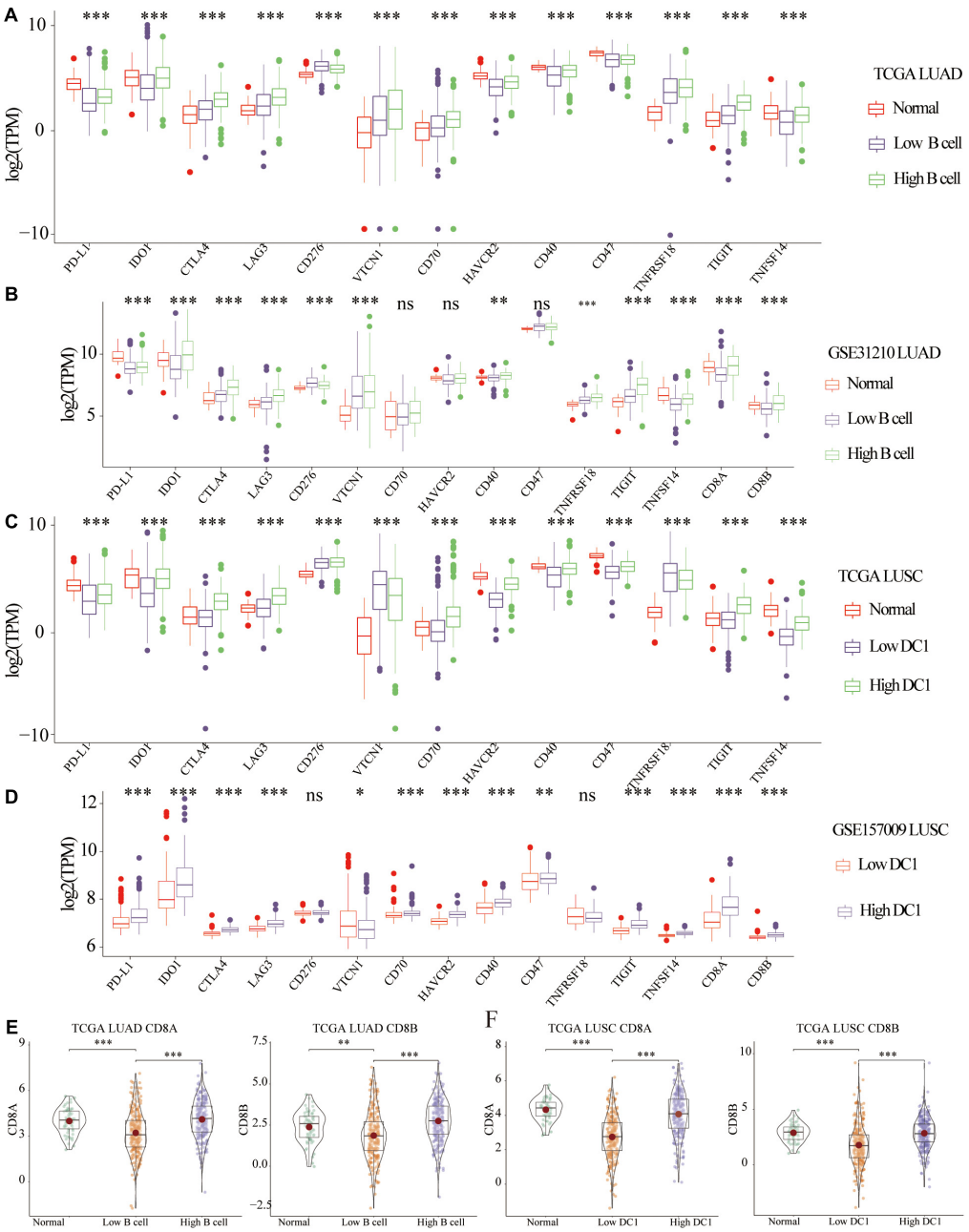

FIGURE 4 | Expression profiles of adaptive immune resistance markers and CD8A and CD8B in LUAD and LUSC. Differential expression of adaptive immune resistance markers among normal, low, and high B cell groups in **(A)** TCGA LUAD and **(B)** GSE31210 LUAD cohorts. Differential expression of adaptive immune resistance markers among normal, low DC1, and high DC1 groups in **(C)** TCGA LUSC and **(D)** GSE157009 LUSC cohorts. Differential expression of CD8A and CD8B in **(B)** GSE31210 LUAD, **(E)** TCGA LUAD, **(D)** GSE157009 LUSC, and **(F)** TCGA LUSC cohorts. *$p < 0.05$ **$p < 0.01$, ***$p < 0.001$.

DC1 and neutrophil were significantly related to the survival of LUSC patients.

The Prognostic Significance of TIICs in Lung Cancer

The prognostic landscapes of TIICs in lung cancer were characterized in forest plots. The univariate Cox regression analysis revealed that B cell was associated with good prognosis [hazard ratio (HR) = 0.044, 95% confidence interval (CI) = 0.008–0.254, $P < 0.001$] in LUAD patients, whereas both DC1 and neutrophil were associated with poor prognosis (HR = 2.397, 95% CI = 1.396–4.118, $P = 0.002$; HR = 8.529, 95% CI = 2.024–35.935, $P = 0.003$) for LUSC patients (**Figure 3A**). The multivariate Cox regression analysis illustrated that B cell was related to good prognosis (HR = 0.015, 95% CI = 0.002–0.127, $P < 0.001$) in

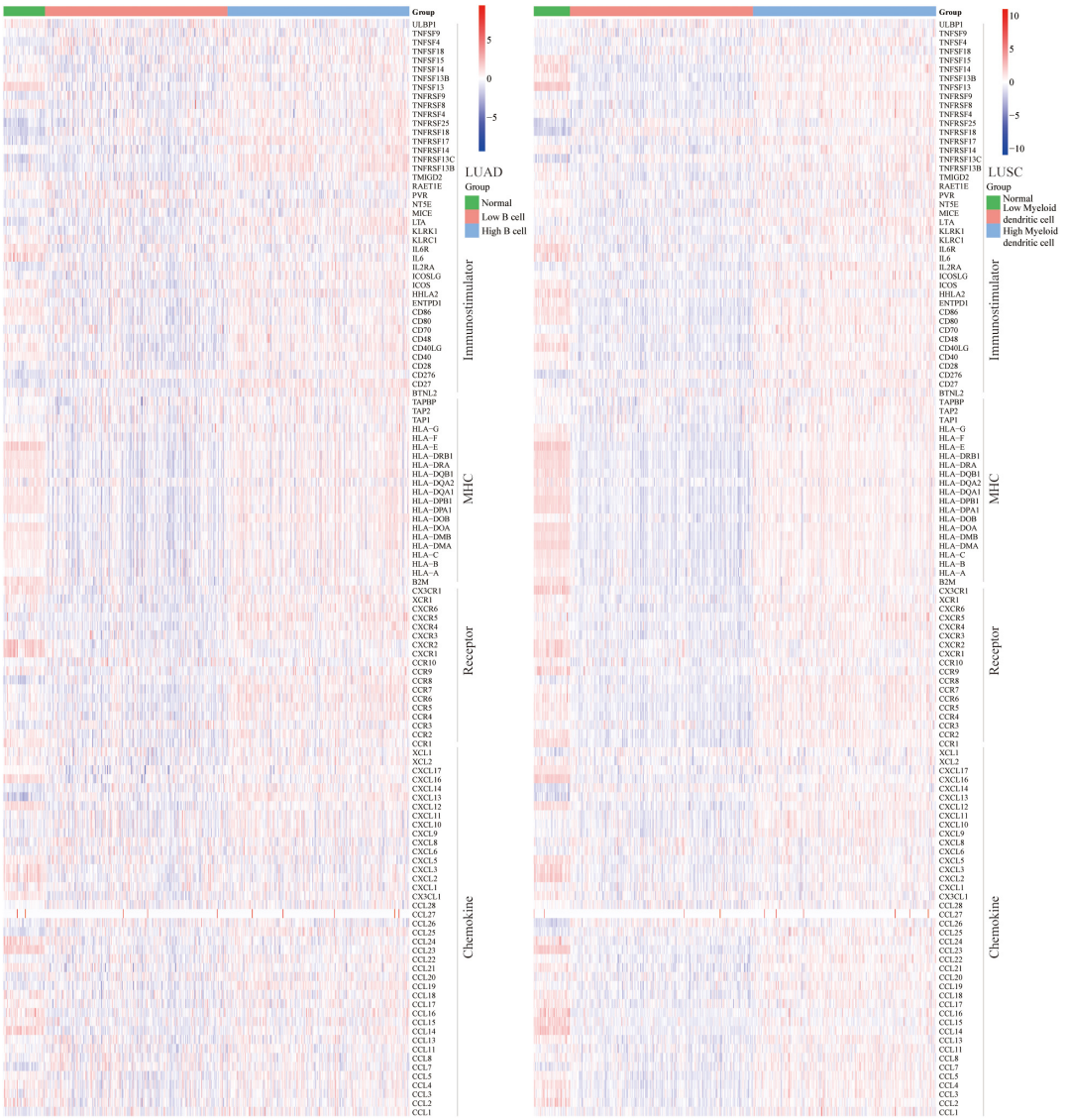

FIGURE 5 | Heatmaps of immunomodulators (immunostimulators, MHC, receptors, and chemokines). Most immunomodulators were upregulated in the high-infiltration group. Each column represents a sample, and each row represents one of the immunomodulators. The expression level of immunomodulators was displayed in different colors, transitioning from blue to red with increasing expression.

LUAD patients, whereas DC1 was related with poor prognosis (HR = 3.100, 95% CI = 1.098–8.756, $P = 0.033$) in LUSC patients (**Figure 3B**). Therefore, B cell and DC1 were independent prognostic factors for LUAD and LUSC patients, respectively.

The Functional Enrichment Analysis of Genes Highly Related to B Cell or DC1 in Lung Cancer

To evaluate the biological functions of B cell and DC1 in the occurrence and development of LUAD and LUSC, respectively, in the TCGA-LUAD and TCGA-LUSC transcriptome data, including 19,464 protein-coding genes, we performed the Spearman correlation analysis. Based on the absolute Spearman correlation coefficient greater than 0.6, we obtained 29 protein-coding genes strongly related to B cell in TCGA-LUAD and 487 protein-coding genes highly related to DC1 in TCGA-LUSC. Then, GO and KEGG enrichment analyses were performed by these 29 and 487 genes, respectively. In terms of GO analysis, 29 protein-coding genes were mainly enriched in B cell activation, whereas 487 protein-coding genes were significantly enriched in T cell activation (**Figure 3C**). In KEGG analysis, Cytokine–cytokine receptor interaction was the most significant pathway of enrichment (**Figure 3D**). It could be seen that B cell and DC1 abundance, as independent prognostic factors, were closely related to the immune activation status of lung cancer patients. Besides, we inferred, for the prognosis of LUAD patients, that activated humoral

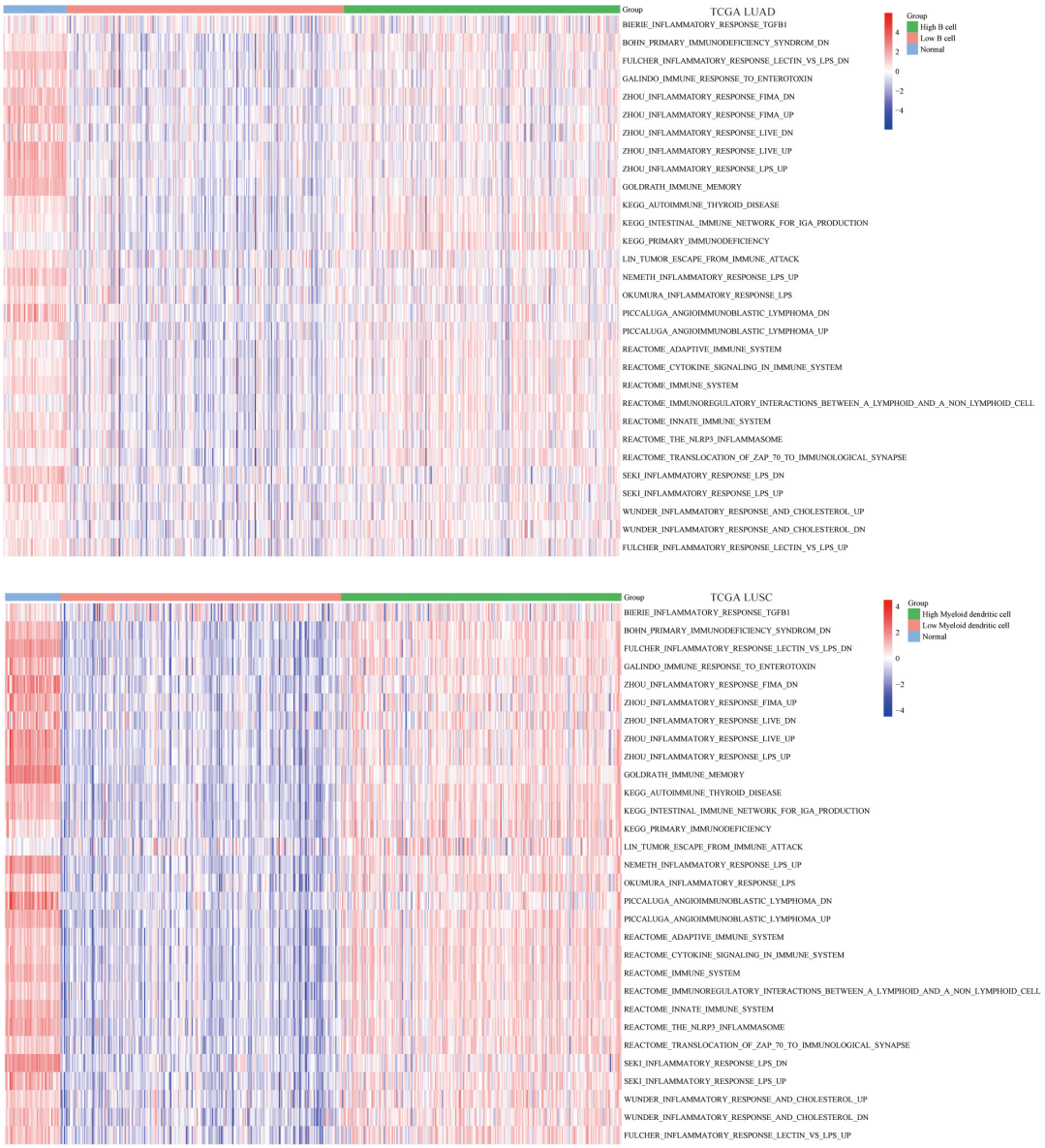

FIGURE 6 | Differences in ssGSEA scores of 30 immune-related pathways among normal, low, and high B cell/DC1 groups in lung cancer. With the increase of B cell/DC1 infiltration, most immune-related pathways were significantly activated.

immunity played more prominent roles, whereas activated cellular immunity played more significant roles in the prognosis of LUSC patients.

Expression Profiles of Adaptive Immune Resistance Markers and CD8A and CD8B in LUAD and LUSC

Enrichment analysis revealed that B cell or DC1 abundance, as independent prognostic factor, was significantly related to the immune activation of the TME of lung cancer. Previous research had shown that ICB therapy, mainly targeting the PD-L1/PD-1 axis, had produced a favorable clinical response in cancer patients (Remon and Besse, 2017). Therefore, we hypothesized that LUAD patients with high B cell infiltration or LUSC patients with high DC1 abundance were more suitable for ICB treatment. According to the median abundance of B cell or DC1 in each tumor sample, all tumor samples were classified into high- and low-infiltration groups. In terms of LUAD patients, most biomarkers, including IDO1, CTLA4, LAG3, CD40, TNFRSF18, TIGIT, and TNFSF14, were significantly increased in tumor tissues with high B cell abundance compared with that of low B cell group (**Figures 4A,B**). For LUSC patients (**Figures 4C,D**), compared with tumor tissues with low DC1 abundance, PD-L1, IDO1, CTLA4, LAG3, CD70, HAVCR2, CD40, CD47, TIGIT, and TNFSF14 were significantly

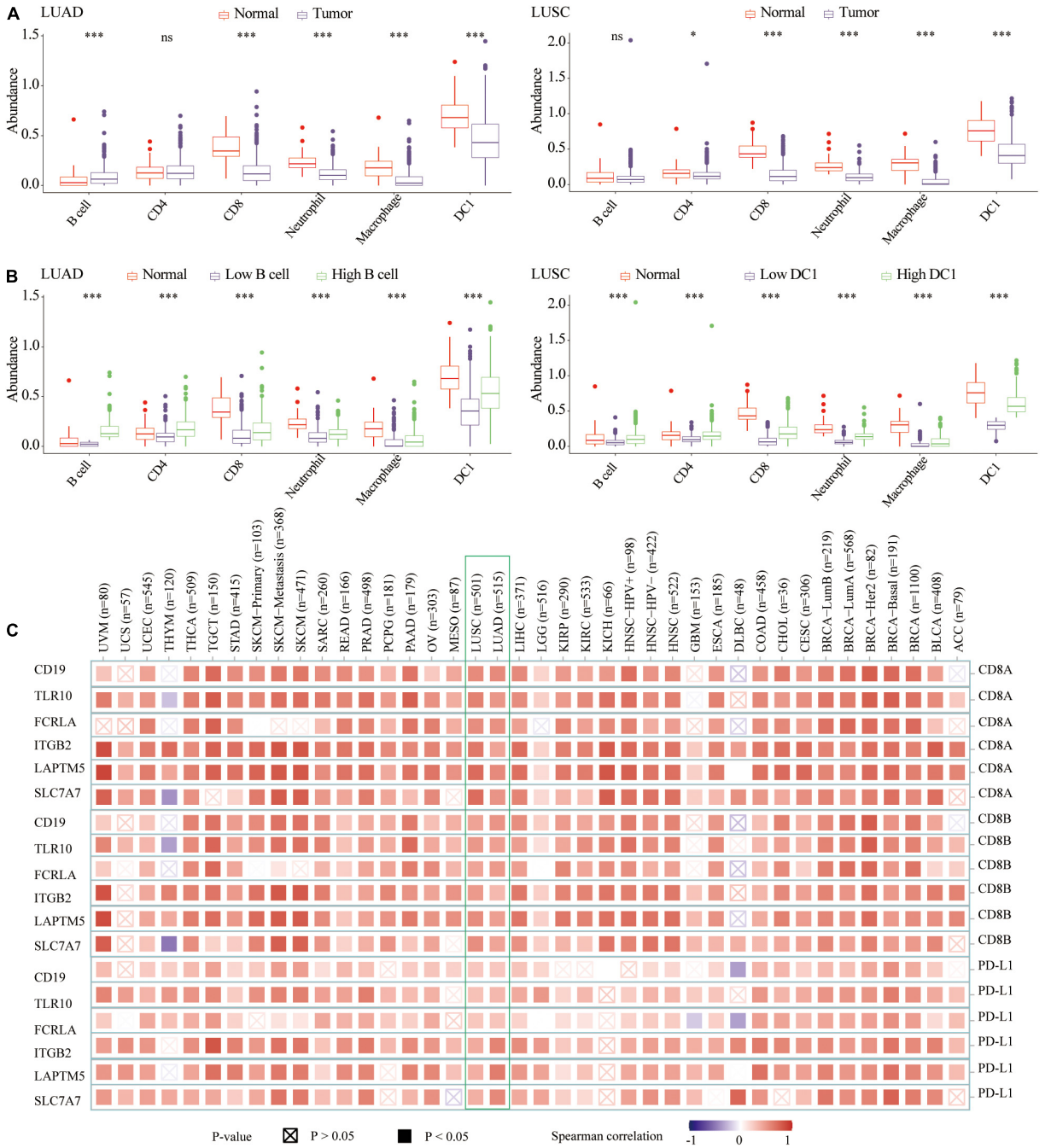

FIGURE 7 | The abundance of six types of TIICs among normal, low, and high B cell/DC1 groups. **(A)** Compared with normal tissues, the abundances of most TIICs were lower in lung cancer tissues. **(B)** For both LUAD and LUSC samples, compared with low B cell/DC1 groups, TIICs all increased significantly in the high B cell/DC1 group. **(C)** In TCGA pan-cancer, hub genes (CD19, TLR10, FCRLA, ITGB2, LAPTM5, and SLC7A7) were significantly related to CD8A, CD8B, and PD-L1. Red represents positive correlation, whereas blue represents negative correlation. The darker the color, the greater the correlation. Solid squares represent $P < 0.05$. $^{*}p < 0.05$, $^{***}p < 0.001$.

increased in low DC1 infiltration tumor tissues. However, in LUAD patients, the expression of CD276 was higher in the low B cell group, whereas in LUSC patients, the expression of VTCN1 was higher in the low DC1 group. For LUAD and LUSC patients, the expression level of most adaptive immune resistance markers in high B cell/DC1 infiltration tumor tissues tended to be normal tissues.

In addition, previous studies had proved that CD8A mRNA levels could predict the ICB response (Fumet et al., 2018). CD8A and CD8B expressions were also significantly correlated

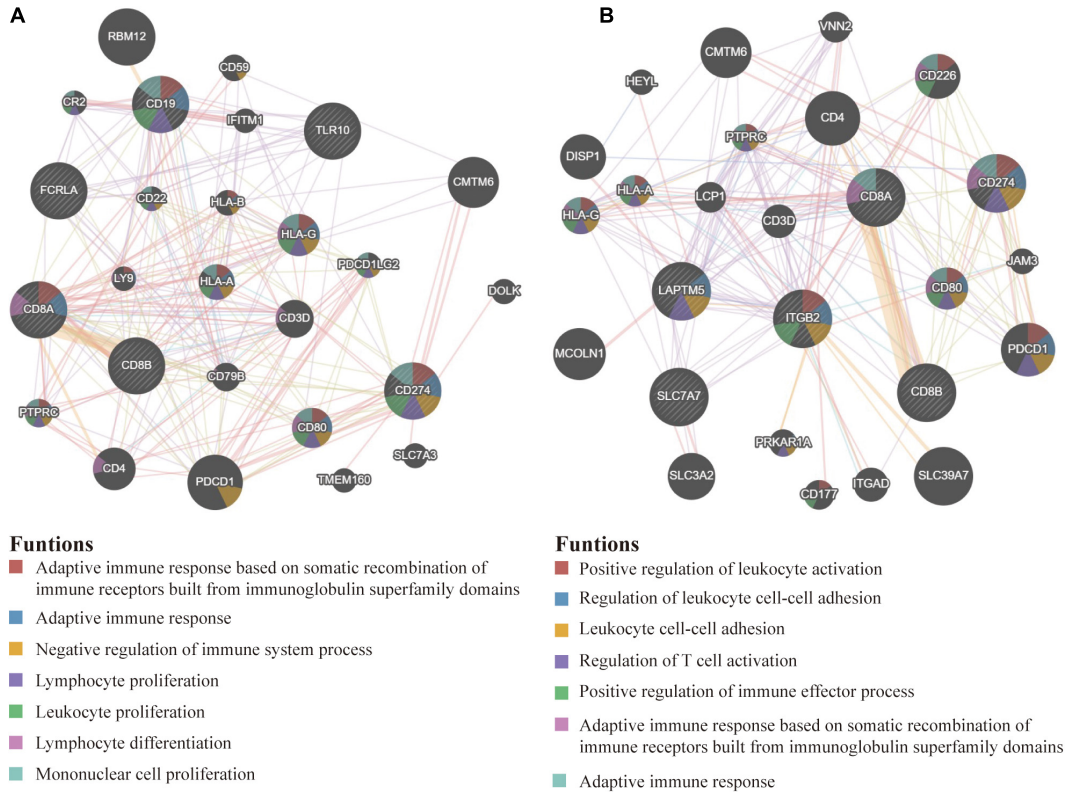

FIGURE 8 | The PPI network. **(A)** The most relevant genes of PD-L1, CD8A, CD8B, CD19, TLR10, and FCRLA are displayed in the PPI network. **(B)** The most relevant genes of PD-L1, CD8A, CD8B, ITGB2, LAPTM5, and SLC7A7 are also shown in the PPI network. Their significant enrichment results are listed below ($P < 0.05$).

with cytolytic activity (Rooney et al., 2015). Compared with low B cell group, high B cell group and normal tissues had higher expression of CD8A and CD8B (**Figures 4B,D,E**). Similarly, high DC1 LUSC and normal tissues had higher CD8A and CD8B expression than low DC1 infiltration tumor samples (**Figures 4B,D,F**).

Correlation Between B Cell, DC1, and Immunomodulators (Immunostimulators, MHC, Receptors, and Chemokines)

To determine the ICB response, we further explored the relationship between abundance of B cell and DC1 and expression of immunostimulators, MHC, receptors, and chemokines. For LUAD and LUSC patients, B cell and DC1 were positively correlated with most immunomodulators (**Figure 5**). Most MHC molecules in the high B cell/DC1 infiltration group were upregulated, indicating that the high-infiltration group's antigen presentation and processing capacity were strengthened. These upregulated chemokines and receptors recruited more CD8 T cells, T_H17 cells, and antigen-presenting cells into the TME of LUAD and LUSC patients. Therefore, we concluded that high B cell/DC1 infiltration shaped an inflamed and immune-activated TME, which was necessary for the success of ICB therapy.

The Abundance of B Cell and DC1 Was Significantly Related to Immune-Related Pathways

Apart from single biomarker and immunomodulators, we further studied the correlation between the abundance of B cell and DC1 and immune-related pathways using the ssGSEA algorithm. The enrichment results indicated that in the high B cell/DC1 infiltration group, most immune-related pathways were significantly activated. Besides, the degree of immune activation of high B cell/DC1 infiltration tumor tissues was equivalent to that of normal tissues, and this part of the tumor tissues tended to be closer to normal tissues (**Figure 6**), which further demonstrated that the high B cell/DC1 infiltration group was immune activated and more suitable for ICB therapy.

The Abundance of TIICs in Lung Cancer

Previous studies had shown that the abundance of TIICs could not only predict the survival of cancer patients, but also reflect the efficacy of immunotherapy (Jiang et al., 2018a; Farhood et al., 2019). In terms of infiltration abundance in LUAD and LUSC, DC1 was the most abundant TIICs. Specifically, compared with normal tissues, there was lower CD8 T cell, neutrophil, macrophage, and DC1 abundance, whereas there was higher B cell infiltration in LUAD tissues. For LUSC tissues, the infiltration

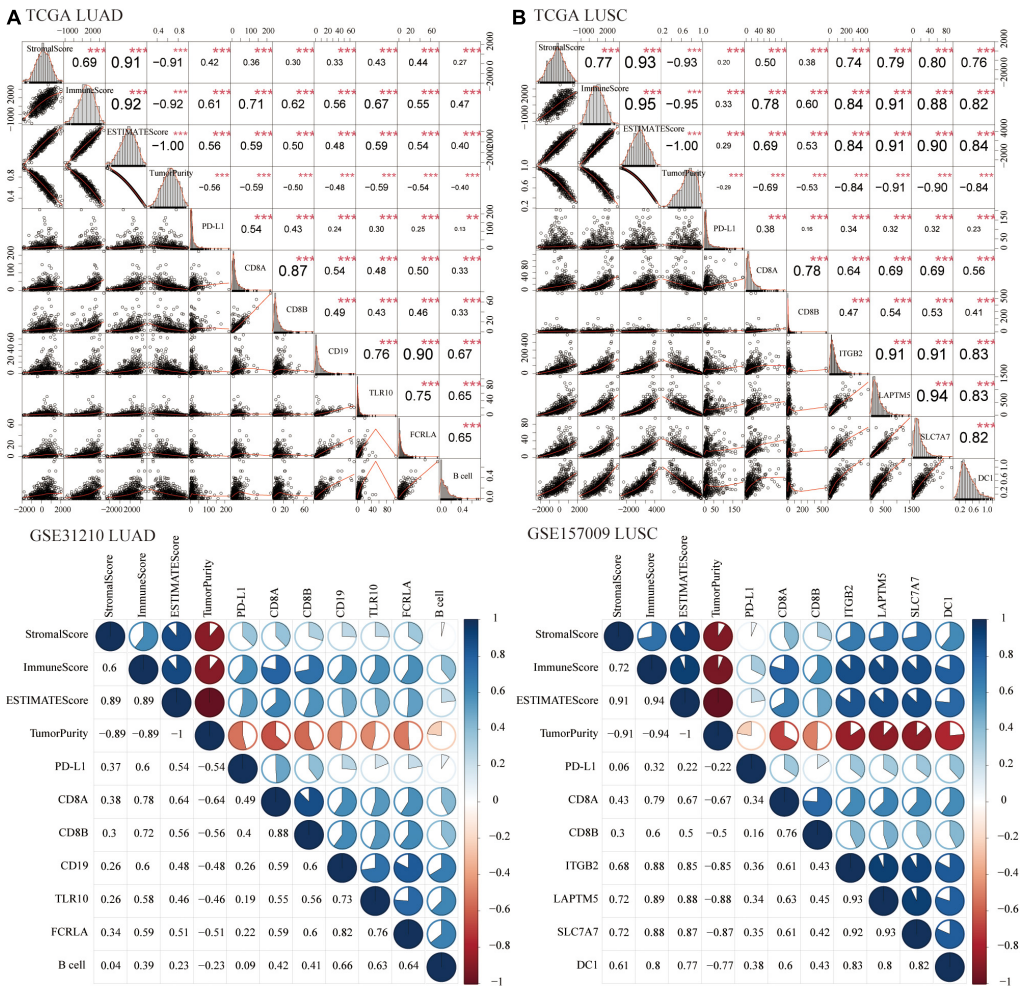

FIGURE 9 | Correlation with the overall tumor microenvironment (TME) score. For LUAD (TCGA and GSE31210) **(A)** and LUSC (TCGA and GSE157009) **(B)** patients, PD-L1, CD8A, CD8B, six hub genes, B cell, and DC1 were significantly positively related to the stromal score, immune score, and ESTIMATE score, whereas they were negatively associated with tumor purity. $^{**}P < 0.01$, $^{***}P < 0.001$.

of CD4 T cell, CD8 T cell, neutrophil, macrophage, and DC1 was lower than that of normal samples (**Figure 7A**). For both LUAD and LUSC samples, compared with the low B cell/DC1 infiltration group, six types of TIICs significantly increased in the high B cell/DC1 group (**Figure 7B**). It could be seen that the high B cell/DC1 group was more like "hot tumor" and would benefit more from immunotherapy.

Correlation Between Abundance of B Cell and DC1 and Clinical Parameters

To judge which lung cancer patients are suitable for immunotherapy from the existing clinical indicators, we analyzed the correlation between abundance of B cell and DC1 and clinical parameters. Combining the TCGA and GSE31210 datasets, we could not draw the same conclusion for which LUAD patients were suitable for immunotherapy. For LUSC of TCGA and GSE157009, female patients had higher DC1 abundance (**Supplementary Figure 1**), suggesting that female patients would benefit more from ICB therapy. Regarding other clinical parameters of LUAD and LUSC patients, no unanimous conclusions were drawn.

Correlation With CD8A, CD8B, PD-L1, TME Score, and Highly Related Genes of B Cell and DC1

To facilitate the clinical application of B cell and DC1, in LUAD (TCGA and GSE31210) and LUSC (TCGA and GSE157009) transcriptome data, we performed the Spearman correlation analysis between abundance of B cell and DC1 and 19,464 protein-coding genes, respectively. Among the top 10 genes most related to B cell in TCGA and GSE31210, we screened three shared genes (CD19, TLR10, and FCRLA). Among the top 10 genes most related to DC1 in TCGA and GSE157009, we also captured three shared genes (ITGB2, LAPTM5, and SLC7A7). For convenience, we called these six genes hub genes (**Supplementary Table 1**). Based on the TIMER2.0, we found

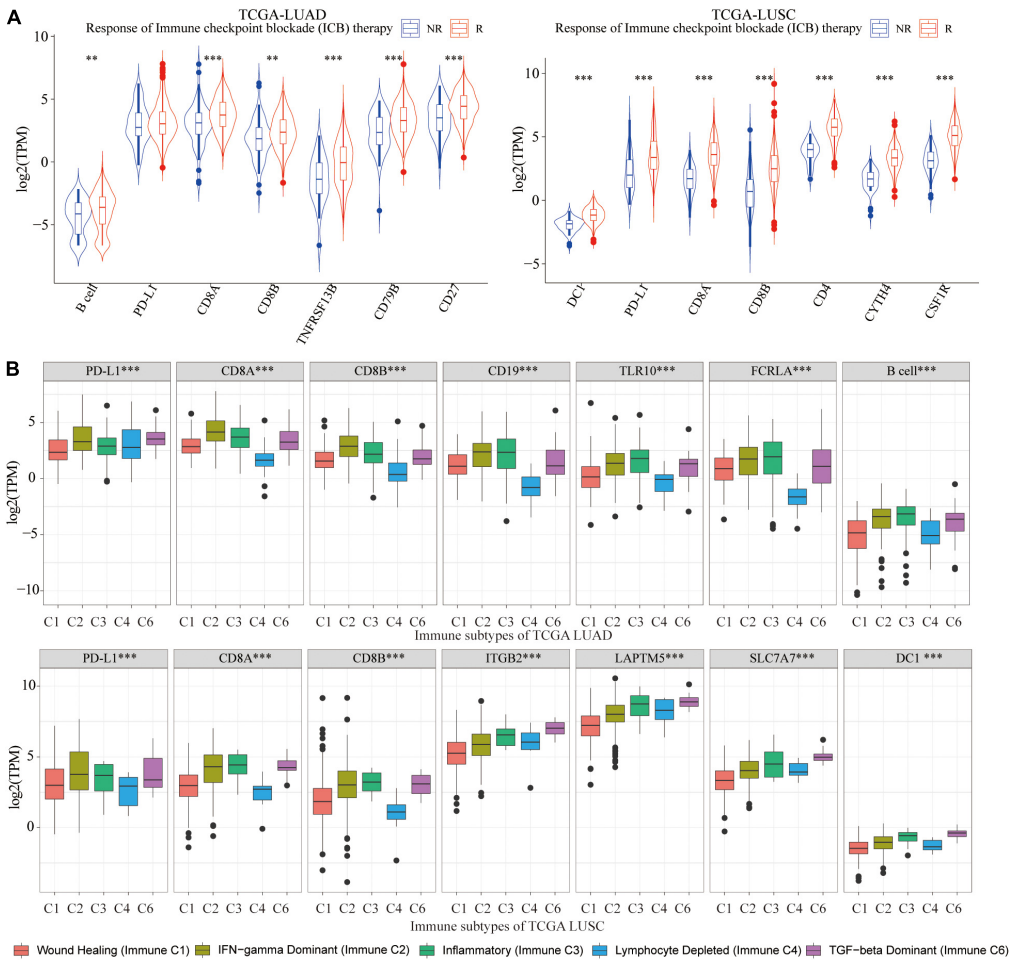

FIGURE 10 | Correlation with ICB treatment and immune subtypes. **(A)** For LUAD, in the ICB response group, B cell abundance, and three hub genes were significantly higher, whereas in LUSC, there were significantly higher abundance of DC1 and expression of three hub genes. **(B)** Among five immune subtypes, immune C2, C3, and C6 had a higher abundance of B cell and DC1 and expression of CD8A, CD8B, and six hub genes. $^{**}p < 0.01$, $^{***}p < 0.001$.

that six hub genes were significantly related to CD8A, CD8B, and PD-L1 in the LUAD and LUSC and most other tumor tissues in TCGA (**Figure 7C**).

The PPI Network

On the GeneMANIA website, we further developed two PPI networks, one of which contained 20 proteins most related to PD-L1, CD8A, CD8B, CD19, TLR10, and FCRLA (**Figure 8A**), and the other contained 20 proteins most related to PD-L1, CD8A, CD8B, ITGB2, LAPTM5, and SLC7A7 (**Figure 8B**). The functional enrichment results of the above two groups of 23 proteins were related to the activation and proliferation of immune cells. This confirmed that six hub genes were significantly related to the activation of immune system.

Correlation With the Overall TME Score

Growing evidence had indicated that stromal score and immune score could be used as novel biomarkers to predict the prognosis and response to immunotherapy of cancer patients (Jiang et al., 2018b; Lambrechts et al., 2018; Ren et al., 2020). Therefore, we calculated the correlation of six hub genes with stromal score and immune score. For LUAD (**Figure 9A**) and LUSC (**Figure 9B**) patients, six hub genes, B cell, and DC1 were significantly positively related to stromal score, immune score, and ESTIMATE score, whereas they were negatively associated with tumor purity, which indicated that lung cancer tissues with high expression of hub genes and abundance of B cell and DC1 were more like "hot tumors," with lower tumor purity and might benefit more from ICB treatment.

The Expression Difference of PD-L1, CD8A, CD8B, and Six Hub Genes Between the ICB Non-response (NR) and Response (R) Groups, Five Immune Subtypes of Lung Cancer

Based on the ImmuCellAI website, lung cancer tissues were classified into the ICB response group (R) and non-response

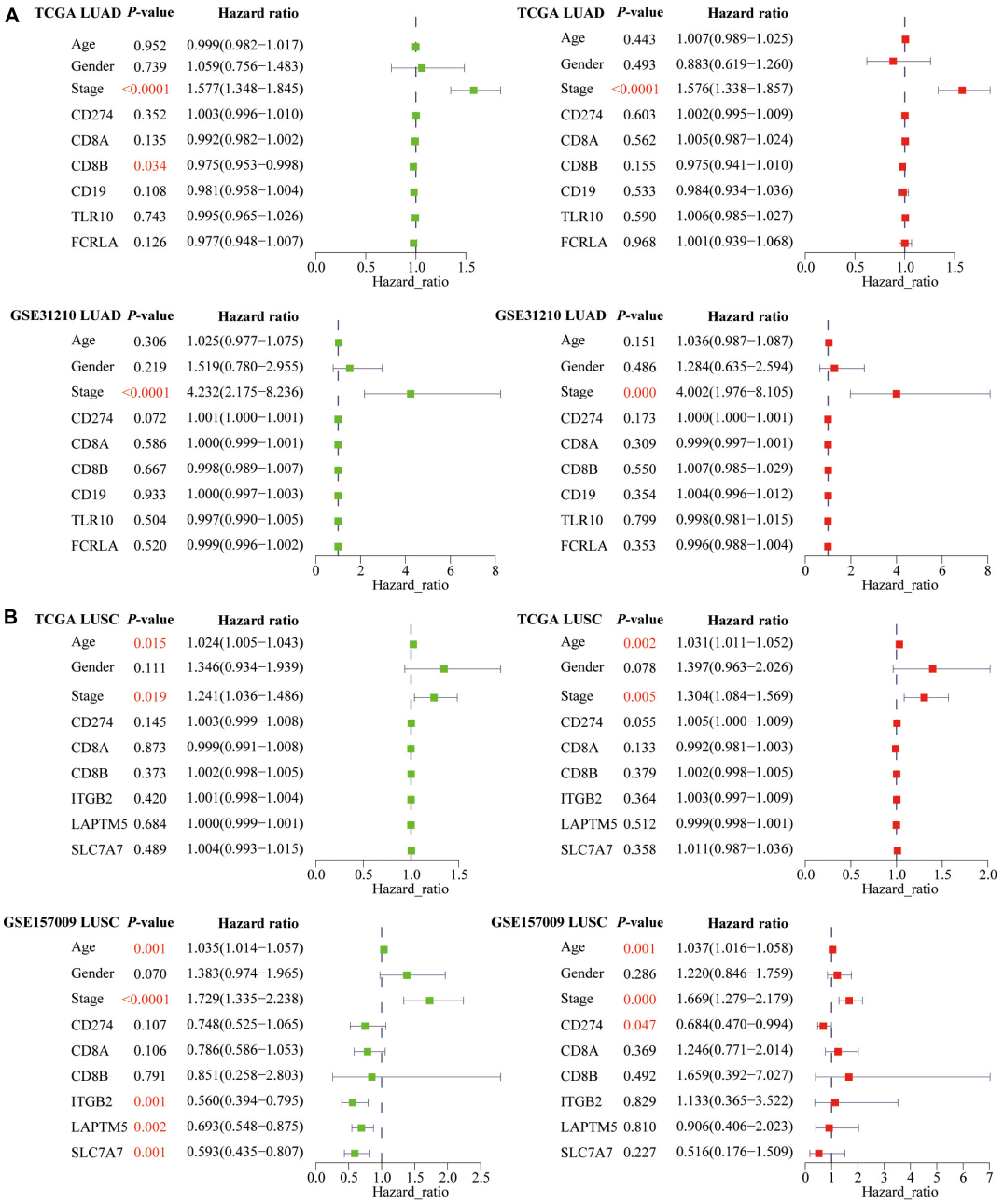

FIGURE 11 | The prognostic significance of PD-L1, CD8A, CD8B, and six hub genes in lung cancer. For **(A)** LUAD and **(B)** LUSC patients, we performed univariate and multivariate Cox regression analyses. Green represents single factor, and red represents multiple factors. *P*-values of independent prognostic factors are marked in red.

group (NR). We draw the conclusion that for LUAD patients who responded well to ICB therapy, there were significantly higher infiltration of B cell and higher expression of CD8A, CD8B, CD19, TLR10, and FCRLA, whereas in LUSC patients who responded well to ICB therapy, there were significantly higher infiltration of DC1 and higher expression of ITGB2, LAPTM5, and SLC7A7 (**Figure 10A**). It could be seen that abundance of B cell and DC1 and expression of six hub genes could be used to evaluate the ICB efficacy for lung cancer patients in advance.

As we all know, TCGA-LUAD and TCGA-LUSC patients were classified into five immune subtypes, including wound healing (immune C1), interferon γ (IFN-γ) dominant (immune C2), inflammatory (immune C3), lymphocyte-depleted (immune C4), and transforming growth factor β (TGF-β) dominant (immune C6). Immune C2, C3, and C6 had higher abundance of B cell and DC1, CD8A, CD8B, and hub genes (**Figure 10B**), which indicated that immune C2, C3, and C6 lung cancer patients were suitable for immunotherapy and would benefit more from ICB therapy.

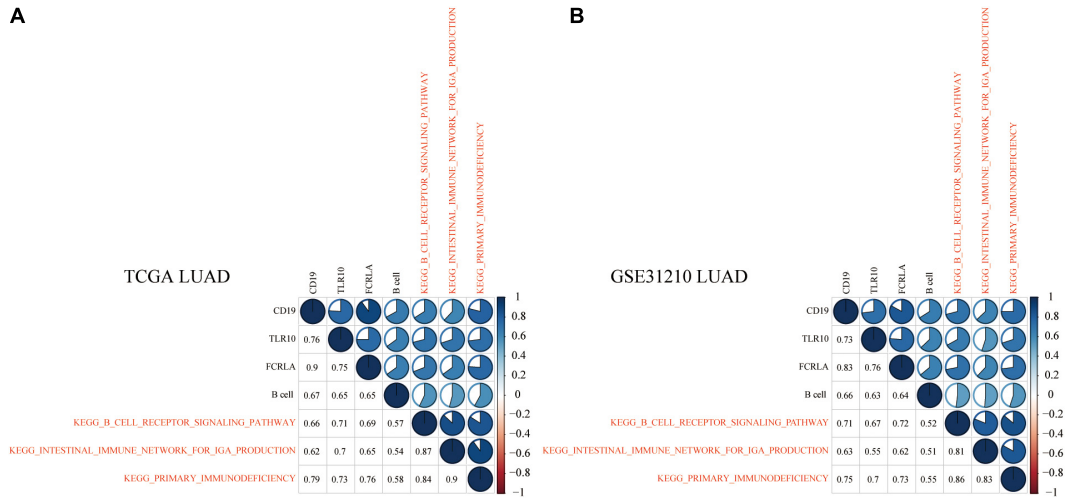

FIGURE 12 | In LUAD tissues of TCGA **(A)** and GSE31210 **(B)**, the above three shared KEGG pathways were highly related to B cell and CD19, TLR10, and FCRLA and are marked in red.

The Prognostic Significance of PD-L1, CD8A, CD8B, Six Hub Genes, Age, Gender, and Stage in Lung Cancer

In addition to the predictive effect of ICB efficacy, we also studied the prognostic significance of PD-L1, CD8A, CD8B, and six hub genes. Based on the univariate and multivariate Cox regression analyses, we only found that PD-L1 was an independent prognostic factor for LUSC patients (**Figure 11B**). Besides, among three clinical parameters, stage was an independent factor for LUAD patients (**Figure 11A**), whereas age and stage were independent factors for LUSC patients ($P < 0.05$) (**Figure 11B**).

Identifying Significant and Universally Relevant KEGG Pathways

To explore KEGG pathways that were commonly associated with B cell, DC1, and six hub genes, the ssGSEA algorithm was used to quantify the enrichment score of 186 KEGG pathways in each LUAD and LUSC sample. Taking the Spearman correlation coefficient greater than 0.5 as the threshold, among 186 KEGG pathways, there were 3 and 27 KEGG pathways, which were significantly enriched in LUAD (TCGA and GSE31210) and LUSC (TCGA and GSE157009) cohorts, respectively. Shared enrichment pathways in TCGA and GSE31210 are marked in red (**Figure 12**). Besides, common enrichment pathways in TCGA and GSE157009 also were highlighted in red (**Figure 13**).

KEGG Pathways Related to the Prognosis and the ICB Efficacy Prediction of Lung Cancer Patients

To further explore the molecular mechanisms of B cell and DC1 in predicting the prognosis and the efficacy of immunotherapy simultaneously, based on the median of ssGSEA scores, LUAD and LUSC patients were divided into high- and low-score groups, respectively. As shown in **Figures 14A,B**, shared KEGG pathways, KEGG B Cell Receptor Signaling Pathway, KEGG Intestinal Immune Network for IGA Production, and KEGG Primary Immunodeficiency, were the molecular mechanisms by which B cell predicted the prognosis and the efficacy of ICB of LUAD patients ($P < 0.05$). For LUSC patients, among the above 27 shared KEGG pathways, KEGG Neuroactive Ligand Receptor Interaction, KEGG Prion Diseases, KEGG Complement And Coagulation Cascades, and KEGG FC Epsilon RI Signaling Pathway were the molecular mechanisms of DC1 that both predicted the prognosis and the ICB efficacy of LUSC patients ($P < 0.05$) (**Figures 14C,D**). The above seven KEGG pathways were expected to become new immunotherapy targets, and more research was urgently needed.

DISCUSSION

According to the latest cancer statistics, lung cancer is the second most common cancer, ranking first of cancer-related deaths (Siegel et al., 2020). Therefore, its prognosis and treatment problems need to be solved urgently. With the free opening of public databases, including TCGA and GEO, various prognostic signatures, such as immune-related (Li et al., 2017), glycolysis-related (Zhang et al., 2019a), autophagy-associated (Liu et al., 2019), hypoxia-associated (Mo et al., 2020), metabolism-associated (He et al., 2020), ferroptosis-related (Gao et al., 2021), and TME-associated (Ma et al., 2020) signature, had been established recently. However, previous signatures focused only on the prognosis and did not consider the choice of treatment options for lung cancer patients, especially whether to choose immunotherapy. However, these features focus only on the prognosis, without considering the treatment of lung cancer. In our study, we follow novel findings. B cell was an independent factor for LUAD patients, whereas DC1 was an independent factor for LUSC patients. In many

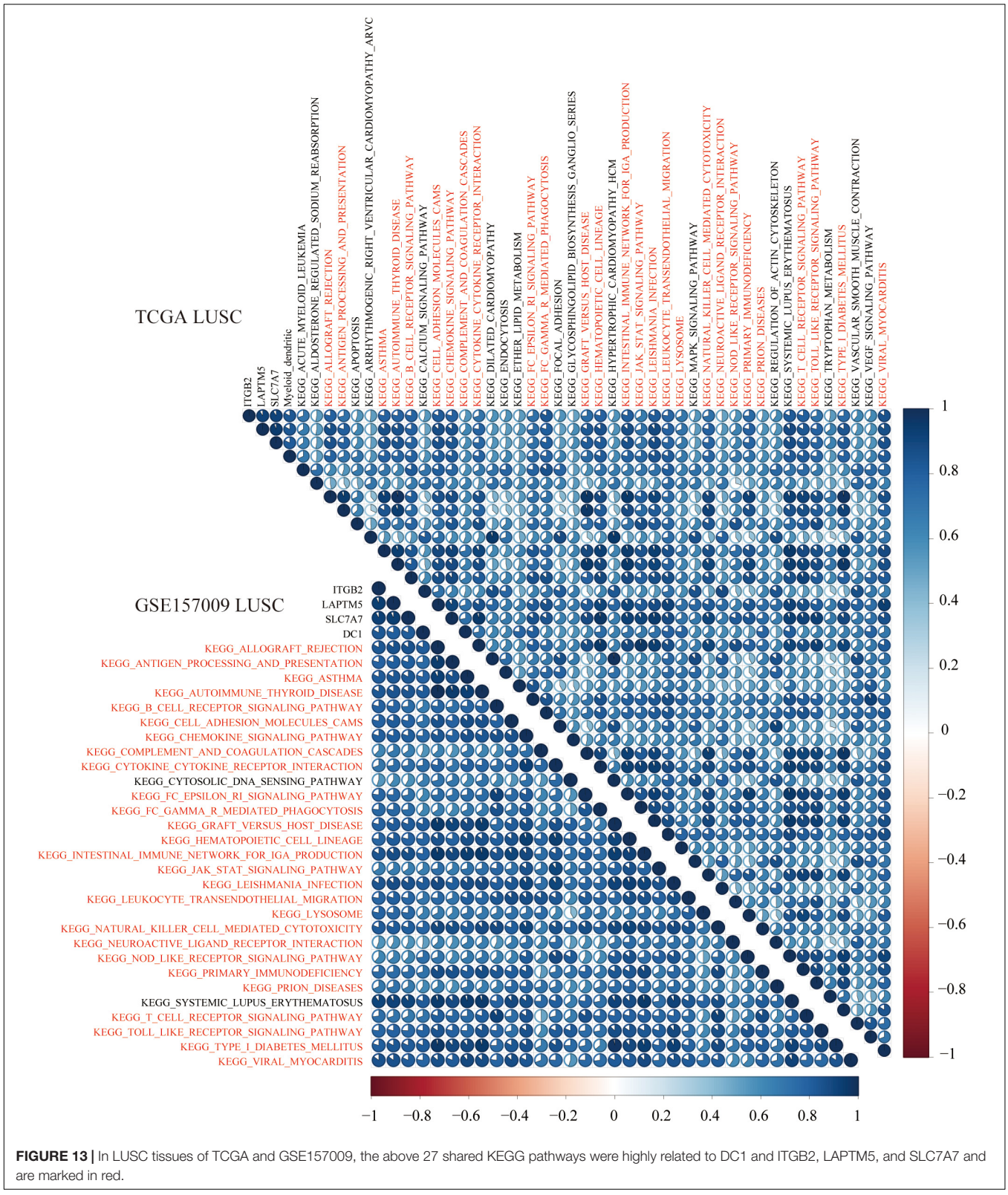

FIGURE 13 | In LUSC tissues of TCGA and GSE157009, the above 27 shared KEGG pathways were highly related to DC1 and ITGB2, LAPTM5, and SLC7A7 and are marked in red.

respects, the high B cell/DC1 infiltration shaped an inflamed and immune-activated TME of lung cancer tissues, including adaptive immune resistance markers, CD8A, CD8B, immunomodulators (immunostimulants, MHC, receptors, and chemokines), and immune-related pathways. Besides, tumor tissues in the high-infiltration group were more similar to adjacent normal tissues,

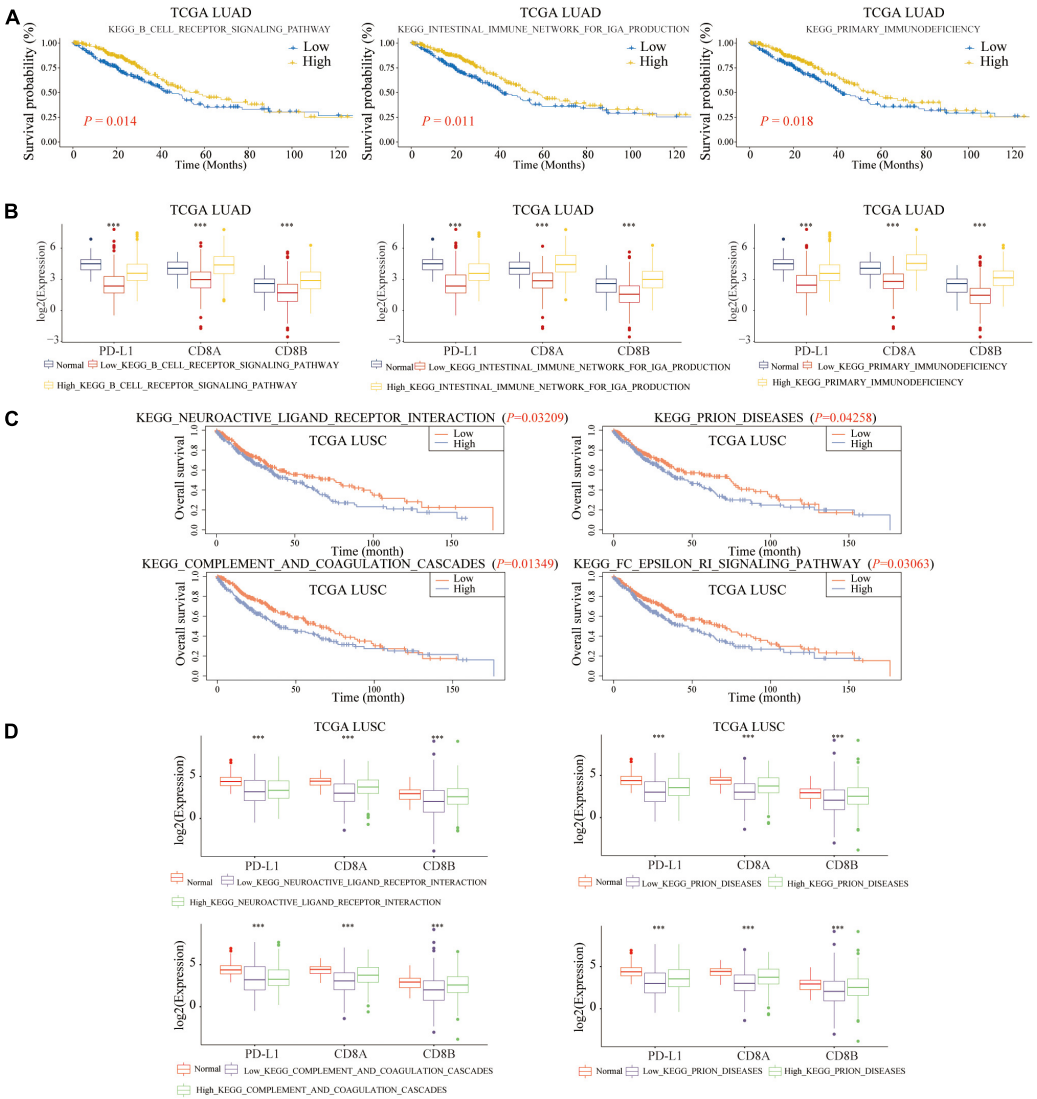

FIGURE 14 | Molecular mechanisms of B cell and DC1 predicting the OS and ICB efficacy of LUAD and LUSC patients. For LUAD patients, the above three KEGG pathways clarified the potential mechanisms of B cell predicting **(A)** the ICB efficacy and **(B)** the OS. The above four pathways elaborated the molecular mechanisms of DC1 predicting **(C)** the ICB efficacy and **(D)** the OS in LUSC patients. ***$p < 0.001$.

whose TME was necessary for the success of ICB therapy. Among five types of immune subtypes of TCGA-LUAD and TCGA-LUSC, IFN-γ–dominant (immune C2), inflammatory (immune C3), and TGF-β–dominant (immune C6) subtypes might be more suitable for ICB therapy. Among 186 KEGG pathways, KEGG B Cell Receptor Signaling Pathway, KEGG Intestinal Immune Network for IGA Production, and KEGG Primary Immunodeficiency were significantly related to infiltration abundance of B cell. Moreover, they were the specific molecular mechanisms by which B cell predicted the ICB efficacy and prognosis of LUAD patients. Similarly, there were four KEGG pathways that clarified the molecular mechanisms of DC1 predicting the prognosis and the ICB efficacy of LUSC patients.

To facilitate clinical application, in the lung cancer transcriptome, including 19,464 protein-coding genes, we extracted the three most relevant genes of B cell (CD19, TLR10, and FCRLA) and DC1 (ITGB2, LAPTM5, and SLC7A7), respectively. Previous immune-related studies on these six genes were as follows.

CD19 is a member of the immunoglobulin gene superfamily and a reliable marker for pre-B cells. The expression of CD19 protein is restricted to B cell lymphocytes. Previous studies have confirmed that it acts as a co-receptor for the B cell antigen receptor complex (BCR). CD19 can decrease the threshold for activation of downstream signaling pathways and for triggering B cell responses to antigens (de Rie et al., 1989; Carter and Fearon, 1992). In short, CD19 molecules play a regulatory role in B cell proliferation and differentiation.

TLR10 is a member of the TLR family that plays a fundamental role in pathogen recognition and activation of innate immunity.

Specifically, TLR10 can inhibit the activation and differentiation of monocytes, thereby affecting the DC-mediated adaptive immune response (Hess et al., 2017a). In terms of adaptive immune response, TLR10 is a B cell intrinsic suppressor of adaptive immune responses (Hess et al., 2017b).

There is relatively little research on FCRLA. Fc receptor-like A is selectively expressed in B cells and may be involved in their differentiation and the development of lymphomas (Inozume et al., 2007; Reshetnikova et al., 2012).

Integrin subunit beta 2 (ITGB2) encodes an integrin β chain and is a receptor for ICAM3 and VCAM1. In terms of immune function, ITGB2 regulates the cytotoxicity of natural killer cell (Barber et al., 2004) and is involved in leukocyte adhesion and transmigration of leukocytes including T cells and neutrophils (Ostermann et al., 2002; Bai et al., 2017).

Lysosomal protein transmembrane 5 (LAPTM5) encodes a transmembrane receptor that is associated with lysosomes (Kawai et al., 2014) and plays a crucial role in hematopoiesis (Zhang et al., 2019b). In terms of innate immunity, LAPTM5 protein is a positive regulator of proinflammatory signaling pathways in macrophages (Glowacka et al., 2012). For adaptive immune, LAPTM5 downregulates the level of BCR on the surface of B cells and inhibits B cell activation (Ouchida et al., 2010). LAPTM5 deficiency results in elevated T cell receptor expression on T cells after CD3 stimulation, as well as enhanced T cell responses *in vitro* and *in vivo* (Ouchida et al., 2008).

Solute carrier family 7 member 7 (SLC7A7) encodes the light subunit of a cationic amino acid transporter. Previous studies on SLC7A7 in immunity are as follows. In NSCLC, SLC7A7 is a prognostic biomarker correlated with immune infiltrates (Dai et al., 2021). For T cell acute lymphoblastic leukemia, SLC7A7 inhibits cell apoptosis and promotes cell migration and invasion (Ji et al., 2018). Downregulation of SLC7A7 triggers an inflammatory phenotype in human macrophages and airway epithelial cells (Rotoli et al., 2018).

The functional enrichment analysis of genes significantly related to B cell and DC1 mainly focused on B cell activation and T cell activation in LUAD and LUSC, respectively. Therefore, we concluded that activated humoral immunity might be more critical for the prognosis and the ICB efficacy prediction of LUAD patients, whereas activated cellular immunity might be more crucial for the prognosis and the prediction of ICB efficacy for LUSC patients.

Unlike LUSC patients, for LUAD patients, there was no difference between ICB response and non-response group on the expression of PD-L1. It could be seen that for LUAD patients, PD-L1 could not effectively predict the efficacy of ICB treatment.

CONCLUSION

In terms of prognosis, LUAD patients with high B cell infiltration had longer OS, whereas LUSC patients with high DC1 infiltration had shorter OS. In terms of immunotherapy efficacy prediction, lung cancer patients with high B cell/DC1 infiltration, whose TME was inflamed and immune activated, were suitable for ICB therapy. The six hub genes and seven KEGG pathways might become novel potential targets for immunotherapy. Immune C2, C3, and C6 subtypes of lung cancer patients might benefit more from ICB therapy. It is necessary to conduct studies in large cohorts to confirm these findings.

DATA AVAILABILITY STATEMENT

The datasets presented in this study can be found in online repositories. The names of the repository/repositories and accession number(s) can be found in the article/ **Supplementary Material**.

AUTHOR CONTRIBUTIONS

SZ and XL provided direction and concept. XL, XS, and JL analyzed the data and wrote the manuscript. XL and SZ made revisions to the manuscript. All authors have read and approved the final manuscript.

FUNDING

This work was supported by a grant from Scientific Research Seed Fund of Peking University First Hospital (No. 2021SF22).

ACKNOWLEDGMENTS

Our team is very grateful for the openness of TCGA's public data and the Timer2.0 website, as well as the developers of R software and R packages.

SUPPLEMENTARY MATERIAL

The Supplementary Material for this article can be found online at: https://www.frontiersin.org/articles/10.3389/fcell.2021.707143/full#supplementary-material

REFERENCES

Bai, M., Grieshaber-Bouyer, R., Wang, J., Schmider, A. B., Wilson, Z. S., Zeng, L., et al. (2017). CD177 modulates human neutrophil migration through activation-mediated integrin and chemoreceptor regulation. *Blood* 130, 2092–2100. doi: 10.1182/blood-2017-03-768507

Barber, D. F., Faure, M., and Long, E. O. (2004). LFA-1 contributes an early signal for NK cell cytotoxicity. *J. Immunol.* 173, 3653–3659. doi: 10.4049/jimmunol.173.6.3653

Carter, R. H., and Fearon, D. T. (1992). CD19: lowering the threshold for antigen receptor stimulation of B lymphocytes. *Science* 256, 105–107. doi: 10.1126/science.1373518

Chen, Y. P., Zhang, Y., Lv, J. W., Li, Y. Q., Wang, Y. Q., He, Q. M., et al. (2017). Genomic analysis of tumor microenvironment immune types across 14 solid cancer types: immunotherapeutic implications. *Theranostics* 7, 3585–3594. doi: 10.7150/thno.21471

Dai, W., Feng, J., Hu, X., Chen, Y., Gu, Q., Gong, W., et al. (2021). SLC7A7 is a prognostic biomarker correlated with

immune infiltrates in non-small cell lung cancer. *Cancer Cell Int.* 21:106.

de Rie, M. A., Schumacher, T. N., Van Schijndel, G. M., Van Lier, R. A., and Miedema, F. (1989). Regulatory role of CD19 molecules in B-cell activation and differentiation. *Cell Immunol.* 118, 368–381. doi: 10.1016/0008-8749(89)90385-7

Farhood, B., Najafi, M., and Mortezaee, K. (2019). CD8(+) cytotoxic T lymphocytes in cancer immunotherapy: a review. *J. Cell. Physiol.* 234, 8509–8521. doi: 10.1002/jcp.27782

Fumet, J. D., Richard, C., Ledys, F., Klopfenstein, Q., Joubert, P., Routy, B., et al. (2018). Prognostic and predictive role of CD8 and PD-L1 determination in lung tumor tissue of patients under anti-PD-1 therapy. *Br. J. Cancer* 119, 950–960. doi: 10.1038/s41416-018-0220-9

Gao, X., Tang, M., Tian, S., Li, J., and Liu, W. (2021). A ferroptosis-related gene signature predicts overall survival in patients with lung adenocarcinoma. *Future Oncol.* 17, 1533–1544. doi: 10.2217/fon-2020-1113

Glowacka, W. K., Alberts, P., Ouchida, R., Wang, J. Y., and Rotin, D. (2012). LAPTM5 protein is a positive regulator of proinflammatory signaling pathways in macrophages. *J. Biol. Chem.* 287, 27691–27702. doi: 10.1074/jbc.m112.355917

Hänzelmann, S., Castelo, R., and Guinney, J. (2013). GSVA: gene set variation analysis for microarray and RNA-seq data. *BMC Bioinformatics* 14:7. doi: 10.1186/1471-2105-14-7

He, L., Chen, J., Xu, F., Li, J., and Li, J. (2020). Prognostic implication of a metabolism-associated gene signature in lung adenocarcinoma. *Mol. Ther. Oncolytics* 19, 265–277. doi: 10.1016/j.omto.2020.09.011

He, R., and Zuo, S. (2019). A robust 8-Gene prognostic signature for early-stage non-small cell lung cancer. *Front. Oncol.* 9:693. doi: 10.3389/fonc.2019.00693

Hess, N. J., Felicelli, C., Grage, J., and Tapping, R. I. (2017a). TLR10 suppresses the activation and differentiation of monocytes with effects on DC-mediated adaptive immune responses. *J. Leukoc. Biol.* 101, 1245–1252. doi: 10.1189/jlb.3a1116-492r

Hess, N. J., Jiang, S., Li, X., Guan, Y., and Tapping, R. I. (2017b). TLR10 is a B cell intrinsic suppressor of adaptive immune responses. *J. Immunol.* 198, 699–707. doi: 10.4049/jimmunol.1601335

In, J., and Lee, D. K. (2019). Survival analysis: part II - applied clinical data analysis. *Korean J. Anesthesiol.* 72, 441–457. doi: 10.4097/kja.19183

Inozume, T., Mitsui, H., Okamoto, T., Matsuzaki, Y., Kawakami, Y., Shibagaki, N., et al. (2007). Dendritic cells transduced with autoantigen FCRLA induce cytotoxic lymphocytes and vaccinate against murine B-cell lymphoma. *J. Invest. Dermatol.* 127, 2818–2822. doi: 10.1038/sj.jid.5700909

Ji, X., Yang, X., Wang, N., Kang, M., Wang, Y., Rong, L., et al. (2018). Function of SLC7A7 in T-Cell acute lymphoblastic leukemia. *Cell Physiol. Biochem.* 48, 731–740. doi: 10.1159/000491899

Jiang, P., Gu, S., Pan, D., Fu, J., Sahu, A., Hu, X., et al. (2018a). Signatures of T cell dysfunction and exclusion predict cancer immunotherapy response. *Nat. Med.* 24, 1550–1558. doi: 10.1038/s41591-018-0136-1

Jiang, Y., Zhang, Q., Hu, Y., Li, T., Yu, J., Zhao, L., et al. (2018b). ImmunoScore signature: a prognostic and predictive tool in gastric cancer. *Ann. Surg.* 267, 504–513. doi: 10.1097/sla.0000000000002116

Kawai, Y., Ouchida, R., Yamasaki, S., Dragone, L., Tsubata, T., and Wang, J. Y. (2014). LAPTM5 promotes lysosomal degradation of intracellular CD3ζ but not of cell surface CD3ζ. *Immunol. Cell Biol.* 92, 527–534. doi: 10.1038/icb.2014.18

Lambrechts, D., Wauters, E., Boeckx, B., Aibar, S., Nittner, D., Burton, O., et al. (2018). Phenotype molding of stromal cells in the lung tumor microenvironment. *Nat. Med.* 24, 1277–1289. doi: 10.1038/s41591-018-0096-5

Li, B., Cui, Y., Diehn, M., and Li, R. (2017). Development and validation of an individualized immune prognostic signature in early-stage nonsquamous non-small cell lung cancer. *JAMA Oncol.* 3, 1529–1537. doi: 10.1001/jamaoncol.2017.1609

Li, T., Fu, J., Zeng, Z., Cohen, D., Li, J., Chen, Q., et al. (2020). TIMER2.0 for analysis of tumor-infiltrating immune cells. *Nucleic Acids Res.* 48, W509–W514.

Liberzon, A., Subramanian, A., Pinchback, R., Thorvaldsdóttir, H., Tamayo, P., and Mesirov, J. P. (2011). Molecular signatures database (MSigDB) 3.0. *Bioinformatics* 27, 1739–1740. doi: 10.1093/bioinformatics/btr260

Lin, H. Y., Cheng, C. H., Chen, D. T., Chen, Y. A., and Park, J. Y. (2016). Coexpression and expression quantitative trait loci analyses of the angiogenesis gene-gene interaction network in prostate cancer. *Transl. Cancer Res.* 5, S951–S963.

Liu, Y., Wu, L., Ao, H., Zhao, M., Leng, X., Liu, M., et al. (2019). Prognostic implications of autophagy-associated gene signatures in non-small cell lung cancer. *Aging (Albany NY)* 11, 11440–11462. doi: 10.18632/aging.102544

Ma, C., Luo, H., Cao, J., Zheng, X., Zhang, J., Zhang, Y., et al. (2020). Identification of a novel tumor microenvironment-associated eight-gene signature for prognosis prediction in lung adenocarcinoma. *Front. Mol. Biosci.* 7:571641. doi: 10.3389/fmolb.2020.571641

Miao, Y. R., Zhang, Q., Lei, Q., Luo, M., Xie, G. Y., Wang, H., et al. (2020). ImmuCellAI: a unique method for comprehensive T-Cell subsets abundance prediction and its application in cancer immunotherapy. *Adv. Sci. (Weinh)* 7:1902880. doi: 10.1002/advs.201902880

Mo, Z., Yu, L., Cao, Z., Hu, H., Luo, S., and Zhang, S. (2020). Identification of a hypoxia-associated signature for lung adenocarcinoma. *Front. Genet.* 11:647. doi: 10.3389/fgene.2020.00647

Ostermann, G., Weber, K. S., Zernecke, A., Schröder, A., and Weber, C. (2002). JAM-1 is a ligand of the beta(2) integrin LFA-1 involved in transendothelial migration of leukocytes. *Nat. Immunol.* 3, 151–158. doi: 10.1038/ni755

Ouchida, R., Kurosaki, T., and Wang, J. Y. (2010). A role for lysosomal-associated protein transmembrane 5 in the negative regulation of surface B cell receptor levels and B cell activation. *J. Immunol.* 185, 294–301. doi: 10.4049/jimmunol.1000371

Ouchida, R., Yamasaki, S., Hikida, M., Masuda, K., Kawamura, K., Wada, A., et al. (2008). A lysosomal protein negatively regulates surface T cell antigen receptor expression by promoting CD3zeta-chain degradation. *Immunity* 29, 33–43. doi: 10.1016/j.immuni.2008.04.024

Pagès, F., Kirilovsky, A., Mlecnik, B., Asslaber, M., Tosolini, M., Bindea, G., et al. (2009). In situ cytotoxic and memory T cells predict outcome in patients with early-stage colorectal cancer. *J. Clin Oncol.* 27, 5944–5951. doi: 10.1200/jco.2008.19.6147

Perez-Moreno, P., Brambilla, E., Thomas, R., and Soria, J. C. (2012). Squamous cell carcinoma of the lung: molecular subtypes and therapeutic opportunities. *Clin. Cancer Res.* 18, 2443–2451. doi: 10.1158/1078-0432.ccr-11-2370

Remon, J., and Besse, B. (2017). Immune checkpoint inhibitors in first-line therapy of advanced non-small cell lung cancer. *Curr. Opin. Oncol.* 29, 97–104. doi: 10.1097/cco.0000000000000351

Ren, Q., Zhu, P., Zhang, H., Ye, T., Liu, D., Gong, Z., et al. (2020). Identification and validation of stromal-tumor microenvironment-based subtypes tightly associated with PD-1/PD-L1 immunotherapy and outcomes in patients with gastric cancer. *Cancer Cell Int.* 20:92.

Reshetnikova, E. S., Mechetina, L. V., Volkova, O. Y., Guselnikov, S. V., Chikaev, N. A., Kövesdi, D., et al. (2012). Differential expression of FCRLA in naïve and activated mouse B cells. *Cell Immunol.* 272, 182–192. doi: 10.1016/j.cellimm.2011.10.013

Rooney, M. S., Shukla, S. A., Wu, C. J., Getz, G., and Hacohen, N. (2015). Molecular and genetic properties of tumors associated with local immune cytolytic activity. *Cell* 160, 48–61. doi: 10.1016/j.cell.2014.12.033

Rotoli, B. M., Barilli, A., Visigalli, R., Ingoglia, F., Milioli, M., Di Lascia, M., et al. (2018). Downregulation of SLC7A7 triggers an inflammatory phenotype in human macrophages and airway epithelial cells. *Front. Immunol.* 9:508. doi: 10.3389/fimmu.2018.00508

Shang, X., Li, J., Wang, H., Li, Z., Lin, J., Chen, D., et al. (2020). CMTM6 is positively correlated with PD-L1 expression and immune cells infiltration in lung squamous carcinoma. *Int. Immunopharmacol.* 88:106864. doi: 10.1016/j.intimp.2020.106864

Siegel, R. L., Miller, K. D., and Jemal, A. (2020). Cancer statistics, 2020. *CA Cancer J. Clin.* 70, 7–30.

Subramanian, A., Tamayo, P., Mootha, V. K., Mukherjee, S., Ebert, B. L., Gillette, M. A., et al. (2005). Gene set enrichment analysis: a knowledge-based approach for interpreting genome-wide expression profiles. *Proc. Natl. Acad. Sci. U S A.* 102, 15545–15550. doi: 10.1073/pnas.0506580102

Sung, H., Ferlay, J., Siegel, R. L., Laversanne, M., Soerjomataram, I., Jemal, A., et al. (2021). Global cancer statistics 2020: GLOBOCAN estimates of incidence and mortality worldwide for 36 cancers in 185 countries. *CA Cancer J. Clin.* 71, 209–249. doi: 10.3322/caac.21660

Waniczek, D., Lorenc, Z., Śnietura, M., Wesecki, M., Kopec, A., and Muc-Wierzgoń, M. (2017). Tumor-Associated macrophages and regulatory T cells

infiltration and the clinical outcome in colorectal cancer. *Arch. Immunol. Ther. Exp. (Warsz)* 65, 445–454. doi: 10.1007/s00005-017-0463-9

Warde-Farley, D., Donaldson, S. L., Comes, O., Zuberi, K., Badrawi, R., Chao, P., et al. (2010). The GeneMANIA prediction server: biological network integration for gene prioritization and predicting gene function. *Nucleic Acids Res.* 38, W214–W220.

Yoshihara, K., Shahmoradgoli, M., Martínez, E., Vegesna, R., Kim, H., Torres-Garcia, W., et al. (2013). Inferring tumour purity and stromal and immune cell admixture from expression data. *Nat. Commun.* 4:2612.

Zhang, L., Zhang, Z., and Yu, Z. (2019a). Identification of a novel glycolysis-related gene signature for predicting metastasis and survival in patients with lung adenocarcinoma. *J. Transl. Med.* 17:423.

Zhang, Z., Parker, M. P., Graw, S., Novikova, L. V., Fedosyuk, H., Fontes, J. D., et al. (2019b). O-GlcNAc homeostasis contributes to cell fate decisions during hematopoiesis. *J. Biol. Chem.* 294, 1363–1379. doi: 10.1074/jbc.ra118.005993

Zuo, S., Wei, M., Zhang, H., Chen, A., Wu, J., Wei, J., et al. (2019). A robust six-gene prognostic signature for prediction of both disease-free and overall survival in non-small cell lung cancer. *J. Transl. Med.* 17:152.

Conflict of Interest: The authors declare that the research was conducted in the absence of any commercial or financial relationships that could be construed as a potential conflict of interest.

Publisher's Note: All claims expressed in this article are solely those of the authors and do not necessarily represent those of their affiliated organizations, or those of the publisher, the editors and the reviewers. Any product that may be evaluated in this article, or claim that may be made by its manufacturer, is not guaranteed or endorsed by the publisher.

Copyright © 2021 Liu, Shang, Li and Zhang. This is an open-access article distributed under the terms of the Creative Commons Attribution License (CC BY). The use, distribution or reproduction in other forums is permitted, provided the original author(s) and the copyright owner(s) are credited and that the original publication in this journal is cited, in accordance with accepted academic practice. No use, distribution or reproduction is permitted which does not comply with these terms.

frontiers in Cell and Developmental Biology

ORIGINAL RESEARCH
published: 03 August 2021
doi: 10.3389/fcell.2021.704853

Interleukin 32 Promotes Foxp3$^+$ Treg Cell Development and CD8$^+$ T Cell Function in Human Esophageal Squamous Cell Carcinoma Microenvironment

Li Han[1†], Shiyu Chen[1†], Zheyi Chen[1], Bingqian Zhou[1], Yingxia Zheng[1] and Lisong Shen[1,2*]*

[1] Department of Laboratory Medicine, Xin Hua Hospital, Shanghai Jiao Tong University School of Medicine, Shanghai, China,
[2] Faculty of Medical Laboratory Science, Shanghai Jiao Tong University School of Medicine, Shanghai, China

OPEN ACCESS

Edited by:
Zimu Deng,
Shanghai Institute of Biochemistry and Cell Biology, Chinese Academy of Sciences (CAS), China

Reviewed by:
Zhaohui Du,
Fred Hutchinson Cancer Research Center, United States
Taibo Li,
Johns Hopkins University, United States
Can Cui,
Yale University, United States

***Correspondence:**
Lisong Shen
lisongshen@hotmail.com
Yingxia Zheng
zhengyingxia@xinhuamed.com.cn

† These authors have contributed equally to this work

Specialty section:
This article was submitted to Molecular and Cellular Pathology, a section of the journal Frontiers in Cell and Developmental Biology

Received: 04 May 2021
Accepted: 29 June 2021
Published: 03 August 2021

Citation:
Han L, Chen S, Chen Z, Zhou B, Zheng Y and Shen L (2021) Interleukin 32 Promotes Foxp3$^+$ Treg Cell Development and CD8$^+$ T Cell Function in Human Esophageal Squamous Cell Carcinoma Microenvironment. Front. Cell Dev. Biol. 9:704853. doi: 10.3389/fcell.2021.704853

Proinflammatory cytokine interleukin 32 (IL-32) is involved in infectious diseases and cancer, but what subtypes of immune cells express IL-32 and its roles in tumor microenvironment (TME) have not been well discussed. In this study, we applied bioinformatics to analyze single-cell RNA sequencing data about tumor-infiltrating immune cells from esophageal squamous cell carcinoma (ESCC) TME and analyzed IL-32 expression in different immune cell types. We found CD4$^+$ regulatory T cells (Treg cells) express the highest level of IL-32, while proliferating T and natural killer cells expressed relatively lower levels. Knocking down of IL-32 reduced Foxp3 and interferon gamma (IFNγ) expressions in CD4$^+$ and CD8$^+$ T cells, respectively. IL-32 was positively correlated with Foxp3, IFNG, and GZMB expression but was negatively correlated with proliferation score. IL-32 may have a contradictory role in the TME such as it promotes IFNγ expression in CD8$^+$ T cells, which enhances the antitumor activity, but at the same time induces Foxp3 expression in CD4$^+$ T cells, which suppresses the tumor immune response. Our results demonstrate different roles of IL-32 in Treg cells and CD8$^+$ T cells and suggest that it can potentially be a target for ESCC cancer immunosuppressive therapy.

Keywords: IL-32, regulatory T cells, CD8$^+$ T cells, single-cell RNA seq, ESCC

INTRODUCTION

Interleukin 32 (IL-32) is a novel cytokine related to cancer and immune diseases. It is also one of the essential members of the inflammatory cytokine networks, which express in immune cells and non-immune cells. Inflammatory cytokines, including IL2, IL-1β, and IFNγ, induce the secretion of IL-32 (Rosenow and Menzler, 2013). In early studies, IL-32 was upregulated in several inflammatory diseases, such as rheumatoid arthritis, inflammatory bowel disease, allergic rhinitis, and multiple sclerosis (Cagnard et al., 2005; Shioya et al., 2007; Jeong et al., 2011; Morsaljahan et al., 2017). However, several recent studies have found that IL-32 negatively regulates immune function in some immune diseases such as asthma (Xin et al., 2018), HIV infection

(Palstra et al., 2018), Alzheimer disease (Yun et al., 2015), and non-alcoholic fatty liver disease (Dali-Youcef et al., 2019). IL-32 was further reported to be associated with the occurrence and development of various malignant tumors such as gastric cancer, lung cancer, and cutaneous T-cell lymphoma (Sorrentino and Di Carlo, 2009; Kang et al., 2012; Yousif et al., 2013; Tsai et al., 2014; Gruber et al., 2020), suggesting it has a critical role in tumor development. However, what types of tumor-infiltrating lymphocytes express IL-32 and the exact role of IL-32 in these cells are still unclear and need further study.

Regulatory T cells (Treg cells) are an integral part of the immune system to maintain immunological tolerance. At the same time, they suppress the antitumor immune response, thereby triggering tumor immune escape (Togashi et al., 2019). Previous studies have found that IL-32 could be detected in esophageal squamous cell carcinoma (ESCC) immortalized cell lines. Besides, the combination of IL-32 expression on tumor cells and Treg infiltration was selected as the independent prognostic factor in ESCC (Nabeki et al., 2015). However, the role and the significance of IL-32 in infiltrating Treg cells in the tumor microenvironment (TME) still need to be explored.

Our study utilized the published single-cell RNA sequencing (scRNA-seq) data to analyze the potential expression and function characteristics of IL-32 in immune cells in the microenvironment of ESCC. IL-32 was primarily expressed in T and natural killer (NK) cells. However, B cells and monocytes/macrophages expressed a lower level. Interestingly, we found Treg cells express the highest IL-32 than other T cell subsets. IL-32 had positively correlated with Foxp3, IFNγ and GZMB expression but was negatively associated with proliferation score. Furthermore, knocking down of IL-32 decreased Foxp3 expression in the Treg cell–inducing system; additionally, inhibited IL-32 expression in $CD8^+$ T cells diminished IFNγ production. According to these results, we speculate that T cells that express IL-32 may have a contradictory role that promotes IFNγ expression in $CD8^+$ T cells, which enhances the antitumor activity, and induces $CD4^+$ T cells Foxp3 expression, which suppresses tumor immune response.

MATERIALS AND METHODS

ESCC scRNA-Seq Data Acquisition

The raw data of ESCC in this study were downloaded from the Gene Expression Omnibus database (GSE145370), including seven ESCC tumor and paired adjacent tissues (Zheng et al., 2020).

scRNA-Seq Data Analysis

The data analysis pipeline, including transfer from raw files to FASTQ, barcode identification, UMI extraction, filter, and the map read, was the same as the method described in our published article (Zheng et al., 2020). Briefly, 10 × Genomics Cell Ranger (3.0.1 version) pipeline was used to demultiplex raw files into FASTQ files, extract barcodes and UMI, filter, and map reads to the GRCh38 reference genome and generate a matrix containing normalized gene counts versus cells per sample. This output was then imported into the Seurat (v3) R toolkit for quality control and downstream analysis. All functions were run with default parameters unless otherwise specified. Low-quality cells (<400 genes/cell and >10% mitochondrial genes) were excluded. As a result, 80,787 cells with a median of 1,170 detected genes per cell were included in downstream analyses. To remove the batch effect, the datasets collected from different samples were integrated using Seurat v3 with default parameters.

Dimensionality Reduction, Clustering, and Annotation

We then identified a subset of genes that exhibit high cell-to-cell variation in the dataset, which helped to represent the biological signal in downstream analyses. The Seurat function "FindVariableFeatures" was applied to identify the highly variable genes (HVGs). The top 2,000 HVGs were used for data integration. The data were scaled using "ScaleData," and the first 20 principal components were adopted for autoclustering analyses using "FindNeighbors" and "FindClusters" functions. For all 80,787 cells, we identified clusters setting the resolution parameter as 1.5, and the clustering results were visualized with the UMAP scatter plot. The marker genes of each cell cluster were identified using the receiver operating characteristic analysis function provided by the Seurat "FindAll-Markers" function for the top genes with the largest AUC (area under the curve). The whole dataset was then categorized into NK cells, T cells, myeloid cells, mast cells, and other cells (including fibroblast cells and basal cells) according to the known markers: KLRC1, KLRD1 (NK cells), CD3G, CD3D, CD3E, CD2 (T cells), FCGR2A, CSF1R, FCER1A (myeloid cells), CD19, CD79A (B cells), TPSB2, CPA3 (mast cells), KRT19, IGFBP4, and CTSB (basal cells/fibroblasts). Clusters were also confirmed by identifying significantly highly expressed marker genes in each cluster and then comparing them with the known cell type–specific marker genes. For 44634 NK-T cells, we identified clusters setting the resolution parameter as 1.

Correlation Analysis

For the correlation between IL-32 and other genes, we screened cells that detected the expression of two genes (expression values > 0) at the same time. The mean value of gene expression was used as the signature score, and the cells whose IL-32 expression and score were both equal to 0 were eliminated. We considered signature gene lists for the cell cycle score as published information (Navarro-Barriuso et al., 2018). Pearson correlation analysis was used for statistical test.

IL-32 shRNA Lentivirus Transfection *in vitro*

Fresh blood was obtained from healthy volunteers; the written informed consent was obtained. Studies were performed in accordance with the Declaration of Helsinki and were approved by the Research Ethics Board of the Xinhua Hospital, Shanghai Jiao Tong University School of Medicine. Peripheral blood mononuclear cells (PBMCs) were isolated from fresh heparinized

blood by standard density gradient centrifugation with Ficoll-Paque Plus (GE Healthcare). $CD4^+$ and $CD8^+$ T cells were obtained by negative selection using a human $CD4^+$ or $CD8^+$ T cell isolation kit (Miltenyi) and seeded with 5×10^5 cells per well in 96-well plates. The complete medium (RPMI 1640 with 10% fetal bovine serum) was added to 50 ng/mL recombinant human IL-2 (Peprotech) and cultured for 48 h for the cell activation.

IL-32 shRNA lentivirus (Genechem Company) and activated $CD4^+$ and $CD8^+$ T cells were mixed according to MOI = 10 plus the infection enhancer B-1 (Genechem Company). The mixture was centrifuged at 1,200 revolutions/min, 30 min at room temperature. After 24 h, the culture medium was half-exchanged. The transfection efficiency was detected by green fluorescent protein fluorescence expression under the microscope and detects mRNA level using real-time polymerase chain reaction (PCR) at 72 h.

RNA Isolation and Real-Time PCR

We isolated total RNA from cell pellets using the RNeasy Mini Kit (Qiagen) and obtained first-strand cDNA using the Sensiscript Reverse Transcription Kit (Qiagen) according to the manufacturer's instructions. We determined the mRNA expression of IL-32 and GAPDH (internal control) by real-time PCR using SYBR Green master mix (Applied Biosystems). The primer sequences for IL-32 were as follows: forward 5′-CAG CTC TGA CCT GGT GCT GT -3′, reverse 5′-CCC AGT CTC AGG CAT TCT TTA T-3′, and those for GAPDH were forward 5′-GTG AAG GTC GGA GTC AAC G-3′ and reverse 5′-TGA GGT CAA TGA AGG GGT C-3′. Thermocycler conditions comprised an initial holding at 50°C for 2 min and then at 95°C for 10 min, which was followed by a two-step PCR program consisting of 95°C for 15 s and 60°C for 60 s for 40 cycles. We collected and analyzed data using an ABI Prism 7500 sequence detection system (Applied Biosystems). We expressed all data as a fold increase or decrease relative to the expression of GAPDH. The expression of IL-32 in a given sample was presented as $2^{-\Delta Ct,}$ where $\Delta Ct = Ct_{IL-32} - Ct_{GAPDH}$.

Treg Induction

$CD4^+$ T cells were stimulated with anti-CD3 (2 μg/mL) (eBioscience), anti-CD28 (1 μg/mL) (eBioscience), IL-2 (50 ng/mL) (R&D Systems), and transforming growth factor β (20 ng/mL) (R&D Systems) and cultured for 3 days for Treg cell induction.

Flow Cytometry

The $CD4^+$ and $CD8^+$ T cells were collected after the cell stimulation and Treg induction for 72 h. Surface markers were stained with appropriate antibody CD4-PerCPcy 5.5, CD8-PE-CY7 at room temperature for 30 min and washed twice by phosphate-buffered saline (PBS). For intracellular protein staining, cells were stimulated with the cell stimulation cocktail plus protein transport inhibitors (eBioscience) for 5 h. Then, the cells were fixed and permeabilized with Cytofix/Cytoperm buffer and were stained with antibodies IFNγ-ACP-cy7, Foxp3-eFluor450, and isotype control according to the manufacturer's instructions. Flow cytometric was performed with a FACS Canto II instrument (BD Bioscience), and the analysis was by FlowJo software (TreeStar). All the flow antibodies were from eBioscience.

Survival Analysis

The relationship between IL-32 expression and survival of ESCC patients was analyzed by an online website[1] (Gyorffy et al., 2010). The survival was analyzed with Kaplan–Meier method, using the log-rank test to determine the difference.

Statistical Analysis

Statistical significance was determined by using the GraphPad Prism 5.0 (GraphPad, Inc.) and R (v4.0.4). Measured data were presented as the mean ± SEM; two-tailed Student *t* test was applied to compare quantitative data, whereas other statistical methods are described in the above "Methods" sections and in the figure legends.

RESULTS

IL-32 Is Overexpressed in T and NK Cells in the TME

We used published scRNA-seq data to analyze the IL-32 expression in ESCC $CD45^+$ tumor-infiltrating immune cells (Zheng et al., 2020). According to the scRNA-seq data annotation and canonical marker, we classified several dominant cell subsets in immune cells, such as T cells, B cells, NK cells, myeloid cells, mast cells, and "other cells" that stand for the non-immune cells (**Figures 1A,B**). First, we analyzed IL-32 expression in disparate immune cell subsets. Seurat function "FindMarkers" was applied, and the *p* value adjustment was presented using Bonferroni correction based on the total number of genes in the dataset by default. Like the previous reports, IL-32 expression was higher in T and NK cells (Dahl et al., 1992; Cheon et al., 2011; **Figures 1C,D**). However, B cells, myeloid, mast cells, and other cells barely expressed IL-32 (**Figures 1C,D**). We further analyzed IL-32 expression between the tumor and adjacent tissues. Data showed that IL-32 expression in T and NK cells in tumor tissues was slightly higher in comparison to the adjacent tissues (**Figure 1E**). A recent report noted that IL-32 acted as an essential growth factor for human cutaneous T-cell lymphoma cells (Suga et al., 2014). IL-32 also augmented the cytotoxic effect of NK-92 cells on the cancer cells through activation of DR3 and caspase-3 cell signaling (Park et al., 2012). Our data suggest that IL-32 is potentially involved in the regulative function of T and NK cells and plays an important role in tumor surveillance.

IL-32 Is Dominant in $CD4^+$ Treg Cells

T and NK cells are the primary cell types for antitumor activity in the TME; thus, we next determined the IL-32 expression in different T and NK cell subsets. First, we unsupervised reclustering the $CD4^+$ T, $CD8^+$ T, and NK cells from ESCC (**Figures 2A,B**). According to the annotation (Zheng et al., 2020),

[1] http://kmplot.com/analysis/index.php? p = service.

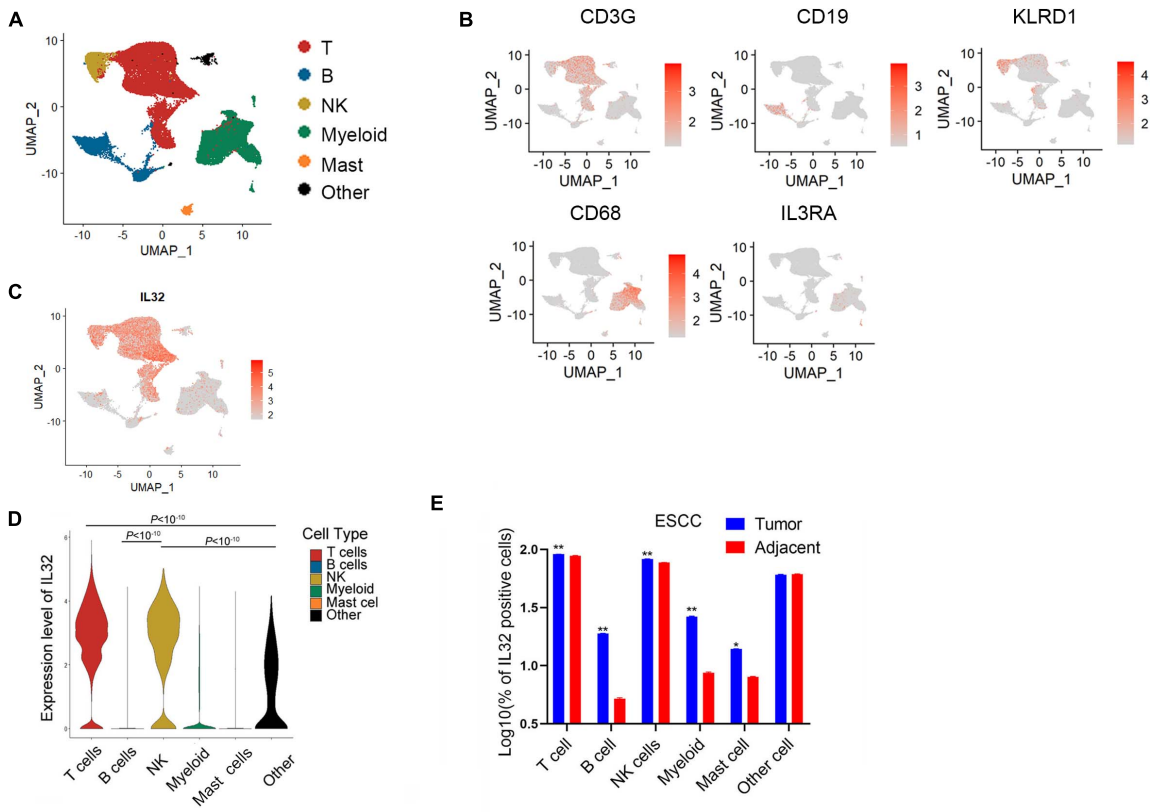

FIGURE 1 | Overexpression of IL-32 in T and NK cells in the ESCC TME. **(A)** UMAP plot of immune cells from the tumor tissues of seven ESCC patients to visualize cell-type clusters based on the expression of known marker genes, main clusters shown in different colors. **(B)** Expression levels of relative marker genes illustrated as UMAP plots. The expression was measured as the log2 (count + 1). **(C)** Expression levels of IL-32 illustrated as UMAP plots. The expression was measured as the log2 (count + 1). **(D)** Violin plot shows the IL-32 expression in T cell, B cell, NK cell, myeloid, mast cell, and other cell subsets in the ESCC. *p* Value adjustment was performed using Bonferroni correction then was calculated by Wilcoxon signed rank test. **(E)** Box plot shows the IL-32–positive cells between the tumor and adjacent group in T cell, B cell, NK cell, myeloid, mast cell, and other cell subsets of ESCC ($n = 7$). The data were measured as the log10 (% of positive cells). *p* Value was calculated by two-tailed Student *t* test. $^{**}p < 10^{-10}$, $^{*}p < 0.001$.

we grouped the $CD4^+$ T cells into naive, Th, proliferation, and Treg cells, and $CD8^+$ T cells into cytotoxic, proliferation, and exhausted subsets. NK cells were divided into cytotoxic, tolerogenic, and proliferation subsets (**Figures 2C,D**). We then compared IL-32 expression among groups. Seurat function "FindMarkers" was applied, and the *p* value adjustment was performed using Bonferroni correction based on the total number of genes in the dataset by default. IL-32 expression in $CD4^+$ T cells was significantly higher than that in $CD8^+$ T and NK cells (**Figure 2E**). Interestingly, in $CD4^+$ T cells, IL-32 expression was much higher in Treg cells. While in $CD8^+$ T and NK cells, IL-32 expression was much higher in cytotoxic cells. Interestingly, the proliferation CD4, CD8, and NK cell subsets expressed relatively lower levels of IL-32 (**Figures 2F–H**). We further evaluated the IL-32 expression in the tumor and adjacent tissues T cell subsets. Date showed that in $CD4^+$ T cells, naive CD4 and Treg cells in tumor expressed much more IL-32 than adjacent tissue (**Figure 2I**), and in $CD8^+$ T cell subsets, IL-32 expression was much higher in adjacent than tumor tissues (**Figure 2J**). In NK cells, the cytotoxic and exhausted subset IL-32 expression was much higher in tumor tissue (**Figure 2K**). These data suggest that ESCC TME may induce or inhibit IL-32 expression in different T cell subsets.

IL-32 Negatively Correlates With Cell Cycle Score While It Positively Correlates With Foxp3 and Cytotoxic Molecules IFNG and GZMB

Our previous data showed that IL-32 expression was far higher in Treg cells than proliferation T cells, and IL-32 has been illustrated to be the inflammatory cytokine. Next, we developed the correlations between IL-32 and Treg cell transcription factor such as Foxp3 and IKZF2 (Barbi et al., 2014; Ng et al., 2019), cell cycle (G1S and G2M), and cytotoxic molecules IFNG and GAMB, respectively. As expected, IL-32 expression was positively correlated with Foxp3 and IKZF2 in $CD4^+$ T cells (**Figure 3A**), and GZMB and IFNG in $CD8^+$ T cells (**Figure 3B**) in ESCC patients. However, IL-32 expression was negatively correlated with cell cycle scores in $CD4^+$ (**Figure 3C**) and $CD8^+$ T cells, respectively (**Figure 3D**). Furthermore, we used the ESCA bulk RNA sequencing data from TCGA and analyzed

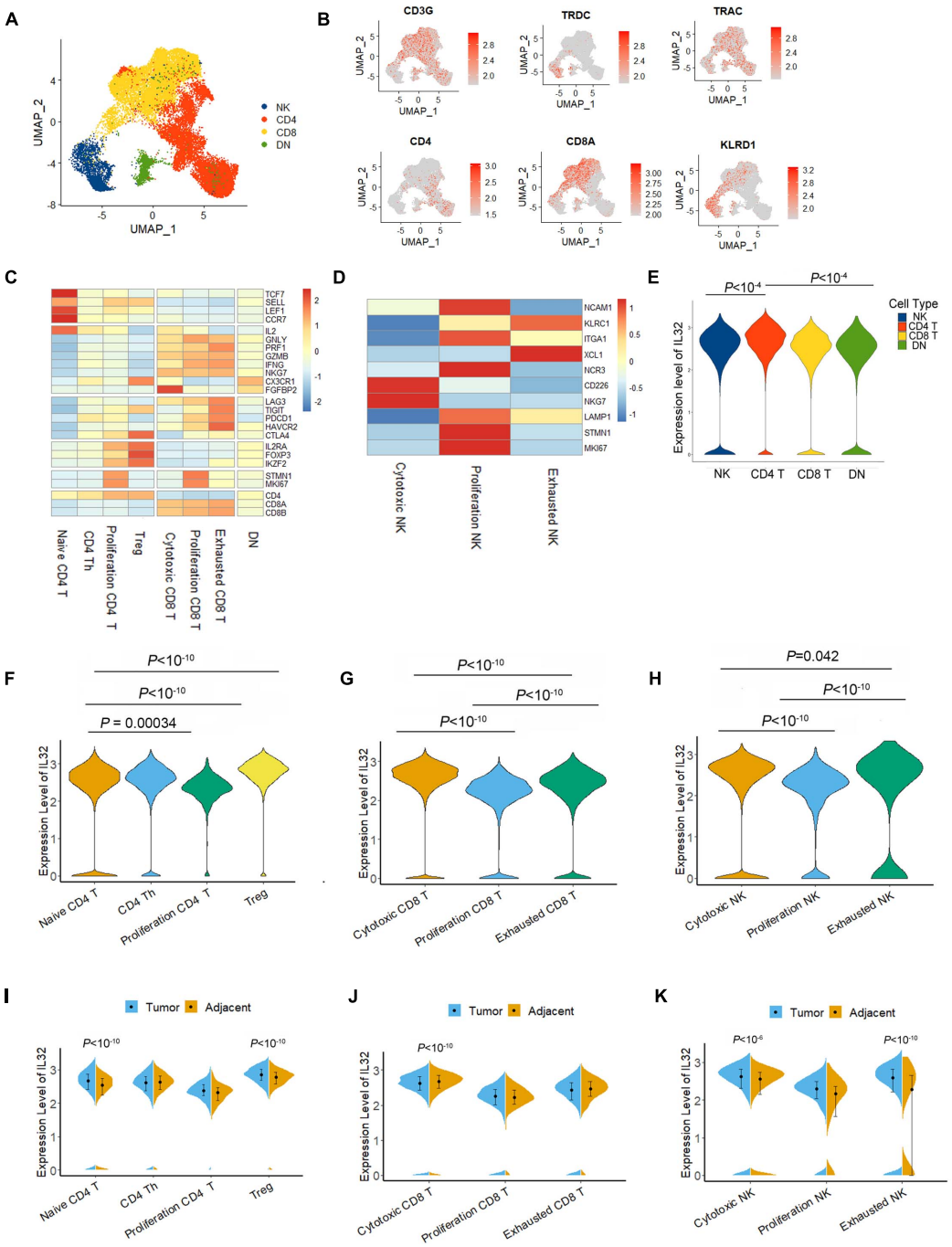

FIGURE 2 | IL-32 expression in subtypes of T and NK cells. **(A)** UMAP plot of T and NK cells from the tumor tissues of seven ESCC patients, showing the formation of main $CD4^{+}$T cells, $CD8^{+}$ T cells, NK cells, and CD4/CD8 low expression cells (DN). Each dot corresponds to a single cell, colored according to the cell cluster. **(B)** Expression levels of relative marker genes illustrated as UMAP plots. The expression was measured as the log2 (count + 1). **(C)** Heatmap of *Z* score normalized log2 (count + 1) expression of selected T cell function–associated genes in each cell cluster. **(D)** Heatmap of *Z* score normalized log2 (count + 1) expression of selected NK cell function–associated genes in each cell cluster. **(E)** Violin plot compared the IL-32 expression in NK, CD4 T, CD8 T, and DN T cells in the ESCC. The expressions of IL-32 were measured as the log2 (count + 1). **(F)** Violin plot shows the IL-32 expression among naive CD4 T, CD4 Th, proliferation CD4, and Treg cell subsets in ESCC. **(G)** Violin plot shows the IL-32 expression in cytotoxic CD8, proliferation CD8, and exhausted CD8 T cells in ESCC. **(H)** Violin plot shows the IL-32 expression in cytotoxic NK, proliferation NK, and exhausted NK cell subsets in ESCC. *p* Value adjustment was performed using Bonferroni correction and then was calculated by Wilcoxon signed rank test for panels **(E–G)**. **(I)** Violin plot shows the IL-32 expression in tumor and adjacent CD4 T cell subsets. **(J)** Violin plot shows the IL-32 expression in tumor and adjacent CD8 T cell subsets. **(K)** Violin plot shows the IL-32 expression in tumor and adjacent NK cell subsets. The expression of above figures was measured as the log2 (count + 1). Each plot represents the interquartile range (IQR, the range between the 25th and 75th percentile) with the midpoint of the data. *p* Value was calculated by Wilcoxon signed rank test.

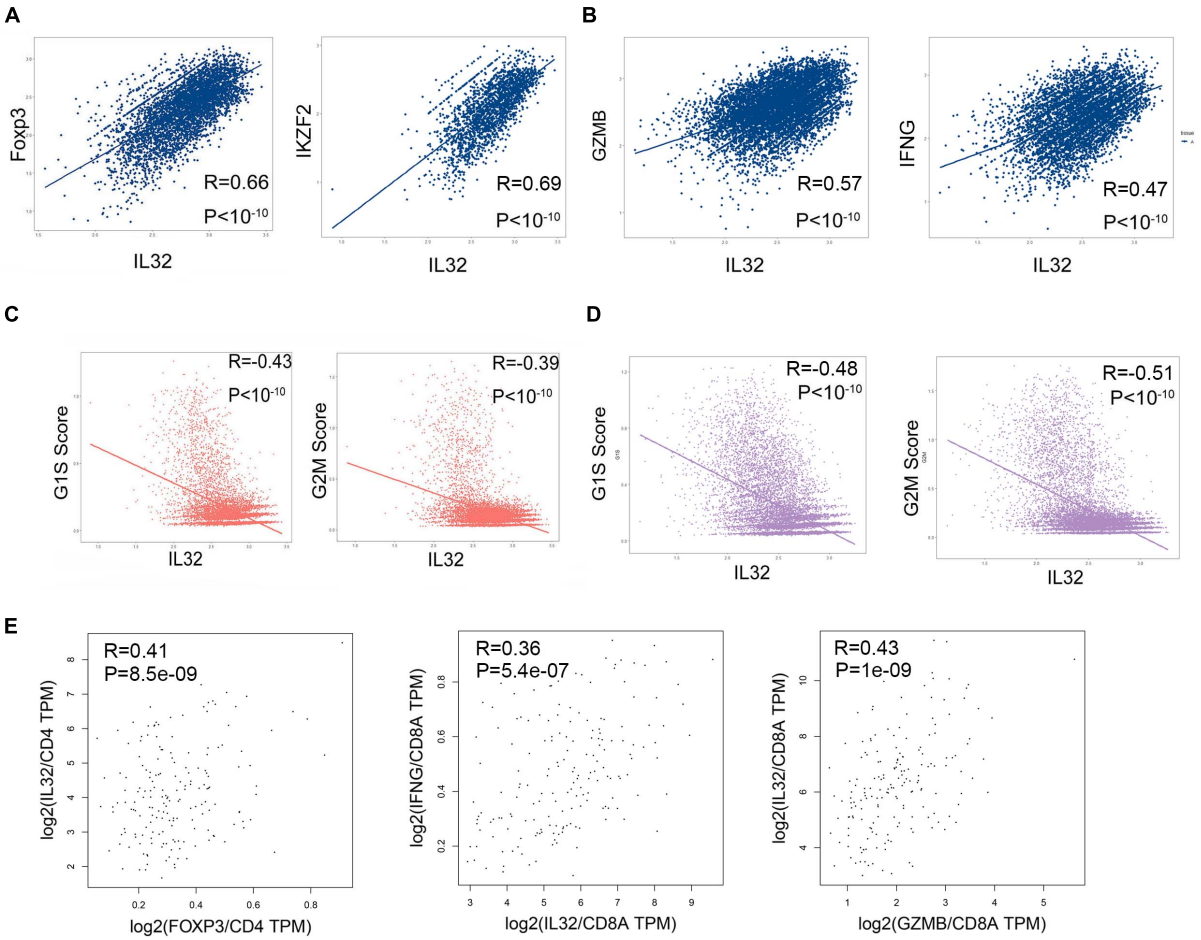

FIGURE 3 | Correlation between IL-32, cell cycle scores, and multiple gene expressions. **(A)** Pearson correlation coefficient demonstrates the correlation between IL-32 and Foxp3, IFZF2 in $CD4^+$ T cells from ESCC tumor tissues. **(B)** Pearson correlation coefficient demonstrates the correlation between IL-32 and GZMB and IFNG in $CD8^+$ T cells from ESCC tumor tissues. **(C)** Pearson correlation coefficient demonstrates the correlations between IL-32 and G1S scores and G2M scores in $CD4^+$ T cells from ESCC tumor tissues. **(D)** Pearson correlation coefficient demonstrates the correlations between IL-32 and G1S scores and G2M scores in $CD8^+$ T cells from ESCC tumor tissues. **(E)** The correlations between IL-32 and Foxp3 expression (left panel), gene expression was normalized in CD4; the correlation between IL32 and IFNG expression (middle panel) and GZMB expression (right panel), gene expression was normalized in CD8a, from ESCA bulk RNA sequence data. The *R* value represents the correlation between the *x* and *y* axis values, $R > 0$ means a positive correlation, $R < 0$ means a negative correlation, and $p < 0.01$ indicates that the correlation was statistically significant.

the correlationship between IL-32 and Foxp3 in $CD4^+$ T cells, GZMB, and IFNG in $CD8^+$ T cells. Consistent with scRNA-seq data, IL-32 expression was positively correlated with Foxp3, GZMB, and IFNG (**Figure 3E**). These data suggest that IL-32 might be involved in Treg cell function and cytotoxic $CD8^+$ T cell function.

Knockdown of IL-32 Gene Inhibits the Development of Treg Cells and IFNγ Production in $CD8^+$ T Cells

To demonstrate the relationship between IL-32 and Treg cells, we performed shRNA to knock down IL-32 expression in $CD4^+$ T cells and detected the Foxp3 expression in the *in vitro* Treg cell induction system. Data showed that when $CD4^+$ T cells were knocked down of IL-32, the IL-32 mRNA expression was significantly decreased (**Figure 4A**). Foxp3 expression was significantly decreased in the knockdown group than the control group following the stimulation or Treg cell induction system (**Figure 4B**). Additionally, when the CD8 T cells were knocked down of IL-32, IFNγ production in $CD8^+$ T cells was decreased relative to the control group (**Figure 4C**). These results demonstrated that IL-32 might have duality and play different roles in the Treg and cytotoxic $CD8^+$ T cell development, and the underlying mechanisms need to be elaborated in the future study.

We further used Kaplan–Meier plotter to analyze the patient survival; 81 ESCC patients from the dataset were included. The group of patients with a high level of IL-32 expression was compared to the low-level groups. Increasing expression of IL-32 was not positively or negatively associated with the overall survival or disease-free survival of ESCC patients (**Figure 4D**).

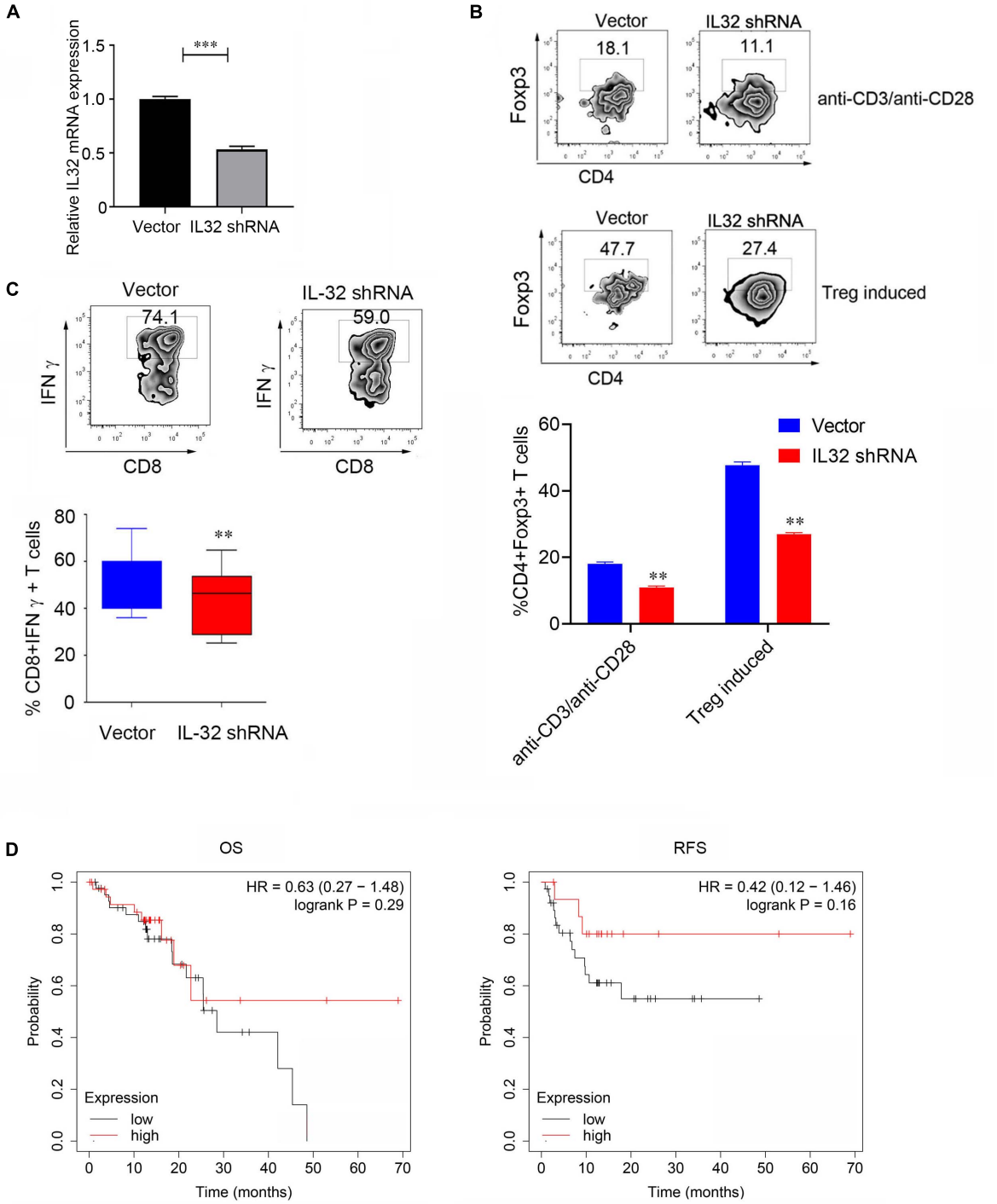

FIGURE 4 | Decreasing Foxp3 and IFNγ expression after IL-32 was knockdown. **(A)** The relative mRNA expression between control (vector) group and lentivirus transduction (IL-32 shRNA) group. *p* Value was calculated by two-tailed Student *t* test. **(B)** Proportions of $CD4^+$ $Foxp3^+$ Treg cells between the virus transfection with IL-32 shRNA and vector groups in $CD4^+$ T cells isolated from PBMCs of healthy donors *in vitro*. The stimulation conditions were using the anti-CD3, anti-CD28 antibodies (top) activated $CD4^+$ T cell and IL-2, transforming growth factor β induces Treg production (bottom). One of the three similar experiments is presented; data are presented as the mean ± SEM; *p* value was calculated by two-tailed Student *t*-test. **(C)** Flow cytometry measures the IFNγ expression in $CD8^+$ T cells transfected with IL-32 shRNA and vector group. One of the three similar experiments is presented; data are presented as the mean ± SEM; *p* value was calculated by two-tailed Student *t* test. **(D)** Kaplan–Meier plot was used to analyze the overall survival (**left**) and disease-free survival (**right**) of IL-32 expression with the ESCC patients ($n = 81$) from the TCGA data.

One possible reason is that only 81 ESCC patients were included in the analysis. The lack of significance is most likely due to the smaller sample size; the other reason is that the different role of IL-32 in Treg and cytotoxic CD8 T cells might be responsible for these effects. In the subsequent study, more patients will be needed to obtain much more definite conclusions.

DISCUSSION

IL-32 has been reported to regulate cell growth, metabolism, and immune regulation. Therefore, it participates in the pathological regulation and protection of inflammatory diseases and cancer. Kim and colleagues recently demonstrated that IL-32γ functions through a cytoplasmic event, not a paracrine or autocrine pathway, suggesting that IL-32γ functions as a non–cytokine-like molecule in hepatitis B virus (HBV) suppression (Kim et al., 2018). Previous studies defined that IL-32 was upregulated in patients with several inflammatory diseases and was induced by inflammatory responses. However, several reports suggested that IL-32 was downregulated in several inflammatory diseases, including asthma, HIV infection disease, neuronal diseases, metabolic disorders, and experimental colitis (Hong et al., 2017). Furthermore, some recent data indicated that IL-32 induced anti-inflammatory cytokines, such as IL-10 (Kang et al., 2009) and the immunosuppressive molecules such as IDO in macrophages through STAT3 and nuclear factor κB pathway, and promoted multiple myeloma development (Smith et al., 2011; Yan et al., 2019). These data suggest that IL-32 may play different roles in different immune cells and perform different activities in inflammatory disease. Nevertheless, what exact types of T and NK cell subsets express IL-32 and its significance have not been well addressed.

Using the published ESCC scRNA-seq data, we found that IL-32 expression was dominated in T and NK cells, consistent with the previous study (Kim et al., 2005; Cheon et al., 2011; Park et al., 2012). Our study further analyzed the T cell and NK cell subset IL-32 expression and pointed that Treg cells express a much higher level of IL-32 than other T cell subsets. In contrast, proliferation exhausted T and NK cells expressed a much lower level of IL-32 in ESCC. IL-32 was negatively correlated with the cell cycle and but was positively correlated with the expression of Foxp3 and cytotoxic molecules IFNG and GZMB. In human melanoma, colon cancer, breast cancer, and other cancer types, IL-32 can be induced by tumor necrosis factor (TNFα and IFNγ to inhibit cancer development, and its high expression may be related to the therapeutic effect of PD1 (Bhat et al., 2017; Paz et al., 2019). The upregulation of IL-32 for colon cancer and prostate cancer can enhance the killing function of NK cells. In addition, IL-32 can activate the expression of several cytokines, such as IL-6, TNFα, and IFNγ in immune cells, and inhibits HIV-1 (Nold et al., 2008). In our experiment, we found that when $CD8^+$ T cells were knocked down of IL-32, IFNγ expression decreased, suggesting that IL-32 may be involved in the development of cytotoxic $CD8^+$ T cells. Consistent with the previous studies that IL-32 may be involved in the secretion of IFNγ, Th1, and the maintenance of killer T cells in HIV (Santinelli et al., 2019).

The high expression of IL-32 in ESCC tumor cells combined with a high proportion of Treg cell infiltration was associated with a poor prognosis and suggests that IL-32 may indeed have a specific relationship with the differentiation of T cells, the secretion of cytokines, and even the development of Tregs in the TME. IL-32 has nine alternative spliced isoforms; IL-32α and IL-32β isoforms are thought to be the major isoforms predominantly expressed in the various cells (Hong et al., 2017). Until now, IL-32 isoform secretions are very confusing and unclear; some controversy even exists. IL-32γ isoform is thought to be a secreted cytokine that possesses a hydrophobic signal peptide in its N-terminus. However, IL-32β is detected in intracellular fraction, IL-32α is not secreted in anti-CD3 antibody-activated human T cell, and IL-32β found in the supernatant is derived from the cytoplasm of apoptotic T cells (Kim et al., 2005; Goda et al., 2006). In our experiment, we found that when $CD8^+$ T cells were knocked down of IL-32, IFNγ expression decreased; similarly, Foxp3 expression reduced when IL-32 shRNA was knocked down in $CD4^+$ T cells, suggesting that IL-32 may be involved in the development of cytotoxic $CD8^+$ T cells and Treg cells, but how it works, based on an autocrine or cell-intrinsic fashion, is not clear and needs to be addressed in the future work. In summary, our data showed that IL-32 might have antitumor and anti-immune response in ESCC TME. IL-32 may promote $CD8^+$ T cell IFNγ expression that enhances the antitumor activity, but at the same time induce $CD4^+$ T cell Foxp3 expression, which could suppress tumor immune response. Our study demonstrated that blocking IL-32 may reduce Treg cell development, or increasing IL-32 expression may enhance cytotoxic $CD8^+$ T cell function in the ESCC tumor immunotherapy.

DATA AVAILABILITY STATEMENT

Publicly available datasets were analyzed in this study. The names of the repository/repositories and accession number(s) can be found in the article/supplementary material.

ETHICS STATEMENT

The studies involving human participants were reviewed and approved by The Ethical Committee of Xin Hua Hospital, Shanghai Jiao Tong University School of Medicine. The patients/participants provided their written informed consent to participate in this study.

AUTHOR CONTRIBUTIONS

LS and YZ designed the experiments. LH, SC, ZC, and BZ performed and analyzed the experimental data. LS, YZ, and LH wrote the manuscript, with all authors contributing to writing and providing feedback.

FUNDING

This work was supported by grants from the National Natural Science Foundation of China (81873863 and 82071753 to YZ and 81672363 to LS), the Shanghai Municipal Education Commission—Gaofeng Clinical Medicine Grant Support (20161315 to YZ), the Key Specialty Development Program of Xin Hua Hospital and Shanghai Municipal Health Commission (to LS), Medicine and Engineering Cross Research Foundation of Shanghai Jiao Tong University (Project No. YG2017ZD02 to LS), and Municipal Science and Technology Commission (Project No. 17441902300 to LS).

REFERENCES

Barbi, J., Pardoll, D., and Pan, F. (2014). Treg functional stability and its responsiveness to the microenvironment. *Immunol. Rev.* 259, 115–139. doi: 10.1111/imr.12172

Bhat, S., Gardi, N., Hake, S., Kotian, N., Sawant, S., Kannan, S., et al. (2017). Impact of intra-tumoral IL17A and IL32 gene expression on T-cell responses and lymph node status in breast cancer patients. *J. Cancer Res. Clin. Oncol.* 143, 1745–1756. doi: 10.1007/s00432-017-2431-5

Cagnard, N., Letourneur, F., Essabbani, A., Devauchelle, V., Mistou, S., Rapinat, A., et al. (2005). Interleukin-32, CCL2, PF4F1 and GFD10 are the only cytokine/chemokine genes differentially expressed by in vitro cultured rheumatoid and osteoarthritis fibroblast-like synoviocytes. *Eur. Cytokine Netw.* 16, 289–292.

Cheon, S., Lee, J. H., Park, S., Bang, S. I., Lee, W. J., Yoon, D. Y., et al. (2011). Overexpression of IL-32alpha increases natural killer cell-mediated killing through up-regulation of Fas and UL16-binding protein 2 (ULBP2) expression in human chronic myeloid leukemia cells. *J. Biol. Chem.* 286, 12049–12055. doi: 10.1074/jbc.M110.159756

Dahl, C. A., Schall, R. P., He, H. L., and Cairns, J. S. (1992). Identification of a novel gene expressed in activated natural killer cells and T cells. *J. Immunol.* 148, 597–603.

Dali-Youcef, N., Vix, M., Costantino, F., El-Saghire, H., Lhermitte, B., Callari, C., et al. (2019). Interleukin-32 contributes to human nonalcoholic fatty liver disease and insulin resistance. *Hepatol. Commun.* 3, 1205–1220. doi: 10.1002/hep4.1396

Goda, C., Kanaji, T., Kanaji, S., Tanaka, G., Arima, K., Ohno, S., et al. (2006). Involvement of IL-32 in activation-induced cell death in T cells. *Int. Immunol.* 18, 233–240. doi: 10.1093/intimm/dxh339

Gruber, T., Kremenovic, M., Sadozai, H., Rombini, N., Baeriswyl, L., Maibach, F., et al. (2020). IL-32gamma potentiates tumor immunity in melanoma. *JCI Insight* 5:e138772. doi: 10.1172/jci.insight.138772

Gyorffy, B., Lanczky, A., Eklund, A. C., Denkert, C., Budczies, J., Li, Q., et al. (2010). An online survival analysis tool to rapidly assess the effect of 22,277 genes on breast cancer prognosis using microarray data of 1,809 patients. *Breast Cancer Res. Treat.* 123, 725–731. doi: 10.1007/s10549-009-0674-9

Hong, J. T., Son, D. J., Lee, C. K., Yoon, D. Y., Lee, D. H., and Park, M. H. (2017). Interleukin 32, inflammation and cancer. *Pharmacol. Ther.* 174, 127–137. doi: 10.1016/j.pharmthera.2017.02.025

Jeong, H. J., Shin, S. Y., Oh, H. A., Kim, M. H., Cho, J. S., and Kim, H. M. (2011). IL-32 up-regulation is associated with inflammatory cytokine production in allergic rhinitis. *J. Pathol.* 224, 553–563. doi: 10.1002/path.2899

Kang, J. W., Choi, S. C., Cho, M. C., Kim, H. J., Kim, J. H., Lim, J. S., et al. (2009). A proinflammatory cytokine interleukin-32beta promotes the production of an anti-inflammatory cytokine interleukin-10. *Immunology* 128(1 Suppl.), e532–e540. doi: 10.1111/j.1365-2567.2008.03025.x

Kang, Y. H., Park, M. Y., Yoon, D. Y., Han, S. R., Lee, C. I., Ji, N. Y., et al. (2012). Dysregulation of overexpressed IL-32alpha in hepatocellular carcinoma suppresses cell growth and induces apoptosis through inactivation of NF-kappaB and Bcl-2. *Cancer Lett.* 318, 226–233. doi: 10.1016/j.canlet.2011.12.023

Kim, D. H., Park, E. S., Lee, A. R., Park, S., Park, Y. K., Ahn, S. H., et al. (2018). Intracellular interleukin-32gamma mediates antiviral activity of cytokines against hepatitis B virus. *Nat. Commun.* 9:3284. doi: 10.1038/s41467-018-05782-5

Kim, S. H., Han, S. Y., Azam, T., Yoon, D. Y., and Dinarello, C. A. (2005). Interleukin-32: a cytokine and inducer of TNFalpha. *Immunity* 22, 131–142. doi: 10.1016/j.immuni.2004.12.003

Morsaljahan, Z., Rafiei, A., Valadan, R., Abedini, M., Pakseresht, M., and Khajavi, R. (2017). Association between interleukin-32 polymorphism and multiple sclerosis. *J. Neurol. Sci.* 379, 144–150. doi: 10.1016/j.jns.2017.05.045

Nabeki, B., Ishigami, S., Uchikado, Y., Sasaki, K., Kita, Y., Okumura, H., et al. (2015). Interleukin-32 expression and Treg infiltration in esophageal squamous cell carcinoma. *Anticancer Res.* 35, 2941–2947.

Navarro-Barriuso, J., Mansilla, M. J., and Martinez-Caceres, E. M. (2018). Searching for the transcriptomic signature of immune tolerance induction-biomarkers of safety and functionality for tolerogenic dendritic cells and regulatory macrophages. *Front. Immunol.* 9:2062. doi: 10.3389/fimmu.2018.02062

Ng, M. S. F., Roth, T. L., Mendoza, V. F., Marson, A., and Burt, T. D. (2019). Helios enhances the preferential differentiation of human fetal CD4(+) naive T cells into regulatory T cells. *Sci. Immunol.* 4:eaav5947. doi: 10.1126/sciimmunol.aav5947

Nold, M. F., Nold-Petry, C. A., Pott, G. B., Zepp, J. A., Saavedra, M. T., Kim, S. H., et al. (2008). Endogenous IL-32 controls cytokine and HIV-1 production. *J. Immunol.* 181, 557–565. doi: 10.4049/jimmunol.181.1.557

Palstra, R. J., de Crignis, E., Roling, M. D., van Staveren, T., Kan, T. W., van Ijcken, W., et al. (2018). Allele-specific long-distance regulation dictates IL-32 isoform switching and mediates susceptibility to HIV-1. *Sci. Adv.* 4:e1701729. doi: 10.1126/sciadv.1701729

Park, M. H., Song, M. J., Cho, M. C., Moon, D. C., Yoon, D. Y., Han, S. B., et al. (2012). Interleukin-32 enhances cytotoxic effect of natural killer cells to cancer cells via activation of death receptor 3. *Immunology* 135, 63–72. doi: 10.1111/j.1365-2567.2011.03513.x

Paz, H., Tsoi, J., Kalbasi, A., Grasso, C. S., McBride, W. H., Schaue, D., et al. (2019). Interleukin 32 expression in human melanoma. *J. Transl. Med.* 17:113. doi: 10.1186/s12967-019-1862-y

Rosenow, F., and Menzler, K. (2013). Invasive EEG studies in tumor-related epilepsy: when are they indicated and with what kind of electrodes? *Epilepsia* 54(Suppl.9), 61–65. doi: 10.1111/epi.12446

Santinelli, L., Statzu, M., Pierangeli, A., Frasca, F., Bressan, A., Pinacchio, C., et al. (2019). Increased expression of IL-32 correlates with IFN-gamma, Th1 and Tc1 in virologically suppressed HIV-1-infected patients. *Cytokine* 120, 273–281. doi: 10.1016/j.cyto.2019.01.012

Shioya, M., Nishida, A., Yagi, Y., Ogawa, A., Tsujikawa, T., Kim-Mitsuyama, S., et al. (2007). Epithelial overexpression of interleukin-32alpha in inflammatory bowel disease. *Clin. Exp. Immunol.* 149, 480–486. doi: 10.1111/j.1365-2249.2007.03439.x

Smith, A. J., Toledo, C. M., Wietgrefe, S. W., Duan, L., Schacker, T. W., Reilly, C. S., et al. (2011). The immunosuppressive role of IL-32 in lymphatic tissue during HIV-1 infection. *J. Immunol.* 186, 6576–6584. doi: 10.4049/jimmunol.1100277

Sorrentino, C., and Di Carlo, E. (2009). Expression of IL-32 in human lung cancer is related to the histotype and metastatic phenotype. *Am. J. Respir. Crit. Care Med.* 180, 769–779. doi: 10.1164/rccm.200903-0400OC

Suga, H., Sugaya, M., Miyagaki, T., Kawaguchi, M., Fujita, H., Asano, Y., et al. (2014). The role of IL-32 in cutaneous T-cell lymphoma. *J. Invest. Dermatol.* 134, 1428–1435. doi: 10.1038/jid.2013.488

Togashi, Y., Shitara, K., and Nishikawa, H. (2019). Regulatory T cells in cancer immunosuppression - implications for anticancer therapy. *Nat. Rev. Clin. Oncol.* 16, 356–371. doi: 10.1038/s41571-019-0175-7

Tsai, C. Y., Wang, C. S., Tsai, M. M., Chi, H. C., Cheng, W. L., Tseng, Y. H., et al. (2014). Interleukin-32 increases human gastric cancer cell invasion associated with tumor progression and metastasis. *Clin. Cancer Res.* 20, 2276–2288. doi: 10.1158/1078-0432.CCR-13-1221

Xin, T., Chen, M., Duan, L., Xu, Y., and Gao, P. (2018). Interleukin-32: its role in asthma and potential as a therapeutic agent. *Respir. Res.* 19:124. doi: 10.1186/s12931-018-0832-x

Yan, H., Dong, M., Liu, X., Shen, Q., He, D., Huang, X., et al. (2019). Multiple myeloma cell-derived IL-32gamma increases the immunosuppressive function of macrophages by promoting indoleamine 2,3-dioxygenase (IDO) expression. *Cancer Lett.* 446, 38–48. doi: 10.1016/j.canlet.2019.01.012

Yousif, N. G., Al-Amran, F. G., Hadi, N., Lee, J., and Adrienne, J. (2013). Expression of IL-32 modulates NF-kappaB and p38 MAP kinase pathways in human esophageal cancer. *Cytokine* 61, 223–227. doi: 10.1016/j.cyto.2012.09.022

Yun, H. M., Kim, J. A., Hwang, C. J., Jin, P., Baek, M. K., Lee, J. M., et al. (2015). Neuroinflammatory and AMYLOIDOGENIC ACTIVITies of IL-32beta in Alzheimer's disease. *Mol. Neurobiol.* 52, 341–352. doi: 10.1007/s12035-014-8860-0

Zheng, Y., Chen, Z., Han, Y., Han, L., Zou, X., Zhou, B., et al. (2020). Immune suppressive landscape in the human esophageal squamous cell carcinoma microenvironment. *Nat. Commun.* 11:6268. doi: 10.1038/s41467-020-20019-0

Conflict of Interest: The authors declare that the research was conducted in the absence of any commercial or financial relationships that could be construed as a potential conflict of interest.

Publisher's Note: All claims expressed in this article are solely those of the authors and do not necessarily represent those of their affiliated organizations, or those of the publisher, the editors and the reviewers. Any product that may be evaluated in this article, or claim that may be made by its manufacturer, is not guaranteed or endorsed by the publisher.

Copyright © 2021 Han, Chen, Chen, Zhou, Zheng and Shen. This is an open-access article distributed under the terms of the Creative Commons Attribution License (CC BY). The use, distribution or reproduction in other forums is permitted, provided the original author(s) and the copyright owner(s) are credited and that the original publication in this journal is cited, in accordance with accepted academic practice. No use, distribution or reproduction is permitted which does not comply with these terms.

frontiers in Cell and Developmental Biology

ORIGINAL RESEARCH
published: 30 August 2021
doi: 10.3389/fcell.2021.727762

Ferroptosis Driver *SOCS1* and Suppressor *FTH1* Independently Correlate With M1 and M2 Macrophage Infiltration in Head and Neck Squamous Cell Carcinoma

Zhang-Wei Hu[1,2], Yi-Hui Wen[1,2], Ren-Qiang Ma[1,2], Lin Chen[1,2], Xue-Lan Zeng[1,2], Wei-Ping Wen[1,2,3] and Wei Sun[1,2]**

[1] Department of Otolaryngology, The First Affiliated Hospital, Sun Yat-sen University, Guangzhou, China, [2] Otorhinolaryngology Institute, Sun Yat-sen University, Guangzhou, China, [3] Department of Otolaryngology, The Sixth Affiliated Hospital of Sun Yat-sen University, Guangzhou, China

OPEN ACCESS

Edited by:
Qian Xiao,
Rutgers Cancer Institute of New Jersey, United States

Reviewed by:
Sohini Roy,
Vanderbilt University Medical Center, United States
Zheng Wei,
Yale University, United States
Guang Lei,
Hunan Cancer Hospital, Xiangya School of Medicine, Central South University, China

***Correspondence:**
Wei Sun
sunwei26@mail.sysu.edu.cn
Wei-Ping Wen
wenwp@mail.sysu.edu.cn

Specialty section:
This article was submitted to Molecular and Cellular Pathology, a section of the journal Frontiers in Cell and Developmental Biology

Received: 19 June 2021
Accepted: 11 August 2021
Published: 30 August 2021

Citation:
Hu Z-W, Wen Y-H, Ma R-Q, Chen L, Zeng X-L, Wen W-P and Sun W (2021) Ferroptosis Driver SOCS1 and Suppressor FTH1 Independently Correlate With M1 and M2 Macrophage Infiltration in Head and Neck Squamous Cell Carcinoma. Front. Cell Dev. Biol. 9:727762. doi: 10.3389/fcell.2021.727762

Objective: To investigate the role of ferroptosis, an iron-dependent form of non-apoptotic cell death, in the head and neck squamous cell carcinoma (HNSCC) immune microenvironment.

Materials and Methods: A list of ferroptosis-related genes was obtained from the FerrDb database. Gene expression data were acquired from the cancer genome atlas (TCGA) and analyzed using the R language. Protein–protein interaction analysis was conducted using STRING and GeneMANIA. The correlations between gene expression levels and a patient's survival were analyzed using GEPIA, the Kaplan–Meier estimate, and a multivariate Cox proportional hazards model. The expression results were verified using Oncomine and Human Protein Atlas data. We used the TIMER, GEPIA2, GEPIA2021, and TIMER2 databases to investigate the relationships between gene expression and infiltrating immune cells.

Results: Analysis of differentially expressed genes (DEGs) identified nine each ferroptosis drivers and ferroptosis suppressors, among which four genes correlated with survival as follows: two drivers (*SOCS1*, *CDKN2A*) associated with better survival and two suppressors (*FTH1*, *CAV1*) associated with poorer survival. Multivariate Cox survival analysis identified *SOCS1* and *FTH1* as independent prognostic factors for HNSCC, and their higher expression levels were verified using Oncomine and HPA data. The results acquired using TIMER, GEPIA2, GEPIA2021, and TIMER2 data revealed that the driver *SOCS1* and the suppressor *FTH1* independently correlated with M1 and M2 macrophage infiltration.

Conclusions: The ferroptosis driver *SOCS1* and suppressor *FTH1* are independent prognostic factors and that correlate with M1 and M2 macrophage infiltration in HNSCC. Targeting ferroptosis-immunomodulation may serve as a strategy to enhance the activity of immunotherapy.

Keywords: ferroptosis, suppressor of cytokine signaling-1, ferritin heavy chain, tumor microenvironment, immune therapy

INTRODUCTION

Head and neck squamous cell carcinoma (HNSCC) is the sixth most common cancer worldwide (Siegel et al., 2020). In 2016, the United States Food and Drug Administration approved immunotherapy as second-line monotherapy for recurrent or metastatic HNSCC, and in 2019, as front-line treatment of inoperable HNSCC (Ferris et al., 2016; Seiwert et al., 2016; Burtness et al., 2019). Despite great progress in immunotherapy, only a small subset of patients with HNSCC respond to immune checkpoint inhibitors (Johnson et al., 2020), mainly because of the immunosuppressive microenvironment associated with tumor immunosuppressive cells, including tumor-associated macrophages (TAMs, also called M2d), regulatory T cells (Tregs), and other immunomodulatory cells (Watermann et al., 2021). Thus, decreasing the populations of such cells may serve as a strategy to improve the patients' objective response rates to immunotherapy.

Ferroptosis, a term coined in 2012, is an iron-dependent form of non-apoptotic cell death (Dixon et al., 2012). On one hand, in tumor microenvironment ferroptosis seems to have a dual role in tumor promotion and suppression, depending on releasing damage-associated molecular patterns and activating immune response (Chen et al., 2021). On the other hand, ferroptosis is thought to have synergistic effects to suppress tumor growth in combination with other anti-tumor drugs, including immune checkpoint inhibitors (Roh et al., 2016; Wang et al., 2019). Currently, numerous studies focus on the role of ferroptosis in tumors, particularly in tumor cells and infiltrating antitumor immune cells (Wang et al., 2019; Chen et al., 2021). However, the role of ferroptosis in the functions of infiltrating immunosuppressive cells is unknown. We previously found that the expression of the ferroptosis suppressor gene *FTH1* positively correlated with macrophages in most solid tumors (Hu et al., 2021), indicating an important role for ferroptosis in regulating tumor immunity.

In the present study, we mined data acquired from FerrDb to comprehensively analyze the correlations between ferroptosis-related genes, including drivers and suppressors, as well as with tumor-infiltrating immune cells in HNSCC, with the goal of uncovering the potential role of ferroptosis in the immune response to HNSCC.

MATERIALS AND METHODS

Data Sources

The expression levels of genes and clinical information regarding HNSCC were acquired from the cancer genome atlas (TCGA)[1] through the UCSC Xena tool.[2] The use of such open-access data did not require approval from the local ethics committee.

[1]https://genomecancer.ucsc.edu/

[2]https://xenabrowser.net/

Ferroptosis-Related Genes and Differentially Expressed Genes

A list of ferroptosis-related genes was obtained from the FerrDb database (Zhou and Bao, 2020)[3] that includes 98 ferroptosis driver genes and 94 ferroptosis suppressor genes (**Supplementary Table 1**). Differentially expressed genes (DEGs) were analyzed using the empirical Bayes method with adjusted *p*-value (Benjamini and Hochberg FDR) through R (version 3.6.3), RStudio (version 1.2.5033), and the R LIMMA package (Linear Models for Microarray Data, version 3.42.2). Genes with $\log_2$FC absolute value higher than 1 and *q*-value lower than 0.01 were considered as DEGs. The correlations between genes were investigated using the Pearson's correlation analysis.

Protein–Protein Interaction Analysis

Protein–protein interactions (PPIs) were analyzed using the Search Tool for the Retrieval of Interacting Genes/Proteins dataset (STRING, version 11.0b)[4] and the GeneMANIA dataset[5] that provides a biological network integration method for predicting gene function.

Univariate and Multivariate Analyses of Prognosis

Correlations between the expression levels of ferroptosis-related genes and overall survival (OS) were separately analyzed through

[3]http://www.zhounan.org/ferrdb/

[4]https://string-db.org/

[5]http://www.genemania.org

TABLE 1 | Baseline characteristics of the cancer genome atlas (TCGA) data.

Characteristic	n (%)	Characteristic	n(%)
Normal	82 (100%)	HNSCC	528 (100%)
Age		**Age**	
Mean	62.3	Mean	61.4
Range	26.2–87.7	Range	20.0–90.1
Gender		**Gender**	
Male	57 (69.5%)	Male	386 (73.1%)
Female	25 (30.5%)	Female	142 (26.9%)
Metastatic	2 (100%)	T	
Age		T1	49 (9.3%)
Mean	61.6	T2	140 (26.5%)
Range	55.7–67.5	T3	101 (19.1%)
Gender		T4	175 (33.1%)
Male	1 (50%)	Unknown	63 (11.9%)
Female	1 (50%)	N	
		N0	180 (34.1%)
		N+	248 (47.0%)
		Unknown	100 (18.9%)
		Stage	
		I	27 (5.1%)
		II	74 (14.0%)
		III	82 (15.5%)
		IV	270 (51.1%)
		Unknown	75 (14.2%)

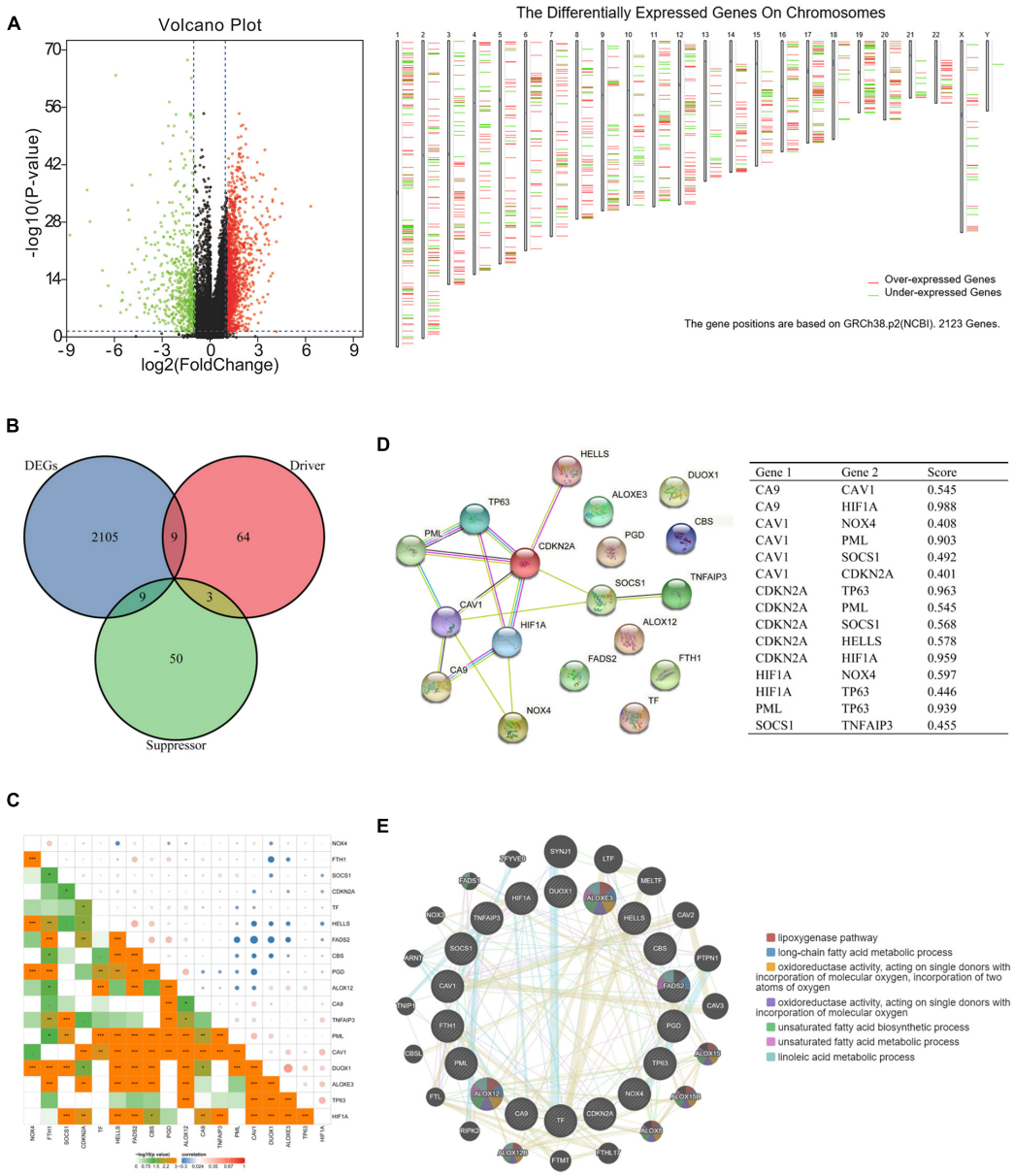

Gene 1	Gene 2	Score
CA9	CAV1	0.545
CA9	HIF1A	0.988
CAV1	NOX4	0.408
CAV1	PML	0.903
CAV1	SOCS1	0.492
CAV1	CDKN2A	0.401
CDKN2A	TP63	0.963
CDKN2A	PML	0.545
CDKN2A	SOCS1	0.568
CDKN2A	HELLS	0.578
CDKN2A	HIF1A	0.959
HIF1A	NOX4	0.597
HIF1A	TP63	0.446
PML	TP63	0.939
SOCS1	TNFAIP3	0.455

FIGURE 1 | Ferroptosis-related differentially expressed genes (DEGs) and protein–protein interaction (PPI) analysis. **(A)** Volcano plot and chromosomal localizations of DEGs in head and neck squamous cell carcinoma (HNSCC) ("limma" analysis) **(B)** Venn diagram of common genes encoding ferroptosis drivers and suppressors that correlated with DEGs (R package analysis). **(C)** The correlation of expressions between each two genes of the 18 selected ferroptosis-related genes. **(D)** Annotation of ferroptosis-related differentially expressed proteins and their co-expression scores (STRING analysis). **(E)** PPI network of ferroptosis-related DEGs (GeneMANIA analysis), ALOXE3 and ALOXE12 were primarily related to the lipoxygenase pathway, while ALOXE3, ALOXE12, FADS2 were primarily related to the long-chain fatty acid metabolic process.

Gene Expression Profiling Interactive Analysis (GEPIA)[6] with 50% cutoff and the Kaplan–Meier Plotter[7] with auto select best cutoff. Multivariate Cox proportional hazard model analysis was implemented using RStudio (version 1.2.5033) and the R SURVIVAL package (version 3.2-3).

Oncomine Platform and the Human Protein Atlas

The mRNA levels of SOCS1 and FTH1 for the datasets GSE2379, GSE3524, GSE6791, and PMID14729608 were acquired from the Oncomine Platform.[8] Through GraphPad Prism 7.0, the two-tailed unpaired *t*-test assuming equal variances was

[6]http://gepia.cancer-pku.cn/index.html

[7]http://kmplot.com/analysis/

[8]https://www.oncomine.org

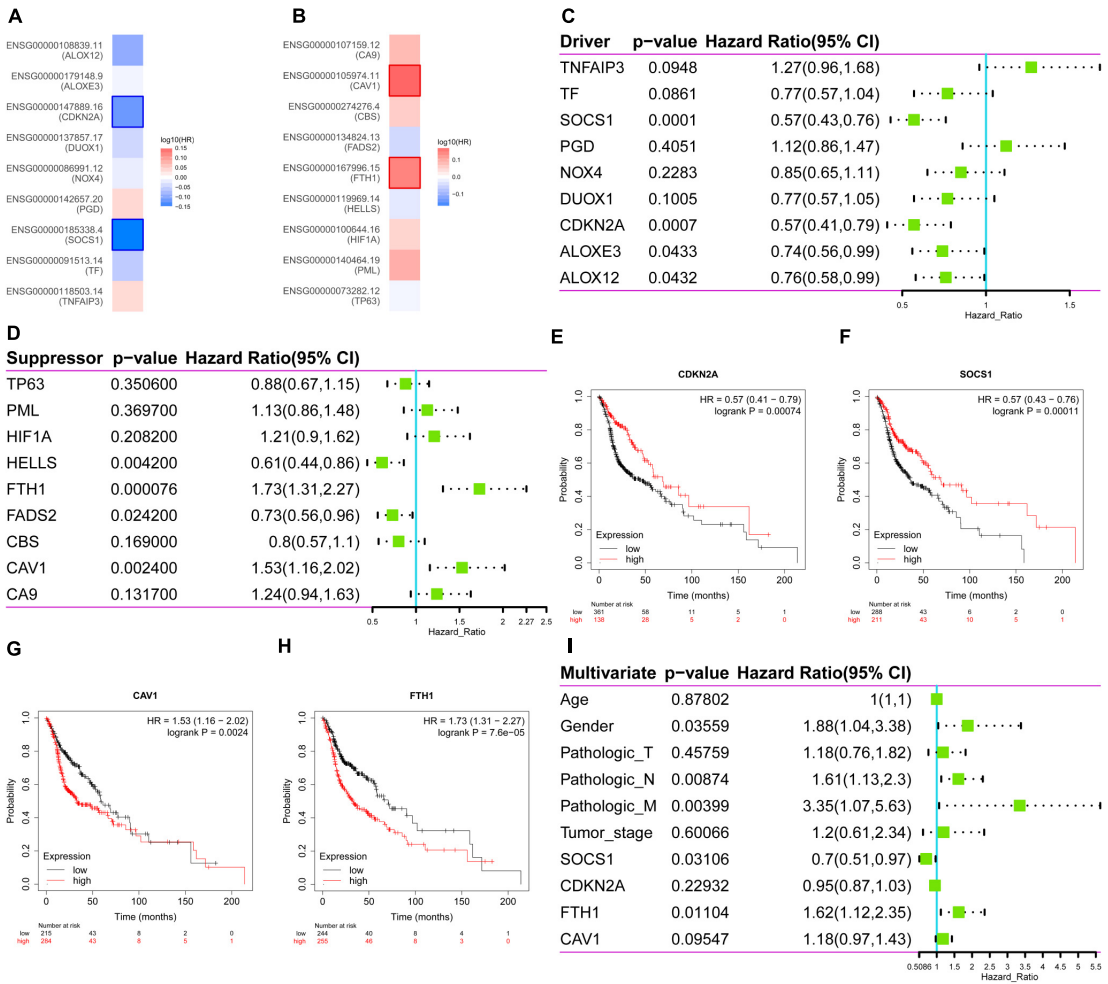

FIGURE 2 | Survival analysis of the expression levels of the ferroptosis driver and suppressor genes in HNSCC. **(A)** The ferroptosis drivers *CDKN2A* and *SOCS1* correlated with longer overall survival (OS). **(B)** The ferroptosis suppressors *CAV1* and *FTH1* correlated with poorer OS. **(C–H)** Correlations between ferroptosis driver and suppressor genes and OS (Kaplan–Meier Plotter). **(I)** Multivariate Cox survival analysis showed that *SOCS1* (HR 0.7, 95%CI 0.51–0.97, $p < 0.05$) and *FTH1* (HR 1.62, 95%CI 1.12–2.35, $p < 0.05$) were independent prognostic factors for HNSCC.

performed to analyze differences in gene expression. Moreover, protein immunohistochemistry for SOCS1 and FTH1 in normal and tumor tissues were obtained from the Human Protein Atlas (HPA).[9]

Analysis of Immune Cell Infiltration

The correlations between gene expression and immune cell infiltration (B cells, CD8+ T cells, CD4+ T cells, macrophages, neutrophils, and dendritic cells) were investigated using the Tumor IMmune Estimation Resource (TIMER)[10] tool. We used GEPIA2[11] to perform pairwise gene correlation analysis. We estimated immune infiltration using the CIBERSORT, CIBERSORT-ABS, QUANTISEQ, MCP-COUNTER, XCELL, and EPIC algorithms through the TIMER2 resource.[12] We investigated gene expression levels in various immune cells by CIBERSORT through the GEPIA2021.[13]

RESULTS

Patients' Baseline Characteristics

In total, the gene expression data and clinical characteristics of 528 HNSCC, 2 metastatic and 82 normal tissue samples from the TCGA database were included in the study. Patients' baseline characteristics including age at diagnosis, sex, pathological T, pathological N, pathological M, and tumor stage are presented in **Table 1**.

[9]https://www.proteinatlas.org/

[10]https://cistrome.shinyapps.io/timer/

[11]http://gepia2.cancer-pku.cn/#index

[12]http://timer.comp-genomics.org/

[13]http://gepia2021.cancer-pku.cn/

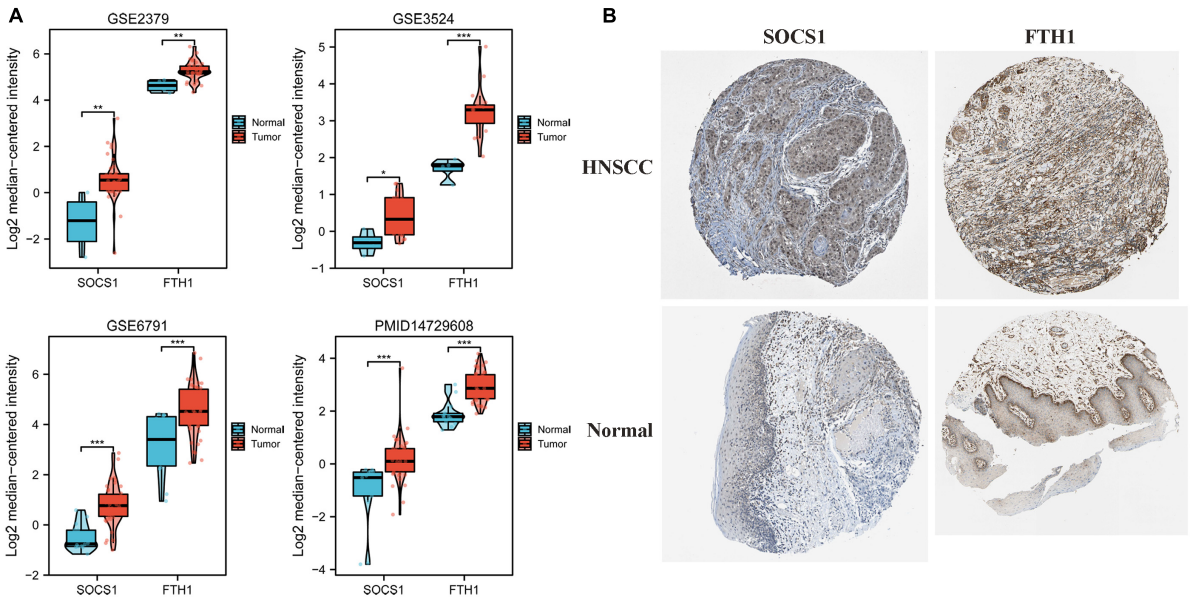

FIGURE 3 | Analysis of *SOCS1* and *FTH1* gene expression using Oncomine and the HPA. **(A)** Validation of higher *SOCS1* and *FTH1* gene expression levels using the datasets GSE2379 (*SOCS1*, $t = 3.569$, $p = 0.0010$; *FTH1*, $t = 3.168$, $p = 0.003$), GSE3524 (*SOCS1*, $t = 2.332$, $p = 0.0315$; *FTH1*, $t = 4.362$, $p = 0.0004$), GSE6791 (*SOCS1*, $t = 5.449$, $p < 0.0001$; *FTH1*, $t = 4.153$, $p = 0.0001$), and PMID14729608 (*SOCS1*, $t = 4.217$, $p < 0.0001$; *FTH1*, $t = 5.917$, $p < 0.0001$). **(B)** SOCS1 and FTH1 protein levels in HNSCC were higher in HNSCC compared with those in normal tissues.

Gene Expression Screening and PPI Analysis

To explore the differentially expressed ferroptosis-related genes in HNSCC, mRNA expression was analyzed with the TCGA database. In total, we identified 2123 DEGs (**Figure 1A**), among which nine were ferroptosis-related drivers (*TNFAIP3*, *TF*, *SOCS1*, *PGD*, *NOX4*, *DUOX1*, *CDKN2A*, *ALOXE3*, *ALOX12*) and nine were ferroptosis-related suppressors (*TP63*, *PML*, *HIF1A*, *HELLS*, *FTH1*, *FADS2*, *CBS*, *CAV1*, *CA9*) (**Figure 1B**). Pearson correlation analysis was conducted to assess the correlations of expressions between each two genes of the above 18 ferroptosis related genes (**Figure 1C**). It showed that most of the gene expressions have statistical correlations and the detailed results were shown in the **Supplementary Table 2**. Then, we used STRING to analyze the PPI network, and the gene annotations and scores are listed in **Figure 1D** and **Supplementary Table 3**. The results of GeneMANIA revealed that ALOXE3 and ALOXE12 are primarily related to the lipoxygenase pathway, and ALOXE3, ALOXE12, FADS2 are primarily related to the long-chain fatty acid metabolic process (**Figure 1E**).

SOCS1 and *FTH1* Are Independent Prognostic Factors

Then, the correlations between ferroptosis-related DEGs and survival were analyzed, respectively through GEPIA (**Figures 2A,B**) and Kaplan–Meier Plotter (**Figures 2C,D**). Four common genes that correlated with survival were identified as follows: two drivers, *CDKN2A* (HR 0.57, 95%CI 0.41–0.79, $p = 7.4 \times 10^{-4}$) (**Figure 2E**); *SOCS1* (HR 0.57, 95%CI 0.43–0.76, $p = 1.1 \times 10^{-4}$) (**Figure 2F**); and two suppressors, *CAV1*, (HR 1.53, 95%CI 1.16–2.02, $p = 2.4 \times 10^{-3}$) (**Figure 2G**) and *FTH1* (HR 1.73, 95%CI 1.31–2.27, $p = 7.6 \times 10^{-5}$) (**Figure 2H**). Multivariate Cox survival analysis showed that *SOCS1* (HR 0.7, 95%CI 0.51–0.97, $p < 0.05$) and *FTH1* (HR 1.62, 95%CI 1.12–2.35, $p < 0.05$) were independent prognostic factors for HNSCC (likelihood ratio test $p = 3 \times 10^{-6}$, Wald test $p = 5 \times 10^{-6}$, score log-rank test $p = 9 \times 10^{-9}$) (**Figure 2I**).

SOCS1 and *FTH1* Are Expressed at Elevated Levels in HNSCC

Given these findings that ferroptosis-related DEGs *SOCS1* and *FTH1* were independent prognostic factors in HNSCC, we next validated their higher levels using Oncomine and HPA data. The significantly higher *SOCS1* and *FTH1* mRNA levels in HNSCC compared with those in normal tissues were validated using the datasets GSE2379 (*SOCS1*, $t = 3.569$, $p = 0.0010$; *FTH1*, $t = 3.168$, $p = 0.003$), GSE3524 (*SOCS1*, $t = 2.332$, $p = 0.0315$; *FTH1*, $t = 4.362$, $p = 0.0004$), GSE6791 (*SOCS1*, $t = 5.449$, $p < 0.0001$; *FTH1*, $t = 4.153$, $p = 0.0001$), and PMID14729608 (*SOCS1*, $t = 4.217$, $p < 0.0001$; *FTH1*, $t = 5.917$, $p < 0.0001$) (**Figure 3A**). The protein levels of SOCS1 and FTH1 were correspondingly higher in HNSCC compared with those in normal tissues using HPA data (**Figure 3B**).

FTH1 mRNA Levels Positively Correlate With Lymph Node Metastasis

Furthermore, we analyzed the correlations between the mRNA levels of *SOCS1* and *FTH1* and clinical information (**Figures 4A–L**). *SOCS1* (**Figure 4A**, $t = 10.74$, $p < 0.001$) and *FTH1*

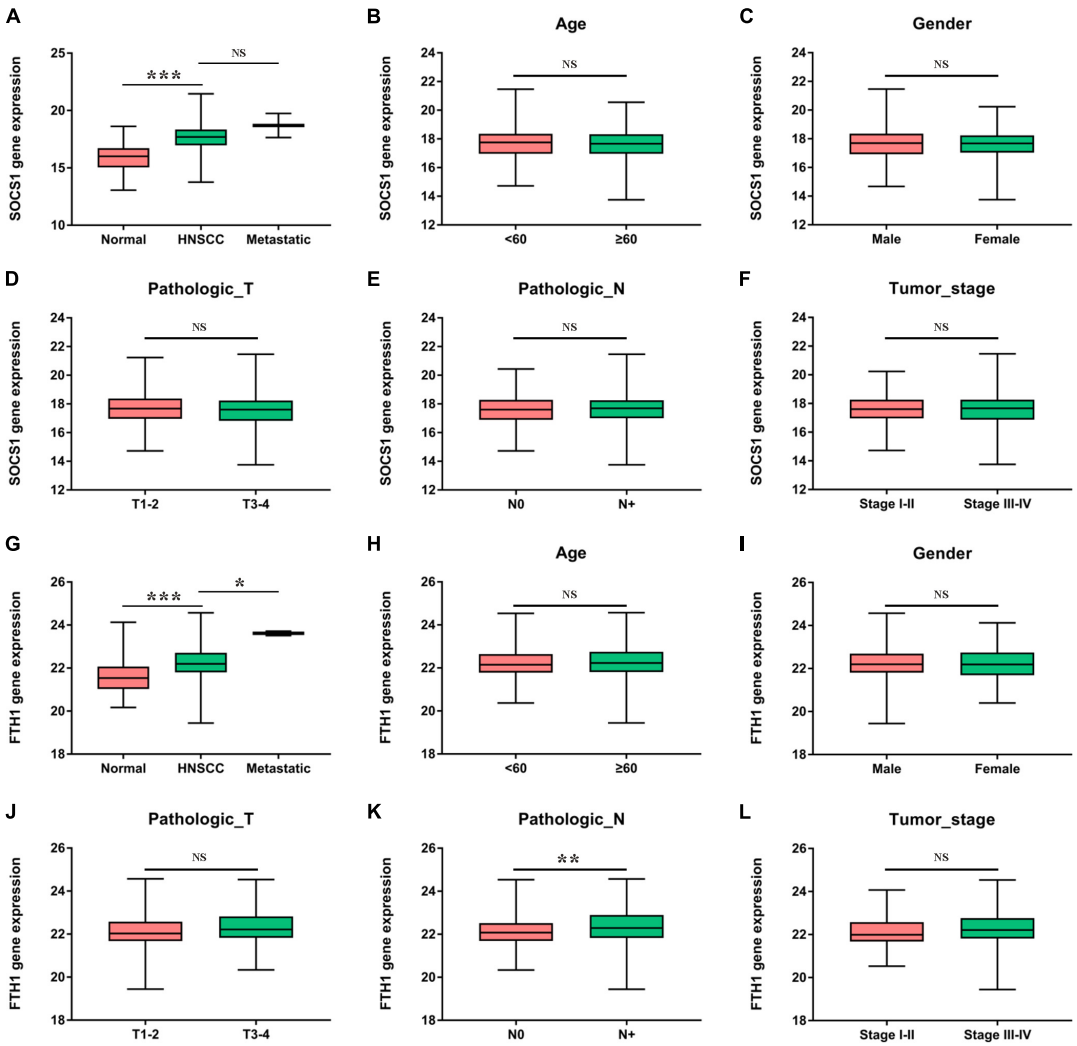

FIGURE 4 | Clinical significance of *SOCS1* and *FTH1* gene expression in HNSCC. **(A)** *SOCS1* levels were significantly higher in HNSCC compared with those of normal tissues ($t = 10.74$, $p < 0.001$). **(B–F)** There was no statistically significant difference between *SOCS1* levels and age, sex, pathological T stage, pathological N stage, or tumor stage. **(G)** The levels of *FTH1* were significantly higher in HNSCC compared with those in normal tissues ($t = 4.976$, $p < 0.001$) and were significantly associated with metastatic sites ($t = 2.569$, $p = 0.0105$). **(H–L)** *FTH1* levels were significantly higher in HNSCC with node metastasis compared with HNSCC without such metastasis (*K*, $t = 2.764$, $p = 0.0060$), and there was no significant difference between *FTH1* levels and age, sex, pathological T stage, or tumor stage.

(**Figure 4G**, $t = 4.976$, $p < 0.001$) mRNA levels were higher in HNSCC tissues compared with those in normal tissues. Furthermore, *FTH1* mRNA levels were higher in HNSCC with lymph node metastasis than without (**Figure 4K**, $t = 2.764$, $p = 0.0060$), consistent with the results of protein expression in our previous work (Hu et al., 2019).

SOCS1 Expression Positively Correlates With M1 Macrophages, and *FTH1* Expression Positively Correlates With M2 Macrophages and TAMs

Finally, we conducted correlation analysis of the mRNA levels of *SOCS1* and *FTH1* and infiltrating immune cells. The TIMER data showed that the mRNA levels of *SOCS1* (**Figure 5A**) and *FTH1* (**Figure 5B**) were significantly associated with the infiltration of macrophages and B cells, regardless of HPV status (*SOCS1* and B cells, $R = 0.246$, $p = 5.69 \times 10^{-8}$; *SOCS1* and macrophages, $R = 0.204$, $p = 6.36 \times 10^{-6}$; *FTH1* and B cells, $R = 0.128$, $p = 5.04 \times 10^{-3}$; *FTH1* and macrophages, $R = 0.343$, $p = 9.11 \times 10^{-5}$).

Then, GEPIA2 data were used to further analyze the correlation between *SOCS1* and *FTH1* levels and B-cell infiltration of tumors (**Supplementary Figures 1A,B**, *SOCS1* and B cells, $R = 0.25$, $p = 1.2 \times 10^{-8}$; *FTH1* and B cells, $R = -0.12$, $p = 7.6 \times 10^{-3}$) and macrophages through their immune cell signatures. The results of GEPIA2 verified the above correlations between *SOCS1* and *FTH1* levels and macrophage infiltration (**Figure 6** and **Supplementary Figures 1C–H**). Furthermore, *SOCS1* expression was mainly related to M1 macrophages

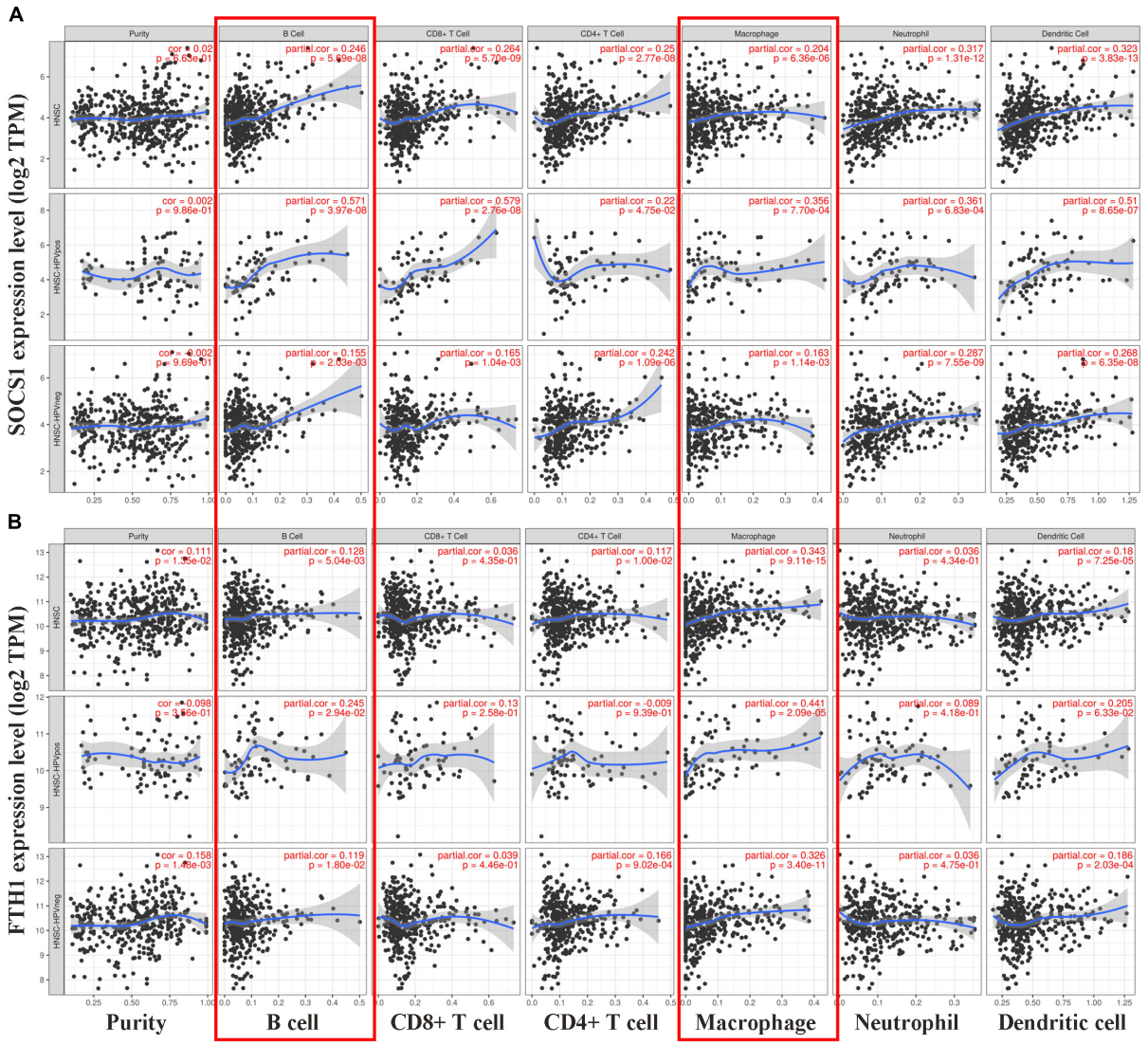

FIGURE 5 | Correlations between *SOCS1* and *FTH1* expression and immune cell infiltration in HNSCC (TIMER). **(A)** *SOCS1* mRNA levels positively correlated with B cell and macrophage infiltration, independent of HPV status (*SOCS1* and B cells, $R = 0.246$, $p = 5.69 \times 10^{-8}$; *SOCS1* and macrophages, $R = 0.204$, $p = 6.36 \times 10^{-6}$). **(B)** *FTH1* mRNA levels positively correlated with B cell and macrophage infiltration, independent of HPV status (*FTH1* and B cells, $R = 0.128$, $p = 5.04 \times 10^{-3}$; *FTH1* and macrophages, $R = 0.343$, $p = 9.11 \times 10^{-5}$).

($R = 0.19$, $p = 9.5 \times 10^{-6}$) (**Figure 6A**), while *FTH1* expression was significantly associated with M2 ($R = 0.21$, $p = 8 \times 10^{-7}$) (**Figure 6E**), TAMs ($R = 0.14$, $p = 1.9 \times 10^{-3}$) (**Figure 6F**), M2a ($R = 0.14$, $p = 1.3 \times 10^{-3}$) (**Supplementary Figure 1F**), M2b ($R = 0.17$, $p = 1.1 \times 10^{-4}$) (**Supplementary Figure 1G**), and M2c ($R = 0.13$, $p = 3.2 \times 10^{-3}$) (**Supplementary Figure 1H**).

Moreover, TIMER2.0 analysis further confirmed the correlations between *SOCS1* and *FTH1* levels and macrophage infiltration (A, EPIC, *SOCS1*, and macrophages, *Rho* = 0.295, $p = 2.46 \times 10^{-11}$; B, XCELL, *SOCS1*, and macrophages, *Rho* = 0.127, $p = 4.75 \times 10^{-3}$; C, CIBERSORT, *SOCS1*, and M1 macrophages, *Rho* = 0.197, $p = 1.11 \times 10^{-5}$; D, CIBERSORT, *SOCS1*, and M2 macrophages, *Rho* = −0.12, $p = 7.56 \times 10^{-3}$; E, TIDE, *SOCS1*, and M2 macrophages, *Rho* = −0.19, $p = 2.23 \times 10^{-5}$; F, EPIC, *FTH1*, and macrophages, *Rho* = 0.258, $p = 6.42 \times 10^{-9}$; G, XCELL, *FTH1*, and macrophages, *Rho* = 0.232, $p = 1.97 \times 10^{-7}$; H, CIBERSORT, *FTH1*, and M1 macrophages, *Rho* = 0.22, $p = 8.2 \times 10^{-7}$; I, CIBERSORT, *FTH1*, and M2 macrophages, *Rho* = 0.15, $p = 8.39 \times 10^{-4}$; J, TIDE, *FTH1*, and M2 macrophages *Rho* = 0.119, $p = 8.16 \times 10^{-3}$) (**Figure 7**).

Lastly, we investigated *SOCS1* and *FTH1* gene expression levels in various immune cells by CIBERSORT through GEPIA2021, the results revealed that M1 Macrophage has the highest median value of *SOCS1*, while M2 Macrophage has the highest median value of *FTH1* (**Supplementary Figure 2**).

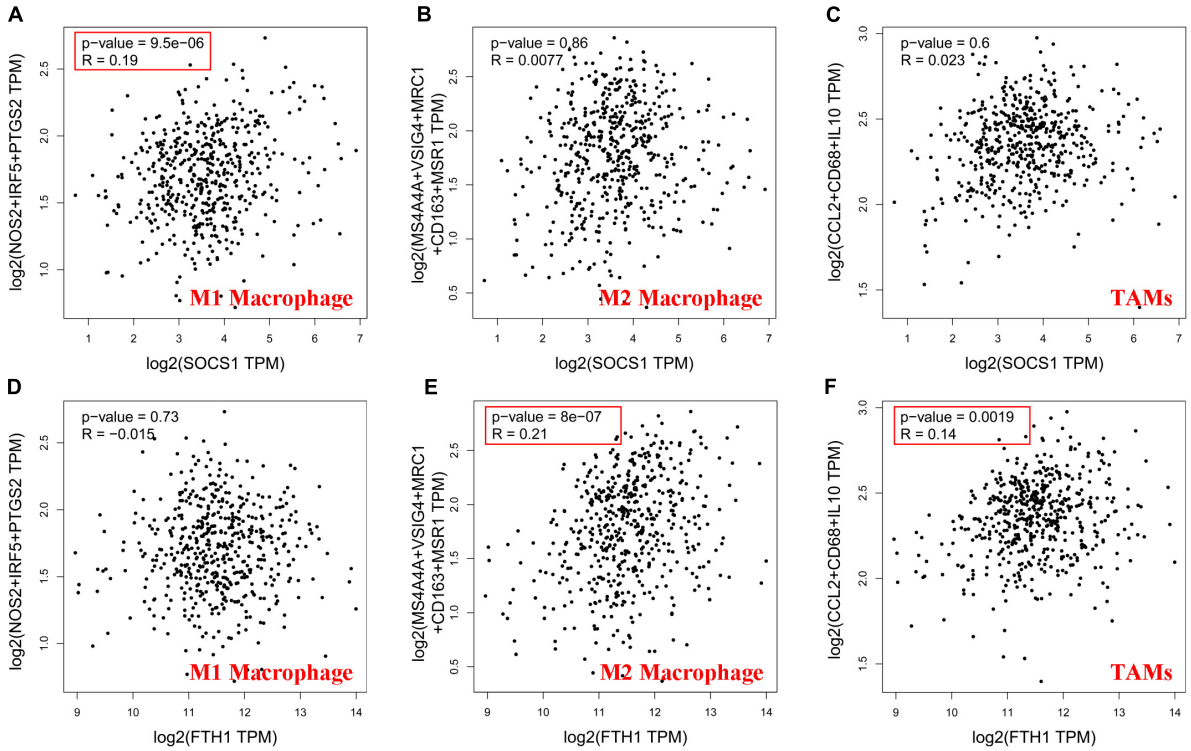

FIGURE 6 | Significance of the correlations between *SOCS1* and *FTH1* expression and markers of macrophages (GEPIA2). **(A)** *SOCS1* and M1 ($R = 0.19$, $p = 9.5 \times 10^{-6}$). **(B)** *SOCS1* and M2 ($R = 0.0077$, $p = 0.86$). **(C)** *SOCS1* and TAMs ($R = 0.023$, $p = 0.6$). **(D)** *FTH1* and M1 ($R = -0.015$, $p = 0.73$). **(E)** *FTH1* and M2 ($R = 0.21$, $p = 8 \times 10^{-7}$). **(F)** *FTH1* and TAMs ($R = 0.14$, $p = 1.9 \times 10^{-3}$).

DISCUSSION

Increasing recognition that ferroptosis plays complex roles in tumor biology fueled intense interest in its potential for developing novel cancer therapeutics (Lei et al., 2020; Chen et al., 2021). The induction of ferroptosis requires iron accumulation, lipid peroxidation, and membrane damage (Zheng and Conrad, 2020). Furthermore, a large quantity of iron is required to support the rapid proliferation cancer cells in most solid tumors (Torti and Torti, 2013; Manz et al., 2016). For example, we previously found that HNSCC tissue accumulates iron, particularly in metastatic tissue (Hu et al., 2019). Moreover, cancer cells maintain high metabolic activity and a higher load of reactive oxygen species (Jiang et al., 2021). Therefore, we believe that it is reasonable to assume that tumor cells are susceptible to ferroptosis. Furthermore, tumor cells may upregulate the expression of ferroptosis suppressors to counteract the driver to inhibit the antitumor function of ferroptosis (Rojo et al., 2018).

Here we show that the levels of ferroptosis driver *SOCS1* (Saint-Germain et al., 2017) and suppressor *FTH1* (Du et al., 2019) positively correlated among each other and were upregulated in HNSCC compared with their levels in normal tissues. The *SOCS1* gene, which resides on human chromosome 16p13.3, encodes a 211 amino-acid polypeptide chain (Yandava et al., 1999). The main function of *SOCS1* is to suppress cell signaling and promote ubiquitination through recruiting E3 ubiquitin ligases (Ying et al., 2019). *SOCS1* induces ferroptosis through p53 target genes and downregulation of the expression of SLC7A11 (Saint-Germain et al., 2017). Thus, *SOCS1* functions as a tumor suppressor, and the inhibition of this function may promote cancer progression or relapse. For example, a study of 83 patients with esophageal cancer found that exosome-associated miR-19b-3p promotes tumor progression by inhibiting *SOCS1* expression (Deng et al., 2021). Moreover, loss of SPTBN1 expression induces liver cancer through downregulation of *SOCS1* expression as well (Lin et al., 2021). In nasopharyngeal carcinoma, LINC00669 protects *SOCS1* from ubiquitinating STAT1, which promotes cancer cell proliferation and invasion (Qing et al., 2020). Here we show that *SOCS1* was differentially expressed at higher levels in HNSCC and served as a significant and independent prognostic factor for HNSCC, consistent with its role in hepatocellular carcinoma (Khan et al., 2020).

FTH1, the functional subunit of the major iron storage protein ferritin, possesses ferroxidase activity and efficiently reduces the toxicity of Fe^{2+} (Salatino et al., 2019). Furthermore, *FTH1* protect cancer cells from ferroptosis (Sun et al., 2016; Du et al., 2019). Here, we show that *FTH1* was expressed at higher levels in HNSCC compared with those of normal tissues, which is consistent with the findings of our previous study (Hu et al., 2019). Furthermore, *FTH1* served as an independent prognostic factor of poorer prognosis, in contrast to *SOCS1*.

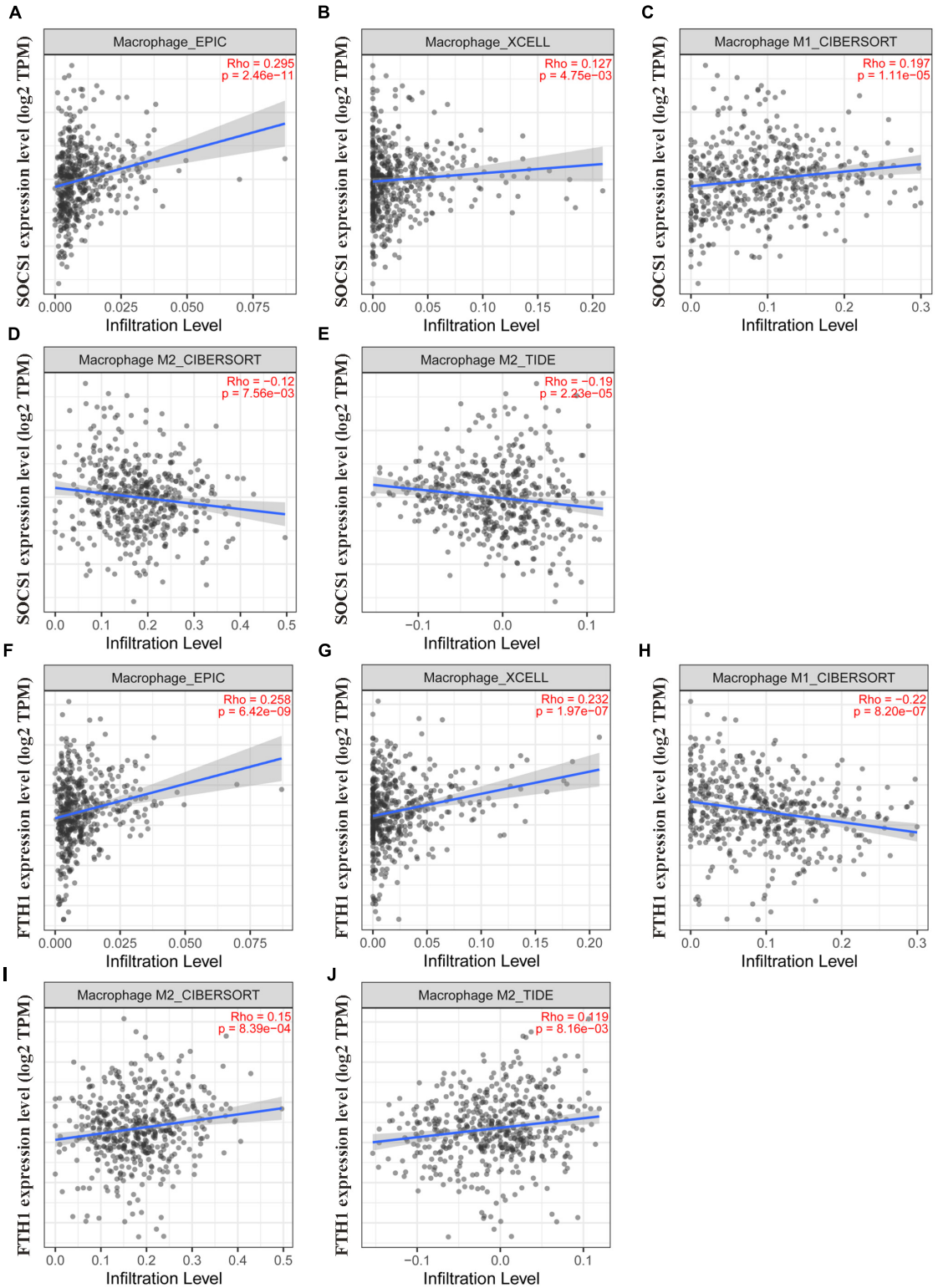

FIGURE 7 | Validation of the significant correlations between *SOCS1* and *FTH1* expression and macrophages (TIMER2.0). **(A)** EPIC, *SOCS1*, and macrophages ($R = 0.295$, $p = 2.46 \times 10^{-11}$). **(B)** XCELL, *SOCS1*, and macrophages ($R = 0.127$, $p = 4.75 \times 10^{-3}$). **(C)** CIBERSORT, *SOCS1*, and M1 macrophages ($R = 0.197$, $p = 1.11 \times 10^{-5}$). **(D)** CIBERSORT, *SOCS1*, and M2 macrophages ($R = -0.12$, $p = 7.56 \times 10^{-3}$). **(E)** TIDE, *SOCS1*, and M2 macrophages ($R = -0.19$, $p = 2.23 \times 10^{-5}$). **(F)** EPIC, *FTH1*, and macrophages ($R = 0.258$, $p = 6.42 \times 10^{-9}$). **(G)** XCELL, *FTH1*, and macrophages ($R = 0.232$, $p = 1.97 \times 10^{-7}$). **(H)** CIBERSORT, *FTH1*, and M1 macrophages ($R = -0.22$, $p = 8.2 \times 10^{-7}$). **(I)** CIBERSORT, *FTH1*, and M2 macrophages ($R = 0.15$, $p = 8.39 \times 10^{-4}$). **(J)** TIDE, *FTH1*, and M2 macrophages ($R = 0.119$, $p = 8.16 \times 10^{-3}$).

The multiple roles of ferroptosis in tumor immunity is attracting intense interest, which mainly focuses on CD8+ T cells that induce ferroptosis of cancer cells through secreting interferon gamma (Wang et al., 2019). In contrast, CD36-mediated ferroptosis impairs antitumor activity through dampening the functions of CD8+ T cells (Ma et al., 2021). The macrophage in the tumor immune microenvironment may exert dual influences on tumors depending on their phenotypic polarization (Wang et al., 2020; Maller et al., 2021). For example, in the M1–M2 macrophage polarization system, macrophages are typically divided into an antitumor M1, classically activated subtype, in the presence of high levels of TNF, NOS2, or MHC2. The alternative subtype, protumor M2 macrophages, are activated in the presence of high levels of ARG1, IL-10, CD163, CD204, or CD206 (Mantovani et al., 2002; Mantovani and Locati, 2013). Additionally, based on the different cytokine expression profiles, M2 could be further subdivided into M2a, M2b, M2c, and M2d (aka. tumor-associated macrophage, TAM), all of them share the immunosuppressive functions (Avila-Ponce De León et al., 2021). Furthermore, in tumors the microenvironment tends to induce M2-like TAMs (Shan et al., 2020).

To our knowledge, few studies focus on the role of ferroptosis in tumor infiltrating macrophages. Our previous analysis of diverse cancers found that in HNSCC, *FTH1* expression positively correlates with infiltration by macrophages of most solid tumors (Hu et al., 2021). Nevertheless, we were unable to identify the subtypes. Here we show that *FTH1* expression positively correlated with M2-macrophage infiltration and that in contrast, the ferroptosis driver *SOCS1* was mainly associated with M1-macrophage infiltration. We therefore hypothesize that the balance between the driver *SOCS1* and suppressor *FTH1* influence macrophage polarization through the regulation of ferroptosis.

An increasing number of studies focus on therapeutic targeting of TAMs, which mainly include depletion and repolarization of macrophages (DeNardo and Ruffell, 2019). The main methods used to deplete TAMs include the inhibition of CCL2–CCR2 signaling or the activity of the CSF1–CSF1R axis, both of which reduce the numbers of TAMs in tumor sites and improve the efficacy of immunotherapy (Kalbasi et al., 2017; Peranzoni et al., 2018; Wang et al., 2018). However, the macrophage is the primary phagocyte and antigen-presenting cell in the TME, and the depletion of TAMs inhibit their latent immune stimulatory function. Thus, repolarization of TAMs from the M2 to the M1 phenotype may serve as a more efficacious approach to improving the efficacy of immunotherapy (Goossens et al., 2019). We speculate that this may be achieved through the induction of ferroptosis in HNSCC through increasing the expression of *SOCS1* or decreasing that of *FTH1*.

In summary, we show here that the ferroptosis driver *SOCS1* and suppressor *FTH1* served as independent prognostic factors that independently correlate with M1 and M2 macrophage infiltration in HNSCC, suggesting that inducing ferroptosis directly influences the infiltration of M1–M2 macrophages. The targeting of ferroptosis-immunomodulation may therefore serve as a strategy to enhance the activity of immunotherapy.

DATA AVAILABILITY STATEMENT

Publicly available datasets were analyzed in this study. This data can be found here: https://genomecancer.ucsc.edu/; https://xenabrowser.net/; http://www.zhounan.org/ferrdb/; https://string-db.org/; http://www.genemania.org; http://gepia.cancer-pku.cn/index.html; http://kmplot.com/analysis/; https://www.oncomine.org; https://www.proteinatlas.org/; https://cistrome.shinyapps.io/timer/; http://gepia2.cancer-pku.cn/#index; http://timer.comp-genomics.org/; http://gepia2021.cancer-pku.cn/; and http://cis.hku.hk/TISIDB/.

AUTHOR CONTRIBUTIONS

Z-WH, WS, and W-PW conceived and designed the study. Y-HW, X-LZ, and LC downloaded the data, while Z-WH and R-QM analyzed the data. Z-WH wrote the manuscript. All authors read and approved the final manuscript.

FUNDING

This study was supported by the National Natural Science Foundation of China (NSFC) grants 82020108009, 81870696 (W-PW) and 81972527 (WS), Guangdong Natural Science Foundation of China grant 2018B030312008 (W-PW), Guangdong Research Program of Key Fields in Province 2020B1111300003 (W-PW), and the Key-Area Research and Development of Guangdong Province 2020B1111190001 (W-PW).

SUPPLEMENTARY MATERIAL

The Supplementary Material for this article can be found online at: https://www.frontiersin.org/articles/10.3389/fcell.2021.727762/full#supplementary-material

Supplementary Figure 1 | Correlations between *SOCS1* and *FTH1* gene expressions and markers of B cell, M2a, M2b, and M2c (GEPIA2). **(A)** *SOCS1* and B cell ($R = 0.25$, $p = 1.2 \times 10^{-8}$). **(B)** *FTH1* and B cell ($R = -0.12$, $p = 7.6 \times 10^{-3}$). **(C)** *SOCS1* and M2a ($R = -0.011$, $p = 0.8$). **(D)** *SOCS1* and M2b ($R = 0.005$, $p = 0.91$). **(E)** *SOCS1* and M2c ($R = 0.08$, $p = 6.8 \times 10^{-2}$). **(F)** *FTH1* and M2a ($R = 0.14$, $p = 1.3 \times 10^{-3}$). **(G)** *FTH1* and M2b ($R = 0.17$, $p = 1.1 \times 10^{-4}$). **(H)** *FTH1* and M2c ($R = 0.13$, $p = 3.2 \times 10^{-3}$).

Supplementary Figure 2 | *SOCS1* and *FTH1* gene expressions in various immune cells by CIBERSORT (GEPIA2021). M1 Macrophage has the highest median value of *SOCS1* (median value 3.3212), while M2 Macrophage has the highest median value of *FTH1* (median value 5.4181).

Supplementary Table 1 | A list of ferroptosis related genes from the FerrDb database.

Supplementary Table 2 | Correlations of expressions between each two genes of the 18 selected ferroptosis related genes.

Supplementary Table 3 | Annotation of ferroptosis-related differentially expressed proteins and their co-expression scores (STRING analysis).

REFERENCES

Avila-Ponce De León, U., Vázquez-Jiménez, A., Matadamas-Guzman, M., Pelayo, R., and Resendis-Antonio, O. (2021). Transcriptional and microenvironmental landscape of macrophage transition in cancer: a boolean analysis. *Front. Immunol.* 12:642842. doi: 10.3389/fimmu.2021.642842

Burtness, B., Harrington, K. J., Greil, R., Soulières, D., Tahara, M., de Castro, G., et al. (2019). Pembrolizumab alone or with chemotherapy versus cetuximab with chemotherapy for recurrent or metastatic squamous cell carcinoma of the head and neck (KEYNOTE-048): a randomised, open-label, phase 3 study. *Lancet* 394, 1915–1928. doi: 10.1016/S0140-6736(19)32591-7

Chen, X., Kang, R., Kroemer, G., and Tang, D. (2021). Broadening horizons: the role of ferroptosis in cancer. *Nat. Rev. Clin. Oncol.* 18, 280–296. doi: 10.1038/s41571-020-00462-0

DeNardo, D. G., and Ruffell, B. (2019). Macrophages as regulators of tumour immunity and immunotherapy. *Nat. Rev. Immunol.* 19, 369–382. doi: 10.1038/s41577-019-0127-6

Deng, Y., Julaiti, A., Ran, W., and He, Y. (2021). Bone marrow mesenchymal stem cells-derived exosomal microRNA-19b-3p targets SOCS1 to facilitate progression of esophageal cancer. *Life Sci.* 278, 1–8. doi: 10.1016/j.lfs.2021.119491

Dixon, S. J., Lemberg, K. M., Lamprecht, M. R., Skouta, R., Zaitsev, E. M., Gleason, C. E., et al. (2012). Ferroptosis: an iron-dependent form of nonapoptotic cell death. *Cell* 149, 1060–1072. doi: 10.1016/j.cell.2012.03.042

Du, J., Wang, T., Li, Y., Zhou, Y., Wang, X., Yu, X., et al. (2019). DHA inhibits proliferation and induces ferroptosis of leukemia cells through autophagy dependent degradation of ferritin. *Free Radic. Biol. Med.* 131, 356–369. doi: 10.1016/j.freeradbiomed.2018.12.011

Ferris, R. L. Jr., Blumenschein, G., Fayette, J., Guigay, J., Colevas, A. D., Licitra, L., et al. (2016). Nivolumab for recurrent squamous-cell carcinoma of the head and neck. *New Engl. J. Med.* 375, 1856–1867. doi: 10.1056/NEJMoa1602252

Goossens, P., Rodriguez-Vita, J., Etzerodt, A., Masse, M., Rastoin, O., Gouirand, V., et al. (2019). Membrane cholesterol efflux drives tumor-associated macrophage reprogramming and tumor progression. *Cell Metab.* 29, 1376–1389. doi: 10.1016/j.cmet.2019.02.016

Hu, Z., Chen, L., Ma, R., Wei, F., Wen, Y., Zeng, X., et al. (2021). Comprehensive analysis of ferritin subunits expression and positive correlations with tumor-associated macrophages and T regulatory cells infiltration in most solid tumors. *Aging (Albany, N. Y.)* 13, 11491–11506. doi: 10.18632/aging.202841

Hu, Z., Wang, L., Han, Y., Li, F., Zheng, A., Xu, Y., et al. (2019). Ferritin: a potential serum marker for lymph node metastasis in head and neck squamous cell carcinoma. *Oncol. Lett.* 17, 314–322. doi: 10.3892/ol.2018.9642

Jiang, X., Stockwell, B. R., and Conrad, M. (2021). Ferroptosis: mechanisms, biology and role in disease. *Nat. Rev. Mol. Cell Biol.* 22, 266–282. doi: 10.1038/s41580-020-00324-8

Johnson, D. E., Burtness, B., Leemans, C. R., Lui, V., Bauman, J. E., and Grandis, J. R. (2020). Head and neck squamous cell carcinoma. *Nat. Rev. Dis. Primers* 6:92. doi: 10.1038/s41572-020-00224-3

Kalbasi, A., Komar, C., Tooker, G. M., Liu, M., Lee, J. W., Gladney, W. L., et al. (2017). Tumor-derived CCL2 mediates resistance to radiotherapy in pancreatic ductal adenocarcinoma. *Clin. Cancer Res.* 23, 137–148. doi: 10.1158/1078-0432.CCR-16-0870

Khan, M., Ghosh, A., Variya, B., Santharam, M. A., Ihsan, A. U., Ramanathan, S., et al. (2020). Prognostic significance of SOCS1 and SOCS3 tumor suppressors and oncogenic signaling pathway genes in hepatocellular carcinoma. *BMC Cancer* 20:774. doi: 10.1186/s12885-020-07285-3

Lei, G., Zhang, Y., Koppula, P., Liu, X., Zhang, J., Lin, S. H., et al. (2020). The role of ferroptosis in ionizing radiation-induced cell death and tumor suppression. *Cell Res.* 30, 146–162. doi: 10.1038/s41422-019-0263-3

Lin, L., Chen, S., Wang, H., Gao, B., Kallakury, B., Bhuvaneshwar, K., et al. (2021). SPTBN1 inhibits inflammatory responses and hepatocarcinogenesis via the stabilization of SOCS1 and downregulation of p65 in hepatocellular carcinoma. *Theranostics* 11, 4232–4250. doi: 10.7150/thno.49819

Ma, X., Xiao, L., Liu, L., Ye, L., Su, P., Bi, E., et al. (2021). CD36-mediated ferroptosis dampens intratumoral CD8(+) T cell effector function and impairs their antitumor ability. *Cell Metab.* 33, 1001–1012. doi: 10.1016/j.cmet.2021.02.015

Maller, O., Drain, A. P., Barrett, A. S., Borgquist, S., Ruffell, B., Zakharevich, I., et al. (2021). Tumour-associated macrophages drive stromal cell-dependent collagen crosslinking and stiffening to promote breast cancer aggression. *Nat. Mater.* 20, 548–559. doi: 10.1038/s41563-020-00849-5

Mantovani, A., and Locati, M. (2013). Tumor-associated macrophages as a paradigm of macrophage plasticity, diversity, and polarization: lessons and open questions. *Arterioscler. Thromb. Vasc. Biol.* 33, 1478–1483. doi: 10.1161/ATVBAHA.113.300168

Mantovani, A., Sozzani, S., Locati, M., Allavena, P., and Sica, A. (2002). Macrophage polarization: tumor-associated macrophages as a paradigm for polarized M2 mononuclear phagocytes. *Trends Immunol.* 23, 549–555. doi: 10.1016/s1471-4906(02)02302-5

Manz, D. H., Blanchette, N. L., Paul, B. T., Torti, F. M., and Torti, S. V. (2016). Iron and cancer: recent insights. *Ann. N. Y. Acad. Sci.* 1368, 149–161. doi: 10.1111/nyas.13008

Peranzoni, E., Lemoine, J., Vimeux, L., Feuillet, V., Barrin, S., Kantari-Mimoun, C., et al. (2018). Macrophages impede CD8 T cells from reaching tumor cells and limit the efficacy of anti-PD-1 treatment. *Proc. Natl. Acad. Sci. U.S.A.* 115, E4041–E4050. doi: 10.1073/pnas.1720948115

Qing, X., Tan, G. L., Liu, H. W., Li, W., Ai, J. G., Xiong, S. S., et al. (2020). LINC00669 insulates the JAK/STAT suppressor SOCS1 to promote nasopharyngeal cancer cell proliferation and invasion. *J. Exp. Clin. Cancer Res.* 39, 1–16. doi: 10.1186/s13046-020-01674-z

Roh, J., Kim, E. H., Jang, H. J., Park, J. Y., and Shin, D. (2016). Induction of ferroptotic cell death for overcoming cisplatin resistance of head and neck cancer. *Cancer Lett.* 381, 96–103. doi: 10.1016/j.canlet.2016.07.035

Rojo, D. L. V. M., Chapman, E., and Zhang, D. D. (2018). NRF2 and the hallmarks of cancer. *Cancer Cell.* 34, 21–43. doi: 10.1016/j.ccell.2018.03.022

Saint-Germain, E., Mignacca, L., Vernier, M., Bobbala, D., Ilangumaran, S., and Ferbeyre, G. (2017). SOCS1 regulates senescence and ferroptosis by modulating the expression of p53 target genes. *Aging (Albany, N.Y.)* 9, 2137–2162. doi: 10.18632/aging.101306

Salatino, A., Aversa, I., Battaglia, A. M., Sacco, A., Di Vito, A., Santamaria, G., et al. (2019). H-Ferritin affects cisplatin-induced cytotoxicity in ovarian cancer cells through the modulation of ROS. *Oxid. Med. Cell. Longev.* 2019, 1–13. doi: 10.1155/2019/3461251

Seiwert, T. Y., Burtness, B., Mehra, R., Weiss, J., Berger, R., Eder, J. P., et al. (2016). Safety and clinical activity of pembrolizumab for treatment of recurrent or metastatic squamous cell carcinoma of the head and neck (KEYNOTE-012): An open-label, multicentre, phase 1b trial. *Lancet Oncol.* 17, 956–965. doi: 10.1016/S1470-2045(16)30066-3

Shan, K., Feng, N., Cui, J., Wang, S., Qu, H., Fu, G., et al. (2020). Resolvin D1 and D2 inhibit tumour growth and inflammation via modulating macrophage polarization. *J. Cell. Mol. Med.* 24, 8045–8056. doi: 10.1111/jcmm.15436

Siegel, R. L., Miller, K. D., and Jemal, A. (2020). Cancer statistics, 2020. *CA Cancer J. Clin.* 70, 7–30. doi: 10.3322/caac.21590

Sun, X., Ou, Z., Chen, R., Niu, X., Chen, D., Kang, R., et al. (2016). Activation of the p62-Keap1-NRF2 pathway protects against ferroptosis in hepatocellular carcinoma cells. *Hepatology* 63, 173–184. doi: 10.1002/hep.28251

Torti, S. V., and Torti, F. M. (2013). Iron and cancer: more ore to be mined. *Nat. Rev. Cancer.* 13, 342–355. doi: 10.1038/nrc3495

Wang, Q., Lu, Y., Li, R., Jiang, Y., Zheng, Y., Qian, J., et al. (2018). Therapeutic effects of CSF1R-blocking antibodies in multiple myeloma. *Leukemia* 32, 176–183. doi: 10.1038/leu.2017.193

Wang, W., Green, M., Choi, J. E., Gijón, M., Kennedy, P. D., Johnson, J. K., et al. (2019). CD8(+) T cells regulate tumour ferroptosis during cancer immunotherapy. *Nature.* 569, 270–274. doi: 10.1038/s41586-019-1170-y

Wang, W., Marinis, J. M., Beal, A. M., Savadkar, S., Wu, Y., Khan, M., et al. (2020). RIP1 kinase drives Macrophage-Mediated adaptive immune tolerance in pancreatic cancer. *Cancer Cell.* 38, 585–590. doi: 10.1016/j.ccell.2020.09.020

Watermann, C., Pasternack, H., Idel, C., Ribbat-Idel, J., Brägelmann, J., Kuppler, P., et al. (2021). Recurrent HNSCC harbor an immunosuppressive tumor immune microenvironment suggesting successful tumor immune evasion. *Clin. Cancer Res.* 27, 632–644. doi: 10.1158/1078-0432.CCR-20-0197

Yandava, C. N., Pillari, A., and Drazen, J. M. (1999). Radiation hybrid and cytogenetic mapping of SOCS1 and SOCS2 to chromosomes 16p13 and 12q, respectively. *Genomics* 61, 108–111. doi: 10.1006/geno.1999.5937

Ying, J., Qiu, X., Lu, Y., and Zhang, M. (2019). SOCS1 and its potential clinical role in tumor. *Pathol. Oncol. Res.* 25, 1295–1301. doi: 10.1007/s12253-019-00612-5

Zheng, J., and Conrad, M. (2020). The metabolic underpinnings of ferroptosis. *Cell Metab.* 32, 920–937. doi: 10.1016/j.cmet.2020.10.011

Zhou, N., and Bao, J. (2020). FerrDb: a manually curated resource for regulators and markers of ferroptosis and ferroptosis-disease associations. *Database* 21, 1–8. doi: 10.1093/database/baaa021

Conflict of Interest: The authors declare that the research was conducted in the absence of any commercial or financial relationships that could be construed as a potential conflict of interest.

Publisher's Note: All claims expressed in this article are solely those of the authors and do not necessarily represent those of their affiliated organizations, or those of the publisher, the editors and the reviewers. Any product that may be evaluated in this article, or claim that may be made by its manufacturer, is not guaranteed or endorsed by the publisher.

Copyright © 2021 Hu, Wen, Ma, Chen, Zeng, Wen and Sun. This is an open-access article distributed under the terms of the Creative Commons Attribution License (CC BY). The use, distribution or reproduction in other forums is permitted, provided the original author(s) and the copyright owner(s) are credited and that the original publication in this journal is cited, in accordance with accepted academic practice. No use, distribution or reproduction is permitted which does not comply with these terms.

frontiers in Cell and Developmental Biology

ORIGINAL RESEARCH
published: 23 September 2021
doi: 10.3389/fcell.2021.736540

Characterization of Molecular Heterogeneity Associated With Tumor Microenvironment in Clear Cell Renal Cell Carcinoma to Aid Immunotherapy

Weimin Zhong[1†], Yinan Li[2,3†], Yichu Yuan[4†], Hongbin Zhong[1,3†], Chaoqun Huang[1], Jiwei Huang[5], Yao Lin[6*] and Jiyi Huang[1,2,3*]*

[1] The Fifth Hospital of Xiamen, Xiamen, China, [2] Department of Nephrology, The First Affiliated Hospital of Xiamen University, Xiamen, China, [3] Department of Clinical Medicine, Fujian Medical University, Fuzhou, China, [4] Department of Urology, Second Affiliated Hospital, Zhejiang University School of Medicine, Hangzhou, China, [5] Department of Urology, Renji Hospital, Shanghai Jiao Tong University School of Medicine, Shanghai, China, [6] Central Laboratory at the Second Affiliated Hospital of Fujian Traditional Chinese Medical University, Collaborative Innovation Center for Rehabilitation Technology, Fujian University of Traditional Chinese Medicine, Fuzhou, China

OPEN ACCESS

Edited by:
Xuejun Sun,
Xi'an Jiaotong University, China

Reviewed by:
Jinhui Liu,
Nanjing Medical University, China
Lianze Chen,
China Medical University, China

***Correspondence:**
Jiwei Huang
jiweihuang@outlook.com
Yao Lin
yaolin@fjtcm.edu.cn
Jiyi Huang
hjy0602@163.com

[†] These authors have contributed equally to this work

Specialty section:
This article was submitted to Molecular and Cellular Pathology, a section of the journal Frontiers in Cell and Developmental Biology

Received: 05 July 2021
Accepted: 03 September 2021
Published: 23 September 2021

Citation:
Zhong W, Li Y, Yuan Y, Zhong H, Huang C, Huang J, Lin Y and Huang J (2021) Characterization of Molecular Heterogeneity Associated With Tumor Microenvironment in Clear Cell Renal Cell Carcinoma to Aid Immunotherapy. Front. Cell Dev. Biol. 9:736540. doi: 10.3389/fcell.2021.736540

Clear cell renal cell carcinoma (ccRCC) is the most common type of kidney cancer and has strong immunogenicity. A systematically investigation of the tumor microenvironment (TME) in ccRCC could contribute to help clinicians develop personalized treatment and facilitate clinical decision-making. In this study, we analyzed the immune-related subtype of ccRCC on the basis of immune-related gene expression data in The Cancer Genome Atlas (TCGA, *N* = 512) and E-MTAB-1980 (*N* = 101) dataset, respectively. As a result, two subtypes (C1 and C2) were identified by performing non-negative matrix factorization clustering. Subtype C1 was characterized by increased advance ccRCC cases and immune-related pathways. A higher immune score, stromal score, TMB value, Tumor Immune Dysfunction and Exclusion (TIDE) prediction score, and immune checkpoint genes expression level were also observed in C1. In addition, the C1 subtype might benefit from chemotherapy and immunotherapy. The patients in subtype C2 had more metabolism-related pathways, higher tumor purity, and a better prognosis. Moreover, some small molecular compounds for the treatment of ccRCC were identified between the two subtypes by using the Connectivity Map (CMap) database. Finally, we constructed and validated an immune-related (IR) score to evaluate immune modification individually. A high IR score corresponded to a favorable prognosis compared to a low IR score, while more advanced tumor stage and grade cases were enriched in the low IR score group. The two IR score groups also showed a distinct divergence among immune status, TME, and chemotherapy. The external validation dataset (E-MTAB-1980) and another immunotherapy cohort (IMvigor 210) demonstrated

that patients in the high IR score group had a significantly prolonged survival time and clinical benefits compared to the low IR score group. Together, characterization of molecular heterogeneity and IR signature may help develop new insights into the TME of ccRCC and provide new strategies for personalized treatment.

Keywords: clear cell renal cell carcinoma, molecular subtype, tumor microenvironment, chemo drugs, immunotherapy, immune checkpoint blockade, IR score

INTRODUCTION

Clear cell renal cell carcinoma (ccRCC) is a typical subtype of renal cell carcinoma (RCC), which is responsible for 70–80% of RCC cases (Martel and Lara, 2003). It was estimated that, in 2019, there would be 73,820 new cases and 14,770 deaths from ccRCC in America, which seriously affects human health (Siegel et al., 2016; Gao et al., 2020). Currently, the most common treatment strategy is surgical intervention, including laparoscopic partial nephrectomy (LPN) and radical nephrectomy (LN) (Porpiglia et al., 2014; Ahmad and Finelli, 2019). However, about 20∼30% of diagnostic RCC cases are metastatic (Gitlitz and Figlin, 2003; Yang et al., 2012). Moreover, despite early-stage RCC patients achieving a 5-year overall survival (OS) rate of 90%, the 5-year OS rate of metastatic or advance-stage RCC patients was less than 10% (Chaffer and Weinberg, 2011; Hirata et al., 2011). Cumulative studies have shown that targeted therapy is an effective method for the treatment of ccRCC, especially for metastatic cRCC patients (Grüllich, 2018). Targeted agents including axitinib (Escudier and Gore, 2011), pazopanib (Sternberg et al., 2010), sorafenib (Gordon, 2008), and sunitinib (Motzer, 2007) have made some progress in metastatic patients. However, the therapeutics were not effective for all patients and some showed drug resistance (Buchler et al., 2015; Baig et al., 2006). Thus, there is an urgent need to identify some molecular subtypes that may have implications on drug selection.

Tumor immunotherapy is a promising treatment method for tumors and has become a research hotspot in tumor therapy, and its efficacy is tightly associated with the TME (Wang et al., 2020). PD-1/PD-L1 is an important immunotherapy target for the treatment of ccRCC (Motzer et al., 2018). One study discovered that RCC patients with positive PD-L1 expression had a higher overall response rate to PD-1/PD-L1 treatment when compared to negative PD-L1 expression (Topalian et al., 2012). Moreover, dis-regulated genes also had an impact on the TME. Studies have shown that high expression level of HMGB1 in ccRCC can induce IL-10 secretion by T regulatory cells and decrease the anti-tumor activity of CD8+T cells (Li et al., 2017). Tim-3 expression in renal cell carcinoma is associated with the invasion of T cells and was considered as a novel therapeutic target for immunotherapy of ccRCC (Cai et al., 2015).

In the present study, we systematically investigated the immune-related (IR) molecular heterogeneity of ccRCC based on IR gene expression. We identified two subtypes with distinct immune microenvironment characteristics and immunotherapy response. These results lay a foundation for the further study of ccRCC immunotherapy and developing a personalized treatment.

MATERIALS AND METHODS

Dataset Collection and Processing

The gene expression data and corresponding clinical information of ccRCC were downloaded from The Cancer Genomics Atlas (TCGA[1]) and ArrayExpress database (E-MTAB-1980[2]), respectively. Among them, the TCGA dataset (training dataset) consisted of 539 ccRCC samples, and the E-MTAB-1980 dataset (external validation dataset) included 101 ccRCC samples (Sato et al., 2013). To obtain a reliable result, we excluded the samples with a survival time less than 30 days, and finally a total of 613 ccRCC (512 samples retrieved from TCGA, 101 samples retrieved from the E-MTAB-1980 dataset) samples were included in the downstream analysis. Moreover, the IR gene symbol names were retrieved from the Immunology Database and Analysis Portal (ImmPort[3]) database (Bhattacharya et al., 2018).

Molecular Subtypes Identification

The IR molecular subtype was identified by performing non-negative matrix factorization (NMF) clustering analysis in the "NMF" R package[4] (Gillis, 2020). Principal component analysis (PCA) was performed to identify the robustness and reliability of the molecular subtype. Gene Set Variation Analysis (GSVA) was applied to identify the molecular function of each subtype (Hänzelmann et al., 2013). The reproducibility of the subtypes in the E-MTAB-1980 and TCGA datasets was identified by using the subclass mapping algorithm.

Exploration of the Relationship Between Subtype and Immune Cell Infiltration

To assess the immune cell infiltration of ccRCC, we firstly retrieved 28 IR cell gene sets from a previously reported article (Charoentong et al., 2016). We then applied the ssGSEA methods to estimate the relative abundance of each immune cell in ccRCC through using the "GSVA" R package (Hänzelmann et al., 2013). Moreover, the TME including immune score, stromal score, and tumor purity of each patient was calculated using the ESTIMATE algorithm[5]. The divergence between immune cell infiltration level, TME, and molecular subtype was evaluated using Wilcoxon rank sum test analysis.

[1]https://portal.gdc.cancer.gov/

[2]https://www.ebi.ac.uk/arrayexpress/

[3]https://www.immport.org/

[4]https://cran.r-project.org/web/packages/NMF/index.html

[5]http://r-forge.r-project.org

Evaluating the Benefit of Each Subtype From Immunotherapy and Four Chemo Drugs

The chemotherapeutic response of each ccRCC sample was evaluated through the online database Genomics of Drug Sensitivity in Cancer (GDSC[6]) (Yang et al., 2016). Four common ccRCC treatment chemo drugs including Sorafenib, Sunitinib, Pazopanib, and Axitinib were selected (Liu et al., 2019). The prediction process was completed by using the "pRRophetic" R package and the half-maximal inhibitory concentration (IC50) of each ccRCC patient was calculated by using the ridge regression algorithm (Geeleher et al., 2014). The parameters were set as default. In addition, we also applied the Tumor Immune Dysfunction and Exclusion (TIDE)[7] algorithm to evaluate the clinical response of ccRCC (Jiang et al., 2018).

Small Molecular Compounds Prediction for the Treatment of Clear Cell Renal Cell Carcinoma

To predict the small molecule compounds of ccRCC, we first identified the differentially expressed genes (DEGs) between subtypes C1 and C2 using the "limma" R package with $|\log FC| > 1$ and adjusted P-value < 0.05 (Ritchie et al., 2015). Then the DEGs were uploaded to the Connective Map (CMap) database, respectively (Lamb et al., 2006). The small molecule compounds were further predicted based on the enrichment value and P-value.

Gene Ontology Terms and Kyoto Encyclopedia of Genes and Genomes Pathway Enrichment Analysis

To investigate the molecular function of DEGs, we performed gene ontology (GO) and kyoto encyclopedia of genes and genomes (KEGG) enrichment analysis to explore the molecular functions and pathways through the "ClusterProfiler" R package. Significant GO terms or pathways were screened with the cutoff adjusted P-value < 0.05 (Yu et al., 2012).

Construction of Immune-Related Score

Firstly, we used univariate Cox regression analysis to select the prognostic DEGs with a P-value < 0.05, and a total of 274 prognostic genes were selected for further analysis. Then, we performed PCA analysis to construct an IR relevant score. PC1 and PC2 were selected as the signature scores. The advantage of this method is that the score is concentrated on the set with the largest block of related (or anti-related) genes, while the weight is not combined with the contribution of the genes tracked by other set members (Zhang et al., 2020):

$IR = \Sigma\ (PC1_i + PC2_i)$, where i represent the expression of each prognostic signature gene. To validate the prognostic value and clinical benefit, RNAseq datasets of 348 patients with bladder cancer were retrieved from the IMvigor 210 dataset (Mariathasan et al., 2018).

[6]https://www.cancerrxgene.org/

[7]http://tide.dfci.harvard.edu/login/

Statistical Analysis

All the analyses was carried out in the R/3.6.1 environment. The continuous data were evaluated using the Wilcoxon rank sum test. A log-rank test Kaplan–Meier (KM) curve was applied to evaluate the survival divergence of different subtypes. In addition, the Fisher test was employed to calculated the difference for the categorical data. For all tests, a P-value < 0.05 was regarded as statistically significant.

RESULTS

Identification of Molecular Subtypes of Clear Cell Renal Cell Carcinoma

To investigate the IR subtype of ccRCC, we firstly retrieved the reads count data from the TCGA database and transformed it into TPM values. We then used the NMF algorithm to cluster the patients based on the IR gene expression data. To ensure a robust clustering result, we first removed the low expression level genes and subsequently included the selected genes in univariate Cox regression analysis. The genes with a P-value less than 0.05 were subjected to NMF clustering analysis in the TCGA dataset. The cophenetic correlation coefficients were applied to determine the optimal k value, and $k = 2$ was then selected as the optimal cluster number after a comprehensive consideration (**Figure 1A**). As shown in **Figure 1B**, when $k = 2$, we observed that the two subtypes (named C1 and C2) had clear boundaries, suggesting a stable and reliable clustering for the ccRCC sample. PCA was further applied to validate the assignments of the two subtypes. As shown in **Figure 1C**, the two-dimensional PCA distribution and the two subtypes had similar consistency. The survival curve revealed that C2 had a significantly better survival outcome when compared to C1 in overall survival (P-value < 0.001) (**Figure 1D**). In addition, we also performed NMF clustering analysis in the E-MTAB-1980 dataset, and the clustering result showed two distinct molecular subtypes, which was consistent with the training dataset result (**Supplementary Figures 1A–C**). The survival difference in the external validation dataset also showed a significant survival difference between the two subtypes (**Supplementary Figure 1D**) (P-value < 0.05). To validate the reproducibility of the molecular subtypes in the TCGA and E-MTAB-1980 datasets, we used the subclass mapping algorithm to compare the expression profiles of the subtypes from the two datasets. As **Supplementary Figure 2** shows, we discovered that subtype C1 ($N = 162$) from TCGA was significantly associated with subtype C2 ($N = 35$) from the E-MTAB-1980 dataset, while subtype C2 ($N = 350$) from TCGA was significantly related to subtype C1 ($N = 66$) from the E-MTAB-1980 dataset (Bonferroni-corrected P-value = 0.003996).

Function Enrichment of the Molecular Subtype

To investigate the function of the two subtypes, we performed Gene Set Variation Analysis (GSVA) for the

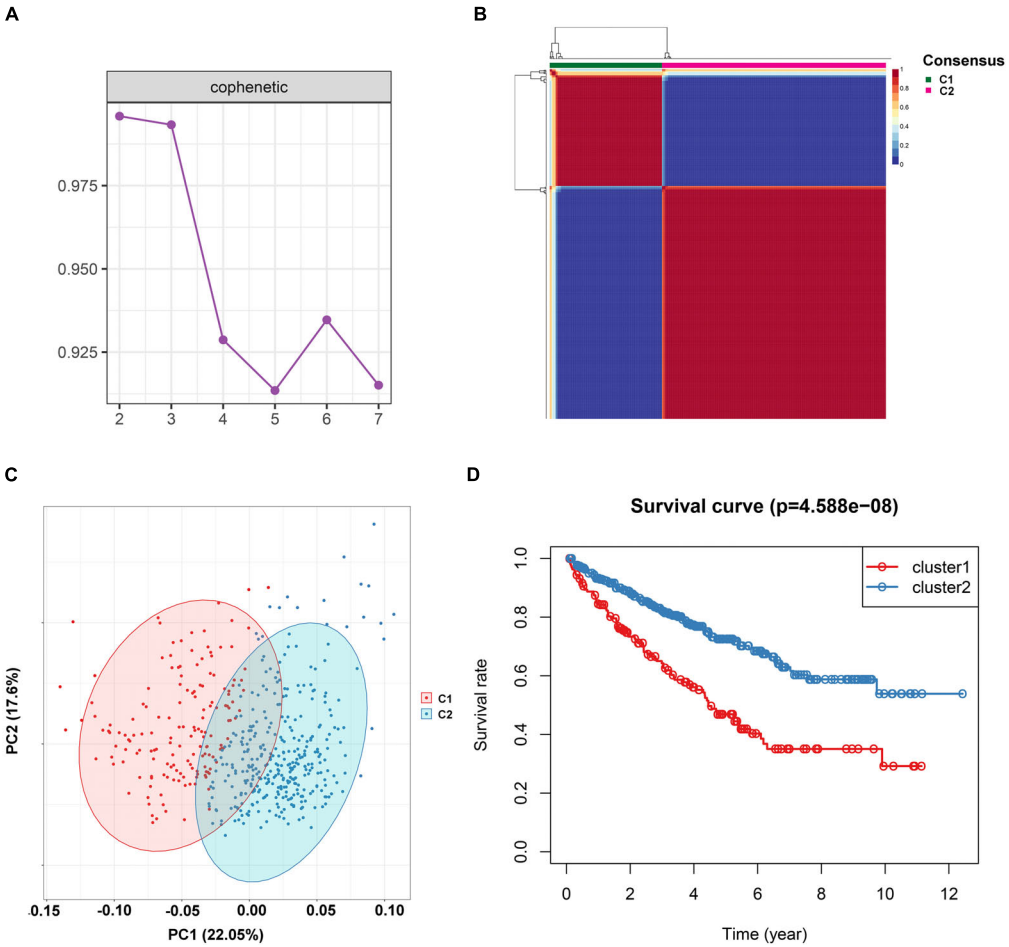

FIGURE 1 | Non-negative matrix factorization clustering analysis to identify potential molecular subtypes of ccRCC based on the immune-related gene expression in TCGA dataset. **(A)** The cophenetic correlation coefficient for the cluster number from 2 to 7. **(B)** Consensus matrix heatmap when $k = 2$. **(C)** Principal component analysis (PCA) for the 512 ccRCC patients, each dot represents a single sample. **(D)** KM survival curve analysis for the overall survival of the two subtypes in ccRCC.

all gene expression datasets based on the subtypes. We then calculated the pathway activity for each sample. We discovered that metabolism-related pathways including fatty acid metabolism, beta alanine metabolism, tryptophan metabolism, and the propanoate metabolism pathway were upregulated in C2, while the p53 signaling pathway, natural killer cell-mediated cytotoxicity, cytokine cytokine receptor interaction, intestinal immune network for IGA production, and primary immunodeficiency pathway were enriched in C1 (**Supplementary Figure 3**).

The Relationship Between Molecular Subtype and Tumor Microenvironment

The tumor microenvironment (TME) is essential for immune function and has diverse clinical implications for immunotherapy. The divergence of immune cell infiltration and the TME were then explored in the two subtypes. The 28 immune cells' infiltration level of each ccRCC patient was evaluated by applying the ssGSEA algorithm. As shown in **Figure 2A**, we observed that the level of activated B cells, CD4 T cells, CD8 T cells, central memory T cells, immature B cells, and T helper cells were significantly high in C1, while CD56dim natural killer cells and neutrophil cells presented at a lower level in C1. Moreover, we also calculated the immune score, stromal score, and tumor purity of each ccRCC sample using the ESTIMATE algorithm. We found that the immune and stromal score were significantly higher in subtype C1 when compared to subtype C2 (**Figures 2B,C**). However, the tumor purity showed a reverse trend that was lower in C1 (**Figure 2D**).

Evaluation of Immunotherapeutic Response in the Clear Cell Renal Cell Carcinoma Subtypes

Recently, the immune checkpoint blockade has become a benchmark in the treatment of many tumors. Therefore, we subsequently explored the expression level of some known immune checkpoints including CD274 (PD-L1), PDCD1LG2

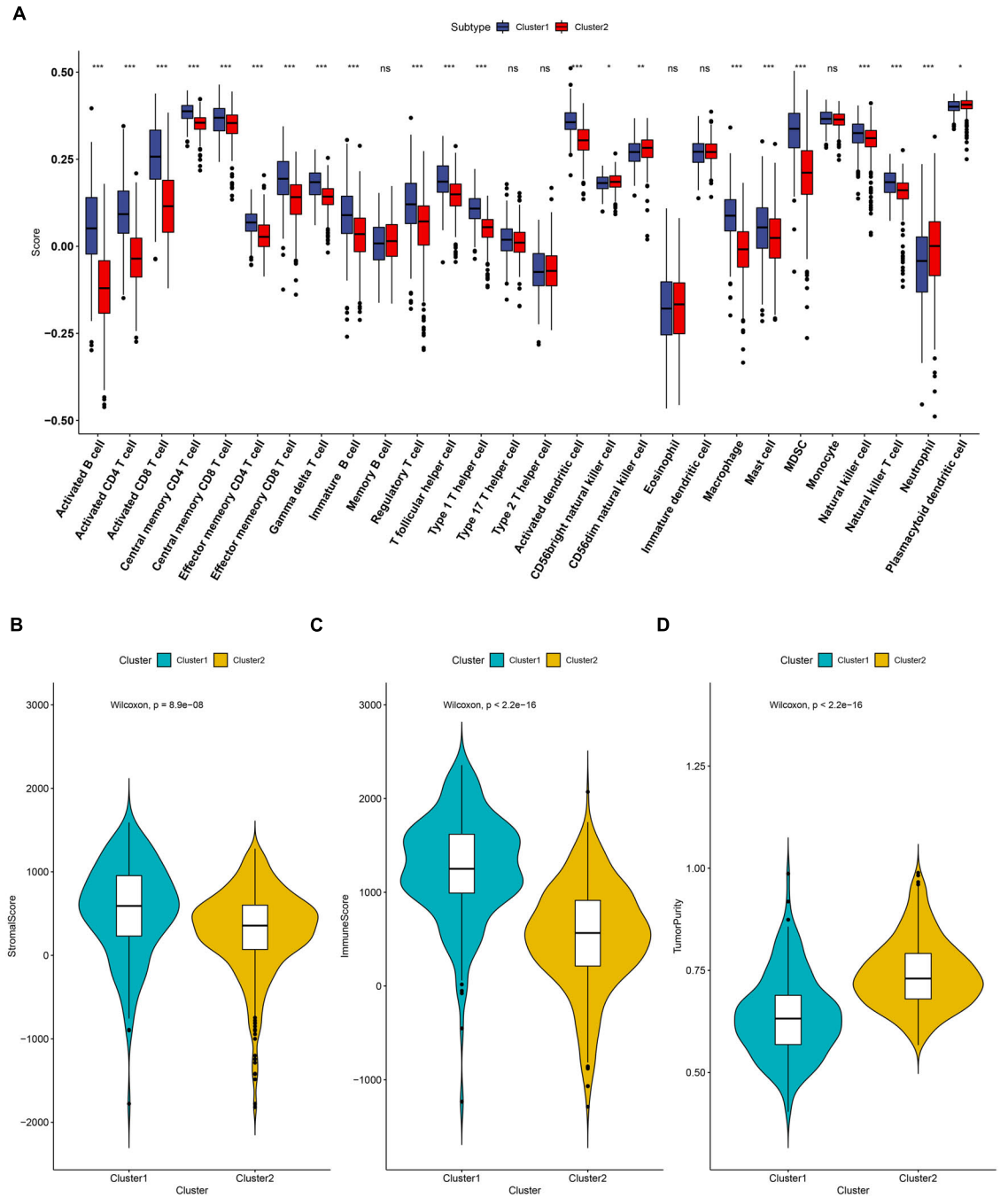

FIGURE 2 | The landscape of immune cell infiltration in the two subtypes. **(A)** Twenty-eight immune cells' infiltration levels that were calculated by the ssGSEA algorithm in the two subtypes. The comparisons of stromal score **(B)**, immune score **(C)** and tumor purity **(D)** between the two subtypes. ns: not significant, $^{*}P < 0.05$, $^{**}P < 0.01$, $^{***}P < 0.001$.

(PD-L2), PDCD1 (PD-1), LAG3, TIGIT, and CTLA4. As shown in **Figures 3A–F**, we found that the PD-L2, PD-1, LAG3, TIGIT, CTLA4 expression levels in subtype C1 were higher than in C2, indicating that patients in subtype C1 with a high expression of immune checkpoint inhibitors were more likely to form an immunosuppressive microenvironment, further leading to tumor immune escape (Dunn et al., 2002). The tumor mutational burden (TMB) has been demonstrated to be an effective predictor of immunotherapy response. In our result, we identified that the TMB level in subtype C2 was significantly lower than C1, which is consistent with a previous report where ccRCC patients' overall survival corresponded to a low TMB

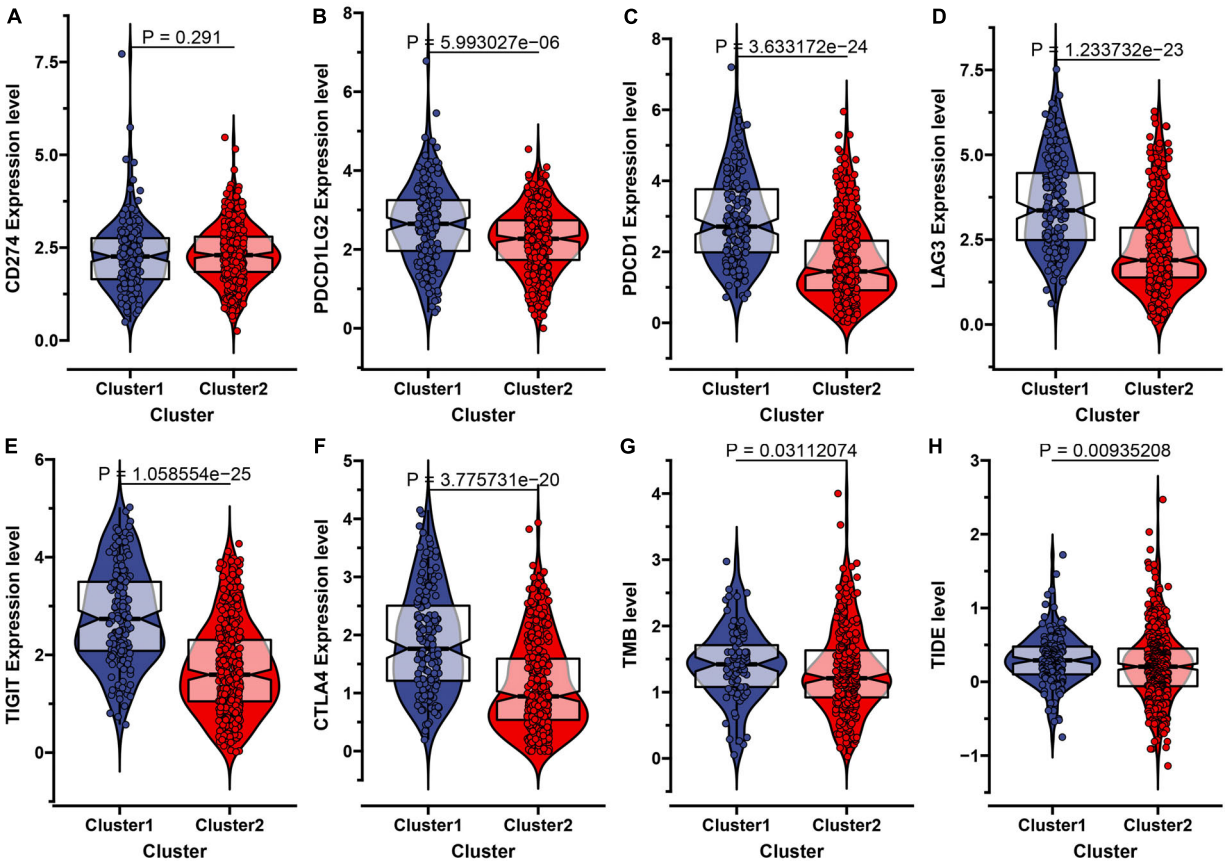

FIGURE 3 | Evaluation of the immunotherapeutic response of the two subtypes in ccRCC. **(A–F)** The expression level of six immune checkpoint inhibitors including CD274 (PD-L1), PDCD1LG2 (PD-L2), PDCD1 (PD-1), LAG3, TIGIT, and CTLA-4 in the two molecular subtypes. **(G)** The comparisons of TMB value between the two subtypes. **(H)** The Tumor Immune Dysfunction and Exclusion (TIDE) prediction score of the two subtypes.

level (**Figure 3G**; Huang et al., 2021). We also used the TIDE algorithm to estimate immunotherapy response and discovered that the TIDE value in subtype C1 was significantly higher than in C2, indicating that C2 was more likely to respond to immunotherapy (**Figure 3H**).

Chemo Drugs for the Treatment of Different Subtypes

Despite the fact that the curative effect of chemotherapy is limited in ccRCC, especially in advanced ccRCC, and considering that chemotherapy is the conventional therapy method for ccRCC, we thus attempted to evaluate the response of the two subtypes to four chemo drugs (Axitinib, Pazopanib, Sorafenib, Sunitinib). Therefore, we applied the ridge regression algorithm to train the GDSC cell line dataset, and obtained satisfactory prediction accuracy through 10-fold cross-validation. The IC50 value was estimated for each ccRCC sample according to the predictive model. As shown in **Figures 4A–D**, apart from Axitinib (*P*-value = 0.058), most of the chemo drugs including Pazopanib (*P*-value = 1.09e-14), Sorafenib (*P*-value = 2.14e-07), and Sunitinib (*P*-value = 4.82e-14) showed a lower IC_{50} value in subtype C1, which indicated that patients in C1 were more likely to respond well to chemo drugs.

Immunotherapy Response Prediction and Small Molecular Compounds Identification Between the Two Subtypes

Currently, immune checkpoint inhibitors are regarded as the routine drugs for the treatment of advanced ccRCC cases (Parikh and Bajwa, 2020). Here, we investigated the likelihood of response to immunotherapy by using the TIDE algorithm, and it demonstrated that patients in subtype C2 (108/350 = 0.309) were more likely to respond to immunotherapy than those in C1 (25/162 = 0.154) (Fisher exact test *P*-value = 0.0002). In addition to the TIDE prediction, we also compared the expression level of the two subtypes and identified another published dataset that included 47 patients with melanoma that responded to immune checkpoint inhibitors therapy by performing submap mapping analysis (Roh et al., 2017). Considering the worse prognosis of C1, we were delighted to discover that patients in subtype C1 were more sensitive to anti-PD-L1 therapy (**Figure 5A**). To identify the small molecular compounds of the ccRCC subtypes, we first performed differentially expressed analysis between C1 and C2.

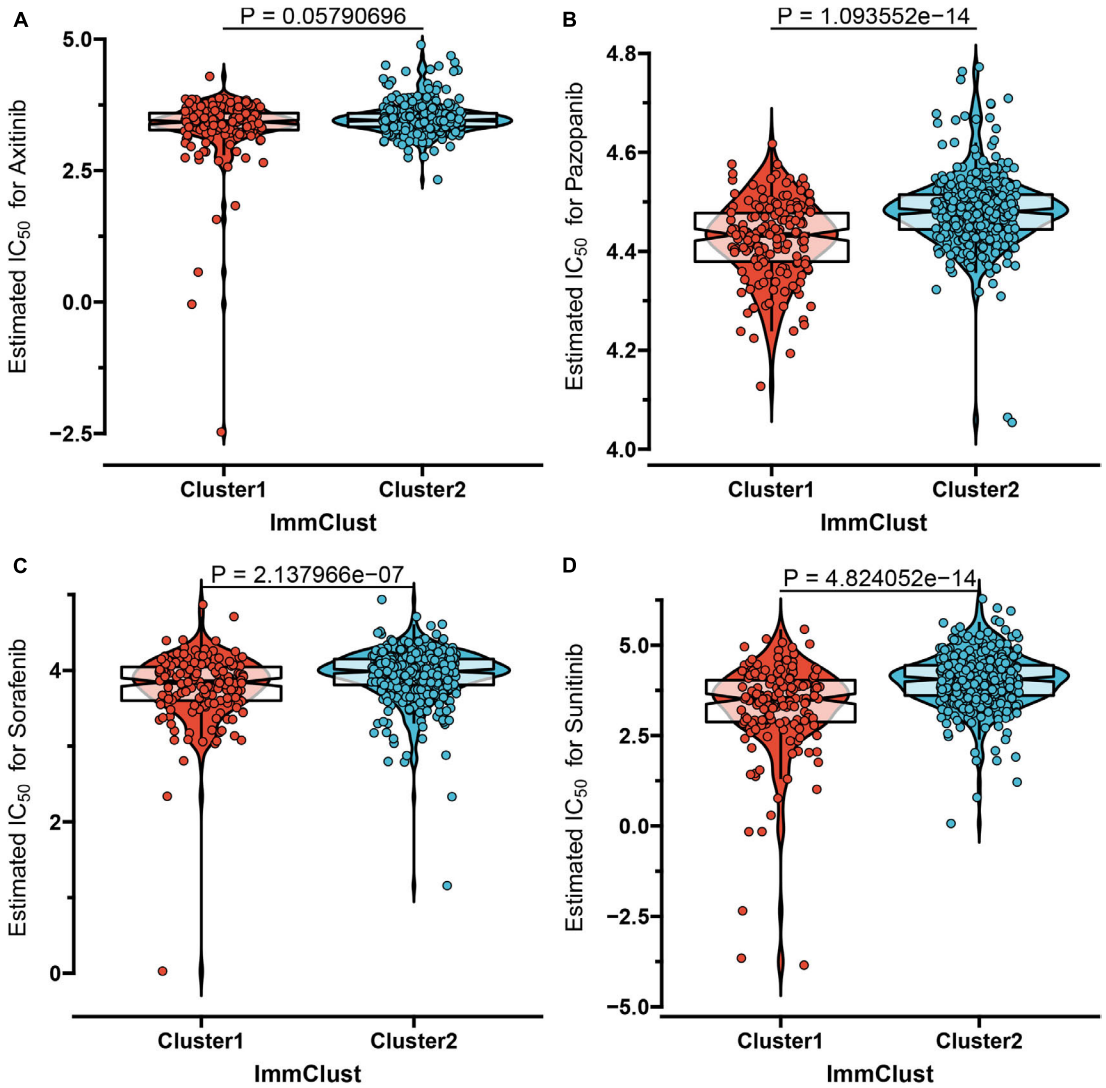

FIGURE 4 | The IC_{50} values of four chemo drugs in the two molecular subtypes of ccRCC including Axitinib **(A)**, Pazopanib **(B)**, Sorafenib **(C)**, and Sunitinib **(D)**.

A total of 349 DEGs were identified, including 99 upregulated genes and 250 downregulated genes (**Supplementary Table 1**). These genes were then uploaded to the CMap database and the compounds with an absolute enrichment value more than 0.5 were retained. As a result, CMap mode-of-action (MoA) analysis of the 19 compounds indicated 16 mechanisms of action shared by the above drugs. As shown in **Figure 5B**, we can observed that scoulerine and suloctidil shared the MoA of adrenergic receptor antagonist, and alclometasone and piretanide shared the MoA of alucocorticoid receptor agonist. These results might provide potential therapeutic targets for the subtypes.

Generation of Immune-Related Gene Signatures and Functional Annotation

To further uncover the function role of each molecular subtype, we firstly performed univariate Cox regression analysis on the 349 DEGs, and a total of 274 prognostic DEGs were identified. We then using the "clusterProfiler" R package to conduct GO and KEGG enrichment analysis on the 274 DEGs. As shown in **Figure 6A**, we discovered that the genes were mainly enriched in complement activation, B cell-mediated immunity, and humoral immune response in the biological processes (**Supplementary Table 2**). Moreover, the complement and coagulation cascades, NF-kappa B signaling pathway, and cytokine-cytokine receptor interaction were observed in the KEGG pathway enrichment result (**Figure 6B** and **Supplementary Table 3**). Interestingly, these GO terms and pathway results were similar to the GSEA results. We further conducted NMF clustering analysis based on the 274 DEGs to categorize patients into different immune genomic subtypes. Interestingly, two immune genomic subtypes (named gene clusters A and B) were identified (**Figures 7A,B**). The KM curve analysis result suggested that patients in gene cluster B had a better prognosis than A (P-value < 0.001)

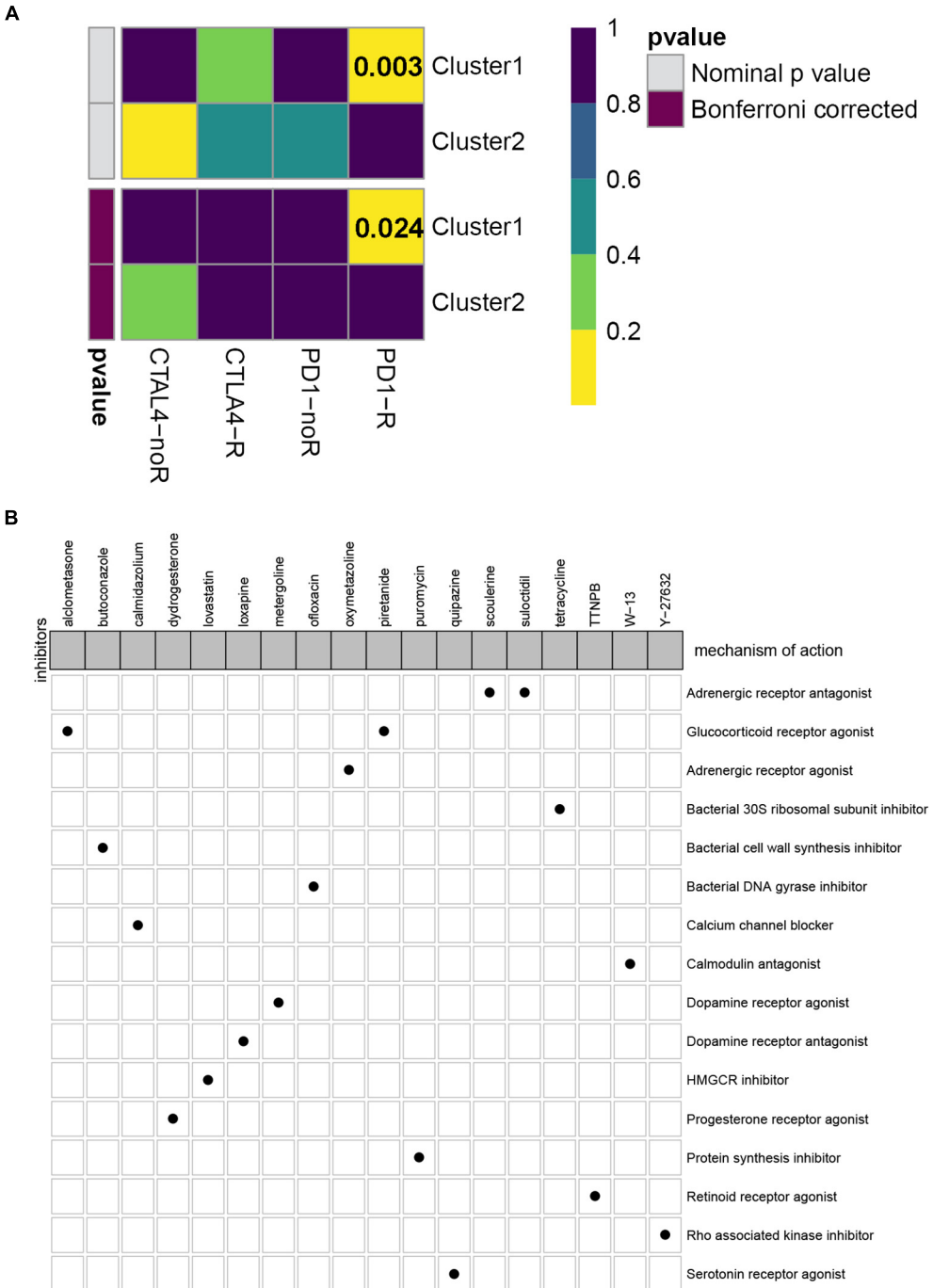

FIGURE 5 | Evaluation of potential compounds and immunotherapy response to the two subtypes. **(A)** Submap analysis demonstrated that cluster 1 had more sensitivity to the programmed cell death protein 1 inhibitor (Bonferroni-corrected, $P = 0.024$). **(B)** CMap database analysis identified candidate drugs targeting the two molecular subtypes based on the DEGs.

(**Figure 7C**). In addition, the PCA analysis could completely distinguish ccRCC samples between A and B (**Figure 7D**). Interestingly, we observed that most of the cases from subtype C2 were in gene cluster A (291/350 = 83.14%), while 96.30% (156/162) of cases from subtype C1 were classified into gene cluster B (**Supplementary Figure 4**). These results indicated that these DEGs were immune phenotype-related genes and might explain why gene cluster A was relevant to worse survival outcome. We further assessed the relationship between the gene clusters and clinical trait. As shown in **Figure 8**, we observed

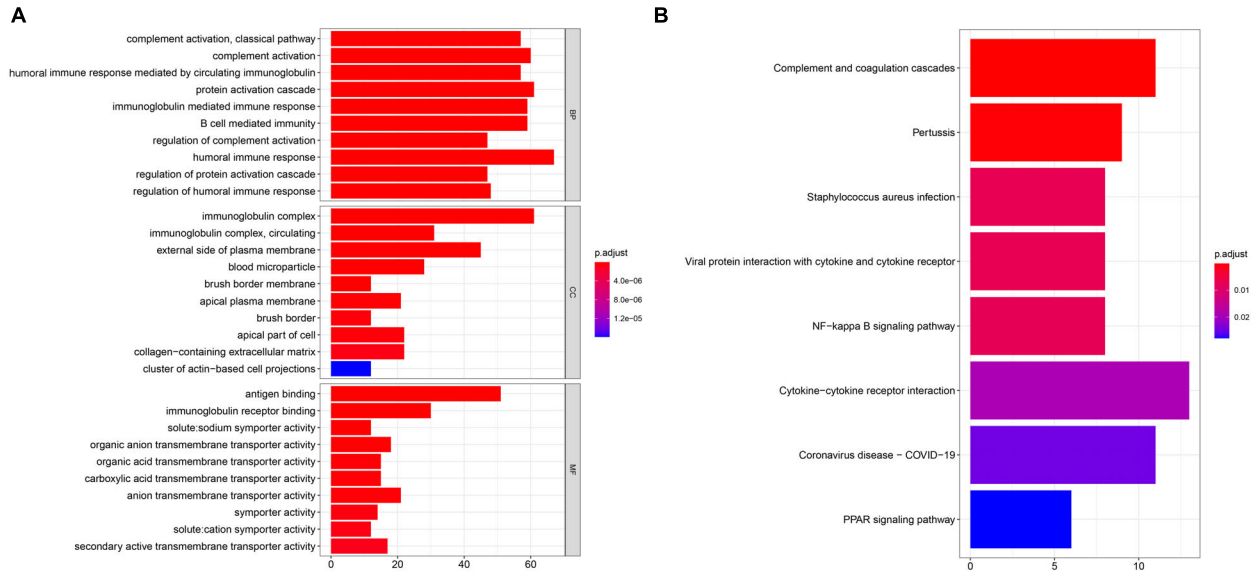

FIGURE 6 | GO **(A)** and KEGG **(B)** enrichment analysis was performed to identify potential function and pathway of DEGs.

that most low-grade cases were enriched in gene cluster B, while advanced stage and grade cases were mainly focused on gene cluster A. Surprisingly, the patients in gene cluster B had large consistency with subtype C1. We also explored the difference of immune checkpoint expression between gene clusters A and B. As expected, except PD-L1 (**Figure 9A**), we found all immune checkpoints including PD-L2, PD-1, LAG3, TIGIT, and CTLA4 had a lower expression level in gene cluster B (**Figures 9B–F**). However, the infiltration level of activated B cells, activated CD4 T cells, activated CD8 T cells, central memory T cells, immature B cells, and T helper cells were higher in gene cluster A (**Figure 9G**).

Immune Score Construction

Considering the individual heterogeneity and complexity of IR subtypes, we developed a scoring system to quantify the immune pattern of individual patients with ccRCC based on 274 DEGs, named as the IR score. The KM curve analysis revealed that those with a high IR score had a better survival outcome (**Figure 10A**). To determine whether IR score can serve as a prognostic predictor, we performed ROC analysis and found that the IR score had the potential capability to ascertain the prognosis of ccRCC (**Figure 10B**). We further investigated the relationship between IR and clinical trait (grade and stage), and demonstrated that IRS was negatively correlated with grade and stage (**Figures 10C,D**). We also evaluated whether IR can serve as an independent prognostic factor via Cox regression analysis. As shown in **Supplementary Figure 5A**, we found that IR was a prognostic factor among the clinical factors in the univariate Cox regression analysis (P-value < 0.001), while there was no significant divergence in the multivariate Cox regression analysis (**Supplementary Figure 5B**). We further evaluated the immune cell infiltration and immune microenvironment, and observed that a high infiltration level of activated B cells, CD4 T cells, CD8 T cells, central memory T cells, immature B cells, and T helper cells was enriched in the low score group, while the level of CD56dim natural killer cells and neutrophils was higher in the high score group (**Supplementary Figure 6**). In addition, the immune and stromal scores were higher in subtype C1 when compared to subtype C2, whereas the level of tumor purity was low in the IR score group (**Supplementary Figures 7A–C**). Considering that the curative effect of chemotherapy is limited in ccRCC, we subsequently examined the sensitivity of the four chemo drugs to the IR score group. As shown in **Figure 11**, we found that the patients in the low IR score group showed more sensitivity to chemo drugs, indicating that the low IR score group may benefit more from chemo drugs. Finally, we identified several small molecular compounds between the low and high IR score groups. Among these compounds, ciprofibrate and clofibrate shared the MoA of PPAR receptor agonist, tiabendazole shared the MoA of angiogenesis inhibitor, and digitoxigenin shared the MoA of ATPase inhibitor (**Supplementary Figure 8**).

Validation of the Immune-Related Score and the Role in Predicting Immunotherapeutic Benefits

To validate the prognostic value of the IR score, we retrieved the disease-free survival (DFS), disease-specific survival (DSS), and progression-free survival (PFS) datasets of ccRCC. As shown in **Figures 12A–C**, we discovered that a significant survival difference between the high IR score and low IR score groups existed in these datasets. We also validated it in the external validation dataset, and found that patients in the high IR score group had a better survival outcome (**Figure 12D**). The immunotherapy represented by PD-L1 and PD-1 blockades has achieved unprecedented success in cancer treatment. We

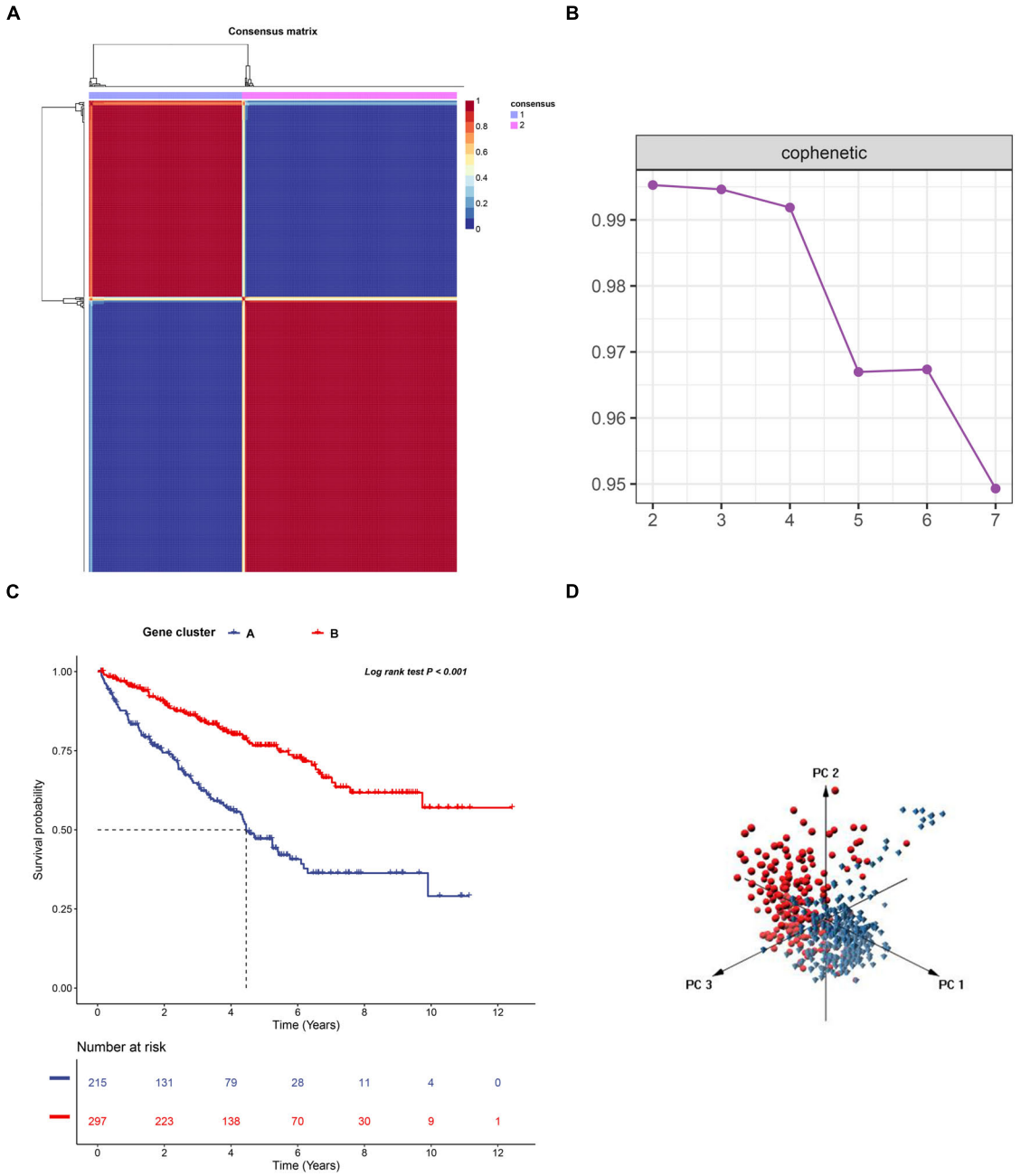

FIGURE 7 | The non-negative matrix factorization (NMF) clustering analysis to identify the genomic subtype of ccRCC based on the 274 DEGs. **(A)** Consensus matrix heatmap when $k = 2$. **(B)** The cophenetic correlation coefficient for the cluster number from 2 to 7. **(C)** KM survival curve analysis for the overall survival of the two subtypes in ccRCC. **(D)** Principal component analysis (PCA) for the 512 ccRCC patients, each dot represents a single sample.

then explored whether the IR score could predict patient response to PD-L1 and CTLA-4 blockade therapy based on IMvigor210. As expected, we were delighted to see that patients with a high IR score showed significant clinical benefits and prolonged survival (**Figure 12E**). The immune response and positive therapeutic benefits of patients in the distinct IR score group to immune checkpoint blockade treatment was further validated (**Figure 12F**).

DISCUSSION

Clear cell renal cell carcinoma is a heterogeneous disease that is associated with a poor prognosis in the advanced stage. How to prolong patient survival time and reduce death in advanced ccRCC remains a difficult clinical problem (Gao et al., 2020). Moreover, ccRCC has strong immunogenicity. ccRCC is characterized by a substantial number of inflammatory

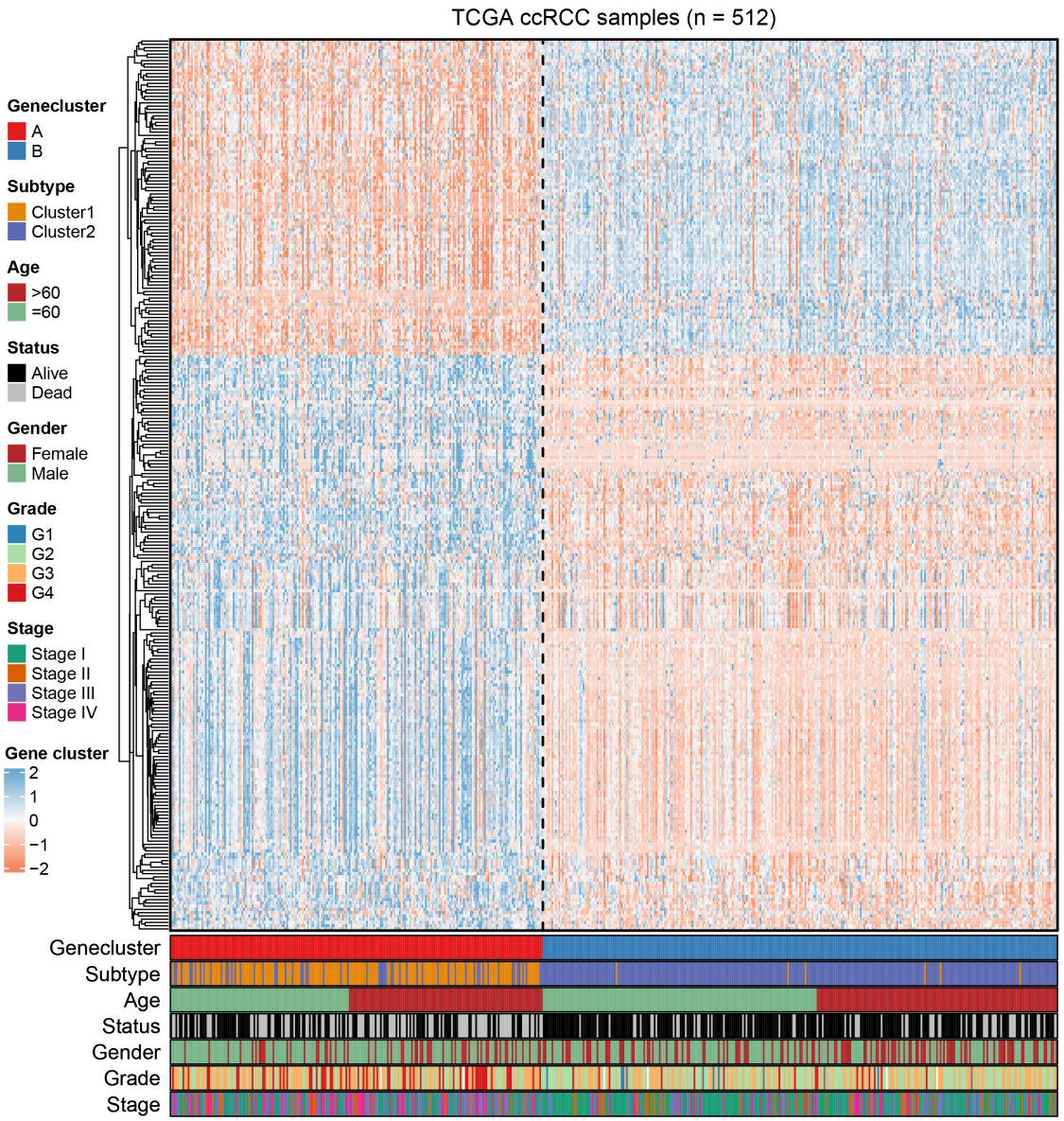

FIGURE 8 | The NMF clustering of DEGs in TCGA cohorts to categorize patients into two genomic subtypes (A and B). The gene clusters, immune-related subtype, tumor stage, age, survival status, gender, grade, and age were termed as patient annotations.

cells including NK cells, macrophages, T cells, and NK cells. Immune suppression is usually generated in the TME in advanced ccRCC through multiple mechanisms to avoid immune attack. For example, mechanisms weaken the presentation of effective antigens, reduce the impact of T cells, and promote immune tolerance, which are vital to tumor occurrence and development (Noessner et al., 2012). Thus, the TME plays a crucial role in the development of ccRCC. In recent years, immunotherapy has emerged as a new pillar for the treatment of tumors (Rini et al., 2019). The immune checkpoint blockade has attracted a lot of attention and has achieved remarkable results in immunotherapy, such as the use of PD-1/PD-L1 inhibitors and CTLA-4 inhibitors (Chae et al., 2018). However, the curative effects for some patients are still not satisfactory (Gulati and Vaishampayan, 2020). Several studies have demonstrated that individualized variation may contribute to the phenomenon (Takagi et al., 2020). Thus, exploring and understanding the subtypes of ccRCC will contribute to a better understanding of the heterogeneity of this disease (Jiang et al., 2020).

The ImmPort database collected a large number of known IR genes, which facilitated a comprehensive analysis of the role of IR genes in ccRCC (Bhattacharya et al., 2018). Wan et al. (2019) constructed a risk model to predict the prognosis of ccRCC based on seven IR genes including LAU, ISG15, IRF9, ARG2, RNASE2, SEMA3G, and UCN. Liao et al. (2021)

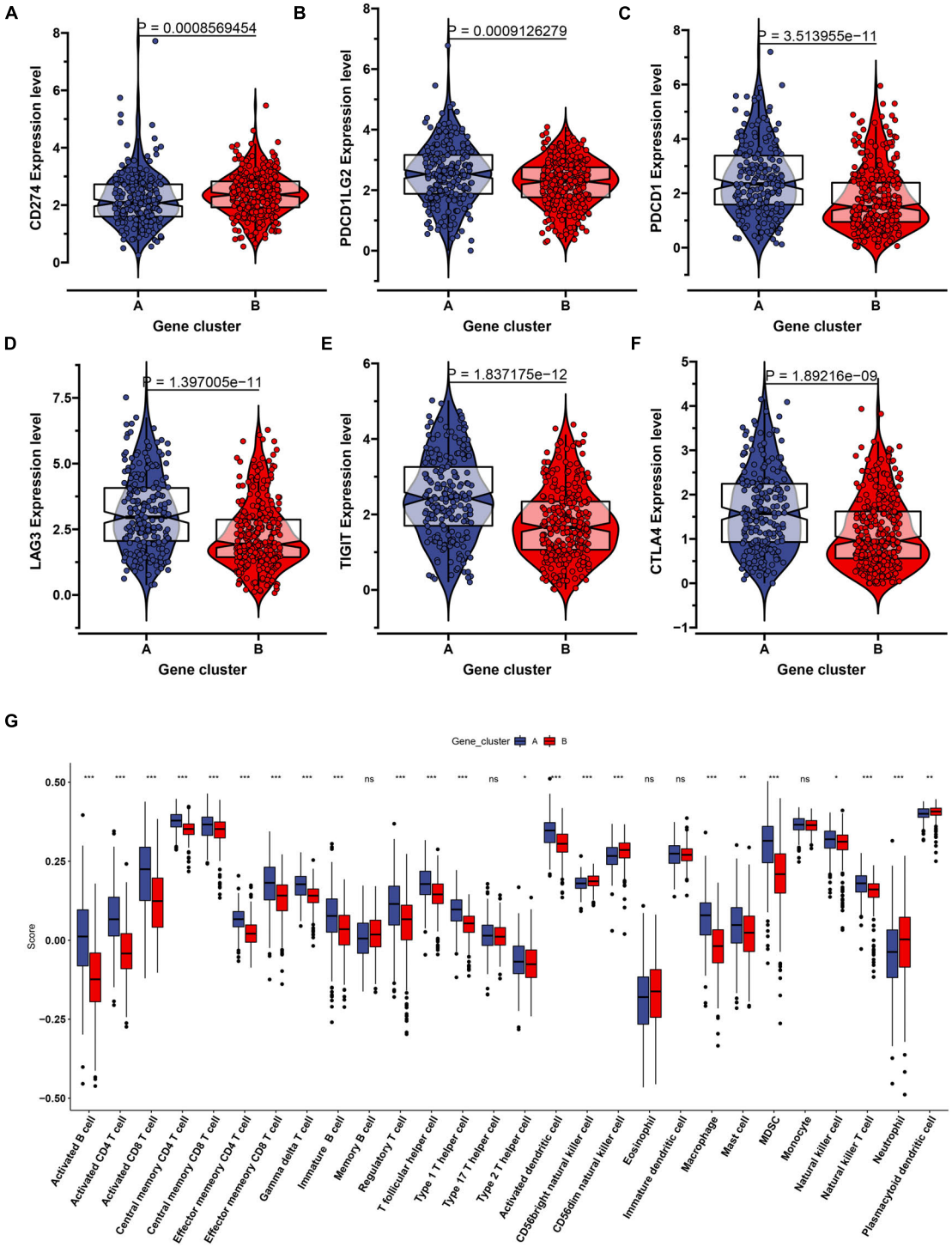

FIGURE 9 | The evaluation of the immune checkpoint and immune cell infiltration in the two genomic clusters. The expression level of six immune checkpoint including CD274 **(A)**, PDCD1LG2 **(B)**, PDCD1 **(C)**, LAG3 **(D)**, TIGIT **(E)**, CTLA4 **(F)** were showed in the two genomic clusters. **(G)** Twenty eight immune cells infiltration level were compared in the two genomic clusters. ns: not significant, $^{*}P < 0.05$, $^{**}P < 0.01$, $^{***}P < 0.001$.

used four prognostic IR genes (CRABP2, LTB4R, PTGER1, and TEK) to establish a gene signature to predict the prognosis of ccRCC. Zou and Hu (2020) developed a 14 IR gene signature to predict clinical outcome of kidney renal clear cell carcinoma. However, these studies mainly focused on the prognostic gene value and did not consider the heterogeneity and complexity of ccRCC. Thus, making a comprehensive analysis of IR subtypes will not only provide new insights into the molecular

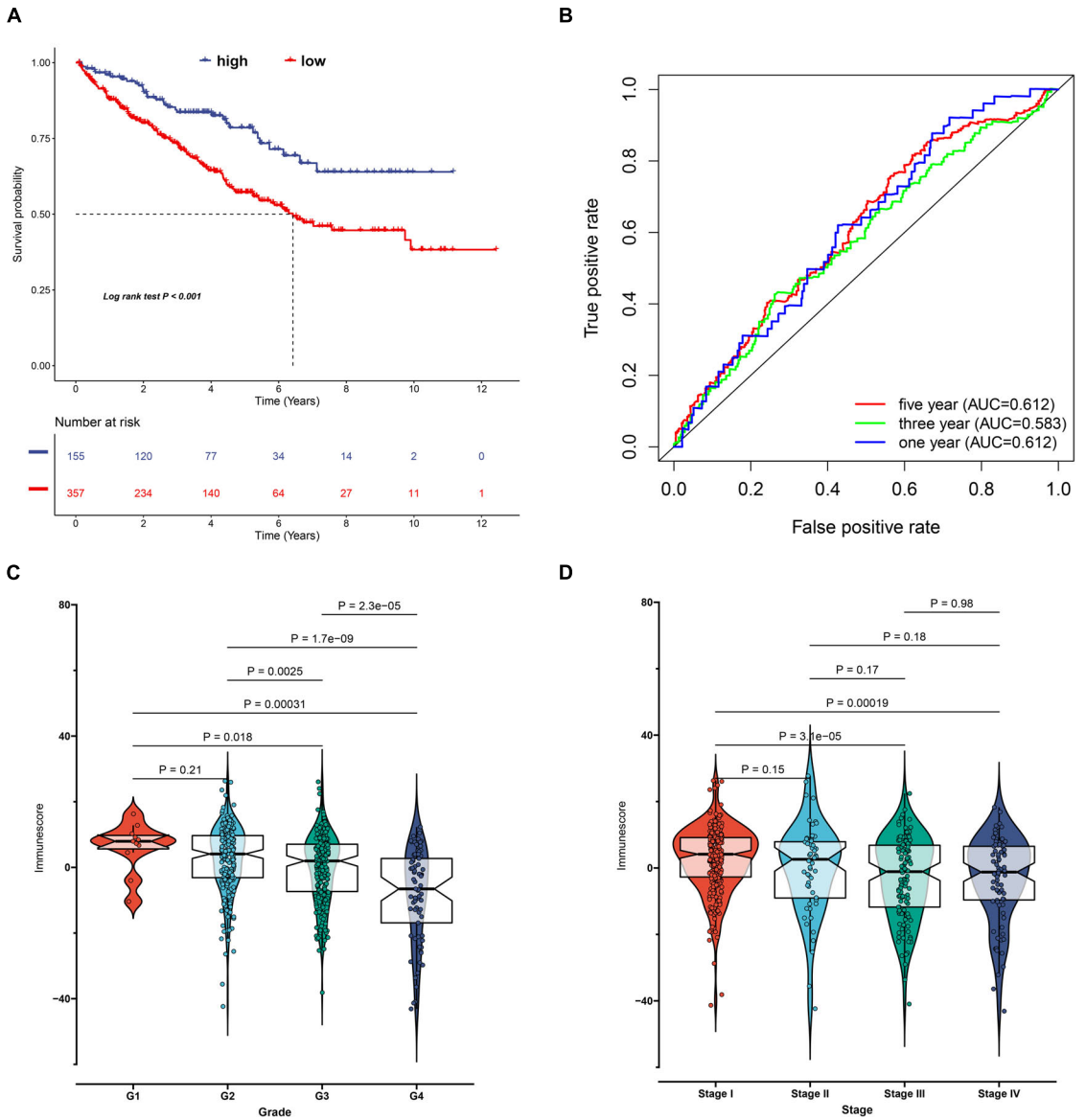

FIGURE 10 | Construction of immune-related (IR) score via principal component analysis. **(A)** Kaplan–Meier curves for patients with high and low IR score subgroups in TCGA cohort. **(B)** The receiver operator curve analysis for the IR score. The relationship between IR score and tumor grade **(C)** and stage **(D)**.

mechanism of ccRCC but also help us to better develop a personalized treatment in ccRCC. In the present study, we identified two IR molecular subtypes of ccRCC according to the gene expression profile. We found that patients in subtype C2 had a better survival outcome than those in C1. We then compared several known immune checkpoint's (PD-L1, PD-L2, PD-1, LAG3, TIGIT, IDO1, CTLA-4) expression levels between the two subtypes. We found that most of the immune checkpoint inhibitors had a higher expression level in C1 when compared to C2. The previously studies reported that patients with a high expression level of immune checkpoint genes were more likely to form an immunosuppressive microenvironment and promote tumor immune escape (Dunn et al., 2002). These results suggest that patients in C1 may benefit from immune checkpoint inhibitor therapies. The TME (immune score, stromal score, and immune purity) and immune cell infiltration have been reported to be tightly associated with the prognosis and immunotherapy of cancers (Luo et al., 2020). Thus, we also investigated the relationship between subtype and TME and immune cell infiltration. Interestingly, we found that patients in subtype C1 tended to have a higher expression level of $CD8^+$ and $CD4^+$ T cell infiltration than those in C2. This indicates that the anti-tumor effect of high T cell infiltration is offset by the strong immunosuppressive pathway activated by over-expressed immune checkpoint proteins (Matsushita et al., 2016; Hua et al., 2020). However, further research is needed to

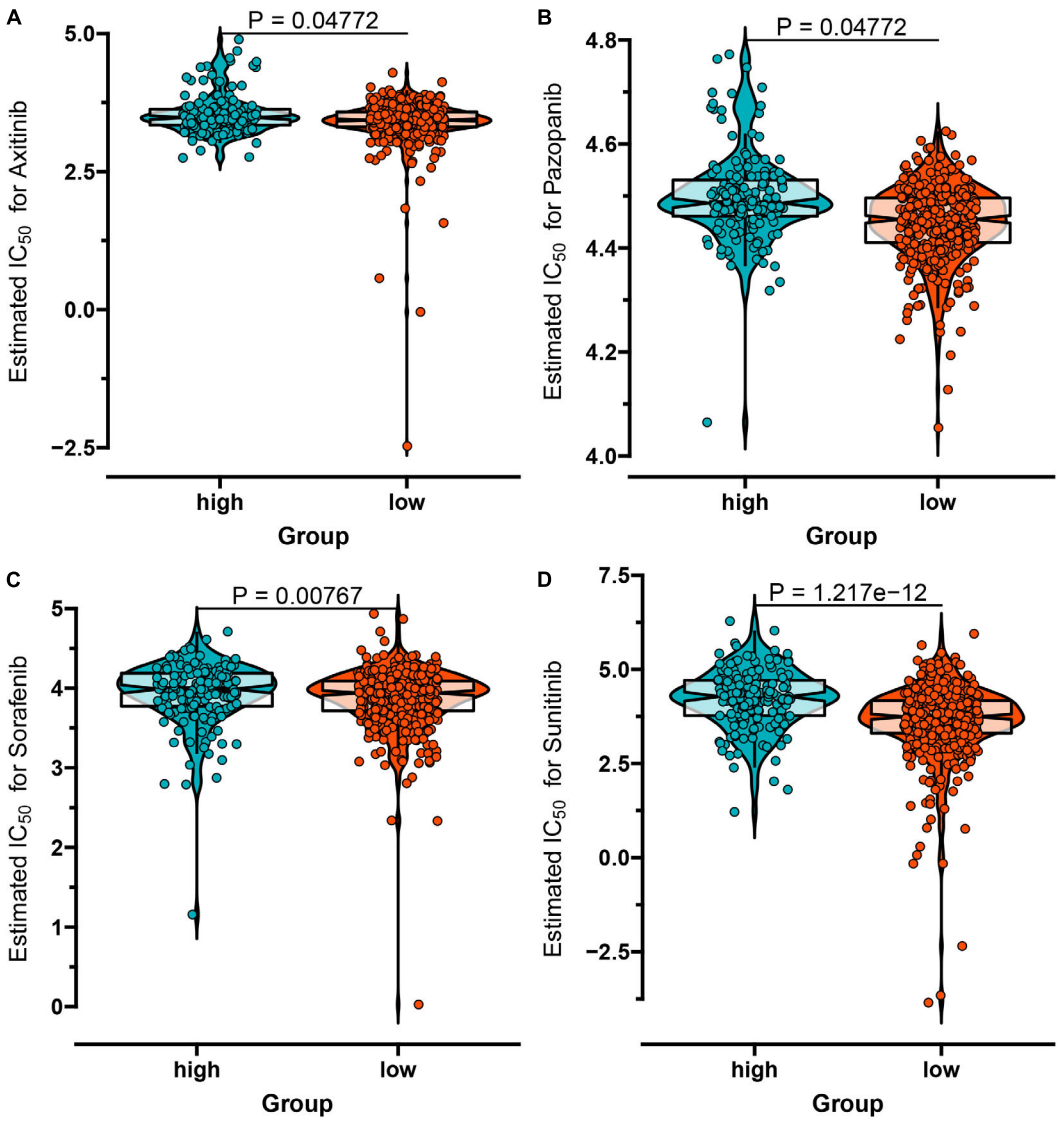

FIGURE 11 | The IC_{50} values of four chemo drugs in the IR score group of ccRCC including Axitinib **(A)**, Pazopanib **(B)**, Sorafenib **(C)**, and Sunitinib **(D)**.

demonstrate the potential molecular interactions between the molecular subtype and the immune cells of tumor immune status in ccRCC. In addition, we also discovered that the immune score and stromal score were higher in C1 when compared to C2. Previous studies have reported that high immune score and stromal score corresponded to poor survival (Luo et al., 2020). These findings were consistent with our results. Similarly, TMB value also showed a similar conclusion with the previous studies that presented a high level in C1, but a lower level in the C2 subtype (Huang et al., 2021).

Cumulative studies have demonstrated that chemo drugs including axitinib, pazopanib, sorafenib, and sunitinib have achieved some progress in advanced ccRCC cases (Koudijs et al., 2018). Here, we investigated the curative effect of four common chemo drugs for the subtypes C1 and C2. Interestingly, most of the IC_{50} values of chemo drugs in the C1 subtype were lower than subtype C2, suggesting that patients in subtype C1 were more sensitive to chemo drugs and may benefit from these drugs. In addition, we also identified 18 small molecular compounds and 16 mechanisms of action for the treatment of the molecular subtypes. These drugs included adrenergic receptor antagonist (scoulerine and suloctidil), glucocorticoid receptor agonist (alclometasone and piretanide), adrenergic receptor agonist (oxymetazoline), protein synthesis inhibitor (puromycin), and HMGCR inhibitor (lovastatin). We also discovered other candidate drugs which might pave the way for implementation of subtype treatments for ccRCC patients.

To further reveal the molecular function and pathway that are involved in the subtypes, we conducted GSVA

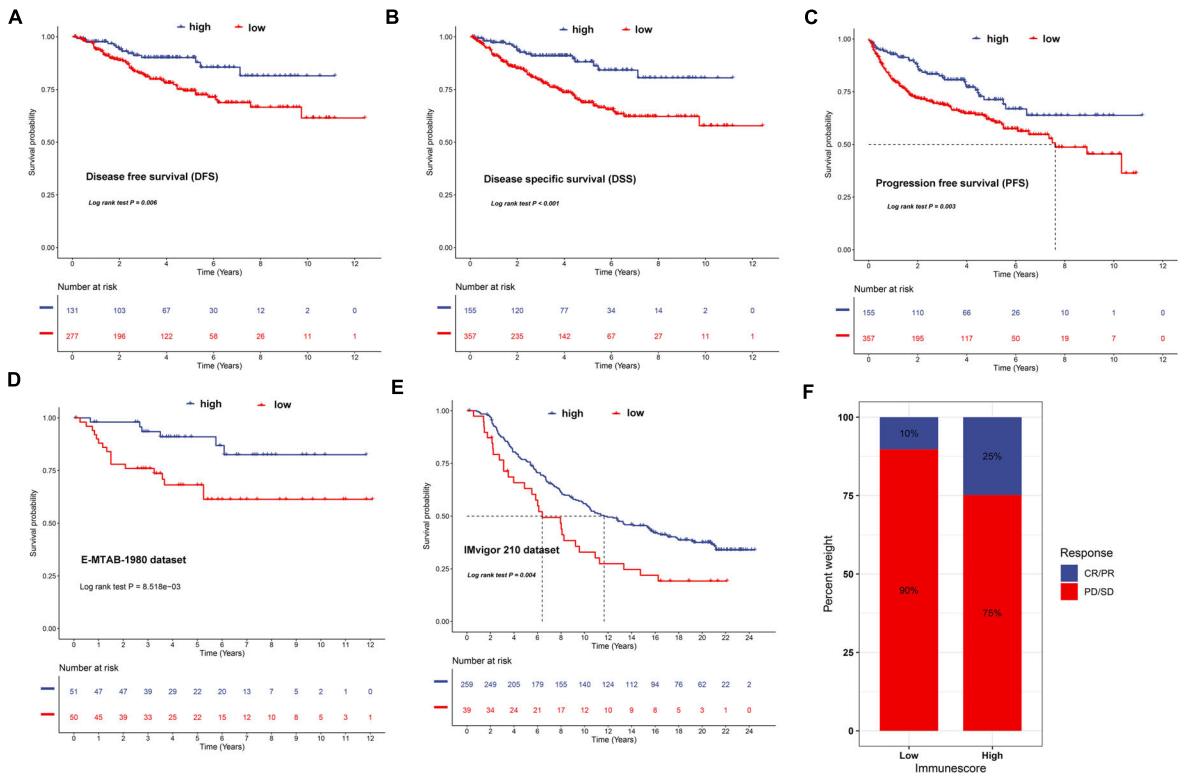

FIGURE 12 | Validation of the prognostic value of IR in disease-free survival **(A)**, disease-special survival **(B)**, and progression-free survival **(C)** of ccRCC, E-MTAB-1980 dataset **(D)**, and IMvigor210 cohort **(E)**, respectively. **(F)** The proportion of patients with response to PD-L1 blockade immunotherapy in low or high IR score groups. Responder/non-responder: 10%/90% in the low IR score groups and 25%/75% in the high IR score groups.

enrichment analysis for the two subtypes. We found that C2 corresponded to metabolism-related pathway, while C1 was associated with p53 signaling and cytokine-cytokine receptor interaction pathways. Studies have revealed that cytokine-cytokine receptor interaction is an important IR pathway that regulates the interaction between cytokines in tumors and is involved in the development and occurrence of tumors (Lee and Rhee, 2017). Considering that subtype C1 has a poor prognosis and more advanced ccRCC patients, it is reasonable that tumor-related pathways were enriched in subtype C1. In addition, we also performed limma analysis and obtained 274 DEGs between C1 and C2, and pathway enrichment results showed that DEGs mainly focused on the complement and coagulation cascades, NF-kappa B signaling pathway, and cytokine-cytokine receptor interaction, which is similar with our previously result, indicating that these DEGs were regarded as immune phenotype-related gene signatures. Similar to the IR gene clustering results, we also identified two genomic clusters based on these DEGs. The two genomic clusters were significantly related to distinct survival outcomes and TME landscapes. Due to the poor prognosis of ccRCC, more potential and valuable biomarkers are urgently needed. Zhang et al. (2021) developed an IR lncRNA-based model (AC012236.1, AC078778.1, AC078950.1, AC087318.1, and AC092535.4) for survival prediction in ccRCC. Liao et al. (2021) developed and validated the prognostic value of IR genes (CRABP2, LTB4R, PTGER1, and TEK) in ccRCC. Xiang et al. (2021) developed a four IR lncRNA signature for the prognosis of ccRCC through WGCNA analysis and Cox regression analysis. However, these risk models may be unstable and easily influenced by the gene expression level, especially considering the strong immunogenicity and heterozygosity of ccRCC. Thus, to guide therapeutic strategies for individual patients more precisely, we further constructed a IR score to quantify the IR patterns of individual tumors. The IR scores were closely associated with clinical information and can also serve as a prognostic biomarker for ccRCC survival. In addition, the prognostic value and therapeutic benefits of IR score were further validated in an external validation dataset and the IMvigor 210 cohort (Mariathasan et al., 2018).

Although we identified two molecular subtypes and constructed an IR score based on expression profile data of ccRCC, several limitations should be noted. Firstly, the samples with clinical information in the external validation dataset were relatively few and need to be expanded. Besides, due to the absence of an appropriate ICI-based ccRCC dataset, we used the different immunotherapy dataset across different malignancies (urothelial cancer) to validate the effects of IR score. Finally, all the discoveries were based on the dataset analysis and

in vitro and *in vivo* experiments need to be performed to further verify these results.

In conclusion, we comprehensively investigated IR subtypes among 613 ccRCC samples based on the IR gene expression data, and systematically linked these subtypes with TME characteristics. We also evaluated the difference of chemo drug sensitivity and immunotherapy response between the subtypes. Finally, we developed an IR score to quantify the immune pattern of individual patients with ccRCC. These results may contribute to promoting our understanding of the characteristics of TME infiltration and provide new strategies for personalized treatment.

DATA AVAILABILITY STATEMENT

The original contributions presented in the study are included in the article/**Supplementary Material**, further inquiries can be directed to the corresponding author/s.

AUTHOR CONTRIBUTIONS

JwH, YaL, and JyH designed the study. CH, YiL, and YY collected the clinical information and gene expression data. WZ and YY analyzed the data. WZ, YiL, and HZ wrote and revised the manuscript. All the authors contributed to the article and approved the submitted version.

FUNDING

This study was supported by the Health Science Research Personnel Training Program of Fujian Province (2017-CXB-22), Fujian Science and Technology Plan Guiding Projects (2019D026), and Xiamen Medical Advantage Subspecialty Vascular Access Construction Fund ([2018] 296). Moreover, we also thank the support of the research program fund of the fifth hospital of Xiamen.

ACKNOWLEDGMENTS

We appreciate TCGA and the ArrayExpress database for providing the original study data. Moreover, our deepest gratitude goes to the reviewers and editors for their careful work and thoughtful suggestions that have helped improve this article substantially.

SUPPLEMENTARY MATERIAL

The Supplementary Material for this article can be found online at: https://www.frontiersin.org/articles/10.3389/fcell.2021.736540/full#supplementary-material

Supplementary Figure 1 | The non-negative matrix factorization (NMF) clustering analysis to identify potential molecular subtypes of ccRCC based on the immune-related gene expression in the E-MTAB-1980 dataset. **(A)** The cophenetic correlation coefficient for the cluster number from 2 to 7. **(B)** Consensus matrix heatmap when $k = 2$. **(C)** Principal component analysis (PCA) for the 101 ccRCC patients, each dot represents a single sample. **(D)** KM survival curve analysis for the two subtypes.

Supplementary Figure 2 | Subclass mapping analysis revealed that subtype cluster 1 from TCGA was significantly associated with subtype cluster 2 from the E-MTAB-1980 dataset, while subtype cluster 2 from TCGA was significantly related to subtype cluster 1 from the E-MTAB-1980 dataset (Bonferroni-corrected P-value = 0.003996).

Supplementary Figure 3 | Gene Set Variant Analysis (GSVA) for the two subtypes on the basis of the 512 samples.

Supplementary Figure 4 | Sankey plot showing the changes of immune-related molecular subtypes, gene cluster, IR score, and patient survival status.

Supplementary Figure 5 | Identification of the independence of the IR score and clinical information through univariate Cox regression analysis **(A)** and multivariate Cox regression analysis **(B)**.

Supplementary Figure 6 | The landscape of immune cells in the two IR score groups.

Supplementary Figure 7 | The comparisons of the stromal score **(A)**, immune score **(B)**, and tumor purity **(C)** in the IR score groups.

Supplementary Figure 8 | Identification of small molecular compounds by using the CMap drug database between the high IR score and low IR score groups.

REFERENCES

Ahmad, A., and Finelli, A. (2019). Renal function outcomes following radical or partial nephrectomy for localized renal cell carcinoma: should urologists rely on preoperative variables to predict renal function in the long term? *Eur. Urol.* 75, 773–774. doi: 10.1016/j.eururo.2018.12.027

Baig, M. A., Lin, Y. S., Rasheed, J., and Mittman, N. (2006). Renal medullary carcinoma. *J. Natl. Med. Assoc.* 98, 1171–1174.

Bhattacharya, S., Dunn, P., Thomas, C., Smith, B., Schaefer, H., Chen, J., et al. (2018). ImmPort, toward repurposing of open access immunological assay data for translational and clinical research. *Sci. Data* 5:180015. doi: 10.1038/sdata.2018.15

Buchler, T., Bortlicek, Z., Poprach, A., Pavlík, T., Veskrnova, V., Honzirkova, M., et al. (2015). Outcomes for patients with metastatic renal cell carcinoma achieving a complete response on targeted therapy: a registry-based analysis. *Eur. Urol.* 70, 469–475. doi: 10.1016/j.eururo.2015.12.031

Cai, C., Xu, Y.-F., Wu, Z.-J., Dong, Q., Li M-y, Olson, J., et al. (2015). Tim-3 expression represents dysfunctional tumor infiltrating T cells in renal cell carcinoma. *World J. Urol.* 34, 561–567. doi: 10.1007/s00345-015-1656-1657

Chae, Y., Arya, A., Iams, W., Cruz, M., Chandra, S., Choi, J., et al. (2018). Current landscape and future of dual anti-CTLA4 and PD-1/PD-L1 blockade immunotherapy in cancer; lessons learned from clinical trials with melanoma and non-small cell lung cancer (NSCLC). *J. ImmunoTherapy Cancer* 6:39. doi: 10.1186/s40425-018-0349-343

Chaffer, C., and Weinberg, R. (2011). A perspective on cancer cell metastasis. *Science (New York, NY)* 331, 1559–1564. doi: 10.1126/science.1203543

Charoentong, P., Finotello, F., Angelova, M., Mayer, C., Efremova, M., Rieder, D., et al. (2016). Pan-cancer immunogenomic analyses reveal genotype-immunophenotype relationships and predictors of response to checkpoint blockade. *Cell Rep.* 18, 248–262.

Dunn, G., Bruce, A., Ikeda, H., and Old, L. (2002). Cancer immunoediting: from immunosurveillance to tumor escape. *Nat. Immunol.* 3, 991–998. doi: 10.1038/ni1102-991

Escudier, B., and Gore, M. (2011). Axitinib for the management of metastatic renal cell carcinoma. *Drugs RD* 11, 113–126. doi: 10.2165/11591240-000000000-00000

Gao, X., Yang, J., and Chen, Y. (2020). Identification of a four immune-related genes signature based on an immunogenomic landscape analysis of clear cell renal cell carcinoma. *J. Cell. Physiol.* 235, 9834–9850. doi: 10.1002/jcp.29796

Geeleher, P., Cox, N., and Huang, R. (2014). pRRophetic: an R Package for prediction of clinical chemotherapeutic response from tumor gene expression levels. *PLoS One* 9:e107468. doi: 10.1371/journal.pone.0107468

Gillis, N. (2020). *Nonnegative Matrix Factorization*. Philadelphia, PA: SIAM.

Gitlitz, B., and Figlin, R. (2003). Cytokine-based therapy for metastatic renal cell cancer. *Urol. Clin. North Am.* 30, 589–600. doi: 10.1016/S0094-0143(03)00027-22

Gordon, M. S. (2008). Sorafenib in advanced clear-cell renal-cell carcinoma. *Yearbook Oncol.* 2008, 95–96. doi: 10.1016/S1040-1741(08)79114-79110

Grüllich, C. (2018). Prospective single center trial of next-generation sequencing analysis in metastatic renal cell cancer: the MORE-TRIAL. *Future Sci. OA* 4:FSO299. doi: 10.4155/fsoa-2017-2150

Gulati, S., and Vaishampayan, U. (2020). Current state of systemic therapies for advanced renal cell carcinoma. *Curr. Oncol. Rep.* 22:26. doi: 10.1007/s11912-020-0892-891

Hänzelmann, S., Castelo, R., and Guinney, J. (2013). GSVA: gene set variation analysis for microarray and RNA-Seq data. *BMC Bioinformatics* 14:7. doi: 10.1186/1471-2105-14-17

Hirata, H., Hinoda, Y., Ueno, K., Nakajima, K., Ishii, N., and Dahiya, R. (2011). MicroRNA-1826 directly targets beta-catenin (CTNNB1) and MEK1 (MAP2K1) in VHL-inactivated renal cancer. *Carcinogenesis* 33, 501–508. doi: 10.1093/carcin/bgr302

Hua, X., Juan, C., Su, Y., and Liang, C. (2020). Identification of an immune-related risk signature for predicting prognosis in clear cell renal cell carcinoma. *Aging* 12, 2302–2332. doi: 10.18632/aging.102746

Huang, J., Li, Z., Fu, L., Lin, D., Wang, C., Wang, X., et al. (2021). Comprehensive characterization of tumor mutation burden in clear cell renal cell carcinoma based on the three independent cohorts. *J. Cancer Res. Clin. Oncol.* 147:1745. doi: 10.1007/s00432-020-03299-3293

Jiang, P., Gu, S., Pan, D., Fu, J., Sahu, A., Hu, X., et al. (2018). Signatures of T cell dysfunction and exclusion predict cancer immunotherapy response. *Nat. Med.* 24, 1550–1558. doi: 10.1038/s41591-018-0136-131

Jiang, Y., Gou, X., Wei, Z., Tan, J., Yu, H., Zhou, X., et al. (2020). Bioinformatics profiling integrating a three immune-related long non-coding RNA signature as a prognostic model for clear cell renal cell carcinoma. *Cancer Cell Int.* 20:116. doi: 10.1186/s12935-020-01242-1247

Koudijs, K., Scheltinga, A., Böhringer, S., Schimmel, K., and Guchelaar, H.-J. (2018). Personalised drug repositioning for clear cell renal cell carcinoma using gene expression. *Sci. Rep.* 8:5250. doi: 10.1038/s41598-018-23195-23198

Lamb, J., Crawford, E., Peck, D., Modell, J., Blat, I., Wrobel, M., et al. (2006). The connectivity map: using gene-expression signatures to connect small molecules, genes, and disease. *Science (New York, NY)* 313, 1929–1935. doi: 10.1126/science.1132939

Lee, M., and Rhee, I. (2017). Cytokine signaling in tumor progression. *Immune Network* 17:214. doi: 10.4110/in.2017.17.4.214

Li, J., Sun, J., Rong, R., Li, L., Shang, W., Song, D., et al. (2017). HMGB1 promotes myeloid-derived suppressor cells and renal cell carcinoma immune escape. *Oncotarget* 8, 63290–63298. doi: 10.18632/oncotarget.18796

Liao, Z., Yao, H., Wei, J., Feng, Z., Chen, W., Luo, J., et al. (2021). Development and validation of the prognostic value of the immune-related genes in clear cell renal cell carcinoma. *Trans. Androl. Urol.* 10, 1607–1619. doi: 10.21037/tau-20-1348

Liu, Y., Zhou, L., Chen, Y., Liao, B., Ye, D., Wang, K., et al. (2019). Hypertension as a prognostic factor in metastatic renal cell carcinoma treated with tyrosine kinase inhibitors: a systematic review and meta-analysis. *BMC Urol.* 19:49. doi: 10.1186/s12894-019-0481-485

Luo, J., Xie, Y., Zheng, Y., Wang, C., Qi, F., Hu, J., et al. (2020). Comprehensive insights on pivotal prognostic signature involved in clear cell renal cell carcinoma microenvironment using the ESTIMATE algorithm. *Cancer Med.* 9, 4310–4323. doi: 10.1002/cam4.2983

Mariathasan, S., Turley, S., Nickles, D., Castiglioni, A., Yuen, K., Wang, Y., et al. (2018). TGFβ attenuates tumour response to PD-L1 blockade by contributing to exclusion of T cells. *Nature* 554, 544–554. doi: 10.1038/nature25501

Martel, C., and Lara, P. (2003). Renal cell carcinoma: current status and future directions. *Crit. Rev. Oncology/Hematol.* 45, 177–190. doi: 10.1016/S1040-8428(02)00076-78

Matsushita, H., Sato, Y., Karasaki, T., Nakagawa, T., Kume, H., Ogawa, S., et al. (2016). Neoantigen load, antigen presentation machinery, and immune signatures determine prognosis in clear cell renal cell carcinoma. *Cancer Immunol. Res.* 4, 463–471. doi: 10.1158/2326-6066.CIR-15-0225

Motzer, R. J., Hutson, T. E., Tomczak, P., Michaelson, M. D., Bukowski, R. M., Rixe, O., et al. (2007). Sunitinib versus interferon alfa in metastatic renal-cell carcinoma. *N. Engl. J. Med.* 356, 115–124. doi: 10.1056/NEJMoa065044

Motzer, R., Tannir, N., McDermott, D., Aren, O., Melichar, B., Choueiri, T., et al. (2018). Nivolumab plus ipilimumab versus sunitinib in advanced renal-cell carcinoma. *N. Engl. J. Med.* 378, 1277–1290. doi: 10.1056/nejmoa1712126

Noessner, E., Brech, D., Mendler, A., Masouris, I., Schlenker, R., and Prinz, P. (2012). Intratumoral alterations of dendritic-cell differentiation and CD8+ T-cell anergy are immune escape mechanisms of clear cell renal cell carcinoma. *Oncoimmunology* 1, 1451–1453. doi: 10.4161/onci.21356

Parikh, M., and Bajwa, P. (2020). Immune checkpoint inhibitors in the treatment of renal cell carcinoma. *Sem. Nephrol.* 40, 76–85. doi: 10.1016/j.semnephrol.2019.12.009

Porpiglia, F., Bertolo, R., Amparore, D., Cattaneo, G., and Fiori, C. (2014). Mini-Retroperitoneoscopic clampless partial nephrectomy for "low-complexity" renal tumours (PADUA Score <= 8). *Eur. Urol.* 66, 778–783. doi: 10.1016/j.eururo.2014.06.001

Rini, B., Battle, D., Figlin, R., George, D., Hammers, H., Hutson, T., et al. (2019). The society for immunotherapy of cancer consensus statement on immunotherapy for the treatment of advanced renal cell carcinoma (RCC). *J. ImmunoTherapy Cancer* 7:81. doi: 10.1186/s40425-019-0813-818

Ritchie, M., Phipson, B., Wu, D., Hu, Y., Law, C., Shi, W., et al. (2015). LIMMA powers differential expression analyses for RNA-sequencing and microarray studies. *Nucleic Acids Res.* 43:e47. doi: 10.1093/nar/gkv007

Roh, W., Chen, P.-L., Reuben, A., Spencer, C. N., Prieto, P., Miller, J., et al. (2017). Integrated molecular analysis of tumor biopsies on sequential CTLA-4 and PD-1 blockade reveals markers of response and resistance. *Sci. Trans. Med.* 9:eaah3560. doi: 10.1126/scitranslmed.aah3560

Sato, Y., Yoshizato, T., Shiraishi, Y., Maekawa, S., Okuno, Y., Kamura, T., et al. (2013). Integrated molecular analysis of clear-cell renal cell carcinoma. *Nat. Genet.* 45, 860–867. doi: 10.1038/ng.2699

Siegel, R., Miller, K., and Jemal, A. (2016). Cancer statistics, 2017. *CA Cancer J. Clin.* 67, 7–30. doi: 10.3322/caac.21387

Sternberg, C., Davis, I., Mardiak, J., Lee, E., Wagstaff, J., Barrios, C., et al. (2010). Pazopanib in locally advanced or metastatic renal cell carcinoma: results of a randomized Phase III trial. *J. Clin. Oncol.* 28, 1061–1068. doi: 10.1200/JCO.2009.23.9764

Takagi, T., Yoshida, K., Wada, A., Kondo, T., Fukuda, H., Ishihara, H., et al. (2020). Predictive factors for recurrence after partial nephrectomy for clinical T1 renal cell carcinoma: a retrospective study of 1227 cases from a single institution. *Int. J. Clin. Oncol.* 25, 892–898. doi: 10.1007/s10147-020-01632-x

Topalian, S., Hodi, F., Brahmer, J., Gettinger, S., Smith, D., McDermott, D., et al. (2012). Safety, activity, and immune correlates of Anti–PD-1 antibody in cancer. *N. Engl. J. Med.* 366, 2443–2454. doi: 10.1056/NEJMoa1200690

Wan, B., Liu, B., Huang, Y., Yu, G., and Lv, C. (2019). Prognostic value of immune-related genes in clear cell renal cell carcinoma. *Aging* 11, 11474–11489. doi: 10.18632/aging.102548

Wang, Z., Xu, H., Zhu, L., He, T., Lv, W., and Wu, Z. (2020). Establishment and evaluation of a 6-Gene survival risk assessment model related to lung adenocarcinoma microenvironment. *BioMed Res. Int.* 2020, 1–8. doi: 10.1155/2020/6472153

Xiang, Z., Shen, E., Li, M., Hu, D., Zhang, Z., and Yu, S. (2021). Potential prognostic biomarkers related to immunity in clear cell renal cell carcinoma using bioinformatic strategy. *Bioengineered* 12, 1773–1790. doi: 10.1080/21655979.2021.1924546

Yang, L., Shi, L., Fu, Q., Xiong, H., Zhang, M., and Yu, S. (2012). Efficacy and safety of sorafenib in advanced renal cell carcinoma patients: results from a long-term study. *Oncol. Lett.* 3, 935–939. doi: 10.3892/ol.2012.585

Yang, W., Lightfoot, H., Bignell, G., Behan, F., Cokelear, T., Haber, D., et al. (2016). Genomics of Drug Sensitivity in Cancer (GDSC): a resource for biomarker discovery in cancer cells. *Eur. J. Cancer* 69:S82. doi: 10.1016/S0959-8049(16)32839-32838

Yu, G., Wang, L.-G., Han, Y., and He, Q.-Y. (2012). clusterProfiler: an R Package for comparing biological themes among gene clusters. *Omics* 16, 284–287. doi: 10.1089/omi.2011.0118

Zhang, B., Wu, Q., Li, B., Wang, D., Wang, L., and Zhou, Y. (2020). M6A regulator-mediated methylation modification patterns and tumor microenvironment infiltration characterization in gastric cancer. *Mol. Cancer* 19:53. doi: 10.1186/s12943-020-01170-1170

Zhang, Z., Tang, Y., Liu, Y., Zhuang, H., Lin, E., Xie, L., et al. (2021). A novel immune-related lncRNA-Based model for survival prediction in clear cell renal cell carcinoma. *J. Immunol. Res.* 2021, 1–37. doi: 10.1155/2021/9921466

Zou, Y., and Hu, C. (2020). A 14 immune-related gene signature predicts clinical outcomes of kidney renal clear cell carcinoma. *PeerJ* 8:e10183. doi: 10.7717/peerj.10183

Conflict of Interest: The authors declare that the research was conducted in the absence of any commercial or financial relationships that could be construed as a potential conflict of interest.

Publisher's Note: All claims expressed in this article are solely those of the authors and do not necessarily represent those of their affiliated organizations, or those of the publisher, the editors and the reviewers. Any product that may be evaluated in this article, or claim that may be made by its manufacturer, is not guaranteed or endorsed by the publisher.

Copyright © 2021 Zhong, Li, Yuan, Zhong, Huang, Huang, Lin and Huang. This is an open-access article distributed under the terms of the Creative Commons Attribution License (CC BY). The use, distribution or reproduction in other forums is permitted, provided the original author(s) and the copyright owner(s) are credited and that the original publication in this journal is cited, in accordance with accepted academic practice. No use, distribution or reproduction is permitted which does not comply with these terms.

frontiers in Cell and Developmental Biology

ORIGINAL RESEARCH
published: 24 September 2021
doi: 10.3389/fcell.2021.709241

Characterization of Immune-Related Long Non-coding RNAs to Construct a Novel Signature and Predict the Prognosis and Immune Landscape of Soft Tissue Sarcoma

Zhengjun Lin[1,2], Ke Pang[1], Hongli Li[3], Xianghong Zhang[1], Jia Wan[1], Tao Zheng[1], Tang Liu[1] and Weijun Peng[3]**

[1] Department of Orthopedics, The Second Xiangya Hospital, Central South University, Changsha, China, [2] Xiangya School of Medicine, Central South University, Changsha, China, [3] Department of Integrated Traditional Chinese and Western Medicine, The Second Xiangya Hospital, Central South University, Changsha, China

OPEN ACCESS

Edited by:
Zimu Deng,
Shanghai Institute of Biochemistry and Cell Biology, Chinese Academy of Sciences (CAS), China

Reviewed by:
Nicolas Sylvius,
University of Leicester, United Kingdom
Renyuan Zhang,
University at Buffalo, United States

***Correspondence:**
Tang Liu
liutang1204@csu.edu.cn
Weijun Peng
pengweijun87@csu.edu.cn

Specialty section:
This article was submitted to Molecular and Cellular Pathology, a section of the journal Frontiers in Cell and Developmental Biology

Received: 13 May 2021
Accepted: 06 September 2021
Published: 24 September 2021

Citation:
Lin Z, Pang K, Li H, Zhang X, Wan J, Zheng T, Liu T and Peng W (2021) Characterization of Immune-Related Long Non-coding RNAs to Construct a Novel Signature and Predict the Prognosis and Immune Landscape of Soft Tissue Sarcoma. Front. Cell Dev. Biol. 9:709241. doi: 10.3389/fcell.2021.709241

Background: Increasing evidence has demonstrated that immune-related long non-coding RNAs (irlncRNAs) are critically involved in tumor initiation and progression and associated with the prognosis of various cancers. However, their role in soft tissue sarcoma (STS) remains significantly uninvestigated.

Materials and Methods: Gene expression profiles were extracted from The Cancer Genome Atlas (TCGA) and Genotype-Tissue Expression (GTEx) for the identification of irlncRNAs. Univariate analysis and modified least absolute shrinkage and selection operator (LASSO) penalized regression analysis were employed to determine differently expressed irlncRNA (DEirlncRNA) pairs of prognostic value, and subsequently, a risk signature based on DEirlncRNA pairs was established. Furthermore, Kaplan–Meier analysis and the area under the receiver operating characteristic curve (AUC) were used to assess survival differences and the predictive accuracy of the risk signature, respectively. Lastly, the correlation of irlncRNAs with immune characteristics and chemosensitivity in patients with STS were further investigated.

Results: A total of 1088 irlncRNAs were identified, and 311 irlncRNAs were distinguished as DEirlncRNAs. A total of 130 DEirlncRNA pairs were further identified as prognostic markers, and 14 pairs were selected for establishing a risk signature. The irlncRNA-based risk signature functioned as an independent prognostic marker for STS. Compared with the patients in the high-risk group, those in the low-risk group exhibited a better prognosis and were more sensitive to several chemotherapeutic agents. In addition, the irlncRNA-based risk signature was significantly associated with immune scores, infiltrating immune cells, and the expression of several immune checkpoints.

Conclusion: In conclusion, our data revealed that the irlncRNA-based risk signature resulted in reliable prognosis, effectively predicted the immune landscape of patients with STS and was significantly correlated with chemosensitivity, thus providing insights into the potential role of irlncRNAs as prognostic biomarkers and novel therapeutic targets for STS.

Keywords: soft tissue sarcomas, immune-related lncRNAs, prognostic signature, immune microenvironment, chemosensitivity

INTRODUCTION

Soft tissue sarcomas (STS), a rare and heterogeneous group of human malignancies with mesenchymal origin (Bourcier et al., 2019; Ratan and Patel, 2016), although only account for about 1% in all human malignancies, consist of more than 50 different distinct subtypes, but they only account for about 1% in all human malignancies (Jo and Fletcher, 2014; Poon and Quek, 2018). Despite surgery, radiotherapy and neoadjuvant chemotherapy, approximately 50% of patients with STS develop distant metastases, and the 5-year survival rate of patients with advanced STS is as low as approximately 28% (Italiano et al., 2011; Kim et al., 2019). Therefore, it is necessary to identify novel targets and develop more effective therapeutic strategies to improve the prognosis of patients with STS.

Recently, the tumor immune microenvironment has been proven to play a regulatory role in tumor progression. It comprises complex components, including multiple infiltrating immune cell types, immune checkpoints, immune-related molecules and signaling pathways, which are all critically involved in cancer development and immunotherapy (Zhang et al., 2019). It can not only inhibit tumor progression by killing tumor cells but also promote tumor progression by establishing conditions that facilitate the growth of tumor cells (Schreiber et al., 2011). For instance, cancer cells can evade immune system attack through immune checkpoints that inhibit immune functions, thus contributing to immune tolerance (Abril-Rodriguez and Ribas, 2017). Cancer immunotherapy has exhibited remarkable efficacy in cancer treatment over the past decades. Recently, multiple immune checkpoint inhibitors have been used for the treatment of several cancers, such as melanoma, renal cancer and lung cancer (Abril-Rodriguez and Ribas, 2017). Although immunotherapy has also been used for STS treatment in several clinical trials, its therapeutic efficacy and prolonged effects require further improvement (Ayodele and Razak, 2020). Therefore, further investigation should focus on exploring promising immune-related biomarkers and developing effective immunotherapeutic strategies for patients with STS. Moreover, numerous studies have investigated the promising potential of immunotherapy based on complex mechanisms that control the tumor immune microenvironment, such as diverse cellular components, signaling pathways and epigenetic modifications (Nguyen and Spranger, 2020; Rusek et al., 2015). However, the detailed regulatory networks of the tumor immune microenvironment have not been conclusively identified.

Long non-coding RNAs (lncRNAs) are a class of RNA transcripts longer than 200 nucleotides that do not code for proteins (Yang et al., 2019). Increasing evidence has revealed that lncRNAs play an important role in multiple physiological processes and human diseases, including human malignancies (Luo et al., 2021; Ransohoff et al., 2018; Schmitz et al., 2016). It has been found that a large number of lncRNAs are dysregulated during cancer progression, and multiple lncRNAs can serve as oncogenic or tumor suppressor genes in several cancers (Bhan et al., 2017; Liang et al., 2020). They can function as fundamental regulators of immune cell activities and immune-related gene expression, thereby modulating the tumor immune microenvironment in human malignancies (Huang et al., 2018). For instance, lncRNA SATB2-AS1, which was downregulated in colorectal cancer tissues, was correlated with tumor immune cell infiltration and affected tumor immune response by targeting SATB2 (Xu et al., 2019). In diffuse large B-cell lymphoma (DLBCL), SNHG14 can stimulate crosstalk between CD8+ T cells and DLBCL cells and induce CD8+ T cells by directly targeting the immune checkpoints PD-1/PD-L1 (Zhao et al., 2019). Recently, several studies have reported that immune-related lncRNAs (irlncRNAs) are correlated with the prognosis and clinicopathological parameters of patients with human malignancies and may facilitate the prognosis of multiple cancers (Wang et al., 2021b,a; Xu et al., 2021). However, the role of irlncRNAs in STS remains largely unknown, and no study has investigated the prognostic and clinicopathological value of irlncRNAs in patients with STS.

Therefore, our study was aimed to explore the association of irlncRNAs with prognosis, immune characteristics and chemosensitivity of STS for identifying the potential of irlncRNAs as prognostic biomarkers and novel therapeutic targets for STS.

Abbreviations: irlncRNAs, immune-related long non-coding RNAs; STS, soft tissue sarcomas; TCGA, The Cancer Genome Atlas; GTEx, genotype-tissue expression; DEirlncRNA, differently expressed irlncRNA; AUC, area under the ROC curve; lncRNAs, long non-coding RNAs; DLBCL, diffuse large B cell lymphoma; AIC, akaike information criterion; IC50, half inhibitory centration; GRCh38, Genome Reference Consortium Human Build 38; DDLPS, dedifferentiated liposarcoma; LMS, leiomyosarcoma; MFS, myxofibrosarcoma; SS, synovial sarcoma; UPS, undifferentiated pleomorphic sarcoma; SS, synovial sarcoma; IDO1, Indoleamine 2, 3-dioxygenase 1; Trp, tryptophan; CAR-T, chimeric antigen receptor T.

MATERIALS AND METHODS

Dataset

RNA-seq data were acquired from The Cancer Genome Atlas Sarcoma (TCGA-SARC) and Genotype-Tissue Expression

(GTEx) datasets from the Genomic Data Commons (GDC) using the UCSC Xena browser[1] (Goldman et al., 2015). The corresponding demographics (age and gender) and clinical characteristics (survival status, overall survival time, histological type, margin status, metastasis status, and confirmed recurrence and radiation therapy) were obtained from the TCGA-SARC database. The GTEx dataset provided RNA-seq data of 54 non-diseased tissue samples from approximately 1000 individuals. RNA-seq data were eventually collected from 78 normal soft tissue samples and 259 tumor samples from 259 patients. RNA-seq data from both TCGA-SARC and GTEx datasets were normalized to FPKM values for further investigation.

Annotation of Long Non-coding RNAs

The lncRNA annotation file of Genome Reference Consortium Human Build 38 (GRCh38) was obtained from GENCODE[2] to annotate lncRNAs of the gene expression files downloaded from the TCGA and GTEx datasets. A total of 14,081 lncRNAs identified in both datasets were enrolled in this study.

Identification of Immune-Related Long Non-coding RNAs

A total of 2483 immune-related genes were extracted from the ImmPort database[3] (**Supplementary Material**). Pearson correlation analysis was implemented to confirm irlncRNAs (with $|\text{Pearson R}| > 0.5$ and $P < 0.001$), and 1088 lncRNAs were considered as irlncRNAs. Subsequently, differentially expressed irlncRNAs (DEirlncRNAs) were extracted through differential analyses between 259 tumor and 78 normal samples using the "limma" R package. The expression differences were evaluated based on their log2 fold change (log2 FC) and false discovery rate (FDR), with the thresholds set at $|\text{log2FC}| > 2$ and FDR < 0.05. A total of 589 irlncRNAs were confirmed as DEirlncRNAs.

Construction of Differently Expressed Immune-Related Long Non-coding RNAs Pairs

Differently Expressed irlncRNAs were paired using a loop-iteration method, and a 0-or-1 matrix was established by assigning C for each DEirlncRNA pair based on the expression level of both lncRNA A and lncRNA B: If the expression level of lncRNA A was higher than that of lncRNA B, C was bound to 1; otherwise, C was bound to 0. Subsequently, the established 0-or-1 matrix was checked ulteriorly. A DEirlncRNA pair was considered to have no prognostic value if the expression level of lncRNA pairs was 0 or 1 because pairs without a certain rank did not effectively predict the prognosis. If the value of a DEirlncRNA pair as 0 or 1 accounted for more than 80% samples enrolled in our study, it was considered to have no relationship with the prognosis of STS. Therefore, DEirlncRNA pairs with values 0 or 1 were selected for further investigation if they constituted more than 20% and less than 80% samples.

[1]https://xenabrowser.net/

[2]https://www.gencodegenes.org/human/

[3]https://immport.niaid.nih.gov

Construction and Validation of Risk Signature

A total of 259 STS patients were randomly divided into a training cohort and a validation cohort at a ratio of 1:1 in R, including 130 patients in the training cohort and 129 patients in the validation cohort. The risk model construction was performed in the training cohort, and external validation in the validation cohort was critical when establishing the risk model. Univariate Cox regression analysis was conducted for profiling the prognostic DEirlncRNA pairs. The least absolute shrinkage and selection operator (LASSO) analysis was performed to identify the most significant prognostic DEirlncRNA pairs for constructing a risk signature employing the 'glmnet' R package. LASSO analysis was performed for 1000 iterations, and random stimulation was performed 1000 times in each iteration. The time required by each DEirlncRNA pair enrolled in the risk model for 1000-iteration LASSO analysis was recorded, and DEirlncRNA pairs that were recorded > 100 times were included in the risk signature for further investigation. The risk score for each patient with STS was calculated based on the coefficients of every DEirlncRNA pair using the following formula: $RiskScore = \sum_{i=0}^{n} \beta_i * Gi$. The area under the curve (AUC) values of each risk model were calculated to determine the optimal risk signature. When the maximum AUC value was reached, the calculation procedure was terminated. The predictive ability of the risk signature for 1-/3-/5-year overall survival was assessed using the "survivalROC" R package. In addition, the Akaike Information Criterion (AIC) value of each point on the receiver operating characteristic (ROC) curve for estimating the 5-year overall survival was calculated to find the maximum inflection point, which was identified as the cut-off value of the risk scores. All patients were then categorized into the high-risk and low-risk groups based on the cut-off value identified in the training set. Kaplan–Meier (K-M) survival curves along with the log-rank test were used to identify differences in overall survival between the two groups using the R packages "survival" and "survminer." As for the validation of the risk signature, all the above analyses were conducted to assess the risk signature in the validation cohort.

To further investigate the clinicopathological significance of the risk signature, the chi-square test was performed to explore the relationship between the risk signature and clinicopathological characteristics using the R package "ComplexHeatmap." The results were visualized on a band diagram, and statistical significance was labeled as follows: $P < 0.001$ = ***, $P < 0.01$ = **, and $P < 0.05$ = *. We further used the Wilcoxon signed-rank test to assess differences in the risk scores among subgroups based on clinicopathological characteristics, and the results were visualized on a box diagram.

Investigation of Immune Characteristics

The abundance of immune cells was analyzed using XCELL (Aran et al., 2017; Aran, 2020), TIMER (Li et al., 2017; Li T. et al., 2020), QUANTISEQ (Finotello et al., 2019; Plattner et al., 2020), MCPcounter (Dienstmann et al., 2019), EPIC (Racle et al., 2017), CIBERSORT-ABS (Tamminga et al., 2020), and CIBERSORT (Chen et al., 2018; Zhang et al., 2020). The immune, stromal

and microenvironment scores were analyzed using XCELL. The relationship between the risk signature and infiltrating immune cells was analyzed using Spearman correlation analysis, and the correlation coefficients were visualized on a bubble diagram. The differences in immune cell infiltration between the high- and low-risk groups were analyzed using the Wilcoxon signed-rank test and were visualized using boxplots. The procedure was conducted using the R packages "ggplot2" and "ggpur."

Investigation of Chemotherapeutic Efficacy

The half maximal inhibitory concentration (IC50) of chemotherapeutic agents was calculated to assess the capability of the irlncRNA-based risk signature in predicting the chemotherapeutic efficacy in patients with STS. The Wilcoxon signed-rank test was used to compare IC50 between the high- and low-risk groups. The procedure was conducted and the results were visualized using the "pRRophetic" and "ggplot2" R packages.

Statistical Analysis

R version 4.0.2 was used for statistical analyses and visualization. Limma package version 3.44.3 K-M survival curves along with the log-rank test were employed to evaluate the survival differences between the two groups. Univariate and multivariate Cox regression analyses were conducted to validate the independent role of the risk signature in the prognosis of patients with STS. Time-dependent ROC analysis was performed for assessing the predictive significance of the risk signature. A P value < 0.05 was considered statistically significant.

RESULTS

Identification of Differently Expressed Immune-Related Long Non-coding RNAs

The procedure of our study is demonstrated in **Figure 1**. We extracted the gene expression profiling data, including 78 normal and 259 tumor samples, from the TCGA and GTEx datasets. The clinicopathological characteristics of patients with STS included in the analysis are provided in **Table 1**. A total of 259 patients with STS were enrolled in our study, including 58 with dedifferentiated liposarcoma (DDLPS), 104 with leiomyosarcoma (LMS), 25 with myxofbrosarcoma (MFS), 10 with synovial sarcoma (SS), 51 with undifferentiated pleomorphic sarcoma (UPS), and 11 with other STS types. Subsequently, we identified 14,081 lncRNAs in both datasets and extracted the expression matrices of 2483 immune-related genes from the datasets. We further conducted Pearson correlation analysis to identify irlncRNAs. The lncRNAs that were associated with one or more immune-related genes ($|$ Pearson R$|$ > 0.5 *and* $P < 0.001$) were defined as irlncRNAs. A total of 1088 lncRNAs were confirmed as irlncRNAs. Furthermore, 311 irlncRNAs were distinguished as DEirlncRNAs, including 45 upregulated and 266 downregulated irlncRNAs, by examining the expression profiles of 259 tumor tissues and 78 normal tissues (**Supplementary Table 1**). The mostly differentially expressed 100 DEirlncRNAs were visualized on the heatmap and volcano plot (**Supplementary Figure 1**).

Construction of Differently Expressed Immune-Related Long Non-coding RNAs Pairs and a Risk Signature

To further establish DEirlncRNA pairs among 311 DEirlncRNAs, we used a loop-iteration method and constructed a 0-or-1 matrix. As a result, a total of 35455 valid DEirlncRNA pairs were established. Subsequently, we selected 130 prognostic DEirlncRNA pairs using univariate Cox regression analysis. By conducting modified LASSO Cox analysis based on 130 prognostic DEirlncRNA pairs, 40 DEirlncRNA pairs were employed to establish a risk assessment model, and 14 pairs were further enrolled in a Cox proportional hazard model using the stepwise method (**Figures 2A–C**). All patients were divided into the following two cohorts: 130 in the training cohort and 129 in the validation cohort. Furthermore, we calculated the 5-year AUC values of each model to identify the maximum value for an optimal model, and the result indicated that the highest 5-year AUC value was 0.898 (**Figure 3A**). Using these AIC values, the maximum inflection point on the 5-year ROC was identified as the cut-off value (**Figure 3B**). All patients with STS in the training cohort were divided into the following two groups based on the cut-off value: 54 patients in the high-risk group and 76 in the low-risk group. Subsequently, we calculated AUC values to assess the performance of the nomogram in predicting the overall survival of patients in the training cohort. The AUC values of 1-, 3-, and 5-year survival were 0.905, 0.850, and 0.898, respectively (**Figure 3C**). Furthermore, we compared the AUC values of 5-year survival of the risk signature with other clinicopathological features, and the results revealed that the risk signature was more accurate than other predictors (**Figure 3D**). K-M analysis was employed for assessing the differences in overall survival between the high- and low-risk groups. The result revealed that high-risk patients had a remarkably shorter survival time than that of low-risk patients ($P < 0.001$; **Figure 3E**). The risk scores and survival status of each patient are shown in **Figures 3F,G**; patients in the high-risk group had worse clinical outcomes. In addition, the results of univariate Cox analysis suggested that the risk signature was significantly correlated with overall survival (hazard ratio [HR], 1.399; 95% confidence interval [CI], 1.207–1.620; $P < 0.001$; **Figure 3H**). The results of multivariate Cox analysis demonstrated that the risk signature functioned as an independent prognostic marker for patients with STS (HR, 1.328; 95% CI, 1.168–1.510; $P < 0.001$; **Figure 3I**). Univariate Cox analysis also revealed that the margin status (HR, 2.835; 95% CI, 1.418–5.670; $P = 0.003$; **Figure 3H**), and the metastasis status (HR, 2.776; 95% CI, 1.397–5.514; $P = 0.004$; **Figure 3H**) was closely associated with the prognosis of patients, and multivariate Cox analysis further indicated that the margin status (HR, 2.391; 95% CI, 1.133–5.046; $P = 0.022$; **Figure 3I**), and the metastasis status (HR, 3.635; 95% CI, 1.687–7.834; $P < 0.001$; **Figure 3I**) functioned as an independent prognostic variable.

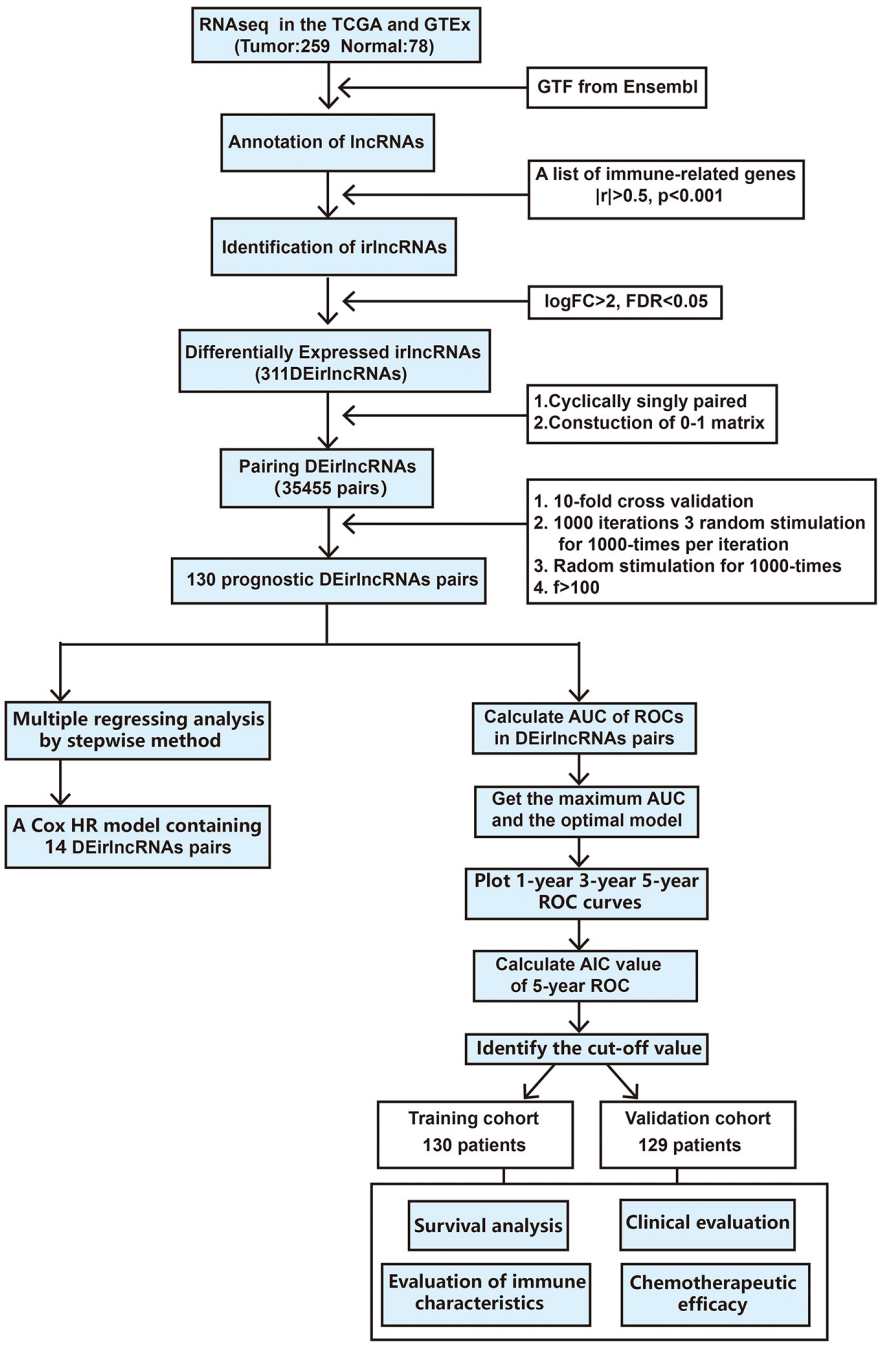

FIGURE 1 | Flowchart of this study.

Validation of Immune-Related Long Non-coding RNAs-Based Risk Signature

We further validated the predictive value of the risk signature in the independent validation cohort. A total of 129 patients with STS were included in the independent validation cohort. The 1-/3-/5-year AUC values were 0.739, 0.824, and 0.808, respectively, which indicated the satisfactory performance of the risk signature in the cohort (**Figure 4A**). In addition, the 5-year AUC value of the risk signature was also significantly higher than that of other clinicopathological variables, indicating that the risk signature was more accurate than other predictors (**Figure 4B**). Survival analysis indicated that the overall survival of high-risk patients was significantly worse than that of their low-risk counterparts ($P < 0.001$; **Figure 4C**). The risk score and survival status plots of patients demonstrated that the survival time and survival rate were decreased with an increasing risk

TABLE 1 | Clinical characteristics of STS patients in the training set and the validation set.

Characteristics (*n*; %)	TGCA-SARC (*n* = 259)	Training set (*n* = 130)	Validation set (*n* = 129)
Age			
≤60	128 (49.4)	67 (51.5)	61 (47.3)
>60	131 (50.6)	63 (48.5)	68 (52.7)
Gender			
Male	118 (45.6)	62 (47.7)	56 (43.4)
Female	141 (54.4)	68 (52.3)	73 (56.6)
Histological type			
DDLPS	58 (22.4)	27 (20.8)	31 (24.0)
LMS	104 (40.2)	50 (38.5)	54 (41.8)
MFS	25 (9.6)	12 (9.2)	13 (10.1)
SS	10 (3.9)	4 (3.1)	6 (4.7)
UPS	51 (19.7)	29 (22.3)	22 (17.1)
Other	11 (4.2)	8 (6.1)	3 (2.3)
Metastasis			
Yes	56 (21.6)	28 (21.5)	28 (21.7)
No	120 (46.3)	58 (44.6)	62 (48.1)
Unknow	83 (32.0)	44 (33.9)	39 (30.2)
Margin status			
Positive	73 (28.1)	37 (28.5)	36 (27.9)
Negative	136 (52.4)	68 (52.3)	68 (52.7)
Unknow	50 (19.3)	25 (19.2)	25 (19.4)
Recurrence			
Yes	29 (11.2)	14 (10.8)	15 (11.6)
No	143 (55.2)	72 (55.4)	71 (55.1)
Unknow	87 (33.6)	44 (33.8)	43 (33.3)
Radiotherapy			
Yes	74 (28.6)	45 (34.6)	29 (22.5)
No	179 (69.1)	83 (63.9)	96 (74.4)
Unknow	6 (2.3)	2 (1.5)	4 (3.1)

A total of 259 patients with STS were enrolled in our study, including 58 with DDLPS, 104 with LMS, 25 with MFS, 10 with SS, 51 with UPS, and 11 with other STS types. They were randomly divided into the training set (130 patients), and the validation set (129 patients). DDLPS, dedifferentiated liposarcoma; LMS, leiomyosarcoma; MFS, myxofibrosarcoma; SS, synovial sarcoma; UPS, undifferentiated pleomorphic sarcoma.

score (**Figures 4D,E**). Moreover, univariate analysis confirmed the significant correlation between risk scores and prognosis (HR, 1.087; 95% CI, 1.040–1.015; $P < 0.001$; **Figure 4F**), and multivariate analysis further confirmed the role of the risk score as an independent prognostic factor in STS (HR, 1.120; 95% CI, 1.054–1.190; $P < 0.001$; **Figure 4G**). In conclusion, all these results were consistent with those of the training cohort, thus verifying the prognostic significance of the risk model in STS.

Analysis of Clinical Parameters Using the Risk Signature

To further verify the clinicopathological significance of the irlncRNA-based risk signature, we conducted chi-square tests to evaluate the correlation between the risk scores and clinicopathological characteristics of patients with STS. The heatmap demonstrated that the risk score might be correlated with the margin status of patients, and the scatter diagrams obtained by the Wilcoxon signed-rank test identified that the high-risk score was significantly associated with metastasis ($P = 0.0022$), and positive margin status ($P = 0.0019$) (**Figures 4H–J**).

Correlation of the Risk Signature With Immune Characteristics

After constructing the irlncRNA-based risk signature, we further assessed its association with immune characteristics in STS. The results of the Wilcoxon signed-rank test revealed that the high-risk score was positively correlated with infiltrating immune cells such as macrophage M0, resting mast cells and resting natural killer (NK) cells, whereas the high-risk score was negatively correlated with CD4+ T cells, CD8+ T cells, monocytes, macrophage M1 and memory B cells (**Supplementary Figure 2**). Currently acknowledged methods including XCELL, TIMER, QUANTISEQ, MCPcounter, EPIC, CIBERSORT-ABS and CIBERSORT were employed to analyze the relationship between the abundance of infiltrating immune cells and risk scores, and the results of Spearman correlation analysis were demonstrated on a lollipop-shaped diagram (**Figure 5A** and **Supplementary Table 2**). In addition, the low-risk group had higher immune, microenvironment and stromal scores, which were evaluated using XCELL (**Figures 5B–D**). In addition, the risk score exhibited a significant correlation with the expression of several immune checkpoints. The high-risk group exhibited lower expression of IDO1, CD96, CD200, CD27, TIGIT, and CD47 than that exhibited by the low-risk group (**Figures 5E–J**). These results indicated that the risk signature was closely related to the abundance of immune cells and microenvironment scores and might predict immunotherapeutic efficacy in patients with STS.

Correlation of the Risk Signature With Chemotherapeutic Efficacy

The potential of the risk signature in predicting chemotherapeutic efficacy in patients with STS was also investigated. The results revealed that a low-risk score was significantly related to higher IC50 of several chemotherapeutics, including doxorubicin ($P = 0.0031$), gemcitabine ($P = 0.0047$), mitomycin C ($P = 0.017$), docetaxel ($P = 0.049$), etoposide ($P = 0.017$), and embelin ($P = 0.00055$), indicating that the irlncRNA-based risk signature effectively predicted chemotherapeutic efficacy in patients with STS (**Figure 6**).

DISCUSSION

The present study is the first of its kind to construct a novel irlncRNA-based risk signature and comprehensively investigate the potential role of irlncRNAs in STS. In this study, 259 patients were enrolled from the TCGA dataset; 35455 DEirlncRNA pairs were constructed, and 130 pairs were further confirmed as prognostic markers for STS. Of the 130 pairs, 14 were selected to construct the irlncRNA-based risk signature. Several lncRNAs, such as LINC02454, lncRNA PDCD4-AS1 and LINC02446, used in the risk signature have been reported to play a critical role

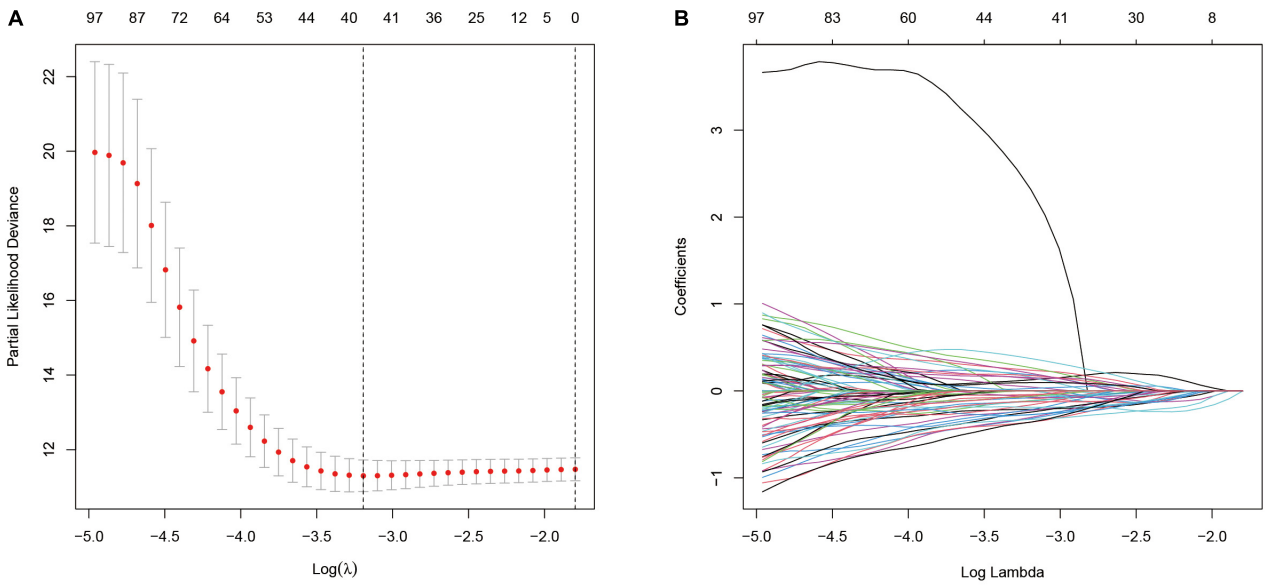

C

	pvalue	Hazard ratio
AC087276.2|AC008443.4	0.004	1.830(1.218−2.749)
PRDM16−DT|AL022318.1	<0.001	0.470(0.314−0.703)
PRDM16−DT|AC012462.3	0.009	0.555(0.356−0.865)
DNM3OS|PDCD4−AS1	0.010	1.730(1.141−2.625)
AC008050.1|AC020658.5	0.005	0.560(0.372−0.842)
AC002546.1|AC112721.1	0.007	0.515(0.317−0.834)
AC002546.1|AC092718.4	0.001	31.297(3.914−250.234)
AC007389.5|AL359853.1	0.004	0.554(0.370−0.830)
AC007389.5|AC074135.1	<0.001	0.488(0.323−0.738)
AC007389.5|AL591686.1	<0.001	0.398(0.250−0.635)
HOXC13−AS|TRBV11−2	0.009	1.704(1.145−2.538)
AL359397.1|LINC02454	0.006	0.566(0.377−0.849)
AL359397.1|LINC02446	0.002	1.959(1.284−2.989)
AL359397.1|AP003071.3	<0.001	2.032(1.362−3.031)

FIGURE 2 | Selection of DEirlncRNA pairs for the risk signature. **(A,B)** LASSO analysis with minimal lambda value. **(C)** Forest plot of the prognostic ability of 14 DEirlncRNA pairs identified by Cox proportional hazard regression included in the risk signature by the stepwise method.

in cancer progression. For instance, LINC02454 was previously reported to be upregulated in papillary thyroid cancer, was closely related to various clinicopathological features, including large tumor size, advanced clinical stage and lymph node metastasis and served as a diagnostic and prognostic biomarker for papillary thyroid cancer (Cai et al., 2018; Li Z. et al., 2021; Tan et al.,

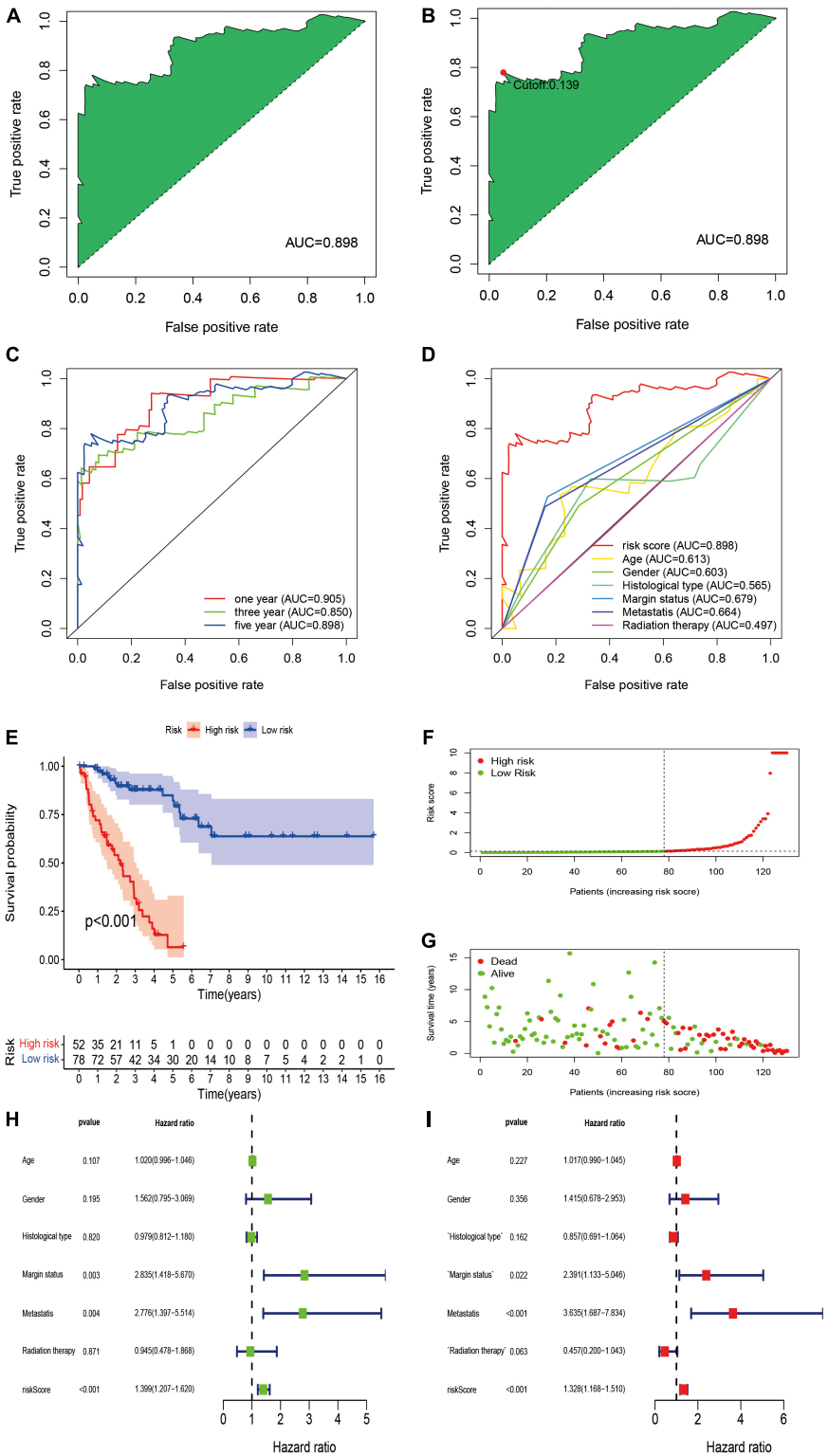

FIGURE 3 | Construction of DEirlncRNA pairs-based risk signature in the training cohort. **(A)** The ROC of the optimal DEirlncRNA pairs-based risk signature with the highest AUC. **(B)** Identification of the cut-off point on the ROC curve by the AIC. **(C)** The 1-, 3-, and 5-year ROC curves of the optimal model. **(D)** Comparison of the 5-year ROC curve with other clinical characteristics. **(E)** Kaplan–Meier analysis of patients in the high risk and low risk groups. Patients in the low-risk group experienced a longer survival time. **(F,G)** Distributions of risk scores and survival status of STS patients. **(H,I)** Univariate and multivariate Cox regression analyses of clinical factors and prognostic risk signature for overall survival. Univariate and multivariate analyses revealed that risk score was an independent prognostic predictor.

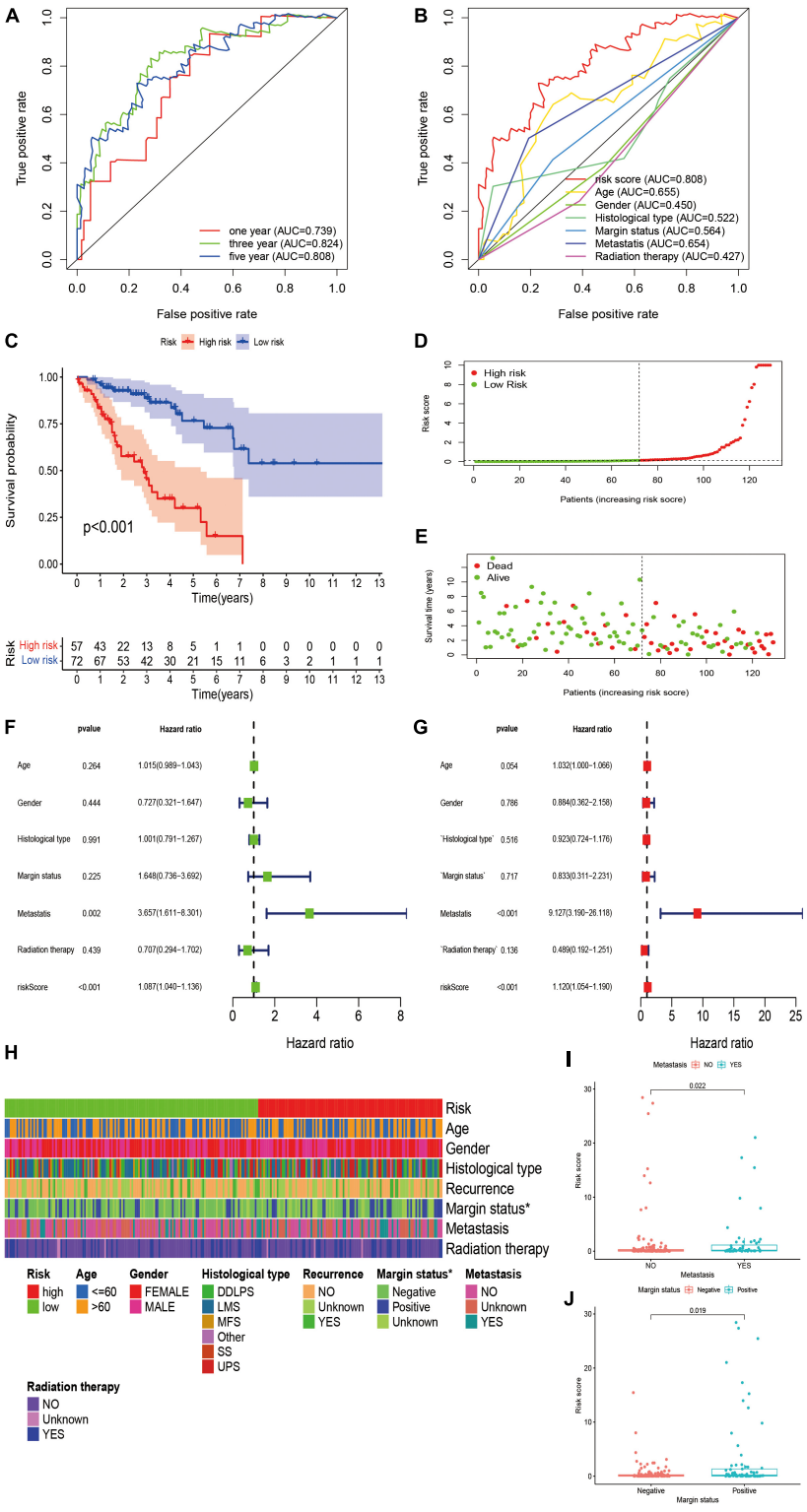

FIGURE 4 | Validation and clinical evaluation of the irlncRNA-based risk signature. **(A)** The 1-, 3-, and 5-year ROC curves of the risk signature in the validation cohort. **(B)** Comparison of the 5-year ROC curve with other clinical characteristics. **(C)** Kaplan–Meier analysis of patients in the high risk and low risk groups. Patients in the low-risk group experienced a longer survival time. **(D,E)** Distributions of risk scores and survival status of STS patients. **(F,G)** Univariate and multivariate Cox regression analyses of clinical factors and prognostic risk signature for overall survival. Univariate and multivariate analyses revealed that risk score was an independent prognostic predictor in the validation cohort. **(H–J)** Evaluation of the association between the risk signature and clinical parameters. A strip chart **(H)** along with the scatter diagram showed that **(I)** metastasis, and **(J)** margin status were significantly correlated with the risk score.

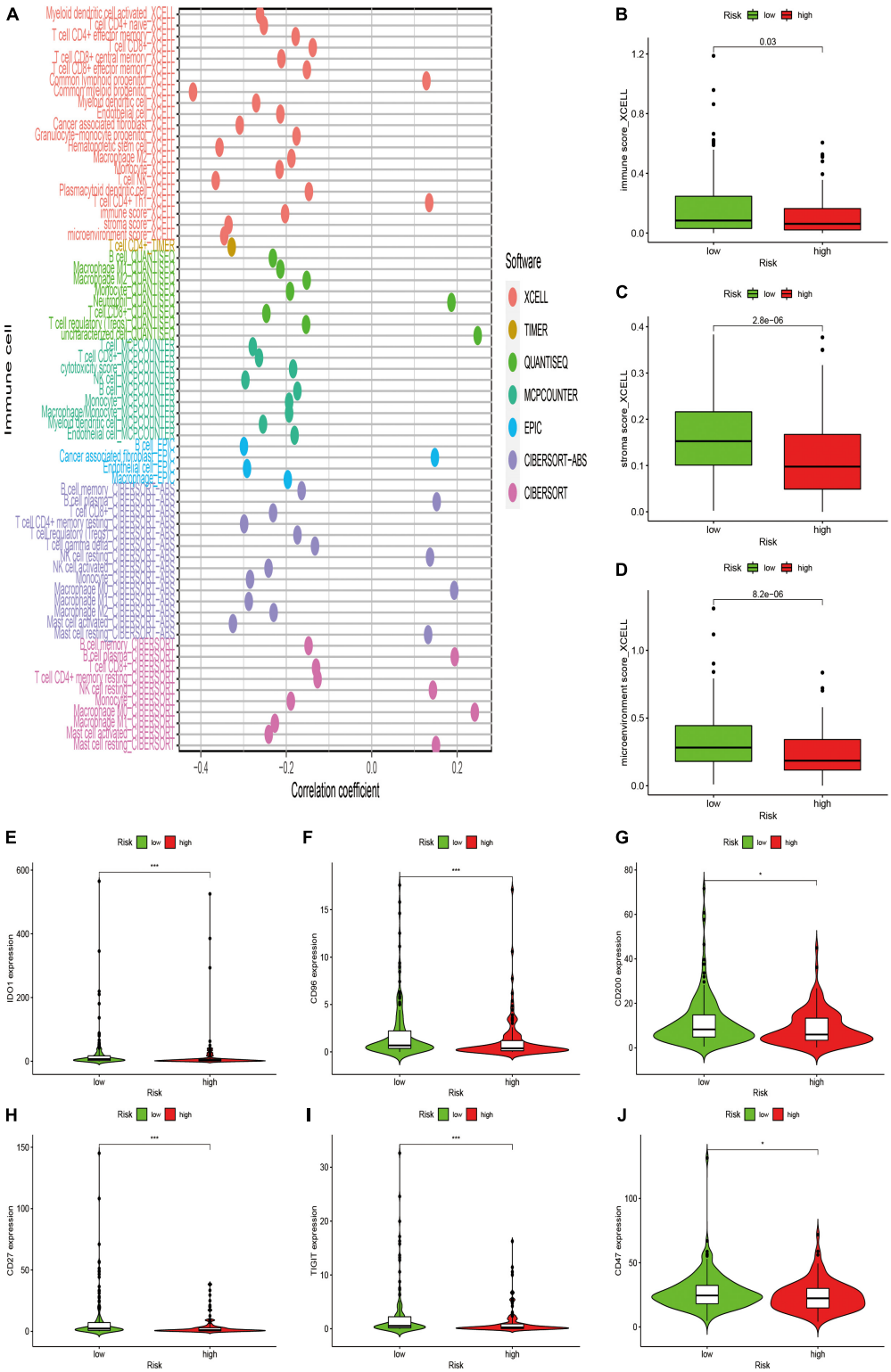

FIGURE 5 | Estimation of the associations between immune characteristics and the risk signature. **(A)** Diagram of Spearman correlation analysis between immune cells infiltration and the risk signature. Patients in the high-risk group were more positively associated with tumor-infiltrating immune cells such as macrophage M0, and NK resting cells, whereas they were negatively associated with CD8+ T cells, CD4+ T cells, and monocytes. **(B–D)** The correlation between the risk signature and immune score by XCELL. Patients in the high-risk group had a lower **(B)** immune, **(C)** stromal scores, and **(D)** microenvironment scores. **(E–J)** The expression levels of immune checkpoints in the high-risk and low-risk groups. High risk scores were negatively correlated with upregulated **(E)** IDO1, **(F)** CD96, **(G)** CD200, **(H)** CD27, **(I)** TIGIT, and **(J)** CD47 levels.

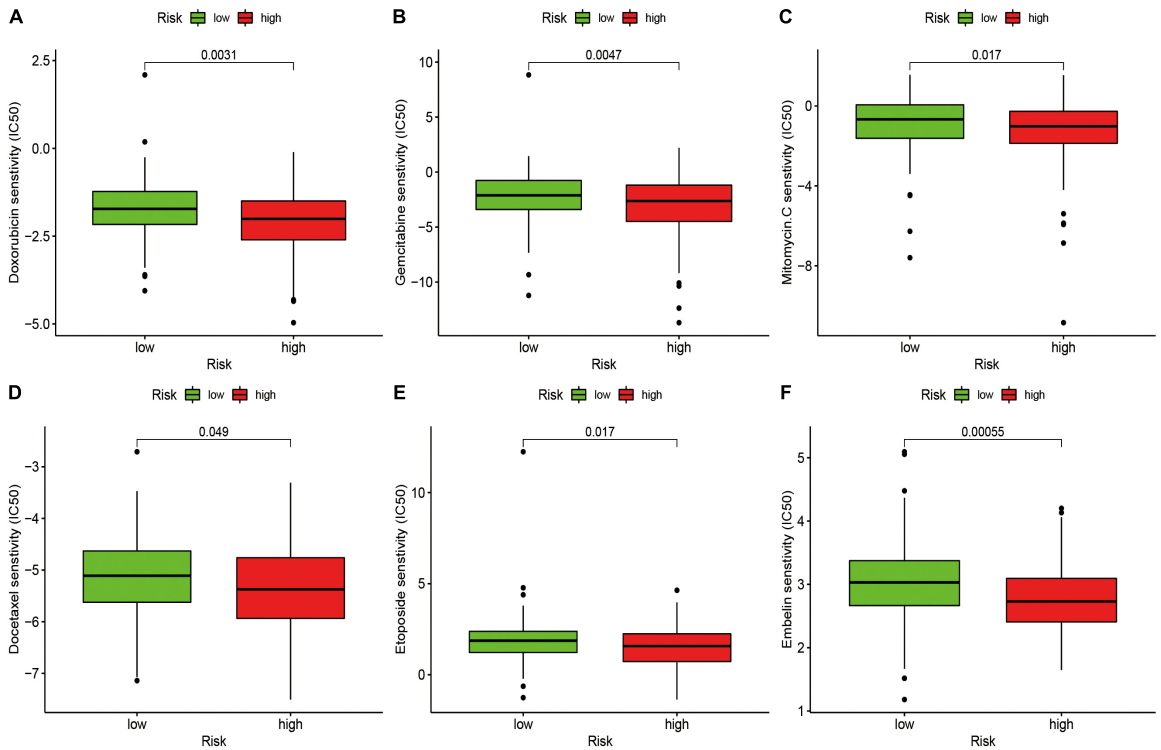

FIGURE 6 | Estimation of the Associations between Chemosensitivity and the Risk Signature. The ICl50 of **(A)** doxorubicin, **(B)** gemcitabine, **(C)** mitomycin C, **(D)** docetaxel, **(E)** etoposide, and **(F)** embelin in the high-risk and low-risk groups. The risk signature acted as a potential predictor for chemosensitivity as high-risk scores were associated with a lower IC50 for chemotherapeutics including doxorubicin, gemcitabine, mitomycin C, docetaxel, etoposide, and embelin.

2020). Via sponging miR-10b-5p to upregulate *IQGAP2*, lncRNA PDCD4-AS1, a downregulated in both triple-negative breast cancer tissues and cell lines and can suppress tumor progression (Jadaliha et al., 2018; Wang et al., 2021c). In addition, via inhibiting the mTOR signaling pathway by directly binding to the EIF3G protein, exogenous overexpression of LINC02446 could inhibit cellular proliferation, migration and invasion in bladder cancer (Zhang et al., 2021). It has been found that LncRNA HOXC13-AS can serve as an oncogene in multiple human malignancies (Li X. et al., 2019; Li W. et al., 2020; Liu et al., 2019). For example, HOXC13-AS has been reported to promote the proliferation of breast cancer cells and tumor growth via epigenetically inhibiting PTEN expression by sponging miR-497-5p in both vivo and vitro (Li X. et al., 2019). However, further investigation is required because only a few studies have investigated the role of these irlncRNAs in STS.

Previous studies have focussed on the potential role of irlncRNAs in cancer progression and constructed risk models based on irlncRNAs with promising predictive significance in various cancers (Wang et al., 2021b). To the best of our knowledge, these risk models were mostly based on the exact expression levels of irlncRNAs. In this study, we established a novel irlncRNA-based algorithm for patients with STS that did not require the exact expression of irlncRNAs. This novel algorithm only required the determination of irlncRNA pairs with either higher or lower expression levels instead of the exact expression levels of irlncRNAs, which minimized sample errors caused by varying expression levels and made our risk model more reliable and convenient. We first confirmed DEirlncRNAs using a differential co-expression analysis and paired DEirlncRNAs using an improved loop-iteration method with a 0-or-1 screening matrix. Furthermore, we selected the most remarkable DEirlncRNA pairs for constructing the novel algorithm using a modified Lasso penalized modeling method to improve the prognostic potential and facilitate the clinical application of the risk signature (Sveen et al., 2012). This modified Lasso penalized modeling method mainly included cross-validation, multiple repeats and random stimulation. It was conducted by incorporating the factors into a Cox regression model based on the rank of occurrence frequency instead of the intersection of occurrence because frequency can reveal the effectiveness of the factor. Moreover, we used an improved method to construct the risk model as follows: Every AUC value of each risk model was calculated to identify the maximum value and confirm the most ideal DEirlncRNA pair for establishing the risk signature. In addition, instead of the median value, the AIC value was identified as the cut-off point for distinguishing the subgroups because it is superior to conventional prognostic models in dividing patients into the high- and low-risk groups. The time-dependent AUC values of 5-year overall survival were higher than 0.80 and the AUC value of the risk signature was significantly higher than that of other clinical characteristics,

indicating the reliable predictive ability and superiority of our irlncRNA-based risk model. Both univariate and multivariate regression analyses were further conducted, which revealed that the risk signature functioned as an independent prognostic marker for patients with STS. In addition, the high-risk group exhibited worse overall survival, and the risk signature was associated with metastasis and histological types of STS. These findings confirmed the prognostic and clinicopathological value of the irlncRNA-based risk signature in STS.

As expected, we found that the irlncRNA-based risk signature was significantly associated with the tumor immune microenvironment of STS. The immune, stromal and microenvironment scores calculated using XCELL were significantly higher in the low-risk group. Previous studies have found that stromal and microenvironment scores calculated using XCELL were positively associated with a reliable prognosis of patients with cancer (Deng et al., 2019; Zou et al., 2020). To examine the association between risk scores and infiltrating immune cell types, seven common acceptable methods were employed for estimating the abundance of infiltrating immune cells, including XCELL, TIMER, QUANTISEQ, MCPcounter, EPIC, CIBERSORT-ABS, and CIBERSORT. Owing to the complexity and defects of these methods, we further performed an integrating analysis for each infiltrating immune cell type. The results demonstrated that the low-risk group exhibited a higher infiltration level of immune cells including CD4 + T cells, CD8 + T cells, activated mast cells, macrophage M1, monocytes and activated NK cells and a lower infiltration level of activated memory CD4 + T cells, resting NK cells and macrophage M0. Infiltrating immune cells in the tumor immune microenvironment are critically involved in cancer initiation and development and exhibit a significant correlation with the clinical outcome of patients. Previous studies have revealed that a higher abundance of macrophage M0 was significantly correlated with worse prognosis and clinical outcomes, whereas an abundance of macrophage M1 led to a reliable prognosis in several cancers. Our results were consistent with those of previous studies (Huang et al., 2019; Yuan et al., 2015). Furthermore, it has been reported that the infiltration of CD4 + and CD8 + T cells can be regarded as a reliable prognostic factor in sarcomas (Ostroumov et al., 2018). Moreover, an abundance of CD4 + and CD8 + T cells plays an important role in tumor response to immunotherapies. Alspach et al. have reported that the anti-tumor efficacy of immune checkpoint blockade therapy requires the activation of CD4 + and CD8 + T cells in sarcomas (Alspach et al., 2019). In conclusion, our risk signature was significantly associated with immune cell infiltration and confirmed its correlation with the prognosis of patients with STS.

Targeting immune checkpoints provide novel insights into cancer therapy, and several immune checkpoint inhibitors, such as PD-1/PD-L1 and CTLA-4 inhibitors, have been used for the treatment of multiple cancers, including melanoma, kidney cancer and non-small cell lung cancer (Li B. et al., 2019; Postow et al., 2018). Recently, the efficacy of immune checkpoint inhibitors in STS was investigated in multiple clinical trials; however, these trials reported controversial results. The low response rate to immune checkpoint inhibitors in some patients with STS may be a major hurdle in improving immunotherapeutic efficacy (Zhu et al., 2020). Therefore, effective biomarkers that can predict response to immune checkpoint inhibitors in patients with STS should be developed, which may improve prognosis by enhancing the efficacy of the inhibitors. In this study, we investigated the potential role of irlncRNAs as predictors for immune checkpoint expression. The results revealed that the risk score was negatively correlated with the expression of IDO1, CD96, CD200, CD27, TIGIT, and CD47. Indoleamine 2,3-dioxygenase 1 (IDO1), an important immune checkpoint, is a rate-limiting metabolic enzyme that contributes to the conversion of the essential amino acid tryptophan (Trp) into kynurenines (Munn and Mellor, 2016). Emerging evidence indicates that IDO1 is highly expressed in various human malignancies and is important for regulating cancer progression and tumor immune microenvironment (Bishnupuri et al., 2019; Xiang et al., 2019). In addition, IDO1 exhibits great prognostic and clinicopathological significance for patients with cancer. However, the prognostic value is inconsistent among different cancers (Zhai et al., 2018). A study reported that high IDO1 expression was correlated with prolonged survival time in patients with UPS, which was consistent with our results (Ishihara et al., 2021). B7-H3 (CD276), a member of the B7-CD28 family, is also a crucial immune checkpoint member that can suppress the functions of T cells (Flem-Karlsen et al., 2020). It has been found that B7-H3 is upregulated in multiple human cancers, and B7-H3 overexpression is closely related to poor prognosis and clinical outcomes (Flem-Karlsen et al., 2020). Because of the low expression of B7-H3 in normal tissues, it has become a promising target for cancer immunotherapy, and several therapeutic strategies that target B7-H3, such as small-molecule inhibitors and chimeric antigen receptor T (CAR-T) cell technology, have been used for the treatment of cancer in clinical trials (Picarda et al., 2016). Recent studies have investigated CAR-T cell immunotherapy that targets B7-H3 in bone sarcoma models in vivo, with a significantly prolonged survival time. Therefore, B7-H3 CAR-T cell therapy may also be an effective immunotherapeutic strategy for patients with STS. Our study provided a promising biomarker for predicting the expression of immune checkpoints and immunotherapeutic efficacy in patients with STS. However, the exact expression pattern and potential role of these immune checkpoints in STS remain undefined. Comprehensive and in-depth studies are necessary for investigating the expression and role of these immune checkpoints and the capability of the irlncRNA-based risk signature to predict immunotherapeutic efficacy in patents with STS.

Although there has been advancement in chemotherapy for patients with STS in the past decades, many patients eventually develop intrinsic or acquired resistance to chemotherapeutic agents, thereby contributing to limited chemotherapeutic efficacy and a poor prognosis. Therefore, we further assessed the predictive value of the irlncRNA-based risk signature to assess chemosensitivity in patients with STS. The results revealed that the irlncRNA-based risk signature effectively predicted the response of patients to doxorubicin, gemcitabine, docetaxel, mitomycin C and embelin. Doxorubicin, an anthracycline

antibiotic that can inhibit the synthesis of both DNA and RNA by embedding into DNA base pairs, has become the most effective and commonly used chemotherapeutic agent for patients with STS (Ratan and Patel, 2016). Owing to STS progression or the development of resistance to first-line chemotherapy, a combination of gemcitabine and docetaxel is used as a standard second-line treatment for patients with STS (Ratan and Patel, 2016). Therefore, our risk signature may function as a promising predictor of chemotherapeutic efficacy, thereby expanding new avenues for selecting the most suitable chemotherapy for each patient with STS.

However, this quality study also has several limitations. The findings are based on clinical samples downloaded from the GDC TCGA-SARC dataset instead of our cohort. The results of the present study should be further validated in patients of our cohort. Furthermore, the correlation between irlncRNAs and STS immune characteristics were not investigated in experiments, and the detailed mechanism by which irlncRNAs modulate STS immune microenvironment remains unknown. Lastly, the novel risk signature should be further validated in larger clinical samples before incorporating it into diagnostic and therapeutic practice.

CONCLUSION

We comprehensively investigated the potential functions and clinical value of irlncRNAs in STS. We established a novel risk signature based on DEirlncRNA pairs for patients with STS. The novel risk signature was significantly correlated with immune characteristics and effectively predicted chemotherapeutic efficacy in patients with STS, thereby serving as a reliable prognostic factor. We identified the prognostic and clinicopathological value of irlncRNAs as well as the correlation between irlncRNAs and immune microenvironment in STS, thus highlighting the promising role of irlncRNAs as clinical biomarkers and novel therapeutic targets for patients with STS.

DATA AVAILABILITY STATEMENT

The datasets presented in this study can be found in online repositories. The names of the repository/repositories and accession number(s) can be found in the article/ **Supplementary Material**.

AUTHOR CONTRIBUTIONS

ZL: writing – original draft, data curation, and formal analysis. KP and XZ: writing – original draft. HL and TZ: writing – review and editing, and visualization. JW: formal analysis. TL and WP: writing – review and editing, supervision, and funding acquisition. All authors contributed to the writing and revision of the manuscript, knew the content of it, and approved its submission.

FUNDING

This study was supported by grants from National Natural Science Foundation of China (Grant Nos. 81871783 and 82072441).

ACKNOWLEDGMENTS

We acknowledge TCGA and GTEx database for providing their platforms and contributors for uploading their meaningful datasets.

SUPPLEMENTARY MATERIAL

The Supplementary Material for this article can be found online at: https://www.frontiersin.org/articles/10.3389/fcell.2021.709241/full#supplementary-material

REFERENCES

Abril-Rodriguez, G., and Ribas, A. (2017). SnapShot: Immune checkpoint inhibitors. *Cancer Cell.* 31, 841–848. doi: 10.1016/j.ccell.2017.05.010

Alspach, E., Lussier, D. M., Miceli, A. P., Kizhvatov, I., DuPage, M., Luoma, A. M., et al. (2019). MHC-II neoantigens shape tumour immunity and response to immunotherapy. *Nature* 574, 696–701. doi: 10.1038/s41586-019-1671-8

Aran, D. (2020). Cell-type enrichment analysis of bulk transcriptomes using xCell. *Methods Mol. Biol.* 2120, 263–276. doi: 10.1007/978-1-0716-0327-7_19

Aran, D., Hu, Z., and Butte, A. J. (2017). xCell: digitally portraying the tissue cellular heterogeneity landscape. *Genome Biol.* 18:220. doi: 10.1186/s13059-017-1349-1

Ayodele, O., and Razak, A. R. A. (2020). Immunotherapy in soft-tissue sarcoma. *Curr. Oncol.* 27, 17–23. doi: 10.3747/co.27.5407

Bhan, A., Soleimani, M., and Mandal, S. S. (2017). Long noncoding RNA and cancer: A new paradigm. *Cancer Res.* 77, 3965–3981. doi: 10.1158/0008-5472.CAN-16-2634

Bishnupuri, K. S., Alvarado, D. M., Khouri, A. N., Shabsovich, M., Chen, B., Dieckgraefe, B. K., et al. (2019). IDO1 and Kynurenine pathway metabolites activate PI3K-Akt signaling in the neoplastic colon epithelium to promote cancer cell proliferation and inhibit apoptosis. *Cancer Res.* 79, 1138–1150. doi: 10.1158/0008-5472.CAN-18-0668

Bourcier, K., Le Cesne, A., Tselikas, L., Adam, J., Mir, O., Honore, C., et al. (2019). Basic knowledge in soft tissue sarcoma. *Cardiovasc. Intervent. Radiol.* 42, 1255–1261. doi: 10.1007/s00270-019-02259-w

Cai, W. Y., Chen, X., Chen, L. P., Li, Q., Du, X. J., and Zhou, Y. Y. (2018). Role of differentially expressed genes and long non-coding RNAs in papillary thyroid carcinoma diagnosis, progression, and prognosis. *J. Cell. Biochem.* 119, 8249–8259. doi: 10.1002/jcb.26836

Chen, B., Khodadoust, M. S., Liu, C. L., Newman, A. M., and Alizadeh, A. A. (2018). Profiling Tumor Infiltrating Immune Cells with CIBERSORT. *Methods Mol. Biol.* 1711, 243–259. doi: 10.1007/978-1-4939-7493-1_12

Deng, L., Lu, D., Bai, Y., Wang, Y., Bu, H., and Zheng, H. (2019). Immune profiles of tumor microenvironment and clinical prognosis among women with triple-negative breast cancer. *Cancer Epidemiol. Biomarkers Prev.* 28, 1977–1985. doi: 10.1158/1055-9965.EPI-19-0469

Dienstmann, R., Villacampa, G., Sveen, A., Mason, M. J., Niedzwiecki, D., Nesbakken, A., et al. (2019). Relative contribution of clinicopathological variables, genomic markers, transcriptomic subtyping and microenvironment features for outcome prediction in stage II/III colorectal cancer. *Ann. Oncol.* 30, 1622–1629. doi: 10.1093/annonc/mdz287

Finotello, F., Mayer, C., Plattner, C., Laschober, G., Rieder, D., Hackl, H., et al. (2019). Molecular and pharmacological modulators of the tumor immune contexture revealed by deconvolution of RNA-seq data. *Genome Med.* 11:34. doi: 10.1186/s13073-019-0655-5

Flem-Karlsen, K., Fodstad, O., and Nunes-Xavier, C. E. (2020). B7-H3 immune checkpoint protein in human cancer. *Curr. Med. Chem.* 27, 4062–4086. doi: 10.2174/0929867326666190517115515

Goldman, M., Craft, B., Swatloski, T., Cline, M., Morozova, O., Diekhans, M., et al. (2015). The UCSC cancer genomics browser: update 2015. *Nucleic Acids Res.* 43, D812–D817. doi: 10.1093/nar/gku1073

Huang, D., Chen, J., Yang, L., Ouyang, Q., Li, J., Lao, L., et al. (2018). NKILA lncRNA promotes tumor immune evasion by sensitizing T cells to activation-induced cell death. *Nat. Immunol.* 19, 1112–1125. doi: 10.1038/s41590-018-0207-y

Huang, R., Meng, T., Chen, R., Yan, P., Zhang, J., Hu, P., et al. (2019). The construction and analysis of tumor-infiltrating immune cell and ceRNA networks in recurrent soft tissue sarcoma. *Aging (Albany NY)* 11, 10116–10143. doi: 10.18632/aging.102424

Ishihara, S., Yamada, Y., Iwasaki, T., Yoshimoto, M., Toda, Y., Kohashi, K., et al. (2021). PDL1 and IDO1 expression in undifferentiated pleomorphic sarcoma: The associations with tumor infiltrating lymphocytes, dMMR and HLA class I. *Oncol. Rep.* 45, 379–389. doi: 10.3892/or.2020.7837

Italiano, A., Mathoulin-Pelissier, S., Cesne, A. L., Terrier, P., Bonvalot, S., Collin, F., et al. (2011). Trends in survival for patients with metastatic soft-tissue sarcoma. *Cancer* 117, 1049–1054. doi: 10.1002/cncr.25538

Jadaliha, M., Gholamalamdari, O., Tang, W., Zhang, Y., Petracovici, A., Hao, Q., et al. (2018). A natural antisense lncRNA controls breast cancer progression by promoting tumor suppressor gene mRNA stability. *PLoS Genet.* 14:e1007802. doi: 10.1371/journal.pgen.1007802

Jo, V. Y., and Fletcher, C. D. (2014). WHO classification of soft tissue tumours: an update based on the 2013 (4th) edition. *Pathology* 46, 95–104. doi: 10.1097/PAT.0000000000000050

Kim, H. S., Nam, C. M., Jang, S. Y., Choi, S. K., Han, M., Kim, S., et al. (2019). Characteristics and treatment patterns of patients with advanced soft tissue sarcoma in Korea. *Cancer Res. Treat* 51, 1380–1391. doi: 10.4143/crt.2018.476

Li, B., Chan, H. L., and Chen, P. (2019). Immune checkpoint inhibitors: basics and challenges. *Curr. Med. Chem.* 26, 3009–3025. doi: 10.2174/0929867324666170804143706

Li, T., Fan, J., Wang, B., Traugh, N., Chen, Q., Liu, J. S., et al. (2017). TIMER: A web server for comprehensive analysis of tumor-infiltrating immune cells. *Cancer Res.* 77, e108–e110. doi: 10.1158/0008-5472.CAN-17-0307

Li, T., Fu, J., Zeng, Z., Cohen, D., Li, J., Chen, Q., et al. (2020). TIMER2.0 for analysis of tumor-infiltrating immune cells. *Nucleic Acids Res.* 48, W509–W514. doi: 10.1093/nar/gkaa407

Li, W., Zhu, Q., Zhang, S., Liu, L., Zhang, H., and Zhu, D. (2020). HOXC13-AS accelerates cell proliferation and migration in oral squamous cell carcinoma via miR-378g/HOXC13 axis. *Oral Oncol.* 111:104946. doi: 10.1016/j.oraloncology.2020.104946

Li, X., Wang, Q., Rui, Y., Zhang, C., Wang, W., Gu, J., et al. (2019). HOXC13-AS promotes breast cancer cell growth through regulating miR-497-5p/PTEN axis. *J. Cell. Physiol.* 234, 22343–22351. doi: 10.1002/jcp.28800

Li, Z., Lin, W., Zheng, J., Hong, W., Zou, J., Zhang, T., et al. (2021). Identification of immune-related lncRNAs to improve the prognosis prediction for patients with papillary thyroid cancer. *Biosci. Rep.* 41:BSR20204086. doi: 10.1042/BSR20204086

Liang, Y., Song, X., Li, Y., Chen, B., Zhao, W., Wang, L., et al. (2020). LncRNA BCRT1 promotes breast cancer progression by targeting miR-1303/PTBP3 axis. *Mol. Cancer* 19:85. doi: 10.1186/s12943-020-01206-5

Liu, N., Wang, Z., Liu, D., and Xie, P. (2019). HOXC13-AS-miR-122-5p-SATB1-C-Myc feedback loop promotes migration, invasion and EMT process in glioma. *Onco. Targets Ther.* 12, 7165–7173. doi: 10.2147/OTT.S220027

Luo, Y., Zheng, S., Wu, Q., Wu, J., Zhou, R., Wang, C., et al. (2021). Long noncoding RNA (lncRNA) EIF3J-DT induces chemoresistance of gastric cancer via autophagy activation. *Autophagy* 2021, 1–19. doi: 10.1080/15548627.2021.1901204

Munn, D. H., and Mellor, A. L. (2016). In the tumor microenvironment: inflammation, counter-regulation, and tolerance. *Trends Immunol.* 37, 193–207. doi: 10.1016/j.it.2016.01.002

Nguyen, K. B., and Spranger, S. (2020). Modulation of the immune microenvironment by tumor-intrinsic oncogenic signaling. *J. Cell. Biol.* 219:e201908224. doi: 10.1083/jcb.201908224

Ostroumov, D., Fekete-Drimusz, N., Saborowski, M., Kuhnel, F., and Woller, N. (2018). CD4 and CD8 T lymphocyte interplay in controlling tumor growth. *Cell. Mol. Life Sci.* 75, 689–713. doi: 10.1007/s00018-017-2686-7

Picarda, E., Ohaegbulam, K. C., and Zang, X. (2016). Molecular pathways: targeting B7-H3 (CD276) for human cancer immunotherapy. *Clin. Cancer Res.* 22, 3425–3431. doi: 10.1158/1078-0432.CCR-15-2428

Plattner, C., Finotello, F., and Rieder, D. (2020). Deconvoluting tumor-infiltrating immune cells from RNA-seq data using quanTIseq. *Methods Enzymol.* 636, 261–285. doi: 10.1016/bs.mie.2019.05.056

Poon, E., and Quek, R. (2018). Soft tissue sarcoma in Asia. *Chin. Clin. Oncol.* 7:46. doi: 10.21037/cco.2018.08.06

Postow, M. A., Sidlow, R., and Hellmann, M. D. (2018). Immune-related adverse events associated with immune checkpoint blockade. *N. Engl. J. Med.* 378, 158–168. doi: 10.1056/NEJMra1703481

Racle, J., de Jonge, K., Baumgaertner, P., Speiser, D. E., and Gfeller, D. (2017). Simultaneous enumeration of cancer and immune cell types from bulk tumor gene expression data. *Elife* 6:e26476. doi: 10.7554/eLife.26476.049

Ransohoff, J. D., Wei, Y., and Khavari, P. A. (2018). The functions and unique features of long intergenic non-coding RNA. *Nat. Rev. Mol. Cell Biol.* 19, 143–157. doi: 10.1038/nrm.2017.104

Ratan, R., and Patel, S. R. (2016). Chemotherapy for soft tissue sarcoma. *Cancer* 122, 2952–2960. doi: 10.1002/cncr.30191

Rusek, A. M., Abba, M., Eljaszewicz, A., Moniuszko, M., Niklinski, J., and Allgayer, H. (2015). MicroRNA modulators of epigenetic regulation, the tumor microenvironment and the immune system in lung cancer. *Mol. Cancer* 14:34. doi: 10.1186/s12943-015-0302-8

Schmitz, S. U., Grote, P., and Herrmann, B. G. (2016). Mechanisms of long noncoding RNA function in development and disease. *Cell. Mol. Life Sci.* 73, 2491–2509. doi: 10.1007/s00018-016-2174-5

Schreiber, R. D., Old, L. J., and Smyth, M. J. (2011). Cancer immunoediting: integrating immunity's roles in cancer suppression and promotion. *Science* 331, 1565–1570. doi: 10.1126/science.1203486

Sveen, A., Agesen, T. H., Nesbakken, A., Meling, G. I., Rognum, T. O., Liestol, K., et al. (2012). ColoGuidePro: a prognostic 7-gene expression signature for stage III colorectal cancer patients. *Clin. Cancer Res.* 18, 6001–6010. doi: 10.1158/1078-0432.CCR-11-3302

Tamminga, M., Hiltermann, T. J. N., Schuuring, E., Timens, W., Fehrmann, R. S., and Groen, H. J. (2020). Immune microenvironment composition in non-small cell lung cancer and its association with survival. *Clin. Transl. Immunol.* 9:e1142. doi: 10.1002/cti2.1142

Tan, J., Liu, L., Zuo, Z., Song, B., Cai, T., Ding, D., et al. (2020). Overexpression of novel long intergenic noncoding RNA LINC02454 is associated with a poor prognosis in papillary thyroid cancer. *Oncol. Rep.* 44, 1489–1501. doi: 10.3892/or.2020.7712

Wang, D., Wang, Z., Zhang, L., and Sun, S. (2021a). LncRNA PDCD4-AS1 alleviates triple negative breast cancer by increasing expression of IQGAP2 via miR-10b-5p. *Transl. Oncol.* 14:100958. doi: 10.1016/j.tranon.2020.100958

Wang, J., Shen, C., Dong, D., Zhong, X., Wang, Y., and Yang, X. (2021b). Identification and verification of an immune-related lncRNA signature for predicting the prognosis of patients with bladder cancer. *Int. Immunopharmacol.* 90:107146. doi: 10.1016/j.intimp.2020.107146

Wang, J., Yin, X., Zhang, Y. Q., and Ji, X. (2021c). Identification and validation of a novel immune-related four-lncRNA signature for lung adenocarcinoma. *Front. Genet.* 12:639254. doi: 10.3389/fgene.2021.639254

Xiang, Z., Li, J., Song, S., Wang, J., Cai, W., Hu, W., et al. (2019). A positive feedback between IDO1 metabolite and COL12A1 via MAPK pathway to promote gastric cancer metastasis. *J. Exp. Clin. Cancer Res.* 38:314. doi: 10.1186/s13046-019-1318-5

Xu, M., Xu, X., Pan, B., Chen, X., Lin, K., Zeng, K., et al. (2019). LncRNA SATB2-AS1 inhibits tumor metastasis and affects the tumor immune cell microenvironment in colorectal cancer by regulating SATB2. *Mol. Cancer* 18:135. doi: 10.1186/s12943-019-1063-6

Xu, Q., Wang, Y., and Huang, W. (2021). Identification of immune-related lncRNA signature for predicting immune checkpoint blockade and prognosis

in hepatocellular carcinoma. *Int. Immunopharmacol.* 92:107333. doi: 10.1016/j.intimp.2020.107333

Yang, C., Shen, C., Feng, T., and Li, H. (2019). Noncoding RNA in NK cells. *J. Leukoc Biol.* 105, 63–71. doi: 10.1002/JLB.1RU0518-197RR

Yuan, A., Hsiao, Y. J., Chen, H. Y., Chen, H. W., Ho, C. C., Chen, Y. Y., et al. (2015). Opposite effects of M1 and M2 macrophage subtypes on lung cancer progression. *Sci. Rep.* 5:14273. doi: 10.1038/srep14273

Zhai, L., Ladomersky, E., Lenzen, A., Nguyen, B., Patel, R., Lauing, K. L., et al. (2018). IDO1 in cancer: a Gemini of immune checkpoints. *Cell. Mol. Immunol.* 15, 447–457. doi: 10.1038/cmi.2017.143

Zhang, H., Li, R., Cao, Y., Gu, Y., Lin, C., Liu, X., et al. (2020). Poor clinical outcomes and immunoevasive contexture in intratumoral IL-10-producing macrophages enriched gastric cancer patients. *Ann. Surg.* 2020:4037. doi: 10.1097/SLA.0000000000004037

Zhang, W. H., Wang, W. Q., Gao, H. L., Yu, X. J., and Liu, L. (2019). The tumor immune microenvironment in gastroenteropancreatic neuroendocrine neoplasms. *Biochim. Biophys. Acta Rev. Cancer* 1872:188311. doi: 10.1016/j.bbcan.2019.188311

Zhang, X., Zhang, J., Zhao, W., Dong, X., Xin, P., Liu, X., et al. (2021). Long non-coding RNA LINC02446 suppresses the proliferation and metastasis of bladder cancer cells by binding with EIF3G and regulating the mTOR signalling pathway. *Cancer Gene Ther.* doi: 10.1038/s41417-020-00285-2 [Epub ahead of print].

Zhao, L., Liu, Y., Zhang, J., Liu, Y., and Qi, Q. (2019). LncRNA SNHG14/miR-5590-3p/ZEB1 positive feedback loop promoted diffuse large B cell lymphoma progression and immune evasion through regulating PD-1/PD-L1 checkpoint. *Cell. Death Dis.* 10:731. doi: 10.1038/s41419-019-1886-5

Zhu, M. M. T., Shenasa, E., and Nielsen, T. O. (2020). Sarcomas: Immune biomarker expression and checkpoint inhibitor trials. *Cancer Treat Rev.* 91:102115. doi: 10.1016/j.ctrv.2020.102115

Zou, Z., Ha, Y., Liu, S., and Huang, B. (2020). Identification of tumor-infiltrating immune cells and microenvironment-relevant genes in nasopharyngeal carcinoma based on gene expression profiling. *Life Sci.* 263:118620. doi: 10.1016/j.lfs.2020.118620

Conflict of Interest: The authors declare that the research was conducted in the absence of any commercial or financial relationships that could be construed as a potential conflict of interest.

Publisher's Note: All claims expressed in this article are solely those of the authors and do not necessarily represent those of their affiliated organizations, or those of the publisher, the editors and the reviewers. Any product that may be evaluated in this article, or claim that may be made by its manufacturer, is not guaranteed or endorsed by the publisher.

Copyright © 2021 Lin, Pang, Li, Zhang, Wan, Zheng, Liu and Peng. This is an open-access article distributed under the terms of the Creative Commons Attribution License (CC BY). The use, distribution or reproduction in other forums is permitted, provided the original author(s) and the copyright owner(s) are credited and that the original publication in this journal is cited, in accordance with accepted academic practice. No use, distribution or reproduction is permitted which does not comply with these terms.

frontiers in Cell and Developmental Biology

ORIGINAL RESEARCH
published: 28 September 2021
doi: 10.3389/fcell.2021.717601

Tumor Immune Microenvironment Landscape in Glioma Identifies a Prognostic and Immunotherapeutic Signature

*Chunyu Zhang[1†], Lirui Guo[1†], Zhongzhou Su[2†], Na Luo[3,4], Yinqiu Tan[5], Pengfei Xu[6], Liguo Ye[1], Shiao Tong[1], Haitao Liu[7], Xiaobin Li[2], Qianxue Chen[1] and Daofeng Tian[1]**

[1] Department of Neurosurgery, Wuhan University, Renmin Hospital, Wuhan, China, [2] Department of Neurosurgery, Huzhou Central Hospital, Affiliated Central Hospital Huzhou University, Huzhou, China, [3] Peking University China-Japan Friendship School of Clinical Medicine, Beijing, China, [4] Department of Neurosurgery, China-Japan Friendship Hospital, Beijing, China, [5] Department of Neurosurgery, Union Hospital, Tongji Medical College, Huazhong University of Science and Technology, Wuhan, China, [6] Sun Yat-sen University, The Seventh Affiliated Hospital, Shenzhen, China, [7] Department of Cardiothoracic Surgery, Jiaxing University, The First Affiliated Hospital, Jiaxing, China

OPEN ACCESS

Edited by:
Xuejun Sun,
Xi'an Jiaotong University, China

Reviewed by:
Wanzun Lin,
Fudan University, China
Shengchao Xu,
Central South University, China
Taibo Li,
Johns Hopkins University, United States
Wei Chong,
Tianjin Medical University Cancer Institute and Hospital, China

***Correspondence:**
Daofeng Tian
tiandaofeng@163.com

[†] These authors have contributed equally to this work

Specialty section:
This article was submitted to Molecular and Cellular Pathology, a section of the journal Frontiers in Cell and Developmental Biology

Received: 31 May 2021
Accepted: 03 August 2021
Published: 28 September 2021

Citation:
Zhang C, Guo L, Su Z, Luo N, Tan Y, Xu P, Ye L, Tong S, Liu H, Li X, Chen Q and Tian D (2021) Tumor Immune Microenvironment Landscape in Glioma Identifies a Prognostic and Immunotherapeutic Signature. Front. Cell Dev. Biol. 9:717601. doi: 10.3389/fcell.2021.717601

The tumor immune microenvironment (TIME) has been recognized to be associated with sensitivity to immunotherapy and patient prognosis. Recent research demonstrates that assessing the TIME patterns on large-scale samples will expand insights into TIME and will provide guidance to formulate immunotherapy strategies for tumors. However, until now, thorough research has not yet been reported on the immune infiltration landscape of glioma. Herein, the CIBERSORT algorithm was used to unveil the TIME landscape of 1,975 glioma observations. Three TIME subtypes were established, and the TIMEscore was calculated by least absolute shrinkage and selection operator (LASSO)–Cox analysis. The high TIMEscore was distinguished by an elevated tumor mutation burden (TMB) and activation of immune-related biological process, such as IL6-JAK-STAT3 signaling and interferon gamma (IFN-γ) response, which may demonstrate that the patients with high TIMEscore were more sensitive to immunotherapy. Multivariate analysis revealed that the TIMEscore could strongly and independently predict the prognosis of gliomas [Chinese Glioma Genome Atlas (CGGA) cohort: hazard ratio (HR): 2.134, $p < 0.001$; Gravendeel cohort: HR: 1.872, $p < 0.001$; Kamoun cohort: HR: 1.705, $p < 0.001$; The Cancer Genome Atlas (TCGA) cohort: HR: 2.033, $p < 0.001$; the combined cohort: HR: 1.626, $p < 0.001$], and survival advantage was evident among those who received chemotherapy. Finally, we validated the performance of the signature in human tissues from Wuhan University (WHU) dataset (HR: 15.090, $p = 0.008$). Our research suggested that the TIMEscore could be applied as an effective predictor for adjuvant therapy and prognosis assessment.

Keywords: glioma, TIME landscape, prognosis, CIBERSORT, immune

INTRODUCTION

Glioma is one of the most common malignancies in the world, with high morbidity and mortality owing to their localization and often locally invasive growth (Siegel et al., 2019). It remains the tumor with the highest incidence in the central nervous system (CNS), accounting for about 25% of primary intracranial neoplastic lesions (Weller et al., 2015; Louis et al., 2016). Meanwhile, about

50% of all gliomas with new diagnosis are classified as glioblastoma (GBM), which is the most malignant type of brain cancer (Ostrom et al., 2014). GBMs have extremely depressing prognosis, with less than 5% of observations surviving beyond 5 years when diagnosed. With the development of research, there are remarkable achievements in exploring the molecular pathogenesis of gliomas, such as the isocitrate dehydrogenase (IDH) status and O^6-methylguanine-DNA methyltransferase promoter (MGMTp) methylation. These findings accelerate the improvement of diagnostics, classification systems, and precision therapy. However, glioma remains incurable with current clinical interventions, which traditionally include surgical resection followed by radiotherapy in combination with concurrent and maintenance temozolomide. Further investigations are essential into identification of new molecular targets, tools for prognostic assessment, and development of therapeutic regimens that provide the potentiality for improved events in the near future.

Nowadays, cancer immunotherapy by immune checkpoint blockade (ICB) has achieved great accomplishments in cancer of the bladder, head and neck squamous cell carcinoma (HNSCC), etc. (Powles et al., 2014; Garon et al., 2015; Economopoulou et al., 2016). However, recent studies have shown that the significant limitations of ICB are a large portion of the population has low or even no response to inhibitors (Rugo et al., 2018), or develop therapeutic resistance (Restifo et al., 2016), or experience severe side effects that put sand in the wheels of clinical treatments (Pitt et al., 2016). There are several important works aiming at understanding immunotherapeutic efficacy in glioma. Clinical trials of anti-PD-1 (nivolumab) immunotherapy in unselected recurrent GBM patients reveal no significant prognosis improvement, and the latest research on nivolumab in newly diagnosed GBMs has failed to show a remarkable clinical response (Chamberlain and Kim, 2017; Shen et al., 2020). These clinical results are the basis of several possibilities that GBM may have undergone such important immune reprogramming during tumor development that it has a high degree of immunosuppression and immune evasion and cannot respond to checkpoint lockouts and other immunotherapies (Sampson et al., 2020).

A growing body of research suggests that the tumor immune microenvironment (TIME) acts a critical role in tumorigenesis and treatment response (Ino et al., 2013; Shigeoka et al., 2013; Makkouk and Weiner, 2015). For example, TIME may develop several chemical and physical characteristics, beneficial to tumor progression, such as hypoxia, and increased extracellular matrix (ECM) stiffness (Barbera-Guillem et al., 2002; Bingle et al., 2002; Yu et al., 2009; Noman et al., 2014; Corbet et al., 2020). Moreover, TIME dysregulates immune effector cells resulting in suppression of immune response by recruiting cells represented by tumor-associated microglia/macrophages (TAMs), regulatory T cells (Tregs), and myeloid-derived suppressor cells (MDSCs; Badie and Schartner, 2000; Chen and Mellman, 2017; Sullivan et al., 2020). In recent years, investigations into glioma cells have indicated that CNS-resident cells or tumor infiltrative cells are inhibitory to anti-tumor immunity, such as microglia and monocytes (Grauwet and Chiocca, 2016; Varvel et al., 2016). And monocytic cells in GBM account for about 50% of the total cell counts, in comparison with <1% of cells in tumor-free brain (Badie and Schartner, 2000). Especially, anti-inflammatory M2 macrophages, polarizing from macrophages, express cytokines including interleukin 10 (IL-10), transforming growth factor (TGF)-β, and angiogenesis-associated cytokines, such as vascular endothelial growth factor (VEGF), contributing to disease progression and immune suppression (Saraiva and O'Garra, 2010; Syed, 2016; De Palma et al., 2017; Batlle and Massagué, 2019; Sawant et al., 2019).

With the advent of high-throughput technologies and advance of deconvolution algorithms such as CIBERSORT and quanTIseq (Chen et al., 2018; Finotello et al., 2019), the immune contents in the TIME could be evaluated based on RNA sequencing data. And the infiltrative fractions of immune cells calculated on CIBERSORT method have proven to be as solid as results from experimental measures such as immunohistochemistry and flow cytometry (Fu et al., 2018). This methodology has been used in cancers for exploring the association between prognosis and immunotherapy response and resistance and TIME infiltrates (Zeng et al., 2019; Fan et al., 2020; Zhang et al., 2020). However, to date, the comprehensive analysis of landscape of immune cell infiltration in glioma has not yet been completely explicated.

In the present study, CIBERSORT algorithm was employed to calculate the fractions of 22 immune cell categories based on 1,975 glioma RNA-seq profiles. Systematic correlation was calculated among the TIME infiltration patterns and clinicopathologic characteristics of glioma. As a result, we established a TIMEscore, which might act as a strong and accurate biomarker for assessment of clinical outcomes and response to immunotherapy for glioma patients.

MATERIALS AND METHODS

Obtaining and Preprocessing Public Glioma Datasets

We methodically orderly systematically retrieved three databases – The Cancer Genome Atlas (TCGA), Chinese Glioma Genome Atlas (CGGA), and GlioVis – for publicly available glioma gene expression datasets. Samples with no survival information were excluded from following analysis. Totally, we obtained four datasets of 1,975 glioma samples. The microarray datasets (Gravendeel and Kamoun) generated by Affymetrix were downloaded from GlioVis database[1] (Bowman et al., 2017). For fragments per kilobase million (FPKM), normalized gene expression data of CGGA and TCGA cohorts were obtained from CGGA database[2] and TCGA database.[3] RNA sequencing data with FPKM values were converted into transcripts per kilobase million (TPM) values, which were more similar to the transcripts produced by microarrays and were more comparable between samples (Wagner et al., 2012). The detailed clinical characteristics of observations enrolled are displayed in **Supplementary Table 1**. Sequencing data were

[1]http://gliovis.bioinfo.cnio.es/

[2]http://www.cgga.org.cn/

[3]https://portal.gdc.cancer.gov/

processed and analyzed on R project (version 4.0.3). Finally, we used the "ComBat" algorithm to decrease the likelihood of batch effects as a result of non-biological technical biases among the four cohorts (Leek et al., 2012). Finally, six immune infiltrates of TCGA glioma set were obtained from TIMER webtool.[4]

Consensus Clustering for Tumor-Infiltrating Immune Cells

R package CIBERSORT was employed to conduct quantification of the infiltration fractions of 22 immune cells in glioma samples. One thousand permutations was preset here (Chen et al., 2018), and the reference 547 gene sets (LM22 signature) were obtained from the CIBERSORT website. We applied unsupervised clustering analysis, that is, *k*-means method, into identification of TIME patterns and patient classification in the meta-dataset. This procedure was carried out by the R package ConsensuClusterPlus. Repetition of 1,000 times was preset to guarantee the stability of classification.

Differentially Expressed Genes Related to the Tumor Immune Microenvironment Patterns

For detection of genes correlated with the TIME patterns, we grouped patients according to TIME subtypes on the basis of immune cell infiltration. Differentially expressed genes (DEGs) among the three subtypes were detected out of 12,572 genes and identified by R package limma, which performed the empirical Bayesian algorithm to calculate changes in expression levels based on *t*-test (Ritchie et al., 2015). And we applied the Benjamini–Hochberg (B-H) procedure to transform the *p*-value to false discovery rate (FDR). Genes were considered remarkably varied with FDR < 0.05 and absolute log2 fold-change > 1.0.

Functional Annotation Analysis

Gene enrichment analysis based on the package clusterProfiler was carried out on TIME-associated DEGs (Yu et al., 2012). Gene Ontology (GO) and Kyoto Encyclopedia of Genes and Genomes (KEGG) results with a cutoff of FDR < 0.05 were considered statistically significant. Pathways between TIME groups A, B, and C were identified by conducting gene set variation analysis (GSVA) of the adjusted expression data in all glioma samples. HALLMARK gene sets from the Molecular Signatures Database (MSigDB) were downloaded and chosen as the reference set.

Generation of TIMEscore and Survival Analysis

The flow of establishment of TIMEscore was designed as follows. First, the univariate Cox regression analysis was performed to calculate the association between the DEGs and the overall survival (OS) of patients with glioma. Then, a least absolute shrinkage and selection operator (LASSO)–Cox model with 10-fold validation was used to narrow down the prognosis-related variables and calculate coefficients of the left DEGs. Then, the expression of selective genes (*EXPi*) and their corresponding regression coefficients(*COEFi*) were used to construct TIMEscore. And the formula was as follows:

$$\text{TIMEscore} = \sum_{1}^{n} (EXPi) \times (COEFi)$$

Prognostic clinical covariates such as age and IDH status of glioma patients determined based on univariate Cox regression analysis were filtered out. Finally, multivariate Cox regression analysis was employed to verify independently the prognosis-predicting feature of the TIMEscore based on R package survminer, even after being adjusted by the prognosis-associated clinical covariates.

Human Samples

The research was approved by the Ethics Committee of Wuhan University [approval number: 2012LKSZ (010) H]. In total, 88 tissue samples from patients with glioma were acquired during surgical operation, covering 34 low-grade gliomas (LGGs) and 54 GBMs; and we designated the set as Wuhan University (WHU) dataset. The tissues were snap-frozen in liquid nitrogen and preserved for experimental purposes. All participants provided written informed consent.

Quantitative Real-Time Polymerase Chain Reaction

Total RNA extraction was conducted by the TRIzol reagent (Invitrogen, Carlsbad, CA, United States). The PrimeScript RT Reagent Kit (RR047A; Takara, Tokyo, Japan) was employed to accomplish cDNA synthesis. RNA expression quantification was conducted on SYBR Premix Ex Taq II (RR820A; Takara, Tokyo, Japan), following the tutorials from manufacturers; and quantitative real-time (qRT-PCR) was performed on Bio-Rad CFX Manager (Bio-Rad Laboratories, Hercules, CA, United States). The $2^{-\Delta\Delta Ct}$ method was applied, and GAPDH was set as the reference. The primer sequences are displayed in **Supplementary Table 2**.

Statistical Analysis

When comparing variables between two groups, statistical significance was calculated by the Wilcoxon test and, among more than two groups, by the Kruskal–Wallis test. Correlative degree was assessed by Spearman's correlation method. The optimal cut points were obtained by the R package survminer to divide patients into the low- and high TIMEscore groups in each dataset for reduction of the computational batch effect. The Kaplan–Meier (K-M) method was employed to visualize the survival curves, and log-rank test to estimate the statistical significance of survival differences between the subgroups. R package forestplot was introduced to visualize the results of subgroup analysis of TIMEscore in glioma datasets. The hazard ratio (HR) in univariate analysis was calculated using the univariate Cox analysis. The independent prognosis-predicting indicators were identified by multivariate Cox regression analysis. R package survivalROC was employed to visualize receiver operating characteristic (ROC) curves and compute the area under the curve (AUC) to estimate the performance in prognostic

[4]https://cistrome.shinyapps.io/timer/

assessment of TIMEscore at 1-, 3-, and 5-year OS and progression-free survival (PFS). All heatmaps were accomplished by the R package pheatmap. OncoPrint was employed to display mutation landscapes of TCGA glioma sets including TCGA-GBM and TCGA-LGG cohorts, conducted by R package maftools (Mayakonda et al., 2018). The chi-square test was utilized to identify the gene somatic mutation frequency differences between the TIMEscore subgroups. All statistical analyses were carried out on R project (v4.0.3). All tests were two-sided, and $p < 0.05$ was regarded as significant.

RESULTS

Landscape of Glioma Tumor Immune Microenvironment

The workflow of our research is displayed in **Supplementary Figure 1**. First, original batch effect and batch effect removal of multiple transcriptomic data was carried out by Combat method; and results are displayed in **Supplementary Figures 2A,B**. Then, we performed the CIBERSORT to quantify the fractions of 22 immune cells in glioma samples (**Supplementary Table 3**). On the basis of 1,975 samples of the combined cohorts (Gravendeel, Kamoun, CGGA, and TCGA), unsupervised clustering was performed. We identified three independent TIME cell infiltration subtypes (**Figure 1A**, **Supplementary Figures 2C–G**, and **Supplementary Table 4**), and there were significant survival differences among the divided (log-rank test, $p < 0.001$; **Figure 1B**). Subgroup survival analysis revealed that the TIME clusters could remarkably distinguish the patients with worst prognosis in LGG subgroup (log-rank test, $p < 0.001$; **Supplementary Figure 3A**), yet not in GBM (log-rank test, $p > 0.05$; **Supplementary Figure 3B**). In addition, the correlation heatmap was drawn to display the immune cell interactions in glioma tissues (**Figure 1C**). To further elucidate the underlying biologic underpinnings that contribute to three distinct phenotypes, immune cell compositions among the three groups was compared (**Figure 1D**). TIME cluster A was identified to be related to an advantageous outcome with a median survival up to 697 days, which was characterized by high infiltrations of M1 macrophages, plasma cells activated CD4 + T memory cells, T follicular helper (Tfh) cells, activated NK cells, activated mast cells, and naive B cells, while there is a lack of infiltrations of CD8 + T cells and activated dendritic cells (aDCs). TIME cluster B experienced a median survival of 609 days, which was marked by median cell infiltration levels such as activated mast cells, and M0, M1, and M2 macrophages. The observations in TIME cluster C witnessed a worst OS, with only median survival of 504 days, and displayed the evaluated infiltration of such as immune-inhibiting cells such as monocytes, M0 macrophages, M2 macrophages, and Tregs and relatively high infiltrative levels of antitumor-involved CD8 + T cells and aDCs.

Because of the remarkable survival differences between TIME clusters A, B, and C, we, therefore, explored the biological differences using GSVA with all transcripts. As a result, we found that gene sets related to tumorigenic and immune-related processes were significantly enriched in TIME gene cluster C, including epithelial–mesenchymal transition (EMT), p53 pathway signaling, interferon alpha response, and IL6-JAK-STAT3 signaling (**Figure 2A** and **Supplementary Table 5**). Immune response-related biological process was enriched in TIME cluster A, such as tumor necrosis factor-α (TNFA) signaling *via* NFκB pathway. Pathological processes such as hypoxia and angiogenesis were also enriched in cluster B (**Figure 2A** and **Supplementary Table 5**).

Then we characterized the alterations in cytokines and chemokines levels among clusters. *CXCL10*, *CXCL9*, *GZMA*, *GZMB*, *PRF1*, *CD8A*, *IFNG*, *TBX2*, and *TNF* were regarded as immune-activated genes; IDO1, CD274, HAVCR2, PDCD1, CTLA4, LAG3, and PDCD1LG2 as immune checkpoint-associated molecules; and VIM, ACTA2, COL4A1, TGFBR2, ZEB1, CLDN3, SMAD9, and TWIST1 as EMT pathway-related molecules. TIME cluster A exhibited the high expression profiles of ZEB1, TNF, and LAG3; while GZMA, CXCL9, CXCL10, and CD8A were relatively overexpressed in TIME cluster C. EMT is a common process of paramount importance in glioma occurrence and invasion (Du et al., 2017; Brabletz et al., 2018). As depicted in **Figure 2B**, TIME cluster C revealed comparatively the highest expression levels of VIM, COL4A1, and TWIST1 and the lowest levels of ZEB1 and SMAD9 among the three, which is consistent with the results of GSVA step that EMT process relatively activated in TIME cluster C. And upregulated TNF in TIME cluster A might be involved in the activation of TNFA signaling *via* NFκB pathway. Cluster B revealed moderate expression levels of the above-mentioned markers (**Figure 2B**). Recent research has shown that neoplasms with an immune-inflamed phenotype are characterized by the existence of plentiful immune cells such as monocytic cells, which are located adjacent to the tumor core (Chen and Mellman, 2017). Meanwhile, tumor with immune-inflamed phenotype may exhibit high expression of PD-L1 in some cases. The results from the above analysis revealed that cluster C could be classified to be immune-inflamed. Cluster B was classified as immune-desert phenotype, characterized by a paucity of T cells, demonstrating the suppression of anti-tumor immunity. Cluster A was categorized into an immune-excluded phenotype, characterized by B cell-mediated adaptive immune response. In this category, recent research proposed that immune cells are located in the surrounding nest of tumor cells rather than penetrate the tumor tissues (Chen and Mellman, 2017).

Gene Annotation and Construction of the TIMEscore

To acquire prognosis-related quantitative indicator of TIME landscape in glioma observations, 39 DEGs calculated by the limma package were used for further analyses (**Supplementary Figures 4A,B**). As can be seen in **Supplementary Figure 4**, most genes were dysregulated between TIME clusters A and C; for example, *TNF* and *CCL4* were significantly upregulated in TIME cluster A; *FCGBP*, *IGFBP2*, and *METTL7B* in cluster C; while no gene expression significantly changed in TIME cluster B. Then functional annotation analysis revealed that in GO analysis, DEGs were mainly enriched in leukocyte differentiation, a positive regulation of neuroinflammatory response, which was considered to be related with immune regulation. KEGG

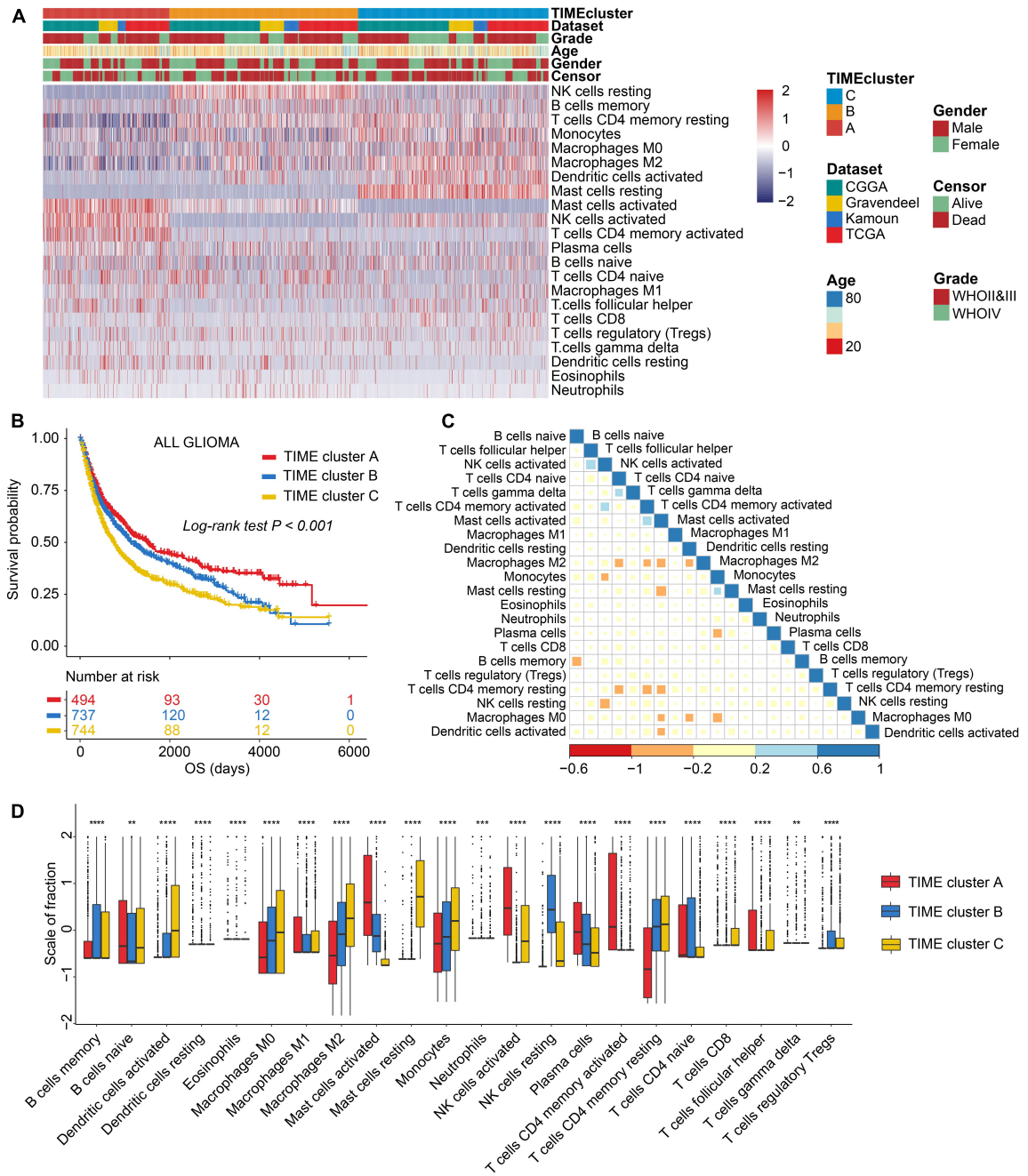

FIGURE 1 | The landscape of immune cell infiltrations in the tumor immune microenvironment (TIME) of glioma. **(A)** Unsupervised cluster of tumor-infiltrating immune cells in four glioma sets. Rows refer to glioma immune infiltrates, columns samples, and colors infiltrative levels; red represents high levels and blue low levels. **(B)** Kaplan–Meier (K-M) curves for overall survival (OS) of all glioma samples grouped by TIME subtypes. **(C)** Correlation analysis of 22 immune cells. Blue represents negative correlation and red positive. **(D)** Comparing the infiltrative levels of immune cells among three TIME patterns by the Kruskal–Wallis test. ns, $p > 0.05$; *$p < 0.05$; **$p < 0.01$; ***$p < 0.001$; and ****$p < 0.0001$.

analysis demonstrated that genes were enriched in modulation of Toll-like receptor, IL-17, TNF, and MAPK signaling pathway (**Supplementary Table 6**). In the following research, the major focus was on the CGGA set, with the most detailed and complete follow-up data. We first used univariate Cox analysis to filter out genes associated with prognosis of glioma, and there were 33 DEGs left ($p < 0.05$, **Supplementary Figure 5**). Then, a LASSO–Cox regression model with 10-fold cross-validation was used to contract the variables again and make the model optimized by filtering out seven genes: *METTL7B*, *IGFBP2*, *GDAP1L1*, *CRTAC1*, *CHI3L1*, *CHGB*, and *ANXA1* (**Figures 3A,B**). We established a signature consisting of

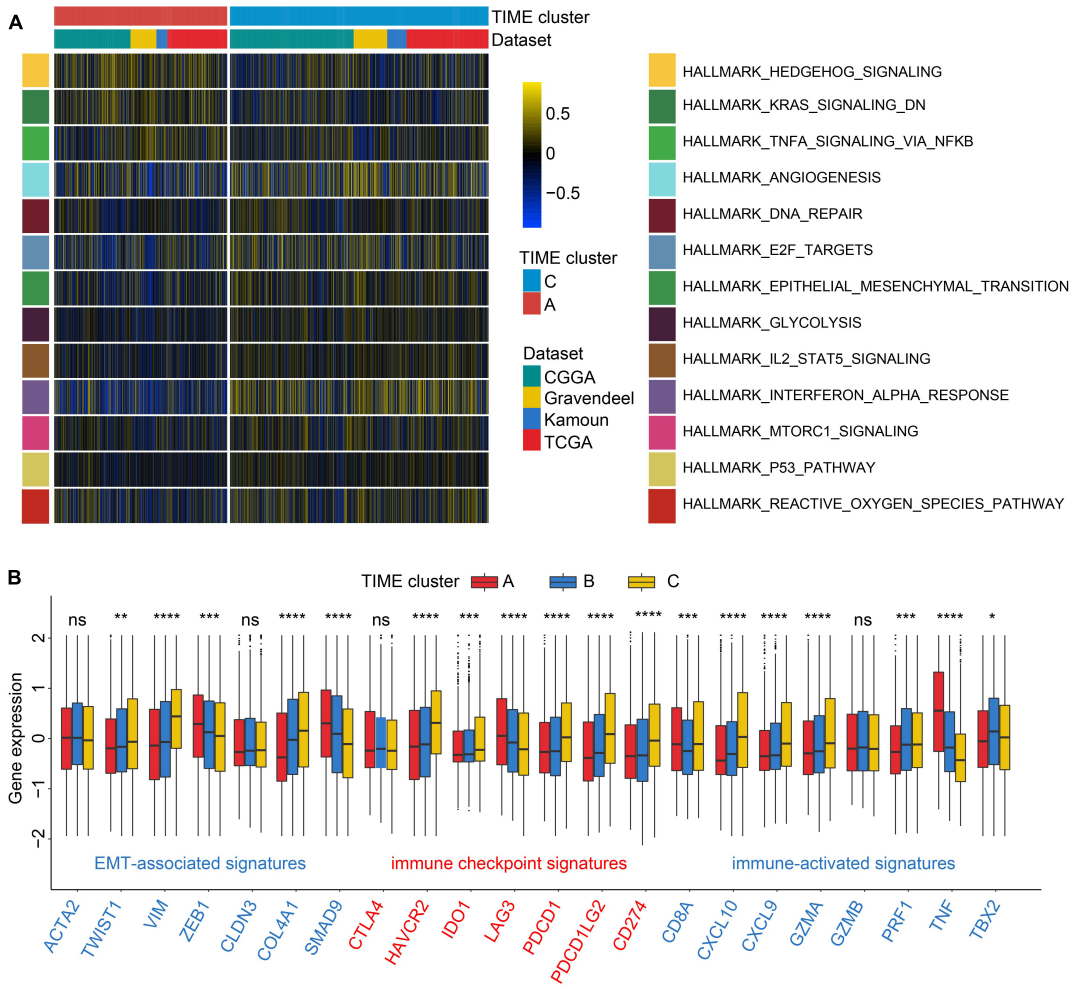

FIGURE 2 | Enrichment analysis and association of transcriptome traits and TIME phenotypes in the Chinese Glioma Genome Atlas (CGGA) cohort. **(A)** Gene set variation analysis (GSVA) revealed P53 and IL2-STAT3 signaling pathways were enriched in TIME cluster C; and TNFA *via* NFκB signaling pathway and downregulation of kirsten rat sarcoma viral oncogen (KRAS) were enriched in TIME cluster A. Color represents pathway enrich scores: color blue refers to high score and yellow low. **(B)** TIME patterns were discriminated by distinct expression levels of signatures related to epithelial–mesenchymal transition (EMT), immune checkpoint, and immune activation by the Kruskal–Wallis test. ns, $p > 0.05$; *$p < 0.05$; **$p < 0.01$; ***$p < 0.001$; and ****$p < 0.0001$.

seven mRNAs to estimate the TIMEscore for each patient, on the basis of the expression values of mRNAs multiplied by the corresponding regression coefficients (**Figure 3C**): $\text{TIMEscore} = \text{EXP}_{\text{ANXA1}} \times 0.076412216 + \text{EXP}_{\text{CHGB}} \times -0.050949893 + \text{EXP}_{\text{CHI3L1}} \times 0.012208032 + \text{EXP}_{\text{CRTA}} \times -0.096289744 + \text{EXP}_{\text{GDAP1L1}} \times -0.016843218 + \text{EXP}_{\text{IGFBP2}} \times 0.109118581 + \text{EXP}_{\text{METTL7B}} \times 0.007038053$.

The TIMEscore Predicts Glioma Prognosis

As previously described, glioma stratification was based on the optimal cutoff calculated by the R package survminer. We separated the observations into two groups according to the cutoff value of TIMEscore. The K-M curves showed that the patients with high TIMEscore had remarkably worse OS (median OS, 506 days) in comparison with the low TIMEscore group in CGGA cohort (median OS, 1,250 days; log-rank test, $p < 0.001$; **Figure 3D**). **Supplementary Figures 6A,B** depict that patients divided into TIME cluster A had the lowest TIMEscore, cluster B the medium, and C the highest, demonstrating that a high TIMEscore was linked to TIME cluster C and a disadvantageous outcome. To be specific, we inquired into the question that whether application of adjuvant therapy disturbed the potency of the TIMEscore to predict glioma prognosis. As a result, the survival advantage was evident in patients with low TIMEscore and receiving adjuvant chemotherapy or radiotherapy (log-rank test, $p < 0.001$; **Figures 3E,F**). Moreover, the predicting potency of TIMEscore was proven to be solid in Gravendeel ($n = 263$), Kamoun ($n = 145$), TCGA ($n = 640$), and the total glioma cohort ($n = 1{,}975$; log-rank test, $p < 0.001$; **Figures 4A–D**). Also, the assessment of PFS in TCGA set based on the signature showed consistent results (log-rank test, $p < 0.001$, **Figure 4E**). The AUCs revealed that TIMEscore was a strong and accurate

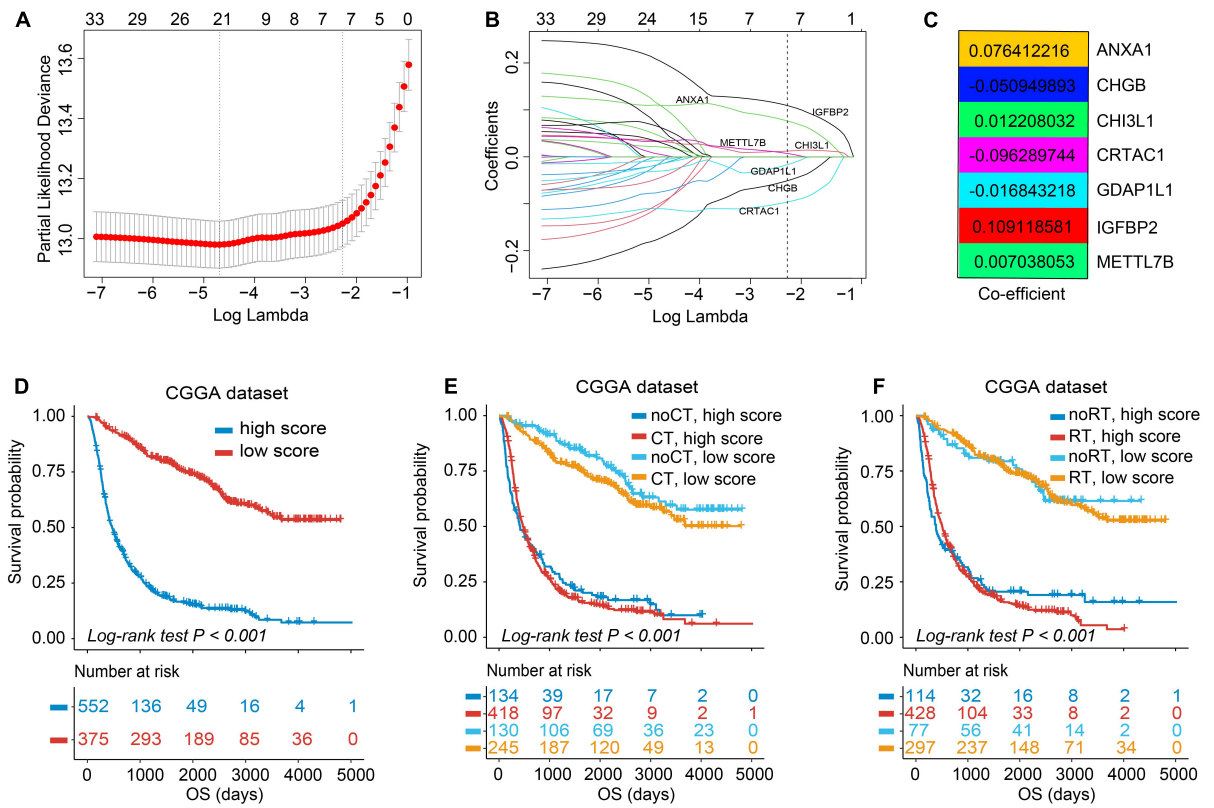

FIGURE 3 | Feature selection using least absolute shrinkage and selection operator (LASSO)–Cox regression and establishment of TIMEscore. **(A)** Tuning parameter selection (λ) in the LASSO–Cox model used 10-fold cross-validation *via* minimum criteria. Dotted vertical lines were drawn at the optimal values by using the minimum criteria and the 1 standard error of the minimum criteria (the 1 – SE criteria). λ value of 0.103, with log (λ); –2.273 was chosen (1 – SE criteria) based on 10-fold cross-validation. **(B)** A coefficient profile plot of LASSO–Cox coefficient profiles of the 33 variates. **(C)** Heatmap of coefficients calculated from LASSO–Cox analysis of seven mRNAs. **(D)** K-M curve of survival differences between high and low TIMEscore groups, in CGGA sets. **(E,F)** K-M curve of survival differences between high and low TIMEscore groups when receiving adjuvant chemotherapy **(E)** and radiotherapy **(F)**.

indicator for glioma OS at predicting 1-year survival (all cohorts: 0.75; CGGA: 0.77; Gravendeel: 0.88; Kamoun: 0.77; and TCGA: 0.69) and PFS in TCGA cohort (AUC = 0.69); at predicting 3-year survival (all cohorts: 0.78; CGGA: 0.84; Gravendeel: 0.81; Kamoun: 0.47; and TCGA: 0.75) and PFS in TCGA cohort (AUC = 0.71); and at predicting 5-year survival (all cohorts: 0.78; CGGA: 0.85; Gravendeel: 0.78; Kamoun: 0.47; and TCGA: 0.71) and PFS in TCGA cohort (AUC = 0.72). And we noticed except in the Kamoun cohort that the AUC values at predicting 3- and 5-year OS and PFS were all around 0.70, or even more than 0.70 in TCGA, Gravendeel, CGGA, and all glioma cohorts. Notably, in the Kamoun cohort, there are only two patients who survived over 3 years, so results of 3- and 5-year ROC in this cohort might be statically incorrect. The short lives might be partly caused by the human race and small-size samples in the Kamoun cohort (**Figure 4F** and **Supplementary Figures 7A–E**). In subgroup survival analysis, remarkable differences in OS between TIMEscore groups were obtained in CGGA sets (HR = 5.81, 95% CI: 4.73–7.41). Simultaneously, the prognosis-predicting value of the constructed prognostic marker was also confirmed in the other four cohorts (Gravendeel: HR = 4.50, 95% CI: 3.33–6.09; Kamoun: HR = 7.24, 95% CI: 3.62–14.47; TCGA: HR = 3.19; 95% CI: 2.44–4.16, the combined set: HR = 4.38, 95% CI: 3.83–5.01, $p < 0.001$; **Figure 4G**). A similar finding was also observed in TCGA_PFS cohort (HR = 2.99, 95% CI: 2.29–3.91, and $p < 0.001$). **Table 1** and **Supplementary Table 7** reveal that TIMEscore was detected and validated as an independent and cogent prognosis-associated indicator for OS in the CGGA, Gravendeel, TCGA, Kamoun, and combined cohort and for PFS in TCGA cohort. Finally, clinical tissues were selected for external validation, and the results demonstrated that high TIMEscore could predict the poor prognosis (log-rank test, $p < 0.001$, **Supplementary Figure 8A**), and ROC analysis validated the reliability of public findings (AUC: 1 year, 0.66; 3 years, 0.92; 5 years, 0.97; **Supplementary Figure 8B**). Meanwhile, the signature was still verified as a potent and independent marker for glioma, again in WHU set (HR = 15.09; 95% CI: 2.06–110.51, $p = 0.008$, **Supplementary Figure 8C**).

Association of TIMEscore With Different Clinical Subgroups

To further inspect the predicting firmness of TIMEscore, the predictive power was calculated in patients with different gender,

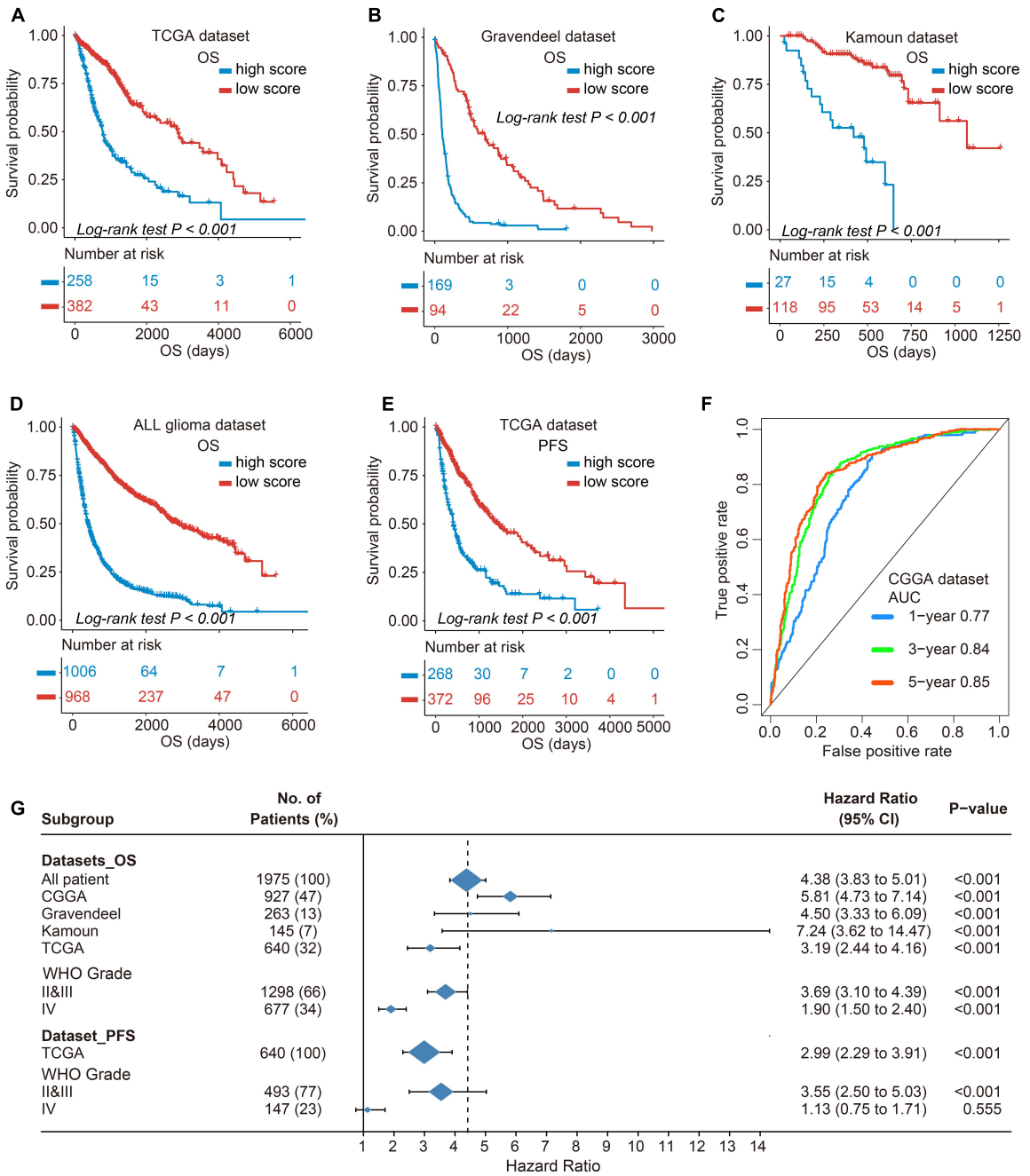

FIGURE 4 | Validation of prognostic value of TIMEscore and subgroup survival analysis. **(A–E)** K-M curve of OS differences between high and low TIMEscore groups in The Cancer Genome Atlas (TCGA), Gravendeel, Kamoun, and four merged cohorts, and progression-free survival (PFS) in TCGA sets. **(F)** Receiver operating characteristic (ROC) curves estimating the predicting value of the TIMEscore in the CGGA set for OS at 1, 3, and 5 years. **(G)** Forest plot of subgroup analyses assessing prognosis-predicting value between TIMEscore groups in glioma datasets and WHO grade. Hazard ratio (HR) > 1.0 demonstrates that high TIMEscore is an unfavorable prognostic indicator.

age, WHO grade, 1p19q codeletion status, IDH mutation status, and MGMTp methylation status in CGGA cohort.

We found that except for patients with a mean age >43 years, which are associated with relatively high TIMEscore, female patients and patients with 1p19q coding deletion or IDH mutation or WHO II and III were all statistically related to low TIMEscore (**Figures 5A–F**). Similar consequences could be found in TCGA cohort (**Supplementary Figures 9A–F**). Furthermore, the K-M curves demonstrated that the disadvantageous and advantageous survival groups were still distinguished based on TIMEscore even across all clinicopathologic subgroups (log-rank test, $p < 0.001$;

Figures 5G–I and **Supplementary Figures 10A–C**), which demonstrated that the seven-mRNA-based signature provided statistically significant OS stratification.

Correlation of TIMEscore and Immune Infiltrates

By comparing immune cell infiltrations between the TIME groups, we found CD8 + T cells, activated NK cells, M2 macrophages, aDCs, and memory B cells remarkably infiltrated in the high TIMEscore group; and CD4 + T cells, naive T cells, activated memory CD4, and monocytes in the low TIMEscore subgroup (**Supplementary Figure 11A**). Then, we validated the reliability of the correlative results between TIMEscore and immune infiltrates based on six immune infiltrates of TCGA glioma set from TIMER webtool.

As shown in **Figures 6A–F**, similar consequences could be acquired through TIMER webtool. There were positive relations between TIMEscore and immune infiltrates in glioma microenvironment. Notably, TIMEscore had the strongest correlative degree with macrophage infiltration (R = 0.42, p < 2.2e−16), in comparison with others (B cells: R = 0.18, p = 8.1e−06; CD4 + T cells: R = 0.26, p = 1.4e−11; CD8 + T cells: R = 0.19, p = 1.9e−06; neutrophils: R = 0.23, p = 2.6e−09; and dendritic cells: R = 0.38, p < 2.2e−16). Meanwhile, in **Figure 6G**, in the high TIMEscore group, there were high infiltration levels of B cells, CD4 + T cells, CD8 + T cells, neutrophils, and dendritic cells (Wilcoxon test, p < 0.05). Finally, we also found that immune checkpoints such as CD274, PDCD1, and CTLA4 showed relatively high expression in high TIMEscore set (**Supplementary Figure 11B**). GSVA analysis between high and low TIMEscore groups revealed that immune-related biological processes such as IL6-JAK-STAT3 signaling, interferon gamma (IFN-γ) response, and inflammatory response were relatively activated in the high TIMEscore group; on the contrary, Wnt/beta-catenin pathway activation and dysregulation of kirsten rat sarcoma viral oncogen (KRAS) signaling pathway were found in the low TIMEscore group (**Supplementary Table 8**).

Correlation Between Tumor Immune Microenvironment Features and Cancer Somatic Genome

Recently, a great deal of research has demonstrated that tumors with an increased tumor mutation burden (TMB) in all possibility harbor the improved response to cancer immunotherapy (Nanda et al., 2016; Hellmann et al., 2018). TCGA cohort has the complete mutation files of glioma, providing solid foundations for this research. Given the important role played by TMB in clinical practice, we attempted to explore the intrinsic association between the TMB and TIMEscore. And TMB values were compared in gliomas within the high and low TIMEscore subgroups. As shown in **Figure 7A**, patients with high TIMEscore displayed a remarkably increased TMB, in contrast to subjects in the low TIMEscore set (Wilcoxon test, p < 0.001), which indicated immunotherapy might benefit gliomas with relatively high TIMEscore. Next, we used the R package survminer to obtain an optimal cutoff of TMB to categorize the gliomas into two subgroups, and there were significant survival differences after being grouped using the K-M curve (log-rank test, p < 0.001, **Figure 7B**). Considering the correlation between TMB and TIMEscore, we calculated the collaborative influence of both factors on glioma. Stratification analysis demonstrated that a seven-mRNA-based signature could still independently predict glioma prognosis, even in the presence of TMB value interference (log-rank test, p < 0.001, **Figure 7C**). Therefore, these findings

TABLE 1 | Cox regression analysis of the clinical variables, and survival in the Chinese Glioma Genome Atlas (CGGA) and The Cancer Genome Atlas (TCGA) cohorts.

Covariate	CGGA_OS cohort			TCGA_OS cohort			TCGA_PFS cohort		
	HR	95% CI	*P*	HR	95% CI	*p*	HR	95% CI	*p*
Univariate Cox regression analysis									
TIMEscore	2.718	2.450–3.016	**<0.001**	2.184	1.877–2.543	**<0.001**	1.839	1.629–2.077	**<0.001**
Gender	1.036	0.878–1.223	0.675	1.092	0.824–1.447	0.541	1.045	0.837–1.305	0.697
Age	1.028	1.021–1.036	**<0.001**	1.074	1.062–1.086	**<0.001**	1.040	1.032–1.048	**<0.001**
Grade	4.115	3.467–4.885	**<0.001**	10.88	7.783–15.221	**<0.001**	5.598	4.392–7.135	**<0.001**
IDH status	3.039	2.560–3.608	**<0.001**	8.84	6.561–11.91	**<0.001**	6.826	5.351–8.707	**<0.001**
1p19q status	4.368	3.312–5.759	**<0.001**	3.82	2.449–5.957	**<0.001**	3.333	2.397–4.634	**<0.001**
MGMTp status	1.202	1.009–1.432	**0.039**	3.223	2.419–4.294	**<0.001**	2.856	2.241–3.639	**<0.001**
Multivariate Cox regression analysis									
TIMEscore	2.042	1.734–2.405	**<0.001**	1.847	1.435–2.377	**<0.001**	1.434	1.159–1.774	**0.001**
Age	1.009	1.002–1.016	**0.016**	1.053	1.039–1.067	**<0.001**	1.014	1.004–1.025	**0.006**
Grade	2.000	1.597–2.503	**<0.001**	5.020	3.065–8.223	**<0.001**	2.799	1.796–4.361	**<0.001**
IDH status	0.796	0.622–1.017	0.068	1.240	0.695–2.214	0.467	2.074	1.263–3.407	**0.004**
1p19q status	1.959	1.426–2.693	**<0.001**	1.628	0.959–2.765	0.071	1.440	0.959–2.163	0.079
MGMTp status	1.071	0.888–1.292	0.475	1.275	0.905–1.798	0.165	1.212	0.901–1.628	0.203

HR, hazard ratio; CI, confidence interval; CGGA, Chinese Glioma Genome Atlas; TCGA, The Cancer Genome Atlas; IDH, isocitrate dehydrogenase; MGMTp, O^6-methylguanine-DNA methyltransferase promoter.

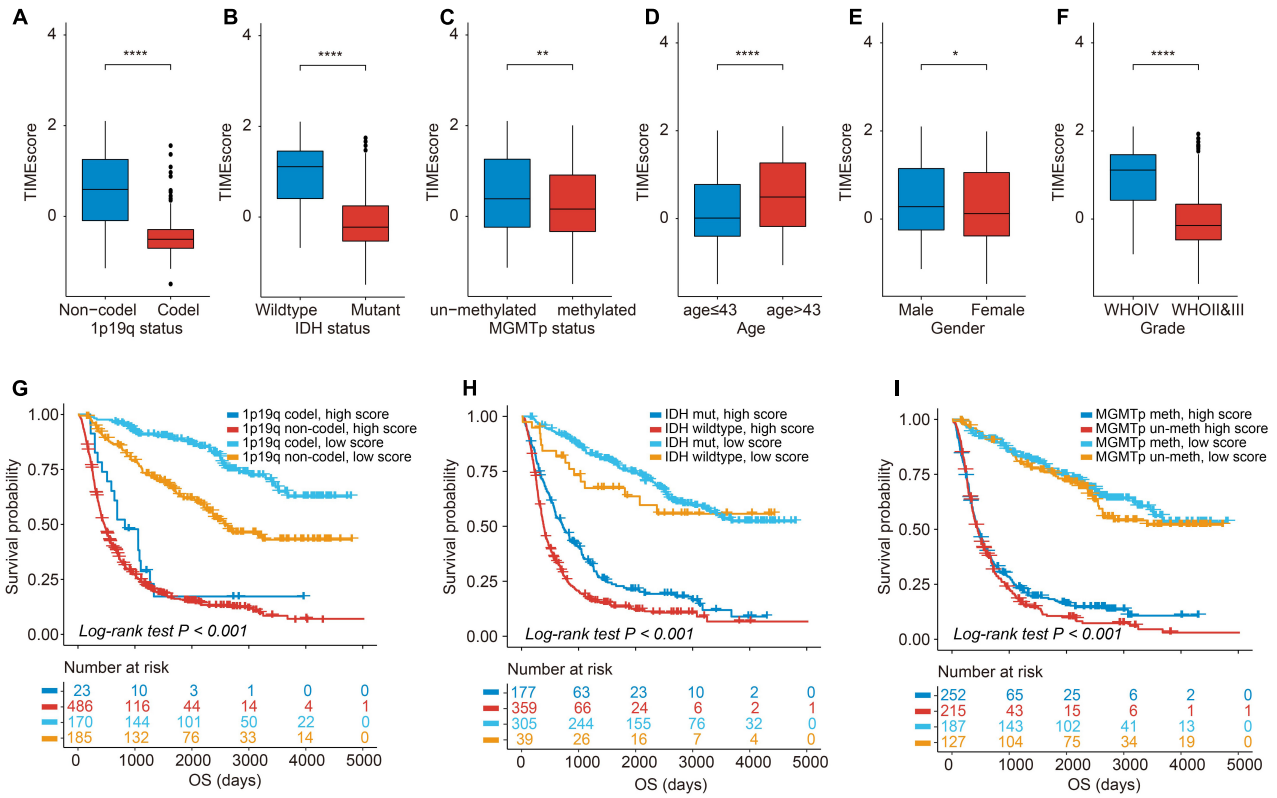

FIGURE 5 | Association of TIMEscore and glioma clinicopathologic features. **(A–F)** Barplot of TIMEscore in groups with different clinicopathologic characteristics in CGGA set, compared with the Wilcoxon test. **(G–I)** K-M curves for patients with glioma in the CGGA cohort stratified by 1p19q codeletion status **(G)**, isocitrate dehydrogenase (IDH) mutation status **(H)**, O^6-methylguanine-DNA methyltransferase (MGMT) methylation status **(I)**, and TIMEscore. *$p < 0.05$; **$p < 0.01$; ***$p < 0.001$; and ****$p < 0.0001$.

demonstrated that TIMEscore could in all probability serve as a potential predicting indicator independent of TMB and an effective tool to screen beneficiaries of immunotherapy. Furthermore, we analyzed the landscape of somatic variants in TCGA glioma set between the TIMEscore subgroups by maftools. The top 20 genes with the highest alteration frequency were demonstrated in **Figures 7D,E**. Meanwhile, we also analyzed the gene with different alteration frequencies between the two groups. And we found that genes were significantly different such as *IDH1*, *CIC*, *EGFR*, *PTEN*, *FUBP1*, *TTN*, *NOTCH1*, *COL6A3*, *NF1*, *DNAH3*, *RYR2*, *IDH2*, *MYOCD*, *F8*, *ROS1*, *SETD2*, *LRP2*, *FBN2*, and *HCN1* (**Supplementary Table 9**). These findings may contribute to gain insights into glioma TIME compositions and gene mutations in immunotherapy.

DISCUSSION

Increasing research has demonstrated that the immune cell dysfunction within the glioma TIME boosts disorders of immune regulation and thus triggers the related malignant biological properties and poor outcomes of cancer patients. In the current study, we comprehensively analyzed landscape of interactions between the clinical features and the infiltrative cells in a meta-cohort of 1,975 glioma samples. A TIMEscore comprising seven selected mRNA features in glioma was developed by LASSO–Cox regression model. The prognostic signature developed and validated was expected to be an indicator for predicting glioma prognosis and for more effective adjuvant therapy.

Clinical trials of immunotherapy against cancer of kidney, non-small cell lung cancer (NSCLC), and HNSCC have achieved a lot (Garon et al., 2015; Motzer et al., 2015; Ferris et al., 2016), demonstrating excellent viability of the promising regimes. However, in glioma field, few studies succeed (Weller et al., 2017; Long et al., 2018; Woroniecka et al., 2018), due to the great intratumor heterogeneity and unique TIME such as dramatic T-cell malfunctions and high infiltrates of TAM (Sampson et al., 2020). In the case of the treatment strategies and prognosis assessment for glioma, the specific marker construction remains a far-reaching challenge.

The emphasis of our research was laid on the interactions of TIME with the molecular characteristics in glioma, so we first extracted immune-related genes between the TIME clusters. When analyzing functions of TIME-associated genes, our research suggested that in the GO analysis, the mRNAs were enriched in regulation of leukocyte differentiation, positive regulation of neuroinflammatory response, and mononuclear cell

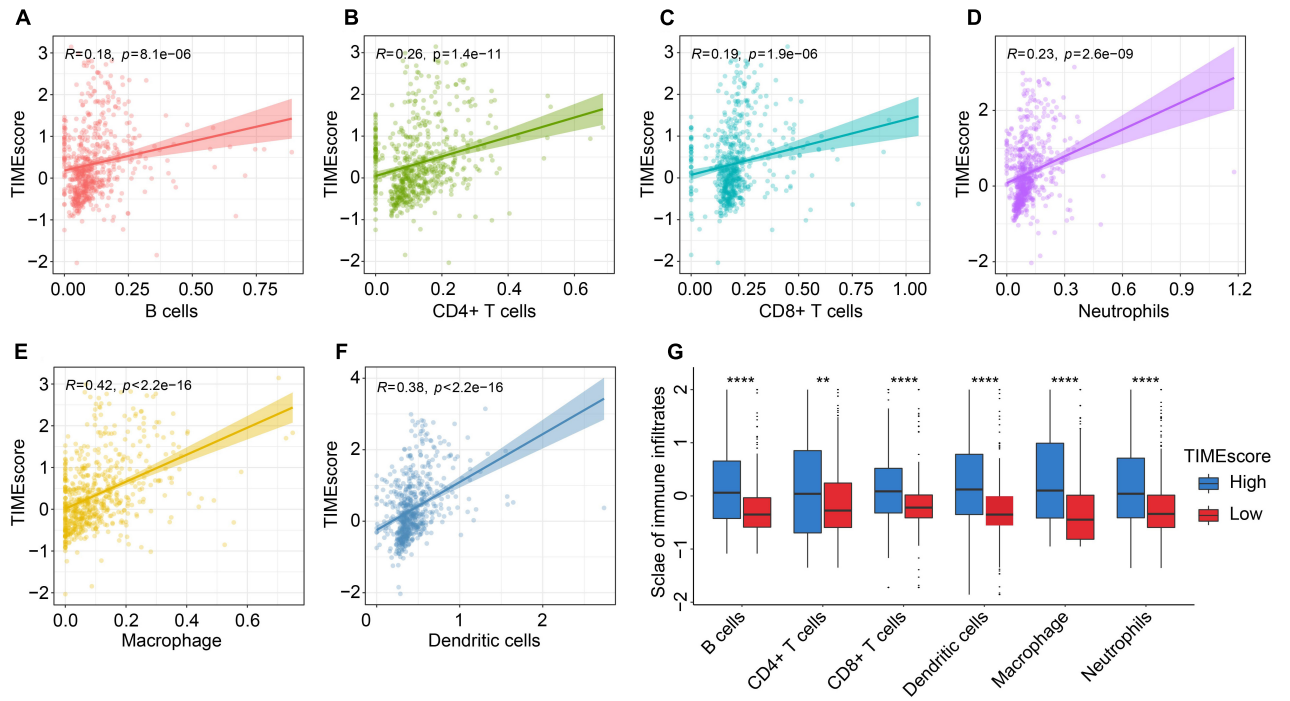

FIGURE 6 | Correlation between the TIMEscore and tumor immune infiltrates using TIMER method. **(A–G)** Scatter diagrams of correlation of TIMEscore and B cells **(A)**, CD4 + T cells **(B)**, CD8 + T cells **(C)**, neutrophils **(D)**, macrophage **(E)**, and dendritic cells **(F)**. **(G)** Barplots of six immune cell infiltrative levels between high and low TIMEscore groups. *$p < 0.05$; **$p < 0.01$; ***$p < 0.001$; and ****$p < 0.0001$.

migration, which are considered to be related with immune regulation. In KEGG analysis, we found that the genes were significantly implicated in modulation of Toll-like receptor signaling pathway, IL-17 signaling pathway, TNF signaling pathway, and MAPK signaling pathway. These findings revealed that the DEGs between TIME clusters might play a role of significant importance in immune regulation (Iwasaki and Medzhitov, 2004; Liu et al., 2007; Veldhoen, 2017; Chen et al., 2021). For the DEGs involved in the construction of TIMEscore, METTL7B overexpression could promote glioma progression and bring an inverse prognosis to gliomas (Xiong et al., 2021); upregulated IGFBP2 in glioma has been considered as a suppressor of phosphorylation of FcγRIIB and a promoter of vasculogenic mimicry formation (Liu et al., 2019a,b); the overexpressed ANXA1 could accelerate glioma malignancy behaviors by upregulating the PI3K/Akt signaling (Wei et al., 2021); CHI3L1 and CRTAC1 have been reported to be related to glioma prognosis (Deluche et al., 2019; Xiao et al., 2020); and GDAP1L1 is expressed exclusively in human brain neuron, acting as a marker for distinguishing neuron from others such as astrocytes (Bardy et al., 2016). However, no research has been reported on GDAP1L1 in glioma.

To gain further insights into biological differences among TIME clusters, we probed into infiltrative fractions of immune cells. The results suggested that TIME cluster C had abundant infiltrations of immune-inhibitory cells, such as monocytes, M0 macrophages, M2 macrophages, and Tregs. Although high infiltration of CD8 + T cells was observed in cluster C, the cells may be in a dysfunctional state such as hyper-exhaustion (Gajewski et al., 2013; Spranger et al., 2013). Meanwhile, immune checkpoints such as PD-L1 and PD1 and proinflammatory and effector cytokines such as CXCL9 and CXCL10 can also be detected by mRNA analysis in TIME cluster C. According to recent research, TIME cluster C can be classified into immune-inflamed phenotype (Chen and Mellman, 2017). This feature reveals the existence of a preexisting anticancer immunity that could possibly be blocked by immunosuppression in the tumor bed (Rosenberg et al., 2016). Currently, response to immunotherapy most often occur in patients with inflammatory tumors, indicating potential clinical benefits from immunotherapy for these patients (Powles et al., 2014; Garon et al., 2015).

Previous research demonstrated that M2 macrophages could secrete several immune suppressors such as IL-10 and TGF-β and could downregulate IL-12 and IL-6, contributing to the suppression of T-cell activation and proliferation in tumor microenvironment (Sica et al., 2006; Qian and Pollard, 2010), as well as inducing the infiltration of Tregs (Ino et al., 2013; Shigeoka et al., 2013). Infiltration of Tregs has been recognized as a crucial mechanism in modulating immune system homeostasis and immune tolerance of the body. For example, Tregs could secrete immunosuppressive cytokines such as TGF-β, IL-10, and IL-35 (Sullivan et al., 2020); inhibit antigen presentation functions of dendritic cells and CD4 + T helper cells; and generate tumor-specific CD8 + cytotoxic T lymphocytes (CTLs), which act as barriers of anti-tumor immune response and

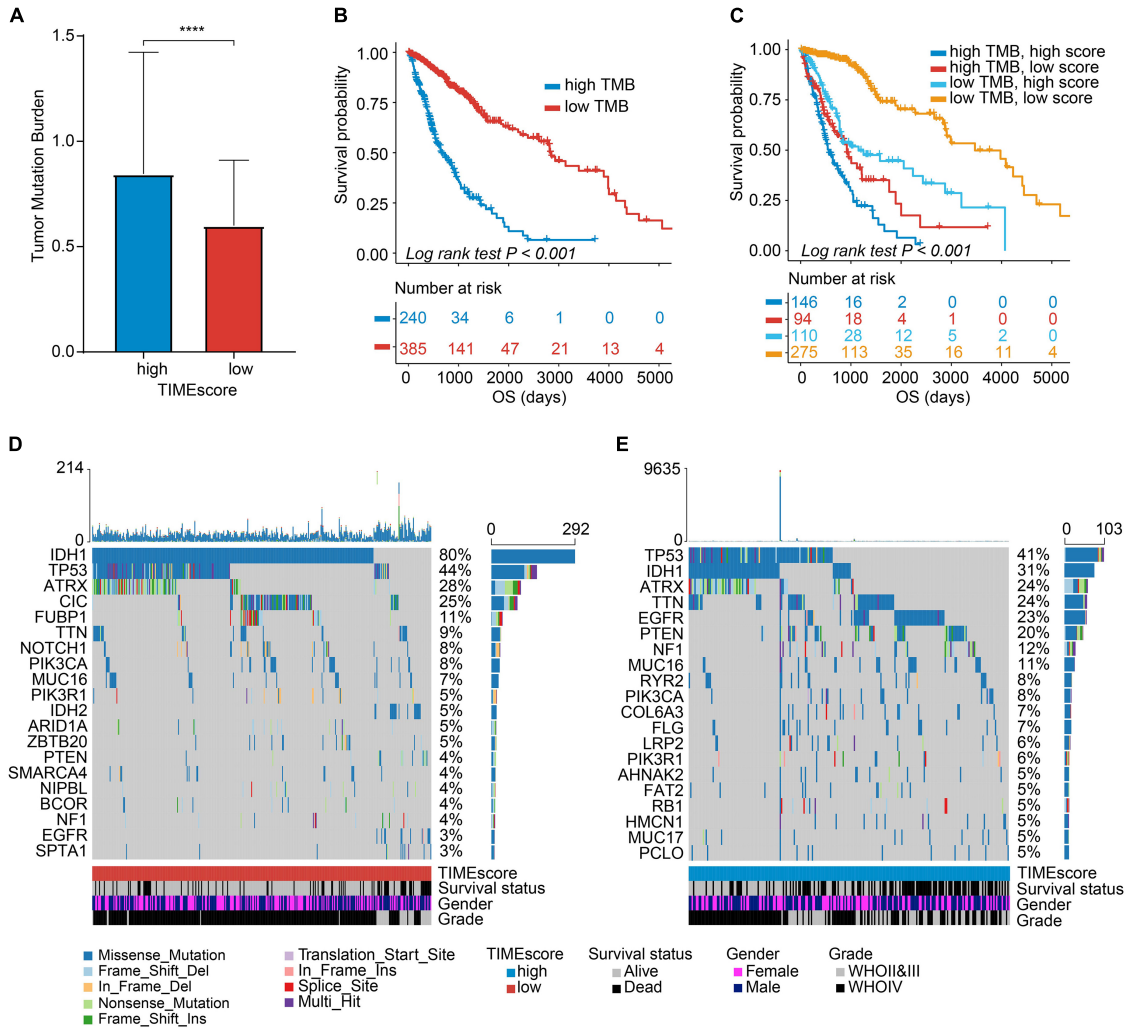

FIGURE 7 | Correlation between the TIMEscore and somatic variants. **(A)** Tumor mutation burden (TMB) differences in the high and low TIMEscore subgroups. Wilcoxon test, $p < 0.0001$. **(B)** K-M curves for high and low TMB groups of TCGA glioma cohort. **(C)** K-M curves for patients in TCGA glioma cohort stratified by both TMB and TIMEscore. **(D,E)** The oncoPrint was constructed using low TIMEscore on the left **(D)** and high TIMEscore on the right **(E)**. The columns represent samples. $^{*}p < 0.05$; $^{**}p < 0.01$; $^{***}p < 0.001$; and $^{****}p < 0.0001$.

result in the motivation of tumor immune escape. With the use of GSVA algorithm, oncogenic and immune-associated processes such as EMT, angiogenesis, IFN-γ response, and pathways such as p53 and IL6-JAK-STAT3 signaling pathways were relatively activated in TIME cluster C. The distinctive features suggested by GSVA further confirm the coexistence of slight preexisting anticancer immunity and overwhelming immunosuppressing processes in the tumor bed. Recent research reveals that CD8 + T-cell-derived IFN-γ can function as a driver and contributor of Treg fragility to boost anti-neoplasm immunity (Overacre-Delgoffe et al., 2017). In glioma TIME, IL6-JAK-STAT3 signaling pathway acts a critical role in driving tumor cell proliferation, invasion, and metastasis and negatively regulates immune response (Johnson et al., 2018). Meanwhile, research reveals that overactivation of STAT3 negatively regulates effector T cells and DCs and positively modulates infiltrations of MDSCs and Tregs. Conversely, TIME cluster A exhibited the presence of abundant immune cells such as activated NK cells, activated CD4 + T memory cells, plasma cells, and M1 macrophages, while lacking the infiltration of CD8 + T cells and aDCs. Previous research classified this type of immune-infiltrating characteristics as an immune-excluded phenotype (Salmon et al., 2012; Joyce and Fearon, 2015). For the infiltrative category, the immune cells do not penetrate the parenchyma of glioma, instead of retaining in the stroma-sounding nests of tumor cells, which makes it seem that the immune cells are actually inside the tumor (Vesely and Schreiber, 2013). Cluster B was characterized by scant activated and priming T cells and was associated with immune tolerance, corresponding to the immune-desert phenotype (Vesely and Schreiber, 2013).

Immunotherapeutic monoclonal antibodies that obstruct the PD-1 or PD-L1 could bring about durable responses in tumor

patients (Mariathasan et al., 2018). With the advancement of immunotherapy in clinical trials, several studies demonstrate that TMB values and expression of immune checkpoints such as PD1 are not practical indicators to discriminate beneficiaries of immunotherapy for glioma (McGrail et al., 2021). The construction of predictors for immune checkpoint inhibitor is, therefore, encouraging. Accumulating studies support the opinions that the TIME has profound effects on glioma outcomes and on efficiency of immunotherapy. Considering the individual heterogeneity of the immune environment, we constructed and validated a scoring system that was defined as TIMEscore to quantify the TIME pattern for an individual glioma. Comprehensive analysis demonstrated that the constructed TIMEscore was an independent prognostic biomarker for glioma, and patients in the low TIMEscore group were blessed with advantageous OS and PFS, in comparison with counterparts in the high TIMEscore group. The findings were validated in TCGA, Gravendeel, and Kamoun sets; in the merged cohorts of CGGA, TCGA, Gravendeel, Kamoun datasets; and even in the clinical samples. Meanwhile, the subgroups meta-analysis further identified the strong performance of the signature in the cohorts mentioned above. By applying ROC analysis, the TIMEscore revealed the high accuracy in predicting glioma OS and PFS, demonstrating its high potentiality in clinical practice.

By analyzing the correlation between TIMEscore and clinicopathologic characteristics, we found that the signature was significantly decreased in patients with 1p19q codeletion, IDH mutant, and MGMTp methylation molecular subtype. The consequences displayed the high probability of TIMEscore applied to estimate patients' clinical and pathological characteristics including WHO grade, IDH status, MGMTp status, 1p19q status, and TMB. 1p19q codeletion and MGMTp methylation have been confirmed to be beneficial to survival and markers for patients with high sensitivity to adjuvant chemotherapy in guiding the post-surgery treatment (Morris and Lassman, 2010; Omuro and DeAngelis, 2013). Furthermore, a recent study confirms that 1p19q codeleted WHO II and III gliomas are accompanied with decreased levels of immune infiltrates and epigenetic silencing of immune checkpoints, compared with the 1p19q non-codeletion counterparts, leading to the unsuitable immunotherapy for 1p19q codeleted LGGs (Lv et al., 2021). IDH mutation is an early event in the formation of several diffuse gliomas, which is considered to be the strongest prognostic factor for glioma (Han et al., 2020). For example, the median survival time of IDH mutant GBM is 31 months, which is more than twice the median survival time of 15 months in wild-type GBM (Yan et al., 2009), is consistent with our analysis in **Figure 5B** and **Supplementary Figure 9B**. Meanwhile, recent research reveals IDH mutation-derived D-2-hydroxyglutarate (D-2-HG) serves as a potent negative modulator for anti-tumor T-cell immunity. D-2-HG inhibits adenosine triphosphate (ATP)-dependent T-cell receptor signaling pathway, putting sand in the wheels of activating T cells in brain malignancy. Through suppressing the molecule, called signal transducer and activator of transcription 1 (STAT1), D-2-HG could result in a reduction of CD8 + T-cell immigration into the glioma region (Kohanbash et al., 2017). For WHO grading of glioma, recent research reveals the tight relations between WHO IV glioma, that is, the GBM, and immune infiltrates in that GBM has higher infiltrates of immune cells such as microglia, macrophages, and MDSCs (Komohara et al., 2008; Raychaudhuri et al., 2011), which is consistent with the findings displayed in **Figures 5B**, 6E that the TIMEscore positively correlated with the WHO grade and monocytic cell infiltrates.

When analyzing the correlation between TIMEscore and immune cell infiltrations, high TIMEscore was related to higher infiltrative proportion of immune cells like aDCs, CD8 + T cells, and macrophages and higher immunotherapy-related gene expression such as LAG3, IDO1, CTLA4, and PDCD1. We also observed that the patients in the high TIMEscore group demonstrated higher TMB values in TCGA glioma cohort. The above findings supported that patients in high TIMEscore might be more sensitive to immunotherapy. Although several prognostic markers have been explored in glioma field, our TIME signature based on large-scale population could be more accurate and independent in predicting the glioma prognosis, compared with indicators established (AUC: 1 year, 0.685; 3 years, 0.619; and 5 years, 0.621) (Qiu et al., 2020). Meanwhile, our comprehensive analysis revealed that the TIMEscore could also act as a potential predictor for clinical adjuvant therapy, such as radiotherapy, chemotherapy, or even immunotherapy.

CONCLUSION

In conclusion, we comprehensively analyzed the TIME landscape of glioma, providing insights into the TIME infiltrative characteristics. Meanwhile, a TIMEscore system established here might boost the clinical prognosis assessment and development of treatment regimens for gliomas.

DATA AVAILABILITY STATEMENT

The datasets presented in this study can be found in online repositories: TCGA: https://portal.gdc.cancer.gov/; CGGA: http://www.cgga.org.cn/; and GLIOVIS: http://gliovis.bioinfo.cnio.es/.

ETHICS STATEMENT

The research was approved by the Ethics Committee of Wuhan University [approval number: 2012LKSZ (010) H]. The patients/participants provided their written informed consent to participate in this study.

AUTHOR CONTRIBUTIONS

CZ: concept and design. CZ, HL, and NL: data collection and analysis. CZ, PX, ST, and LY: drafting the manuscript.

CZ, YT, LG, ZS, and XL: revision. QC and DT: supervision for the study. All authors contributed to the article and approved the submitted version.

FUNDING

This work was supported by the Hubei Province Health and Family Planning Scientific Research Project (WJ2017M019).

ACKNOWLEDGMENTS

We gratefully appreciated research help from Jinping Zhang and Yue Zhou.

SUPPLEMENTARY MATERIAL

The Supplementary Material for this article can be found online at: https://www.frontiersin.org/articles/10.3389/fcell.2021.717601/full#supplementary-material

REFERENCES

Badie, B., and Schartner, J. M. (2000). Flow cytometric characterization of tumor-associated macrophages in experimental gliomas. *Neurosurgery* 46, 957–961.

Barbera-Guillem, E., Nyhus, J. K., Wolford, C. C., Friece, C. R., and Sampsel, J. W. (2002). Vascular endothelial growth factor secretion by tumor-infiltrating macrophages essentially supports tumor angiogenesis, and IgG immune complexes potentiate the process. *Cancer Res.* 62, 7042–7049.

Bardy, C., van den Hurk, M., Kakaradov, B., Erwin, J. A., Jaeger, B. N., Hernandez, R. V., et al. (2016). Predicting the functional states of human iPSC-derived neurons with single-cell RNA-seq and electrophysiology. *Mol. Psychiatry* 21, 1573–1588. doi: 10.1038/mp.2016.158

Batlle, E., and Massagué, J. (2019). Transforming growth factor-β signaling in immunity and cancer. *Immunity* 50, 924–940. doi: 10.1016/j.immuni.2019.03.024

Bingle, L., Brown, N. J., and Lewis, C. E. (2002). The role of tumour-associated macrophages in tumour progression: implications for new anticancer therapies. *J. Pathol.* 196, 254–265. doi: 10.1002/path.1027

Bowman, R. L., Wang, Q., Carro, A., Verhaak, R. G. W., and Squatrito, M. (2017). GlioVis data portal for visualization and analysis of brain tumor expression datasets. *Neuro Oncol.* 19, 139–141. doi: 10.1093/neuonc/now247

Brabletz, T., Kalluri, R., Nieto, M. A., and Weinberg, R. A. (2018). EMT in cancer. *Nat. Rev. Cancer* 18, 128–134. doi: 10.1038/nrc.2017.118

Chamberlain, M. C., and Kim, B. T. (2017). Nivolumab for patients with recurrent glioblastoma progressing on bevacizumab: a retrospective case series. *J. Neurooncol.* 133, 561–569. doi: 10.1007/s11060-017-2466-0

Chen, A. Y., Wolchok, J. D., and Bass, A. R. (2021). TNF in the era of immune checkpoint inhibitors: friend or foe? *Nat. Rev. Rheumatol.* 17, 213–223. doi: 10.1038/s41584-021-00584-4

Chen, B., Khodadoust, M. S., Liu, C. L., Newman, A. M., and Alizadeh, A. A. (2018). Profiling tumor infiltrating immune cells with CIBERSORT. *Methods Mol. Biol.* 1711, 243–259. doi: 10.1007/978-1-4939-7493-1_12

Chen, D. S., and Mellman, I. (2017). Elements of cancer immunity and the cancer-immune set point. *Nature* 541, 321–330. doi: 10.1038/nature21349

Corbet, C., Bastien, E., Santiago de Jesus, J. P., Dierge, E., Martherus, R., Vander Linden, C., et al. (2020). TGFβ2-induced formation of lipid droplets supports acidosis-driven EMT and the metastatic spreading of cancer cells. *Nat. Commun.* 11:454. doi: 10.1038/s41467-019-14262-3

De Palma, M., Biziato, D., and Petrova, T. V. (2017). Microenvironmental regulation of tumour angiogenesis. *Nat. Rev. Cancer* 17, 457–474. doi: 10.1038/nrc.2017.51

Deluche, E., Bessette, B., Durand, S., Caire, F., Rigau, V., Robert, S., et al. (2019). CHI3L1, NTRK2, 1p/19q and IDH status predicts prognosis in glioma. *Cancers (Basel)* 11:544. doi: 10.3390/cancers11040544

Du, L., Tang, J.-H., Huang, G.-H., Xiang, Y., and Lv, S.-Q. (2017). The progression of epithelial-mesenchymal transformation in gliomas. *Chin. Neurosurg. J.* 3:23. doi: 10.1186/s41016-017-0086-3

Economopoulou, P., Agelaki, S., Perisanidis, C., Giotakis, E. I., and Psyrri, A. (2016). The promise of immunotherapy in head and neck squamous cell carcinoma. *Ann. Oncol.* 27, 1675–1685. doi: 10.1093/annonc/mdw226

Fan, T., Zhu, M., Wang, L., Liu, Y., Tian, H., Zheng, Y., et al. (2020). Immune profile of the tumor microenvironment and the identification of a four-gene signature for lung adenocarcinoma. *Aging* 13, 2397–2417. doi: 10.18632/aging.202269

Ferris, R. L., Blumenschein, G. Jr., Fayette, J., Guigay, J., Colevas, A. D., Licitra, L., et al. (2016). Nivolumab for recurrent squamous-cell carcinoma of the head and neck. *N. Engl. J. Med.* 375, 1856–1867. doi: 10.1056/NEJMoa1602252

Finotello, F., Mayer, C., Plattner, C., Laschober, G., Rieder, D., Hackl, H., et al. (2019). Molecular and pharmacological modulators of the tumor immune contexture revealed by deconvolution of RNA-seq data. *Genome Med.* 11:34. doi: 10.1186/s13073-019-0638-6

Fu, H., Zhu, Y., Wang, Y., Liu, Z., Zhang, J., Xie, H., et al. (2018). Identification and validation of stromal immunotype predict survival and benefit from adjuvant chemotherapy in patients with muscle-invasive bladder cancer. *Clin. Cancer Res.* 24, 3069–3078. doi: 10.1158/1078-0432.CCR-17-2687

Gajewski, T. F., Woo, S.-R., Zha, Y., Spaapen, R., Zheng, Y., Corrales, L., et al. (2013). Cancer immunotherapy strategies based on overcoming barriers within the tumor microenvironment. *Curr. Opin. Immunol.* 25, 268–276. doi: 10.1016/j.coi.2013.02.009

Garon, E. B., Rizvi, N. A., Hui, R., Leighl, N., Balmanoukian, A. S., Eder, J. P., et al. (2015). Pembrolizumab for the treatment of non-small-cell lung cancer. *N. Engl. J. Med.* 372, 2018–2028. doi: 10.1056/NEJMoa1501824

Grauwet, K., and Chiocca, E. A. (2016). Glioma and microglia, a double entendre. *Nat. Immunol.* 17, 1240–1242. doi: 10.1038/ni.3586

Han, S., Liu, Y., Cai, S. J., Qian, M., Ding, J., Larion, M., et al. (2020). IDH mutation in glioma: molecular mechanisms and potential therapeutic targets. *Br. J. Cancer* 122, 1580–1589. doi: 10.1038/s41416-020-0814-x

Hellmann, M. D., Ciuleanu, T. E., Pluzanski, A., Lee, J. S., Otterson, G., Audigier-Valette, C., et al. (2018). Abstract CT077: nivolumab (nivo) + ipilimumab (ipi) vs platinum-doublet chemotherapy (PT-DC) as first-line (1L) treatment (tx) for advanced non-small cell lung cancer (NSCLC): initial results from CheckMate 227. *Cancer Res.* 78(13 Suppl), CT077–CT077. doi: 10.1158/1538-7445.am2018-ct077

Ino, Y., Yamazaki-Itoh, R., Shimada, K., Iwasaki, M., Kosuge, T., Kanai, Y., et al. (2013). Immune cell infiltration as an indicator of the immune microenvironment of pancreatic cancer. *Br. J. Cancer* 108, 914–923. doi: 10.1038/bjc.2013.32

Iwasaki, A., and Medzhitov, R. (2004). Toll-like receptor control of the adaptive immune responses. *Nat. Immunol.* 5, 987–995.

Johnson, D. E., O'Keefe, R. A., and Grandis, J. R. (2018). Targeting the IL-6/JAK/STAT3 signalling axis in cancer. *Nat. Rev. Clin. Oncol.* 15, 234–248. doi: 10.1038/nrclinonc.2018.8

Joyce, J. A., and Fearon, D. T. (2015). T cell exclusion, immune privilege, and the tumor microenvironment. *Science* 348, 74–80. doi: 10.1126/science.aaa6204

Kohanbash, G., Carrera, D. A., Shrivastav, S., Ahn, B. J., Jahan, N., Mazor, T., et al. (2017). Isocitrate dehydrogenase mutations suppress STAT1 and CD8+ T cell accumulation in gliomas. *J. Clin. Invest.* 127, 1425–1437. doi: 10.1172/jci90644

Komohara, Y., Ohnishi, K., Kuratsu, J., and Takeya, M. (2008). Possible involvement of the M2 anti-inflammatory macrophage phenotype in growth of human gliomas. *J. Pathol.* 216, 15–24. doi: 10.1002/path.2370

Leek, J. T., Johnson, W. E., Parker, H. S., Jaffe, A. E., and Storey, J. D. (2012). The sva package for removing batch effects and other unwanted variation in high-throughput experiments. *Bioinformatics* 28, 882–883. doi: 10.1093/bioinformatics/bts034

Liu, Y., Li, F., Yang, Y. T., Xu, X. D., Chen, J. S., Chen, T. L., et al. (2019a). IGFBP2 promotes vasculogenic mimicry formation via regulating CD144 and MMP2

expression in glioma. *Oncogene* 38, 1815–1831. doi: 10.1038/s41388-018-0525-4

Liu, Y., Shepherd, E. G., and Nelin, L. D. (2007). MAPK phosphatases–regulating the immune response. *Nat. Rev. Immunol.* 7, 202–212.

Liu, Y., Song, C., Shen, F., Zhang, J., and Song, S. W. (2019b). IGFBP2 promotes immunosuppression associated with its mesenchymal induction and FcγRIIB phosphorylation in glioblastoma. *PLoS One* 14:e0222999. doi: 10.1371/journal.pone.0222999

Long, K. B., Young, R. M., Boesteanu, A. C., Davis, M. M., Melenhorst, J. J., Lacey, S. F., et al. (2018). CAR T cell therapy of non-hematopoietic malignancies: detours on the road to clinical success. *Front. Immunol.* 9:2740. doi: 10.3389/fimmu.2018.02740

Louis, D. N., Perry, A., Reifenberger, G., von Deimling, A., Figarella-Branger, D., Cavenee, W. K., et al. (2016). The 2016 world health organization classification of tumors of the central nervous system: a summary. *Acta Neuropathol.* 131, 803–820. doi: 10.1007/s00401-016-1545-1

Lv, L., Zhang, Y., Zhao, Y., Wei, Q., Zhao, Y., and Yi, Q. (2021). Effects of 1p/19q codeletion on immune phenotype in low grade glioma. *Front. Cell. Neurosci.* 15:704344. doi: 10.3389/fncel.2021.704344

Makkouk, A., and Weiner, G. J. (2015). Cancer immunotherapy and breaking immune tolerance: new approaches to an old challenge. *Cancer Res.* 75, 5–10. doi: 10.1158/0008-5472.CAN-14-2538

Mariathasan, S., Turley, S. J., Nickles, D., Castiglioni, A., Yuen, K., Wang, Y., et al. (2018). TGFβ attenuates tumour response to PD-L1 blockade by contributing to exclusion of T cells. *Nature* 554, 544–548. doi: 10.1038/nature25501

Mayakonda, A., Lin, D. C., Assenov, Y., Plass, C., and Koeffler, H. P. (2018). Maftools: efficient and comprehensive analysis of somatic variants in cancer. *Genome Res.* 28, 1747–1756. doi: 10.1101/gr.239244.118

McGrail, D. J., Pilié, P. G., Rashid, N. U., Voorwerk, L., Slagter, M., Kok, M., et al. (2021). High tumor mutation burden fails to predict immune checkpoint blockade response across all cancer types. *Ann. Oncol.* 32, 661–672. doi: 10.1016/j.annonc.2021.02.006

Morris, P. G., and Lassman, A. B. (2010). Medical oncology: optimizing chemotherapy and radiotherapy for anaplastic glioma. *Nat. Rev. Clin. Oncol.* 7, 428–430. doi: 10.1038/nrclinonc.2010.98

Motzer, R. J., Escudier, B., McDermott, D. F., George, S., Hammers, H. J., Srinivas, S., et al. (2015). Nivolumab versus everolimus in advanced renal-cell carcinoma. *N. Engl. J. Med.* 373, 1803–1813. doi: 10.1056/NEJMoa1510665

Nanda, R., Chow, L. Q. M., Dees, E. C., Berger, R., Gupta, S., Geva, R., et al. (2016). Pembrolizumab in patients with advanced triple-negative breast cancer: phase Ib KEYNOTE-012 study. *J. Clin. Oncol.* 34, 2460–2467. doi: 10.1200/JCO.2015.64.8931

Noman, M. Z., Desantis, G., Janji, B., Hasmim, M., Karray, S., Dessen, P., et al. (2014). PD-L1 is a novel direct target of HIF-1α, and its blockade under hypoxia enhanced MDSC-mediated T cell activation. *J. Exp. Med.* 211, 781–790. doi: 10.1084/jem.20131916

Omuro, A., and DeAngelis, L. M. (2013). Glioblastoma and other malignant gliomas: a clinical review. *JAMA* 310, 1842–1850. doi: 10.1001/jama.2013.280319

Ostrom, Q. T., Bauchet, L., Davis, F. G., Deltour, I., Fisher, J. L., Langer, C. E., et al. (2014). The epidemiology of glioma in adults: a "state of the science" review. *Neuro Oncol.* 16, 896–913.

Overacre-Delgoffe, A. E., Chikina, M., Dadey, R. E., Yano, H., Brunazzi, E. A., Shayan, G., et al. (2017). Interferon-γ drives T fragility to promote anti-tumor immunity. *Cell* 169, 1130–1141.e11. doi: 10.1016/j.cell.2017.05.005

Pitt, J. M., Vétizou, M., Daillère, R., Roberti, M. P., Yamazaki, T., Routy, B., et al. (2016). Resistance mechanisms to immune-checkpoint blockade in cancer: tumor-intrinsic and -extrinsic factors. *Immunity* 44, 1255–1269. doi: 10.1016/j.immuni.2016.06.001

Powles, T., Eder, J. P., Fine, G. D., Braiteh, F. S., Loriot, Y., Cruz, C., et al. (2014). MPDL3280A (anti-PD-L1) treatment leads to clinical activity in metastatic bladder cancer. *Nature* 515, 558–562. doi: 10.1038/nature13904

Qian, B.-Z., and Pollard, J. W. (2010). Macrophage diversity enhances tumor progression and metastasis. *Cell* 141, 39–51. doi: 10.1016/j.cell.2010.03.014

Qiu, H., Li, Y., Cheng, S., Li, J., He, C., and Li, J. (2020). A prognostic microenvironment-related immune signature via ESTIMATE (PROMISE Model) predicts overall survival of patients with glioma. *Front. Oncol.* 10:580263. doi: 10.3389/fonc.2020.580263

Raychaudhuri, B., Rayman, P., Ireland, J., Ko, J., Rini, B., Borden, E. C., et al. (2011). Myeloid-derived suppressor cell accumulation and function in patients with newly diagnosed glioblastoma. *Neuro Oncol.* 13, 591–599. doi: 10.1093/neuonc/nor042

Restifo, N. P., Smyth, M. J., and Snyder, A. (2016). Acquired resistance to immunotherapy and future challenges. *Nat. Rev. Cancer* 16, 121–126. doi: 10.1038/nrc.2016.2

Ritchie, M. E., Phipson, B., Wu, D., Hu, Y., Law, C. W., Shi, W., et al. (2015). limma powers differential expression analyses for RNA-sequencing and microarray studies. *Nucleic Acids Res.* 43:e47. doi: 10.1093/nar/gkv007

Rosenberg, J. E., Hoffman-Censits, J., Powles, T., van der Heijden, M. S., Balar, A. V., Necchi, A., et al. (2016). Atezolizumab in patients with locally advanced and metastatic urothelial carcinoma who have progressed following treatment with platinum-based chemotherapy: a single-arm, multicentre, phase 2 trial. *Lancet* 387, 1909–1920. doi: 10.1016/S0140-6736(16)00561-4

Rugo, H. S., Delord, J.-P., Im, S.-A., Ott, P. A., Piha-Paul, S. A., Bedard, P. L., et al. (2018). Safety and antitumor activity of pembrolizumab in patients with estrogen receptor-positive/human epidermal growth factor receptor 2-negative advanced breast cancer. *Clin. Cancer Res.* 24, 2804–2811. doi: 10.1158/1078-0432.CCR-17-3452

Salmon, H., Franciszkiewicz, K., Damotte, D., Dieu-Nosjean, M.-C., Validire, P., Trautmann, A., et al. (2012). Matrix architecture defines the preferential localization and migration of T cells into the stroma of human lung tumors. *J. Clin. Invest.* 122, 899–910. doi: 10.1172/JCI45817

Sampson, J. H., Gunn, M. D., Fecci, P. E., and Ashley, D. M. (2020). Brain immunology and immunotherapy in brain tumours. *Nat. Rev. Cancer* 20, 12–25. doi: 10.1038/s41568-019-0224-7

Saraiva, M., and O'Garra, A. (2010). The regulation of IL-10 production by immune cells. *Nat. Rev. Immunol.* 10, 170–181. doi: 10.1038/nri2711

Sawant, D. V., Yano, H., Chikina, M., Zhang, Q., Liao, M., Liu, C., et al. (2019). Adaptive plasticity of IL-10 and IL-35 T cells cooperatively promotes tumor T cell exhaustion. *Nat. Immunol.* 20, 724–735. doi: 10.1038/s41590-019-0346-9

Shen, S., Chen, L., Liu, J., Yang, L., Zhang, M., Wang, L., et al. (2020). Current state and future of co-inhibitory immune checkpoints for the treatment of glioblastoma. *Cancer Biol. Med.* 17, 555–568. doi: 10.20892/j.issn.2095-3941.2020.0027

Shigeoka, M., Urakawa, N., Nakamura, T., Nishio, M., Watajima, T., Kuroda, D., et al. (2013). Tumor associated macrophage expressing CD204 is associated with tumor aggressiveness of esophageal squamous cell carcinoma. *Cancer Sci.* 104, 1112–1119. doi: 10.1111/cas.12188

Sica, A., Schioppa, T., Mantovani, A., and Allavena, P. (2006). Tumour-associated macrophages are a distinct M2 polarised population promoting tumour progression: potential targets of anti-cancer therapy. *Eur. J. Cancer* 42, 717–727. doi: 10.1016/j.ejca.2006.01.003

Siegel, R. L., Miller, K. D., and Jemal, A. (2019). Cancer statistics, 2019. *CA Cancer J. Clin.* 69, 7–34. doi: 10.3322/caac.21551

Spranger, S., Spaapen, R. M., Zha, Y., Williams, J., Meng, Y., Ha, T. T., et al. (2013). Up-regulation of PD-L1, IDO, and T(regs) in the melanoma tumor microenvironment is driven by CD8(+) T cells. *Sci. Transl. Med.* 5:200ra116. doi: 10.1126/scitranslmed.3006504

Sullivan, J. A., Tomita, Y., Jankowska-Gan, E., Lema, D. A., Arvedson, M. P., Nair, A., et al. (2020). Treg-cell-derived IL-35-coated extracellular vesicles promote infectious tolerance. *Cell Rep.* 30, 1039–1051.e5. doi: 10.1016/j.celrep.2019.12.081

Syed, V. (2016). TGF-β signaling in cancer. *J. Cell. Biochem.* 117, 1279–1287. doi: 10.1002/jcb.25496

Varvel, N. H., Neher, J. J., Bosch, A., Wang, W., Ransohoff, R. M., Miller, R. J., et al. (2016). Infiltrating monocytes promote brain inflammation and exacerbate neuronal damage after status epilepticus. *Proc. Natl. Acad. Sci. U.S.A.* 113, E5665–E5674. doi: 10.1073/pnas.1604263113

Veldhoen, M. (2017). Interleukin 17 is a chief orchestrator of immunity. *Nat. Immunol.* 18, 612–621. doi: 10.1038/ni.3742

Vesely, M. D., and Schreiber, R. D. (2013). Cancer immunoediting: antigens, mechanisms, and implications to cancer immunotherapy. *Ann. N. Y. Acad. Sci.* 1284, 1–5. doi: 10.1111/nyas.12105

Wagner, G. P., Kin, K., and Lynch, V. J. (2012). Measurement of mRNA abundance using RNA-seq data: RPKM measure is inconsistent among samples. *Theory Biosci.* 131, 281–285. doi: 10.1007/s12064-012-0162-3

Wei, L., Li, L., Liu, L., Yu, R., Li, X., and Luo, Z. (2021). Knockdown of annexin-A1 inhibits growth, migration and invasion of glioma cells by suppressing the PI3K/Akt signaling pathway. *ASN Neuro* 13:17590914211001218. doi: 10.1177/17590914211001218

Weller, M., Butowski, N., Tran, D. D., Recht, L. D., Lim, M., Hirte, H., et al. (2017). Rindopepimut with temozolomide for patients with newly diagnosed, EGFRvIII-expressing glioblastoma (ACT IV): a randomised, double-blind, international phase 3 trial. *Lancet Oncol.* 18, 1373–1385. doi: 10.1016/s1470-2045(17)30517-x

Weller, M., Wick, W., Aldape, K., Brada, M., Berger, M., Pfister, S. M., et al. (2015). Glioma. *Nat. Rev. Dis. Primers* 16:15017. doi: 10.1038/nrdp.2015.17

Woroniecka, K., Chongsathidkiet, P., Rhodin, K., Kemeny, H., Dechant, C., Farber, S. H., et al. (2018). T-cell exhaustion signatures vary with tumor type and are severe in glioblastoma. *Clin. Cancer Res.* 24, 4175–4186. doi: 10.1158/1078-0432.Ccr-17-1846

Xiao, K., Liu, Q., Peng, G., Su, J., Qin, C. Y., and Wang, X. Y. (2020). Identification and validation of a three-gene signature as a candidate prognostic biomarker for lower grade glioma. *PeerJ* 8:e8312. doi: 10.7717/peerj.8312

Xiong, Y., Li, M., Bai, J., Sheng, Y., and Zhang, Y. (2021). High level of METTL7B indicates poor prognosis of patients and is related to immunity in glioma. *Front. Oncol.* 11:650534. doi: 10.3389/fonc.2021.650534

Yan, H., Parsons, D. W., Jin, G., McLendon, R., Rasheed, B. A., Yuan, W., et al. (2009). IDH1 and IDH2 mutations in gliomas. *N. Engl. J. Med.* 360, 765–773. doi: 10.1056/NEJMoa0808710

Yu, G., Wang, L. G., Han, Y., and He, Q. Y. (2012). clusterProfiler: an R package for comparing biological themes among gene clusters. *Omics* 16, 284–287. doi: 10.1089/omi.2011.0118

Yu, H., Pardoll, D., and Jove, R. (2009). STATs in cancer inflammation and immunity: a leading role for STAT3. *Nat. Rev. Cancer* 9, 798–809.

Zeng, D., Li, M., Zhou, R., Zhang, J., Sun, H., Shi, M., et al. (2019). Tumor microenvironment characterization in gastric cancer identifies prognostic and immunotherapeutically relevant gene signatures. *Cancer Immunol. Res.* 7, 737–750. doi: 10.1158/2326-6066.CIR-18-0436

Zhang, B., Wu, Q., Li, B., Wang, D., Wang, L., and Zhou, Y. L. (2020). m(6)A regulator-mediated methylation modification patterns and tumor microenvironment infiltration characterization in gastric cancer. *Mol. Cancer* 19:53. doi: 10.1186/s12943-020-01170-0

Conflict of Interest: The authors declare that the research was conducted in the absence of any commercial or financial relationships that could be construed as a potential conflict of interest.

Publisher's Note: All claims expressed in this article are solely those of the authors and do not necessarily represent those of their affiliated organizations, or those of the publisher, the editors and the reviewers. Any product that may be evaluated in this article, or claim that may be made by its manufacturer, is not guaranteed or endorsed by the publisher.

Copyright © 2021 Zhang, Guo, Su, Luo, Tan, Xu, Ye, Tong, Liu, Li, Chen and Tian. This is an open-access article distributed under the terms of the Creative Commons Attribution License (CC BY). The use, distribution or reproduction in other forums is permitted, provided the original author(s) and the copyright owner(s) are credited and that the original publication in this journal is cited, in accordance with accepted academic practice. No use, distribution or reproduction is permitted which does not comply with these terms.

frontiers in Cell and Developmental Biology

ORIGINAL RESEARCH
published: 29 October 2021
doi: 10.3389/fcell.2021.721897

Prognosis and Immunotherapy Significances of a Cancer-Associated Fibroblasts-Related Gene Signature in Gliomas

Zhimin Chen[1†], Shenghua Zhuo[2†], Guiying He[3†], Jingzhi Tang[1], Weijie Hao[1], Wei-Qiang Gao[1], Kun Yang[2] and Huiming Xu[1]**

[1] State Key Laboratory of Oncogenes and Related Genes, Renji-MedX Clinical Stem Cell Research Center, Ren Ji Hospital, School of Medicine, Shanghai Jiao Tong University, Shanghai, China, [2] Department of Neurosurgery, The First Affiliated Hospital of Hainan Medical University, Haikou, China, [3] Department of Neurology, Shenzhen Nanshan People's Hospital, The 6th Affiliated Hospital of Shenzhen University Health Science Center, Shenzhen, China

OPEN ACCESS

Edited by:
Xuejun Sun,
Xi'an Jiaotong University, China

Reviewed by:
Bo Xia,
New York University, United States
Renyuan Zhang,
University at Buffalo, United States

***Correspondence:**
Kun Yang
chbyk1379@163.com
Huiming Xu
quxuhm123@163.com

[†] These authors have contributed equally to this work

Specialty section:
This article was submitted to Molecular and Cellular Pathology, a section of the journal Frontiers in Cell and Developmental Biology

Received: 07 June 2021
Accepted: 22 September 2021
Published: 29 October 2021

Citation:
Chen Z, Zhuo S, He G, Tang J, Hao W, Gao W-Q, Yang K and Xu H (2021) Prognosis and Immunotherapy Significances of a Cancer-Associated Fibroblasts-Related Gene Signature in Gliomas. Front. Cell Dev. Biol. 9:721897. doi: 10.3389/fcell.2021.721897

As a cold tumor, malignant glioma has strong immunosuppression and immune escape characteristics. The tumor microenvironment (TME) provides the "soil" for the survival of malignant tumors, and cancer-associated fibroblasts (CAFs) are the architects of matrix remodeling in TME. Therefore, CAFs have potent regulatory effects on the recruitment and functional differentiation of immune cells, whereby they synthesize and secrete numerous collagens, cytokines, chemokines, and other soluble factors whose interaction with tumor cells creates an immunosuppressive TME. This consequently facilitates the immune escape of tumor cells. Targeting CAFs would improve the TME and enhance the efficacy of immunotherapy. Thus, regulation of CAFs and CAFs-related genes holds promise as effective immunotherapies for gliomas. Here, by analyzing the Chinese Glioma Genome Atlas and the Cancer Genome Atlas database, the proportion of CAFs in the tumor was revealed to be associated with clinical and immune characteristics of gliomas. Moreover, a risk model based on the expression of CAFs-related six-gene for the assessment of glioma patients was constructed using the least absolute shrinkage and selection operator and the results showed that a high-risk group had a higher expression of the CAFs-related six-genes and lower overall survival rates compared with those in the low-risk group. Additionally, patients in the high-risk group exhibited older age, high tumor grade, isocitrate dehydrogenase wildtype, 1p/19q non-codeletion, O-6-methylguanine-DNA methyltransferase promoter unmethylation and poor prognosis. The high-risk subtype had a high proportion CAFs in the TME of glioma, and a high expression of immune checkpoint genes. Analysis of the Submap algorithm indicated that the high-risk patients could show potent response to anti-PD-1 therapy. The established risk prediction model based on the expression of six CAFs-related genes has application prospects as an independent prognostic indicator and a predictor of the response of patients to immunotherapy.

Keywords: glioma, cancer-associated fibroblasts, tumor microenvironment, immunotherapy, prognosis, risk score

INTRODUCTION

Glioma is the most common form of a primary malignant brain tumor in adults. In particular, glioblastoma (GBM) is one of the most lethal and highly aggressive cancer, associated with low survival, less than 1 year (Lapointe et al., 2018). Although current evidence indicates surgical resection as the main treatment approach for gliomas, postoperative radiotherapy, and chemotherapy can also be administered according to the specific condition of patients. However, most gliomas are difficult to completely be removed by surgery without affecting normal brain functions due to the growth properties and its special local anatomy characteristics. Some patients also do not respond well to radiotherapy and chemotherapy, and consequently, develop rapid recurrence after standard therapy (Tan et al., 2020). Despite recent progress in the development of new drugs, researchers are facing challenges in developing therapeutics for gliomas due to biological properties, including the blood-brain barrier, tumor specificity of gliomas, and immune environments (Aldape et al., 2019).

The tumor microenvironment (TME), as the "soil" for tumor survival, is crucial for tumor survival and is closely associated with the malignant behavior of tumor cells equivalent to "seed." Compelling evidence shows that tumor cells interact with the extracellular matrix (ECM), immune cells, chemokines, and cytokines to create a favorable microenvironment for the proliferation and metastasis of tumors (Maman and Witz, 2018). The microenvironment of different tumors is diverse. For instance, in glioma, tumors can cooperate with peritumoral cells through chemokines and cytokines, direct contact, extracellular vesicles, nanotubes and microtubules, to promote tumor proliferation, brain invasion, angiogenesis and immunosuppression. This consequently creates a microenvironment conducive to the growth of malignant tumors (Broekman et al., 2018). Therefore, an in-depth understanding of the interactions between tumor cells and peritumoral cells may provide a new perspective to managing gliomas.

Interestingly, cancer-associated fibroblasts (CAFs) are an important component of stromal cells in TME and an "architect" of matrix remodeling, which are closely related to the prognosis of solid tumors (Cox, 2021). In TME, CAFs play a key role in the induction of Epithelial-mesenchymal Transition (EMT), and the maintenance of the pool of cancer stem cells and drug resistance by interacting with tumor cells and immune cells and releasing a variety of soluble factors (Su et al., 2018; Erin et al., 2020). Moreover, CAFs regulate tumor immunity and promote immune escape and resistance to cancer immunotherapy (Liu et al., 2019a). Therefore, targeting CAFs would not only inhibit the "seed" of cancer but also transform the "soil" into a microenvironment that inhibits tumor growth, and consequently transform the "enemy" that promotes tumor progression into a "friend" that inhibits tumor growth or metastasis (Chen and Song, 2019). Also, CAFs are activated to different degrees at different stages of tumor development. Studies have shown that different cytokines secreted by CAFs can play a pro-cancer or anti-cancer role (Liu et al., 2019b; Wang et al., 2021).

It is also noteworthy that because glioma is a "cold " tumor, immunotherapy has poor efficacy against the malignancy (Jackson et al., 2019). As such, to improve the efficacy of immunotherapy, transforming the "cold" environment into a "hot" one without causing neurotoxicity is imperative. Additionally, novel immunotherapeutic approaches, including oncolytic virus and adoptive T cell therapy, may exploit the T cell response to overcome the "cold" state of glioma, such as GBM (Buerki et al., 2018). Intriguingly, CAFs are co-expressed with the Fibroblast Activation Protein α (FAPα) and the Platelet-derived Growth Factor Receptor (PDGFR), which are the main components of stromal cells in GBM. Oncolytic adenoviruses have also been shown to specifically target GBM cells and CAFs (Li et al., 2020).

Cancer-associated fibroblasts are highly heterogeneous in terms of tissue origin, phenotype and function (Louault et al., 2020), but their function in the glioma microenvironment is yet to be fully elucidated. In the present study, we analyzed the sequencing data of glioma cohorts from the Chinese Glioma Genome Atlas (CGGA) database by the Estimate Proportion of Immune and Cancer cells (EPIC) algorithm (Racle et al., 2017; Liu et al., 2020), which is a common method to analyze the cell types based on the gene expression profile of the different type of cells, to quantify the expression of CAFs, then further analyze the relationship among CAFs and clinical features, tumor purity, immune score, stromal score, ESTIMATE score and stemness score of gliomas. Differentially expressed genes related to prognosis in the high and low expression subtypes of CAFs were also screened. Moreover, the risk scores of gliomas were assessed according to the expression of six genes identified as independent prognostic factors via the Least Absolute Shrinkage and Selection Operator (LASSO) regression analysis and validated in the Cancer Genome Atlas (TCGA) database. The established risk signature containing six CAFs-related-genes strongly correlates with the clinical and immune characteristics of glioma, including immune cells, immune checkpoints, and immunotherapy.

MATERIALS AND METHODS

Data Collection

The RNA sequencing datasets [mRNAseq_693, mRNAseq_325 and mRNA sequencing (non-glioma as a control)] and the corresponding clinical and molecular information, including sex, age, grade, IDH status, 1p/19q status, MGMT promoter, and survival status information, were retrieved from the CGGA database[1] (Zhao et al., 2021). The data were categorized into the training cohort [including 625 cases of low-grade gliomas (LGG) and 388 cases of GBM] and the testing cohort (comprising transcriptome data from 698 cases of gliomas in TCGA database from the Genomic Data Commons Data Portal (GDC).[2] Additionally, the FPKM data was converted into TPM for subsequent analysis. The mRNAseq_693 and mRNAseq_325

[1]http://www.cgga.org.cn/

[2]https://portal.gdc.cancer.gov/

data were merged into one metadata set, and batch effects were removed using the combat function in the SVA R package.

Quantification of Different Cell Types in the Tumor Microenvironment

Estimate Proportion of Immune and Cancer cells (Racle et al., 2017) is an effective algorithm used to simultaneously estimate the proportion of cancer and immune cell types according to the gene expression in tumors based on a unique set of RNA-seq reference gene expression profiles described previously (Tirosh et al., 2016). It allows for accurate prediction of the proportion of cancer and non-malignant cell types even in the absence of *a priori* information about cancer cells. In this study, the reference profiles from tumor-infiltrating cells were used as the parameter, whereas the TPM data of CGGA glioma were used as input data. The proportion of CAF was estimated using the R package "EPIC" to explore the changes of matrix components in gliomas. CIBERSORT is a tool that deconvolutes the expression matrix of human immune cell subtypes based on the principle of linear support vector regression. Researchers also apply this tool to determine immune cell composition, which comprises 22 immune cell subtypes, based on the specific gene expression data of the cells (Newman et al., 2015). We analyzed gene expression data with standard annotation using CIBERSORT source code in relative mode. The algorithm was run using the LM22 signature and 100 permutations. For each sample, the final CIBERSORT output estimates were normalized to sum to one such that it could be interpreted directly as cell fractions for comparison across different immune cell types and datasets. Immune infiltration analysis based on a single-sample gene set enrichment analysis (ssGSEA) score can also be employed to explore the degree of immune infiltration of gliomas. It defines an enrichment score representing the absolute degree of enrichment of the gene set in each sample in each dataset. ssGSEA-based evaluation of the level of immune infiltration in a sample according to the expression levels of immune cell-specific marker genes demonstrated the immune infiltration landscape of gliomas (Bindea et al., 2013). The ESTIMATE package was used to estimate tumor immune score and tumor purity (Yoshihara et al., 2013). The stemness index of glioma was calculated according to the expression of tumor stem cell genes (Miranda et al., 2019). Submap[3] algorithms (Hoshida et al., 2007) were further utilized to predict the clinical response to immune checkpoint blocking therapy for PD-1 and CTLA4 in the low-and high-risk score groups. P-value < 0.05 denoted statistical significance.

Identification of Risk Genes and Calculation of Risk Score

Data were grouped into high subtype and low subtype according to the median value of CAFs. This was followed by the analysis of the differences between the mRNAseq_325 and mRNAseq_693 CGGA data. Differentially expressed genes (DEGs) were obtained according to a fold change (logFC) > 1.5 and $P < 0.05$. Genes with $P < 0.001$ and genes associated with prognosis were screened through univariate Cox regression analysis. A total of 329 genes were identified from mRNAseq_325 and 116 from the mRNAseq_693 CGGA database. Crossing the two sets of genes yielded 104 genes. Furthermore, multivariate Cox regression analysis was performed to identify 11 genes related to glioma overall survival (OS) ($P < 0.001$). Subsequently, LASSO analysis was employed, to minimize the risk of overfitting a prognostic model and construct a risk model (Tibshirani, 1997). The LASSO was utilized for variable selection and shrinkage via the "glmnet" package in R software (Simon et al., 2011). The independent variable in the regression was the normalized expression matrix of candidates for prognostic factors. The response variable was the OS time and state of the patients in the CGGA cohort. The penalty parameter (λ) of the model was constructed through tenfold cross-validations, followed by the minimum criteria (i.e., the value of λ corresponding to the lowest partial likelihood deviance). The risk score of the patients was calculated according to the normalized expression level of the prognostic gene signature and their corresponding regression coefficients according to the formula: risk score = $e^{\text{sum(each gene's expression} \times \text{corresponding coefficient)}}$. Finally, patients were divided into high and low risk groups according to the median risk score.

Establishment of the Nomogram

The nomogram incorporated age, grade, 1p/19q status based on the CGGA cohort. The prognostic risk score model was established via the "RMS" package in R. The consistency between predicted survival rate and actual survival rate using time-dependent calibration curves, and verified in the TCGA cohort. The concordance index (C index) was calculated to evaluate the effectiveness of the model in prognosis prediction. The C index ranged between 0.5 and 1.0; notably, a higher index denoted the better the performance of the model in predicting survival rate.

Functional Enrichment Analysis

Spearman's correlation analysis was used to reveal the genes associated with the risk score; here, the correlation coefficient ≥ 0.4 was selected. Genes related to risk scores were sorted according to the calculated correlation coefficient. Next, Gene Set Enrichment Analysis (GSEA) was performed with the "clusterProfiler" R package (Yu et al., 2012), using "h.all.v7.0.entrez.gmt" as a reference gene set. P values were adjusted using the Benjamini and Hochberg methods. P-value < 0.05 implied statistically significant differences. Lastly, the results of the first five enrichment analysis were visualized using "enrichplot" and "ggplot2" (Wickham, 2016) R software package.

Statistical Analysis

Patients in the CGGA training and TCGA validation cohorts were categorized into the high- and low-risk subtypes according to the median risk score. Wilcoxon rank-sum test was applied to compare the high- and low-risk subtypes. Differences among three or more subtypes of patients were tested using the K-W test. Kaplan-Meier analysis and log-rank test were employed to analyze survival rates between low-risk and high-risk subtypes. Univariate and multivariate Cox regression analyses identified

[3]https://cloud.genepattern.org/gp

the independent factors associated with the OS of glioma. All statistical analyses were conducted in R software (version 4.0.3), and $P < 0.05$ denoted statistical significance ($^{*}P < 0.05$, $^{**}P < 0.01$, $^{***}P < 0.001$, $^{****}P < 0.0001$).

RESULTS

Cancer-Associated Fibroblasts Are Closely Related to the Clinical Progression of Gliomas

A detailed flow chart of this analysis is shown in **Figure 1**. Using EPIC, the proportion of CAFs was calculated in different glioma samples in the CGGA cohort. The mRNAseq_693 and mRNAseq_325 datasets in the CGGA cohort were merged and batch discrepancies were eliminated. Subsequently, the proportion of CAFs was calculated in gliomas in the training cohort. Patients were then stratified into high and low CAFs subtypes according to the median of CAFs. The prognosis of the high-CAFs subtype was worse than the low-CAFs subtype (log-rank, $P < 0.0001$; **Figure 2A**). According to the WHO (2016) grading guidelines, patients with high CAFs showed poor prognosis in Oligodendroglioma with IDH mutation and 1p/19q co-deletion, Astrocytoma with IDH mutant, Astrocytoma with IDH wildtype, GBM with IDH mutant, and GBM with IDH wildtype (**Supplementary Figure 1**). In addition, both univariate and multivariate Cox regression analyses verified that the proportion of CAFs is an independent risk predictor for gliomas (**Figures 2B,C**). On the other hand, the high proportion of CAF is mainly enriched in glioma patients with higher age ($P < 0.0001$), high WHO grade ($P < 0.001$), IDH wildtype status ($P < 0.001$), 1p/19q non-codeletion status ($P < 0.001$), and MGMT promoter un-methylated status ($P < 0.01$). However, CAFs did not differ between genders (**Figures 2D–I**). To eliminate the effect of data consolidation in mRNAseq_693 and mRNAseq_325 datasets, the proportion of CAFs in both datasets was calculated, respectively, which yielded a similar result to the merged dataset (**Supplementary Figure 2**). Results suggest that the proportion of CAFs is of promise as an independent predictor for the prognosis and progression of gliomas.

A High Proportion of Cancer-Associated Fibroblasts Is Associated With Immune Landscape and Stemness of Gliomas

Cancer-associated fibroblasts as the architect of matrix remodeling in TME may affect cell components of TME and promote progression of tumor malignancy. In this study, the ESTIMATE and GSVA packages in R were used to estimate tumor purity, immune score, stromal score, ESTIMATE score, and stemness score of gliomas in the CGGA cohort. A high proportion of CAFs was revealed to be associated with the glioma patients with low tumor purity, high stromal score, high ESTIMATE score, and high stemness score ($P < 0.0001$; **Figures 2J–N**). At the same time, the prognosis of glioma patients characterized by low tumor purity, high immune score, high stromal score, high ESTIMATE score, and high stemness score was poor ($P < 0.0001$, **Supplementary Figures 3A–E**). The findings suggest the association of low tumor purity, high immune score, high stromal score, high ESTIMATE score, and high stemness score with a high proportion of CAFs and the OS of glioma patients.

Construction of Prognostic Gene Signatures of Cancer-Associated Fibroblasts Which Are Related to the Status Gliomas

After calculating the proportion of CAFs in the CGGA mRNAseq_693 and mRNAseq_325 cohorts, the training cohorts were stratified into high and low subtypes according to the median of CAFs. Subsequently, univariate Cox regression analysis was conducted on both datasets of DEGs to screen for genes related to prognosis (with $P < 0.001$). Through a crossover analysis of the two DEGs sets, 104 genes were obtained. Eleven genes related to the total survival of glioma patients were obtained via multivariate Cox regression analysis ($P < 0.001$). The risk of overfitting was minimized using the LASSO regression algorithm. The risk score was calculated according to the expression level and regression coefficient of six genes (ABCC3, CTHRC1, MSR1, PDLIM1, TNFRSF12A, and CHI3L2) (**Figures 3A,B**). The risk score = (ABCC3 × 0.00530703547540297) + (PDLIM1 × 0.00158225241997429) + (CHI3L2 × 0.0000527762285183538) + (MSR1 × 0.00118065457455651) + (CTHRC1 × 0.00479963348819953) + (TNFRSF12A × 0.00212454022154963). The formula was also used to calculated risk scores for the glioma patients in the TCGA validation cohorts. Of note, the six genes associated with the risk of glioma were highly expressed in the high-risk group (**Figure 3C**). There were significant differences in risk scores among patients with different ages in terms of first diagnosis ($P < 0.001$), WHO grade ($P < 0.0001$), IDH ($P < 0.0001$), 1p/19q ($P < 0.0001$) and MGMT promoter ($P < 0.001$). These six genes were also mainly highly expressed in high-grade glioma and IDH wildtype groups (**Supplementary Figures 4A–L**). These results strongly demonstrated that the risk model, based on the six genes is closely associated with the clinical progression of glioma, therefore, could be employed as a risk prediction model for glioma.

Survival Analysis and Pathological Features Between High- and Low-Risk Patients

Kaplan-Meier analysis showed that the OS of the high-risk subtype was worse compared to that of the low-risk subtype ($P < 0.0001$; **Figure 4A**). Additionally, the risk score was related to a prognostic value in gliomas, stratified according to the WHO guidelines (2016) for the grading of tumors. The high-risk subtype was related to the low OS of the patients with Oligodendroglioma with IDH mutant and 1p/19q co-deletion, Astrocytoma with IDH mutant, Astrocytoma with IDH wildtype, GBM with IDH mutant, and GBM with IDH wildtype (**Supplementary Figure 5**). Next, we performed a multivariate Cox regression analysis of the risk score and clinical-pathological

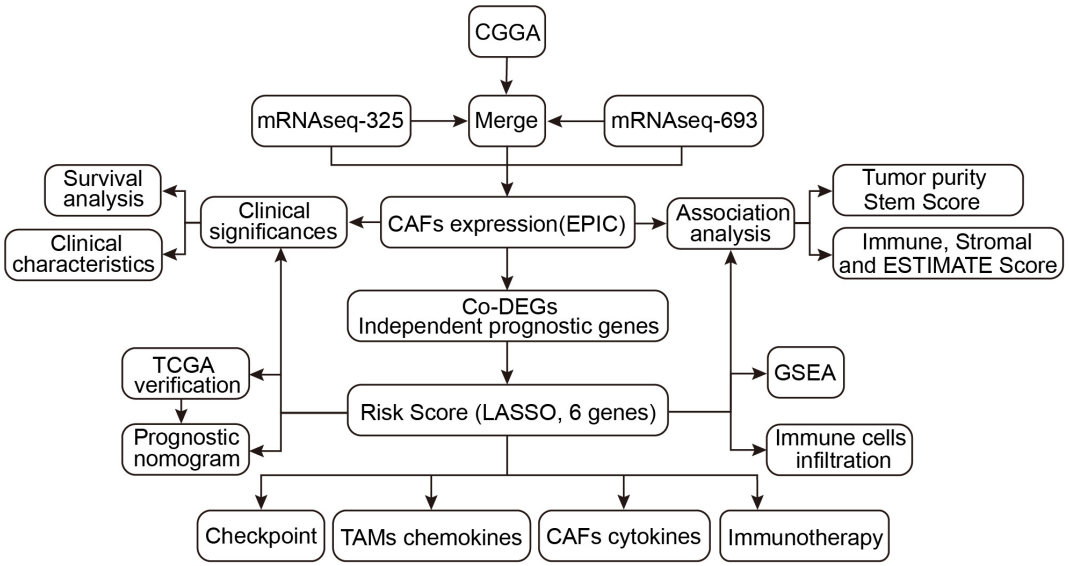

FIGURE 1 | Flowchart of the study.

features of glioma patients. Results demonstrated that risk score is an independent risk factor to predict the OS in patients with glioma (HR = 1.731, 95% CI = 1.341–2.237, $P < 0.001$; **Figure 4B**). The heatmap showed that high glioma mortality is related to an increased risk score (**Figure 4C**). Furthermore, through ROC curve analysis, the accuracy of risk score as a prognostic factor for glioma was validated. Results showed that the risk score could predict the OS of the CGGA cohorts (5-year, AUC = 0.789). Of note, higher CAFs (AUC = 0.7994), tumor histology (AUC = 0.7822), IDH status (AUC = 0.8066), 1p/19q status (AUC = 0.8163) and MGMT promotor status (AUC = 0.5641) was shown in the high-risk group than in the lower group (**Figures 4D–I**). Moreover, glioma data from TCGA was utilized to validate the risk score. The LASSO regression analysis was performed on the TCGA data to calculate the patients' risk scores using similar regression coefficients. Subsequently, K-M survival analysis of the TCGA data was performed to assess the risk model. Results demonstrated lower OS in the high-risk subtype than that in the low-risk subtype (**Supplementary Figure 6A**). Univariate Cox regression analysis was conducted to explore the prognostic value of the risk score. Results showed a significant correlation of the risk score with OS in TCGA LGG-GBM (HR = 4.255, 95% CI = 3.538–5.117, $P < 0.001$, **Supplementary Figure 6B**). Moreover, multivariate Cox regression analysis demonstrated that the risk score was an independent prognostic indicator (HR = 1.888, 95% CI = 1.438–2.4, $P < 0.001$, **Supplementary Figure 6C**). ROC curve analysis revealed that the risk model had a strong predictive value for the OS of glioma patients (**Supplementary Figure 6D**). Furthermore, six CAFs-related genes were highly expressed in TCGA LGG-GBM cohorts, particularly in the high-risk subtype (**Supplementary Figure 6E**), consistent with the results of CGGA cohorts. Taken together, the results provided evidence that the high-risk subtype is associated with low OS rate and some clinical-pathological features, therefore, has application prospects as a risk model based on the specific expression of the six genes.

The Risk Model for Individual Prognostic Prediction

Nomogram is a powerful tool used to quantitatively determine individual risk in the clinical setting by integrating various risk factors. Herein, using a six CAFs-related genes signature, a nomogram was constructed based on age, grade, 1p/19q gene deletion status, and risk score to predict the probability of 3- and 5-year OS. Meanwhile, the calculated C index was 0.760. Each factor was graded according to its contribution to OS (**Figure 5A**). The calibration curve showed a consistent actual survival rate with the predicted survival rate (**Figures 5B,C**). The accuracy of the prognostic prediction model was verified in the TCGA cohort, and the calculated C index was 0.844. The correction chart demonstrated that the 3- and 5-year OS corroborated with the predicted values (**Figures 5D,E**). These data demonstrate that the risk model is relatively accurate and can improve the ability to estimate individual prognosis.

The Immune Landscape Between Different Risk Subtypes

To determine the potential biological processes of risk score, Spearman's correlation analysis was performed to identify the genes related to the risk score. Genes with Spearman correlation coefficient ≥ 0.4 were used for GSEA analysis. Results revealed that genes associated with risk score were mainly associated with epithelial-mesenchymal transformation ($P < 0.0001$, $q < 0.0001$), hypoxia ($P < 0.0001$, $q < 0.0001$), inflammation ($P < 0.0001$, $q < 0.0001$), interferon-gamma response ($P < 0.0001$, $q < 0.0001$), and

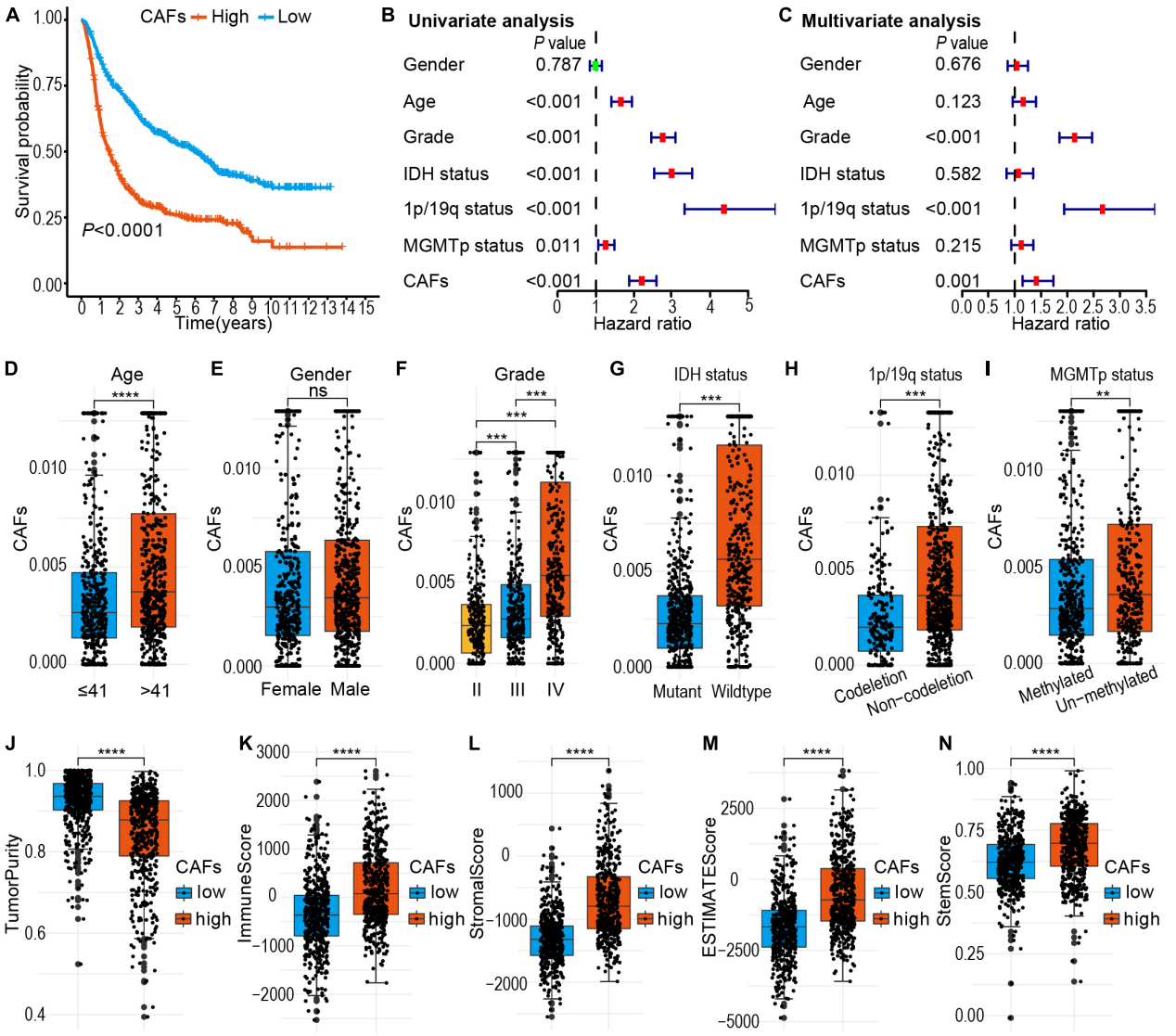

FIGURE 2 | Predictive values of cancer-associated fibroblasts (CAFs) in the survival of glioma patients and its relationship with pathological characteristics. **(A)** Comparison of overall survival between low and high CAFs subtypes in the Chinese Glioma Genome Atlas (CGGA) database. **(B)** Univariate Cox regression analysis. Forest plot of the association between CAFs and glioma survival. **(C)** Multivariate Cox regression analysis showed that the CAFs was an independent predictor of gliomas. **(D–N)** Distribution of the CAFs in patients stratified according to age **(D)**, gender **(E)**, WHO grade **(F)**, isocitrate dehydrogenase (IDH) status **(G)**, 1p/19q status **(H)**, O-6-methylguanine-DNA methyltransferase (MGMT) promoter status **(I)**, Tumor purity **(J)**, Immune score **(K)**, Stromal score **(L)**, ESTIMATE score **(M)**, and Stemness score **(N)**. ****$P < 0.0001$; ***$P < 0.001$; **$P < 0.01$; ns, no significant.

NFkB-mediated TNFα signal transduction ($P < 0.0001$, $q < 0.0001$; **Figure 6A**). Furthermore, the ESTIMATE and GSVA packages in R were employed to estimate tumor purity, immune score, stromal score, ESTIMATE score, stemness score, and the proportion of immune cells in the CGGA cohort. Results showed that the high-risk subtype was associated with a high proportion of CAFs, high stemness score, high stromal score, high immune score, the high ESTIMATE score, and low tumor purity ($P < 0.0001$; **Figure 6B**). In addition, aDC, pDC, iDC, T helper cells, macrophage, Th2 cells, Treg cells, and B cells were rich in high-risk subtype, whereas neutrophil, Th1 cells were rich in low-risk subtypes (**Figure 6B**). To further verify that immunosuppressive cells were mainly enriched in the high-risk group, a histogram was generated and the proportion of immune cells in the CGGA data was calculated via the CIBERSORT algorithm. Results revealed that immunosuppressive cells, including Tregs and M2 macrophages, were mainly concentrated in the high-risk subtype (**Supplementary Figures 7A,B**). Intriguingly, the proportion of immune cells calculated by ssGSEA and the CIBERSORT algorithm showed that $CD4^+$, $CD8^+$ T cells, and NK cells were also enriched in the high-risk subtype (**Supplementary Figure 7C**).

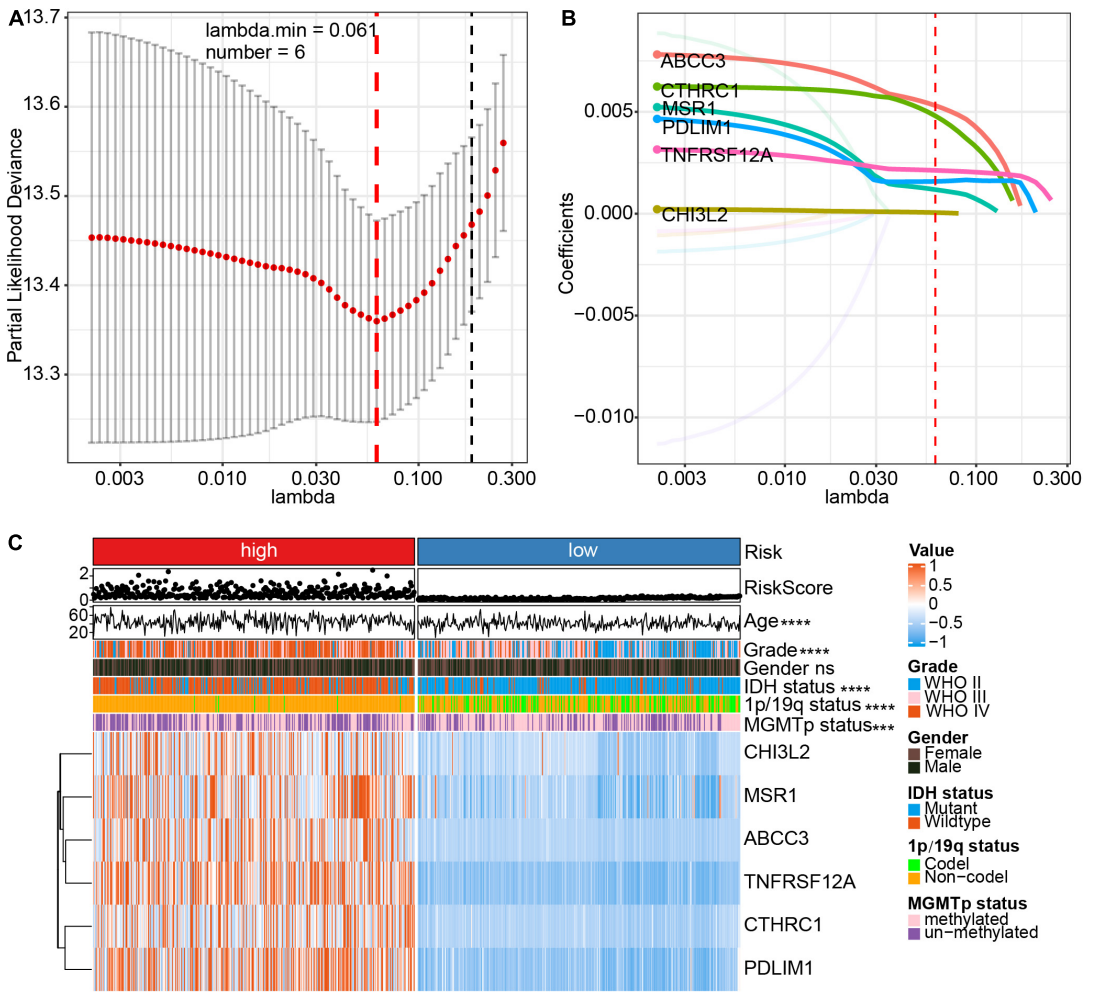

FIGURE 3 | Identification of a CAFs-related six-gene risk signature for overall survival risk characteristics by least absolute shrinkage and selection operator (LASSO) regression analysis in CGGA cohort. **(A)** Cross-validation for tuning parameter (lambda) screening in the LASSO regression model. **(B)** LASSO coefficient spectrum of six genes in gliomas. **(C)** The heatmap shows the association between risk and clinic pathological characteristics of the six-gene risk signature. LASSO, least absolute shrinkage and selection operator. ****$P < 0.0001$; ***$P < 0.001$; ns, no significant.

The Immune Checkpoint Landscape Between Different Risk Subtypes

Previously, T cells and NK cells exhaustion have been demonstrated to potentially facilitate cancer cells to escape host immunity, which is linked to poor prognosis (Gonzalez-Gugel et al., 2016; Zarour, 2016). In the present work, most of these exhaustion markers [TIGIT (Manieri et al., 2017), CEACAM1 (Huang et al., 2015), CTLA4 (Krummel and Allison, 1996; Postow et al., 2015), LAG3 (Ruffo et al., 2019), PD-1 (Ishida et al., 1992; Postow et al., 2015), PD-L1 (Postow et al., 2015), and TIM3 (Huang et al., 2015)] were highly expressed in the high-risk subtype (**Figure 7A**), indicating an elevated level of immune exhaustion in the tumors of high-risk glioma patients. It is well known that CAFs can promote the transformation of M1 macrophages to M2 and induce the secretion of related cytokines to promote tumor invasion, angiogenesis, and change the immune landscape of tumors (Farhood et al., 2019; An et al., 2020). Therefore, we explored the expression of chemokines and cytokines secreted by CAFs in the high-risk subtype and the low-risk subtype. M2 macrophage chemokines (IL10, IL13, CSF1, TGFB1, TGFB2, and TGFB3) were found to be highly positively correlated, whereas M1 macrophage chemokines (HMGB1, TNF) were weakly positively correlated with risk score (Zhang et al., 2021; **Figures 7B,C**). Additionally, analysis of the expression of chemokines and cytokines secreted by CAFs in the high-risk subtype and the low-risk subtype demonstrated that most of the cytokines secreted by CAFs were highly expressed in the high-risk subtype (**Figure 7D**). Patients with a high-risk score exhibited a type I interferon response, type II interferon response, and the activation of pro-inflammatory functions (**Supplementary Figure 7C**). These observations provided evidence that patients with a high-risk score are eligible for and respond to immunotherapy. Furthermore, subclass mapping was applied to compare the expression profile of the high- and low-risk subtypes with another

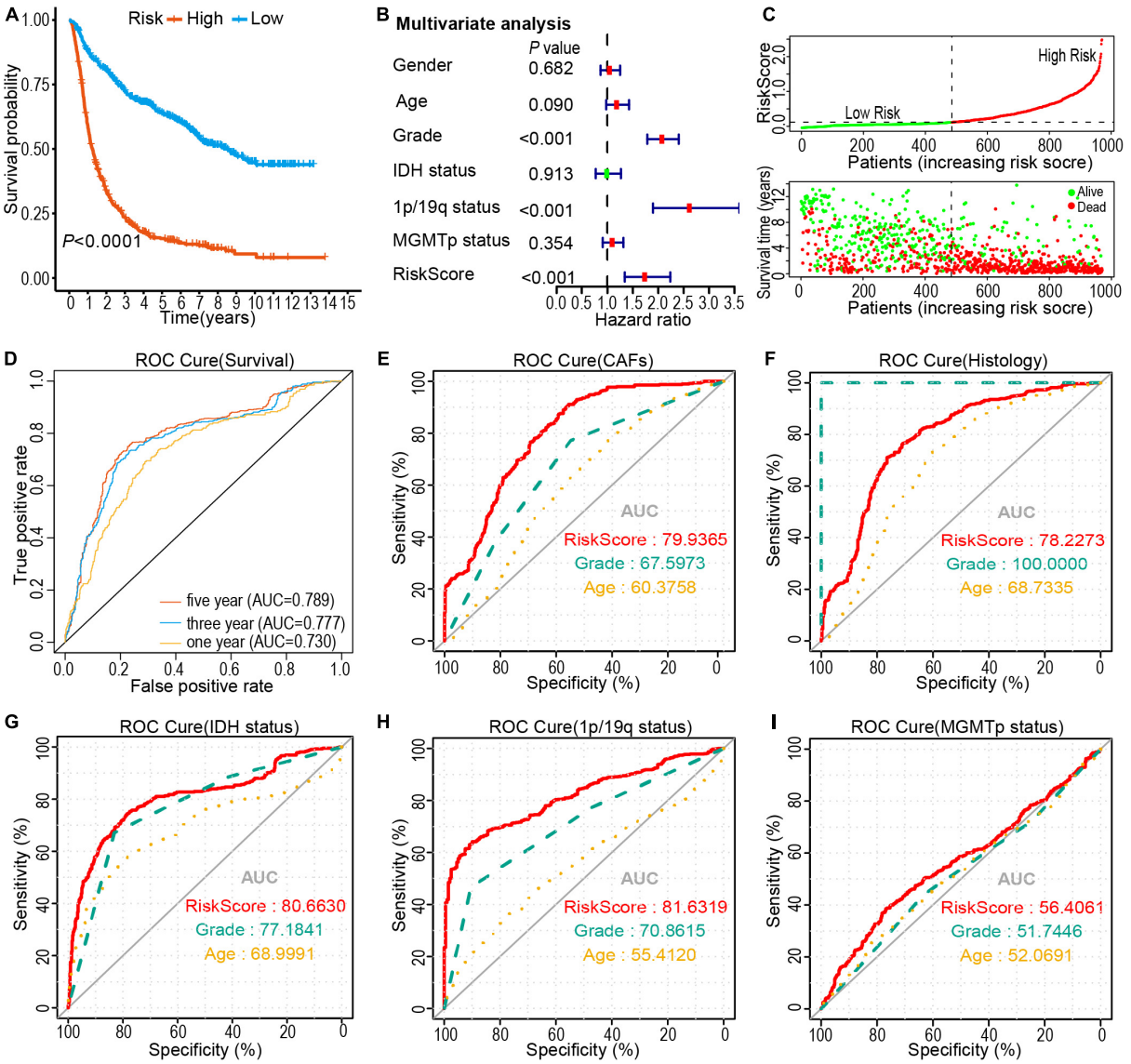

FIGURE 4 | Prognostic significance of risk signature derived risk score in the CGGA cohort. **(A)** Kaplan-Meier analysis of CGGA glioma patients was stratified by median risk. **(B)** Multivariate Cox regression analysis showed that the risk signature was an independent predictor of gliomas. **(C)** Risk score distribution, patient survival time, and glioma status. The black dotted line is the optimal threshold for classifying patients into low-and high-risk subtypes. **(D–I)** A high-risk score is associated with a lower survival rate for gliomas. ROC curves showed the predictive efficiency of risk characteristics, overall survival **(D)**, CAFs **(E)**, Histology **(F)**, IDH status **(G)**, 1p/19q status **(H)**, and MGMT promoter methylation status **(I)**.

published dataset containing 47 patients with melanoma that responded to immunotherapies (Roh et al., 2017). The high-risk subtype showed potent responses to anti–PD-1 therapy (Bonferroni correction $P = 0.01$; **Figure 7E**).

DISCUSSION

The present study, through analysis of the CGGA and TCGA databases of glioma, revealed that CAFs are associated with clinical and immunological characteristics of gliomas. More evidence shows that CAFs are an independent prognostic factor and CAFs are enriched in patients with a poor survival rate, older age, high tumor grade, IDH wild-type, 1p/19q non-codeletion, and MGMT promoter unmethylation (**Figures 2A-I**). This work has also demonstrated the association of a high proportion of CAFs in glioma patients with low tumor purity and high immune score, high stromal score, ESTIMATE score, and high stemness score (**Figures 2J-N**). By intersecting the two DEGs sets and conducting a further screen through multivariate Cox regression analysis, the remaining prognostic genes were used for LASSO regression analysis. Assessment of the risk score was based on the expression of six CAFs-related genes (ABCC3, CTHRC1, MSR1, PDLIM1, TNFRSF12A, and CHI3L2) (**Figure 3**). Similar

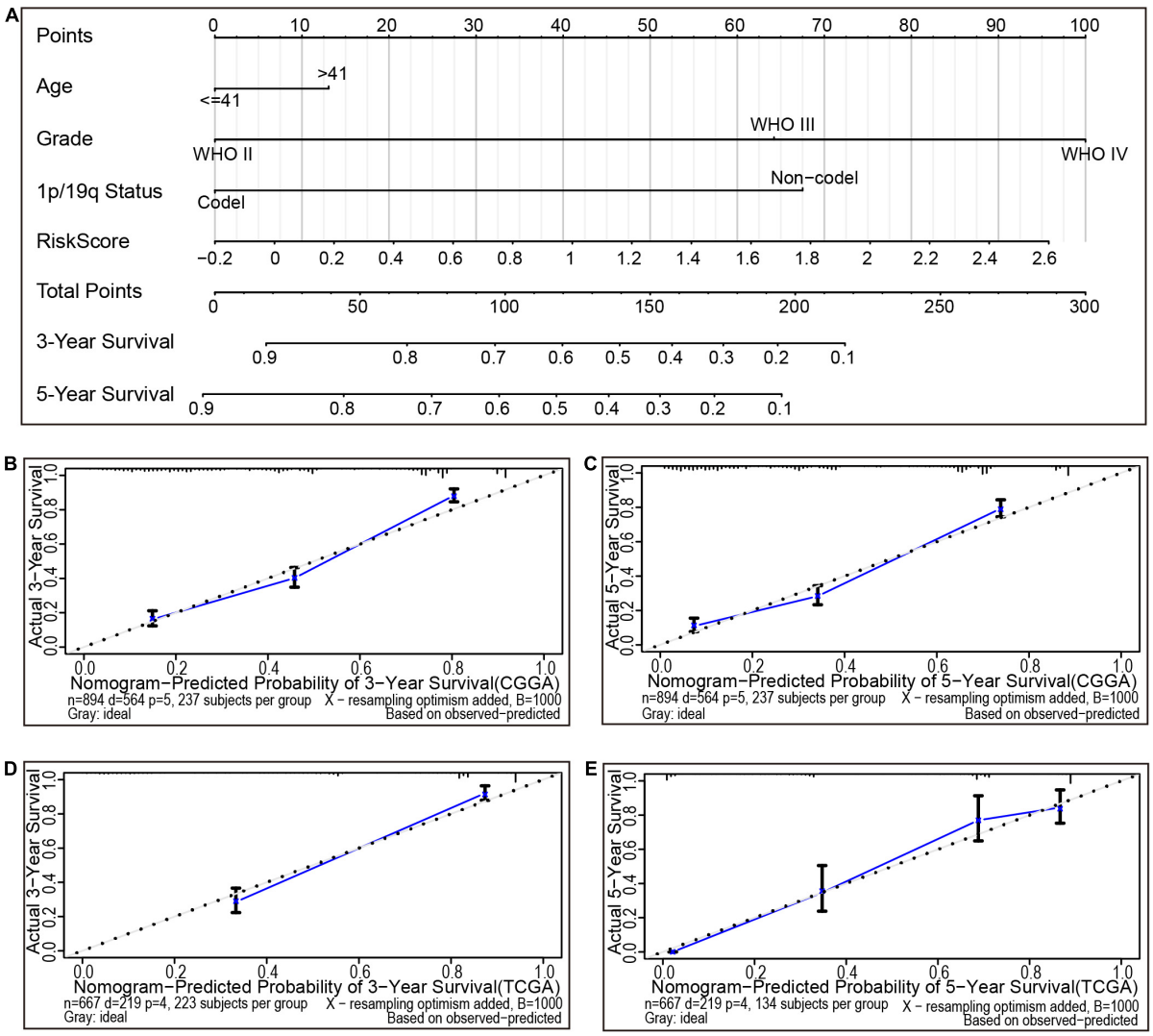

FIGURE 5 | The nomogram can predict the prognosis of gliomas. **(A)** A nomogram of the gliomas cohort (training set) was used to predict overall survival. **(B,C)** A calibration plot was used to predict the 3-year **(B)** and 5-year survival **(C)** in the CGGA cohorts (training set). Calibration plots for 3-year **(D)** and 5-year survival **(E)** in the Cancer Genome Atlas (TCGA) cohort (testing set). The X- and Y-axis represent the Nomogram prediction and actual survival, respectively. The solid line represents the nomogram of the forecast and the vertical line represents the 95% confidence interval.

to the proportion of CAFs, the risk score was correlated with a survival rate, clinical characteristics, tumor purity, immune score, stromal score, ESTIMATE score, and stemness score. These data strongly demonstrate that the risk score holds great promise as an independent prognostic factor for glioma (**Figure 4**). Furthermore, independent prognostic factors were used to construct a nomogram to directly predict individual OS based on six CAFs-related-gene signature risk score (**Figure 5**). It was revealed that the main enriched pathways in the tumor, including epithelial-mesenchymal transformation (Shintani et al., 2016), hypoxia (Lappano et al., 2020), inflammatory Response (Ershaid et al., 2019), interferon-gamma response (Broad et al., 2021), and NFkB-mediated TNFα signal transduction (Katanov et al., 2015) were closely related to the function of CAFs. These observations indicate that risk scores can fully reflect the function of CAFs (**Figure 6A**). To explore the role of the risk score in the TME, ssGSEA, and CIBERSORT were employed to evaluate immune cell infiltration. Percentage analysis of immune cells demonstrated that gliomas were mainly enriched with macrophages and few T cells. Also, significant differences in the abundance of immune cells between the high-and low-risk subtypes were noted. Th1 cells were mainly enriched in the low-risk subtype while immunosuppressive cells such as Th2 cells, Tregs, and M2 macrophages were mainly enriched in the high-risk category. Furthermore, $CD4^+$ T cells, $CD8^+$ T cells, and NK cells were highly enriched in the high-risk subtype (**Figure 6B** and **Supplementary Figure 7**). In addition, high-risk patients were shown to express high levels of markers of immune cell exhaustion (**Figure 7A**). These data demonstrate that although immune-activated cells are highly expressed in

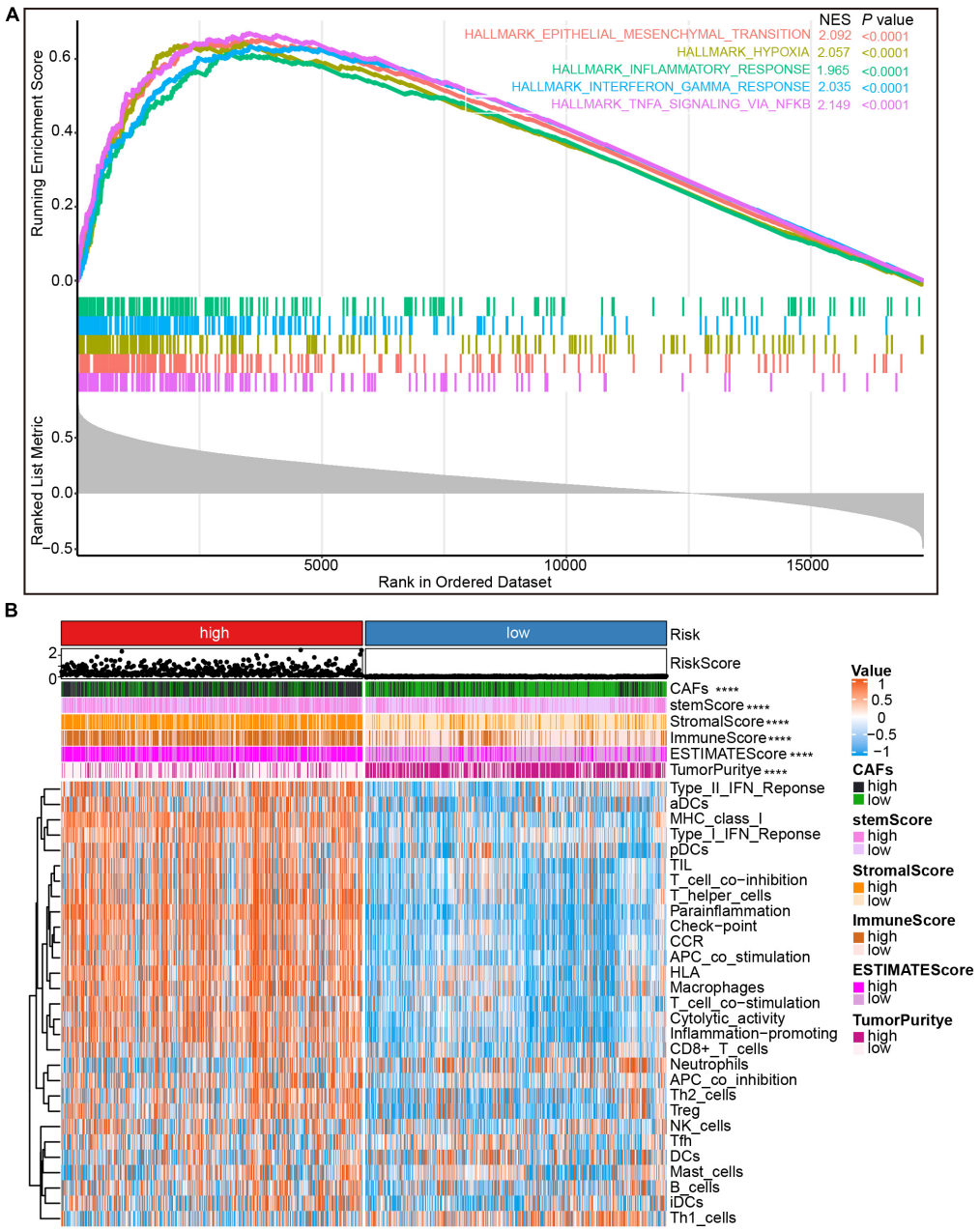

FIGURE 6 | Gene set enrichment analysis (GSEA) and immune cell infiltration analysis. **(A)** The GSEA of genes positively correlated with risk score. **(B)** Heatmap showing immune cells infiltration by ssGSEA algorithm between low- and high-risk groups in the CGGA cohort. NES, normalized enrichment score. ****$P < 0.0001$.

the high-risk group, it is possible that they are in a state of functional inhibition.

High expression of immune-related cytokines and chemokines in high-risk subtypes provide evidence on the relationship between CAFs and tumor-associated macrophages (TAMs) (**Figures 7B–D**). Studies show that recruitment of TAMs into the glioma environment may induce immunosuppression and tumor promotion effects (Hambardzumyan et al., 2016). Moreover, CAFs may promote the polarization of macrophages to M2 macrophages and exert an immunosuppressive effect in TME, and more, CAFs can secret cytokines and chemokines to interact with various immune cells in the tumor environment, contributing to the malignant transformation of tumors and resistance to treatment (Linares et al., 2020). Therefore, secretion factors from CAFs are promising indicators for tumor diagnosis and prognosis, and as drug targets.

Previous evidence indicates that CCL2 in the glioma microenvironment promotes the recruitment of Tregs and myeloid-derived suppressor cells (MDSCs) (Chang et al., 2016). On the other hand, $CD70^{+}$ CAFs are independent markers for

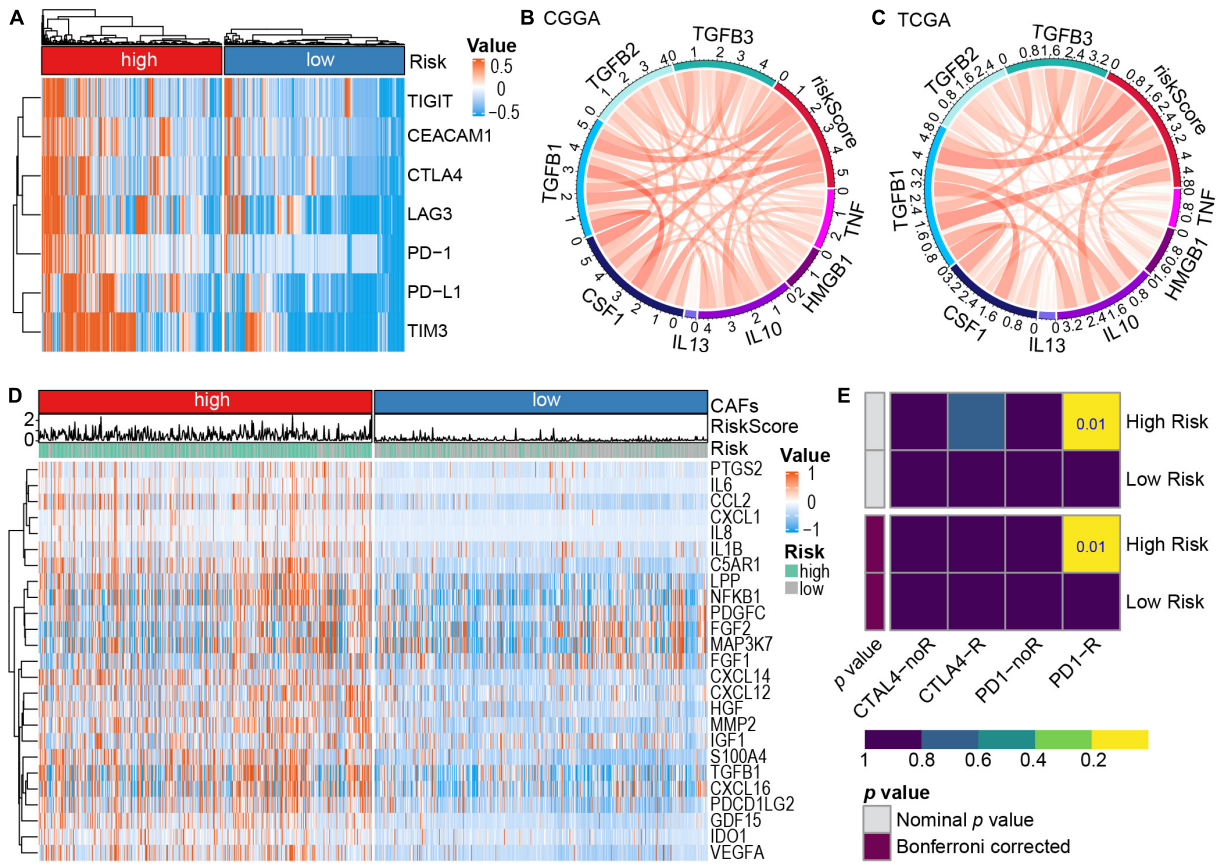

FIGURE 7 | The role of risk signature in immune microenvironment and immunotherapy. **(A)** Expression of immune cell exhaustion marker genes in the high- and low-risk subtypes. **(B,C)** Correlation between representative macrophage chemokines and risk score, CGGA dataset **(B)**, TCGA dataset **(C)**. M1 macrophage chemokines (TNF, HMGB1), M2 macrophage chemokines (IL10, IL13, CSF1, TGFB1, TGFB2, and TGFB3). **(D)** Cytokines secreted by CAFs high expression in the high-risk subtype. **(E)** Predicting response to immunotherapy (anti-PD-1 and anti-CTLA4) in the high-and low-risk subtype based on the Submap algorithms.

poor prognosis in invasive colorectal cancer, they potentially increase the infiltration of Tregs and promote the immune escape of tumor cells (Jacobs et al., 2018). Immunosuppression mediated by high expression of PD-L1 in gliomas has been demonstrated to be potentially associated with the infiltration of TAMs and M2 polarization (Zhu et al., 2020). Studies have also shown that the differentiation and survival of macrophages are dependent on the colony-stimulating Factor-1 (CSF-1), and IL6 and the granulocyte-macrophage colony-stimulating factor (GM-CSF) secreted by CAFs, which promote the differentiation of monocytes into M2-like TAMs (Cho et al., 2018). Consistently, Pyonteck et al. (2013) found that targeting TAMs with the CSF-1R inhibitor significantly improves the survival rate of GBM mice. These pieces of evidence indicate that CAFs and their secreted factors orchestrate with the immune cells in the TME to promote glioma progression.

Increasing evidence has shown that T cell dysfunction contributes to tumor immune escape in patients with gliomas (Mirzaei et al., 2017; Woroniecka et al., 2018). In the presence of adenosine, activation of $CD8^+$ T cells effectuates a decrease in the expression of IFN-γ and tumor necrosis factor-α (TNF-α), thereby inhibiting anti-tumor response (Takenaka et al., 2019). Moreover, $CD8^+$ T cells during tumorigenesis mediate the immune editing of immunogenic tumor clones, contributing to immune escape in murine glioma (Kane et al., 2020). The present study, based on the six-gene signature of CAFs, reported a higher expression of immune checkpoint molecules in high-risk subtype tumors. It was notable that the functions of CAFs rely on immune checkpoint activation, which induces the loss of antigen specificity in $CD8^+$ T cells and blocks the activity of T cells (Lakins et al., 2018). Furthermore, evidence indicates that to inhibit $CD8^+$ T cells, CAFs can secrete high levels of IL-6, which remodel the immunosuppressive TME (Kato et al., 2018). Previous researchers also demonstrated that CAFs can recruit and balance $CD4^+$ effector T cell subsets (Th1 and Th2), promoting the recruitment and differentiation of Tregs, and facilitate the transformation of macrophages to the M2 phenotype through frequent interactions with TAMs. Additionally, CAFs can inhibit the ability of $CD8^+$ T cells to kill tumor cells. To achieve this, CAFs reduce T cell infiltration, blocking both the cytotoxic activity of T cells and T-cell communication in the TME (An et al., 2020; Baker et al., 2021). Taken together, these findings support the view that CAFs potentially inhibit $CD8^+$ T function, promote the formation of

MDSC, and establish an immunosuppressive TME to facilitate the immune escape of tumor cells.

Additionally, the present work revealed the activation of the inflammation-promoting function, type I IFN response, and type II IFN response in the high-risk subtype (**Figure 6B** and **Supplementary Figure 7C**). The expression levels of immune checkpoint-related genes were also higher in the high-risk subtype (**Figure 7A**), demonstrating that immunosuppressed patients in the high-risk category may respond to immune checkpoint blockers. By predicting the response and resistance of different risk subtypes to immune checkpoint blockers therapy, it was intriguing that patients with high-risk scores showed higher responses to anti-PD-1 therapy (**Figure 7E**). As such, patients in the high-risk subtype are likely to be more responsive to immunotherapy. These results demonstrate that the risk score based on the expression of the six CAFs-related genes is promising as a novel and reliable method for evaluating the prognosis and clinical response to immunotherapy of glioma patients.

More evidence shows that CAFs-induced inhibition of immunosuppression may further enhance the response of tumors to immunotherapy. Current evidence shows several therapeutic strategies that target CAFs, including (i) targeting cytokines and chemokines (such as TGF-β or IL6) through immunotherapy, directly consuming CAFs (such as FAP-DNA vaccine) via cell surface labeling; (ii) targeting CAFs through the elimination of endothelial progenitors using bevacizumab, normalizing activated CAFs (e.g., using VDR ligand calcipotriol); (iii) targeting CAFs-derived extracellular matrix proteins or their related signal transduction in animal models (Chen and Song, 2019; Liu et al., 2019a). Moreover, selectively targeting CAFs using nanomedicine has been revealed to enhance the infiltration of cytotoxic T cells and inhibits tumor growth (Zhen et al., 2017). More importantly, the synergistic effect of blocking immune checkpoint molecules and targeting CAFs can be achieved by remodeling the immunosuppressive microenvironment and achieving an immunotherapeutic response (Feig et al., 2013). Normalization of CAFs may eliminate the tumor-promoting effect and increase the sensitivity of treatment (Öhlund et al., 2014; Vennin et al., 2019). Collectively, CAFs secrete cytokines in the TME during glioma progression, interact with immune cells, mediate the formation of the immunosuppressive microenvironment and induce the transformation to the malignant phenotype. Therefore, an improved understanding of the interaction of CAFs with anti-tumor immunity is crucial in establishing effective immunotherapy. In this regard, approaches such as spatial transcriptomics, single-cell RNA sequencing (Moncada et al., 2020), and organoids (Xu et al., 2021) can be employed to comprehensively understand the Spatio-temporal dynamics of CAFs as they interact with tumor and immune cells and their role in TME of gliomas.

To the best of our knowledge, this is the first study to explore the clinical features of CAFs in gliomas and establish a prognostic signature, based on CAFs for predicting the survival outcome of glioma patients and immunotherapy efficacy. The results are based on public data sets analysis, therefore, more exploration is warranted on heterogeneity in different patient groups, including intertumoral or intratumoral heterogeneity. Also, the biological functions of six CAFs-related genes as a prognostic signature should be explored deeply. Notably, the roles of CAFs vary in different patients given the complex and diverse immune microenvironment of gliomas. Thus, the precise effects of CAFs and their interaction with tumor cells and immune cells deserve further clarification.

CONCLUSION

Increased CAFs infiltration in gliomas is significantly correlated with older age, high tumor grade, IDH status, 1p/19q status and MGMT promoter status, tumor purity, immune score, stromal score, ESTIMATE score, stemness score, and patient prognosis. The established risk prediction model, based on the expression of six CAFs-related genes, has application prospects as an independent prognostic indicator. The risk model holds great promise in predict prognosis and immunotherapy response in glioma patients.

DATA AVAILABILITY STATEMENT

The datasets presented in this study can be found in online repositories. The names of the repository/repositories and accession number(s) can be found in the article/ **Supplementary Material**.

AUTHOR CONTRIBUTIONS

HX and KY conceived and designed the study and drafted the manuscript. ZC, SZ, and GH performed data analysis and wrote the manuscript. JT, WH, and W-QG revised the manuscript. All authors reviewed the manuscript.

FUNDING

This study was supported by the National Natural Science Foundation of China (Grant Nos. 31571399 and 82060456) and Finance Science and Technology Project of Hainan Province (Grant No. ZDYF2019129).

ACKNOWLEDGMENTS

The authors gratefully acknowledge contributions from the CGGA and TCGA network.

SUPPLEMENTARY MATERIAL

The Supplementary Material for this article can be found online at: https://www.frontiersin.org/articles/10.3389/fcell.2021.721897/full#supplementary-material

REFERENCES

Aldape, K., Brindle, K. M., Chesler, L., Chopra, R., Gajjar, A., Gilbert, M. R., et al. (2019). Challenges to curing primary brain tumours. *Nat. Rev. Clin. Oncol.* 16, 509–520. doi: 10.1038/s41571-019-0177-5

An, Y., Liu, F., Chen, Y., and Yang, Q. (2020). Crosstalk between cancer-associated fibroblasts and immune cells in cancer. *J. Cell Mol. Med.* 24, 13–24. doi: 10.1111/jcmm.14745

Baker, A. T., Abuwarwar, M. H., Poly, L., Wilkins, S., and Fletcher, A. L. (2021). Cancer-associated fibroblasts and T cells: from mechanisms to outcomes. *J. Immunol.* 206, 310–320. doi: 10.4049/jimmunol.2001203

Bindea, G., Mlecnik, B., Tosolini, M., Kirilovsky, A., Waldner, M., Obenauf, A. C., et al. (2013). Spatiotemporal dynamics of intratumoral immune cells reveal the immune landscape in human cancer. *Immunity* 39, 782–795. doi: 10.1016/j.immuni.2013.10.003

Broad, R. V., Jones, S. J., Teske, M. C., Wastall, L. M., Hanby, A. M., Thorne, J. L., et al. (2021). Inhibition of interferon-signalling halts cancer-associated fibroblast-dependent protection of breast cancer cells from chemotherapy. *Br. J. Cancer* 124, 1110–1120. doi: 10.1038/s41416-020-01226-4

Broekman, M. L., Maas, S. L. N., Abels, E. R., Mempel, T. R., Krichevsky, A. M., and Breakefield, X. O. (2018). Multidimensional communication in the microenvirons of glioblastoma. *Nat. Rev. Neurol.* 14, 482–495. doi: 10.1038/s41582-018-0025-8

Buerki, R. A., Chheda, Z. S., and Okada, H. (2018). Immunotherapy of primary brain tumors: facts and hopes. *Clin. Cancer Res.* 24, 5198–5205. doi: 10.1158/1078-0432.CCR-17-2769

Chang, A. L., Miska, J., Wainwright, D. A., Dey, M., Rivetta, C. V., Yu, D., et al. (2016). CCL2 Produced by the Glioma Microenvironment is essential for the recruitment of regulatory T Cells and myeloid-derived suppressor cells. *Cancer Res.* 76, 5671–5682. doi: 10.1158/0008-5472.CAN-16-0144

Chen, X., and Song, E. (2019). Turning foes to friends: targeting cancer-associated fibroblasts. *Nat. Rev. Drug Discov.* 18, 99–115. doi: 10.1038/s41573-018-0004-1

Cho, H., Seo, Y., Loke, K. M., Kim, S. W., Oh, S. M., Kim, J. H., et al. (2018). Cancer-stimulated CAFs enhance monocyte differentiation and protumoral TAM activation via IL6 and GM-CSF secretion. *Clin. Cancer Res.* 24, 5407–5421. doi: 10.1158/1078-0432.CCR-18-0125

Cox, T. R. (2021). The matrix in cancer. *Nat. Rev. Cancer* Online ahead of print. doi: 10.1038/s41568-020-00329-7

Erin, N., Grahovac, J., Brozovic, A., and Efferth, T. (2020). Tumor microenvironment and epithelial mesenchymal transition as targets to overcome tumor multidrug resistance. *Drug Resist. Updat.* 53:100715. doi: 10.1016/j.drup.2020.100715

Ershaid, N., Sharon, Y., Doron, H., Raz, Y., Shani, O., Cohen, N., et al. (2019). NLRP3 inflammasome in fibroblasts links tissue damage with inflammation in breast cancer progression and metastasis. *Nat. Commun.* 10:4375. doi: 10.1038/s41467-019-12370-8

Farhood, B., Najafi, M., and Mortezaee, K. (2019). Cancer-associated fibroblasts: secretions, interactions, and therapy. *J. Cell Biochem.* 120, 2791–2800. doi: 10.1002/jcb.27703

Feig, C., Jones, J. O., Kraman, M., Wells, R. J., Deonarine, A., Chan, D. S., et al. (2013). Targeting CXCL12 from FAP-expressing carcinoma-associated fibroblasts synergizes with anti-PD-L1 immunotherapy in pancreatic cancer. *Proc. Natl. Acad. Sci. U.S.A.* 110, 20212–20217. doi: 10.1073/pnas.1320318110

Gonzalez-Gugel, E., Saxena, M., and Bhardwaj, N. (2016). Modulation of innate immunity in the tumor microenvironment. *Cancer Immunol. Immunother.* 65, 1261–1268. doi: 10.1007/s00262-016-1859-9

Hambardzumyan, D., Gutmann, D. H., and Kettenmann, H. (2016). The role of microglia and macrophages in glioma maintenance and progression. *Nat. Neurosci.* 19, 20–27. doi: 10.1038/nn.4185

Hoshida, Y., Brunet, J. P., Tamayo, P., Golub, T. R., and Mesirov, J. P. (2007). Subclass mapping: identifying common subtypes in independent disease data sets. *PLoS One* 2:e1195. doi: 10.1371/journal.pone.0001195

Huang, Y. H., Zhu, C., Kondo, Y., Anderson, A. C., Gandhi, A., Russell, A., et al. (2015). CEACAM1 regulates TIM-3-mediated tolerance and exhaustion. *Nature* 517, 386–390. doi: 10.1038/nature13848

Ishida, Y., Agata, Y., Shibahara, K., and Honjo, T. (1992). Induced expression of PD-1, a novel member of the immunoglobulin gene superfamily, upon programmed cell death. *EMBO J.* 11, 3887–3895. doi: 10.1002/j.1460-2075.1992.tb05481.x

Jackson, C. M., Choi, J., and Lim, M. (2019). Mechanisms of immunotherapy resistance: lessons from glioblastoma. *Nat. Immunol.* 20, 1100–1109. doi: 10.1038/s41590-019-0433-y

Jacobs, J., Deschoolmeester, V., Zwaenepoel, K., Flieswasser, T., Deben, C., Van den Bossche, J., et al. (2018). Unveiling a CD70-positive subset of cancer-associated fibroblasts marked by pro-migratory activity and thriving regulatory T cell accumulation. *Oncoimmunology* 7:e1440167. doi: 10.1080/2162402X.2018.1440167

Kane, J. R., Zhao, J., Tsujiuchi, T., Laffleur, B., Arrieta, V. A., Mahajan, A., et al. (2020). CD8(+) T-cell-Mediated immunoediting influences genomic evolution and immune evasion in murine gliomas. *Clin. Cancer Res.* 26, 4390–4401. doi: 10.1158/1078-0432.CCR-19-3104

Katanov, C., Lerrer, S., Liubomirski, Y., Leider-Trejo, L., Meshel, T., Bar, J., et al. (2015). Regulation of the inflammatory profile of stromal cells in human breast cancer: prominent roles for TNF-alpha and the NF-kappaB pathway. *Stem Cell Res. Ther.* 6:87. doi: 10.1186/s13287-015-0080-7

Kato, T., Noma, K., Ohara, T., Kashima, H., Katsura, Y., Sato, H., et al. (2018). Cancer-associated fibroblasts affect intratumoral CD8(+) and FoxP3(+) T Cells Via IL6 in the tumor microenvironment. *Clin. Cancer Res.* 24, 4820–4833. doi: 10.1158/1078-0432.CCR-18-0205

Krummel, M. F., and Allison, J. P. (1996). CTLA-4 engagement inhibits IL-2 accumulation and cell cycle progression upon activation of resting T cells. *J. Exp. Med.* 183, 2533–2540. doi: 10.1084/jem.183.6.2533

Lakins, M. A., Ghorani, E., Munir, H., Martins, C. P., and Shields, J. D. (2018). Cancer-associated fibroblasts induce antigen-specific deletion of CD8 (+) T Cells to protect tumour cells. *Nat. Commun.* 9:948. doi: 10.1038/s41467-018-03347-0

Lapointe, S., Perry, A., and Butowski, N. A. (2018). Primary brain tumours in adults. *Lancet* 392, 432–446. doi: 10.1016/S0140-6736(18)30990-5

Lappano, R., Talia, M., Cirillo, F., Rigiracciolo, D. C., Scordamaglia, D., Guzzi, R., et al. (2020). The IL1beta-IL1R signaling is involved in the stimulatory effects triggered by hypoxia in breast cancer cells and cancer-associated fibroblasts (CAFs). *J. Exp. Clin. Cancer Res.* 39:153. doi: 10.1186/s13046-020-01667-y

Li, M., Li, G., Kiyokawa, J., Tirmizi, Z., Richardson, L. G., Ning, J., et al. (2020). Characterization and oncolytic virus targeting of FAP-expressing tumor-associated pericytes in glioblastoma. *Acta Neuropathol. Commun.* 8:221. doi: 10.1186/s40478-020-01096-0

Linares, J., Marin-Jimenez, J. A., Badia-Ramentol, J., and Calon, A. (2020). Determinants and functions of CAFs secretome during cancer progression and therapy. *Front. Cell Dev. Biol.* 8:621070. doi: 10.3389/fcell.2020.621070

Liu, B., Chen, X., Zhan, Y., Wu, B., and Pan, S. (2020). Identification of a gene signature for renal cell carcinoma-associated fibroblasts mediating cancer progression and affecting prognosis. *Front. Cell Dev. Biol.* 8:604627. doi: 10.2139/ssrn.3688868

Liu, T., Han, C., Wang, S., Fang, P., Ma, Z., Xu, L., et al. (2019a). Cancer-associated fibroblasts: an emerging target of anti-cancer immunotherapy. *J. Hematol. Oncol.* 12:86. doi: 10.1186/s13045-019-0770-1

Liu, T., Zhou, L., Li, D., Andl, T., and Zhang, Y. (2019b). Cancer-associated fibroblasts build and secure the tumor microenvironment. *Front. Cell Dev. Biol.* 7:60. doi: 10.3389/fcell.2019.00060

Louault, K., Li, R. R., and DeClerck, Y. A. (2020). Cancer-associated fibroblasts: understanding their heterogeneity. *Cancers* 12:3108. doi: 10.3390/cancers12113108

Maman, S., and Witz, I. P. (2018). A history of exploring cancer in context. *Nat. Rev. Cancer* 18, 359–376. doi: 10.1038/s41568-018-0006-7

Manieri, N. A., Chiang, E. Y., and Grogan, J. L. (2017). TIGIT: a key inhibitor of the cancer immunity cycle. *Trends Immunol.* 38, 20–28. doi: 10.1016/j.it.2016.10.002

Miranda, A., Hamilton, P. T., Zhang, A. W., Pattnaik, S., Becht, E., Mezheyeuski, A., et al. (2019). Cancer stemness, intratumoral heterogeneity, and immune response across cancers. *Proc. Natl. Acad. Sci. U.S.A.* 116, 9020–9029. doi: 10.1073/pnas.1818210116

Mirzaei, R., Sarkar, S., and Yong, V. W. (2017). T cell exhaustion in glioblastoma: intricacies of immune checkpoints. *Trends Immunol.* 38, 104–115. doi: 10.1016/j.it.2016.11.005

Moncada, R., Barkley, D., Wagner, F., Chiodin, M., Devlin, J. C., Baron, M., et al. (2020). Integrating microarray-based spatial transcriptomics and single-cell RNA-seq reveals tissue architecture in pancreatic ductal adenocarcinomas. *Nat. Biotechnol.* 38, 333–342. doi: 10.1038/s41587-019-0392-8

Newman, A. M., Liu, C. L., Green, M. R., Gentles, A. J., Feng, W., Xu, Y., et al. (2015). Robust enumeration of cell subsets from tissue expression profiles. *Nat. Methods* 12, 453–457. doi: 10.1038/nmeth.3337

Öhlund, D., Elyada, E., and Tuveson, D. (2014). Fibroblast heterogeneity in the cancer wound. *J. Exp. Med.* 211, 1503–1523. doi: 10.1084/jem.20140692

Postow, M. A., Callahan, M. K., and Wolchok, J. D. (2015). Immune checkpoint blockade in cancer therapy. *J. Clin. Oncol.* 33, 1974–1982. doi: 10.1200/JCO.2014.59.4358

Pyonteck, S. M., Akkari, L., Schuhmacher, A. J., Bowman, R. L., Sevenich, L., Quail, D. F., et al. (2013). CSF-1R inhibition alters macrophage polarization and blocks glioma progression. *Nat. Med.* 19, 1264–127237. doi: 10.1038/nm.3337

Racle, J., de Jonge, K., Baumgaertner, P., Speiser, D. E., and Gfeller, D. (2017). Simultaneous enumeration of cancer and immune cell types from bulk tumor gene expression data. *Elife* 6:e26476. doi: 10.7554/eLife.26476.049

Roh, W., Chen, P. L., Reuben, A., Spencer, C. N., Prieto, P. A., Miller, J. P., et al. (2017). Integrated molecular analysis of tumor biopsies on sequential CTLA-4 and PD-1 blockade reveals markers of response and resistance. *Sci. Transl. Med.* 9:eaah3560. doi: 10.1126/scitranslmed.aah3560

Ruffo, E., Wu, R. C., Bruno, T. C., Workman, C. J., and Vignali, D. A. A. (2019). Lymphocyte-activation gene 3 (LAG3): the next immune checkpoint receptor. *Semin. Immunol.* 4:101305. doi: 10.1016/j.smim.2019.101305

Shintani, Y., Fujiwara, A., Kimura, T., Kawamura, T., Funaki, S., Minami, M., et al. (2016). IL-6 secreted from cancer-associated fibroblasts mediates chemoresistance in NSCLC by increasing epithelial-mesenchymal transition signaling. *J. Thorac. Oncol.* 11, 1482–1492. doi: 10.1016/j.jtho.2016.05.025

Simon, N., Friedman, J., Hastie, T., and Tibshirani, R. (2011). Regularization paths for Cox's proportional hazards model via coordinate descent. *J. Stat. Softw.* 39, 1–13. doi: 10.18637/jss.v039.i05

Su, S., Chen, J., Yao, H., Liu, J., Yu, S., Lao, L., et al. (2018). CD10(+)GPR77(+) cancer-associated fibroblasts promote cancer formation and chemoresistance by sustaining cancer stemness. *Cell* 172, 841–856.e816. doi: 10.1016/j.cell.2018.01.009

Takenaka, M. C., Gabriely, G., Rothhammer, V., Mascanfroni, I. D., Wheeler, M. A., Chao, C. C., et al. (2019). Control of tumor-associated macrophages and T cells in glioblastoma via AHR and CD39. *Nat. Neurosci.* 22, 729–740. doi: 10.1038/s41593-019-0370-y

Tan, A. C., Ashley, D. M., López, G. Y., Malinzak, M., Friedman, H. S., and Khasraw, M. (2020). Management of glioblastoma: state of the art and future directions. *CA Cancer J. Clin.* 70, 299–312. doi: 10.3322/caac.21613

Tibshirani, R. (1997). The lasso method for variable selection in the Cox model. *Stat. Med.* 16, 385–395. doi: 10.1002/(SICI)1097-0258(19970228)16:4<385::AID-SIM380>3.0.CO;2-3

Tirosh, I., Izar, B., Prakadan, S. M., Wadsworth, M. H., Treacy, D., Trombetta, J. J., et al. (2016). Dissecting the multicellular ecosystem of metastatic melanoma by single-cell RNA-seq. *Science* 352, 189–196. doi: 10.1126/science.aad0501

Vennin, C., Mélénec, P., Rouet, R., Nobis, M., Cazet, A. S., Murphy, K. J., et al. (2019). CAF hierarchy driven by pancreatic cancer cell p53-status creates a pro-metastatic and chemoresistant environment via perlecan. *Nat. Commun.* 10:3637. doi: 10.1038/s41467-019-10968-6

Wang, Z., Yang, Q., Tan, Y., Tang, Y., Ye, J., Yuan, B., et al. (2021). Cancer-associated fibroblasts suppress cancer development: the other side of the coin. *Front. Cell Dev. Biol.* 9:613534. doi: 10.3389/fcell.2021.613534

Wickham, H. (2016). *ggplot2: Elegant Graphics for Data Analysis*. New York: Springer-Verlag. doi: 10.1007/978-3-319-24277-4

Woroniecka, K. I., Rhodin, K. E., Chongsathidkiet, P., Keith, K. A., and Fecci, P. E. (2018). T-cell dysfunction in glioblastoma: applying a new framework. *Clin. Cancer Res.* 24, 3792–3802. doi: 10.1158/1078-0432.CCR-18-0047

Xu, R., Zhou, X., Wang, S., and Trinkle, C. (2021). Tumor organoid models in precision medicine and investigating cancer-stromal interactions. *Pharmacol. Ther.* 218:107668. doi: 10.1016/j.pharmthera.2020.107668

Yoshihara, K., Shahmoradgoli, M., Martínez, E., Vegesna, R., Kim, H., Torres-Garcia, W., et al. (2013). Inferring tumour purity and stromal and immune cell admixture from expression data. *Nat. Commun.* 4:2612. doi: 10.1038/ncomms3612

Yu, G., Wang, L. G., Han, Y., and He, Q. Y. (2012). clusterProfiler: an R package for comparing biological themes among gene clusters. *OMICS* 16, 284–287. doi: 10.1089/omi.2011.0118

Zarour, H. M. (2016). Reversing T-cell dysfunction and exhaustion in cancer. *Clin. Cancer Res.* 22, 1856–1864. doi: 10.1158/1078-0432.CCR-15-1849

Zhang, Y., Liu, L., Qiu, Q., Zhou, Q., Ding, J., Lu, Y., et al. (2021). Alternative polyadenylation: methods, mechanism, function, and role in cancer. *J. Exp. Clin. Cancer Res.* 40:51. doi: 10.1186/s13046-021-01852-7

Zhao, Z., Zhang, K. N., Wang, Q., Li, G., Zeng, F., Zhang, Y., et al. (2021). Chinese Glioma Genome Atlas (CGGA): a comprehensive resource with functional genomic data from Chinese Gliomas. *Genomics Proteomics Bioinform.* 19, 1–12. doi: 10.1016/j.gpb.2020.10.005

Zhen, Z., Tang, W., Wang, M., Zhou, S., Wang, H., Wu, Z., et al. (2017). Protein nanocage mediated fibroblast-activation protein targeted photoimmunotherapy to enhance cytotoxic T Cell infiltration and tumor control. *Nano Lett.* 17, 862–869. doi: 10.1021/acs.nanolett.6b04150

Zhu, Z., Zhang, H., Chen, B., Liu, X., Zhang, S., and Zong, Z. (2020). PD-L1-mediated immunosuppression in glioblastoma is associated with the infiltration and M2-polarization of tumor-associated macrophages. *Front. Immunol.* 11:588552. doi: 10.3389/fimmu.2020.588552

Conflict of Interest: The authors declare that the research was conducted in the absence of any commercial or financial relationships that could be construed as a potential conflict of interest.

Publisher's Note: All claims expressed in this article are solely those of the authors and do not necessarily represent those of their affiliated organizations, or those of the publisher, the editors and the reviewers. Any product that may be evaluated in this article, or claim that may be made by its manufacturer, is not guaranteed or endorsed by the publisher.

Copyright © 2021 Chen, Zhuo, He, Tang, Hao, Gao, Yang and Xu. This is an open-access article distributed under the terms of the Creative Commons Attribution License (CC BY). The use, distribution or reproduction in other forums is permitted, provided the original author(s) and the copyright owner(s) are credited and that the original publication in this journal is cited, in accordance with accepted academic practice. No use, distribution or reproduction is permitted which does not comply with these terms.

frontiers in Cell and Developmental Biology

ORIGINAL RESEARCH
published: 09 November 2021
doi: 10.3389/fcell.2021.760800

Heme Oxygenase-1 Predicts Risk Stratification and Immunotherapy Efficacy in Lower Grade Gliomas

Wenrui Ye[1], Zhixiong Liu[1,2], Fangkun Liu[1] and Cong Luo[3]**

[1] Department of Neurosurgery, Xiangya Hospital, Central South University (CSU), Changsha, China, [2] National Clinical Research Center for Geriatric Disorders, Xiangya Hospital, Central South University (CSU), Changsha, China, [3] Department of Urology, Xiangya Hospital, Central South University (CSU), Changsha, China

Background: Gliomas are the most common tumors in human brains with unpleasing outcomes. Heme oxygenase-1 (*HMOX1*, *HO-1*) was a potential target for human cancers. However, their relationship remains incompletely discussed.

Methods: We employed a total of 952 lower grade glioma (LGG) patients from TCGA and CGGA databases, and 29 samples in our hospital for subsequent analyses. Expression, mutational, survival, and immune profiles of *HMOX1* were comprehensively evaluated. We constructed a risk signature using the LASSO Cox regression model, and further generated a nomogram model to predict survival of LGG patients. Single-cell transcriptomic sequencing data were also employed to investigated the role of *HMOX1* in cancer cells.

Results: We found that *HMOX1* was overexpressed and was related to poorer survival in gliomas. *HMOX1*-related genes (HRGs) were involved in immune-related pathways. Patients in the high-risk group exhibited significantly poorer overall survival. The risk score was positively correlated with the abundance of resting memory CD4+ T cells, M1, M2 macrophages, and activated dendritic cells. Additionally, immunotherapy showed potent efficacy in low-risk group. And patients with lower *HMOX1* expression were predicted to have better response to immunotherapies, suggesting that immunotherapies combined with *HMOX1* inhibition may execute good responses. Moreover, significant correlations were found between *HMOX1* expression and single-cell functional states including angiogenesis, hypoxia, and metastasis. Finally, we constructed a nomogram which could predict 1-, 3-, and 5-year survival in LGG patients.

Conclusion: *HMOX1* is involved in immune infiltration and predicts poor survival in patients with lower grade glioma. Importantly, *HMOX1* were related to oncological functional states including angiogenesis, hypoxia, and metastasis. A nomogram integrated with the risk signature was obtained to robustly predict glioma patient outcomes, with the potential to guide clinical decision-making.

Keywords: glioma, heme oxygenase-1, prognosis, risk signature, single-cell sequencing

OPEN ACCESS

Edited by:
Qian Xiao,
Rutgers Cancer Institute of New Jersey, United States

Reviewed by:
Zheng Wei,
Yale University, United States
Zhi Chai,
Icahn School of Medicine at Mount Sinai, United States

****Correspondence:***
Fangkun Liu
liufangkun@csu.edu.cn
Cong Luo
2204150121@csu.edu.cn

Specialty section:
This article was submitted to Molecular and Cellular Pathology, a section of the journal Frontiers in Cell and Developmental Biology

Received: *18 August 2021*
Accepted: *11 October 2021*
Published: *09 November 2021*

Citation:
Ye W, Liu Z, Liu F and Luo C (2021) Heme Oxygenase-1 Predicts Risk Stratification and Immunotherapy Efficacy in Lower Grade Gliomas. Front. Cell Dev. Biol. 9:760800. doi: 10.3389/fcell.2021.760800

INTRODUCTION

Gliomas, originating from intrinsic constituent cells of the brain, are the most common primary tumors there (Sanai et al., 2005). Before genome-wide molecular profiling researches revealed the comprehensive genomic landscape of human gliomas (Brat et al., 2015; Suzuki et al., 2015), glioma classification was largely based on their microscopic and immunohistochemical features. Development at the molecular biology level identifies novel biomarkers for optimized classification strategy and promising treatment targets. Predictive biomarkers recognized and used in clinics mainly included isocitrate dehydrogenase (IDH) mutation, the discovery of which constituted a key breakthrough in the understanding of WHO grade II/III gliomas (Yan et al., 2009). Besides, the presence of O6-methylguanine-DNA methyltransferase (MGMT) promoter methylation predicts benefit from temozolomide-based chemotherapy in patients with IDH-wildtype glioma (Wick et al., 2012). Furthermore, 1p/19q codeletion is predictive for benefit from combined radiotherapy and chemotherapy (with procarbazine, lomustine, and vincristine) in two phase III trials (Cairncross et al., 2013; van den Bent et al., 2013). Novel pathogenesis-based treatments targeting oncogenic signaling pathways such as BRAF mutation (Robinson et al., 2014), epidermal growth factor receptor (EGFR) amplification (Phillips et al., 2016), and fibroblast growth factor receptor (FGFR)-TACC fusion (Stefano et al., 2015) harbored the potential for LGG treatment.

Although these molecular subclassifications deepened our understanding of tumorigenesis and personalized therapeutics, a certain LGG population still acquired resistance to these targeted therapies. Furthermore, gliomas are not considered highly immunogenic due to the low mutational loads, besides they are featured by severe immunosuppression mediated by immune-inhibitory factors, such as programmed cell-death 1 ligand 1 (PDCD1LG1) and secreted transforming growth factor β (Nduom et al., 2015). Therefore, we hope that newly identified biomarkers can overcome immunosuppression, exploit antitumor immune responses, and guide individualized treatments.

Heme oxygenase is an essential enzyme in heme catabolism as it cleaves cellular heme to form biliverdin. *HMOX1* overexpression is observed in various solid malignancies, including bladder (Miyata et al., 2014), breast (Noh et al., 2013), colon (Yin et al., 2014), glioma (Gandini et al., 2014), lung (Degese et al., 2012), prostate (Maines and Abrahamsson, 1996), and gastric (Yin et al., 2012), cancers. Although HMOX1 prevents DNA damage under normal conditions, *HMOX1* overexpression paradoxically promotes cancer cell proliferation and invasiveness at late phase of tumorigenesis (Was et al., 2006; Ph et al., 2013). Targeting HMOX1 was effective for hormone-refractory prostate cancer (Alaoui-Jamali et al., 2009) and it has been shown to reverse imatinib resistance in myeloid leukemia (Mayerhofer et al., 2008). Several imidazole-based non-porphyrin HMOX1 inhibitors were recently developed, which exhibited selectivity toward HMOX1 (Pittalà et al., 2013). Meanwhile, they showed potent anti-tumor activities both *in vitro* and *in vivo*, with the potential for clinical applications (Salerno et al., 2013). In a nutshell, these findings shed a light on the future for targeting HMOX1 to promote cancer immunotherapy.

Currently, several clinical trials are attempting to explore the clinical benefits of targeting HMOX1 (or related molecules) in the treatment of lower grade gliomas and other solid cancers (**Supplementary Table 1**). We comprehensively analyzed two independent glioma cohorts, as well as samples from our institution, to explore the *HMOX1* profiling in the context of gliomas. In addition, an HRG-based risk signature was established to predict the outcome of patients diagnosed with primary lower grade gliomas. The multifaceted performance of the IIRS was also examined to reveal its superior predictive ability of response to immunotherapy.

MATERIALS AND METHODS

Data Extraction

Transcriptomic, copy number variations (CNV), and clinical data were extracted from The Cancer Genome Atlas (TCGA) and Chinese Glioma Genome Atlas (CGGA) databases, and 952 samples with lower grade glioma were finally included. 508 samples extracted from the TCGA database were defined as the training set, while 444 from the CGGA database were set as the validation set. Normal or glioblastoma (GBM, WHO grade IV glioma) samples were excluded.

Expression, Mutational, and Survival Analysis

We evaluated the expression distribution of *HMOX1* between tumor and normal tissues in TCGA pan-cancers. *HMOX1* expression between different clinic-related subgroups were explored in both cohorts. The associations between *HMOX1* expression and patient outcomes, including overall survival (OS), disease specific survival (DSS), and progression free interval (PFI), in TCGA pan-cancer sets were evaluated using univariate Cox analysis and displayed using R package "forestplot." And the survival curves were correspondingly established by Kaplan-Meier analysis to evaluate the relationship of LGG patients' prognosis and *HMOX1* expression level as well as mutation status.

Immune Infiltration Analysis in Lower Grade Gliomas

The Estimation of Stromal and Immune cells in Malignant Tumor tissues using Expression data (ESTIMATE; R package "estimate") analysis was employed to measure the tumor purity. Meanwhile, we used the CIBERSORT and the Tumor Immune Estimation Resource (TIMER) algorithm to assess the fractions of human immune infiltrating cell types (Li et al., 2017; Chen et al., 2018). The abundance of these cells was compared between groups with either high or low *HMOX1* expression levels (according to the median value) in WHO grade II/III gliomas. Besides, the correlations between *HMOX1* and tumor stemness, tumor mutational burden, as well as microsatellite instability (MSI) were assessed based on

TABLE 1 | The characteristics of include cohorts.

Characteristics	TCGA (*n* = 508)		CGGA (*n* = 444)		Samples (*n* = 29)	
	N	%	N	%	N	%
Age (y)						
≤40	251	49.41	229	51.58	6	20.69
>40	257	50.59	214	48.20	23	79.31
NA	0	0.00	1	0.23	0	0.00
Gender						
Female	282	55.51	193	43.47	6	20.69
Male	226	44.49	251	56.53	23	79.31
Grade						
II	246	48.43	189	42.57	12	41.38
III	262	51.57	255	57.43	17	58.62
Histological type						
A	128	25.20	271	61.04	9	31.03
OA	188	37.01	30	6.76	0	0.00
O	192	37.80	142	31.98	3	10.34
NA	0	0.00	1	0.23	17	58.62
***IDH1* status**						
Wildtype	34	6.69	96	21.62	6	20.69
Mutation	91	17.91	307	69.14	18	62.07
NA	383	75.39	41	9.23	5	17.24
Radiation therapy						
Yes	142	27.95	315	70.95	0	0.00
No	119	23.43	102	22.97	0	0.00
NA	247	48.62	27	6.08	29	100.00
Chemotherapy						
Yes	277	54.53	285	64.19	0	0.00
No	229	45.08	132	29.73	0	0.00
NA	2	0.39	27	6.08	29	100.00

A, astrocytoma; IDH1, isocitrate dehydrogenase 1; NA, not available; O, oligodendroglioma; OA, oligoastrocytoma.

Spearman's correlation analysis, which were displayed as radar charts using R package "radar."

Immunohistochemical Staining and RNA Sequencing of Glioma Samples

We included 29 glioma samples from the Department of Neurosurgery, Xiangya Hospital from February 2019 to February 2021. Patients with recurrent gliomas, glioblastomas, or other cancers, or serious underlying diseases were excluded. Five fresh glioma samples were collected and then immediately stored in 4% paraformaldehyde in room temperature. Slides were sequentially incubated in graded ethanol after deparaffinization for 3 h at 60 degrees. Antigen was exposed using citrate buffer (pH = 6.0). After blocking, slides were treated with anti-*HMOX1* (rabbit, AiFang biological AF300167, 1:100) in antibody diluent (abcam ab64211), and subsequent HRP Goat anti-rabbit IgG (H+L) secondary antibody (ABclonal AS014, 1:1,000).

We acquired scanned images on immunohistochemical sections using a digital scanner, and the area of tissue measurement was automatically read using an image analysis system (Servicebio). The positive grade was divided as follows: 0 for negative staining (without staining); 1 for weakly positive (light yellow staining); 2 for moderately positive (brownish yellow staining); and 3 for strongly positive (tan staining). The histochemistry score (H-score) was calculated to reflect the degree of positivity using the following formula:

$$H - Score = \sum_{i=0}^{3} (p_i \times i)$$

In the formula, "p_i" indicates percentage of negative/weak/moderate/strong intensity area. "i" represents the positive grade. H-score ranges from 0 to 300, where a higher H-score means a stronger positivity.

Twenty-four samples were collected and then stored in liquid nitrogen for further sequencing on a BGISEQ-500 platform (BGI-Shenzhen, China). The gene expression levels were calculated using RSEM (v1.2.12). This study was approved by the Ethics Committee of Xiangya Hospital (No. 2017121019). The written informed consents were obtained in advance from all participants or their family representatives.

Construction and Validation of Risk Signature Based on *HMOX1*-Related Genes

We calculated the correlations between *HMOX1* and other genes to identify HRGs (| correlation coefficient| > 0.6; false discovery rate (FDR) < 0.001), which were recorded for subsequent functional enrichment analysis. Gene Ontology (GO) and Kyoto Encyclopedia of Genes and Genomes (KEGG) terms were used to explore the biological functions of the gene set. Next, we developed a HRGs based prognostic signature for the LGG patients by performing the least absolute shrinkage and selection operator (LASSO) Cox regression analysis based on the R package "glmnet" (Friedman et al., 2020), The risk score calculating formula is:

$$Risk\ score\ =\ \sum_{i=1}^{n}(\beta_i\ \times\ x_i)$$

Where "n" means the number of genes, "β_i" is the coefficient for each gene, "x_i" means the expression value (log transformed) of each gene. The predicted protein-protein interactions (PPI) among these model genes were achieved by GeneMANIA.[1] And their correlations were also calculated.

We then calculated the risk score for the patients, and divided them into low- and high-risk groups according to the median risk score. The relationships between risk signature and survival as well as other clinicopathological characteristics were also assessed.

Prediction of Therapy Efficacy, Correlation With Pathways in Single Cell Landscape, and Drug Response

The efficacies of four therapies (radiotherapy, chemotherapy, targeted therapy, and immunotherapy) in high-risk and low-risk groups were evaluated.

The Tumor immune dysfunction and exclusion (TIDE) was used to assess the response of LGG patients to the immunotherapies (Jiang et al., 2018). Three resources for therapeutic biomarker discovery in cancer cells, including Genomics of Drug Sensitivity in Cancer (GDSC), Cancer Therapeutics Response Portal (CTRP), and Cancer Cell Line Encyclopedia (CCLE), were employed to evaluate the relationship between drug sensitivity [half maximal inhibitory concentration (IC50)] and mRNA expression of genes.

Single-cell RNA sequencing data derived from the single-cell dataset GSE84465 which contains four cell groups and 3,590 cells (2,342 tumor cells and 1,248 periphery cells) (Darmanis et al., 2017). The correlations between gene expression and functional states including angiogenesis, apoptosis, cell cycle, differentiation, DNA damage, DNA repair, epithelial-mesenchymal transition (EMT), hypoxia, inflammation, invasion, metastasis, proliferation, quiescence, and stemness, were calculated based on the CancerSEA database[2] (Yuan et al., 2019).

Establishment of Nomogram

We constructed a nomogram integrating clinical information and prognostic signature by R package "rms" using the variables screened out by Cox regression analysis, which could predict the 1-, 3-, and 5-year overall survival of LGG patients in an intuitionistic and easy-to-utilize manner. Calibration plots and C-indexes were obtained to access the predictive accuracy of the model.

Statistical Analyses

We used Kaplan-Meier curve combined log-rank test to evaluate the patient survival. Subgroups were stratified on the basis of clinical, pathological, and molecular features including age (≤ 40 or > 40-year-old), gender (male or female), grade (II or III), histological type (astrocytoma, oligoastrocytoma, or oligodendroglioma), and *IDH1* status (mutant or wildtype). When comparing variables between groups, we used Wilcoxon test or Kruskal-Wallis test. Most statistical analyses were achieved via R language (version 4.0.3). And $P < 0.05$ was considered statistically significant.

RESULTS

Heme Oxygenase-1 Is Overexpressed in Lower Grade Glioma

The flow chart of our study was displayed as **Supplementary Figure 1**. And the characteristics of included patients were summarized in **Table 1**. *HMOX1* expression levels were significantly elevated in tumor samples compared to normal controls (**Figures 1A,B**). Importantly, this trend remained consistent at single-cell level (**Figure 1C**). Similarly, glioma tissue had elevated protein level of HMOX1 than normal cerebral cortex tissue (**Figures 1D,E**). In the TCGA cohort, youngers (≤40 years old) and males had relatively higher *HMOX1* expression levels (**Figure 1F**), while no significant difference was observed in CGGA cohort (**Figure 1G**), which could be partially attributed to the heterogeneity between cohorts.

Furthermore, we comprehensively investigated the expression distribution of HMOX1 at tissue and cell levels in HPA database (**Supplementary Figure 2**). In normal tissues, HMOX1 was enriched in lymphoid tissues, especially spleen (**Supplementary Figure 2A**). Regarding cell types, HMOX1 demonstrated a high expression level in blood and immune cells including monocytes, macrophages, Kupffer cells, and Hofbauer cells (**Supplementary Figure 2B**). And in both tumor tissues and cell lines, HMOX1 was found to be elevated in glioma tissues and cells (U-138 MG and U-87 MG; **Supplementary Figures 2C,D**).

Moreover, the mutational profiles of *HMOX1* have been illustrated in **Supplementary Figure 3**. Amplification stood as the most common mutation type in LGG cohort (**Supplementary Figure 3A**). R123H/C site alteration was frequently observed

[1] http://genemania.org/

[2] http://biocc.hrbmu.edu.cn/CancerSEA

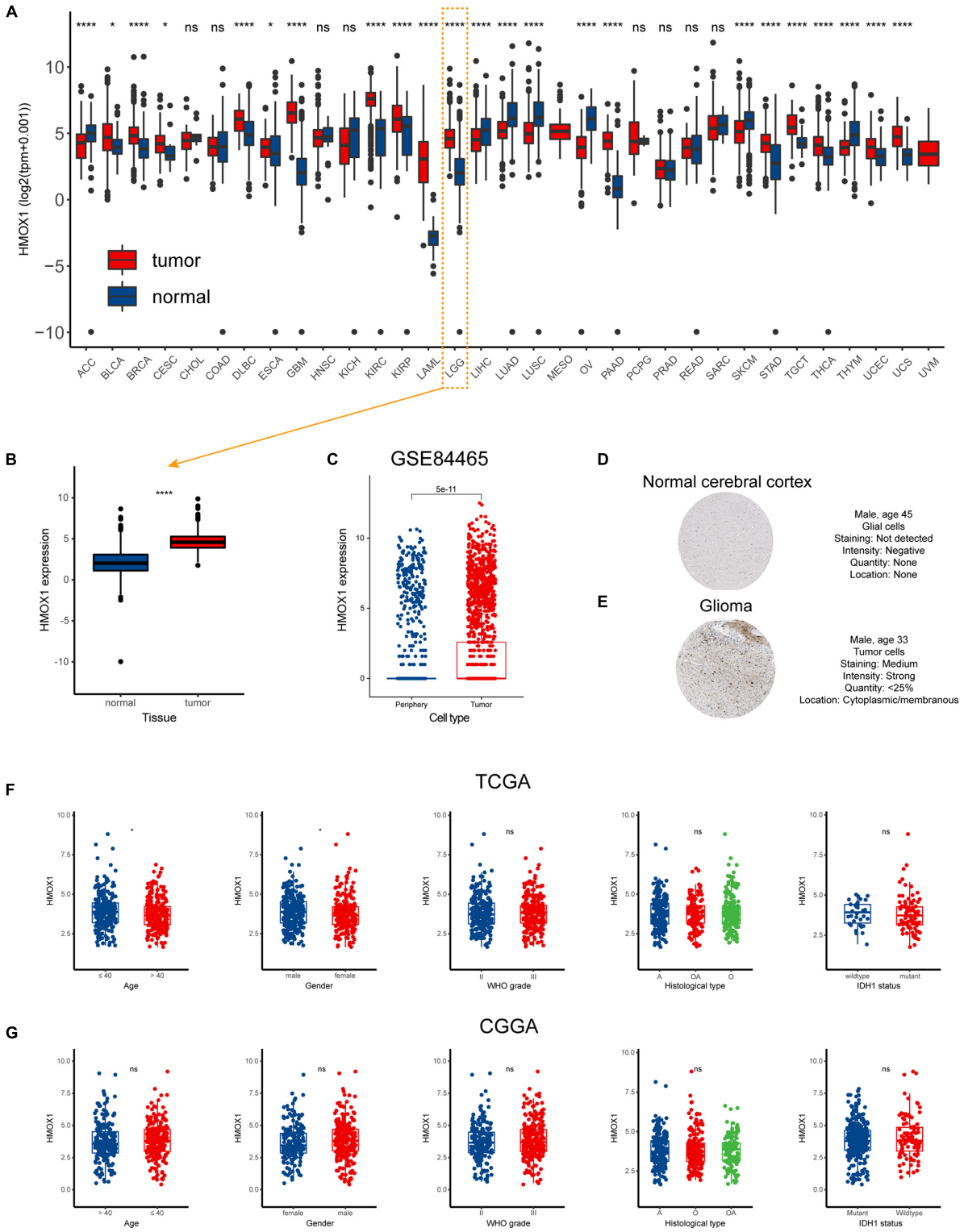

FIGURE 1 | Expression profiles of *HMOX1* in human normal and cancer tissues. **(A)** *HMOX1* expression levels in TCGA pan-cancers. **(B)** *HMOX1* mRNA expression levels in LGG and normal brain tissues. **(C)** *HMOX1* mRNA expression levels in tumor and periphery single cells in GSE84465 cohort. **(D,E)** Representative IHC images of HMOX1 protein expression in normal cerebral cortex and glioma. **(F,G)** The *HMOX1* expression of different subgroups for age, gender, WHO grade, histological type, and IDH1 status in the TCGA and CGGA cohorts. $^{*}p < 0.05$, $^{****}p < 0.0001$, ns, not significant. A, astrocytoma; O, oligodendroglioma; OA, oligoastrocytoma; WHO, World Health Organization; IDH1, isocitrate dehydrogenase 1.

among *HMOX1* mutations (**Supplementary Figure 3B**). Compared to the *HMOX1*-wildtpe group, *HMOX1*-mutant group shared significantly higher mutation frequencies of *TP53*, *TTN*, *MCM5* in pan-cancers (**Supplementary Figure 3C**), and higher mutation frequencies of *MCM5*, *APOL6*, *MB* in lower grade gliomas (**Supplementary Figure 3D**).

Heme Oxygenase-1 Predicts Poorer Survival Outcome in Lower Grade Glioma

Elevated *HMOX1* expression was significantly correlated with an unfavorable OS, DSS, and PFI in both uveal melanoma (UVM) and LGG (**Figures 2A–C**). Subsequent Kaplan-Meier survival analysis showed that $HMOX1^{high}$ patients had significantly poorer OS ($p = 0.0020$), poorer DSS ($p = 0.0064$), and poorer PFI ($p = 0.0240$) in TCGA cohort (**Figures 2D–F**). Furthermore, LGG patients with *HMOX1* wildtype had better survival than those with *HMOX1* mutation (**Figures 2G–I**). Specifically, patients with *HMOX1* CNV deletion demonstrated the worst prognosis which can be explained by the fact that lower CNV (deletion when < 0) represented higher *HMOX1* gene expression, as CNV was negatively correlated with expression for *HMOX1* (**Supplementary Figures 4A,B**). Notably, when exploring the impact of the CNV status on the prognosis of glioma patients, the sample sizes varied considerably. Briefly, there were 416 individuals in the HMOX1 "wild type" group vs. only 26 in the "amplification" group. This between-group variation is highly likely to contribute to a misinterpretation of statistical results.

Heme Oxygenase-1 Participates in Immune Infiltration and Tumor Microenvironment

Positively correlations were observed between *HMOX1* expression and regulatory T cells (Tregs), activated CD4+ memory T cells, as well as M2 macrophages (**Figure 3A**) in most cancer types. Regarding LGG, significant correlations were observed between higher *HMOX1* expression with increased abundance of naïve B cells, resting CD4+ memory T cells, Tregs, and M2 macrophages, but with decreased abundance of memory B cells and naive CD4+ T cells (**Figure 3B**). Furthermore, a negative relationship existed between *HMOX1* expression and tumor purity in lower grade gliomas, as it positively correlated with stromal, immune, and ESTIMATE scores (**Figures 3C–E**). Moreover, we found that the abundances of CD4+ T cells, neutrophils, macrophages, and dendritic cells were positively associated with *HMOX1* expression based on TIMER algorithm (**Figure 3F**).

To further explore the specific correlations between *HMOX1* and subpopulations of M2 macrophages. We summarized the functions, inducers, and surface markers of M2a∼d macrophages (Colin et al., 2014; Martinez and Gordon, 2014; Wang et al., 2019). Then we calculated the correlation between *HMOX1* and each marker to reflect the correlations between *HMOX1* mRNA expression and subclassified M2 macrophages (**Table 2**). The results showed that *HMOX1* expression was strongly correlated with M2b macrophages, as it was significantly correlated with M2b markers including CD86 ($R = 0.752$, $p < 0.0001$; **Supplementary Figure 4C**), HLA-DR ($R = 0.705$, $p < 0.0001$; **Supplementary Figure 4D**), HLA-DP ($R = 0.672$, $p < 0.0001$; **Supplementary Figure 4E**), and HLA-DQ ($R = 0.621$, $p < 0.0001$; **Supplementary Figure 4F**).

Using our own samples, we validated that grade III gliomas had higher HMOX1 protein expression compared with grade II gliomas (**Figure 4A**). The detailed immunohistochemical staining results were summarized in **Supplementary Table 2**. Furthermore, we confirmed the positive relationships between *HMOX1* expression levels and immune infiltrates including B cell and resting memory CD4+ T cell (**Figures 4B,C**), which was in consistent with the results obtained from the TCGA cohort. However, the poor correlations between *HMOX1* expression and cancer stemness, TMB, and MSI (**Figures 3G–I**) indicated that *HMOX1* was unlikely to influence oncogenic processes by engaging in genetic alterations or epigenetic modifications. Furthermore, *HMOX1* was significantly correlated with several recognized immune checkpoints including leukocyte associated immunoglobulin like receptor 1 (LAIR1), CD80, programmed cell death 1 ligand 2 (PDCD1LG2), CD40, and CD86 (**Supplementary Figure 4G**).

Risk Signature Construction in the Training Set

We identified 505 HRGs ($|\text{Spearman R}| > 0.6$, FDR < 0.001). Mainly located on cytoplasmic vesicle membrane, HRGs participated molecular functions such as immune receptor activity and interactions. In terms of biological processes, the gene set was mainly involved in leukocyte activity involved in immune response, leukocyte activation, positive regulation of immune response, etc. (**Figure 5A**). Regarding KEGG pathways, HRGs were intimately involved in tumor immunity such as NOD-like receptor signaling pathway, cytokine-cytokine receptor interaction, and NK cell mediated cytotoxicity (**Figure 5A**).

A total of 377 HRGs were significantly prognostic in the training set following a univariate Cox analysis ($p < 0.05$). A LASSO Cox analysis was performed on training dataset and a risk signature was then constructed containing 27 genes (**Figure 5B**). The result of PCA analysis indicated that the signature could discriminate lower grade gliomas from GBM and normal brain tissues (**Figure 5C**). Moreover, the coefficients and univariate Cox analysis results were displayed in **Figures 5D,E** and **Supplementary Table 3**. Protein-protein interactions and transcriptomic correlations were also illustrated in **Figures 5F,G**.

External and Subgroup Validation Demonstrates Stability of the Risk Signature

Risk plots and survival diagrams were displayed as **Figure 6A**. Kaplan-Meier curve indicated that high-risk LGG patients had significantly poorer prognosis ($p < 0.0001$, **Figure 6B**). The time-dependent ROC curves exhibited a promising ability of the model to predict OS in the training cohort (1-year AUC = 0.83, 3-year AUC = 0.88, 5-year AUC = 0.91; **Figure 6C**). The results were similar in the external CGGA cohort (**Figure 6D**). Higher risk

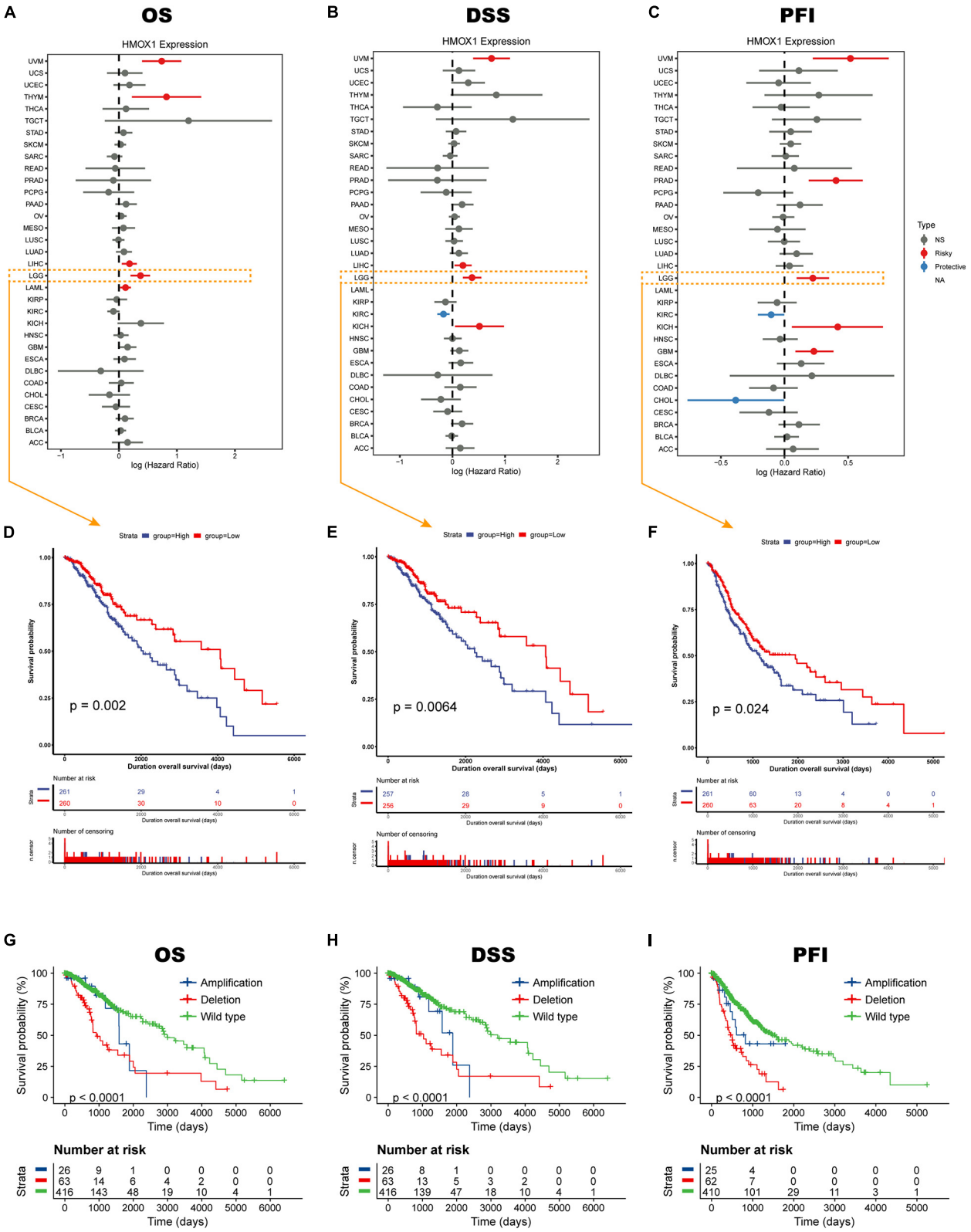

FIGURE 2 | Survival profiles of *HMOX1* in cancers. Relationships between *HMOX1* expression and **(A)** OS, **(B)** DSS, **(C)** PFI across 33 cancer types in TCGA database. **(D–F)** Kaplan-Meier survival curves based on *HMOX1* expression. **(G–I)** Kaplan-Meier survival curves based on *HMOX1* CNV status.

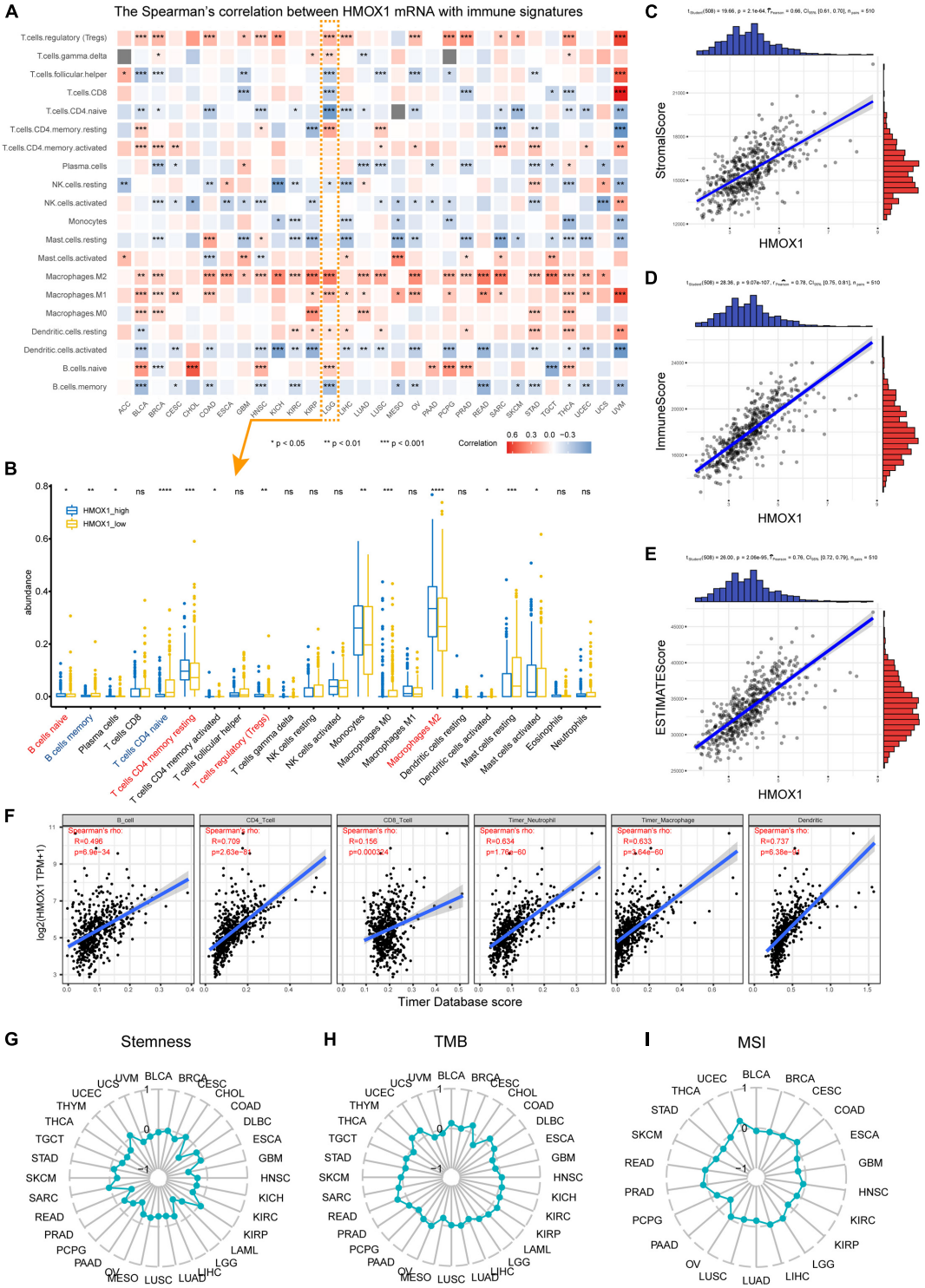

FIGURE 3 | Immune infiltration profiles of *HMOX1*. **(A)** Correlations between *HMOX1* expression and immune infiltrates in pan-cancers. **(B)** The abundance of immune infiltrates between *HMOX1*^{high} and *HMOX1*^{low} groups in LGG cohort based on CIBERSORT algorithm. **(C–E)** Correlations between *HMOX1* expression and stromal, immune, ESTIMATE scores. **(F)** The correlations between *HMOX1* expression and immune infiltrates in LGG cohort based on TIMER algorithm. **(G–I)** Correlations between *HMOX1* expression and stemness indexes, TMB, MSI in pan-cancers. $^{*}p < 0.05$, $^{**}p < 0.01$, $^{***}p < 0.001$. TMB, tumor mutation burden; MSI, microsatellite instability.

TABLE 2 | The correlations between *HMOX1* and M2 macrophage phenotypes in LGG based on cell markers.

M2 Macrophage phenotype	Functions	Inducers	Markers and surface molecules	Gene name	Spearman's rho	*p*-value
M2a macrophage	Type II inflammation;	IL-4	CD163	*CD163*	0.584	1.49E-48
	Allergy;	IL-13	CD200R1	*CD200R1*	0.279	1.15E-10
	Killing and encapsulation of parasites;		CD301	*CLEC10A*	0.513	4.70E-36
	Anti-inflammation;		CXCR1	*CXCR1*	0.161	2.37E-04
	Wound healing.		CXCR2	*CXCR2*	0.526	4.28E-38
			CD209	*CD209*	0.267	6.65E-10
			Dectin-1	*CLEC7A*	**0.649**[a]	4.28E-63
			FCERA	*FCER1A*	0.441	6.18E-26
			IL-1R2	*IL1R2*	0.280	9.59E-11
			IL-4R	*IL4R*	0.589	2.03E-49
			CD206	*MRC1*	0.090	0.0409
M2b macrophage	Th2 activation;	Lipopolysaccharides	CD86	*CD86*	**0.752**[a]	5.48E-59
	Immunoregulation;	Immune complexes	HLA-DR	*HLA-DRA*	**0.705**[a]	1.30E-78
	Promoting infection;	IL1R/TLR ligands	HLA-DP	*HLA-DPA1*	**0.672**[a]	5.00E-69
	Tumor progression.		HLA-DQ	*HLA-DQA1*	**0.621**[a]	2.70E-56
			IL-4R	*IL4R*	0.589	2.03E-49
			CD206	*MRC1*	0.090	0.0409
M2c macrophage	Immunosuppression;	IL-10	CCR2	*CCR2*	0.506	6.69E-35
	Tissue remodeling;	TGF-β	CD150	*SLAMF1*	0.427	2.86E-24
	Phagocytosis.	Glucocorticoid	CD163	*CD163*	0.584	1.49E-48
			IL-4R	*IL4R*	0.589	2.03E-49
			CD206	*MRC1*	0.090	0.0409
			SR-AI	*MSR1*	**0.758**[a]	1.72E-97
			TLR1	*TLR1*	**0.685**[a]	8.93E-73
M2d macrophage	Tumor progression;	TLR+A2R ligands	iNOS	*NOS2*	−0.232	9.24E-08
	Angiogenesis.		TNF-α (low)	*TNF*	0.310	5.67E-13
			IL-12 (low)	*IL12A*	0.089	0.0440
			VEGF	*VEGFA*	0.095	0.0305

[a]*Rho greater than 0.6 was bold.*

CXCR1, C-X-C chemokine receptor type 1; CXCR2, C-X-C chemokine receptor type 2; CLEC7A, C-type lectin domain family 7, member A; FCER1A, Fc fragment of IgE; MRC1, Mannose receptor, C type 1; CCR2, Chemokine (C-C motif) receptor 2; SLAMF1, Signaling lymphocytic activation molecule family member 1; MSR1, Macrophage scavenger receptor 1; TLR1, Toll-like receptor 1; NOS2, Nitric oxide synthase 2, inducible; VEGFA, Vascular endothelial growth factor A.

scores also indicated poorer OS ($p < 0.0001$, **Figure 6E**). The risk model still exhibited stable and high predication ability (1-year AUC = 0.75, 3-year AUC = 0.77, 5-year AUC = 0.78; **Figure 6F**). Furthermore, we performed a stratification analysis and found that the risk model retained the ability to predict OS in various subgroups in both cohorts (**Figures 6G,H**).

Risk Signature Correlates With Clinicopathological Characteristics, Immune Microenvironment, and Therapeutic Efficacy

Sankey diagrams were displayed showing the distribution of risk score and clinicopathologic characteristics among LGG patients (**Figures 7A,B**). LGG patients with increasing age and higher WHO grade possessed higher risk scores. Besides, an individual patient would have a higher risk score if his pathologic type of glioma was an astrocytoma or if he carried a wildtype IDH1 (**Figures 7C,D**). As for the immune microenvironment of glioma, samples with higher risk demonstrated higher percentages of resting CD4+ memory T cells, M1, M2 macrophages, and activated dendritic cells in both cohorts (**Figures 7E,F** and **Supplementary Table 4**).

As for the association between risk signature and therapeutic benefit, most therapies showed poor efficacy in both low-risk (**Figures 8A–C**) and high-risk groups (**Figures 8E–G**) in the TCGA cohort. However, patients who had lower risk scores exhibited uniquely better prognosis if they had undergone immunotherapies ($p = 0.0078$; **Figure 8D**). But the condition was not observed in the high-risk group ($p = 0.0620$; **Figure 8H**).

We then decoded the different functional states of malignant cells and target molecules at single-cell resolution and discovered three functional states which were significantly related to *HMOX1*, including angiogenesis (correlation = 0.44, $p < 0.001$;

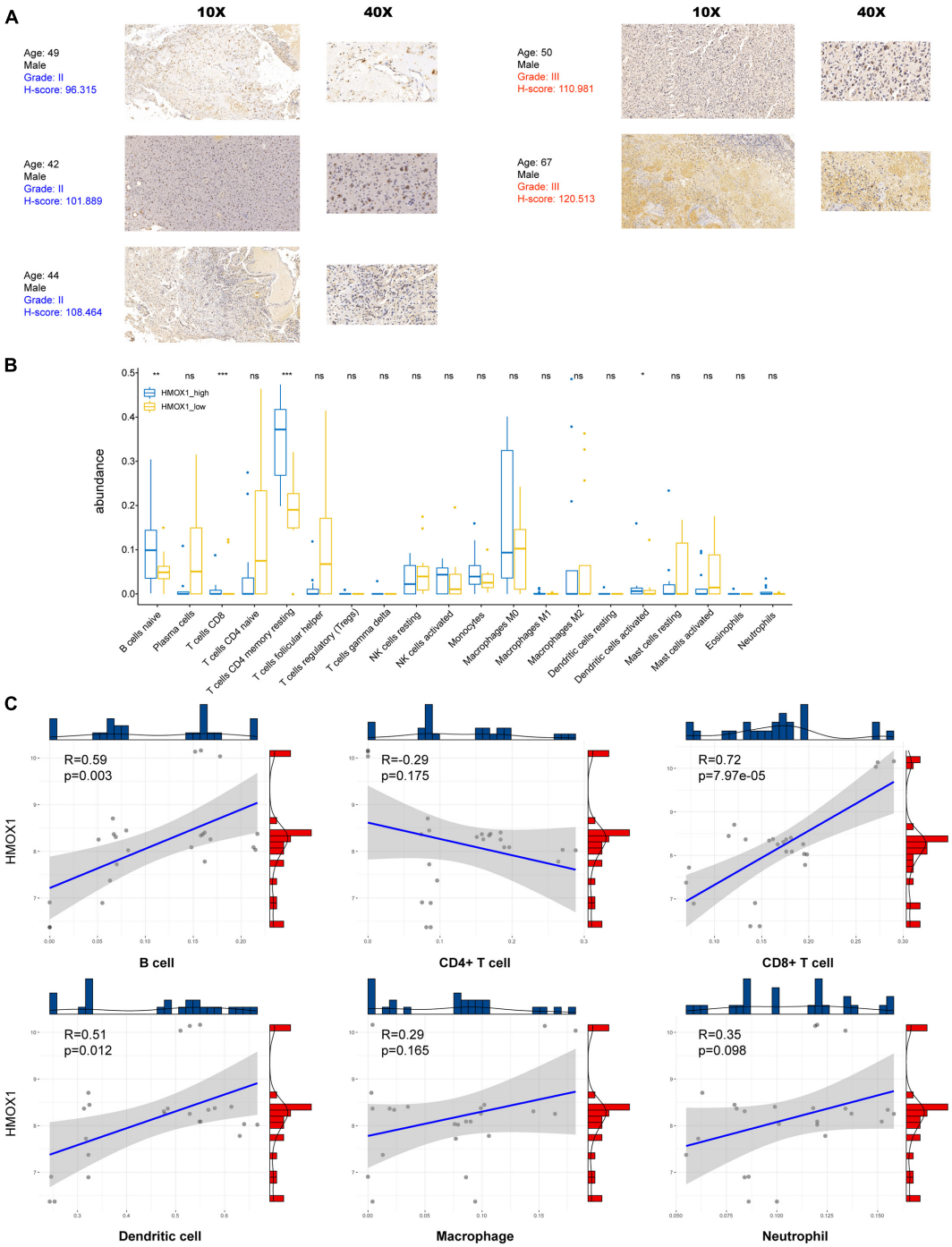

FIGURE 4 | Validation by using glioma samples from Xiangya Hospital. **(A)** Immunohistochemical staining results of five samples in Xiangya hospital. **(B)** The abundance of immune infiltrates between *HMOX1*^{high} and *HMOX1*^{low} groups in 24 glioma samples. **(C)** The correlations between *HMOX1* expression and immune infiltrates in 24 glioma samples. $^{*}p < 0.05$, $^{**}p < 0.01$, $^{***}p < 0.001$, ns, not significant.

Figure 8I), hypoxia (correlation = 0.40, $p < 0.001$; **Figure 8J**), and metastasis (correlation = 0.31, $p < 0.01$; **Figure 8K**). Furthermore, patients with lower *HMOX1* expression levels had high TIDE scores and exhibited better responses to the immunotherapies (**Figure 8L**). This is in consistent with the results of prediction of therapy efficacy in different risk subgroups. In addition, three drug databases were accessed to find relationship between drug sensitivity and *HMOX1* expression. TKI258 (dovitinib) showed significant sensitivity in the CCLE database (**Supplementary Figure 5A**). WZ3105 and Repligen 136

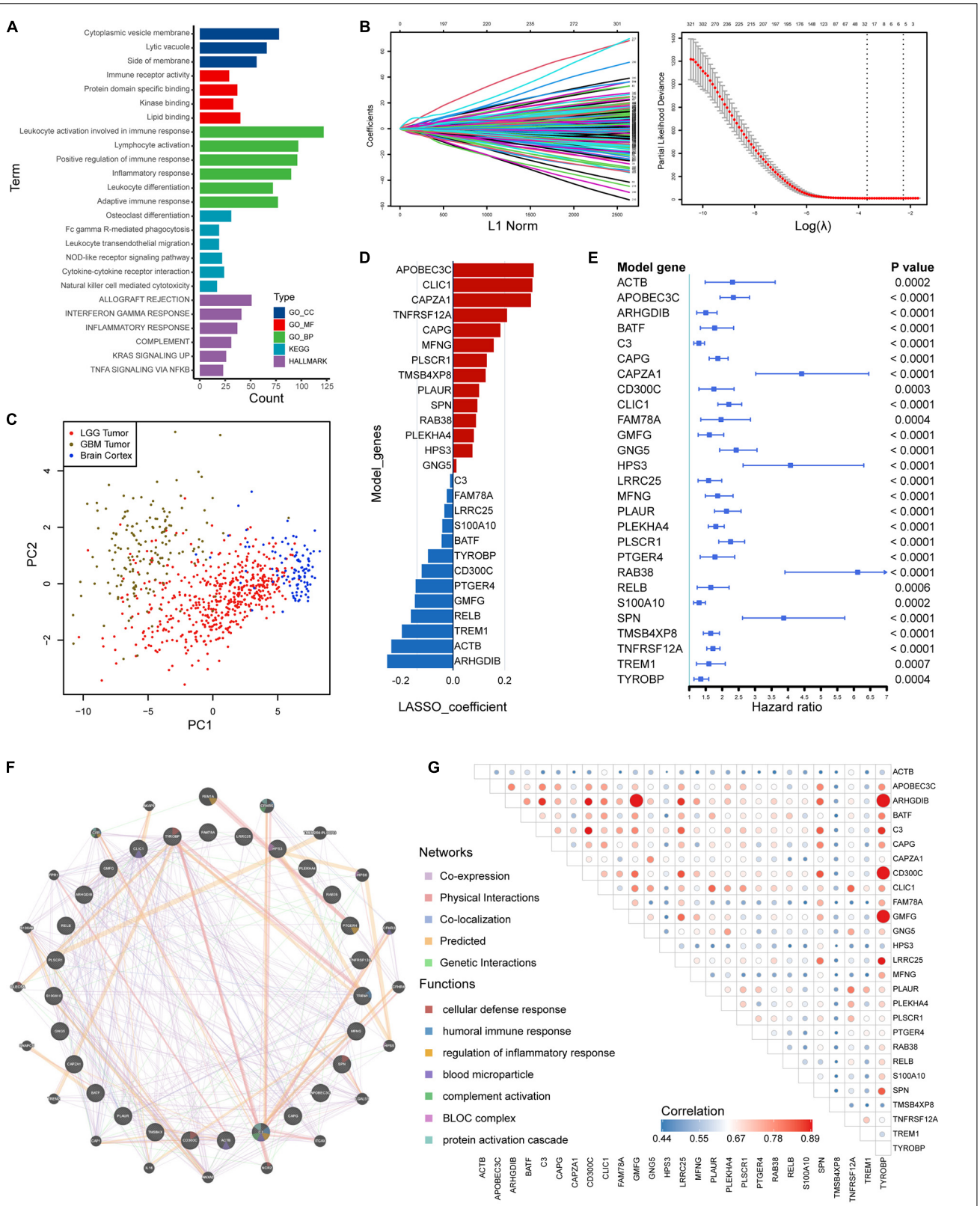

FIGURE 5 | Construction of risk signature based on HRGs in the training set. **(A)** Enrichment analyses based on HRGs. **(B,C)** LASSO analysis with eligible lambda value. **(C)** PCA analysis assessing the signature. **(D)** LASSO coefficients of the model genes. **(E)** Univariate analysis results of the model genes. **(F)** Protein-protein interactions of products of included genes. **(G)** Correlations among the model genes. GO, Gene Ontology; KEGG, Kyoto Encyclopedia of Genes and Genomes.

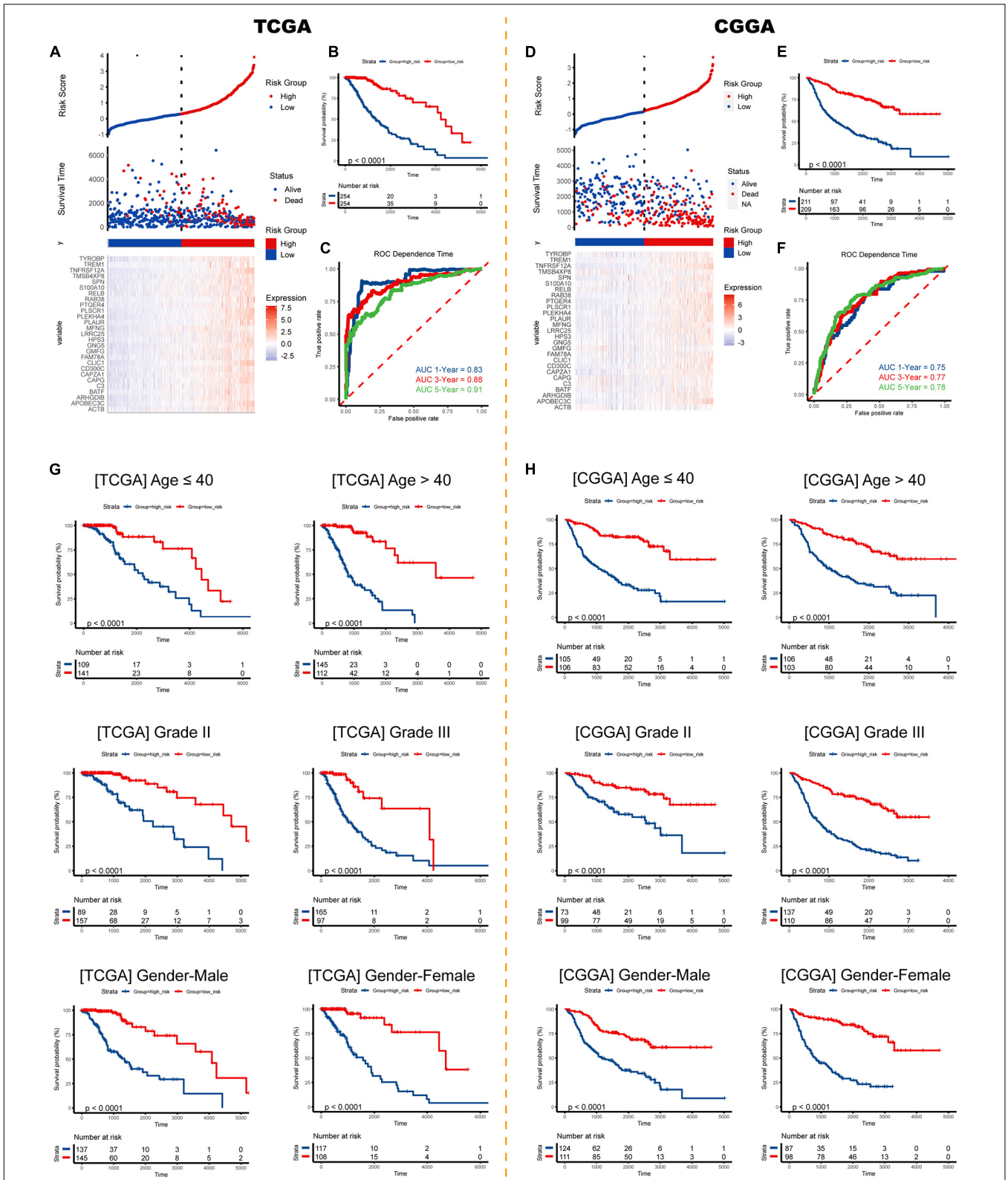

FIGURE 6 | Validation of the risk signature. Risk score, survival status, and expression pattern of model genes in the **(A)** TCGA cohort and **(D)** CGGA cohort. Kaplan-Meier analysis of patients in the high- and low-risk groups in the **(B)** TCGA cohort and **(E)** CGGA cohort. Time-dependent ROC analysis of risk score in predicting prognoses in the TCGA cohort **(C)** and the CGGA cohort **(F)**. Survival analyses in subgroups in the **(G)** TCGA cohort and **(H)** CGGA cohort. ROC, receiver operating characteristic.

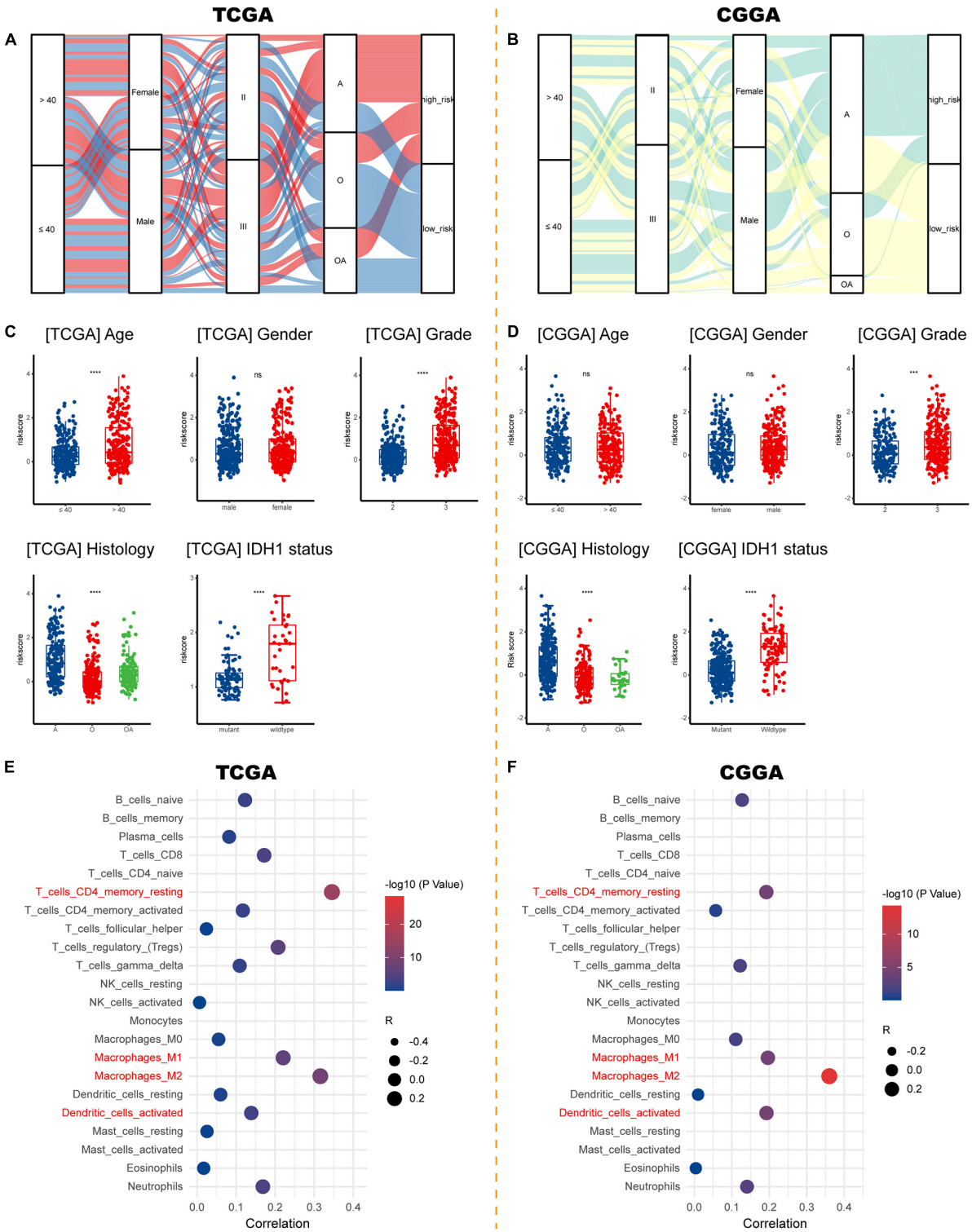

FIGURE 7 | Correlations between risk signature and clinicopathological characteristics. **(A,B)** Sankey diagrams showing the distribution of risk score and clinicopathologic characteristics in the TCGA and CGGA cohorts. **(C,D)** The risk score in different subgroups stratified by age, gender, WHO grade, histological type, and IDH1 status in the TCGA and CGGA cohorts. **(E,F)** Correlations between risk score and immune infiltration in the TCGA and CGGA cohorts. ***$p < 0.001$, ****$p < 0.0001$, ns, not significant. A, astrocytoma; O, oligodendroglioma; OA, oligoastrocytoma; IDH1, isocitrate dehydrogenase 1.

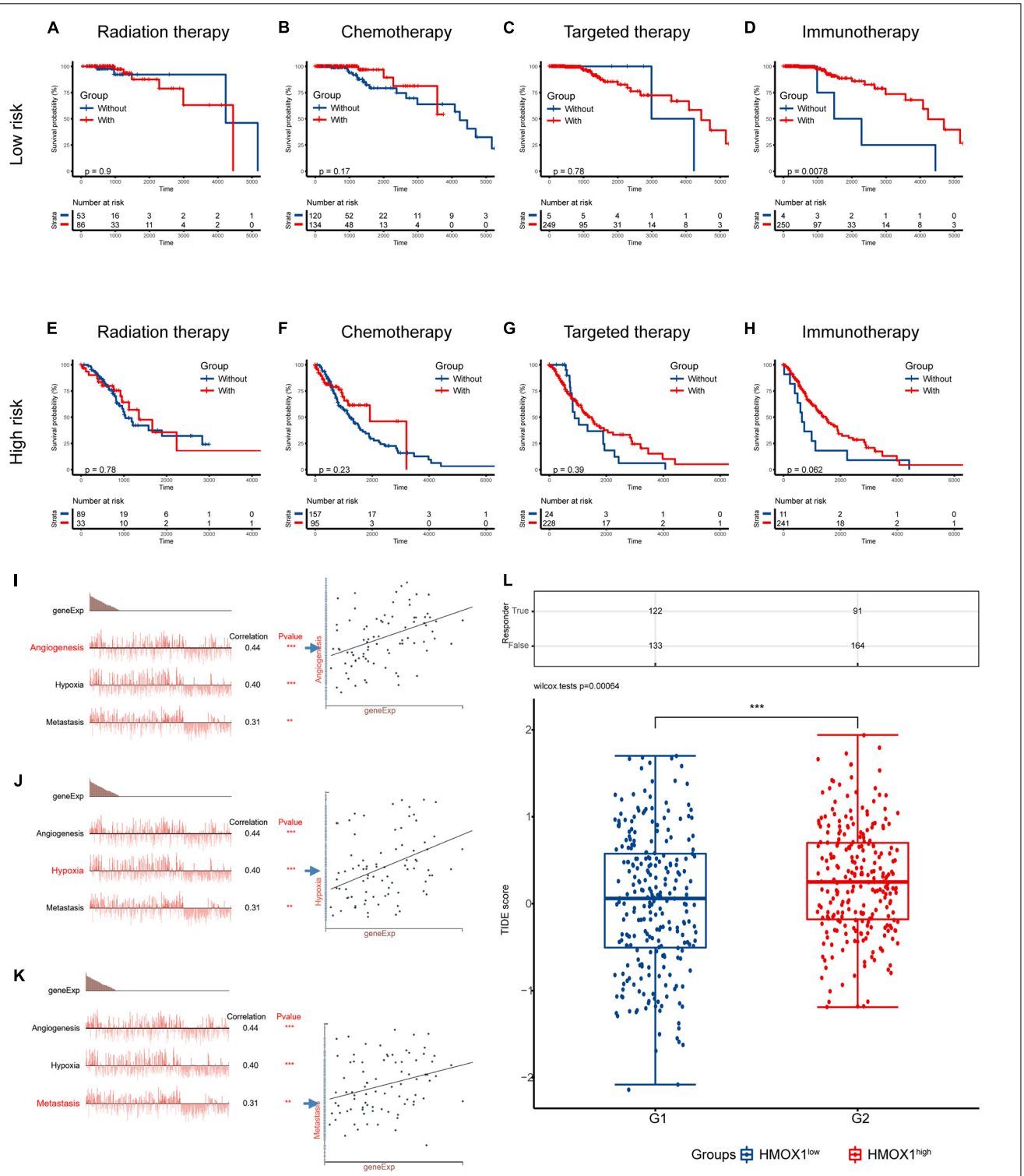

FIGURE 8 | Validation using collected samples and prediction of therapy efficacy. **(A–D)** The efficacies of radiation therapy, chemotherapy, targeted therapy, and immunotherapy in the TCGA cohort. **(E–H)** The efficacies of radiation therapy, chemotherapy, targeted therapy, and immunotherapy in the CGGA cohort. **(I–K)** The relationship between functional states and *HMOX1* expression based on single-cell sequencing. **(L)** Prediction of response to immunotherapy using TIDE algorithm. $^{**}p < 0.01$, $^{***}p < 0.001$. TIDE, Tumor Immune Dysfunction and Exclusion.

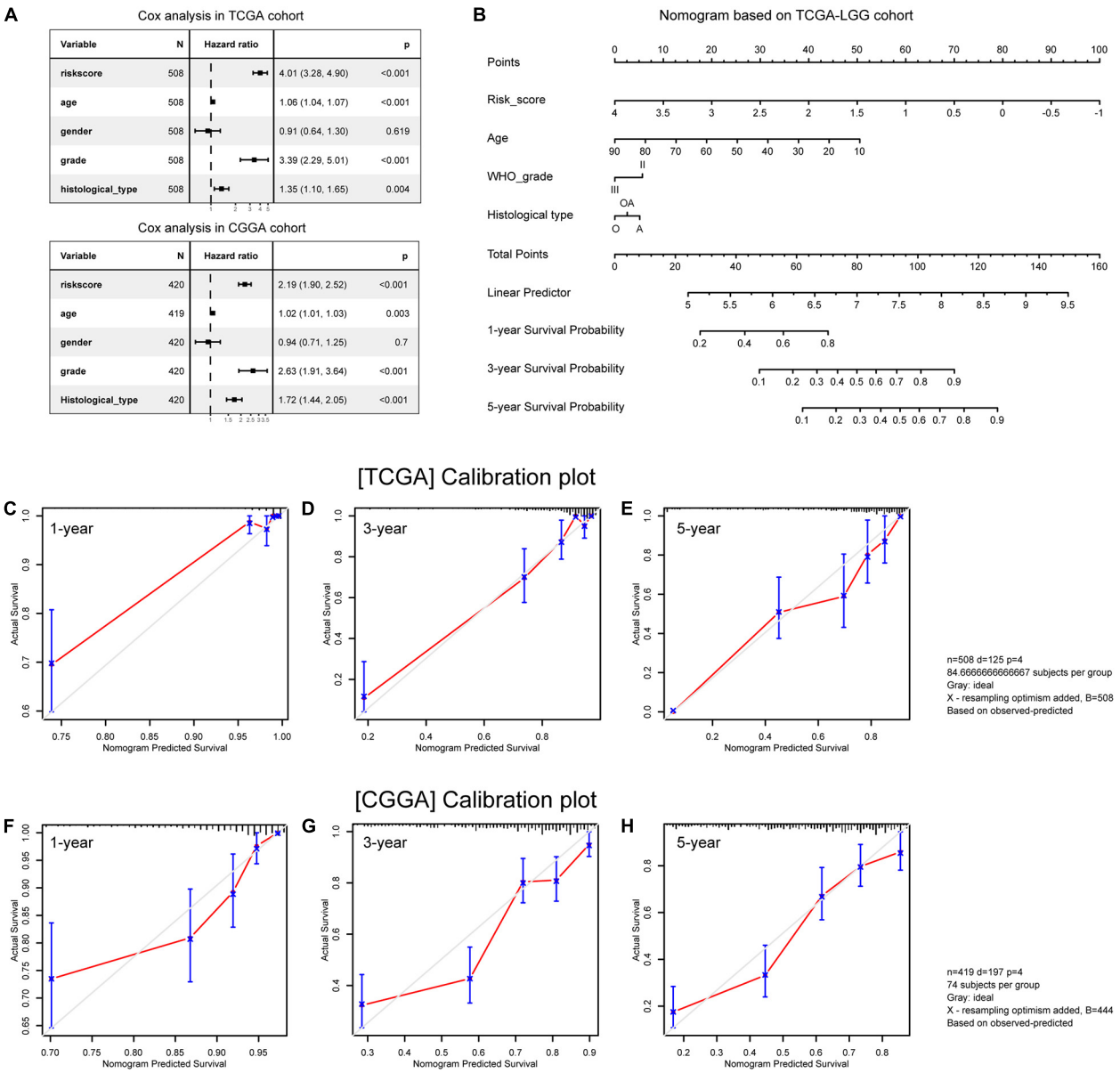

FIGURE 9 | Construction and validation of the nomogram. **(A)** Multivariate analysis results. **(B)** Nomogram based on risk score, age, WHO grade, and histological type. **(C–E)** Calibration plots of the nomogram for predicting the probability of OS at 1-, 3-, and 5-year in the TCGA cohort. **(F–H)** Calibration plots of the nomogram for predicting the probability of OS at 1-, 3-, and 5-year in the CGGA cohort. A, astrocytoma; O, oligodendroglioma; OA, oligoastrocytoma.

were selected from the CTRP (**Supplementary Figure 5B**) and GDSC (**Supplementary Figure 5C**) drug banks, respectively.

Construction and Validation of the Nomogram

Multivariate Cox analyses showed that age at first pathological diagnosis, WHO grade, histological type, and risk score were independent predictors of OS in both cohorts (**Figure 9A**). We then constructed a nomogram model incorporating these prognostic variables as a clinically applicable quantitative tool to predict survival in patients with primary lower grade gliomas (**Figure 9B**). The calibration plots demonstrated satisfactory predictive performance of the nomogram in both training (**Figures 9C–E**) and validation (**Figures 9F–H**) cohorts.

DISCUSSION

Molecular profiling of lower grade gliomas, common tumors in the human brain, has enhanced insights of molecular oncology and identified few prognostic and therapeutic targets. Over the past decades, surgical section following radiotherapy and chemotherapy still serve as the mainstream means for

glioma treatment. Due to the unique microenvironment and low mutational burden, gliomas acquire immunosuppressive phenotypes and poorly response to established immunotherapies. Clinicians thus need renewed molecular targets for better response rate as well as improved prognosis. Comprehensive bioinformatic analyses were used at multiple levels of expression, survival, and biological function to demonstrate the essential role of *HMOX1*. *HMOX1* and the risk signature are reliable predictors of LGG prognosis, and targeting *HMOX1* will help clinicians optimize the management of lower grade glioma patients in future preclinical and clinical practice.

The mechanism can be explained by the antioxidant role of HMOX1 in malignancies. Heme oxygenase-1 is a phase II enzyme that responds to adverse conditions, such as oxidative stress, cellular injury, and diseases. Its diverse roles in tumorigenesis have been well reviewed (Nitti et al., 2017; Chiang et al., 2018). Furthermore, HMOX1 has been widely recognized to play a cytoprotective role in tumor cells to overcome the assault of enhanced oxidative stress in the tumor microenvironment, thereby preventing the cancer cells from apoptosis and autophagy (Chiang et al., 2018). On the other hand, our study found that HMOX1 was enriched in blood and immune cells, especially monocytes and macrophages, which were thought to be risk factors for the overall survival of glioma patients (Zhang et al., 2021a,b). Therefore, a higher *HMOX1* expression level represented a stronger resistance to oxidative stress and a higher abundance of risk immune cell types, resulting an unfavorable outcome for LGG patients.

We observed that *HMOX1* expression was increased in lower grade gliomas at both tissue and single-cell levels, and such increase was associated with worse OS, DSS, and PFI in patients with LGG. Thereafter we suspect that *HMOX1* might influence the malignant properties and patient outcomes by intervening immune infiltration in the TME, as it was significantly associated with tumor purity, immune checkpoints' levels, immune infiltration abundance, as well as immune-oncological pathways. These findings were partially validated by our own samples.

In this study, 27of 377 prognostically valuable HRGs were screened out to establish a risk signature. Among them, *ARHGDIB* (Su et al., 2019), *LRRC25* (Zhang et al., 2020), *PLAUR* (Tan et al., 2020), and *TREM1* (Kong et al., 2020) were selected as prognostic hub genes in lower grade glioma in previous bioinformatic analyses. Besides, *GMFG* (Lan et al., 2021), *GNG5* (Yang et al., 2020), *S100A10* (Zhang et al., 2021c), *TNFRSF12A* (Tran et al., 2006), and *TYROBP* (Lu et al., 2021) were found to be upregulated and correlated with worse prognosis in LGG. Importantly, *CAPG* was identified as a prognosis factor correlated with macrophages in gliomas (Wei et al., 2020; Prescher et al., 2021). Moreover, a recent study reported that targeting *CLIC1* reduced gliomagenesis in tumoral stem or progenitor cells, indicating *CLIC1* as a potential target and prognostic biomarker there (Wang et al., 2012; Setti et al., 2013). Briefly, previous literature indicated that the model genes and encoded proteins were related to the progression of gliomas, which were perfectly consistent to our risk signature. The risk signature we constructed may reflect the distribution of immune infiltrates involved in the TME, as well as reliably and independently predicts prognosis of patients with primary gliomas. In addition, combining the constructed signature with clinicopathological features, we obtained a nomogram with strong predictive power which is of potential in clinical utilization.

Intriguingly, both the risk signature and *HMOX1* expression are correlated with fractions of infiltrating cells, especially resting memory CD4+ T cells and M2 macrophages. Resting memory CD4+ T cells were indicated to play an vital role in latent HIV-1 infection (Siliciano and Siliciano, 2015), its functions is yet warranted to be discovered in glioma. Additionally, abundance of M2 macrophages was associated with immune suppressive phenotype and short-term relapse after radiation therapy (Wang et al., 2017). Moreover, M2b macrophages are the most closely related to *HMOX1* in M2 macrophage subsets. Considering its involvement in type 2 helper T (Th2) activation, immunomodulation, and tumor progression, combined with the fact that Th2/Th1 ratio is a poor prognostic marker in gliomas (Kumar et al., 2006), we have good reasons to believe that HMOX1 is involved in immunoregulation in glioma microenvironment, driving tumors toward more malignant properties as well as a worse prognosis. Further work is certainly imperative for the validation of *HMOX1* functions in lower grade glioma. Besides, selectively targeting *HMOX1* was effective for therapy resistance in various cancers (Mayerhofer et al., 2008; Alaoui-Jamali et al., 2009). Several recently developed imidazole based non-porphyrin *HMOX1* inhibitors are highly selective for *HMOX1* without affecting other heme-containing proteins (Pittalà et al., 2013), and show potent antitumor activities in preclinical models (Salerno et al., 2013), exhibiting high-quality prospects for clinical use.

A key finding in our study is that immunotherapy demonstrated unique superiority in the low-risk group as patients with vs. without immunotherapy exhibited significantly better survival. Considering that patients with lower *HMOX1* expression had lower TIDE score and showed higher response rate to immunotherapy, we conclude that *HMOX1*, as well as *HMOX1*-based risk signature, is capable for predicting the immunotherapy efficacy in lower grade gliomas. Regarding the mechanisms, we found that both *HMOX1* and risk signature were correlated with M2 macrophages. An important and promising observation for cancer immunotherapy is that macrophages can direct T or B cell responses in the presence or absence of specific antigens (Mills et al., 2016). In particular, M2 macrophages induce T cells into Treg and other T cell type responses without anticancer activity via innate signals such as transforming growth factor-β (TGF-β) and interleukin 10 (IL-10) (Mills et al., 2000; Ruffell and Coussens, 2015). Therefore, we believe that the key to the sensitivity of immunotherapies to the risk score is that the *HMOX1*-based risk score well reflects the distribution of M2 macrophages in gliomas.

There were several limitations in our study. First, our sample size is too small to be completely convinced. Second, only one cohort with single-cell sequencing data was employed to evaluated the functions of *HMOX1* in glioma. Third, we included

27 genes in our risk signature, proposing a great challenge for experimental validation. Finally, The TCGA dataset does not provide details of adjuvant therapy and, in particular, immunotherapy, which reduces the generalizability of our conclusions. Unfortunately, we do not have such a LGG dataset to study the immunotherapy response. Although we used patients from the CGGA database (validation set) to validate the results obtained from the TCGA database (training set) and showed good concordance, we believe that a larger multi-center cohort of glioma patients who undergo immunotherapy will provide insight into this issue.

In our study, we employed data from independent cohorts to explore the expression profile of heme oxygenase-1 in glioma. *HMOX1* influences immune infiltration as well as survival prognosis of LGG patients. Importantly, *HMOX1* were related to oncological functional states including angiogenesis, hypoxia, and metastasis. A risk signature and nomogram based on HRGs have robust predict power as well as the potential for clinical applications.

DATA AVAILABILITY STATEMENT

The datasets presented in this study can be found in online repositories. The names of the repository/repositories and accession number(s) can be found in the article/ **Supplementary Material**.

ETHICS STATEMENT

The studies involving human participants were reviewed and approved by the Ethics Committee of Xiangya Hospital. The patients/participants provided their written informed consent to participate in this study.

AUTHOR CONTRIBUTIONS

WY performed the data analysis, interpreted the data, and prepared the draft. FL collected the samples in our cohort and they were responsible for the subsequent RNA sequencing of them. CL performed the visualization. ZL and FL revised the manuscript. CL and FL designed the research and supervised all the work. All authors have read and approved the final manuscript, and agree to be accountable for the content of the work.

FUNDING

This work was supported by the National Natural Science Foundation of China (Grant No. 82001223) and the Natural Science Foundation for Young Scientist of Hunan Province, China (Grant No. 2019JJ50952).

ACKNOWLEDGMENTS

We thank all reviewers for their comments, which have greatly improved the quality of our manuscript.

SUPPLEMENTARY MATERIAL

The Supplementary Material for this article can be found online at: https://www.frontiersin.org/articles/10.3389/fcell.2021.760800/full#supplementary-material

Supplementary Figure 1 | Flow chart of the whole study. FDR, false discovery rate; LASSO, least absolute shrinkage and selection operator.

Supplementary Figure 2 | The comprehensive illustration of HMOX1 expression in different tissues and cell types downloading from the HPA database (https://www.proteinatlas.org/). **(A)** The expression of *HMOX1* in normal tissues. **(B)** The expression of *HMOX1* in normal cells (including single cells). **(C)** The expression of *HMOX1* in tumor tissues. **(G)** The expression of *HMOX1* in cell lines.

Supplementary Figure 3 | Mutational profiles of *HMOX1*. **(A)** Summary of *HMOX1* mutations in TCGA pan-cancers. **(B)** The general mutation count of *HMOX1*. **(C,D)** Differential altered genes between HMOX1-altered and HMOX1-unaltered groups in pan-cancer and LGG cohort. $^{*}p < 0.05$. CNV, copy number variation.

Supplementary Figure 4 | (A) CNV distribution of *HMOX1* in LGG tumor samples. **(B)** Spearman correlation between *HMOX1* CNV and mRNA expression in LGG. **(C–F)** Correlations between *HMOX1* and M2b macrophage markers. **(G)** Correlations between *HMOX1* expression and recognized immune checkpoints. $^{*}p < 0.05$, $^{**}p < 0.01$, $^{***}p < 0.001$. CNV, copy number variation; Homo. Amp., homogenous amplification; Homo. Del., homogenous deletion; Hete. Amp., heterogenous amplification; Hete. Del., heterogenous deletion.

Supplementary Figure 5 | Prediction of drug responses in the **(A)** Cancer Cell Line Encyclopedia (CCLE), **(B)** Cancer Therapeutics Response Portal (CTRP), and **(C)** Genomics of Drug Sensitivity in Cancer (GDSC) banks. $^{*}p < 0.05$.

REFERENCES

Alaoui-Jamali, M. A., Bismar, T. A., Gupta, A., Szarek, W. A., Su, J., Song, W., et al. (2009). A novel experimental heme oxygenase-1–targeted therapy for hormone-refractory prostate cancer. *Cancer Res.* 69, 8017–8024. doi: 10.1158/0008-5472.CAN-09-0419

Brat, D. J., Verhaak, R. G. W., Aldape, K. D., Yung, W. K. A., Salama, S. R., Cooper, L. A. D., et al. (2015). Comprehensive, integrative genomic analysis of diffuse lower-grade gliomas. *N. Engl. J. Med.* 372, 2481–2498. doi: 10.1158/1538-7445.AM2014-936

Cairncross, G., Wang, M., Shaw, E., Jenkins, R., Brachman, D., Buckner, J., et al. (2013). Phase III trial of chemoradiotherapy for anaplastic oligodendroglioma: long-term results of RTOG 9402. *J. Clin. Oncol.* 31, 337–343. doi: 10.1200/JCO.2012.43.2674

Chen, B., Khodadoust, M. S., Liu, C. L., Newman, A. M., and Alizadeh, A. A. (2018). Profiling tumor infiltrating immune cells with CIBERSORT. *Methods Mol. Biol.* 1711, 243–259. doi: 10.1007/978-1-4939-7493-1_12

Chiang, S.-K., Chen, S.-E., and Chang, L.-C. A. (2018). Dual role of heme oxygenase-1 in cancer cells. *Int. J. Mol. Sci.* 20:39. doi: 10.3390/ijms20010039

Colin, S., Chinetti-Gbaguidi, G., and Staels, B. (2014). Macrophage phenotypes in atherosclerosis. *Immunol. Rev.* 262, 153–166. doi: 10.1111/imr.12218

Darmanis, S., Sloan, S. A., Croote, D., Mignardi, M., Chernikova, S., Samghababi, P., et al. (2017). Single-cell RNA-Seq analysis of infiltrating neoplastic cells at the migrating front of human glioblastoma. *Cell Rep.* 21, 1399–1410. doi: 10.1016/j.celrep.2017.10.030

Degese, M. S., Mendizabal, J. E., Gandini, N. A., Gutkind, J. S., Molinolo, A., Hewitt, S. M., et al. (2012). Expression of heme oxygenase-1 in non-small cell lung cancer (NSCLC) and its correlation with clinical data. *Lung Cancer* 77, 168–175. doi: 10.1016/j.lungcan.2012.02.016

Friedman, J., Hastie, T., Tibshirani, R., Narasimhan, B., Tay, K., and Simon, N. (2020). *Lasso and Elastic-Net Regularized Generalized Linear Models [R package glmnet version 4.0-2]*.

Gandini, N. A., Fermento, M. E., Salomón, D. G., Obiol, D. J., Andrés, N. C., Zenklusen, J. C., et al. (2014). Heme oxygenase-1 expression in human gliomas and its correlation with poor prognosis in patients with astrocytoma. *Tumor Biol.* 35, 2803–2815. doi: 10.1007/s13277-013-1373-z

Jiang, P., Gu, S., Pan, D., Fu, J., Sahu, A., Hu, X., et al. (2018). Signatures of T cell dysfunction and exclusion predict cancer immunotherapy response. *Nat. Med.* 24, 1550–1558. doi: 10.1038/s41591-018-0136-1

Kong, Y., Feng, Z.-C., Zhang, Y.-L., Liu, X.-F., Ma, Y., Zhao, Z.-M., et al. (2020). Identification of immune-related genes contributing to the development of glioblastoma using weighted gene co-expression network analysis. *Front. Immunol.* 11:1281. doi: 10.3389/fimmu.2020.01281

Kumar, R., Kamdar, D., Madden, L., Hills, C., Crooks, D., O'Brien, D., et al. (2006). Th1/Th2 cytokine imbalance in meningioma, anaplastic astrocytoma and glioblastoma multiforme patients. *Oncol. Rep.* 15, 1513–1516. doi: 10.3892/or.15.6.1513

Lan, A., Ren, C., Wang, X., Tong, G., and Yang, G. (2021). Bioinformatics and survival analysis of glia maturation factor-γ in pan-cancers. *BMC Cancer* 21:423. doi: 10.1186/s12885-021-08163-2

Li, T., Fan, J., Wang, B., Traugh, N., Chen, Q., Liu, J. S., et al. (2017). TIMER: a web server for comprehensive analysis of tumor-infiltrating immune cells. *Cancer Res.* 77, e108–e110. doi: 10.1158/0008-5472.CAN-17-0307

Lu, J., Peng, Y., Huang, R., Feng, Z., Fan, Y., Wang, H., et al. (2021). Elevated TYROBP expression predicts poor prognosis and high tumor immune infiltration in patients with low-grade glioma. *BMC Cancer* 21:723. doi: 10.1186/s12885-021-08456-6

Maines, M. D., and Abrahamsson, P.-A. (1996). Expression of heme oxygenase-1 (HSP32) in human prostate: normal, hyperplastic, and tumor tissue distribution. *Urology* 47, 727–733. doi: 10.1016/S0090-4295(96)00010-6

Martinez, F. O., and Gordon, S. (2014). The M1 and M2 paradigm of macrophage activation: time for reassessment. *F1000 Med. Rep.* 6:13. doi: 10.12703/P6-13

Mayerhofer, M., Gleixner, K. V., Mayerhofer, J., Hoermann, G., Jaeger, E., Aichberger, K. J., et al. (2008). Targeting of heat shock protein 32 (Hsp32)/heme oxygenase-1 (HO-1) in leukemic cells in chronic myeloid leukemia: a novel approach to overcome resistance against imatinib. *Blood* 111, 2200–2210. doi: 10.1182/blood-2006-11-055723

Mills, C. D., Kincaid, K., Alt, J. M., Heilman, M. J., and Hill, A. M. (2000). M-1/M-2 macrophages and the Th1/Th2 paradigm. *J. Immunol.* 164, 6166–6173. doi: 10.4049/jimmunol.164.12.6166

Mills, C. D., Lenz, L. L., and Harris, R. A. (2016). A breakthrough: macrophage-directed cancer immunotherapy. *Cancer Res.* 76, 513–516. doi: 10.1158/0008-5472.CAN-15-1737

Miyata, Y., Kanda, S., Mitsunari, K., Asai, A., and Sakai, H. (2014). Heme oxygenase-1 expression is associated with tumor aggressiveness and outcomes in patients with bladder cancer: a correlation with smoking intensity. *Transl. Res.* 164, 468–476. doi: 10.1016/j.trsl.2014.06.010

Nduom, E. K., Weller, M., and Heimberger, A. B. (2015). Immunosuppressive mechanisms in glioblastoma. *Neuro Oncol.* 17, vii9–vii14. doi: 10.1093/neuonc/nov151

Nitti, M., Piras, S., Marinari, U. M., Moretta, L., Pronzato, M. A., and Furfaro, A. L. (2017). HO-1 induction in cancer progression: a matter of cell adaptation. *Antioxidants* 6:29. doi: 10.3390/antiox6020029

Noh, S. J., Bae, J. S., Jamiyandorj, U., Park, H. S., Kwon, K. S., Jung, S. H., et al. (2013). Expression of nerve growth factor and heme oxygenase-1 predict poor survival of breast carcinoma patients. *BMC Cancer* 13:516. doi: 10.1186/1471-2407-13-516

Ph, L., Wm, L., and Ly, C. (2013). TRC8 suppresses tumorigenesis through targeting heme oxygenase-1 for ubiquitination and degradation. *Oncogene* 32, 2325–2334. doi: 10.1038/onc.2012.244

Phillips, A. C., Boghaert, E. R., Vaidya, K. S., Mitten, M. J., Norvell, S., Falls, H. D., et al. (2016). ABT-414, an antibody drug conjugate targeting a tumor-selective EGFR epitope. *Mol. Cancer Ther.* 15, 661–669. doi: 10.1158/1535-7163.MCT-15-0901

Pittalà, V., Salerno, L., Romeo, G., Modica, M. N., and Siracusa, M. A. (2013). A focus on heme oxygenase-1 (HO-1) inhibitors. *Curr. Med. Chem.* 20, 3711–3732. doi: 10.2174/0929867311320300003

Prescher, N., Hänsch, S., Knobbe-Thomsen, C. B., Stühler, K., and Poschmann, G. (2021). The migration behavior of human glioblastoma cells is influenced by the redox-sensitive human macrophage capping protein CAPG. *Free Radic. Biol. Med.* 167, 81–93. doi: 10.1016/j.freeradbiomed.2021.02.038

Robinson, G. W., Orr, B. A., and Gajjar, A. (2014). Complete clinical regression of a BRAF V600E-mutant pediatric glioblastoma multiforme after BRAF inhibitor therapy. *BMC Cancer* 14:258. doi: 10.1186/1471-2407-14-258

Ruffell, B., and Coussens, L. M. (2015). Macrophages and therapeutic resistance in cancer. *Cancer Cell* 27, 462–472. doi: 10.1016/j.ccell.2015.02.015

Salerno, L., Pittalà, V., Romeo, G., Modica, M. N., Siracusa, M. A., Giacomo, C. D., et al. (2013). Evaluation of novel aryloxyalkyl derivatives of imidazole and 1,2,4-triazole as heme oxygenase-1 (HO-1) inhibitors and their antitumor properties. *Bioorg. Med. Chem.* 21, 5145–5153. doi: 10.1016/j.bmc.2013.06.040

Sanai, N., Alvarez-Buylla, A., and Berger, M. S. (2005). Neural stem cells and the origin of gliomas. *N. Engl. J. Med.* 353, 811–822. doi: 10.1056/NEJMra043666

Setti, M., Savalli, N., Osti, D., Richichi, C., Angelini, M., Brescia, P., et al. (2013). Functional role of CLIC1 ion channel in glioblastoma-derived stem/progenitor cells. *J. Natl. Cancer Inst.* 105, 1644–1655. doi: 10.1093/jnci/djt278

Siliciano, J. M., and Siliciano, R. F. (2015). The remarkable stability of the latent reservoir for HIV-1 in resting memory CD4+ T Cells. *J. Infect. Dis.* 212, 1345–1347. doi: 10.1093/infdis/jiv219

Stefano, A. L. D., Fucci, A., Frattini, V., Labussiere, M., Mokhtari, K., Zoppoli, P., et al. (2015). Detection, characterization and inhibition of FGFR-TACC fusions in IDH wild type glioma. *Clin. Cancer Res.* 21, 3307–3317. doi: 10.1158/1078-0432.CCR-14-2199

Su, J., Long, W., Ma, Q., Xiao, K., Li, Y., Xiao, Q., et al. (2019). Identification of a tumor microenvironment-related eight-gene signature for predicting prognosis in lower-grade gliomas. *Front. Genet.* 10:1143. doi: 10.3389/fgene.2019.01143

Suzuki, H., Aoki, K., Chiba, K., Sato, Y., Shiozawa, Y., Shiraishi, Y., et al. (2015). Mutational landscape and clonal architecture in grade II and III gliomas. *Nat. Genet.* 47, 458–468. doi: 10.1038/ng.3273

Tan, Y. Q., Li, Y. T., Yan, T. F., Xu, Y., Liu, B. H., Yang, J. A., et al. (2020). Six immune associated genes construct prognostic model evaluate low-grade glioma. *Front. Immunol.* 11:606164. doi: 10.3389/fimmu.2020.606164

Tran, N. L., McDonough, W. S., Savitch, B. A., Fortin, S. P., Winkles, J. A., Symons, M., et al. (2006). Increased fibroblast growth factor-inducible 14 expression levels promote glioma cell invasion via Rac1 and nuclear factor-κB and correlate with poor patient outcome. *Cancer Res.* 66, 9535–9542. doi: 10.1158/0008-5472.CAN-06-0418

van den Bent, M. J., Brandes, A. A., Taphoorn, M. J. B., Kros, J. M., Kouwenhoven, M. C. M., Delattre, J.-Y., et al. (2013). Adjuvant procarbazine, lomustine, and vincristine chemotherapy in newly diagnosed anaplastic oligodendroglioma: long-term follow-up of EORTC brain tumor group study 26951. *J. Clin. Oncol.* 31, 344–350. doi: 10.1200/JCO.2012.43.2229

Wang, L., He, S., Tu, Y., Ji, P., Zong, J., Zhang, J., et al. (2012). Elevated expression of chloride intracellular channel 1 is correlated with poor prognosis in human gliomas. *J. Exp. Clin. Cancer Res.* 31:44. doi: 10.1186/1756-9966-31-44

Wang, L. X., Zhang, S. X., Wu, H. J., Rong, X. L., and Guo, J. (2019). M2b macrophage polarization and its roles in diseases. *J. Leukoc. Biol.* 106, 345–358. doi: 10.1002/JLB.3RU1018-378RR

Wang, Q., Hu, B., Hu, X., Kim, H., Squatrito, M., Scarpace, L., et al. (2017). Tumor evolution of glioma-intrinsic gene expression subtypes associates with immunological changes in the microenvironment. *Cancer Cell* 32:152. doi: 10.1016/j.ccell.2017.06.003

Was, H., Cichon, T., Smolarczyk, R., Rudnicka, D., Stopa, M., Chevalier, C., et al. (2006). Overexpression of heme oxygenase-1 in murine melanoma: increased proliferation and viability of tumor cells, decreased survival of mice. *Am. J. Pathol.* 169, 2181–2198. doi: 10.2353/ajpath.2006.051365

Wei, J., Feng, L., and Wu, L. (2020). Integrated analysis identified CAPG as a prognosis factor correlated with immune infiltrates in lower−grade glioma. *Clin. Transl. med.* 10:e51. doi: 10.1002/ctm2.51

Wick, W., Platten, M., Meisner, C., Felsberg, J., Tabatabai, G., Simon, M., et al. (2012). Temozolomide chemotherapy alone versus radiotherapy

alone for malignant astrocytoma in the elderly: the NOA-08 randomised, phase 3 trial. *Lancet Oncol.* 13, 707–715. doi: 10.1016/S1470-2045(12)70164-X

Yan, H., Parsons, D. W., Jin, G., McLendon, R., Rasheed, B. A., Yuan, W., et al. (2009). IDH1 and IDH2 mutations in gliomas. *N. Engl. J. Med.* 360, 765–773. doi: 10.1056/NEJMoa0808710

Yang, B., Han, Z.-Y., Wang, W.-J., Ma, Y.-B., and Chu, S.-H. (2020). GNG5 is an unfavourable independent prognostic indicator of gliomas. *J. Cell. Mol. Med.* 24, 12873–12878. doi: 10.1111/jcmm.15923

Yin, H., Fang, J., Liao, L., Maeda, H., and Su, Q. (2014). Upregulation of heme oxygenase-1 in colorectal cancer patients with increased circulation carbon monoxide levels, potentially affects chemotherapeutic sensitivity. *Bmc Cancer* 14:436. doi: 10.1186/1471-2407-14-436

Yin, Y., Liu, Q., Wang, B., Chen, G., Xu, L., and Zhou, H. (2012). Expression and function of heme oxygenase-1 in human gastric cancer. *Exp. Biol. Med.* 237, 362–371. doi: 10.1258/ebm.2011.011193

Yuan, H., Yan, M., Zhang, G., Liu, W., Deng, C., Liao, G., et al. (2019). CancerSEA: a cancer single-cell state atlas. *Nucleic Acids Res.* 47, D900–D908. doi: 10.1093/nar/gky939

Zhang, M., Wang, X., Chen, X., Guo, F., and Hong, J. (2020). Prognostic value of a stemness index-associated signature in primary lower-grade glioma. *Front. Genet.* 11:441. doi: 10.3389/fgene.2020.00441

Zhang, N., Dai, Z., Wu, W., Wang, Z., Cao, H., Zhang, Y., et al. (2021a). The predictive value of monocytes in immune microenvironment and prognosis of glioma patients based on machine learning. *Front. Immunol.* 12:656541. doi: 10.3389/fimmu.2021.656541

Zhang, N., Zhang, H., Wang, Z., Dai, Z., Zhang, X., Cheng, Q., et al. (2021b). Immune infiltrating cells-derived risk signature based on large-scale analysis defines immune landscape and predicts immunotherapy responses in glioma tumor microenvironment. *Front. Immunol.* 12:691811. doi: 10.3389/fimmu.2021.691811

Zhang, Y., Yang, X., Zhu, X.-L., Bai, H., Wang, Z.-Z., Zhang, J.-J., et al. (2021c). S100A gene family: immune-related prognostic biomarkers and therapeutic targets for low-grade glioma. *Aging (Albany NY)* 13, 15459–15478. doi: 10.18632/aging.203103

Conflict of Interest: The authors declare that the research was conducted in the absence of any commercial or financial relationships that could be construed as a potential conflict of interest.

Publisher's Note: All claims expressed in this article are solely those of the authors and do not necessarily represent those of their affiliated organizations, or those of the publisher, the editors and the reviewers. Any product that may be evaluated in this article, or claim that may be made by its manufacturer, is not guaranteed or endorsed by the publisher.

Copyright © 2021 Ye, Liu, Liu and Luo. This is an open-access article distributed under the terms of the Creative Commons Attribution License (CC BY). The use, distribution or reproduction in other forums is permitted, provided the original author(s) and the copyright owner(s) are credited and that the original publication in this journal is cited, in accordance with accepted academic practice. No use, distribution or reproduction is permitted which does not comply with these terms.

frontiers in Cell and Developmental Biology

ORIGINAL RESEARCH
published: 10 January 2022
doi: 10.3389/fcell.2021.784199

Immune Landscape Refines the Classification of Colorectal Cancer With Heterogeneous Prognosis, Tumor Microenvironment and Distinct Sensitivity to Frontline Therapies

Zaoqu Liu[1,2†], Yaxin Guo[3,4,5†], Xiuxiu Yang[6], Chen Chen[7], Dandan Fan[5], Xiaoke Wu[8], Chaohua Si[7], Yanxin Xu[1], Bo shao[1], Zhuang Chen[1], Qin Dang[1], Wenming Cui[1], Xinwei Han[2], Zhenyu Ji[5]* and Zhenqiang Sun[1]**

[1]Department of Colorectal Surgery, The First Affiliated Hospital of Zhengzhou University, Zhengzhou, China, [2]Department of Interventional Radiology, The First Affiliated Hospital of Zhengzhou University, Zhengzhou, China, [3]School of Basic Medical Sciences, Zhengzhou University, Zhengzhou, China, [4]Academy of Medical Sciences, Zhengzhou University, Zhengzhou, China, [5]Henan Institute of Medical and Pharmaceutical Sciences, Zhengzhou University, Zhengzhou, China, [6]Department of Hematology, Tongji Hospital, Tongji Medical College, Huazhong University of Science and Technology, Wuhan, China, [7]School of Life Sciences, Zhengzhou University, Zhengzhou, China, [8]Department of Neurology, The First Affiliated Hospital of Zhengzhou University, Zhengzhou, China

The immune microenvironment has profound impacts on the initiation and progression of colorectal cancer (CRC). Therefore, the goal of this article is to identify two robust immune subtypes in CRC, further provide novel insights for the underlying mechanisms and clinical management. In this study, two CRC immune subtypes were identified using the consensus clustering of immune-related gene expression profiles in the *meta*-GEO dataset (n = 1,198), and their reproducibility was further verified in the TCGA-CRC dataset (n = 638). Subsequently, we characterized the immune escape mechanisms, gene alterations, and clinical features of two immune subtypes. Cluster 1 (C1) was defined as the "immune cold subtype" with immune cell depletion and deficiency, while cluster 2 (C2) was designed as the "immune hot subtype", with abundant immune cell infiltration and matrix activation. We also underlined the potential immune escape mechanisms: lack of MHC molecules and defective tumor antigen presentation capacity in C1, increased immunosuppressive molecules in C2. The prognosis and sensitivity to 5-FU, Cisplatin and immunotherapy differed between two subtypes. According to the two immune subtypes, we developed a prognosis associated risk score (PARS) with the accurate performance for predicting the prognosis. Additionally, two nomograms for overall survival (OS) and disease-free survival (DFS) were further constructed to facilitate clinical management.

Abbreviations: CRC: Colorectal cancer; GEO: Gene Expression Omnibus; TCGA: The Cancer Genome Atlas; ssGSEA: Single sample gene set enrichment analysis; CDF: Cumulative distribution function; PAC: Proportion of ambiguous clustering; IGP: In-group proportion; GSVA: Gene set variation analysis; TMB: Tumor mutation burden; AS: Aneuploidy scores; HRD: Homologous recombination defects; MSI: Microsatellite instability; CTAs: Cancer/testis-antigens; APS: Antigen processing and presenting machinery scores; CNV: Copy number variation; SMGs: Significant mutation genes; NMF: Non-negative matrix factorization; DEGs: Differentially expressed genes; OS: Overall survival; DFS: disease free survival; ROCs: Receiver operating characteristic curves; AUC: Area under the ROC curve.

OPEN ACCESS

Edited by:
Zimu Deng,
Shanghai Institute of Biochemistry and Cell Biology (CAS), China

Reviewed by:
Manuel Fuentes,
University of Salamanca, Spain
Faming Zhao,
Huazhong University of Science and Technology, China
Xingyu Wang,
First Affiliated Hospital of Anhui Medical University, China

***Correspondence:**
Xinwei Han
fcchanxw@zzu.edu.cn
Zhenyu Ji
jizhenyu@zzu.edu.cn
Zhenqiang Sun
fccsunzq@zzu.edu.cn

†These authors have contributed equally to this work

Specialty section:
This article was submitted to Molecular and Cellular Pathology, a section of the journal Frontiers in Cell and Developmental Biology

Received: 27 September 2021
Accepted: 20 December 2021
Published: 10 January 2022

Citation:
Liu Z, Guo Y, Yang X, Chen C, Fan D, Wu X, Si C, Xu Y, shao B, Chen Z, Dang Q, Cui W, Han X, Ji Z and Sun Z (2022) Immune Landscape Refines the Classification of Colorectal Cancer With Heterogeneous Prognosis, Tumor Microenvironment and Distinct Sensitivity to Frontline Therapies. Front. Cell Dev. Biol. 9:784199. doi: 10.3389/fcell.2021.784199

Overall, our research provides new references and insights for understanding and refining the CRC.

Keywords: colorectal cancer, genomic alteration, mutational signature, molecular subtype, prognosis, metastasis

INTRODUCTION

Colorectal cancer (CRC) is a malignant tumor that originates from resident somatic stem cells and colorectal epithelial tissue (Perekatt et al., 2018). According to the anatomical location, CRC can be divided into colon cancer and rectal cancer. Adenocarcinoma is the most common pathological type of CRC, and very few are squamous cell carcinoma. Currently, the clinical staging system of CRC based on histopathology and medical imaging has limited ability in the clinical management of CRC (Benson et al., 2018; Weiser, 2018). Recently, the molecular classification improved the staging system and provides clues for mining CRC treatment targets (Calon et al., 2015). However, these molecular classification studies were primarily focused on tumor cell-intrinsic characteristics and did not consider the key roles of tumor immunity and tumor microenvironment in tumor progression.

Previous studies reported that the immune system and immune-related genes played vital roles in tumor initiation, progression, prognosis, recurrence, and chemotherapy and immunotherapy benefits (Terzic et al., 2010; Ye et al., 2019; Bruni et al., 2020; Liu et al., 2021c; Liu et al., 2021e). A TCGA-pancancer study conducted extensive immunogenomic analysis and identified six pancancer immune subtypes (PISs): wound healing (PIS1), IFN-gamma dominant (PIS2), inflammatory (PIS3), lymphocyte depleted (PIS4), immunologically quiet (PIS5), and TGF-beta dominant (PIS6), which spans across traditional cancer classifications based on anatomical site of origin and suggests that certain therapeutic approaches may be considered regardless of tumor location and histology (Thorsson et al., 2018).

Recently, immune checkpoint inhibitors (ICIs) have shown amazing therapeutic effects in a variety of tumors (Brahmer et al., 2012; Topalian et al., 2012; Wolchok et al., 2017). However, not all patients could benefit from immunotherapy, which might be due to the involvement of tumor immune escapes. Tumor immune escapes refer to the phenomenon that tumor cells evade recognition and attack by the immune system through a variety of mechanisms, thereby continuing to survive and proliferate. In this study, we aimed to identify two robust immune subtypes with differences in tumor immune escapes, molecular alterations, and clinical outcomes, to further advance the understanding and clinical management of CRC.

MATERIALS AND METHODS

Dataset Source and Preprocessing

Public gene-expression data and full clinical annotation were searched in Gene-Expression Omnibus (GEO) and the Cancer Genome Atlas (TCGA) databases. A total of 1836 patients from eight eligible CRC cohorts including GSE17536 (n = 177), GSE17537 (n = 55), GSE29621 (n = 65), GSE38832 (n = 122), GSE39084 (n = 70), GSE39582 (n = 585), GSE72970 (n = 124), and TCGA-CRC (n = 638) were pooled in this study for further analysis. All GEO datasets were from the GPL570 platform. Basic information of datasets included in this study were shown in **Supplementary Table S1**. The Robust Multi-Array Average algorithm (RMA) algorithm was utilized to normalize the GEO microarrays. The Combat function implemented in the SVA package was applied to remove the batch effects among the GEO datasets (**Supplementary Figure S1A,B**). The TCGA RNA-seq data was converted into log2 (TPM+1) format. The clinical information, mutation, copy number variant (CNV), and methylation data of TCGA-CRC were downloaded from the TCGA official website. Additionally, we also included three immunotherapy cohorts (Roh cohort, GSE100797, and GSE78220) for subclass mapping (SubMap) analysis (Roh et al., 2017). Complete response (CR) and partial response (PR) were regarded as immunotherapy responders while stable disease (SD) and progressive disease (PD) were regarded as immunotherapy non-responders, and patients who were not evaluable (NE) were removed. All the expression data were further transformed into Z-score.

Gene Source

A total of 1793 immune-related genes were enrolled from the ImmPort database. A total of 728 immune cell consensus biomarkers were extracted from a previous report (Charoentong et al., 2017). To account for yet unknown immune-related genes, we included genes that were significantly correlated with at least one gene in the meta-GEO cohort. The thresholds were set as the absolute value of Spearman correlation >0.7 and false discovery rate (FDR) < 0.05. Eventually, a total of 2,798 genes were recruited for further analysis in this study (**Supplementary Table S2**).

Identification of Immune Subtypes and Gene Modules

Based on 1,198 samples in the meta-GEO cohort, we used the ConsensusClusterPlus package to perform consensus clustering. This procedure was repeated 1,000 times to ensure the stability of classification. The number of clusters K was set to 2–9, and the sampling ratio of the sample was set to 0.8. Unsupervised clustering methods (K-means) were used to identify immune subtypes for further analysis (based on Euclidean distance). To identify immune gene modules, we also applied the consensus clustering using the same settings and parameters. Cumulative distribution function (CDF) and proportion of ambiguous clustering (PAC) were used to identify the optimal K.

Validation of Immune Subtypes

To further evaluate the reproducibility of the clusters generated from consensus clustering in the meta-GEO cohort, the in-group proportion (IGP) statistical analysis was employed to demonstrate the existence of these clusters in the TCGA-CRC validation cohort. The IGP was defined as the proportion of samples in a group whose nearest neighbors were also in the same group (Kapp and Tibshirani, 2007). We firstly calculated a centroid for each cluster found in the meta-GEO cohort, each sample in the TCGA cohort was classified to a cluster whose centroid had the highest Pearson correlation with a centroid. Later, the clusterRepro package was utilized to perform IGP statistical analysis, and the statistical significance of IGP was assessed with 1,000 permutations (Kapp and Tibshirani, 2007). The *p*-value and IGP statistics were used to estimate cluster quality as in the previous study (Liu et al., 2021b; Liu et al., 2021f).

Functional Annotation and Immune Cells Infiltration Assessment

The gene-set enrichment analysis (GSEA) was performed between two subtypes, and gene terms with FDR <0.05 were significant. We also applied the gene-set variation analysis (GSVA) to find the specific Hallmark pathways of each subtype. The single sample gene-set enrichment analysis (ssGSEA) algorithm was used to evaluate the infiltration abundance of 30 different types of tumor microenvironment (TME) cells. Considering that fibroblasts and epithelial cells are also important cellular components in TME, thus, in addition to including consensus biomarkers of 28 immune cells, we also included 40 marker genes of fibroblasts and endothelial cells from a previous study (**Supplementary Table S3**) (Becht et al., 2016).

Collection and Investigation of Immune Escape Indicators

A series of tumor immune-related indicators (**Supplementary Table S4**), including stromal and leukocyte fractions, nonsilent mutation rate, neoantigen burden, cancer testis antigens (CTA) score, aneuploidy score, intratumor heterogeneity, number of segments, number or fraction of segments with loss of heterozygosity (LOH), fraction altered, homologous recombination deficiency (HRD), BCR/TCR diversity (Shannon Entropy and Richness) score (Thorsson et al., 2018), microsatellite instability (MSI) score (Bonneville et al., 2017), cytolytic activity (Rooney et al., 2015), antigen processing and presenting machinery score (APS) (Wang et al., 2019) and the expression of immunomodulator molecules (Liu et al., 2021d; Liu et al., 2021h), were enrolled or calculated for the investigation of potential immune escape mechanisms in the four clusters. Moreover, multi-omics regulation of 75 immunomodulator molecules was further analyzed (**Supplementary Table S5**).

Genomic Alterations

We used the MutationPattern package to convert the mutation data into a matrix of 96 mutation spectra. Then the NMF package was performed to extract mutation signatures of the two immune subtypes. The MutSigCV algorithm was executed to identify significant mutation genes (SMGs). The screening criteria for frequently mutated genes (FMG) are set to $q < 0.05$ and mutation frequency >10%. GISTIC 2.0 was used to identify chromosome arms or chromosome segments that are significantly amplified or deleted. Segments with $q < 0.05$ and copy number variation frequency >0.3 are considered as driver segments.

Treatment Prediction for Immune Subtypes

We use the pRRophetic package to predict the sensitivity of the two subtypes to Cisplatin. The sensitivity was quantified by IC50. The lower the value, the stronger the sensitivity. As in previous studies, the TIDE and SubMap algorithms were utilized to predict the response of the two subtypes to immunotherapy (Liu et al., 2021a; Liu et al., 2021e; Liu et al., 2021g).

Generation of a Prognosis Signature

To identify a prognosis signature for facilitating the clinical management of CRC, we constructed a pipeline. 1) The limma package was utilized to screen differentially expressed genes (DEGs) between C1 and C2 in both meta cohorts and TCGA cohort respectively, and the filtration criteria were adjust-p <0.05 and $|\log_2 \text{fold change}| > 1$. The overlapping DEGs in both cohorts were defined as consensus DEGs (CDEGs). 2) For the CDEGs expression matrix, we next transformed it into the gene pairs matrix. The gene pair was concerned about the mathematical relationship between the mRNA expression of two genes, and ignored the batch effects of different platforms and facilitated the clinical application. For example, for a gene pair (gene1 and gene2), if the expression of gene1 was greater than gene2 in sample x, the gene pair value in the sample was labeled as 1, otherwise it was labeled as 0. 3) If a gene pair had more than 90% of the same value in all samples, the gene pair was removed. 4) Univariate Cox regression analysis extracted the gene pair with predominant prognostic significance for further analysis (adjust-p <0.05 and |HR-1| >0.5; HR: Hazard ratio). 5) The Lasso regression was employed to fit a well-behaved model for predicting overall survival (OS), and the minimal lambda value determined the number of gene pairs and the optimal model. The final model was as follows: risk score = $\sum$ Value (gene pair) * Coef (gene pair), where Value (gene pair) denoted the value of a gene pair (0/1) and Coef (gene pair) represented its regression coefficient. The risk score was termed prognosis associated risk score (PARS). 6) We calculated the PARS of each patient and performed the Kaplan-Meier survival analysis for OS and DFS. The univariate Cox regression was applied to reveal the prognosis value in various cohorts. The receiver operator characteristic (ROC) curves and Concordance index (C-index) were utilized to assess the performance of PARS in predicting prognosis. 7) In order to ensure the stability of the signature, the process of constructing the model was performed in the *meta*-GEO cohorts, and the TCGA-CRC cohort was used for validation.

Statistical Analysis

The Fisher's exact test was used to evaluate the co-occurrence or rejection of FMGs. The Spearman or Pearson correlation analysis

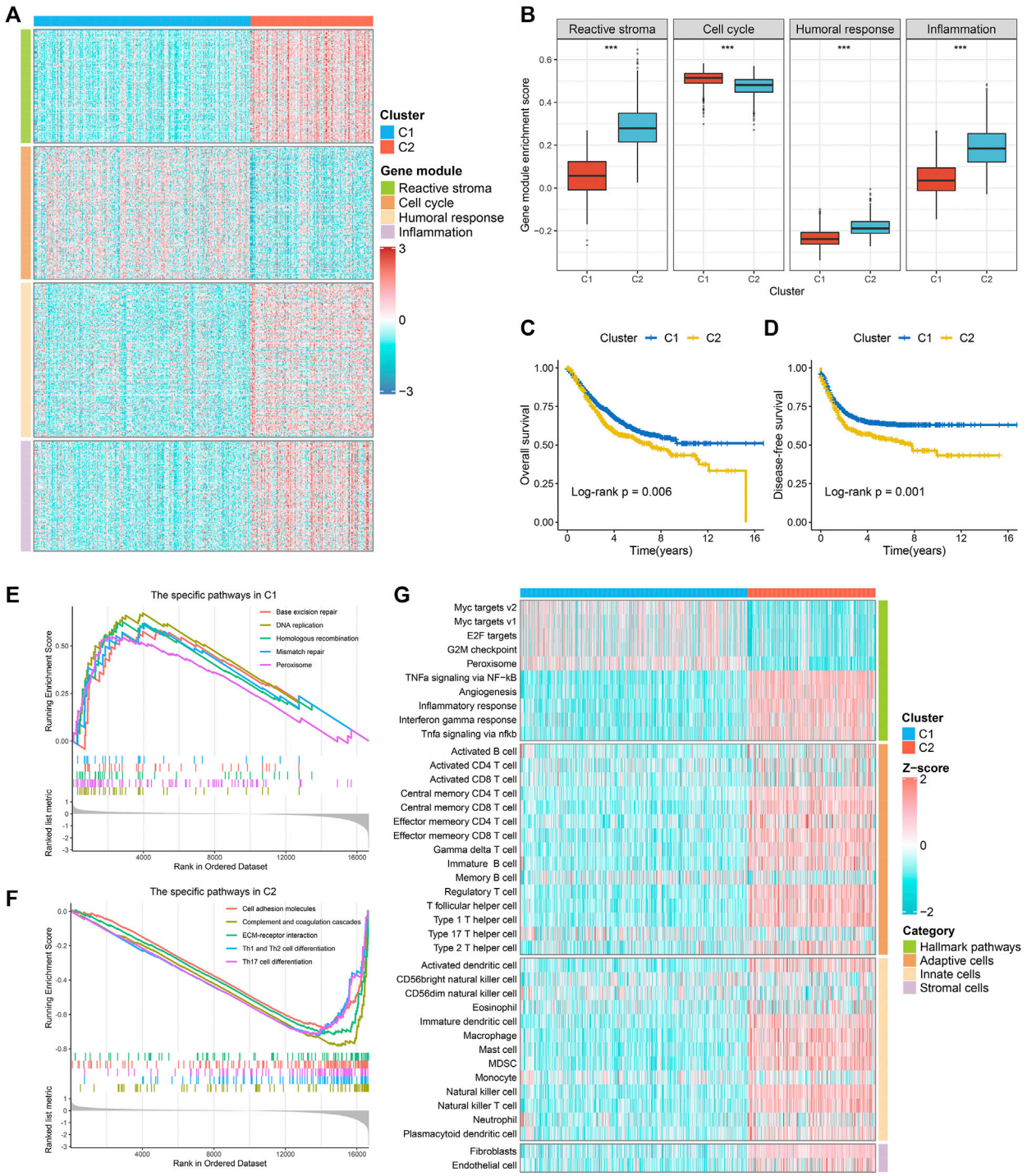

FIGURE 1 | The specific functions and survival status of each subtype in the *meta*-GEO cohort. **(A)** The expression profiles of gene modules between two subtypes. **(B)** The ssGSEA algorithm was performed to quantify the relative abundance of four gene modules between two subtypes. **(C,D)** Kaplan-Meier survival analysis of overall survival **(C)** and disease-free survival **(D)** according to the two subtypes. **(E,F)**. GSEA was performed to identify specific KEGG pathways in C1 **(E)** and C2 **(F)**. **(G)**. The hallmark analysis (GSVA) and immune cell infiltration estimation (ssGSEA) of two subtypes.

was used to calculate the correlation coefficient of two variables. The comparison between the two groups was carried out by Wilcoxon rank sum test, when three or more groups were compared by Kruskal-Wallis test. The Kaplan-Meier method was used to generate survival curves for prognostic analysis, and the log-rank test was used to determine the significance of

differences. The univariate Cox regression analysis was used to calculate the hazard ratio (HR) of the variables, and multiple Cox regression was used to determine independent prognostic factors. The ROC curves were analyzed by the timeROC package. The enrichment analysis was performed by the clusterProfiler package. The survminer package was applied to determine the optimal cut-off value of PARS for the Kaplan-Meier survival analysis. The maftools R package was utilized to analyze data and visualize the mutation waterfall plots. All statistical values were tested by two-sided test, and $p < 0.05$ was considered statistically significant.

RESULTS

Immune Subtypes and Gene Modules

Based on the immune-related gene expression profiles, we identified two robust immune subtypes (C1 and C2) in the *meta*-GEO discovery cohort (**Suppplementary Figure S1C**). The CDF curves and PAC analysis verified the results (**Supplementary Figures S1D,E**). In the two-dimensional PCA analysis, the spatial distribution contours of the two subtypes basically did not overlap (**Supplementary Figure S1F**). To ensure the reproducibility and robustness of the immune subtypes derived from the GEO cohort, we further calculated the IGP statistic to validate the immune subtypes in the TCGA-CRC validation cohort. These two immune subtypes were highly consistent between the discovery and validation cohorts, with the corresponding IGP values at 91.3 and 93.7%, respectively (all, $p < 0.001$). In addition, we also identified four gene modules (GM1-4) (**Supplementary Figures S2A–C**). Enrichment analysis showed that GM1-4 was mainly related to reactive stroma, cell cycle, humoral response, and inflammation, respectively (**Supplementary Figure S2D**). As shown in **Figures 1A,B** and **Supplementary Figures S3A,B**, GM1/3/4 was higher in C2, while GM2 was superior in C1. Overall, C2 was biased towards immune activation and matrix activation, and C1 was biased towards cell proliferation. Survival analysis revealed that C1 had better OS and disease-free survival (DFS) than C2 (**Figures 1C,D** and **Supplementary Figures S3CD**). GSEA analysis showed that C2 was mainly enriched in matrix activation and immune activation related pathways (**Figure 1E** and **Supplementary Figure S3E**), while C1 was mainly enriched in cell proliferation related pathways (**Figure 1F** and **Supplementary Figure S3F**). We further identified the specific Hallmark pathway of each immune subtype. The results were consistent with the GSEA analysis: C2 was mainly related to matrix activation and immune activation, and C1 mainly enriched cell proliferation related pathways (**Figure 1G** and **Supplementary Figure S3G**). The ssGSEA algorithm was further used to evaluate the infiltration abundance of TME cells in the training and the validation datasets. It was observed that C1 showed relatively low infiltration of immune cells, while C2 showed high infiltration abundance in most immune cells (**Figure 1G** and **Supplementary Figure S3G**). A TCGA-pancancer study proposed six immune clusters: wound healing (PIS1), IFN-gamma dominant (PIS2), inflammatory (PIS3), lymphocyte depleted (PIS4), immunologically quiet (PIS5), and TGF-beta dominant (PIS6) (Thorsson et al., 2018). In TCGA-CRC cohort, the PIS5 was absent, and only five PISs were identified in CRC, predominantly PIS1 (77.1%) and C2 (17.4%) (Soldevilla et al., 2019). In our subtypes, C1 and C2 both had the highest proportion of PIS1, notably PIS1 was more identified in C1, whereas PIS2 was particularly dominant in C2. Of note, there was no PIS6 in C1 (**Supplementary Figure S4**).

Exogenous Immune Escape Mechanisms

To further explore the regulatory mechanisms of the immune subtypes, we focused on the TCGA-CRC cohort, which possessed comprehensive omics data. We firstly investigated the exogenous immune escape mechanisms. Previous studies indicated that exogenous immune escape may include three major aspects: absence of leukocytes, presence of immunosuppressive cells, and release of abundant immunosuppressive cytokines (Schreiber et al., 2011; Beatty and Gladney, 2015). The relative abundance distributions of two immune subtypes in TME cells fraction, innate immune cells, adaptive immune cells and stromal cells were summarized in **Figure 2A**. C2 was characterized by higher levels of TME cell fraction, innate immune cells, adaptive immune cells and stromal cells. We also used leukocyte fraction and stromal fraction as indicators for further verification (Thorsson et al., 2018). The results are consistent with above, compared with C2, C1 showed lower levels in leukocyte fraction and stromal fraction (**Supplementary Figure S5A,B**). Therefore, it was speculated that the exogenous immune escape mechanism of C1 was ascribe to the lack of immune cells, while the exogenous immune escape mechanism of C2 was ascribe to the larger proportion of immunosuppressive cells and stromal cells.

Intrinsic Immune Escape Mechanisms

We further explored the potential intrinsic immune escape mechanisms in two major facets: tumor immunogenicity and immune checkpoint molecules. The main elements of tumor immunogenicity are genome instability and antigen presentation ability. 17 elements associated with tumor immunogenicity were estimated. The heatmap and box plots illustrated the levels of these 17 indicators between C1 and C2 (**Figure 2B** and **Supplementary Figures S5C–S)**. Overall, C2 displayed higher immunogenicity relative to C1, such as BCR, TCR, cytolytic activity, and SNV and indel neoantigens (**Figure 2B** and **Supplementary Figures S5C–S**). To systematically measure the efficiency of antigen processing and presentation, we used the expression of MHC molecules (**Figure 2C**) and APS (**Supplementary Figure S5T**) as the main basis for evaluation. The results showed that C2 had higher APS and MHC-related molecules expression level compared with C1. Thus, the endogenous immune escape mechanism of C1 might be the low immunogenicity and impaired antigen presentation ability.

Furthermore, we further explored the expressions and multi-omics regulations of immunomodulators between two subtypes (**Figure 2C**). The results showed that C2 had both higher costimulatory and coinhibitory molecules than C1, which suggested C2 may upregulate the immune checkpoint

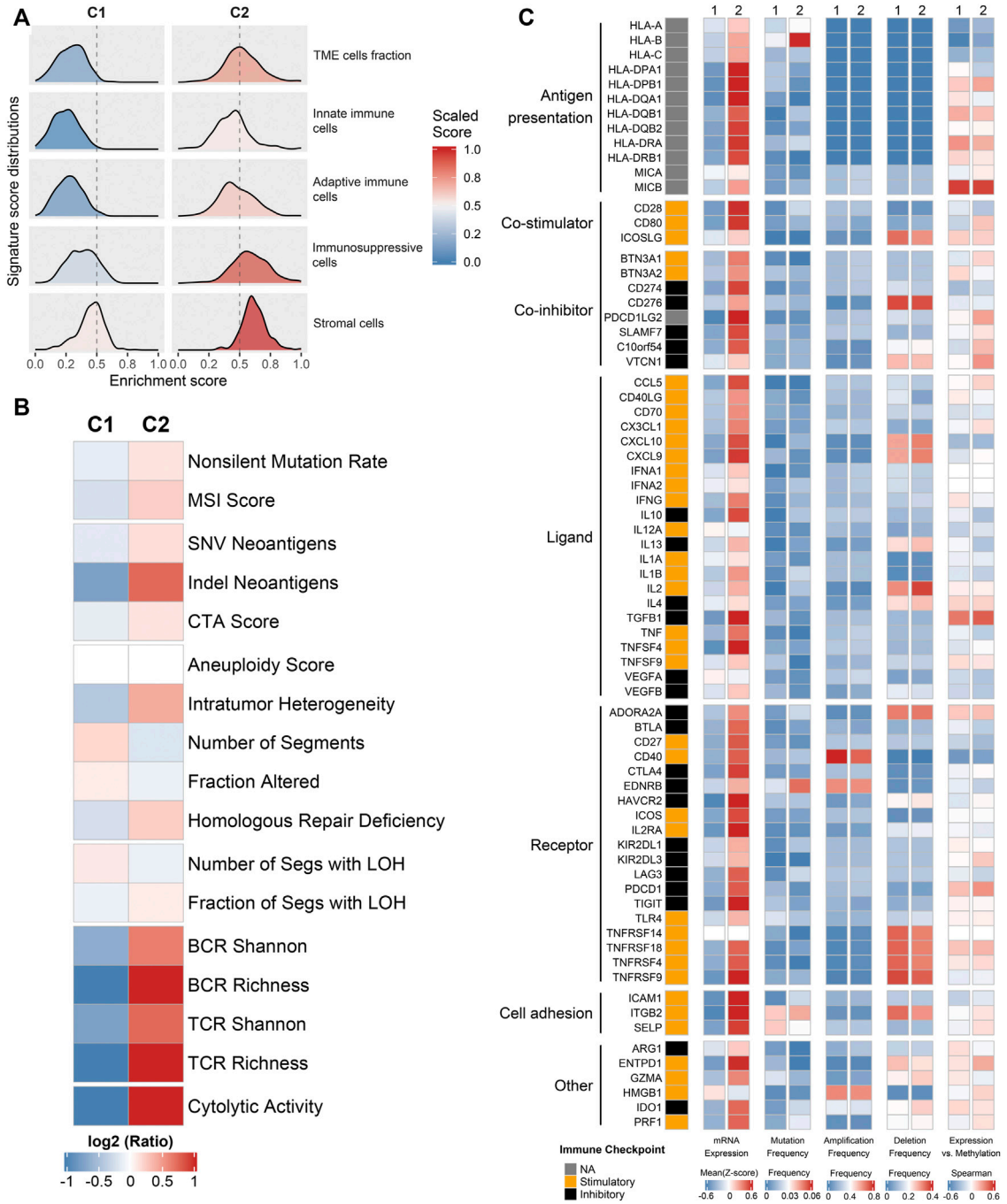

FIGURE 2 | Potential immune escape mechanisms of each phenotype. **(A)** The relative abundance distributions of two immune subtypes in TME cells fraction, innate immune cells, adaptive immune cells, and stromal cells. **(B)** The expression levels of 17 tumor immunogenicity indicators of in C1 and C2. **(C)** Multi-omics analysis of 75 immunomodulators in two subtypes.

molecules (such as CD274 and PDCD1LG2) to avoid immune surveillance. The mutation frequency of some indicators varies significantly between two phenotypes. For instance, HLA-B and EDNRB had a higher mutation frequency in C2 (**Figure 2C**). It was noteworthy that the differential expression of immunomodulators between the two subtypes could not be explained by CNV (all $p > 0.05$) (**Figure 2C**). The negative correlation between DNA methylation and gene expression indicated epigenetic silencing, such as CD80 (**Figure 2C**). The different characteristics of immunomodulators between immune subtypes provided clues for the discovery of new immunity therapy targets.

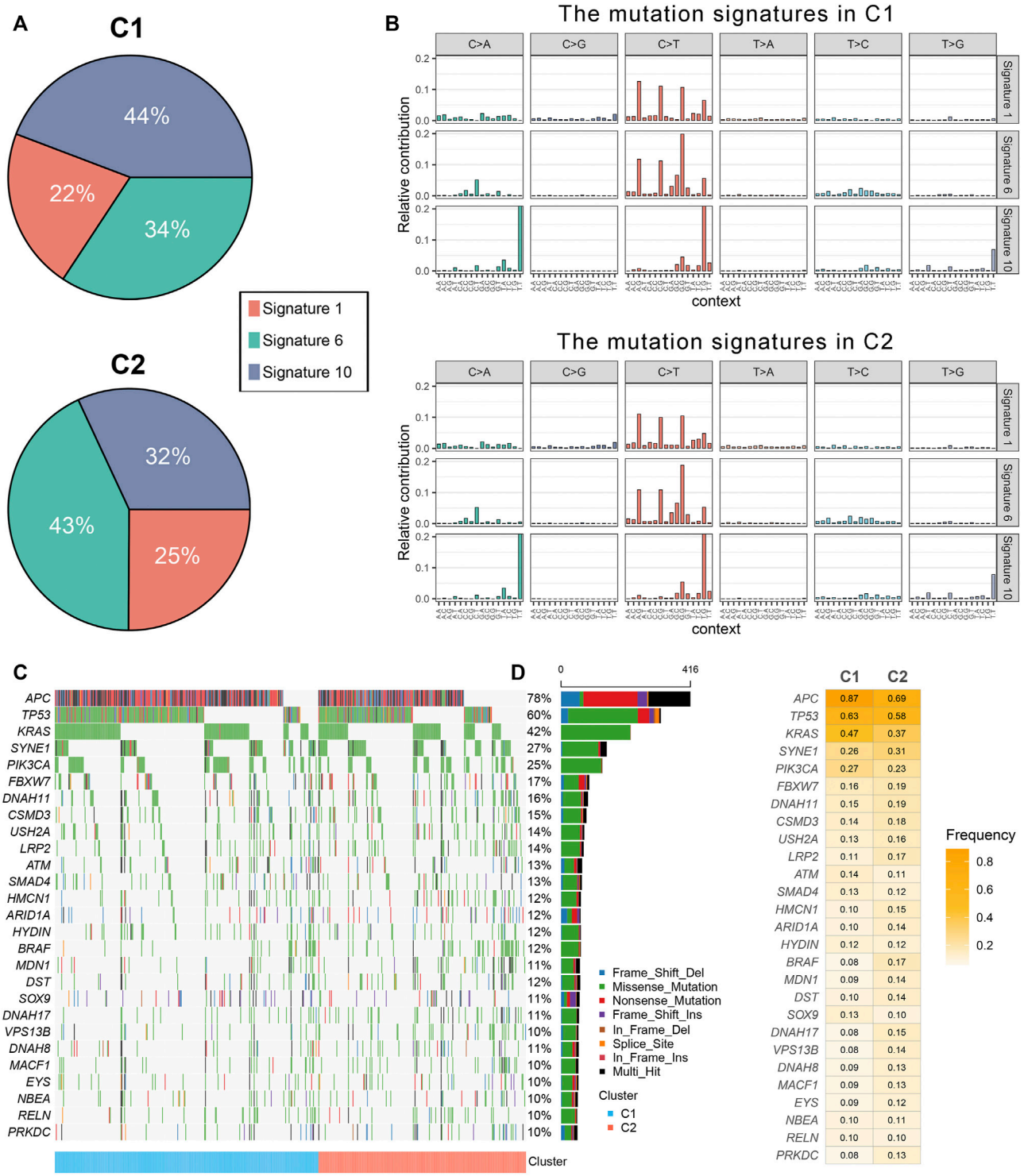

FIGURE 3 | The mutational landscape of two immune subtypes. **(A)** Three mutation signatures were extracted from two immune subtype and named according to the COSMIC signature. The proportion of each mutation signature, which reflects the likely carcinogenic factors. **(B)** The relative contribution of three signature in C1 and C2. **(C,D)** The mutational landscape **(C)** and frequency **(D)** of 27 significant mutation genes (SMGs) in two subtypes.

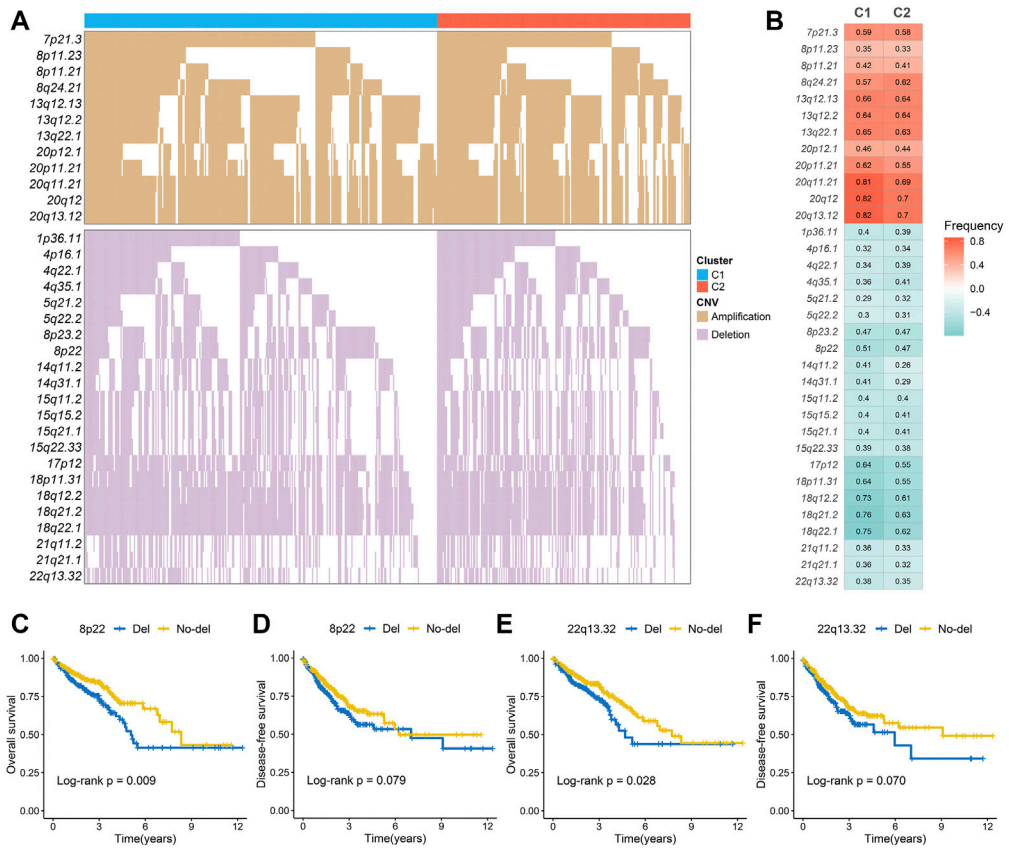

FIGURE 4 | The copy number variations of two immune subtypes. **(A,B)** The waterfall plot **(A)** and alteration frequency **(B)** of significantly amplified and loss chromosomal segments in C1 and C2. **(C,D)**. Kaplan-Meier survival analysis of overall survival **(C)** and disease-free survival **(D)** according to the 8p22 deletion. **(E,F)** Kaplan-Meier survival analysis of overall survival **(E)** and disease-free survival **(F)** according to the 22q13.32 deletion.

Genomic Alterations of Immune Subtypes

The mutation spectrums were decoded to analyze its potential biological carcinogenic factors. The NMF package was used to identify three mutation signatures for two immune subtypes (**Figure 3A**). The cosine similarity between the extracted mutation signature and thirty COSMIC signatures were shown in **Supplementary Figure S6A-B** (Alexandrov et al., 2015). **Figure 3B** showed the proportion of each mutation signature, which reflects the predominant carcinogenic factors. Signature 10 accounted for the highest proportion in C1, indicating that carcinogenic factor was mainly related to altered activity of the error-prone polymerase POLE. Signature six accounted for the highest proportion in C2, indicating that carcinogenic factor was mainly related to microsatellite instability (MSI). Additionally, although not significant, the tumor mutation burden (TMB) of C2 was greater than C1 (**Supplementary Figure S6C**). In total, 27 FMGs were identified (**Figure 3C**). The co-occurrence or elusive of these 27 genes were shown in **Supplementary Figure S6D**. Univariate cox regression further revealed the prognostic value of these 27 FMGs (**Supplementary Figure S7A,B**). Among these genes, USH2A and KRAS were poor prognostic factors. In addition, we also investigated the mutation frequency of FMGs in each cluster. It was found that mutations in APC, TP53, and KRAS were enriched in C1 although C2 had the higher TMB (**Figure 3D**). GISTIC 2.0 recognized the significantly amplified and loss chromosomal segments in the TCGA-CRC cohort (**Supplementary Figures S8A,B**). The results showed that there was no significant difference in the CNV load of the two immune subtypes (**Supplementary Figure S8C**). Of the 34 driver segments, 12 were amplified and 22 were loss (**Figure 4A**). C1 was characterized by the more frequent alterations encompassing 20p11.21, 20q11.21, 20q12, and 20q13.12 amplifications as well as 17p12, 18p11.31, 18q12.2, 18q21.2, and 18q22.1 loss (**Figure 4B**). Univariate Cox regression further revealed the prognostic value of these 34 segments (**Supplementary Figures S9A,B**). Kaplan-Meier survival analysis suggested that the deletions of 8p22 and 22q13.32 were significantly associated with poor OS and DFS (**Figures 4C–F**).

Clinical Characteristics of Different Immune Subtypes

We examined the distribution of clinical characteristics including age, gender, TNM stage, AJCC-stage, MSI, and 5-FU response rates. There was no significant difference in age and gender

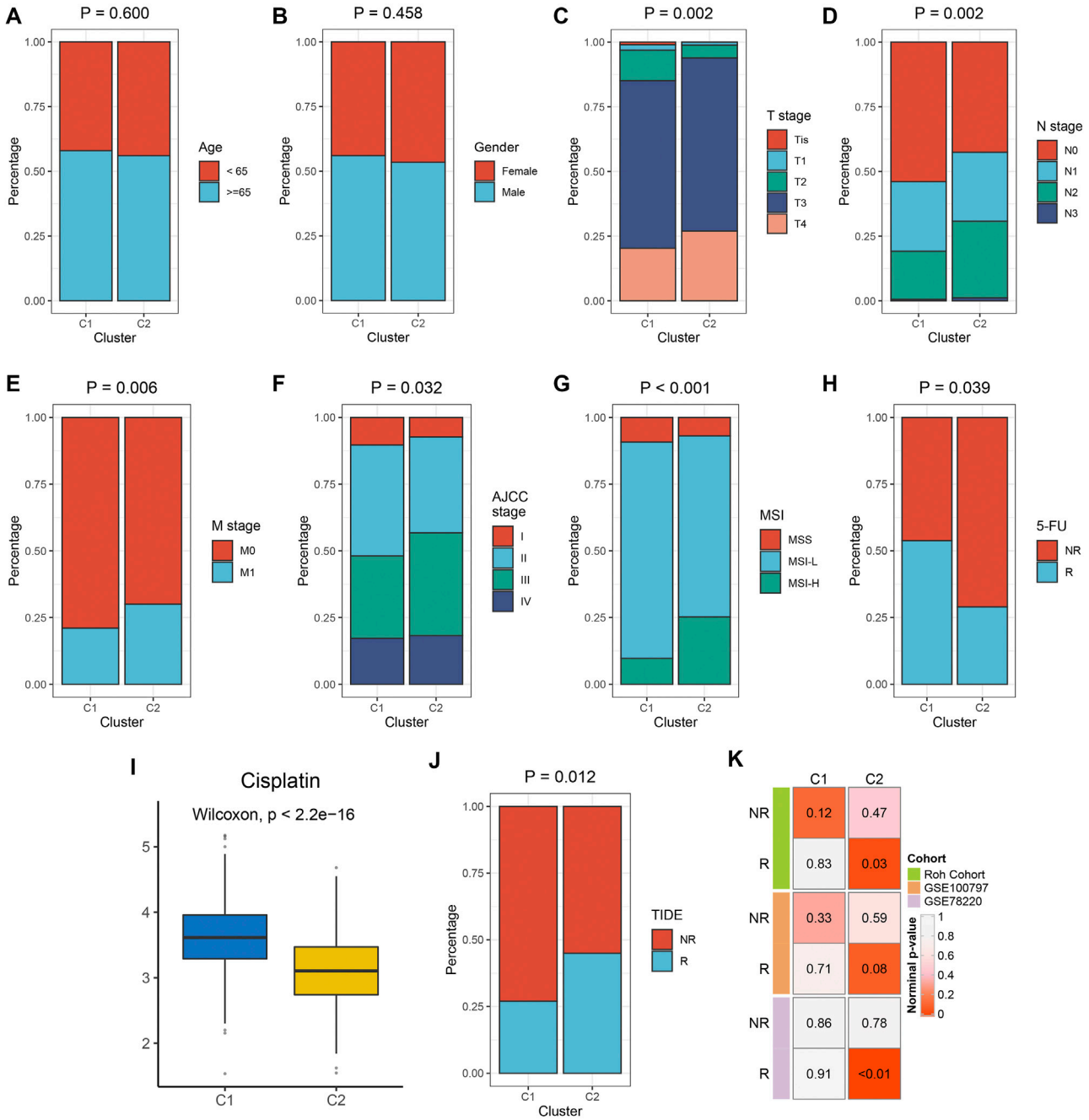

FIGURE 5 | The clinical significance of the two immune subtypes in the *meta*-GEO cohort. **(A–H)** Composition percentages of clinical characteristics such as age **(A)**, gender **(B)**, T stage **(C)**, N stage **(D)**, M stage **(E)**, AJCC stage **(F)**, MSI **(G)**, and 5-FU response **(H)** between C1 and C2. **(I)** The IC50 distribution of Cisplatin between two subtypes. **(J)** Composition percentages of immunotherapy response estimated by TIDE algorithm between C1 and C2. **(K)** Submap analysis revealed that C2 was sensitive to immunotherapy.

distribution among the two subtypes. C1 had a higher response rate of 5-FU. C2 had higher levels of T stage, N stage, distant transfer, AJCC-stage, and MSI-status (**Figures 5A–H**). The prediction of pRRophetic indicates that C2 was more sensitive to Cisplatin (**Figure 5I**). The previous results indicate that C2 belonged to the immune hot subtype but was in an immunosuppressive state; C1 belonged to the immune cold subtype. Therefore, we further explored the sensitivity of immune phenotypes to immunotherapy. The TIDE algorithm showed that C2 had a higher proportion of responders to immunotherapy (**Figure 5J**). SubMap also showed that C2 was more prone to respond to immunotherapy (**Figure 5K**).

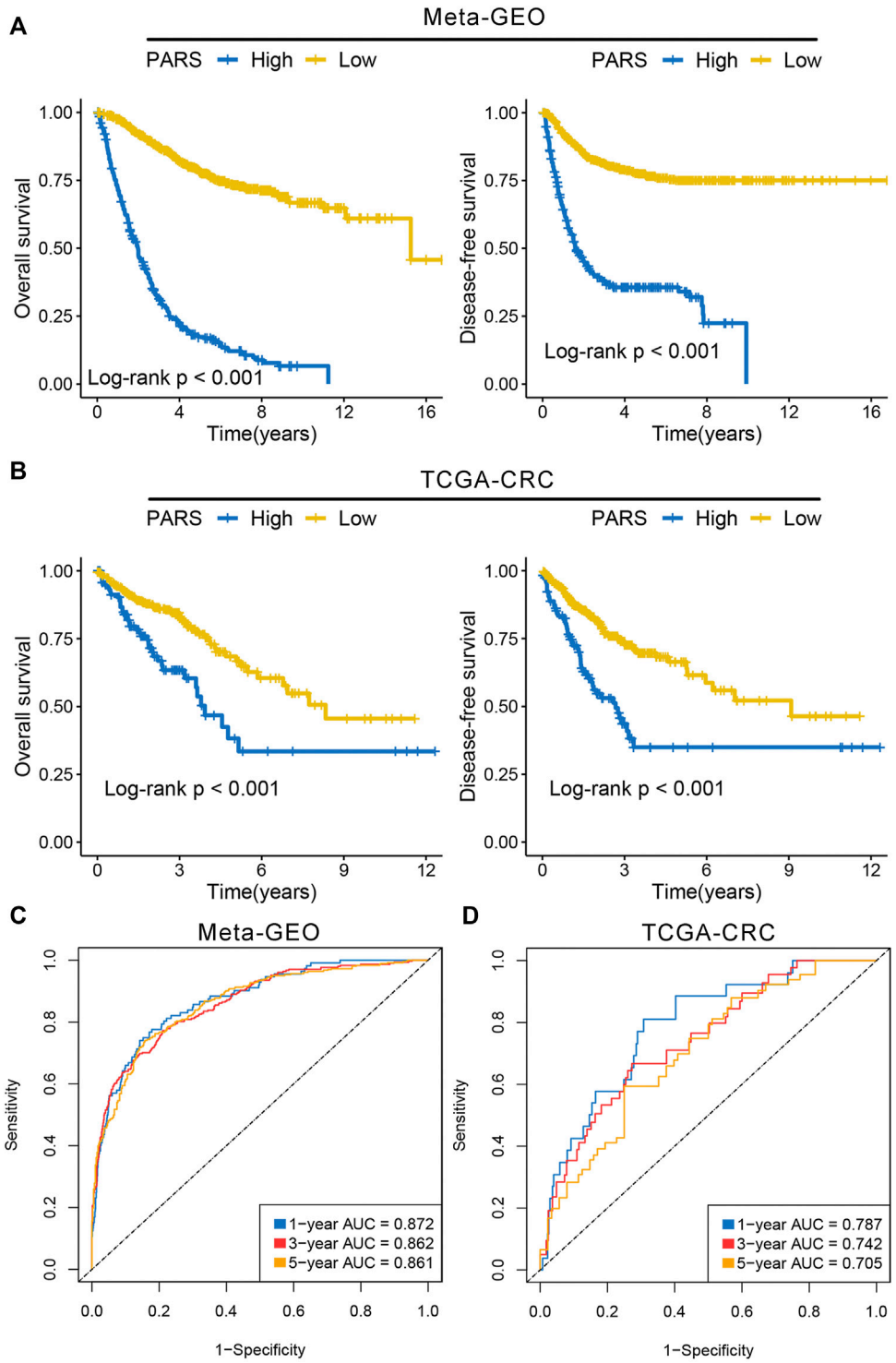

FIGURE 6 | Development of prognosis associated risk score. **(A)** Kaplan-Meier survival analysis of overall survival and disease-free survival according to PARS in the *meta*-GEO cohort. **(B)** Kaplan-Meier survival analysis of overall survival and disease-free survival according to PARS in the TCGA-CRC cohort. **(C,D)** ROC curves of PARS in the *meta*-GEO **(C)** and TCGA-CRC **(D)** cohorts.

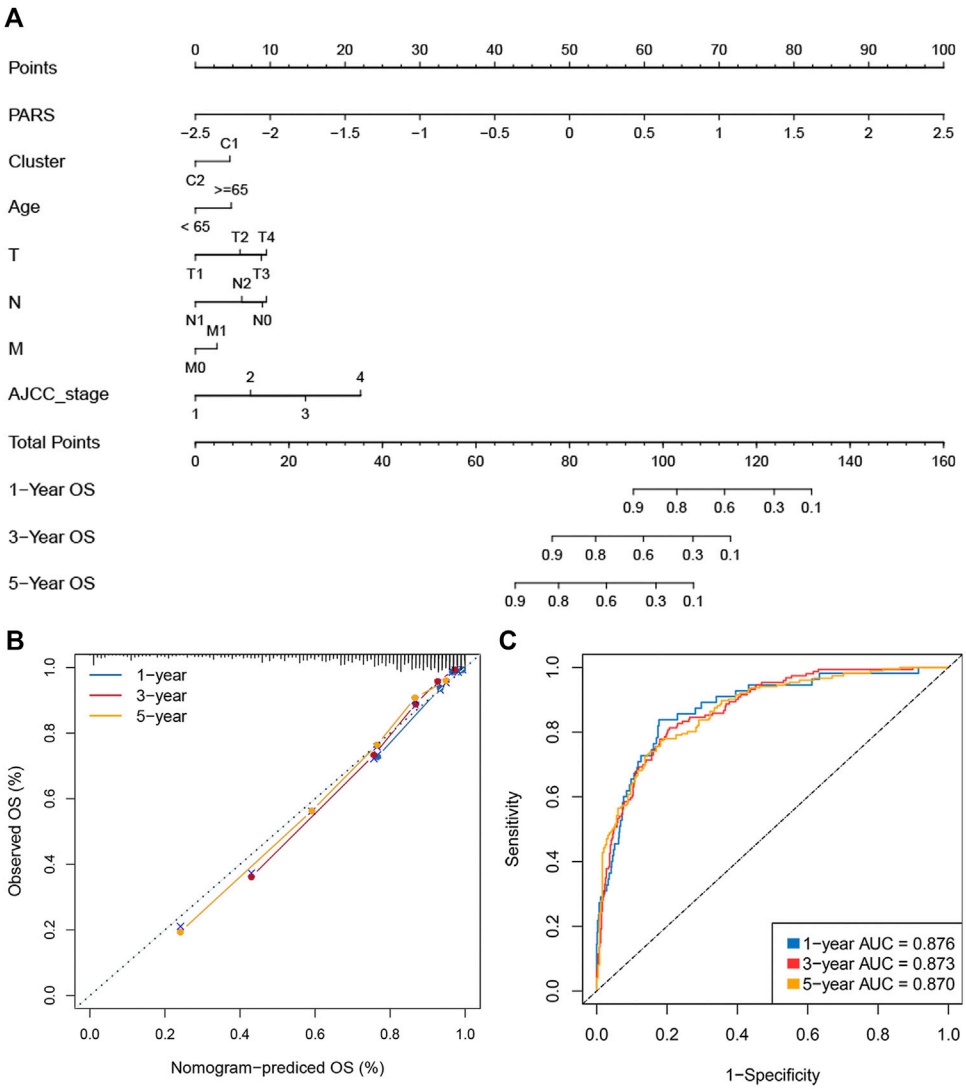

FIGURE 7 | Construction of a nomogram for evaluating prognosis. **(A)** Nomogram for predicting the 1-, 3-, and 5 years OS of CRC patients. **(B)** Calibration analysis of our nomogram in evaluating the 1-, 3-, and 5years OS. **(C)**. ROC curve for evaluating the performance of nomogram in predicting the 1-, 3-, and 5 years OS.

Supplementary Figure S10 showed similar results in the TCGA-CRC validation set.

Development of Prognosis Associated Risk Score

We identified 388 and 572 DEGs in *meta*-GEO cohorts and TCGA-CRC cohort, respectively (**Supplementary Figure S11A,B**). The overlapping DEGs in both cohorts eventually determined 312 CDEGs (**Supplementary Figure S11C**). The biological process (BP) and KEGG pathway enrichment analysis of these CDEGs revealed plenty of immune related functions such as cytokine-cytokine receptor interaction, response to stimulus and immune system process (**Supplementary Figures S11D,E**). Based on the constructed pipeline, we further transformed the CDEGs expression matrix into the gene pairs matrix, and further screened 980 gene pairs with significantly prognosis significance (adjust-p <0.05; **Supplementary Table S6**). Subsequently, the Lasso regression was performed to develop the optimal model, and it was determined by the optimal lambda = 0.0324 (**Supplementary Figure S11F** and **Supplementary Table S7**). We calculated the PARS of each patient, and divided the patients into high risk and low risk groups. The Kaplan-Meier analysis suggested the patients with high PARS tended to possess a worse OS and DFS relative to patients with low PARS in both *meta*-GEO cohorts and TCGA-CRC cohort (**Figures 6A,B**). The area under the ROC curves (AUCs) of predicting 1-year, 3 years, and 5 years OS were 0.872, 0.862 and 0.861 in the *meta*-GEO cohort, 0.787, 0.742 and 0.705 in the TCGA-CRC cohort (**Figures 6C,D**). The C-index was 0.815 [95%CI: 0.795–0.835] and 0.738 [95%CI: 0.675–0.801] in the *meta*-GEO cohort and TCGA-CRC cohort, respectively. We

also found C1 had lower PARS compared with C2 in both meta cohorts and TCGA cohort (**Supplementary Figures S11G,H**), which was in line with the prognostic characteristic of immune subtypes. These results indicated PARS was a robust and promising signature for prognosis.

Construction of a Nomogram for Evaluating Prognosis

The immune subtypes, age, gender, TNM stage, AJCC stage, and MSI status were subjected into the univariate Cox regression analysis of OS and DFS. Multivariate cox regression analysis found that PARS and Cluster are independent prognostic factors of OS. For DFS, only PARS was an independent prognostic factor (**Supplementary Table S8**). We selected statistically significant variables to further construct nomograms (**Supplementary Table S8** and **Figures 7A,B**). The nomogram was used to assess the 1-, 3-, and 5 years survival rates of a single patient. We use ROC and calibration plots to evaluate the nomogram. The calibration curves showed a good assistant between the nomogram prediction and the observed value (**Figure 7B**). The AUCs for 1-, three- and 5-years were 0.876, 0.873, and 0.870, respectively (**Figure 7C**). These results indicated that the nomograms had excellent performance. The above indicated the nomogram was reliable, which could facilitate the clinical managements of CRC.

DISCUSSION

More and more patients with solid tumors benefit from immunotherapy (Doi et al., 2018; Song et al., 2018; Ganesh et al., 2019). However, the effective response and survival benefits to immunotherapy are usually limited to a small subset of patients. In this study, we identified two robust CRC immune subtypes through consensus clustering and found that each immune subtype had distinct immune escape mechanisms, genome alterations, and clinical characteristics. This study provides an innovative CRC classification concept, and immunological classification may have clinical guiding significance for personalized immunotherapy. Our work reflects innovation in several important ways.

Firstly, the unsatisfactory response efficiency of immunotherapy might be due to tumor immune escape. Therefore, it was very necessary to explore the immune escape mechanisms of different immune subtypes. We analyzed the cellular and molecular characteristics of these two immune subtypes. It was found that the exogenous immune escape mechanism of C1 was the lack of immune cells, especially immune killer cells, while the exogenous immune escape mechanism of C2 was the increase of immunosuppressive cells and stromal cells. In addition, the endogenous immune escape of C1 was mainly due to low immunogenicity and impaired antigen presentation ability. C2 was more immunogenic, but the increase of immunosuppressive molecules may be the reason for its endogenous immune escape. Different immune escape mechanisms might be the key impediments to the development of immunotherapy for two subtypes.

Secondly, different carcinogenic factors lead to different mutation spectrums. Therefore, we tried to analyze its potential biological carcinogenic factors through the tumor mutation spectrum. We found that signature 10 has the highest proportion in C1, indicating that carcinogens are mainly related to changes in the activity of the error-prone polymerase POLE. Signature six accounted for the highest proportion in C2, indicating that its main carcinogenesis was related to MSI. By identifying FMGs, we found APC, TP53, and KRAS mutations were enriched in C1 although C2 had the higher TMB. In addition, C1 was characterized by the more frequent alterations encompassing 20p11.21, 20q11.21, 20q12, and 20q13.12 amplifications as well as 17p12, 18p11.31, 18q12.2, 18q21.2, and 18q22.1 loss. These results revealed the molecular landscape of two subtypes.

Next, our research provided clues for choosing clinical treatment options. Analysis of clinical characteristics of different immune subtypes may help to accurately select chemotherapy drugs. C1 has a higher response rate of 5-FU while C2 was more sensitive to Cisplatin. In addition, our results might facilitate the selection of suitable patients for immunotherapy. Two algorithms including TIDE and SubMap demonstrated that C2 was more likely to respond to immunotherapy.

Finally, we proposed a gene pair pipeline to develop a predictive model. The gene pair was concerned about the mathematical relationship between the mRNA expression of two genes and ignored the batch effects of different platforms and facilitated the clinical application. Our PARS model had the accurate performance for predicting OS. To further advance the managements of CRC, we constructed a nomogram for evaluating individual patient risk. Overall, our PARS and nomogram displayed stable and robust performance in the *meta*-GEO and TCGA-CRC cohorts and might be promising tools in clinical settings.

Prior to this study, a few reports identified molecular subtypes based on gene expression profiles or mutational signatures (Guinney et al., 2015; Dunne et al., 2017; Liu et al., 2021h). To the best of our knowledge, this is the first study to date comprehensively delineating the immune and molecular landscape of CRC according to the expression files of scale sample and the broad-spectrum immune genes. Two identified immune subtypes displayed substantial differences in immunology, genomic alterations, and clinical features. This raises the intriguing issue of how to optimally regulate the host immune response so that patients are mobilized toward more favorable states, providing a roadmap to more successful immunotherapy. Combined with the difference in Cisplatin sensitivity and molecular alterations between the two subtypes, this may provide references for precise treatment of CRC. Thus, this study has potential therapeutic implications for the rational design of combination immunotherapy strategies. Although our cluster is promising, some limitations should be acknowledged. First, due to lack of data, we only considered the inter-individual heterogeneity, but did not consider the intra-tumor

heterogeneity. Second, the sensitivity to Cisplatin and immunotherapy was evaluated via machine learning algorithms, further clinical validation is necessary.

In conclusion, our research provides a new classification strategy for CRC. The two subtypes were characterized by distinct immune escape mechanisms, molecular alterations, clinical characteristics, and prognosis. Additionally, our PARS and nomogram were robust and promising indicators for assessing the prognosis of CRC patients. Our study provided deep insights and novel clinical management strategies for CRC.

DATA AVAILABILITY STATEMENT

The datasets presented in this study can be found in online repositories. The names of the repository/repositories and accession number(s) can be found in the article/ **Supplementary Material**.

ETHICS STATEMENT

The patient data in this work were acquired from the publicly available datasets whose informed consent of patients were complete.

AUTHOR CONTRIBUTIONS

ZS, ZJ, XH, and ZL designed this work. ZL and YG integrated and wrote this manuscript. ZL analyzed the data. XY, CC, and DF edited and revised the manuscript. XW, CS, and YX assisted with data acquisition. BS, ZC, QD, and WC contributed to the expertise. All authors read and approved the final manuscript.

FUNDING

This study was supported by The National Natural Science Foundation of China (81972663, U2004112); Key Scientific Research Projects of Institutions of Higher Education in Henan Province (19A310024); The National Natural Science Foundation of Henan Province (182300410342); and The Health Commission Technology Talents Overseas Training Project of Henan Province (2018140).

SUPPLEMENTARY MATERIAL

The Supplementary Material for this article can be found online at: https://www.frontiersin.org/articles/10.3389/fcell.2021.784199/full#supplementary-material

REFERENCES

Alexandrov, L. B., Jones, P. H., Wedge, D. C., Sale, J. E., Campbell, P. J., Nik-Zainal, S., et al. (2015). Clock-like Mutational Processes in Human Somatic Cells. *Nat. Genet.* 47 (12), 1402–1407. doi:10.1038/ng.3441

Beatty, G. L., and Gladney, W. L. (2015). Immune Escape Mechanisms as a Guide for Cancer Immunotherapy. *Clin. Cancer Res.* 21 (4), 687–692. doi:10.1158/1078-0432.CCR-14-1860

Becht, E., Giraldo, N. A., Lacroix, L., Buttard, B., Elarouci, N., Petitprez, F., et al. (2016). Estimating the Population Abundance of Tissue-Infiltrating Immune and Stromal Cell Populations Using Gene Expression. *Genome Biol.* 17 (1), 218. doi:10.1186/s13059-016-1070-5

Benson, A. B., Venook, A. P., Al-Hawary, M. M., Cederquist, L., Chen, Y.-J., Ciombor, K. K., et al. (2018). NCCN Guidelines Insights: Colon Cancer, Version 2.2018. *J. Natl. Compr. Canc Netw.* 16 (4), 359–369. doi:10.6004/jnccn.2018.0021

Bonneville, R., Krook, M. A., Kautto, E. A., Miya, J., Wing, M. R., Chen, H.-Z., et al. (2017). Landscape of Microsatellite Instability across 39 Cancer Types. *JCO Precision Oncol.* 2017, 1–15. doi:10.1200/PO.17.00073

Brahmer, J. R., Tykodi, S. S., Chow, L. Q. M., Hwu, W.-J., Topalian, S. L., Hwu, P., et al. (2012). Safety and Activity of Anti-PD-L1 Antibody in Patients with Advanced Cancer. *N. Engl. J. Med.* 366 (26), 2455–2465. doi:10.1056/NEJMoa1200694

Bruni, D., Angell, H. K., and Galon, J. (2020). The Immune Contexture and Immunoscore in Cancer Prognosis and Therapeutic Efficacy. *Nat. Rev. Cancer* 20 (11), 662–680. doi:10.1038/s41568-020-0285-7

Calon, A., Lonardo, E., Berenguer-Llergo, A., Espinet, E., Hernando-Momblona, X., Iglesias, M., et al. (2015). Stromal Gene Expression Defines Poor-Prognosis Subtypes in Colorectal Cancer. *Nat. Genet.* 47 (4), 320–329. doi:10.1038/ng.3225

Charoentong, P., Finotello, F., Angelova, M., Mayer, C., Efremova, M., Rieder, D., et al. (2017). Pan-cancer Immunogenomic Analyses Reveal Genotype-Immunophenotype Relationships and Predictors of Response to Checkpoint Blockade. *Cell Rep.* 18 (1), 248–262. doi:10.1016/j.celrep.2016.12.019

Doi, T., Piha-Paul, S. A., Jalal, S. I., Saraf, S., Lunceford, J., Koshiji, M., et al. (2018). Safety and Antitumor Activity of the Anti-programmed Death-1 Antibody Pembrolizumab in Patients with Advanced Esophageal Carcinoma. *Jco* 36 (1), 61–67. doi:10.1200/JCO.2017.74.9846

Dunne, P. D., Alderdice, M., O'Reilly, P. G., Roddy, A. C., McCorry, A. M. B., Richman, S., et al. (2017). Cancer-cell Intrinsic Gene Expression Signatures Overcome Intratumoural Heterogeneity Bias in Colorectal Cancer Patient Classification. *Nat. Commun.* 8, 15657. doi:10.1038/ncomms15657

Ganesh, K., Stadler, Z. K., Cercek, A., Mendelsohn, R. B., Shia, J., Segal, N. H., et al. (2019). Immunotherapy in Colorectal Cancer: Rationale, Challenges and Potential. *Nat. Rev. Gastroenterol. Hepatol.* 16 (6), 361–375. doi:10.1038/s41575-019-0126-x

Guinney, J., Dienstmann, R., Wang, X., de Reyniès, A., Schlicker, A., Soneson, C., et al. (2015). The Consensus Molecular Subtypes of Colorectal Cancer. *Nat. Med.* 21 (11), 1350–1356. doi:10.1038/nm.3967

Kapp, A. V., and Tibshirani, R. (2007). Are Clusters Found in One Dataset Present in Another Dataset? *Biostatistics* 8 (1), 9–31. doi:10.1093/biostatistics/kxj029

Liu, Z., Liu, L., Jiao, D., Guo, C., Wang, L., Li, Z., et al. (2021a). Association of RYR2 Mutation with Tumor Mutation Burden, Prognosis, and Antitumor Immunity in Patients with Esophageal Adenocarcinoma. *Front. Genet.* 12, 669694. doi:10.3389/fgene.2021.669694

Liu, Z., Liu, L., Lu, T., Wang, L., Li, Z., Jiao, D., et al. (2021b). Hypoxia Molecular Characterization in Hepatocellular Carcinoma Identifies One Risk Signature and Two Nomograms for Clinical Management. *J. Oncol.* 2021, 1–20. doi:10.1155/2021/6664386

Liu, Z., Lu, T., Li, J., Wang, L., Xu, K., Dang, Q., et al. (2021c). Clinical Significance and Inflammatory Landscape of aNovel Recurrence-Associated Immune Signature in Stage II/III Colorectal Cancer. *Front. Immunol.* 12. doi:10.3389/fimmu.2021.702594

Liu, Z., Lu, T., Wang, L., Liu, L., Li, L., and Han, X. (2021d). Comprehensive Molecular Analyses of a Novel Mutational Signature Classification System with Regard to Prognosis, Genomic Alterations, and Immune Landscape in Glioma. *Front. Mol. Biosci.* 8, 682084. doi:10.3389/fmolb.2021.682084

Liu, Z., Lu, T., Wang, Y., Jiao, D., Li, Z., Wang, L., et al. (2021e). Establishment and Experimental Validation of an Immune miRNA Signature for Assessing

Prognosis and Immune Landscape of Patients with Colorectal Cancer. *J. Cell Mol Med* 25 (14), 6874–6886. doi:10.1111/jcmm.16696

Liu, Z., Wang, L., Liu, L., Lu, T., Jiao, D., Sun, Y., et al. (2021f). The Identification and Validation of Two Heterogenous Subtypes and a Risk Signature Based on Ferroptosis in Hepatocellular Carcinoma. *Front. Oncol.* 11, 619242. doi:10.3389/fonc.2021.619242

Liu, Z., Weng, S., Xu, H., Wang, L., Liu, L., Zhang, Y., et al. (2021g). Computational Recognition and Clinical Verification of TGF-β-Derived miRNA Signature with Potential Implications in Prognosis and Immunotherapy of Intrahepatic Cholangiocarcinoma. *Front. Oncol.* 11, 757919. doi:10.3389/fonc.2021.757919

Liu, Z., Zhang, Y., Dang, Q., Wu, K., Jiao, D., Li, Z., et al. (2021h). Genomic Alteration Characterization in Colorectal Cancer Identifies a Prognostic and Metastasis Biomarker: FAM83A|Ido1. *Front. Oncol.* 11, 632430. doi:10.3389/fonc.2021.632430

Perekatt, A. O., Shah, P. P., Cheung, S., Jariwala, N., Wu, A., Gandhi, V., et al. (2018). SMAD4 Suppresses WNT-Driven Dedifferentiation and Oncogenesis in the Differentiated Gut Epithelium. *Cancer Res.* 78 (17), 4878–4890. doi:10.1158/0008-5472.CAN-18-0043

Roh, W., Chen, P.-L., Reuben, A., Spencer, C. N., Prieto, P. A., Miller, J. P., et al. (2017). Integrated Molecular Analysis of Tumor Biopsies on Sequential CTLA-4 and PD-1 Blockade Reveals Markers of Response and Resistance. *Sci. Transl. Med.* 9 (379). doi:10.1126/scitranslmed.aah3560

Rooney, M. S., Shukla, S. A., Wu, C. J., Getz, G., and Hacohen, N. (2015). Molecular and Genetic Properties of Tumors Associated with Local Immune Cytolytic Activity. *Cell* 160 (1-2), 48–61. doi:10.1016/j.cell.2014.12.033

Schreiber, R. D., Old, L. J., and Smyth, M. J. (2011). Cancer Immunoediting: Integrating Immunity's Roles in Cancer Suppression and Promotion. *Science* 331 (6024), 1565–1570. doi:10.1126/science.1203486

Soldevilla, B., Carretero-Puche, C., Gomez-Lopez, G., Al-Shahrour, F., Riesco, M. C., Gil-Calderon, B., et al. (2019). The Correlation between Immune Subtypes and Consensus Molecular Subtypes in Colorectal Cancer Identifies Novel Tumour Microenvironment Profiles, with Prognostic and Therapeutic Implications. *Eur. J. Cancer* 123, 118–129. doi:10.1016/j.ejca.2019.09.008

Song, W., Tiruthani, K., Wang, Y., Shen, L., Hu, M., Dorosheva, O., et al. (2018). Trapping of Lipopolysaccharide to Promote Immunotherapy against Colorectal Cancer and Attenuate Liver Metastasis. *Adv. Mater.* 30 (52), 1805007. doi:10.1002/adma.201805007

Terzić, J., Grivennikov, S., Karin, E., and Karin, M. (2010). Inflammation and colon Cancer. *Gastroenterology* 138 (6), 2101–2114. doi:10.1053/j.gastro.2010.01.058

Thorsson, V., Gibbs, D. L., Brown, S. D., Wolf, D., Bortone, D. S., Ou Yang, T. H., et al. (2018). The Immune Landscape of Cancer. *Immunity* 48 (4), 812–e14. e814. doi:10.1016/j.immuni.2018.03.023

Topalian, S. L., Hodi, F. S., Brahmer, J. R., Gettinger, S. N., Smith, D. C., McDermott, D. F., et al. (2012). Safety, Activity, and Immune Correlates of Anti-PD-1 Antibody in Cancer. *N. Engl. J. Med.* 366 (26), 2443–2454. doi:10.1056/NEJMoa1200690

Wang, S., He, Z., Wang, X., Li, H., and Liu, X.-S. (2019). Antigen Presentation and Tumor Immunogenicity in Cancer Immunotherapy Response Prediction. *Elife* 8. doi:10.7554/eLife.49020

Weiser, M. R. (2018). AJCC 8th Edition: Colorectal Cancer. *Ann. Surg. Oncol.* 25 (6), 1454–1455. doi:10.1245/s10434-018-6462-1

Wolchok, J. D., Chiarion-Sileni, V., Gonzalez, R., Rutkowski, P., Grob, J.-J., Cowey, C. L., et al. (2017). Overall Survival with Combined Nivolumab and Ipilimumab in Advanced Melanoma. *N. Engl. J. Med.* 377 (14), 1345–1356. doi:10.1056/NEJMoa1709684

Ye, L., Zhang, T., Kang, Z., Guo, G., Sun, Y., Lin, K., et al. (2019). Tumor-Infiltrating Immune Cells Act as a Marker for Prognosis in Colorectal Cancer. *Front. Immunol.* 10, 2368. doi:10.3389/fimmu.2019.02368

Conflict of Interest: The authors declare that the research was conducted in the absence of any commercial or financial relationships that could be construed as a potential conflict of interest.

Publisher's Note: All claims expressed in this article are solely those of the authors and do not necessarily represent those of their affiliated organizations, or those of the publisher, the editors and the reviewers. Any product that may be evaluated in this article, or claim that may be made by its manufacturer, is not guaranteed or endorsed by the publisher.

Copyright © 2022 Liu, Guo, Yang, Chen, Fan, Wu, Si, Xu, shao, Chen, Dang, Cui, Han, Ji and Sun. This is an open-access article distributed under the terms of the Creative Commons Attribution License (CC BY). The use, distribution or reproduction in other forums is permitted, provided the original author(s) and the copyright owner(s) are credited and that the original publication in this journal is cited, in accordance with accepted academic practice. No use, distribution or reproduction is permitted which does not comply with these terms.

frontiers in Cell and Developmental Biology

ORIGINAL RESEARCH
published: 02 February 2022
doi: 10.3389/fcell.2021.760929

Immune Characteristics of LYN in Tumor Microenvironment of Gliomas

Chonghua Jiang[1,2†], *Hao Zhang*[1,2†], *Wantao Wu*[2,3], *Zeyu Wang*[1,2], *Ziyu Dai*[1,2], *Liyang Zhang*[1,2,4,5*], *Zhixiong Liu*[1,2*] *and Quan Cheng*[1,2*]

[1]Department of Neurosurgery, Xiangya Hospital, Central South University, Changsha, China, [2]National Clinical Research Center for Geriatric Disorders, Xiangya Hospital, Central South University, Changsha, China, [3]Department of Oncology, Xiangya Hospital, Central South University, Changsha, China, [4]Department of Medicine, The University of Oklahoma Health Sciences Center, Oklahoma City, OK, United States, [5]Clinical Diagnosis and Therapeutic Center of Glioma, Xiangya Hospital, Central South University, Changsha, China

OPEN ACCESS

Edited by:
Xuejun Sun,
Xi'an Jiaotong University, China

Reviewed by:
Chengming Liu,
Chinese Academy of Medical Sciences and Peking Union Medical College, China
Peng Huang,
Okayama University, Japan
Wenfeng Lin,
Okayama University Graduate School of Medicine, Japan, in collaboration with reviewer PH

***Correspondence:**
Quan Cheng
chengquan@csu.edu.cn
Zhixiong Liu
zhixiongliu@csu.edu.cn
Liyang Zhang
zhangliyang@csu.edu.cn

[†]These authors have contributed equally to this work

Specialty section:
This article was submitted to Molecular and Cellular Pathology, a section of the journal Frontiers in Cell and Developmental Biology

Received: 19 August 2021
Accepted: 20 December 2021
Published: 02 February 2022

Citation:
Jiang C, Zhang H, Wu W, Wang Z, Dai Z, Zhang L, Liu Z and Cheng Q (2022) Immune Characteristics of LYN in Tumor Microenvironment of Gliomas. Front. Cell Dev. Biol. 9:760929. doi: 10.3389/fcell.2021.760929

The prognosis of gliomas is poor and there are limited therapeutic approaches. Immunotherapy has become a promising treatment for gliomas. Here, we explored the expression pattern of Lck/yes-related protein tyrosine kinase (LYN) in gliomas and assessed its value as an immunotherapy biomarker. Transcriptional data was mined from two publicly available datasets, TCGA and CGGA, and used to investigate the correlation between LYN and clinical characteristics including patient prognosis, somatic mutation, and immune infiltrating features in gliomas. Besides, the correlation between LYN and classical immune checkpoint molecules was explored. Glioma samples obtained from the Xiangya Hospital cohort were used for immunohistochemistry staining. High expression level of LYN was observed in advanced gliomas and other cancer types, which predicted a worse prognosis. LYN stratified patients' survival in the Xiangya cohort and was also significantly associated with infiltrating immune cell types and inflammatory activities in the tumor microenvironment. LYN was involved in tumor mutation, correlated with the regulation of oncogenic genes, and also showed a significant positive correlation with PD-L1. LYN can be a potential diagnostic marker and immunotherapy marker in gliomas.

Keywords: glioma, lyn, microenvironment, immune suppression, prognostic marker, PD-L1

INTRODUCTION

Gliomas are the most malignant tumors. The latest world health organization (WHO) category defines grade 2 and grade 3 glioma as diffuse lower-grade glioma (LGG), and grade 4 gliomas as glioblastoma (GBM). Although the classical treatment options of surgery and adjuvant chemoradiotherapy are reported, the median overall survival rate of glioma patients is still less than 10 years (Zhang et al., 2019). Besides, it is noteworthy that, although patients with LGG enjoy a relatively favorable prognosis, most LGG eventually progress to GBM (Claus et al., 2015). The dismal outcome, tumor recurrence, and inevitable drug resistance reveal the urgent need to explore potential

Abbreviations: CGGA, Chinese Glioma Genome Atlas; FPKM, Fragments per kilobase million; GBM, glioblastoma multiforme; GSVA, gene sets variation analysis; ICIs, immune checkpoints inhibitors; LGG, lower-grade glioma; LYN, Lck/yes-related protein tyrosine kinase; OS, overall survival; PD-1, programmed death 1; PD-L1, programmed death ligand 1; ROC, Receiver operating characteristic; TCGA, The Cancer Genome Atlas; TPM, transcripts per kilobase million; WHO, world health organization.

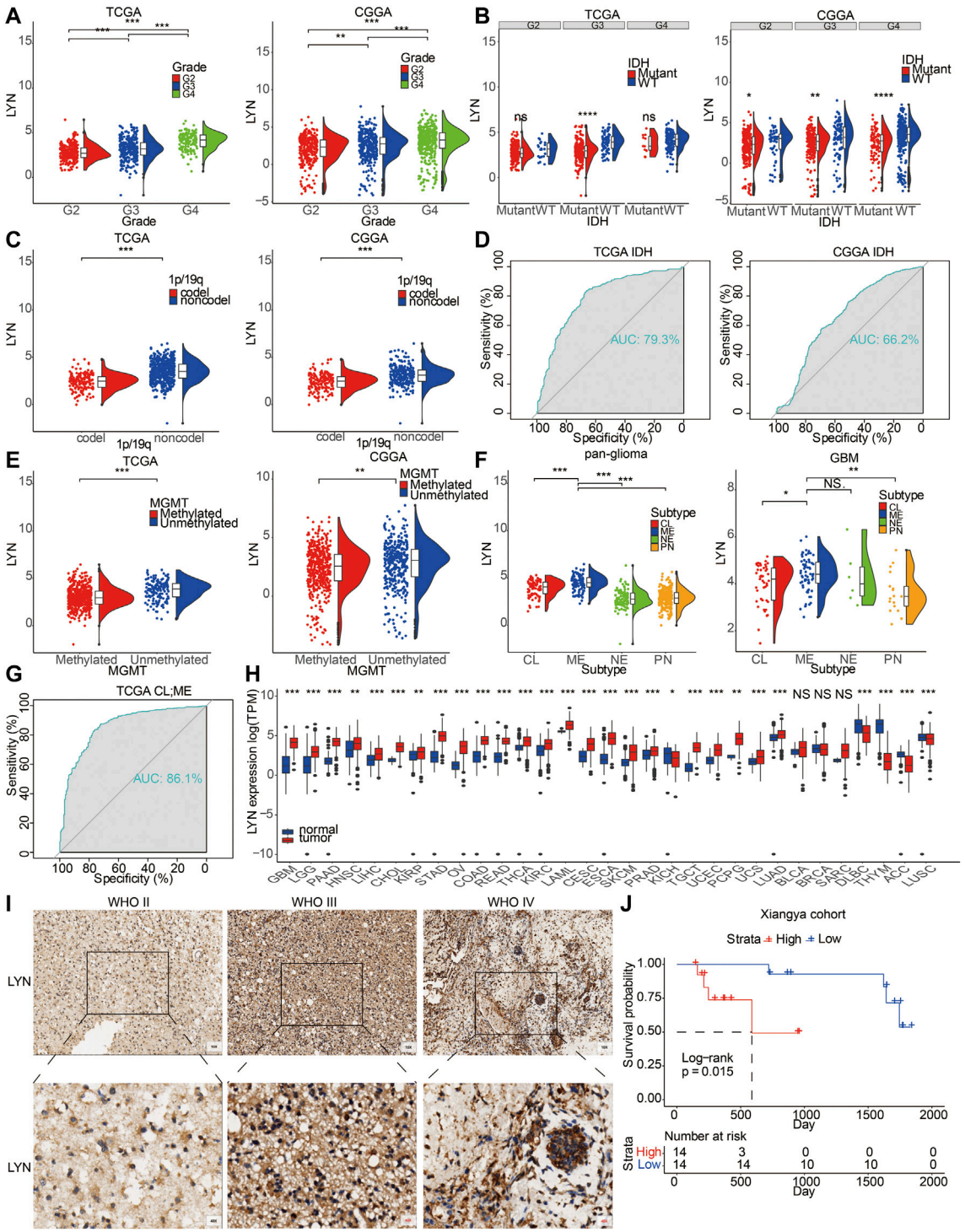

FIGURE 1 | LYN expression correlated with diverse pahological characteristics **(A)**. LYN expression in different WHO grades in TCGA and CGGA **(B)**. LYN expression in different IDH state in TCGA and CGGA **(C)**. LYN expression in different 1p/19q status from TCGA and CGGA dataset **(D)**. ROC curves showed LYN as a predictor of IDH mutation **(E)**. LYN expression in different MGMT promotor status from TCGA and CGGA dataset **(F)**. LYN expression in GBM samples and glioma samples based on molecular subtypes in TCGA **(G)**. ROC curves of LYN in predicting classical and mesenchymal subtype glioma **(H)**. LYN expression in different cancers from TCGA dataset. $^{*}p < 0.05$, $^{**}p < 0.01$, $^{***}p < 0.001$ **(I)**. Immunohistochemistry staining results of LYN in Xiangya cohort **(J)**. Kaplan—Meier curve of overall survival in Xiangya cohort based on the staining intensity of LYN. *p*-value was obtained from the log-rank test.

biomarkers involved in the tumorigenic mechanism of gliomas and develop potential therapeutic targets for treatment of glioma patients (Zhang et al., 2021a).

Gene markers are becoming increasingly attractive in tumor research, including predicting tumor progression and treatment efficiency, reducing the recurrence rate, and prolonging patients' survival (Zhang et al., 2021b). Immune checkpoint molecules have been identified as effective markers in predicting the immunotherapeutic effect in various cancer types (Zhang et al., 2021c). Programmed death 1 (PD-1) and its ligand, programmed death-ligand 1 (PD-L1), have exhibited remarkable prognostic and therapeutic value (Billon et al., 2019; Dong et al., 2021). Previous studies with immune checkpoint inhibitors (ICIs) targeting PD1 and PD-L1 have demonstrated durable clinical responses and prolonged survival in solid tumors (Ribas and Wolchok, 2018). Notably, the reliability and efficacy of PD-1 and PD-L1 as immunosuppressive biomarkers have been explored and confirmed (Dunn-Pirio and Vlahovic, 2017; Dong et al., 2021). Given the positive rate of PD-L1 in the majority of gliomas, multiple clinical trials with PD-1/PD-L1 inhibitors in gliomas are ongoing.

As a member of protein tyrosine kinases, LYN critically regulates essential cellular processes including cell growth and cell differentiation. LYN is found predominantly in myeloid cells, B lymphocytes, and cell types outside of the hematopoietic compartment (Uhlén et al., 2015). Studies have demonstrated that LYN regulates positive and negative pathways in B cell-mediated immunity (Brodie et al., 2018). Moreover, LYN profoundly affects the innate immune responses by controlling the activation of dendritic and NK cells (Krebs et al., 2012).

In this study, we speculated that LYN may be another promising biomarker for immunotherapy in glioma patients. Using transcriptomic data from two datasets, we investigated the expression level, clinical features, and functional annotation of LYN. Notably, we found the co-expression pattern of LYN and PD-L1 in glioma microenvironment. LYN could also significantly predict the anti-PD-1 and anti-CTLA-4 immunotherapy responses.

RESULTS

LYN Expression Correlates With Malignant Phenotypes in Gliomas

LYN expression in GBM samples was higher than that in LGG samples (**Figure 1A**). In this study, LYN expression was observed in IDH wild-type gliomas (**Figure 1B**). It should be noted that LYN expression in TCGA was only significantly different in grade 3, while there were differences in all three grades in CGGA. The seemingly contradictory result could be explained by the insufficient samples in TCGA (672 samples) compared with CGGA (1,018 samples). Besides, the median value of LYN in WT group was generally higher than that in mutant group in all three grades in TCGA. ROC curve proved the predictive value of LYN expression in glioma patients with IDH mutation or IDH wildtype in TCGA and CGGA (**Figure 1D**). Furthermore, LYN showed high expression in histopathologically malignant glioma samples (**Supplementary Figure S1B**) and 1p/19q non-codeletion glioma samples (**Figure 1C**). LYN expression was more enriched in unmethylated glioma samples (**Figure 1E**). As shown in **Figure 1F**, LYN expression was more enriched in the classical (CL) and mesenchymal (ME) subtypes compared with proneural (PN) and neural (NE) subtypes in TCGA (**Figure 1F**). Meanwhile, the ROC curve indicated that LYN expression effectively predicted CL and ME subtypes (**Figure 1G**).

Patients with recurrent gliomas were detected with higher level of LYN expression compared with patients with primary gliomas (**Supplementary Figure S1E**). LYN showed higher expression in glioma patients with progressive disease than in glioma patients with complete remission (**Supplementary Figure S1F**). Additionally, LYN expression was higher in contrast-enhanced (CE) regions than in non-contrast-enhanced (NCE) and normal tissues (NT) (**Supplementary Figure S1C**). Besides, based on the tumor anatomic structure of GBM, LYN expression was more enriched in hyperplastic blood vessels (**Supplementary Figure S1D**). LYN protein level was also found to be upregulated with increase of WHO grades based on the IHC staining results of glioma samples (n = 40) from the Xiangya hospital cohort (**Figure 1I**). The expression level of LYN also stratified glioma patients' survival in the Xiangya cohort (**Figure 1J**). The clinical information of the Xiangya cohort was provided in **Supplementary Table S1**.

Further, LYN expression levels in HMC-1 (mast cell), HEL (human erythroleukemia cells), U-698 (human B cell lymphoma), HDLM-2 (human Hodgkin lymphoma), and Karpas-707 (human myeloma) cell lineages were relatively high based on Cancer Cell Line Encyclopedia (CCLE) (**Supplementary Figure S1A**). Likewise, LYN was highly expressed in various cancer types (**Figure 1H**).

LYN Expression Predicts Worse Survival of Glioma Patients

Next, the prognostic value of LYN expression was explored. Patients with high LYN expression exhibited significantly lower overall survival (OS) than patients with low LYN expression in TCGA and CGGA (**Figures 2A,B**). Moreover, LYN expression was negatively related to progression-free interval (PFI) and disease-specific survival (DSS) in glioma patients (**Supplementary Figure S2**). ROC curve further indicated that LYN was a sensitive marker for 3-years and 5-years survival (**Supplementary Figure S1G**). The prognostic value of LYN was further validated using other datasets including CGGA325, CGGA693, array300, and GSE108474 (**Supplementary Figure S3**). Although the survival difference in GBM samples from TCGA (p = 0.16), CGGAarray (p = 0.55), and GSE108474 (p = 0.65) was not statistically significant, this could be attributed to the insufficient samples volume in these three datasets as the tendency in survival difference was evident that high LYN expression could

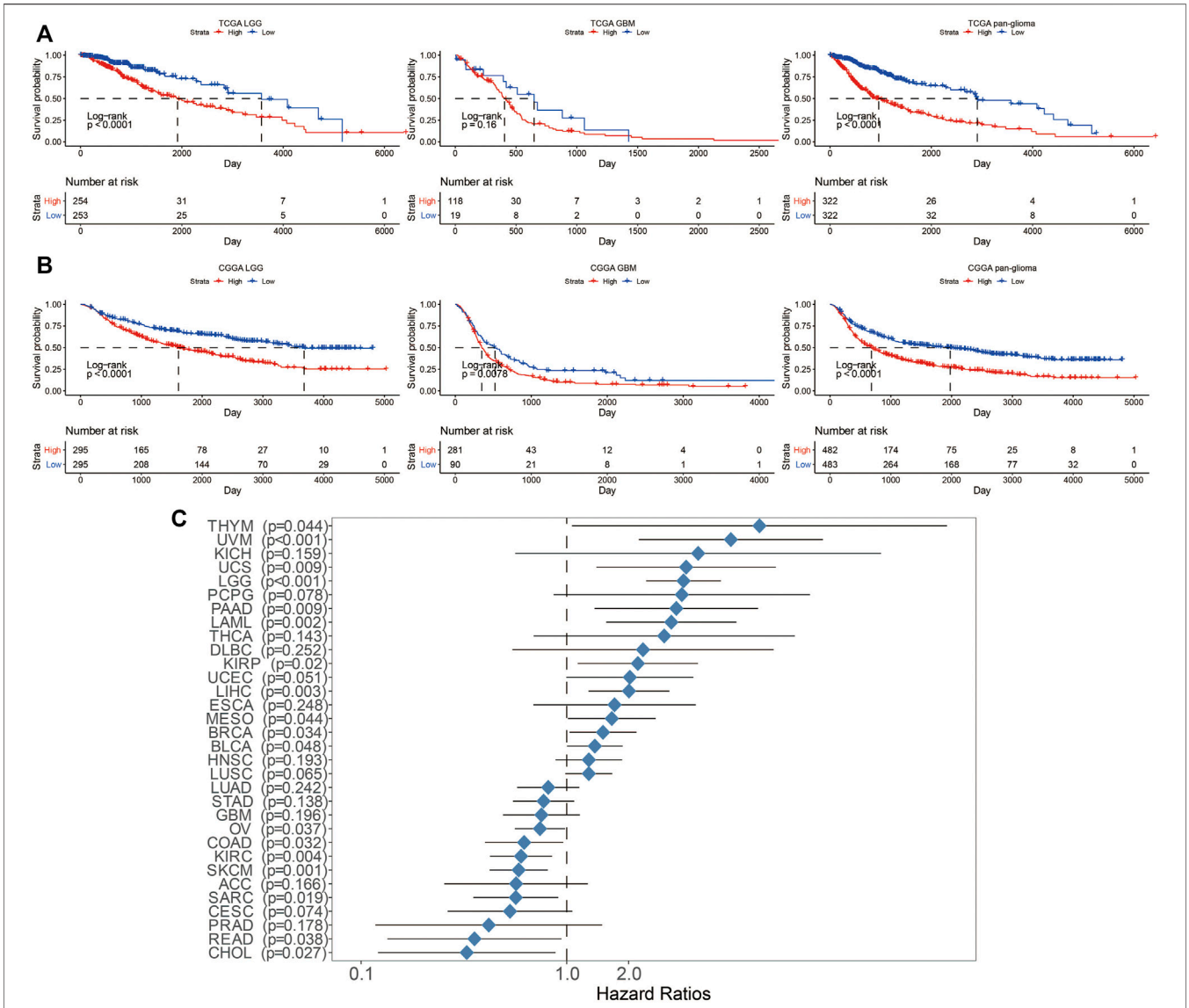

FIGURE 2 | Survival analysis in glioma patients with different levels of LYN expression. Kaplan–Meier curve of OS in glioma samples in **(A)**. TCGA and **(B)**. CGGA. *p*-values were calculated based on log-rank test **(C)**. Univariate cox regression analysis evaluating prognostic value of LYN expression in different cancer types regarding OS in TCGA. The length of horizontal line represents the 95% confidence interval. The vertical dotted line represents the HR of cancer patients. HR < 1.0 indicates that high LYN expression is a favorable prognostic biomarker.

predict worse survival. In the pan-cancer analysis, LYN indicated worse OS in thymoma (THYM), uveal melanoma (UVM), uterine carcinosarcoma (UCS), acute myeloid leukemia (LAML), kidney renal papillary cell carcinoma (KIRP), uterine corpus endometrial carcinoma (UCEC), liver hepatocellular carcinoma (LIHC), mesothelioma (MESO), breast invasive carcinoma (BRCA), ovarian serous pancreatic adenocarcinoma (PAAD), and testicular germ cell tumors (TGCT) (**Supplementary Figure S4**). We further revealed that LYN expression was a hazardous marker in eleven cancer types and a favorable marker in seven cancer types (**Figure 2C**).

In TCGA, high LYN expression was associated with reduced survival in glioma patients regarding different IDH statuses (p = 0.0454, p = 0.1062, respectively; **Figure 3**), radiotherapy statuses ($p < 0.001$, respectively; **Figure 3**), 1p19q statuses ($p < 0.001$, p = 0.1533, respectively; **Figure 3**), and MGMT promotor statuses ($p = 0.0074$, $p < 0.001$, respectively; **Figure 3**). Likewise, in CGGA, high LYN expression predicted worse survival in glioma patients regarding different IDH statuses (p = 0.0331, $p < 0.001$, respectively; **Figure 3**), radiotherapy statuses (p = 0.0961, $p <$ 0.001, respectively; **Figure 3**), chemotherapy statuses ($p = 0.1377$, $p = 0.0735$, respectively; **Figure 3**), 1p19q statuses ($p < 0.001$, p = 0.2452, respectively; **Figure 3**), and with MGMT promotor

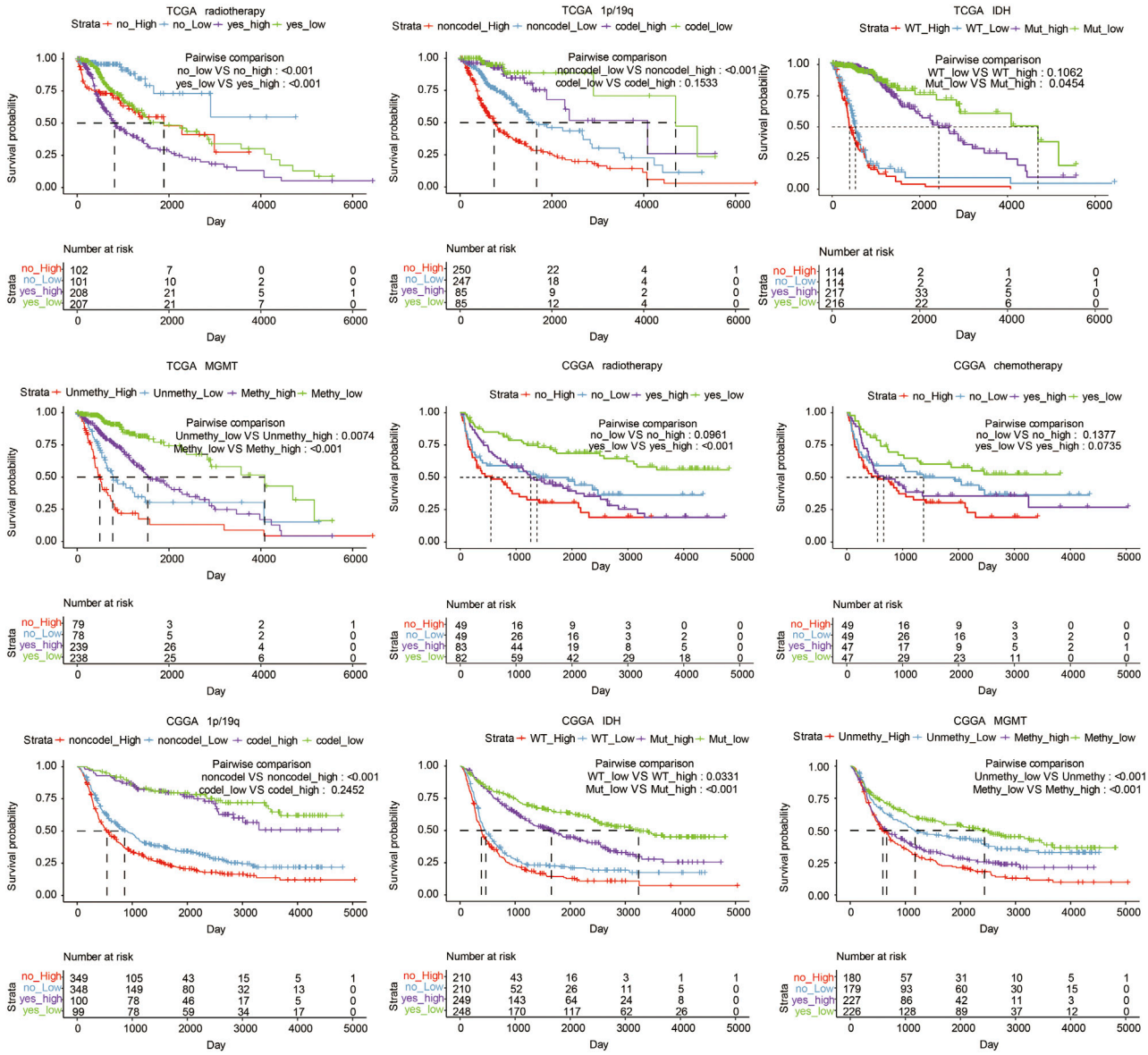

FIGURE 3 | Overall survival in glioma patients with different status, including radiotherapy, chemotherapy, 1p19q, MGMT, and IDH in TCGA and CGGA datasets.

statuses ($p < 0.001$, respectively; **Figure 3**). Notably, glioma patients receiving radiotherapy experienced reduced survival in TCGA ($p < 0.001$, respectively; **Figure 3**), which suggested that LGG patients might negatively respond to radiotherapy.

LYN Expression Correlates With Genomic Alterations

Glioma samples with CN loss expressed significantly higher level of LYN mRNA than diploid (**Figure 4A**). A global CNA profile was obtained in glioma samples with low LYN expression and glioma samples with high LYN expression (**Figures 4B,C**). Glioma samples with high LYN expression had frequent amplification of chr7 and deletion of chr10 (**Figure 4B**), while glioma samples with low LYN expression had frequent deletion of 1p and 19q (**Figure 4B**). In glioma samples with high LYN expression, oncogenic driver genes such as EGFR (7p11.2) and CDK4 (12q14.1) were frequently amplified, while tumor suppressor gene PTEN (10q23.31) and CDKN2A (9p21.3) were frequently deleted (**Figure 4C**). Additionally, TP53 (39%), PTEN (23%), EGFR (22%), TTN (20%) were frequently mutated in the LYN high expression cluster, while IDH1 (80%) and CIC (32%) were frequently mutated in the LYN low expression cluster (**Figure 4D**). It should be noted that ATRX had similar mutation rate in LYN high expression cluster and LYN low expression cluster, which indicated that the mutation of ATRX might be independent of LYN expression.

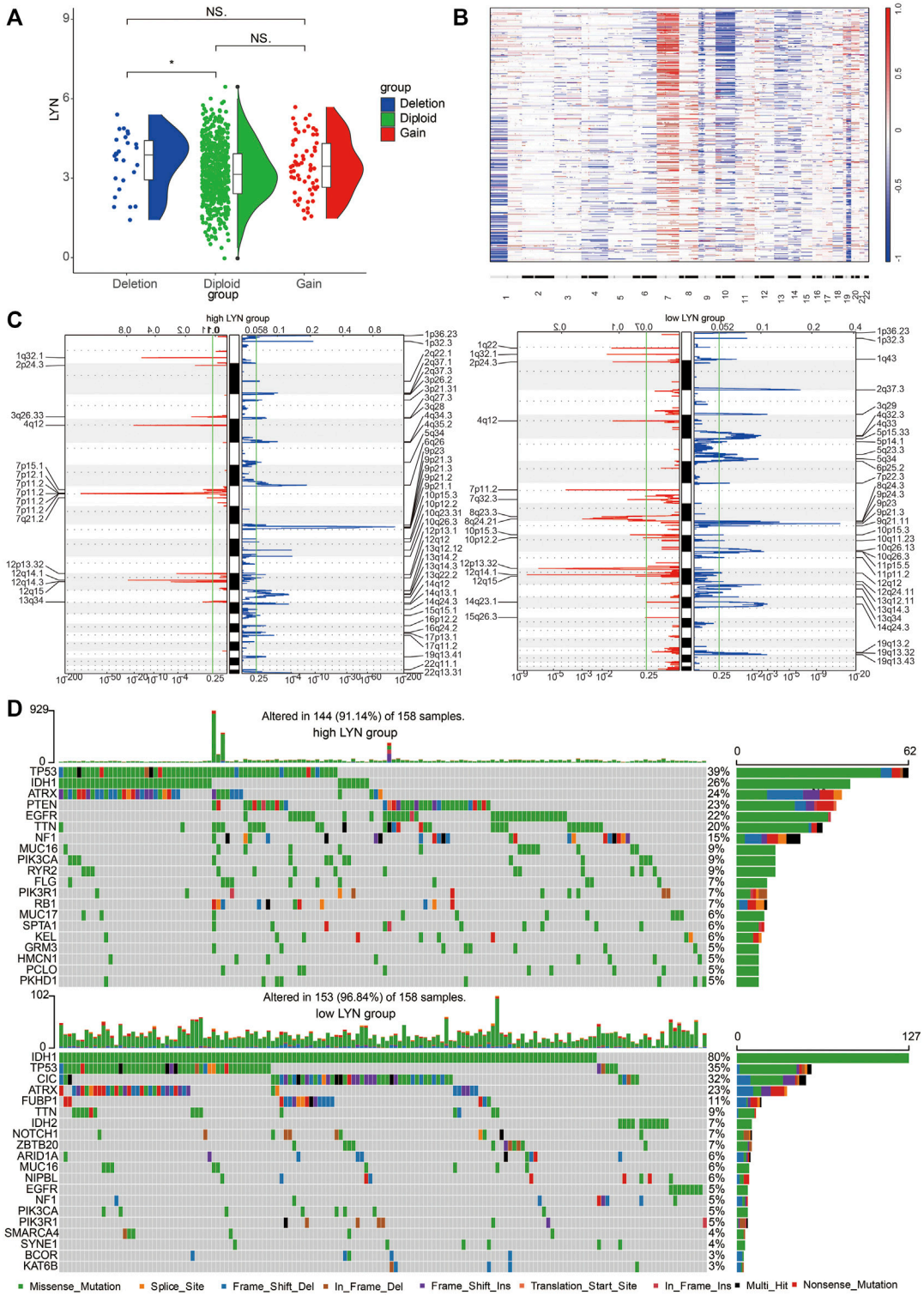

FIGURE 4 | Different genomic alterations are related to LYN expression **(A)**. Relationship between LYN expression and copy number variation in TCGA. NS, *, **, and *** indicate $p < 0.05$, $p < 0.01$, $p < 0.001$, and no significant difference, respectively **(B)**. The overall CNA profile based on LYN expression. 22 human chromosomes are numbered 1 to 22 consecutively **(C)**. Genomic events in glioma samples with low and high LYN expression based on GISTIC 2.0. Chromosomal locations of amplification peaks (red) and deletions peaks (blue) are presented **(D)**. Different genomic alterations in glioma samples with low and high LYN expression.

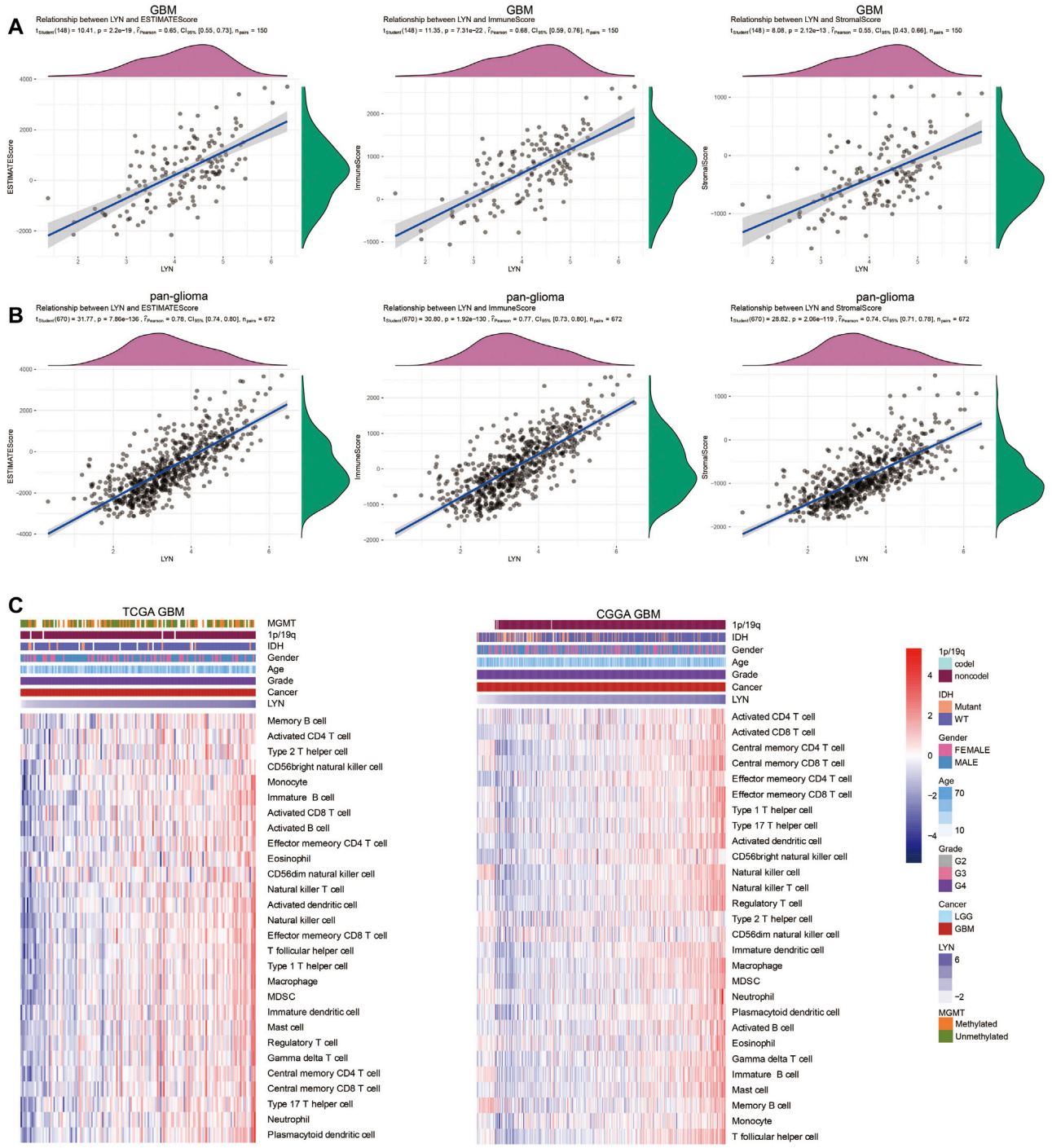

FIGURE 5 | LYN correlates with immune infiltration **(A)**. The correlation between LYN and Estimate Score, Immune Score, and Stromal Score in GBM samples in TCGA **(B)**. The correlation between LYN and Estimate Score, Immune Score, and Stromal Score in pan-glioma samples in CGGA **(C)**. Heatmaps illustrating the relationship between LYN and 28 immune cell types in TCGA GBM samples and CGGA GBM samples, respectively. The expression values are z-transformed. High expression values are colored red and low expression values are colored blue.

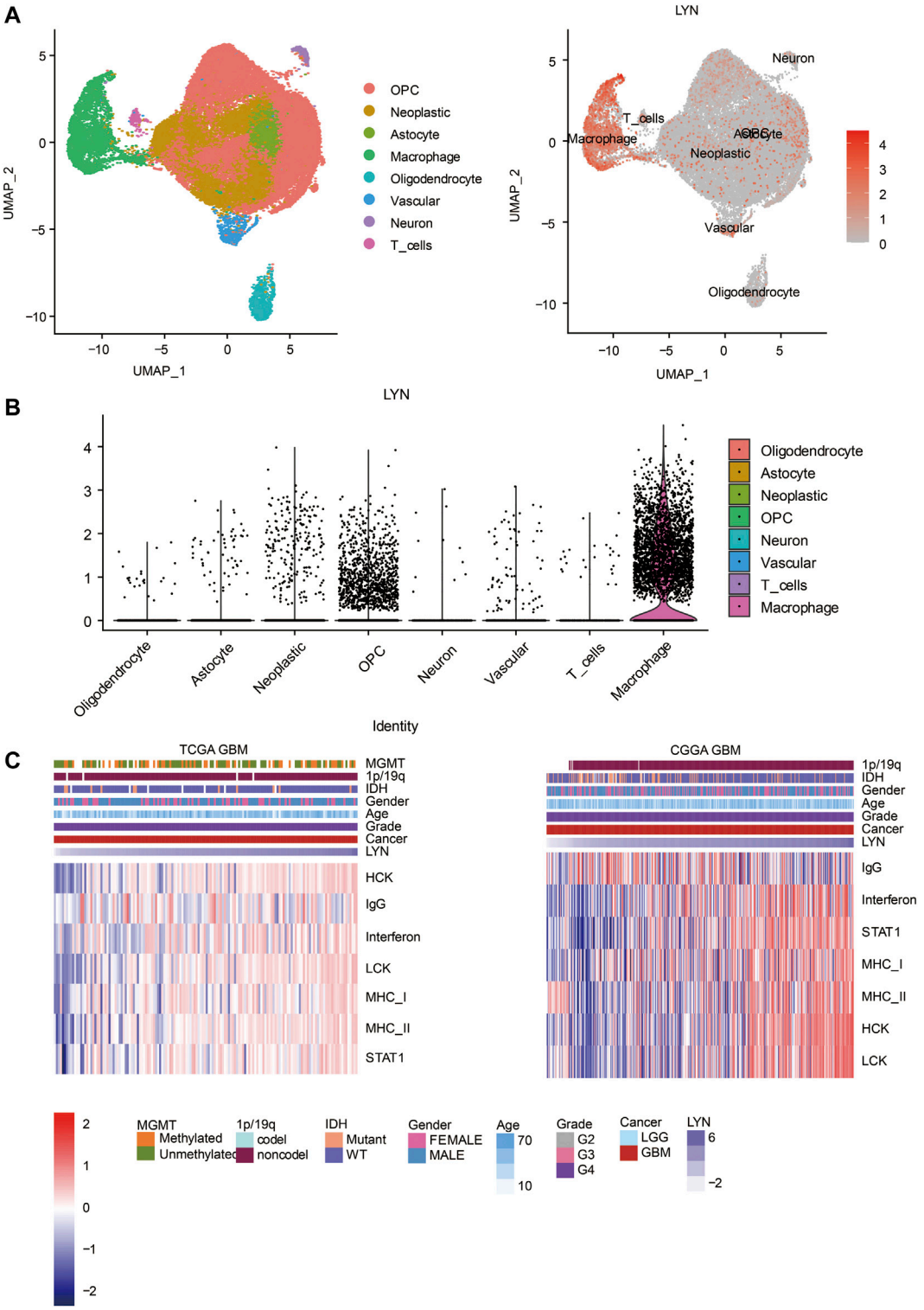

FIGURE 6 | Single cell sequencing analysis **(A)**. UMAP plot showing 8 cell clusters. Gray area represents all clustered cells. The red dot represents cell expressing LYN **(B)**. The expression level of LYN in 8 cell clusters **(C)**. Heatmaps illustrating LYN related inflammatory activities in TCGA GBM and CGGA GBM, respectively. The expression values are z-transformed. High expression values are colored red and low expression values are colored blue.

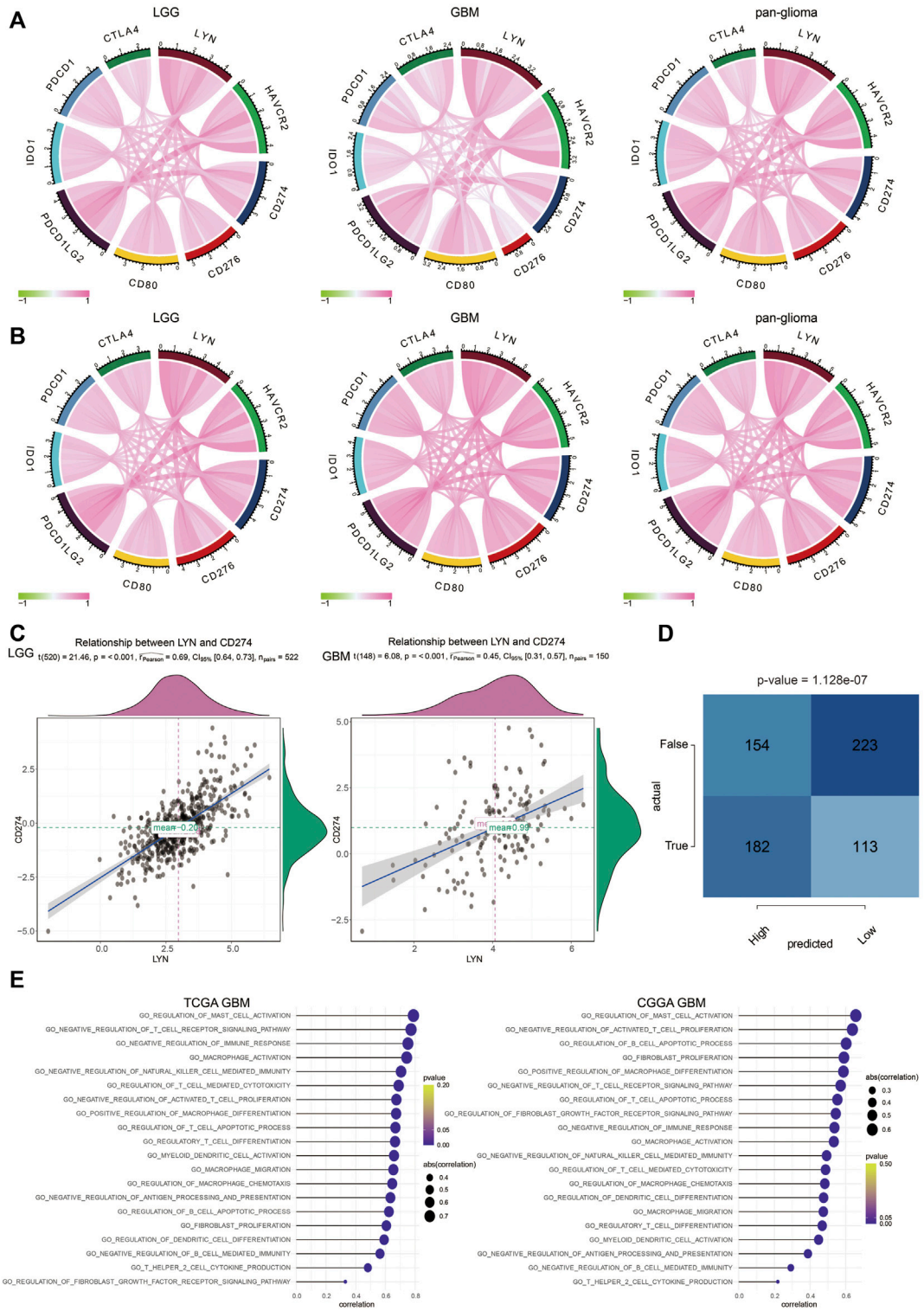

FIGURE 7 | LYN is associated with immunosuppressive activities **(A)**. The correlation between LYN and classical immune checkpoints in TCGA dataset **(B)**. The correlation between LYN and classical immune checkpoints in CGGA dataset **(C)**. The correlation between LYN and CD274 (PD-L1) in LGG and GBM in TCGA **(D)**. Contingency table showing the predictive value of LYN expression in immunotherapy responses based on TIDE algorithm **(E)**. The correlation between LYN and immune related signaling pathways in TCGA GBM and CGGA GBM samples in GO analysis.

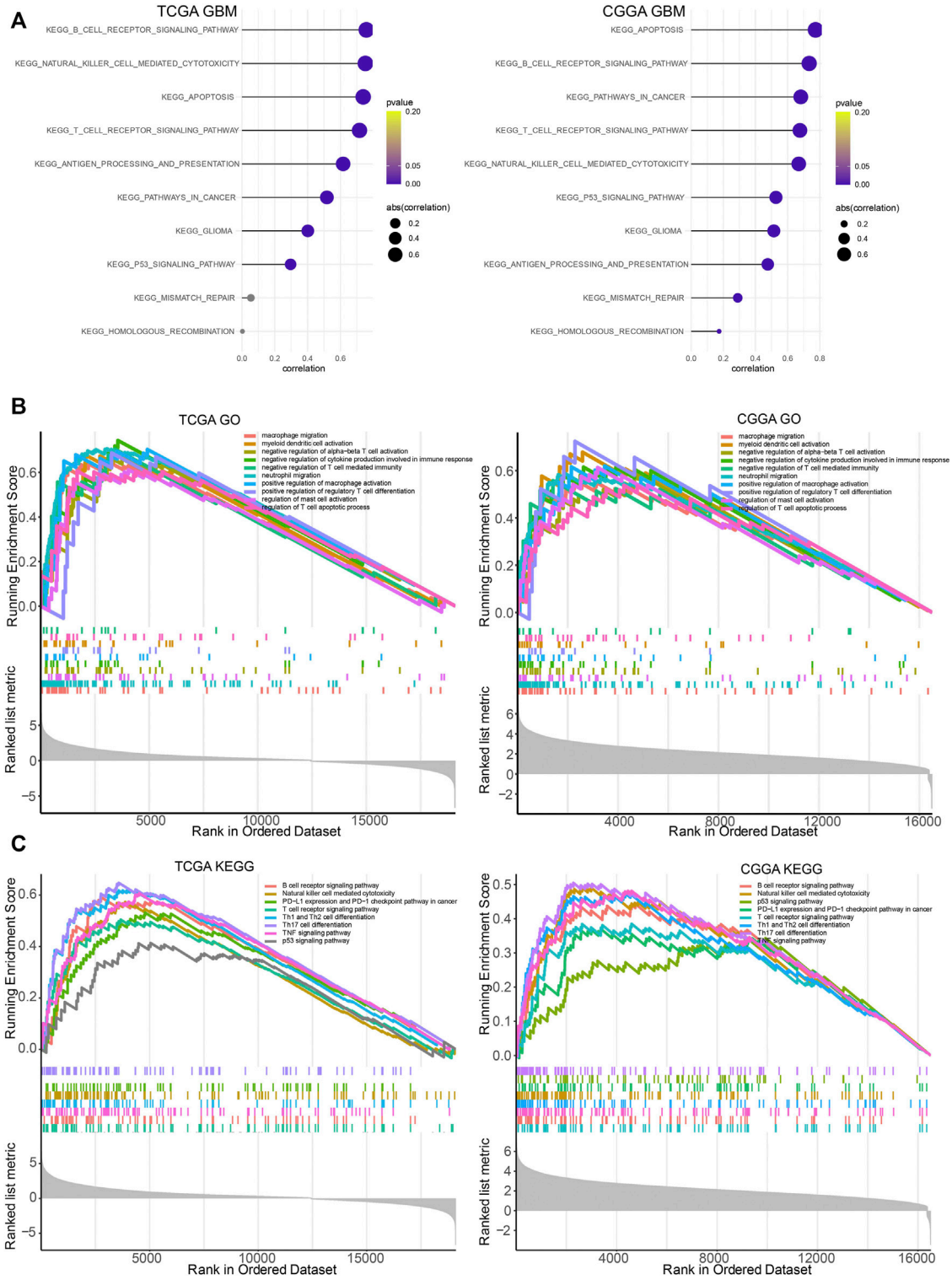

FIGURE 8 | LYN related immune processes **(A)**. The correlation between LYN and immune related signaling pathways in TCGA GBM and CGGA GBM samples in KEGG analysis **(B)**. GSEA of LYN in TCGA and CGGA in GO **(C)**. GSEA of LYN in TCGA and CGGA in KEGG.

LYN Mediates Tumor Immune Microenvironment

We identified the relationship between LYN and ESTIMATE scores. LYN was found to positively correlate with immune score, stromal score, and ESTIMATE score in GBM samples (**Figure 5A**) and glioma samples (**Figure 5B**). LYN expression was positively associated with a variety of immune infiltrating cell types responsible for an anti-tumor response in GBM samples (**Figures 5C,D**) and glioma samples (**Supplementary Figures S5A,B**). Additionally, based on the CIBERSORT algorithm, high LYN expression positively correlated with M2 macrophages, neutrophils (**Supplementary Figures S5C,D**). In single-cell sequencing analysis of GBM samples, after regressing out the patient effects, eight clusters of cells were identified (**Figure 6A**). The expression pattern of LYN in the eight-cell types was shown in **Figure 6A**. Moreover, the relative expression level of LYN was shown in **Figure 6B**, which confirmed that LYN highly correlated with macrophage and oligodendrocyte precursor cell (OPC). This result suggested that the abnormal high expression of LYN in GBM could be potentially caused by immune infiltrating microenvironment dominated by macrophages. Besides, LYN expression correlated with inflammatory signature genes in glioma samples (**Supplementary Figures S6A,B**) and GBM samples (**Figure 6C**) in TCGA and CGGA.

LYN Correlates With Other Immune Checkpoint Molecules and Immune-Related Pathways in Gliomas

As shown in **Figures 7A,B**, LYN positively correlated with classical immune checkpoint molecules in glioma samples in TCGA and CGGA. The correlation between LYN and PD-L1 was further analyzed in LGG and GBM samples, and the correlation was found to be higher in LGG than GBM (**Figure 7C**). Moreover, LYN expression in glioma patients could significantly predict anti-PD-1 and anti-CTLA-4 immunotherapy responses based on the TIDE algorithm (**Figure 7D**). Given that, LYN was more conceivably involved in the process of modulating immunosuppression-related signaling pathways by combining with other immune checkpoints in the LGG microenvironment.

LYN was found to positively correlate with regulation of B cell immunity, T cell proliferation, regulatory T cell differentiation, T cell apoptotic process, CD4 positive alpha-beta T cell activation, and regulation of T cell differentiation in GBM samples (**Figure 7E**) and glioma samples (**Supplementary Figures S7A,B**) in TCGA and CGGA based on GSVA results of GO terms. Thus, these findings indicated that LYN critically regulated the tumor immune environment in gliomas. In GSVA results of KEGG terms, LYN was associated with apoptosis, pathways in cancer, p53 signaling pathway, and mismatch repair in GBM samples (**Figure 8A**) and glioma samples (**Supplementary Figures S7C,D**) in both datasets. The GSEA results in GO (**Figure 8B**) and KEGG (**Figure 8C**) further confirmed that LYN correlated with immune suppressive activity and tumor proliferation in TCGA and CGGA.

Identification of Gene Modules Associated With LYN Expression

WGCNA analysis was used to determine the most correlated function of LYN based on the cluster dendrogram of LYN-related genes (**Figure 9A**). Genes were grouped into five modules, and the correlation coefficient between the identified modules and the expression level of LYN was calculated (**Figures 9B,D**). Notably, the brown module exhibited the highest correlation coefficient with a high LYN expression level (**Figure 9B**, $r = 0.7$, $p < 8e\text{-}102$). A significant correlation for genes in the brown module is illustrated in the plots of module membership and gene significance (**Figure 9C**, $r = 0.91$, $p < 1e\text{-}200$). GO analysis revealed that neutrophil activation and chemotaxis, negative regulation of T cell proliferation and activation, and chemokine-mediated signaling pathways were the most related gene functions associated with the high expression of LYN (**Figure 9E**). KEGG analysis revealed that Th17 cell differentiation, IL-17 signaling pathway, Th1 and Th2 cell differentiation, as well as NF-kappa B signaling pathway, were the pathways most related to the high expression of LYN (**Figure 9F**).

DISCUSSION

Immunotherapy is a rising star in tumor treatment, and immune checkpoint blockade has demonstrated promising results. Given the increasing attention to incorporate ICB in the treatment of gliomas, exploring novel and potential immune checkpoint molecules are significant. Based on large-scale bioinformatics analysis, we comprehensively delineated the clinical characteristic landscape of LYN in the immune infiltrating microenvironment of gliomas. Our work revealed that LYN was upregulated in higher grade gliomas. LYN expression was also highly correlated with IDH wildtype in GBM and served as a sensitive marker of IDH status. Besides, LYN was enriched in CL and ME subtype of gliomas, which indicated worse survival, and LYN was associated with 1p19q non-codeletion and unmethylated MGMT promoter, both of which predicted worse survival in glioma patients. LYN was mostly localized in hyperplastic blood vessels region that created a permissive environment for tumor growth.

LYN has been reported to promote the proliferation and migration of glioma cells and inversely correlates with patient survival (Dhruv et al., 2014; Lewis-Tuffin et al., 2015; Moncayo et al., 2018). In this study, LYN was associated with worse survival in both LGG and GBM patients. Additionally, genomic alternations analysis revealed that LYN expression was positively associated with somatic mutations and CNVs. Amplification of oncogenic drivers including PDGFRA, EGFR, and CDK4 were detected in high LYN expression samples, while tumor suppressor genes including CDKN2A/CDKN2B and PTEN had a deletion peak in high LYN expression samples. However, only in*in vivo* and *in vitro* experiments with LYN being knocked down or overexpressed in cells or animals, could we prove that these high frequency mutations are closely related to

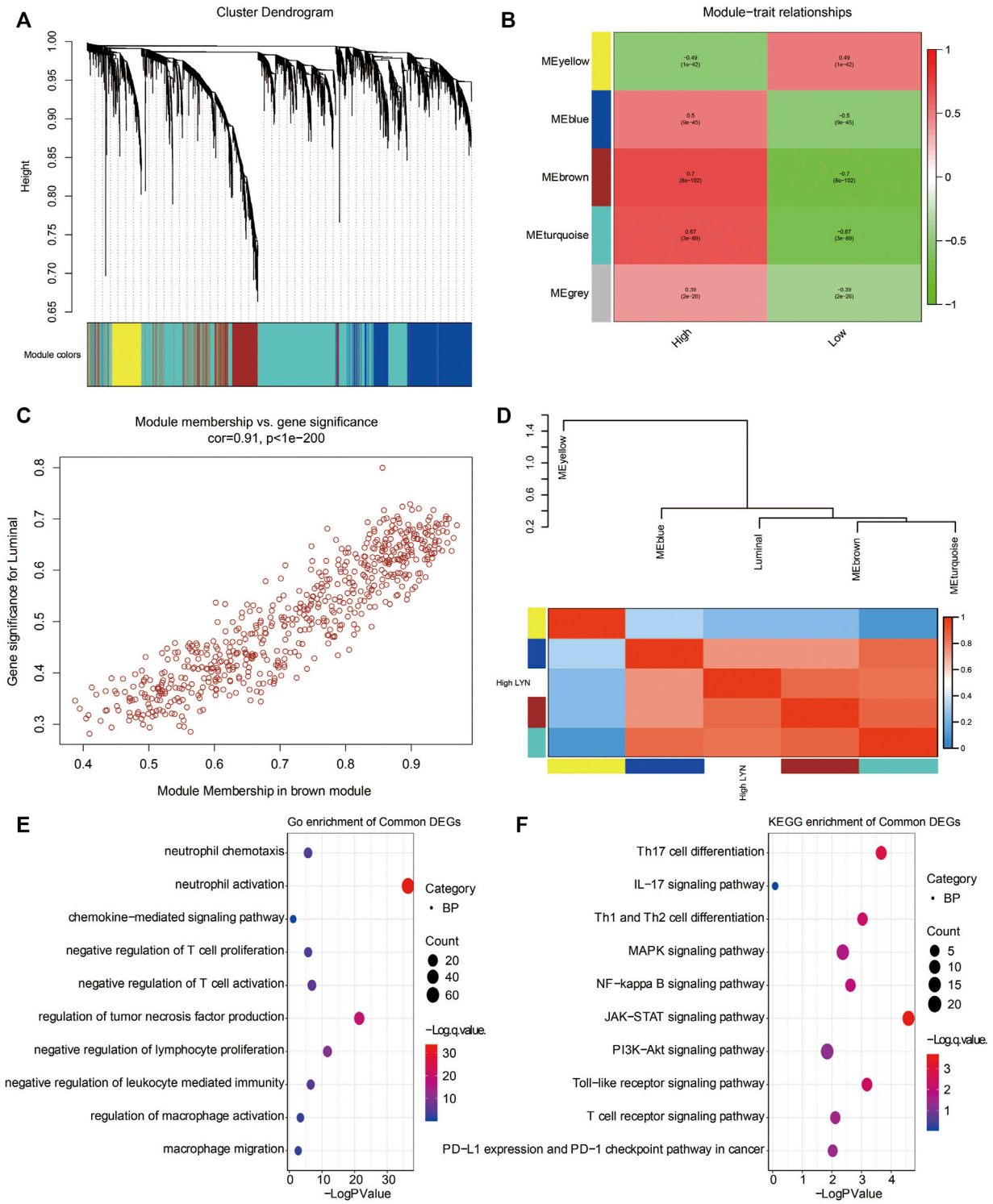

FIGURE 9 | WGCNA exploring LYN-related gene module **(A)**. WGCNA was performed to identify five modules **(B)**. Four modules (nongrey) were identified with the brown module showing the highest correlation ($r = 0.7$, $P = 8e\text{-}102$) with high LYN expression **(C)**. The gene significance highly correlated with module membership of the genes in the brown module **(D)**. The clustering results of the identified modules **(E)**. GO enrichment analysis of the genes extracted from brown module **(F)**. KEGG enrichment analysis of the genes extracted from brown module.

LYN. The abnormal higher mutation rate of tumor suppressor gene, TP53, in LYN high expression cluster was intriguing and also needed to be explored. Taken together, these results indicated that LYN regulated glioma cell progression and proliferation, and high LYN expression could predict the survival rate of glioma patients.

Previous studies have demonstrated that LYN regulates the development and function of multiple immune cells, such as macrophage, dendritic cells (Yang et al., 2018), T cells (Fallacara et al., 2019), and B cells (Brodie et al., 2018). This study further showed that LYN was involved in the glioma immune microenvironment. Besides, LYN was found to have a positive correlation with estimate score, immune score and stromal score, all of which were negatively correlated with the prognosis of glioma patients (Jia et al., 2018). LYN also positively correlated with various immune infiltrating cells, including Tregs, M2 macrophage, and MDSC, which contribute to an immunosuppressive microenvironment in gliomas (Marvel and Gabrilovich, 2015; Zhang et al., 2021d; Zhang et al., 2021e; Zhang et al., 2021f). GSVA in GO confirmed that LYN was involved in macrophage activation, macrophage migration, fibroblast proliferation, myeloid dendritic cell activation, regulatory T cell differentiation, and negative regulation of activated T cell proliferation. Additionally, GSVA in KEGG and GSEA showed that LYN negatively regulated the immune system in gliomas and promoted the proliferation of glioma cells. Besides, a correlation was observed between inflammatory signatures and LYN. Taken together, these results revealed the immunosuppressive role played by LYN in gliomas.

Immune checkpoint blockage enhances anti-tumor immune response. Several classical immune checkpoint molecules including PD-1, PD-L1, LAG3, and TIM3, have been shown to cause disorders of the immune system (Li et al., 2018). The classical PD-1/PD-L1 axis directly promotes the invasion and progression of GBM cells (Litak et al., 2019). In this study, LYN remarkably correlated with multiple classical immune checkpoint molecules. Special attention was paid to the connection between LYN and PD-L1, and LYN showed a correlation with PD-L1 in LGG and GBM. These results showed that LYN could potentially mediate the function of immune checkpoint molecules.

Taken together, we described the characteristics of LYN in gliomas based on bioinformatics analysis of several datasets. LYN predicted malignant gliomas and served as a prognostic marker indicating worse survival of glioma patients. Moreover, LYN facilitated the establishment of an immune-suppressive and favorable glioma microenvironment. However, there is a need for research to investigate LYN as a potential immune checkpoint molecule, which can promote the clinical management of glioma patients receiving immunotherapy.

MATERIALS AND METHODS

Data Collection

The transcriptome data of LYN was collected from glioma samples in TCGA and CGGA databases. 672 glioma samples were downloaded from TCGA (https://xenabrowser.net/). Three CGGA cohorts, including mRNAseq_693 (693 glioma samples), mRNAseq_325 (325 glioma samples), and CGGAarray (300 glioma samples), were downloaded from CGGA (http://www.cgga.org.cn/) and included in this study. CGGA325 and CGGA693 were combined as CGGA dataset after removing batch effect using the R package sva. 414 glioma samples from GSE108474 dataset were downloaded from the GEO database (https://www.ncbi.nlm.nih.gov/geo/). Fragments per kilobase million (FPKM) values of gene matrix were transformed into transcripts per kilobase million (TPM) values. RNA-seq data of tumor localization in patients with GBM was downloaded from the Ivy Glioblastoma Atlas Project (http://glioblastoma.alleninstitute.org/). A total of 8,295 normal samples were collected from GTEX (http://commonfund.nih.gov/GTEx/) and TCGA databases. Single-cell sequencing dataset was downloaded from GSE138794 (Wang et al., 2019) in the Gene Expression Omnibus (GEO; https://www.ncbi.nlm.nih.gov/) database. Eight scRNA sequencing samples of GBM were included in the analysis. Tumor tissues were from glioma patients underwent surgery in Xiangya Hospital, Central South University. Written informed consent was obtained from all patients.

Immunohistochemistry

Paraffin-embedded tissue sections were obtained from human gliomas (WHO grades II-IV) and used for IHC staining. 40 samples were used for LYN. The sections were incubated with the LYN primary antibody (Rabbit) (1:50; Proteintech; Wuhan, China) after blockage with 5% BSA. The antibody reaction was visualized after 3, 3′-diaminobenzidine (DAB) development, and sections were counterstained with hematoxylin.

Biological Function Annotation of LYN

Somatic mutations and copy number alterations (CNAs) of glioma samples were downloaded from TCGA. GISTIC 2.0 (https://gatkforums.broadinstitute.org) was performed for enrichment of genetic alteration events. CIBERSORT algorithm was performed for quantifying the expression level of 22 immune cell types (Newman et al., 2015). The gene sets variation analysis (GSVA) and gene set enrichment analysis (GSEA) were applied to investigate the immune-related and tumor-related processes of LYN. ssGSEA was used for the enrichment pattern of the 28 immune cell types. TIDE algorithm was applied to evaluate the predictive value of LYN in anti-PD-1 and anti-CTLA-4 immunotherapy responses (Jiang et al., 2018).

Single Cell RNA-Sequencing

Single-cell expression matrix was processed using R package Seurat V3.1.2. Expression data was normalized by "NormalizeData", and 2000 highly variable genes (HVGs) was identified after performing "FindVariableGenes". "FindIntegrationAnchors" and "Integratedata" was applied to merge eight GBM samples of single-cell sequencing (Stuart et al., 2019). Principal component analysis (PCA) was performed as previously described. Finally, "UMAP" was adopted for visualization of cell clusters with patient effects regressed out.

Weighted Gene Co-expression Network Analysis

R package WGCNA was applied to explore the LYN related genes. After performing the correlation analysis between LYN and the gene expression matrix in TCGA, 3923 LYN related genes (correlation efficient >0.4) were used as the input of WGCNA. A power of $\beta = 8$ and a scale-free R2 = 0.84 were determined and set as soft-threshold parameters for a scale-free topology network. The calculated scale-free distribution topological matrix determined the softConnectivity for constructing sample dendrogram. The labeledHeatmap was used for depicting the module-trait relationship. The internal gene significance of each module was calculated and visualized using verboseScatterplot. Genes within the identified module with the highest gene significance were extracted for GO and KEGG enrichment analysis.

Statistical Analysis

The datasets were divided into high and low groups based on the median and cutoff expression level of LYN in pan-gliomas, LGG, and GBM, respectively. Kaplan-Meier survival curves were generated using R package survival. The oneway analysis of variance was used to determine the LYN expression levels among multiple groups. The Wilcoxon rank testing was applied for determining the LYN expression levels in relation to different pathological characteristics between two groups. R package pROC was used for generation of receiver operating characteristic (ROC) curves. The classifier of ROC curve was built based on IDH status (WT vs. mutant) and molecular subtypes (classical, mesenchymal vs. proneural, neural). Pearson's correlation coefficient was used for calculation of correlation coefficient. R version 3.6.3 was used for all statistical analyses. p-values < 0.05 were set as the criteria of statistically significant.

CONCLUSION

LYN was associated with malignancy of gliomas and served as a prognostic marker of glioma patients. Besides, LYN facilitated the establishment of an immune-suppressive and favorable glioma microenvironment. At single cell sequencing level, LYN was abundantly expressed by tumor associated macrophages and T cells. Furthermore, the robust relationship between LYN and PD-L1 indicated that LYN might be a potent immune checkpoint molecule in predicting immunotherapy response.

DATA AVAILABILITY STATEMENT

The original contributions presented in the study are included in the article/**Supplementary Material**, further inquiries can be directed to the corresponding authors.

AUTHOR CONTRIBUTIONS

Study design: LZ, ZL, and QC. Foundation support: LZ, ZL, and QC. Acquisition and analysis of data: LZ, CJ, HZ, QC, WW, and ZW. Drafting the manuscript and revising for submission quality: LZ, CJ, HZ, and QC. Reviewing and approving the final vision: LZ, ZL, and QC. All authors read and approved the final manuscript.

FUNDING

This work was funded by the National Natural Science Foundation of China (NO. 82073893, NO. 82172685, NO. 81703622, NO. 81402249, NO. 81873635), China Postdoctoral Science Foundation (NO. 2018M633002), Hunan Provincial Natural Science Foundation of China (NO. 2018JJ3838, NO. 2019JJ50963), Hunan provincial health and Health Committee Foundation of China (C2019186), Xiangya Hospital Central South University postdoctoral foundation.

SUPPLEMENTARY MATERIAL

The Supplementary Material for this article can be found online at: https://www.frontiersin.org/articles/10.3389/fcell.2021.760929/full#supplementary-material

REFERENCES

Billon, E., Finetti, P., Bertucci, A., Niccoli, P., Birnbaum, D., Mamessier, E., et al. (2019). PDL1 Expression Is Associated with Longer Postoperative, Survival in Adrenocortical Carcinoma. *Oncoimmunology* 8, e1655362. doi:10.1080/2162402X.2019.1655362

Brodie, E. J., Infantino, S., Low, M. S. Y., and Tarlinton, D. M. (2018). Lyn, Lupus, and (B) Lymphocytes, a Lesson on the Critical Balance of Kinase Signaling in Immunity. *Front. Immunol.* 9, 401. doi:10.3389/fimmu.2018.00401

Claus, E. B., Walsh, K. M., Wiencke, J. K., Molinaro, A. M., Wiemels, J. L., Schildkraut, J. M., et al. (2015). Survival and Low-Grade Glioma: the Emergence of Genetic Information. *Foc.* 38, E6. doi:10.3171/2014.10.FOCUS12367

Dhruv, H. D., Whitsett, T. G., Jameson, N. M., Patel, F., Winkles, J. A., Berens, M. E., et al. (2014). Tumor Necrosis Factor-like Weak Inducer of Apoptosis (TWEAK) Promotes Glioblastoma Cell Chemotaxis via Lyn Activation. *Carcin* 35, 218–226. doi:10.1093/carcin/bgt289

Dong, D., Zhang, W., Xiao, W., Wu, Q., Cao, Y., Gao, X., et al. (2021). A GRN Autocrine-dependent FAM135B/AKT/mTOR Feedforward Loop Promotes Esophageal Squamous Cell Carcinoma Progression. *Cancer Res.* 81, 910–922. doi:10.1158/0008-5472.CAN-20-0912

Dunn-Pirio, A. M., and Vlahovic, G. (2017). Immunotherapy Approaches in the Treatment of Malignant Brain Tumors. *Cancer* 123, 734–750. doi:10.1002/cncr.30371

Fallacara, A. L., Passannanti, R., Mori, M., Iovenitti, G., Musumeci, F., Greco, C., et al. (2019). Identification of a New Family of Pyrazolo[3,4-D]pyrimidine Derivatives as Multitarget Fyn-Blk-Lyn Inhibitors Active on B- and T-Lymphoma Cell Lines. *Eur. J. Med. Chem.* 181, 111545. doi:10.1016/j.ejmech.2019.07.048

Jia, D., Li, S., Li, D., Xue, H., Yang, D., and Liu, Y. (2018). Mining TCGA Database for Genes of Prognostic Value in Glioblastoma Microenvironment. *Aging* 10, 592–605. doi:10.18632/aging.101415

Jiang, P., Gu, S., Pan, D., Fu, J., Sahu, A., Hu, X., et al. (2018). Signatures of T Cell Dysfunction and Exclusion Predict Cancer Immunotherapy Response. *Nat. Med.* 24, 1550–1558. doi:10.1038/s41591-018-0136-1

Krebs, D. L., Chehal, M. K., Sio, A., Huntington, N. D., Da, M. L., Ziltener, P., et al. (2012). Lyn-dependent Signaling Regulates the Innate Immune Response by Controlling Dendritic Cell Activation of NK Cells. *J.I.* 188, 5094–5105. doi:10.4049/jimmunol.1103395

Lewis-Tuffin, L. J., Feathers, R., Hari, P., Durand, N., Li, Z., Rodriguez, F. J., et al. (2015). Src Family Kinases Differentially Influence Glioma Growth and Motility. *Mol. Oncol.* 9, 1783–1798. doi:10.1016/j.molonc.2015.06.001

Li, X., Wang, B., Gu, L., Zhang, J., Li, X., Gao, L., et al. (2018). Tim-3 Expression Predicts the Abnormal Innate Immune Status and Poor Prognosis of Glioma Patients. *Clinica Chim. Acta* 476, 178–184. doi:10.1016/j.cca.2017.11.022

Litak, J., Mazurek, M., Grochowski, C., Kamieniak, P., and Roliński, J. (2019). PD-L1/PD-1 Axis in Glioblastoma Multiforme. *Ijms* 20, 5347. doi:10.3390/ijms20215347

Marvel, D., and Gabrilovich, D. I. (2015). Myeloid-derived Suppressor Cells in the Tumor Microenvironment: Expect the Unexpected. *J. Clin. Invest.* 125, 3356–3364. doi:10.1172/JCI80005

Moncayo, G., Grzmil, M., Smirnova, T., Zmarz, P., Huber, R. M., Hynx, D., et al. (2018). SYK Inhibition Blocks Proliferation and Migration of Glioma Cells and Modifies the Tumor Microenvironment. *Neuro Oncol.* 20, 621–631. doi:10.1093/neuonc/noy008

Newman, A. M., Liu, C. L., Green, M. R., Gentles, A. J., Feng, W., Xu, Y., et al. (2015). Robust Enumeration of Cell Subsets from Tissue Expression Profiles. *Nat. Methods* 12, 453–457. doi:10.1038/nmeth.3337

Ribas, A., and Wolchok, J. D. (2018). Cancer Immunotherapy Using Checkpoint Blockade. *Science* 359, 1350–1355. doi:10.1126/science.aar4060

Stuart, T., Butler, A., Hoffman, P., Hafemeister, C., Papalexi, E., Mauck, W. M., 3rd, et al. (2019). Comprehensive Integration of Single-Cell Data. *Cell* 177, 1888–1902. doi:10.1016/j.cell.2019.05.031

Uhlén, M., Fagerberg, L., Hallström, B. M., Lindskog, C., Oksvold, P., Mardinoglu, A., et al. (2015). Tissue-based Map of the Human Proteome. *Science* 347, 1260419. doi:10.1126/science.1260419

Wang, L., Babikir, H., Müller, S., Yagnik, G., Shamardani, K., Catalan, F., et al. (2019). The Phenotypes of Proliferating Glioblastoma Cells Reside on a Single Axis of Variation. *Cancer Discov.* 9, 1708–1719. doi:10.1158/2159-8290.CD-19-0329

Yang, Y., Wang, C., Cheng, P., Zhang, X., Li, X., Hu, Y., et al. (2018). CD180 Ligation Inhibits TLR7- and TLR9-Mediated Activation of Macrophages and Dendritic Cells through the Lyn-SHP-1/2 Axis in Murine Lupus. *Front. Immunol.* 9, 2643. doi:10.3389/fimmu.2018.02643

Zhang, H., Dai, Z., Wu, W., Wang, Z., Zhang, N., Zhang, L., et al. (2021). Regulatory Mechanisms of Immune Checkpoints PD-L1 and CTLA-4 in Cancer. *J. Exp. Clin. Cancer Res.* 40, 184. doi:10.1186/s13046-021-01987-7

Zhang, H., Luo, Y.-B., Wu, W., Zhang, L., Wang, Z., Dai, Z., et al. (2021). The Molecular Feature of Macrophages in Tumor Immune Microenvironment of Glioma Patients. *Comput. Struct. Biotechnol. J.* 19, 4603–4618. doi:10.1016/j.csbj.2021.08.019

Zhang, H., Wang, R., Yu, Y., Liu, J., Luo, T., and Fan, F. (2019). Glioblastoma Treatment Modalities besides Surgery. *J. Cancer* 10, 4793–4806. doi:10.7150/jca.32475

Zhang, H., Wang, Z., Dai, Z., Wu, W., Cao, H., Li, S., et al. (2021). Novel Immune Infiltrating Cell Signature Based on Cell Pair Algorithm Is a Prognostic Marker in Cancer. *Front. Immunol.* 12, 694490. doi:10.3389/fimmu.2021.694490

Zhang, L., Liu, F., Weygant, N., Zhang, J., Hu, P., Qin, Z., et al. (2021). A Novel Integrated System Using Patient-Derived Glioma Cerebral Organoids and Xenografts for Disease Modeling and Drug Screening. *Cancer Lett.* 500, 87–97. doi:10.1016/j.canlet.2020.12.013

Zhang, N., Dai, Z., Wu, W., Wang, Z., Cao, H., Zhang, Y., et al. (2021). The Predictive Value of Monocytes in Immune Microenvironment and Prognosis of Glioma Patients Based on Machine Learning. *Front. Immunol.* 12, 656541. doi:10.3389/fimmu.2021.656541

Zhang, N., Zhang, H., Wang, Z., Dai, Z., Zhang, X., Cheng, Q., et al. (2021). Immune Infiltrating Cells-Derived Risk Signature Based on Large-Scale Analysis Defines Immune Landscape and Predicts Immunotherapy Responses in Glioma Tumor Microenvironment. *Front. Immunol.* 12, 691811. doi:10.3389/fimmu.2021.691811

Conflict of Interest: The authors declare that the research was conducted in the absence of any commercial or financial relationships that could be construed as a potential conflict of interest.

Publisher's Note: All claims expressed in this article are solely those of the authors and do not necessarily represent those of their affiliated organizations, or those of the publisher, the editors and the reviewers. Any product that may be evaluated in this article, or claim that may be made by its manufacturer, is not guaranteed or endorsed by the publisher.

Copyright © 2022 Jiang, Zhang, Wu, Wang, Dai, Zhang, Liu and Cheng. This is an open-access article distributed under the terms of the Creative Commons Attribution License (CC BY). The use, distribution or reproduction in other forums is permitted, provided the original author(s) and the copyright owner(s) are credited and that the original publication in this journal is cited, in accordance with accepted academic practice. No use, distribution or reproduction is permitted which does not comply with these terms.

frontiers in Cell and Developmental Biology

ORIGINAL RESEARCH
published: 21 February 2022
doi: 10.3389/fcell.2022.815596

Identification of Tumor Antigens and Immune Subtypes in Lung Adenocarcinoma for mRNA Vaccine Development

Ran Xu[1,2], *Tong Lu*[1,2], *JiaYing Zhao*[1,2], *Jun Wang*[1,2], *Bo Peng*[1,2] *and LinYou Zhang*[1]*

[1]Department of Thoracic Surgery, The Second Affiliated Hospital of Harbin Medical University, Harbin, China, [2]Harbin Medical University, Harbin, China

Cancer vaccines are emerging as a viable strategy for cancer treatment. In the current study, we screened for genes associated with the prognosis of patients with lung adenocarcinoma and positively correlated with antigen-presenting cell infiltration and identified KLRG1 and CBFA2T3 as potential tumor antigens for mRNA vaccines in lung adenocarcinoma (LUAD). Further analyses of immune subtypes revealed that patients with early-stage LUAD, high immune cell infiltration, high immune checkpoint expression, and low tumor mutation burden might benefit from mRNA vaccination. Moreover, we identified four biomarkers that can be used to assess mRNA vaccination suitability. We also identified potentially sensitive anti-cancer drugs for populations not suitable for vaccination by means of anti-cancer drug susceptibility prediction. Overall, we provided a new perspective for mRNA vaccine treatment strategies for LUAD and emphasized the importance of precise and personalized treatments.

Keywords: lung adenocarcinoma, mRNA vaccine, tumor antigens, antigen presentation, individualized treatment

OPEN ACCESS

Edited by:
Qian Xiao,
Rutgers Cancer Institute of New Jersey, United States

Reviewed by:
Xing Huang,
Zhejiang University, China
Yuanyong Wang,
People's Liberation Army General Hospital, China

***Correspondence:**
LinYou Zhang
lyzhang@hrbmu.edu.cn

Specialty section:
This article was submitted to Molecular and Cellular Pathology, a section of the journal Frontiers in Cell and Developmental Biology

Received: *15 November 2021*
Accepted: *31 January 2022*
Published: *21 February 2022*

Citation:
Xu R, Lu T, Zhao J, Wang J, Peng B and Zhang L (2022) Identification of Tumor Antigens and Immune Subtypes in Lung Adenocarcinoma for mRNA Vaccine Development. Front. Cell Dev. Biol. 10:815596. doi: 10.3389/fcell.2022.815596

INTRODUCTION

Lung cancer is the leading malignant disease death cause (Siegel et al., 2021) with a 5-years survival rate of 4–17% (Hirsch et al., 2017). Lung adenocarcinoma (LUAD) is the most common lung cancer pathological subtype and great progress has been made recently regarding individualized and precise treatments. To date, surgery is the primary treatment for early-stage LUAD but surgical opportunities are often missed in asymptomatic patients (Tanoue et al., 2015; Abbas 2018). Therefore, alternatives are required for those lung cancer patients that cannot undergo surgery. In these cases, other important treatment strategies can be used, such as targeted therapy (e.g., targeting EGFR mutations) and immunotherapy (Mayekar and Bivona 2017; Osmani et al., 2018). However, resistance to EGFR-TKI or low immune checkpoint expression remains challenging (Wu and Shih 2018; Santarpia et al., 2020). Hence, a new strategy for the precise treatment of LUAD needs to be developed.

Abbreviations: LUAD, lung adenocarcinoma; TCGA, The Cancer Genome Atlas; GSVA, gene set variation analysis; ssGSEA, single-sample gene set enrichment analysis; APCs, Antigen-presenting cells; IC50, Half maximal inhibitory concentration; GO, Gene oncology; KEGG, Kyoto Encyclopedia of Genes and Genomes; ICP, Immune checkpoint; ICD, Immunogenic cell death modulators.

Recently, the development of vaccines to treat cancer has received significant attention from researchers worldwide (Sullenger and Nair 2016). The main challenge in cancer vaccine development lies in finding specific and personalized tumor cell antigens that will be activated and prepare a patient's immune system to recognize cancer cells, eliminating immune escape possibilities (Bowen et al., 2018; Sahin and Tureci 2018). Among the different types of vaccines, mRNA vaccines have advantages such as being easy to prepare; mRNA does not integrate into the host's genome and they can be degraded by RNases in cells, increasing their long-term safety (Pardi et al., 2018). The clinical safety of mRNA vaccines was indeed confirmed after their vast clinical application in COVID-19 prevention (Polack et al., 2020). Currently, several mRNA cancer vaccines are undergoing clinical trials (Li et al., 2014; Wang et al., 2018; Cafri et al., 2020), but no relevant reports on mRNA vaccines for LUAD have been reported.

In the current study, we investigated potential tumor antigens of LUAD that could be used to develop mRNA vaccines. We found two potential tumor antigens involved in antigen-presenting cell infiltration in LUAD and associated with a better prognosis. Moreover, we determined the characteristics of patients eligible for mRNA vaccination after grouping populations according to immune subtypes. Altogether, our findings provided new ideas for mRNA vaccines development and personalized treatment strategies for LUAD.

METHODS

Identification of Significantly Altered Copy Number Variant Chromosomal Regions, Gene Mutations, and Prognosis-Related Genes

To analyze the copy number variation of candidate genes in TCGA-LUAD, we used TCGAbiolinks R package (Colaprico et al., 2016) to download "Masked Copy Number Segment" data, and the GISTIC 2.0 software (https://cloud.genepattern.org/) (Mermel et al., 2011)was used to identify chromosomal regions with significant copy number variations. The threshold for significant amplifications and/or deletions was set as a q-value < 0.01. The R package "maftools" (Mayakonda et al., 2018) was used to visualize the mutation landscape. To analyze the functional enrichment of genes affected by copy numbers variations, the "clusterprofiler" R package (Yu et al., 2012) was used. Analyses of all prognosis-related genes in the TCGA-LUAD cohort were performed using the GEPIA2 database (http://gepia2.cancer-pku.cn/#survival). Patients was grouped according to the median value of each gene expression, and *p-value* < 0.05 was considered significant for prognosis.

Identification of Potential mRNA Vaccine Antigens in Lung Adenocarcinoma

Correlation analyses between the gene expression of potential vaccine antigens and immune cells were conducted using the TIMER database (https://cistrome.shinyapps.io/timer/). The GEPIA2 database (Tang et al., 2019) was used to analyze antigen gene expression and survival in LUAD patients. The expression of antigen genes in patients in different stages was visualized using the "ggplot2" R package (https://CRAN.R-project.org/package=ggplot2).

Identification of Immunophenotyping in Lung Adenocarcinoma Patients

After retrieving immune-related gene sets from the IMMPORT database (https://www.immport.org/shared/home), immune-related gene expressions were extracted from the TCGA-LUAD cohort FPKM data. The "ConsensusClusterPlus" R package (Wilkerson and Hayes 2010) was used to distinguish the immune subtypes. The clustering algorithm used the k-means of Euclidean distance, the total number of subsampling is set to 50, 80% of the total sample proportion is selected for each resampling, and the maximum number of clusters is set to 9. The optimal K was determined using the elbow method and ensuring that the number of patients in each cluster was ≥100. Survival analysis between clusters was performed using the "survival" R package. Hallmark gene set analysis for each sample was conducted using the "GSVA" R package (Hanzelmann et al., 2013), and the Hallmark gene set was from the Msigdb database (Liberzon et al., 2015). Poisson distribution was set up during the analysis and the pathway contained at least 10 genes. Heat maps were plotted using the "pheatmap" R package (https://CRAN.R-project.org/package=pheatmap).

Analysis of Tumor Immune Infiltration Microenvironment

The "Estimate" algorithm was used to calculate the immune stromal cell score for each sample. Since the Estimate package does not output tumor purity by default for data from the sequencing platform, the tumor purity of the samples was calculated manually according to the previously published literature (Yoshihara et al., 2013).

$$\text{Tumour purity} = \cos(0.6049872018 + 0.0001467884 * \text{ESTIMATE score})$$

The gene sets used to assess infiltrating immune cells for all samples were obtained from previously published articles (Supplementary Table S1) (Charoentong et al., 2017) Immune checkpoints and immunogenic cell death modulators genes were referred to previously published articles (Huang et al., 2021a).

Identification of Mutations Among Clusters

The "maftool" R package was used to visualize the gene mutation landscape among clusters and to calculate the tumor mutation burden for each sample. Additionally, the MutsigCV software was used to identify LUAD driver mutations in the cohort (Lawrence et al., 2013). Human Genome Assembly GRCh38 was used as the reference genome in the analysis (https://www.ncbi.nlm.nih.gov/

grc/human/data?asm=GRCh38). Significant mutations were defined as a q-value < 0.05, and driver mutated genes were chromosomally mapped using the "RCircos" R package (Zhang et al., 2013).

Weighted Gene Co-expression Network Analysis

The WGCNA was performed using the "WGCNA" R package (Langfelder and Horvath 2008) and normalized expressions of immune-related genes. After clustering the samples, no outlying samples were found. Hence, all samples were included in subsequent analyses. First, the Person correlation coefficient between any two genes is calculated and a similarity matrix is built by the results. The optimal soft threshold power "$\beta = 3$" is then obtained by unitary linear regression matching so that R2 > 0.85, and the similarity matrix is transformed into an adjacency matrix according to the optimal soft threshold power, which is then transformed into a topological overlap matrix (TOM). Eventually, we used 1-Tom as the distance to cluster the genes. The minimum number of genes per module was set to 20. To further analyze the modules, we calculated the dissimilarity of the module eigengenes, set the sensitivity to 2, and no modules were merged. Nine modules were identified after the soft threshold was set at three. Then, the correlation between modules and cluster classification were analyzed. KEGG functional enrichment analysis of genes in modules of interest was performed using "Clusterprofiler". The predictive ability of each gene for prognosis was assessed using ROC curves plotted by the "timeROC" R package (https://CRAN.R-project.org/package=timeROC). Genes with an area under the curve (AUC) > 0.6 were considered as better predictive biomarkers.

Anticancer Drug Sensitivity Analyses

The Genomics of Drug Sensitivity in Cancer (GDSC) database (Yang et al., 2013) is a database for therapeutic biomarker discovery in cancer cells. The R package "pRRophetic" (Geeleher et al., 2014)was used to construct a ridge regression model according to the GDSC cell line expression and TCGA-LUAD expression profiles, to assess the sensitivity of each sample to multiple anti-cancer drugs. Immunotherapy response was predicted using the TIDE (Tumor Immune Dysfunction and Exclusion) online tool (http://tide.dfci.harvard.edu/) (Jiang et al., 2018; Fu et al., 2020).

RESULTS

Identification of Potential Tumor Antigens of Lung Adenocarcinoma

Variations in copy number and mutations caused by genomic instability are crucial in cancer development (Bailey et al., 2021). Also, tumor cell heterogeneity caused by these variations drives phenotypic adaptation during tumor progression, leading to drug resistance (Sansregret et al., 2018). Therefore, to find tumor-specific antigens in LUAD as potential mRNA vaccine targets, we first investigated the chromosomal variation landscape in LUAD using the GISTIC software (Mermel et al., 2011). We considered genes affected by regions with significant chromosomal amplification and/or deletion as potential mRNA vaccine targets (**Figures 1A,B**). Moreover, we analyzed the landscape of gene mutations in LUAD patients. We found that missense and nonsense mutations occurred at higher frequencies and a single nucleotide variant was the most frequent mutation type (**Figure 1C**). Next, we performed a KEGG enrichment analysis of the copy number variant genes. Results showed that these genes were involved in the regulation of different cancer and immune-related pathways, demonstrating that these genes could be used as potential targets for cancer mRNA vaccines (**Figure 1D**). We also used all genes with mutations in the TCGA database as candidate targets for mRNA vaccines. Relevant genes retrieved from the GEPIA database that could affect patients' overall survival and disease-free survival were used for screening. Fianlly, we obtained 13 LUAD-specific antigens (TTK, BUB1B, ASB2, HJURP, CBFA2T3, PTGFRN, HSPA4, ST6GAL1, CENPU, KLRG1, GTF3C6, OIP5, VDAC3) that could affect patients prognosis (**Figure 1E**). These tumor antigens hold promise as new therapeutic targets against immune escape of tumor cells.

Potential Antigen Expression Correlates With Patient's Survival and Antigen-Presenting Cells

The immunogenicity of mRNA vaccine is the key to whether it can effectively activate the immune system. The higher immunogenicity represents that it can be recognized and processed by antigen-presenting cells and presented to T cells, which plays an important role in the immune recognition, immune response, and immune regulation. Antigen presenting cells are a major route for mRNA vaccine-mediated lymphocyte generation of immune memory and anti-tumor immunity (Cafri et al., 2020; Xu et al., 2020). Therefore, we investigated the relationship between the antigen candidates obtained above and three immune cell types that act as antigen-presenting (B cells, dendritic cells, and macrophages) to screen for optimal LAUD antigens. Dendritic cells play a vital role in the initiation and regulation of innate and adaptive immunities (Wculek et al., 2020). Moreover, B cells act as antigen-presenting cells by mediating memory T cells activation (Popi et al., 2016). We found that the expression of two, CBFA2T3 and KLRG1, of the 13 antigen candidates was significantly positively correlated with APCs expressions (**Figures 2A,B**). This result suggested that mRNA vaccines based on these two antigens might induce immune system activation after injection. After grouping based on the expression of these two potential antigens in LUAD patients, we observed that patients with high CBFA2T3 and KLRG1 expressions had a better prognosis. This also indicated that patients with high expression of these two genes may have a more conducive immune microenvironment for survival (**Figure 2C**). Then, we investigated the expression of KLRG1 and CBFA2T3 in different tumor stages (**Figures 2D,E**). The results show that these two genes are highly expressed in early-stage patients, reflecting that mRNA vaccines designed based on these two tumor antigens may produce better immunogenicity in

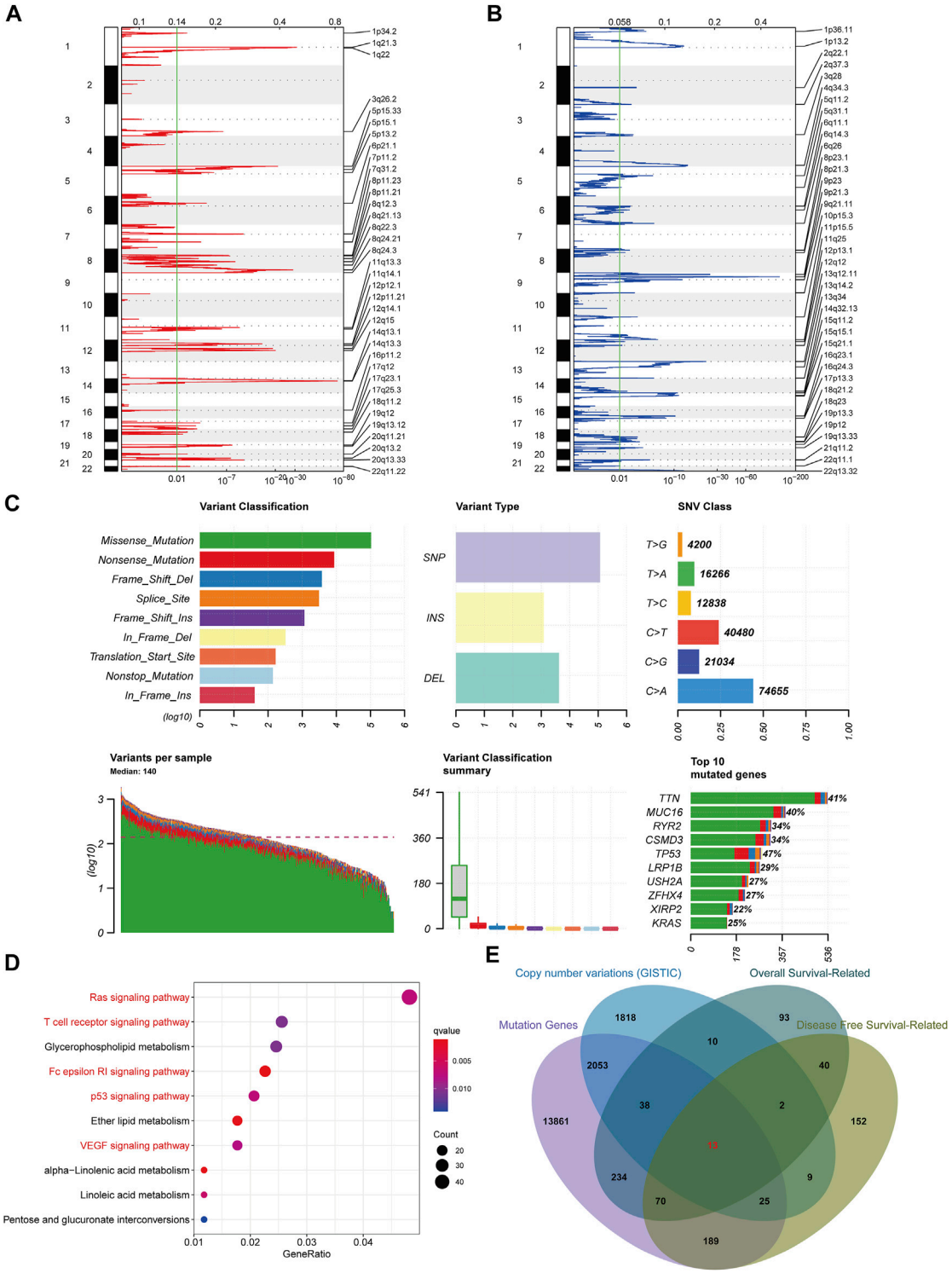

FIGURE 1 | Screening for potential tumor antigens in lung adenocarcinoma. **(A)** Identification of chromosomal copy number amplification regions. **(B)** Identification of chromosomal copy number deletion regions. **(C)** Summary of gene mutations in lung adenocarcinoma. **(D)** KEGG functional enrichment analysis of genes in regions of chromosomal copy number variation. **(E)** Identification of instability genes associated with prognosis.

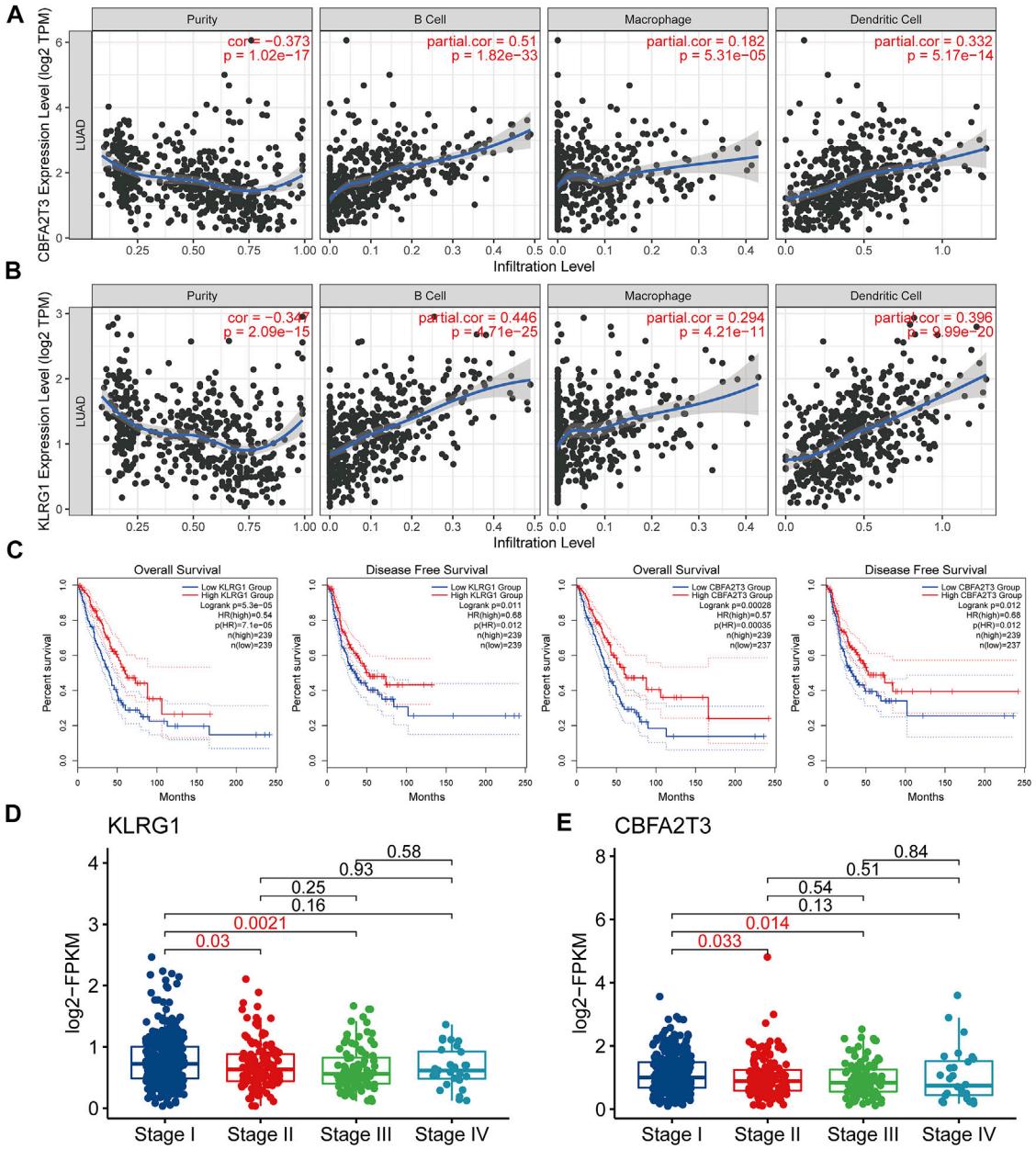

FIGURE 2 | Identification of tumor antigens in lung adenocarcinoma that can be used to develop mRNA vaccines **(A)** The expression of CBFA2T3 is positively correlated with the infiltration of a variety of antigen-presenting cells. **(B)** The expression of KLRG1 is positively correlated with the infiltration of a variety of antigen-presenting cells. **(C)** CBFA2T3 and KLRG1 are associated with overall survival and disease-free survival in patients with lung adenocarcinoma. **(D–E)** Expression of CBFA2T3 and KLRG1 in different stages of patients with lung adenocarcinoma.

early-stage patients. After grouping the cohorts according to the expression of these two potential antigens and performing a GSEA-based KEGG enrichment analysis, we observed an enrichment of multiple immune-related pathways in the highly expressed population (**Figures 3A,B**). In contrast, their low expression was associated with active cell cycle pathways (**Figures 3C,D**). Compared with other disease vaccines, therapeutic cancer vaccines mainly play a therapeutic role rather than prevention (DeMaria and Bilusic 2019), which should be clarified for the appropriate population, so we next identified the characteristics of lung adenocarcinoma patients suitable for mRNA vaccination.

Identification of Immune Subtypes in Lung Adenocarcinoma Patients

Immune subtypes can reflect the current tumor microenvironment status of patients and the patient's current

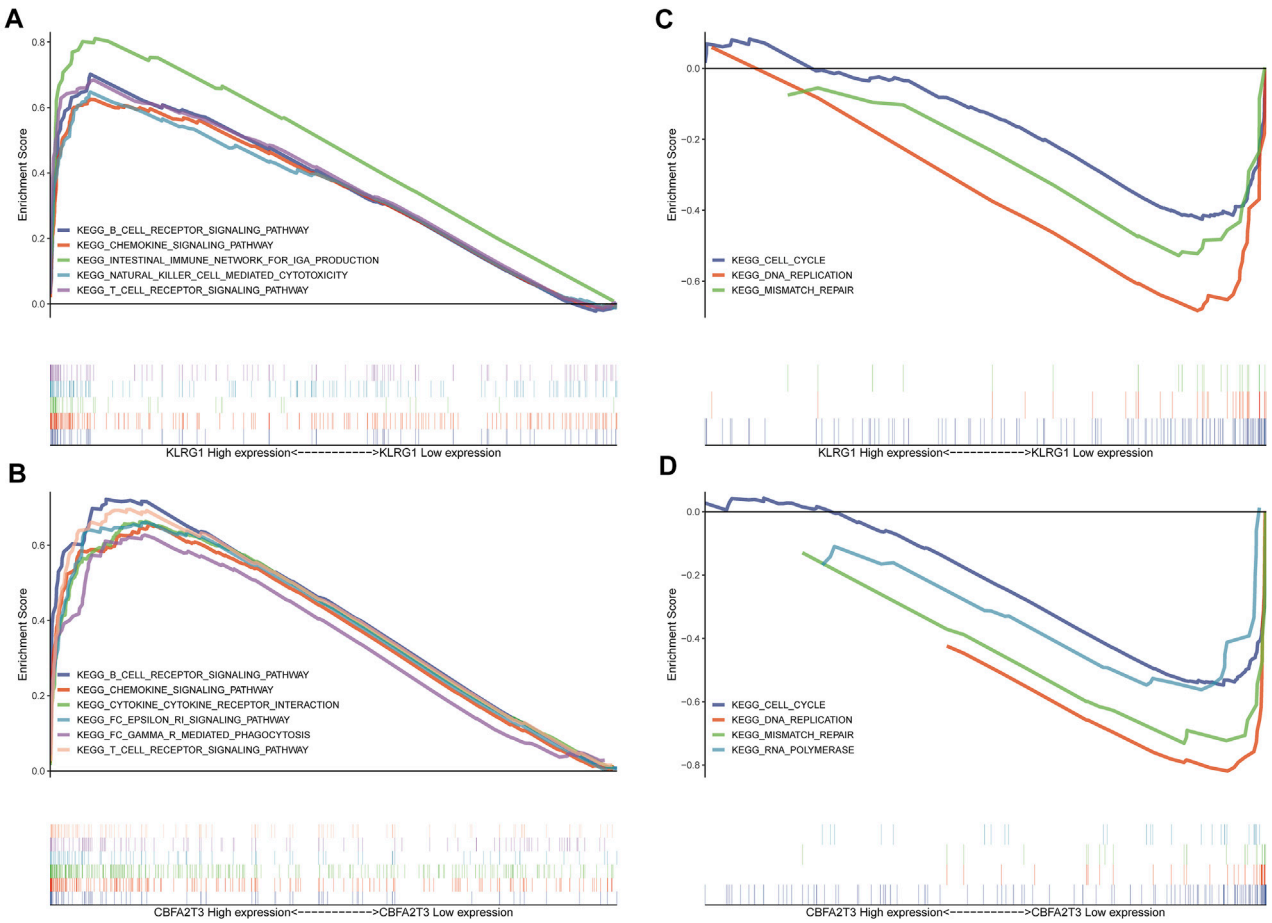

FIGURE 3 | Expression of tumor antigens is associated with a variety of immune pathways and cell cycle pathways **(A–B)** Patients with high expression of KLRG1 and CBFA2T3 have more active immune-related pathways. **(C–D)** Patients with low expression of KLRG1 and CBFA2T3 have a more active cell cycle.

immune status correlates with the effect of immune-related therapy (Ye et al., 2021a). Hence, we used immune-related genes in the TCGA-LUAD cohort to identify different patient populations and to assess their suitability for mRNA vaccination. Using consensus clustering, we identified four LUAD patients subtypes with different immune characteristics (**Figures 4A–C**). Clusters A and B had the best prognosis among the four subtypes, suggesting that the LUAD tumor microenvironment might affect prognoses (**Figure 4D**). The enrichment analysis of cancer hallmarks comparing Clusters A and B (better prognoses) to C and D subtypes (worse prognoses) also showed multiple immune-related pathways enriched for A and B (**Figure 4E**). Therefore, vaccination of Clusters A and B patients might produce a robust immune response. Additionally, after analyzing patients in different stages, we observed a higher proportion of Clusters A and B in patients with stages I and II, consistently with the results in **Figures 2D,E**. These results demonstrated that early-stage tumors patients are more sensitive to vaccination (**Figure 4F**). Notably, KLRG1 and CBFA2T3 were highly expressed in Clusters A and B (**Figure 4G**). Our results indicate that patients with Cluster A and B have an active current immune status and higher expression of the two tumor antigens identified. Cluster A and B may therefore have better immunogenicity for mRNA vaccines. Altogether, these results suggested that patients from Clusters A and B are more suitable for mRNA vaccination using these antigens.

Characteristics of the Tumor Immune Microenvironment in Various Immune Clusters

To further characterize the tumor microenvironment of each immune cluster, we first assessed immune and stromal scores using the ESTIMATE algorithm (**Figures 5A–D**). Clusters A and B had higher immune and stromal scores, while tumor purity was lower, suggesting that the proportion of tumor-infiltrating immune cells was higher in these samples. Also, we quantified various infiltrating immune cells using previously published immune cell gene sets (**Figure 5E**). After contrasting Clusters A and B with C and D, the data suggested that A and B might behave as “hot” immune subtypes, while C and D as “cold” subtypes (**Figure 5F**). Additionally, along with high KLRG1 and

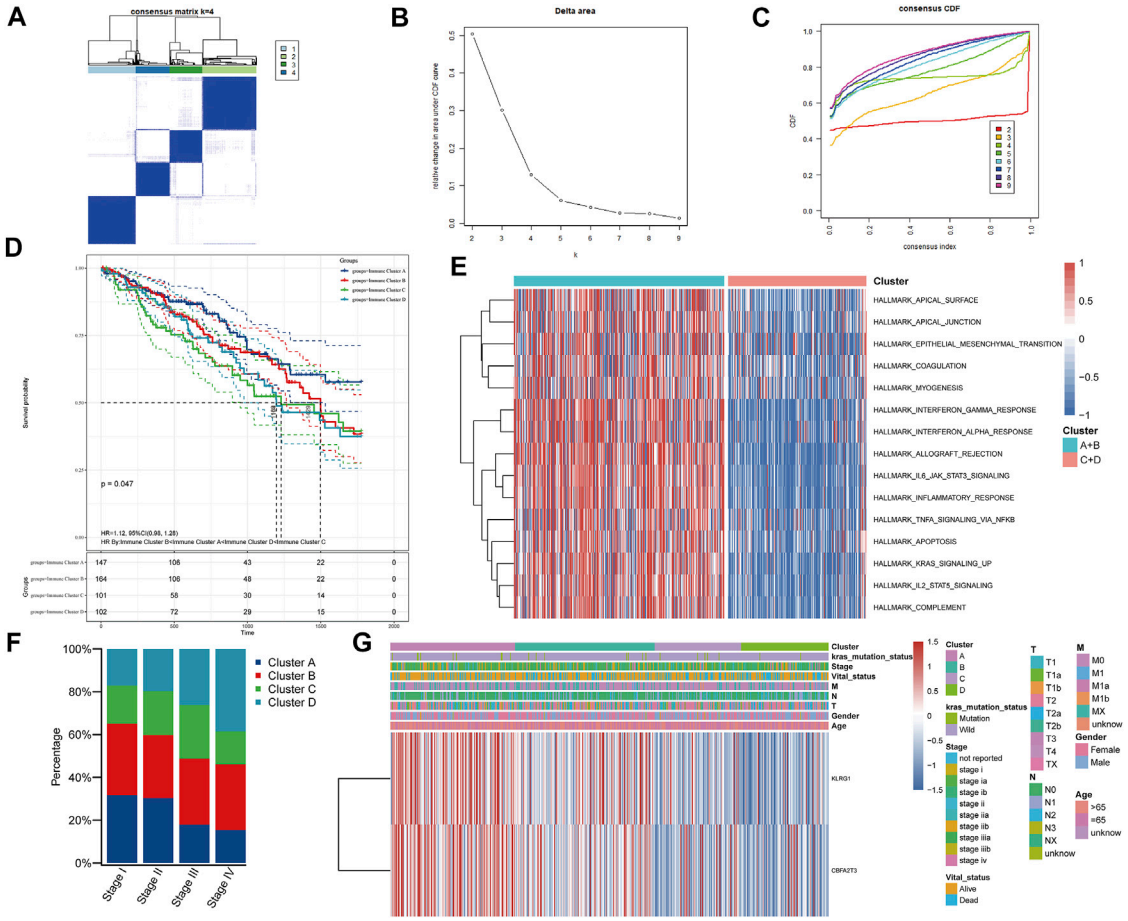

FIGURE 4 | Identification of immune clusters in patients with lung adenocarcinoma. **(A–C)** Patients with lung adenocarcinoma were divided into four immune clusters according to the expression of immune-related genes. **(D)** Survival analysis of patients with different immune clusters. **(E)** GSVA enrichment analysis of cancer Hallmarks in patients with different immune clusters. **(F)** Distribution of immune clusters in patients with different stages. **(G)** Heat map of tumor antigen expression and clinical parameters.

CBFA2T3 expressions (**Figure 3G**), clusters A and B may have a higher responsiveness to mRNA vaccination. Further, we contrasted Clusters A and B and showed that most immune cells were more infiltrated in Cluster A than in B. Therefore, Cluster A patients might be the most appropriate population to be vaccinated (**Figure 5G**). Moreover, we found a range of immune checkpoints and high expression of immunogenic cell death modulators in Cluster A, indicating that this population would also have better effects on immunotherapy (**Figures 5H,I**).

Relationship Between Immune Clusters and Tumor Mutation Burden

Then, we summarized the mutation landscape of all clusters and observed that KRAS had a higher mutation frequency in all of them (**Figure 6A**). Various studies have reported that KRAS mutations can lead to resistance to EGFR-TKIs that are widely used (Lehmann et al., 2019; McFall et al., 2019; Scheffler et al., 2019). Thus, mRNA vaccines may constitute an alternative treatment strategy for these populations. After calculating the TMB, Cluster A presented lower TMB (**Figure 6B**). Therefore, this low TMB could be correlated with vaccination suitability. We also used the MutSigCV algorithm to assess tumor-driver gene mutations and determined their location on the chromosome (**Figure 6C**). After visualizing the driver mutation genes in each patient, we observed that the co-mutation frequency of EGFR and KRAS was rare in Cluster A, indicating that EGFR-TKIs are still a promising treatment strategy for these patients. Hence, we believe that patients should be evaluated, and, for example, target gene sequencing should be performed before considering vaccination (**Figure 6D**).

Identification of Immune Gene Co-expression Module in Lung Adenocarcinoma

Immune-related genes were clustered using the WGCNA algorithm, and "three" was chosen as the soft threshold power based on the scale-free fit index and average connectivity (**Figures 7A–C**). Ten modules were identified among all immune-related genes (**Figure 7D**). After investigating the association between

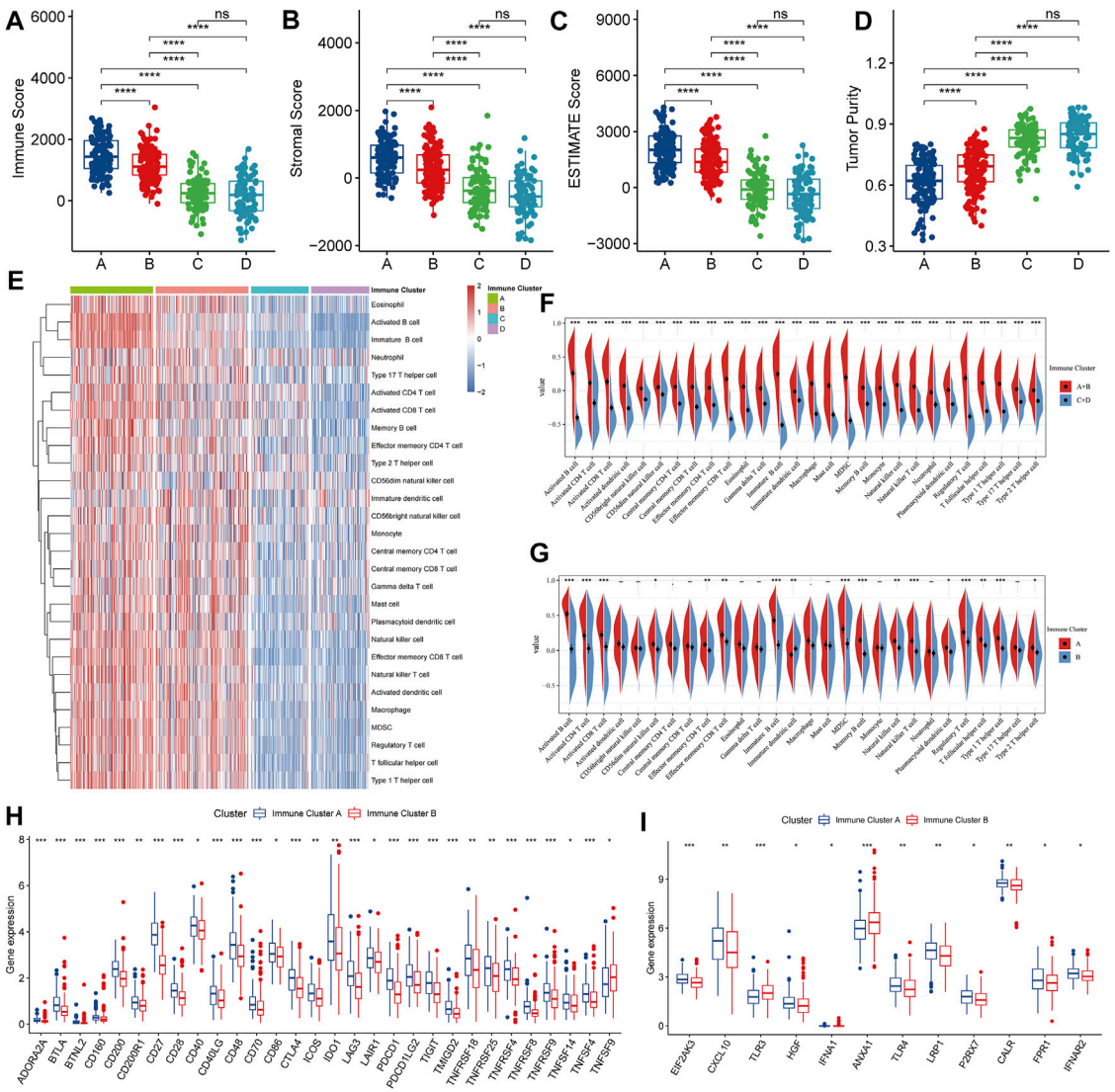

FIGURE 5 | Identification of tumor immune cell infiltration in patients with different clusters. **(A–D)** Immune-stromal scores and tumor purity of patients in each cluster were assessed by the ESTIMATE algorithm. **(E)** Heat map of immune cell infiltration levels assessed based on ssGSEA enrichment. **(F–G)** Comparison of immune cell infiltration levels between clusters. **(H)** Comparison of immune checkpoint expression between clusters. **(I)** Immunogenic cell death modulators genes expression comparison between clusters.

modules and phenotypes, we observed that the "blue" module was characteristic of Cluster A (suitable for vaccination) (**Figure 7E**). After extracting the genes from the blue module, the Gene Ontology (GO) enrichment analysis results showed that these genes were involved in the activation and proliferation of various immune cells (**Figure 7F**). Further, we investigated the predictive ability of these genes for the prognosis in the Cluster A population. We identified four genes (BECN1, RAET1E, PTGS2, TAPBP) with a good predictive ability for the prognosis (ROC curves AUC >0.6) (**Figures 7G–J**). Moreover, BECN1 was experimentally validated in a previous article as an important initiator molecule of autophagy and inhibited the growth of lung adenocarcinoma cells (Han et al., 2018) and it also plays a role in the regulation of the immune system (Cui et al., 2016), while PTGS2 was also confirmed as a prognostic biomarker for lung adenocarcinoma (Castelao et al., 2003). Therefore, these four genes could be used as biomarkers after mRNA vaccination.

Immune Clusters Are Associated With Anti-Cancer Drug Sensitivity

To explore therapeutic strategies for clusters that are not suitable for mRNA vaccination, we used drug sensitivity data from the Genomics of Drug Sensitivity in Cancer (GDSC) database as a training set to predict common anti-cancer drug sensitivity in TCGA-LUAD cohort samples. Surprisingly, after contrasting clusters, we found that cisplatin - a drug widely used to treat advanced lung cancer - had a lower half-maximal inhibitory

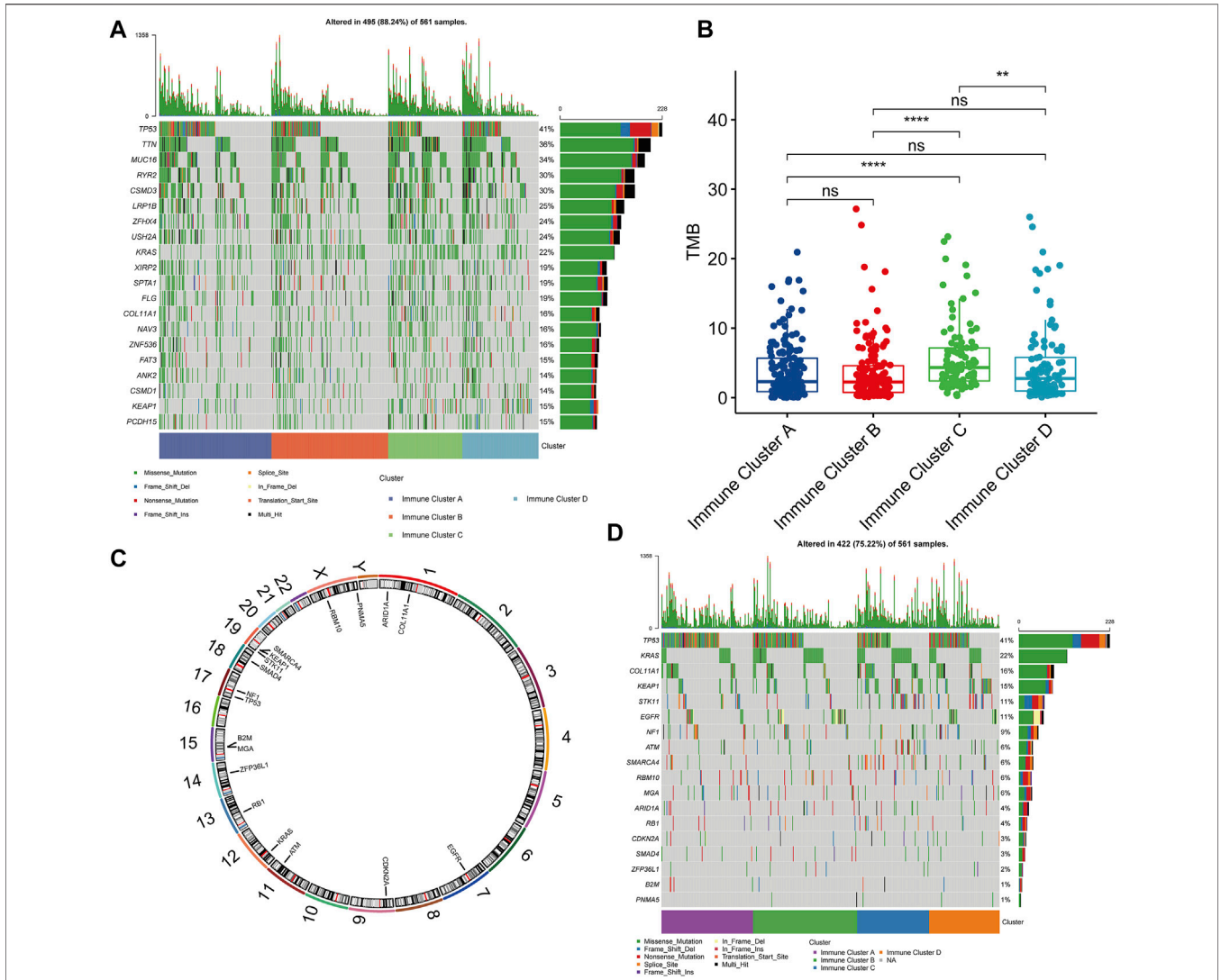

FIGURE 6 | Gene Mutation Landscapes in Patients with Different Clusters. **(A)** Top 20 genes in mutation frequency in all clusters. **(B)** Comparison of tumor mutation burden in different clusters. **(C)** Chromosomal localization of tumor driver mutated genes identified by MutSigCV algorithm. **(D)** Distribution of tumor driver mutant genes in clusters.

concentration (IC50) in clusters not suitable for vaccination, such as C and D (**Figure 8A**). This implied that Clusters C and D might be chemosensitive. We also found potentially sensitive anti-cancer drugs in Clusters C and D (**Figures 8B–E**). For Cluster A and B (suitable for vaccination), we observed a low IC50 for gefitinib (**Figure 8F**). This might be associated with the higher EGFR mutation frequency observed above (**Figure 6D**). Similarly, we found other potentially sensitive anti-cancer drugs suitable for Clusters A and B (**Figure 8G-L**). The TIDE score effectively reflects the potential benefit of immunotherapy and is superior to the prediction of immune checkpoint expression and mutations. When we used the TIDE online tool for immunotherapy response prediction in the overall cohort, we found that Cluster A and B tumor immune dysfunction scores were high (**Supplementary Figure S1A–B**), which reflects that they may not be sensitive to immune checkpoint blockade, so although Cluster A and B have higher immune checkpoint expression, but they may not be effective for immunotherapy. The mRNA vaccine may be a potentially effective alternative therapeutic strategy. Altogether, immune Clusters A and B were not only suitable for mRNA vaccination but also may be sensitive to targeted therapy. On the other hand, immune Clusters C and D might be more sensitive to chemotherapy. Differences in treatment sensitivity between different immune clusters also reflected the heterogeneity among tumors, emphasizing the importance of individualized treatments.

DISCUSSION

Recently, due to the broad clinical application of mRNA vaccines, their feasibility and safety have been confirmed (Polack et al.,

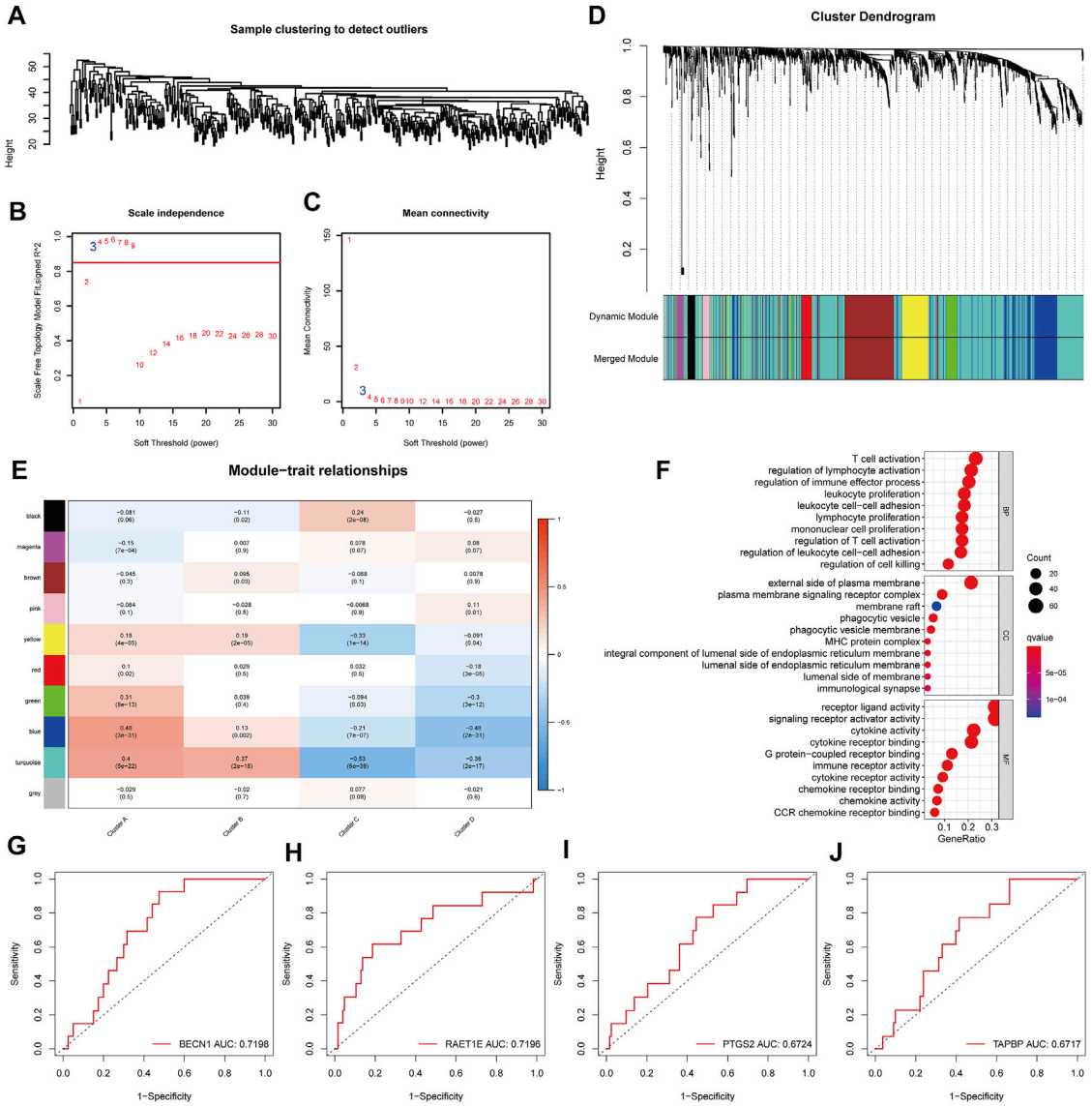

FIGURE 7 | Identification of gene co-expression network and identification of biomarkers in the suitable vaccinated population. **(A–D)** Identification of WGCNA gene modules. **(E)** Correlation analysis between gene modules and immune clusters. **(F)** Gene Ontology (GO) functional enrichment analysis of genes in the blue module. **(G–J)** Four potential prognostic biomarkers in cluster A patients eligible for mRNA vaccination.

2020). These vaccines have good prospects in cancer treatment, but more research is needed (Sahin and Tureci 2018). Mining tumor antigens with better immunogenicity and immunoreactivity in different cancers is the key to mRNA vaccine development. In the current study, we identified KLRG1 and CBFA2T3 as potential antigenic targets that could be used to develop mRNA vaccines for LUAD. Further analyses of immune subtypes identified a patient population that would benefit the most from vaccination. We also identified four biomarkers (BECN1, RAET1E, PTGS2, and TAPBP) that could be used to monitor vaccine response. Finally, we identified potentially sensitive anti-cancer drugs in the populations unsuitable for vaccination through drug sensitivity analyses. During the study, we found that the patient population with high immune checkpoint expression may not be sensitive to immune checkpoint blockade therapy due to immune system disorders, so mRNA vaccines may be another potential therapeutic strategy, but further studies are needed to verify our view. Overall, we identified two tumor antigens in LUAD - KLRG1 and CBFA2T3 - that could be used to develop mRNA vaccines. Also, we identified potential individualized treatment strategies for patients with different immune subtypes.

Tumor antigens can activate various antigen-presenting cells. Thus, inducing tumor-specific immunity and immune memory can be used in the development of tumor mRNA vaccines (Khan et al., 2021). KLRG1 has been reported as a prognosis biomarker

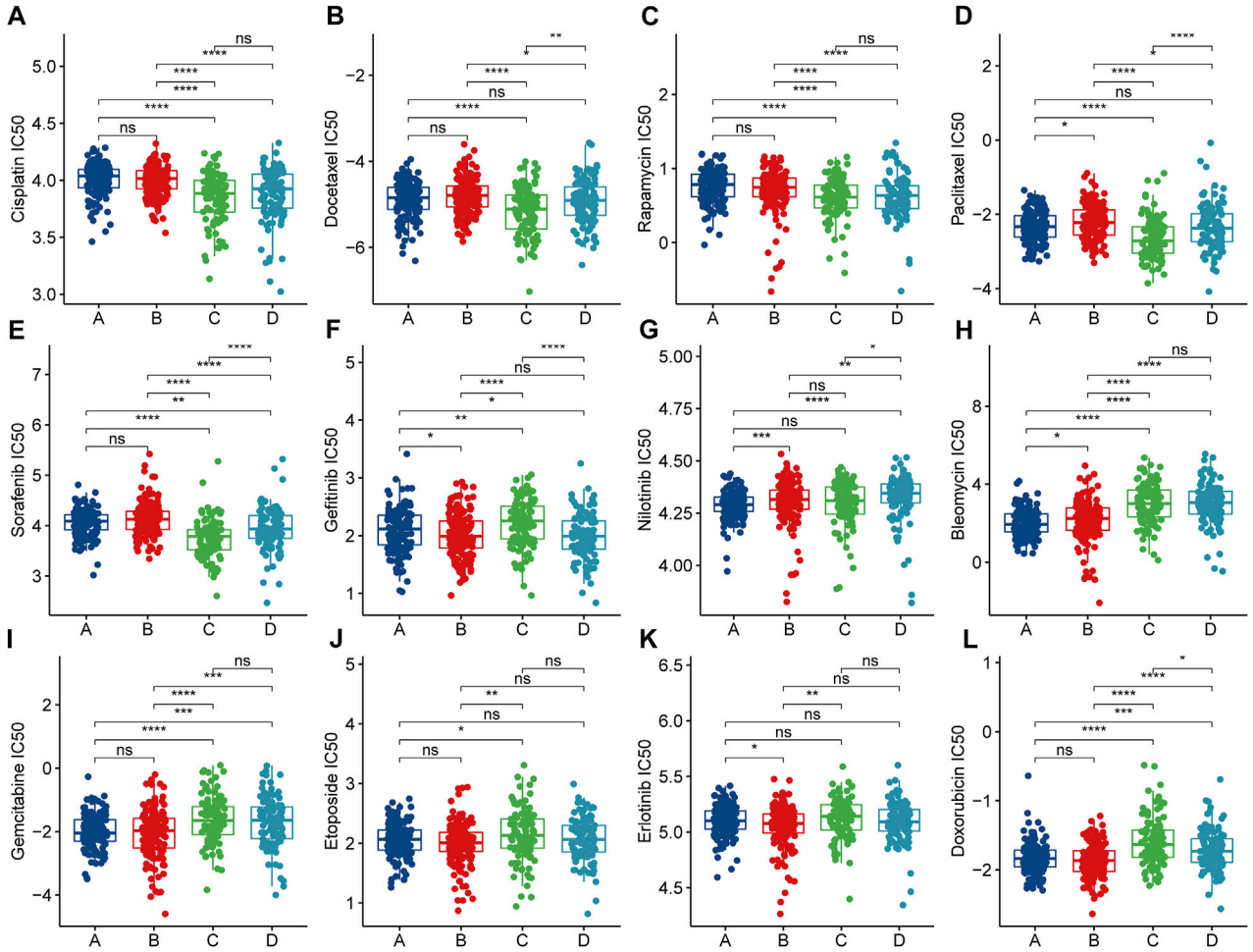

FIGURE 8 | Anticancer Drug Sensitivity Analysis in Patients with Different Clusters. **(A–L)** Half maximal inhibitory concentration (IC50) of multiple anticancer drugs in patients with different clusters.

in LUAD patients and is associated with response to immunotherapy (Yang et al., 2021). Additionally, combined blockade of KLRG1 with PD-1 can promote NK and T cell anti-tumor immunity (Tata et al., 2021). On the contrary, there has also been reported that high KLRG1 expression is associated with low proliferation of lung adenocarcinoma cells, however, KLRG1 expression is often low in lung adenocarcinoma cells, and associated with adverse effects of immunotherapy (Yang et al., 2021). The cancer-promoting and cancer-suppressing effects of KLRG1 appear paradoxical in response to immunotherapy and the effects of the cell cycle of the tumor cells themselves. But an article reported that KLRG1+effector CD8+T cells can effectively promote anti-tumor immunity after differentiation and loss of KLRG1 expression (Herndler-Brandstetter et al., 2018). Therefore, we believed that the development of KLRG1 as an mRNA vaccine could help to stimulate KLRG1+Effector CD8+T Cells to differentiate into memory T cells of other lineages and produce effective anti-tumor immunity. Using KLRG1 as an mRNA vaccine can achieve anti-tumor immunity by activating the immune system without altering KLRG1 expression in cancer cells themselves to affect the cell cycle. In our current study, we found a positive correlation between KLRG1 and the infiltration of different antigen-presenting cells, revealing that KLRG1 could induce tumor immunity and immune memory, and could be used as a potential tumor antigen for mRNA vaccines. Also, KLRG1 can be a marker of immune cell senescence, and the expansion of oligoclonal senescent T cells may negatively impact immunotherapy (Ferrara et al., 2021). Therefore, using KLRG1 as a tumor antigen, APCs will be trained to recognize and remove KLRG1-expressing tumor cells and senescent immune cells, becoming a new LUAD treatment strategy. CBFA2T3 has been reported as a tumor suppressor in lung cancer and can be an independent prognostic marker in LUAD (Zhang et al., 2018; Chen et al., 2021). Furthermore, we showed that CBFA2T3 expression was positively correlated with higher antigen-presenting cell infiltration. Hence, CBFA2T3 can potentially be used as a tumor antigen in future mRNA vaccines. In recent years, tumor antigen receptor chimeric T-cell immunotherapy (CAR-T) has also become a hot topic, and its main mechanism is to

engineer T cells isolated from patients to directly recognize and kill tumor cells (Feins et al., 2019). However, due to the low expression of the two genes in lung adenocarcinoma, the benefit of CART-T therapy may not be as good as that of mRNA vaccine, and mRNA vaccine also has the advantages of easier preparation and more economy.

Compared with live attenuated and inactivated vaccines, mRNA vaccines reduce problems associated with endotoxin and infection, and mRNA vaccines do not cause insertional mutagenesis caused by genomic integration compared with DNA vaccines and viral vector-based vaccines (Kim et al., 2021). Although mRNA vaccines are promising, they are easily degraded by extracellular ribonucleases (RNases) due to the difficulty of mRNA as an anionic molecule to counteract the electrostatic repulsion of cell membranes (Kowalski et al., 2019). Therefore, the design of delivery vectors is the key to whether mRNA vaccines can work.

Identification of different immune subtypes contributes to the development of precise treatment strategies (Charoentong et al., 2017). Thus, we classified LUAD patients by immune-related gene expression and identified four immune subtypes with different prognoses. Also, we described the different immune subtype landscapes and analyzed the potential benefits of using mRNA vaccines for each subtype. Notably, we identified a population of patients suitable for mRNA vaccination. This population was formed by early-stage patients with high immune cell infiltration, high immune checkpoints, immunogenic cell death modulators expression, and low TMB. The most relevant characteristic gene modules of this population were found by WGCNA, and four biomarkers that could be used as vaccination responses were found in these modules. Although previous studies have described LUAD immune subtypes (Wu et al., 2021; Zhao et al., 2021; Zhou et al., 2021), in the present study, we associated immune subtypes and mRNA vaccination for the first time. Drug sensitivity analysis of different immune subtypes showed significant differences in drug sensitivity among different subtypes, not only providing a reference for treatment strategies for populations not suitable for vaccination but also revealing the importance of individualized treatment.

Overall, we provided new ideas for the development of mRNA vaccines for LUAD treatment. Further, detailed analyses of immune subtypes revealed the characteristics of the population suitable for mRNA vaccination and emphasized the importance of personalized treatment. Although there have been previous tumor antigen-related studies of other cancers (Huang et al., 2021a; Huang et al., 2021b; Ye et al., 2021b; Zhong et al., 2021), the study of lung adenocarcinoma is the first, our study also reveals the characteristics of the appropriate vaccinated population and finds optional prognostic biomarkers for the potential vaccinated population. In addition, we provide a reference for potentially beneficial treatment strategies through drug sensitivity analysis of lung adenocarcinoma patients with different immune subtypes and finally emphasize the importance of individualized treatment.

DATA AVAILABILITY STATEMENT

The original contributions presented in the study are included in the article/**Supplementary Material**, further inquiries can be directed to the corresponding author.

AUTHOR CONTRIBUTIONS

RX was responsible for analyzing data and writing the article. TL, JZ, JW, and BP were responsible for plotting figures. LZ was accountable for the guidance of the idea of the article and the review of the article.

FUNDING

National Key R&D Plan (No. 2017YFC1308700), the Ministry of Science and Technology of the People's Republic of China.

ACKNOWLEDGMENTS

The survival analysis in this paper uses the GEPIA2 online tool (http://gepia2.cancer-pku.cn). Correlation analysis between gene expression and immune cell infiltration was performed using the TIMER online tool (https://cistrome.shinyapps.io/timer/). The graphical abstract was created with BioRender (https://biorender.com/).

SUPPLEMENTARY MATERIAL

The Supplementary Material for this article can be found online at: https://www.frontiersin.org/articles/10.3389/fcell.2022.815596/full#supplementary-material

REFERENCES

Abbas, A. E. (2018). Surgical Management of Lung Cancer: History, Evolution, and Modern Advances. *Curr. Oncol. Rep.* 20 (12), 98. doi:10.1007/s11912-018-0741-7

Bailey, C., Black, J. R. M., Reading, J. L., Litchfield, K., Turajlic, S., McGranahan, N., et al. (2021). Tracking Cancer Evolution through the Disease Course. *Cancer Discov.* 11 (4), 916–932. doi:10.1158/2159-8290.CD-20-1559

Bowen, W. S., Svrivastava, A. K., Batra, L., Barsoumian, H., and Shirwan, H. (2018). Current Challenges for Cancer Vaccine Adjuvant Development. *Expert Rev. Vaccin.* 17 (3), 207–215. doi:10.1080/14760584.2018.1434000

Cafri, G., Gartner, J. J., Zaks, T., Hopson, K., Levin, N., Paria, B. C., et al. (2020). mRNA Vaccine-Induced Neoantigen-specific T Cell Immunity in Patients with Gastrointestinal Cancer. *J. Clin. Invest.* 130 (11), 5976–5988. doi:10.1172/JCI134915

Castelao, J. E., Bart, R. D., 3rd, DiPerna, C. A., Sievers, E. M., and Bremner, R. M. (2003). Lung Cancer and Cyclooxygenase-2. *Ann. Thorac. Surg.* 76 (4), 1327–1335. doi:10.1016/s0003-4975(03)00334-5

Charoentong, P., Finotello, F., Angelova, M., Mayer, C., Efremova, M., Rieder, D., et al. (2017). Pan-cancer Immunogenomic Analyses Reveal Genotype-Immunophenotype Relationships and Predictors of Response to Checkpoint Blockade. *Cel Rep.* 18 (1), 248–262. doi:10.1016/j.celrep.2016.12.019

Chen, Y., Shen, L., Chen, B., Han, X., Yu, Y., Yuan, X., et al. (2021). The Predictive Prognostic Values of CBFA2T3, STX3, DENR, EGLN1, FUT4, and PCDH7 in Lung Cancer. *Ann. Transl Med.* 9 (10), 843. doi:10.21037/atm-21-1392

Colaprico, A., Silva, T. C., Olsen, C., Garofano, L., Cava, C., Garolini, D., et al. (2016). TCGAbiolinks: an R/Bioconductor Package for Integrative Analysis of TCGA Data. *Nucleic Acids Res.* 44 (8), e71. doi:10.1093/nar/gkv1507

Cui, J., Jin, S., and Wang, R.-F. (2016). The BECN1-USP19 axis Plays a Role in the Crosstalk between Autophagy and Antiviral Immune Responses. *Autophagy* 12 (7), 1210–1211. doi:10.1080/15548627.2016.1173801

DeMaria, P. J., and Bilusic, M. (2019). Cancer Vaccines. *Hematol. Oncol. Clin. North Am.* 33 (2), 199–214. doi:10.1016/j.hoc.2018.12.001

Feins, S., Kong, W., Williams, E. F., Milone, M. C., and Fraietta, J. A. (2019). An Introduction to Chimeric Antigen Receptor (CAR) T-cell Immunotherapy for Human Cancer. *Am. J. Hematol.* 94 (S1), S3–S9. doi:10.1002/ajh.25418

Ferrara, R., Naigeon, M., Auclin, E., Duchemann, B., Cassard, L., Jouniaux, J.-M., et al. (2021). Circulating T-Cell Immunosenescence in Patients with Advanced Non-small Cell Lung Cancer Treated with Single-Agent PD-1/pd-L1 Inhibitors or Platinum-Based Chemotherapy. *Clin. Cancer Res.* 27 (2), 492–503. doi:10.1158/1078-0432.CCR-20-1420

Fu, J., Li, K., Zhang, W., Wan, C., Zhang, J., Jiang, P., et al. (2020). Large-scale Public Data Reuse to Model Immunotherapy Response and Resistance. *Genome Med.* 12 (1), 21. doi:10.1186/s13073-020-0721-z

Geeleher, P., Cox, N., and Huang, R. S. (2014). pRRophetic: an R Package for Prediction of Clinical Chemotherapeutic Response from Tumor Gene Expression Levels. *PLoS One* 9 (9), e107468. doi:10.1371/journal.pone.0107468

Han, T., Guo, M., Gan, M., Yu, B., Tian, X., and Wang, J.-B. (2018). TRIM59 Regulates Autophagy through Modulating Both the Transcription and the Ubiquitination of BECN1. *Autophagy* 14 (12), 2035–2048. doi:10.1080/15548627.2018.1491493

Hänzelmann, S., Castelo, R., and Guinney, J. (2013). GSVA: Gene Set Variation Analysis for Microarray and RNA-Seq Data. *BMC Bioinformatics* 14, 7. doi:10.1186/1471-2105-14-7

Herndler-Brandstetter, D., Ishigame, H., Shinnakasu, R., Plajer, V., Stecher, C., Zhao, J., et al. (2018). KLRG1+ Effector CD8+ T Cells Lose KLRG1, Differentiate into All Memory T Cell Lineages, and Convey Enhanced Protective Immunity. *Immunity* 48 (4), 716–729. doi:10.1016/j.immuni.2018.03.015

Hirsch, F. R., Scagliotti, G. V., Mulshine, J. L., Kwon, R., Curran, W. J., Jr., Wu, Y.-L., et al. (2017). Lung Cancer: Current Therapies and New Targeted Treatments. *The Lancet* 389 (10066), 299–311. doi:10.1016/S0140-6736(16)30958-8

Huang, X., Tang, T., Zhang, G., and Liang, T. (2021a). Identification of Tumor Antigens and Immune Subtypes of Cholangiocarcinoma for mRNA Vaccine Development. *Mol. Cancer* 20 (1), 50. doi:10.1186/s12943-021-01342-6

Huang, X., Zhang, G., Tang, T., and Liang, T. (2021b). Identification of Tumor Antigens and Immune Subtypes of Pancreatic Adenocarcinoma for mRNA Vaccine Development. *Mol. Cancer* 20 (1), 44. doi:10.1186/s12943-021-01310-0

Jiang, P., Gu, S., Pan, D., Fu, J., Sahu, A., Hu, X., et al. (2018). Signatures of T Cell Dysfunction and Exclusion Predict Cancer Immunotherapy Response. *Nat. Med.* 24 (10), 1550–1558. doi:10.1038/s41591-018-0136-1

Khan, P., Siddiqui, J. A., Lakshmanan, I., Ganti, A. K., Salgia, R., Jain, M., et al. (2021). RNA-based Therapies: A Cog in the Wheel of Lung Cancer Defense. *Mol. Cancer* 20 (1), 54. doi:10.1186/s12943-021-01338-2

Kim, J., Eygeris, Y., Gupta, M., and Sahay, G. (2021). Self-assembled mRNA Vaccines. *Adv. Drug Deliv. Rev.* 170, 83–112. doi:10.1016/j.addr.2020.12.014

Kowalski, P. S., Rudra, A., Miao, L., and Anderson, D. G. (2019). Delivering the Messenger: Advances in Technologies for Therapeutic mRNA Delivery. *Mol. Ther.* 27 (4), 710–728. doi:10.1016/j.ymthe.2019.02.012

Langfelder, P., and Horvath, S. (2008). WGCNA: an R Package for Weighted Correlation Network Analysis. *BMC Bioinformatics* 9, 559. doi:10.1186/1471-2105-9-559

Lawrence, M. S., Stojanov, P., Polak, P., Kryukov, G. V., Cibulskis, K., Sivachenko, A., et al. (2013). Mutational Heterogeneity in Cancer and the Search for New Cancer-Associated Genes. *Nature* 499 (7457), 214–218. doi:10.1038/nature12213

Lehmann, S. G., Seve, M., Vanwonterghem, L., Michelland, S., Cunin, V., Coll, J.-L., et al. (2019). A Large Scale Proteome Analysis of the Gefitinib Primary Resistance Overcome by KDAC Inhibition in KRAS Mutated Adenocarcinoma Cells Overexpressing Amphiregulin. *J. Proteomics* 195, 114–124. doi:10.1016/j.jprot.2019.01.009

Li, J., Sun, Y., Jia, T., Zhang, R., Zhang, K., and Wang, L. (2014). Messenger RNA Vaccine Based on Recombinant MS2 Virus-like Particles against Prostate Cancer. *Int. J. Cancer* 134 (7), 1683–1694. doi:10.1002/ijc.28482

Liberzon, A., Birger, C., Thorvaldsdóttir, H., Ghandi, M., Mesirov, J. P., and Tamayo, P. (2015). The Molecular Signatures Database Hallmark Gene Set Collection. *Cel Syst.* 1 (6), 417–425. doi:10.1016/j.cels.2015.12.004

Mayakonda, A., Lin, D.-C., Assenov, Y., Plass, C., and Koeffler, H. P. (2018). Maftools: Efficient and Comprehensive Analysis of Somatic Variants in Cancer. *Genome Res.* 28 (11), 1747–1756. doi:10.1101/gr.239244.118

Mayekar, M. K., and Bivona, T. G. (2017). Current Landscape of Targeted Therapy in Lung Cancer. *Clin. Pharmacol. Ther.* 102 (5), 757–764. doi:10.1002/cpt.810

McFall, T., Diedrich, J. K., Mengistu, M., Littlechild, S. L., Paskvan, K. V., Sisk-Hackworth, L., et al. (2019). A Systems Mechanism for KRAS Mutant Allele-specific Responses to Targeted Therapy. *Sci. Signal.* 12 (600), eaaw8288. doi:10.1126/scisignal.aaw8288

Mermel, C. H., Schumacher, S. E., Hill, B., Meyerson, M. L., Beroukhim, R., and Getz, G. (2011). GISTIC2.0 Facilitates Sensitive and Confident Localization of the Targets of Focal Somatic Copy-Number Alteration in Human Cancers. *Genome Biol.* 12 (4), R41. doi:10.1186/gb-2011-12-4-r41

Osmani, L., Askin, F., Gabrielson, E., and Li, Q. K. (2018). Current WHO Guidelines and the Critical Role of Immunohistochemical Markers in the Subclassification of Non-small Cell Lung Carcinoma (NSCLC): Moving from Targeted Therapy to Immunotherapy. *Semin. Cancer Biol.* 52 (Pt 1), 103–109. doi:10.1016/j.semcancer.2017.11.019

Pardi, N., Hogan, M. J., Porter, F. W., and Weissman, D. (2018). mRNA Vaccines - a new era in Vaccinology. *Nat. Rev. Drug Discov.* 17 (4), 261–279. doi:10.1038/nrd.2017.243

Polack, F. P., Thomas, S. J., Kitchin, N., Absalon, J., Gurtman, A., Lockhart, S., et al. (2020). Safety and Efficacy of the BNT162b2 mRNA Covid-19 Vaccine. *N. Engl. J. Med.* 383 (27), 2603–2615. doi:10.1056/NEJMoa2034577

Popi, A. F., Longo-Maugéri, I. M., and Mariano, M. (2016). An Overview of B-1 Cells as Antigen-Presenting Cells. *Front. Immunol.* 7, 138. doi:10.3389/fimmu.2016.00138

Sahin, U., and Türeci, Ö. (2018). Personalized Vaccines for Cancer Immunotherapy. *Science* 359 (6382), 1355–1360. doi:10.1126/science.aar7112

Sansregret, L., Vanhaesebroeck, B., and Swanton, C. (2018). Determinants and Clinical Implications of Chromosomal Instability in Cancer. *Nat. Rev. Clin. Oncol.* 15 (3), 139–150. doi:10.1038/nrclinonc.2017.198

Santarpia, M., Aguilar, A., Chaib, I., Cardona, A. F., Fancelli, S., Laguia, F., et al. (2020). Non-Small-Cell Lung Cancer Signaling Pathways, Metabolism, and PD-1/pd-L1 Antibodies. *Cancers* 12 (6), 1475. doi:10.3390/cancers12061475

Scheffler, M., Ihle, M. A., Hein, R., Merkelbach-Bruse, S., Scheel, A. H., Siemanowski, J., et al. (2019). K-ras Mutation Subtypes in NSCLC and Associated Co-occuring Mutations in Other Oncogenic Pathways. *J. Thorac. Oncol.* 14 (4), 606–616. doi:10.1016/j.jtho.2018.12.013

Siegel, R. L., Miller, K. D., Fuchs, H. E., and Jemal, A. (2021). Cancer Statistics, 2021. *CA A. Cancer J. Clin.* 71 (1), 7–33. doi:10.3322/caac.21654

Sullenger, B. A., and Nair, S. (2016). From the RNA World to the Clinic. *Science* 352 (6292), 1417–1420. doi:10.1126/science.aad8709

Tang, Z., Kang, B., Li, C., Chen, T., and Zhang, Z. (2019). GEPIA2: an Enhanced Web Server for Large-Scale Expression Profiling and Interactive Analysis. *Nucleic Acids Res.* 47 (W1), W556–W560. doi:10.1093/nar/gkz430

Tanoue, L. T., Tanner, N. T., Gould, M. K., and Silvestri, G. A. (2015). Lung Cancer Screening. *Am. J. Respir. Crit. Care Med.* 191 (1), 19–33. doi:10.1164/rccm.201410-1777CI

Tata, A., Dodard, G., Fugère, C., Leget, C., Ors, M., Rossi, B., et al. (2021). Combination Blockade of KLRG1 and PD-1 Promotes Immune Control of Local and Disseminated Cancers. *Oncoimmunology* 10 (1), 1933808. doi:10.1080/2162402X.2021.1933808

Wang, Y., Zhang, L., Xu, Z., Miao, L., and Huang, L. (2018). mRNA Vaccine with Antigen-specific Checkpoint Blockade Induces an Enhanced Immune Response

against Established Melanoma. *Mol. Ther.* 26 (2), 420–434. doi:10.1016/j.ymthe.2017.11.009

Wculek, S. K., Cueto, F. J., Mujal, A. M., Melero, I., Krummel, M. F., and Sancho, D. (2020). Dendritic Cells in Cancer Immunology and Immunotherapy. *Nat. Rev. Immunol.* 20 (1), 7–24. doi:10.1038/s41577-019-0210-z

Wilkerson, M. D., and Hayes, D. N. (2010). ConsensusClusterPlus: a Class Discovery Tool with Confidence Assessments and Item Tracking. *Bioinformatics* 26 (12), 1572–1573. doi:10.1093/bioinformatics/btq170

Wu, G., Wang, Q., Zhu, T., Fu, L., Li, Z., Wu, Y., et al. (2021). Identification and Validation of Immune-Related LncRNA Prognostic Signature for Lung Adenocarcinoma. *Front. Genet.* 12, 681277. doi:10.3389/fgene.2021.681277

Wu, S.-G., and Shih, J.-Y. (2018). Management of Acquired Resistance to EGFR TKI-Targeted Therapy in Advanced Non-small Cell Lung Cancer. *Mol. Cancer* 17 (1), 38. doi:10.1186/s12943-018-0777-1

Xu, S., Yang, K., Li, R., and Zhang, L. (2020). mRNA Vaccine Era-Mechanisms, Drug Platform and Clinical Prospection. *Int. J. Mol. Sci.* 21 (18), 6582. doi:10.3390/ijms21186582

Yang, W., Soares, J., Greninger, P., Edelman, E. J., Lightfoot, H., Forbes, S., et al. (2013). Genomics of Drug Sensitivity in Cancer (GDSC): a Resource for Therapeutic Biomarker Discovery in Cancer Cells. *Nucleic Acids Res.* 41 (Database issue), D955–D961. doi:10.1093/nar/gks1111

Yang, X., Zheng, Y., Han, Z., and Zhang, X. (2021). Functions and Clinical Significance of KLRG1 in the Development of Lung Adenocarcinoma and Immunotherapy. *BMC Cancer* 21 (1), 752. doi:10.1186/s12885-021-08510-3

Ye, L., Wang, L., Yang, J. a., Hu, P., Zhang, C., Tong, S. a., et al. (2021a). Identification of Tumor Antigens and Immune Landscape in Glioblastoma for mRNA Vaccine Development. *Front. Genet.* 12, 701065. doi:10.3389/fgene.2021.701065

Ye, L., Wang, L., Yang, J. a., Hu, P., Zhang, C., Tong, S. a., et al. (2021b). Identification of Tumor Antigens and Immune Subtypes in Lower Grade Gliomas for mRNA Vaccine Development. *J. Transl Med.* 19 (1), 352. doi:10.1186/s12967-021-03014-x

Yoshihara, K., Shahmoradgoli, M., Martínez, E., Vegesna, R., Kim, H., Torres-Garcia, W., et al. (2013). Inferring Tumour Purity and Stromal and Immune Cell Admixture from Expression Data. *Nat. Commun.* 4, 2612. doi:10.1038/ncomms3612

Yu, G., Wang, L.-G., Han, Y., and He, Q.-Y. (2012). clusterProfiler: an R Package for Comparing Biological Themes Among Gene Clusters. *OMICS: A J. Integr. Biol.* 16 (5), 284–287. doi:10.1089/omi.2011.0118

Zhang, D.-L., Qu, L.-W., Ma, L., Zhou, Y.-C., Wang, G.-Z., Zhao, X.-C., et al. (2018). Genome-wide Identification of Transcription Factors that Are Critical to Non-small Cell Lung Cancer. *Cancer Lett.* 434, 132–143. doi:10.1016/j.canlet.2018.07.020

Zhang, H., Meltzer, P., and Davis, S. (2013). RCircos: an R Package for Circos 2D Track Plots. *BMC Bioinformatics* 14, 244. doi:10.1186/1471-2105-14-244

Zhao, Q.-Y., Liu, L.-P., Lu, L., Gui, R., and Luo, Y.-W. (2021). A Novel Intercellular Communication-Associated Gene Signature for Prognostic Prediction and Clinical Value in Patients with Lung Adenocarcinoma. *Front. Genet.* 12, 702424. doi:10.3389/fgene.2021.702424

Zhong, H., Liu, S., Cao, F., Zhao, Y., Zhou, J., Tang, F., et al. (2021). Dissecting Tumor Antigens and Immune Subtypes of Glioma to Develop mRNA Vaccine. *Front. Immunol.* 12, 709986. doi:10.3389/fimmu.2021.709986

Zhou, T., Yang, P., Tang, S., Zhu, Z., Li, X., Yang, Z., et al. (2021). Classification of Lung Adenocarcinoma Based on Immune Checkpoint and Screening of Related Genes. *J. Oncol.* 2021, 1–12. doi:10.1155/2021/5512325

Conflict of Interest: The authors declare that the research was conducted in the absence of any commercial or financial relationships that could be construed as a potential conflict of interest.

Publisher's Note: All claims expressed in this article are solely those of the authors and do not necessarily represent those of their affiliated organizations, or those of the publisher, the editors and the reviewers. Any product that may be evaluated in this article, or claim that may be made by its manufacturer, is not guaranteed or endorsed by the publisher.

Copyright © 2022 Xu, Lu, Zhao, Wang, Peng and Zhang. This is an open-access article distributed under the terms of the Creative Commons Attribution License (CC BY). The use, distribution or reproduction in other forums is permitted, provided the original author(s) and the copyright owner(s) are credited and that the original publication in this journal is cited, in accordance with accepted academic practice. No use, distribution or reproduction is permitted which does not comply with these terms.

frontiers in Cell and Developmental Biology

ORIGINAL RESEARCH
published: 21 February 2022
doi: 10.3389/fcell.2021.799278

BCL2A1 and CCL18 Are Predictive Biomarkers of Cisplatin Chemotherapy and Immunotherapy in Colon Cancer Patients

Taohua Yue[1†], Xiangzheng Liu[2†], Shuai Zuo[1], Jing Zhu[1], Jichang Li[1], Yucun Liu[1], Shanwen Chen[1] and Pengyuan Wang[1*]*

[1]*Division of General Surgery, Peking University First Hospital, Peking University, Beijing, China,* [2]*Department of Thoracic Surgery, Peking University First Hospital, Peking University, Beijing, China*

OPEN ACCESS

Edited by:
Zimu Deng,
Chinese Academy of Sciences (CAS), China

Reviewed by:
Bo Liang,
Nanjing University of Chinese Medicine, China
Hualin Song,
Tianjin Medical University Cancer Institute and Hospital, China
Bin Zhao,
Xiamen University, China

***Correspondence:**
Pengyuan Wang
pengyuan_wang_bjmu@163.com
Shanwen Chen
shanwen_chen_bjmu@163.com

[†]These authors have contributed equally to this work and share first authorship

Specialty section:
This article was submitted to Molecular and Cellular Pathology, a section of the journal Frontiers in Cell and Developmental Biology

Received: *21 October 2021*
Accepted: *29 December 2021*
Published: *21 February 2022*

Citation:
Yue T, Liu X, Zuo S, Zhu J, Li J, Liu Y, Chen S and Wang P (2022) BCL2A1 and CCL18 Are Predictive Biomarkers of Cisplatin Chemotherapy and Immunotherapy in Colon Cancer Patients. Front. Cell Dev. Biol. 9:799278. doi: 10.3389/fcell.2021.799278

Background: Cisplatin enhances the antitumor T cell response, and the combination of PD-L1 blockade produces a synergistic therapeutic effect. However, the clinical correlation between cisplatin and immunotherapy in colon cancer (CC) is unknown.

Methods: Using the "pRRophetic" package, we calculated the IC50 of cisplatin. The correlation between cisplatin IC50, cisplatin resistance–related genes (CCL18 and BCL2A1), and immunotherapy were preliminarily verified in TCGA and further validated in independent cohorts (GSE39582 and GSE17538), cisplatin-resistant CC cell line DLD1, and our own clinical specimens. Classification performance was evaluated using the AUC value of the ROC curve. Scores of immune signatures, autophagy, ferroptosis, and stemness were quantified using the ssGSEA algorithm.

Results: Based on respective medians of three CC cohorts, patients were divided into high- and low-IC50 groups. Compared with the high IC50 group, the low-IC50 group had significantly higher tumor microenvironment (TME) scores and lower tumor purity. Most co-signaling molecules were upregulated in low IC50 group. CC patients with good immunotherapy efficacy (MSI, dMMR, and more TMB) were more attributable to the low-IC50 group. Among seven shared differentially expressed cisplatin resistance–related genes, CCL18 and BCL2A1 had the best predictive efficacy of the above immunotherapy biomarkers. For wet experimental verification, compared with cisplatin-resistant DLD1, similar to PD-L1, CCL18 and BCL2A1 were significantly upregulated in wild-type DLD1. In our own CC tissues, the mRNA expression of CCL18, BCL2A1, and PD-L1 in dMMR were significantly increased. The high group of CCL18 or BCL2A1 had a higher proportion of MSI, dMMR, and more TMB. IC50, CCL18, BCL2A1, and PD-L1 were closely related to scores of immune-related pathways, immune signatures, autophagy, ferroptosis, and stemness. The microRNA shared by BCL2A1 and PD-L1, hsa-miR-137, were significantly associated with CCL18, BCL2A1, and PD-L1, and downregulated in low-IC50 group. The activity of the TOLL-like receptor signaling pathway affected the sensitivity of CC patients to cisplatin and immunotherapy. For subtype analysis, immune C2, immune C6, HM-indel, HM-SNV, C18, and C20 were equally sensitive to cisplatin chemotherapy and immunotherapy.

Conclusions: CC patients sensitive to cisplatin chemotherapy were also sensitive to immunotherapy. CCL18 and BCL2A1 were novel biomarkers for cisplatin and immunotherapy.

Keywords: chemotherapy, immunotherapy, BCL2A1, CCL18, PD-L1, colon cancer

INTRODUCTION

According to Global Cancer Statistics 2020, colon cancer (CC) is the second most common cause of cancer-related deaths worldwide, whose incidence rate ranks third (Sung et al., 2021). From the histological classification, it is mainly colon adenocarcinoma (COAD), which accounts for about three quarters. It can be seen that CC is a global health problem that needs to be solved urgently.

In addition to surgery, CC can be treated with radiotherapy and chemotherapy, molecular targeted therapy, and emerging immunotherapy (Dekker et al., 2019; Johdi and Sukor, 2020). Immunotherapy refers to a treatment method that artificially enhances or suppresses the immune function of the body to achieve the purpose of curing diseases. Previous studies show that biomarkers for immunotherapy include tumor microenvironment (TME) scores (Xia et al., 2021), tumor infiltrating immune cell (TIIC) abundance (Zeng et al., 2020), expression of immune-related genes (co-inhibitory molecules (T cell and APC cell), Type I and II IFN response molecules, co-stimulatory molecules (T cell and APC cell), cytolytic activity molecules) (Liu X et al., 2021), microsatellite stability (MSI), deficient mismatch repair (dMMR), tumor mutational burden (TMB) (Halama et al., 2016; Duffy and Crown, 2019), immune-related signatures, pathways, somatic mutation frequency (Peng et al., 2016), and activity of autophagy (Ramakrishnan et al., 2012; Sirichanchuen et al., 2012), ferroptosis (Kim et al., 2018; Wang W et al., 2019), and stemness (Hu et al., 2019; Unver, 2021).

Previous research proves that cisplatin augments antitumor T cell responses, leading to a potent therapeutic effect in combination with PD-L1 blockade (Luo et al., 2019; Wakita et al., 2019). Then, we studied the connection between cisplatin chemotherapy and immunotherapy in CC and tried to reveal which CC patients were suitable for cisplatin chemotherapy and immunotherapy and molecular characteristics.

In our study, based on the "pRRophetic" package and transcriptome data, we predicted the half maximal inhibitory concentration (IC50) of cisplatin in CC patients (TCGA, GSE39582, and GSE17538). Based on the biomarkers for immunotherapy, we concluded that the low-IC50 group of CC patients might benefit more from immunotherapy. Besides this, the cisplatin resistance–related genes CCL18 and BCL2A1 could predict the sensitivity of cisplatin chemotherapy and immunotherapy in CC patients, simultaneously. For wet experimental verification, in wild-type and cisplatin-resistant DLD1 cell lines verified by CCK8 experiments, similar to PD-L1, CCL18 and BCL2A1 could predict the efficacy of cisplatin chemotherapy. In the CC specimens of our hospital, compared with pMMR tissues, the mRNA expression of CCL18, BCL2A1, and PD-L1 in dMMR were significantly increased.

Previous studies show that PD-L1 and chemotherapy resistance interact with each other in the biological and functional cascade through microRNA regulation (Xu et al., 2016). On the ENCORI website, we extracted shared miRNAs of PD-L1, CCL18, and BCL2A1. Results showed that hsa-miR-137 was the most potentially predictive miRNA for cisplatin chemotherapy and immunotherapy.

Both functional enrichment analysis (GO-MF and KEGG) and gene set enrichment analysis (GSEA) were applied for the identification of pathways that could explain the functions of IC50 of cisplatin, CCL18, and BCL2A1. Results indicate that the KEGG_TOLL_LIKE_RECEPTOR_SIGNALING_PATHWAY was associated with the sensitivity of COAD patients to cisplatin chemotherapy and immunotherapy. CCL18 and BCL2A1 might play a predictive role through the KEGG_TOLL_LIKE_RECEPTOR_SIGNALING_PATHWAY. Subgroup analysis confirmed that CC patients of immune C2, immune C6, HM-indel, HM-SNV, C18, C20, and High_CCL18_High_BCL2A1 were equally sensitive to cisplatin chemotherapy and immunotherapy.

MATERIALS AND METHODS

Data Source

Gene expression data of CC samples were collected from public data sets at the TCGA (https://portal.gdc.cancer.gov/) and Gene Expression Omnibus (GEO) database (https://www.ncbi.nlm.nih.gov/geo/). For TCGA data, fragment per kilobase of transcript per million mapped reads (FPKM) was converted to TPM (transcript per kilobase of exon model per million mapped reads) and used in our study. Log2 transformation was used for normalization of GEO chip data (GSE39582 and GSE17538). After removing the missing values, our study included 419 TCGA-COAD patients, 566 GSE39582 CC patients, and 238 GSE17538 CC patients.

Chemosensitivity Assessment

Based on transcriptome data of TCGA, GSE39582, and GSE17538 cohorts, the "pRRophetic" package was used to evaluate cisplatin chemotherapy sensitivity (Geeleher et al., 2014) and presented it in the form of the half maximal inhibitory concentration (IC50). According to the respective medians of cisplatin IC50, CC patients of each cohort were divided into low- and high-IC50 groups, respectively.

The TME Score and Tumor Purity

The TME score enabled us to reflect the behavior and response of the cancer cells to a treatment process (Wang et al., 2018). A previous study proves that low tumor purity (the proportion of tumor cells in the TME) was associated with heavy mutation

burden and intense immune phenotype in CC tissues (Mao et al., 2018). Estimation of STromal and Immune cells in MAlignant Tumor tissues using Expression data (ESTIMATE) is a method for estimating infiltrating nontumor cells (immune and stromal cells) in the TME based on gene expression profiles and two gene signatures (the immune and stromal signatures) (Wang H et al., 2019). Next, we inferred the purity of each patient's tumor (Yoshihara et al., 2013).

Quantification of TIICs

The TIIC abundance was a robust biomarker for immunotherapeutic response and immunophenotype determination (Zeng et al., 2020). The TIMER2.0 is a systematic platform for evaluations of the clinical influence of various TIICs in diverse cancer (Li T et al., 2020). Based on the TIMER2.0, we quantified the abundance of three types of innate TIICs and three types of adaptive TIICs in the CC microenvironment.

Differentially Expressed Genes (DEGs)

For TCGA, DEGs between high- and low-IC50 samples were identifies using the "DEseq2" package (Kang et al., 2020). As a method of differential analysis of transcriptome count data, due to the shrinkage estimators for fold change (FC) and dispersion, DESeq2 improves the interpretability and stability of estimation (Love et al., 2014). For GSE39582 and GSE17538, DEGs between high- and low-IC50 tissues were identified using the "Limma" package. The adjusted p-value < .05 and $|FC| > 2$ were used as the cutoff criteria to filter DEGs (Wu et al., 2019).

Receiver Operating Characteristic (ROC)

With the help of the "pROC" package (Robin et al., 2011), we built the ROC curve (high vs. low IC50, high vs. low PD-L1, and high vs. low pathway score).

TMB

TMB is defined as the total number of gene encoding errors, base replacement, gene insertion or deletion errors per million bases (Schumacher et al., 2015). The 38 Mb is routinely taken based on the length of the human exon, so the TMB estimate for each sample is equal to the total mutation frequency/38 (Lv et al., 2020).

Establishment of the Cisplatin-Resistant Cell Line DLD1

The resistant cell line DLD1 was established *in vitro* by intermittent exposure to different concentrations of cisplatin (S1166, selleck) in stepwise increments of time. Starting with a concentration of 5 μmol/L, cisplatin was added to the cells when they grew to ~80% confluence. After 24 h, the remaining cells were cultured in cisplatin-free DMEM medium. When the surviving cells were restored to exponential growth, the next concentration of 5 FU (increase of 1 μmol/L) was then added. The cisplatin-resistant cell line DLD1 was established 9 months after the treatment was initiated, and the resistant phenotype was established.

Measurement of Cell Viability

The CCK-8 assay was used to detect cell viability according to the manufacturer's instructions. In short, DLD1 wild-type and cisplatin-resistance cells were cultured until ~80% confluence, completely digested and added to each well (5000 cells/well) of a 96-well plate (Corning, United States). After 48 h of incubation, CCK-8 solution was added to each well of the 96-well plate. Finally, we used the microplate reader to read the OD value.

RNA Isolation and Quantitative Reverse Transcription PCR (qRT-PCR)

The total RNA (DLD1 cell line and six pairs of CC tissues) was isolated according to the protocol of TRIZOL reagent (Life Technologies). The mRNA expressions of CCL18, BCL2A1, PD-L1, and β-actin were measured by the real-time PCR system (Applied Biosystems, Carlsbad, United States). The data were obtained by normalizing CCL18, BCL2A1, and PD-L1 gene Ct (cycle threshold) values with corresponding β-actin Ct and then analyzed with the 2-ΔΔCt Ct method (Xu et al., 2015). The primer sequences are as follows: CCL18 forward primer (5′-CTCTGCTGCCTCGTCTATACC-3′), CCL18 reverse primer (5′-CTTGGTTAGGAGGATGACACCT-3′), BCL2A1 forward primer (5′-TACAGGCTGGCTCAGGACTAT-3′), BCL2A1 reverse primer (5′-CGCAACATTTTGTAGCACTCTG-3′), PD-L1 forward primer (5′-TGGCATTTGCTGAACGCATTT-3′), PD-L1 reverse primer (5′-TGCAGCCAGGTCTAATTG TTTT-3′), β-actin forward primer (5′-CATGTACGTTGCTAT CCAGGC-3′) and β-actin reverse primer (5′-CTCCTTAATGTC ACGCACGAT-3′).

Correlation Diagram

The correlations between DEGs, PD-L1, and TME score were studied by Spearman's correlation analysis and visualized using the "corrplot" and "PerformanceAnalytics" packages in R software.

The Single-Sample GSEA (ssGSEA)

The 30 immune-related pathways (Shang et al., 2020) were retrieved on the GSEA website (https://www.gsea-msigdb.org/gsea/msigdb/genesets.jsp?collection=CC).

Using immune (**Supplementary Table S1**), autophagy (**Supplementary Table S2**), and ferroptosis (**Supplementary Table S3**) signatures, we quantified the immune, autophagy, and ferroptosis activities by the "GSVA" package and ssGSEA method (Hänzelmann et al., 2013).

Heatmap

Heatmaps were constructed through the "pheatmap" package in R. Columns represent COAD tissues, and rows represent immune-related biomarkers. The levels of biomarkers were displayed in different colors, which transition from blue to red with increasing expression.

Mutation Waterfall Charts

Somatic mutation data in the "masked somatic mutation" type was processed by VarScan2 (Koboldt et al., 2012). The "maftools"

package was used to process and visualize the somatic mutation data of TCGA (Mayakonda et al., 2018).

Autophagy-Related Genes (ARGs) and Ferroptosis-Related Genes

On the Human Autophagy Database (HADb, http://www.autophagy.lu/), we collected 232 ARGs (**Supplementary Table S2**) (Galluzzi et al., 2017). The ferroptosis-related genes were downloaded from FerrDb (**Supplementary Table S3**) (http://www.zhounan.org/ferrdb/) (Zhou and Bao, 2020).

The UCSC XENA Database

On the UCSC XENA database (https://pancanatlas.xenahubs.net), an online exploration tool for public and private, multi-omic and clinical/phenotype data, we obtained TCGA-COAD patients' immune subtype classification, molecular subtype classification, tumor stemness score based on RNAseq, icluster classification (Goldman et al., 2020), and visualized using R software.

Functional Enrichment Analysis

To research the biofunctions of CCL18 and BCL2A1, the R "clusterProfiler" package (Yu et al., 2012) was used to perform functional annotations among 80 protein-coding genes with a correlation greater than 0.6 with CCL18 and BCL2A1, which included three categories of GO (biological processes (BP), molecular functions (MF), and cellular components (CC)) and KEGG enrichment analysis. Using the "treemap" package (Liu L et al., 2021), we visualized the results of functional enrichment analysis.

The Encyclopedia of RNA Interactomes (ENCORI)

Using ENCORI (http://starbase.sysu.edu.cn/index.php), which is an open-source platform for studying miRNA–mRNA interactions, the miRNA differential expression and miRNA-target co-expression of CCL18, BCL2A1, and PD-L1 were examined.

GSEA

The KEGG gene set (186 pathways) was downloaded from the MSigDB database (https://www.gsea-msigdb.org/gsea/msigdb/index.jsp) (Subramanian et al., 2005). Based on software GSEA_4.0.1, we performed the GSEA. Enrichment FDR values were based on 1000 permutations. Nominal p-value < .05 and FDR <0.25 were considered to be statistical significance (Cheng et al., 2021).

Statistical Analysis

All statistical analyses in our study were performed using R software (version 4.0.3). Due to COAD transcriptome data, immune cell abundance, and ssGSEA scores do not follow a normal distribution, differences between two groups were tested by the Wilcoxon test. $p < .05$ was considered statistically significant: $^{*}p < .05$, $^{**}p < .01$, $^{***}p < .001$, $^{****}p < .0001$.

RESULTS

Estimation of TME Score and TIIC Abundance

The flow chart of this research is shown in **Figure 1**. Previous studies show that the TME score and tumor purity (the proportion of tumor cells in the TME) were novel features to measure the efficacy of immunotherapy (Gong et al., 2020). Specifically, a high TME score or low-purity tumors exhibited a strong immunophenotype (Zhang et al., 2017). It was reported that cisplatin therapy could increase antitumor immune response by reducing immunosuppressive cells of the TME. Therefore, we studied the relationship between cisplatin chemotherapy and the TME in CC. Compared with the high-IC50 group, CC tissues in the low-IC50 group had higher stromal, immune, and ESTIMATE scores (**Figure 2A**) and lower tumor purity (**Figure 2B**), which suggests that the low-IC50 group are more like "hot tumors." Furthermore, we investigated differences of the abundance of three types of innate TIICs and three types of adaptive TIICs in the TME. Combining the above three cohorts, the samples in the low-IC50 group had significantly higher infiltration of CD8+T cells, neutrophils, macrophages, and myeloid dendritic cells (MDCs) (**Figure 2C**). Therefore, we conclude that the immunophenotype of the low-IC50 group was different from that of the high-IC50 group and CC tissues sensitive to cisplatin chemotherapy were more like hot tumors and might be more sensitive to immunotherapy.

Differences in the Expression of Immune-Related Genes

To further clarify whether the low-IC50 group would benefit more from immunotherapy, we studied differences in the expression of co-inhibitory molecules of APC and T cells (**Figure 3A**), IFNG response molecules (**Figure 3B**), co-stimulatory molecules of APC and T cells (**Figure 3C**), and cytolytic activity molecules (**Figure 3D**) between low- and high-IC50 groups. The expression of most immune-related genes was significantly higher in the low-IC50 group, indicating that the CC in the low IC50 group had a stronger immunophenotype and would benefit more from immunotherapy.

Other Predictive Biomarkers for Immunotherapy

Next, we explored the relationship between the IC50 and other hallmarks of genomic instability (biomarkers for immunotherapy), including MSI, dMMR, and TMB (Halama et al., 2016; Duffy and Crown, 2019). Compared with the high-IC50 group, the low-IC50 group had a higher proportion of MSI (**Figure 4A**), dMMR (**Figure 4B**), and more TMB (**Figure 4C**). Similarly, patients of MSI, dMMR, and more TMB had lower IC50 (**Figures 4D–F**). The diagnostic power of cisplatin IC50 was evaluated using the area under the curve (AUC) of the ROC. The IC50 had excellent diagnostic performance for MSI (**Figure 4G**)

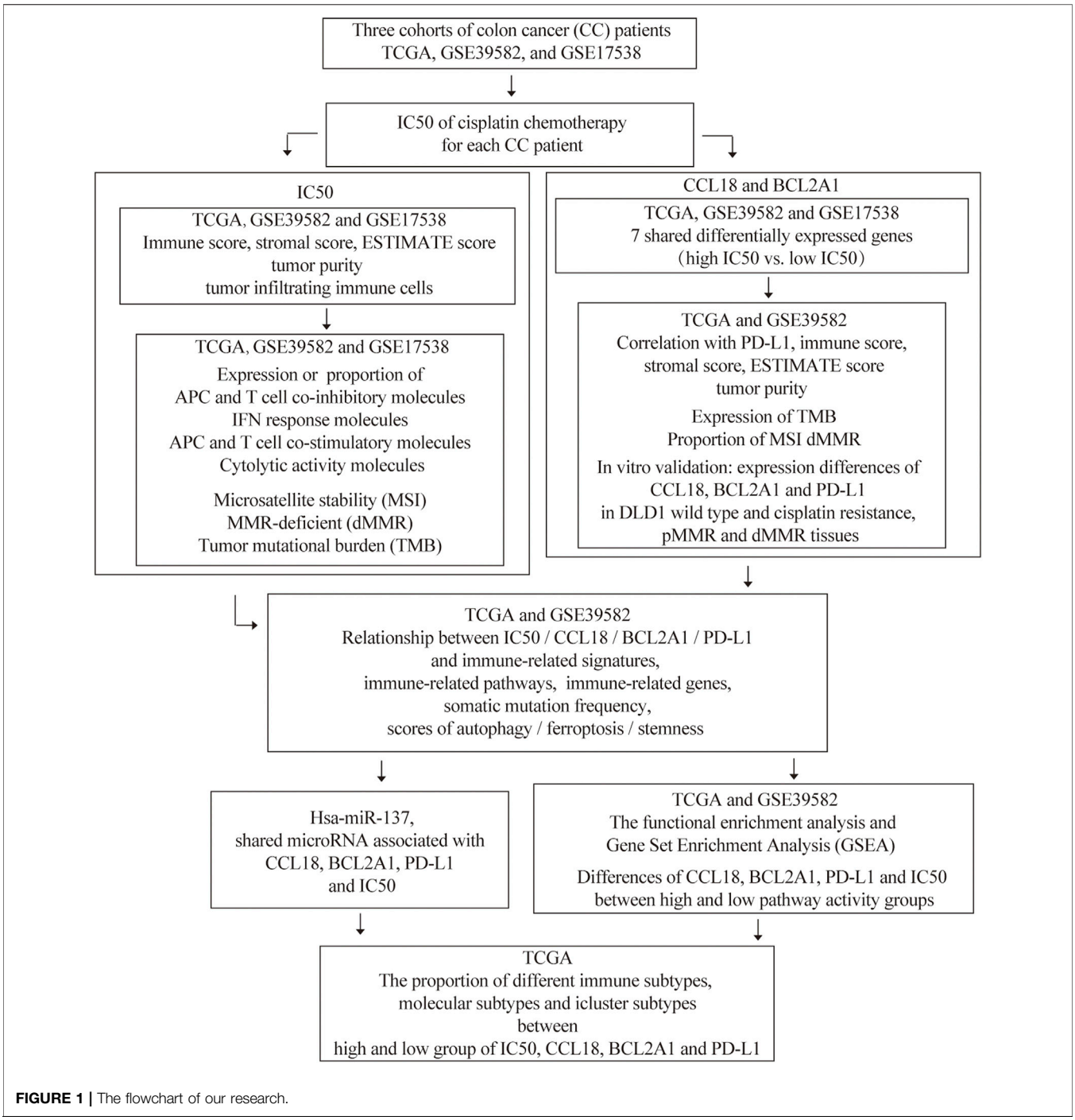

FIGURE 1 | The flowchart of our research.

and MMR (**Figure 4H**), and general diagnostic performance for TMB (**Figure 4I**). From this, we conclude that CC patients who were sensitive to cisplatin chemotherapy were more likely to be sensitive to immunotherapy.

Cisplatin Resistance–Related Genes

To explore the transcriptomic signatures associated with cisplatin resistance, we conducted differential expression analysis between the low- and high-IC50 groups in three cohorts, respectively. Utilizing the DEseq2 (TCGA) and limma (GSE39582 and GSE17538) algorithms, a total of seven shared DEGs were screened (**Figure 5A**), all of which were downregulated in the high-IC50 group (**Figure 5B**). Diagnostic power (high vs. low IC50) (high vs. low PD-L1) of these seven genes were also evaluated using the AUC of the ROC. Combining three data sets, for the quantification of IC50, CCL18, TMEM45A, TNFAIP6, and BCL2A1 had higher diagnostic efficiency (AUC > 0.7) (**Figure 5C**). For the quantification of PD-L1 expression (biomarker in cancer

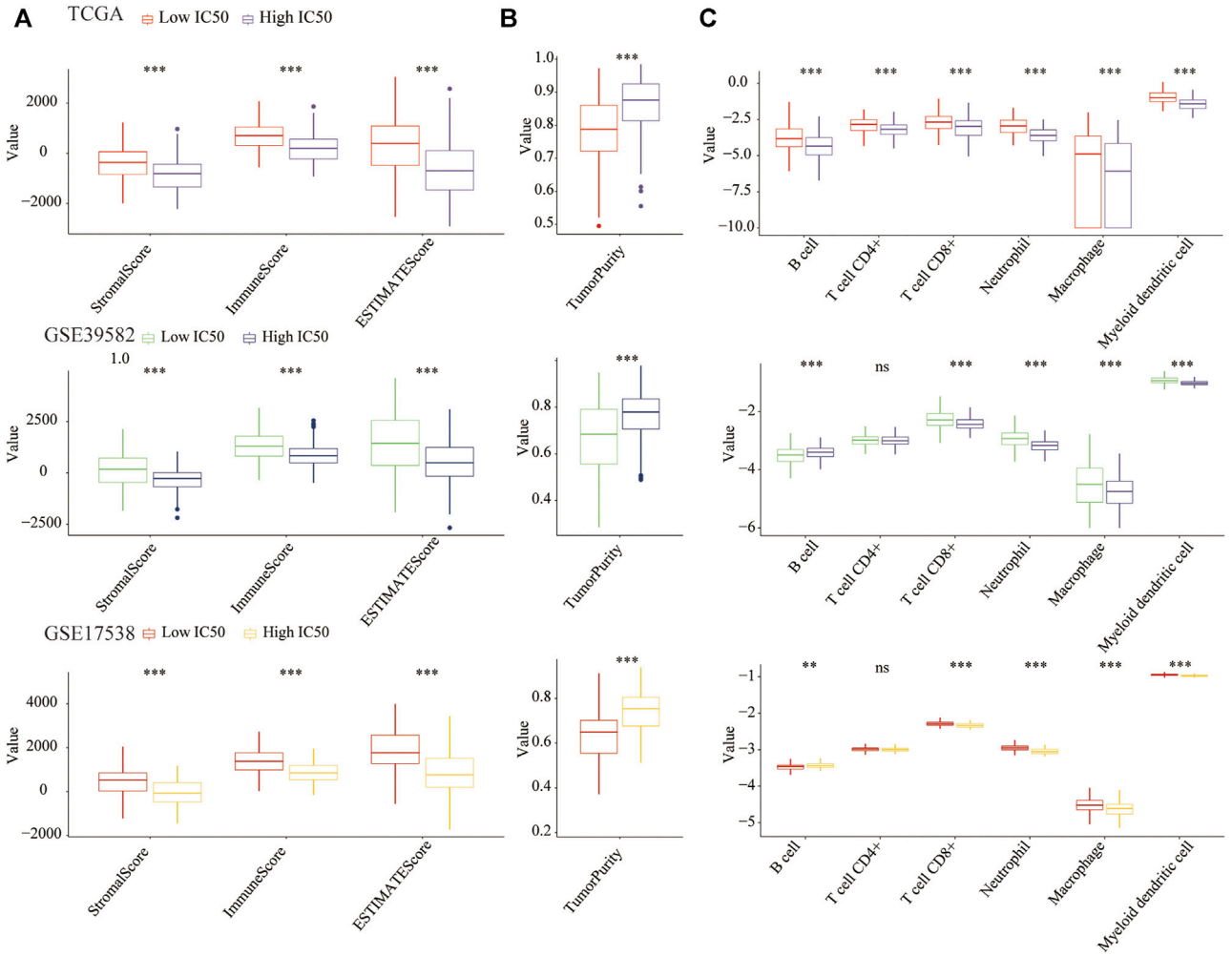

FIGURE 2 | The COAD tissues of the low-IC50 group were more like hot tumors. **(A)** The stromal, immune, and ESTIMATE scores of the low-IC50 group were significantly higher than those of the low-IC50 group. **(B)** The tumor purity of CC tissue was significantly lower in the low-IC50 group. **(C)** Comparison of abundance of six kinds of tumor infiltrating immune cells between low- and high-IC50 groups. $^{**}p < .01$, $^{***}p < .001$.

immunotherapy), CCL18, TNFAIP6, and BCL2A1 had higher diagnostic efficiency (AUC > 0.7) (**Figure 5D**). We concluded that the mechanisms for the low-IC50 group to benefit from immunotherapy might be closely related to the increased expression of CCL18, TNFAIP6, and BCL2A1.

Correlation of Cisplatin Resistance–Related Genes With PD-L1 Expression and the TME Score

In the above three cohorts, we further performed Spearman correlation analysis among PD-L1 and seven cisplatin resistance–related genes. Taking the correlation coefficient greater than 0.5 as the threshold, CCL18 and BCL2A1 were significantly associated with PD-L1 (**Figure 6A**). Besides this, similar to PD-L1, CCL18 and BCL2A1 were also significantly positively correlated with TME score (stromal, immune, and ESTIMATE scores), whereas negatively associated with tumor purity (**Figure 6B**). It could be seen that the expression of cisplatin resistance–related genes, CCL18 and BCL2A1, were significantly related to the immunophenotype of the TME.

Compared with DLD1 wild-type, the survival rate of drug-resistant DLD1 increased significantly when the concentration of cisplatin was more than 10 μmol/L (**Figure 6C**). For *in vitro* verification, compared with DLD1 wild-type, the expression of CCL18, BCL2A1, and PD-L1 was significantly decreased in cisplatin-resistant DLD1 (**Figure 6D**). Next, we evaluated the CCL18, BCL2A1, and PD-L1 mRNA expression in six pairs CC tissues (pMMR vs. dMMR) of our hospital. The patient's consent was obtained in advance, and informed consent was signed. Compared with pMMR tissues, the mRNA expression of CCL18, BCL2A1, and PD-L1 in dMMR was significantly increased (**Figure 6E**). The *in vitro* wet experiments were consistent with the abovementioned bioinformatics analysis

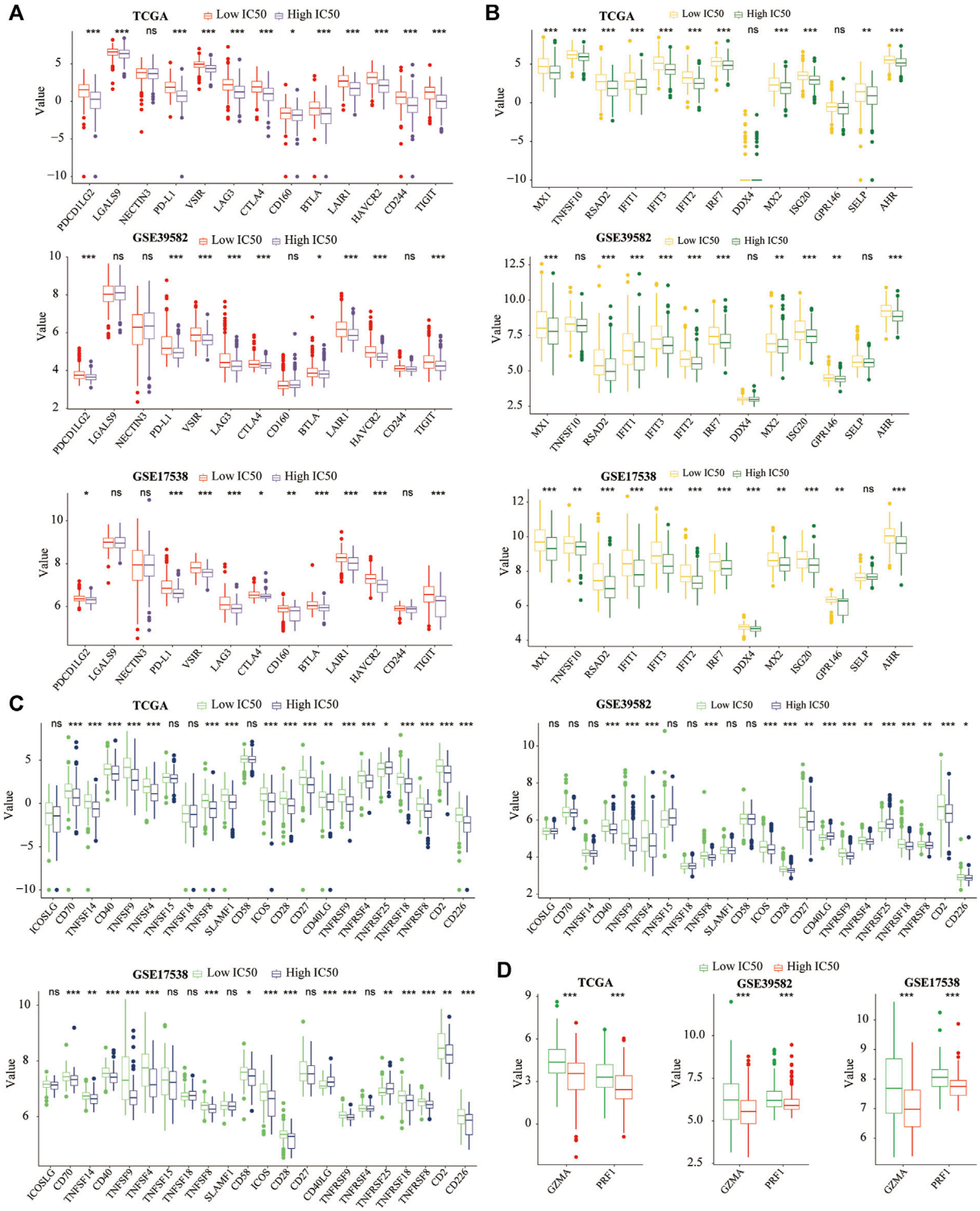

FIGURE 3 | Differences of immune-related genes. The most **(A)** co-inhibitory molecules, **(B)** IFN response molecules, **(C)** co-stimulatory molecules, **(D)** cytolytic activity molecules were significantly higher in the low-IC50 group. *$p < .05$, **$p < .01$, ***$p < .001$.

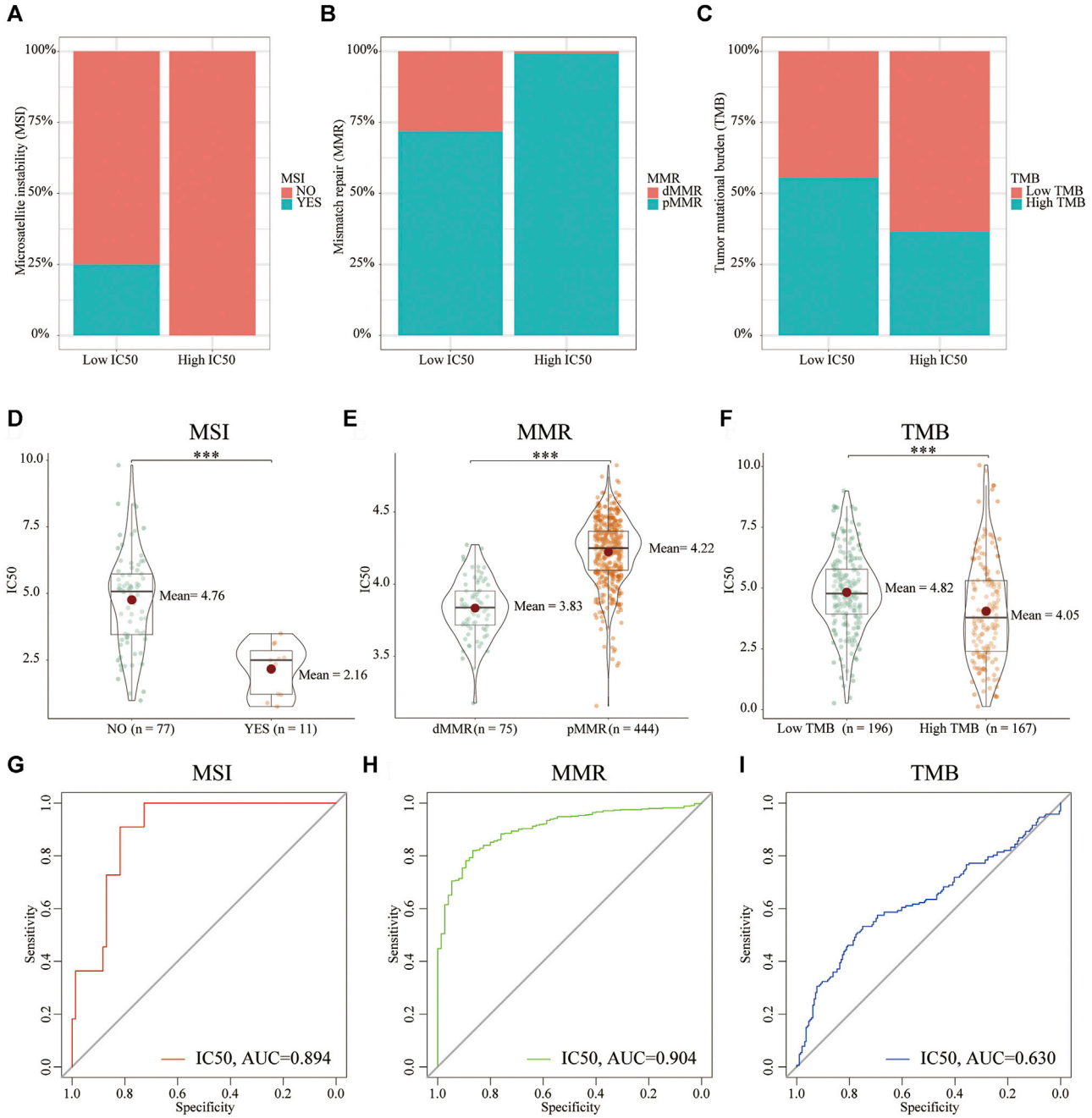

FIGURE 4 | The relationship between hallmarks of genomic instability and IC50. Compared with the high-IC50 group, the low-IC50 group had a higher proportion of **(A)** MSI, **(B)** dMMR, and **(C)** more TMB. CC patients in the **(D)** MSI, **(E)** dMMR, **(F)** high TMB group had significantly lower IC50 for cisplatin chemotherapy. The IC50 had excellent diagnostic performance for **(G)** MSI and **(H)** dMMR,= and **(I)** general diagnostic performance for TMB. ***$p < .001$.

conclusion, that is, CC tissues that were sensitive to cisplatin chemotherapy might be more sensitive to immunotherapy.

The Relationship Between CCL18, BCL2A1, and Hallmarks of Genomic Instability

To further determine whether CCL18 and BCL2A1 could be used as predictive biomarkers for cancer immunotherapy, such as cisplatin IC50, we investigated their relationship with hallmarks of genomic instability (biomarkers for immunotherapy). In contrast with the low group of CCL18, BCL2A1, and PD-L1, the corresponding high group had a higher proportion of MSI (**Figure 7A**), dMMR (**Figure 7B**), and more TMB (**Figure 7C**).

Based on respective medians of CCL18 and BCL2A1, CC patients were divided into four groups, including

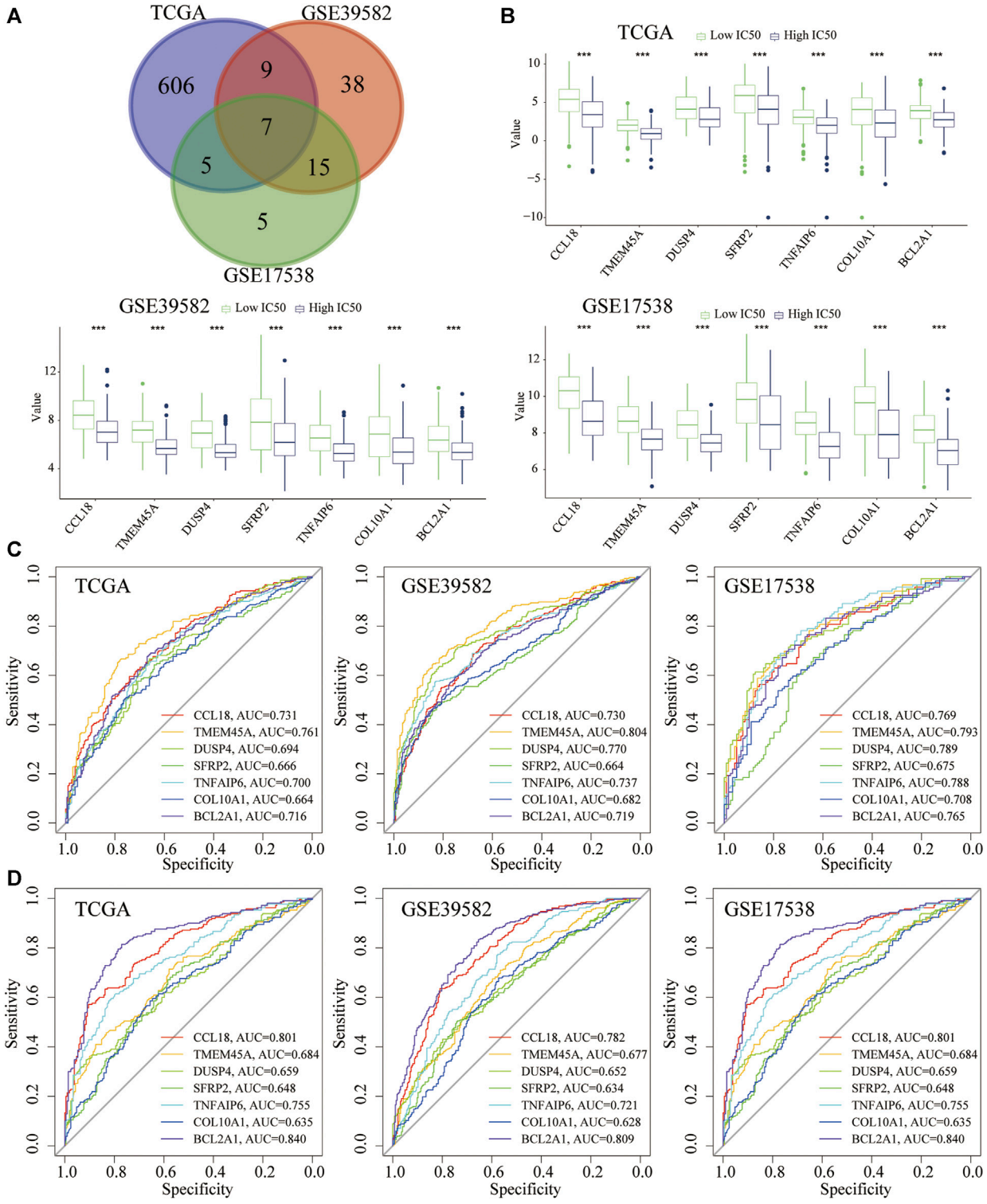

FIGURE 5 | DEGs related to cisplatin resistance and their diagnostic performance. **(A)** The seven shared DEGs (High vs. low IC50). **(B)** The seven shared genes were significantly overexpressed in the low-IC50 group. **(C)** Diagnostic performance (high or low IC50) of seven genes. **(D)** Diagnostic performance (high or low PD-L1) of seven genes. ***$p < .001$.

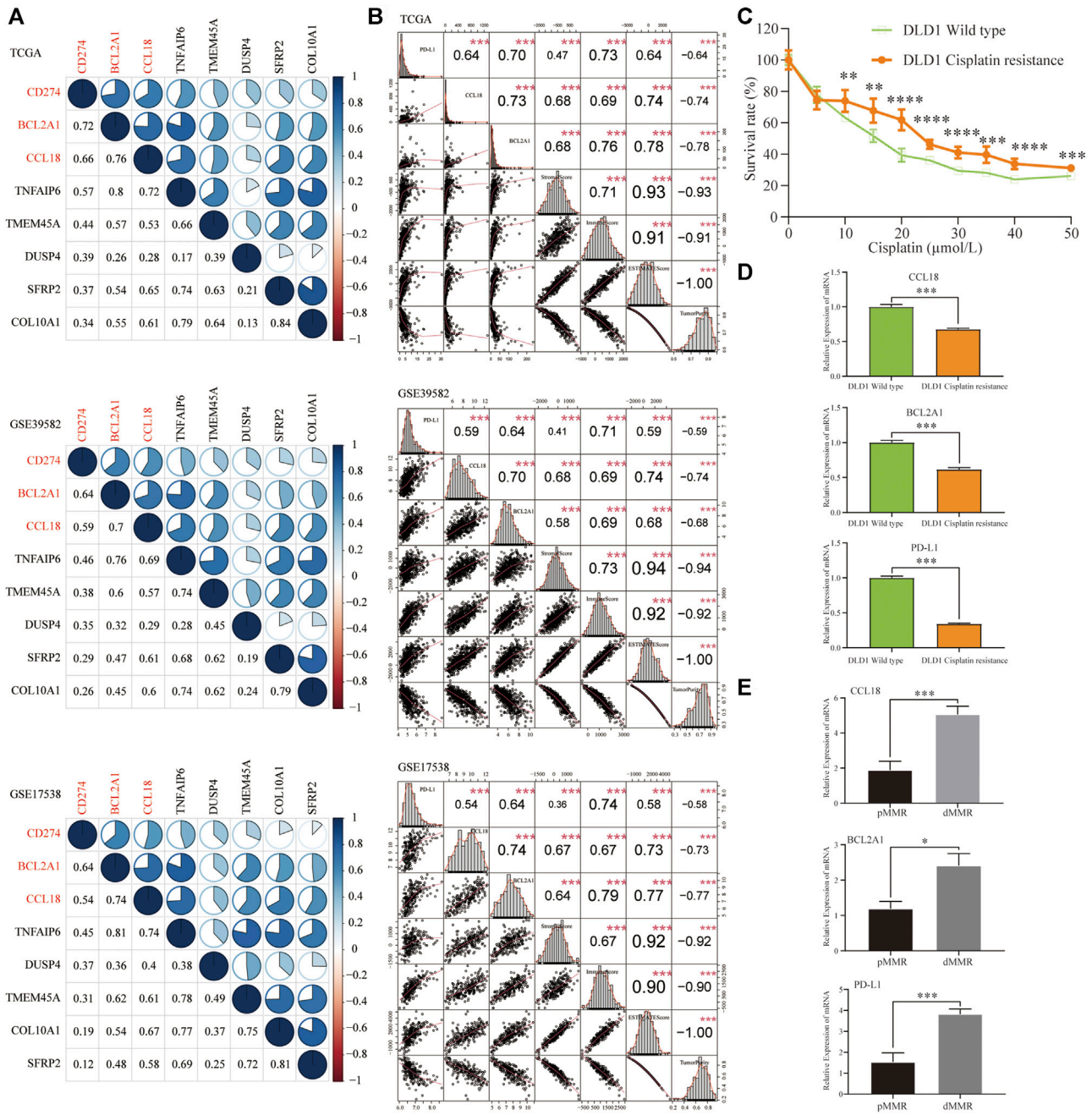

FIGURE 6 | Correlation of seven resistance-related genes with PD-L1 expression, the TME scores, tumor purity, and *in vitro* validation. In three COAD cohorts, **(A)** CCL18 and BCL2A1 had a higher correlation with PD-L1 (Spearman's correlation coefficient >0.5) **(B)** Similar to PD-L1, CCL18 and BCL2A1 were significantly positively correlated with stromal, immune, and ESTIMATE scores and significantly negatively correlated with tumor purity. In cisplatin-resistant DLD1 cell line **(C)**, similar to PD-L1, CCL18 and BCL2A1 were significantly downregulated **(D)**. **(E)** Compared with pMMR tissues, the mRNA expression of CCL18, BCL2A1 and PD-L1 in dMMR was significantly increased. $^{**}p < .01$, $^{***}p < .001$, $^{****}p < .0001$.

Low_CCL18_Low_BCL2A1, Low_CCL18_High_BCL2A1, High_CCL18_Low_BCL2A1 and High_CCL18_High_BCL2A1. Low_CCL18_High_BCL2A1 and High_CCL18_High_BCL2A1 patients had a higher proportion of MSI (**Figure 7D**). BCL2A1 was better than CCL18 in terms of MSI prediction. For MMR, High_CCL18_High_BCL2A1 patients had the highest proportion of dMMR (**Figure 7E**). For TMB, High_CCL18_High_BCL2A1 patients had the highest TMB (**Figure 7F**). Therefore, compared with the other three groups, High_CCL18_High_BCL2A1 patients would benefit more from chemotherapy or immunotherapy. Besides this, For MSI prediction, BCL2A1 had a better prediction of the efficacy of

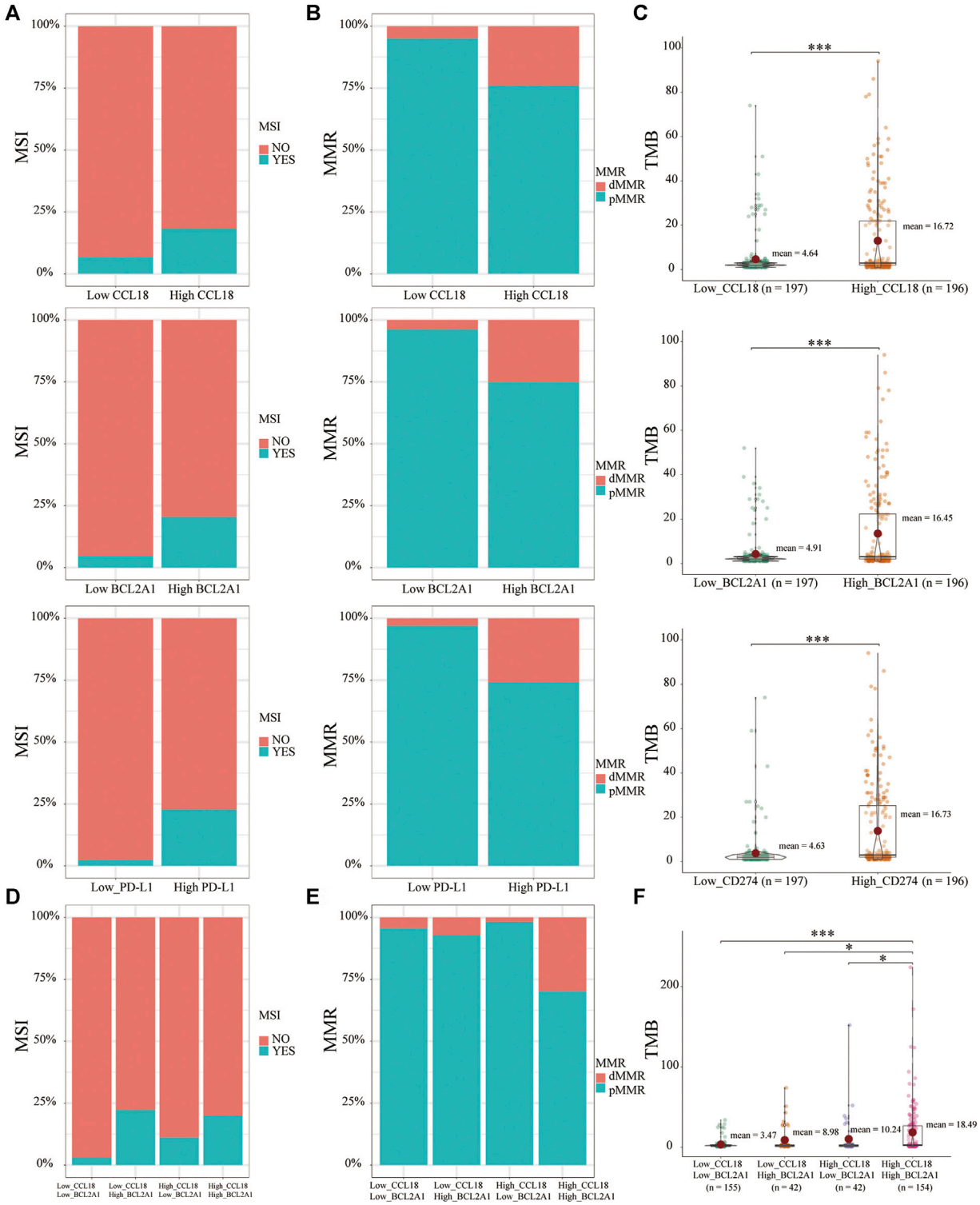

FIGURE 7 | The relationship between MSI, dMMR, TMB, and CCL18, BCL2A1. Similar to PD-L1, the high CCL18 or BCL2A1 group had a greater proportion of **(A)** MSI, **(B)** dMMR, and **(C)** more TMB. **(D)** Low_CCL18_High_BCL2A1 and High_CCL18_High_BCL2A1 groups had a greater proportion of MSI. Compared with the other three groups, the High_CCL18_High_BCL2A1 group had the highest proportion of **(E)** dMMR and the most **(F)** TMB. *$p < .05$, ***$p < .001$.

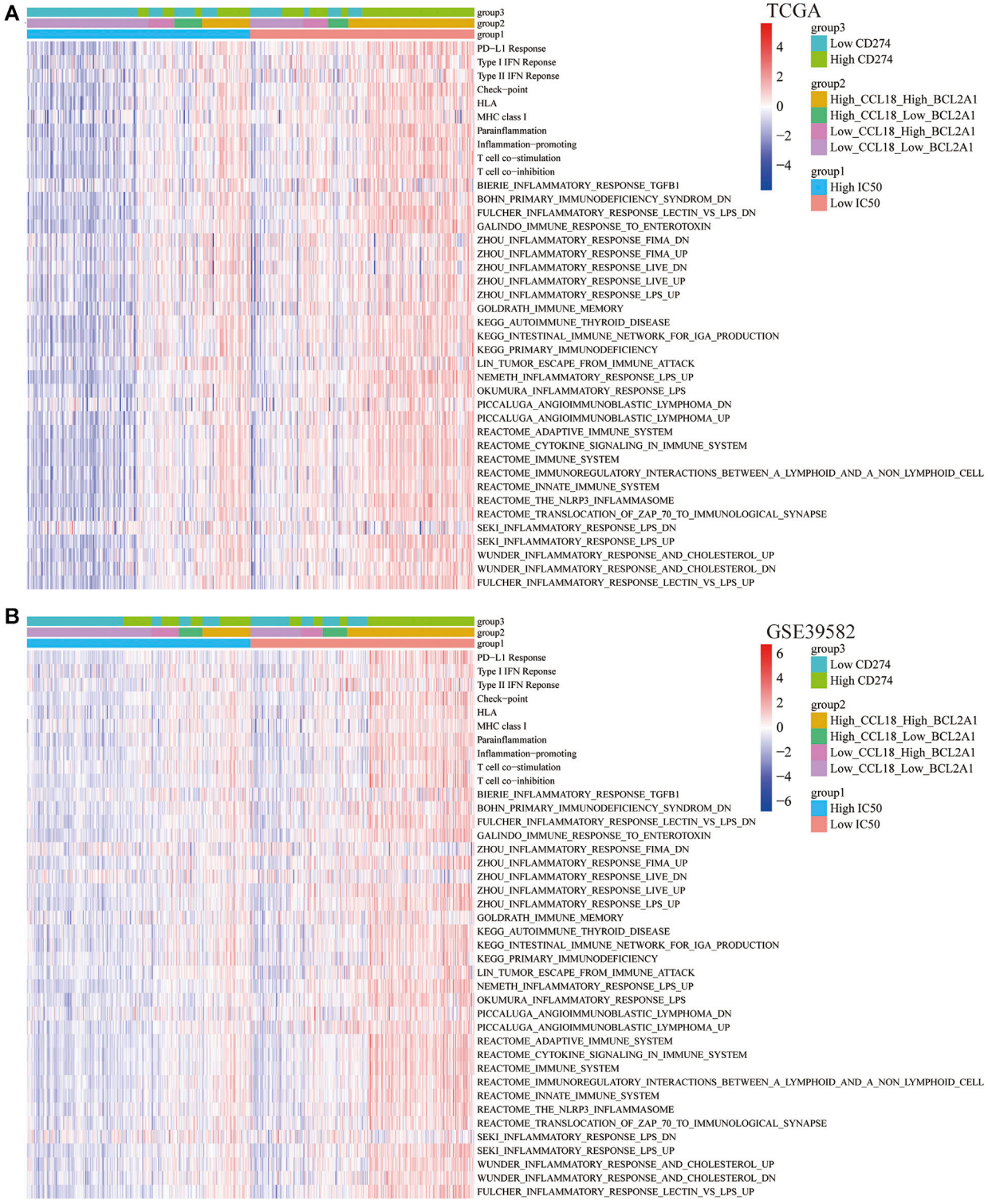

FIGURE 8 | Correlation of immune signatures and pathways. In **(A)** TCGA and **(B)** GSE39582, the score of most immune signatures and pathways were significantly higher in the low-IC50 group and High_CCL18_High_BCL2A1 group.

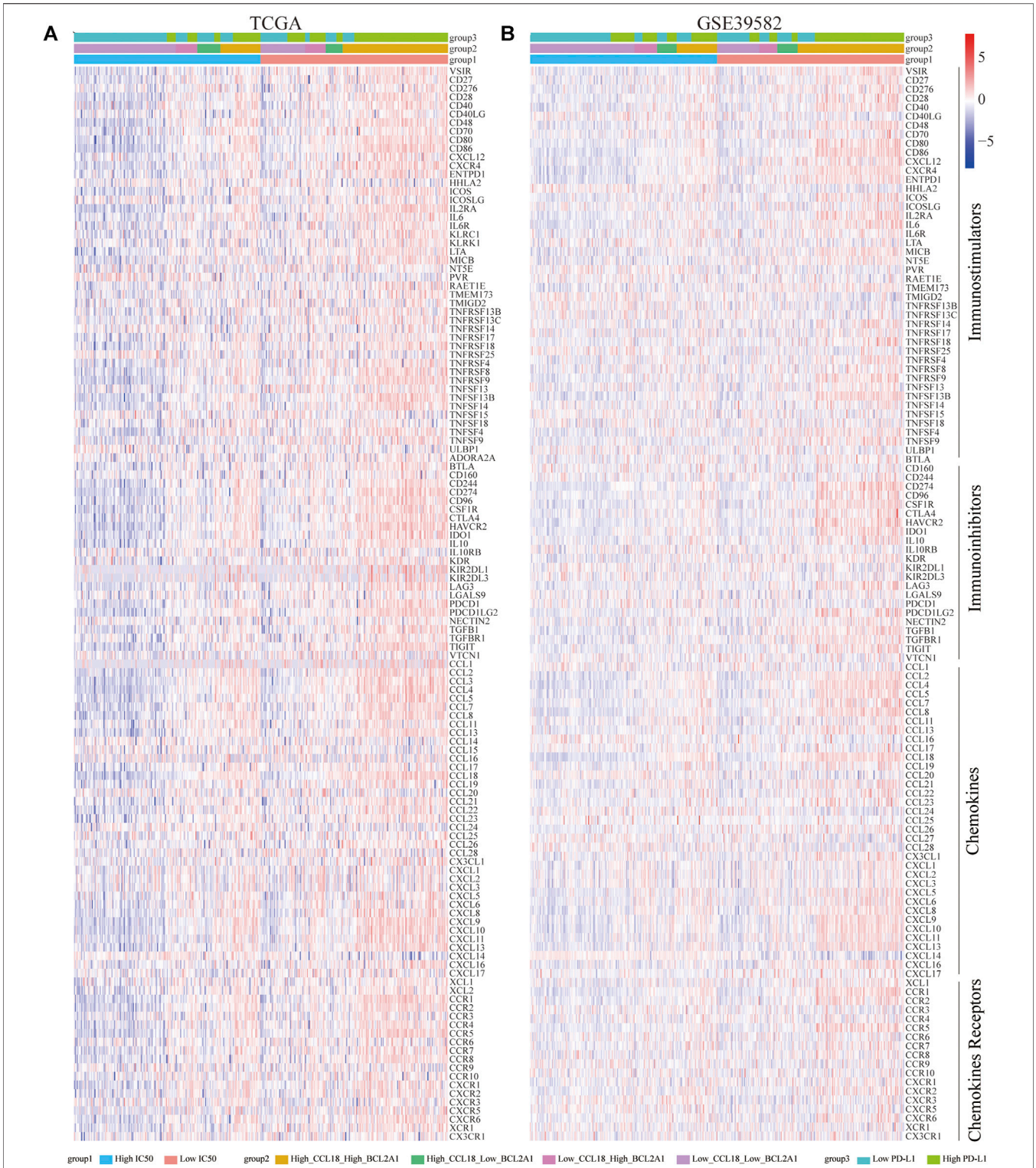

FIGURE 9 | Correlation of immunomodulators (immunostimulators, immunoinhibitors, chemokines, and chemokine receptors). In **(A)** TCGA and **(B)** GSE39582, most immunomodulators were significantly upregulated in the low-IC50 group and High_CCL18_High_BCL2A1 group.

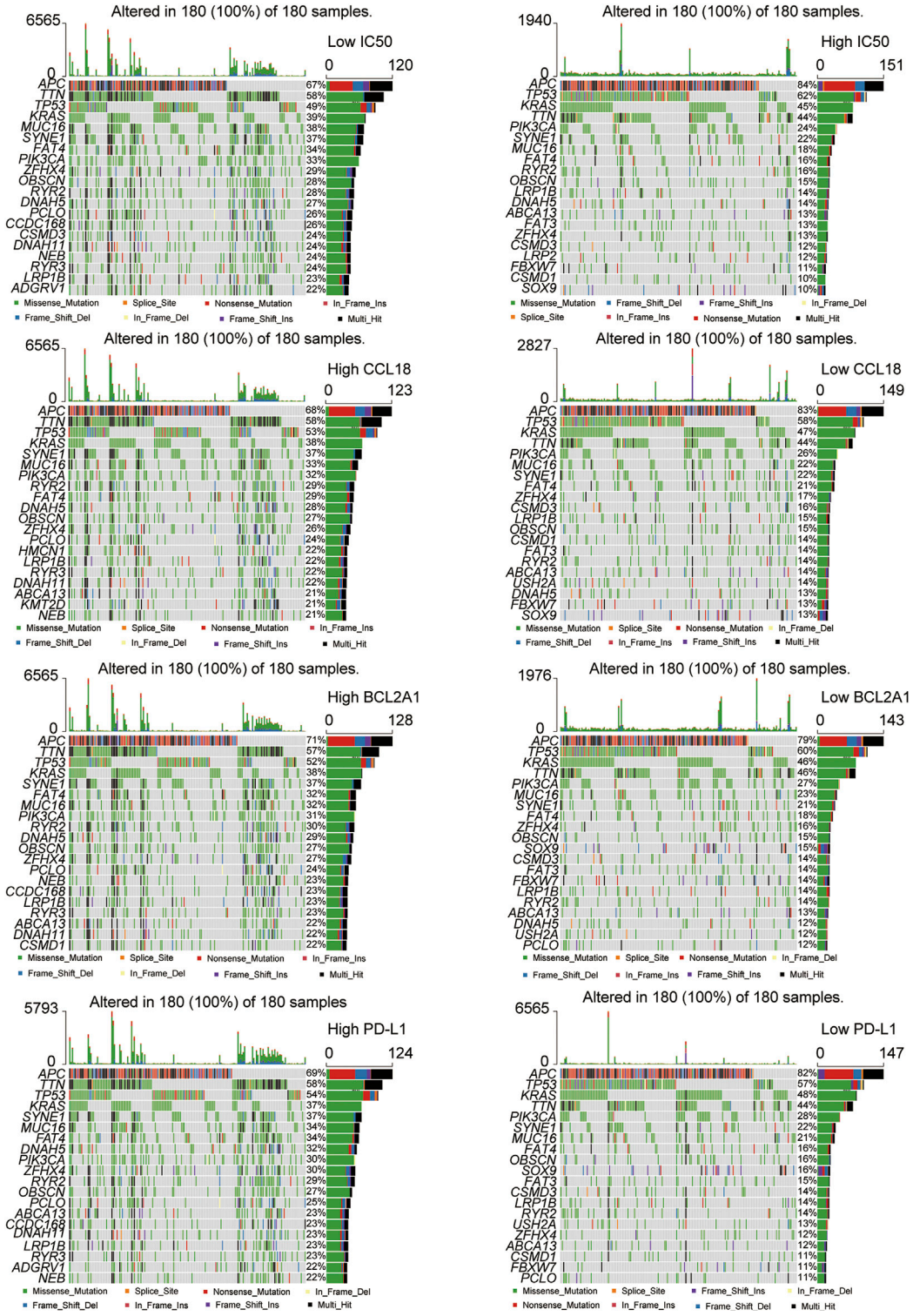

FIGURE 10 | The landscapes of somatic mutations. The low-IC50 group and the high CCL18 or BCL2A1 or PD-L1 group had more somatic mutation frequencies.

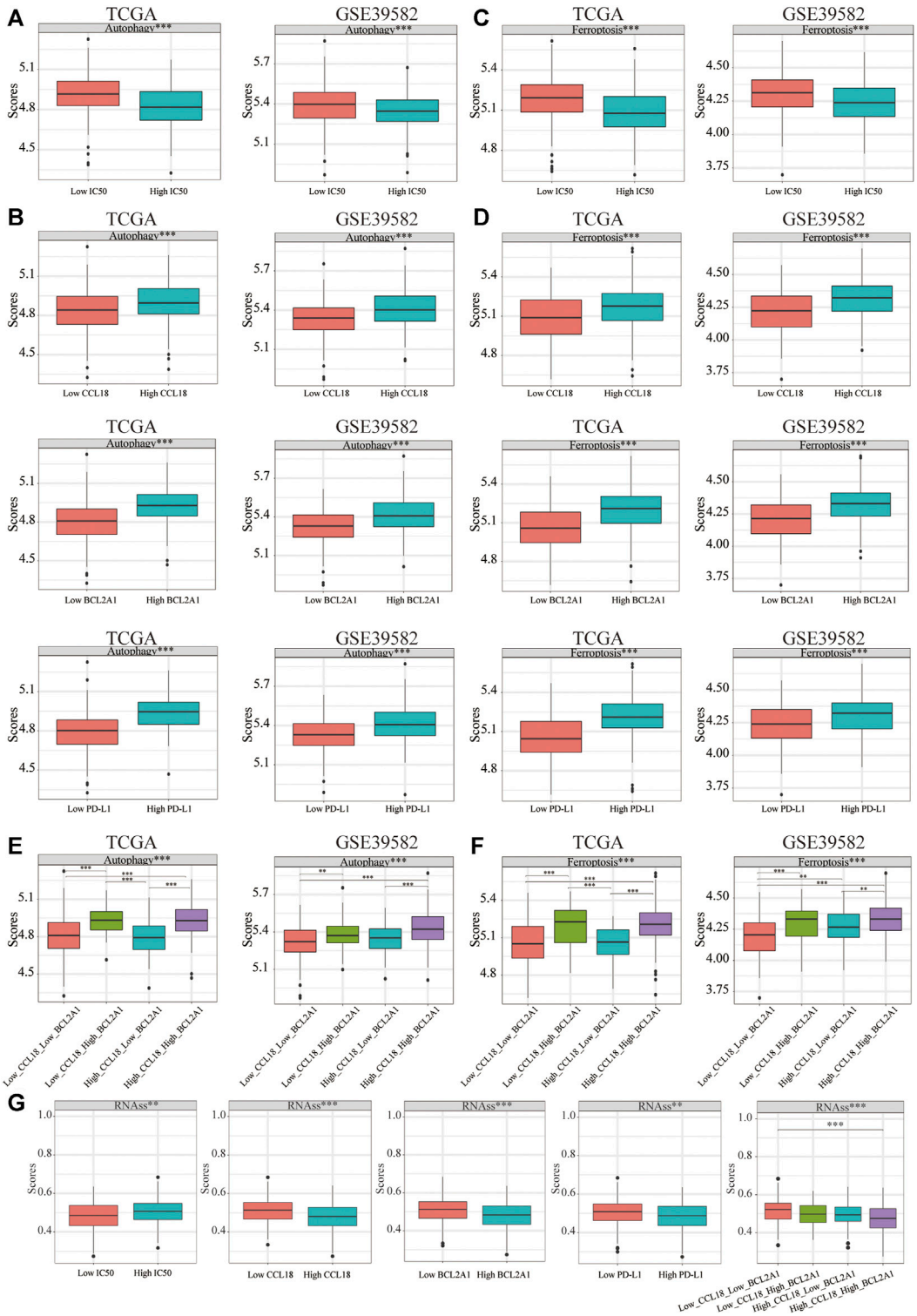

FIGURE 11 | The difference of autophagy, ferroptosis, and stemness scores. In TCGA and GSE39582, the autophagy score of **(A)** the low-IC50 group and **(B)** high group of CCL18 or BCL2A1 or PD-L1 were significantly higher. Similarly, for ferroptosis, the score of **(C)** the low-IC50 group and **(D)** high group of CCL18 or BCL2A1 or PD-L1 were significantly higher. **(E**,**F)** The autophagy or ferroptosis score of High_CCL18_High_BCL2A1 patients were significantly higher than that of Low_CCL18_Low_BCL2A1 and High_CCL18_Low_BCL2A1 patients. The autophagy or ferroptosis score of Low_CCL18_High_BCL2A1 patients were significantly higher than that of Low_CCL18_Low_BCL2A1 patients. **(G)** The stemness score of the low IC50 group and high group of CCL18 or BCL2A1 or PD-L1 was significantly upregulated. The stemness score of High_CCL18_High_BCL2A1 patients was significantly upregulated than that of Low_CCL18_Low_BCL2A1 patients. $^{**}p < .01$, $^{***}p < .001$.

immunotherapy. Based on the expression of CCL18 and BCL2A1, we could partly predict the sensitivity of immunotherapy in CC patients.

Scores of Immune Signatures and Immune Pathways and Expression of Immunomodulators

Based on the ssGSEA algorithm, we calculated the scores of 10 immune signatures and 30 immune pathways and further forecasted their relationship with cisplatin IC50, CCL18, BCL2A1, and PD-L1. Results indicate that, with the increasing expression of CCL18 and BCL2A1, most immune responses were activated as well as immune-related pathways (**Figures 8A,B**). Besides this, for immunomodulators, whether it was immunostimulators, immunoinhibitors, chemokines, or chemokine receptors, most of them were significantly positively correlated with the expression of CCL18 and BCL2A1 (**Figures 9A,B**). Cisplatin resistance–related genes CCL18 and BCL2A1 could partly predict the efficacy of immunotherapy in CC patients.

The Landscapes of Gene Mutations

Gene mutations caused cancer patients to be sensitive or resistant to immune drugs, affecting clinical drug selection and treatment effects (Peng et al., 2016). Therefore, we investigated the landscapes of gene mutations in the low and high groups of TCGA-COAD patients. Similar to the PD-L1 high group, for the low-IC50 group and high-CCL18 or BCL2A1 group, among the 20 most frequently mutated genes, there were more TTN, MUC16, SYNE1, FAT4, PIK3CA, ZFHX4, OBSCN, RYR3, DNAH5, PCLO, DNAH11, NEB, and LRP1B mutation and less APC, TP53, and KRAS mutation (**Figure 10**). It could be seen that gene mutation frequencies were closely related to immunotherapy response in CC patients.

Difference of Autophagy, Ferroptosis, and Stemness Scores

Previous studies confirm that autophagy mediated the sensitivity of tumor cells to immunotherapy after chemotherapy (Ramakrishnan et al., 2012). In our study, in the TCGA and GSE39582 data sets, compared with the low-IC50 group, the autophagy score of the high-IC50 group was significantly decreased (**Figure 11A**), which was consistent with previous study that autophagy activators could inhibit the cisplatin resistance of tumor cells (Sirichanchuen et al., 2012). Compared with the low group of CCL18 or BCL2A1 or PD-L1, the autophagy score of corresponding high group was significantly increased (**Figure 11B**), which was consistent with the conclusions of previous studies that enhanced autophagy would increase the sensitivity of immunotherapy (Jiang et al., 2019; Xia et al., 2021).

Ferroptosis, the bright new star in immunotherapy, could enhance the efficacy of immunotherapy (Wang W et al., 2019). Besides this, ferroptosis inducers could enhance chemotherapeutic drug sensitivity (Kim et al., 2018). Similar to the difference in autophagy score, the low-IC50 group and the high-CCL18 or BCL2A1 or PD-L1 group had higher ferroptosis scores (**Figures 11C,D**). Among the four groups, the autophagy or ferroptosis score of High_CCL18_High_BCL2A1 patients were significantly higher than that of Low_CCL18_Low_BCL2A1 and High_CCL18_Low_BCL2A1 patients. The autophagy or ferroptosis score of Low_CCL18_High_BCL2A1 patients were significantly higher than that of Low_CCL18_Low_BCL2A1 patients (**Figures 11E,F**). The difference between autophagy and ferroptosis further verified that CCL18 and BCL2A1 were closely related to the sensitivity of immunotherapy in CC patients.

Previous study confirms that the stemness of immune T cells promotes antitumor effects (Li W et al., 2020). Therefore, we analyzed the stemness score difference between low and high IC50 or CCL18 or BCL2A1 or PD-L1 groups. (**Figure 11G**) The high-IC50 group and low-CCL18 or BCL2A1 or PD-L1 group had a higher stemness score. The stemness score of High_CCL18_High_BCL2A1 patients was significantly lower than that of Low_CCL18_Low_BCL2A1 patients. Therefore, we speculated that the outcome of chemotherapy and immunotherapy for CC patients with high stemness score might not be good (**Figure 12**).

MicroRNA Correlation

The mechanism of drug resistance is very extensive in cytology, including a variety of key genes and pathways. The genetic variation of these key factors can lead to the occurrence of drug resistance in tumor cells. Among them, microRNA is one of these key genes (Ma et al., 2010). On the ENCORI database, we excavated the respective miRNAs of CCL18, BCL2A1, and PD-L1 and finally screened the two miRNAs shared by BCL2A1 and PD-L1, hsa-miR-514a-5p and hsa-miR-137 (**Figure 12A**). Hsa-miR-137 was significantly positively associated with CCL18, BCL2A1, and PD-L1 (**Figure 12B**), and upregulated in CC (**Figure 12C**) and the high-IC50 group (**Figure 12D**). Previous studies confirm that hsa-miR-137 was closely related to the occurrence and development (Smith et al., 2015; Huang et al., 2016), chemotherapy sensitivity (Guo et al., 2017) of cancer, and could also regulate the autophagy (Wang Z et al., 2019), ferroptosis (Luo et al., 2018), and stemness (Sakaguchi et al., 2016) of cancer cells. To a certain extent, this confirms the conclusions of our analysis. However, the roles of hsa-miR-137 in cancer immunotherapy were never mentioned, which needed to be explored in depth. For the other microRNA, hsa-miR-514a-5p was only positively significantly associated with BCL2A1. Therefore, we did not study it further.

The Functional Enrichment Analysis (GO and KEGG) and GSEA

To explore the underlying mechanisms of CCL18 and BCL2A1, among 19,584 protein-coding genes in the TCGA and 20,183 protein-coding genes in the GSE39582, based on the Spearman correlation coefficient greater than 0.6, we unearthed 80 genes related to both CCL18 and BCL2A1 and performed GO (**Figure 13A**) and KEGG (**Figure 13B**) analysis.

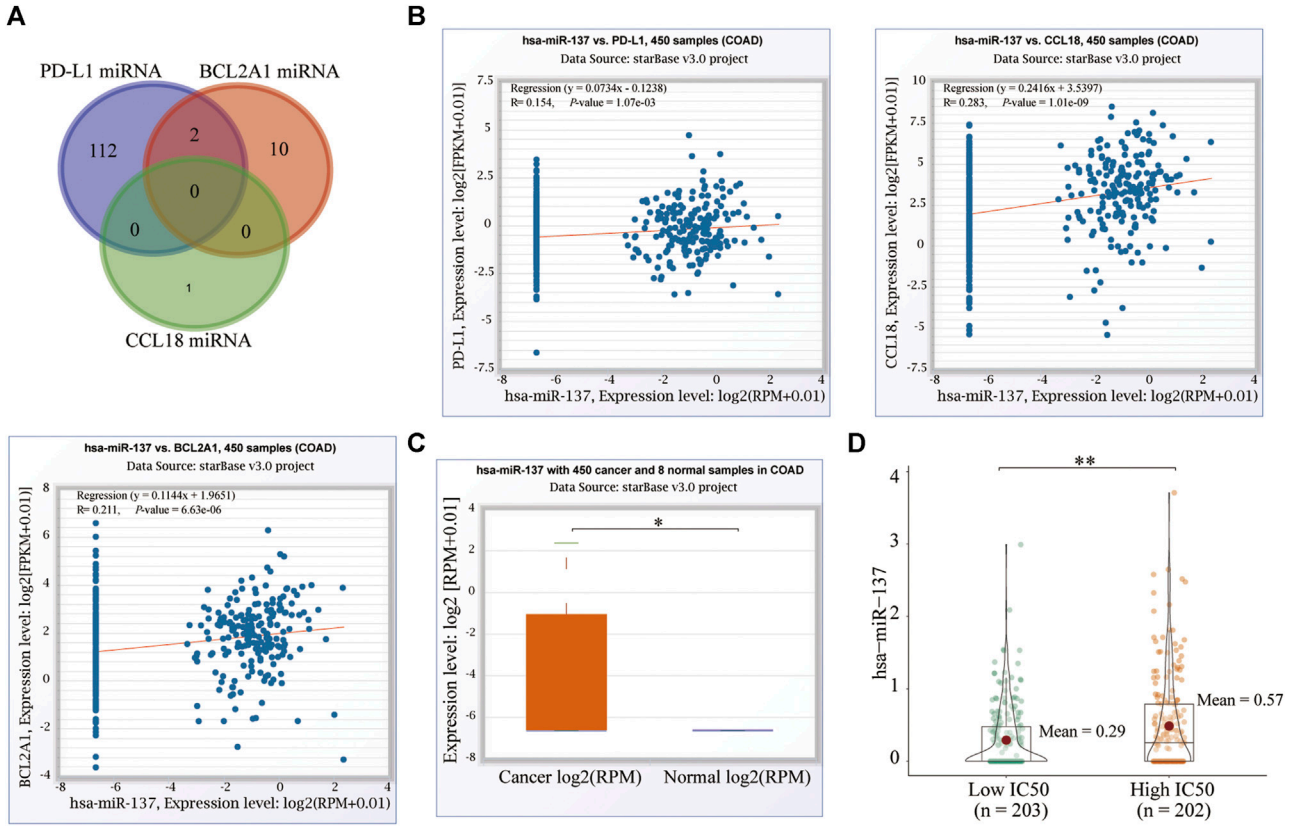

FIGURE 12 | MicroRNAs correlation and **(A)** shared miRNAs of PD-L1, CCL18, and BCL2A1. **(B)** One of the common miRNAs of PD-L1 and BCL2A1, hsa-miR-137, was significantly related to PD-L1, BCL2A1, and CCL18. **(C)** Hsa-miR-137 was significantly upregulated in CC tissues and the highIC50 group. *$p < 0.05$, **$p < .01$.

For BP, MF, and KEGG, CCL18 and BCL2A1 were significantly related to immune and inflammatory response. For CC, CCL18 and BCL2A1 were significantly related to granule membrane. Besides this, results of GO-MF and KEGG were both significantly related to the function of Toll-like receptors. Toll-like receptors might be involved in the resistance process of chemotherapy and immunotherapy in CC patients.

To further study potential pathways for chemotherapy-sensitive tumor cells to benefit from immunotherapy and the molecular mechanisms of CCL18 and BCL2A1, we performed GSEA among 186 KEGG pathways, including the Toll-like receptor signaling pathway. Results indicate that the low-IC50 group and high-CCL18 or BCL2A1 or PD-L1 group were significantly associated with KEGG_ANTIGEN_PROCESSING_AND_PRESENTATION and KEGG_TOLL_LIKE_RECEPTOR_SIGNALING_PATHWAY (**Figure 13C**). Downregulating the activity of these two pathways might help increase the sensitivity of drug-resistant tumor cells to cisplatin chemotherapy and immunotherapy.

Differences in the Scores of two Enrichment Pathways

Using the ssGSEA method, we quantified the scores of the above two key pathways. Based on the respective medians of the pathway score, CC patients were divided into high and low groups. In the high group of two key pathways, the expression of CCL18, BCL2A1, and PD-L1 increased significantly, whereas the IC50 decreased significantly (**Figures 14A,B**). Diagnostic power (high vs. low IC50) of two pathways were also evaluated using the AUC of the ROC. The diagnostic power of KEGG_TOLL_LIKE_RECEPTOR_SIGNALING_PATHWAY was higher than KEGG_ANTIGEN_PROCESSING_AND_PRESENTATION (**Figures 14C**). This corresponded to the Toll-like receptor function of the previous GO-MF and KEGG results. The Toll-like receptor signaling pathway might play a pivotal role in the response to chemotherapy and immunotherapy and was a key target to increase treatment sensitivity.

Subtype Analysis of TCGA-COAD Patients

To understand the pathogenesis of fatal malignant tumors, 33 types of tumors in the TCGA were classified into different subtypes according to the genomic characteristics (Liu et al., 2018; Thorsson et al., 2018; Swanson et al., 2019). We explored the proportion of different immune subtypes, molecular subtypes and icluster subtypes of a TCGA-COAD cohort. Among five types of immune subtypes of TCGA-COAD, the proportion of IFN-γ dominant (immune C2) and TGF-beta dominant (Immune C6) patients in the low-IC50 group, high CCL18 or BCL2A1 or PD-L1 group, and

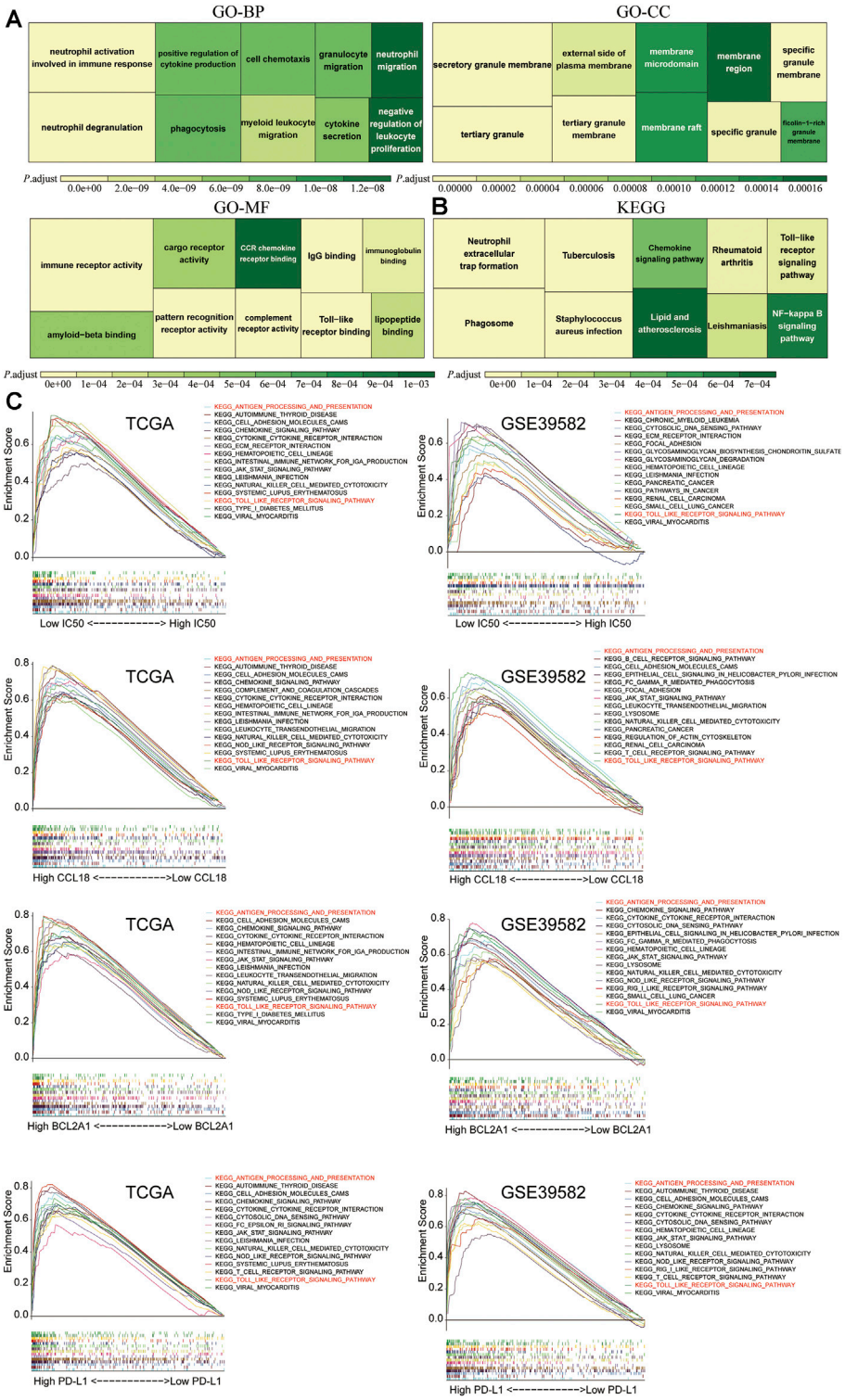

FIGURE 13 | The functional enrichment analysis and GSEA. The **(A)** GO and **(B)** KEGG analysis of 80 genes significantly related to CCL18 and BCL2A1 (Spearman's correlation coefficient >0.6) in TCGA and GSE39582. **(C)** In TCGA and GSE39582, between the high and low groups of IC50, CCL18, BCL2A1, and PD-L1, among 186 KEGG pathways, there were two shared significant enrichment pathways, which are marked in red.

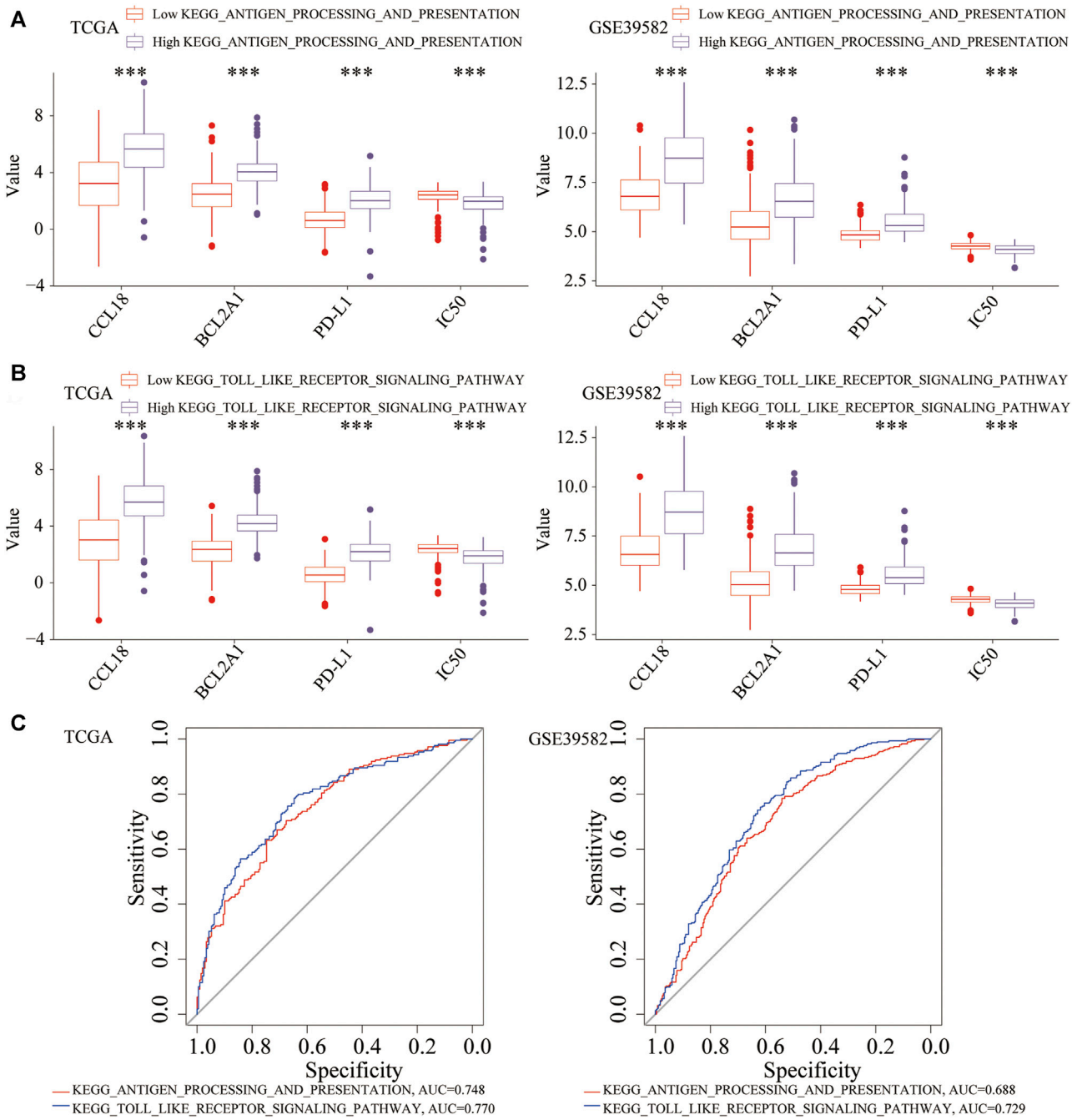

FIGURE 14 | The relationship between two key pathways and the expression of CCL18, BCL2A1, PD-L1, and IC50. In the high **(A)** KEGG_ANTIGEN_PROCESSING_AND_PRESENTATION or **(B)** KEGG_TOLL_LIKE_RECEPTOR_SIGNALING_PATHWAY group, CCL18, BCL2A1 and PD-L1 were significantly upregulated, and the IC50 was significantly downregulated. **(C)** Diagnostic efficacy of the two pathways (high vs. low IC50). ***$p < .001$.

High_CCL18_High_BCL2A1 group increased significantly (**Figures 15A,B**), indicating that these patients were suitable for cisplatin chemotherapy and immunotherapy. Among four types of molecular subtypes of TCGA-COAD, patients of HM-indel and HM-SNV might benefit more from cisplatin chemotherapy and immunotherapy (**Figures 15C,D**). Using the iCluster and Cluster of Cluster Assignments (COCAs) method (Swanson et al., 2019), CC patients were mainly divided into five types, of which C18 and C20 patients were mainly attributable to low-IC50 group, high-CCL18 or BCL2A1 or PD-L1 group, and High_CCL18_High_BCL2A1 group (**Figures 15E,F**). It could be seen that C18 and C20 patients might benefit more from cisplatin chemotherapy and immunotherapy.

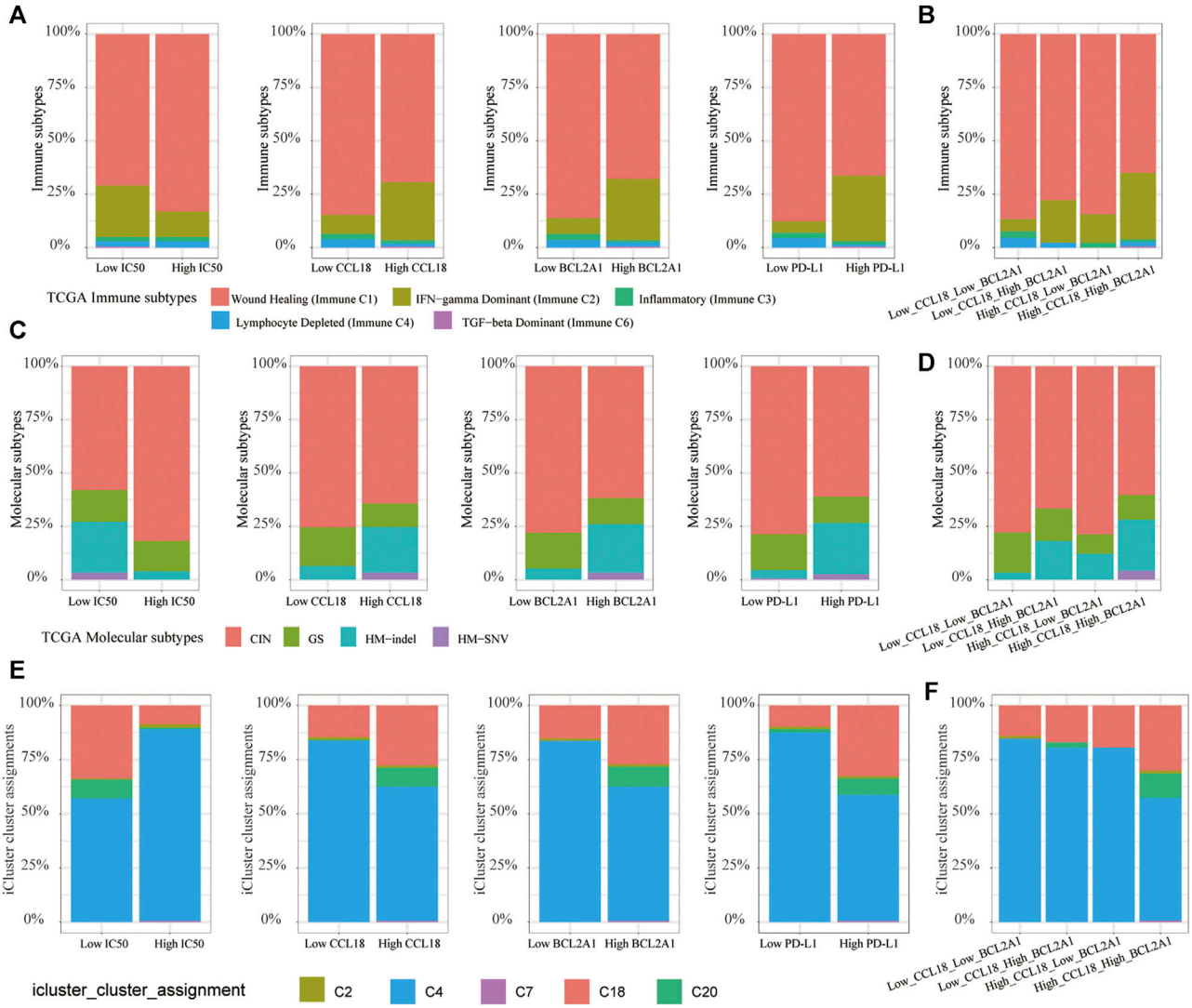

FIGURE 15 | TCGA-COAD subtype analysis. **(A,B)** The proportion of immune C2 and C6 increased significantly in the low-IC50 group, high CCL18 or BCL2A1 or PD-L1 group, and High_CCL18_High_BCL2A1 group. **(C–F)** The low-IC50 group, high group of CCL18 or BCL2A1 or PD-L1 and Low_CCL18_Low_BCL2A1 group had a higher proportion of HM-indel, HM-SNV, C18 and C20.

DISCUSSION

As one of the leading causes of cancer-related death, the treatment of COAD has always been highly concerned. The immune TME occupies an important position in the process of tumor occurrence, invasion, metastasis, and treatment tolerance, indicating that we can start from the perspective of the immune microenvironment to explore novel ant-tumor targets.

With the increasing popularity of immunotherapy, it has brought hope to cancer patients. However, not all patients can respond well to immunotherapy (Ganesh et al., 2019). Therefore, the development of immune-related biomarkers with high accurate value is essential to predict the efficacy of immunotherapy in COAD patients.

In this study, we found that CCL18 and BCL2A1 could predict the efficacy of chemotherapy and immunotherapy at the same time. At the subtype level, COAD patients of immune C2, immune C6, HM-indel, HM-SNV, C18 and C20 were suitable for chemotherapy and immunotherapy. At the genetic level, High_CCL18_High_BCL2A1 patients might benefit the most from chemotherapy and immunotherapy. Low_CCL18_High_BCL2A1 patients had a high proportion of MSI, which was close to that of High_CCL18_High_BCL2A1 patients. In addition, the proportion of immune C2 and HM-indel in Low_CCL18_High_BCL2A1 patients was higher than that of High_CCL18_Low_BCL2A1. From this, we concluded that BCL2A1 was better than CCL18 in predicting the sensitivity of COAD patients to chemotherapy and immunotherapy.

To study the potential mechanisms of CCL18 and BCL2A1, GSEA and functional enrichment analysis were conducted. Results show that the expression changes of CCL18 and BCL2A1 mainly affected the Toll-like receptor signaling pathway, which provides clues for further research.

For hsa-miR-137, a previous study confirmed its correlation with chemotherapy sensitivity. Hsa-miR-137 chemosensitized CC cells to the chemotherapeutic drug oxaliplatin by targeting YBX1 (Guo et al., 2017). Silencing OIP5-AS1 and upregulating hsa-miR-137 expression significantly intensified growth inhibition of drug-resistant CC cells and improved the sensitivity of CC cells to Oxaliplatin (Liang et al., 2020). Besides this, hsa-miR-137 was closely related to the occurrence of early colorectal cancer (Huang et al., 2016). Hsa-miR-137 acted as a tumor-suppressive miRNA in CCs and negatively regulated the progression of CC (Smith et al., 2015). Hsa-miR-137 was also closely related to ferroptosis (Luo et al., 2018), stemness (Sakaguchi et al., 2016), and autophagy (Wang Z et al., 2019) of cancer cells. However, the roles of hsa-miR-137 in immunotherapy had never been explored, and more molecular biology experiments were urgently needed.

CCL18 is a member of the secreted protein cytokine family involved in immunoregulatory and inflammatory processes (Babu et al., 2009). BCL2A1 is the underdog in the BCL2 family (Vogler, 2012). Previous studies confirm their association with chemotherapy resistance (Eisele et al., 2007; Yajima et al., 2009; Lane et al., 2015; Sagara et al., 2016; Lin et al., 2020). Besides, both CCL18 and BCL2A1 were significantly related to the occurrence and development of cancer (Yu et al., 2019; Korbecki et al., 2020). This study confirmed their prediction of immunotherapy sensitivity, and we looked forward to more wet experiments to verify it in the future.

The advantages of this paper are as follows: in this study, the relationship between cisplatin chemotherapy and immunotherapy was explored in detail by bioinformatics methods and verified *in vitro* by cell experiment and clinical specimens. The disadvantages of this paper were as follows: for CC patients, we proposed cisplatin chemotherapy combined with immunotherapy for the first time, which urgently needs more *in vitro* and *in vivo* research, including animal experiments.

CONCLUSION

COAD patients who were sensitive to cisplatin chemotherapy might also benefit more from immunotherapy. CCL18 and BCL2A1 could simultaneously predict the sensitivity of COAD patients to chemotherapy and immunotherapy. High_CCL18_High_BCL2A1 patients were suitable for combination therapy (chemotherapy and immunotherapy). CCL18, BCL2A1, TOLL-like receptor signaling pathway, and hsa-miR-137 might be novel potential chemotherapy and immunotherapy targets.

DATA AVAILABILITY STATEMENT

The datasets presented in this study can be found in online repositories. The names of the repository/repositories and accession number(s) can be found in the article/ **Supplementary Material**.

AUTHOR CONTRIBUTIONS

This research was designed by PW and SC. The manuscript was written by TY. The data analysis was performed by TY, SZ, JZ, JL, YL and SC. The surgical specimens used in this article was collected by TY and XL. The in vitro experimental verification was done by TY and XL.

FUNDING

This research was supported by the National Natural Science Foundation of China (No. 81902384 and No. 81770522), the National Science and Technology Major Project of China (No. 2018ZX10723204), and the Scientific Research Seed Fund of Peking University First Hospital (No. 2019SF01).

ACKNOWLEDGMENTS

We sincerely thank the maintainers of the TCGA and GEO database, the TIMER2.0, ENCORI, MSigDB, UCSC Xena website and the developers of R packages.

SUPPLEMENTARY MATERIAL

The Supplementary Material for this article can be found online at: https://www.frontiersin.org/articles/10.3389/fcell.2021.799278/full#supplementary-material

REFERENCES

Babu, S., Kumaraswami, V., and Nutman, T. B. (2009). Alternatively Activated and Immunoregulatory Monocytes in Human Filarial Infections. *J. Infect. Dis.* 199, 1827–1837. doi:10.1086/599090

Cheng, Z., Vermeulen, M., Rollins-Green, M., DeVeale, B., and Babak, T. (2021). Cis-regulatory Mutations with Driver Hallmarks in Major Cancers. *iScience* 24, 102144. doi:10.1016/j.isci.2021.102144

Dekker, E., Tanis, P. J., Vleugels, J. L. A., Kasi, P. M., and Wallace, M. B. (2019). Colorectal Cancer. *The Lancet* 394, 1467–1480. doi:10.1016/s0140-6736(19)32319-0

Duffy, M. J., and Crown, J. (2019). Biomarkers for Predicting Response to Immunotherapy with Immune Checkpoint Inhibitors in Cancer Patients. *Clin. Chem.* 65, 1228–1238. doi:10.1373/clinchem.2019.303644

Eisele, L., Klein-Hitpass, L., Chatzimanolis, N., Opalka, B., Boes, T., Seeber, S., et al. (2007). Differential Expression of Drug Resistance-Related Genes Between Sensitive and Resistant Blasts in Acute Myeloid Leukemia. *Acta Haematol.* 117, 8–15. doi:10.1159/000096854

Galluzzi, L., Bravo-San Pedro, J. M., Levine, B., Green, D. R., and Kroemer, G. (2017). Pharmacological Modulation of Autophagy: Therapeutic Potential and Persisting Obstacles. *Nat. Rev. Drug Discov.* 16, 487–511. doi:10.1038/nrd.2017.22

Ganesh, K., Stadler, Z. K., Cercek, A., Mendelsohn, R. B., Shia, J., Segal, N. H., et al. (2019). Immunotherapy in Colorectal Cancer: Rationale, Challenges and Potential. *Nat. Rev. Gastroenterol. Hepatol.* 16, 361–375. doi:10.1038/s41575-019-0126-x

Geeleher, P., Cox, N., and Huang, R. S. (2014). pRRophetic: An R Package for Prediction of Clinical Chemotherapeutic Response from Tumor Gene Expression Levels. *PloS one* 9, e107468. doi:10.1371/journal.pone.0107468

Goldman, M. J., Craft, B., Hastie, M., Repečka, K., McDade, F., Kamath, A., et al. (2020). Visualizing and Interpreting Cancer Genomics Data via the Xena Platform. *Nat. Biotechnol.* 38, 675–678. doi:10.1038/s41587-020-0546-8

Gong, Z., Zhang, J., and Guo, W. (2020). Tumor Purity as a Prognosis and Immunotherapy Relevant Feature in Gastric Cancer. *Cancer Med.* 9, 9052–9063. doi:10.1002/cam4.3505

Guo, Y., Pang, Y., Gao, X., Zhao, M., Zhang, X., Zhang, H., et al. (2017). MicroRNA-137 Chemosensitizes Colon Cancer Cells to the Chemotherapeutic Drug Oxaliplatin (OXA) by Targeting YBX1. *Cbm* 18, 1–9. doi:10.3233/cbm-160650

Halama, N., Zoernig, I., Berthel, A., Kahlert, C., Klupp, F., Suarez-Carmona, M., et al. (2016). Tumoral Immune Cell Exploitation in Colorectal Cancer Metastases Can Be Targeted Effectively by Anti-CCR5 Therapy in Cancer Patients. *Cancer cell* 29, 587–601. doi:10.1016/j.ccell.2016.03.005

Hänzelmann, S., Castelo, R., and Guinney, J. (2013). GSVA: Gene Set Variation Analysis for Microarray and RNA-Seq Data. *BMC bioinformatics* 14, 7. doi:10.1186/1471-2105-14-7

Hu, J. L., Wang, W., Lan, X. L., Zeng, Z. C., Liang, Y. S., Yan, Y. R., et al. (2019). CAFs Secreted Exosomes Promote Metastasis and Chemotherapy Resistance by Enhancing Cell Stemness and Epithelial-Mesenchymal Transition in Colorectal Cancer. *Mol. Cancer* 18, 91. doi:10.1186/s12943-019-1019-x

Huang, Y.-C., Lee, C.-T., Lee, J.-C., Liu, Y.-W., Chen, Y.-J., Tseng, J. T., et al. (2016). Epigenetic Silencing of miR-137 Contributes to Early Colorectal Carcinogenesis by Impaired Aurora-A Inhibition. *Oncotarget* 7, 76852–76866. doi:10.18632/oncotarget.12719

Jiang, G. M., Tan, Y., Wang, H., Peng, L., Chen, H. T., Meng, X. J., et al. (2019). The Relationship Between Autophagy and the Immune System and its Applications for Tumor Immunotherapy. *Mol. Cancer* 18, 17. doi:10.1186/s12943-019-0944-z

Johdi, N. A., and Sukor, N. F. (2020). Colorectal Cancer Immunotherapy: Options and Strategies. *Front. Immunol.* 11, 1624. doi:10.3389/fimmu.2020.01624

Kang, K., Xie, F., Mao, J., Bai, Y., and Wang, X. (2020). Significance of Tumor Mutation Burden in Immune Infiltration and Prognosis in Cutaneous Melanoma. *Front. Oncol.* 10, 573141. doi:10.3389/fonc.2020.573141

Kim, E. H., Shin, D., Lee, J., Jung, A. R., and Roh, J. L. (2018). CISD2 Inhibition Overcomes Resistance to Sulfasalazine-Induced Ferroptotic Cell Death in Head and Neck Cancer. *Cancer Lett.* 432, 180–190. doi:10.1016/j.canlet.2018.06.018

Koboldt, D. C., Zhang, Q., Larson, D. E., Shen, D., McLellan, M. D., Lin, L., et al. (2012). VarScan 2: Somatic Mutation and Copy Number Alteration Discovery in Cancer by Exome Sequencing. *Genome Res.* 22, 568–576. doi:10.1101/gr.129684.111

Korbecki, J., Olbromski, M., and Dzięgiel, P. (2020). CCL18 in the Progression of Cancer. *Int. J. Mol. Sci.* 21, 21. doi:10.3390/ijms21217955

Lane, D., Matte, I., Garde-Granger, P., Laplante, C., Carignan, A., Rancourt, C., et al. (2015). Inflammation-regulating Factors in Ascites as Predictive Biomarkers of Drug Resistance and Progression-free Survival in Serous Epithelial Ovarian Cancers. *BMC cancer* 15, 492. doi:10.1186/s12885-015-1511-7

Li, T., Fu, J., Zeng, Z., Cohen, D., Li, J., Chen, Q., et al. (2020). TIMER2.0 for Analysis of Tumor-Infiltrating Immune Cells. *Nucleic Acids Res.* 48, W509–W514. doi:10.1093/nar/gkaa407

Li, W., Lu, L., Lu, J., Wang, X., Yang, C., Jin, J., et al. (2020). cGAS-STING-mediated DNA Sensing Maintains CD8+ T Cell Stemness and Promotes Antitumor T Cell Therapy. *Sci. Transl Med.* 12. doi:10.1126/scitranslmed.aay9013

Liang, J., Tian, X.-F., and Yang, W. (2020). Effects of Long Non-coding RNA Opa-Interacting Protein 5 Antisense RNA 1 on Colon Cancer Cell Resistance to Oxaliplatin and its Regulation of microRNA-137. *Wjg* 26, 1474–1489. doi:10.3748/wjg.v26.i13.1474

Lin, P., Li, J., Ye, F., Fu, W., Hu, X., Shao, Z., et al. (2020). KCNN4 Induces Multiple Chemoresistance in Breast Cancer by Regulating BCL2A1. *Am. J. Cancer Res.* 10, 3302–3315. doi:10.1016/j.gene.2011.11.010

Liu, L., Chandrashekar, P., Zeng, B., Sanderford, M. D., Kumar, S., and Gibson, G. (2021). TreeMap: A Structured Approach to fine Mapping of eQTL Variants. *Bioinformatics (Oxford, England)* 37, 1125–1134. doi:10.1093/bioinformatics/btaa927

Liu, X., Shang, X., Li, J., and Zhang, S. (2021). The Prognosis and Immune Checkpoint Blockade Efficacy Prediction of Tumor-Infiltrating Immune Cells in Lung Cancer. *Front. Cel Dev. Biol.* 9, 707143. doi:10.3389/fcell.2021.707143

Liu, Y., Sethi, N. S., Hinoue, T., Schneider, B. G., Cherniack, A. D., Sanchez-Vega, F., et al. (2018). Comparative Molecular Analysis of Gastrointestinal Adenocarcinomas. *Cancer cell* 33, 721–735.e8. doi:10.1016/j.ccell.2018.03.010

Love, M. I., Huber, W., and Anders, S. (2014). Moderated Estimation of Fold Change and Dispersion for RNA-Seq Data with DESeq2. *Genome Biol.* 15, 550. doi:10.1186/s13059-014-0550-8

Luo, M., Wu, L., Zhang, K., Wang, H., Zhang, T., Gutierrez, L., et al. (2018). miR-137 Regulates Ferroptosis by Targeting Glutamine Transporter SLC1A5 in Melanoma. *Cell Death Differ* 25, 1457–1472. doi:10.1038/s41418-017-0053-8

Luo, R., Firat, E., Gaedicke, S., Guffart, E., Watanabe, T., and Niedermann, G. (2019). Cisplatin Facilitates Radiation-Induced Abscopal Effects in Conjunction with PD-1 Checkpoint Blockade Through CXCR3/CXCL10-Mediated T-Cell Recruitment. *Clin. Cancer Res.* 25, 7243–7255. doi:10.1158/1078-0432.ccr-19-1344

Lv, J., Zhu, Y., Ji, A., Zhang, Q., and Liao, G. (2020). Mining TCGA Database for Tumor Mutation Burden and Their Clinical Significance in Bladder Cancer. *Biosci. Rep.* 40, 40. doi:10.1042/BSR20194337

Ma, J., Dong, C., and Ji, C. (2010). MicroRNA and Drug Resistance. *Cancer Gene Ther.* 17, 523–531. doi:10.1038/cgt.2010.18

Mao, Y., Feng, Q., Zheng, P., Yang, L., Liu, T., Xu, Y., et al. (2018). Low Tumor Purity Is Associated with Poor Prognosis, Heavy Mutation Burden, and Intense Immune Phenotype in Colon Cancer. *Cmar* 10, 3569–3577. doi:10.2147/cmar.s171855

Mayakonda, A., Lin, D.-C., Assenov, Y., Plass, C., and Koeffler, H. P. (2018). Maftools: Efficient and Comprehensive Analysis of Somatic Variants in Cancer. *Genome Res.* 28, 1747–1756. doi:10.1101/gr.239244.118

Peng, W., Chen, J. Q., Liu, C., Malu, S., Creasy, C., Tetzlaff, M. T., et al. (2016). Loss of PTEN Promotes Resistance to T Cell-Mediated Immunotherapy. *Cancer Discov.* 6, 202–216. doi:10.1158/2159-8290.cd-15-0283

Ramakrishnan, R., Huang, C., Cho, H.-I., Lloyd, M., Johnson, J., Ren, X., et al. (2012). Autophagy Induced by Conventional Chemotherapy Mediates Tumor Cell Sensitivity to Immunotherapy. *Cancer Res.* 72, 5483–5493. doi:10.1158/0008-5472.can-12-2236

Robin, X., Turck, N., Hainard, A., Tiberti, N., Lisacek, F., Sanchez, J.-C., et al. (2011). pROC: An Open-Source Package for R and S+ to Analyze and Compare ROC Curves. *BMC bioinformatics* 12, 77. doi:10.1186/1471-2105-12-77

Sagara, A., Igarashi, K., Otsuka, M., Karasawa, T., Gotoh, N., Narita, M., et al. (2016). Intrinsic Resistance to 5-Fluorouracil in a Brain Metastatic Variant of Human Breast Cancer Cell Line, MDA-MB-231BR. *PloS one* 11, e0164250. doi:10.1371/journal.pone.0164250

Sakaguchi, M., Hisamori, S., Oshima, N., Sato, F., Shimono, Y., and Sakai, Y. (2016). miR-137 Regulates the Tumorigenicity of Colon Cancer Stem Cells through the Inhibition of DCLK1. *Mol. Cancer Res.* 14, 354–362. doi:10.1158/1541-7786.mcr-15-0380

Schumacher, T. N., Kesmir, C., and van Buuren, M. M. (2015). Biomarkers in Cancer Immunotherapy. *Cancer cell* 27, 12–14. doi:10.1016/j.ccell.2014.12.004

Shang, X., Li, J., Wang, H., Li, Z., Lin, j., Chen, D., et al. (2020). CMTM6 Is Positively Correlated with PD-L1 Expression and Immune Cells Infiltration in Lung Squamous Carcinoma. *Int. immunopharmacology* 88, 106864. doi:10.1016/j.intimp.2020.106864

Sirichanchuen, B., Pengsuparp, T., and Chanvorachote, P. (2012). Long-term Cisplatin Exposure Impairs Autophagy and Causes Cisplatin Resistance in Human Lung Cancer Cells. *Mol. Cel Biochem* 364, 11–18. doi:10.1007/s11010-011-1199-1

Smith, A. R., Marquez, R. T., Tsao, W.-C., Pathak, S., Roy, A., Ping, J., et al. (2015). Tumor Suppressive microRNA-137 Negatively Regulates Musashi-1 and Colorectal Cancer Progression. *Oncotarget* 6, 12558–12573. doi:10.18632/oncotarget.3726

Subramanian, A., Tamayo, P., Mootha, V. K., Mukherjee, S., Ebert, B. L., Gillette, M. A., et al. (2005). Gene Set Enrichment Analysis: A knowledge-Based Approach for Interpreting Genome-wide Expression Profiles. *Proc. Natl. Acad. Sci.* 102, 15545–15550. doi:10.1073/pnas.0506580102

Sung, H., Ferlay, J., Siegel, R. L., Laversanne, M., Soerjomataram, I., Jemal, A., et al. (2021). Global Cancer Statistics 2020: GLOBOCAN Estimates of Incidence and Mortality Worldwide for 36 Cancers in 185 Countries. *CA A. Cancer J. Clin.* 71, 209–249. doi:10.3322/caac.21660

Swanson, D. M., Lien, T., Bergholtz, H., Sørlie, T., and Frigessi, A. (2019). A Bayesian Two-way Latent Structure Model for Genomic Data Integration Reveals Few Pan-Genomic Cluster Subtypes in a Breast Cancer Cohort. *Bioinformatics (Oxford, England)* 35, 4886–4897. doi:10.1093/bioinformatics/btz381

Thorsson, V., Gibbs, D. L., Brown, S. D., Wolf, D., Bortone, D. S., Ou Yang, T. H., et al. (2018). The Immune Landscape of Cancer. *Immunity* 48, 812–e14. doi:10.1016/j.immuni.2018.03.023

Unver, N. (2021). Cancer Stemness as a Target for Immunotherapy Is Shaped by Proinflammatory Stress. *Cscr* 16, 792–800. doi:10.2174/1574888x15666200309145901

Vogler, M. (2012). BCL2A1: the Underdog in the BCL2 Family. *Cel Death Differ* 19, 67–74. doi:10.1038/cdd.2011.158

Wakita, D., Iwai, T., Harada, S., Suzuki, M., Yamamoto, K., and Sugimoto, M. (2019). Cisplatin Augments Antitumor T-Cell Responses Leading to a Potent Therapeutic Effect in Combination with PD-L1 Blockade. *Anticancer Res.* 39, 1749–1760. doi:10.21873/anticanres.13281

Wang, H., Wu, X., and Chen, Y. (2019). Stromal-Immune Score-Based Gene Signature: A Prognosis Stratification Tool in Gastric Cancer. *Front. Oncol.* 9, 1212. doi:10.3389/fonc.2019.01212

Wang, J. J., Lei, K. F., and Han, F. (2018). Tumor Microenvironment: Recent Advances in Various Cancer Treatments. *Eur. Rev. Med. Pharmacol. Sci.* 22, 3855–3864. doi:10.26355/eurrev_201806_15270

Wang, W., Green, M., Choi, J. E., Gijón, M., Kennedy, P. D., Johnson, J. K., et al. (2019). CD8+ T Cells Regulate Tumour Ferroptosis During Cancer Immunotherapy. *Nature* 569, 270–274. doi:10.1038/s41586-019-1170-y

Wang, Z.-C., Huang, F.-Z., Xu, H.-B., Sun, J.-C., and Wang, C.-F. (2019). MicroRNA-137 Inhibits Autophagy and Chemosensitizes Pancreatic Cancer Cells by Targeting ATG5. *Int. J. Biochem. Cel Biol.* 111, 63–71. doi:10.1016/j.biocel.2019.01.020

Wu, M., Li, X., Zhang, T., Liu, Z., and Zhao, Y. (2019). Identification of a Nine-Gene Signature and Establishment of a Prognostic Nomogram Predicting Overall Survival of Pancreatic Cancer. *Front. Oncol.* 9, 996. doi:10.3389/fonc.2019.00996

Xia, H., Green, D. R., and Zou, W. (2021). Autophagy in Tumour Immunity and Therapy. *Nat. Rev. Cancer* 21, 281–297. doi:10.1038/s41568-021-00344-2

Xu, S., Tao, Z., Hai, B., Liang, H., Shi, Y., Wang, T., et al. (2016). miR-424(322) Reverses Chemoresistance via T-Cell Immune Response Activation by Blocking the PD-L1 Immune Checkpoint. *Nat. Commun.* 7, 11406. doi:10.1038/ncomms11406

Xu, Y., Wang, C., Zhang, Y., Jia, L., and Huang, J. (2015). Overexpression of MAGE-A9 Is Predictive of Poor Prognosis in Epithelial Ovarian Cancer. *Sci. Rep.* 5, 12104. doi:10.1038/srep12104

Yajima, T., Ochiai, H., Uchiyama, T., Takano, N., Shibahara, T., and Azuma, T. (2009). Resistance to Cytotoxic Chemotherapy-Induced Apoptosis in Side Population Cells of Human Oral Squamous Cell Carcinoma Cell Line Ho-1-N-1. *Int. J. Oncol.* 35, 273–280. doi:10.3892/ijo_00000337

Yoshihara, K., Shahmoradgoli, M., Martínez, E., Vegesna, R., Kim, H., Torres-Garcia, W., et al. (2013). Inferring Tumour Purity and Stromal and Immune Cell Admixture from Expression Data. *Nat. Commun.* 4, 2612. doi:10.1038/ncomms3612

Yu, B., You, W., Chen, G., Yu, Y., and Yang, Q. (2019). MiR-140-5p Inhibits Cell Proliferation and Metastasis by Regulating MUC1 via BCL2A1/MAPK Pathway in Triple Negative Breast Cancer. *Cell Cycle* 18, 2641–2650. doi:10.1080/15384101.2019.1653107

Yu, G., Wang, L. G., Han, Y., and He, Q. Y. (2012). clusterProfiler: an R Package for Comparing Biological Themes Among Gene Clusters. *OMICS: A J. Integr. Biol.* 16, 284–287. doi:10.1089/omi.2011.0118

Zeng, D., Ye, Z., Wu, J., Zhou, R., Fan, X., Wang, G., et al. (2020). Macrophage Correlates with Immunophenotype and Predicts Anti-PD-L1 Response of Urothelial Cancer. *Theranostics* 10, 7002–7014. doi:10.7150/thno.46176

Zhang, C., Cheng, W., Ren, X., Wang, Z., Liu, X., Li, G., et al. (2017). Tumor Purity as an Underlying Key Factor in Glioma. *Clin. Cancer Res.* 23, 6279–6291. doi:10.1158/1078-0432.ccr-16-2598

Zhou, N., and Bao, J. (2020). FerrDb: A Manually Curated Resource for Regulators and Markers of Ferroptosis and Ferroptosis-Disease Associations. *Database (Oxford)* 2020, 2020. doi:10.1093/database/baaa021

Conflict of Interest: The authors declare that the research was conducted in the absence of any commercial or financial relationships that could be construed as a potential conflict of interest.

Publisher's Note: All claims expressed in this article are solely those of the authors and do not necessarily represent those of their affiliated organizations, or those of the publisher, the editors and the reviewers. Any product that may be evaluated in this article, or claim that may be made by its manufacturer, is not guaranteed or endorsed by the publisher.

Copyright © 2022 Yue, Liu, Zuo, Zhu, Li, Liu, Chen and Wang. This is an open-access article distributed under the terms of the Creative Commons Attribution License (CC BY). The use, distribution or reproduction in other forums is permitted, provided the original author(s) and the copyright owner(s) are credited and that the original publication in this journal is cited, in accordance with accepted academic practice. No use, distribution or reproduction is permitted which does not comply with these terms.

frontiers in Cell and Developmental Biology

ORIGINAL RESEARCH
published: 03 March 2022
doi: 10.3389/fcell.2022.828916

Siglec Receptors Modulate Dendritic Cell Activation and Antigen Presentation to T Cells in Cancer

*Jinyu Wang[1], Michela Manni[1], Anne Bärenwaldt[1], Ronja Wieboldt[1], Nicole Kirchhammer[1], Robert Ivanek[1,2], Michal Stanczak[1], Alfred Zippelius[1,3], David König[1,3], Natalia Rodrigues Manutano[1] and Heinz Läubli[1,3]**

[1]Department of Biomedicine, University Hospital and University of Basel, Basel, Switzerland, [2]Swiss Institute of Bioinformatics, Basel, Switzerland, [3]Division of Oncology, Department of Theragnostic, University Hospital Basel, Basel, Switzerland

Interactions between sialylated glycans and sialic acid-binding immunoglobulin-like lectin (Siglec) receptors have been recently described as potential new immune checkpoint that can be targeted to improve anticancer immunity. Myeloid cells have been reported to express a wide range of different Siglecs; however, their expression and functions on cancer-associated dendritic cells (DCs) were not fully characterized. We found that classical conventional DCs (cDCs) from cancer patient samples have a high expression of several inhibitory Siglecs including Siglec-7, Siglec-9, and Siglec-10. In subcutaneous murine tumor models, we also found an upregulation of the inhibitory Siglec-E receptor on cancer-associated cDCs. DC lines and bone marrow-derived DCs (BMDCs) with expression of these inhibitory Siglecs showed impaired maturation states on transcriptome and protein level. Furthermore, ablation of these inhibitory Siglecs from DCs enhanced their capability to prime antigen-specific T cells and induce proliferation. Our work provides a deeper understanding of the influence of inhibitory Siglecs on DCs and reveals a potential new target to improve cancer immunotherapy.

Keywords: sialic acid, tumor immunology, glyco-immune checkpoint, antigen, antigen processing

OPEN ACCESS

Edited by:
Qian Xiao,
Rutgers Cancer Institute of New Jersey, United States

Reviewed by:
Sjoerd Schetters,
Flanders Institute for Biotechnology, Belgium
Ling Ni,
Tsinghua University, China

****Correspondence:***
Heinz Läubli
heinz.laeubli@unibas.ch

Specialty section:
This article was submitted to Molecular and Cellular Pathology, a section of the journal Frontiers in Cell and Developmental Biology

Received: *04 December 2021*
Accepted: *21 January 2022*
Published: *03 March 2022*

Citation:
Wang J, Manni M, Bärenwaldt A, Wieboldt R, Kirchhammer N, Ivanek R, Stanczak M, Zippelius A, König D, Rodrigues Manutano N and Läubli H (2022) Siglec Receptors Modulate Dendritic Cell Activation and Antigen Presentation to T Cells in Cancer. Front. Cell Dev. Biol. 10:828916. doi: 10.3389/fcell.2022.828916

INTRODUCTION

The treatment of cancer with immune checkpoint inhibitors (ICI) has significantly improved the prognosis of cancer patients (Topalian et al., 2015; Zou et al., 2016; Chen and Mellman, 2017; Ribas and Wolchok, 2018). However, most patients respond only shortly or not at all to ICI treatment. Therefore, a better understanding of immunosuppression status during cancer progression is of importance for enhanced therapeutic efficacy. Tumor cell hypersialylation has been reported as one of the tumor-intrinsic factors dampening anti-tumor immunity (Fraschilla and Pillai, 2017). Aberrant glycosylation status in the tumor micro-environment (TME) is associated with tumor invasion and metastasis (Hakomori, 1996). Sialoglycans derived from altered glycosylation can be recognized by inhibitory sialic acid-binding immunoglobulin-like lectins (Siglecs), characterized by their intracellular immunoreceptor tyrosine-based inhibitory motifs (ITIM) (Crocker et al., 2007; Macauley et al., 2014; Nitschke, 2014; Varki et al., 2015; Pearce and Läubli, 2016). Cancer cells are reported to exploit this mechanism as a survival strategy, through overexpression of sialyltransferases, scavenging of food-derived Neu5Gc, or expression of 9-O-acetyl-GD3 (Tangvoranuntakul et al., 2003; Kniep et al., 2006; Hedlund et al., 2008; Pearce and Läubli, 2016).

Recent studies demonstrated that several inhibitory Siglecs are involved in immunosuppression of T cells, NK cells, neutrophils, and macrophages (Läubli et al., 2014a; Läubli et al., 2014b; Hudak et al., 2014; Jandus et al., 2014; Beatson et al., 2016; Stanczak et al., 2018; Barkal et al., 2019; Wang et al., 2019). Dendritic cells (DCs) play a central role as antigen-presenting cells in the tumor tissue and draining lymph nodes to prime tumor-specific T cell response (Broz et al., 2014; Roberts et al., 2016; Salmon et al., 2016; Spranger et al., 2017; Binnewies et al., 2019). Previous reports have demonstrated that Siglec receptors can impact DC function (Ding et al., 2016; Perdicchio et al., 2016; Silva et al., 2016). For example, inhibitory Siglec-G on DCs has been linked to inhibition of antigen cross-presentation in murine models (Ding et al., 2016). Moreover, interactions of sialic acid-containing carbohydrates on antigens with Siglec-E can modulate DC activation (Perdicchio et al., 2016). However, the expression and function of inhibitory Siglecs on cancer-associated DCs is still not well understood. Here, we study the expression of human and murine Siglec receptors in cancer and the functional implication of such receptors on DCs.

MATERIALS AND METHODS

Patient Samples

The local ethics committee in Basel, Switzerland, approved the sample collection and the use of the corresponding clinical data (Ethikkommission Nordwestschweiz, EKNZ, Basel Stadt, Switzerland, EKNZ 2018-01990). Informed consent was obtained from all patients prior to sample collection. Tumor samples were collected locally at the University Hospital Basel, digested, and processed, and single-cell suspensions were frozen. Human peripheral blood mononuclear cells (PBMCs) were isolated by density gradient centrifugation from buffy coats obtained from University Hospital Basel. Single-cell suspension of PBMCs were frozen in liquid nitrogen.

Animal Strains

Siglec-E^{flox} mice were generated in collaboration with Biocytogen Company and crossed with CD11c-cre mice kindly provided by Prof. Daniela Finke. Siglec-E systemic knockout (EKO) mice was obtained from the group of Prof. Ajit Varki. Siglec-9 transgenic mice were previously reported (Läubli et al., 2014b). To generate a high frequency of Siglec-9-expressing mouse bone marrow-derived DCs (BMDCs), Siglec-9^{flox} mice were crossed with XCR1-cre mice. All mouse experiments were approved by the local ethics committee (Basel Stadt, Switzerland) and performed in accordance with the Swiss federal regulations.

Cell Lines

Mouse colorectal cancer cell line MC38 was kindly provided by our collaborator from Hannover. tdTomato-expressing MC38 cell line was generated by our lab through lentiviral transduction, with the Luc2-tdTomato plasmid kindly provided by Prof. Gregor Hutter. OVA-expressing MC38 (MC38-OVA) cell line was kindly provided by Prof. Mark Smyth. Chinese Hamster Ovary cell line with FMS-like tyrosine kinase 3 ligand secretion capability (CHO-Flt3L) was kindly provided by Dr. Panagiotis Tsapogas. Mouse immature dendritic cell line Sp37A3 was kindly provided by Merck KGaA.

Cell Line Culture

Mouse cancer cell lines were maintained in Dulbecco's Modified Eagle Medium (Sigma, United States) supplemented with 10% heat-inactivated fetal bovine serum (PAA Laboratories, Germany), 1 mM sodium pyruvate (Gibco, United States), 1× MEM non-essential amino acid solution (Sigma, United States), and 100 μg/ml streptomycin and 100 U/ml penicillin (Gibco, United States).

CHO-Flt3L cells were maintained in Iscove's Modified Dulbecco's Medium (Sigma, United States) supplemented with 5% heat-inactivated fetal bovine serum (PAA Laboratories, Germany).

Sp37A3 mouse dendritic cell line and relative genetically modified lines were maintained in Iscove's Modified Dulbecco's Medium (Sigma, United States) supplemented with 10% heat-inactivated fetal bovine serum (PAA Laboratories, Germany), 1 mM sodium pyruvate (Gibco, United States), 1× MEM non-essential amino acid solution (Sigma, United States), 100 μg/ml streptomycin and 100 U/ml penicillin (Gibco, United States), 0.05 mM 2-mercaptoethanol (Gibco, United States), 20 ng/ml recombinant mouse GM-CSF (Peprotech, United Kingdom), and 20 ng/ml recombinant mouse M-CSF (Peprotech, United Kingdom).

Mice Primary Bone Marrow Cell Culture

Mouse BMDCs were generated by plating five million bone marrow cells freshly isolated from the tibia and femur into 10-cm dishes. During the 7-day cultivation, the bone marrow cells were maintained in RPMI-1640 Medium (Sigma, United States) supplemented with 10% heat-inactivated fetal bovine serum (PAA Laboratories, Germany), 1 mM sodium pyruvate (Gibco, United States), 1× MEM non-essential amino acid solution (Sigma, United States), 100 μg/ml streptomycin and 100 U/ml penicillin (Gibco, United States), 0.05 mM 2-mercaptoethanol (Gibco, United States), and 10 ng/ml mouse GM-CSF (Peprotech, United Kingdom) in several first experiments.

Animal Tumor Models

For tumor-bearing mice experiments, 7–12 weeks old mice were used. Then, 5×10^5 tumor cells were injected subcutaneously into the right thoracic flank. Tumor size and health score were measured and monitored three times per week. Perpendicular tumor diameters were measured by a caliper and tumor volume calculated according to the following formula: tumor volume = $(d^2 \times D)/2$, where d and D represent the shortest and longest diameters of the tumors (in millimeter), respectively. For tumor growth experiments, mice were sacrificed once tumor size reached 1,500 mm^3. For tumor-infiltrating DC phenotype and functionality experiments, mice were sacrificed once tumor size reached 300–500 mm^3.

Tumor Digests and PBMC Isolation

For the preparation of single-cell suspensions from both human and mouse tumors, tumors were collected, and surgical specimens were mechanically dissociated and subsequently digested using accutase (PAA Laboratories, Germany), collagenase IV (Worthington, United States), hyaluronidase (Sigma, United States), and DNase type IV (Sigma, United States) for 1 h at 37°C under constant agitation. Cell suspensions were filtered through 70-μm mesh twice and lysed for red blood cells using RBC lysis buffer (eBioscience, United States). PBMCs were isolated by density gradient centrifugation using Histopaque-1077 (Sigma, United States) from buffy coats. Mice splenocytes were isolated by mechanical disruption using the end of a 1-ml syringe, lysed for red blood cells using RBC lysis buffer, then digested with Collagenase D (Roche, Switzerland) and DNase I (Roche, Switzerland). Samples were either used directly or frozen (in 90% FBS, 10% DMSO) and stored in liquid nitrogen until the time of analysis.

Generation of Siglec-E Knockout Sp37A3 Cells

Siglec-E-deficient Sp37A3 cells were generated by using CRISPR/Cas9-mediated gene editing. Guide RNAs were designed online based on published data (http://greenlisted.cmm.ki.se/). Guide RNAs with the following sequences were synthesized by Microsynth (Switzerland): forward: 5′—CAC CGG AGG GTC AGA ACC CCC AAG—3′; reverse: 5′—AAA CCT TGG GGG TTC TGA CCC TCC—3′. Then, they were cloned into the lentiCRISPRv2 puro vector (Addgene plasmid #98290). Lentivirus with empty vectors or modified vectors were used to transduce the original Sp37A3 cell line. Single-cell clones with right phenotype were sorted into 96-well plates. After their recovery and expansion, individual clones were screened again for Siglec-E expression. Multiple clones were selected and pooled to avoid clonal selection.

Genetically Modified Sp37A3 Cell RNA Sequencing Analysis

Control empty vector-transduced (CtrV) and EKO Sp37A3 cells were taken from culture. Then, 1×10^6 cells were seeded in six-well plates and pulsed with 0.1 mg/ml EndoFit Ovalbumin (Invivogen, United States) for 2 h. Then, cells were washed and stimulated for maturation by 0.1 ug/ml lipopolysaccharides (Sigma, United States) for 24 h. Cells were washed, and RNA samples were prepared by RNeasy Plus Micro Kit (Qiagen, Germany). The cDNA library was prepared, and next-generation sequencing of the library and data analysis was performed *n*th. Reads were aligned to the mouse genome (UCSC version mm10) with STAR (version 2.7.0c) with default parameters except for allowing up to 10 genome hits (outFilterMultimapNmax 10), reporting only one location for hits with equal score (outSAMmultNmax 1), and for filtering reads without evidence in spliced junction table (outFilterType "BySJout"). The output was sorted and indexed with SAMtools (v 1.9). Read and alignment quality was evaluated using the qQCReport function of the Bioconductor package QuasR (v 1.30.0). The featureCounts function from Bioconductor package Rsubread (v 2.4.3) was used to count the number of reads (5′ ends) overlapping with the exons of each gene assuming an exon union model (with used gene model provided by Ensembl v101). The data were normalized by applying the TMM method from Bioconductor edgeR package (version 3.32.1). Only genes having log2 CPM counts bigger than 0 in at least two samples were kept for further analyses. The principal component analysis was based on 25% of most variable genes in the dataset. The differentially expressed genes were identified using the quasi-likelihood (QL) method implemented in edgeR package (version 3.32.1) using replicate ID as covariate. Genes with FDR smaller than . . . and minimum log2 fold change of . . . were used and considered as differentially expressed.

Neuraminidase Treatment and Maturation Analysis

CtrV and EKO Sp37A3 cells were seeded and stimulated for 24 h with sialidase. Prior to the stimulation, CtrV and EKO Sp37A3 cells were treated with 10 mU/ml neuraminidase from *Vibrio cholerae* (VCN, Sigma) for 30 min. Maturation was measured by analysis of MHC II expression.

CtrV and EKO Sp37A3 Cell Cytokine/Chemokine Array Analysis

CtrV and EKO Sp37A3 cells were seeded and pulsed. After 36 h of LPS stimulation, culture supernatant was collected, frozen, and sent in dry ice for a 44-plex Cytokine/Chemokine Array test (Eve Technologies, Canada). Cytokine and chemokine concentrations were analyzed and presented by Eve Technologies (Canada).

DC and Antigen-Specific T Cell Co-Culture

BMDCs or Sp37A3 cells were seeded 4×10^4 cells per well in 96-well plate. Then, cells were pulsed with 0.1 mg/ml OVA protein (Invivogen, United States) or left unpulsed for 2 h. DCs were washed and stimulated by 0.1 μg/ml LPS for overnight. OVA antigen-specific OT-I $CD8^+$ T cells and OT-II $CD4^+$ T cells were isolated from spleens of indicated mice, respectively, by MACS (Stemcell, Canada). T cells were labelled with CellTrace Violet (CTV, Invitrogen, United States) and added into wells, at 2×10^5 cells per well. T cell activation and proliferation was checked after certain timepoints as described in each experiment.

Multicolor Flow Cytometry

For multicolor flow cytometry, dead cells and doublets were excluded in all analyses (also **Supplementary Figure S1**). Corresponding isotype antibodies or fluorescence-minus-one (FMO) samples were used as a control, in particular for the Siglec stainings. All tumor samples were analyzed with a Fortessa LSR II flow cytometer (BD Biosciences). For infiltration analysis, mice were euthanized, and tumors were mechanically dissociated and digested as described for the human sample preparation.

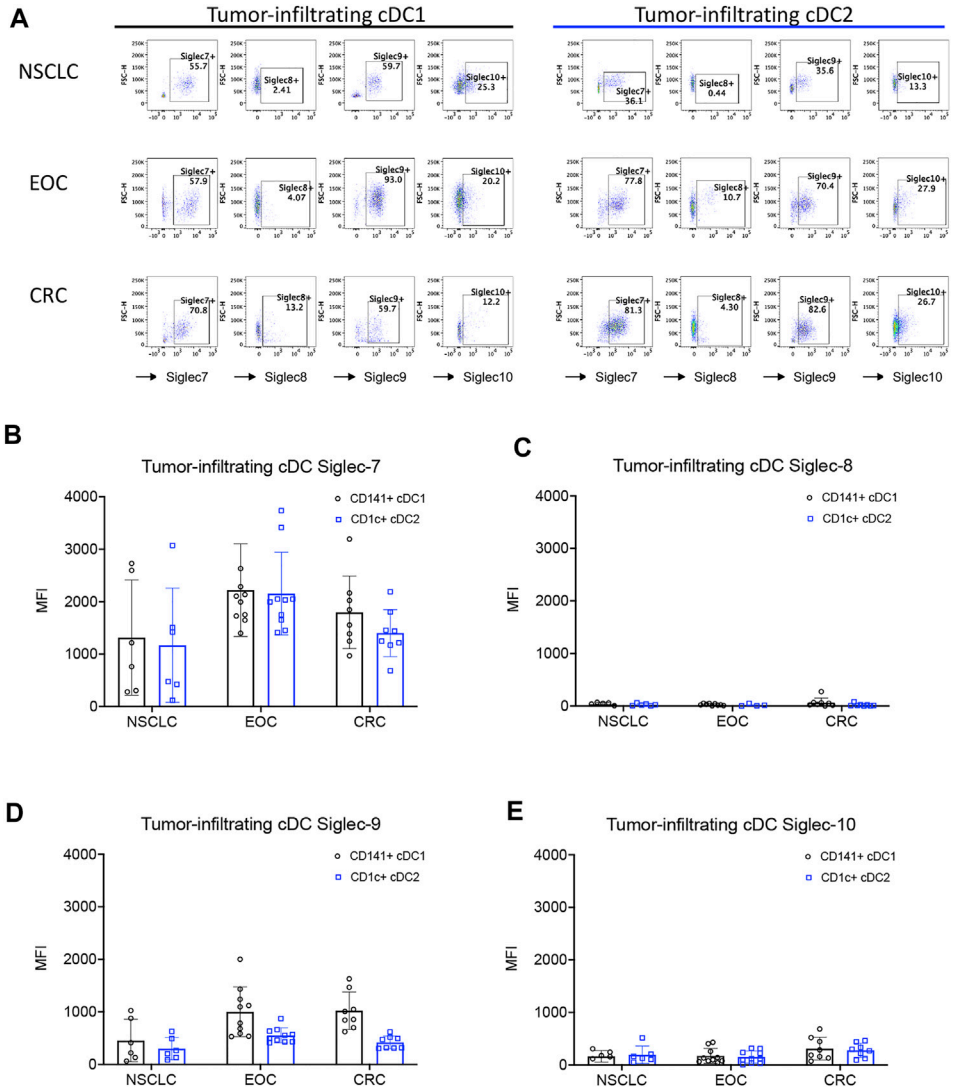

FIGURE 1 | Expression of inhibitory Siglecs on human tumor-infiltrating DCs. **(A)** Representative examples of Siglec receptor expression determined by flow cytometry on different cDC subsets from primary patient samples. **(B–E)** The expression levels of inhibitory Siglecs on DCs from primary tumor samples of patients with non-small cell lung cancer (NSCLC), epithelial ovarian cancer (EOC), and colorectal cancer (CRC). Data are presented as mean ± SD.

Statistical Analysis

Statistical analysis was performed using Prism 9 (GraphPad, United States). Different comparison strategies were indicated in each specific figure respectively.

RESULTS

Tumor-infiltrating conventional dendritic cells express inhibitory Siglec receptors in humans.

Previous reports have shown that Siglec receptors are expressed on myeloid cells, including cDCs (Chen et al., 2009; Ding et al., 2016; Fraschilla and Pillai, 2017; Barenwaldt and Laubli, 2019; Ruffin et al., 2019). However, the expression and functions of these receptors on intratumoral cDCs from patients with different types of cancer are poorly understood. Therefore, we tested the expression of several inhibitory Siglec receptors on tumor-infiltrating conventional DCs (Ti-cDCs) from different types of cancers including epithelial ovarian cancer (EOC), non-small cell lung cancer (NSCLC), and colorectal cancer (CRC) by flow cytometry (**Figure 1A** and **Supplementary Figures S1A, S2**). We found a significant proportion of both type 1 and type 2 cDC-expressing inhibitory Siglec receptors. Across the different cancer types tested, Siglec-7 and Siglec-9 were consistently expressed by a higher percentage of Ti-cDCs compared to other Siglecs. Siglec-10 showed low to intermediate expression levels on Ti-cDCs, while Siglec-8 expression was even less frequent. The results of geometric mean fluorescence intensity (MFI) for each inhibitory Siglecs also revealed higher expression levels of Siglec-7 and Siglec-9 compared to the other two Siglecs

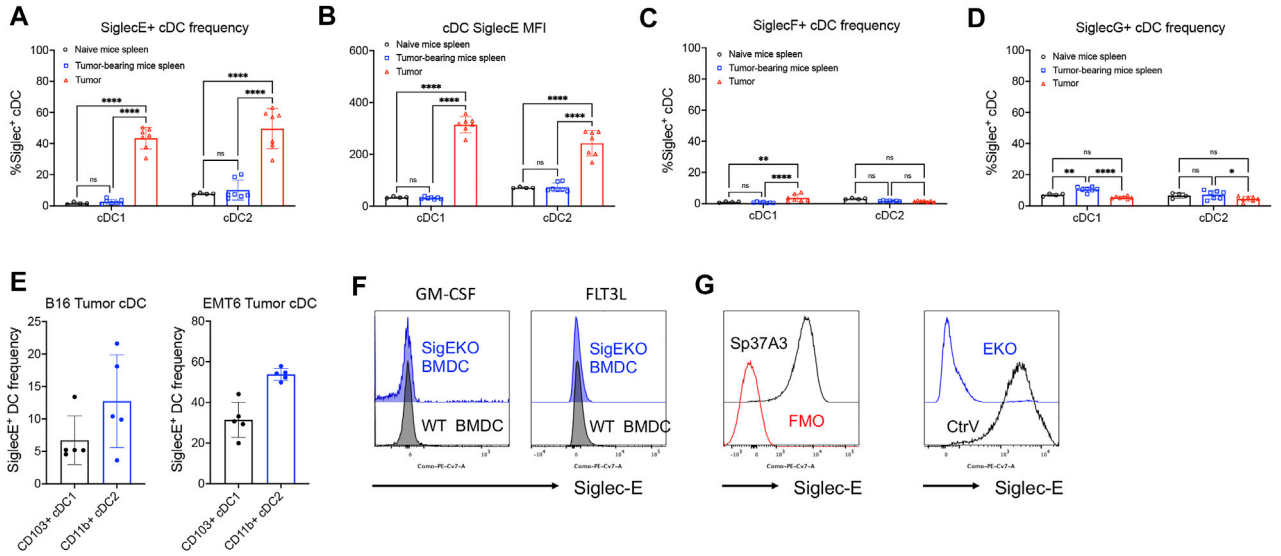

FIGURE 2 | Inhibitory Siglec-E expression is significant on mouse tumor-associated DCs. **(A–D)** The expression patterns of several murine inhibitory Siglecs on cDCs isolated from naive C57BL/6 mice spleens, MC38 tumor-bearing mouse spleens, and primary subcutaneous tumors were analyzed by flow cytometry. **(A)** SiglecE + cDC frequency, **(B)** SiglecE MFI, **(C)** SiglecF + cDC frequency, and **(D)** SiglecG + cDC frequency. **(E)** Siglec-E expression on tumor cDC subsets from B16 melanoma and EMT6 breast cancer mouse models. **(F)** Siglec-E expression of BMDCs from wildtype (WT, black line) and systemic Siglec-E knockout (EKO, blue line) mice after 7-day *in vitro* culture supplemented with GM-CSF or FLT3L. **(G)** The expression of Siglec-E on Sp37A3 cell line (black line) versus FMO control (red line). Siglec-E expression of Siglec-E knockout (EKO) Sp37A3 cells and empty control vector (CtrV)-transduced Sp37A3 cells. Data are presented as mean ± SD, and two-way ANOVA was used for two-way comparisons (*$p < 0.0332$, **$p < 0.0021$, ***$p < 0.0002$, and ****$p < 0.0001$).

(**Figures 1B–E**; **Supplementary Figures S1, S2**). Similar expression patterns of these Siglec receptors were also observed on plasmacytoid dendritic cells (pDCs), although to a lower percentage (**Supplementary Figure S3**). Taken together, this data demonstrates that inhibitory Siglecs are expressed on human cancer-associated DCs and could be potentially involved in the regulation of these cells.

Siglec-E Expression Is Upregulated on Intratumoral DCs

To further investigate the function of Siglec receptors on cDCs during cancer progression, we next analyzed the expression of several inhibitory Siglec receptors in mice. DCs were isolated from the spleen of healthy C57BL/6 wildtype mice or from the spleen and tumor tissue of MC38 tumor-bearing mice. The expression of inhibitory Siglec-E, -F, and -G was analyzed by flow cytometry (**Figures 2A–D**; **Supplementary Figure S4**). We observed that these inhibitory Siglecs were only expressed by very small proportions of spleen cDCs from either naïve mice or MC38 subcutaneous tumor-bearing mice. However, Siglec-E expression, but not Siglec-F and Siglec-G, was quite pronounced on both Ti-cDC subsets, suggesting a unique role of this molecule on DC biology or functions during tumor progression (**Figures 2A,B**). The expression of Siglec-E on Ti-cDCs was also confirmed in two other murine tumor models, including the B16 melanoma and the EMT6 breast cancer model in C57BL/6 and BALB/c mice, respectively (**Figures 2E,F**).

Siglec-E-Deficient DCs Are More Responsive to Stimulation

To explore the possible function of Siglec-E expression on DCs in an *in vitro* system, we next analyzed the expression of Siglec-E on BMDC. Neither GM-CSF- nor FLT3L-derived BMDC expressed significant Siglec-E levels as compared to cells derived from Siglec-E-deficient mice (**Figure 2G**). We then screened several murine DC cell lines for Siglec-E expression. Among them, an immature DC cell line Sp37A3, generated from C57BL/6 mouse spleen (Bros et al., 2007), showed significant expression of Siglec-E (**Figure 2H**). Thus, we next used a CRISPR-Cas9-based lentivirus transduction system to deplete *Siglece* in Sp37A3 cells (EKO Sp37A3 cells). After pooling several single clones that were confirmed to have minimal or no Siglec-E expression, we successfully generated EKO Sp37A3 line, along with an empty CtrV Sp37A3 line (**Figure 2H**). We then directly explored whether Siglec-E influences DC activation and maturation. We first analyzed markers of DC maturation on the newly generated CtrV Sp37A3 and EKO Sp37A3 cell lines. The DC phenotypic maturation markers we investigated, including MHC-I, MHC-II, and CD40, all showed significant upregulation on EKO Sp37A3 cells compared to the Siglec-E-expressing Sp37A3 cells (**Figures 3A–C**). We further investigated how treatment with neuraminidase influences activation of CtrV Sp37A3 and EKO Sp37A3 cell lines. Indeed, desialylation led to an increased maturation and MHC II expression on the DC cell lines (**Figure 3D**). To confirm these findings *in vivo*, we generated $CD11c^{cre}SigE^{flox/flox}$ mice (ELOX mice) that display specific

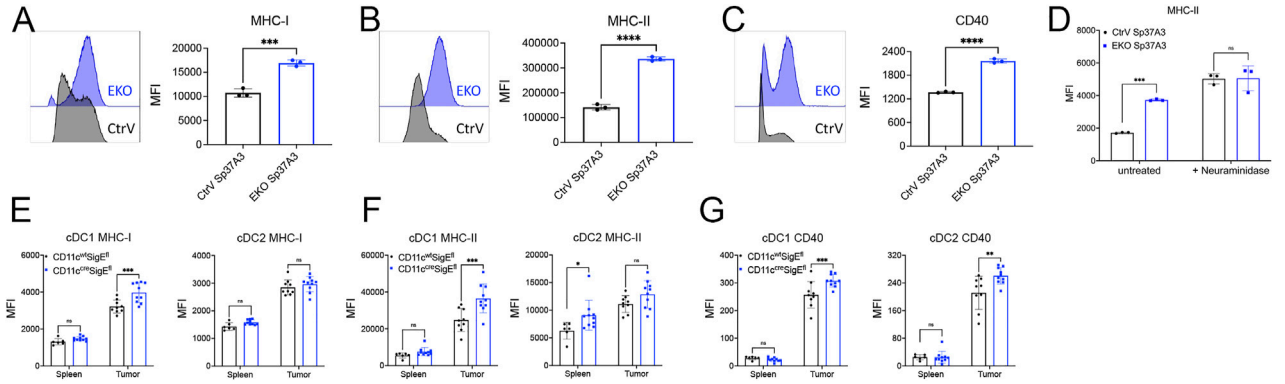

FIGURE 3 | Siglec-E-deficient DCs showed enhanced phenotypic maturation. **(A–C)** Flow cytometry analysis of the expression levels of several DC maturation markers on CtrV Sp37A3 cells (black) and EKO Sp37A3 cells (blue), including MHC-I **(A)**, MHC-II **(B)**, and CD40 **(C)**. **(D)** treatment of CtrV Sp37A3 cells (black) and EKO Sp37A3 cells (blue) with neuraminidase and maturation with LPS was measured by the expression of MHC II. **(E–G)** Maturation markers on spleen and tumor-infiltrating cDCs isolated from MC38 subcutaneous tumor models of CD11c^{cre}SigE^{fl} mice (blue) and littermates (CD11c^{wt}SigE^{fl}, black) by flow cytometry. Data are presented as mean (±SD). Two-way ANOVA was used for two-way comparisons, and unpaired *t* test was used for one-way comparisons (*$p < 0.0332$, **$p < 0.0021$, ***$p < 0.0002$, and ****$p < 0.0001$).

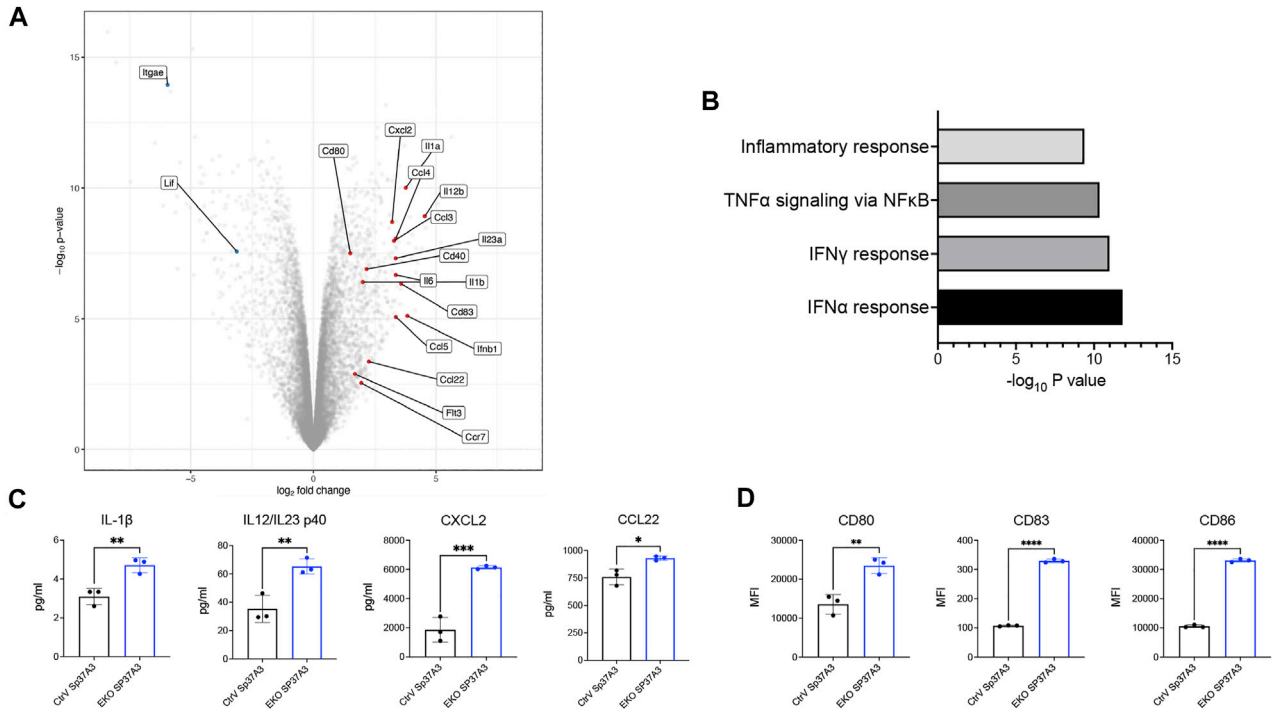

FIGURE 4 | Siglec-E-deficient DCs showed elevated maturation status upon stimulation. **(A)** Volcano plot of differentially expressed genes between EKO SP37A3 and CtrV Sp37A3 cells. **(B)** GSEA of the most significantly activated pathways in EKO Sp37A3 cells. **(C)** Cytokine and chemokine production and **(D)** activator and co-stimulatory markers of CtrV (black) and EKO (blue) Sp37A3 cells. Data are presented as mean (±SD), and unpaired *t* test was used for one-way comparisons (*$p <$ 0.0332, **$p < 0.0021$, ***$p < 0.0002$, and ****$p < 0.0001$).

SiglecE deficiency from the CD11c-expressing cells with the cre recombinase, affecting mainly cDCs. As expected, naïve spleen cDCs from ELOX mice and their littermates do not show significant differences in maturation (**Supplementary Figure S5**). However, similar to the *in vitro* data, intratumoral cDCs showed a significant increase of MHC-I, MHC-II, and CD40 markers on tumor-infiltrating cDC1 cells lacking Siglec-E compared to cDC1 cells from littermate control mice (**Figures 3D–F**). Only CD40 was significantly increased in cDC2 from ELOX mice but not MHC-I and MHC-II (**Figures 3D–F**). Taken

together, our newly generated Sp37A3 cell lines appeared to be appropriate models to study the roles of Siglec-E on cDCs.

Siglec-E Regulates DC Activation and Cytokine Secretion

As Sp37A3 cell line was reported as an immature cell line (Bros et al., 2007), we next investigated how our newly generated cell lines respond to antigen and maturation stimuli. We compared the transcriptional profile of OVA-pulsed, LPS-stimulated CtrV and EKO Sp37A3 by bulk RNA sequencing. The EKO Sp37A3 cells upregulated the mRNA levels of co-stimulatory molecules, multiple chemokines, and cytokines including CD80, CD40, CCL2, CCL4, CCL5, and IL-23 (**Figure 4A**). Gene Set Enrichment Analysis (GSEA) suggests that several pathways were differentially activated in cells lacking Siglec-E (**Figure 4B**). In particular, EKO Sp37A3 cells showed stronger upregulation of type I and II interferon (IFN-α and IFN-γ)-related responses, tumor necrosis factor alpha (TNF-α) response, and general inflammatory response (**Figure 4B**). To validate these findings at protein level, we collected cell culture supernatants of OVA-pulsed, LPS-stimulated Sp37A3 cells and performed a Mouse Cytokine/Chemokine Array assay. Among the 44 cytokines and chemokines, the levels of interleukin (IL)-1β, IL-12, or IL-23 p40 subunit (IL12/IL23 p40); CXCL2; and CCL22 showed different secretion patterns between the two Sp37A3 lines (**Figure 4C** and **Supplementary Figure, S6A,B**). Similar to the *in vitro* and *in vivo* data, analysis of the surface maturation markers and co-stimulatory molecules on protein level also showed that EKO Sp37A3 cells showed and increased activation profile compared to CtrV Sp37A3 cells (**Figure 4D** and **Supplementary Figure S6C**). Taken together, these results indicate that the EKO Sp37A3 show a higher activation and maturation status upon stimulation compared to the Siglec-E expressing control cell line. This data suggests that Siglec-E can modulate cDC activation and potentially also influence antigen presentation.

Inhibitory Siglecs Modulate Antigen Presentation

In order to understand whether the antigen presentation of cDCs is affected by the expression of Siglec-E, we studied antigen handling including uptake, processing, and presentation in Sp37A3 cells. First, we analyzed antigen endocytosis of the Sp37A3 cells with fluorescent-labelled soluble OVA antigen or tumor cell-associated antigens. No difference of antigen uptake was observed between EKO and control cDCs (**Supplementary Figures S7A,B**). Furthermore, we co-cultured the Sp37A3 cells with live fluorescent-labelled or GFP-expressing MC38 tumor cells. Neither the frequency of fluorescent-positive DCs nor the MFI showed any significant change (**Supplementary Figures S7C,D**). As mannose receptor (MR) was reported to be the key mediator of soluble OVA antigen uptake by DCs (Burgdorf et al., 2006), we also examined its expression levels on both Sp37A3 cells. However, we observed even less MR expression on the EKO Sp37A3 cells, suggesting MR is of less importance in our scenario (**Supplementary Figure S7E**). Since antigen uptake was not affected by the Siglec-E expression, we then investigated whether Siglec-E expression affects antigen processing. We pulsed EKO Sp37A3 and control Sp37A3 cells with DQ-OVA and followed processing by measuring the fluorescent signal. We measured the fluorescence at several timepoints and found that the EKO Sp37A3 DCs showed a stronger fluorescent signal compared to control Sp37A3 cells, suggesting a more efficient antigen processing (**Supplementary Figure S7F**). To understand whether this leads to better antigen presentation, we used OVA-pulsed Sp37A3 cells to co-culture with either antigen-specific T cells from OT-I and OT-II transgenic mice or T cell proliferation was analyzed after CTV staining, and activation was studied by CD25 and CD69 expression on T cells. Even though both MHC-I and MHC-II molecules are expressed at higher levels in EKO Sp37A3 cells, mainly OT-II $CD4^+$ T cells showed better activation and proliferation during co-culture (**Figures 5A–F**). As sialic acids were previously reported to favor regulatory T cell (Tregs) polarization of naïve OT-II cells (Perdicchio et al., 2016), we tested the frequency of Foxp3+ Tregs at the end of the co-culture time and found only very low frequency of the $CD4^+$ OT-II cells differentiated into Tregs (**Supplementary Figure S7G**). We also tested the potential effect on cross-presentation by using heat-shocked wildtype or OVA-expressing MC38 tumor cells (MC38-wt or MC38-OVA) to replace soluble OVA antigen. Heat-shocked MC38-OVA cells induced a strong OT-I $CD8^+$ T cell activation and proliferation, but no difference was observed between the two Sp37A3 lines (**Supplementary Figures S7H–J**). Furthermore, differences between cell lines were still visible when not maturated with LPS (**Supplementary Figure S8**). To investigate whether the overexpression of an inhibitory Siglec would influence DC antigen presentation, we used the Siglec-9 transgenic mouse crossed to CD11c-Cre mice (Läubli et al., 2014b; Stanczak et al., 2018). Unlike mouse Siglec-E, naive BMDCs generated from these transgenic mice showed expression of human Siglec-9. Similar to our observations on Siglec-E-expressing DCs, OT-II $CD4^+$ T cells co-cultured with OVA antigen-pulsed Siglec-9-positive BMDCs represented less activation and proliferation (**Figures 5G–I**). Taken together, these results suggested that the expression of inhibitory Siglecs could modulate antigen processing and presentation to $CD4^+$ T cells.

DISCUSSION

In this work, we show that inhibitory Siglec receptors are expressed on DCs in cancer patients and can modulate DC activation and antigen presentation to T cells. Although several inhibitory Siglecs have been reported to influence myeloid cell functions in cancer, the understanding of the role of Siglec receptors on DCs in particular in the context of cancer is rather limited (Bax et al., 2007; Ding et al., 2016; Perdicchio et al., 2016; Silva et al., 2016). In our analysis, we found that several inhibitory Siglecs are observed on cDCs from human cancer patients and in murine tumor models. In various patient biopsies

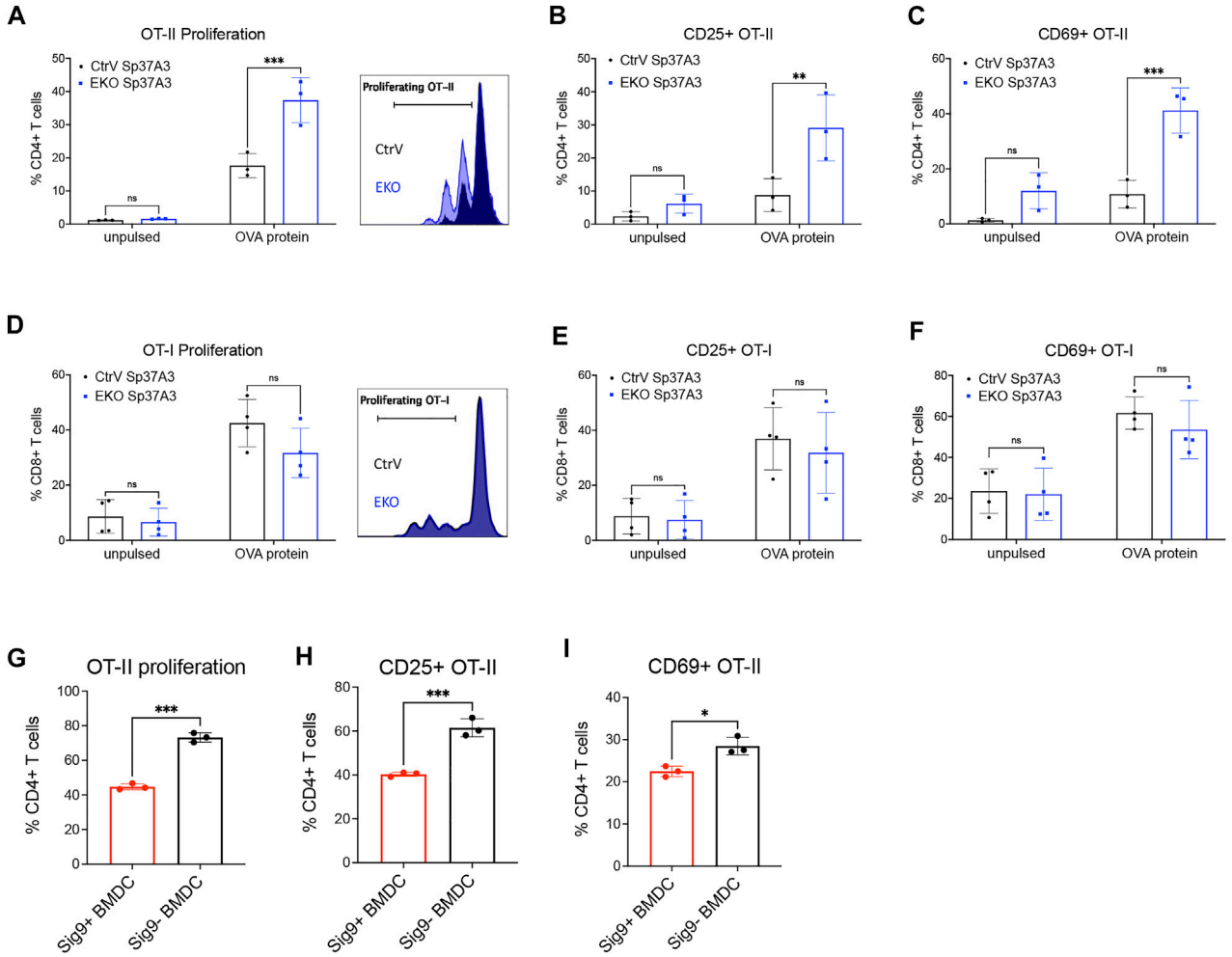

FIGURE 5 | Inhibitory Siglecs impair DC antigen presentation to CD4$^+$ T cells. **(A–F)** 48-h *in vitro* co-culture of OVA-pulsed CtrV or EKO Sp37A3 cells with **(A–C)** CD4$^+$ OT-II T cells or **(D–F)** CD8$^+$ OT-I T cells. Data was pooled from several independent experiments, and each datapoint represents the average of the technical replicates in individual experiments. **(G–I)** 72-h *in vitro* co-culture of OVA-pulsed Siglec-9-positive (red) or Siglec-9-negative (black) BMDCs with CD4$^+$ OT-II T cells. Data are presented as mean (±SD). Two-way ANOVA was used for two-way comparisons, and unpaired *t* test was used for one-way comparisons (*$p < 0.0332$, **$p < 0.0021$, ***$p < 0.0002$, and ****$p < 0.0001$).

from different cancer types, we detected a high expression of several inhibitory Siglecs on Ti-cDCs, in particular Siglec-7 and Siglec-9. Also, in different tumor models, we found an increased expression of Siglec-E, which is a functional paralog of human Siglec-9. Previous works have described Siglecs on DCs (Bax et al., 2007; Chen et al., 2009; Kawasaki et al., 2014; Ding et al., 2016; Affandi et al., 2020; Perez-Zsolt et al., 2021). For example, Siglec-7 has been targeted on human monocyte-derived DCs to deliver antigen (Kawasaki et al., 2014). In another study, Siglec-10 (and Siglec-G in mice) had been demonstrated to influence the response to damage-induced stress (Chen et al., 2009).

In order to study the functional role of inhibitory Siglec receptors on DCs, we tried to use BMDCs from wildtype and Siglec-E-deficient mice. However, although myeloid bone marrow cells express a high level of Siglec-E, BMDCs are not expressing Siglec-E. Previous studies have also found similar results when comparing to complete Siglec-E-deficient animals (Nagala et al., 2017). We therefore screened several mouse DC cell lines for functional testing. The C57BL/6 background mouse spleen-derived DC cell line Sp37A3 expresses high level of Siglec-E. By comparison of Siglec-E-deficient (EKO) and control (CtrV) Sp37A3 DCs, we found that Siglec-E ablation increased DC maturation. This *in vitro* finding was confirmed on mouse tumor-infiltrating DCs utilizing a conditional Siglec-E knockout mouse model. Further examination by transcriptomic analysis showed an elevated secretion of cytokines and chemokines, as well as surface co-stimulatory molecules. In a previous work, the loss of Siglec-G led to an increased response to damage-associated signaling molecules including high mobility group box 1 (HMGB1), IL-6, and TNF-α (Chen et al., 2009). The lack of Siglec-G on DCs also led to improved cross-presentation

of antigens (Ding et al., 2016). In the same work, Siglec-G-deficient DCs also led to an improved anti-tumoral immune response (Ding et al., 2016). In our study, the lack of Siglec-E had no direct influence on cross-presentation but led to an increased DC activation, enhanced antigen processing, and induced a stronger T cell proliferation, predominantly in $CD4^+$ T cells. A previous work has demonstrated that increased lysosomal processing could influence MHC II presentation while not so much modulating MHC I presentation (Samie and Cresswell, 2015). We found an increased processing when Siglec-E was deleted in DC cell lines, which could potentially explain the difference on MHC I and MHC II presentation and T cell stimulation. The role of inhibitory Siglecs on MHC II-mediated antigen presentation was also confirmed by a mouse BMDC model, which was engineered to express human Siglec-9. The Siglec-9-expressing BMDCs showed a worse antigen-specific $CD4^+$ T cell activation, demonstrating that the overexpression of an inhibitory Siglec receptor can inhibit antigen presentation and T cell activation.

Interactions between Siglec receptors and sialoglycans have been recently described as a potential new immune checkpoint to improve anti-cancer immunity, in particular on innate immune cells (Beatson et al., 2016; RodrÍguez et al., 2018; Duan and Paulson, 2020). A recent manuscript demonstrated that sialoglycans on pancreatic cancer cells can engage Siglec-7 and Siglec-9 receptors on tumor-associated macrophages and thereby promote cancer progression (Rodriguez et al., 2021). Interactions of Siglec-10 on TAMs with sialoglycans have shown to promote cancer (Barkal et al., 2019). In addition, blockade of GD-2, a new Siglec-7 ligand, enhanced antitumor immunity in combination with CD47 blockade (Theruvath et al., 2022). Here, we further demonstrate that Siglecs might play a role in antigen processing and presentation and targeting sialoglycan–Siglec interactions in cancer could potentially influence the anti-tumor immunity mediated by DCs.

The limitation of our analysis is mainly the *in vitro* character of our functional studies. Further analysis is certainly needed in animal models that can support a functional role for Siglec receptors on DCs. Moreover, the exact molecular mechanisms on how improved antigen processing and T cell stimulation are mediated in Siglec-deficient DCs remain also elusive and require more work.

In summary, we found several inhibitory Siglec receptors expressed on cDCs in primary cancer samples. Inhibitory Siglecs on cDCs can modulate DC activation, antigen processing, and T cell activation. Our findings provide new insights into mechanisms involved in Siglec-mediated immune escape in cancer.

DATA AVAILABILITY STATEMENT

The datasets presented in this study can be found in online repositories. The names of the repository/repositories and accession number(s) can be found as follows: https://www.ncbi.nlm.nih.gov/geo/, GSE190700.

ETHICS STATEMENT

The studies involving human participants were reviewed and approved by the Ethikkommission Nordwestschweiz, EKNZ, Basel Stadt, Switzerland. The patients/participants provided their written informed consent to participate in this study. The animal study was reviewed and approved by the local ethics committee, Basel Stadt, Switzerland. Written informed consent was obtained from the owners for the participation of their animals in this study.

AUTHOR CONTRIBUTIONS

HL and NR conceived and planned the project. JW, MM, AB, RW, NK, MS, and NR performed experiments and interpreted the results. DK provided samples. RI performed the bioinformatical analysis. JW, MM, AZ, and HL wrote the manuscript. All authors contributed to the article and approved the submitted version.

FUNDING

This work was supported by the Krebsliga Beider Basel (KLBB, to HL), the Schoenemakers-Mülller Foundation (to HL), and the Swiss National Science Foundation (SNSF Nr. 310030_184720/1 to HL).We thank Petra Herzig, Reto Ritschard, and Mélanie Buchi for their technical assistance.

ACKNOWLEDGMENTS

We also thank all the patients who allowed us to use their materials and made this work possible.

SUPPLEMENTARY MATERIAL

The Supplementary Material for this article can be found online at: https://www.frontiersin.org/articles/10.3389/fcell.2022.828916/full#supplementary-material

REFERENCES

Affandi, A. J., Grabowska, J., Olesek, K., Lopez Venegas, M., Barbaria, A., Rodríguez, E., et al. (2020). Selective Tumor Antigen Vaccine Delivery to Human CD169+antigen-Presenting Cells Using Ganglioside-Liposomes. *Proc. Natl. Acad. Sci. USA* 117, 27528–27539. doi:10.1073/pnas.2006186117

Bärenwaldt, A., and Läubli, H. (2019). The Sialoglycan-Siglec Glyco-Immune Checkpoint - a Target for Improving Innate and Adaptive Anti-cancer Immunity. *Expert Opin. Ther. Targets* 23, 839–853. doi:10.1080/14728222.2019.1667977

Barkal, A. A., Brewer, R. E., Markovic, M., Kowarsky, M., Barkal, S. A., Zaro, B. W., et al. (2019). CD24 Signalling through Macrophage Siglec-10 Is a Target for Cancer Immunotherapy. *Nature* 572, 392–396. doi:10.1038/s41586-019-1456-0

Bax, M., García-Vallejo, J. J., Jang-Lee, J., North, S. J., Gilmartin, T. J., Hernández, G., et al. (2007). Dendritic Cell Maturation Results in Pronounced Changes in Glycan Expression Affecting Recognition by Siglecs and Galectins. *J. Immunol.* 179, 8216–8224. doi:10.4049/jimmunol.179.12.8216

Beatson, R., Tajadura-Ortega, V., Achkova, D., Picco, G., Tsourouktsoglou, T.-D., Klausing, S., et al. (2016). The Mucin MUC1 Modulates the Tumor Immunological Microenvironment through Engagement of the Lectin Siglec-9. *Nat. Immunol.* 17, 1273–1281. doi:10.1038/ni.3552

Binnewies, M., Mujal, A. M., Pollack, J. L., Combes, A. J., Hardison, E. A., Barry, K. C., et al. (2019). Unleashing Type-2 Dendritic Cells to Drive Protective Antitumor CD4+ T Cell Immunity. *Cell* 177, 556–571. doi:10.1016/j.cell.2019.02.005

Bros, M., Jährling, F., Renzing, A., Wiechmann, N., Dang, N.-A., Sutter, A., et al. (2007). A Newly Established Murine Immature Dendritic Cell Line Can Be Differentiated into a Mature State, but Exerts Tolerogenic Function upon Maturation in the Presence of Glucocorticoid. *Blood* 109, 3820–3829. doi:10.1182/blood-2006-07-035576

Broz, M. L., Binnewies, M., Boldajipour, B., Nelson, A. E., Pollack, J. L., Erle, D. J., et al. (2014). Dissecting the Tumor Myeloid Compartment Reveals Rare Activating Antigen-Presenting Cells Critical for T Cell Immunity. *Cancer cell* 26, 638–652. doi:10.1016/j.ccell.2014.09.007

Burgdorf, S., Lukacs-Kornek, V., and Kurts, C. (2006). The Mannose Receptor Mediates Uptake of Soluble but Not of Cell-Associated Antigen for Cross-Presentation. *J. Immunol.* 176, 6770–6776. doi:10.4049/jimmunol.176.11.6770

Chen, D. S., and Mellman, I. (2017). Elements of Cancer Immunity and the Cancer-Immune Set point. *Nature* 541, 321–330. doi:10.1038/nature21349

Chen, G.-Y., Tang, J., Zheng, P., and Liu, Y. (2009). CD24 and Siglec-10 Selectively Repress Tissue Damage-Induced Immune Responses. *Science* 323, 1722–1725. doi:10.1126/science.1168988

Crocker, P. R., Paulson, J. C., and Varki, A. (2007). Siglecs and Their Roles in the Immune System. *Nat. Rev. Immunol.* 7, 255–266. doi:10.1038/nri2056

Ding, Y., Guo, Z., Liu, Y., Li, X., Zhang, Q., Xu, X., et al. (2016). The Lectin Siglec-G Inhibits Dendritic Cell Cross-Presentation by Impairing MHC Class I-Peptide Complex Formation. *Nat. Immunol.* 17, 1167–1175. doi:10.1038/ni.3535

Duan, S., and Paulson, J. C. (2020). Siglecs as Immune Cell Checkpoints in Disease. *Annu. Rev. Immunol.* 38, 365–395. doi:10.1146/annurev-immunol-102419-035900

Fraschilla, I., and Pillai, S. (2017). Viewing Siglecs through the Lens of Tumor Immunology. *Immunol. Rev.* 276, 178–191. doi:10.1111/imr.12526

Hakomori, S. (1996). Tumor Malignancy Defined by Aberrant Glycosylation and Sphingo(glyco)lipid Metabolism. *Cancer Res.* 56, 5309–5318.

Hedlund, M., Padler-Karavani, V., Varki, N. M., and Varki, A. (2008). Evidence for a Human-specific Mechanism for Diet and Antibody-Mediated Inflammation in Carcinoma Progression. *Proc. Natl. Acad. Sci.* 105, 18936–18941. doi:10.1073/pnas.0803943105

Hudak, J. E., Canham, S. M., and Bertozzi, C. R. (2014). Glycocalyx Engineering Reveals a Siglec-Based Mechanism for NK Cell Immunoevasion. *Nat. Chem. Biol.* 10, 69–75. doi:10.1038/nchembio.1388

Jandus, C., Boligan, K. F., Chijioke, O., Liu, H., Dahlhaus, M., Démoulins, T., et al. (2014). Interactions between Siglec-7/9 Receptors and Ligands Influence NK Cell-dependent Tumor Immunosurveillance. *J. Clin. Invest.* 124, 1810–1820. doi:10.1172/jci65899

Kawasaki, N., Rillahan, C. D., Cheng, T.-Y., Van Rhijn, I., Macauley, M. S., Moody, D. B., et al. (2014). Targeted Delivery of Mycobacterial Antigens to Human Dendritic Cells via Siglec-7 Induces Robust T Cell Activation. *J. Immunol.* 193, 1560–1566. doi:10.4049/jimmunol.1303278

Kniep, B., Kniep, E., Özkucur, N., Barz, S., Bachmann, M., Malisan, F., et al. (2006). 9-O-acetyl GD3 Protects Tumor Cells from Apoptosis. *Int. J. Cancer* 119, 67–73. doi:10.1002/ijc.21788

Läubli, H., Alisson-Silva, F., Stanczak, M. A., Siddiqui, S. S., Deng, L., Verhagen, A., et al. (2014a). Lectin Galactoside-Binding Soluble 3 Binding Protein (LGALS3BP) Is a Tumor-Associated Immunomodulatory Ligand for CD33-Related Siglecs. *J. Biol. Chem.* 289, 33481–33491. doi:10.1074/jbc.m114.593129

Läubli, H., Pearce, O. M. T., Schwarz, F., Siddiqui, S. S., Deng, L., Stanczak, M. A., et al. (2014b). Engagement of Myelomonocytic Siglecs by Tumor-Associated Ligands Modulates the Innate Immune Response to Cancer. *Proc. Natl. Acad. Sci. USA* 111, 14211–14216. doi:10.1073/pnas.1409580111

Macauley, M. S., Crocker, P. R., and Paulson, J. C. (2014). Siglec-mediated Regulation of Immune Cell Function in Disease. *Nat. Rev. Immunol.* 14, 653–666. doi:10.1038/nri3737

Nagala, M., Mckenzie, E., Richards, H., Sharma, R., Thomson, S., Mastroeni, P., et al. (2017). Expression of Siglec-E Alters the Proteome of Lipopolysaccharide (LPS)-Activated Macrophages but Does Not Affect LPS-Driven Cytokine Production or Toll-like Receptor 4 Endocytosis. *Front. Immunol.* 8, 1926. doi:10.3389/fimmu.2017.01926

Nitschke, L. (2014). CD22 and Siglec-G Regulate Inhibition of B-Cell Signaling by Sialic Acid Ligand Binding and Control B-Cell Tolerance. *Glycobiology* 24, 807–817. doi:10.1093/glycob/cwu066

Pearce, O. M. T., and Läubli, H. (2016). Sialic Acids in Cancer Biology and Immunity. *Glycobiology* 26, 111–128. doi:10.1093/glycob/cwv097

Perdicchio, M., Ilarregui, J. M., Verstege, M. I., Cornelissen, L. A. M., Schetters, S. T. T., Engels, S., et al. (2016). Sialic Acid-Modified Antigens Impose Tolerance via Inhibition of T-Cell Proliferation and De Novo Induction of Regulatory T Cells. *Proc. Natl. Acad. Sci. USA* 113, 3329–3334. doi:10.1073/pnas.1507706113

Perez-Zsolt, D., Munoz-Basagoiti, J., Rodon, J., Elosua-Bayes, M., Raich-Regue, D., Risco, C., et al. (2021). SARS-CoV-2 Interaction with Siglec-1 Mediates Trans-infection by Dendritic Cells. *Cell Mol Immunol* 18, 2676. doi:10.1038/s41423-021-00794-6

Ribas, A., and Wolchok, J. D. (2018). Cancer Immunotherapy Using Checkpoint Blockade. *Science* 359, 1350–1355. doi:10.1126/science.aar4060

Roberts, E. W., Broz, M. L., Binnewies, M., Headley, M. B., Nelson, A. E., Wolf, D. M., et al. (2016). Critical Role for CD103+/CD141+ Dendritic Cells Bearing CCR7 for Tumor Antigen Trafficking and Priming of T Cell Immunity in Melanoma. *Cancer Cell* 30, 324–336. doi:10.1016/j.ccell.2016.06.003

RodrÍguez, E., Schetters, S. T. T., and Van Kooyk, Y. (2018). The Tumour Glyco-Code as a Novel Immune Checkpoint for Immunotherapy. *Nat. Rev. Immunol.* 18, 204–211. doi:10.1038/nri.2018.3

Rodriguez, E., Boelaars, K., Brown, K., Eveline Li, R. J., Kruijssen, L., Bruijns, S. C. M., et al. (2021). Sialic Acids in Pancreatic Cancer Cells Drive Tumour-Associated Macrophage Differentiation via the Siglec Receptors Siglec-7 and Siglec-9. *Nat. Commun.* 12, 1270. doi:10.1038/s41467-021-21550-4

Ruffin, N., Gea-Mallorquí, E., Brouiller, F., Jouve, M., Silvin, A., See, P., et al. (2019). Constitutive Siglec-1 Expression Confers Susceptibility to HIV-1 Infection of Human Dendritic Cell Precursors. *Proc. Natl. Acad. Sci. USA* 116, 21685–21693. doi:10.1073/pnas.1911007116

Salmon, H., Idoyaga, J., Rahman, A., Leboeuf, M., Remark, R., Jordan, S., et al. (2016). Expansion and Activation of CD103 + Dendritic Cell Progenitors at the Tumor Site Enhances Tumor Responses to Therapeutic PD-L1 and BRAF Inhibition. *Immunity* 44, 924–938. doi:10.1016/j.immuni.2016.03.012

Samie, M., and Cresswell, P. (2015). The Transcription Factor TFEB Acts as a Molecular Switch that Regulates Exogenous Antigen-Presentation Pathways. *Nat. Immunol.* 16, 729–736. doi:10.1038/ni.3196

Silva, M., Silva, Z., Marques, G., Ferro, T., Gonçalves, M., Monteiro, M., et al. (2016). Sialic Acid Removal from Dendritic Cells Improves Antigen Cross-Presentation and Boosts Anti-tumor Immune Responses. *Oncotarget* 7, 41053–41066. doi:10.18632/oncotarget.9419

Spranger, S., Dai, D., Horton, B., and Gajewski, T. F. (2017). Tumor-residing Batf3 Dendritic Cells Are Required for Effector T Cell Trafficking and Adoptive T Cell Therapy. *Cancer Cell* 31, 711–723. doi:10.1016/j.ccell.2017.04.003

Stanczak, M. A., Siddiqui, S. S., Trefny, M. P., Thommen, D. S., Boligan, K. F., Von Gunten, S., et al. (2018). Self-associated Molecular Patterns Mediate Cancer Immune Evasion by Engaging Siglecs on T Cells. *J. Clin. Invest.* 128, 4912–4923. doi:10.1172/jci120612

Tangvoranuntakul, P., Gagneux, P., Diaz, S., Bardor, M., Varki, N., Varki, A., et al. (2003). Human Uptake and Incorporation of an Immunogenic Nonhuman Dietary Sialic Acid. *Proc. Natl. Acad. Sci.* 100, 12045–12050. doi:10.1073/pnas.2131556100

Theruvath, J., Menard, M., Smith, B. A. H., Linde, M. H., Coles, G. L., Dalton, G. N., et al. (2022). Anti-GD2 Synergizes with CD47 Blockade to Mediate Tumor Eradication. *Nat. Med.* online ahead of print. doi:10.1038/s41591-021-01625-x

Topalian, S. L., Drake, C. G., and Pardoll, D. M. (2015). Immune Checkpoint Blockade: a Common Denominator Approach to Cancer Therapy. *Cancer cell* 27, 450–461. doi:10.1016/j.ccell.2015.03.001

Varki, A., Cummings, R. D., Esko, J. D., Stanley, P., Hart, G. W., Aebi, M., et al. (2015). *Essentials of Glycobiology*. Cold Spring Harbor (NY): Cold Spring Harbor Laboratory Press.

Wang, J., Sun, J., Liu, L. N., Flies, D. B., Nie, X., Toki, M., et al. (2019). Siglec-15 as an Immune Suppressor and Potential Target for Normalization Cancer Immunotherapy. *Nat. Med.* 25, 656–666. doi:10.1038/s41591-019-0374-x

Zou, W., Wolchok, J. D., and Chen, L. (2016). PD-L1 (B7-H1) and PD-1 Pathway Blockade for Cancer Therapy: Mechanisms, Response Biomarkers, and Combinations. *Sci. Transl. Med.* 8, 328rv4. doi:10.1126/scitranslmed.aad7118

Conflict of Interest: HL received travel grants and consultant fees from Bristol-Myers Squibb (BMS) and Merck, Sharp and Dohme (MSD). HL received research support from BMS, GlycoEra, Novartis and Palleon Pharmaceuticals.

The remaining authors declare that the research was conducted in the absence of any commercial or financial relationships that could be construed as a potential conflict of interest.

Publisher's Note: All claims expressed in this article are solely those of the authors and do not necessarily represent those of their affiliated organizations, or those of the publisher, the editors and the reviewers. Any product that may be evaluated in this article, or claim that may be made by its manufacturer, is not guaranteed or endorsed by the publisher.

Copyright © 2022 Wang, Manni, Bärenwaldt, Wieboldt, Kirchhammer, Ivanek, Stanczak, Zippelius, König, Rodrigues Manutano and Läubli. This is an open-access article distributed under the terms of the Creative Commons Attribution License (CC BY). The use, distribution or reproduction in other forums is permitted, provided the original author(s) and the copyright owner(s) are credited and that the original publication in this journal is cited, in accordance with accepted academic practice. No use, distribution or reproduction is permitted which does not comply with these terms.

frontiers in Cell and Developmental Biology

REVIEW
published: 08 March 2022
doi: 10.3389/fcell.2022.830208

Key Players of the Immunosuppressive Tumor Microenvironment and Emerging Therapeutic Strategies

Kevin Park[1,2], *Mysore S. Veena*[1,2] *and Daniel Sanghoon Shin*[1,2,3,4]*

[1]Department of Medicine, Division of Hematology/Oncology, Los Angeles, CA, United States, [2]VA Greater Los Angeles Healthcare System, University of California, Los Angeles (UCLA), Los Angeles, CA, United States, [3]Molecular Biology Institute, Los Angeles, CA, United States, [4]Jonsson Comprehensive Cancer Center, Los Angeles, CA, United States

The tumor microenvironment (TME) is a complex, dynamic battlefield for both immune cells and tumor cells. The advent of the immune checkpoint inhibitors (ICI) since 2011, such as the anti-cytotoxic T-lymphocyte associated protein (CTLA)-4 and anti-programmed cell death receptor (PD)-(L)1 antibodies, provided powerful weapons in the arsenal of cancer treatments, demonstrating unprecedented durable responses for patients with many types of advanced cancers. However, the response rate is generally low across tumor types and a substantial number of patients develop acquired resistance. These primary or acquired resistance are attributed to various immunosuppressive elements (soluble and cellular factors) and alternative immune checkpoints in the TME. Therefore, a better understanding of the TME is absolutely essential to develop therapeutic strategies to overcome resistance. Numerous clinical studies are underway using ICIs and additional agents that are tailored to the characteristics of the tumor or the TME. Some of the combination treatments are already approved by the Food and Drug Administration (FDA), such as platinum-doublet chemotherapy, tyrosine kinase inhibitor (TKI) -targeting vascular endothelial growth factor (VEGF) combined with anti-PD-(L)1 antibodies or immuno-immuno combinations (anti-CTLA-4 and anti-PD-1). In this review, we will discuss the key immunosuppressive cells, metabolites, cytokines or chemokines, and hypoxic conditions in the TME that contribute to tumor immune escape and the prospect of relevant clinical trials by targeting these elements in combination with ICIs.

Keywords: tumor microenvironment, cancer, immune escape, immune checkpoint inhibitors, immunotherapy, clinical trials

OPEN ACCESS

Edited by:
Qian Xiao,
Rutgers Cancer Institute of New Jersey, United States

Reviewed by:
Lianjun Zhang,
Suzhou Institute of Systems Medicine (ISM), China
Carlos Del Fresno,
University Hospital La Paz Research Institute (IdiPAZ), Spain
Lin Zhang,
University of California, San Diego, United States

***Correspondence:**
Daniel Sanghoon Shin
dsshin@mednet.ucla.edu

Specialty section:
This article was submitted to Molecular and Cellular Pathology, a section of the journal Frontiers in Cell and Developmental Biology

Received: *06 December 2021*
Accepted: *14 February 2022*
Published: *08 March 2022*

Citation:
Park K, Veena MS and Shin DS (2022) Key Players of the Immunosuppressive Tumor Microenvironment and Emerging Therapeutic Strategies. Front. Cell Dev. Biol. 10:830208. doi: 10.3389/fcell.2022.830208

INTRODUCTION

The tumor microenvironment (TME) is composed of tumor cells, various associated cells of the host, and surrounding extracellular matrix components consisting of various cytokines, chemokines, proteases, many enzymes, microvesicles, and other secreted molecules. The host cell population of the TME mainly consists of fibroblasts, endothelial cells, granulocytes, lymphocytes, and macrophages (Mantovani et al., 2008). Constant spatio-temporal changes in the TME composition are highly complex in nature as the tumor advances in time. In addition to adapting to the changing TME, cancer cells escape destruction by the host immune system by

manipulating their own immunogenicity, producing immunosuppressive mediators, and attaining immunomodulatory phenotypes.

To circumvent immunosuppression, immunotherapy rose to stardom since the approval of the first immune checkpoint inhibitor (ICI), ipilimumab, in 2011. Ipilimumab is a monoclonal antibody (mAb) targeting cytotoxic T-lymphocyte associated protein (CTLA-4), demonstrating increased lymphocyte counts and $CD4^+/CD8^+$ T cell percentages in melanoma patients correlated to improved survival (Martens et al., 2016). Since its initial success in melanoma patients, it has received Food and Drug Administration (FDA) approvals in combination with nivolumab (anti-programmed cell death receptor (PD-1) antibody) for the treatment of poor-risk advanced renal cell carcinoma (RCC), microsatellite instability-high or mismatch repair deficient metastatic colorectal cancer (CRC), hepatocellular carcinoma (HCC) previously treated with sorafenib and advanced non-small cell lung cancer (NSCLC) or malignant pleural mesothelioma. Thus, the era of immunotherapy began, indicated by the 18% decrease in the overall mortality rate for metastatic melanoma from 2013 to 2016 - a trend attributable to the effects of ICI therapies (Cable et al., 2021).

However, ICI monotherapy suffers from low response rates of about 13% and moderately high rates of immune-related adverse events, with incidences of 72 and 66% in anti-CTLA-4 and anti-PD-(L)1 therapies, respectively (Sun and Lu, 2020). In 2019, a retrospective, cross-sectional study found that about 39% the U.S. population of cancer patients were eligible for immunotherapy treatment (Haslam et al., 2020). This unfavorable outlook is attributable to the multidimensional TME which continuously devises additional mechanisms of resistance, limiting both initial and prolonged responses to immunotherapies (Bagchi et al., 2021).

To enhance both the response rates and number of candidates for ICI therapies, a comprehensive understanding of the TME is imperative to tackle the resistance to ICI therapies exhibited by the majority of patients. Many clinical trials today are investigating the combination of different immunotherapies or immunotherapy and chemotherapy together in a multifaceted approach, targeting more than one ICIs within the TME to maximize response rates and circumvent resistance (Bagchi et al., 2021). Beyond combination regimens involving ICIs, multi-agent treatments involving the use of therapeutic agents to disable the immunosuppressive cells contributing to ICI resistance is expected to greatly augment immunotherapy. In this review we will discuss the key players contributing to the immunosuppressive TME, the possibility and potential of combination regimens involving multiple cell types, and current clinical trials being conducted to target these aspects within the TME.

$CD8^+$ CYTOTOXIC T CELLS

Cytotoxic $CD8^+$ T cells are undoubtedly the major players in immunotherapy today, carrying out cytolytic activities against tumor cells. Effector $CD8^+$ T cell activation is dependent on the recognition of an antigen-major histocompatibility complex (MHC) on a tumor cell; upon successful recognition, $CD8^+$ T cells release granules that contain perforin, granzyme, and the Fas ligand into the immunological synapse to carry out effector functions (**Figure 1A**) (Iwahori, 2020). $CD8^+$ T cells exist in different cytotoxic T cell (Tc) subsets: the Tc1 subset is responsible for the aforementioned production of granzyme B, perforin, and cytokines such as IFN-γ and tumor necrosis factor (TNF)-α. Tc2 cells do not produce as much IFN-γ as Tc1 cells but maintain a comparable level of cytotoxic activities via granzyme B, while Tc22 similarly express granzyme B to provide antitumor activities and comprise up to 35% of expanded effector T cells from tumors (St Paul et al., 2020; St Paul and Ohashi, 2020). Contrastingly, the Tc9 and Tc17 subsets demonstrate poor cytolytic functions due to their low levels of granzyme B (St Paul and Ohashi, 2020). Tc polarization can be affected by a variety of factors: tumor-associated macrophages (TAMs) from HCC patients were shown to induce Tc17 polarization *in vitro*, intestinal dendritic cells (DCs) were found to induce Tc9 polarization upon antigen cross-presentation, and Langerhans cells were shown to induce Tc22 polarization (Fujita et al., 2009; Kuang et al., 2010; Chang et al., 2013). While the role of the TME in driving Tc cell polarization has yet to be described, the composition of Tc subsets within a tumor can serve as a significant factor determining the response rates to ICI therapies.

$CD8^+$ T cells additionally express immune checkpoint molecules to limit their functions, a mechanism harnessed by tumor cells to induce T cell exhaustion and promote cancer progression (Raskov et al., 2021). In an attempt to revitalize the T cell's effector functions, interleukin (IL)-2 therapy was approved by the FDA for the treatment of renal cell carcinoma and metastatic melanoma in 1992 and 1998, respectively (Wrangle et al., 2018). Interleukin (IL)-2 signaling is required to sustain the effector T cell (Teff)'s cytolytic activity and induce their proliferation (Pipkin et al., 2010); however, a recent study by Liu et al. revealed IL-2's newfound role in driving T cell exhaustion instead, uncovering its inhibitory potential (Liu et al., 2021).

Co-Inhibitory Molecules and Related Therapies

Immunotherapy today instead relies on inhibitors to block signals leading to T cell dysfunction, effectively removing the restraints on the effector cells (**Figure 1A**). While ICI therapies have displayed promising results, they struggle heavily from limited accessibility and performance. In a retrospective cross-sectional study by Haslam et al. from 2011 to 2019, 36.1–38.5% of U.S. patients with cancer were estimated to be eligible for ICIs while the response rates to the therapies were projected to be 10.9–11.4% (Haslam et al., 2020).

To improve the efficacy of ICIs, combination therapies using both anti-PD-1 and anti-CTLA-4 checkpoint inhibitors are approved for few types of cancers and under investigation for several others. As reviewed by Toor et al. (2020) and Jiang et al. (2019), CTLA-4 and PD-1 are the most targeted inhibitory

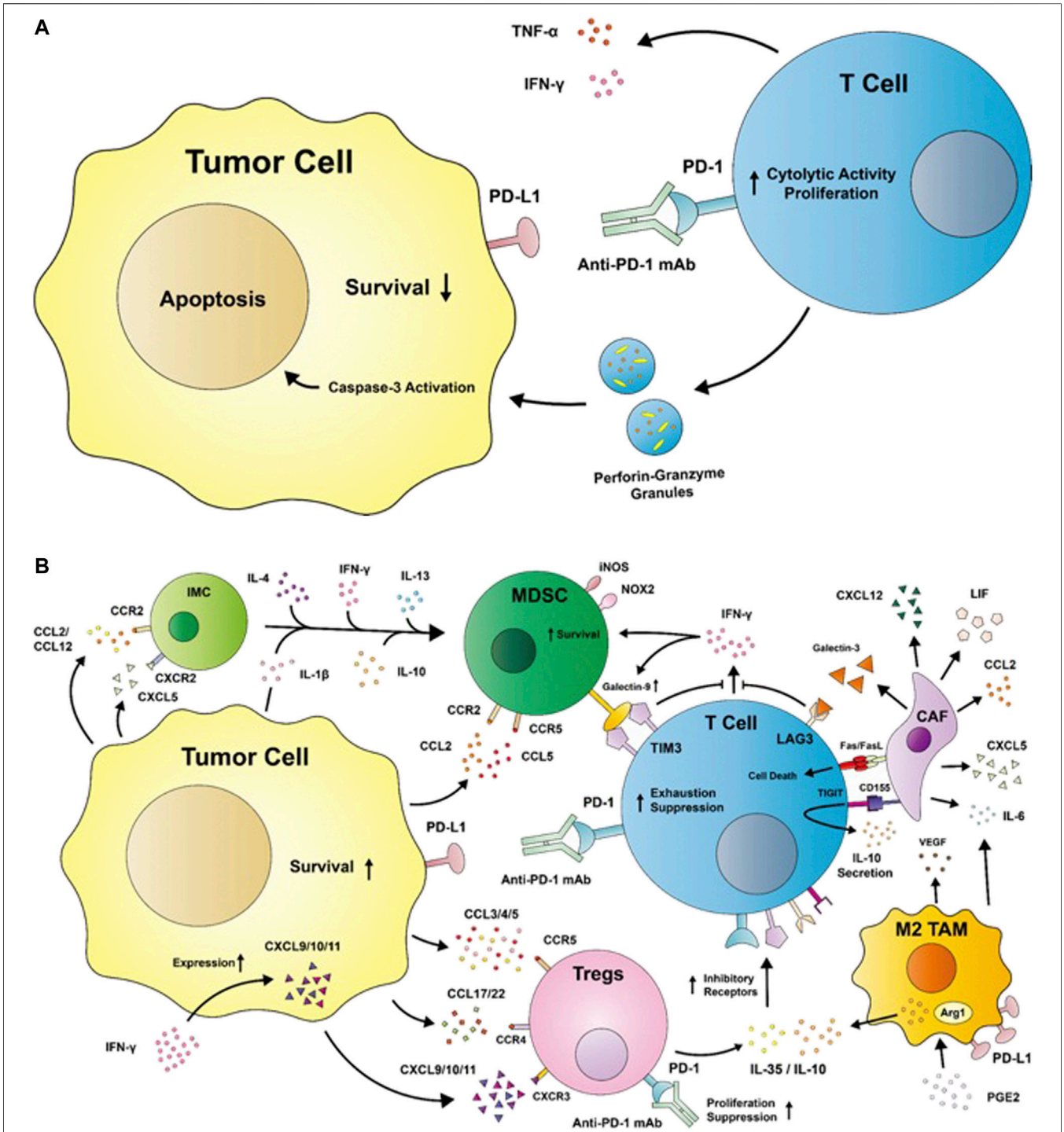

FIGURE 1 | (A) A diagram depicting the restoration of effector T cell antitumor activities by immune checkpoint inhibitors such as the anti-programmed cell death protein 1 (PD-1) monoclonal antibody. T cells secrete cytokines such as tumor necrosis factor (TNF) -α and interferon (IFN) -γ to generate an inflammatory environment while releasing granules with perforin and granzyme B to induce tumor apoptosis. **(B)** Immunosuppression in the TME. Tumor cells release chemokines such as C-C motif ligands (CCLs) and C-X-C motif ligands (CXCLs), which interact with C-C motif receptors (CCRs) and C-X-C motif receptors (CXCRs), respectively, to recruit immunosuppressive cells such as regulatory T cells (Tregs), myeloid-derived suppressor cells (MDSCs), M2-like tumor-associated macrophages (TAMs), and cancer-associated fibroblasts (CAFs) into the tumor microenvironment. Tregs secrete interleukin (IL)-35 and IL-10 to induce the upregulation of inhibitory receptors such as PD-1, T cell immunoglobulin and mucin-domain containing 3 (TIM3), T cell immunoglobulin and immunoreceptor tyrosine-based inhibitory motif domain (TIGIT), and lymphocyte activation gene 3 (LAG3). The binding of anti-PD-1 mAb to Tregs has the potential to increase its suppressive functions. The engagement of inhibitory receptors impairs T cell antitumor activities by suppressing IFN-γ and inducing T cell exhaustion by promoting its secretion of anti-inflammatory cytokines. M2-like TAMs

(*Continued*)

FIGURE 1 | are induced by the prostaglandin E2 (PGE2)—abundant TME to upregulate the expression of arginase 1 (Arg1) and IL-10, and secrete factors like IL-6 and vascular epithelial growth factor (VEGF) to promote tumor immune escape and migration. Tumors recruit both immature myeloid cells (IMCs) and MDSCs into the TME, where the expansion of IMCs into MDSCs are induced by factors such as IL-1β, IL-4, IL-10, IL-13, and IFN-γ. MDSCs exert immunosuppression via the expression of the TIM3 ligand galectin-9, inducible nitric oxide synthase (iNOS), and nicotinamide adenine dinucleotide phosphate oxidase (NOX) 2. iNOS and NOX2 produce nitric oxide and reactive oxygen species, which are detrimental to proper immune functions. CAFs secrete a variety of factors such as CXCL5, CXCL12, CCL2, and leukemia inhibitory factor (LIF), which serve immunosuppressive functions. CAFs are additionally capable of inducing T cell death with Fas ligand (FasL). CCR: C-C motif receptor; CD: cluster of differentiation; PD-L1: programmed cell death protein ligand 1.

pathways involved in the immune escape by tumors. In patients with previously untreated unresectable stage III or IV melanomas, nivolumab plus ipilimumab demonstrated greater objective response rate (ORR), median overall survival (OS) and progression-free survival (PFS) than ipilimumab alone (Wolchok et al., 2021). Similarly, in patients with ovarian cancer, nivolumab plus ipilimumab exhibited both increased ORR and PFS than nivolumab alone within 6 months of enrollment (Zamarin et al., 2020). Given these promising results, ipilimumab in combination with nivolumab has gained FDA approval for the treatment of several cancer types, such as melanoma, advanced RCC, CRC, HCC, metastatic NSCLC, and malignant pleural mesothelioma (Ipilimumab FDA, 2021). Combination therapy, however, is not without its limitations; for example, the relatively brief PFS reported by Zamarin et al. indicates its short-lived benefits (Zamarin et al., 2020). Likewise, while the Checkmate 032 trial (NCT01928394) in recurrent small-cell lung cancer (SCLC) patients revealed a greater ORR for the nivolumab plus ipilimumab group than nivolumab alone, it failed to replicate the same trends for both OS and PFS (Ready et al., 2020). The increased toxicity due to the combination regimen is also a major concern. Patients receiving combination treatments have higher, more severe incidences of treatment-related adverse events (TRAEs) than single-agent treatments, although the respective TRAEs are generally manageable (Warner and Postow, 2018; Cheng et al., 2020; Wolchok et al., 2021). Ready et al. proposed the discontinuation of the combination treatment due to increased toxicity as a possible explanation for the similar OS and PFS between the two groups, but their claims have not been verified (Ready et al., 2020).

Currently, clinical trials are evaluating the efficacy of ipilimumab and nivolumab combination in various cancer types to expand its use for the treatment of breast cancer, esophageal cancer, head and neck cancer, Hodgkin's lymphoma, and SCLC (Kooshkaki et al., 2020). Research into different approaches to minimize side effects and increase response rates are undergoing as well. For instance, the first-in-human phase I clinical trial of CRISPR–Cas9 (clustered regularly interspaced short palindromic repeats associated with Cas9 endonuclease) - engineered T cells prevent the expression of co-inhibitory molecules by deleting the *TRAC*, *TRBC* and *PDCD1* loci, demonstrating the potential of CRISPR gene-editing for immunotherapy (NCT04417764 (Wang,MD, 2020) and NCT03525782 (Chen, 2018)) (Stadtmauer et al., 2020; Sun and Lu, 2020). Further studies are warranted to increase the duration of clinical benefits from the combination therapies by incorporating additional agents, and to determine whether the discontinuation of treatment due to the increased toxicity of combination regimens has a significant effect on clinical outcomes.

Combination therapy is appealing in its ability to target more than one immune checkpoint molecule, leaving tumor cells with less options for immune escape. As such, additional inhibitory receptors contributing to T cell dysfunction in the TME have been identified. T cell immunoglobulin and mucin-domain containing 3 (TIM3) promotes $CD8^+$ T cell apoptosis or exhaustion upon binding to its ligands, galectin-9 (gal-9), phosphatidylserine, high-mobility group protein B1, and carcinoembryonic antigen cell adhesion molecule 1 (Huang et al., 2015; Kang et al., 2015; Acharya et al., 2020). Gal-9 is produced by cells such as T cells, B cells, macrophages, gastrointestinal epithelial cells, endothelial cells, and fibroblasts, and is upregulated in response to IFN-γ (**Figure 1B**). Binding of gal-9 releases Bat3 from the intracellular tail of TIM3 to ultimately result in T cell inhibition. Carcinoembryonic antigen cell adhesion molecule 1 also similarly releases Bat3 from TIM3 upon binding to TIM3 to inhibit T cell receptor (TCR) signaling, and is expressed on activated T cells, DCs, monocytes, macrophages, and tumor cells (Acharya et al., 2020). TIM3 expression is driven by IL-27, which engages the IL-27 nuclear factor, interleukin 3-regulated axis to cooperate with T-bet and induce IL-10 expression by T cells (Zhu et al., 2015).

Targeting TIM3 has promising potential to overcome resistance acquired after initial immunotherapy. The most abundant tumor infiltrating lymphocyte (TIL) population in multiple solid tumors were found to be $CD8^+$ TILs expressing both TIM3 and PD-1, and targeting both co-inhibitory molecules was shown to rescue exhausted $CD8^+$ T cells (Tian and Li, 2021). T cells in murine models of lung adenocarcinoma upregulated TIM3 expression, displaying a positive correlation with the duration of PD-1 blockade administered to the mice. TIM3 blockade following anti-PD-1 resistance increased survival, suggesting the upregulation of TIM3 surface expression as a means of ICI resistance (Koyama et al., 2016). Hence, by identifying and targeting additional co-inhibitory molecules in the TME, more durable ORRs can be expected. The development of TIM3 mAbs are currently under investigation for use with anti-PD-1/PD-L1 therapies. The combination therapy of TIM3 and PD-1/PD-L1 monoclonal antibodies, cobolimab and dostarlimab, respectively, have shown promising results in phase I trials of NSCLC patients resistant to anti-PD-1/PD-L1 therapy alone, displaying increased clinical activity in addition to manageable toxicity (Wolf et al., 2020). Phase II and III trials of the combination therapy are currently ongoing to validate its efficacy and safety (NCT04655976 (GlaxoSmithKline, 2021)) **Table 1**.

T cell immunoglobulin and immunoreceptor tyrosine-based inhibitory motif domain (TIGIT) is expressed on $CD4^+$ and $CD8^+$ T cells, natural killer (NK) cells, and regulatory T cells (Tregs), where its expression is upregulated following activation (Harjunpää and Guillerey, 2020). Binding of TIGIT to CD155 (poliovirus receptor PVR) expressed on tumor cells results in the decreased secretion of pro-inflammatory cytokines such as IFN-γ, IL-17a, and TNF-α, and an increased secretion of the anti-inflammatory cytokine IL-10 (**Figure 1B**) (Zhang C. et al., 2020). TIGIT inhibits T cell function by decreasing T cell activation, IL-2 production, and TCR-mediated proliferation (Lozano et al., 2012). TIGIT's receptor, CD155, is highly expressed on DCs, fibroblasts, endothelial cells and tumor cells within the TME, creating a highly immunosuppressive environment (**Figure 1B**). The engagement of the TIGIT/CD155 axis by T cells and DCs, respectively, inhibits T cell functions by inducing a tolerogenic DC phenotype. TIGIT's competing receptors to CD155 include CD226 (DNAM-1) and CD96, both of which have lower affinity to CD155 than TIGIT (Yu et al., 2009). CD226 especially has potential positive effects on T cells upon engagement to CD155 by promoting T-bet-mediated IFN-γ production. However, TIGIT's higher affinity for CD155 impedes the anti-tumoral CD226/CD155 axis, inhibiting anti-tumoral activities through competition (Lozano et al., 2012).

Anti-TIGIT treatments demonstrated efficacy in preclinical trials of multiple myeloma and head and neck squamous cell carcinoma (HNSCC) by decreasing tumor progression in a $CD8^+$ T cell-dependent manner (Guillerey et al., 2018; Wu et al., 2019). Targeting the TIGIT/CD155 axis is appealing as TIGIT and CD155 were each found to be highly expressed by Tregs and MDSCs, respectively, where CD155s expression by stromal or epithelial cells in particular was associated with worse survival in HNSCC patients (Wu et al., 2019). Etiglimab is an anti-TIGIT mAb currently undergoing clinical trials in combination therapy with nivolumab for the treatment of locally advanced or metastatic tumors, in addition to platinum-resistant carcinoma (NCT04761198 (Mereo BioPharma, 2021) and NCT05026606 (M.D. Anderson Cancer Center, 2021a)). Etiglimab demonstrated promising results in preclinical trials by preventing human melanoma growth in mice reconstituted with human hematopoietic stem cells. Other monoclonal antibodies to TIGIT, such as vibostolimab, domvanalimab, BMS-986207, and ASP8374 are in phase I and II clinical trials to confirm their efficacies and safety profiles in monotherapy or combination therapies with pembrolizumab, nivolumab, ipilimumab, pemetrexed, or carboplatin (NCT04738487 (Merck Sharp and Dohme Corp., 2021) and NCT02913313 (Bristol-Myers Squibb, 2021)) (Harjunpää and Guillerey, 2020). Recent updates on the trials testing anti-TIGIT with anti-PD-(L)1 combination treatments appear to be promising; it is highly anticipated that these combination treatments may able to provide improvement in response rates (Rodriguez-Abreu et al., 2020; Chau et al., 2021) **Table 1**.

Exhausted $CD8^+$ T cells express the lymphocyte activation gene 3 (LAG3/CD223) in response to prolonged activation (Huard et al., 1994). In melanoma, LAG3 can bind to MHC-IIs upregulated on tumor cells, upregulating MAPK/Erk and phosphatidylinositol-3-kinase (PI3K)/Akt pathways to confer melanoma cells resistance to Fas-mediated and drug-induced apoptosis (Hemon et al., 2011). LAG3-MHC-II binding additionally recruits tumor-specific $CD4^+$ T cells, decreasing the $CD8^+$ T cell response (Donia et al., 2015). Galectin-3 (gal-3) is another LAG3 ligand expressed by epithelial, myeloid, and stromal cells, including cancer-associated fibroblasts (CAFs) (Dumic et al., 2006; Dong et al., 2018). Binding of gal-3 to LAG3 on $CD8^+$ T cells leads to the decreased expression of pro-inflammatory cytokines such as IFN-γ, TNF-α, and IL-6 (**Figure 1B**) (Kouo et al., 2015). Other LAG3 ligands include LSECtin expressed on DCs and fibrinogen-like protein 1, which similarly leads to the inhibition of IFN-γ secretion by Teffs, suppression of IL-2 induction, and TNF-α and IFN-γ secretion (Xu et al., 2014; Wang et al., 2019).

Monoclonal antibodies to LAG3, such as relatlimab (BMS-986016), LAG525, BI754111, MK-4280, Sym022, TSR-033, REGN3767, and INCAGN2385-101 are currently undergoing phase I and II clinical trials as monotherapy or combination therapy with anti-PD-1/PD-L1 mAbs to treat multiple myeloma, SCLC, NSCLC, gastric/esophageal adenocarcinoma, and CRC. Antagonistic bispecific antibodies to LAG3, such as MGD013, FS118, and xmab22841, respectively targeting PD-1, PD-L1, and CTLA-4 in addition to LAG3 are also in clinical trials (NCT04653038 (Zai Lab (Shanghai) Co., Ltd., 2020) and NCT03440437 (F-star Therapeutics Limited, 2021)) **Table 1**. Murine models of chronic lymphocytic leukemia (CLL) treated with both anti-PD-1 and anti-LAG3 displayed a significantly lower number of CLL cells in the spleen, along with a decrease in Tregs and an increase in Teffs (Wierz et al., 2018). Relatlimab in combination with nivolumab has shown efficacy in melanoma patients with LAG3 expression in at least 1% of tumor-associated immune cells, demonstrating an ORR of 18% (n = 33). In contrast, melanoma patients with LAG3 expression in less than 1% of their immune cells had an average ORR of 5% (n = 22), indicating that LAG3 inhibition therapy may be a specific, targeted therapy for patients with high expression of LAG3 in their TME (Ascierto et al., 2017). Although the combination therapy of anti-LAG3 and anti-PD-1/PD-L1 mAbs have resulted in durable responses in 9.9% of patients (n = 121), the exact mechanism contributing to the synergy is unknown (Maruhashi et al., 2020).

Targeting LAG3 faces unique challenges due to the different role of soluble LAG3 (sLAG3). sLAG3 carries out antitumoral activities by allowing DCs to mature and attack tumor cells. sLAG3 exhibits a positive correlation with $CD8^+$ T cells, secretion of IL-12 and IFN-γ, and survival in murine models of gastric cancer (GC) (He et al., 2016; Li et al., 2018, 3). These characteristics of sLAG3 opens avenues for its potential use as a therapeutic agent for certain cancer types, but also indicates the possibility of LAG3 inhibitors interacting with sLAG3. Therefore, while LAG3 inhibitors are promising treatment options, their molecular mechanisms of action in combination regimens with PD-1, their effects on sLAG3, and mechanisms of resistance to anti-LAG3 therapies warrant further investigation (Barrueto et al., 2020).

REGULATORY T CELLS

Characterized as $CD4^+CD25^+FoxP3^+$ T cells, Tregs are responsible for carrying out immunosuppressive activities in the TME to drive tumor progression. IL-10 secretion by Tregs inhibits the production of pro-inflammatory cytokines such as TNF-α, IL-1β, IL-6, and IL-12 in macrophages in a signal transducer and activator of transcription (STAT) 3-dependent pathway (Lang et al., 2002), and suppresses downstream signaling of CD28 in T cells via the Janus kinase (JAK) 1 and tyrosine kinase 2 pathways (Taylor et al., 2006). Tregs additionally secrete IL-35, a member of the IL-12 family that inhibits $CD4^+$ and $CD8^+$ Teff proliferation via the IL-35 receptor-mediated activation of STAT4 and STAT1. IL-10 and IL-35 additionally increases the expression of inhibitory molecules on $CD8^+$ T cells, making them susceptible to exhaustion and suppression (**Figure 1B**) (Sawant et al., 2019). IL-35 has the ability to induce a regulatory population of T cells that do not express FoxP3, which exhibits potent immunosuppressive capacities *in vivo* (Collison et al., 2010). Upon induction, Tregs rely on IL-2 for their maturation and function, using CD25 as the receptor for the cytokine. Because Tregs are unable to produce IL-2, Tregs consume large quantities of IL-2 from the TME and impair T cell functions by depriving the cytokine from the TME (Li C. et al., 2020).

Tregs rely on the C-C motif receptor (CCR) 4/C-C motif ligand (CCL) 22 or CCR4/CCL17 pathway for chemotaxis (**Figure 1B**). In a study by Curiel et al. (2004), tumor Tregs with high expressions of CCR4 interacted with CCL22 or CCL17 secreted by tumor cells or TAMs to facilitate their recruitment into the TME (Iellem et al., 2001; Curiel et al., 2004; Dadey et al., 2020). These $CCR4^+$ tumor Tregs have been characterized as the most suppressive subset, allowing them to abundantly infiltrate tumor sites in multiple cancers such as gastric and esophageal cancers (Sugiyama et al., 2013). Tumor cells and MDSCs in the TME are able to secrete CCL3, CCL4, and CCL5, interacting with CCR5 on Tregs and attracting them into the TME (Tan et al., 2009; Schlecker et al., 2012). The pro-inflammatory conditions in the TME created by IFN-γ further promotes Treg recruitment by inducing the expression of C-X-C motif ligand (CXCL) 9, CXCL10, and CXCL11, all three of which are ligands for C-X-C motif receptor (CXCR) 3 (Müller et al., 2007; Redjimi et al., 2012; Tokunaga et al., 2018). CXCR3 is expressed on Tregs via T-BET and similarly induced by the pro-inflammatory conditions within the TME (Koch et al., 2009).

Tregs are capable of synergizing with other immunosuppressive immune cells within the TME, such as the myeloid-derived suppressor cells (MDSCs). CD80/CTLA-4 interactions between MDSCs and Tregs, respectively, can augment the suppressive functions of Tregs (Yang et al., 2006), while IL-35 secreted by Tregs can induce MDSC accumulation and increase immunosuppressive effects in the TME (Wang Z. et al., 2021). Tregs also express the nucleases CD39 and CD73 on their surfaces, catalyzing the conversion of ATP or ADP into AMP and AMP into adenosine, respectively (Li C. et al., 2020). Adenosine binds to the A2A adenosine receptor (A2AR) expressed on the surface of immune cells that evoke different responses depending on the target. On $CD4^+$ and $CD8^+$ T cells, the engagement of the A2AR-mediated pathway leads to the inhibition of T cell function by restricting their proliferation, cytotoxicity, and cytokine secretion (Ohta et al., 2012). In contrast, A2AR stimulation on Tregs not only leads to their proliferation, but also inhibits the IL-2 production by Teffs (Zarek et al., 2008; Ohta et al., 2012).

OX40 is a co-stimulatory molecule part of the tumor necrosis factor receptor superfamily expressed on the surfaces of activated T cells, neutrophils, and NK cells. Its receptor, OX40L (CD252), is expressed on antigen-presenting cells such as DCs, activated B cells, and macrophages. In Tregs, OX40 expression is constitutive and its ligation dampens their suppressive abilities by limiting their proliferation and generation of IL-10 producing type 1 Tregs (Fu Y. et al., 2020; Kuang et al., 2020). However, in a study of HCC patients with and without cirrhosis, it has been implied that OX40 signaling may contribute towards the survival and proliferation of Tregs. The cirrhotic microenvironment can induce the development of highly suppressive $OX40^+$ Tregs, where $OX40L^+$ TAMs provide signals to expand Tregs and promote the development of HCC from cirrhosis (Piconese et al., 2014). In a later study in HCC patients, HCC tumors were shown to express high levels of OX40, where IL-2 could upregulate OX40 expression and interact with the molecule to drive Treg proliferation. In HCC tumors with high OX40 expression, despite the greater activation of Teffs, they do not correlate to increased antitumor activities, suggesting the involvement of functionally defective $CD8^+$ T cells or immune checkpoint molecules (Xie et al., 2018). Additional work to characterize the aspects of the HCC TME contributing to the conflicting role of OX40 would be of great benefit to fully understand its effects on Tregs.

Like T cells, Tregs express immune checkpoint molecules on their surfaces. Tregs can target DCs with co-inhibitory receptors such as CTLA-4 and LAG3 (Li C. et al., 2020). Tregs constitutively express CTLA-4 on their surfaces (Read et al., 2000), impairing the upregulation of CD80 and CD86 on DCs and limiting the activation of naive T cells by inhibiting CD28 signaling (Wing et al., 2008). Binding of CTLA-4 to CD80/CD86 on the surfaces of DCs also upregulates indoleamine 2,3-dioxygenase (IDO) to produce kynurenine, a metabolite of tryptophan that suppresses Teff function and promotes Treg synthesis (Mellor and Munn, 2004; Li C. et al., 2020). Upon Treg activation and in the presence of Teffs, Tregs upregulate the expression of LAG3, which is essential for their immunosuppressive functions (Huang et al., 2004). Increased frequencies of $LAG3^+$ Tregs were found in the PBMCs of cancer patients, which expand in the TME to secrete IL-10 and transforming growth factor beta 1 (TGF-β1) (Camisaschi et al., 2010). However, in the context of Type 1 diabetes, $LAG3^+$ Tregs exhibited limited proliferation and function, contributing to autoimmunity by failing to induce immunosuppression (Zhang et al., 2017). Further studies into LAG3's role in Treg function are required to elucidate the mechanisms behind its variable activity in the tumor and autoimmune settings.

TIM3 and PD-1 are co-inhibitory molecules often co-expressed on the surfaces of Tregs. TIM3$^+$ Tregs exhibited higher suppressive capacities relative to TIM3$^-$ Tregs towards T helper (Th) 1 and Th17 cells, with TIM3 expression being correlated to worse prognosis in lung cancer (Gao et al., 2012; Gautron et al., 2014). Similarly, TIGIT activation exerts potent inhibitory effects on Teffs and NK cells, but contrastingly enhances the immunosuppressive activities of Tregs. Ligation of TIGIT on Tregs induces their Fgl2 production and secretion, which suppresses Teff proliferation, promotes Th2 polarization, inhibits Th1 and Th17 activities, and induces IL-10 and IL-4 expression (Joller et al., 2014). In melanoma patients, TIGIT$^+$ Tregs exhibited greater immunosuppressive capabilities and stability than TIGIT- Tregs by increasing the expression of CTLA-4, CD39, PD-1, and TIM3 (Fourcade et al., 2018). However, PD-1 expression by Tregs have been shown to limit their proliferation and suppressive capacities (Franceschini et al., 2009), exhibiting an exhausted phenotype marked by increased secretion of IFN-γ (Lowther et al., 2016). This may imply that while anti-PD-1 therapies may restore Teff functions, they may also renew the immunosuppressive abilities of Tregs. In fact, Kamada et al. revealed the presence of highly proliferative, suppressive effector Treg cells in GC patients undergoing hyperprogressive disease after anti-PD-1 treatment, suggesting the therapy's undesired effects on Tregs (**Figure 1B**) (Kamada et al., 2019).

Treg-Based Therapies

In addition to the aforementioned ICI therapies, approaches to disable or deplete immunosuppressive cell populations like Tregs within the TME are pursued to augment the anti-tumoral activities of Teffs **Table 1**. Like the anti-PD-1 treatment, ICIs may achieve different results on Tregs compared to those on Teffs. For example, anti-CTLA-4 mAbs ipilimumab and tremelimumab were found to increase the density of CD4$^+$ and CD8$^+$ T cells in tumor tissues but not deplete Tregs (Sharma et al., 2019). By modifying the Fc-region of the anti-CTLA-4 mAb, Ha et al. increased the antibody-dependent cell-mediated cytotoxicity (ADCC) of the inhibitor to deplete activated Tregs highly expressing CTLA-4. However, antigen stimulation results in the expansion of CTLA-4$^+$ antigen-specific CD8$^+$ T cells, where the high ADCC-CTLA-4 mAb causes the depletion of the Teff population along with Tregs. With the high ADCC-CTLA-4 mAb, the authors recommend the administration of Treg depletion regimen before antigenic stimulation (Ha et al., 2019).

An alternative approach is the anti-CD25 mAb, which binds to CD25 highly expressed on Tregs relative to Teffs. While anti-CD25 mAbs failed to create remarkable responses, Fc-optimized anti-CD25 mAbs were successful in selectively depleting tumor-infiltrating Tregs and increasing the Teff to Treg ratio (Arce Vargas et al., 2017). However, the major concern with anti-CD25 mAb is its ability to interact with IL-2 and block IL-2 signaling crucial to sustain Teffs, resulting in reduced antitumoral activities by decreasing granzyme B expression. Solomon et al. synthesized a modified anti-CD25 mAb, RO7296682 (RG6292), capable of depleting Tregs while preserving IL-2 signaling on Teffs. The non-IL-2 blocking anti-CD25 mAb demonstrated higher activation of CD8$^+$ T cells than the Fc-optimized anti-CD25 mAbs, creating synergistic effects with anti-PD-1 therapies in murine models (Solomon et al., 2020). A phase I trial is currently underway with the combination of RO7296682 and atezolizumab to determine its safety and tolerability in patients with advanced solid tumors (NCT04642365 (Hoffmann-La Roche, 2021)).

Strategies to target more than one molecule by the use of bispecific antibodies are rising as an alternative therapeutic option. The pairing of ICIs and co-stimulatory checkpoint molecules is in essence a combination regimen and highly attractive as it can simultaneously drive Teff functions while preventing suppressive cells such as Tregs from depressing the immune response (Galon and Bruni, 2019). ATOR-1015 is a bispecific antibody to CTLA-4 and OX40, which are two receptors highly expressed on Tregs. Agonistic OX40 mAbs were shown to drive Teff proliferation while inhibiting Treg survival and functions in preclinical settings (Voo et al., 2013). ATOR-1015 has shown to induce localized Treg depletion and T cell activation *in vitro* while decreasing tumor growth and improving survival in murine models by enhancing anti-PD-1 treatments. Despite these preclinical findings, the safety profile of ATOR-1015 has yet to be assessed and requires further investigation to evaluate its ability to deplete Tregs (Kvarnhammar et al., 2019). ATOR-1015 is currently undergoing clinical trials to assess its safety and tolerability in patients with solid tumors (NCT03782467 (Alligator Bioscience AB, 2021)). Similarly, there has been the development of the bispecific antibody KY1055, which combines the agonist for inducible T cell co-stimulator and PD-L1-mAb. KY1055 was able to increase the ratio of CD8$^+$ Teffs to Tregs and deplete Tregs *in vivo*, but has yet to enter clinical trials (Sainson et al., 2021). Clinical studies comparing the efficacy of agonist-inhibitor bispecific antibodies to single antibodies will help better elucidate the benefits they offer.

Antibody drug conjugates (ADCs) are novel approaches to deliver drugs to targets in a highly specific manner (Dees et al., 2021). A preclinical trial demonstrated the ability of a CD25-targeted, pyrrolobenzodiazepine dimer-based ADC to induce durable antitumor activity by inducing a durable and robust depletion of Tregs. When delivered in combination with anti-PD-1 therapy, there was a greater increase in CD8$^+$ TILs, suggesting its synergy with ICIs (Zammarchi et al., 2020). The CD25-targeted, PBD dimer-based ADC, ADCT-301, is currently undergoing phase I clinical trials in patients with lymphoma, leukemia, and various advanced solid tumors (NCT04639024 (Gwynn Long MD, 2021) and NCT03621982 (ADC Therapeutics S.A., 2021)). The importance of precisely targeting Tregs to allow Teffs from exerting antitumoral effects is crucial to augment ICI therapies today, and it is anticipated that combination therapies involving the depletion of Tregs will help achieve greater and prolonged responses.

MYELOID-DERIVED SUPPRESSOR CELLS

MDSCs are another example of immunosuppressive cells within the TME, comprised of heterogeneous, immature myeloid cells

(IMCs) generated by emergency myelopoiesis. Emergency myelopoiesis is triggered to meet the high demands of leukocytes generated by pathological conditions, increasing the production of myelomonocytic cells in the bone marrow to supply innate immune cells needed to combat infections (Takizawa et al., 2012). While IMCs normally differentiate into mature neutrophils, macrophages, and DCs upon entering peripheral blood and tissues, tumor-derived soluble factors and pro-inflammatory cytokines in the TME such as IFN-γ, IL-1β, IL-4, and IL-10 instead drive the differentiation of IMCs into MDSCs and later into immunosuppressive macrophages and DCs (**Figure 1B**) (Bunt et al., 2006; Gallina et al., 2006; Gabrilovich et al., 2012). Tumor cells additionally facilitate the development of MDSCs by secreting CCL2, CCL12, CXCL5 to attract IMCs into the TME while also secreting growth factors that recruit MDSCs in the bone marrow (Huang et al., 2007; Yang et al., 2008; Gabrilovich et al., 2012).

In the TME, MDSCs are activated by tumor-derived TGF-β and drive the proliferation of Tregs (Ghiringhelli et al., 2005). The primary subtypes of MDSCs include polymorphonuclear (PMN) - MDSCs and monocytic (M) - MDSCs. M-MDSCs suppress the immune system via secretion of anti-inflammatory cytokines like IL-10, additionally employing inducible nitric oxide synthase (iNOS) to produce nitric oxide (NO) (**Figure 1B**). NO has been shown to inhibit the T cell response by promoting T cell apoptosis, decreasing IL-2-mediated signaling, and preventing MHC-II expression. M-MDSCs are recruited to the TME primarily by tumor-derived CCL2 and CCL5, while PMN-MDSCs are recruited by CCL2 and CCL3 (Qian et al., 2011; Reichel et al., 2012; Chun et al., 2015). PMN-MDSCs produce high levels of reactive oxygen species (ROS) with high levels of NADPH oxidase (NOX) 2, resulting in increased recruitment of MDSCs to the TME, disruption of the immune cells' DNA, and impaired differentiation of MDSCs into DCs. NO and ROS together produce peroxynitrite, which nitrifies both the TCR and T cell-specific chemokines to restrict T cells' activation and migration (Safarzadeh et al., 2018). Furthermore, both subtypes are capable of producing arginase-1 (arg1), which depletes L-arginine from the TME (Yang et al., 2020) By consuming L-arginine and sequestering L-cysteine from the TME, T cells are deprived of essential amino acids required for their activation, function, and proliferation (Safarzadeh et al., 2018). M-MDSCs are additionally able to provide inhibitory signals by the expression of gal-9, which binds to TIM-3 expressed on $CD8^+$ T cells to impair their IFN-γ secretions and confer resistance to anti-PD-1 therapy (**Figure 1B**) (Limagne et al., 2019).

MDSC expansion in the TME is driven by factors from tumor cells, stromal cells, and immune cells (Safarzadeh et al., 2018). Factors such as Toll-like receptor (TLR) 4, IL-4, IL-1β, TGFβ, and IFN-γ activate pathways such as STAT1, STAT3, STAT6, and NF-kB to sustain MDSC survival and function (**Figure 1B**) (Gabrilovich and Nagaraj, 2009; Law et al., 2017). One of the main transcription factors regulating MDSC expansion is STAT3, where GM-CSF, macrophage (M)-CSF, and vascular endothelial growth factor (VEGF) activate its downstream signaling. STAT3 is speculated to play a role in driving MDSC proliferation and block the differentiation of IMCs into various mature myeloid cells (Nefedova et al., 2004; Law et al., 2017). Upon STAT3 inhibition, a decrease in MDSC populations and an increase in antitumor activities were observed (Kortylewski et al., 2005). However, Kumar et al. discovered that upon the downregulation of STAT3 activity by hypoxia-induced CD45 protein tyrosine phosphatases, MDSCs are rapidly differentiated into tumor-promoting TAMs (Kumar et al., 2017). While this may raise some concerns about using STAT3 inhibitors to decrease MDSC populations in the TME, a study by Hellsten et al. assessing the performance of galiellalactone, a STAT3 inhibitor, revealed a significant decrease in the generation of M-MDSC but no increase in tumor-promoting TAMs (Hellsten et al., 2019).

MDSC-Based Therapies

Unlike other cell populations, targeting MDSCs for therapy faces significant challenges due to the cell population being largely heterogeneous with no consensus on the surface markers for MDSC identification (Law et al., 2020). Therefore, various approaches such as disabling the function, recruitment, or expansion of MDSCs by targeting chemokines or signaling pathways have been explored. Because MDSCs exert potent immunosuppressive activities in the TME and contribute towards tumor growth, a combination of both MDSC-targeted therapies and ICIs is becoming increasingly attractive (**Table 1**). Attempts to use chemotherapeutic agents such as 5-fluorouracil and oxaliplatin, which decrease the MDSC population, in combination with anti-PD-1 therapy in murine models of GC were successful in increasing the antitumor response and Teff tumor infiltration. Kim et al. additionally confirmed that MDSCs contributed to resistance towards anti-PD-1 therapy; during later stages of GC where MDSC accumulation was more significant, anti-PD-1 monotherapy elicited minimal responses compared to its administration during the early stages of GC when less MDSCs were present in the TME (Kim et al., 2021). Therefore, targeting MDSCs prior to or in combination with ICIs is the next step to evoke greater antitumor responses in patients.

Additional therapeutic options to deplete MDSCs include the aforementioned STAT3 inhibitor galiellalactone and the tyrosine kinase inhibitor sunitinib, which in combination decreased MDSC populations from the TME to restore antitumor activities. While sunitinib received FDA approval for the treatment of gastrointestinal stromal tumors, advanced and recurrent RCC, and progressive pancreatic neuroendocrine tumors, galiellalactone has yet to enter clinical trials (Hellsten et al., 2019; Law et al., 2020). An example of a therapeutic strategy aimed towards preventing the recruitment of MDSCs is the CXCR2 inhibitor, which interacts with CXCR2 and CXCR5 (Katoh et al., 2013). CXCR2 inhibition using the small molecule inhibitor SX-682 enhanced the effects of adoptively transferred T cells or NK cells by abrogating MDSC infiltration into the TME (Sun et al., 2019; Greene et al., 2020). SX-682 is currently undergoing clinical evaluation in patients with metastatic melanoma as monotherapy or in combination with pembrolizumab (NCT03161431 (Syntrix Biosystems, Inc., 2021)). Another CXCR2 inhibitor AZD5069 (NCT02499328

(AstraZeneca, 2020, 2)) is currently in phase 1b/2 clinical trial for the treatment of advanced solid tumors and metastatic HNSCC. MDSCs additionally rely on the colony-stimulating factor-1 receptor (CSF-1R)/CSF-1 axis for their recruitment, allowing for the inhibition of CSF-1R as an alternative option. The small molecule inhibitor of CSF-1R, PLX3397 (pexidartinib), led to the increased infiltration of lymphocytes into the tumor with higher IFN-γ secretion (Mok et al., 2014). PLX3397 is currently in phase III for the treatment of tenosynovial giant cell tumor (NCT04488822 (Daiichi Sankyo Co., Ltd., 2021)). However, because anti-CSF-1R therapies suffer from limited therapeutic benefits when administered alone, approaches to use them in combination with ICI therapies or adopted T cell therapies are currently under evaluation and will be discussed later (Ries et al., 2015).

Epigenetic reprogramming is another avenue that can be taken to neutralize MDSCs' immunosuppressive activities by targeting their effector molecules (Christmas et al., 2018). Entinostat, a class I histone deacetylase inhibitor, was shown to decrease tumor growth and increase survival in murine models of lung cancer and RCC in combination with anti-PD-1/PD-L1 therapy. Orillion et al. discovered that entinostat significantly reduced arg-1, iNOS, and cyclooxygenase-2 (COX-2) to inhibit immunosuppressive activities in the TME, making tumors more susceptible to immune responses by effector cells (Orillion et al., 2017; Law et al., 2020). Clinical trials are currently underway to examine the activity of entinostat in combination with pembrolizumab to treat lymphoma (NCT03179930 (Memorial Sloan Kettering Cancer Center, 2021)) and melanoma (NCT03765229 (UNC Lineberger Comprehensive Cancer Center, 2021)).

TUMOR-ASSOCIATED MACROPHAGES

As opposed to Tregs or MDSCs, TAMs can support either tumor progression or eradication. Macrophages in the TME exist in a dynamic spectrum of phenotypes across tumor types, dependent on tumor stage and tissue-specific regulation (Li X. et al., 2019). TAMs can be characterized into two major phenotypes: M1 classically activated macrophages and M2 alternatively activated macrophages (Zhang S.-Y. et al., 2020). M1 macrophages can be induced by proinflammatory stimuli, such as IFN-γ, TNF-α, granulocyte-macrophage CSF, and TLR ligands. The transcription factors interferon regulatory factor (IRF) 3 and 5 regulate M1 polarization and the expression of type I interferons. On the other hand, M2 macrophage polarization is driven by immunosuppressive stimuli such as TGF-β, IL-4, IL-10, and IL-13, which activate downstream STAT3 and STAT6 transcription factors (Park-Min et al., 2005; Sinha et al., 2005; Xin et al., 2009; Wang et al., 2014). α-ketoglutarate, the downstream product of glutaminolysis, drives M2-like polarization through fatty acid oxidation (FAO) and Jmjd3-dependent epigenetic reprogramming of M2 genes (Liu et al., 2017).

M1 macrophages promote beneficial anti-tumor effects by driving the Th1 response and via the secretion of TNF-α, IL-1, IL-6, IL-12, Type I IFN, CXCL1-3, CXCL5, and CXCL8-10. M2 macrophages contrastingly perform immunosuppressive functions by supporting the Th2 response and secreting IL-10, TGF-β, CCL17, CCL18, CCL22, and CCL24 (Wang et al., 2014; Wu et al., 2020). M2 macrophages also direct tumor progression via the secretion of adrenomedullin and (VEGF) to promote angiogenesis and expression of PD-L1 to allow immune escape of tumor cells (**Figure 1B**) (Chen et al., 2011; Jayasingam et al., 2019). TAMs themselves are recruited into the TME by tumor-derived adenosine, the CCL2/CCR2 axis, the CXCL12/CXCR4 axis, and the VEGF receptor pathway; tumor cells, stromal cells, and macrophages are responsible for the production of chemokines necessary to attract TAMs and MDSCs into the TME (Qian et al., 2011; Hughes et al., 2015; Montalbán Del Barrio et al., 2016; Li X. et al., 2019).

Succinate and prostaglandin E2 (PGE2) are abundant molecules in the TME accountable for TAM-dependent tumor progression. Tumor cells have dysfunctions in succinate dehydrogenase, an enzyme involved in tumor suppression. Succinate accumulates in tumor cells due to the dysfunction of succinate dehydrogenase, and high amounts of succinate released by tumor cells into the TME activates succinate receptor 1 (SUCNR1) expressed on macrophages (Selak et al., 2005; Chen et al., 2021). The subsequent activation generates pro-tumor TAMs, driven by the SUCNR1-triggered-PI3K—hypoxia inducible factor (HIF)-1α axis. In return, activated TAMs increase tumor cell migration by secreting IL-6 (Wu et al., 2020). Similarly, high levels of PGE2 in the TME is associated with tumor progression and poor prognosis (Wang and Dubois, 2010). The inflammatory conditions at tumor sites drive the catalysis of PGE2 from arachidonic acid by COX-2 (Mizuno et al., 2019). PGE2 induces M2-like polarization in macrophages via the phosphorylation of cAMP-responsive element binding pathway, increasing CCAAT enhancer binding protein β expression and ultimately upregulating *Arg1*, *IL-10*, and *Mrc1* gene expressions (**Figure 1B**) (Na et al., 2015). Prima et al. (2017) uncovered PGE2's role in PD-L1 regulation by showing that inhibitors of COX-2, microsomal PGE2 synthase 1, and overexpression of PGE2-degrading enzyme 15-hydroxyprostaglandin dehydrogenase resulted in decreased PD-L1 expression in TAMs (Prima et al., 2017).

Unlike succinate and PGE2, retinoic acid (RA) is a molecule with ambiguous effects on tumor progression. RA *in vitro* exhibited antitumor properties by decreasing TGF-β1 secretion in tumor cells, impairing their abilities to activate macrophages that secrete VEGF and IL-8 (Liss et al., 2002). All-trans-retinoic acid treatment of prostate cancer cells showed a decreased proliferation of pro-tumoral TAMs, impairing their immunosuppressive capacities by disrupting their cytokine secretion and surface molecule expression (Tsagozis et al., 2014). However, Devalaraja et al. (2020) elucidated the role of tumor cell-derived RA in inhibiting the differentiation of monocytes into immunostimulatory DCs and instead driving the differentiation of pro-tumoral TAMs (Devalaraja et al., 2020). RA downregulates the transcription factor IRF4, and reducing the RA level in the TME induces monocyte differentiation into immunostimulatory antigen-presenting cells and restores T cell activity against tumors. The difference between RA and tumor

cell-derived RA leading to contrasting effects need to be better understood.

TAM-Based Therapies

Along with Tregs and MDSCs, immunosuppressive TAMs are among the main players contributing towards immunotherapy resistance. Treatments to disable the immunosuppressive activities of TAMs in the TME has great potential to be used in combination with ICIs. TAM-targeted therapies today focus on restricting their recruitment, depleting them from the TME, or converting them from M2 to the M1 phenotype **Table 1** (Li X. et al., 2019).

Inflammatory cytokines such as IFN-γ and TNF-α induce the production of CSF-1 by tumor cells, which prompts M2 TAM activation or recruitment into the TME (Satriano et al., 1993; Neubert et al., 2018). While anti-CSF-1R treatments demonstrated limited efficacy alone (Ries et al., 2015), anti-CSF1R treatment in combination with anti-PD-1 therapy significantly decreased M2 TAMs while increasing the number of $CD4^+$ and $CD8^+$ TILs in murine models of melanoma (Neubert et al., 2018). In murine models of mesothelioma, it was demonstrated that mesothelioma tumor cells and $CD8^+$ upregulated PD-L1 and PD-1, respectively, in response to anti-CSF-1R therapy alone, emphasizing the importance of incorporating anti-PD-1 therapy into anti-CSF-1R treatment regimens (Magkouta et al., 2021). Anti-CSF-1R therapy moreover was shown to induce the apoptosis of $CSF\text{-}1R^+$ macrophages, serving as a means to deplete them from the TME (Ries et al., 2014). A clinical trial evaluating the combination of the CSF-1R inhibitor MCS110 and anti-PD-1 mAb PDR001 was recently completed, although a report on its efficacy and tolerability has yet to be published (Novartis Pharmaceuticals, 2021). The inhibition of other TAM-recruiting chemokines such as CCL2 and CXCR4 resulted in decreased tumor growth and progression in preclinical trials; however, their performances in combination with ICIs have not yet been evaluated (Li et al., 2017; Zhou et al., 2018).

Another way of targeting TAMs is to promote their conversion from an immunosuppressive phenotype into an antitumoral, proinflammatory phenotype. Tumor cells express CD47 on their surfaces, which engages the signal regulatory protein alpha (SIRPα) receptor on macrophages to provide a "don't eat me" signal (Li X. et al., 2019). SIRPα-IgG1 Fc (TTI-621) is a recombinant fusion protein with the SIRPα domain and the Fc domain responsible for providing the prophagocytic signals required for antitumor activities (Ansell et al., 2021). Because TTI-621 demonstrated promising antitumor activities *in vitro* and in murine models of lymphoma (Lin et al., 2017; Petrova et al., 2017), the safety and efficacy of TTI-621 was evaluated in a phase I study as a monotherapy or in combination with rituximab or nivolumab (NCT02663518 (Trillium Therapeutics Inc., 2021)). TTI-621 overall was well-tolerated and elicited objective responses without causing anemia, highlighting its potential as a therapeutic agent using macrophages as its primary effector cells (Ansell et al., 2021). The synergy between SIRPα-IgG1 Fc and anti-PD-1 mAb can be attributed to their combined ability to reverse the M2-like polarization of TAMs and induce their M1-like phenotype instead (Zhao et al., 2021).

PI3Kγ is a molecule expressed in myeloid cells but not cancer cells, responsible for myeloid cell recruitment during inflammation and cancer. PI3Kγ inhibition demonstrated promising therapeutic potentials to induce the transition from M2 to M1-like TAMs, staggering tumor growth and survival by increasing MHC-II expression and proinflammatory cytokine secretion while decreasing the production of immunosuppressive factors in tumors and TAMs. In murine models of HNSCC, PI3Kγ inhibition synergized with anti-PD-1 therapies, contributing to greater survival and effective antitumoral activities by increasing immune response gene expressions and Teff recruitment to the TME at higher levels than PI3Kγ inhibition alone (Kaneda et al., 2016). Like CSF-1R therapies, PI3Kγ therapies are anticipated to benefit greatly from combination regimens with ICIs. IPI-549, a small molecule inhibitor of PI3Kγ, was found to increase PD-1 and CTLA-4 expressions on Teff upon administration, where additional ICI treatments are anticipated to neutralize their effects. Indeed, in ICI-resistant murine models, the combination of anti-CTLA-4 or anti-PD-1 mAbs with IPI-549 significantly delayed tumor growth in comparison to ICI monotherapies (De Henau et al., 2016). IPI-549 is actively undergoing clinical evaluation in combination with nivolumab (NCT03980041 and NCT02637531) and atezolizumab (NCT03961698) for the treatment of various cancers (Infinity Pharmaceuticals, Inc., 2021a; Infinity Pharmaceuticals, Inc., 2021b; Infinity Pharmaceuticals, Inc., 2021c).

CANCER-ASSOCIATED FIBROBLASTS

CAFs are defined by their ability to degrade the ECM, increase angiogenesis, and promote tumor growth and invasiveness (Mishra et al., 2011). In the TME, epithelial cancer cells release growth factors into the TME that mediate fibroblast activation, such as TGF-β, platelet-derived growth factor, hepatocyte growth factor (HGF), and epidermal growth factor. Resident fibroblasts can be activated by TGF-β binding to the ubiquitous type II serine/threonine kinase receptor TGF-βRII, where it activates TGF-βRI and SMAD. TGF-β/SMAD mediates the exosomal secretion of CXCL12/CXCR4 chemokines by CAFs, where CXCL12 promotes cancer malignancy by increasing tumor cell proliferation, migration, and angiogenesis (Kuzet and Gaggioli, 2016). HGF can induce the conversion of normal fibroblasts into CAFs and promotes tumor proliferation, migration, and ultimately cancer progression (Wu et al., 2013).

CAF-derived Effects on Immune Cell Subtypes

CAFs affect a variety of myeloid cells, such as MDSCs, TAMs, and DCs. CXCL12 within the TME are primarily derived from CAFs (Feig et al., 2013), which recruit myeloid cells into the TME. Similarly, CXCL1 attracts PMN-MDSCs into the TME (Kumar et al., 2017). CAFs additionally secrete IL-6, inducing IDO

production in DCs (Cheng et al., 2016). CXCL12/CXCR4 expression by CAFs is mediated by PGE2 and TGF-β, where the activation of the CXCL12/CXCR4 pathway helps to maintain the elevated TGF-β expression in CAFs (Kojima et al., 2010, 20; Obermajer et al., 2011). The CXCL12/CXCR4 pathway also contributes to T cell exclusion, where CXCL12 inhibitors restored the infiltration of T cells into the TME (Zboralski et al., 2017). Leukemia inhibitory factor (LIF) secreted by CAFs induces the expression of genes related to an oncogenic phenotype, such as CCL2, CCL3, CCL7, CD206, and CD163, but decreases the expression of CXCL9. While CCL2 is an essential chemokine to attract myeloid cells into the TME (Barrett and Puré, 2020), CXCL9 is an important chemoattractant for the migration of $CD8^+$ T cells. LIF additionally inhibits the ability of TAMs to recruit cytotoxic T cells into the TME by using enhancer of zeste 2 polycomb repressive complex 2 subunit to silence the CXCL9 gene (Pascual-García et al., 2019). While CAFs indirectly increase the CCL2 concentration in the TME by inducing CCL2 expression in TAMs, fibroblast activation protein-positive CAFs are capable of secreting their own CCL2s by activating the fibroblastic STAT3 through a JAK2 signaling pathway (**Figure 1B**) (Yang et al., 2016).

The depletion of alpha-smooth muscle actin $(\alpha\text{-SMA})^+$ CAFs led to the acceleration of tumor growth by increasing the recruitment of Tregs into the TME, suggesting a potential positive effect by CAFs in regulating T cell activity against cancer progression (Özdemir et al., 2014). However, the role of CAFs in regulating T cell activity appears to be more complex. In esophageal tumor tissues, $CD8^+$ TILs were found to be negatively correlated to CAFs, while $FoxP3^+$ TILs exhibited a positive correlation with CAFs. Co-culture of cancer cells and CAFs yielded high concentrations of IL-6, where blocking the IL-6 signaling resulted in decreased tumor growth and increased accumulation of $CD8^+$ TILs in tumor tissues. As IL-6 is known to inhibit the TGF-β-dependent differentiation of naive T cells into Tregs (Kimura and Kishimoto, 2010), the role of IL-6 in the TME needs to be better elucidated (Kato et al., 2018).

Specific subsets of CAFs in breast cancer were found to retain $CD4^+$ $CD25^+$ T cells at their surfaces through OX40L, PD-L2, and junctional adhesion molecule 2 pathways to promote their differentiation into Tregs through B7H3 (CD276), CD73, and dipeptidyl-peptidase 4. The molecules described have potential roles in anti-tumor immunity: B7H3 is an immune checkpoint molecule, CD73 is involved in the adenosine pathway (Barrett and Puré, 2020), and dipeptidyl-peptidase 4 cleaves CXCL10, a chemokine with the capacity to recruit Teffs into the TME, into an antagonist to its own receptor CXCR3 (Costa et al., 2018). Furthermore, CAFs possess the ability to cross-present antigens complexed to MHC class I molecules and are involved in the direct killing of Teffs via the expression of Fas ligand and PD-L2. The ligands engage the immune checkpoints Fas and PD-1 on the surfaces of T cells to induce their death and dysfunction (**Figure 1B**) (Lakins et al., 2018). The expression of PD-L1 and PD-L2 by CAFs reduces the infiltration of $CD8^+$ T cells (Cho et al., 2011). CAFs can additionally increase the expression of PD-L1 on tumor cell surfaces by expressing CXCL5, which engages CXCR2 on tumor cells and upregulates PD-L1 by activating PI3K/AKT signaling (Li Z. et al., 2019). TGF-β also has multiple roles in preventing the T cell response to tumors; not only does TGF-β induce the differentiation of CAFs, which increases TGF-β1 signaling in tumors, but it also inhibits $CD8^+$ T cell expansion and function. However, because TGF-β is important for tissue homeostasis, targeting its downstream targets such as NADPH oxidase 4 (NOX4) can be a safer approach to restoring T cell anti-tumor activity restricted by TGF-β. The inhibitor of NOX4 was shown to prevent CAF differentiation and convert it to a normal fibroblast-like cell (Ford et al., 2020).

CAF-Based Therapies

Therapies targeting CAFs have largely been unsuccessful due to the difficulties presented by the cell type. Development of approaches targeted at CAFs face challenges due to the heterogeneity of CAFs and the inability of murine models to emulate the stromal reactions that take place in the human TME (Hanley and Thomas, 2020). While TGF-β inhibition in combination with anti-PD-1 therapy was found to increase $CD8^+$ infiltration into tumors (Mariathasan et al., 2018), no decrease in CAF levels within the TME or $CD8^+$ levels at the tumor margin was observed in CAF-rich models. Although TGF-β inhibition prevents CAF activation, it fails to reverse the CAF phenotype, suggesting its limited therapeutic potential (Ford et al., 2020).

As such, the small molecule inhibitor of NOX4 has been shown to be a promising option to overcome resistance to ICI therapies by targeting CAFs downstream of TGF-β signaling. In murine models of colorectal cancer, CAFs indeed conferred tumor cells resistance to anti-PD-1 treatments by increasing CTLA-4 expression on $CD8^+$ T cells. While CTLA-4 inhibition on CAF-rich lung cancer tumors demonstrated antitumor effects, it had minimal effects on T cells or tumors with low levels of CAFs. The NOX4 inhibitor GKT137831 (setanaxib) instead neutralized the immunosuppressive activity of CAFs by downregulating functional CAF markers such as α-SMA and collagen-1. With increased $CD8^+$ cell tumor infiltration, GKT137831 additionally induced the increased expression of PD-L1 by colorectal tumor cell. The combination of GKT137831 and anti-PD-1 therapy resulted in the greater tumor infiltration by $CD8^+$ T cells and overall survival relative to anti-PD-1 therapy alone. Surprisingly, the depletion of TAMs using anti-CSF-1R inhibitors on CAF-rich tumors had minimal effects, suggesting the importance of characterizing the immune microenvironment to identify their primary immunosuppressive cell populations (Ford et al., 2020). GKT137831 has yet to enter clinical trials as monotherapy or in combination with ICIs.

Instead of turning off the signals necessary for CAF maintenance, a different strategy is to activate signals that maintain the "normal" fibroblast phenotype. In CRC, high vitamin D receptor (VDR) expression by CAFs was associated with longer CRC patient survival (Ferrer-Mayorga et al., 2017). VDR functions as a master transcriptional regulator, where its activation suppresses tumor-supporting signaling pathways (Sherman et al., 2014). The most active vitamin D metabolite,

1α,25-dihydroxyvitamin D_3 ($1,25(OH)_2D_3$), reduced the expression of activated fibroblast marker *S100A4* and the ability of CAFs to induce CRC cell migration. This effect was observed across fibroblasts not only from CRC patients but from human lung, foreskin, and mouse embryo tissues (Ferrer-Mayorga et al., 2017). In the context of pancreatic cancer, pancreatic stellate cells (PSCs), the predominant fibroblast in the TME of the pancreas, have impaired tumor-promoting capacities in response to vitamin D receptor (VDR) engagement VDR signaling was shown to support signaling pathways to promote a quiescent state of PSCs and increase chemotherapy efficacy (Sherman et al., 2014). The VDR agonist paricalcitol is currently in phase I and II clinical trials in combination therapy with the chemotherapeutic agent gemcitabine to evaluate its safety and efficacy in treating pancreatic cancer (NCT03520790 (Perez, 2021) and NCT04617067 (Cancer Trials Ireland, 2021)) **Table 1**.

Despite these potential therapeutic benefits of VDR, Gorchs et al. recently discovered the conflicting roles of VDR agonists in pancreatic cancer therapies. Calcipotriol, a vitamin D_3 analogue, was shown to increase the expression of α-SMA but reduce the secretion of IL-6 and LIF. Additionally, calcipotriol decreased the CAFs' proliferative and migratory capacities, potentially reversing their immunosuppressive phenotypes. Surprisingly, calcipotriol significantly reduced $CD8^+$ T cell function and proliferation, primarily by vitamin D's ability to promote tolerogenic DCs and produce Tregs (Xie et al., 2017; Gorchs et al., 2020). However, calcipotriol increased the expression of PD-L1 on CAFs but decreased their PD-L2 expression, creating an opportunity for anti-PD-1 therapies to circumvent the pro-tumoral effects. Preclinical studies on VDR agonist treatments face further challenges due to the difference in VDR signaling between murine and human biology (Gorchs et al., 2020). Further clinical evaluation is therefore required to validate the efficacy of VDR agonists in affecting human CAF activities.

Another signaling pathway of interest has been the CXCL12/CXCR4 pathway, which recruits immunosuppressive cells while excluding Teffs. NOX-A12 is an RNA oligonucleotide drug that binds CXCL12 with high affinity and effectively inhibits the interactions with its ligands, CXCR4 and CXCR7. In preclinical studies, NOX-A12 synergized with anti-PD-1/PD-L1 therapy by enhancing Teff infiltration into the tumor (Zboralski et al., 2017). Clinical trials of NOX-A12 in combination with pembrolizumab for the treatment of microsatellite-stable CRC or pancreatic cancer demonstrated excellent overall tolerability and efficacy even in heavily pretreated patients who underwent multiple lines of chemotherapy. Responses were attributable to the increased $CD3^+$ T cell infiltration and interferon production. However, the authors did not biopsy tumor samples that received the combination treatment, leaving the post-treatment characterization of the TME left much to be desired (Suarez-Carmona et al., 2021). Currently, NOX-A12 is undergoing additional phase II clinical trials in combination with pembrolizumab to evaluate both its safety and toxicity of the therapy in the context of microsatellite-stable metastatic pancreatic cancer (NCT04901741 (NOXXON Pharma AG, 2021)) **Table 1**. Identifying the synergistic mechanisms between CXCL12 inhibitors and ICIs will help determine the most effective treatment regimens.

TUMOR HYPOXIA

Hypoxia provides tumor growth advantage by exercising several immune suppressive mechanisms (Hompland et al., 2021). It is well established that hypoxic conditions create increased mutational burden in tumor cells leading to heterogeneity and eventual immune escape (Noman et al., 2019; Terry et al., 2020). Tumor hypoxia shields cancer cells from immune surveillance by modulating various regulatory pathways. An immediate outcome of hypoxia is the upregulation and stabilization of the transcription factor HIF. Of the different hypoxia inducible factors, HIF-1α plays an integral role in conferring resistance to immune cell attack by transcriptional regulation of key survival genes in tumors.

Under hypoxic conditions, immune-suppressive actions can additionally be triggered by over-expression of VEGF and activation of VEGF receptor. The master regulator HIF-1α activates immune-suppressive effects by recruiting and stimulating immune-suppressor cells (Treg, MDSC), inducing secretion of immune-suppressive Th2-type cytokines, and inhibiting antitumor immune responses. The latter inhibitory effect is carried out mainly by suppressing the effects of immune cells such as NK, natural killer T (NKT), $CD4^+$ and $CD8^+$ T cells, curtailing antigen-presenting DC cells, and reducing immune-stimulatory Th1-type cytokines (Vaupel and Multhoff, 2018).

Cancer cells adapt to low oxygen levels of hypoxia by metabolic shift, deriving their energy by converting glucose to lactate rather than by aerobic glycolysis/TCA cycle. Even though energy yield in glycolysis is much lower in glycolysis compared to TCA cycle (2 ATPs compared to 36 ATPs), tumor cells utilize the available resources for catabolic processes. In this way, they take the advantage of the situation by producing more biomass for sustainability rather than just increased energy production. Due to increased aerobic glycolysis, lactic acid is generated and released into the TME creating an acidic milieu that is inhospitable for immune cells (Lardner, 2001; Brand et al., 2016; Lim et al., 2020). Tumor acidity could also have a profound effect on the bioactivity and distribution of antibodies, thus potentially dampening the clinical efficacy of therapeutic antibodies (Huber et al., 2017).

However, the effector functions of immune cells that are inhibited by lactic acid and an acidic TME have been experimentally demonstrated to be reversible in a variety of immune cell types across different cancers (Calcinotto et al., 2012). Thus, if the acidic TME can be buffered back to a physiological condition, the anticancer functions of various immune cells can likely be restored—uncovering a potential for an extremely powerful form of immunotherapy. In a preclinical study, Pilon-Thomas et al. examined the effect of pH buffering in the context of cancer immunotherapy (Pilon-Thomas et al., 2016). Bicarbonate administration was added on to the treatment regimen involving anti-PD-1 antibodies, where the

combination showed improved antitumor response in different tumor types to indicate that reversing tumor acidity could be a better treatment option in immune checkpoint blockade therapies. Though the exact mechanism was not apparent, it was evident that more T cell homing to the tumor site could have a played role in tumor suppression. In another study reported by Chafe et al., carbonic anhydrase IX inhibition by SLC-0111 showed decreased TME acidification in part due to reduced glycolytic metabolism of tumor cells, which in turn increased immune activity (Chafe et al., 2019).

Hypoxia-Targeting Therapies

Among the biomarkers for predicting the outcome of immunotherapy, the hypoxic milieu is often overlooked even though it is the basic niche from which complications arise. The extent of hypoxia in a tumor could be an important biomarker to estimate immunotherapy outcomes (Wang B. et al., 2021). A hypoxia-immune based gene signature was constructed by Yang et al. in triple negative breast cancer as a predictive model for risk stratification and survival (Yang et al., 2021). Their model was derived from the existing data in different databases, identifying six cross-cohort prognostic hypoxia-immune related gene signature. The robustness of this model was also validated among different groups of triple negative breast cancer patients, highlighting the importance of hypoxic TME when considering immunotherapy. Furthermore, the negative impact of hypoxia on the tumor immune response by modifying the expression of main immune checkpoints could be advantageous for developing innovative combination approaches (Noman et al., 2019) **Table 1**. As such, it has been suggested that targeting the hypoxic TME would enhance immunotherapy to a great extent (Abou Khouzam et al., 2020). Several immunotherapy studies targeting the hypoxic TME have also been carried out under preclinical and clinical settings, which include the use of hypoxia-activated prodrugs and the inhibition of HIF signaling (Terry et al., 2018).

Hypoxia activated prodrugs are drugs that undergo bioreduction in low-oxygen conditions to yield cytotoxic metabolites. Currently, several hypoxia activated prodrugs are available, where TH-302 (evofosfamide) is widely used as a combinatorial agent in immunotherapy (Guise et al., 2014; Phillips, 2016; Noman et al., 2019). Under hypoxic conditions, TH-302 is reported to reduce the expression of HIF-1α, induce cytotoxicity by DNA crosslinking, and inhibit cell proliferation (Meng et al., 2012). In an *in vivo* mouse study, TH-302 in combination with PD-1 and CTLA-4 inhibitors significantly suppressed prostate cancer and extended the survival period. In this study, immunotherapy alone was not efficient as the hypoxic regions in prostate cancer models lacked T cell infiltration, creating immunotherapy resistance zones. Adding TH-302 to the therapeutic regimen resulted in the suppression of MDSCs while also increasing the recruitment of T cells into hypoxic tumor regions (Jayaprakash et al., 2018). TH-302 also showed favorable results in controlling soft tissue sarcoma when used in combination with Adriamycin (Phillips et al., 2013). TH-302 also showed favorable results in controlling soft tissue sarcoma when used in combination with Adriamycin (Phillips et al., 2013), and similarly, Jamieson et al. reported that the combined therapy of TH-302 and CTLA-4 blockade improved the survival rate in a HNSCC model compared to the use of a single agent alone (Jamieson et al., 2018). In a recent clinical trial, TH-302 is included in the combination therapy with ipilimumab and Adriamycin, where in the latter case, it is used against cancer models of pancreatic, prostate, and melanoma. The results of this ongoing clinical trial (NCT03098160 (Threshold Pharmaceuticals, 2017)) are much awaited to evaluate its performance. However, as promising as they are in overcoming therapy resistance in tumors, hypoxia activated prodrugs have not always been successful in the clinic. The main reason for suggested for this shortcoming is the lack of patient stratification based on tumor hypoxia status, which is highly variable among patients. Thus, the stratification of patients is an essential factor to achieve successful therapy with the hypoxia activated prodrugs (Spiegelberg et al., 2019).

Inhibition of HIF signaling is also one of the avenues to enhance immunotherapy in several cancers exhibiting immunotherapy resistance. Developing pharmacological agents to modulate HIF-1α signaling has inspired significant interest in recent times. Several drug sub-types have been described to inhibit HIF-1α activity and include inhibitors of HIF-1α/HIF-1β dimerization (e.g. acriflavine), HIF-1α degradation (e.g.Bisphenol A), HIF-1α protein synthesis and stability (e.g. Glyceollins) (Semenza, 2012; Ellinghaus et al., 2013; Scholz and Taylor, 2013). In a technique mimicking the mode of activation of acriflavine, HIF-1α transcriptional activity was compromised by deleting the domain essential for dimerization with HIF-1β, leading to successful inhibition of melanoma (Lequeux et al., 2021). In RCC, adding HIF inhibitors has boosted the immunotherapy outcome in therapy resistant patients. Collective data now indicates that combinations of immune checkpoint inhibitors, HIF signaling inhibitors, and cytokines are powerful regimens to address this cancer type (Considine and Hurwitz, 2019). In a phase I clinical trial, another HIF-2α inhibitor, PT2385, in combination with anti-PD1 mAb exerted a higher synergistic inhibitory effect on clear cell RCC in comparison with single agent treatment alone (Ban et al., 2021).

In recent times, hyperbaric Oxygen therapy (HBO) is also gaining momentum as a treatment modality in some of the cancer types with elevated HIFs. HBO mainly targets the HIF axis to suppress cancers, although additional primary or secondary targets of the therapy cannot be ruled out (Zhang et al., 2021). Most recently, HBO therapy has been combined with immunotherapy in a phase I trial (2021–2024) to treat cancer patients with resistance to previous immunotherapy (NCT05031949 (bixiangzhang, 2021)). The study will explore the efficacy and safety of HBO therapy plus camrelizumab as a second-line treatment.

EXOSOMES

Exosomes consist of EVs containing molecules such as lipids, proteins, short RNAs, long noncoding RNAs (lncRNAs), and microRNAs (miRNAs) (D'Asti et al., 2016). Exosomes produced

by cancer cells are classified as tumor-derived exosomes (TEX), responsible for facilitating immunosuppression by mediating the development, maturation, and function of immune cells within the TME (Whiteside, 2016). Besides affecting immune cells, tumor cells can secrete TEX to induce angiogenesis or self-proliferation for their own maintenance, or promote the transformation of normal cells into cancer or cancer-promoting cells (Skog et al., 2008). Exosomes from stromal cells, such as fibroblasts, were additionally shown to support tumor growth by providing nutrients, inhibiting apoptosis of tumor cells, and driving their proliferation (Gurunathan et al., 2019).

LncRNAs

The delivery of lncRNAs via exosomes can promote tumor progression. LncRNA from TEX promotes angiogenesis by stimulating circulating angiogenic cells. The lncRNA HOX antisense intergenic RNA (HOTAIR) contained in TEX from glioma cells affects endothelial cells by promoting their expressions of VEGF-A (Sun et al., 2018). In bladder cancer, HOTAIR promotes the invasion of urothelial bladder cancer cells by upregulating the genes associated with EMT, such as the Snail family transcriptional repressor 1, Laminin subunit gamma 2, and laminin subunit beta 3 (Berrondo et al., 2016). In the context of CRC, the expression level of the exosomal lncRNA 91H was found to be positively associated with the risk of tumor relapse or metastasis in a heterogeneous nuclear ribonucleoprotein K-dependent mechanism (Gao et al., 2018). Similarly, the lncRNA H19 promotes HCC growth, angiogenesis, and metastasis by upregulating VEGF in endothelial cells and promoting the adhesion of CSC-like liver cells to endothelial cells (Matouk et al., 2007; Conigliaro et al., 2015; Niu et al., 2017).

miRNAs

Another type of RNA that can be carried within exosomes are microRNAs. Tregs secrete exosomes containing miR-150-5p and miR-142-3p to cause DC dysfunction in addition to delivering exosomal miR-let-7d to Th1 cells, crippling their effector functions. Tumor cells create an immunosuppressive TME by secreting exosomes carrying miRNAs such as miR-21 to induce M2-like polarization in monocytes, while exosomal miR-21 promotes the activation of MDSCs to drive immunosuppression within the TME (Tan et al., 2020). miR-122 is another miRNA-containing TEX secreted by breast cancer cells, reducing glucose uptake in normal, noncancerous cells by downregulating their expression of pyruvate kinase. Reduction of glucose consumption by other cells promotes cancer growth by increasing glucose availability to tumors, and supports cancer metastasis by influencing pre-metastatic niches to facilitate tumor cell colonization and metastatic formation (Fong et al., 2015).

TEXs carrying miRNAs and circular RNAs (circRNA) can serve as mediums facilitating tumor immune escape and conferring tumor cells resistance to immunotherapy. In the context of glioma, hypoxic glioma-derived exosomes were found to carry miR-1246, which induces M2 macrophage polarization in the TME to drive tumor progression and survival. MiR-1246 targets the telomeric repeat binding factor 2 interacting protein, which subsequently activates STAT3 and inhibits the NF-kB signaling pathway in macrophages, ultimately contributing to immunosuppression (Qian et al., 2020). Furthermore, endoplasmic reticulum stress on HCC cells were found to release exosomes containing miR-23a-3p to TAMs. MiR-23a-3p inhibited the TAM's phosphatase and tensin homolog expression, activating the PI3K-AKT pathway to upregulate their PD-L1 expression (Pascut et al., 2020). Ubiquitin-like with PHD and RING finger domain 1 (UHRF1) is a molecule usually overexpressed in cancer, which is normally responsible for the regulation of DNA methylation. In the context of HCC, the overexpression of UHRF1 promotes tumorigenesis and cancer progression. Not only is the UHRF1-derived circRNA (circUHRF1) closely correlated to poor HCC prognosis, but the HCC-derived exosomal circUHRF1 also degrades the miR-449c-5p in NK cells to upregulate their TIM3 expressions. CircUHRF1 is also implicated to confer resistance to anti-PD-1/PD-L1 therapy, as demonstrated by the increased sensitivity of circUHRF-1-knockdown HCC cells to anti-PD-1/PD-L1 treatment (Zhang P.-F. et al., 2020).

Proteins

Besides RNA, exosomes can contain proteins to drive resistance to immunotherapies (Sun et al., 2018). For example, tumor-derived exosomal PD-L1 has been implicated for its role in driving resistance to anti-PD-1/PD-L1 therapy. Tumor cells secrete exosomes containing PD-L1 both on its surface and inside the exosome, upon which can be transferred to neighboring cells without PD-L1 expression and bind to PD-1 to impair T cell activation (Yang et al., 2018). The expression of PD-L1 on these vesicles is upregulated by IFN-γ (Chen et al., 2018). Exosomal PD-L1 display greater immunosuppressive effects than soluble PD-L1, primarily due to the effect of exosomal MHC-I interaction with TCR enhancing the inhibitory effect of exosomal PD-L1. Like PD-L1 on tumor cells, exosomal PD-L1 unleashes devastating immunosuppressive effects on T cells, promoting the apoptosis of $CD8^+$ T cells, suppressing their proliferation and effector functions, and instead driving the inhibitory activities of Tregs (Yin et al., 2021). The pre-treatment levels of circulating exosomal PD-L1 was significantly higher for melanoma patients who did not respond to pembrolizumab. However, if anti-PD-1/PD-L1 therapy blocks the interaction between PD-1 and PD-L1, how would exosomal PD-L1 confer resistance if it is blocked in the same way? One possible explanation for this phenomenon is that high pre-treatment levels of exosomal PD-L1 may have driven T cells to a point of exhaustion beyond rescue by anti-PD-1/PD-L1 therapy (Chen et al., 2018). Another speculated mechanism is that the delivered anti-PD-L1 mAbs may not be sufficient to block both the exosomal and surface-expressed PD-L1, ultimately leading to T cell inhibition. However, the exact mechanism of exosomal PD-L1-derived resistance still remains elusive, and therapeutic approaches to deplete exosomal PD-L1 from the TME can be investigated, as its removal led to enhanced responses to anti-PD-1/PD-L1 treatments (Yin et al., 2021).

TABLE 1 | List of current cancer immunotherapy clinical trials.

Treatment	Targets	Disease	Phase	Trial identifier
T Cell-based Therapies				
nivolumab or nivolumab/ipilimumab or nivolumab/ipilimumab/ cobimetinib	PD-1, CTLA-4, MEK pathway	Advanced/Metastatic Solid Tumors	I/II	NCT01928394
PD-1 knockout engineered T cell	PD-1	Advanced HCC	I	NCT04417764
Anti-MUC1 CAR T cells and/or PD-1 knockout engineered T cells in comparison to nivolumab	PD-1	Advanced NSCLC	I/II	NCT03525782
cobolimab, dostarlimab, Docetaxel	TIM3, PD-1	Advanced NSCLC	II/III	NCT04655976
etigilimab and nivolumab	TIGIT, PD-1	Advanced/Metastatic Solid Tumors	I/II	NCT04761198
etigilimab and nivolumab	TIGIT, PD-1	Platinum-Resistant Recurrent CCO, PP, or FT Cancer	II	NCT05026606
pembrolizumab and vibostolimab	PD-1, TIGIT	Metastatic NSCLC	III	NCT04738487
BMS-986207, nivolumab, and ipilumumab	TIGIT, PD-1, CTLA-4	Solid Tumors	I/II	NCT02913313
MGD013 (tebotelimab)	PD-1, LAG3	Melanoma	I	NCT04653038
FS118	PD-1, LAG3	SCCHN	I/II	NCT03440437
Treg-based Therapies				
RO7296682 and atezolizumab	CD25, PD-L1	Advanced Solid Tumors	I	NCT04642365
ATOR-1015	CTLA-4, OX40	Solid Tumors	I	NCT03782467
ADCT-301	CD25	AML, MDS, or MDS/MPN	II	NCT04639024
ADCT-301 and pembrolizumab	CD25, PD-1	Advanced Solid Tumors	I	NCT03621982
MDSC-based Therapies				
SX-682 and pembrolizumab	CXCR2, PD-1	Metastatic Melanoma	I	NCT03161431
durvalumab with AZD9150 or AZD5069	PD-L1, STAT3, CXCR2	Advanced Solid Tumors, Relapsed Metastatic SCCHN	II	NCT02499328
pexidartinib (PLX3397)	CSF-1R	Tenosynovial Giant Cell Tumor	III	NCT04488822
Entinostat and pembrolizumab	HDAC, PD-1	Relapsed and Refractory Lymphoma	II	NCT03179930
Entinostat and pembrolizumab	HDAC, PD-1	Stage III/IV Melanoma	II	NCT03765229
TAM-based Therapies				
TTI-621 and rituximab or nivolumab	SIRPα, CD20, PD-1	Hematologic Malignancies and Solid Tumors	I	NCT02663518
IPI-549 and nivolumab	PI3Kγ, PD-1	Advanced Urothelial Carcinoma	II	NCT03980041
IPI-549 and nivolumab	PI3Kγ, PD-1	Advanced Solid Tumors	I	NCT02637531
IPI-549 and atezolizumab/Paclitaxel/bevacizumab	PI3Kγ, PD-L1, VEGF	Triple-Negative Breast Cancer or RCC		NCT03961698
CAF-based Therapies				
Paricalcitol, Gemcitabine, and Nab-paclitaxel	VDR	Metastatic Pancreatic Cancer	I/II	NCT03520790
Paricalcitol, Gemcitabine, and Nab-paclitaxel	VDR	Advanced Pancreatic Cancer	II	NCT04617067
Olaptesed pegol (NOX-A12), pembrolizumab and Nanoliposomal Irinotecan or Gemcitabine/Nab-Paclitaxel	CXCL12, PD-1	Metastatic Pancreatic Cancer	II	NCT04901741
Hypoxia-based Therapies				
Evofosfamide and ipilimumab	CTLA-4	Pancreatic Cancer, Melanoma, SCCHN, Prostate Cancer	I	NCT03098160
Hyperbaric oxygen therapy and camrelizumab	PD-1	Advanced/Metastatic HCC	I	NCT05031949
Exosome-based Therapies				
Mesenchymal Stromal Cells-derived Exosomes with KRAS G12D siRNA	KRAS	Metastatic Pancreatic Cancer	I	NCT03608631

HCC: hepatocellular carcinoma, NSCLC: Non-small cell lung cancer, MUC1: Mucin 1, CAR: chimeric antigen receptor, CCO: clear cell ovarian, PP: primary peritoneal, FT: fallopian tube, AML: acute myeloid leukemia, MDS: myelodysplastic syndrome, MDS/MPN: myeloproliferative neoplasm, SCCHN: Squamous cell carcinoma of head and neck HDAC: Histone deacetylase RCC: renal cell carcinoma, VDR: Vitamin D Receptor, MEK: Mitogen-activated Extracellular kinase, SIRP α: Signal Regulatory Protein α, PI3Kγ: Phosphoinositide 3-kinase γ, VEGF: vascular endothelial growth factor, CXCL: Chemokine (C-X-C) motif ligand, CXCR: Chemokine (C-X-C) motif receptor, CD: cluster of differentiation, CSF-1R: Colony Stimulating Factor 1 Receptor, STAT3: Signal Transducer And Activator Of Transcription 3.

Exosome-based Therapies

Exosomes can be utilized as immunotherapy mediums to deliver appropriate stimulatory signals and carry out effective antitumor immune responses. For example, DC-derived exosomes (DCexos), which contain MHC I, MHC II, and CD86 can activate $CD4^+$ and $CD8^+$ T cells (Viaud et al., 2010). DCexos

loaded with melanoma antigen gene tumor antigens were found to induce melanoma antigen gene-specific T cell responses and increase NK cell lytic activities (Morse et al., 2005). While DCexos, as inert vehicles, exhibit resistance to tumor-derived suppressive factors in addition to their greater bioavailability and biostability, they fail to induce appropriate levels of T cell activation and suffer from low response rates (Fu C. et al., 2020). Instead, synthetic exosomes (iExosomes) can be engineered to incorporate a variety of agents to induce antitumor responses. iExosomes loaded with oxaliplatin (OXA), a chemotherapeutic agent for the treatment of pancreatic ductal adenocarcinoma, and gal-9 small interfering RNA (siRNA) were delivered to the tumor sites of murine pancreatic cancer models. The respective exosomes displayed specific pancreatic tumor-targeting abilities and the downregulation of gal-9 by pancreatic tumor cells to ultimately induce the M1-like polarization of local TAMs. While exosomes loaded with OXA or gal-9 siRNA were unsuccessful in restraining tumor growth alone, their combination regimen significantly decreased tumor size and prolonged survival relative to the effects of the conventional chemotherapeutic agent gemcitabine (Zhou et al., 2021).

Another promising target is the KRAS oncogene, which is a primary drug target in lung cancer. Mutation in KRAS lock it in an active state, sending downstream signals that cause cancer by increasing cell proliferation and survival (Stephen et al., 2014). However, inhibitors targeting KRAS directly faces challenges due to the absence of deep hydrophobic pockets available for binding on the KRAS molecule itself (Cox et al., 2014). As such, the delivery of EFTX-D1, a siRNA selectively targeting the most common mutated KRAS genes such as G12C, G12D, and G13D, has been explored as a therapeutic approach. EFTX-D1 was able to decrease both the levels of oncogenic KRAS mRNA and protein levels, but *in vivo* preclinical trials are yet to be conducted (Papke et al., 2021). In agreement with Papke et al., the authors agree that the nanoparticle delivery of EFTX-D1 using iExosomes will be the next step to evaluate the KRAS inhibitor's performance, possibly in combination with ICIs. The ongoing clinical trial delivering KRAS G12D siRNA in mesenchymal stromal cell-derived iExosomes to pancreatic cancer patients with KRAS G12D mutations will be beneficial to elucidate the challenges and therapeutic efficacy of delivering KRAS siRNAs with iExosomes (NCT03608631 (M.D. Anderson Cancer Center, 2021b)) **Table 1**.

A different approach is to target exosomes using GW4869, which prevents the secretion of exosomes by inhibiting neutral sphingomyelinases (Menck et al., 2017). In the context of breast cancer cells, the administration of GW4869 ameliorated the metabolic changes in the TME caused by CAF-derived exosomes in preclinical trials. CAF-derived exosomes contributed to the immunosuppressive TME by decreasing the oxygen consumption rate by tumor cells and increasing lactate levels, where GW4869 administration partially negated this metabolic change (Li Y. et al., 2020, 3). However, the off-target effects of GW4869 administration needs to be assessed in detail, or ways to specifically target certain CAF-derived exosomes are required for maximal benefits.

CONCLUDING REMARKS

Without a doubt, ICI immunotherapy revolutionized the landscape of cancer treatments in the last decade. While immunotherapy exhibits remarkable potential, there are numerous obstacles within the TME that make it difficult to achieve high response rates and sustained benefits for patients. Immunosuppressive cells, hypoxic conditions, metabolites, and exosomes are among the many factors that contribute to immunotherapy resistance.

Today, there are numerous clinical trials being conducted investigating the different combinations of immunotherapies, which exhibit greater response rate and efficacy. It is evident that targeting multiple inhibitory pathways in the TME contributing to immune escape is a promising approach to enhance anti-tumor activities by immune cells and staunch tumor progression. Incorporating other ICIs beyond anti-CTLA-4 or anti-PD-1/PD-L1 to be used in combination therapies will be the next step in overcoming resistance to immunotherapies involving ICIs, offering patients additional options. Additionally, disabling or clearing the TME of immunosuppressive populations or compounds responsible for ICI resistance will allow T cells to exert their antitumoral effects. Broadening our knowledge of the TME will ultimately bring us closer to the goals of increasing both the number of patients eligible for ICI therapies and the response rates to treatments.

AUTHOR CONTRIBUTIONS

KP and MV drafted the manuscript and performed literature searches. KP prepared the figures and table. DS devised the idea and overall structure of the review. KP, MV, and DS participated in the peer review and finalization of the manuscript.

REFERENCES

Abou Khouzam, R., Goutham, H. V., Zaarour, R. F., Chamseddine, A. N., Francis, A., Buart, S., et al. (2020). Integrating Tumor Hypoxic Stress in Novel and More Adaptable Strategies for Cancer Immunotherapy. *Semin. Cancer Biol.* 65, 140–154. doi:10.1016/j.semcancer.2020.01.003

Acharya, N., Sabatos-Peyton, C., and Anderson, A. C. (2020). Tim-3 Finds its Place in the Cancer Immunotherapy Landscape. *J. Immunother. Cancer* 8, e000911. doi:10.1136/jitc-2020-000911

ADC Therapeutics S.A (2021). A Phase 1b, Open-Label, Dose-Escalation and Dose-Expansion Study to Evaluate the Safety, Tolerability, Pharmacokinetics, and Antitumor Activity of Camidanlumab Tesirine (ADCT-301) as Monotherapy or in Combination in Patients with Selected Advanced Solid Tumors. *clinicaltrials.gov*. Available at: https://clinicaltrials.gov/ct2/show/NCT03621982 (Accessed November 21, 2021).

Alligator Bioscience (2021). A First-In-Human, Multicenter, Open-Label, Phase 1 Study in Patients with Advanced And/or Refractory Solid Malignancies to Evaluate the Safety of Intravenously Administered ATOR-1015. *clinicaltrials.gov*. Available at: https://clinicaltrials.gov/ct2/show/NCT03782467 (Accessed November 25, 2021).

Ansell, S. M., Maris, M. B., Lesokhin, A. M., Chen, R. W., Flinn, I. W., Sawas, A., et al. (2021). Phase I Study of the CD47 Blocker TTI-621 in Patients with Relapsed or Refractory Hematologic Malignancies. *Clin. Cancer Res.* 27, 2190–2199. doi:10.1158/1078-0432.CCR-20-3706

Arce Vargas, F., Furness, A. J. S., Solomon, I., Joshi, K., Mekkaoui, L., Lesko, M. H., et al. (2017). Fc-Optimized Anti-CD25 Depletes Tumor-Infiltrating Regulatory T Cells and Synergizes with PD-1 Blockade to Eradicate Established Tumors. *Immunity* 46, 577–586. doi:10.1016/j.immuni.2017.03.013

Ascierto, P. A., Bono, P., Bhatia, S., Melero, I., Nyakas, M. S., Svane, I.-M., et al. (2017). Efficacy of BMS-986016, a Monoclonal Antibody that Targets Lymphocyte Activation Gene-3 (LAG-3), in Combination with Nivolumab in Pts with Melanoma Who Progressed during Prior Anti-PD-1/pd-L1 Therapy (Mel Prior IO) in All-Comer and Biomarker-Enriched Populations. *Ann. Oncol.* 28, v611–v612. doi:10.1093/annonc/mdx440.011

AstraZeneca (2020). A Phase 1b/2, Open-Label, Multicentre Study Assessing the Safety, Tolerability, Pharmacokinetics, and Preliminary Anti-tumor Activity of MEDI4736 in Combination with AZD9150 or AZD5069 in Patients with Advanced Solid Malignancies and Subsequently Comparing AZD9150 and AZD5069 Both as Monotherapy and in Combination with MEDI4736 as Second Line Treatment in Patients with Recurrent And/or Metastatic Squamous Cell Carcinoma of the Head and Neck. *clinicaltrials.gov*. Available at: https://clinicaltrials.gov/ct2/show/NCT02499328 (Accessed November 21, 2021).

Bagchi, S., Yuan, R., and Engleman, E. G. (2021). Immune Checkpoint Inhibitors for the Treatment of Cancer: Clinical Impact and Mechanisms of Response and Resistance. *Annu. Rev. Pathol. Mech. Dis.* 16, 223–249. doi:10.1146/annurev-pathol-042020-042741

Ban, H. S., Uto, Y., and Nakamura, H. (2021). Hypoxia-inducible Factor (HIF) Inhibitors: a Patent Survey (2016-2020). *Expert Opin. Ther. Patents* 31, 387–397. doi:10.1080/13543776.2021.1874345

Barrett, R. L., and Puré, E. (2020). Cancer-associated Fibroblasts and Their Influence on Tumor Immunity and Immunotherapy. *eLife* 9, e57243. doi:10.7554/eLife.57243

Barrueto, L., Caminero, F., Cash, L., Makris, C., Lamichhane, P., and Deshmukh, R. R. (2020). Resistance to Checkpoint Inhibition in Cancer Immunotherapy. *Translational Oncol.* 13, 100738. doi:10.1016/j.tranon.2019.12.010

Berrondo, C., Flax, J., Kucherov, V., Siebert, A., Osinski, T., Rosenberg, A., et al. (2016). Expression of the Long Non-coding RNA HOTAIR Correlates with Disease Progression in Bladder Cancer and Is Contained in Bladder Cancer Patient Urinary Exosomes. *PLoS ONE* 11, e0147236. doi:10.1371/journal.pone.0147236e0147236

bixiangzhang (2021). A Single-center, Single-Arm, Non-randomized Clinical Study to Evaluate the Efficacy and Safety of Hyperbaric Oxygen Therapy Plus Camrelizumab as a Second-Line Treatment in Advanced/Metastatic Hepatocellular Carcinoma. *clinicaltrials.gov*. Available at: https://clinicaltrials.gov/ct2/show/NCT05031949 (Accessed November 25, 2021).

Brand, A., Singer, K., Koehl, G. E., Kolitzus, M., Schoenhammer, G., Thiel, A., et al. (2016). LDHA-associated Lactic Acid Production Blunts Tumor Immunosurveillance by T and NK Cells. *Cel Metab.* 24, 657–671. doi:10.1016/j.cmet.2016.08.011

Bristol-Myers Squibb (2021). Phase 1/2a First-In-Human Study of BMS-986207 Monoclonal Antibody Alone and in Combination with Nivolumab or with Nivolumab and Ipilimumab in Advanced Solid Tumors. *clinicaltrials.gov*. Available at: https://clinicaltrials.gov/ct2/show/NCT02913313 (Accessed November 25, 2021).

Bunt, S. K., Sinha, P., Clements, V. K., Leips, J., and Ostrand-Rosenberg, S. (2006). Inflammation Induces Myeloid-Derived Suppressor Cells that Facilitate Tumor Progression. *J. Immunol.* 176, 284–290. doi:10.4049/jimmunol.176.1.284

Cable, J., Greenbaum, B., Pe'er, D., Bollard, C. M., Bruni, S., Griffin, M. E., et al. (2021). Frontiers in Cancer Immunotherapy-A Symposium Report. *Ann. N.Y. Acad. Sci.* 1489, 30–47. doi:10.1111/nyas.14526

Calcinotto, A., Filipazzi, P., Grioni, M., Iero, M., De Milito, A., Ricupito, A., et al. (2012). Modulation of Microenvironment Acidity Reverses Anergy in Human and Murine Tumor-Infiltrating T Lymphocytes. *Cancer Res.* 72, 2746–2756. doi:10.1158/0008-5472.CAN-11-1272

Camisaschi, C., Casati, C., Rini, F., Perego, M., De Filippo, A., Triebel, F., et al. (2010). LAG-3 Expression Defines a Subset of CD4+CD25highFoxp3+ Regulatory T Cells that Are Expanded at Tumor Sites. *J.I.* 184, 6545–6551. doi:10.4049/jimmunol.0903879

Cancer Trials Ireland (2021). Phase II, Open Label Clinical Trial of Paricalcitol in Combination with Gemcitabine/Nab-Paclitaxel Therapy in Advanced Pancreatic Cancer. *clinicaltrials.gov*. Available at: https://clinicaltrials.gov/ct2/show/NCT04617067 (Accessed November 21, 2021).

Chafe, S. C., McDonald, P. C., Saberi, S., Nemirovsky, O., Venkateswaran, G., Burugu, S., et al. (2019). Targeting Hypoxia-Induced Carbonic Anhydrase IX Enhances Immune-Checkpoint Blockade Locally and Systemically. *Cancer Immunol. Res.* 7, 1064–1078. doi:10.1158/2326-6066.CIR-18-0657

Chang, S.-Y., Song, J.-H., Guleng, B., Cotoner, C. A., Arihiro, S., Zhao, Y., et al. (2013). Circulatory Antigen Processing by Mucosal Dendritic Cells Controls CD8+ T Cell Activation. *Immunity* 38, 153–165. doi:10.1016/j.immuni.2012.09.018

Chau, I., Doki, Y., Ajani, J. A., Xu, J., Wyrwicz, L., Motoyama, S., et al. (2021). Nivolumab (NIVO) Plus Ipilimumab (IPI) or NIVO Plus Chemotherapy (Chemo) versus Chemo as First-Line (1L) Treatment for Advanced Esophageal Squamous Cell Carcinoma (ESCC): First Results of the CheckMate 648 Study. *JCO* 39, LBA4001. doi:10.1200/JCO10.1200/jco.2021.39.15_suppl.lba4001

Chen, D., Zhang, X., Li, Z., and Zhu, B. (2021). Metabolic Regulatory Crosstalk between Tumor Microenvironment and Tumor-Associated Macrophages. *Theranostics* 11, 1016–1030. doi:10.7150/thno.51777

Chen, G., Huang, A. C., Zhang, W., Zhang, G., Wu, M., Xu, W., et al. (2018). Exosomal PD-L1 Contributes to Immunosuppression and Is Associated with Anti-PD-1 Response. *Nature* 560, 382–386. doi:10.1038/s41586-018-0392-8

Chen, P., Huang, Y., Bong, R., Ding, Y., Song, N., Wang, X., et al. (2011). Tumor-associated Macrophages Promote Angiogenesis and Melanoma Growth via Adrenomedullin in a Paracrine and Autocrine Manner. *Clin. Cancer Res.* 17, 7230–7239. doi:10.1158/1078-0432.CCR-11-1354

Chen, S. (2018). A Clinical Study of Anti-MUC1 CAR T Cells and PD-1 Knockout Engineered T Cells for Patients with Advanced Non-small Cell Lung Cancer. *clinicaltrials.gov*. Available at: https://clinicaltrials.gov/ct2/show/NCT03525782 (Accessed November 21, 2021).

Cheng, A.-L., Hsu, C., Chan, S. L., Choo, S.-P., and Kudo, M. (2020). Challenges of Combination Therapy with Immune Checkpoint Inhibitors for Hepatocellular Carcinoma. *J. Hepatol.* 72, 307–319. doi:10.1016/j.jhep.2019.09.025

Cheng, J.-t., Deng, Y.-n., Yi, H.-m., Wang, G.-y., Fu, B.-s., Chen, W.-j., et al. (2016). Hepatic Carcinoma-Associated Fibroblasts Induce Ido-producing Regulatory Dendritic Cells through IL-6-mediated STAT3 Activation. *Oncogenesis* 5, e198. doi:10.1038/oncsis.2016.7

Cho, Y.-A., Yoon, H.-J., Lee, J.-I., Hong, S.-P., and Hong, S.-D. (2011). Relationship between the Expressions of PD-L1 and Tumor-Infiltrating Lymphocytes in Oral Squamous Cell Carcinoma. *Oral Oncol.* 47, 1148–1153. doi:10.1016/j.oraloncology.2011.08.007

Christmas, B. J., Rafie, C. I., Hopkins, A. C., Scott, B. A., Ma, H. S., Cruz, K. A., et al. (2018). Entinostat Converts Immune-Resistant Breast and Pancreatic Cancers into Checkpoint-Responsive Tumors by Reprogramming Tumor-Infiltrating MDSCs. *Cancer Immunol. Res.* 6, 1561–1577. doi:10.1158/2326-6066.CIR-18-0070

Chun, E., Lavoie, S., Michaud, M., Gallini, C. A., Kim, J., Soucy, G., et al. (2015). CCL2 Promotes Colorectal Carcinogenesis by Enhancing Polymorphonuclear Myeloid-Derived Suppressor Cell Population and Function. *Cel Rep.* 12, 244–257. doi:10.1016/j.celrep.2015.06.024

Collison, L. W., Chaturvedi, V., Henderson, A. L., Giacomin, P. R., Guy, C., Bankoti, J., et al. (2010). IL-35-mediated Induction of a Potent Regulatory T Cell Population. *Nat. Immunol.* 11, 1093–1101. doi:10.1038/ni.1952

Conigliaro, A., Costa, V., Lo Dico, A., Saieva, L., Buccheri, S., Dieli, F., et al. (2015). CD90+ Liver Cancer Cells Modulate Endothelial Cell Phenotype through the Release of Exosomes Containing H19 lncRNA. *Mol. Cancer* 14, 155. doi:10.1186/s12943-015-0426-x

Considine, B., and Hurwitz, M. E. (2019). Current Status and Future Directions of Immunotherapy in Renal Cell Carcinoma. *Curr. Oncol. Rep.* 21, 34. doi:10.1007/s11912-019-0779-1

Costa, A., Kieffer, Y., Scholer-Dahirel, A., Pelon, F., Bourachot, B., Cardon, M., et al. (2018). Fibroblast Heterogeneity and Immunosuppressive Environment in Human Breast Cancer. *Cancer Cell* 33, 463–479. doi:10.1016/j.ccell.2018.01.011

Cox, A. D., Fesik, S. W., Kimmelman, A. C., Luo, J., and Der, C. J. (2014). Drugging the Undruggable Ras: mission Possible? *Nat. Rev. Drug Discov.* 13, 828–851. doi:10.1038/nrd4389

Curiel, T. J., Coukos, G., Zou, L., Alvarez, X., Cheng, P., Mottram, P., et al. (2004). Specific Recruitment of Regulatory T Cells in Ovarian Carcinoma Fosters Immune Privilege and Predicts Reduced Survival. *Nat. Med.* 10, 942–949. doi:10.1038/nm1093

Dadey, R. E., Workman, C. J., and Vignali, D. A. A. (2020). Regulatory T Cells in the Tumor Microenvironment. *Adv. Exp. Med. Biol.* 1273, 105–134. doi:10.1007/978-3-030-49270-010.1007/978-3-030-49270-0_6

Daiichi Sankyo Co., Ltd (2021). Multicenter Single Arm Study of the Efficacy and Safety of Pexidartinib in Adult Subjects with Tenosynovial Giant Cell Tumor. *clinicaltrials.gov*. Available at: https://clinicaltrials.gov/ct2/show/NCT04488822 (Accessed November 21, 2021).

D'Asti, E., Chennakrishnaiah, S., Lee, T. H., and Rak, J. (2016). Extracellular Vesicles in Brain Tumor Progression. *Cell Mol Neurobiol* 36, 383–407. doi:10.1007/s10571-015-0296-1

De Henau, O., Rausch, M., Winkler, D., Campesato, L. F., Liu, C., Cymerman, D. H., et al. (2016). Overcoming Resistance to Checkpoint Blockade Therapy by Targeting PI3Kγ in Myeloid Cells. *Nature* 539, 443–447. doi:10.1038/nature20554

Dees, S., Ganesan, R., Singh, S., and Grewal, I. S. (2021). Regulatory T Cell Targeting in Cancer: Emerging Strategies in Immunotherapy. *Eur. J. Immunol.* 51, 280–291. doi:10.1002/eji.202048992

Devalaraja, S., To, T. K. J., Folkert, I. W., Natesan, R., Alam, M. Z., Li, M., et al. (2020). Tumor-Derived Retinoic Acid Regulates Intratumoral Monocyte Differentiation to Promote Immune Suppression. *Cell* 180, 1098–1114. doi:10.1016/j.cell.2020.02.042

Dong, R., Zhang, M., Hu, Q., Zheng, S., Soh, A., Zheng, Y., et al. (2018). Galectin-3 as a Novel Biomarker for Disease Diagnosis and a Target for Therapy (Review). *Int. J. Mol. Med.* 41, 599–614. doi:10.3892/ijmm.2017.3311

Donia, M., Andersen, R., Kjeldsen, J. W., Fagone, P., Munir, S., Nicoletti, F., et al. (2015). Aberrant Expression of MHC Class II in Melanoma Attracts Inflammatory Tumor-specific CD4+ T- Cells, Which Dampen CD8+ T-Cell Antitumor Reactivity. *Cancer Res.* 75, 3747–3759. doi:10.1158/0008-5472.CAN-14-2956

Dumic, J., Dabelic, S., and Flögel, M. (2006). Galectin-3: an Open-Ended story. *Biochim. Biophys. Acta (Bba) - Gen. Subjects* 1760, 616–635. doi:10.1016/j.bbagen.2005.12.020

Ellinghaus, P., Heisler, I., Unterschemmann, K., Haerter, M., Beck, H., Greschat, S., et al. (2013). BAY 87-2243, a Highly Potent and Selective Inhibitor of Hypoxia-induced Gene Activation Has Antitumor Activities by Inhibition of Mitochondrial Complex I. *Cancer Med.* 2, 611–624. doi:10.1002/cam4.112

F-star Therapeutics Limited (2021). A Phase 1/2, Open-Label, First-In-Human Study to Evaluate the Safety and Anti-tumor Activity of FS118, a LAG-3/pd-L1 Bispecific Antibody, in Patients with Advanced Malignancies. *clinicaltrials.gov*. Available at: https://clinicaltrials.gov/ct2/show/NCT03440437 (Accessed November 25, 2021).

Feig, C., Jones, J. O., Kraman, M., Wells, R. J. B., Deonarine, A., Chan, D. S., et al. (2013). Targeting CXCL12 from FAP-Expressing Carcinoma-Associated Fibroblasts Synergizes with Anti-PD-L1 Immunotherapy in Pancreatic Cancer. *Proc. Natl. Acad. Sci.* 110, 20212–20217. doi:10.1073/pnas.1320318110

Ferrer-Mayorga, G., Gómez-López, G., Barbáchano, A., Fernández-Barral, A., Peña, C., Pisano, D. G., et al. (2017). Vitamin D Receptor Expression and Associated Gene Signature in Tumour Stromal Fibroblasts Predict Clinical Outcome in Colorectal Cancer. *Gut* 66, 1449–1462. doi:10.1136/gutjnl-2015-310977

Fong, M. Y., Zhou, W., Liu, L., Alontaga, A. Y., Chandra, M., Ashby, J., et al. (2015). Breast-cancer-secreted miR-122 Reprograms Glucose Metabolism in Premetastatic Niche to Promote Metastasis. *Nat. Cel Biol* 17, 183–194. doi:10.1038/ncb3094

Ford, K., Hanley, C. J., Mellone, M., Szyndralewiez, C., Heitz, F., Wiesel, P., et al. (2020). NOX4 Inhibition Potentiates Immunotherapy by Overcoming Cancer-Associated Fibroblast-Mediated CD8 T-Cell Exclusion from Tumors. *Cancer Res.* 80, 1846–1860. doi:10.1158/0008-5472.CAN-19-3158

Fourcade, J., Sun, Z., Chauvin, J.-M., Ka, M., Davar, D., Pagliano, O., et al. (2018). CD226 Opposes TIGIT to Disrupt Tregs in Melanoma. *JCI Insight* 3, 121157. doi:10.1172/jci.insight.121157

Franceschini, D., Paroli, M., Francavilla, V., Videtta, M., Morrone, S., Labbadia, G., et al. (2009). PD-L1 Negatively Regulates CD4+CD25+Foxp3+ Tregs by Limiting STAT-5 Phosphorylation in Patients Chronically Infected with HCV. *J. Clin. Invest.* 119, 551–564. doi:10.1172/JCI36604

Fu, C., Zhou, L., Mi, Q.-S., and Jiang, A. (2020a). DC-based Vaccines for Cancer Immunotherapy. *Vaccines* 8, 706. doi:10.3390/vaccines8040706

Fu, Y., Lin, Q., Zhang, Z., and Zhang, L. (2020b). Therapeutic Strategies for the Costimulatory Molecule OX40 in T-Cell-Mediated Immunity. *Acta Pharmaceutica Sinica B* 10, 414–433. doi:10.1016/j.apsb.2019.08.010

Fujita, H., Nograles, K. E., Kikuchi, T., Gonzalez, J., Carucci, J. A., and Krueger, J. G. (2009). Human Langerhans Cells Induce Distinct IL-22-producing CD4+ T Cells Lacking IL-17 Production. *Proc. Natl. Acad. Sci.* 106, 21795–21800. doi:10.1073/pnas.0911472106

Gabrilovich, D. I., and Nagaraj, S. (2009). Myeloid-derived Suppressor Cells as Regulators of the Immune System. *Nat. Rev. Immunol.* 9, 162–174. doi:10.1038/nri2506

Gabrilovich, D. I., Ostrand-Rosenberg, S., and Bronte, V. (2012). Coordinated Regulation of Myeloid Cells by Tumours. *Nat. Rev. Immunol.* 12, 253–268. doi:10.1038/nri3175

Gallina, G., Dolcetti, L., Serafini, P., Santo, C. D., Marigo, I., Colombo, M. P., et al. (2006). Tumors Induce a Subset of Inflammatory Monocytes with Immunosuppressive Activity on CD8+ T Cells. *J. Clin. Invest.* 116, 2777–2790. doi:10.1172/JCI28828

Galon, J., and Bruni, D. (2019). Approaches to Treat Immune Hot, Altered and Cold Tumours with Combination Immunotherapies. *Nat. Rev. Drug Discov.* 18, 197–218. doi:10.1038/s41573-018-0007-y

Gao, T., Liu, X., He, B., Nie, Z., Zhu, C., Zhang, P., et al. (2018). Exosomal lncRNA 91H Is Associated with Poor Development in Colorectal Cancer by Modifying HNRNPK Expression. *Cancer Cel Int* 18, 11. doi:10.1186/s12935-018-0506-2

Gao, X., Zhu, Y., Li, G., Huang, H., Zhang, G., Wang, F., et al. (2012). TIM-3 Expression Characterizes Regulatory T Cells in Tumor Tissues and Is Associated with Lung Cancer Progression. *PLoS One* 7, e30676. doi:10.1371/journal.pone.0030676

Gautron, A.-S., Dominguez-Villar, M., de Marcken, M., and Hafler, D. A. (2014). Enhanced Suppressor Function of TIM-3+FoxP3+regulatory T Cells. *Eur. J. Immunol.* 44, 2703–2711. doi:10.1002/eji.201344392

Ghiringhelli, F., Me´nard, C., Terme, M., Flament, C., Taieb, J., Chaput, N., et al. (2005). CD4+CD25+ Regulatory T Cells Inhibit Natural Killer Cell Functions in a Transforming Growth Factor-β-dependent Manner. *J. Exp. Med.* 202, 1075–1085. doi:10.1084/jem.20051511

GlaxoSmithKline (2021). A Randomized, Open Label Phase 2/3 Study Comparing Cobolimab + Dostarlimab + Docetaxel to Dostarlimab + Docetaxel to Docetaxel Alone in Participants with Advanced Nonsmall Cell Lung Cancer Who Have Progressed on Prior Anti-PD-(L)1 Therapy and Chemotherapy (COSTAR Lung). *clinicaltrials.gov*. Available at: https://clinicaltrials.gov/ct2/show/NCT04655976 (Accessed November 21, 2021).

Gorchs, L., Ahmed, S., Mayer, C., Knauf, A., Fernández Moro, C., Svensson, M., et al. (2020). The Vitamin D Analogue Calcipotriol Promotes an Anti-tumorigenic Phenotype of Human Pancreatic CAFs but Reduces T Cell Mediated Immunity. *Sci. Rep.* 10, 17444. doi:10.1038/s41598-020-74368-3

Greene, S., Robbins, Y., Mydlarz, W. K., Huynh, A. P., Schmitt, N. C., Friedman, J., et al. (2020). Inhibition of MDSC Trafficking with SX-682, a CXCR1/2 Inhibitor, Enhances NK-Cell Immunotherapy in Head and Neck Cancer Models. *Clin. Cancer Res.* 26, 1420–1431. doi:10.1158/1078-0432.CCR-19-2625

Guillerey, C., Harjunpää, H., Carrié, N., Kassem, S., Teo, T., Miles, K., et al. (2018). TIGIT Immune Checkpoint Blockade Restores CD8+ T-Cell Immunity against Multiple Myeloma. *Blood* 132, 1689–1694. doi:10.1182/blood-2018-01-825265

Guise, C. P., Mowday, A. M., Ashoorzadeh, A., Yuan, R., Lin, W.-H., Wu, D.-H., et al. (2014). Bioreductive Prodrugs as Cancer Therapeutics: Targeting Tumor Hypoxia. *Chin. J. Cancer* 33, 80–86. doi:10.5732/cjc.012.10285

Gurunathan, S., Kang, M.-H., Jeyaraj, M., Qasim, M., and Kim, J.-H. (2019). Review of the Isolation, Characterization, Biological Function, and Multifarious Therapeutic Approaches of Exosomes. *Cells* 8, 307. doi:10.3390/cells8040307

Gwynn Long MD (2021). An Open-Label Pilot Study to Evaluate the Safety and Efficacy of ADCT-301 in Patients with Relapsed or Refractory Acute Myeloid Leukemia, Myelodysplastic Syndrome, or Myeloproliferative Neoplasms. *clinicaltrials.gov*. Available at: https://clinicaltrials.gov/ct2/show/NCT04639024 (Accessed November 21, 2021).

Ha, D., Tanaka, A., Kibayashi, T., Tanemura, A., Sugiyama, D., Wing, J. B., et al. (2019). Differential Control of Human Treg and Effector T Cells in Tumor Immunity by Fc-Engineered Anti-CTLA-4 Antibody. *Proc. Natl. Acad. Sci. USA* 116, 609–618. doi:10.1073/pnas.1812186116

Hanley, C. J., and Thomas, G. J. (2020). T-cell Tumour Exclusion and Immunotherapy Resistance: a Role for CAF Targeting. *Br. J. Cancer* 123, 1353–1355. doi:10.1038/s41416-020-1020-6

Harjunpää, H., and Guillerey, C. (2020). TIGIT as an Emerging Immune Checkpoint. *Clin. Exp. Immunol.* 200, 108–119. doi:10.1111/cei.13407

Haslam, A., Gill, J., and Prasad, V. (2020). Estimation of the Percentage of US Patients with Cancer Who Are Eligible for Immune Checkpoint Inhibitor Drugs. *JAMA Netw. Open* 3, e200423. doi:10.1001/jamanetworkopen.2020.0423

He, Y., Rivard, C. J., Rozeboom, L., Yu, H., Ellison, K., Kowalewski, A., et al. (2016). Lymphocyte-activation Gene-3, an Important Immune Checkpoint in Cancer. *Cancer Sci.* 107, 1193–1197. doi:10.1111/cas.12986

Hellsten, R., Lilljebjörn, L., Johansson, M., Leandersson, K., and Bjartell, A. (2019). The STAT3 Inhibitor Galiellalactone Inhibits the Generation of MDSC-like Monocytes by Prostate Cancer Cells and Decreases Immunosuppressive and Tumorigenic Factors. *Prostate* 79, 1611–1621. doi:10.1002/pros.23885

Hemon, P., Jean-Louis, F., Ramgolam, K., Brignone, C., Viguier, M., Bachelez, H., et al. (2011). MHC Class II Engagement by its Ligand LAG-3 (CD223) Contributes to Melanoma Resistance to Apoptosis. *J.I.* 186, 5173–5183. doi:10.4049/jimmunol.1002050

Hoffmann-La Roche (2021). An Open-Label, Multicenter, Phase Ib Study to Evaluate the Safety, Tolerability, Pharmacokinetics, Pharmacodynamics, and Preliminary Anti-tumor Activity of RO7296682 in Combination with Atezolizumab in Participants with Advanced And/or Metastatic Solid Tumors. *clinicaltrials.gov*. Available at: https://clinicaltrials.gov/ct2/show/NCT04642365 (Accessed November 21, 2021).

Hompland, T., Fjeldbo, C. S., and Lyng, H. (2021). Tumor Hypoxia as a Barrier in Cancer Therapy: Why Levels Matter. *Cancers* 13, 499. doi:10.3390/cancers13030499

Huang, B., Lei, Z., Zhao, J., Gong, W., Liu, J., Chen, Z., et al. (2007). CCL2/CCR2 Pathway Mediates Recruitment of Myeloid Suppressor Cells to Cancers. *Cancer Lett.* 252, 86–92. doi:10.1016/j.canlet.2006.12.012

Huang, C.-T., Workman, C. J., Flies, D., Pan, X., Marson, A. L., Zhou, G., et al. (2004). Role of LAG-3 in Regulatory T Cells. *Immunity* 21, 503–513. doi:10.1016/j.immuni.2004.08.010

Huang, Y.-H., Zhu, C., Kondo, Y., Anderson, A. C., Gandhi, A., Russell, A., et al. (2015). CEACAM1 Regulates TIM-3-Mediated Tolerance and Exhaustion. *Nature* 517, 386–390. doi:10.1038/nature13848

Huard, B., Gaulard, P., Faure, F., Hercend, T., and Triebel, F. (1994). Cellular Expression and Tissue Distribution of the Human LAG-3-Encoded Protein, an MHC Class II Ligand. *Immunogenetics* 39, 213–217. doi:10.1007/BF00241263

Huber, V., Camisaschi, C., Berzi, A., Ferro, S., Lugini, L., Triulzi, T., et al. (2017). Cancer Acidity: An Ultimate Frontier of Tumor Immune Escape and a Novel Target of Immunomodulation. *Semin. Cancer Biol.* 43, 74–89. doi:10.1016/j.semcancer.2017.03.001

Hughes, R., Qian, B.-Z., Rowan, C., Muthana, M., Keklikoglou, I., Olson, O. C., et al. (2015). Perivascular M2 Macrophages Stimulate Tumor Relapse after Chemotherapy. *Cancer Res.* 75, 3479–3491. doi:10.1158/0008-5472.CAN-14-3587

Iellem, A., Mariani, M., Lang, R., Recalde, H., Panina-Bordignon, P., Sinigaglia, F., et al. (2001). Unique Chemotactic Response Profile and Specific Expression of Chemokine Receptors Ccr4 and Ccr8 by Cd4+Cd25+ Regulatory T Cells. *J. Exp. Med.* 194, 847–854. doi:10.1084/jem.194.6.847

Infinity Pharmaceuticals, Inc (2021a). A Phase 1/1b First-In-Human, Dose-Escalation Study to Evaluate the Safety, Tolerability, Pharmacokinetics, and Pharmacodynamics of IPI-549 Monotherapy and in Combination with Nivolumab in Subjects with Advanced Solid Tumors. *clinicaltrials.gov*. Available at: https://clinicaltrials.gov/ct2/show/NCT02637531 (Accessed January 13, 2022).

Infinity Pharmaceuticals, Inc (2021b). A Phase 2, Multi-Arm, Multicenter, Open-Label Study to Evaluate the Efficacy and Safety of IPI-549 Administered in Combination with Front-Line Treatment Regimens in Patients with Locally Advanced And/or Metastatic Triple-Negative Breast Cancer or Renal Cell Carcinoma. *clinicaltrials.gov*. Available at: https://clinicaltrials.gov/ct2/show/NCT03961698 (Accessed January 13, 2022).

Infinity Pharmaceuticals, Inc (2021c). A Phase 2, Multicenter, Randomized, Double-Blind, Active-Control Study to Evaluate the Efficacy and Safety of Nivolumab Administered in Combination with IPI-549 Compared to Nivolumab Monotherapy in the Treatment of Patients with Immune Therapy-Naïve, Advanced Urothelial Carcinoma. *clinicaltrials.gov*. Available at: https://clinicaltrials.gov/ct2/show/NCT03980041 (Accessed January 13, 2022).

Ipilimumab FDA (2021). Highlights of Prescribing Information. Label Available at: https://www.accessdata.fda.gov/drugsatfda_docs/label/2021/125377s121lbl.pdf (Accessed December 2, 2021).

Iwahori, K. (2020). Cytotoxic CD8+ Lymphocytes in the Tumor Microenvironment. *Adv. Exp. Med. Biol.* 1224, 53–62. doi:10.1007/978-3-030-35723-810.1007/978-3-030-35723-8_4

Jamieson, S. M. F., Tsai, P., Kondratyev, M. K., Budhani, P., Liu, A., Senzer, N. N., et al. (2018). Evofosfamide for the Treatment of Human Papillomavirus-Negative Head and Neck Squamous Cell Carcinoma. *JCI Insight* 3, 122204. doi:10.1172/jci.insight.122204

Jayaprakash, P., Ai, M., Liu, A., Budhani, P., Bartkowiak, T., Sheng, J., et al. (2018). Targeted Hypoxia Reduction Restores T Cell Infiltration and Sensitizes Prostate Cancer to Immunotherapy. *J. Clin. Invest.* 128, 5137–5149. doi:10.1172/JCI96268

Jayasingam, S. D., Citartan, M., Thang, T. H., Mat Zin, A. A., and Ch'ng, E. S. (2019). Evaluating the Polarization of Tumor-Associated Macrophages into M1 and M2 Phenotypes in Human Cancer Tissue: Technicalities and Challenges in Routine Clinical Practice. *Front. Oncol.* 9, 1512. doi:10.3389/fonc.2019.01512

Jiang, X., Wang, J., Deng, X., Xiong, F., Ge, J., Xiang, B., et al. (2019). Role of the Tumor Microenvironment in PD-L1/pd-1-Mediated Tumor Immune Escape. *Mol. Cancer* 18, 10. doi:10.1186/s12943-018-0928-4

Joller, N., Lozano, E., Burkett, P. R., Patel, B., Xiao, S., Zhu, C., et al. (2014). Treg Cells Expressing the Coinhibitory Molecule TIGIT Selectively Inhibit Proinflammatory Th1 and Th17 Cell Responses. *Immunity* 40, 569–581. doi:10.1016/j.immuni.2014.02.012

Kamada, T., Togashi, Y., Tay, C., Ha, D., Sasaki, A., Nakamura, Y., et al. (2019). PD-1+ Regulatory T Cells Amplified by PD-1 Blockade Promote Hyperprogression of Cancer. *Proc. Natl. Acad. Sci. USA* 116, 9999–10008. doi:10.1073/pnas.1822001116

Kaneda, M. M., Messer, K. S., Ralainirina, N., Li, H., Leem, C. J., Gorjestani, S., et al. (2016). PI3Kγ Is a Molecular Switch that Controls Immune Suppression. *Nature* 539, 437–442. doi:10.1038/nature19834

Kang, C.-W., Dutta, A., Chang, L.-Y., Mahalingam, J., Lin, Y.-C., Chiang, J.-M., et al. (2015). Apoptosis of Tumor Infiltrating Effector TIM-3+CD8+ T Cells in colon Cancer. *Sci. Rep.* 5, 15659. doi:10.1038/srep15659

Kato, T., Noma, K., Ohara, T., Kashima, H., Katsura, Y., Sato, H., et al. (2018). Cancer-Associated Fibroblasts Affect Intratumoral CD8+ and FoxP3+ T Cells via IL6 in the Tumor Microenvironment. *Clin. Cancer Res.* 24, 4820–4833. doi:10.1158/1078-0432.CCR-18-0205

Katoh, H., Wang, D., Daikoku, T., Sun, H., Dey, S. K., and DuBois, R. N. (2013). CXCR2-expressing Myeloid-Derived Suppressor Cells Are Essential to Promote Colitis-Associated Tumorigenesis. *Cancer Cell* 24, 631–644. doi:10.1016/j.ccr.2013.10.009

Kim, W., Chu, T. H., Nienhüser, H., Jiang, Z., Del Portillo, A., Remotti, H. E., et al. (2021). PD-1 Signaling Promotes Tumor-Infiltrating Myeloid-Derived Suppressor Cells and Gastric Tumorigenesis in Mice. *Gastroenterology* 160, 781–796. doi:10.1053/j.gastro.2020.10.036

Kimura, A., and Kishimoto, T. (2010). IL-6: Regulator of Treg/Th17 Balance. *Eur. J. Immunol.* 40, 1830–1835. doi:10.1002/eji.201040391

Koch, M. A., Tucker-Heard, G. s., Perdue, N. R., Killebrew, J. R., Urdahl, K. B., and Campbell, D. J. (2009). The Transcription Factor T-Bet Controls Regulatory T Cell Homeostasis and Function during Type 1 Inflammation. *Nat. Immunol.* 10, 595–602. doi:10.1038/ni.1731

Kojima, Y., Acar, A., Eaton, E. N., Mellody, K. T., Scheel, C., Ben-Porath, I., et al. (2010). Autocrine TGF- and Stromal Cell-Derived Factor-1 (SDF-1) Signaling Drives the Evolution of Tumor-Promoting Mammary Stromal Myofibroblasts. *Proc. Natl. Acad. Sci.* 107, 20009–20014. doi:10.1073/pnas.1013805107

Kooshkaki, O., Derakhshani, A., Hosseinkhani, N., Torabi, M., Safaei, S., Brunetti, O., et al. (2020). Combination of Ipilimumab and Nivolumab in Cancers: From Clinical Practice to Ongoing Clinical Trials. *Ijms* 21, 4427. doi:10.3390/ijms21124427

Kortylewski, M., Kujawski, M., Wang, T., Wei, S., Zhang, S., Pilon-Thomas, S., et al. (2005). Inhibiting Stat3 Signaling in the Hematopoietic System Elicits Multicomponent Antitumor Immunity. *Nat. Med.* 11, 1314–1321. doi:10.1038/nm1325

Kouo, T., Huang, L., Pucsek, A. B., Cao, M., Solt, S., Armstrong, T., et al. (2015). Galectin-3 Shapes Antitumor Immune Responses by Suppressing CD8+ T Cells via LAG-3 and Inhibiting Expansion of Plasmacytoid Dendritic Cells. *Cancer Immunol. Res.* 3, 412–423. doi:10.1158/2326-6066.CIR-14-0150

Koyama, S., Akbay, E. A., Li, Y. Y., Herter-Sprie, G. S., Buczkowski, K. A., Richards, W. G., et al. (2016). Adaptive Resistance to Therapeutic PD-1 Blockade Is Associated with Upregulation of Alternative Immune Checkpoints. *Nat. Commun.* 7, 10501. doi:10.1038/ncomms10501

Kuang, D.-M., Peng, C., Zhao, Q., Wu, Y., Zhu, L.-Y., Wang, J., et al. (2010). Tumor-activated Monocytes Promote Expansion of IL-17-producing CD8+ T Cells in Hepatocellular Carcinoma Patients. *J.I.* 185, 1544–1549. doi:10.4049/jimmunol.0904094

Kuang, Z., Jing, H., Wu, Z., Wang, J., Li, Y., Ni, H., et al. (2020). Development and Characterization of a Novel Anti-OX40 Antibody for Potent Immune Activation. *Cancer Immunol. Immunother.* 69, 939–950. doi:10.1007/s00262-020-02501-2

Kumar, V., Donthireddy, L., Marvel, D., Condamine, T., Wang, F., Lavilla-Alonso, S., et al. (2017). Cancer-Associated Fibroblasts Neutralize the Anti-tumor Effect of CSF1 Receptor Blockade by Inducing PMN-MDSC Infiltration of Tumors. *Cancer Cell* 32, 654–668. doi:10.1016/j.ccell.2017.10.005

Kuzet, S.-E., and Gaggioli, C. (2016). Fibroblast Activation in Cancer: when Seed Fertilizes Soil. *Cell Tissue Res* 365, 607–619. doi:10.1007/s00441-016-2467-x

Kvarnhammar, A. M., Veitonmäki, N., Hägerbrand, K., Dahlman, A., Smith, K. E., Fritzell, S., et al. (2019). The CTLA-4 X OX40 Bispecific Antibody ATOR-1015 Induces Anti-tumor Effects through Tumor-Directed Immune Activation. *J. Immunotherapy Cancer* 7, 103. doi:10.1186/s40425-019-0570-8

Lakins, M. A., Ghorani, E., Munir, H., Martins, C. P., and Shields, J. D. (2018). Cancer-associated Fibroblasts Induce Antigen-specific Deletion of CD8 + T Cells to Protect Tumour Cells. *Nat. Commun.* 9, 948. doi:10.1038/s41467-018-03347-0

Lang, R., Patel, D., Morris, J. J., Rutschman, R. L., and Murray, P. J. (2002). Shaping Gene Expression in Activated and Resting Primary Macrophages by IL-10. *J. Immunol.* 169, 2253–2263. doi:10.4049/jimmunol.169.5.2253

Lardner, A. (2001). The Effects of Extracellular pH on Immune Function. *J. Leukoc. Biol.* 69, 522–530.

Law, A. M. K., Lim, E., Ormandy, C. J., and Gallego-Ortega, D. (2017). The Innate and Adaptive Infiltrating Immune Systems as Targets for Breast Cancer Immunotherapy. *Endocr. Relat. Cancer* 24, R123–R144. doi:10.1530/ERC-16-0404

Law, A. M. K., Valdes-Mora, F., and Gallego-Ortega, D. (2020). Myeloid-Derived Suppressor Cells as a Therapeutic Target for Cancer. *Cells* 9, 561. doi:10.3390/cells9030561

Lequeux, A., Noman, M. Z., Xiao, M., Van Moer, K., Hasmim, M., Benoit, A., et al. (2021). Targeting HIF-1 Alpha Transcriptional Activity Drives Cytotoxic Immune Effector Cells into Melanoma and Improves Combination Immunotherapy. *Oncogene* 40, 4725–4735. doi:10.1038/s41388-021-01846-x

Li, C., Jiang, P., Wei, S., Xu, X., and Wang, J. (2020a). Regulatory T Cells in Tumor Microenvironment: New Mechanisms, Potential Therapeutic Strategies and Future Prospects. *Mol. Cancer* 19, 116. doi:10.1186/s12943-020-01234-1

Li, N., Jilisihan, B., Wang, W., Tang, Y., and Keyoumu, S. (2018). Soluble LAG3 Acts as a Potential Prognostic Marker of Gastric Cancer and its Positive Correlation with CD8+T Cell Frequency and Secretion of IL-12 and INF-γ in Peripheral Blood. *Cbm* 23, 341–351. doi:10.3233/CBM-181278

Li, X., Liu, R., Su, X., Pan, Y., Han, X., Shao, C., et al. (2019a). Harnessing Tumor-Associated Macrophages as Aids for Cancer Immunotherapy. *Mol. Cancer* 18, 177. doi:10.1186/s12943-019-1102-3

Li, X., Yao, W., Yuan, Y., Chen, P., Li, B., Li, J., et al. (2017). Targeting of Tumour-Infiltrating Macrophages via CCL2/CCR2 Signalling as a Therapeutic Strategy against Hepatocellular Carcinoma. *Gut* 66, 157–167. doi:10.1136/gutjnl-2015-310514

Li, Y., Zhao, Z., Liu, W., and Li, X. (2020b). SNHG3 Functions as miRNA Sponge to Promote Breast Cancer Cells Growth through the Metabolic Reprogramming. *Appl. Biochem. Biotechnol.* 191, 1084–1099. doi:10.1007/s12010-020-03244-7

Li, Z., Zhou, J., Zhang, J., Li, S., Wang, H., and Du, J. (2019b). Cancer-associated Fibroblasts Promote PD-L1 Expression in Mice Cancer Cells via Secreting CXCL5. *Int. J. Cancer*. doi:10.1002/ijc.32278

Lim, A. R., Rathmell, W. K., and Rathmell, J. C. (2020). The Tumor Microenvironment as a Metabolic Barrier to Effector T Cells and Immunotherapy. *Elife* 9, e55185. doi:10.7554/eLife.55185

Limagne, E., Richard, C., Thibaudin, M., Fumet, J.-D., Truntzer, C., Lagrange, A., et al. (2019). Tim-3/galectin-9 Pathway and mMDSC Control Primary and Secondary Resistances to PD-1 Blockade in Lung Cancer Patients. *Oncoimmunology* 8, e1564505. doi:10.1080/2162402X.2018.1564505

Lin, G. H. Y., Chai, V., Lee, V., Dodge, K., Truong, T., Wong, M., et al. (2017). TTI-621 (SIRPαFc), a CD47-Blocking Cancer Immunotherapeutic, Triggers Phagocytosis of Lymphoma Cells by Multiple Polarized Macrophage Subsets. *PLoS ONE* 12, e0187262. doi:10.1371/journal.pone.0187262

Liss, C., Fekete, M. J., Hasina, R., and Lingen, M. W. (2002). Retinoic Acid Modulates the Ability of Macrophages to Participate in the Induction of the Angiogenic Phenotype in Head and Neck Squamous Cell Carcinoma. *Int. J. Cancer* 100, 283–289. doi:10.1002/ijc.10507

Liu, P.-S., Wang, H., Li, X., Chao, T., Teav, T., Christen, S., et al. (2017). α-Ketoglutarate Orchestrates Macrophage Activation through Metabolic and Epigenetic Reprogramming. *Nat. Immunol.* 18, 985–994. doi:10.1038/ni.3796

Liu, Y., Zhou, N., Zhou, L., Wang, J., Zhou, Y., Zhang, T., et al. (2021). IL-2 Regulates Tumor-Reactive CD8+ T Cell Exhaustion by Activating the Aryl Hydrocarbon Receptor. *Nat. Immunol.* 22, 358–369. doi:10.1038/s41590-020-00850-9

Lowther, D. E., Goods, B. A., Lucca, L. E., Lerner, B. A., Raddassi, K., van Dijk, D., et al. (2016). PD-1 marks Dysfunctional Regulatory T Cells in Malignant Gliomas. *JCI Insight* 1, e85935. doi:10.1172/jci.insight.85935

Lozano, E., Dominguez-Villar, M., Kuchroo, V., and Hafler, D. A. (2012). The TIGIT/CD226 axis Regulates Human T Cell Function. *J.I.* 188, 3869–3875. doi:10.4049/jimmunol.1103627

Magkouta, S. F., Vaitsi, P. C., Pappas, A. G., Iliopoulou, M., Kosti, C. N., Psarra, K., et al. (2021). CSF1/CSF1R Axis Blockade Limits Mesothelioma and Enhances Efficiency of Anti-PDL1 Immunotherapy. *Cancers* 13, 2546. doi:10.3390/cancers13112546

Mantovani, A., Allavena, P., Sica, A., and Balkwill, F. (2008). Cancer-related Inflammation. *Nature* 454, 436–444. doi:10.1038/nature07205

Mariathasan, S., Turley, S. J., Nickles, D., Castiglioni, A., Yuen, K., Wang, Y., et al. (2018). TGFβ Attenuates Tumour Response to PD-L1 Blockade by Contributing to Exclusion of T Cells. *Nature* 554, 544–548. doi:10.1038/nature25501

Martens, A., Wistuba-Hamprecht, K., Yuan, J., Postow, M. A., Wong, P., Capone, M., et al. (2016). Increases in Absolute Lymphocytes and Circulating CD4+ and CD8+ T Cells Are Associated with Positive Clinical Outcome of Melanoma Patients Treated with Ipilimumab. *Clin. Cancer Res.* 22, 4848–4858. doi:10.1158/1078-0432.CCR-16-0249

Maruhashi, T., Sugiura, D., Okazaki, I.-M., and Okazaki, T. (2020). LAG-3: from Molecular Functions to Clinical Applications. *J. Immunother. Cancer* 8, e001014. doi:10.1136/jitc-2020-001014

Matouk, I. J., DeGroot, N., Mezan, S., Ayesh, S., Abu-lail, R., Hochberg, A., et al. (2007). The H19 Non-coding RNA Is Essential for Human Tumor Growth. *PLoS One* 2, e845. doi:10.1371/journal.pone.0000845

M.D. Anderson Cancer Center (2021a). EON: A Single-Arm Phase II Study of Etigilimab (OMP-313M32) in Combination with Checkpoint Inhibition (Nivolumab) in Patients with Platinum-Resistant, Recurrent Epithelial Ovarian Cancer. *clinicaltrials.gov*. Available at: https://clinicaltrials.gov/ct2/show/NCT05026606 (Accessed November 21, 2021).

M.D. Anderson Cancer Center (2021b). Phase I Study of Mesenchymal Stromal Cells-Derived Exosomes with KrasG12D siRNA for Metastatic Pancreas Cancer Patients Harboring KrasG12D Mutation. *clinicaltrials.gov*. Available at: https://clinicaltrials.gov/ct2/show/NCT03608631 (Accessed November 25, 2021).

Mellor, A. L., and Munn, D. H. (2004). Ido Expression by Dendritic Cells: Tolerance and Tryptophan Catabolism. *Nat. Rev. Immunol.* 4, 762–774. doi:10.1038/nri1457

Memorial Sloan Kettering Cancer Center (2021). A Phase II Study of Pembrolizumab and Entinostat in Patients with Relapsed and Refractory Lymphomas. *clinicaltrials.gov*. Available at: https://clinicaltrials.gov/ct2/show/NCT03179930 (Accessed November 21, 2021).

Menck, K., Sönmezer, C., Worst, T. S., Schulz, M., Dihazi, G. H., Streit, F., et al. (2017). Neutral Sphingomyelinases Control Extracellular Vesicles Budding from the Plasma Membrane. *J. Extracellular Vesicles* 6, 1378056. doi:10.1080/20013078.2017.1378056

Meng, F., Evans, J. W., Bhupathi, D., Banica, M., Lan, L., Lorente, G., et al. (2012). Molecular and Cellular Pharmacology of the Hypoxia-Activated Prodrug TH-302. *Mol. Cancer Ther.* 11, 740–751. doi:10.1158/1535-7163.MCT-11-0634

Merck Sharp & Dohme Corp (2021). A Phase 3, Multicenter, Randomized, Double-Blind Study of MK-7684 with Pembrolizumab as a Coformulation (MK-7684A) versus Pembrolizumab Monotherapy as First Line Treatment for Participants with PD-L1 Positive Metastatic Non-small Cell Lung Cancer. *clinicaltrials.gov*. Available at: https://clinicaltrials.gov/ct2/show/NCT04738487 (Accessed November 25, 2021).

Mereo BioPharma (2021). A Phase 1b/2 Open-Label Study of the Efficacy and Safety of Etigilimab (MPH313) Administered in Combination with Nivolumab to Subjects with Locally Advanced or Metastatic Solid Tumors (ACTIVATE). *clinicaltrials.gov*. Available at: https://clinicaltrials.gov/ct2/show/NCT04761198 (Accessed November 21, 2021).

Mishra, P., Banerjee, D., and Ben-Baruch, A. (2011). Chemokines at the Crossroads of Tumor-Fibroblast Interactions that Promote Malignancy. *J. Leukoc. Biol.* 89, 31–39. doi:10.1189/jlb.0310182

Mizuno, R., Kawada, K., and Sakai, Y. (2019). Prostaglandin E2/EP Signaling in the Tumor Microenvironment of Colorectal Cancer. *Ijms* 20, 6254. doi:10.3390/ijms20246254

Mok, S., Koya, R. C., Tsui, C., Xu, J., Robert, L., Wu, L., et al. (2014). Inhibition of CSF-1 Receptor Improves the Antitumor Efficacy of Adoptive Cell Transfer Immunotherapy. *Cancer Res.* 74, 153–161. doi:10.1158/0008-5472.CAN-13-1816

Montalbán del Barrio, I., Penski, C., Schlahsa, L., Stein, R. G., Diessner, J., Wöckel, A., et al. (2016). Adenosine-generating Ovarian Cancer Cells Attract Myeloid Cells Which Differentiate into Adenosine-Generating Tumor Associated Macrophages - a Self-Amplifying, CD39- and CD73-dependent Mechanism for Tumor Immune Escape. *J. Immunotherapy Cancer* 4, 49. doi:10.1186/s40425-016-0154-9

Morse, M. A., Garst, J., Osada, T., Khan, S., Hobeika, A., Clay, T. M., et al. (2005). A Phase I Study of Dexosome Immunotherapy in Patients with Advanced Non-small Cell Lung Cancer. *J. Transl Med.* 3, 9. doi:10.1186/1479-5876-3-9

Müller, M., Carter, S. L., Hofer, M. J., Manders, P., Getts, D. R., Getts, M. T., et al. (2007). CXCR3 Signaling Reduces the Severity of Experimental Autoimmune Encephalomyelitis by Controlling the Parenchymal Distribution of Effector and Regulatory T Cells in the Central Nervous System. *J. Immunol.* 179, 2774–2786. doi:10.4049/jimmunol.179.5.2774

Na, Y. R., Jung, D., Yoon, B. R., Lee, W. W., and Seok, S. H. (2015). Endogenous Prostaglandin E2 Potentiates Anti-inflammatory Phenotype of Macrophage through the CREB-C/EBP-β cascade. *Eur. J. Immunol.* 45, 2661–2671. doi:10.1002/eji.201545471

Nefedova, Y., Huang, M., Kusmartsev, S., Bhattacharya, R., Cheng, P., Salup, R., et al. (2004). Hyperactivation of STAT3 Is Involved in Abnormal Differentiation of Dendritic Cells in Cancer. *J. Immunol.* 172, 464–474. doi:10.4049/jimmunol.172.1.464

Neubert, N. J., Schmittnaegel, M., Bordry, N., Nassiri, S., Wald, N., Martignier, C., et al. (2018). T Cell-Induced CSF1 Promotes Melanoma Resistance to PD1 Blockade. *Sci. Transl. Med.* 10. doi:10.1126/scitranslmed.aan3311

Niu, Z.-S., Niu, X.-J., and Wang, W.-H. (2017). Long Non-coding RNAs in Hepatocellular Carcinoma: Potential Roles and Clinical Implications. *Wjg* 23, 5860–5874. doi:10.3748/wjg.v23.i32.5860

Noman, M. Z., Hasmim, M., Lequeux, A., Xiao, M., Duhem, C., Chouaib, S., et al. (2019). Improving Cancer Immunotherapy by Targeting the Hypoxic Tumor Microenvironment: New Opportunities and Challenges. *Cells* 8, 1083. doi:10.3390/cells8091083

Novartis Pharmaceuticals (2021). A Phase Ib/II, Open Label, Multicenter Study of MCS110 in Combination with PDR001 in Patients with Advanced Malignancies. *clinicaltrials.gov*. Available at: https://clinicaltrials.gov/ct2/show/study/NCT02807844 (Accessed January 13, 2022).

NOXXON Pharma AG (2021). An Open-Label Phase 2 Study of Olaptesed Pegol (NOX-A12) Combined with Pembrolizumab and Nanoliposomal Irinotecan/5-FU/Leucovorin or Gemcitabine/Nab-Paclitaxel in Microsatellite-Stable Metastatic Pancreatic Cancer Patients. *clinicaltrials.gov*. Available at: https://clinicaltrials.gov/ct2/show/NCT04901741 (Accessed November 21, 2021).

Obermajer, N., Muthuswamy, R., Odunsi, K., Edwards, R. P., and Kalinski, P. (2011). PGE2-Induced CXCL12 Production and CXCR4 Expression Controls the Accumulation of Human MDSCs in Ovarian Cancer Environment. *Cancer Res.* 71, 7463–7470. doi:10.1158/0008-5472.CAN-11-2449

Ohta, A., Kini, R., Ohta, A., Subramanian, M., Madasu, M., and Sitkovsky, M. (2012). The Development and Immunosuppressive Functions of CD4+ CD25+ FoxP3+ Regulatory T Cells Are under Influence of the Adenosine-A2a Adenosine Receptor Pathway. *Front. Immun.* 3, 190. doi:10.3389/fimmu.2012.00190

Orillion, A., Hashimoto, A., Damayanti, N., Shen, L., Adelaiye-Ogala, R., Arisa, S., et al. (2017). Entinostat Neutralizes Myeloid-Derived Suppressor Cells and Enhances the Antitumor Effect of PD-1 Inhibition in Murine Models of Lung and Renal Cell Carcinoma. *Clin. Cancer Res.* 23, 5187–5201. doi:10.1158/1078-0432.CCR-17-0741

Özdemir, B. C., Pentcheva-Hoang, T., Carstens, J. L., Zheng, X., Wu, C.-C., Simpson, T. R., et al. (2014). Depletion of Carcinoma-Associated Fibroblasts and Fibrosis Induces Immunosuppression and Accelerates Pancreas Cancer with Reduced Survival. *Cancer Cell* 25, 719–734. doi:10.1016/j.ccr.2014.04.005

Papke, B., Azam, S. H., Feng, A. Y., Gutierrez-Ford, C., Huggins, H., Pallan, P. S., et al. (2021). Silencing of Oncogenic KRAS by Mutant-Selective Small Interfering RNA. *ACS Pharmacol. Transl. Sci.* 4, 703–712. doi:10.1021/acsptsci.0c00165

Park-Min, K.-H., Antoniv, T. T., and Ivashkiv, L. B. (2005). Regulation of Macrophage Phenotype by Long-Term Exposure to IL-10. *Immunobiology* 210, 77–86. doi:10.1016/j.imbio.2005.05.002

Pascual-García, M., Bonfill-Teixidor, E., Planas-Rigol, E., Rubio-Perez, C., Iurlaro, R., Arias, A., et al. (2019). LIF Regulates CXCL9 in Tumor-Associated Macrophages and Prevents CD8+ T Cell Tumor-Infiltration Impairing Anti-PD1 Therapy. *Nat. Commun.* 10, 2416. doi:10.1038/s41467-019-10369-9

Pascut, D., Pratama, M. Y., Vo, N. V. T., Masadah, R., and Tiribelli, C. (2020). The Crosstalk between Tumor Cells and the Microenvironment in Hepatocellular Carcinoma: The Role of Exosomal microRNAs and Their Clinical Implications. *Cancers* 12, 823. doi:10.3390/cancers12040823

Perez, K. (2021). Vitamin D Receptor Agonist Paricalcitol Plus Gemcitabine and Nab-Paclitaxel in Patients with Metastatic Pancreatic Cancer. *clinicaltrials.gov*. Available at: https://clinicaltrials.gov/ct2/show/NCT03520790 (Accessed November 21, 2021).

Petrova, P. S., Viller, N. N., Wong, M., Pang, X., Lin, G. H. Y., Dodge, K., et al. (2017). TTI-621 (SIRPαFc): A CD47-Blocking Innate Immune Checkpoint Inhibitor with Broad Antitumor Activity and Minimal Erythrocyte Binding. *Clin. Cancer Res.* 23, 1068–1079. doi:10.1158/1078-0432.CCR-16-1700

Phillips, R. M., Hendriks, H. R., and Peters, G. J. (2013). EORTC-pharmacology and Molecular Mechanism GroupEO9 (Apaziquone): from the Clinic to the Laboratory and Back Again. *Br. J. Pharmacol.* 168, 11–18. doi:10.1111/j.1476-5381.2012.01996.x

Phillips, R. M. (2016). Targeting the Hypoxic Fraction of Tumours Using Hypoxia-Activated Prodrugs. *Cancer Chemother. Pharmacol.* 77, 441–457. doi:10.1007/s00280-015-2920-7

Piconese, S., Timperi, E., Pacella, I., Schinzari, V., Tripodo, C., Rossi, M., et al. (2014). Human OX40 Tunes the Function of Regulatory T Cells in Tumor and Nontumor Areas of Hepatitis C Virus-Infected Liver Tissue. *Hepatology* 60, 1494–1507. doi:10.1002/hep.27188

Pilon-Thomas, S., Kodumudi, K. N., El-Kenawi, A. E., Russell, S., Weber, A. M., Luddy, K., et al. (2016). Neutralization of Tumor Acidity Improves Antitumor Responses to Immunotherapy. *Cancer Res.* 76, 1381–1390. doi:10.1158/0008-5472.CAN-15-1743

Pipkin, M. E., Sacks, J. A., Cruz-Guilloty, F., Lichtenheld, M. G., Bevan, M. J., and Rao, A. (2010). Interleukin-2 and Inflammation Induce Distinct Transcriptional Programs that Promote the Differentiation of Effector Cytolytic T Cells. *Immunity* 32, 79–90. doi:10.1016/j.immuni.2009.11.012

Prima, V., Kaliberova, L. N., Kaliberov, S., Curiel, D. T., and Kusmartsev, S. (2017). COX2/mPGES1/PGE2pathway Regulates PD-L1 Expression in Tumor-Associated Macrophages and Myeloid-Derived Suppressor Cells. *Proc. Natl. Acad. Sci. USA* 114, 1117–1122. doi:10.1073/pnas.1612920114

Qian, B.-Z., Li, J., Zhang, H., Kitamura, T., Zhang, J., Campion, L. R., et al. (2011). CCL2 Recruits Inflammatory Monocytes to Facilitate Breast-Tumour Metastasis. *Nature* 475, 222–225. doi:10.1038/nature10138

Qian, M., Wang, S., Guo, X., Wang, J., Zhang, Z., Qiu, W., et al. (2020). Hypoxic Glioma-Derived Exosomes Deliver microRNA-1246 to Induce M2 Macrophage Polarization by Targeting TERF2IP via the STAT3 and NF-Kb Pathways. *Oncogene* 39, 428–442. doi:10.1038/s41388-019-0996-y

Raskov, H., Orhan, A., Christensen, J. P., and Gögenur, I. (2021). Cytotoxic CD8+ T Cells in Cancer and Cancer Immunotherapy. *Br. J. Cancer* 124, 359–367. doi:10.1038/s41416-020-01048-4

Read, S., Malmström, V., and Powrie, F. (2000). Cytotoxic T Lymphocyte-Associated Antigen 4 Plays an Essential Role in the Function of Cd25+Cd4+ Regulatory Cells that Control Intestinal Inflammation. *J. Exp. Med.* 192, 295–302. doi:10.1084/jem.192.2.295

Ready, N. E., Ott, P. A., Hellmann, M. D., Zugazagoitia, J., Hann, C. L., de Braud, F., et al. (2020). Nivolumab Monotherapy and Nivolumab Plus Ipilimumab in Recurrent Small Cell Lung Cancer: Results from the CheckMate 032 Randomized Cohort. *J. Thorac. Oncol.* 15, 426–435. doi:10.1016/j.jtho.2019.10.004

Redjimi, N., Raffin, C., Raimbaud, I., Pignon, P., Matsuzaki, J., Odunsi, K., et al. (2012). CXCR3+ T Regulatory Cells Selectively Accumulate in Human Ovarian Carcinomas to Limit Type I Immunity. *Cancer Res.* 72, 4351–4360. doi:10.1158/0008-5472.CAN-12-0579

Reichel, C. A., Puhr-Westerheide, D., Zuchtriegel, G., Uhl, B., Berberich, N., Zahler, S., et al. (2012). C-C Motif Chemokine CCL3 and Canonical Neutrophil Attractants Promote Neutrophil Extravasation through Common and Distinct Mechanisms. *Blood* 120, 880–890. doi:10.1182/blood-2012-01-402164

Ries, C. H., Cannarile, M. A., Hoves, S., Benz, J., Wartha, K., Runza, V., et al. (2014). Targeting Tumor-Associated Macrophages with Anti-CSF-1r Antibody Reveals a Strategy for Cancer Therapy. *Cancer Cell* 25, 846–859. doi:10.1016/j.ccr.2014.05.016

Ries, C. H., Hoves, S., Cannarile, M. A., and Rüttinger, D. (2015). CSF-1/CSF-1R Targeting Agents in Clinical Development for Cancer Therapy. *Curr. Opin. Pharmacol.* 23, 45–51. doi:10.1016/j.coph.2015.05.008

Rodriguez-Abreu, D., Johnson, M. L., Hussein, M. A., Cobo, M., Patel, A. J., Secen, N. M., et al. (2020). Primary Analysis of a Randomized, Double-Blind, Phase II Study of the Anti-TIGIT Antibody Tiragolumab (Tira) Plus Atezolizumab (Atezo) versus Placebo Plus Atezo as First-Line (1L) Treatment in Patients with PD-L1-Selected NSCLC (CITYSCAPE). *Jco* 38, 9503. doi:10.1200/jco.2020.38.15_suppl.9503

Safarzadeh, E., Orangi, M., Mohammadi, H., Babaie, F., and Baradaran, B. (2018). Myeloid-derived Suppressor Cells: Important Contributors to Tumor Progression and Metastasis. *J. Cel Physiol* 233, 3024–3036. doi:10.1002/jcp.26075

Sainson, R. C. A., Parveen, N., Borhis, G., Kosmac, M., Okell, T., Taggart, E., et al. (2021). KY1055, a Novel ICOS/PD-L1 Bispecific Antibody, Efficiently Enhances T Cell Activation and Delivers a Potent Anti-tumour Response *In Vivo*. 1.

Satriano, J. A., Hora, K., Shan, Z., Stanley, E. R., Mori, T., and Schlondorff, D. (1993). Regulation of Monocyte Chemoattractant Protein-1 and Macrophage colony-stimulating Factor-1 by IFN-Gamma, Tumor Necrosis Factor-Alpha, IgG Aggregates, and cAMP in Mouse Mesangial Cells. *J. Immunol.* 150, 1971–1978.

Sawant, D. V., Yano, H., Chikina, M., Zhang, Q., Liao, M., Liu, C., et al. (2019). Adaptive Plasticity of IL-10+ and IL-35+ Treg Cells Cooperatively Promotes Tumor T Cell Exhaustion. *Nat. Immunol.* 20, 724–735. doi:10.1038/s41590-019-0346-9

Schlecker, E., Stojanovic, A., Eisen, C., Quack, C., Falk, C. S., Umansky, V., et al. (2012). Tumor-infiltrating Monocytic Myeloid-Derived Suppressor Cells Mediate CCR5-dependent Recruitment of Regulatory T Cells Favoring Tumor Growth. *J.I.* 189, 5602–5611. doi:10.4049/jimmunol.1201018

Scholz, C. C., and Taylor, C. T. (2013). Targeting the HIF Pathway in Inflammation and Immunity. *Curr. Opin. Pharmacol.* 13, 646–653. doi:10.1016/j.coph.2013.04.009

Selak, M. A., Armour, S. M., MacKenzie, E. D., Boulahbel, H., Watson, D. G., Mansfield, K. D., et al. (2005). Succinate Links TCA Cycle Dysfunction to Oncogenesis by Inhibiting HIF-α Prolyl Hydroxylase. *Cancer Cell* 7, 77–85. doi:10.1016/j.ccr.2004.11.022

Semenza, G. L. (2012). Hypoxia-inducible Factors: Mediators of Cancer Progression and Targets for Cancer Therapy. *Trends Pharmacol. Sci.* 33, 207–214. doi:10.1016/j.tips.2012.01.005

Sharma, A., Subudhi, S. K., Blando, J., Scutti, J., Vence, L., Wargo, J., et al. (2019). Anti-CTLA-4 Immunotherapy Does Not Deplete FOXP3+ Regulatory T Cells (Tregs) in Human Cancers. *Clin. Cancer Res.* 25, 1233–1238. doi:10.1158/1078-0432.CCR-18-0762

Sherman, M. H., Yu, R. T., Engle, D. D., Ding, N., Atkins, A. R., Tiriac, H., et al. (2014). Vitamin D Receptor-Mediated Stromal Reprogramming Suppresses Pancreatitis and Enhances Pancreatic Cancer Therapy. *Cell* 159, 80–93. doi:10.1016/j.cell.2014.08.007

Sinha, P., Clements, V. K., and Ostrand-Rosenberg, S. (2005). Reduction of Myeloid-Derived Suppressor Cells and Induction of M1 Macrophages Facilitate the Rejection of Established Metastatic Disease. *J. Immunol.* 174, 636–645. doi:10.4049/jimmunol.174.2.636

Skog, J., Würdinger, T., van Rijn, S., Meijer, D. H., Gainche, L., Curry, W. T., et al. (2008). Glioblastoma Microvesicles Transport RNA and Proteins that Promote Tumour Growth and Provide Diagnostic Biomarkers. *Nat. Cel Biol* 10, 1470–1476. doi:10.1038/ncb1800

Solomon, I., Amann, M., Goubier, A., Arce Vargas, F., Zervas, D., Qing, C., et al. (2020). CD25-Treg-depleting Antibodies Preserving IL-2 Signaling on Effector T Cells Enhance Effector Activation and Antitumor Immunity. *Nat. Cancer* 1, 1153–1166. doi:10.1038/s43018-020-00133-0

Spiegelberg, L., Houben, R., Niemans, R., de Ruysscher, D., Yaromina, A., Theys, J., et al. (2019). Hypoxia-activated Prodrugs and (Lack of) Clinical Progress: The Need for Hypoxia-Based Biomarker Patient Selection in Phase III Clinical Trials. *Clin. Translational Radiat. Oncol.* 15, 62–69. doi:10.1016/j.ctro.2019.01.005

Stadtmauer, E. A., Fraietta, J. A., Davis, M. M., Cohen, A. D., Weber, K. L., Lancaster, E., et al. (2020). CRISPR-engineered T Cells in Patients with Refractory Cancer. *Science* 367. doi:10.1126/science.aba7365

Stephen, A. G., Esposito, D., Bagni, R. K., and McCormick, F. (2014). Dragging Ras Back in the Ring. *Cancer Cell* 25, 272–281. doi:10.1016/j.ccr.2014.02.017

St. Paul, M., and Ohashi, P. S. (2020). The Roles of CD8+ T Cell Subsets in Antitumor Immunity. *Trends Cel Biol.* 30, 695–704. doi:10.1016/j.tcb.2020.06.003

St. Paul, M., Saibil, S. D., Lien, S. C., Han, S., Sayad, A., Mulder, D. T., et al. (2020). IL6 Induces an IL22+ CD8+ T-Cell Subset with Potent Antitumor Function. *Cancer Immunol. Res.* 8, 321–333. doi:10.1158/2326-6066.CIR-19-0521

Suarez-Carmona, M., Williams, A., Schreiber, J., Hohmann, N., Pruefer, U., Krauss, J., et al. (2021). Combined Inhibition of CXCL12 and PD-1 in MSS Colorectal and Pancreatic Cancer: Modulation of the Microenvironment and Clinical Effects. *J. Immunother. Cancer* 9, e002505. doi:10.1136/jitc-2021-002505

Sugiyama, D., Nishikawa, H., Maeda, Y., Nishioka, M., Tanemura, A., Katayama, I., et al. (2013). Anti-CCR4 mAb Selectively Depletes Effector-type FoxP3+CD4+ Regulatory T Cells, Evoking Antitumor Immune Responses in Humans. *Proc. Natl. Acad. Sci.* 110, 17945–17950. doi:10.1073/pnas.1316796110

Sun, J.-Y., and Lu, X.-J. (2020). Cancer Immunotherapy: Current Applications and Challenges. *Cancer Lett.* 480, 1–3. doi:10.1016/j.canlet.2020.03.024

Sun, L., Clavijo, P. E., Robbins, Y., Patel, P., Friedman, J., Greene, S., et al. (2019). Inhibiting Myeloid-Derived Suppressor Cell Trafficking Enhances T Cell Immunotherapy. *JCI Insight* 4, 126853. doi:10.1172/jci.insight.126853

Sun, Z., Yang, S., Zhou, Q., Wang, G., Song, J., Li, Z., et al. (2018). Emerging Role of Exosome-Derived Long Non-coding RNAs in Tumor Microenvironment. *Mol. Cancer* 17, 82. doi:10.1186/s12943-018-0831-z

Syntrix Biosystems, Inc (2021). A Phase 1, Open-Label, Dose-Escalation with Expansion Study of SX-682 in Subjects with Metastatic Melanoma Concurrently Treated with Pembrolizumab. *clinicaltrials.gov*. Available at: https://clinicaltrials.gov/ct2/show/NCT03161431 (Accessed January 10, 2022).

Takizawa, H., Boettcher, S., and Manz, M. G. (2012). Demand-adapted Regulation of Early Hematopoiesis in Infection and Inflammation. *Blood* 119, 2991–3002. doi:10.1182/blood-2011-12-380113

Tan, M. C. B., Goedegebuure, P. S., Belt, B. A., Flaherty, B., Sankpal, N., Gillanders, W. E., et al. (2009). Disruption of CCR5-dependent Homing of Regulatory T Cells Inhibits Tumor Growth in a Murine Model of Pancreatic Cancer. *J. Immunol.* 182, 1746–1755. doi:10.4049/jimmunol.182.3.1746

Tan, S., Xia, L., Yi, P., Han, Y., Tang, L., Pan, Q., et al. (2020). Exosomal miRNAs in Tumor Microenvironment. *J. Exp. Clin. Cancer Res.* 39, 67. doi:10.1186/s13046-020-01570-6

Taylor, A., Verhagen, J., Blaser, K., Akdis, M., and Akdis, C. A. (2006). Mechanisms of Immune Suppression by Interleukin-10 and Transforming Growth Factor-Beta: the Role of T Regulatory Cells. *Immunology* 117, 433–442. doi:10.1111/j.1365-2567.2006.02321.x

Terry, S., Engelsen, A. S. T., Buart, S., Elsayed, W. S., Venkatesh, G. H., and Chouaib, S. (2020). Hypoxia-driven Intratumor Heterogeneity and Immune Evasion. *Cancer Lett.* 492, 1–10. doi:10.1016/j.canlet.2020.07.004

Terry, S., Faouzi Zaarour, R., Hassan Venkatesh, G., Francis, A., El-Sayed, W., Buart, S., et al. (2018). Role of Hypoxic Stress in Regulating Tumor Immunogenicity, Resistance and Plasticity. *Ijms* 19, 3044. doi:10.3390/ijms19103044

Threshold Pharmaceuticals (2017). A Phase 1 Immunotherapy Study of Evofosfamide in Combination with Ipilimumab in Patients with Advanced Solid Malignancies. *clinicaltrials.gov*. Available at: https://clinicaltrials.gov/ct2/show/NCT03098160 (Accessed November 25, 2021).

Tian, T., and Li, Z. (2021). Targeting Tim-3 in Cancer with Resistance to PD-1/pd-L1 Blockade. *Front. Oncol.* 11, 731175. doi:10.3389/fonc.2021.731175

Tokunaga, R., Zhang, W., Naseem, M., Puccini, A., Berger, M. D., Soni, S., et al. (2018). CXCL9, CXCL10, CXCL11/CXCR3 axis for Immune Activation - A Target for Novel Cancer Therapy. *Cancer Treat. Rev.* 63, 40–47. doi:10.1016/j.ctrv.2017.11.007

Toor, S. M., Sasidharan Nair, V., Decock, J., and Elkord, E. (2020). Immune Checkpoints in the Tumor Microenvironment. *Semin. Cancer Biol.* 65, 1–12. doi:10.1016/j.semcancer.2019.06.021

Trillium Therapeutics Inc (2021). A Phase 1a/1b Dose Escalation and Expansion Trial of TTI-621, a Novel Biologic Targeting CD47, in Subjects with Relapsed or Refractory Hematologic Malignancies and Selected Solid Tumors. *clinicaltrials.gov*. Available at: https://clinicaltrials.gov/ct2/show/NCT02663518 (Accessed January 13, 2022).

Tsagozis, P., Augsten, M., and Pisa, P. (2014). All Trans-retinoic Acid Abrogates the Pro-tumorigenic Phenotype of Prostate Cancer Tumor-Associated Macrophages. *Int. Immunopharmacology* 23, 8–13. doi:10.1016/j.intimp.2014.07.037

UNC Lineberger Comprehensive Cancer Center (2021). Breaking Innate PD-1 Inhibitor (PD1i) Resistance Using Epigenetic Modifiers; Antitumor Efficacy and Correlative Analyses of Entinostat Plus Pembrolizumab in Non-inflamed Metastatic Melanoma (MM). *clinicaltrials.gov*. Available at: https://clinicaltrials.gov/ct2/show/NCT03765229 (Accessed November 21, 2021).

Vaupel, P., and Multhoff, G. (2018). Hypoxia-/HIF-1α-Driven Factors of the Tumor Microenvironment Impeding Antitumor Immune Responses and Promoting Malignant Progression. *Adv. Exp. Med. Biol.* 1072, 171–175. doi:10.1007/978-3-319-91287-510.1007/978-3-319-91287-5_27

Viaud, S., Théry, C., Ploix, S., Tursz, T., Lapierre, V., Lantz, O., et al. (2010). Dendritic Cell-Derived Exosomes for Cancer Immunotherapy: What's Next? *Cancer Res.* 70, 1281–1285. doi:10.1158/0008-5472.CAN-09-3276

Voo, K. S., Bover, L., Harline, M. L., Vien, L. T., Facchinetti, V., Arima, K., et al. (2013). Antibodies Targeting Human OX40 Expand Effector T Cells and Block Inducible and Natural Regulatory T Cell Function. *J.I.* 191, 3641–3650. doi:10.4049/jimmunol.1202752

Wang, B., Zhao, Q., Zhang, Y., Liu, Z., Zheng, Z., Liu, S., et al. (2021a). Targeting Hypoxia in the Tumor Microenvironment: a Potential Strategy to Improve Cancer Immunotherapy. *J. Exp. Clin. Cancer Res.* 40, 24. doi:10.1186/s13046-020-01820-7

Wang, D., and Dubois, R. N. (2010). Eicosanoids and Cancer. *Nat. Rev. Cancer* 10, 181–193. doi:10.1038/nrc2809

Wang, J., Sanmamed, M. F., Datar, I., Su, T. T., Ji, L., Sun, J., et al. (2019). Fibrinogen-like Protein 1 Is a Major Immune Inhibitory Ligand of LAG-3. *Cell* 176, 334–347. doi:10.1016/j.cell.2018.11.010

Wang, N., Liang, H., and Zen, K. (2014). Molecular Mechanisms that Influence the Macrophage M1â€"M2 Polarization Balance. *Front. Immunol.* 5, 614. doi:10.3389/fimmu.2014.00614

Wang, Z., Jiang, R., Li, Q., Wang, H., Tao, Q., and Zhai, Z. (2021b). Elevated M-MDSCs in Circulation Are Indicative of Poor Prognosis in Diffuse Large B-Cell Lymphoma Patients. *Jcm* 10, 1768. doi:10.3390/jcm10081768

Wang,MD, W (2020). Safety and Effect Assessment of TACE in Combination with Autologous PD-1 Knockout Engineered T Cells by Percutaneous Infusion in the Paitents with Advanced Hepatocellular Carcinoma. *clinicaltrials.gov*. Available at: https://clinicaltrials.gov/ct2/show/NCT04417764 (Accessed November 21, 2021).

Warner, A. B., and Postow, M. A. (2018). Combination Controversies: Checkpoint Inhibition Alone or in Combination for the Treatment of Melanoma? *Oncology (Williston Park)* 32, 228–234.

Whiteside, T. L. (2016). Exosomes and Tumor-Mediated Immune Suppression. *J. Clin. Invest.* 126, 1216–1223. doi:10.1172/JCI81136

Wierz, M., Pierson, S., Guyonnet, L., Viry, E., Lequeux, A., Oudin, A., et al. (2018). Dual PD1/LAG3 Immune Checkpoint Blockade Limits Tumor Development in a Murine Model of Chronic Lymphocytic Leukemia. *Blood* 131, 1617–1621. doi:10.1182/blood-2017-06-792267

Wing, K., Onishi, Y., Prieto-Martin, P., Yamaguchi, T., Miyara, M., Fehervari, Z., et al. (2008). CTLA-4 Control over Foxp3 + Regulatory T Cell Function. *Science* 322, 271–275. doi:10.1126/science.1160062

Wolchok, J. D., Chiarion-Sileni, V., Gonzalez, R., Grob, J.-J., Rutkowski, P., Lao, C. D., et al. (2022). Long-Term Outcomes with Nivolumab Plus Ipilimumab or Nivolumab Alone versus Ipilimumab in Patients with Advanced Melanoma. *Jco* 40, 127–137. doi:10.1200/JCO.21.02229

Wolf, Y., Anderson, A. C., and Kuchroo, V. K. (2020). TIM3 Comes of Age as an Inhibitory Receptor. *Nat. Rev. Immunol.* 20, 173–185. doi:10.1038/s41577-019-0224-6

Wrangle, J. M., Patterson, A., Johnson, C. B., Neitzke, D. J., Mehrotra, S., Denlinger, C. E., et al. (2018). IL-2 and beyond in Cancer Immunotherapy. *J. Interferon Cytokine Res.* 38, 45–68. doi:10.1089/jir.2017.0101

Wu, J.-Y., Huang, T.-W., Hsieh, Y.-T., Wang, Y.-F., Yen, C.-C., Lee, G.-L., et al. (2020). Cancer-Derived Succinate Promotes Macrophage Polarization and Cancer Metastasis via Succinate Receptor. *Mol. Cel* 77, 213–227. doi:10.1016/j.molcel.2019.10.023

Wu, L., Mao, L., Liu, J.-F., Chen, L., Yu, G.-T., Yang, L.-L., et al. (2019). Blockade of TIGIT/CD155 Signaling Reverses T-Cell Exhaustion and Enhances Antitumor Capability in Head and Neck Squamous Cell Carcinoma. *Cancer Immunol. Res.* 7, 1700–1713. doi:10.1158/2326-6066.CIR-18-0725

Wu, X., Chen, X., Zhou, Q., Li, P., Yu, B., Li, J., et al. (2013). Hepatocyte Growth Factor Activates Tumor Stromal Fibroblasts to Promote Tumorigenesis in Gastric Cancer. *Cancer Lett.* 335, 128–135. doi:10.1016/j.canlet.2013.02.002

Xie, K., Xu, L., Wu, H., Liao, H., Luo, L., Liao, M., et al. (2018). OX40 Expression in Hepatocellular Carcinoma Is Associated with a Distinct Immune Microenvironment, Specific Mutation Signature, and Poor Prognosis. *Oncoimmunology* 7, e1404214. doi:10.1080/2162402X.2017.1404214

Xie, Z., Chen, J., Zheng, C., Wu, J., Cheng, Y., Zhu, S., et al. (2017). 1,25-dihydroxyvitamin D3 -induced Dendritic Cells Suppress Experimental Autoimmune Encephalomyelitis by Increasing Proportions of the Regulatory Lymphocytes and Reducing T Helper Type 1 and Type 17 Cells. *Immunology* 152, 414–424. doi:10.1111/imm.12776

Xin, H., Zhang, C., Herrmann, A., Du, Y., Figlin, R., and Yu, H. (2009). Sunitinib Inhibition of Stat3 Induces Renal Cell Carcinoma Tumor Cell Apoptosis and Reduces Immunosuppressive Cells. *Cancer Res.* 69, 2506–2513. doi:10.1158/0008-5472.CAN-08-4323

Xu, F., Liu, J., Liu, D., Liu, B., Wang, M., Hu, Z., et al. (2014). LSECtin Expressed on Melanoma Cells Promotes Tumor Progression by Inhibiting Antitumor T-Cell Responses. *Cancer Res.* 74, 3418–3428. doi:10.1158/0008-5472.CAN-13-2690

Yang, L., Huang, J., Ren, X., Gorska, A. E., Chytil, A., Aakre, M., et al. (2008). Abrogation of TGFβ Signaling in Mammary Carcinomas Recruits Gr-1+CD11b+ Myeloid Cells that Promote Metastasis. *Cancer Cell* 13, 23–35. doi:10.1016/j.ccr.2007.12.004

Yang, R., Cai, Z., Zhang, Y., Yutzy, W. H., Roby, K. F., and Roden, R. B. S. (2006). CD80 in Immune Suppression by Mouse Ovarian Carcinoma-Associated Gr-1+CD11b+ Myeloid Cells. *Cancer Res.* 66, 6807–6815. doi:10.1158/0008-5472.CAN-05-3755

Yang, X., Lin, Y., Shi, Y., Li, B., Liu, W., Yin, W., et al. (2016). FAP Promotes Immunosuppression by Cancer-Associated Fibroblasts in the Tumor Microenvironment via STAT3-CCL2 Signaling. *Cancer Res.* 76, 4124–4135. doi:10.1158/0008-5472.CAN-15-2973

Yang, X., Weng, X., Yang, Y., Zhang, M., Xiu, Y., Peng, W., et al. (2021). A Combined Hypoxia and Immune Gene Signature for Predicting Survival and

Risk Stratification in Triple-Negative Breast Cancer. *Aging* 13, 19486–19509. doi:10.18632/aging.203360

Yang, Y., Li, C.-W., Chan, L.-C., Wei, Y., Hsu, J.-M., Xia, W., et al. (2018). Exosomal PD-L1 Harbors Active Defense Function to Suppress T Cell Killing of Breast Cancer Cells and Promote Tumor Growth. *Cell Res* 28, 862–864. doi:10.1038/s41422-018-0060-4

Yang, Z., Guo, J., Weng, L., Tang, W., Jin, S., and Ma, W. (2020). Myeloid-derived Suppressor Cells-New and Exciting Players in Lung Cancer. *J. Hematol. Oncol.* 13, 10. doi:10.1186/s13045-020-0843-1

Yin, Z., Yu, M., Ma, T., Zhang, C., Huang, S., Karimzadeh, M. R., et al. (2021). Mechanisms Underlying Low-Clinical Responses to PD-1/pd-L1 Blocking Antibodies in Immunotherapy of Cancer: a Key Role of Exosomal PD-L1. *J. Immunother. Cancer* 9, e001698. doi:10.1136/jitc-2020-001698

Yu, X., Harden, K., C Gonzalez, L., Francesco, M., Chiang, E., Irving, B., et al. (2009). The Surface Protein TIGIT Suppresses T Cell Activation by Promoting the Generation of Mature Immunoregulatory Dendritic Cells. *Nat. Immunol.* 10, 48–57. doi:10.1038/ni.1674

Zai Lab (Shanghai) Co. Ltd (2020). An Open-Label, Multi-Cohort, Multi-center Phase I Study Evaluating the Efficacy and Safety of MGD013 in Patients with Unresectable, Recurrent or Metastatic Malignant Melanoma. *clinicaltrials.gov*. Available at: https://clinicaltrials.gov/ct2/show/NCT04653038 (Accessed November 25, 2021).]

Zamarin, D., Burger, R. A., Sill, M. W., Powell, D. J., Lankes, H. A., Feldman, M. D., et al. (2020). Randomized Phase II Trial of Nivolumab versus Nivolumab and Ipilimumab for Recurrent or Persistent Ovarian Cancer: An NRG Oncology Study. *Jco* 38, 1814–1823. doi:10.1200/JCO.19.02059

Zammarchi, F., Havenith, K., Bertelli, F., Vijayakrishnan, B., Chivers, S., van Berkel, P. H., et al. (2020). CD25-targeted Antibody-Drug Conjugate Depletes Regulatory T Cells and Eliminates Established Syngeneic Tumors via Antitumor Immunity. *J. Immunother. Cancer* 8, e000860. doi:10.1136/jitc-2020-000860

Zarek, P. E., Huang, C.-T., Lutz, E. R., Kowalski, J., Horton, M. R., Linden, J., et al. (2008). A2A Receptor Signaling Promotes Peripheral Tolerance by Inducing T-Cell Anergy and the Generation of Adaptive Regulatory T Cells. *Blood* 111, 251–259. doi:10.1182/blood-2007-03-081646

Zboralski, D., Hoehlig, K., Eulberg, D., Frömming, A., and Vater, A. (2017). Increasing Tumor-Infiltrating T Cells through Inhibition of CXCL12 with NOX-A12 Synergizes with PD-1 Blockade. *Cancer Immunol. Res.* 5, 950–956. doi:10.1158/2326-6066.CIR-16-0303

Zhang, C., Wang, Y., Xun, X., Wang, S., Xiang, X., Hu, S., et al. (2020a). TIGIT Can Exert Immunosuppressive Effects on CD8+ T Cells by the CD155/TIGIT Signaling Pathway for Hepatocellular Carcinoma *In Vitro*. *Vitro. J. Immunother.* 43, 236–243. doi:10.1097/CJI.0000000000000330

Zhang, L., Ke, J., Min, S., Wu, N., Liu, F., Qu, Z., et al. (2021). Hyperbaric Oxygen Therapy Represses the Warburg Effect and Epithelial-Mesenchymal Transition in Hypoxic NSCLC Cells via the HIF-1α/PFKP Axis. *Front. Oncol.* 11, 691762. doi:10.3389/fonc.2021.691762

Zhang, P.-F., Gao, C., Huang, X.-Y., Lu, J.-C., Guo, X.-J., Shi, G.-M., et al. (2020b). Cancer Cell-Derived Exosomal circUHRF1 Induces Natural Killer Cell Exhaustion and May Cause Resistance to Anti-PD1 Therapy in Hepatocellular Carcinoma. *Mol. Cancer* 19, 110. doi:10.1186/s12943-020-01222-5

Zhang, Q., Chikina, M., Szymczak-Workman, A. L., Horne, W., Kolls, J. K., Vignali, K. M., et al. (2017). LAG3 Limits Regulatory T Cell Proliferation and Function in Autoimmune Diabetes. *Sci. Immunol.* 2. doi:10.1126/sciimmunol.aah4569

Zhang, S.-Y., Song, X.-Y., Li, Y., Ye, L.-L., Zhou, Q., and Yang, W.-B. (2020c). Tumor-associated Macrophages: A Promising Target for a Cancer Immunotherapeutic Strategy. *Pharmacol. Res.* 161, 105111. doi:10.1016/j.phrs.2020.105111

Zhao, W., Hu, X., Li, W., Li, R., Chen, J., Zhou, L., et al. (2021). M2-Like TAMs Function Reversal Contributes to Breast Cancer Eradication by Combination Dual Immune Checkpoint Blockade and Photothermal Therapy. *Small* 17, 2007051. doi:10.1002/smll.202007051

Zhou, W., Zhou, Y., Chen, X., Ning, T., Chen, H., Guo, Q., et al. (2021). Pancreatic Cancer-Targeting Exosomes for Enhancing Immunotherapy and Reprogramming Tumor Microenvironment. *Biomaterials* 268, 120546. doi:10.1016/j.biomaterials.2020.120546

Zhou, Y., Cao, H.-B., Li, W.-J., and Zhao, L. (2018). The CXCL12 (SDF-1)/CXCR4 Chemokine axis: Oncogenic Properties, Molecular Targeting, and Synthetic and Natural Product CXCR4 Inhibitors for Cancer Therapy. *Chin. J. Nat. Medicines* 16, 801–810. doi:10.1016/S1875-5364(18)30122-5

Zhu, C., Sakuishi, K., Xiao, S., Sun, Z., Zaghouani, S., Gu, G., et al. (2015). An IL-27/NFIL3 Signalling axis Drives Tim-3 and IL-10 Expression and T-Cell Dysfunction. *Nat. Commun.* 6, 6072. doi:10.1038/ncomms7072

Conflict of Interest: The authors declare that the research was conducted in the absence of any commercial or financial relationships that could be construed as a potential conflict of interest.

Publisher's Note: All claims expressed in this article are solely those of the authors and do not necessarily represent those of their affiliated organizations, or those of the publisher, the editors and the reviewers. Any product that may be evaluated in this article, or claim that may be made by its manufacturer, is not guaranteed or endorsed by the publisher.

Copyright © 2022 Park, Veena and Shin. This is an open-access article distributed under the terms of the Creative Commons Attribution License (CC BY). The use, distribution or reproduction in other forums is permitted, provided the original author(s) and the copyright owner(s) are credited and that the original publication in this journal is cited, in accordance with accepted academic practice. No use, distribution or reproduction is permitted which does not comply with these terms.

frontiers in Cell and Developmental Biology

ORIGINAL RESEARCH
published: 24 March 2022
doi: 10.3389/fcell.2022.808212

ITGAL as a Prognostic Biomarker Correlated With Immune Infiltrates in Gastric Cancer

Junchang Zhang[1,2†], *Han Wang*[1,2†], *Cheng Yuan*[1], *Jing Wu*[1], *Jiannan Xu*[1,2], *Songyao Chen*[1,2], *Changhua Zhang*[1*] and *Yulong He*[1,2*]

[1]Department of Center for Digestive Disease, The Seventh Affiliated Hospital of Sun Yat-sen University, Shenzhen, China, [2]Department of Gastrointestinal Surgery, The First Affiliated Hospital of Sun Yat-sen University, Guangzhou, China

Integrin alpha L (ITGAL) is a member of the integrin family in which the abnormal expression is linked with carcinogenesis and immune regulation. However, the relation between ITGAL and the prognosis of gastric cancer (GC) and tumor-infiltrating lymphocytes (TILs) are not well understood. The differential expressions of ITGAL in human tumors and the clinical prognosis in GC were systematically analyzed *via* multiple databases including Gene Expression Profiling Interaction Analysis (GEPIA), UALCAN, Tumor Immune Estimation Resource (TIMER), and Kaplan–Meier (KM) plotter. TIMER, GEPIA, and TISIDB databases were used to comprehensively investigate the correlation between ITGAL and tumor infiltration immune cells. Also, further results were investigated by immunohistochemistry, qRT-PCR, and Western blot. We found that ITGAL expression in GC samples was considerably increased than in peritumor samples. Sample type, subgroup, cancer stage, lymphatic node stage, and worse survival were strongly related to high ITGAL expression. Moreover, upregulated ITGAL expression was strongly connected with immunomodulators, chemokines, and infiltrating levels of $CD8^+$, $CD4^+$ T cell, B cell, monocyte, neutrophil, macrophage, T-cell regulatory, NK cell, and myeloid dendritic cell in stomach adenocarcinoma (STAD). Specifically, immunohistochemistry and bioinformatic analysis showed that ITGAL expression was shown to have strong relationships with various immunological marker sets including PD1 (T-cell exhaustion marker). In conclusion, ITGAL is a prognostic biomarker for GC patients. It might regulate tumor immune microenvironment leading to poor prognosis. Furthermore, studies are essential to explore therapeutic targeting ITGAL.

Keywords: gastric cancer, integrin alpha L (ITGAL), PD-1, tumor-associated macrophages, prognosis, tumor immune microenvironment

OPEN ACCESS

Edited by:
Zimu Deng,
Shanghai Institute of Biochemistry and Cell Biology (CAS), China

Reviewed by:
Shentong Fang,
China Pharmaceutical University, China
Wende Yang,
Third Affiliated Hospital of Sun Yat-sen University, China

***Correspondence:**
Changhua Zhang
zch2108@163.com
Yulong He
hyl1821@163.com

[†]*These authors have contributed equally to this work*

Specialty section:
This article was submitted to Molecular and Cellular Pathology, a section of the journal Frontiers in Cell and Developmental Biology

Received: *03 November 2021*
Accepted: *14 February 2022*
Published: *24 March 2022*

Citation:
Zhang J, Wang H, Yuan C, Wu J, Xu J, Chen S, Zhang C and He Y (2022) ITGAL as a Prognostic Biomarker Correlated With Immune Infiltrates in Gastric Cancer. Front. Cell Dev. Biol. 10:808212. doi: 10.3389/fcell.2022.808212

INTRODUCTION

Gastric cancer (GC) is the world's third leading cause of cancer-related mortality among common fatal tumors (Bray et al., 2018). Despite considerable improvements in diagnosis and therapy about GC, the prognosis still remains challenging (Luebeck et al., 2013). At present, immunotherapy is a prominent subject in the area of cancer treatment and has been an effective treatment in various types of cancer (Larkin et al., 2015; Motzer et al., 2015; Reck et al., 2016), including gastric cancer (Lote et al., 2015; Procaccio et al., 2017). Nevertheless, not all GC patients benefit from immunotherapy, which may be related to the immune microenvironment of tumors (Davidson

et al., 2015). Therefore, it is an emergent issue to look for specific immune-related biomarkers with GC and discover new immunotherapy targets.

ITGAL, also known as CD11a, encodes an integrin component of LFA-1, which expressed in immune cells (Silva et al., 2008; Kuwano et al., 2010; Sumagin et al., 2010) and regulated intercellular adhesion and the costimulation signaling of lymphocytes (Ley et al., 2007; Samatov et al., 2013). ITGAL, as a member of the integrin family, which play important roles during angiogenesis and cancer development (Silva et al., 2008; Winograd-Katz et al., 2014; Seguin et al., 2015; Xie et al., 2021), also participates in immune reactions, inflammatory processes, and construction of the tumor microenvironment, thus, contributing to the pathogenesis of diverse tumors, such as renal cancer, colorectal cancer, ovarian cancer, melanoma, prostate adenocarcinoma, and head and neck squamous cell carcinoma (Vendrell et al., 2007; Boguslawska et al., 2016; Song et al., 2019; Zhao et al., 2019; Ji et al., 2020). These researchers suggested that ITGAL might have a significant influence on cancer growth and transformation, and may be a novel target in treating a variety of malignancies. However, the possible mechanisms of ITGAL about tumor development and immune engagement with GC are still unknown.

In this present study, the ITGAL expression and its connection to GC patient prognosis were investigated utilizing diverse databases including the Gene Expression Profiling Interaction Analysis (GEPIA), Oncomine, Kaplan–Meier (KM) plotter, and UALCAN datasets. Furthermore, the Tumor Immune Estimation Resource (TIMER) and immunohistochemistry were performed to investigate the relationship of ITGAL with immune-related cells in the distinct tumor microenvironments. This study uncovered the critical involvement of ITGAL in GC and the possible connection and mechanism by which ITGAL may regulate tumor-infiltrating immune cells.

METHODS

Tumor immune estimation resource database analysis

The Tumor Immune Estimation Resource (TIMER2.0) is a web-based interactive platform to analyze immune infiltration systematically in various malignancies (https://timer.cistrome.org/) (Li et al., 2020). The TIMER2.0 database applies six advanced algorithms to provide a more rigorous evaluation of tumor-infiltrating lymphocyte (TIL) levels for The Cancer Genome Atlas (TCGA) or tumor-related data. Additionally, the database can also precisely estimate tumor purity. We investigated ITGAL expression in various malignancies and the relationship between the expression of ITGAL and TILs *via* gene modules. Furthermore, the relationship between ITGAL expression with gene markers of TILs, including markers of CD8+/CD4+ T cells, B cells, monocytes, natural killer (NK) cells, dendritic cells (DCs), TAMs, M1macrophages, M2 macrophages, neutrophils, T cells, and related subtypes, has been analyzed *via* correlation modules. Expression dispersion maps were created between a pair of custom genes for GC and the statistical significance of the correlation and estimation of Spearman, by correlation module. The level of gene expression was shown as log2 RSEM.

Gene expression profiling interaction analysis

The Gene Expression Profiling Interactive Analysis (GEPIA) (Tang et al., 2017) online database (http://gepia.cancer-pku.cn/index.html) is a comprehensive platform that obtained the analysis data from TCGA and The Genotype–Tissue Expression (GTEx) databases. In the present research, we used the GEPIA data source to assess the ITGAL levels in GC samples and healthy samples *via* the "DIY Expression" page.

UALCAN analysis

The UALCAN website provides an extensive and interactive study of bioinformatics applying RNA-seq and clinical data of 31 malignancies from TCGA (Chandrashekar et al., 2017) (http://ualcan.path.uab.edu/). The database can compare gene expression in tumors to healthy samples, and in different tumor stages or subtypes, as well as other clinicopathological features. This research will, respectively, examine the ITGAL expression lever from major clinical features such as tissue type (healthy/tumor), GC stage (stages 1, 2, 3, and 4), lymph node stage (N0 1, 2, and 3), and cancer subgroup.

Kaplan–Meier Plotter (gastric cancer)

The KM plotter (http://kmplot.com/analysis/) could evaluate the survival prognosis of related genes *via* mapping the survival curve using 1,065 GC samples with an average follow-up of 33 months (Lánczky et al., 2016). The prognostic significance of ITGAL in GC, including overall survival (OS), first progression (FP), and post-progression survival (PPS), was investigated using this database. The hazard ratio (HR) with 95% confidence intervals was also estimated, as well as the log-rank p-value. Statistical significance was defined as $p < 0.05$.

TISIDB

TISIDB (http://cis.hku.hk/TISIDB/index.php) is an online platform that combines various heterogeneous data sources to study tumor and immune system interactions. This database may help researchers understand how tumors and immune cells interact, as well as forecast immunotherapy responses and identify new immunotherapy targets. It would become a valuable resource for cancer immunology research and therapy. In this research, TISIDB was utilized to investigate the association of ITGAL with 28 TILs, 45 immunostimulators, 24 immunoinhibitors, 41 chemokines, and 18 receptors in GC (Ru et al., 2019).

Real-time quantitative PCR analysis

According to the instructions, the total RNA of tissue samples was extracted by using MolPure® Cell/Tissue Total RNA Kit (YEASEN CAT#19221ES50). The cDNA of samples was synthesized from 2 μg RNA *via* Evo M-MLV reverse transcription master mix (Accurate Biology, CAT#AG11706).

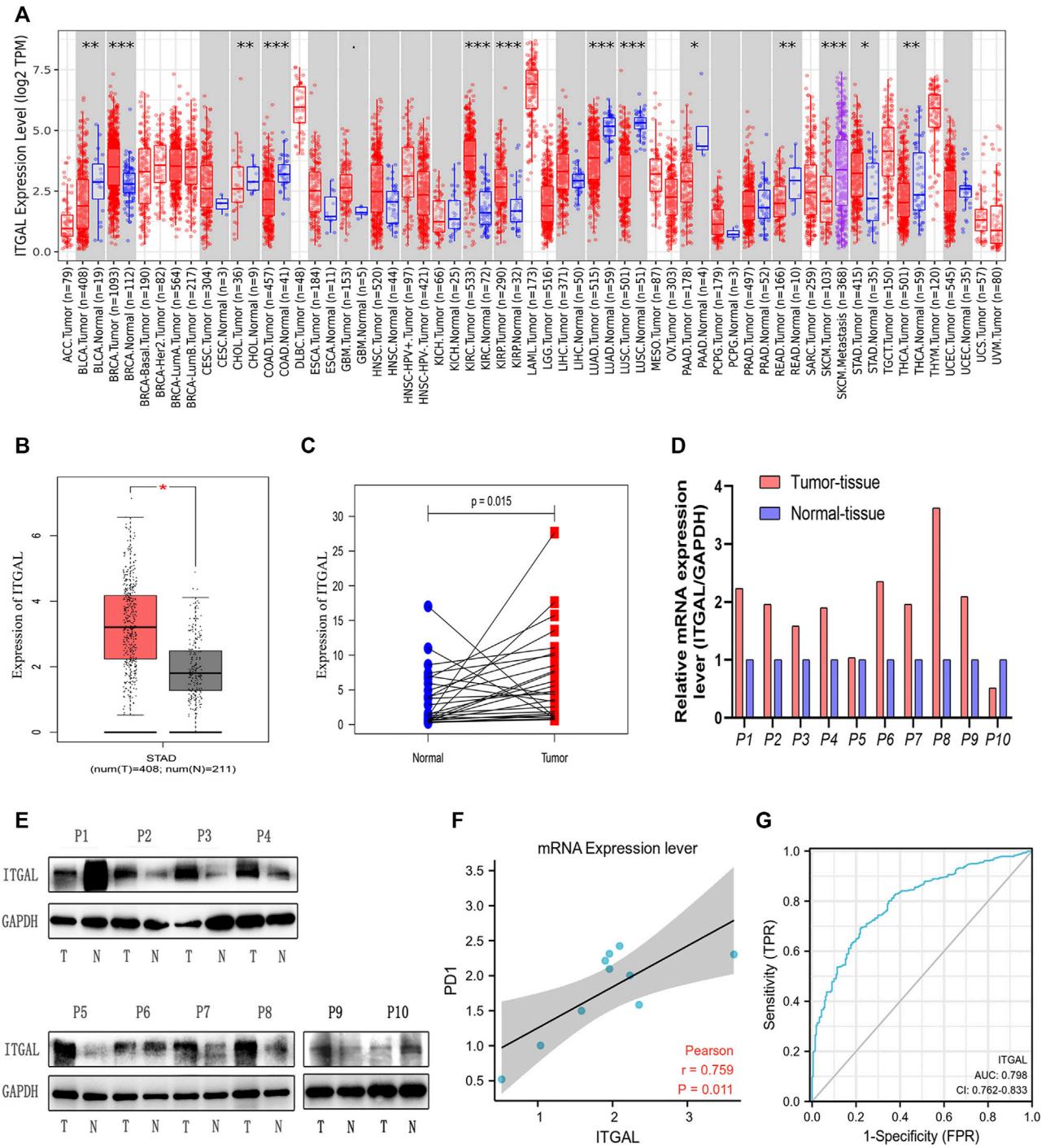

FIGURE 1 | Integrin alpha L (ITGAL) expression levels in different types of human cancers. **(A)** Increased or decreased ITGAL in different tumor types from The Cancer Genome Atlas (TCGA) database were determined by Tumor Immune Estimation Resource (TIMER) (*$p < 0.05$, **$p < 0.01$, ***$p < 0.001$). **(B)** Increased ITGAL in gastric cancer tissues compared with normal tissues in Gene Expression Profiling Interaction Analysis (GEPIA). **(C)** Increased ITGAL expression in gastric cancer compared with the matching normal tissue from TCGA database ($n = 27$). **(D)** The mRNA level of ITGAL in 10 pairs of GC tissues and their paired normal adjacent tissues. **(E)** Western blotting was used to detect the protein level of ITGAL in 10 pairs of GC tissues and their paired adjacent normal tissues. **(F)** The correlation analysis between ITGAL and PD1 mRNA level. **(G)** The receiver-operating characteristic (ROC) curve analysis of ITGAL in gastric cancer (GC) patients.

The qRT-PCR was performed using a SYBR Green Pro Taq HS premixed qPCR kit (Accurate Biology, CAT# AG11701). The ITGAL primer sequence is as follows: forward 5′-CTGCTTTGC CAGCCTCTCTGT-3′ and reverse 5′-GCTCACAGGTATCTG GCTATGG-3′. GAPDH: forward 5′-CGGAGTCAACGGATT TGGTCGT-3′ and reverse 5′-TCTCAGCCTTGACGGTGC

CA-3′. The 2−ΔΔCT calculation method was used to determine the relative target gene level.

Western blotting

Protease inhibitors are used to lyse tissue samples in a radioimmunoprecipitation analysis (RIPA) solution. The BCA protein assay kit (KeyGEN BioTECH, cat#KGP903) was used to valuate the protein concentration. Western blot was performed as previously described (Wang et al., 2021). The following antibodies were used: anti-ITGAL (Abclonal, cat#A1644) and anti-GAPDH (Proteintech, cat#60004-1-Ig).

Immunohistochemistry

This research was conducted on 10 paraffin-embedded GC specimens from the FAHSYSU Department of Pathology. IHC was performed to investigate the expression of ITGAL and PD1, thus, to identify the connection between ITGAL expression and TILs. IHC staining of these specimens were conducted as previously described (Yang et al., 2019). Anti-ITGAL (Abclonal, cat#A1644) and anti-PD1 (Abclonal, cat#A11973) were used for IHC staining. The staining intensity was classified as follows: negative (−), weak (+), moderate (++), and strong (+++).

Statistical analysis

The KM plots were performed to construct survival curves. For KM plots, GEPIA, and TISIDB, HR and *p*-values were described using log-rank test. Spearman's correlation coefficient was calculated to analyze the connection of ITGAL expression with immune infiltration levels, immunomodulators, and chemokines. The strength of correlation was judged to be a very weak correlation if <0.2, weak if <0.4, moderate if <0.6, strong if <0.8, and very strong if <1.0. Statistical significance was defined as $p < 0.05$.

RESULTS

Aberrant integrin alpha L expression in gastric cancer

By applying RNA-seq data from various cancer types in the TCGA, we investigated the differential expression of ITGAL between tumor and surrounding healthy tissues. **Figure 1A** shows the findings. According to the TIMER database, we discovered that ITGAL expression levels are increased in breast invasive carcinoma, kidney renal clear cell carcinoma, kidney renal papillary cell carcinoma, and stomach adenocarcinoma (STAD), but are decreased in colon adenocarcinoma and lung adenocarcinoma compared with peritumor tissues.

To verify these findings in GC, 619 samples from the TCGA database were examined by GEPIA. As **Figure 1B** shows, we discovered that ITGAL mRNA was substantially greater in GC samples (408 cases) than that in healthy samples (211cases) ($p < 0.05$) from TCGA, which was similar with the TIMER database. As we can see from **Figure 1C**, TCGA database showed that ITGAL expression was higher than the matching normal tissue ($n = 27$). Meanwhile, Western blotting and qRT-PCR were performed to examine the ITGAL expression in 10 pairs of GC cases and adjacent healthy tissues. We observed that in most GC tissues, ITGAL mRNA (**Figure 1D**) and protein levels (**Figure 1E**) were higher than the paired adjacent healthy tissues. Interestingly, increased ITGAL mRNA expression was consistent with PD1 (**Figure 1F**), and the AUC was 0.798 (95% CI 0.762–0.833) for ITGAL in GC (**Figure 1G**). The above data indicated that ITGAL was strongly increased in GC tissues and may be potential diagnostic biomarker for GC.

Relationship between integrin alpha L expression and gastric cancer patient clinical pathology

We examined ITGAL expression in relation to several clinical–pathological parameters in patients, including sample type (healthy/primary tumor), tumor stage (stage 1, 2, 3, and 4), lymph node stage (N0 1, 2, and 3), and gastric cancer subgroup by applying UALCAN. As shown in **Figure 2A**, GC samples had substantially higher ITGAL expression than that in healthy samples ($p = 0.0015$). A study of cancer stages revealed that ITGAL in the middle and late-stage cancers was significantly higher expressed than in the early stages, suggesting a potential function for ITGAL in tumor development and migration (**Figure 2B**). ITGAL expression in lymph node stage samples was markedly higher in lymph nodes at all stages of cancer development than normal, indicating that ITGAL is present in malignancy (**Figure 2C**). Furthermore, as demonstrated in **Figure 2D**, ITGAL expression was significantly elevated in diffuse adenocarcinoma compared with normal tissue.

Next, in order to get a well grasp of the significance and possible molecular mechanism of ITGAL expression in tumor development, we observed the correlation between the ITGAL expression and clinical–pathological features of GC in the KM plotter. Upregulated ITGAL expression was linked with a poorer OS and PPS in male and female patients. Specifically, increased ITGAL mRNA expression was associated with poorer OS and PPS in stage 1 (OS HR = 0.22, $p = 0.0062$) and stage 2 (OS HR = 2.18, $p = 0.022$; PPS HR = 3.58, $p = 0.00016$) of GC patients (**Table 1**). Furthermore, we discovered that OS and PPS at stage N1 (OS HR = 2.2, $p = 0.00082$; PPS HR = 3.55, $p = 2.1e{-}08$) and N1 + 2 + 3 (OS HR = 1.55, $p = 0.001$; PPS HR = 1.94, $p = 3.9e{-}06$) were related to ITGAL expression at the same time. These findings suggested that the prognostic significance of ITGAL in GC patients was determined by their clinical features, particularly in early-stage and LN metastases of GC.

Increased integrin alpha L mRNA expression linked to poor overall survival in gastric cancer patients

The findings indicated that GC patients had a higher degree of ITGAL mRNA expression compared with normal controls. Therefore, more investigation was necessary to determine whether ITGAL expression is associated with tumor outcome.

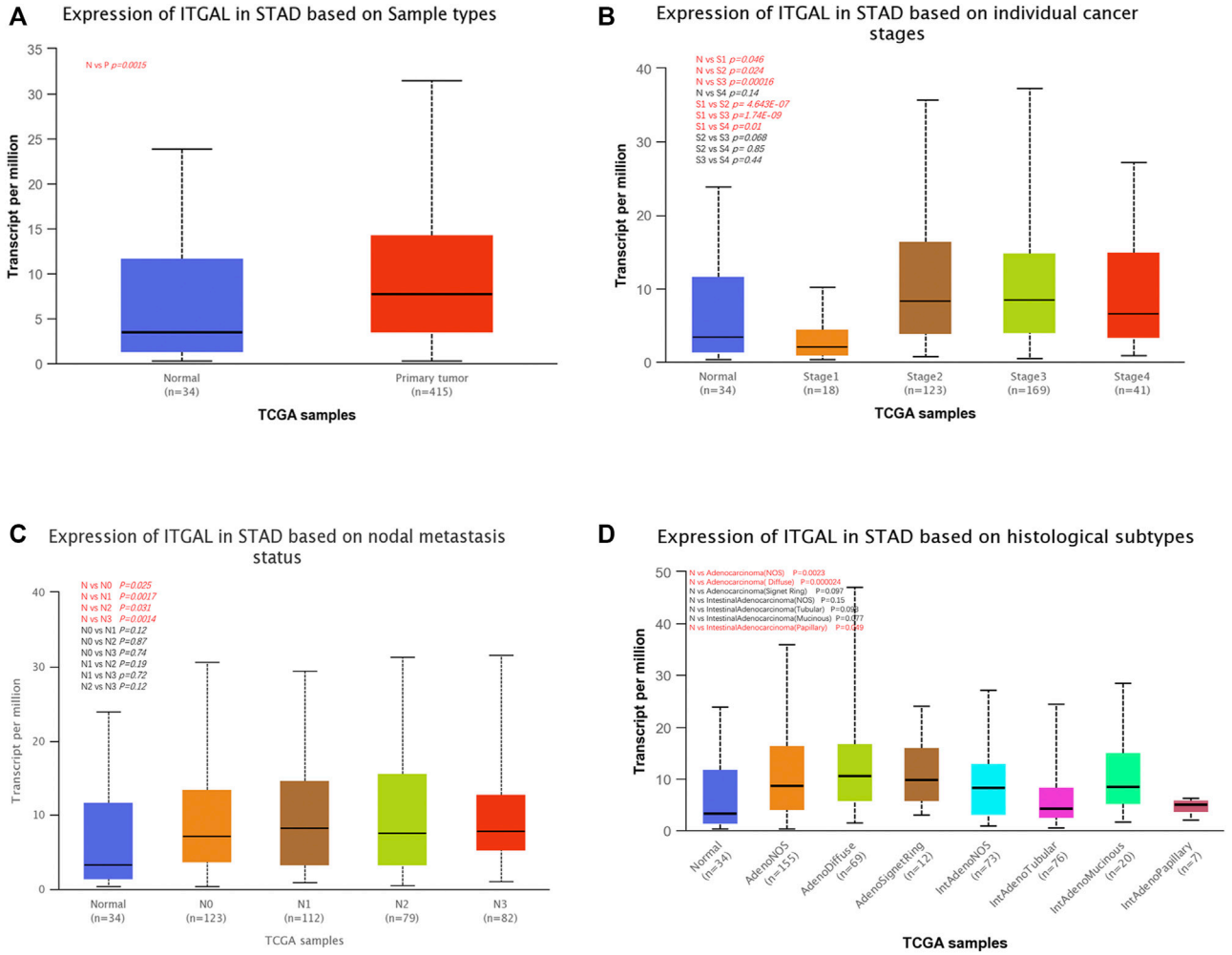

FIGURE 2 | Correlation between ITGAL mRNA expression level and clinicopathological parameters of gastric cancer through the UALCAN database. **(A)** Sample type (normal/primary tumor). **(B)** Cancer stage (stage 1, 2, 3, and 4). **(C)** Lymph node stage (N0 1, 2, and 3). **(D)** Gastric cancer subgroup. N, normal; P, primary tumor; S1, stage 1; S2, stage 2; S3, stage 3; S4, stage 4; STAD, stomach adenocarcinoma.

In the present research, we examined the ITGAL expression and their relationship with prognosis *via* Kaplan–Meier survival curves in order to establish whether ITGAL can be used as a prognostic biomarker in GC. Notably, ITGAL expression was associated with a favorable outcome for GC, and this study showed that increased ITGAL expression was linked with a worse prognosis in the GC cohort 213475-s-at (OS: HR = 1.25, $p = 0.0091$) and 1554240-a-at (OS: HR = 1.47, $p = 0.00057$) (**Figure 3**).

Correlation between immune infiltration and integrin alpha L expression in gastric cancer

Immune infiltration is a key factor associated with tumor progression. Therefore, TISIDB and TIMER platforms were performed to assess ITGAL expression connection to immune cell infiltration levels in STAD. The purity of tumors in clinical cancer samples has a significant impact on the study of immune infiltration using genetic techniques (Yoshihara et al., 2013). Therefore, in this study, ITGAL expression is adversely correlated with the purity of STAD (rho = -0.266, p <1.38e−7). Our results also discovered that ITGAL had a strong correlation with the abundance of TILs (**Figure 4A**). For instance, high-expression level of ITGAL was positively correlated with infiltrating degree of $CD8^+$ T cell (rho = 0.732), $CD4^+$ T cell (rho = 0.466), B cell (rho = 0.719), monocyte (rho = 0.728), neutrophil (rho = 0.574), and macrophage (rho = 0.675), T-cell regulatory (rho = 0.67), NK cell (rho = 0.618), and myeloid dendritic cell (rho = 0.8) (**Figure 4B**). All the p-values were far less than 0.001. These results indicate that ITGAL plays a key function in immune infiltration of GC.

TIMER and GEPIA databases were applied to study the association among ITGAL and different biomarkers of TILs (CD8+/CD4+ T cells, NK cells, B cells, monocytes, DCs,

TABLE 1 | Correlation of integrin alpha L (ITGAL) mRNA expression and clinical prognosis in gastric cancer with different clinicopathological factors by Kaplan–Meier plotter.

Clinicopathological characteristics	Overall survival (*n* = 881)			Post-progression survival (*n* = 503)		
	N	Hazard ratio	p	N	Hazard ratio	p
Sex						
Female	187	1.6 (1.03–2.47)	**0.033**	127	2.63 (1.6–4.31)	**7.1e−05**
Male	349	1.4 (1.03–1.92)	**0.032**	256	1.72 (1.17–2.52)	**0.0055**
Stage						
1	62	0.22 (0.07–0.72)	**0.0062**	31	0.54 (0.12–2.43)	0.41
2	135	2.18 (1.1–4.33)	**0.022**	105	3.58 (1.77–7.23)	**0.00016**
3	197	0.7 (0.47–1.05)	0.084	142	1.3 (0.86–1.99)	0.22
4	140	1.44 (0.93–2.23)	0.09	104	2 (1.14–3.54)	**0.015**
Stage T						
2	241	1.42 (0.92–2.18)	0.11	196	2.19 (1.39–3.45)	**0.00055**
3	204	1.31 (0.93–1.85)	0.12	150	1.49 (1–2.23)	**0.046**
4	28	1.86 (0.77–4.52)	0.16	29	0.6 (0.24–1.5)	0.27
Stage N						
0	74	0.42 (0.17–1.03)	**0.05**	41	1.58 (0.49–5.03)	0.44
1	225	2.2 (1.37–3.53)	**0.00082**	169	3.55 (2.22–5.69)	**2.1e−08**
2	121	0.69 (0.41–1.13)	0.14	105	0.55 (0.32–0.93)	**0.025**
3	76	1.78 (0.92–3.45)	0.085	63	1.69 (0.86–3.33)	0.12
1 + 2 3	422	1.55 (1.19–2.01)	**0.001**	337	1.94 (1.46–2.58)	**3.9e−06**
Stage M						
0	444	1.29 (0.98–1.71)	0.067	342	1.85 (1.37–2.5)	**4.2e−05**
1	56	1.36 (0.7–2.62)	0.36	36	2.33 (0.94–5.81)	0.062
Lauren classification						
Intestinal	269	1.61 (1.12–2.33)	**0.0098**	192	1.93 (1.26–2.95)	**0.002**
Diffuse	240	1.24 (0.87–1.76)	0.23	176	1.71 (1.16–2.51)	**0.0064**
Mixed	29	0.18 (0.05–0.67)	**0.0042**	16	-	-
Differentiation						
Differentiation	121	0.53 (0.33–0.87)	**0.01**	49	0.76 (0.36–1.62)	0.48
Moderately	67	1.62 (0.83–3.17)	0.15	24	0.41 (0.15–1.08)	0.062
HER2						
Positive	202	1.59 (1.09–2.34)	**0.016**	101	2.43 (1.46–4.07)	**0.00048**
Negative	429	1.41 (1.08–1.85)	**0.012**	283	1.81 (1.3–2.53)	**0.00034**

Note. Bold values indicate p < *0.05.*

TAMs, M1macrophages, M2 macrophages, neutrophils, T cells, and related subtypes) in STAD. We found that ITGAL was associated with the majority of TILs markers in STAD. The several functional T cells, including Th1/Th2/Th17/Tfh cells, Tregs, and exhausted T cells were also analyzed. Particularly, ITGAL was strongly linked with the majority of immune marker sets of TILs in STAD (**Table 2**).

Obviously, ITGAL had a significant association with the majority of marker sets of monocytes, TAMs, M2 macrophages, and T cell exhaustion in STAD (**Table 2**). Specifically, this study implicated that PDCD1, PDCD1G2, CTLA4, LAG3, HAVCR2, GZMB of T-cell exhaustion, and chemokine ligand (CCL)-2, CD68, and IL10 of TAMs are all strongly correlated with ITGAL in STAD, as well as IRF5 of M1 phenotype and CD163, VSIG4, MS4A4A of M2 phenotype ($p < 0.0001$; **Figures 5A–E**). Furthermore, according to the GEPIA database, we further assessed the connection of ITGAL expression with the aforementioned markers of TAMs, M2 macrophages, monocytes, and T-cell exhaustion, and the correlations are comparable with that in TIMER (**Table 3**). Therefore, ITGAL may regulate T-cell exhaustion, and macrophage polarization in STAD.

The expression of integrin alpha L is associated with immunomodulators in gastric cancer

Immunomodulators are substances that affect the function of the immune system. This research indicated that ITGAL was significantly connected with immunoinhibitors ($p < 2.2e{-}16$), such as BTLA (rho = 0.843), CD96 (rho = 0.89), CD274 (rho = 0.526), CSF1R (rho = 0.69), HAVCR2 (rho = 0.716), PDCD1 (rho = 0.77), and TIGIT (rho = 0.88) (**Figure 6A**). The expression of ITGAL was also closely associated with immunostimulators ($p < 2.2e{-}16$), including CD27 (rho = 0.849), CD28 (rho = 0.841), CD40 (rho = 0.559), CD48 (rho = 0.88), CD80 (rho = 0.665), CD86 (rho = 0.723), CXCR4 (rho = 0.638), ICOS (rho = 0.793), IL2RA (rho = 0.702), KLRK1 (rho = 0.833), and LTA (rho = 0.819) (**Figure 6B**). These results suggested that ITGAL is intimately engaged in the regulation of

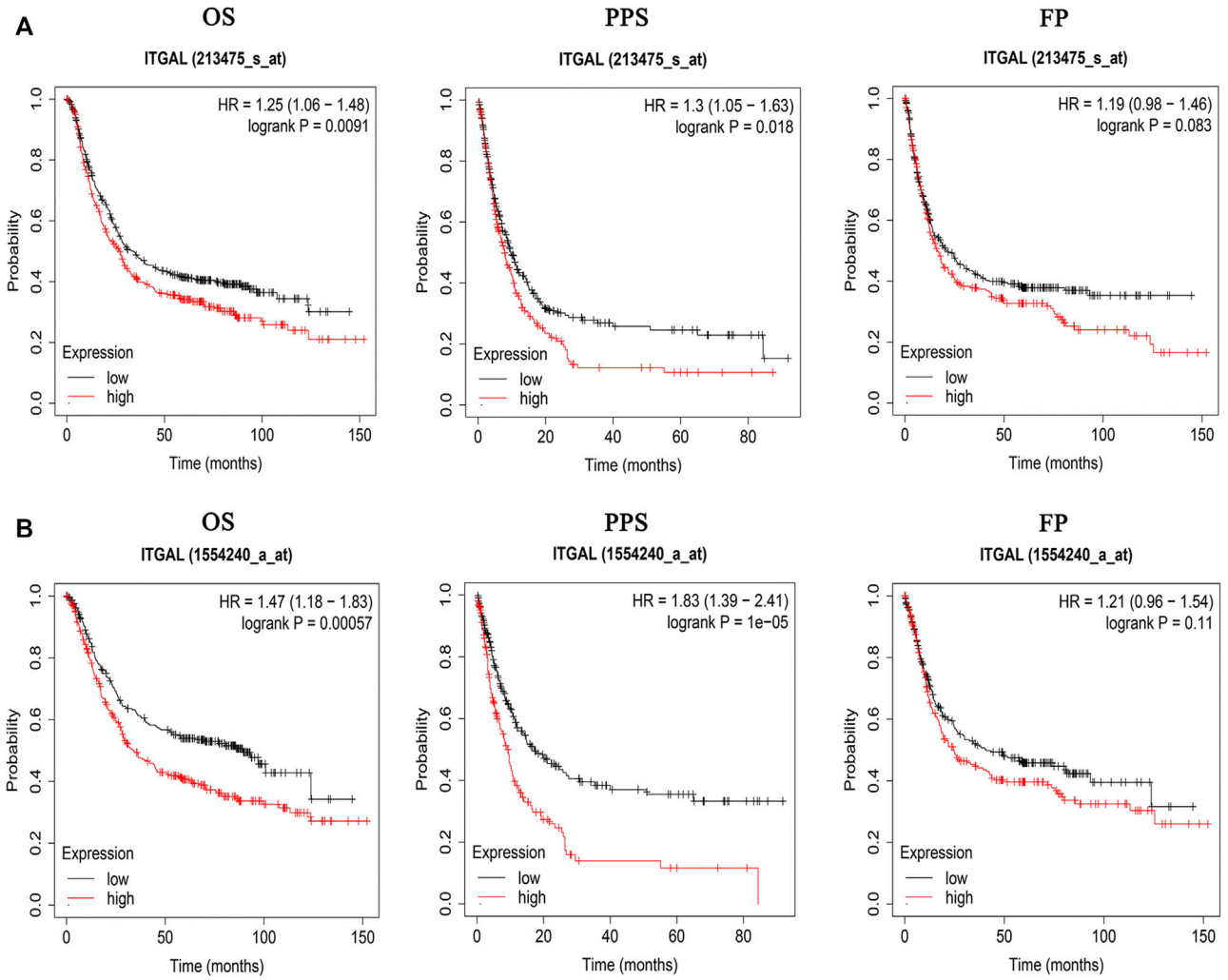

FIGURE 3 | Kaplan–Meier survival curves comparing the high and low expression of ITGAL in gastric cancer in Kaplan–Meier plotter databases. **(A)** Survival curves of OS, PPS, and FP in the gastric cancer cohort (213475-s-at). **(B)** OS, PPS, and FP survival curves of gastric cancer (1554240-a-at). OS, overall survival; PPS, post-progression survival; FP, first progression.

the immune interaction and may modulate tumor immune escape.

Correlation between the integrin alpha L expression and chemokines in gastric cancer

Chemokines play a great function in controlling infiltration degree of immune cell. This research implicated the association between ITGAL expression with chemokines. For example, ITGAL expression was significantly linked with CCL2 (rho = 0.353), CCL3 (rho = 0.353), CCL4 (rho = 0.584), CCL5 (rho = 0.788), CCL8 (rho = 0.347), CCL11 (rho = 0.396), CCL13 (rho = 0.408), CCL17 (rho = 0.54), CCL18 (rho = 0.383), CCL19 (rho = 0.663), CCL21 (rho = 0.471), CCL22 (rho = 0.677), CCL23 (rho = 0.458), CX3CL1 (rho = 0.421), CXCL9 (rho = 0.673), CXCL10 (rho = 0.526), CXCL13 (rho = 0.73), and XCL2 (rho = 0.668) (**Figure 7A**). All the values of p were far less than 0.001. Meanwhile, we demonstrated that ITGAL expression was also significantly correlated with chemokine receptors ($p < 0.001$), including CCR1 (rho = 0.662), CCR2 (rho = 0.797), CCR4 (rho = 0.782), CCR5 (rho = 0.896), CCR6 (rho = 0.379), CCR7 (rho = 0.772), CCR8 (rho = 0.711), CCR9 (rho = 0.344), CCR10 (rho = 0.336), CXCR3 (rho = 0.755), CXCR4 (rho = 0.638), CXCR5 (rho = 0.707), CXCR6 (rho = 0.821), and XCR1 (rho = 0.679) (**Figure 7B**). These results further demonstrated the findings that ITGAL may function as an immunoregulatory factor in GC.

Correlation between integrin alpha L expression and infiltration degree of T-cell exhaustion in gastric cancer

In this research, TIMER and GEPIA databases were performed to investigate whether ITGAL expression had a correlation with

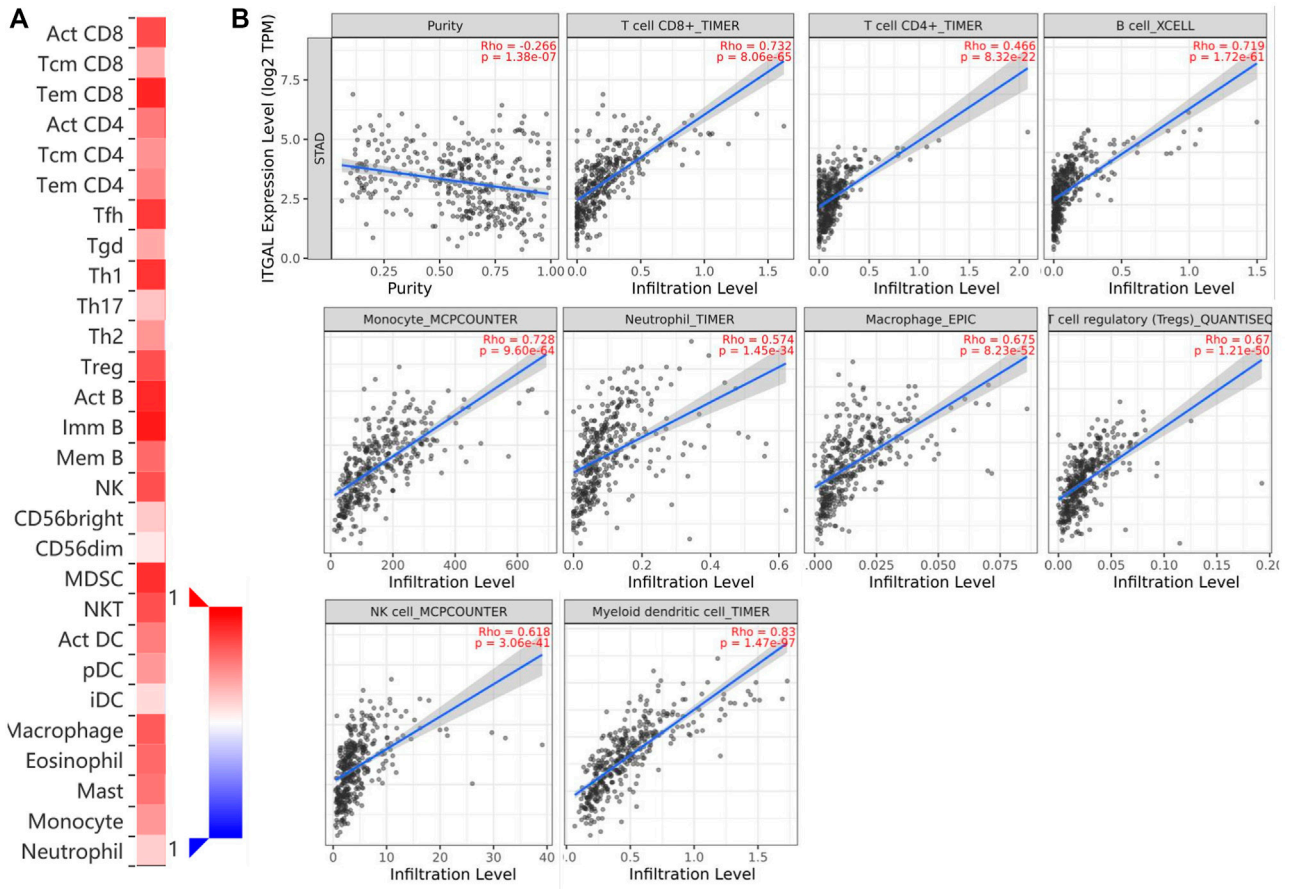

FIGURE 4 | Correlation of ITGAL expression with immune infiltration in gastric cancer. **(A)** Correlation between the expression of ITGAL and the abundance of TILs in gastric cancer available at TISIDB database. **(B)** Correlation of ITGAL expression with infiltration levels of CD8 + T cell, CD4 + T cell, Treg cell, B cell, neutrophil, macrophage, myeloid dendritic cell, natural killer cell, and monocyte in gastric cancer available at TIMER2.0 database. TILs, tumor-infiltrating lymphocytes; TIMER2.0, Tumor Immune Estimation Resource. Color images are available online.

T-cell exhaustion infiltration in GC (**Figure 5 and Table 3**), and ITGAL expression was positively correlated with PD1 (PDCD1) in GC. Therefore, we conducted an immunohistochemical method to determine the association between ITGAL and PD1 expression, and the results are presented in **Figure 8**. By scoring staining intensity, we classified the levels of the expression into four groups: negative (−), weak (+), moderate (++), and strong (+ + +) staining. ITGAL showed strong expression in most GC specimens, and a few specimens showed weak staining. Obviously, PD1 was consistent with ITGAL staining intensity (**Supplementary Figure S1**). The expression level of PD1 was correspondingly high and low in ITGAL strong and weak expression samples. These findings further demonstrated that the upregulated ITGAL corresponds to a higher T-cell exhaustion infiltration degree.

DISCUSSION

In the present research, a comprehensive bioinformatics investigation was performed to systematically analyze the clinical significance and expression lever of ITGAL in GC. Our analyses revealed poor prognosis was consistent with high expression of ITGAL in GC. Furthermore, our data also indicated that ITGAL expression had a close association with infiltration degrees of different immune cells, immunostimulators, immunoinhibitors, chemokines, and receptors in GC. Therefore, our research revealed new insights in understanding the critical function of ITGAL, and it may be a prognostic biomarker linked with immune infiltration of GC.

Integrins, the heterodimers produced by α and β subunit noncovalent binding, not only can regulate intercellular function including cellular adhesion, cell–matrix adhesion, and tumor microenvironment but also control cell proliferation and migration by recognizing specific extracellular ligands (Ruoslahti and Pierschbacher, 1987; Anikeeva et al., 2005; Schwartz et al., 2018). ITGAL, as a member of the integrin family, plays a key function in a variety of immunological processes, including leukocyte–endothelial cell interaction and cytotoxic T-cell-mediated killing (Barber et al., 2004; Giblin and Lemieux, 2006). Although ITGAL has not been thoroughly investigated, it is known that the

TABLE 2 | Correlation analysis between ITGAL and related genes and markers of immune cells in Tumor Immune Estimation Resource (TIMER2.0).

Description	Gene markers	STAD			
		None		Purity	
		Cor	*p*	Cor	*p*
$CD8^+$ T cell	CD8A	0.845	***	0.83	***
	CD8B	0.658	***	0.64	***
T cell (general)	CD3D	0.873	***	0.856	***
	CD3E	0.904	***	0.894	***
	CD2	0.691	***	0.88	***
B cell	CD19	0.893	***	-	-
	CD79A	0.711	***	0.683	***
Monocyte	CD86	0.75	***	0.733	***
	CD115 (CSF1R)	0.712	***	0.716	***
TAM	CCL2	0.414	***	0.373	***
	CD68	0.498	***	0.49	***
	IL10	0.556	***	0.53	***
M1 Macrophage	INOS (NOS2)	0.146	*	0.139	*
	IRF5	0.42	***	0.399	***
	COX2(PTGS2)	−0.053	0.28	−0.098	0.0561
M2 Macrophage	CD163	0.631	***	0.626	***
	VSIG4	0.549	***	0.546	***
	MS4A4A	0.669	***	0.657	***
Neutrophils	CD66b	−0.001	0.978	−0.009	0.859
	CD11b (ITGAM)	0.666	***	0.656	***
	CCR7	0.784	***	0.76	***
Natural killer cell	KIR2DL1	0.339	***	0.312	***
	KIR2DL3	0.31	***	0.269	***
	KIR2DL4	0.416	***	0.382	***
	KIR3DL1	0.39	***	0.382	***
	KIR3DL2	0.481	***	0.45	***
	KIR3DL3	0.137	*	0.153	*
	KIR2DS4	0.341	***	0.321	***
Dendritic cell	HLA-DPB1	0.791	***	0.771	***
	HLA-DQB1	0.616	***	0.57	***
	HLA-DRA	0.733	***	0.71	***
	HLA-DPA1	0.722	***	0.696	***
	BDCA-1(CD1C)	0.616	***	0.583	***
	BDCA-4(NRP1)	0.469	***	0.447	***
	CD11c (ITGAX)	0.718	***	0.713	***
Th1	T -bet (TBX21)	0.882	***	0.877	***
	STAT4	0.83	***	0.826	***
	STAT1	0.527	***	0.533	***
	IFN-γ (IFNG)	0.605	***	0.59	***
	TNF-α (TNF)	0.356	***	0.286	***
Th2	GATA3	0.64	***	0.616	***
	STAT6	0.287	***	0.313	***
	STAT5A	0.631	***	0.622	***
	IL13	0.183	**	0.173	**
Tfh	BCL6	0.324	***	0.301	***
	IL21	0.531	***	0.511	***
Th17	STAT3	0.411	***	0.416	***
	IL17A	0.1	0.0417	0.095	0.0651
Treg	FOXP3	0.801	***	0.779	***
	CCR8	0.738	***	0.733	***
	STAT5B	0.485	***	0.509	***
	TGFβ (TGFB1)	0.499	***	0.485	***
T cell exhaustion	PD-1 (PDCD1)	0.799	***	0.78	***
	PDL1(PDCD1LG2)	0.757	***	0.745	***
	CTLA4	0.702	***	0.668	***
	LAG3	0.735	***	0.718	***
	TIM-3 (HAVCR2)	0.751	***	0.74	***
	GZMB	0.562	***	0.523	***

*Note. STAD, stomach adenocarcinoma; TAM, tumor-associated macrophage; Th, T helper cell; Tfh, Follicular helper T cell; Treg, regulatory T cell; Cor, R value of Spearman's correlation; None, correlation without adjustment; Purity; correlation adjusted by purity. *p < 0.01; **p < 0.001; ***p < 0.0001.*

carcinogenic potential of ITGAL, whose expression levels of ITGAL plays a crucial role in carcinogenic potential, was correlated with renal cancer, ovarian cancer, colorectal cancer, and head and neck squamous cell carcinoma (Vendrell et al., 2007; Boguslawska et al., 2016; Song et al., 2019; Zhao et al., 2019; Ji et al., 2020). However, the possible function of ITGAL in regulating tumor immunity and its clinical significance in GC are still unknown.

Thus, we evaluated ITGAL expression of GC by dependent databases including GEPIA, TIMER, TCGA, and UALCAN. We discovered that ITGAL was an aberrant expression between cancer and paracancerous tissues in various malignancies. Moreover, ITGAL was obviously increased in GC compared with paracancerous samples. These results were consistent with those from TCGA database. We also found that the ITGAL mRNA and protein levels were increased in most GC samples compared with the paired paracancerous samples. These results show that the level of ITGAL expression may serve as a potential diagnostic indicator in GC. Furthermore, to confirm whether ITGAL can be used as a prognostic biomarker, we used the KM plotter database to analyze the correlation between the ITGAL expression and OS, PPS, and FP in GC cohorts (213475-s-at and 1554240-a-at). Notably, analysis of this database indicated that the higher ITGAL expression correlated with HR for worse OS and poor PPS of GC. In addition, upregulated ITGAL expression had a significant correlation with a worse prognosis of GC in stages 1 and 2, N1 and N1 + 2 + 3 with the highest HR for worse OS and in stages 2 and 4, T2 to T3, N1, N2, and N1 + 2 + 3 for worse PPS. Together, these observations strongly support our hypothesis that ITGAL is a prognostic biomarker in GC.

Additionally, this study discovered that ITGAL is strongly related to the degree of immune infiltration in GC. In the cancer microenvironment, it has been demonstrated that immune cell infiltration plays critical roles in the development and progression of cancers (Curigliano, 2018; Klauschen et al., 2018). ITGAL is a tissue-specific integrin that plays a role in inflammatory and immune responses (Lu et al., 2002). Recent studies have revealed that ITGAL could promote T-cell migration *via* reaction to Rho GTPase signaling suppression caused direct CLL cell contact (Ramsay et al., 2013; Haspels et al., 2018). However, whether ITGAL expression is linked with immune infiltration in GC remains unknown. Therefore, we systematically examined the association between ITGAL expression and the degree of immune infiltration in GC. In our experience, this is the first time that ITGAL regulating immune infiltration with GC is identified. Our study showed that ITGAL expression had a strong correlation with TILs including CD8+T cell, CD4+T cell, Treg cell, B cell, neutrophil, TAM, DCs, NK cell, and monocyte. At the same time, increased ITGAL expression was associated with immunostimulators, immunoinhibitors, chemokines, and receptors. In addition, this study also demonstrated the association between ITGAL expression and the TIL marker genes of GC. Obviously, ITGAL expression had an association with M2 macrophage markers,

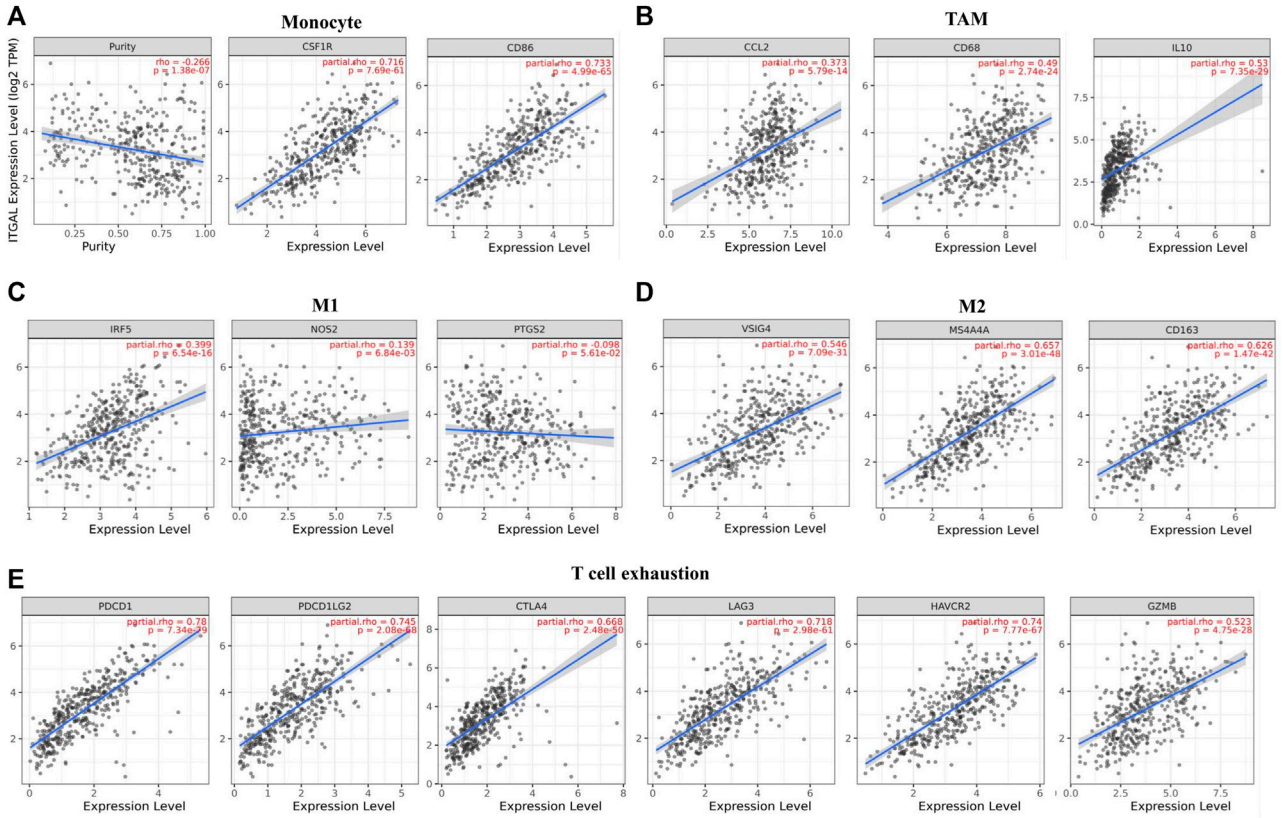

FIGURE 5 | ITGAL expression correlated with monocyte, macrophages, and T cell exhaustion in stomach adenocarcinoma (STAD). Markers include CD86 and CSF1R of monocytes; CCL2, CD68, and IL10 of TAMs; NOS2, IRF5, and PTGS2 of M1 macrophages; and CD163, VSIG4, and MS4A4A of M2 macrophages. Scatterplots of correlations between ITGAL expression and gene markers of monocytes **(A)**, TAMs **(B)**, and M1 **(C)**, M2 macrophages **(D)** and T-cell exhaustion **(E)** in STAD (n = 415).

TABLE 3 | Correlation analysis between ITGAL and related genes and markers of monocyte, macrophages, and T-cell exhaustion in Gene Expression Profiling Interaction Analysis (GEPIA).

Description	Gene markers	STAD			
		Tumor		Normal	
		Cor	*p*	Cor	*p*
Monocyte	CD86	0.75	***	0.79	***
	CD115 (CSF1R)	0.72	***	0.68	***
TAM	CCL2	0.41	***	–0.13	0.45
	CD68	0.47	***	0.45	*
	IL10	0.58	***	0.54	**
M1 Macrophage	INOS (NOS2)	0.16	**	0.16	0.36
	IRF5	0.4	***	0.32	0.06
	COX2(PTGS2)	0.035	0.48	–0.41	0.43
M2 Macrophage	CD163	0.59	***	–0.082	0.64
	VSIG4	0.54	***	0.22	0.2
	MS4A4A	0.68	***	0.14	0.4
T cell exhaustion	PD-1 (PDCD1)	0.75	***	0.88	***
	PDL1(PDCD1LG2)	0.78	***	0.44	*
	CTLA4	0.7	***	0.84	***
	LAG3	0.66	***	0.79	***
	TIM-3 (HAVCR2)	0.76	***	0.74	***
	GZMB	0.5	***	0.71	***

Note. STAD, stomach adenocarcinoma; TAM, tumor-associated macrophages; Tumor, correlation analysis in tumor tissue of TCGA; Normal, correlation analysis in normal tissue of TCGA.
*p < 0.01; **p < 0.001; ***p < 0.0001.

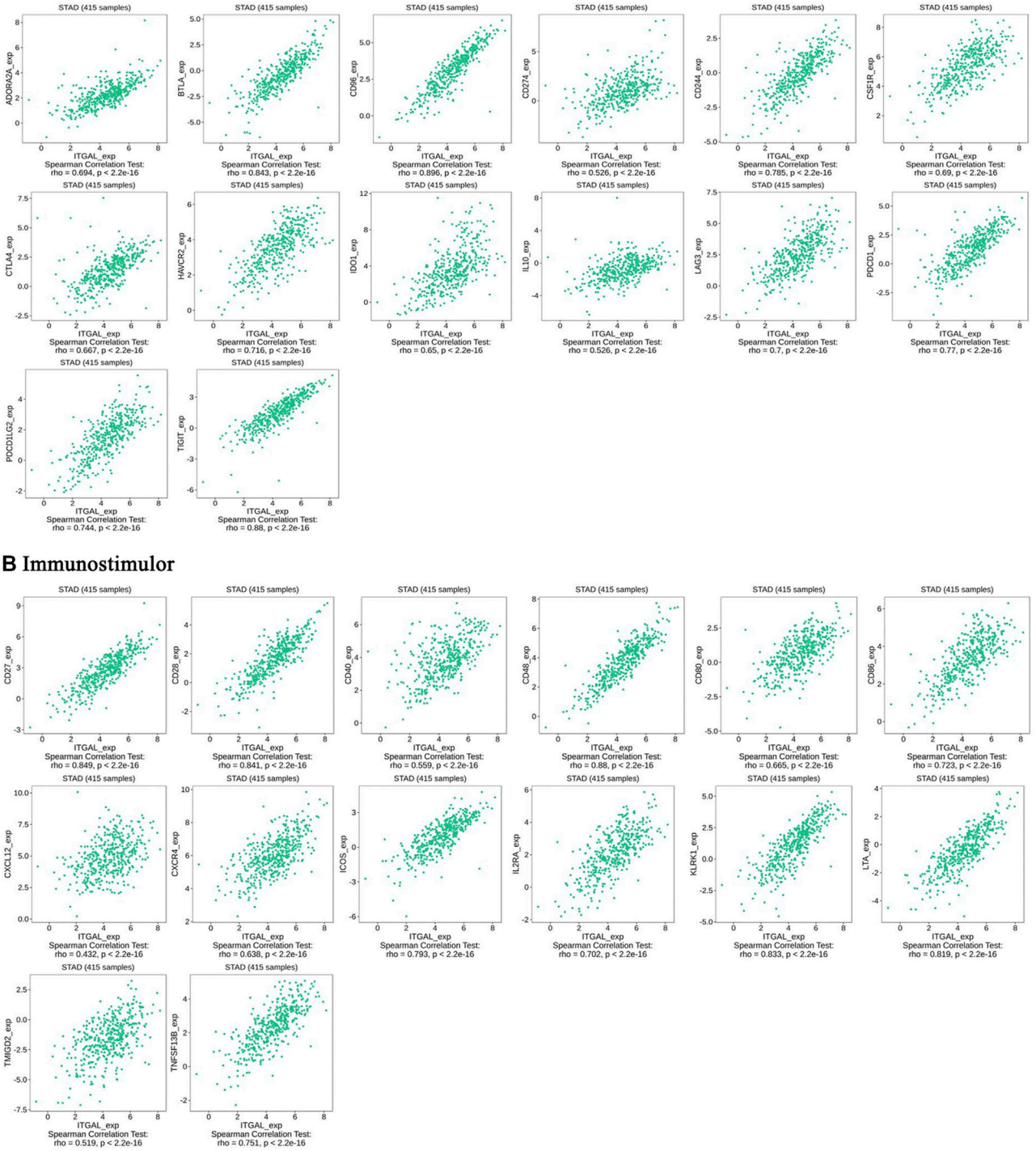

FIGURE 6 | The expression of ITGAL is associated with immunomodulators in gastric cancer. **(A)** Correlation between ITGAL expression and immunoinhibitors in gastric cancer available at TISIDB database. **(B)** Correlation between ITGAL expression and immunostimulators in gastric cancer available at TISIDB database. Color images are available online.

including CD163, VSIG4, and MS4A4A, whereas M1 macrophage markers, such as NOS2 and IRF5, correlated with ITGAL expression in very weak and moderate ways correspondingly. Macrophages, a kind of specialized immune cells, are divided into M1 and M2 macrophages (Jayasingam et al., 2019), and play a crucial function in

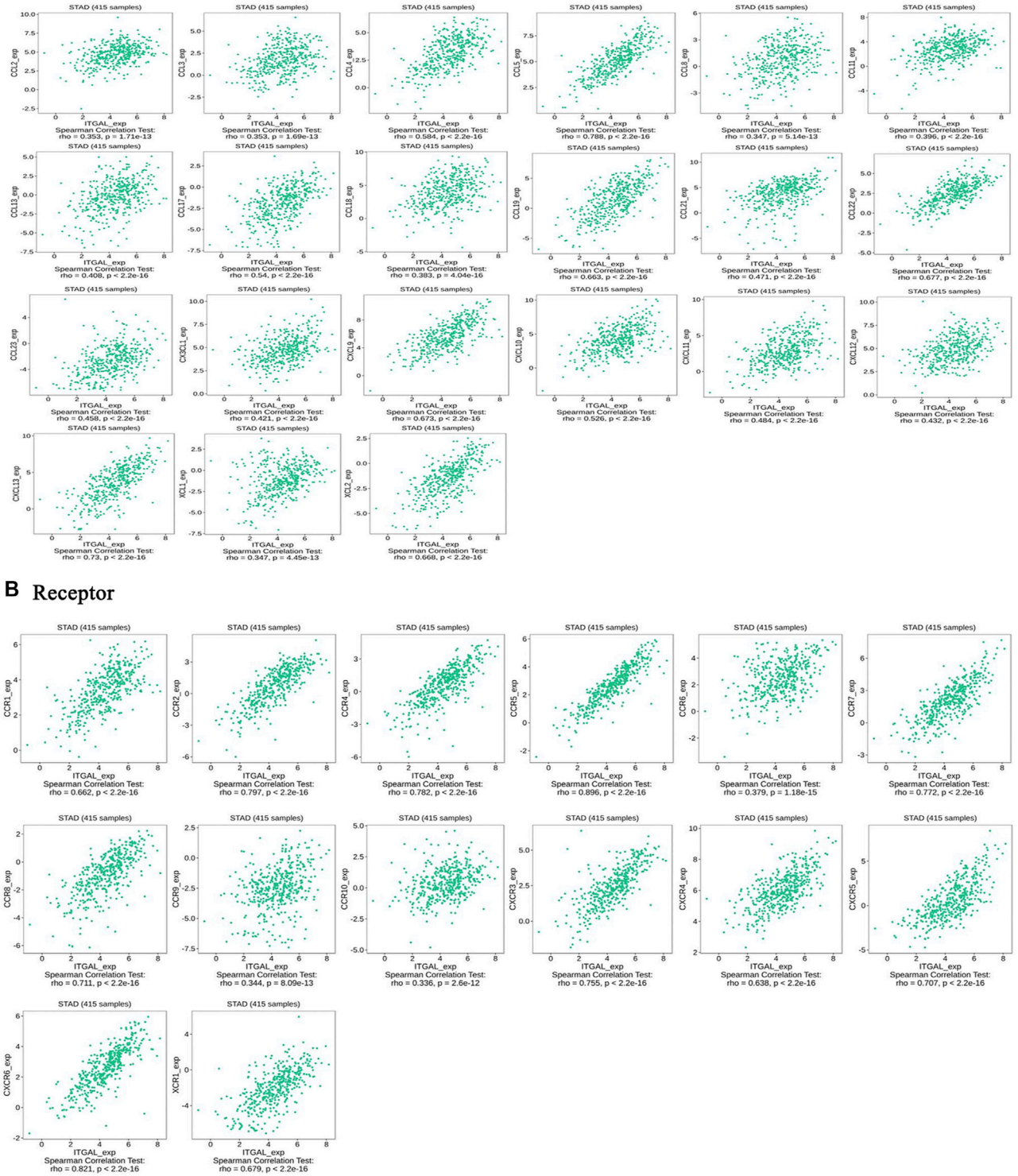

FIGURE 7 | Correlation between the expression of ITGAL and chemokines in gastric cancer. **(A)** Correlation between ITGAL expression and chemokines in gastric cancer available at TISIDB database. **(B)** Correlation between ITGAL expression and chemokine receptors in gastric cancer available at TISIDB database. Color images are available online.

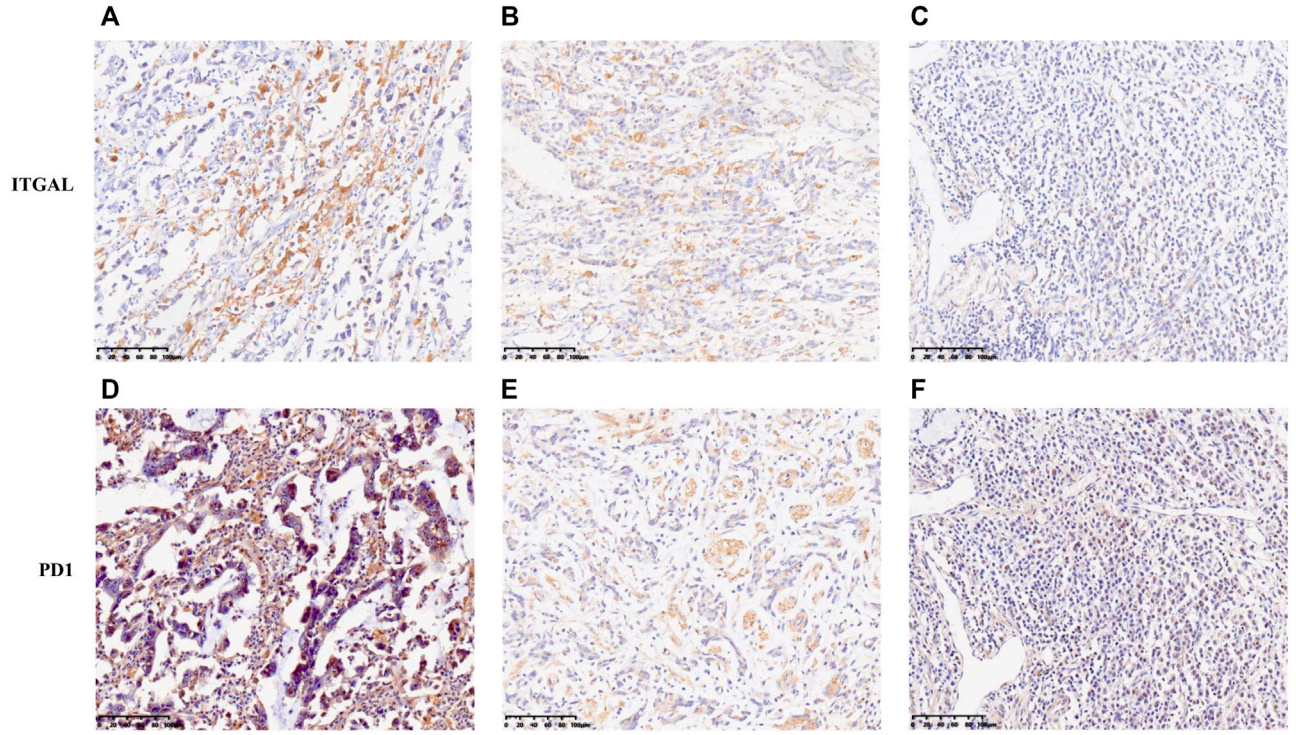

FIGURE 8 | Correlation between ITGAL expression and immune infiltration levers of T-cell exhaustion in gastric cancer. The expression of ITGAL [**(A)** +++, **(B)** ++, **(C)** +]. The expression of PD1 [**(D)** +++, **(E)** ++, **(F)** +]. The expression density of ITGAL and PD1 in gastric cancer tissue was quantitated by scoring staining intensity, including negative (–) and weak (+) staining, moderate (++) and strong (+ + +) staining, respectively.

proliferation (Su et al., 2017), angiogenesis (Sammarco et al., 2018), invasion (Zhang et al., 2018), and metastasis (Song et al., 2017), and immunity of tumor (Wynn et al., 2013). These findings indicate that ITGAL has a potential function to regulate the polarization of TAMs.

Furthermore, upregulated ITGAL expression was strongly correlated with Tregs markers (FOXP3, CCR8) and T-cell exhaustion markers (PD1, CTLA4, LAG3). Immune checkpoint blockade is the main immunotherapeutic strategy. PD1/PDL1, as the important immune checkpoint component, has been verified to regulate the function of TILs. To date, PD1/PDL1 checkpoint blockade therapy is widely performed to various malignancies including GC (Kang et al., 2017; Fuchs et al., 2018; Kim et al., 2018), but some studies discovered that PD-1 has a critical function in tumor antigen tolerance, leading to poor therapeutic effect in some patients with PD1 therapy (Woo et al., 2012; Kang et al., 2017). Therefore, the most important is to improve tumor cell response to immune checkpoint inhibitors and cytokines. Our results revealed that increased ITGAL expression was not only associated with PD1 and CTLA4 but also significantly correlated with cell response to chemokines according to the TISIDB, TIMER, and GEPIA databases. These results reflected that it may be a strategy for enhancing immunotherapy effectiveness by targeting ITGAL. In conjunction with these results, ITGAL played a vital function in recruiting and modulating TILs in GC, and it is worth to continue investigating the molecular mechanism and function of ITGAL in modulating tumor microenvironment.

However, our study has some limitations. A limitation of this study is that most data are based on the online platform databases, which are updated and expanded continuously; therefore, the results of the research may be affected. Second, the information of complications and treatment option is not included in our study. Third, the *in vitro* and *in vivo* experiment is not used to validate the function of ITGAL in GC and the molecular mechanism of ITGAL in GC immunity, but in the future study, we guarantee that we will put more emphasis to the whole baseline information of patients, and experiments will be performed to further validate the projected results.

CONCLUSION

The upregulated ITGAL expression is closely correlated with poor prognosis and enhanced immune infiltration degree including CD8+ T cells, C4+ T cells, macrophages, neutrophils, and myeloid dendritic cells in GC. Moreover, the expression of ITGAL contributes to the regulation of M2 macrophages, Treg, and T-cell exhaustion. Therefore, this

study suggests that ITGAL may, as a prognosis biomarker, highlight its novel potential function in the regulation of immune cell infiltration in GC patients.

DATA AVAILABILITY STATEMENT

The original contributions presented in the study are included in the article/**Supplementary Material**, further inquiries can be directed to the corresponding authors.

ETHICS STATEMENT

The studies involving human participants were reviewed and approved by the ethics committee of the Seventh Affiliated Hospital of Sun Yat-sen University, Shenzhen, Guangdong, China. The patients/participants provided their written informed consent to participate in this study.

AUTHOR CONTRIBUTIONS

YH and CZ designed and supervised the study. JZ and HW carried out the bioinformatics analysis, performed the experiments, and analyzed the data. JZ, HW, CY and JW wrote the paper. JZ, JX, SC, YH and CZ edited the manuscript and provided critical comments. All authors read and approved the final manuscript.

FUNDING

This study was funded by grants from the National Natural Science Foundation of China (81772579), Guangdong Province Science and Technology Plan Projects (2014A020212693), "3&3" Project of The First Affiliated Hospital of Sun Yat-Sen University (YH), and Sanming Project of Medical in Shenzhen (SZSM201911010). All these study sponsors have no roles in the study design, in the collection, analysis, and interpretation of data.

SUPPLEMENTARY MATERIAL

The Supplementary Material for this article can be found online at: https://www.frontiersin.org/articles/10.3389/fcell.2022.808212/full#supplementary-material

Supplementary Figure 1 | Correlation between ITGAL and PD1 expression based on immunohistochemical score.

REFERENCES

Anikeeva, N., Somersalo, K., Sims, T. N., Thomas, V. K., Dustin, M. L., and Sykulev, Y. (2005). Distinct Role of Lymphocyte Function-Associated Antigen-1 in Mediating Effective Cytolytic Activity by Cytotoxic T Lymphocytes. *Proc. Natl. Acad. Sci.* 102 (18), 6437–6442. doi:10.1073/pnas.0502467102

Barber, D. F., Faure, M., and Long, E. O. (2004). LFA-1 Contributes an Early Signal for NK Cell Cytotoxicity. *J. Immunol.* 173 (6), 3653–3659. doi:10.4049/jimmunol.173.6.3653

Boguslawska, J., Kedzierska, H., Poplawski, P., Rybicka, B., Tanski, Z., and Piekielko-Witkowska, A. (2016). Expression of Genes Involved in Cellular Adhesion and Extracellular Matrix Remodeling Correlates with Poor Survival of Patients with Renal Cancer. *J. Urol.* 195 (6), 1892–1902. doi:10.1016/j.juro.2015.11.050

Bray, F., Ferlay, J., Soerjomataram, I., Siegel, R. L., Torre, L. A., and Jemal, A. (2018). Global Cancer Statistics 2018: GLOBOCAN Estimates of Incidence and Mortality Worldwide for 36 Cancers in 185 Countries. *CA: A Cancer J. Clinicians* 68 (6), 394–424. doi:10.3322/caac.21492

Chandrashekar, D. S., Bashel, B., Balasubramanya, S. A. H., Creighton, C. J., Ponce-Rodriguez, I., Chakravarthi, B. V. S. K., et al. (2017). UALCAN: A Portal for Facilitating Tumor Subgroup Gene Expression and Survival Analyses. *Neoplasia* 19 (8), 649–658. doi:10.1016/j.neo.2017.05.002

Curigliano, G. (2018). Gyneco-oncological Genomics and Emerging Biomarkers for Cancer Treatment with Immune-Checkpoint Inhibitors. *Semin. Cancer Biol.* 52 (Pt 2), 253–258. doi:10.1016/j.semcancer.2018.05.004

Davidson, M., Okines, A. F. C., and Starling, N. (2015). Current and Future Therapies for Advanced Gastric Cancer. *Clin. Colorectal Cancer* 14 (4), 239–250. doi:10.1016/j.clcc.2015.05.013

Fuchs, C. S., Doi, T., Jang, R. W., Muro, K., Satoh, T., Machado, M., et al. (2018). Safety and Efficacy of Pembrolizumab Monotherapy in Patients with Previously Treated Advanced Gastric and Gastroesophageal Junction Cancer. *JAMA Oncol.* 4 (5), e180013. doi:10.1001/jamaoncol.2018.0013

Giblin, P., and Lemieux, R. (2006). LFA-1 as a Key Regulator of Immune Function: Approaches toward the Development of LFA-1-Based Therapeutics. *Cpd* 12 (22), 2771–2795. doi:10.2174/138161206777947731

Haspels, H. N., Rahman, M. A., Joseph, J. V., Gras Navarro, A., and Chekenya, M. (2018). Glioblastoma Stem-like Cells Are More Susceptible Than Differentiated Cells to Natural Killer Cell Lysis Mediated through Killer Immunoglobulin-like Receptors-Human Leukocyte Antigen Ligand Mismatch and Activation Receptor-Ligand Interactions. *Front. Immunol.* 9, 1345. doi:10.3389/fimmu.2018.01345

Jayasingam, S. D., Citartan, M., Thang, T. H., Mat Zin, A. A., Ang, K. C., and Ch'ng, E. S. (2019). Evaluating the Polarization of Tumor-Associated Macrophages into M1 and M2 Phenotypes in Human Cancer Tissue: Technicalities and Challenges in Routine Clinical Practice. *Front. Oncol.* 9, 1512. doi:10.3389/fonc.2019.01512

Ji, C., Li, Y., Yang, K., Gao, Y., Sha, Y., Xiao, D., et al. (2020). Identification of Four Genes Associated with Cutaneous Metastatic Melanoma. *Open Med. (Wars)* 15 (1), 531–539. doi:10.1515/med-2020-0190

Kang, Y.-K., Boku, N., Satoh, T., Ryu, M.-H., Chao, Y., Kato, K., et al. (2017). Nivolumab in Patients with Advanced Gastric or Gastro-Oesophageal junction Cancer Refractory to, or Intolerant of, at Least Two Previous Chemotherapy Regimens (ONO-4538-12, ATTRACTION-2): a Randomised, Double-Blind, Placebo-Controlled, Phase 3 Trial. *The Lancet* 390 (10111), 2461–2471. doi:10.1016/s0140-6736(17)31827-5

Kim, S. T., Cristescu, R., Bass, A. J., Kim, K.-M., Odegaard, J. I., Kim, K., et al. (2018). Comprehensive Molecular Characterization of Clinical Responses to PD-1 Inhibition in Metastatic Gastric Cancer. *Nat. Med.* 24 (9), 1449–1458. doi:10.1038/s41591-018-0101-z

Klauschen, F., Müller, K.-R., Binder, A., Bockmayr, M., Hägele, M., Seegerer, P., et al. (2018). Scoring of Tumor-Infiltrating Lymphocytes: From Visual Estimation to Machine Learning. *Semin. Cancer Biol.* 52 (Pt 2), 151–157. doi:10.1016/j.semcancer.2018.07.001

Kuwano, Y., Spelten, O., Zhang, H., Ley, K., and Zarbock, A. (2010). Rolling on E- or P-Selectin Induces the Extended but Not High-Affinity Conformation of LFA-1 in Neutrophils. *Blood* 116 (4), 617–624. doi:10.1182/blood-2010-01-266122

Lánczky, A., Nagy, Á., Bottai, G., Munkácsy, G., Szabó, A., Santarpia, L., et al. (2016). miRpower: a Web-Tool to Validate Survival-Associated miRNAs Utilizing Expression Data from 2178 Breast Cancer Patients. *Breast Cancer Res. Treat.* 160 (3), 439–446. doi:10.1007/s10549-016-4013-7

Larkin, J., Chiarion-Sileni, V., Gonzalez, R., Grob, J. J., Cowey, C. L., Lao, C. D., et al. (2015). Combined Nivolumab and Ipilimumab or Monotherapy in Untreated Melanoma. *N. Engl. J. Med.* 373 (1), 23–34. doi:10.1056/NEJMoa1504030

Ley, K., Laudanna, C., Cybulsky, M. I., and Nourshargh, S. (2007). Getting to the Site of Inflammation: the Leukocyte Adhesion cascade Updated. *Nat. Rev. Immunol.* 7 (9), 678–689. doi:10.1038/nri2156

Li, T., Fu, J., Zeng, Z., Cohen, D., Li, J., Chen, Q., et al. (2020). TIMER2.0 for Analysis of Tumor-Infiltrating Immune Cells. *Nucleic Acids Res.* 48 (W1), W509–W514. doi:10.1093/nar/gkaa407

Lote, H., Cafferkey, C., and Chau, I. (2015). PD-1 and PD-L1 Blockade in Gastrointestinal Malignancies. *Cancer Treat. Rev.* 41 (10), 893–903. doi:10.1016/j.ctrv.2015.09.004

Lu, Q., Ray, D., Gutsch, D., and Richardson, B. (2002). Effect of DNA Methylation and Chromatin Structure onITGAL Expression. *Blood* 99 (12), 4503–4508. doi:10.1182/blood.v99.12.4503

Luebeck, E. G., Curtius, K., Jeon, J., and Hazelton, W. D. (2013). Impact of Tumor Progression on Cancer Incidence Curves. *Cancer Res.* 73 (3), 1086–1096. doi:10.1158/0008-5472.Can-12-2198

Motzer, R. J., Escudier, B., McDermott, D. F., George, S., Hammers, H. J., Srinivas, S., et al. (2015). Nivolumab versus Everolimus in Advanced Renal-Cell Carcinoma. *N. Engl. J. Med.* 373 (19), 1803–1813. doi:10.1056/NEJMoa1510665

Procaccio, L., Schirripa, M., Fassan, M., Vecchione, L., Bergamo, F., Prete, A. A., et al. (2017). Immunotherapy in Gastrointestinal Cancers. *Biomed. Res. Int.* 2017, 4346576. doi:10.1155/2017/4346576

Ramsay, A. G., Evans, R., Kiaii, S., Svensson, L., Hogg, N., and Gribben, J. G. (2013). Chronic Lymphocytic Leukemia Cells Induce Defective LFA-1-Directed T-Cell Motility by Altering Rho GTPase Signaling that Is Reversible with Lenalidomide. *Blood* 121 (14), 2704–2714. doi:10.1182/blood-2012-08-448332

Reck, M., Rodríguez-Abreu, D., Robinson, A. G., Hui, R., Csőszi, T., Fülöp, A., et al. (2016). Pembrolizumab versus Chemotherapy for PD-L1-Positive Non-small-cell Lung Cancer. *N. Engl. J. Med.* 375 (19), 1823–1833. doi:10.1056/NEJMoa1606774

Ru, B., Wong, C. N., Tong, Y., Zhong, J. Y., Zhong, S. S. W., Wu, W. C., et al. (2019). TISIDB: an Integrated Repository portal for Tumor-Immune System Interactions. *Bioinformatics* 35 (20), 4200–4202. doi:10.1093/bioinformatics/btz210

Ruoslahti, E., and Pierschbacher, M. D. (1987). New Perspectives in Cell Adhesion: RGD and Integrins. *Science* 238 (4826), 491–497. doi:10.1126/science.2821619

Samatov, T. R., Tonevitsky, A. G., and Schumacher, U. (2013). Epithelial-mesenchymal Transition: Focus on Metastatic cascade, Alternative Splicing, Non-coding RNAs and Modulating Compounds. *Mol. Cancer* 12 (1), 107. doi:10.1186/1476-4598-12-107

Sammarco, G., Gadaleta, C. D., Zuccalà, V., Albayrak, E., Patruno, R., Milella, P., et al. (2018). Tumor-Associated Macrophages and Mast Cells Positive to Tryptase Are Correlated with Angiogenesis in Surgically-Treated Gastric Cancer Patients. *Int. J. Mol. Sci.* 19, 19. doi:10.3390/ijms19041176

Schwartz, A. D., Hall, C. L., Barney, L. E., Babbitt, C. C., and Peyton, S. R. (2018). Integrin α6 and EGFR Signaling Converge at Mechanosensitive Calpain 2. *Biomaterials* 178, 73–82. doi:10.1016/j.biomaterials.2018.05.056

Seguin, L., Desgrosellier, J. S., Weis, S. M., and Cheresh, D. A. (2015). Integrins and Cancer: Regulators of Cancer Stemness, Metastasis, and Drug Resistance. *Trends Cel Biol.* 25 (4), 234–240. doi:10.1016/j.tcb.2014.12.006

Silva, R., D'Amico, G., Hodivala-Dilke, K. M., and Reynolds, L. E. (2008). Integrins. *Atvb* 28 (10), 1703–1713. doi:10.1161/atvbaha.108.172015

Song, W., Mazzieri, R., Yang, T., and Gobe, G. C. (2017). Translational Significance for Tumor Metastasis of Tumor-Associated Macrophages and Epithelial-Mesenchymal Transition. *Front. Immunol.* 8, 1106. doi:10.3389/fimmu.2017.01106

Song, Y., Pan, Y., and Liu, J. (2019). The Relevance between the Immune Response-Related Gene Module and Clinical Traits in Head and Neck Squamous Cell Carcinoma. *Cmar* 11, 7455–7472. doi:10.2147/cmar.S201177

Su, C., Jia, S., and Liu, H. (2017). Immunolocalization of CD163+ Tumor-Associated Macrophages and Symmetric Proliferation of Ki-67 as Biomarkers to Differentiate New Different Grades of Laryngeal Dysplasia. *Am. J. Clin. Pathol.* 149 (1), 8–16. doi:10.1093/ajcp/aqx107

Sumagin, R., Prizant, H., Lomakina, E., Waugh, R. E., and Sarelius, I. H. (2010). LFA-1 and Mac-1 Define Characteristically Different Intralumenal Crawling and Emigration Patterns for Monocytes and Neutrophils *In Situ*. *J.Immunol.* 185 (11), 7057–7066. doi:10.4049/jimmunol.1001638

Tang, Z., Li, C., Kang, B., Gao, G., Li, C., and Zhang, Z. (2017). GEPIA: a Web Server for Cancer and normal Gene Expression Profiling and Interactive Analyses. *Nucleic Acids Res.* 45 (W1), W98–w102. doi:10.1093/nar/gkx247

Vendrell, E., Ribas, M., Valls, J., Solé, X., Grau, M., Moreno, V., et al. (2007). Genomic and Transcriptomic Prognostic Factors in R0 Dukes B and C Colorectal Cancer Patients. *Int. J. Oncol.* 30 (5), 1099–1107. doi:10.3892/ijo.30.5.1099

Wang, X. K., Zhang, Y. W., Wang, C. M., Li, B., Zhang, T. Z., Zhou, W. J., et al. (2021). METTL16 Promotes Cell Proliferation by Up-regulating Cyclin D1 Expression in Gastric Cancer. *J. Cel Mol Med* 25 (14), 6602–6617. doi:10.1111/jcmm.16664

Winograd-Katz, S. E., Fässler, R., Geiger, B., and Legate, K. R. (2014). The Integrin Adhesome: from Genes and Proteins to Human Disease. *Nat. Rev. Mol. Cel Biol* 15 (4), 273–288. doi:10.1038/nrm3769

Woo, S.-R., Turnis, M. E., Goldberg, M. V., Bankoti, J., Selby, M., Nirschl, C. J., et al. (2012). Immune Inhibitory Molecules LAG-3 and PD-1 Synergistically Regulate T-Cell Function to Promote Tumoral Immune Escape. *Cancer Res.* 72 (4), 917–927. doi:10.1158/0008-5472.Can-11-1620

Wynn, T. A., Chawla, A., and Pollard, J. W. (2013). Macrophage Biology in Development, Homeostasis and Disease. *Nature* 496 (7446), 445–455. doi:10.1038/nature12034

Xie, J., Guo, T., Zhong, Z., Wang, N., Liang, Y., Zeng, W., et al. (2021). ITGB1 Drives Hepatocellular Carcinoma Progression by Modulating Cell Cycle Process through PXN/YWHAZ/AKT Pathways. *Front. Cel Dev. Biol.* 9, 711149. doi:10.3389/fcell.2021.711149

Yang, L., Chen, Z., Xiong, W., Ren, H., Zhai, E., Xu, K., et al. (2019). High Expression of SLC17A9 Correlates with Poor Prognosis in Colorectal Cancer. *Hum. Pathol.* 84, 62–70. doi:10.1016/j.humpath.2018.09.002

Yoshihara, K., Shahmoradgoli, M., Martínez, E., Vegesna, R., Kim, H., Torres-Garcia, W., et al. (2013). Inferring Tumour Purity and Stromal and Immune Cell Admixture from Expression Data. *Nat. Commun.* 4, 2612. doi:10.1038/ncomms3612

Zhang, D., Qiu, X., Li, J., Zheng, S., Li, L., and Zhao, H. (2018). TGF-β Secreted by Tumor-Associated Macrophages Promotes Proliferation and Invasion of Colorectal Cancer via miR-34a-VEGF axis. *Cell Cycle* 17 (24), 2766–2778. doi:10.1080/15384101.2018.1556064

Zhao, X., Lei, Y., Li, G., Cheng, Y., Yang, H., Xie, L., et al. (2019). Integrative Analysis of Cancer Driver Genes in Prostate Adenocarcinoma. *Mol. Med. Rep.* 19 (4), 2707–2715. doi:10.3892/mmr.2019.9902

Conflict of Interest: The authors declare that the research was conducted in the absence of any commercial or financial relationships that could be construed as a potential conflict of interest.

Publisher's Note: All claims expressed in this article are solely those of the authors and do not necessarily represent those of their affiliated organizations, or those of the publisher, the editors, and the reviewers. Any product that may be evaluated in this article, or claim that may be made by its manufacturer, is not guaranteed nor endorsed by the publisher.

Copyright © 2022 Zhang, Wang, Yuan, Wu, Xu, Chen, Zhang and He. This is an open-access article distributed under the terms of the Creative Commons Attribution License (CC BY). The use, distribution or reproduction in other forums is permitted, provided the original author(s) and the copyright owner(s) are credited and that the original publication in this journal is cited, in accordance with accepted academic practice. No use, distribution or reproduction is permitted which does not comply with these terms.

Frontiers in
Cell and Developmental Biology

Explores the fundamental biological processes of life, covering intracellular and extracellular dynamics.

The world's most cited developmental biology journal, advancing our understanding of the fundamental processes of life. It explores a wide spectrum of cell and developmental biology, covering intracellular and extracellular dynamics.

Discover the latest Research Topics

See more →

Frontiers

Avenue du Tribunal-Fédéral 34
1005 Lausanne, Switzerland
frontiersin.org

Contact us

+41 (0)21 510 17 00
frontiersin.org/about/contact